PB82-241159

Air Pollution: Proceedings of the Seventh International Technical Meeting on Air Pollution Modeling and its Application 7-10 September 1976

(U.S.) NATO Committee on the Challenges of Modern Society, Brussels (Belgium)

1976

U.S. Department of Commerce
National Technical Information Service
NTIS

TECHNICAL REPORT DATA

(Please read Instructions on the reverse before completing)

1. REPORT NO. 51

2.

3. RECIPIENT'S ACCESSION NO. PB82-241159

4. TITLE AND SUBTITLE
Air Pollution: Proc. of the 7th International Technical Meeting on Air Pollution Modeling and its Application

5. REPORT DATE 1976

6. PERFORMING ORGANIZATION CODE

7. AUTHOR(S)

8. PERFORMING ORGANIZATION REPORT NO.

9. PERFORMING ORGANIZATION NAME AND ADDRESS
U.S. EPA, RTP
Air Pollution Pilot Study

10. PROGRAM ELEMENT NO.

11. CONTRACT/GRANT NO.

12. SPONSORING AGENCY NAME AND ADDRESS
NATO Committee on the Challenges to Modern Society

13. TYPE OF REPORT AND PERIOD COVERED

14. SPONSORING AGENCY CODE

15. SUPPLEMENTARY NOTES

16. ABSTRACT

Focus is on seven areas: Model validation and application, interregional & regional models, sensitivity analysis and dispersion under low wind speeds, numerical grids and physical modeling, tall stack plume, diffusion parameters and stability categories and innovative modeing techniques.

17. KEY WORDS AND DOCUMENT ANALYSIS

a. DESCRIPTORS	b. IDENTIFIERS/OPEN ENDED TERMS	c. COSATI Field/Group
Air Pollution Air Pollution Modeling		EPA 68A

18. DISTRIBUTION STATEMENT	**19. SECURITY CLASS** *(This Report)*	**21. NO. OF PAGES** 1109
	20. SECURITY CLASS *(This page)*	**22. PRICE**

EPA Form 2220-1 (Rev. 4-77) PREVIOUS EDITION IS OBSOLETE

PB82-241159

COMMITTEE ON THE CHALLENGES OF MODERN SOCIETY

NATO CDSM
OTAN CCMS

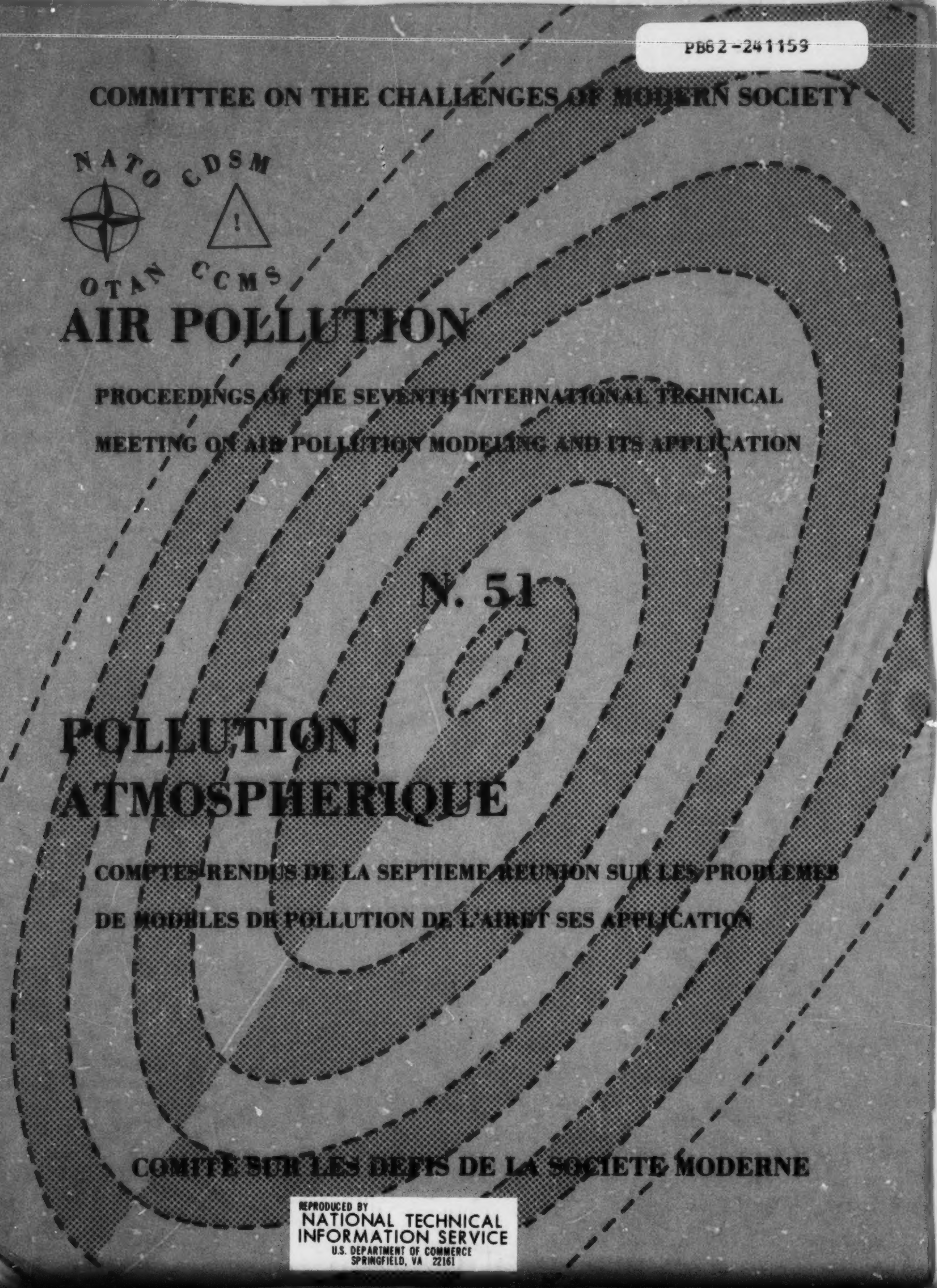

AIR POLLUTION

PROCEEDINGS OF THE SEVENTH INTERNATIONAL TECHNICAL MEETING ON AIR POLLUTION MODELING AND ITS APPLICATION

N. 51

POLLUTION ATMOSPHERIQUE

COMPTES RENDUS DE LA SEPTIEME REUNION SUR LES PROBLEMES DE MODELES DE POLLUTION DE L'AIR ET SES APPLICATION

COMITE SUR LES DEFIS DE LA SOCIETE MODERNE

REPRODUCED BY
NATIONAL TECHNICAL
INFORMATION SERVICE
U.S. DEPARTMENT OF COMMERCE
SPRINGFIELD, VA 22161

PROCEEDINGS OF THE SEVENTH INTERNATIONAL TECHNICAL MEETING ON AIR POLLUTION MODELING AND ITS APPLICATION

7 - 10 September 1976

AIRLIE HOUSE, VIRGINIA
United States of America

A Report of the Air Pollution Pilot Study

NATO Committee on the Challenges to Modern Society

1976

PREFACE

Celebrating the 200 years anniversary of its independence in 1976 the United States of America as co-pilot nation for the Air Pollution Pilot Study "Assessment Methodology and Modeling" invited experts in air pollution modeling as well as users of air quality models or decision makers in air quality management for their seventh International Technical Meeting on Air Pollution Modeling and its Application.

74 international experts representing ten countries (Belgium 3, Canada 7, France 1, Federal Republic of Germany 16, Italy 7, Netherlands 4, Norway 1, Sweden 1, United States of America 32, United Kingdom 2) followed the invitation and appreciated the outstanding hospitality of this country.

Seven topics have been discussed:
Examples of Model Validation and Model Application, Interregional and Regional Models, Sensitivity Analysis and Dispersion under Low Wind Speeds, Numerical Grids and Physical Modeling, Tall Stack Plume, including Sulphate Transformation and Removal, Diffusion Parameters and Stability Categories, Innovative Modeling Techniques.

Special thanks are due to the United States Environmental Protection Agency, RTP, to James R. Hammerle and his staff, for the preparation and organization of the meeting and for making available all technical support required.

The present document contains the papers that were submitted, together with the reports of the several rapporteurs to the different sessions of the meeting, summarizing the discussions which followed each presentation. Like in Frankfurt last year, it was not possible to provide time for an oral presentation of all papers that are published in this document.

The secretariat of the NATO/CCMS Air Pollution Pilot Study again takes the opportunity to thank all authors and rapporteurs for having submitted their presentations and reports so promptly.

Christa Morawa

Secretariat for the NATO/CCMS Air Pollution
Pilot Study
Umweltbundesamt
1 Berlin 33
Bismarckplatz 1

CONTENTS

Opening (and Closing) Remarks ....I - VII

CHAPTER I

Page:

Examples of Model Validation and Model Application 1

1. Two Efficient Gaussian Plume Models Developed at the Texas Air Control Board (R. A. Porter, J. H. Christiansen) 2

2. Air Quality Management Utilizing Air Quality Models (D. M. Rote) 25

3. Applications of Mathematical Models in Pollution Network Planning and Air Quality Control (A. Cavallaro, R. Gualdi, G. Laneve, G. Tebaldi) 50

4. The Validation of a Gaussian Plume Point Source Diffusion Model in a Lake Shore Environment (L. L. Schulman, Th. F. Lavery, St. G. Penansky) 82

5. Rapporteur's Summary Report: J. B. Knox 112

6. Diffusion Model Comparisons to Measured Data in Complex Terrain (R. B. Lantz, G. F. Hoffnagle, S. B. Pahwa) 119

7. The Application of Dispersion Models in a Fjord Valley Area of Norway (B. Sivertsen) 143

8. The Validation of the Gaussian Dispersion Model for Long-Term Average Ground Level Concentrations in the Rijnmond Region (F. T. M. Nieuwstadt, C. M. Verheul, J. Addicks) 169

9. A Dual Tracer Study for the Validation of Models with Respect to High and Low Altitude Source (J. H. Overton, B. K. Lamb, F. H. Shair, W. E. Wilson) ..219

10. Validation of the Immission Frequency Distribution Model in the Region of Antwerpen, Belgium (J. G. Kretzschmar, G. de Baere, J. Vandervee) 235

11. Rapporteur's Summary Report: B. A. Egan 271

CHAPTER II

Page

Interregional and Regional Models 276

12. Preliminary Results of the Application of a Statistical Model on Interregional Transport of SO_2 (B. Dietzer) 277

13. The European Regional Model of Air Pollution (EURMAP) and its Application to Transfrontier Air pollution (M. B. Johnson, D.L. Wolf, R. L. Mancuso) 292

14. Recent Advances in the Simulation of Regional Air Quality (J. B. Knox) 372

15. Rapporteur's Summary Report: H. E. Turner 409

16. Modeling Mountain Air Quality (D. G. Fox, M. A. Fosberg) 413

17. A Regional Scale Model for Computing Deposition and Ground Level Air Concentration of SO_2 and Sulfates from Elevated and Ground Sources (L. L. Wendell, D. C. Powell, R. L. Drake) 428

18. Analytical-Numerical Model for Mesoscale Transport, Transformation and Removal of Air Pollutants (N. V. Gillani, R. B. Husar) 436

19. A Study of Long Range Transport from Visibility Observations, Trajectory Analysis and Local Air Pollution Monitoring Data (R. B. Husar, N. V. Gillani, J. D. Husar, D. E. Patterson) 468

20. Rapporteur's Summary Report: A. Keddie 487

CHAPTER III

Sensitivity Analysis and Dispersion under Low Wind Speed ...490

21. Sensitivity Analysis of the Single Source (CRSTER) Model (W. P. Freas, R. F. Lee) 491

Page

22. Concentration and Index Sensitivity of a Gaussian Plume Model
(W. J. Veigele, R. L. Clayson) 515

23. An Air Quality Dispersion Model Applicable to Calm Conditions
(R. J. Yamartino) 537

24. The Role of Turbulent Diffusion in the Direction of the Mean Wind in a Numerical AQSM
(K. Herrmann) 555

25. Influences of Model Parameters and Sensitivity to Their Variation within the Immissions Forecasting
(L. Kropp, H. Bresser) 582

26. Rapporteur's Summary Report: R. Porter 605

CHAPTER IV

Numerical Grids and Physical Modeling 610

27. Dispersion of Roof-Top Emissions from Isolated Buildings - A Wind Tunnel Study -
(R. S. Thompson, D. J. Lombardi) 611

28. An Efficient Air Quality K-Model
(E. Runca) 628

29. Further Developments in the Application of Shir's Model to the Venice Area
(G. L. Marziano, A. Sutera, L. Gianolio, M. Ciprian) ..651

30. A Three-Dimensional Advective-Diffusive Model for Long Range Sulfate Transport and Transformation
(B. A. Egan, K. S. Rao, A. Bass) 697

31. An Empirical Equation for Simulating Maximum Concentration Values Occuring at Buildings Projecting into the Path of a Plume in the Immediate Vicinity of an Emission Source
(J. Giebel) 715

32. Rapporteur's Summary Report: D. G. Fox 726

Page

CHAPTER V

Tall Stack Plume, including Sulphate Transformation and Removal Processes 730

33. Improved Techniques for Modeling the Dispersion of Tall Stack Plumes
(H. E. Cramer) 731

34. Plume Dispersion from the Sudbury Tall Stack
(F. H. Fanaki, H. E. Turner) 781

35. A Comparison of "STAR" Stability Predictions, Measured Lapse-Rate Stability Classification and Observed Tall Stack Plume Dispersion Parameters
(R. V. Portelli) 813

36. Mathematical Modelling of Chemical Reactions in a Plume
(M. Lusis) 831

37. On SO_2-Removal and Sulfate Formation Processes in the Atmosphere
(D. R. Kalthoff) 856

38. Rapporteur's Summary Report: W. B. Johnson 871

CHAPTER VI

Diffusion Parameters and Stability Categories 875

39. Comparison between Experimentally Measured Diffusion Parameters and the Main Stability Criteria
(L. Santomauro, D. Anfossi, P. Bacci, A. Longhetto) ...876

40. Experimental Study of Atmospheric Diffusion Parameters
(A. Saab, M. Ribon) 896

41. Rapporteur's Summary Report: R. Lee 910

Page

CHAPTER VII

Innovative Modeling Techniques 913

42. Modeling the Atmospheric Dispersal of Radioactive Pollutants Beyond the First Few Hours of Travel (H. ApSimon, A. J. H. Goddard) 914

43. Diffusion and Transport of a Passive Contaminant Over Complex Terrain Under Stable and Unstable Conditions (R. A. Anthes, N. Seaman, D. Kayser) 931

44. On Theoretical Methods for the Solution of Complex Urban Air Pollution Problems (H. Fortak) 948

45. Pollutant Dispersion Simulation by Monte Carlo Techniques (K. H. Müller) 989

46. Mathematical Model for Urban Diffusion of Carbon Monoxide from Motor Vehicles (P. P. Gaddo, F. Corazzari, R. Borgialli, G. Marcenaro G. Marchesi, F. Carbone, G. Ferrante, D. Casella, A. Piccone, S. Chiaiso, E. Damasio) 1013

47. Rapporteur's Summary Report: D. M. Rote 1031

48. Some Considerations about the Stability Categories in the Case of Short Range Diffusion of Atmospheric Releases (P. Cagnetti) 1037

49. Application of the Tennekes-Carson Slab Model of the PBL to the Prediction of Internal Boundary Layer Development (A. Venkatram) 1059

Agenda 1074
Attendees 1085

7 th NATO/CCMS
International Technical Meeting
on Air Pollution Modeling

OPENING (AND CLOSING) REMARKS

by

Erich Weber

Bundesministerium des Innern

- Abteilung Umwelt -

AIRLIE HOUSE, AIRLIE, VIRGINIA
UNITED STATES OF AMERICA
September 7 - 10, 1976

Ladies and Gentlemen,

As representative of the Federal Republic of Germany and chairman of the Pilot Study on Air Pollution, I am very pleased to welcome you at Airlie House. This is the 7th I.T.M. on modeling, and this symposium is for the first time taking place in the United States. I should like to express my thanks to the United States in several respects - it was the delegates of the United States EPA who in 1970 took the initiative and established this symposium, and moreover, the delegates or experts of the United States have in the last few years always gone to the trouble of travelling to Europe for attending this symposium - a fact that greatly relieved us Europeans and highly facilitated our cooperation. I should also like to thank the United States for their invitation to hold the 7th symposium in the United States on the occasion of the bicentennial of Independence Day. After the many years of excellent cooperation we are very pleased with your invitation, and it is only natural for us to accept it.
I think it is time now that the experts from Europe also go to the trouble of travelling over long distances in order to visit this country in the Bicentennial and to celebrate it together with our friends in the United States. Special thanks are due to the United States EPA for enabling us to do this at such an attractive place as Airlie House. Last year the symposium took place in Frankfurt, Germany. It was attended by 71 experts, and 27 papers were presented and discussed. It was the objective

of the Frankfurt symposium to continue the discussions started in Denmark at the 5th symposium in autumn 1974 and to create the basis for a discussion between designers of models and model-users. The three items on the agenda "Current and future applications of air pollution modeling and its application", "Requirements of standardization of AQSM's and requirements of a common data base for AQSM's" and "Validation of AQSM's" were discussed there at length. The results of the lectures and discussions were summarized by one or several rapporteurs. The lectures and the summaries have been published in NATO /CCMS document No. 42 in spring 1976. Due to the quite enthusiastic response of the participants and the limited time that was available, it was unfortunately not possible in every case to provide time for an oral presentation. As far as they were submitted in written form, they were, however, included into the NATO /CCMS document.

By the end of the symposium in Frankfurt, the responsible organizers concluded that any further problems involved in the practical application of AQSM's should not be discussed at the 7th symposium at Airlie House. It appeared to us, that, at the present stage, new problems should be taken up and dealt with. This does not exclude that at the symposium in autumn 1970 or 1979 the problems of model application and the discussion between designers of models and model users will be put on the agenda again. We were, however, of the opinion that here at Airlie House problems should be dealt with that are of importance for the future with regard to scientific research and application. We have chosen several sets of topics that appeared to be of particular importance. You will find them on the agenda of our symposium.

The response to the individual sets of topics on the agenda varied strongly. We had to turn down some papers for oral presentation in the case of several items, while on other items only few papers had been submitted. This does not imply any value judgement.

However, when compiling the agenda for the next symposium which is also to serve the discussion of problems important for the future, we shall have to give particular attention to the results of the discussions here at Airlie House and the reports of the rapporteurs. The rapporteurs' summary reports are of particular importance in this context. They should, if possible, also indicate whether the agenda item referred to will need rediscussion at the next symposium or whether it should be postponed for the time being.

This will be of decisive impact on the agenda of the next symposium planned for autumn 1977.

The programme of this symposium is very extensive.
It is therefore important that the time schedule with regard to lectures and discussions should be adhered to as closely as possible, and I have asked the chairmen of the various sessions to see to it that this requirement is met. At the same time I should like to ask the speakers to transmit the fair copies of their lectures to the secretariate of the Pilot Study, so that we shall be able to complete the NATO / CCMS document on the symposium this very year. I should also like to ask the rapporteurs to finish the summary reports on lectures and discussions already here at Airlie House and to submit them to the secretariate. The rapporteurs' reports may also be submitted in hand writing, though in legible form.

I will not conclude without having expressed my particular thanks to the organizers of this meeting. This applies in particular to the members of the United States EPA who have done excellent work here and who in the next three days will have to tackle many additional problems. I should also like to express my appreciation to Mrs. Christa Morawa and Dr. Dieter Jost who have been responsible for the selection of the presentations and the scientific organization.

Now I should like to give the floor to Dr. Jim Hammerle as delegate of the host country and representative of the United States EPA and then to Dr. Dieter Jost who has taken over the chairmanship at this meeting. I thank you for your cooperation in this symposium and hope it will be successful.

Concluding Remarks

Ladies and Gentlemen,

We have now arrived at the end of this symposium. Let me first give just a few statistical data:

40 papers were read
9 rapporteurs have prepared a summary of the
7 items of the agenda, more than
70 experts

of NATO and non-NATO countries have been participating.

I think this symposium has been very successful. Its character was somewhat different from earlier symposia since the majority of the participants came from the host country. I feel that we, and in particular the participants from Europe, have been able to gather many new impressions. This applies in particular to the organizers of the next I.T.M. on Modeling.
The agenda will be strongly influenced by the impressions gained during the extensive discussions. Apparently some of the points treated here will require further discussion:

We shall take this into consideration when preparing the final agenda. I feel that the problems with regard to modeling at low wind speeds and the questions of the transformation of primary emissions into secondary air pollutants, i. e. the problem of sources and sinks, is of particular importance for the future. The same applies to the questions with regard to the modeling of the transport of air pollutants over long distances or beyond national frontiers.

In conclusion I should like to express my thanks to all participants in this symposium for their active cooperation. I should like to thank in particular the speakers, the chairmen of the various sessions, the organizers and the rapporteurs for their excellent work. Special thanks are due to the United States EPA for their great hospitality.

Dr. Hammerle as representative of the host country and Dr. Renson as delegate of Belgium, the country where the next I.T.M. on Modeling will take place in autumn 1977, will be the last speakers of this conference.

I should like to ask you to pay attention to an information paper that has been distributed and will give you preliminary information on the agenda, place and time of the next symposium in Belgium in autumn 1977. Once more many thanks to you, and I am looking forward to seeing you again.

7 th NATO/CCMS
International Technical Meeting
on Air Pollution Modeling

TOPIC I

EXAMPLES OF MODEL VALIDATION AND MODEL APPLICATION

Two Efficient Gaussian Plume Models
Developed at the Texas Air Control Board

Richard A. Porter, P.E.
Meteorology Section
Texas Air Control Board
Austin, Texas

John H. Christiansen
Data Processing Section
Texas Air Control Board
Austin, Texas

September 8, 1976

7th NATO/CCMS International Technical
Meeting on Air Pollution Modeling

ABSTRACT

Two Gaussian plume mathematical models developed at the Texas Air Control Board incorporate innovative computer techniques that provide results equivalent to other popular Gaussian models with a great savings in computer time. The Texas Climatological Model (TCM) is a long-term model that computes mean pollutant concentrations based on an annual or seasonal joint frequency function of meteorological data. The Texas Episodic Model (TEM) computes ten minute to 24-hour average concentrations based on expected meteorology for the averaging period. Each model incorporates output options that meet the operational requirements of a wide variety of users.

Two Efficient Gaussian Plume Models
Developed at the Texas Air Control Board

Introduction

Air pollution modeling is a vital part of the daily engineering analysis tasks performed by air pollution engineers and scientists in regulatory agencies, industry, consulting services, and in research facilities. At the Texas Air Control Board two Gaussian plume mathematical models have been developed that have received wide acceptance in the air pollution modeling community. The Texas Climatological Model (TCM) provides predictions of long term average concentrations based on annual or seasonal climatology. The Texas Episodic Model (TEM) provides short term average predictions based on specific meteorological scenarios. The models have proved popular because they require less computer time to execute than comparable Gaussian models while providing a variety of features and options that invite wide application by regulatory agencies, industry, consultants, and research scientists. In this paper the input/output features and options of the models are described along with examples of specific applications. The appendix provides a complete mathematical description of the various algorithms of the models.

Texas Climatological Model (TCM)

The Texas Climatological Model (TCM combines the familiar Gaussian plume point source algorithm with a simple area source algorithm proposed by Hanna and Gifford (Hanna, 1971) to calculate expected annual or seasonal mean concentrations from elevated point sources and area sources. The TCM follows the basic concept of the Climatological Dispersion Model (CDM, Busse and Zimmerman, 1973) in that both models are based on the same point source and plume rise equations; however, the TCM differs significantly in execution from the CDM because the point source algorithm is solved by interpolation in a table of precalculated coefficients and a simple equation is used to calculate concentrations due to area sources. As a result of these and other time saving innovations (see Appendix) the TCM is roughly two orders of magnitude faster than the CDM; however, both models predict essentially the same concentrations given the same input data. The TCM is suitable for nonreactive pollutants and relatively flat terrain.

Data input to the TCM consists of: (1) a stability wind rose (the joint frequency of occurrence of 16 wind directions, 6 stability classes, and 6 wind speed classes) for a year or season; (2) point and area sources for one to three pollutants; and (3) air quality monitor data for calibration (optional). Features of the TCM include options for input of up to five stability wind roses (seasonal plus annual climatology), output of a culpability list of the five high contributors to the concentration at each receptor point, self-calibration by linear regression of predicted to observed concentration values, and first order pollutant decay with a decay half-life provision.

Concentrations are calculated by the TCM in a fixed grid array of up to 50 X 50 elements of arbitrary spacing. Calibrated and uncalibrated concentrations calculated by the TCM are available in four formats, any combination of which are available at user option. The formats are: a listing of the concentrations; punched card output for computer plotter mapping; a print plot grid array suitable for hand isoplething; and a listing of the five high contributors to the pollution at each grid point.

Texas Episodic Model (TEM)

The Texas Episodic Model calculates expected mean concentrations for periods of from ten minutes up to 24 hours based on the expected stability class, wind speed and wind direction for the averaging period. The TEM uses the bivariate Gaussian point source algorithm (Turner, 1970) and an area source algorithm suggested by Gifford and Hanna (Gifford and Hanna, 1970). Point and area source data is input in the same format as for the TCM, and the output format options for the TEM and TCM are the same. The TEM also has the same culpability list and decay half-life features as the TCM. In addition the TEM features: (1) consideration of limited mixing depth meteorology including a variable inversions strength factor; (2) selection of a plume rise formula from one of six (Briggs, 1969) according to stability, downwind distance, and plume buoyancy; (3) an automatic grid option that selects the number and spacing of grid points in a way that insures the maximum concentration resulting from each source is included in the output grid array. For speed of calculation TEM solves the bivariate Gaussian equation by interpolation in precalculated tables of coefficients.

APPLICATIONS

Both models are suitable for a wide range of applications, separately and together, depending upon the situation being modeled. Listed below are typical applications of the models by the Texas Air Control Board.

Air Quality Maintenance Planning and Analysis. The Environmental Protection Agency (EPA) requires that the states submit plans that show how air quality standards will be attained and maintained over periods of ten years or more. The TCM and TEM are modeling vehicles tailored to this task. The TCM is first run on a base year for which emissions and observed ambient air quality data are known. The TCM is used to model the base year exercising the self-calibration feature of the model (see Porter & Christiansen, 1976). The emissions for future years are projected and the model run again using the calibration factor established for the base year. The areas that violate the standards can then be examined in greater detail with the culpability list option used to determine which sources are major contributors to the high levels of pollution. The TEM is exercised for the same sources to determine if the short term standards will be violated. Control strategy plans can then be formultaed and tested by modeling to determine their effectiveness. The TCM can be used to investigate the effect of seasonal variation on concentrations with up to five scenarios (four seasons plus annual) of meteorology input to a single model run. The TEM can be used to investigate specific scenarios of meteorological conditions such as low mixing height or very stable atmospheric conditions for which special control strategies should be devised. Because the models can calculate concentrations for large urban areas with many point and area pollution sources while requiring relatively little computer time, modeling can be an efficient and cost effective way to examine the many control strategy options open to the air quality planner.

Analysis of the Impact of New Pollution Sources. The TEM and TCM are routinely employed by TACB engineers when processing applications for construction of new sources by

Texas industries. The models are used to investigate the effectiveness of various emission control devices upon ground level concentrations. The impact of the new facility is determined by modeling the new source alone and by modeling the new source along with all other sources in the area. Modeling results become part of the hearing record if a public hearing is called on the permit request.

Compliance Actions. Modeling sometimes indicates that a specific plant is causing pollution levels in violation of the ambient air standards. When the TACB compliance division is called upon to monitor the facility, the TEM is exercised to specify where monitoring should be done for specific meteorological conditions so that the expected high pollution levels can be observed. The TCM is exercised using growing season meteorology to outline areas in which to search for vegetation damage.

Air Quality Analysis. The TCM and TEM have been used to investigate the sources of high levels of pollution observed at ambient air quality monitors. The culpability list option of the models was used to determine which sources contributed to high levels of pollution. When the model predicted pollution levels were substantially below the observed levels an investigation was conducted for sources not listed in the emissions inventory. The investigations revealed fugitive industrial sources, construction sites, and unpaved roads that had a large impact on monitors that violated the ambient air standards.

Sulfur Dioxide Conversion. The laboratory division of the TACB used X-ray fluorescence to determine the constitution of particulate matter gathered on filters during a special monitoring period in Houston. The TEM is being used to correlate sulfur dioxide emissions to observed sulfate and sulfite concentrations during the test period.

Frequency Distribution Generation. Because of its speed in computation the TEM was selected to be the heart of a new Frequency Distribution Model (TEM/FRED) developed recently at the Texas Air Control Board. In the TEM/FRED model, the TEM is used to predict concentrations for every set of weather conditions encountered in the joint frequency function of meteorological conditions (METSET). These concentrations are processed by the FREquency Distribution (FRED) post processor. The result is a climatological model that predicts the frequency distribution of concentrations at each receptor grid point. FRED then calculates the parameters of the frequency distribution (assuming lognormality), the arithmetic mean, standard deviation, and various percentile concentrations of the lognormal distribution. The validity of the of lognormality is tested by the Kolmogoroff-Smirnov statistic. Both the TCM and TEM/FRED were exercised on the SO_2 data base for Frankfurt, Germany, as a part of the NATO/CCMS Practical Demonstration of Urban Air Quality Simulation Models. Figure 2 presents the Frankfurt area TCM predictions of arithmetic mean concentrations of sulfur dioxide. Figure 3 displays the TEM/FRED geometric mean concentration predictions for the same area.

	STABLE AIR	UNSTABLE AIR
BUOYANCY-DOMINATED	$\Delta h(x) = 1.6F^{1/3} x^{2/3} U^{-1}$ 21 or $\Delta h_{MAX} = 2.4[F/US]^{1/3}$ 22 where $S = 0.02g/T_A$, E stability, $S = 0.035g/T_A$, F stability.	$\Delta h(x) = 1.6F^{1/3} x^{2/3} U^{-1}$ 21 for $x < 3.5x^*$, or $\Delta h_{MAX} = 1.6F^{1/3}(3.5x^*)^{2/3} U^{-1}$ 23 for $x > 3.5x^*$. $x^* = 14F^{5/8}$ if $F < 55$, $x^* = 34F^{2/5}$ if $F > 55$.
MOMENTUM-DOMINATED	$\Delta h_{MAX} = 1.5(VR)^{2/3} U^{-1/3} S^{-1/6}$ 24 S as above.	$\Delta h(x) = 3.78\left(\frac{V^2}{U(V+3U)}\right)^{2/3}\left(\frac{xR^2}{2}\right)^{1/3}$ 25 or $\Delta h_{MAX} = 3VD/U$ (27)

$F = gVR^2(T-T_A)/T$.

T = source temperature, °K.

T_A = ambient temperature, °K.

V = velocity, m/s.

R = radius, m.

D = diameter, m.

x = downwind distance, m.

U = wind speed at physical source height, m/s.

g = acceleration due to gravity, 9.8 m/s^2.

FIGURE 1, TEM Plume Rise Formulae

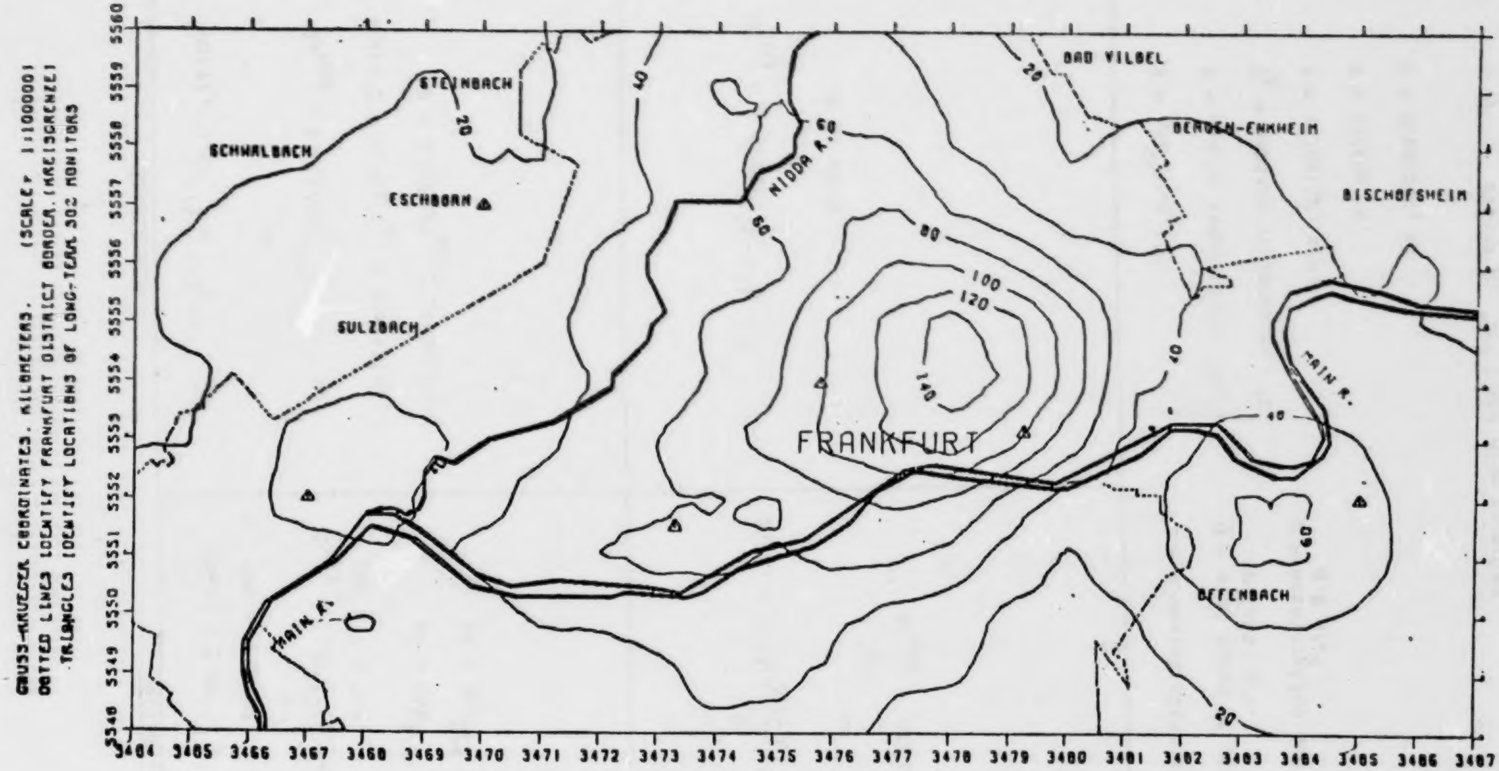
GAUSS-KRUEGER COORDINATES, KILOMETERS. (SCALE: 1:100000)
DOTTED LINES IDENTIFY FRANKFURT DISTRICT BORDER (KREISGRENZE)
TRIANGLES IDENTIFY LOCATIONS OF LONG-TERM SO2 MONITORS
SCHWALBACH
STEINBACH
ESCHBORN
SULZBACH
NIDDA R.
FRANKFURT
BAD VILBEL
BERGEN-ENKHEIM
BISCHOFSHEIM
OFFENBACH
MAIN R.
MAIN R.
20
40
60
80
100
120
140
3404
3405
3406
3407
3408
3409
3410
3411
3412
3413
3414
3415
3416
3417
3418
3419
3420
3421
3422
3423
3424
3425
3426
3427
3548
3549
3550
3551
3552
3553
3554
3555
3556
3557
3558
3559
3560

ERANKFURT AM MAIN - PREDICTIONS OF ANNUAL SO2 CONCENTRATIONS

TCM: F=50. AREA EMISSION RADIUS = 1.5 KM

CONCENTRATIONS IN MICROGRAMS PER CUBIC METER

Figure 2

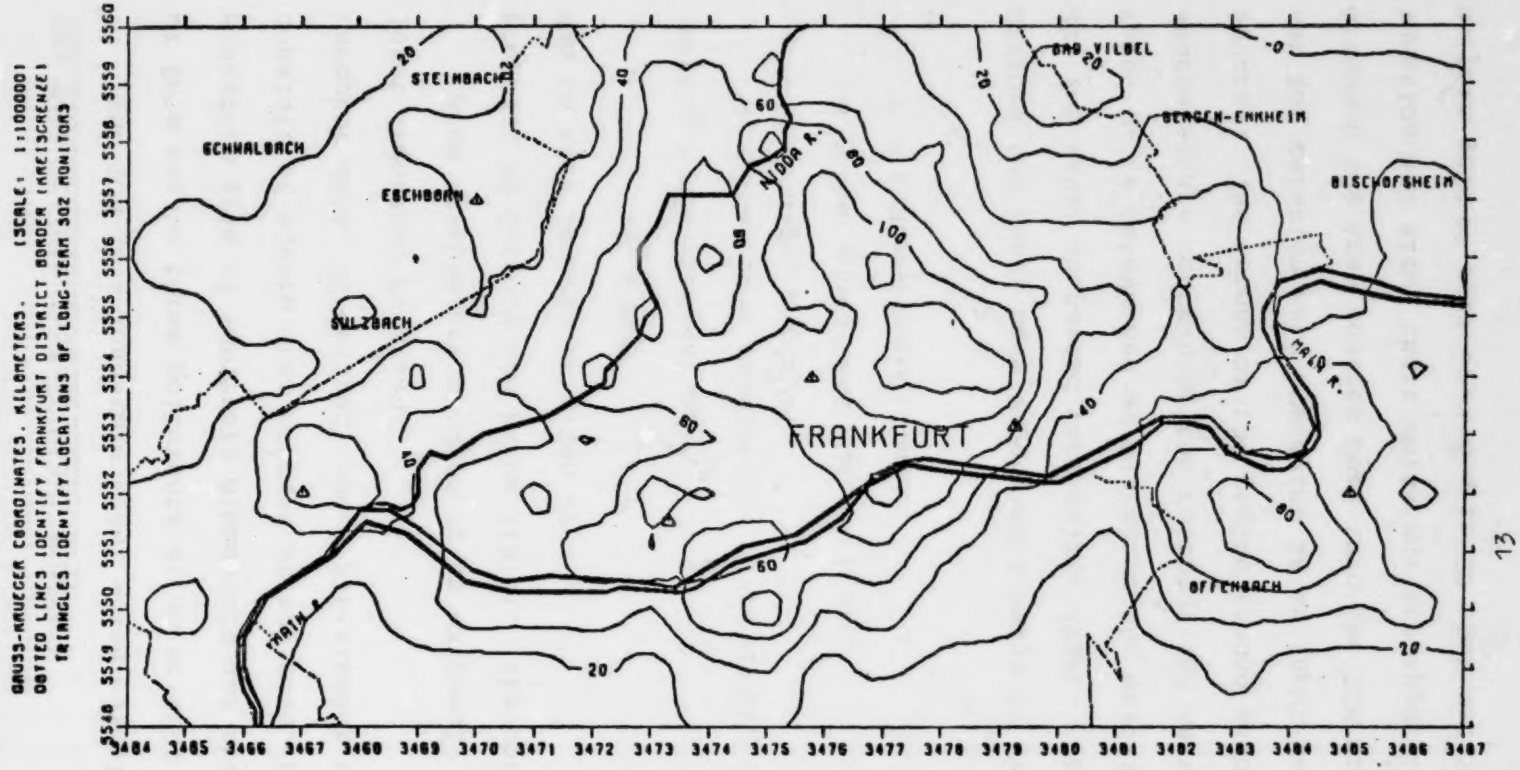
GAUSS-KRUEGER COORDINATES. KILOMETERS. (SCALE: 1:100000)
DOTTED LINES IDENTIFY FRANKFURT DISTRICT BORDER (KREISGRENZE)
TRIANGLES IDENTIFY LOCATIONS OF LONG-TERM SO2 MONITORS
5548
5549
5550
5551
5552
5553
5554
5555
5556
5557
5558
5559
5560
3464
3465
3466
3467
3468
3469
3470
3471
3472
3473
3474
3475
3476
3477
3478
3479
3480
3481
3482
3483
3484
3485
3486
3487
SCHWALBACH
STEINBACH
ESCHBORN
SULZBACH
BAD VILBEL
BERGEN-ENKHEIM
BISCHOFSHEIM
OFFENBACH
FRANKFURT
NIDDA R.
MAIN R.
MAIN R.
20
40
60
80
100
60
40
20
0
20
80
60
20

FRANKFURT AM MAIN - PREDICTIONS OF ANNUAL SO2 CONCENTRATIONS

TEM: GEOMETRIC MEAN

CONCENTRATIONS IN MICROGRAMS PER CUBIC METER

Figure 3

APPENDIX: THE COMPUTER MODEL ALGORITHMS

The Texas Climatological Model (TCM)

The TCM is a long-term model which calculates concentrations of from one to three pollutants at up to 2500 locations in a uniform grid of arbitrary dimensions and spacing. Input consists of square area sources of any size, point sources, receptor data, if desired, and a 576-element meteorological joint frequency function.

Area sources are handled by an extremely simple algorithm proposed by Gifford and Hanna (1973). The concentration due to area sources is given by

$$\chi_A = FQ/U \qquad (1)$$

where χ_A = concentration, $\mu g/m^3$,

Q = area source emission rate in the vicinity of the receptor, $\mu g/m^2/s$,

U = mean ground-level wind speed, m/s,

F = a dimensionless constant.

Gifford and Hanna have suggested a value of $F=50$ for SO_2 and 225 for total suspended particulate (TSP). The area emission rate, Q, is determined by averaging the emissions in the area source square containing the receptor and in the neighboring squares. The extent of the region around each receptor to use for emission rate averaging is an input parameter. Although the area sources read into the TCM may be of any location and size, their emissions are apportioned to a uniform grid of squares, with up to 50 rows and 50 columns of squares. The dimensions and square size of the grid are input parameters. The grid serves an additional purpose. Concentrations are calculated at the center of each grid square. Thus, the TCM can predict concentrations for as many as 2500 receptor points.

The TCM uses steady-state Gaussian plume point source logic, with the crosswind distribution averaged across 22°.5 azimuthal sectors. The only meteorological input required for area source calculations is the mean wind speed, but the point source calculations require a meteorological joint frequency function with 16 22°.5 wind sectors, six wind speed classes (0-3, 4-6, 7-10, 11-16,17-21, and >21 knots), and six stability classes (Turner classes A,B,C,D (day), D (night), and E plus F). Let the concentration due to point source i be given by

$$\chi = (16\times 10^{6}/2\pi) \sum_{\ell=1}^{6} \sum_{m=1}^{6} \phi\,(k_i,\ell,m)\, Q_i S/x, \tag{2}$$

$$S = (2/\sqrt{2\pi}\, U_\ell \sigma_z) \exp\,(-H_i^2/2\sigma_z^2)\, \exp\,(-.692x/U_\ell T_k) \tag{3}$$

with χ = concentration, $\mu g/m^3$,
k_i = the wind sector index appropriate to source i at the receptor
l = wind speed class index,
m = stability class index,
ϕ = meteorological joint frequency function,
Q_i = emission rate of source i, g/s,
H_i = effective height of source i, m,
σ_z = standard deviation of vertical Gaussian concentration distribution,m,

$T_{1/2}$ = half-life for first-order pollutant decay, s,
U_l = central wind speed of class l, m/s,
x = downwind distance, m.

This is the form used by the Climatological Dispersion Model (CDM). The TCM defines a wind speed U_m characteristic of an entire stability class:

$$U_m = \left[\sum_{k=1}^{16}\sum_{\ell=1}^{6}\phi(k,\ell,m)\right]\left[\sum_{k=1}^{16}\sum_{\ell=1}^{6}\phi(k,\ell,m)/U_\ell\right]^{-1}, \qquad (4)$$

This allows the reduction of $\phi(k,l,m)$ to $\phi(k,m)$, with each frequency of the new 96-element joint frequency function being the sum of the six wind speed class elements for each stability class / wind sector combination.

$$\chi = (16x10^6/2\pi)\sum_{m=1}^{6}\phi(k_1,m)\,Q_1 S/x, \qquad (5)$$

$$S = (2/\sqrt{2\pi}\,U_m\sigma_z)\exp(-H_1^2/2\sigma_z^2)\text{ (decay term)}. \qquad (6)$$

Define K =

$$K(x,H,m) = (32x10^6/(2\pi)^{3/2}x\,\sigma_z)\exp(-H_1^2/2\sigma_z^2). \qquad (7)$$

Then finally,

$$\chi = Q_1\sum_{m=1}^{6}(K(x,H,m)\phi(k,m)/U_m)\text{ (decay term)}. \qquad (8)$$

For the TCM, K was precalculated for twenty downwind distances, x = 0.1 to 46.1 km, nine effective source heights, H = 10 to 300 m, and the six stability classes mentioned above. These 1080 K-values (20x9x6) are stored as data tables in the TCM. The dispersion equation (8), is solved by interpolation in the K-tables rather than the time-consuming explicit calculation of the exponentials in equations (2) and (3). Decay terms are also precalculated.

The dispersion parameter σ_z in equation (7) is calculated as in the CDM:

$$\sigma_z = ax^b, \qquad (9)$$

with Busse and Zimmerman's tabulated values of the stability and downwind distance - dependent coefficients a and b.

A Briggs (1969) plume rise formulation is used :

$$H = h + \Delta h,$$

$$\Delta h = 1.6\, F^{1/3}\, (3.5x^*)^{2/3} U^{-1}$$

$$x^* = 14F^{5/8} \text{ if } F \leq 55,$$

$$x^* = 34F^{2/5} \text{ if } F > 55. \qquad (10)$$

$$F = gvr^2(T - T_{ambient})/T,$$

Here H = effective source height, m,
h = physical source height, m,
Δh = plume rise, m,
g = 9.8 m/s^2
v = source exhaust velocity, m/s
r = inside radius of source, m,
T = source temperature, °K
Tambient = ambient temperature, °K

The wind speeds U_1, etc., in equations (3), (4), (6), (8), and (10) are the speeds at the physical height of the source. They are derived from the ground-level wind speed via

$$U = U_o(z/z_o)^P \qquad (11)$$

where U = wind speed at height z, m/s,
U_o= surface wind speed, m/s,
z = height, m,
z_o= anemometer height,m. z_o is set equal to 10m.
P = an exponent dependent on stability class (Busse and Zimmerman, 1973)

Up to five meteorological joint frequency functions along with five sets of point sources and five sets of weighting factors for one set of area sources may be input to the TCM in one computer run. The usual application of this feature is for annual and seasonal predictions for the same study area. There is no limit to the number of area or point sources which may be used as input.

The TCM is "self-calibrating", performing (on request) a first-order least squares regression analysis on calculated vs. observed concentrations in the same computer run.

TCM output is available in any combination of the following four forms:

1. List of predicted concentrations by receptor, one receptor grid column per page.
2. Printer map of the concentrations across the receptor grid, suitable for hand isoplething.
3. Culpability list of the five sources contributing the most to the total concentration at each receptor.

4. Punched cards for computer contour plotting.

Due to the highly efficient area and point source logic and the simplification of the joint frequency function, the TCM gives essentially the same results as the CDM but is some 80 to 400 times faster.

The Texas Episodic Model (TEM)

The TEM is a short-term companion model to the TCM. Both models can use the same source input and have the same options available for displaying output. The TEM calculates concentrations of one or two pollutants at up to 2500 locations in a uniform grid of arbitrary dimensions and spacing. Input consists of square area sources of any size, point sources, and weather data for up to 8 weather "scenarios" for which concentrations are predicted, for sample times of from 10 minutes to 3 hours, with provisions for simulating a 24 hour day through superposition of eight scenarios representing three hours each. Information required for each scenario includes stability class, wind speed, wind direction, ambient temperature, first-order decay half-lives of the two pollutants, mixing height, and an "inversion penetrability factor" which controls the strength of the inversion. An option allows the TEM to search through four different wind directions in each weather scenario instead of the direction specified for the scenario.

Area sources are input as squares of arbitrary size and location. Their emissions are reapportioned by the TEM into a uniform grid of squares, and the area source algorithm operates on this uniform grid. As with the TCM, the grid contains up to 50 rows and 50 columns of squares of any size, and concentrations are calculated at the center of each grid square. The area source algorithm is due to Gifford and Hanna, (1970). Each area source square is affected by its own diffuse emissions and those in the N area source square directly upwind of it:

$$\chi = \sqrt{\frac{2}{\pi}}\ \frac{(\Delta x/2)^{1-b}}{U_o a(1-b)} \left\{ Q_o + \sum_{i=1}^{N} Qi\ [(2i+1)^{1-b} - (2i-1)^{1-b}] \right\} \qquad (12)$$

with

Δx = length of side of area source grid squares, m,

U_o = surface wind speed, m/s,

Q_o = area emission rate of square containing the receptor, $\mu g/m^2$,

Q_i = area emission rates of the upwind area sources, $\mu g/m^2$,

a,b as in equation (9).

In the TEM, N=4. For each wind direction, every area source square lays down the same concentration pattern, scaled by Q. There are 10 possible patterns for N=4, stored as data in the model. To simplify the calculations, equation (12) is used in a source-oriented instead of a receptor-oriented manner—that is, each source square affects itself and the four squares downwind of it.

The TEM employs steady-state bivariate Gaussian plume point source logic. The concentration due to an elevated point source is given by

$$\chi = \frac{10^6 Q}{\pi \sigma_y \sigma_z U} \exp(-y^2/2\sigma_y^2) \exp(-H^2/2\sigma_z^2) \exp(-.692x/UT_{\frac{1}{2}}) \qquad (13)$$

where χ = concentration, $\mu g/m^3$,

Q = emission rate, g/s,

U = wind speed at physical source height, m/s,

H = effective source height, m,

x = downwind distance, m,

y = crosswind distance, m,

$T_{½}$ = first-order pollutant decay half-life, s,

σ_y, σ_z are the standard deviations of the Gaussian concentration distribution, respectively:

$$\sigma_z = ax^b, \tag{14}$$

$$\sigma_y = cx^d, \tag{15}$$

with stability and downwind distance-dependent coefficients a, b, c, and d from Busse and Zimmerman (1973) and Turner (1970). The wind speed U is obtained from the surface wind speed through equation (11). Let K_y and K_z be defined by

$$K_y = \frac{1000}{\sigma_y} \exp\,(-y^2/2\sigma_y{}^2), \tag{16}$$

$$K_z = \frac{1000}{\pi\sigma_z} \exp\,(-H^2/2\sigma_z{}^2). \tag{17}$$

Then equation (13) becomes

$$\chi = \frac{K_y K_z Q}{U}\,(\text{decay term}) \tag{18}$$

K_y was calculated for each of the 1120 combinations of twenty downwind distances from 2 to 60 km, eight crosswind angles ($\mathrm{Tan}^{-1} y/x$) from 0° to 7°, with δ varying from 1° to 5° depending on stability, and seven stability classes (A,B,C,D(day),D(night) E and F). K_z was calculated for each of the 1960 combinations of the same twenty downwind distances, fourteen effective source heights from 10 to 2000 meters, and seven stability classes. These 3080 values are stored in the TEM as data tables. For downwind distances over 2 km, concentrations are calculated by interpolating for the K_y and K_z values appropriate to a given downwind distance, crosswind distance, effective source height, and stability class. Decay factors for each distance are precalculated for each scenario. Such calculations are considerably faster than the explicit solution of equation (13). For downwind distances of less than 2 km, interpolation is not considered sufficiently accurate, so equation (13) is used.

Turner's (1970) treatment of mixing height is used in the TEM. For total vertical mixing below a mixing height of L meters,

$$\chi = \frac{10^6 Q}{\sqrt{2\pi}\sigma_y LU} \exp\left(-y^2/2\sigma_y^2\right), \tag{19}$$

or, in terms of equations (17), (18), and (19),

$$K_z = 398L \tag{20}$$

At $x > 2x_m$, where x_m is a distance such that $\sigma_z = 0.47L$, equation (19) is used. For $x_m \leq 2x_m$, interpolation between results of equations (13) and (19) is employed.

An inversion penetration factor, I, is a program input for each weather scenario. If $H > LI$, the plume escapes the mixing layer. If $L < H \leq LI$, the plume does not escape, and H is set equal to L. Typically, $I \approx 2$.

Plume rise is calculated by one of six formulae, all due to Briggs, (1969). The program chooses the correct formula on the basis of 1) downwind distance, 2) atmospheric stability, and 3) whether the rise of the plume is dominated by thermal buoyancy or momentum. Figure 1 shows the six equations, with the conditions under which they are used.

The TEM has the same options for displaying output as the TCM. The concentrations may be listed, displayed in a printer map, and/or punched onto cards for plotting, and a culpability list of the five sources contributing the most to the total concentration at each receptor may be requested.

Use of equation (18) for point sources and the relatively simple algorithm for area sources make the TEM approximately three to five times faster than other similar but less sophisticated short-term models tested at the Texas Air Control Board, while the careful treatment of plume rise greatly enhances its accuracy.

REFERENCES

G. A. Briggs, Plume Rise, U. S. Atomic Energy Commission, Division of Technical Information, Oak Ridge, Tenn. 1969.

A. D. Busse and J. R. Zimmerman, User's Guide for the Climatological Dispersion Model, U. S. Environmental Protection Agency, Research Triangle Park, N.C. (EPA-R4-73-024), 1973.

F. A. Gifford, Jr., and S. R. Hanna, "Modeling Urban Air Pollution", Atmospheric Environment, vol. 7, 131. 1973

F. A. Gifford, Jr. and S. R. Hanna, "Urban Air Pollution Modelling," paper no. ME-320, Second International Clean Air Congress, Washington, D.C., 1970.

S. R. Hanna, "A Simple Method of Calculating Dispersion from Urban Area Sources," Journal of the APCA 21, 774, 1971.

D. B. Turner, Workbook of Atmospheric Dispersion Estimates, Public Health Service Publication No. 999-AP-26, 1970.

R. A. Porter and John H. Christiansen, "Modeling of Particulate and Sulfur Dioxide in Support of Ten-Year Planning," EPA Conference on Environmental Modeling and Simulation, Cincinnati, Ohio, 1976.

7th International Technical Meeting
on Air Pollution Modeling and its Application

AIR QUALITY MANAGEMENT UTILIZING AIR QUALITY MODELS

by

Donald M. Rote
Energy and Environmental Systems Division

Argonne National Laboratory
9700 South Cass Avenue
Argonne, Illinois 60439

September 7 - 10, 1976
Airlie Virginia
United States of America

AIR QUALITY MANAGEMENT UTILIZING AIR QUALITY MODELS

Donald M. Rote

ABSTRACT

The variety of air quality simulation models and their uses has grown at a rapid rate during the past decade. In particular, as a result of recent legislation at both the national and local levels of government, the need for the development of effective management of air quality has stimulated widespread use of models in increasingly diverse ways.

In an attempt to review the "Current Uses and Requirements for Air Quality Models as a Basis for Comprehensive Air Quality Management Policies and Systems," a project under that title was initiated in April, 1976, under U.S. EPA sponsorship. The results of that review are summarized in the present paper.

Air quality management and factors which govern the use of models in support of such management are discussed. The relationship between the regulatory approaches to air quality control and model utilization is examined. Particular emphasis is placed upon the decisionmaker or air quality manager as a user of models, the problems he is confronted with and the applications for which he uses models. The kinds of information the user requires in order to apply models, the types of models used, and the data requirements of models is also discussed.

INTRODUCTION

Up until the late sixties environmental protection in the various NATO Countries was often only a small add-on function to the many activities of sometimes only remotely related govenernment agencies. Even then the environmentally related functions were often not clearly specified by legislative mandate.

Since then we have been moving along a learning curve in the environmental protection field. Several countries have now had varying degrees of experience with specific legislative mandates for the formation of government agencies charged with specific environmental responsibilities. Others are giving serious thought to such legislation. These experiences might best be characterized as experimental in nature since they represent heretofore untried, large-scale governmental approaches to solving unclearly stated problems with uncertain knowledge and methods. The approaches have not always proven most fruitful, the solutions have not always been better than the problems, and hindsight tells us that there are certain things we should have done or emphasized more than we did. However, we are moving up the learning curve and hopefully those nations still in the stage of formulating policies will be able to take advantage of other nations' experiments. The Sixth Annual Report of the Council on Environmental Quality (CEQ, 1975) of the United States provides an excellent summary of the recent U. S. experiences and is highly recommended to interested readers.

AIR QUALITY MANAGEMENT

Of specific concern in this report is the branch of environmental quality protection which deals with the air quality; we refer to this branch as air quality management. Its responsibility is to direct those activities, in a mutually constructive fashion, which can lead to a quality of the atmosphere which is compatible with:

- prevention of damage to the health of people, plants, animals and to materials,
- our tolerance for nuisances,
- our aesthetic values,
- our ability to control effluents,
- the physical and chemical laws governing the transport and fate of pollutants in the atmosphere,
- acceptable tradeoffs with other segments of the environment,
- and our ability and willingness to pay the costs.

The major activities falling under air quality management can conveniently be listed under two broad categories as follows:

1. Formulation of Policies and Program Planning
    a. Definition of goals, objectives, scope of activities
    b. Resolution of jurisdictional matters involving government agencies at various levels
    c. Formulation of legislation including emission and/or air quality standards
    d. Ensuring program completeness
    e. Determination of supporting needs including various types of research
    f. Policy and program evaluation (cost of effectiveness, updating, revision, analysis of tradeoffs with other environmental sectors)
    g. Analysis of the economic and social consequences of legislation and control programs
    h. Budgetary considerations
2. Implementation of Policies and Programs
    a. Characterization of the air quality
    b. Determination of the nature and extent of effects and damages
    c. Determination of the need for abatement and/or maintenance
    d. Formulation and evaluation of control programs
    e. Implementation of control programs
    f. Surveillance and enforcement

Roles of Air Quality Simulation Models (AQSM) and Regulatory Approaches to Air Quality Management

The roles that air quality simulation models (AQSM) play in air quality management in any given nation depend upon several factors, one of the most important being the nature of the regulatory approaches to air quality control taken in that nation.

Regulatory approaches have recently been discussed by Cirillo, 1976. The approaches include the following:

1. National Ambient Air Quality Standards (NAAQS)
2. Emission Standards for Stationary Sources
3. New Source Performance Standards (NSPS)
4. National Emission Standards for Hazardous Pollutants

5. National Emission Standards for Mobile Sources
6. Regulation of Fuels and Additives
7. Abatement Conferences

It is worthwhile giving brief descriptions of the first few of these approaches since they are of greatest interest here. Note that workers' health standards have been excluded from this list as they do not generally address the health and welfare of the environment and its occupants outside of the working environments.

1. NAAQS

Ambient air quality refers to the concentration of pollutants at any point where the general public has unlimited access. In the U. S., pollutants subject to this approach must be shown to have adverse health and/or welfare effects at concentration levels measured in the ambient air. Several countries including the U. S., Canada, Sweden and Germany have adopted such standards for SO_2, particulate matter and/or smoke, CO, oxidants and various hazardous materials.

This regulatory approach essentially requires that the relationship between emission and ambient concentration be understood in order to formulate appropriate maintenance and control strategies. At the present time the most effective means for quantifying that relationship for both given and projected emission patterns is with AQSM's. This has been referred to as the "critical property" of AQSM's by Ken Calder (1974) in a recent NATO/CCMS talk. Because of this property, AQSM's can make significant contributions to nearly all of the air quality management activities outlined earlier. H. Slater (1974) has pointed out that both modeling and monitoring supplement each other in identifying and quantifying problems and in suggesting solutions. "Both are necessary but neither is sufficient by itself." In his talk, Calder (1974) stresses the fact that models have a very "high decision value" and that this characteristic should justify the expenditure required to properly develop and characterize models. Kropp (1974) also has testified to the important role models play in yes/no decisions on licensing of new sources and land use development plans. Fortak (1974) has written extensively on the importance of utilizing modeling methods for air quality maintenance and both he and Gronskei (1974) among many other authors have stressed the fact that AQSM's provide the necessary link to couple land use planning to air quality maintenance.

It should be recognized, of course, that the use of models and their "high decision value" is a double-edged sword. On the one hand, models serve the managers well. On the other hand, they are troublesome in that decisions based upon their use come under close and sometimes hostile scrutiny in the courts according to Calder (1974). Hence, users not only need confidence in their model applications, but also a basis for supporting their decisions against harsh criticism and legal debate.

2. Emission Standards

Standards governing the emission of many effluents have been adopted by nearly all developed countries. One mode of specifying the degree of emission control is best available or best practicable control technology. The implementation of such a strategy in the U. K. has virtually eliminated the infamous "London Fog" (although it should be noted that there are now indications that the incidence of haze is becoming increasingly evident and has been attributed to mobile source pollution and possible photochemical smog formation). The importance of this approach is that it can be implemented quickly and relatively economically, often with dramatic results. However, there is not guarantee that the resultant air quality will be acceptable from the point of view of health, material-damage, etc. Hence, it can be viewed as a viable first step.

At first glance it would seem that strict adherence to an emission-oriented policy would preclude the use of air quality simulation models. It is certainly true that modeling applications are more extensive in countries having ambient air quality standards, but a survey of model uses reveals a surprisingly large number and variety of uses under such policies. In fact, one can regard models as being part of the technology itself as is the case, for example, of the so-called supplementary or temporary control strategies. (See for example, Egan 1974). In such cases, a simulation model is employed in a real-time mode to predict potential high pollution periods so that emission patterns can be adjusted accordingly. Another interesting type of use for models which could be classified as an application of best practicable technology is to aid in the site selection process for new sources. Even if there are no air quality standards, one may wish to minimize the impact of new sources by optimizing their location with respect to existing air quality and land use patterns. The potential impacts of extensive new development in the Forth Valley stimulated by North Sea oil exploitation have been investigated by Keddie 1975. A method for optimizing source location for a planned deep sea harbor has been discussed by Fortak (1975). The question of what additional controls may be needed if air quality standards are adopted is currently being addressed in various areas within Great Britain according to a discussion with Keddie.

3. NSPS

This type of standard is a variant of the emission control approach which provides the decision maker with the option to promulgate standards on an industry-by-industry basis but without requiring application to existing sources. This prevents the necessity of forcing expensive or unduly burdensome retrofit programs. It also provides motivation for the development of new and improved control hardware since new sources cannot be added without meeting the standards. Such standards while they do not necessarily address the air quality specifically, can allow for analysis of air quality in their design. In particular, one could investigate the need for control on the basis of air quality prior to new source development. Such an investigation and the evaluation of the effectiveness of such controls can be very directly aided through the use of AQSM's.

What Governs the Use of Models in Air Quality Management?

In addition to the regulatory approach to air quality control, other important factors governing the use of AQSM's include the following:

1. Awareness on the part of the user community of the utility of models.
2. Questions regarding the applicability of models and the limits of accuracy under specific conditions.
3. Availability of suitable models to users.
4. Ability of users to utilize models in light of the input, manpower, and computer requirements.

In contrast to the regulatory approach, the modeling community can, if it wishes, rather directly influence these latter four factors. In fact, it behooves the community to improve and expand the utility of and promote the proper use of AQSM in air quality management. The question therefore is, to what extent is this being done, and are there any problems?

Model Developers and Users

K. Jones (1974), of the U. S. EPA has strongly emphasized the urgent need to specify confidence limits for the pollution concentration estimates provided by AQSM's.

In a short, but to the point paper, A. Corlin (1974), Air Pollution Authority, Copenhagen, appeals to us:

"Dear modelers, please provide users and adminstrators
with good and precise information about your models."

In light of reoccuring requests such as these for validity and applicability information, it is curious to look at the results of a recent survey of air quality model data requirements prepared by Science Applications, Inc. for the Electric Power Research Institute (EPRI, 1976). As shown in a summary table (Table 2-1), and please recognize that it is simply a summary, the vast majority of the respondents to the survey, which are model developers, regard their models as both "user ready" and even more regard their models as "validated." At first glance it would appear that the users' request has been answered. However, closer scrutiny suggest that what the model developer regards as "validated" and "user ready" may not be what the user regards as completely satisfactory for his purposes.

Developers, because of funding limitations or other circumstances, are generally unable to amass adequate data bases designed specifically to properly test their models; not to mention address the specific needs of the users. They must use whatever data bases happen to be available to them. These are often hopelessly inadequate because of the size of the data set, the proper variables are not measured, conditions of measurement are too limited, quality of data is poor, etc.

It should be mentioned that one of the main purposes of the EPRI survey was to enable the design of more complete field experiments which can acquire the necessary data to test a wide variety of models. The survey also provides useful information about model characteristics.

The user on the other hand, seems often to have no real appreciation for the magnitude of the effort required to put a model into a "user-oriented" format, and to properly characterize it in that mode.

Part of the problem arises because of the several meanings associated with the term "user." To many model developers, the term refers to anybody other than themselves. This includes other model developers, research scientists and air pollution engineers. Consequently, adequate documentation, from this point of view, tends to emphasize the theoretical aspects of the modeling approach. In the present context, the term "user" applies to a person who is a decision maker and regards an AQSM as more or less a "black box" requiring specified input and providing some output information. One should perhaps distinguish between the person who actually operates the model and one who uses the model results for decision making purposes, but for our purposes, this distinction is not important. The point is, however, that for the user, the model is a tool just as a monitoring instrument. To be used in that mode, the user must be clearly informed of the applicability of the model to his particular application and of the limits of its accuracy.

These remarks suggest that there is a form of "communication gap" between users and developers. A recognition of this communications gap at the 1973 NATO/CCMS Oberursel Meeting presumably lead to a modeler/user workshop at the 1974 NATO/CCMS meeting of the Expert Panel on Air Pollution Modeling, Roskilde, Denmark. Rapporteurs Niemeyer and Fox (1974) mentioned in The Proceeding of that workshop that "in contrast to the many modelers, there were actually very few users in attendance, and this restricted the input of user attitudes into the discussion."

Hopefully, the design of future user/modeler workshops will allow for greater participation on the part of the users.

The Needs of the Users

As a first iteration, we can prepare a list of what we as modelers perceive as the "users" general needs with respect to models:

Information about the general utility of models.

Information and a method by which he can determine the suitability of a particular modeling approach(es) to his particular problem(s).

Information regarding the accuracy of the model relevant to his application.

Information regarding the relationship between the quality of the input data he must supply and the influence of input errors on output errors.

Model users' manual.

Description of model requirements including nature and extent of input data base, computer requirements, and level of expertise required to operate the model.

Appropriate diagnostic tests to check operation of model.

In addition to these general needs, users specifically require models or tools which allow direct comparison between the air quality consequences of decisions affecting pollutant emission patterns and limitations or standards of air quality. Even in jurisdictions not presently governed by ambient air quality standards, it can be anticipated that such standards may be seriously considered and perhaps even adopted. For example, the European Community is presently considering the uniform adoption of air quality standards. An important aspect of such consideration is the analysis of the economic consequences and the need for additional source controls. Such considerations are quantitatively aided by the use of appropriate modeling tools.

Air Quality Standards

It is common to express limits of concentrations of pollutants in the ambient air in terms of the frequency of occurrence of values representing averages over selected time intervals (averaging times). These averaging times are generally separated into short-term intervals of from 1 up to 24 hours and long-term intervals of from 1 month to 1 year. As pointed out by D. Fox (1974), the statement of the standards is often quite specific implies a predictability that may be unreasonable. It should also be pointed out that such standards may even imply a surveillance program that is unreasonable in terms of frequency of measurement, spacing of monitors, etc.

To illustrate the nature of air quality standards, Table 1 lists selected standards for SO_2. Note that both the long- and short-term standards vary from country to country. Since these standards are supposed to address chronic and acute damage, health effects, and welfare considerations one would suppose that more uniform values could be agreed upon. Furthermore, it seems reasonable to expect that it may be possible to ease the burden of determining compliance by attempting to examine the statistical nature of the damage functions and forming standards more compatible with both the statistical nature of the damage function and of the air quality.

Air Quality Simulation Models That Address the Standards

AQSM's have been developed and applied to problems specifically calling for comparison of predictions with air quality standards such as illustrated in Table 1. The Gaussian multi-source type model has proven to be the most useful for such applications both because of relative ease with which such modes can be applied and because such models specifically account for the most commonly occurring source geometries (elevated point and ground-based area sources). Turner's Workbook of Atmospheric Dispersion Estimates (1969) continues to be a highly useful guide to Gaussian Plume type-modeling. A recent two-part report, entitled "Atmospheric Dispersion Parameters in Gaussian Plume Modeling" serves as an excellent review of recent developments and current thinking in this modeling approach. In the first part, A. Weber (1976) reviews current methods

Table 1 Air Quality (Emmission) Standards for SO_2

Political Jurisdiction	Annual Average Standard	Short-term Standard
Sweden		1/2-hr. average not to be exceeded more than 1% of the time in any 30-day period = 25 pphm
Ontario, Canada	2 pphm	1-hr. average not to be exceeded more than once per year (?) = 25 pphm
USA	Primary Standard: = 3.2 pphm Secondary Standard: = 2.4 pphm	Not to be exceeded more than once per year - 1. Primary Standard: 24-hr. average of 14.6 pphm 2. Secondary Standard: 24-hr. average of 10.4 pphm 3-hr. average of 52 pphm
FRG	5.6 pphm	Not to be exceeded more than 5% of the time = 16 pphm

Note: Standards given in (ug/m^3) have been converted to (pphm) at 20° C.

for determining dispersion parameters and makes comparisons with the original Pasquill-Gifford curves. Notable developments such as the use of gradient transfer theory by B. Smith (1973) to improve estimates of vertical dispersion are now being incorporated by many investigators of urban multi-source dispersion problems. The second part by F. Pasquill (1976) considers possible revisions to the Turner Workbook. Specific recommendations are made for estimating the horizontal dispersion from readily available wind data and for changes to the existing vertical dispersion curves.

As pointed out by Fox, 1974, the problem of addressing the long-term standards is fairly well in hand. The short-term standards are quite another matter. As an example, a Gaussian-type model designed specifically for computation of the maximum 24-hour average concentration due to emissions from a single source has been developed by J. Hrenko, D. B. Turner and Zimmerman of the U. S. EPA (1972). As described by the authors, the model uses the "brute force" method of computing the maximum 24-hour average by computing hour-by-hour concentrations (requiring hourly meteorological data), accumulates the computed concentrations into consecutive 24-hour averages (running from midnight to midnight) for one year, and computes the maximum value. The intermediate computations are stored on magnetic tape for additional analysis so that presumably one could compute the entire frequency distribution, if desired. The meteorological data requirements include: 1) hourly surface weather observations (the 1964 year is specified since hourly data was available for many stations in the U. S. that year) from the nearest representative weather station. 2) Daily mixing height information for 1964 obtained from listings from George Holzworth. The single source can consist of up to 19 spatially undifferentiated stacks. Both seasonal and diurnal variations in source strength may be included in the model application. The authors caution users that concentrations may be deviate by factor of 2 or more from measured values. Furthermore, it is cautioned, the computations refer to a specific one-year historical record. In the absence of detailed information, it is guessed that the maximum 24-hour average may vary by a factor of 3 or 4 from year to year. This kind of information is very useful and the authors should be commended for both telling users what to expect and us what is needed.

Long-Term Model Applications

By far, the greatest experience with the application of models involving comparison between estimated and standard air quality values has been with long-term models. These models generally combine both casual and statistical algorithms to generate long-term averages.

Experiences with such models has shown that, provided that both the emission inventory is fairly good and the meteorology is representative of the region of interest, one can expect results to be within 20 to 30 percent of observed averages. This result seems to be relatively insensitive to details of the modeling approach and perhaps this later fact explains why so-called "validations" with very simple models yield results about as good as more sophisticated models. Annual average computations seem to be more sensitive to the quality of the input data than anything else.

Short Term Model Applications

Procedures for computing air quality over time invervals comparable with the short-term standards have been developed, but experience shows that results are not nearly as good when compared with observation as the long-term model computations are. However, it is precisely for the short-term cases that considerable promise exists for improvements through the use of more sophisticated computational methods and more detailed input data. Basically, two approaches have been widely used up to now to compute short-term concentrations. One is to compute concentrations hour-by-hour, using the best available hourly input data. Multi-hour concentrations are, in turn, computed by averaging over the appropriate number of consecutive one-hour concentrations. The alternative approach is to utilize a computational procedure which provides a frequency distribution of calculated concentrations. The latter procedure generally requires a less detailed set of input data and generally makes the assumption that fluctuations from mean emission rates are independent of meteorological conditions including time of day. In reality, of course, both meteorological conditions and emission rates tend to be coupled together through their time-of-day dependence and this coupling can considerably affect air quality concentration of pollutants such as CO and, to some extent, SO_2. The effect of this coupling has been investigated by Wangen and Rote(1975), using a CDM-type model and meteorological frequency distributions stratified by time of day, as well as month of year.

A third approach, based upon peak-to-mean ratio statistics, has been suggested by Montgomery, Carpenter, and Lindley(1971).

Another approach and one which seems rather interesting has been suggested by R. Lamb (1975). It is based upon an alternative statistical modeling technique using "macro-turbulence." This method attepmts to derive concentration statistics and influence functions from Lagrangian statistics. This latter approach has not as of yet been implemented or tested.

Hence, for the present at least, the best way to approach the short-term air quality problem is by a specific hour-by-hour method utilizing the best available hourly emission and meteorological data.

The general conclusion from experience with short-term models seems to be that about 50% of the calculated results are within a factor of two of the observed values on an hour-by-hour basis. Further, it appears, as noted by Fox, 1974, that the accuracy increases with degree of sophistication of the modeling approach.

However, it is very important to stress that a poor data set may not be capable of manifesting significant improvements, regardless of how sophisticated the modeling approach is. In other words, if the emissions data, meteorological data, and observations are all characterized by poor quality, no model is going to look very good. In fact, it may even turn out, through fortuitous cancellation of errors, that a simpler model may look better than a more sophisticated model.

Model Applicability

The problem of providing users with a means of evaluating the suitability of models for application to specific problems is being addressed in an ongoing study at the Environmental Systems Division of Argonne by Rote, et. al., 1976 for the U. S. EPA.

The method is application-oriented and begins by requiring the user to classify his particular application according to various aspects of the situation rather than according to the approximate methods by which these aspects are treated by the model being evaluated. Figure 1 taken from the method documentation which is currently in preparation, illustrates the classification scheme. Following the classification procedure the user forms a 4-digit index that is used to locate information contained within the document that is appropriate to the application of interest. The user is then given guidance as to how to conduct an evaluation of a model for his application. Procedures are incorporated in the method for the evaluation but the use of "cookbook" recipes is avoided.

Model Uses

The utility of models in support of air quality management activities is illustrated in Table 2. The list of model applications presented in this table is based upon a survey of model users in the NATO Countries. Because of factors such as the regulatory approach to air quality control, countries vary widely in the extent to which the listed applications are incorporated into their modeling activities. It is hoped that further discussion of the applications of models will promote continued expansion of model utilization.

Data Requirements of Models

The input requirements of models in general, without reference to particular applications was addressed in the EPRI 1976 model data requirements survey cited earlier. In that report five main groups of input data have been identified as required to run most models. These are siting, source, winds, dispersion, and chemical data. Except for the chemical group, the input requirements in the four remaining groups were classified according to "Minimal Model Inputs," "Further Inputs for Typical Modeling," and "Additional Variables for Some Models." The Table 3-1 of that report is reproduced in Table 3 here for convenience of the reader.

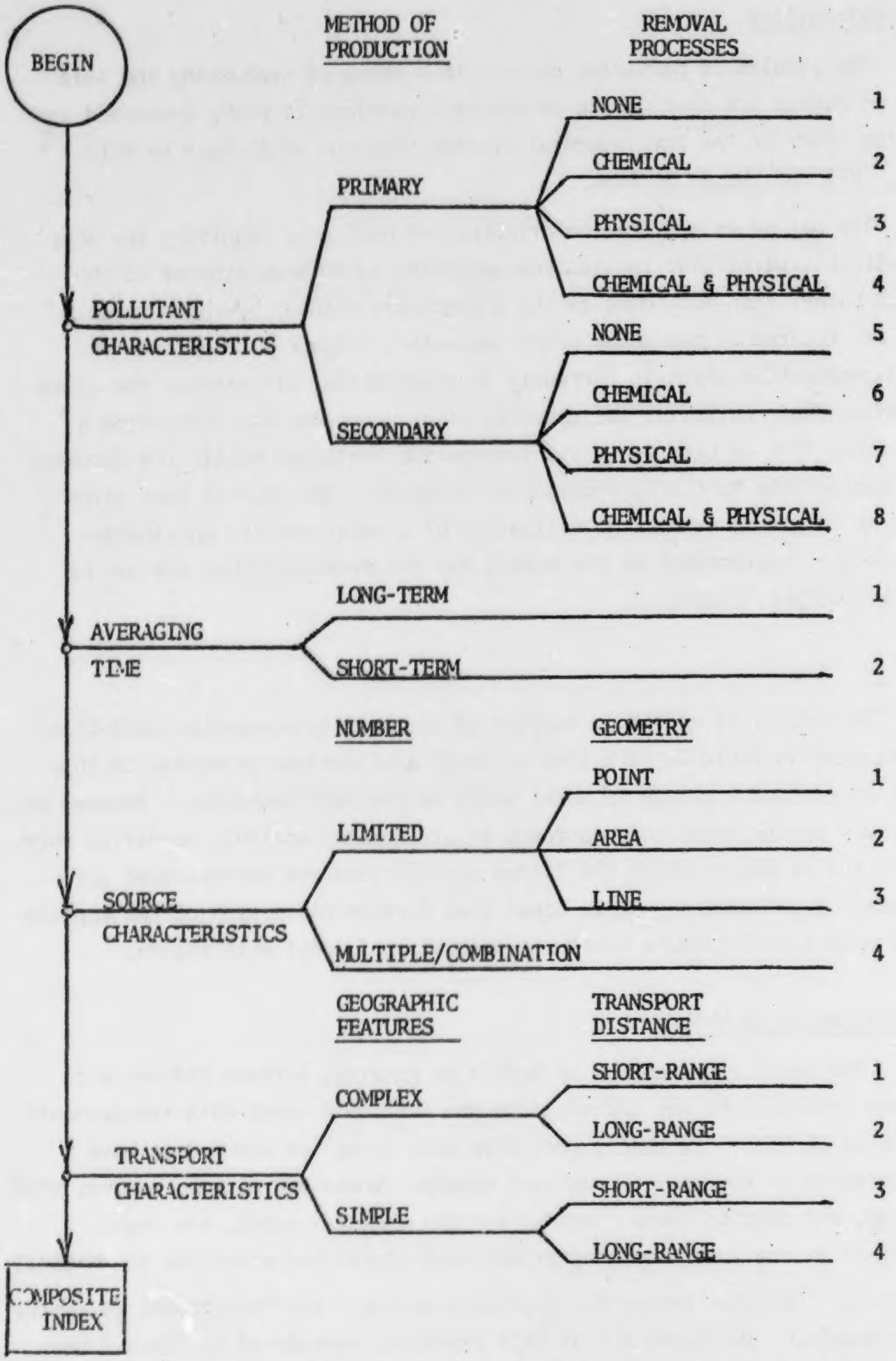
BEGIN
METHOD OF PRODUCTION
REMOVAL PROCESSES
POLLUTANT CHARACTERISTICS
PRIMARY
NONE 1
CHEMICAL 2
PHYSICAL 3
CHEMICAL & PHYSICAL 4
SECONDARY
NONE 5
CHEMICAL 6
PHYSICAL 7
CHEMICAL & PHYSICAL 8
AVERAGING TIME
LONG-TERM 1
SHORT-TERM 2
NUMBER
GEOMETRY
SOURCE CHARACTERISTICS
LIMITED
POINT 1
AREA 2
LINE 3
MULTIPLE/COMBINATION 4
GEOGRAPHIC FEATURES
TRANSPORT DISTANCE
TRANSPORT CHARACTERISTICS
COMPLEX
SHORT-RANGE 1
LONG-RANGE 2
SIMPLE
SHORT-RANGE 3
LONG-RANGE 4
COMPOSITE INDEX

Fig. 1 Schematic Representation of Classification Scheme

TABLE 2

Summary of Air Quality Model Applications

1. Historical Air Quality Trend Analysis (delineation of changes caused by changes in weather, fuel or energy cost and availability, emission controls, etc.)

2. Characterization of Existing Air Quality in Multi-Source Areas (Analysis of ambient concentrations of primary and secondary pollutants)

   2.1 Determination of spatial and temporal air quality patterns
   2.2 Hot spot identification
   2.3 Worst case identification
   2.4 Source culpability determination

      1. by range of source and effect of background
      2. by source class or stack ht
      3. by fuel
      4. by land use type
      5. by geographic location (e.g. windsector)
      6. by political jurisdiction

   2.5 Separation of anthropogenic and natural causes
   2.6 Selection of clean air sites for hospitals, schools, etc.

3. Air Quality Impact Analysis

   3.1 Existing sources
   3.2 Plans involving changes in existing emission patterns

      1. modification of existing sources
      2. addition of new sources
      3. urban expansion and development
      4. commercial/industrial development and expansion
      5. transportation system changes
      6. centralization of space heating facilities
      7. fuel use pattern changes

   3.3 Government policies affecting emission patterns directly or indirectly

   3.4 Review of impact statements by government officials

4. The Integration of Air Quality Impact Analysis and The Planning Process

   4.1 Alternative site selection - minimization of adverse impacts

   4.2 Analysis of tradeoffs with other types of development

5. Long-term Air Quality Control

   5.1 Air Quality standards

      1. formulation
      2. determine economic consequences

   5.2 Control strategy analysis

      1. degree of control required
      2. formulation, evaluation, and optimization of control strategies
      3. determination of requirements for control strategy implementation (fuel and energy requirements, tradeoffs with other environmental impacts, administrative costs, cost to consumers, etc.)

   5.3 Maintenance planning

   5.4 Implementation planning

   5.5 Review of implementation plans by government officials

6. Short-term Air Quality Control

   6.1 Temporary control of selected source types

   6.2 Episode warning and control systems

   6.3 Emergency or accidental spill alert systems

7. Stack Height Calculations

   7.1 Formulation of guidelines for calculation

   7.2 Influence of building wake effects

   7.3 Influence of terrain effects

8. Monitoring Network Design

   8.1 Formulation of guidelines for design

      1. types of data to be taken
      2. measurement frequency
      3. station spacing
      4. supplementing data with model calculations

   8.2 Design optimization

   8.3 Diagnosis of inconsistencies in network data and consistency with emission inventories

9. Emission Inventory Error Diagnois

10. Planning New Measurement or Field Programs

11. Guidelines for Modeling Techniques

    11.1 Investigation of applicability of existing models

    11.2 Formulation of guidelines for applying modeling techniques

    11.3 Determination of needs for new modeling developments

Table 3 Model Input Data Requirements
(Table taken from EPRI, 1976)

Input Data Group	Minimal Model Inputs	Further Inputs For Typical Modeling	Additional Variables For Some Models
Siting	Location of all sources and monitors		
Wind	Mean wind speed and direction	Ground winds at several sites One or more wind profiles Terrain elevations	Geostrophic wind Surface roughness length Friction velocity Pressure gradients
Dispersion	Stability class Mixing depth	One or more vertical temperature profiles	Monin-Obukhov length Wind fluctuations Richardson Number Upward heat flux Surface temperatures
Source	Emission rates Stack gas temperature Volume flux Ambient temperature Stack height Stack diameter		Building dimensions Local winds and temperature profiles Emissions inventory

Gronskei(1975)has reported on "Current and Futures Needs for AQSM's" in which he describes some specific modeling applications and the corresponding information requirements under the general headings of:

1. Environmental Impact Studies
2. Development of Control Strategies
3. Land Use and Transportation Planning
4. Comprehensive Planning
5. Air Pollution Episodes
6. Research on Atmospheric Processes

In that report, Gronskei also makes reference to specific user-oriented models which should be of assistance to users.

Recommendations

Based upon the foregoing information, several recommendations can be formulated:

1. More thought needs to be given to the proper format for communication between users and developers of models. The user/modeler workshop is a good idea but, if such a format is to be used,more emphasis needs to be placed upon needs and less upon new model developments.

2. As a prelude to some larger scale model validation exercises it would be worthwhile to find out what has been learned from previous validations programs. Many studies can be found in the literature which compare model results with observations, with modifications of models, with alternative modeling approaches, etc. These studies have involved a wide variety of climatological conditions, terrain conditions, source emission inventories, meteorological data, as well as a wide range in data quality. It would be very useful to try to condense from all these studies some generally applicable knowledge regarding model applicability, improvements to be expected if the basic model parameters or algorithms are changed, sensitivity of model results to errors in the input data, etc. Often such questions are answered in

different ways with different tests because of biases or peculiarities of the data bases.

A review of those studies should also critically examine the basic design of the model validation exercises and compile a set of recommendations of do's and don'ts for future program designs.

3. In the design of model validation programs a more systematic approach needs to be taken. The current uses of models for air quality management purposes i.e., the needs of model users should be specifically considered in model validation programs. One approach which has been used recently is the formulation of hypotheses which can be tested with the data. However, one should generalize this approach and formulate tested hypotheses which address first the data base itself, secondly the model computations themselves, and thirdly the comparison between the model computations and this observations. The hypotheses which address the data base should be designed to make very clear whether the data is of sufficiently high quality for model evaluation. It is not uncommon in the literature for this aspect of model validation exercises to be completely ignored. As a consequence, the net result of an exercise is that one can not assign fault for poor results or draw useful conclusions. In addition to these types of hypotheses, it is highly desirable that once suitable data bases becomes available, consideration be given to a broader use of the data. For example, by taking subsets of the data one could define numerical experiments to test the applicability of models to a wide variety of problems of data interpolation, extrapolation, short-term prediction, network design, etc. Regression lines and correlation coefficents do not begin to utilize the wealth of information present in high quality data bases.

   The cost of acquiring a rich data base would certainly seem to justify a careful and creative study of what could and should be done with it.

4. More information is required on the applicability of modeling techniques to specific types of problems. Decision makers need a basis for deciding which model to use and what returns they can get for additional expenditures on emission inventory quality and other input data acquisition.

5. One of the most often cited problems with the application of models is the unavailability of proper input data. As far as acquisition of an emission inventory is concerned, more emphasis needs to be placed both on development and testing of inventorying techniques. Perhaps experiments can be designed utilizing the high quality data sets available for St. Louis and Frankfurt to develop and test simplified emission inventory techniques. Both monitoring facilities and models can aid in diagnosing errors in emission inventories and can provide guidance in deciding where additional expenditures on emission inventories are warranted.

   As far as meteorological data is concerned, there seems to be no substitute for some well-placed monitoring stations. Considerable advances have already been made in the development of numerical wind field models (see papers by M. Dickerson, 1975 and C. Sherman, 1975) but they all require good input data. Perhpas the rapid advances in the use of remote sensing equipment and especially the acoustic sounder (see for example Hasenjager, 1975) will place improvements in metrological data within reach of more air quality managers.

REFERENCES

K. L. Calder, *Miscellaneous Questions Relating to the Use of Air Quality Simulation Models*, presented at the 5th meeting of the NATO/CCMS Expert Panel on Air Pollution Modeling (1974).

R. R. Cirillo, Argonne National Laboratory, private communication (1976).

A. Corlin, *The User's Need for Precise Description and Verification of a Model*, presented at the 5th meeting of the NATO/CCMS Expert Panel on Air Pollution Modeling (1974).

M. H. Dickerson, *A Three-Dimensional Mass-Consistent Atmospheric Flux Model for Regions with Complex Topography*, prepared for presentation at First Conf. on Regional and Mesoscale Modeling, Analysis, and Prediction of the American Meteorological Society, May 6-9, 1975, Las Vegas, Nevada (1975).

B. A. Egan, *Modeling for Supplementary Control Systems*, presented at the 5th meeting of the NATO/CCMS Expert Panel on Air Pollution Modeling (1974).

Electric Power Research Institute (EPRI), *Air Quality Models Required Data Characterization*, Project 677-1 (1976).

H. Fortak, *Application of an Air Pollution Model to the Problem of Feasible Industrialization of a Planned Deep-Sea Harbor*, presented at the Seminar held on Air Pollution Modeling in Venice, Nov. 27-28, 1975 (1975).

H. Fortak, *Potential Applications of Mathematical-Meteorological Diffusion Models to the Solution of Problems of Air Quality Maintenance*, presented at the 5th meeting of the NATO/CCMS Expert Panel on Air Pollution Modeling (1974).

D. G. Fox, *Considerations of the U.S. Regional Air Pollution Study*, presented at the 5th meeting of the NATO/CCMS Expert Panel on Air Pollution Modeling (1974).

K. E. Gronskei, *Requirements of Air Quality Models for Land Use Planning*, presented at the 5th meeting of the NATO/CCMS Expert Panel on Air Pollution Modeling (1974).

K. E. Gronskei, *Current and Future Needs for Air Quality Simulation Models* (1975).

S. A. Gustafson, *Computing Optimal Air Pollution Abatement Stategies*, presented at the 5th meeting of the NATO/CCMS Expert Panel on Air Pollution Modeling (1974).

H. Hasenjager, *Examples of Application of a Simple Acoustic Sounder for Observation of Meteorological Parameters Relevant to Air Pollution Studies*, presented at the Seminar held on Air Pollution Modeling in Venice, Nov. 27-28, 1975 (1975).

J. Hrenko, D. B. Turner and J. Zimmerman, *Interim User's Guide for the Single Source Model,* In-House Publication of EPA Division of Meteorology, October 24, 1972.

K. H. Jones, *Introductory Remarks,* presented at the 5th meeting of the NATO/CCMS Expert Panel on Air Pollution Modeling (1974).

A. W. C. Keddie, G. H. Roberts and F. P. Williams, *The Application of Numerical Modeling to Air Pollution in the Fourth Valley* (1975).

L. Kropp, *Use of Dispersion Models During Planning Phases of Industrial and Domestic Regions,* presented at the 5th meeting of the NATO/CCMS Expert Panel on Air Pollution Modeling (1974).

R. G. Lamb, *The Calculation of Long Term Atmospheric Pollutant Concentration Statistics Using the Concept of a Macro-Turbulence,* presented at the Seminar held on Air Pollution Modeling in Venice, Nov. 27-28, 1975 (1975).

T. L. Montgomery, S. B. Carpenter and H. E. Lindley, *The Relationship Between Peak and Mean SO_2 Concentrations,* Conf. on Air Pollution Meteorology of the American Meteorological Society in Cooperation with the Air Pollution Control Association, Raleigh, NC, April 5-9, 1971 (1971).

L. E. Niemeyer and D. G. Fox, *Modeler-User Workshop,* presented at the 5th meeting of the NATO/CCMS Expert Panel on Air Pollution Modeling (1974).

F. Pasquill, *Atmospheric Dispersion Parameters in Gaussian Plume Modeling Part II, Possible Requirements for Change in the Turner Workbook Values,* EPA-60014-76-0306 (1976).

D. Rote, R. R. Cirillo, A. Smith and K. Brubaker, *An Air Quality Simulation Model Evaluation Methodology,* documentation in preparation (1976).

C. A. Sherman, *A Mass-Consistent Model for Wind Fields Over Complex Terrain,* prepared for presentation at First Conf. on Regional Mesoscale Modeling, Analysis, and Prediction of the American Meteorological Society, May 6-9, 1975, Las Vega, Nevada (1975).

D. B. Turner, *Workbook of Atmospheric Dispersion Estimates,* EPA Office of Air Programs Publication, No. AP-26, p. 84 (1969).

L.E. Wangen and D. M. Rote, *The Effects of Temporal Variations in Emissions and Meteorology on Annual Average Concentration Calculations using a Climatological Dispersion Model,* prepared for the U.S. Air Force Weapons Laboratory, Kirtland AFB, New Mexico (1975).

A. H. Weber, *Atmospheric Dispersion Parameters in Gaussian Plume Modeling Part I, Review of Current Systems and Possible Future Developments,* EPA 60014-76-030a (1976).

7th International Technical Meeting
on Air Pollution Modeling and its Application

Title of Paper

APPLICATIONS OF MATHEMATICAL MODELS IN POLLUTION NETWORK PLANNING AND AIR QUALITY CONTROL

Author's Name, Institution

A.CAVALLARO	Laboratorio Provinciale di Igiene e Profilassi
R.GUALDI	Laboratorio Provinciale di Igiene e Profilassi
G.LANEVE	Osservatorio Meteorologico di Brera
G.TEBALDI	Laboratorio Provinciale di Igiene e Profilassi

September 7 - 10, 1976
Airlie Virginia
United States of America

APPLICATIONS OF MATHEMATICAL MODELS IN POLLUTION NETWORK PLANNING AND AIR QUALITY CONTROL

1. **INTRODUCTION**

2. **MATHEMATICAL SIMULATION MODEL**
2.1 Characteristics
2.2 Inventory of emissions
2.3 Reliability

3. **PRACTICAL APPLICATIONS**
3.1 Network planning
3.2 Air quality control
3.3 Simulation of territorial plânning

4. **STATISTICAL MODELS**

5. **ACKNOWLEDGEMENTS**

6. **APPENDIX**

7. **BIBLIOGRAPHY**

SUMMARY

This paper sums up the experiments carried out and the results obtained in the research into air pollution control and prevention in the Province of Milan.

The Provincial Laboratory of Hygiene and Prophylaxis, charged by law with drawing up plans for studying and investigating the matter, turned to the Brera Meteorological Observatory directed by Professor L.Santomauro for help in solving the most sophisticated problems of urban micrometeorology and mathematical models.

This work group planned and built-up a network of chemical and meteorological sensors linked to a centralized computer.

The sampling sites have gradually been increased and connected via leased telephone lines to a central room, the displacement was determined with peculiar analysis, taking the most significant criteria concerning ground pollution into account.

A mathematical model checks the network reliability and the collected values.

In order to examine the amount of air pollution we developed a diffusion model to simulate the dynamics of the Milan atmosphere.

In order to illustrate the model's possibilities, we carried out some tests to simulate the effect of urban and industrial installation in some basic zones according to an inventory both of sources and meteorological conditions.

Commenting on the practical results obtained by the model adopted, we shall make some suggestions as to the possible employment of other models for climatological use.

1. INTRODUCTION

The presence of persistent episodes of heavy pollution over the urban area of Milan during the winter months has made it essential to have an overall picture of how pollution concentrations in the lower atmospheric layers are distributed in space and in time. Since Milan is almost wholly affected by emissions from heating plants, sulphur dioxide was chosen, along with suspended dust, as tracers for monitoring local air pollution distribution.

After a preliminary period of analysis of air samples made with laboratory methods, which gave us an initial understanding of the situation, we used automated techniques suitable for representing a wider area in a synoptical way; we achieved this by increasing the number of sampling sites and by centralizing the data to a process computer. This solution, which is obviously rather costly, has enabled us to have a continuous control in real time of the whole area and to supply the Health Authorities with all the necessary information.

The monitoring data collected over 5 consecutive years served as statistical support for the present report; by studying these data we were able to single out the most heavily polluted areas, to determine the behaviour in time of the phenomena (daily, seasonal, annual), to evaluate the interdependence of the various values, and lastly it conveniently optimized the study of the mathematical model.

As far as siting the sensors was concerned, the choice, of their topographical dislocation was solved, at an initial stage, by applying a logical model, and subsequently a mathematical one. The first is based on representivity criteria according to the strategies to be adopted; to this end a decisional diagram was made in which the elements taken into consideration were grouped into 3 categories: known data, objectives to be reached, and limits to be respected. Each element was assi-

gned with a weight corresponding to its importance.
The initial purpose of the network was to control the city center worst hit by heavy pollution concentrations. For this reason it was decided to place 10 SO_2 monitors and 5 meteo stations in this area, comparable to a circle of 7 km. in diameter. The siting and the instrumentation of the sampling sites are stated in the appendix.
Subsequently, as already said, the validity of the measures and the significance of the sensor was checked with a mathematical model which also gave us useful indications as to future development (§ 4.1).

2. THE MATHEMATICAL SIMULATION MODEL

2.1 Characteristics

The development of a simulation model for the Milanese area aimed at perfecting our understanding of the dynamic behaviour of the urban atmosphere, evaluating the individual contribution of chemical and meteorological components towards episodes of pollution, supplying useful information for territorial planning and lastly, checking the structure of the network.
To this end and on the basis of the knowledge acquired, the ATDL model (Gifford F.A. jr., Hanna S.R., 1971; Hanna S.R., 1972) was adopted.
The choice of this model is justified by the fact that it considers emissions in area sources and point sources. This criterium is suited to the urbana area of Milan in that a census of domestic heating plants shows that only 5% has a potentiality above 4.10^6 Kcal/h and with stacks over 30 m. high (point sources), whereas 95% have a lower potentiality and the average height of the stacks is about 30 m. (area sources) (Fig.1).
It should be remembered that the ATDL model calculates the ground concentration of SO_2 according to emissions (area and point sources) and to

meteorological conditions (wind speed, wind direction distribution normalized to 1, stability classes). This research was done by splitting up the City of Milan into a network of 36 squares, each 2.000 m. wide.

2.2 Inventory of Emissions

At the beginning of the study, in order to calculate the potentiality of the area sources, we made use of the previously mentioned census values; subsequently, so as to supply the model with an up-dated input (organised with a computerized system), we decided to calculate by deduction the emission coefficients ($\mu g\ m^{-2}\ s^{-1}$) for each square. This system, which has given good results in similar applications, in this case turned out to be particularly suitable both because of the acceptably uniform structure of emissions and because of the resources at the researchers' disposal.

The latter are represented by the availability of a detailed record of the volumetry of the buildings (constantly up-dated with urban development), the precise topographical dislocation of which has enabled us to calculate the volumetry contained in each individual square.

For determining the SO_2 emissions we considered the number of installations running on oil and on nafta for each square of the network; then, according to the sulphur content and the fuel consumption used for each unit of volume, it was easy to obtain the corresponding emissions of SO_2; by multiplying the unit value by the total volumetry we obtain the emissions of each square. This arrangement facilitates the use of the model in the field of territorial planning given that the ground concentration is directly referable to the building volumetry.

This procedure was applied only in the months of December since in the Valpadana area December is the most meteorologically stable month.

The emission values concerning the other months were estimated with the day/degree formula.

2.3 Reliability Check

In order to obtain the degree of reliability of the chosen algorithm, in relation to the inputs considered, we carried out tests for 5 cold months from November 1974 to December 1975, extending the research both over long periods (a month), useful for correct practical use, and over short periods (12 hours), useful for a theoretical understanding of the model. Then we calculated the correlation coefficients (tab.1) which vary between 0,6 and 0,9, and 85% is over 0,7.

The analysis of the values observed and calculated on a monthly basis (fig.2) shows that the model reproduces local conditions in the areas examined with satisfactory reality, and also that the values taken are well reproduced without evident alterations.

To have a synoptical view of SO_2 distribution in Milan, we traced the iso-concentration curves (fig.3) according to the monthly values calculated. The graph presented as an example is characteristic of the winter period and shows the presence of concentration nuclei which correspond with the greatest population density, data confirmed by instrumental observations.

3. APPLICATIONS OF THE ATDL MODEL

Considering the good degree of reliability of the ATDL model, it was applied to determine the minimum rate of pollution obtainable with the complete transformation of heating plants; for planning residential and industrial areas and for a better use of the monitors.

3.1 Planning the Network

Since, as we have said, the monitoring network doesn't yet cover the whole urban and metropolitan area of Milan, the study was extended to other zones of the urban network in order to complete the investigation of pollution distribution. Of these, the precedence was given to those subjected to future urbanization and thus susceptible to pollution increases. For this purpose the ATDL model has proved to be an effectively useful instrument since it enables you to single out new sampling zones, to spot redundant positions and lastly, to obtain an accurate image of the situation, even reducing the number of sensors.

An analysis of the isoconcentration curves shows that the sampling sites marked with codes 8, 14 and 9 can be moved elsewhere for better sampling (fig.3). Moreover, a comparison of the calculated values with the sampled ones confirms that the concentrations calculated on a climatological basis taken from the 3 positions mentioned are not representative of the area under control.

- Site n. 8 The model gives values almost constantly higher than those really found by the sensor. An analysis of the site confirms that the instrumental data are not representative of the surrounding area because, given prevalent wind conditions, the air masses reach the sampling site mixed up, presumably because of a grassy park which dilutes the pollution.

  This phenomenon confirms the results of studies carried out on similar topographical situations (Munn R.E.,1966). A study to determine the law which governs the dilution of the pollutant in this case with greater precision is still in progress.

- Site n. 9 The highest values obtained from the sensor can be attributed to the particular sources immediately surrounding the area; these are characterized by low stacks and obsolete installations. Therefore,wishing for synoptical and not detailed values it is necessary to put the equipment elsewhere.

- Site n. 14 This sensor, installed according to topographical criteria at the limit of the urban area opposite a hospital, is now in an intermediate area which is also affected by local conditions.
  Since the calculation reveals a maximum concentration nucleus 1,5 km further north, we presume that analyses in this position can give more valid indications.
  The sensors in position 8 and 9 can be conveniently installed (fig.3) in areas indicated by the model as subject to potential ground concentrations. In this way the same number of sensors controls a wider area (12 km in diameter instead of 7 km); the calculations made by the model give the values relevant to the areas not controlled directly by means of isoconcentration curves.
  Finally, according to the set of historical data collected, we shall make a 3 monthly estimation of the correct functioning of the instruments calculating the differences and evaluating any deviations from the statistically calculated tolerances.

3.2 Air Quality Control

The Mayor of Milan ordered that gas oil should be used instead of nafta in heating plants of over 30.000 Kcal/h. Since the application of this regulation SO_2 concentrations have dropped progressively (fig.4) both as a seasonal average and as temporary peaks. At the present moment 70% of the installations have changed over to oil; therefore, in order to foresee the improvement that will be obtained when there is a 100% change-over, we simulated the pollution for the 5 cold months adopting as meteorological inputs those used in the effective calculation relevant to the period from 11/74 - 3/75.

In order to define the input of the area sources, we considered that oil has a sulphur content three times lower than nafta and that the various sources are uniformly distributed over the whole urban territory. According to these hypotheses we see that 44% of the emissions, in the form of SO_2, is caused by oil plants and thus 56% by those run on nafta. Therefore if this change-over is completed, the calculation indicates a further drop in emissions of 37.4%.

Consequently, calculating the emission coefficients for each square of the network, applying the ATDL model, we got the ground concentrations according to 4 meteorological conditions. An analysis of the values obtained (tab.2) shows that the drop in SO_2 varies from a maximum of 40% (class B) to a minimum of 33% (class E).

3.3 Simulation of the Territorial Plan

One of the plans in progress is that of territorial management.

Given the difficulty of finding historical data on the volumetric urban development and lacking the elements of comparison by which to check the calculations, as a preliminary test we simulated an increase in building in a part of the urban area where the present ground concentration in known, measured and calculated with the ATDL model, and the emission of SO_2 (§ 2.2). The choice fell on a zone situated south of the urban area where further residential complexes are likely to be developed in the near future. The research procedure was based on the hypothesis that an increase in the density of the buildable volumes would increase the emission of sulphur dioxide once by 100% and once by 50%. For the experiment we chose a simulation period of 15 months, split up into 5 seasonal periods.

The results of the calculations are given in tab. 4 where, for each seasonal period, we have shown: the values observed (O) and calculated (C) in the reference zone, as well as the difference between them (O-C); the values calculated with the 100% and the 50% increase in SO_2 emissions (re-

spectively Cs_1 and Cs_2) and the numerical and percentage differences between these and the calculated value ($Cs_1 - C$ and $Cs_2 - C$).
According to this comparison there would be an increase in the same area from 61-75% of SO_2 ground concentration, in the case of a 100% increase, and from 32-38% in the case of a 50% increase.
In the area surrounding the reference zone, at a distance of 2 km the increase of the ground concentration is minimal since it would only be 2.0%. This would confirm that the masses of air above the urban area of Milan and in adiabatic conditions don't move much, as is also shown by the minimum ventilation time (Santomauro L. 1972).
Moreover, if you put the emission percentage in the abscissa of a diagram (fig.5) and the SO_2 ground concentration percentage in the ordinate, the pollution increase is proportional in a linear way to the potentiality of the buildings. These results supply the possibility of dimensioning, at least in theory, the settlements in the areas that are still not heavily built-up, distributing them so as to avoid exceeding the acceptable limits.

4. STATISTICAL MODELS

In order to calculate the behaviour of pollution over the whole urban area, we worked out two statistical models of a climatological type by analyzing the values collected in the 5 year period between 1970/71 and 1974/75. The values considered in this research, apart from SO_2 ground concentrations, are the day/degree, the Stanford index (Stern A. 1973 and others) and fuel consumption.
In order to define the first statistical model, based on multiple regressions, and to demonstrate the validity in the climatological field, the partial correlations are examined between SO_2 + day/degree and between SO_2 + Stanford index. In the first case the result was a regression curve of a parabolic ty

pe (fig. 6), the equation of which is:

$$X = 0{,}068 + 1{,}18 \cdot 10^{-6} X_1^2$$

where X_1 is the monthly day/degree value.

The development of this equation, compared to the linear regression, adapts itself better to the physical reality, especially if you consider the low values of the day/degree; the correlation coefficient is 0. r = 822.

In the second case, i.e. in the partial correlation between SO_2 and the Stanford index which expresses the intensity of the inversion numerically (fig.7) it is seen that the slope of the straight lines is constant in every case, while the value of the intercepting line varies according to the months taken into consideration: this value, which corresponds to the concentration in the absence of inversion in the first 1500 mt is proportional to the fuel consumption and therefore can be related to the day/degree.

The correlation coefficient between the day/degree and the value of the intercepting line is in fact r = 0,937.

From the above we deduce that, for the purposes of a climatological analysis, it is correct to calculate the SO_2 concentrations by means of the multiple regression.

The final equation for the calculation of the SO_2 ground concentration is:

$$X = 0{,}024 + 0{,}11 X_1 + 0{,}012 X_2$$

where X_1 = the daily day/degree

X_2 = the intensity of the inversion and the corresponding correlation coefficients are:

$$r_{x,x_1,x_2} = 0,898$$

$$r_{x,x_1} = 0,787$$

$$r_{x,x_2} = 0,797$$

The results (tab.4) confirm the possibility of following the seasonal pollution indexes in the Milanese area as a whole with this method. The second statistical model enables us to determine a relation which directly involves the quantity of sulphur present in the fuel together with the inversion intensity. And, in fact, for a certain period of validity of the values considered, the ground concentration is in direct proportion to these two values at less than an empirical factor α :

$$X = 0,017 + \alpha \, IS$$

where I = inversion intensity validity interval 5 ÷ 7

S = quantity of sulphur " " 20 ÷ 40 K tons

$$\alpha = \frac{SO_2}{IS}$$

The coefficient α , calculated for the 5 years considered (tab; 9), has proved to be reasonably constant for the whole period and thus it can be considered, at least at the present stage of the research, characteristic of the urban area of Milan. Therefore the report described could be applied in the future to control the effects of the total sulphur quantity contained on the seasonal pollution levels.

5. ACKNOWLEDGEMENTS

I should like to express my particular thanks to Professor L. Santomauro, Director of the Meteorological Observatory of the Brera, Institute of Applied Meteorology, for his encouragement and help in coordinating this re

viewing the text of this report.

6. APPENDIX

Structure of the Milan Network

At the present moment the following monitoring stations are installed and working in the Province of Milan:

- 16 coulometric SO_2 monitors
- 5 meteo stations equipped with sensors for measuring temperature and wind speed and direction.

The instruments that continuously sample the air to be analyzed are linked via telephone lines dedicated to a Philips P855 process computer, which, guided by an automatic timer, sees to the following functions:

a) calculation and printing of the average hourly SO_2 concentration values;

b) hourly printing of the meteorological values;

c) comand and running of calibrations (zero and end of scale) of all the instruments;

d) automatica warning when alarm threshold is exceeded - can be set for each individual station;

e) calculation and printing of the 6-12 and 24 hourly averages;

f) calculation of the Pasquill categories;

g) analogical recording of the concentrations on the stations of particular interest;

h) luminous display of alarm situations on a synoptical panel.

Moreover, the center has:

1 instrument for receiving facsimiles of the isobar maps covering the European area;

1 teletypewriter connected to Linate airport for receiving meteo bulletins.

The organization arranged by the Provincial Laboratory of Hygiene and Prophylaxis has enabled the system to have about a 90% efficiency.

The experience thus acquired both in the field of measuring stations and in the field of data transmission and processing has encouraged the Milan Provincial Authorities to widen and speicify the sampling network.

The new configuration (fig.8) is being built-up and will be finished by the end of September this year. By this date the following will be connected to the computer:

- 25 SO_2 monitors (10 in Milan and 15 over the provincial territory in the towns specified in the enclosed map) Philips PW9755
- 3 automatic dust monitors Philips PW 9790
- 6 meteo stations (among which a tower for a wind and temperature profile); SIAP Bologna VT 5502 VT 5510 TM 5020
- 2 nitrogen oxide monitors; TECO, Philips PW 9760/01 PW 9760/00
- 3 airport noise sensors; Bruel and Kiaer OUTDOOR Microphone type 4921
- centralization of the values detected by peripheral networks.

In order to run this network it was necessary to re-desing the Philips P855 computer giving it greater processing power (56K) so that as well as the organic control of the various types of analyzers, it can supply in real time a series of tables and statistics which give a complete picture of the situation on the controlled sites.

Moreover, all the data collected are recorded on a magnetic tape for further processing.

7. BIBLIOGRAPHY

1) ANNALI DELL'OSSERVATORIO METEOROLOGICO DI BRERA 1973 - Osservazioni meteorologiche eseguite durante l'anno 1974/75.

2) B. BRINGFELT e altri 1971 - A numerical air pollution dispersion model for central Stockolm Atmospheric Environment - Pergamon Press

3) C.CANTONI - A.CAVALLARO R.GUALDI - G.TEBALDI L.SANTOMAURO 1975 - About a diffusion model for a weak atmospheric circulation on urban area - Milano IBM Venezia - Convegno sui modelli matematici.

4) C.CANTONI - R.GUALDI L.SANTOMAURO 1975 - Preliminary report about a diffusion model for Milan urban area. Gifford Hanna model; 6th NATO/CCMS - International Technical Meeting on Air Pollution Modeling; APM 6/1 BATTELLE INSTITUT E.V.

5) A.CAVALLARO - R.GUALDI G.TEBALDI - G.REBUZZINI 1974 - L'inquinamento atmosferico a Milano Acqua e Aria, settembre 1974

6) L.F. ESCUDERO R. DELLANO e coll. 1973 - Metodologia de la Investigacion en Sistemas de Control para Contaminacion Atmosferica Centro de Investigacion VAM-IBM

7) GIFFORD F.A. jr, 1970 - Atmospheric Diffusion in an Urban Area; paper presented 2nd IRPA Conference, Brighton, Engl., May 5, pp 5 + 1 fig.

8) GIFFORD F.A. jr - HANNA R.S. 1970 - Urban Air Pollution Modelling; paper ME-320, 2nd International Clean Air Congress, Washington, Dec.11, 1970

9) HANNA R.S. 1971 - A Simple Method of Calculating Dispersion from Urban Area Sources Jour. of APCA - vol. 21, N.12, p.774, + 5 figs.

10) HANNA R.S. 1972 - Description of ATDL Computer Model for Dispersion from Multiple Sources; 2nd Industrial Air Pollution Control Conference, University of Tennessee ATDL Contrib.File N° 56

11) MUNN R.E. 1973 - Urban Meteorology: some Selected Topics, Bull. Am; Met.Soc.; vol.54 p.90-93

12) PASQUILL F. 1962 - Atmospheric diffusion Van Nostrand London

13) RUNCA E. - MELLI P. ZANNETTI P. 1975 - Simulation of SO_2 - Dispersion in the Venetian area; 6th NATO/CCMS - International Technical Meeting on Air Pollution Modeling; APM 6/4 BATTELLE - INSTITUT E.V.

14) SANTOMAURO L. 1971 - Analysis of Wind Trend in an Urban Area situated on Flat Land; Osservatorio Astr. Milano-Merate; Suppl.Meteor. N.21

15) SANTOMAURO L. 1972 - Proposal for a Mathematical Model of Air Pollution survey in Milan; Proceedings of the 3d Meeting of the Expert Panel on Air Pollution Modeling - NATO/CCMS, N.14, Paris, France, Oct. 2 - 4 Chapt. V.

16) C.C. SHIR - L.J.SHIEN 1973 - A generalized urban air pollution model and its application to the study of SO_2 distribution in the ST. Louis metropolitan area - IBM scientific center - Palo Alto California

17) SMITH M.E. 1968 - Recommended Guide for the Predictions of the Dispersion of Airborne Effluents ASME, IX and 85 pp.

18) STERN A.C. - WOHLERS H.C. BOUBEL R.W. - LOWRY W.P. 1973 - Fundamentals of air pollution

TAB. N°1 - CORRELATION COEFFICIENTS

Station code	November	December	January	February	March
5	—	0.827	0.778	0.859	0.801
6	0.788	0.848	0.788	—	—
7	0.737	0.853	0.859	0.830	0.711
8	0.695	—	—	0.827	0.775
9	—	0.862	0.837	0.853	0.760
10	0.735	0.893	0.900	0.885	0.857
13	0.570	0.814	0.821	0.732	0.682
14	—	0.774	0.736	0.686	0.740
15	0.608	0.723	0.704	0.822	0.768
16	—	0.868	—	0.727	0.605

TAB. N° 2 - SIMULATED SO_2 CONCENTRATION VALUES

Stability class	B				C				D				E			
Months	actual calc.	future calc.	ΔSO_2	%	actual calc.	future calc.	ΔSO_2	%	actual calc.	future calc.	ΔSO_2	%	actual calc.	future calc.	ΔSO_2	%
November ' 74	116.2	74.2	-42.0	39,2	201.5	128.7	-72.8	36,1	359.7	229.9	-129.8	36,1	436.9	277.4	-159.5	36,5
December ' 74	129.5	82.8	-46.7	39,1	225.3	144.0	-81.3	36,1	403.3	257.8	-145.5	36,1	487.0	311.3	-175.7	36,1
January ' 75	148.4	94.8	-53.6	39,1	257,8	164.8	-93.0	36,1	460.8	294.6	-166.2	36,1	556.2	350.7	-205.5	36,9
February ' 75	115.3	67.9	- 47.4	41,1	193.0	128.3	-64.7	33,5	359.2	229.6	-129.6	36,1	419.3	277.3	-142.0	33,9
March ' 75	76.6	51.3	- 25.3	33,0	133.6	89.4	-44.2	33,1	239.6	160.1	- 79.5	33,2	289.4	195.9	- 93.5	32,3

TAB. N° 3 - VARIATIONS IN SO_2 CONCENTRATIONS IN RELATION TO SIMULATED RESIDENTIAL INCREASES

		Station code 15				Station code 8				
Season		Spring 74	Fall 74	Winter 74/75	Spring75	Fall 75	Spring74	Fall 74	Winter74/75	Spring75	Fall 75
0		144	229	427	81	144	190	299	490	109	209
C		146	172	533	73	107	217	256	820	115	162
0 - C		- 2	+ 57	- 106	+ 8	+ 37	- 27	+ 43	- 330	- 6	+ 47
C_{s1} (100%)		241	282	887	128	183	221	260	836	117	164
C_{s2} (50%)		193	227	710	101	145	219	258	828	116	163
$C_{s1} - C$	Δ	95	110	334	55	77	4	4	16	2	2
	%	65	64	61	75	72	1,8	1,6	2,0	1,7	1,2
$C_{s2} - C$	Δ	47	55	177	28	38	2	2	8	1	1
	%	32	32	32	38	35	0,9	0,8	1,0	0,9	0,6

TAB. N°4 - COMPARISON OF COMPUTED (1) AND OBSERVED SO_2 - MONTHLY AVERAGED CONCENTRATIONS

Months	Years	Day/degree (°C)	Invers.int. (I)	SO_2(Calc.) (ppm)	SO_2(P855) (ppm)	diff.(SO_2) (ppm)
October	1972	5,65	2,32	0,11	0,12	- 0,01
"	1973	4,59	2,85	0,11	0,11	0,00
"	1974	8,14	1,40	0,13	0,09	+ 0,04
November	1971	9,84	2,82	0,17	0,19	- 0,02
"	1972	10,29	4,87	0,20	0,24	- 0,04
"	1973	9,78	6,32	0,21	0,22	- 0,01
"	1974	10,44	2,63	0,17	0,14	+ 0,03
December	1971	14,24	16,71	0,38	0,41	- 0,03
"	1972	14,63	5,10	0,25	0,26	- 0,01
"	1973	13,76	6,18	0,25	0,21	+ 0,04
"	1974	12,45	12,82	0,32	0,24	+ 0,08
January	1972	14,13	2,12	0,20	0,28	- 0,08
"	1973	14,52	5,19	0,25	0,25	0,00
"	1974	11,97	6,85	0,24	0,26	- 0,02
"	1975	12,56	7,40	0,25	0,22	+ 0,03
February	1972	11,00	0,95	0,16	0,19	- 0,03
"	1973	11,97	3,51	0,20	0,19	+ 0,01
"	1974	10,10	1,11	0,15	0,16	- 0,01
"	1975	11,85	2,57	0,19	0,18	+ 0,01
March	1972	7,62	1,85	0,13	0,15	- 0,02
"	1973	8,70	2,00	0,14	0,13	+ 0,01
"	1974	8,19	1,07	0,13	0,13	0,00
"	1975	9,10	0,71	0,13	0,11	+ 0,02
October/March	1972/73	10,96	3,83	0,19	0,20	- 0,01
"	1973/74	9,73	4,06	0,18	0,18	0,00
"	1974/75	10,76	4,59	0,20	0,16	+ 0,04

(1) Multiple regression equation: $Z = 0{,}024 + 0{,}011 \cdot x + 0{,}012 \cdot y$

Z = concentration (ppm) x = daily mean value of day/degree

y = seasonal mean value of Inversion Intensity

Correlation coefficient:

$R_{z,x,y} = 0{,}898$ $r_{z,x} = 0{,}797$ $r_{z,y} = 0{,}787$ $r_{x,y} = 0{,}555$

TAB. N°5 - RELATIONSHIP BETWEEN SO_2 - CONCENTRATION, INVERSION INTENSITY AND AMOUNT OF SULFUR FROM COMBUSTION.

Winter (November - March)	SO_2 (ppm)	I	Sulfur (1) (k ton)	q x 10^{-3}
1970 - 71	0,27	5,7	32,45	1.460
1971 - 72	0,24	4,9	33,28	1.472
1972 - 73	0,21	4,1	34,70	1.476
1973 - 74	0,20	4,1	33,20	1.469
1974 - 75	0,18	5,2	23,60	1.467
1970 - 75	0,22	4,8	31,45	1.469

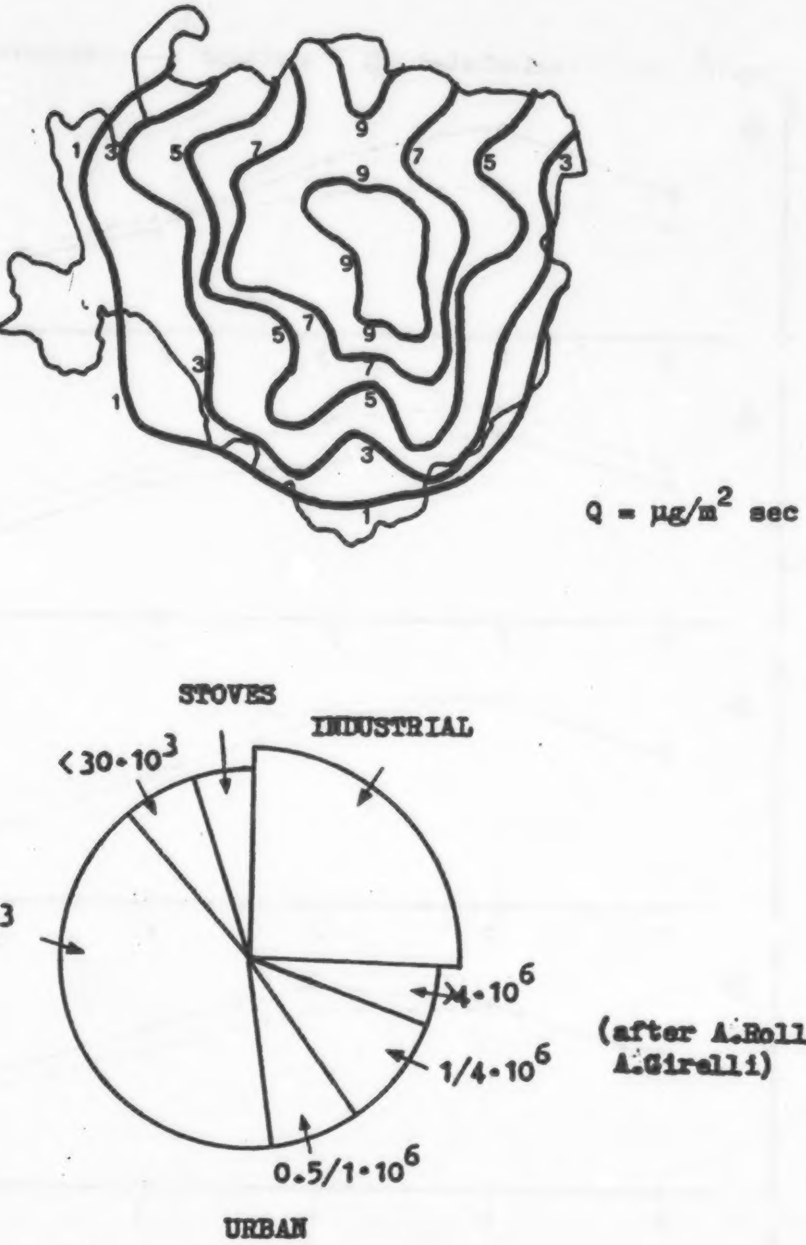

(after A.Rolla, A.Girelli)

FIG. 1 - SPATIAL AND RELATIVE DISTRIBUTION OF SO_2 EMISSIONS

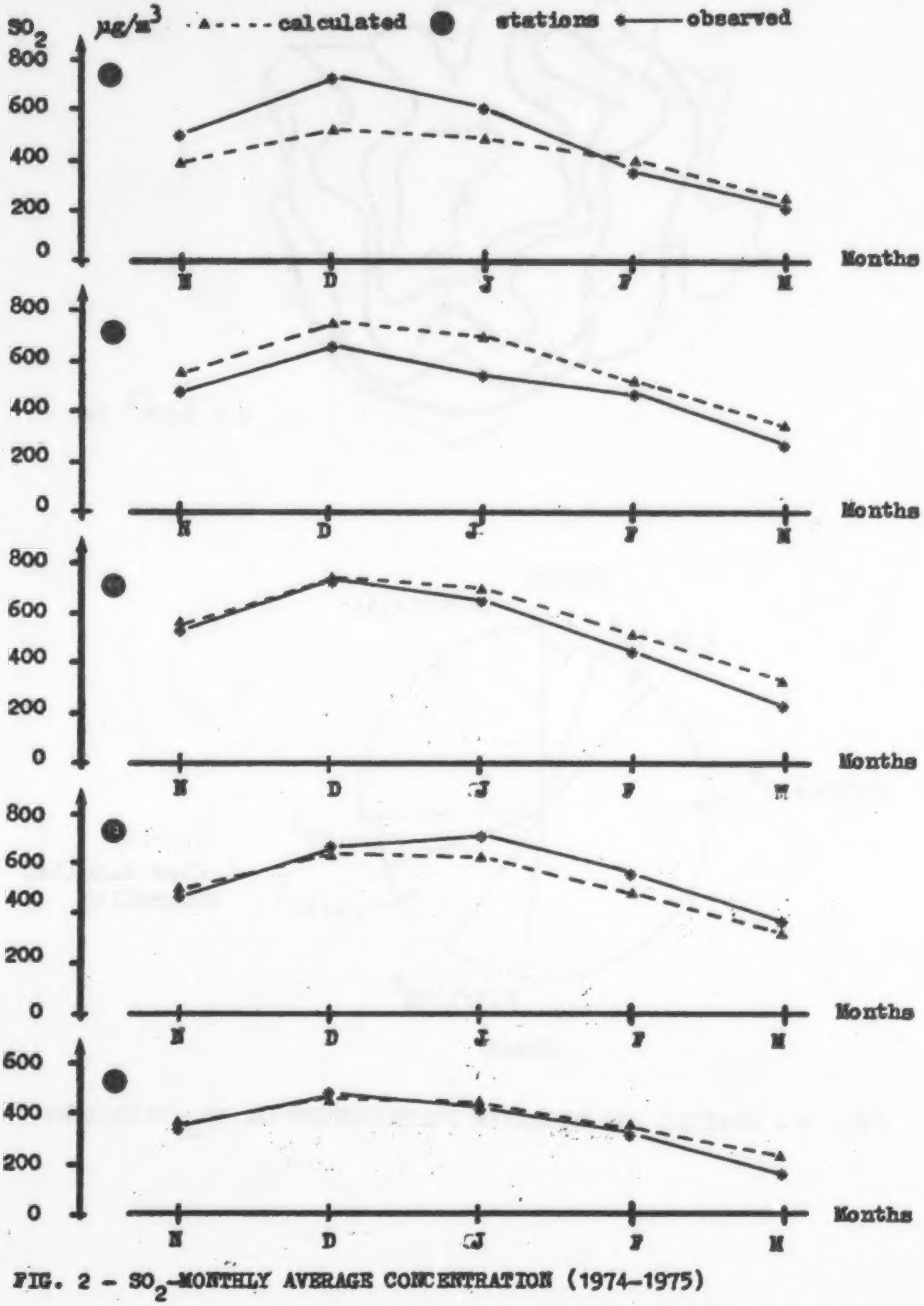

FIG. 2 - SO_2-MONTHLY AVERAGE CONCENTRATION (1974-1975)

JANUARY 1975

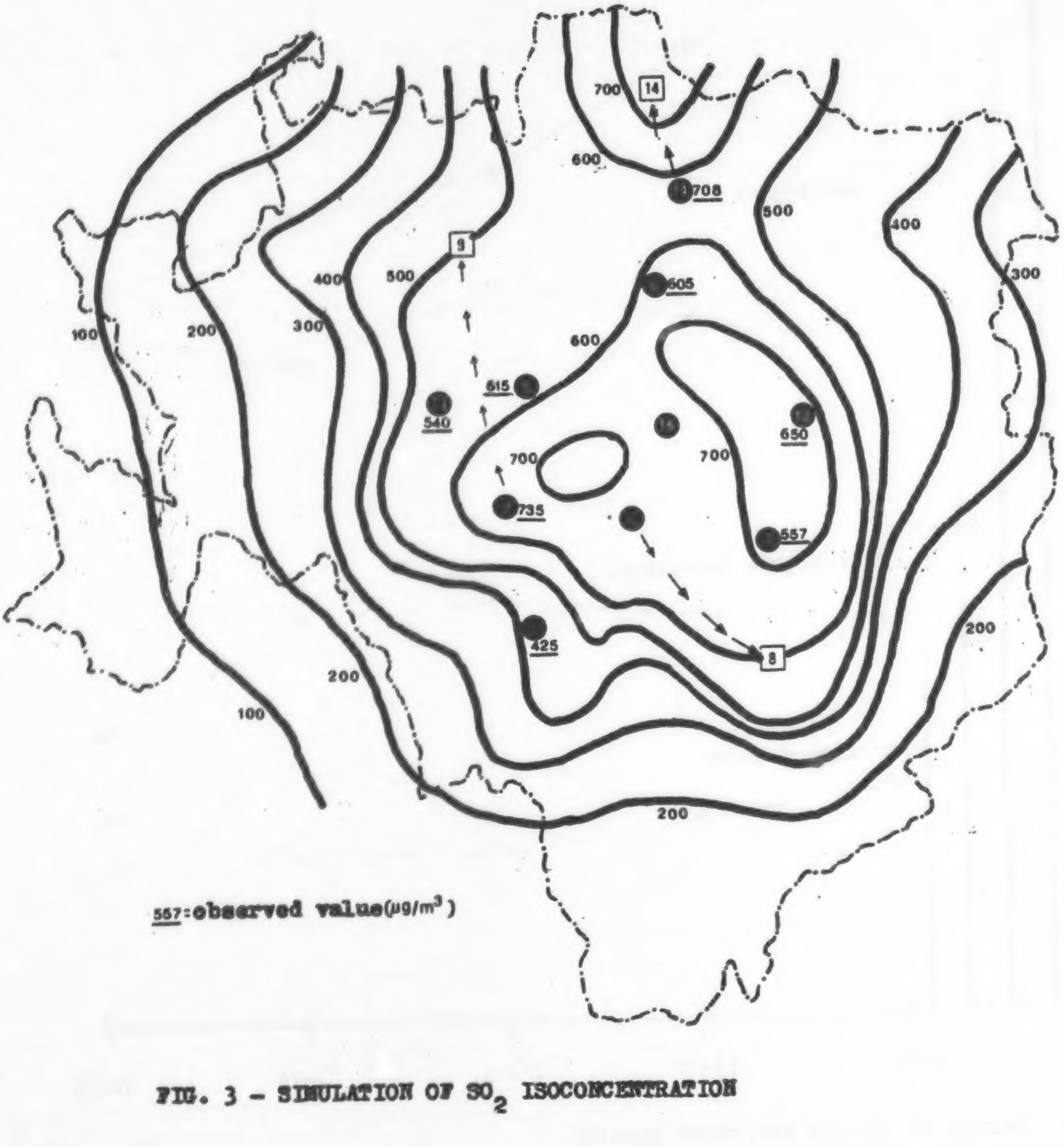
700
14
600
708
500
400
9
500
400
605
300
100
200
300
600
615
540
650
700
700
735
557
425
8
200
200
100
200

557:observed value(µg/m³)

FIG. 3 - SIMULATION OF SO_2 ISOCONCENTRATION

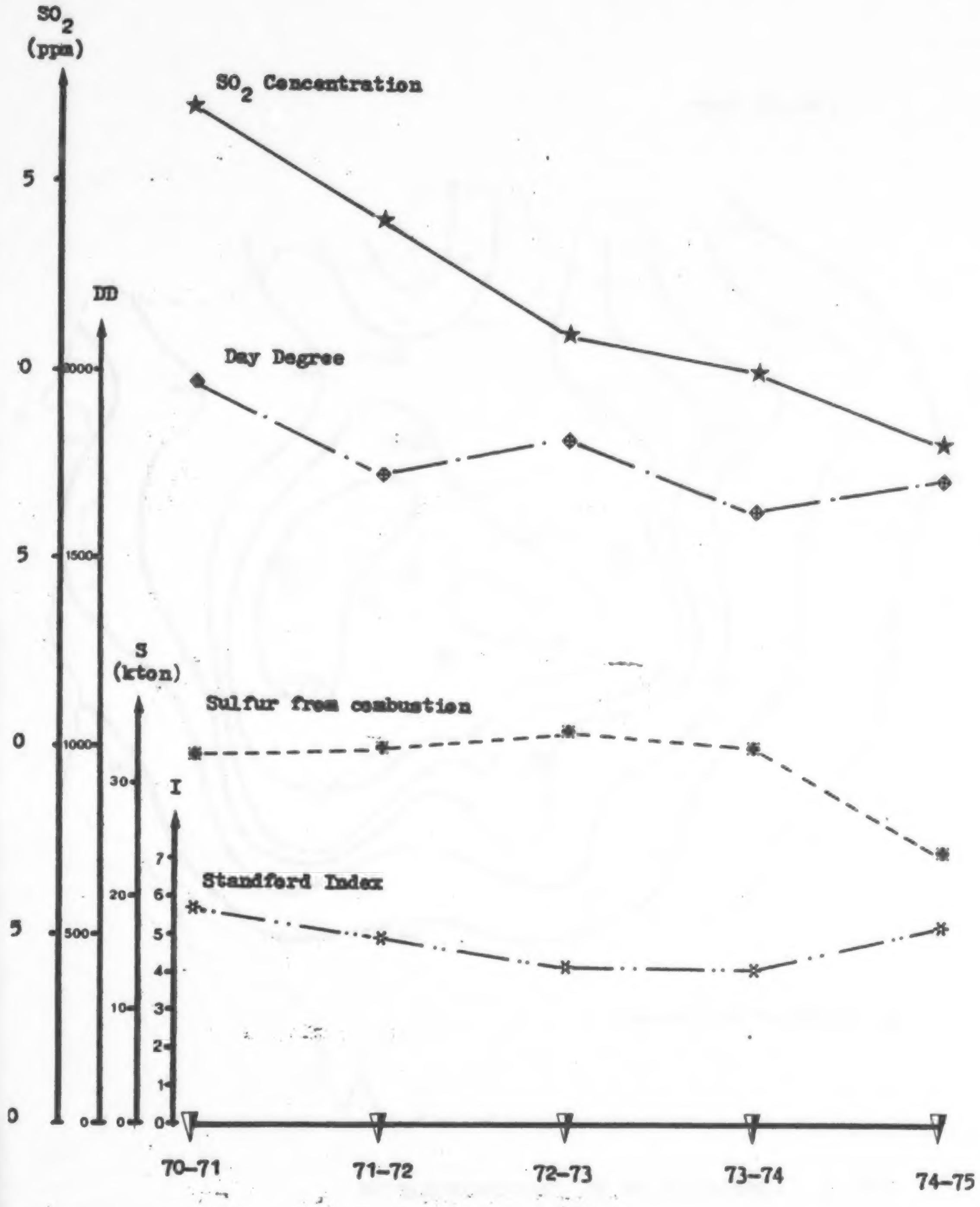

3. 4 - TRENDS IN THE AIR POLLUTION INDICES

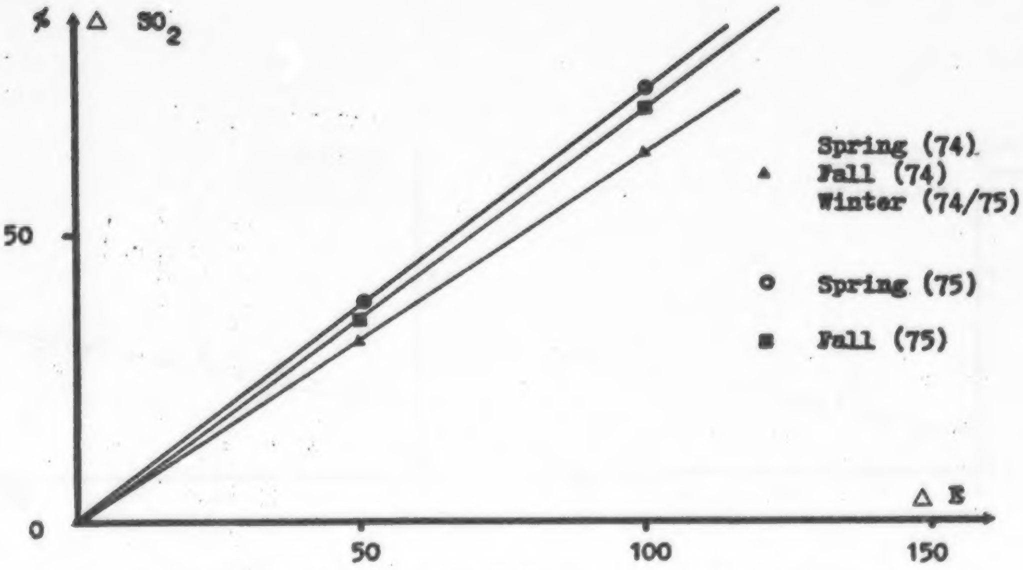

FIG. 5 - VARIATIONS IN SO_2 CONCENTRATIONS IN RELATION TO SIMULATED RESIDENTIAL INCREASES

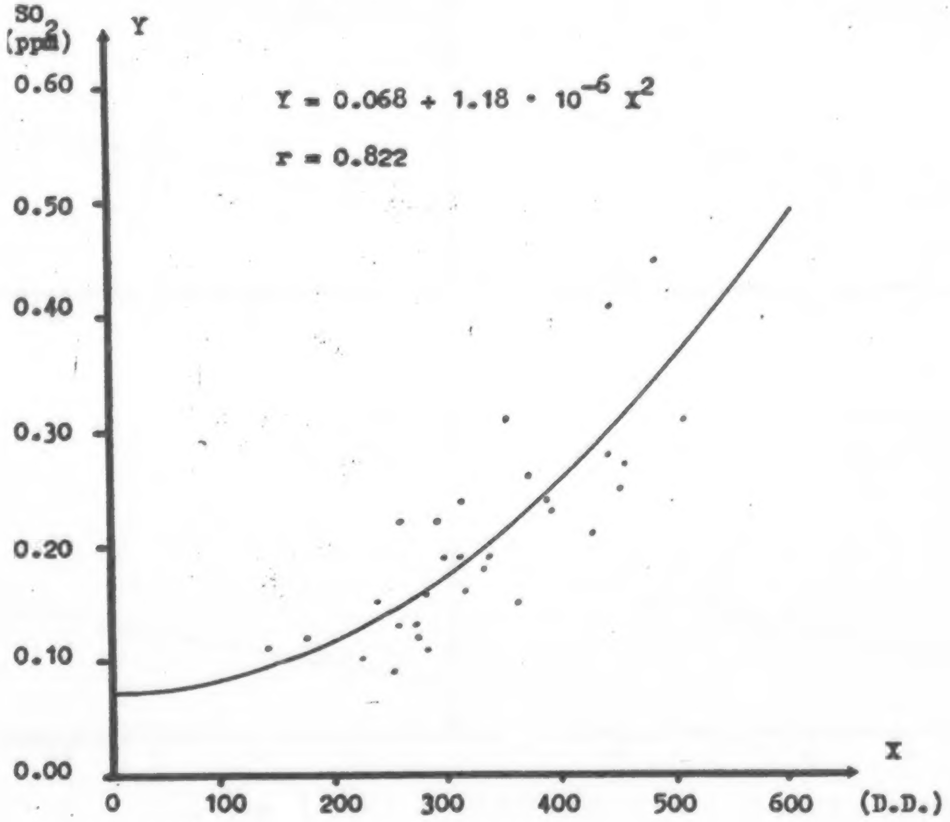

FIG. 6 - RELATIONSHIP BETWEEN DAY-DEGREE AND SO_2

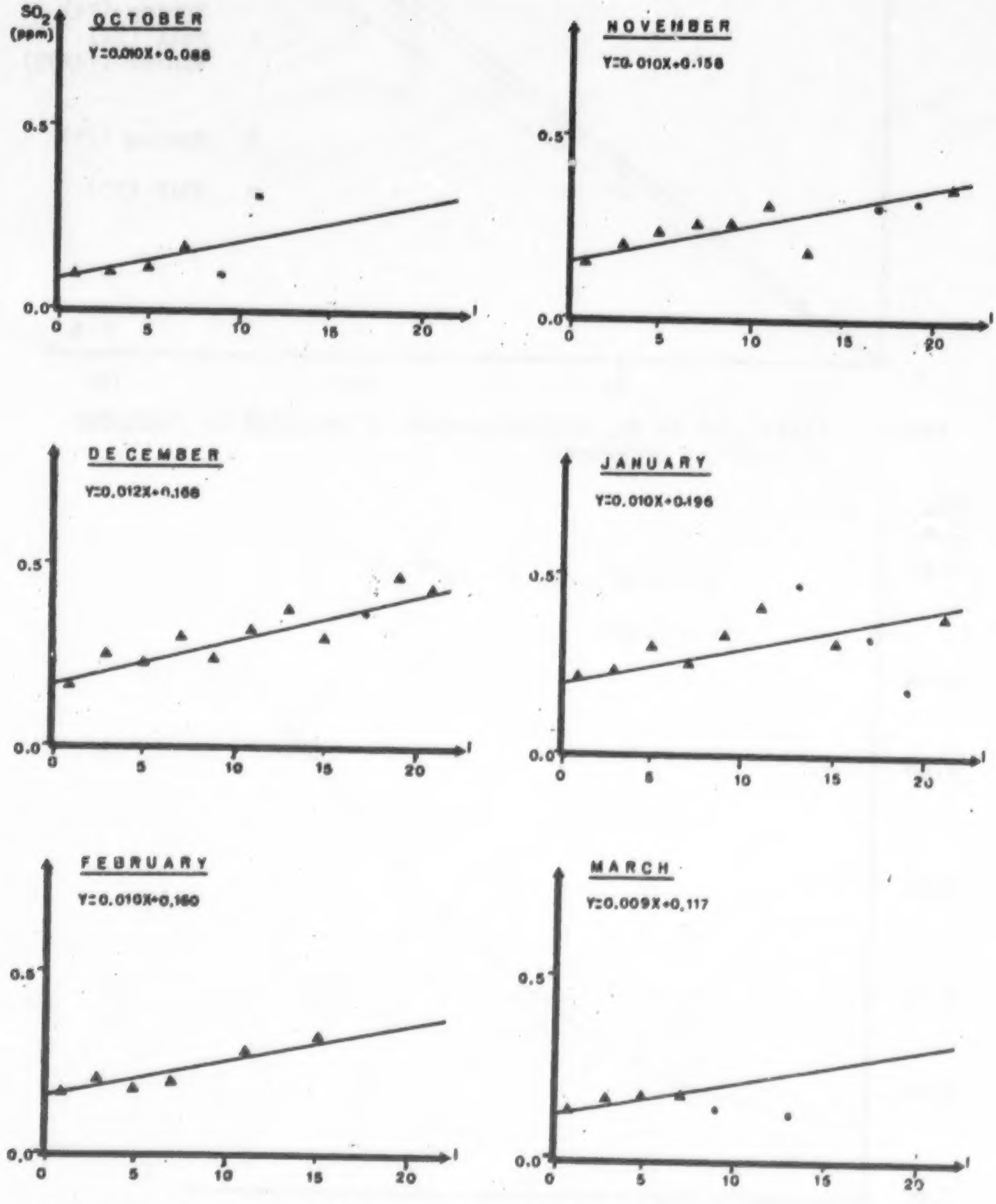

fig.7 REGRESSION LINES BETWEEN I AND SO_2

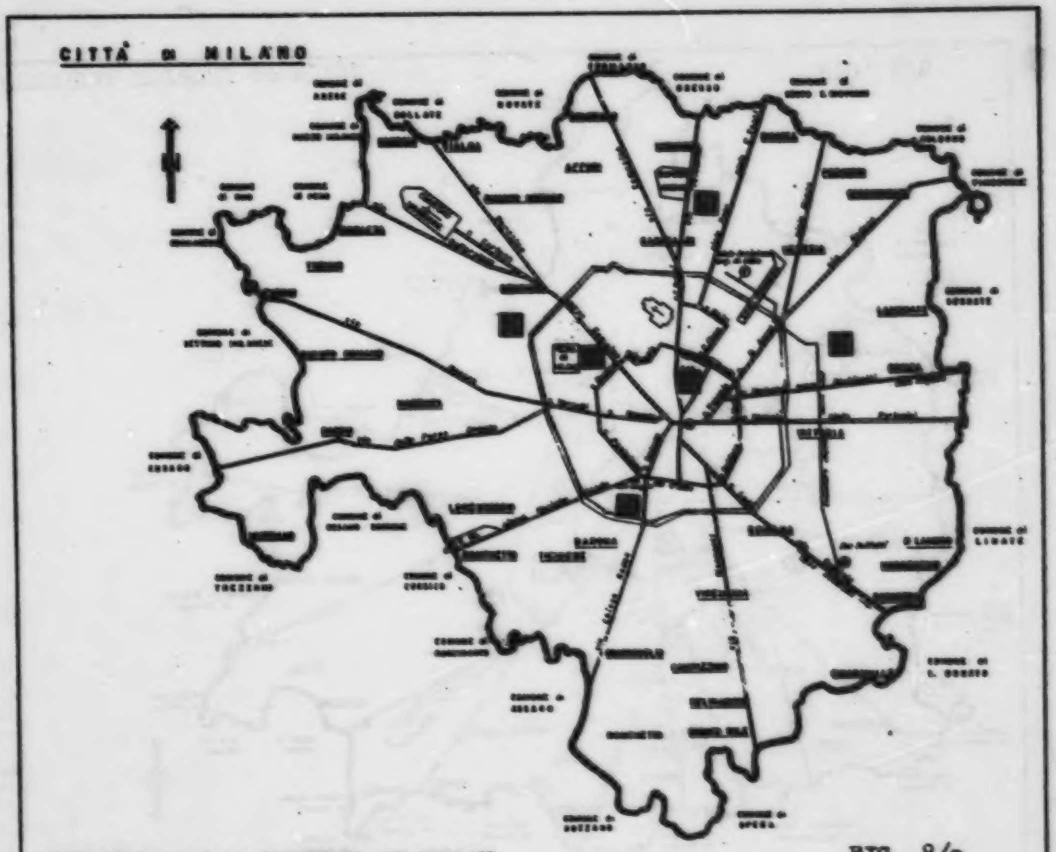
CITTÀ di MILANO

METEOROLOGICAL NETWORK OF MILAN

FIG. 8/a

	T	VV	DV	ΔT	ΔV
■	X	X	X		
■	X	X	X	X	X
■	X	X	X		
■	X	X	X		
■	X	X	X		
■	X	X	X		

■ central control room

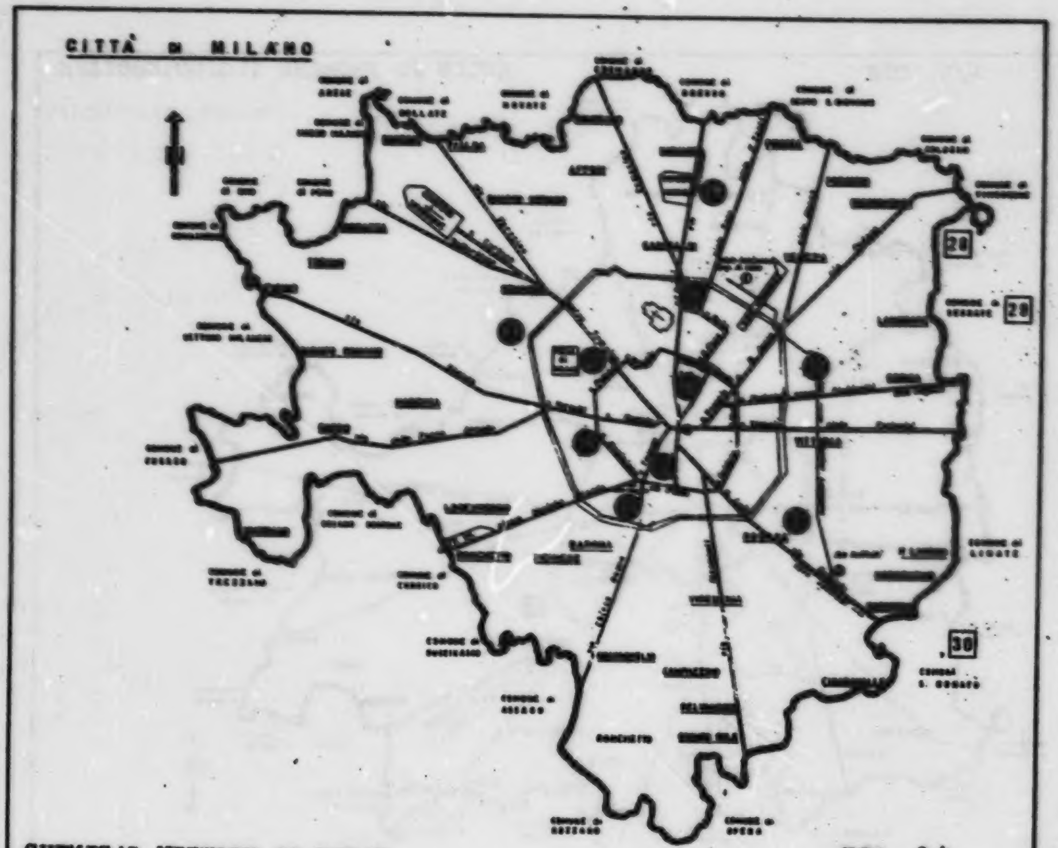
CITTÀ di MILANO

CHEMICAL NETWORK OF MILAN

FIG. 8/b

(1) SO_2
(2) dust
(3) NO_x
(4) noise microphone

	(1)	(2)	(3)	(4)
●	X			
●	X			
●	X			
●	X			
●	X			
●	X	X	X	
●	X	X		
●	X			
●	X	X		
●	X			
28				X
29				X
30				X

● central control room

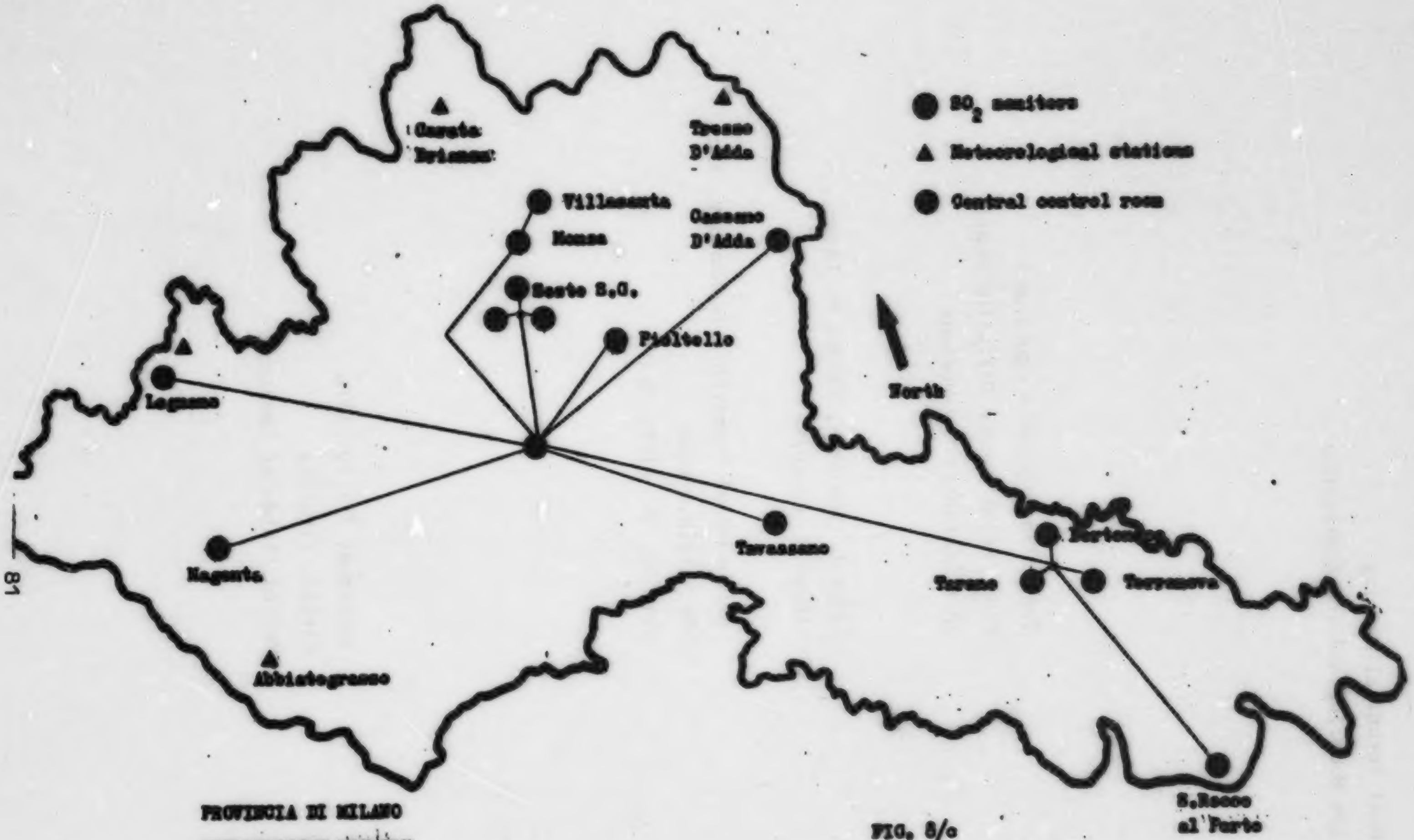

● SO_2 monitors
▲ Meteorological stations
● Central control room
North
Carate Brianza
Trezzo D'Adda
Villasanta
Monza
Cassano D'Adda
Sesto S.G.
Pioltello
Legnano
Magenta
Tavazzano
Bertonico
Turano
Terranova
Abbiategrasso
S.Rocco al Porto

PROVINCIA DI MILANO
METROPOLITAN NETWORK

FIG. 8/c

7th International Technical Meeting
on Air Pollution Modeling and its Application

The Validation of a Gaussian Plume Point Source Diffusion Model in a Lakeshore Environment

Lloyd L. Schulman, Thomas F. Lavery,
Steven G. Penansky

Environmental Research & Technology, Inc.
696 Virginia Road
Concord, MA 01742 U.S.A.

September 7 - 10, 1976
Airlie, Virginia
United States of America

ABSTRACT

A Gaussian plume point source diffusion model was used to predict hourly sulfur dioxide (SO_2) concentrations in the vicinity of a lakeshore electric generating station in western New York State. These model calculations were compared with corresponding SO_2 levels measured at eleven continuous SO_2 monitors during the period 1 November 1974 to 31 October 1975. Concurrent wind direction, wind speed and temperature data used as model input were recorded at two meteorological towers instrumented at 10, 50, and 100 m. Atmospheric mixing depths were derived from both onsite and National Weather Service radiosonde soundings.

Using atmospheric stability classified from wind and temperature measurements at the inland meteorological tower, the model predictions of centerline ground-level concentrations at specified monitor locations were compared with the corresponding observed concentrations. High wind speed neutral conditions generally led to overpredictions by a factor of two or greater. The ratios of the predicted to observed concentrations exhibited a large variance for all stabilities. It was proposed that the relatively cool lake surface temperatures resulted in a more stable atmosphere near the shoreline than was indicated by tower measurements and reduced the plume diffusion for onshore wind directions. The variance of the ratios of the predicted to observed concentrations was reduced by decreasing the magnitude of the diffusion parameters for the various stability classes. The differences between observed and predicted concentrations for both centerline and off-centerline predictions are in large part attributable to errors in estimation of wind direction. Additional differences arise from other inaccuracies in the meteorological and emissions data, the nonhomogeneity of the atmospheric boundary layer, and the inability of the Gaussian plume model to simulate the spatial and temporal variations of the atmosphere.

1. INTRODUCTION

The diffusion of pollution downwind from an elevated, buoyant, continuous point source has been most frequently modeled using the Gaussian plume equation. This simple mathematical expression, whose form is a solution to the Fickian diffusion equation, is largely empirical, relying upon observational diffusion and plume rise data for its application. The model is convenient and often adequate to simulate the primary atmospheric processes that determine ground level pollutant concentrations, namely, plume dilution by the mean wind and plume diffusion by atmospheric turbulence.

The Gaussian character of diffusing plumes has been extensively validated in diffusion experiments (see Slade (1968)). Most of these experiments, however, have been based on ground-level nonbuoyant releases with sampling times on the order of a few minutes. Much less information is available on the relationship of observed and predicted concentrations for elevated, buoyant plumes for averaging times greater than a few minutes. Recent validation studies providing such information have been conducted by a few researchers. Gartrell, Thomas, and Carpenter (1965) and Klug (1974) investigated the dispersion of stack gases from TVA power plants under a variety of meteorological conditions. Moore (1972, 1974) and Mills and Stern (1975) used Gaussian plume models to simulate dispersion from power plants in England and Ohio, respectively, and compared predicted sulfur dioxide (SO_2) concentrations with corresponding one-hour averaged values. Additional studies, however, are required to characterize the accuracy and limitations of Gaussian plume models, especially in different geographic regions.

This report summarizes a study in which a Gaussian plume model was used to predict hourly SO_2 concentrations in the vicinity of a lakeshore power plant. The model calculations were compared with the corresponding observed SO_2 levels measured at eleven continuous SO_2 monitors over the one year study period. Meteorological variables were recorded at two 100 m towers in the vicinity of the plant.

2. THE MODEL

The Environmental Research and Technology, Inc. (ERT) Gaussian plume point source diffusion model (PSDM) was used in the study. The pollutant concentration is expressed by the well known relationship

$$C = \frac{Q}{u\pi\sigma_y\sigma_z} \exp\left(-\frac{y^2}{2\sigma_y{}^2}\right)\left[\exp\left(-\frac{(z-h)^2}{2\sigma_z{}^2}\right) + \exp\left(-\frac{(z+h)^2}{2\sigma_z{}^2}\right)\right]$$

where

C	is the pollutant concentration at height z,
Q	is the point source emission rate,
u	is the mean horizontal wind speed,
σ_y,σ_z	are the standard deviations of the distributions of concentrations in the y (cross-wind) and z (vertical) directions, and are functions of downwind distance, x, and atmospheric stability, and
h	is the effective source height and is equal to the physical stack height (h_s) plus the plume rise (Δh).

PSDM uses the most recent Briggs plume rise equations (Briggs, 1970) to calculate Δh. Both transitional and equilibrium plume rise are calculated. For unstable and neutral conditions:

$$\Delta h = \frac{1.6\ F^{1/3}\ x^{2/3}}{u} \qquad x < 3.5\ x^*$$

$$\Delta h = \frac{1.6\ F^{1/3}\ (3.5\ x^*)^{2/3}}{u} \qquad x \geq 3.5\ x^*$$

where

F = Buoyancy flux of stack emissions (m^4/s^3)

x^* = Downwind distance at which atmospheric turbulence dominates entrainment in plume rise (m)

$$x^* = \begin{cases} 14\ F^{5/8} \text{ if } F \le 55\ m^4/s^3 \\ 34.49\ F^{2/5} \text{ if } F > 55\ m^4/s^3 \end{cases}$$

$3.5\ x^*$ = Downwind distance at which the plume height becomes constant

For stable conditions:

$$\Delta h = \frac{1.6\ F^{1/3} x^{2/3}}{u} \quad x < \pi u s^{-1/2}$$

$$\Delta h = 2.9 \left(\frac{F}{us}\right)^{1/3} \quad x \geq \pi u s^{-1/2}$$

where

$$s = \frac{\partial \theta}{\partial z} \frac{g}{T_a}$$

and

$\frac{\partial \theta}{\partial z}$ is the rate of change of potential temperature with height

g is the acceleration due to gravity

T_a is the ambient temperature

In addition to the meteorological parameters of wind speed, wind direction, and atmospheric stability, the mixing depth must be specified in the model. The mixing depth is assumed to provide an upper limit or lid to the vertical plume diffusion, and as the ground, acts as a reflective surface for the plume. The effects of mixing depth are simulated by a modification to the basic Gaussian equation as given by Bierly and Hewson (1962).

The PSDM program accounts for terrain elevations by permitting the plume to be lifted one-half of the difference between the height of the receptor (the point on the ground for which the concentration is being computed) and the height of the stack base, with the additional restriction that the plume shall always be at least half the height above the ground that it would be if there were no topography.

Several well known characteristics and assumptions of the Gaussian plume equation should be reemphasized.

- The equation requires use of plume shape parameters derived from field experiments. It is necessary, therefore, to use parameters from experiments most representative of the conditions to be studied. Thus, measurements conducted in open, flat land may not produce parameters representative of coastal areas nor areas with hilly terrain.

- The plume equation represents time-averaged concentrations, as determined by the details of the various field experiments. For example, the Pasquill-Gifford horizontal diffusion coefficients are based on three-minute diffusion experiments.
- The Gaussian plume model represents an ensemble average. Any observed concentration is an element of the ensemble and may significantly differ from the mean.
- The model is limited by the simulation of a finite number of stability categories. Actual atmospheric turbulence is continuous over a range of stabilities.
- The equation is representative of steady-state conditions and a homogeneous atmosphere. Its use is less valid when wind speeds, directions, local turbulence rates and atmospheric stability are changing with time or distance.
- Calculations off the centerline are assumed to decrease symmetrically in the cross-plume and vertical directions, following Gaussian distributions in both cases. The exponential variation of predicted concentrations along these directions makes the model very sensitive to changes in wind direction or plume rise. This sensitivity is an observed feature of real plumes and has been discussed by Gifford (1974).

3. VALIDATION DATA BASE

3.1 Air Quality and Meteorological Data

Air quality and meteorological data needed for the hourly validation of PSDM were obtained from a network of eleven air quality monitoring stations, two 100 m meteorological towers, and Buffalo Airport and local radiosonde soundings for the validation period 1 November 1974 through 31 October 1975. Figure 1 presents a topographical map of the region in western New York surrounding the power plant, as well as the locations of the air quality monitors, meteorological towers, and the plant. The lake coastal plain extends inland about 8 km. At this inland distance the terrain slopes upward to the southeast and the ridge line reaches elevations of approximately 450 m above the lake. The inland ridge as well as the lake provide major local influences on the diffusion characteristics of the region.

Wind speed, wind direction, and temperature were recorded at the two meteorological towers at levels of 10, 50, and 100 m. The annual distribution of wind speed and direction derived from observations at the 100 m level of the towers are presented in Figures 2 and 3. The inland tower shows a marked frequency maximum in the west-southwest wind direction. This direction is parallel to the ridge line and is a result of wind channeling. The lakeshore tower shows a more even distribution in the general direction of the prevailing winds.

Stability was determined from the hourly averaged vertical temperature differences between 10 m and 100 m. The classification scheme used is presented in Table 1. It is consistent with the scheme used by the USNRC (1972).

Hourly mixing depths were estimated from daily radiosonde soundings and atmospheric stability. Four months of soundings were taken near the lakeshore tower, and standard National Weather Service soundings from Buffalo comprised the remaining eight months of the year. Afternoon mixing depths were computed using the method of Holzworth (1972). His procedure is basically to extend the maximum afternoon surface temperature upward along the line of constant potential temperature until it intersects the morning 1200 GMT sounding. Hourly mixing depths are then interpolated using a modification of the technique developed by the U. S. EPA (1971).

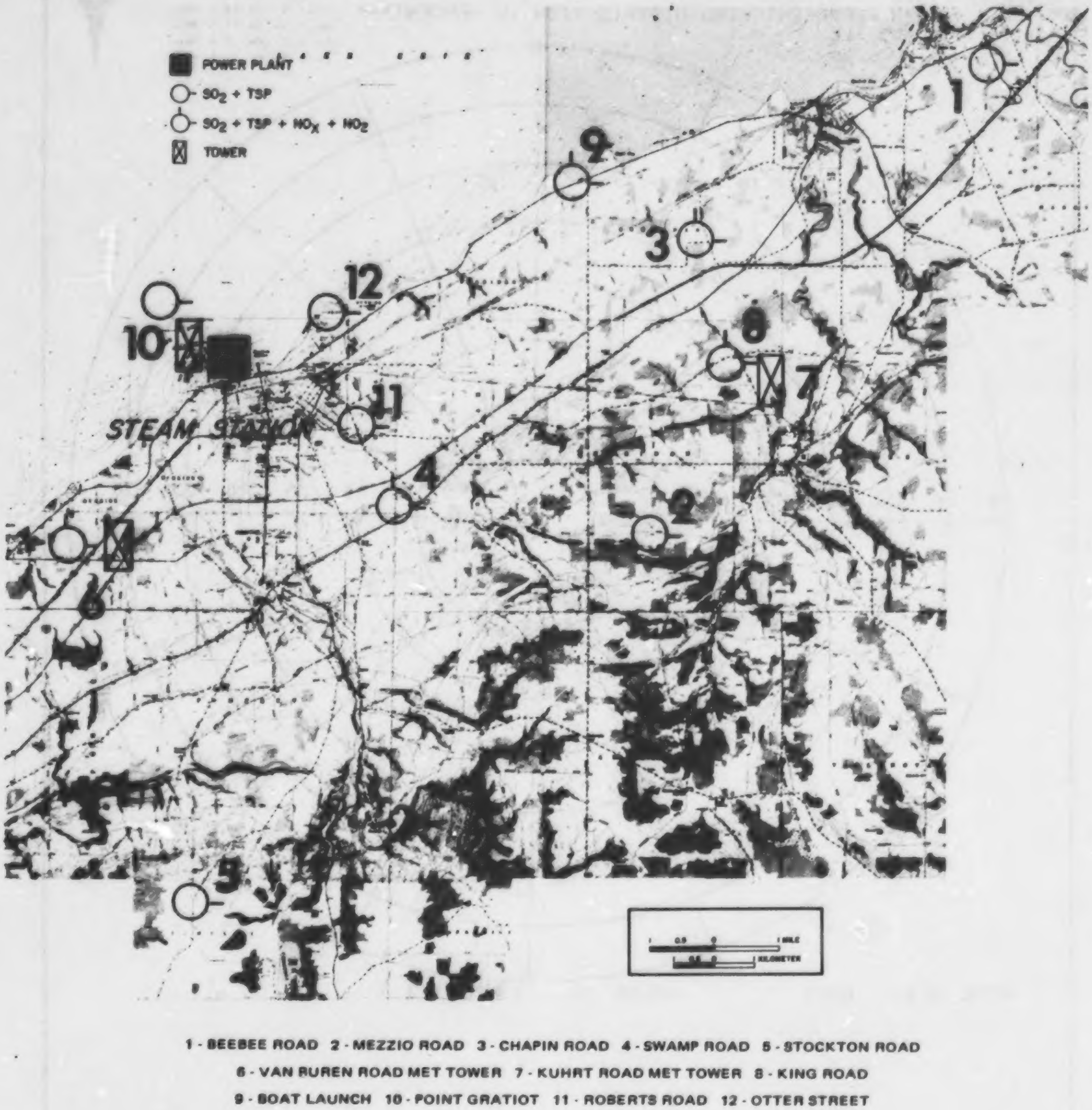
POWER PLANT
SO2 + TSP
SO2 + TSP + NOx + NO2
TOWER
STEAM STATION
1
2
3
4
5
6
7
8
9
10
11
12
0.5
0
1 MILE
KILOMETER
1 - BEEBEE ROAD 2 - MEZZIO ROAD 3 - CHAPIN ROAD 4 - SWAMP ROAD 5 - STOCKTON ROAD
6 - VAN BUREN ROAD MET TOWER 7 - KUHRT ROAD MET TOWER 8 - KING ROAD
9 - BOAT LAUNCH 10 - POINT GRATIOT 11 - ROBERTS ROAD 12 - OTTER STREET

Figure 1 Region of the Validation Study and the Locations of the Air Quality Monitors, Meteorological Towers, and the Plant.

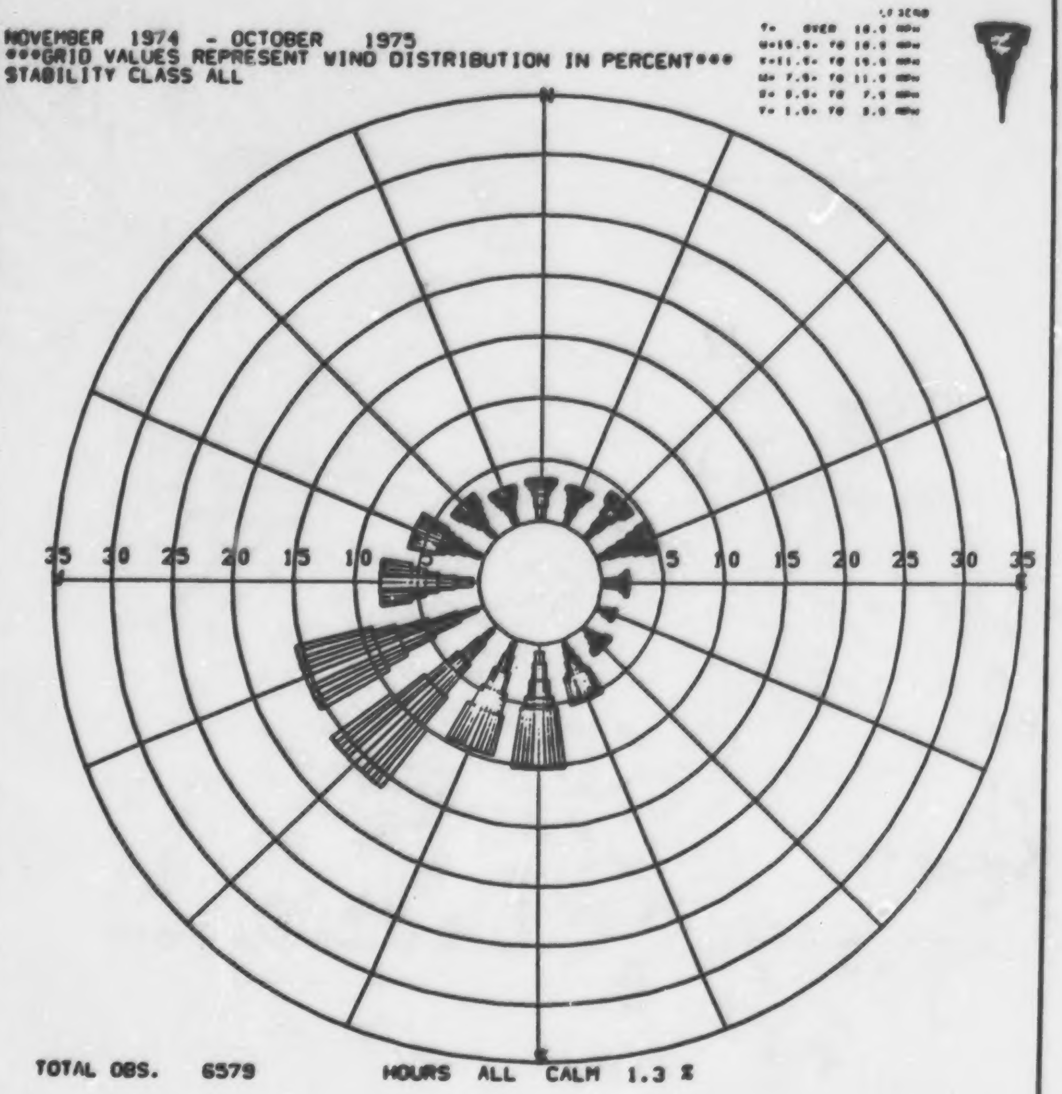

Figure 2 The Annual Distribution of Wind Speed and Direction Derived from Observations at the 100 m Level of the Van Buren Tower

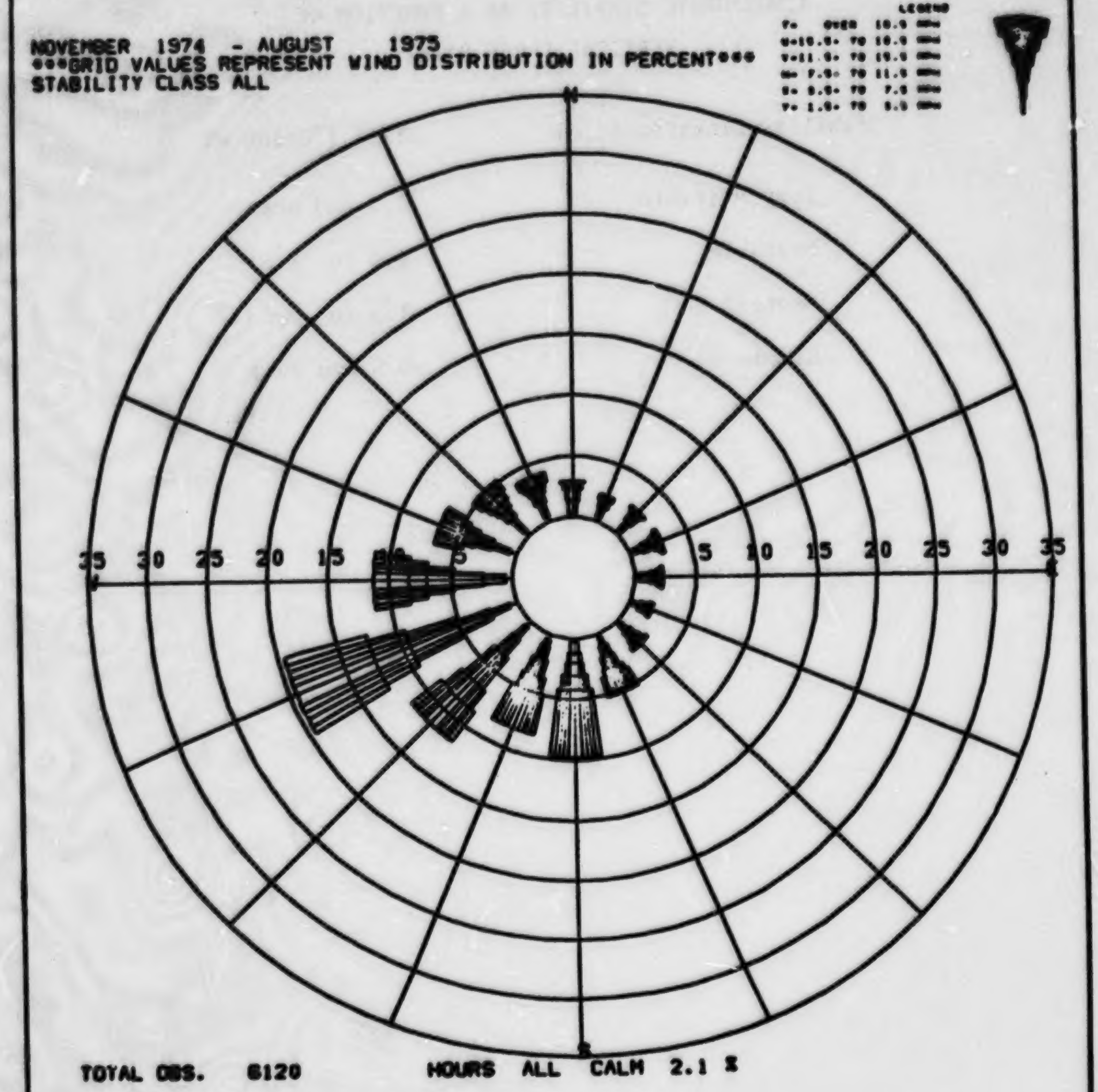

Figure 3 The Annual Distribution of Wind Speed and Direction Derived from Observations at the 100 m Level of the Kuhrt Tower

TABLE 1

ATMOSPHERIC STABILITY AS A FUNCTION OF VERTICAL LAPSE RATE

Stability Classification	ΔT/ΔZ (°C/100 m)
Very Unstable	-1.9 and under
Unstable	-1.9 to -1.5
Neutral	-1.5 to -0.5
Stable	-0.5 and over

3.2 Source Emissions Data

The power plant has a total generating capacity of 628 Mw. Two boiler units have a generating capacity of 96 Mw each and are serviced by individual 95.1 m stacks. The two remaining units have a capacity of 218 Mw each and are breeched into a single 94.5 m stack.

The model validation required hourly averaged SO_2 emission rates and flue gas rates for each of the four units. These were obtained from hourly logs of the power plant operations and weekly coal analyses. The coal heating values and sulfur percentage values were assumed constant for the entire week.

4. VALIDATION PROCEDURES

4.1 Selection of Validation Cases

Meaningful comparison of predicted and observed concentrations required that only those hours of measured values indicating a substantial detection of the plume be studied. These cases were chosen by satisfying either of two sets of criteria.

The first set considered 3-hour periods to identify persistent, significant plume detection at the monitors. The three hours were selected for study if, for each of the hours:

1) the hourly averaged SO_2 concentration at a monitor was greater than 0.05 ppm, and

2) the hourly averaged wind direction at either 100 m tower level was within ±20° of the direction from the plant to the monitor, and

3) the hourly averaged wind speed was greater than or equal to 10 mph at the 100 m levels.

The third condition was imposed to ensure the existence of an organized flow field.

The second set of criteria was simply that a concentration greater than 0.10 ppm be recorded by any of the eleven SO_2 monitors during that hour, regardless of the concurrent meteorological conditions. The union of the sets of hours satisfying each criteria, and for which all the necessary meteorological and emission parameters for model input were available, resulted in a total of 277 cases.

4.2 Computation of Background Concentrations

A background SO_2 concentration for each case was determined from the SO_2 monitoring data, the hourly averaged wind direction at 100 m, and the hourly averaged stability. For each hour a sector extending from the plant and centered on the mean wind was used to define the region of possible plume influence. Thus, the background concentration for each case was computed as the average of the SO_2 concentrations at those monitors lying outside of the sector. The sector angle was made stability dependent and chosen as six standard deviations of the horizontal wind direction. Those standard deviations specified by Slade (1968) (25° for very unstable, 20° for unstable, 10° for neutral and 5° for stable stability) were used in the study.

4.3 Statistical Analyses

The Gaussian plume model was used to predict hourly averaged SO_2 concentrations at each of the monitors using the observed wind speed and wind direction at the 100 m level of the inland tower, mixing depth, temperature, stability class, and plant emissions for each of the 277 cases. The inland meteorological tower data was used in the main portion of the study based upon the results of a preliminary analysis which showed a stronger correlation of predicted and observed values than with data from the lakeshore tower. Diffusion coefficients presented by Smith (1968) and recommended for use with elevated plumes by the American Society of Mechanical Engineers (ASME) were initially used in the model. These ASME coefficients are based on nonbuoyant plume releases at the 108 m level of the Brookhaven National Laboratory tower and are presented in Figure 4.

A comparison of the model predicted concentrations (with background included) and the corresponding observed concentrations was made for each of the 277 hours at the monitor recording the largest observed concentration for each hour. This enabled the study to focus on the ability of the Gaussian model to predict both the locations and magnitudes of the largest observed concentrations.

As a primary guide in evaluating model performance for impact analyses, the cumulative frequency distributions of the maximum observed concentrations and corresponding predicted values were generated. These distributions were used to compare the number and magnitude of the largest observed and predicted concentrations in an overall, and not an hour-by-hour, sense.

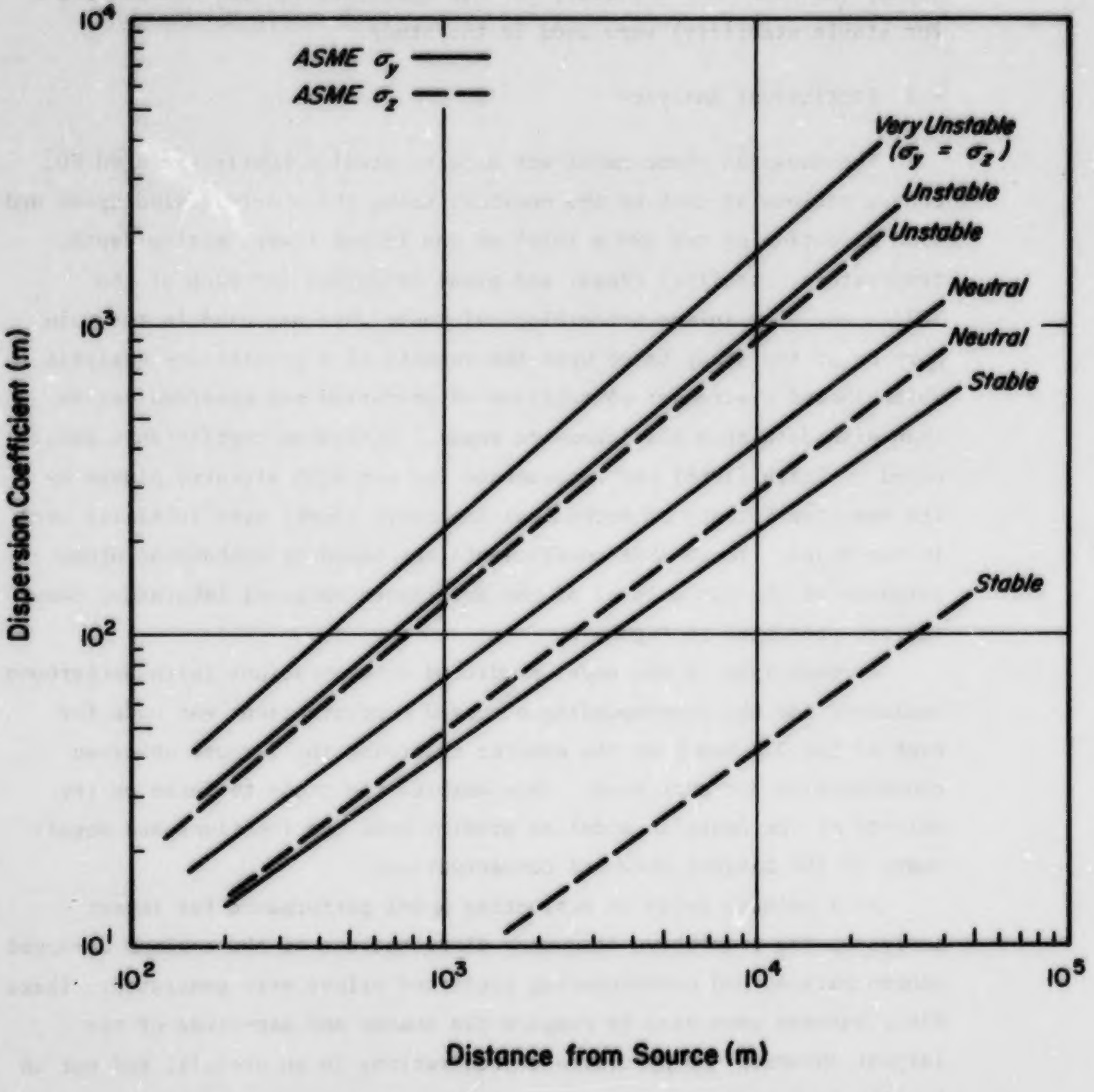

Figure 4   ASME Horizontal (σ_y) and Vertical (σ_z) Diffusion Coefficients

TABLE 2

RATIO OF THE PREDICTED OFF-CENTERLINE TO CENTERLINE CONCENTRATIONS AS A FUNCTION OF ANGLE DEVIATION FROM CENTERLINE DIRECTION AND DOWNWIND DISTANCE FOR NEUTRAL STABILITY

Angle Deviation from Plant to Monitor Direction	Ratio of Off-Centerline to Centerline Concentrations For Downwind Receptor Distance (km)				
(degrees)	3.0	6.0	10.0	15.0	20.0
0	1.0	1.0	1.0	1.0	1.0
2	0.817	0.761	0.710	0.664	0.628
4	0.445	0.334	0.253	0.194	0.155
6	0.161	0.084	0.045	0.024	0.015
8	0.038	0.012	**	**	**
10	**	**	**	**	**
14	**	**	**	**	**
20	**	**	**	**	**

**Less than 0.01

It became apparent after the initial analyses that the complex spatial variations of the flow field in the region of the plant, combined with the known sensitivity of the Gaussian function to directional errors (see Table 2), precluded using the exact wind direction in the study. Instead the centerline concentrations, in which the plume is assumed to travel directly toward the monitor, were used in the analyses.

5. RESULTS OF THE MODEL VALIDATION

Comparisons were made between the maximum observed SO_2 concentrations and the centerline hourly averaged concentrations predicted by the Gaussian plume model at the location of the maximum observed concentration. This comparison is necessarily biased towards overprediction since a monitor only rarely captures the peak cross-wind concentration.

An analysis of the individual, hour-by-hour values showed considerable scatter in the ratios of predicted to observed values. This scatter is probably a direct result of the use of centerline predicted concentrations, and the sensitivity of the locations of the peak predicted concentrations to choices of wind speeds, and to atmospheric stability classifications. For analysis of the impact of a proposed facility, the statistical behavior of a model is often of more importance than the hour-by-hour reliability. Therefore, it is appropriate to examine the frequency distributions of observed and predicted values.

Figure 5 illustrates the cumulative frequency distributions of the observed and predicted concentrations for the 277 cases. The frequency distributions were drawn such that the cumulative frequency of each concentration interval was plotted against the upper limit of that interval. Thus, the highest observed concentration in Figure 5 lies between 0.4-0.5 ppm. The distributions show that more large concentrations are predicted by the model than are observed. In fact, while the model predicts that only 54 percent of the hourly concentrations were below 0.2 ppm, about 90 percent of the observed concentrations were below that figure.

Examination of the observed wind speeds suggested that the temperature lapse rate classification often misrepresented atmospheric stability. Several cases that were classified as unstable or stable stability were also associated with high wind speeds. These cases were most probably neutral.

Wind speed limits were specified for each stability class (very unstable, 8 mph; unstable, 14 mph; and stable, 15 mph). If the limits were exceeded the stability was changed to the next allowable class.

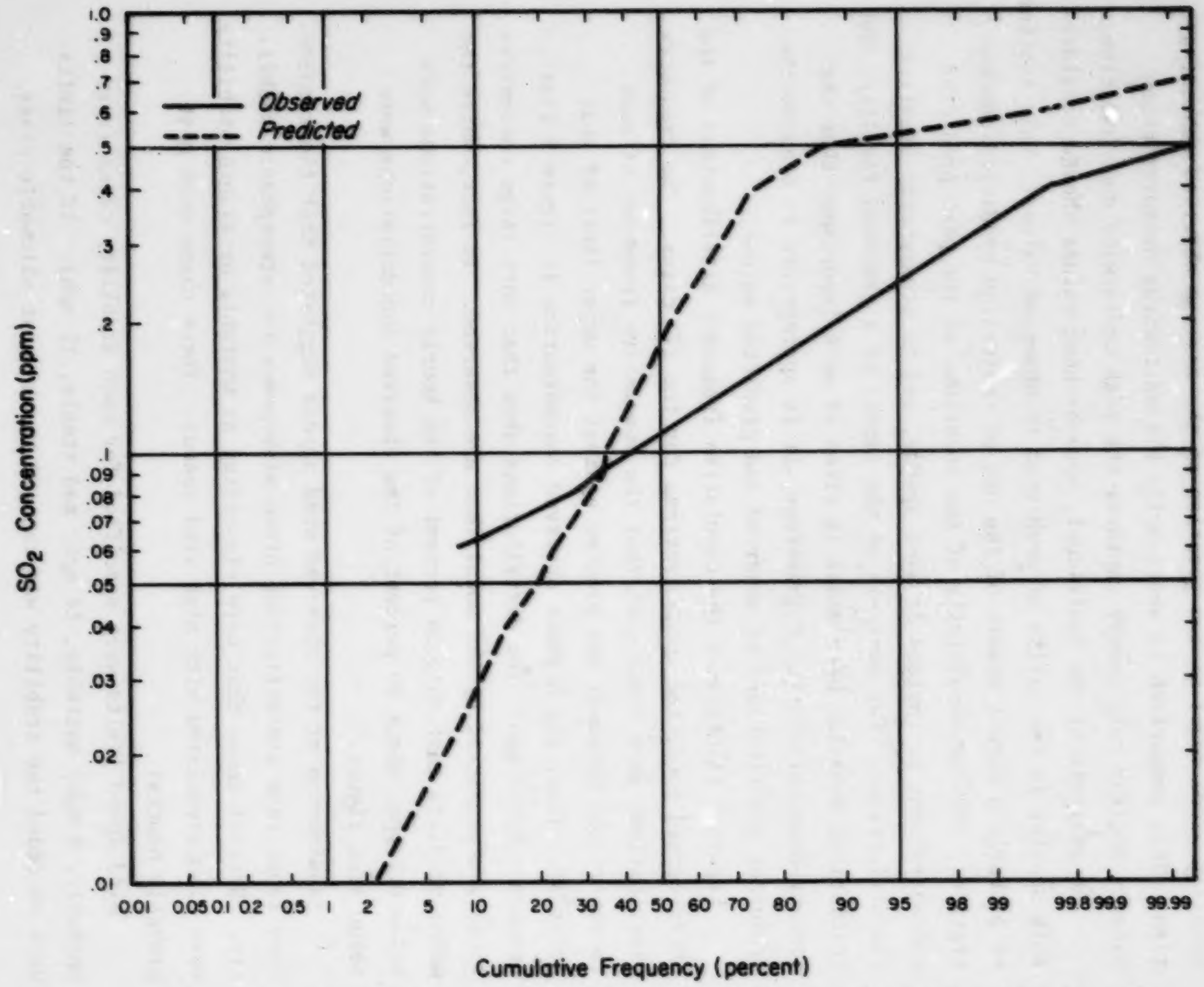

Figure 5 Cumulative Frequency Distributions of the Observed and Predicted Hourly Averaged SO_2 Concentrations for 277 Cases Using the Unmodified Model.

Thus all unstable cases with wind speeds greater than 14 mph, or stable cases with wind speeds greater than 15 mph were reclassified as neutral. Only two cases were labeled as stable with the revised scheme. Because of this limited sample no further evaluation was made of the stable cases.

Using the revised stability classification the Gaussian model was used to predict centerline concentrations for the 275 cases. The cumulative frequency distributions of predicted and observed concentrations are shown in Figure 6. As before, more large concentrations are predicted than are observed. Few differences are noted from the predicted distribution of Figure 5 although the magnitude of the largest prediction has been reduced.

An examination of the downwind distribution of measured SO_2 concentrations, and the corresponding predicted concentrations, indicated that the predicted peak concentrations were often closer to the source than the observed peak concentrations. This could be explained by the influence of the relatively cool lake surface temperatures, an effect more pronounced from the spring to late summer. The stably stratified air over the lake could result in a more stable atmosphere near the shoreline, and hence the plant, than is indicated by tower measurements, and thus reduce the plume diffusion for the onshore wind directions. Another possible contribution to reduced plume diffusion could be the lower turbulence levels at plume height. The plume heights are well above the 108 m tower level used in the Brookhaven National Laboratory diffusion experiments.

After some experimentation, a set of modified (more stable) diffusion coefficients were found to be more effective in predicting the downwind location of the peak concentrations. The modified diffusion coefficients are shown in Figure 7. Very unstable and unstable stabilities are represented by the same coefficients. These coefficients would be equivalent to the dispersion rate for an ASME stability class between unstable and neutral. The neutral horizontal diffusion coefficient remains unchanged from the ASME value. However, the neutral vertical diffusion coefficient would be equivalent to the dispersion rate for an ASME stability class between neutral and stable.

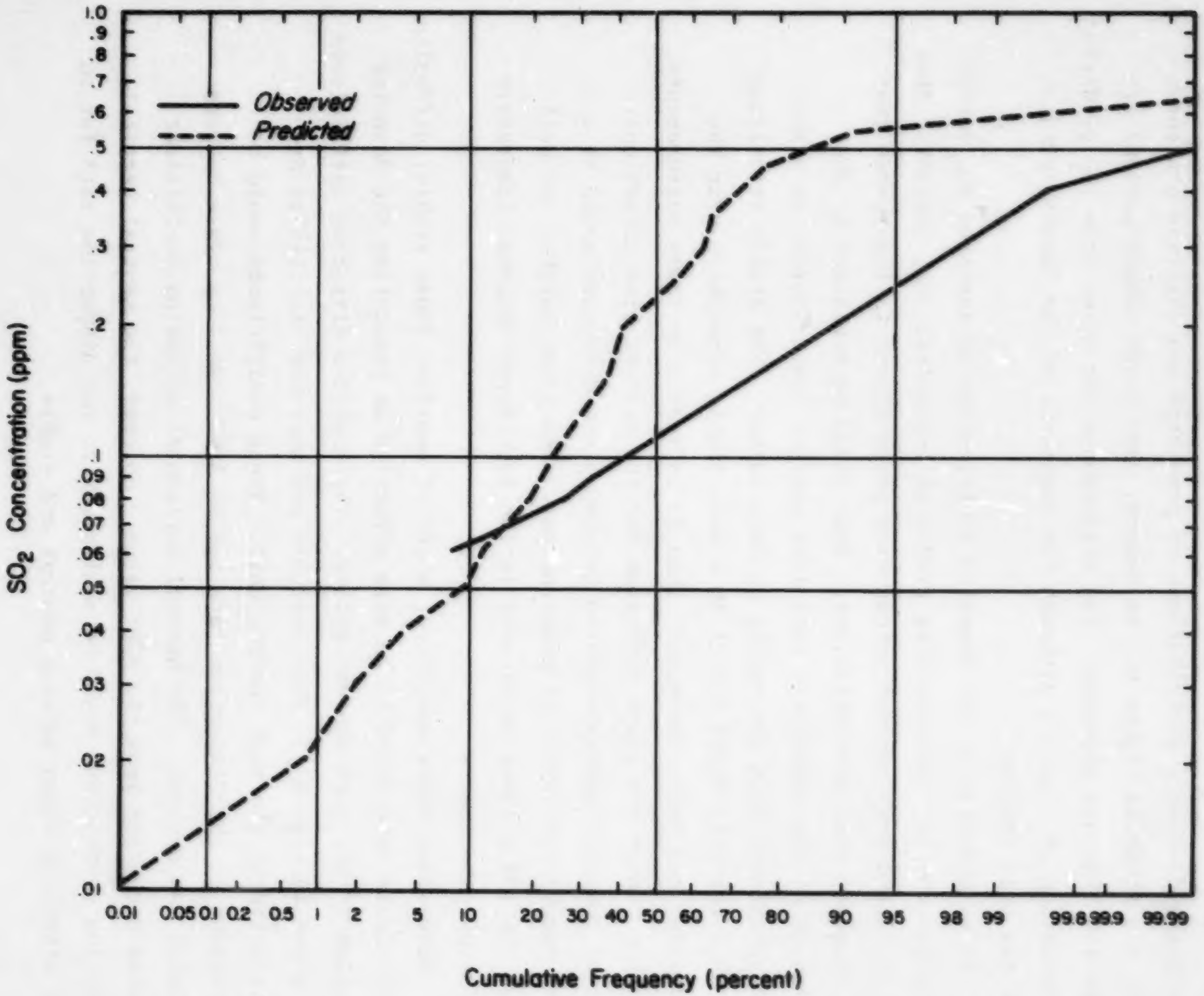

Figure 6 Cumulative Frequency Distributions of the Observed and Predicted Hourly Averaged SO_2 Concentrations for 275 Cases Using the Model with Revised Stability Classifications.

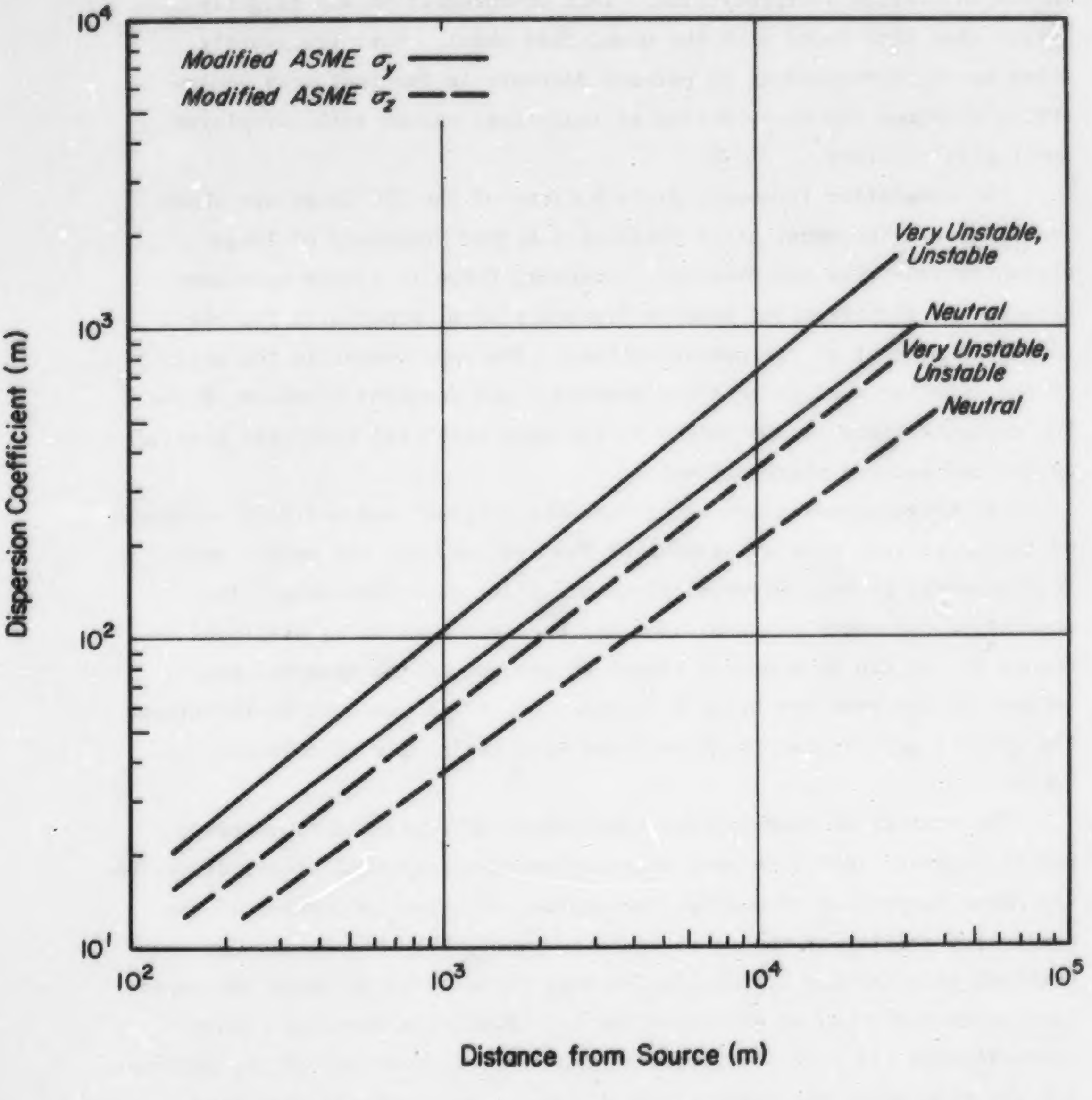

Figure 7 Modified Horizontal (σ_y) and Vertical (σ_z) Diffusion Coefficients

With both the revised stability classifications and the modifications to the ASME diffusion coefficients, the ratios of the 275 centerline Gaussian model predictions to the corresponding maximum observations, showed an average overprediction. This overprediction was slightly larger than that found with the unmodified model. Most importantly, there was a corresponding 25 percent decrease in the root mean square error, although the distribution of individual values still displayed substantial scatter.

The cumulative frequency distributions of the 275 hours are shown in Figure 8. The model still predicts a higher frequency of large concentrations than are observed. However, there is closer agreement between the distributions than in Figures 5 or 6, especially for the largest 5 percent of the concentrations. The improvement in the ability of the model to predict both the magnitude and downwind location of the SO_2 concentrations is due solely to the more selective stability classification and reduced plume diffusion.

Centerline predictions using both the original and modified versions of the model were made at several of the monitors for the entire year (8,760 cases) of SO_2, meteorological and plant emissions data. The cumulative frequency distributions for one such monitor is displayed in Figure 9. As can be expected almost 85 percent of the observed hourly values for the year are below 0.01 ppm. For those non-zero contributions the results are similar to those found with the sample of selected hours.

The scatter of hour-by-hour comparisons of predicted to observed values suggests that with more accurate estimates of wind speed, direction, and plume dispersion throughout the region, a better indication of the predictive ability of the model could be made. This hypothesis was examined in a fashion by considering only those hours in which the upper level wind direction at either of the two towers was oriented within three degrees (±3°) of the direction from the plant to any of the monitors, and the wind speed was greater than 30 mph. The sustained high wind speed should insure more confidence in the direction of the plume and in the uniformity of neutral stability throughout the region, and result in plume detection at the monitors for these cases.

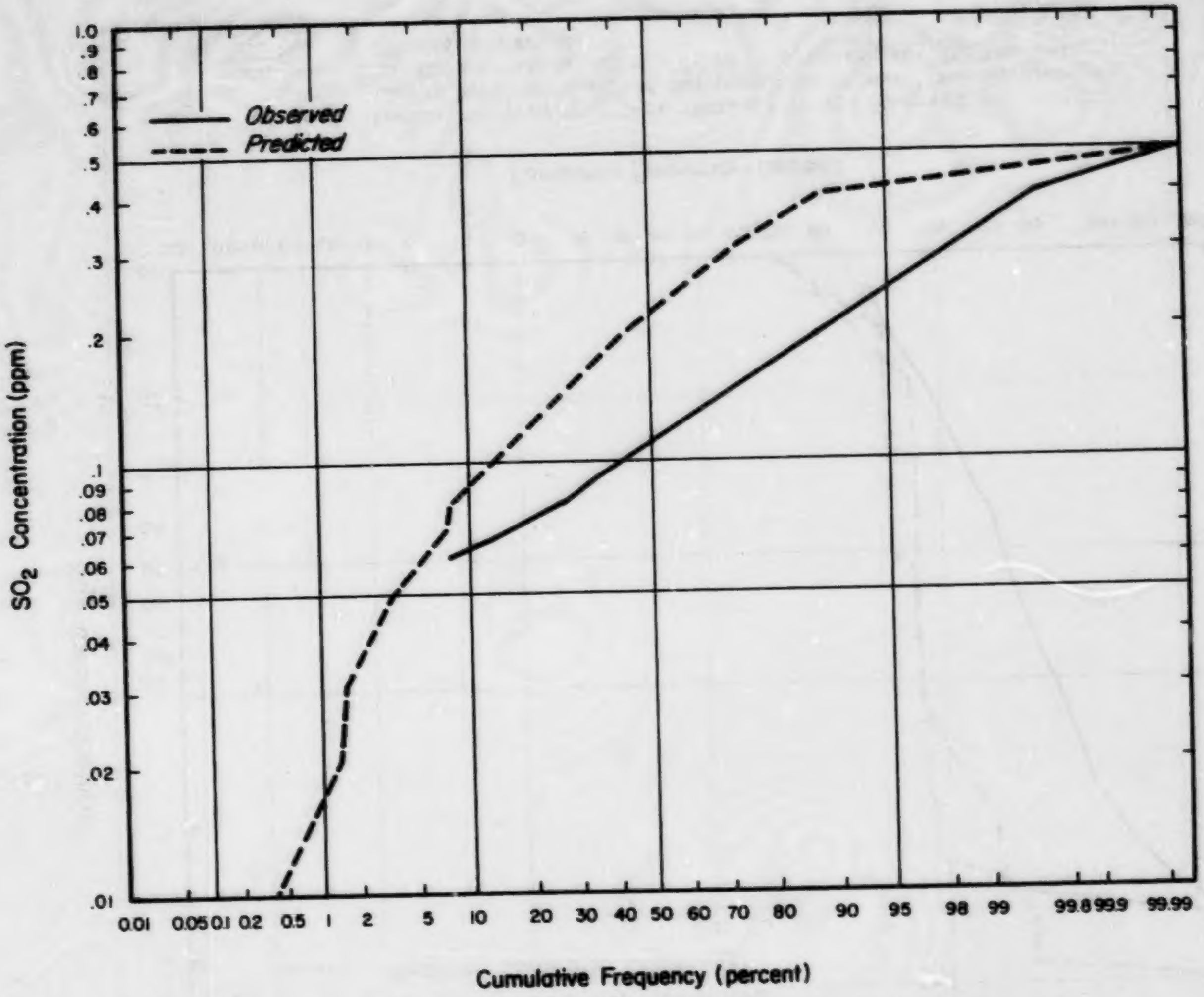

Figure 8 Cumulative Frequency Distributions of the Observed and Predicted Hourly Averaged SO$_2$ Concentrations for 275 Cases Using the Model with Revised Stability Classifications and Modified Diffusion Coefficients.

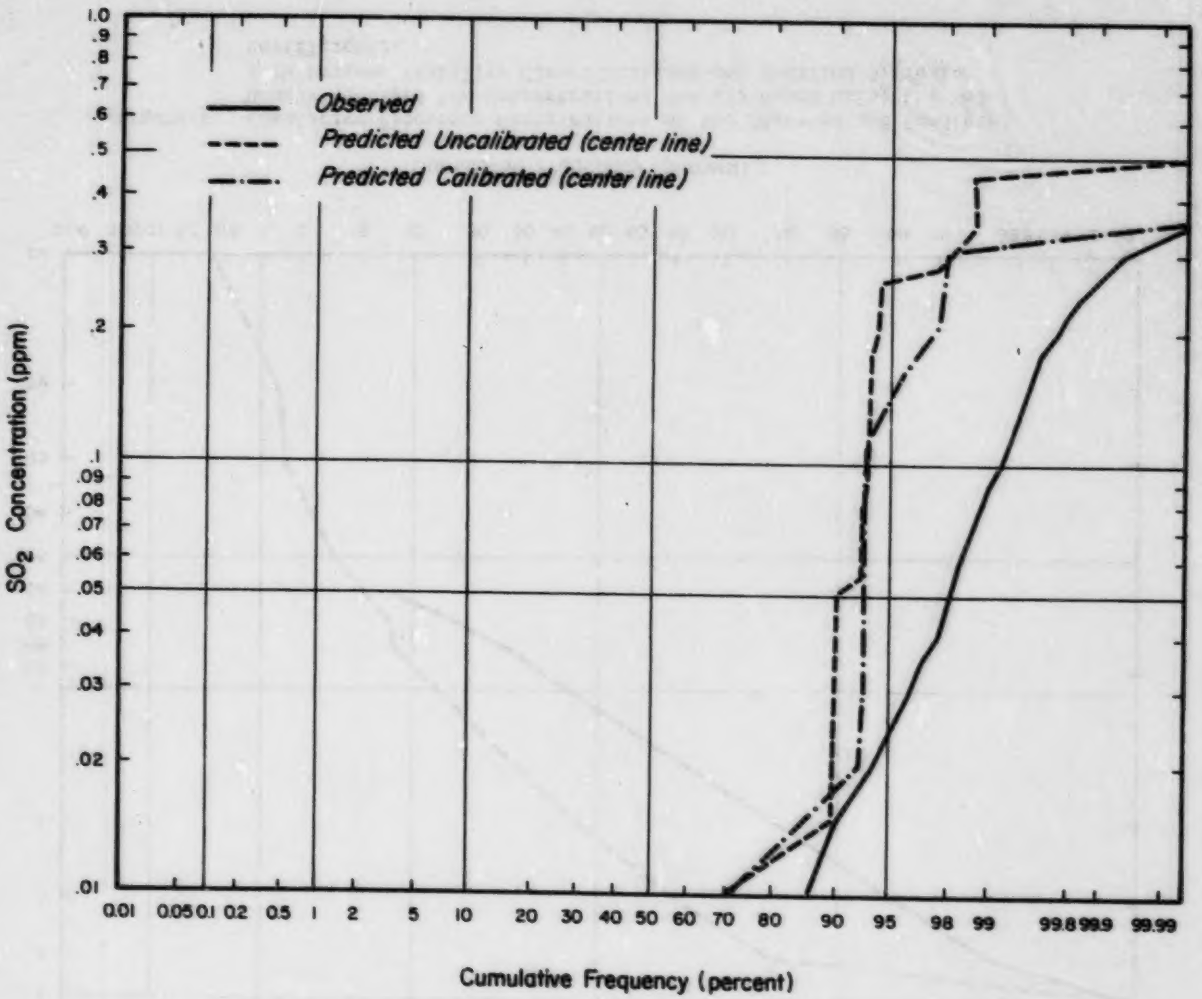

Figure 9 Cumulative Frequency Distributions of the Observed and Predicted (Using both the Modified and Unmodified Models) Hourly Averaged SO_2 Concentrations at the Otter St. Monitor for the One Year Validation Period.

TABLE 3

COMPARISON OF THE RATIOS OF PREDICTED TO OBSERVED HOURLY SO_2 CONCENTRATIONS UNDER CONDITIONS OF HIGH WIND SPEEDS DIRECTED FROM PLANT TO MONITOR*

	Average Ratio	Minimum Ratio	Maximum Ratio
Lakeshore Tower Data			
Centerline	2.63	1.14	12.83
Off-Centerline	1.94	1.04	9.92
Inland Tower Data			
Centerline	2.86	0.90	6.43
Off-Centerline	2.33	0.52	4.19

*Wind Direction within ±3° of orientation of plant to monitors and wind speed greater than 30 mph.

Table 3 summarizes the results of this approach. The Gaussian model overpredicts by about a factor of two for even the off-centerline calculations. The minimum ratio using the off-centerline calculations is just an over unity for the lakeshore tower, and just over one half for the inland tower. It appears that for those special neutral high wind speed cases where the approximate location of the impact can be assured and the value and uniformity of the meteorological inputs known with more certainty, the Gaussian model systematically overpredicted.

6. SUMMARY AND CONCLUSIONS

Using measured meteorological parameters, a Gaussian plume model was used to predict hourly averaged SO_2 concentrations in the vicinity of a lakeshore power plant. The ratios of the predicted to maximum observed concentrations exhibited a large variance for all stabilities. Root mean square errors were the same magnitude as the concentrations themselves. Despite the large variance the model was found to yield an average overprediction. This overprediction was more evident for the neutral, high wind speed cases, where more confidence could be placed in the value and uniformity of the meteorological inputs. Cumulative frequency distributions of the predicted and maximum observed concentrations, although not a measure of an hour-by-hour comparison, showed that more large concentrations were predicted than were observed.

Examination of the downwind location of the maximum predicted concentrations led to the hypothesis that part of the variance could be the result of a more stable plume diffusion than was indicated by measurements of the 100 m tower. It was proposed that the influence of the relatively cool lake surface temperatures and the lower turbulence levels at plume height resulted in the reduced plume diffusion. Some reduction in the root mean square errors, and a better agreement between predicted and observed cumulative frequency distributions, was achieved by changing the stability classifications and the diffusion coefficients. The stability classifications were made functions of both vertical temperature gradient and wind speed, and the diffusion coefficients were modified to reflect the reduced plume diffusion. The remaining variance of the ratios of predicted to maximum observed concentrations can probably be attributed to the limitations of the Gaussian model in representing atmospheric transport and diffusion, errors in estimating meteorological parameters, and errors in the emissions data.

The results of this study have demonstrated that the Gaussian plume model, because of the uncertainties in the meteorology and the emissions, and the limitations of the model, does not accurately predict hourly averaged ground-level SO_2 concentrations for a specified location on an hour-by-hour comparison. However, the Gaussian plume model is adequate for predicting the maximum or average concentrations expected at that specified location over a long time period, or the magnitude, but not precise location, of the maximum hourly averaged ground-level SO_2 concentrations. Substantial improvement in predicting the location of short-term maximum concentrations will require three-dimensional numerical models, and a higher resolution in the meteorological and emissions data available.

REFERENCES

Bierly, E. W., and E. W. Hewson, 1962: Some Restrictive Meteorological Conditions to be Considered in the Design of Stacks. *J. Appl. Meteor.*, 1, 383-390.

Briggs, G. A., 1970: Some Recent Analyses of Plume Rise Observation. Second International Clean Air Congress of the International Union of Air Pollution Prevention Association, Washington, [illegible].C.

Gartrel, F. E., F. W. Thomas, and S. B. Carpenter, 1965: *Full-Scale Study of Dispersion of Stack Gases*. Tennessee Valley Authority, Division of Health and Safety, Chattanooga, Tennessee.

Gifford, F. A., 1974: Sensitivity of the Gaussian Plume Model. *Atmos. Env.* 8, 870-871 (discussion of a technical note).

Holzworth, G. C., 1972: *Mixing Heights, Wind Speeds, and Potential for Urban Air Pollution Throughout the Contiguous United States.* Publication No. AP-101, EPA, Office of Air Programs, Research Triangle Park, North Carolina.

Klug, W., 1974: Dispersion from Tall Stacks. 5th Meeting NATO/CCMS Expert Panel on Air Pollution Modeling, Roskilde, Denmark, June 4-6, 1974.

Mills, M. T., and R. W. Stern, 1975: *Model Validation and Time-Concentration Analysis of Three Power Plants.* EPA document EPA-450/3-76-002, Office of Air and Waste Management, Research Triangle Park, North Carolina.

Moore, D. J., 1972: The Effects of Atmospheric Stability and Wind Speed on the One-Hour Average Ground Level Concentrations of Sulphur Dioxide Emitted from Tall Stacks. *10e Colloque sur les Atmospheres Polluees*, Organise par L'Institut National de Recherche Chimique Appliquee, Paris.

Moore, D. J., 1974: The Prediction of the Mean Hourly Average Maximum Ground-Level Concentration of Sulphur Dioxide at Tilbury. *Atmos. Env.*, 8, 543-554.

Slade, D. H. (ed), 1968: *Meteorology and Atomic Energy 1968*, U. S. Atomic Energy Commission, TID-24190, 445 pp.

Smith, M. E. (ed), 1968: *Recommended Guide for the Prediction of the Dispersion of Airborne Effluents*, Am. Soc. Mech. Eng., New York, 85 pp.

U. S. Environmental Protection Agency, 1971: *Interim Users Guide: CRS-1* Meteorology Laboratory, Research Triangle, Park, North Carolina.

U. S. Nuclear Regulatory Commission, 1972: Regulatory Guide 1.23-Onsite Meteorological Programs, USNRC Division of Reactor Standards, Washington, D.C.

September 14, 1976

Rapporteur Summary Report:

Prepared by J. B. Knox

Covering Papers by: Porter
Rote
Cavallaro, Gualdi, Laneve, Tebaldi
Schulman

Session Title: Examples of Model Validation and Applications.

The papers presented in this session pertain to four separate but important aspects of "Model Validation and Applications:"

(a) The expressed need for an illustration of efficient computer programming and other techniques for lowering costs of the repeated calculations in AQ assessments;

(b) Discussion of the need for model documentation and description to contain enough user-oriented information so that user applicability can be determined by the user;

(c) Description of the 5-year evolutionary work of real-time monitoring of SO_2 in Milan and the use of the ATDL-urban model for system design and assessments of fuel alternatives;

(d) Comparison studies of Gaussian model in presence of water-land discontinuity and complex terrain.

Reduction of Computer Costs: It is clear that most air pollution analysts and users will desire to keep computer costs to a minimum, particularly if technical objectives are not compromised. The dramatic savings in repetitious assessment calculations reported by Mr. Porter exemplify this concept in practice. In years ahead, as models move from research, to validation, and on to applications "user-modeler" communications should focus on optimalization and cost saving procedures that may be of mutual benefit.

Air Pollution Management: The user-modeler relationship.

Through increasing awareness, need, and availability of improved or improving air quality simulation models interactions between the modeling community and the user are destined to be of future importance. Several important aspects of this developing dialogue are identified by Mr. Rote. The author suggests an initial screening procedure for the user to employ to select "a model." It should be noted, however, that the needed dialogue must be two way. Just as the user wishes to select the most economical and adequate model needed for the temporal-spatial requirements of his objective, the modeler desires, just as sincerely, to effect a meaningful, effective application of his model, minimizing the risk of model misuse. The user-modeler dialogue is required to achieve consistency between such obvious matters as source inventory resolution, model zoning selected, the solution resolution matching user-application requirements, and other salient factors. These matters should receive suitable increasing attention in the years ahead as increased reliance on fossil fuels will focus attention on environmental constraints involving more complex assessments.

Urban SO_2 Validation:

The real time monitoring of SO_2 in Milan and the comparison of that data with urban SO_2 model results is an excellent example of the evolutionary and interactive nature of model comparison. Benefits are several and significant: modeling performance is assessed, anomalous station exposures revealed and corrected, and model performance continually tested by the addition of new sampling (or monitoring) stations at places suggested by the model. These attributes of the Milan sutdy are most useful in highlighting additional considerations of the designing future AQ experiments of monitoring networks.

Diffusion Case Studies - Lake Shore and Complex Terrain.

Industrial and power generation sources are by necessity sited namely on lake shores (or river shores) and in near complex terrain. The fate of pollutants released into such complex diffusion environments has been the subject of concern and conflicting results in the past several years. Experimental case studies and emerging regional flow models, of several different types, have shown evidence and promise at this symposium for better capabilities of estimating ground level pollutant concentrations in the presence of complex terrain. It appears that with a reasonable regional flow model approximating the spatial relationship of the pollutant plume to the underlying terrain the estimates of surface air concentrations are greatly improved. Special cases involving boundary layer separation and/or pronounced lee-gravity wave phenomena remain inadequately treated. These cases may not prove to be the cases limiting for air quality maintenance.

JBK:clm

(First 4 papers of 9/8)

Rapporteur - Knox, Joe

Questions - Answers on Papers by Porter, Richard

Question	(Kretzschmar) Although the z dependence of μ is ignored in calculating K_x, K_z, how is the z dependence of μ included in estimates of the effective stack height?
Answer	Any effect of $\mu(z)$ on Hc is included in effective stack-height table look-up contained in the computer program.
Question	(Wendell) Is the TACB model restricted to non-reactive pollutants?
Answer	No. First order decay mechanism can be included.
Question	(Viegele) It has been our experience that computing time is conserved by converting the area, point, and line sources to a single standard source type (e.g. to all effective point sources).
Question	(Nieuwstadt) How well does the TACM model perform in the calculation of effects of new sources?
Answer	One-hour average surface air concentrations, both measured and calculated, compared satisfactorily.
Question	(Fanaki) Did the "flares" observed in your studies fit the accepted effective stack-height (Hc) formulae?
Answer	No. Plumes from flares were not consistent with HC expressions.
Question	(Slater) Could you review the manner in which community growth was included in your studies?
Answer	The source inventory used was for the base year and estimated inventories for years 1980 and 1985.

Question (comment) (Turner) In our opinion, the TACB has done fine work in reducing the computer costs; everyone is interested in reducing cost.

Question - Answers on Paper by Rote, Donald

Question (Fox) In regard to user-oriented information, I have a simple rule - code description should be limited to two pages?

Answer In general, the user-oriented information in UNAMAP is satisfactory on applicability; model applicability should be decided and determined by the user. In general, a two-page code description may not contain sufficient user information for the special cases to be encountered. Two notable examples, wherein more information is needed, include: (a) ground level concentrations resulting from plume impaction; and, (b) the optimization of wind direction at the source to give reasonable estimated peak values of χ a receptors under or near narrow plumes.

Question (comment) (Porter) It is the experience of the TACB that the models developed (by TACB) were misused; in these instances, the modeler's duty is to identify the misuses.

Questions - Answers on the Paper by Mr. Gualdi

NO DISCUSSION

Questions - Answers on Paper by Schulman

Question (Runca) How were the effect of wind shear included in the study?

Answer No wind shear effects were considered; the value of $\bar{\mu}$ was determined by measurement at 100 meter height, the stack height was 95 meters.

Question (Portelli) What atmospheric stability categories were used in the study?

Answer The standard categories as defined in ASME.

Question (Rote) Do you construe your method to have only considered the thermal component of diffusion?

Answer No. There is a specified range of wind speed associated with each atmospheric stability category.

Question (Rote) Were the unstable cases excluded in the study?

Answer: No. There were some 30 unstable cases in the sample of 277 hours of study.

Question (Nagler) Requested clarification of diffusion coefficients?

Answer: Diffusion coefficients were modified to be more stable such that extreme concentrating nearly coincided; in so doing, the RMS error was reduced by a factor of four.

Question (Viegele) Were the meteorological conditions correlated to emissions?

Answer No. Average emissions were used.

Question (Slater) In reality, emissions are time and facility dependent.

Question (Johnson) In an analogous study on Long Island, Johnson reported results in which diffusion coefficient adjustments were indicated by comparison of measurements and calculations - particularly for unstable conditions (as determined by ΔT) with strong wind speeds. However, the dilemma was resolved when an instrumental error was discovered on calibration of the temperature sensors.

Question (Wisse) What influence did the lake have on the mixing height?

Answer The study results indicate that the mixing height had weak influence on the solution (e.g. calculated ground level concentrations).

Seventh International Technical Meeting
on Air Pollution Modeling and Its Application

DIFFUSION MODEL COMPARISONS TO MEASURED DATA IN COMPLEX TERRAIN

R. B. Lantz
C. F. Hoffnagle
S. B. Pahwa
INTERA Environmental Consultants
1201 Dairy Ashford, Suite 200
Houston, Texas 77079

September 7-10, 1976
Airlie, Virginia
United States of America

DIFFUSION MODEL COMPARISONS TO MEASURED DATA IN COMPLEX TERRAIN

R. B. Lantz
G. F. Hoffnagle
S. B. Pahwa

INTERA Environmental Consultants

1. INTRODUCTION

As the energy resources of the western U.S. are developed, the siting of processing and power plants in mountainous or complex terrain areas has become more critical. One of the factors most difficult in evaluation for such complex terrain areas is the dispersion in air of released contaminants.

One of the problems involved is that the mathematical models routinely used to predict air quality have been verified only for flat terrain. In fact, to even apply these traditionally used Gaussian models to elevated terrain requires assumptions (which have since become extremely controversial) about how terrain affects the air flow. Van der Hoven et al[1] utilized such an assumption in evaluating the air quality impact of power plants in the southwestern U.S. His approach undoubtedly set an upper bound on calculated ground level concentrations on elevated terrain by assuming that the plume under stable atmospheric conditions could impact upon terrain which reached the plume centerline elevation. Governmental agencies have made some modifications to relax this original assumption, but still continue to use the same basic plume dispersion formulas with an assumed wind flow as affected by terrain. Within the last five years, a number of authors have proposed air quality models which combine a wind flow calculation along with the plume dispersion estimates[2,3,4].

The reason for the multiplicity of models and the reliance on assumptions is the lack of measured dispersion data in complex terrain situations. Only recently have full-scale diffusion experiments been performed at or near sources located in mountainous terrain. They are:

1. Huntington Canyon[5]: The Air Resources Laboratory (ARL) of the National Oceanic and Atmospheric Administration (NOAA) conducted SF_6 tracer releases in Huntington Canyon, Utah.

2. Navajo Generating Station[6]: An extensive field program of SO_2 monitoring over a six month period at the Navajo Generating Station in northern Arizona. The program was sponsored by the Salt River Project with the cooperation of the Environmental Protection Agency and performed by Rockwell International and Meteorology Research Incorporated.

3. Garfield, Utah[7]: The Air Resources Laboratory released SF_6 from the existing smelter stack at Garfield, Utah.

These three field measuring programs provide consistent data sets for several specific situations where plume interaction with elevated terrain occurred. This body of data is not nearly as detailed and comprehensive as the data which support the Gaussian model over flat terrain, but it provides a start. There are other data in complex terrain, but the data used here are widely available and include significant meteorological information. Unfortunately, most emission sources located in complex terrain usually have only one monitor at elevated terrain positions. This lack of site specific data adds to the requirement for a general model for use in complex terrain circumstances.

What is being sought, therefore, is a good predictive model of atmospheric dispersion in complex terrain. This model should do equally well in various types of terrain and for various differing meteorological situations. It is the hypothesis of this paper that a calculation of the air flow due to the influence of the terrain is essential to the subsequent calculation of the resultant ground level concentrations. Even a rudimentary air flow approximation, if it accounts for atmospheric stability and utilizes the specific three-dimensional terrain of each situation, should be a more accurate and dependable predictor than any generalized air flow assumption.

The three models described below have been utilized in the comparisons to the available data sets. The first two are Gaussian models in common usage in analyzing complex terrain situations for air pollutant dispersion.

The first has become known as the NOAA model. This nomenclature resulted from the use of this model by NOAA in preparing the diffusion model calculations presented in the Southwest Energy Study[1]. For stable atmospheres, the wind is assumed to flow horizontally until intersecting the terrain. This is labeled the "intersecting plume assumption". For neutral and unstable atmospheres, the air flow is assumed to be parallel to the terrain surface and flat terrain calculations are applied.

The second Gaussian model is that presently employed by EPA for making ambient air quality evaluations for rough terrain areas. This model (the version tested was known as C4M3D)[8] is a modification of the plume centerline flow concept used in the NOAA model which allows wind to flow 10 meters over terrain obstacles and, in addition, averages concentrations over a 22.5° angular segment. It also assumes parallel flow in neutral and unstable atmospheres.

The third model is a numerical approach developed by INTERA[2] and is quite different in concept from the Gaussian models. Instead of assuming normal concentration distributions in the crosswind and vertical directions, the model approximates turbulent fluctuations by a Fickian-type eddy diffusivity. These eddy properties are height dependent, as is the wind speed. This differs from the wind and dispersion coefficients averaged over height used in a Gaussian model or even those used in a constant diffusivity model. In addition, the wind flow field in terrain is calculated on a potential flow (hydrodynamic) basis prior to diffusion calculations.

Even so, over flat terrain there is a good agreement between the numerical model and the Gaussian results. The particular height dependence of diffusivity and wind speed which provide this agreement are discussed in Reference 9. Only in cases where terrain modifies the air flow do the INTERA model results differ substantially from either of the Gaussian models.

2. HUNTINGTON CANYON

The data collected in Huntington Canyon by the Air Resources Laboratory (ARL) were intended to provide measurements of plume dispersion in rough, canyon type terrain for comparison with flat terrain results[5]. A model comparison study of this data was supported by EPA[9] and is reported in detail elsewhere.

The basic approach was to release SF_6 tracer and use mobile (helicopter) sampling for centerline dilution concentrations and fixed (canyon wall and floor) sampling for the ground level validation. The helicopter samples were 1 minute samples collected by an air pump which drew samples through a hose hanging 28 m below the aircraft. The ground samples were cumulative over the duration of each test run and were processed to approximate a 1 hour average concentration.

The tracer releases were made at two points. Elevated releases during unstable to neutral stability conditions, Tests 1-6, were made from the top of the stack. (The first unit stack of the Utah Light and Power's Huntington Canyon power plant was already in place.) Wind flows during such conditions were generally upcanyon. The second point of tracer release was from the canyon wall (Test 7) and floor (Tests 8-11) at a distance of about 10 km up the canyon from the power plant stack. These releases were during strong temperature inversions and were always downcanyon flows. The computer generated view downcanyon from those release points is shown schematically in Figure 1.

The available meteorological data was somewhat limited. The various tests were classified as to stability by NOAA personnel. Surface wind speeds were available at several points, as well as the apparent velocities of oil fog (released as a visual tracer) during the SF_6 releases. Measured temperature gradients and cloud cover were also available.

Summary plots of measured versus calculated results for two representative tests, 5 and 10, are presented in Figure 2. The usual Gaussian form of $\chi u/Q$, normalized concentration, has been used to compare the model results to the measured data. Test 5 was an upcanyon flow situation with the SF_6 released from the stack top. The atmospheric stability was judged to be D. The upper dashed line is the Gaussian ground level release line. A factor of 2 reduction, to account for the lack of concentrations reflected from the ground, would represent a good upper envelope of the aerial data. The maximum ground level concentrations occur in the 2 to 4 kilometer distance where the terrain obstacles to flow occur. The numerical model correctly predicts that the maximum ground level concentrations occur on those terrain obstacles and closely approximates the peak value. The Gaussian models, however, because of the parallel flow assumption, ignore the immediate obstacle to flow and place the maximum at the expected downwind distance for D stability thereby also underestimating the concentration.

Test 10 was a stable atmospheric situation classified by the ARL personnel as "more stable than F". F stability has been used, however, in the predictions. The release of SF_6 was from close to ground level and the downvalley stable flow carried the plume past monitors on the floor and sidewalls of the canyon. The results shown in Figure 2 show the ground level release NOAA model results as the highest dashed line which far overestimates the measured values. The EPA model also overestimates many of the points, but comes closer because it averages concentrations over a

22.5° sector, which is similar to the spreading of the valley downwind from the release point. The numerical model provides an excellent upper envelope of the measured data and demonstrates the importance of a terrain wind flow calculation by accurately predicting the concentration at 3 kilometers.

The numerical model calculations, as well as the centerline Gaussian and EPA model results, have been compared with the measurements for the remaining tests. These calculations utilized the reported stability class, wind speed and wind direction with the exception that the downcanyon flows always used a wind oriented along the canyon (approximately 320°). In the downvalley comparisons, wind direction was not important. For the upvalley flows, wind direction has a significant effect on calculated concentrations. Two of the upvalley flow tests were not included. These tests were 2 and 6. The wind direction for these two cases was 120° or even more easterly, and measured ground level concentrations were quite sparse. Test 2, for example, contained only two ground level measurements. As a consequence, we have not made calculations for these two tests with the easterly wind direction.

Statistical comparisons of the measured and calculated results have been made. Of the many statistical comparisons which could have been used, we have chosen a statistic representing the logarithmic mean value ratio of calculated to observed concentrations. This ratio statistic is somewhat more meaningful because all ground concentration points were included. Table I below illustrates the ratio comparison along with a simple arithmetic mean value comparison between calculated and measured values.

TABLE I

Huntington Canyon Statistical Comparisons

Test Number	Measured Mean Values $\mu g/m^3$	Numerical Model		NOAA Model
		Mean Value	Calc/Obs Ratio	Calc/Obs Ratio
1	0.74	0.64	0.43	1.4
3	2.12	2.00	1.10	3.7
4	0.21	0.16	0.59	-
5	0.71	0.91	1.62	5.6
7	0.45	0.73	2.30	14.7
8	9.8	42.7	1.83	14.8
9	9.2	15.2	0.42	-
10	10.2	28.9	1.27	18.9
11	84.6	37.4	0.41	11.8

The results from all tests clearly show the numerical model gave better predictions than did the NOAA model. The EPA model, because of angular segment averaging, fared better than the NOAA model but was a factor of 3 to 5 high for the stable cases (Tests 7-11). These results emphasize the importance of including a calculation of the wind flow as affected by terrain.

Our comparison of the models had been aimed, in general, at calculations as the models would have been used in a predictive study. That is, no attempt was made to adjust diffusion coefficients to give a best match and, for the Gaussian models, no attempt was made to move the plume centerline location so that they best match the measured concentrations. As pointed out previously, the numerical predictive results for Huntington Canyon provide accuracy comparable to Gaussian model results for flat terrain. That is, the addition of a simplified flow model to a calculation based upon Pasquill stability classes has given results for Huntington Canyon comparable to the Gaussian model accuracy with flat terrain. Whereas, the Gaussian model accuracy was significantly decreased by the presence of elevated terrain.

3. NAVAJO GENERATING STATION

The Navajo Generating Station placed its first unit in commercial operation during June of 1974 and its second unit began test operation in December, 1974. Because of differences between the EPA and the Salt River Project, primarily about modeling in complex terrain, an extensive program was undertaken to measure ambient sulfur dioxide concentrations[6]. At issue was the amount of sulfur dioxide removal from stack emissions which would be required to meet the ambient air quality standards. The ambient data, aside from providing a basis for those decisions, naturally provides an excellent set of data for the comparison of model calculations in complex terrain. The experimental program obtained measured data at terrain elevations near the plume centerline under stable conditions. It is these data which are of most concern to EPA and which, thus, constitute the focal point of the model comparisons.

There are several cases where stable plumes apparently resulted in measurable concentrations at those elevated receptors. This is precisely the situation where the models are in the most disagreement. Because of the care with which the continuous monitoring was performed and the backup of aerial concentration measurements and meteorological data, these data become fairly definitive example cases. The other most cited data, for Huntington Canyon, Utah, has often been characterized as not generally applicable because of the "special" situation of a steep walled canyon.

The data from the Navajo study include interaction of the plume with a broad mesa top (the Vermilion Cliffs) at plume height during stable atmospheric conditions. Figure 3 is a map detailing the source, receptors and plume path. This is precisely the situation which is closest to the oft used modeling concept of plume intersection. If the intersection concept were to fail in this case, it would be difficult to find a case more appropriate for its application.

A model comparison study has been performed[12] of the three days with the highest ground level concentrations on Vermilion Cliffs. A detailed example of the comparison for October 16, 1974, the highest concentration day, is provided.

The peak concentration occurred at 1200-1300 MST at one of the four sampling stations along the cliffs. The presence of four stations at essentially the same height provides an excellent opportunity to investigate the lateral dispersion of pollutants as the plume passes up and over the cliff face. The temperature sounding indicated a stable layer, roughly isothermal, in which the plume was trapped and heading toward the cliffs. The aircraft observations reported horizontal dispersion on the order of E stability which spread to D stability σ_y values as the plume passed over terrain. The wind speed measured above the source and on the cliffs averaged in the range of 1.5 to 2.1 meters per second over the period when the plume was traveling toward the cliffs. As the wind speed rose toward the end of the period, the concentrations on the cliffs were significantly reduced.

Because the numerical model first calculates the three-dimensional wind flow field, a review of its results is provided in Figure 4. The particular case shown is for 1.5 meters per second at plume height and F stability. Figure 4-a shows the vertical cross section of winds along the plume centerline (H denotes the effective stack height). Note that there are significant vertical wind velocities at the cliff face and that these are propagated halfway back toward the stack. The grid centers without wind arrows are below terrain and no flow is allowed into those blocks.

Figures 4b and 4c represent two horizontal sections labeled as to position on the left-hand side of 4a. Below the top of the cliff (4b) all flow obviously goes around the terrain. Note that monitor 107a is below the height of this horizontal cross section. Above the cliff (4b) the flow also shows considerable spreading to travel around the terrain obstacle. This spreading agrees with physical concepts of what should happen in this type of flow situation and helps the numerical model simulate the realistic situation.

The model-generated winds at station 105 fit into the pattern of winds measured at that station in both direction and speed, especially in the 2.1 meters per second input wind case.

It is desirable to compare the three models on their ability to predict the various concentrations. The numerical model was utilized with standard input values in order to be comparable to the Gaussian models, i.e. a wind velocity profile and diffusion coefficients which reproduce the Gaussian results for flat terrain situations. Values for the stability classes and the range of wind speeds are indicated on Figure 5. The positions of the monitors are indicated at the top of the figure (note that north is to the left, i.e. the view is back toward the plant), and the hourly average measurements for the two highest hours are plotted. The best comparison to the data occurred with F stability at 1.5 meters per second. For either E or F stability, the predicted concentrations are well within a factor of 2 of the measured values. The non-Gaussian characteristics of the curves are due to the terrain effects. The obstacle, Vermilion Cliffs, is not uniform in the crosswind and the numerical model is responding to those factors. The plume tends to move southwestward along the cliffs keeping monitors to the south of the maximum higher than those to the north. The angle of plume direction to the cliffs is also important to the shape of the calculated profile.

The NOAA model cannot reproduce the lateral dispersion pattern measured. If the peak concentrations of 0.10 ppm were reproduced, requiring 3.5 meters per second winds at E stability if reflection were neglected, the plume would be much too narrow for the pattern observed. Both Gaussian models, the NOAA and the EPA, have been used to predict concentrations on the Vermilion Cliffs. A comparison of values for the maximum ground level concentration with those observed is given in Table II for the three test days selected.

The input values for the various models are as similar as possible, thus providing a valid example of how each performs as a predictor of ground level concentrations. Even though the numerical model performed best at F stability and 1.5 meters per second, a range of speeds and stability has been provided. Because of the variability in wind speed, direction and stability over a few hours time period, a model which did well anywhere within that range should be acceptable. The results, however, indicate that the NOAA model is overestimating the concentrations for all speeds within that range. The predicted values are from a factor of 3 to a factor of 15 too high. As a consequence, it is clear that the plume does not intersect the terrain as postulated in the NOAA model.

TABLE II

Date (Emission Rate, g/sec)	Stability (Wind Speed, m/s)	Peak Hourly Average SO_2 Concentrations, ppm			
		NOAA	EPA	Numerical	Measured
Oct. 16 (583)	F (1.5)	1.25	0.20	0.11	.102
	F (2.1)	0.89	0.14	0.08	
	E (1.5)	0.46	0.11	0.078	
	E (2.1)	0.33	0.08	0.058	
Nov. 24 (478)	F (1.5)	1.02	0.17	0.087	.070
	F (2.1)	0.73	0.12		
	E (1.5)	0.38	0.08		
	E (2.1)	0.27	0.06	0.057	
Dec. 2 (376)	F (1.5)	0.80	0.13	0.066	.069
	F (2.1)	0.57	0.09		
	E (1.5)	0.31	0.07		
	E (2.1)	0.22	0.05	0.048	

The NOAA model assumes that reflection of pollutant from the ground surface is important. In many elevated terrain situations it can be assumed that reflection has little effect and that the intersecting concentration should be calculated as if there were an elevated receptor. Since this is probable for the Vermilion Cliffs situation, all of the above NOAA concentrations might be divided by 2. This would have brought the intersecting plume concept only to within 1.6 times the measured maximum concentration.

The EPA model has predicted values much more consistent with the measured concentrations. The predicted range varied from 0.7 to a factor of 2.4 too high relative to the measured maximum. At the distance of the monitors (24-28 kilometers from the source), the terrain correction, i.e.

plume centerline no closer than 10 meters, reduces the EPA prediction below those of the NOAA model by less than 2%. It is the sector averaging concept which has caused the EPA model predictions to be in the range of the measured concentrations. The answers appear to be correct, but for the wrong physical reason. Sector averaging is also inappropriate because it would imply that all of the monitors would have the same concentration since they all lie within the same 22 1/2° sector. This is clearly not the case since calculating the air flow, as the numerical model does, has provided a simulation of the crosswind pattern of concentration measured at the monitors. Although the EPA model has adequately simulated the maximum measured value, it is unlikely that the model can be used to extrapolate to a variety of other terrain situations since this physical basis is lacking.

The numerical model results are all well within a factor of 2 of the measured maximum concentration. As indicated previously, within the range of acceptable meteorological conditions the model can accurately simulate the crosswind pattern. It should be noted that the numerical model was within a factor of 2 over the entire range. This indicates much less sensitivity to changes in stability than is the case for the Gaussian models. The numerical model decreases 30% from F to E stabilities while the Gaussian models show a 70% decrease. If the three days are used as an example, they are all within 20% of each other in concentration once source strength is considered. Whatever variation in stability they represented resulted in little change in ground level concentration supporting the numerical result. The advantage of calculating the wind field and combining it with the diffusion analysis is thus apparent.

4. GARFIELD, UTAH

During June and July of 1973, NOAA Air Resources Laboratory personnel conducted tracer tests in the mountainous terrain near Garfield, Utah[7]. Figure 6 shows the sampling points in relation to the stack. The numerical and Gaussian models have been compared with these test measurements and the relative merits of these models, especially for unstable conditions, assessed. Sulfur hexafluoride was released from the 122 meter stack of an operating smelter of Kennecott Copper Corporation. NOAA's airborne helicopter and ground level tracer samples were made to evaluate maximum aerial concentrations and ground level concentration distributions. The tracer tests were supported by pibal and surface wind measurements and radiosonde data.

Concentration distributions for three tests (2, 3 and 7) were calculated using the EPA, NOAA and numerical models. Two of these tests (2 and 3) were estimated as Pasquill C stability and the third one (7) as B stability.

Figure 7 illustrates and emphasizes the need for providing a wind flow calculation. During the tests, the airborne samples were used to determine a plume centerline height above ground. Those samples have been smoothed into an observed plume path. The plume centerline paths for the models utilized in the comparison are shown as well. The NOAA (and also the EPA model) assume parallel flow which clearly overestimates the observed plume height. The numerical model, however, reproduces the observed plume centerline path in a reasonable manner. Because of that fact, the ground level concentrations for the numerical model are higher than the Gaussian. The position of maximum ground level concentration, i.e. the upwind side of Sulfur Peak, is accurately predicted by the numerical model wind flow calculation. The Gaussian models place the maximum concentrations downwind of Far Ridge in a clearly inappropriate position. Thus, incorrect placement is also illustrated in Figure 8 where the horizontal pattern of measured concentrations is compared to the output of the numerical and NOAA models. The numerical model simulates a much more realistic pattern of concentrations.

For the three tests which were studied extensively, the following table provides a comparison of the model results to the observed concentrations. The logarithmic mean ratio shows the relative merits of the models in calculating the pattern of ground level concentrations because it weighs each monitor site equally.

TABLE III

Model Comparisons for Test Cases
of Tracer Releases at Garfield, Utah

Test	Model	Ratio Calc/Obs	Logarithmic Mean Ratio
2	Numerical	.90	.82
	NOAA	.26	.20
	EPA	.36	.36
3	Numerical	.45	.44
	NOAA	.35	.26
	EPA	.34	.36
7	Numerical	1.5	1.25
	NOAA	1.5	.78
	EPA	2.69	2.23

In all three tests, the numerical model results were within a factor of 2 1/2. In general, the model overestimated concentrations in Test 7 and underestimated them in Test 3. Test 7, the most unstable case, is suspected of having strong upslope flow induced by surface heating. Because none of the models include this upslope flow, they tend to overestimate concentrations. In Test 3, the NOAA personnel suspect that an elevated inversion increased concentrations at several terrain positions and the models would thus underestimate. It is clear that overall the Gaussian models underestimate the measured concentrations in Tests 2 and 3. This is expected because the plume centerline is assumed to be further from the surface than is actually the case.

The EPA model, when estimating concentrations for unstable atmospheres, also suffers from the same air flow assumptions present in the NOAA model. The plume path and ground level maximum position would be physically unrealistic. The application of sector averaging to the prediction of ground level centerline concentrations might be expected to result in lower concentrations than the NOAA values. However, because few of the measured values are on the centerline, the EPA model predictions are higher than NOAA off-centerline predictions for the same points. This results in predicted concentrations a little better than NOAA for Tests 2 and 3, but still a factor of 3 low. In Test 7 the EPA model results overestimate the measured concentrations by more than both other models.

5. CONCLUSIONS

It seems clear from the measured data presently available that our initial hypothesis was correct. It is significantly better to calculate the expected wind flow in order to make reasonable predictions of ground level concentrations for complex terrain situations. This has been shown for stable, neutral and unstable atmospheric conditions. The Navajo data provide good stable case comparisons; the Garfield data provide good unstable case comparisons and the Huntington Canyon data provide examples of several stability cases in a specific terrain situation. The NOAA model underestimates in unstable cases and overestimates in stable atmospheres. The same trend with atmospheric stability is present with the EPA model. It generally gives improved performance in predicting peak ground level concentrations over the NOAA model for stable conditions because of the angular segment averaging. Its performance for unstable conditions is often worse.

The numerical model, on the other hand, predicts values basically within a factor of 2 of the measured data. This demonstrates a consistency of results in several test terrain conditions and a range of atmospheric stabilities mandatory for a reliable prediction model. The physical realism provided by a wind flow calculation has the benefits of correct plume path calculation, correct prediction of the position of the maximum and correct pattern of ground level concentrations including lateral dispersion over terrain obstacles.

REFERENCES

1. Van der Hoven, I., et al, "Report of Meteorology", SW Energy Study, Appendix E, 1972.

2. Lantz, R. B., Coats, K. H., Kloepfer, C., "A Three-Dimensional Numerical Model for Calculating Spread and Dilution of Air Pollutants", proceedings - Air Pollution, Turbulence and Diffusion Symposium, Las Cruces, NM, December, 1971.

3. Djuric, D., and Thomas, J., "A Numerical Study of Convective Transport of a Gaseous Air Pollutant in Vicinity of Tall Buildings", Air Pollution, Turbulence and Diffusion Symposium, December, 1971.

4. Hotchkiss, R., "Numerical Calculation of Three-Dimensional Flows of Air and Particulates about Structures", Air Pollution, Turbulence and Diffusion Symposium, December, 1971.

5. Start, G., Dickson, C., and Wendell, L., "Diffusion in a Canyon within Rough Mountainous Terrain", NOAA Tech Memo ERLTM-ARL 38, 1974.

6. "Six Month SRP SO_2 Air Quality Monitoring Program", Report to Salt River Project by Rockwell International Science Center, November, 1975.

7. Start, G., Ricks, N. R., and Dickson, C. R., "Effluent Dilutions over Mountainous Terrain", NOAA Air Res. Lab. Draft Tech Memo, December, 1974.

8. Burt, E. W., "Description of Terrain Model (C7M3D)", NDAD, SRAB, Modeling Application Section, 1973, Research Triangle Park, NC.

9. "Evaluation of Selected Air Pollution Dispersion Models Applicable to Complex Terrain", EPA-450/3-75-059 by INTERCOMP in fulfillment of EPA Contract 68-02-1085, July, 1975.

10. Turner, D. B., "Workbook of Atmospheric Dispersion Estimates", PHS Publ. 999-AP-26, 1969.

11. Lantz, R. B., and Hoffnagle, G. F., "Comparison of Plume Dispersion Calculations with Tracer Measurements at Huntington Canyon, Utah", ACPA Paper 75-26.5, Boston, June, 1975.

12. Lantz, R. B., Hoffnagle, G. F., and Mirabella, V. A., "Comparison of Several Models with Ambient Sulfur Dioxide Measurements Near the Navajo Generating Station", APCA Paper 76-34.2, 69th APCA Meeting, Portland, Oregon, June 11, 1976.

HUNTINGTON CANYON TERRAIN

DOWN-CANYON ORIENTATION

Figure 1

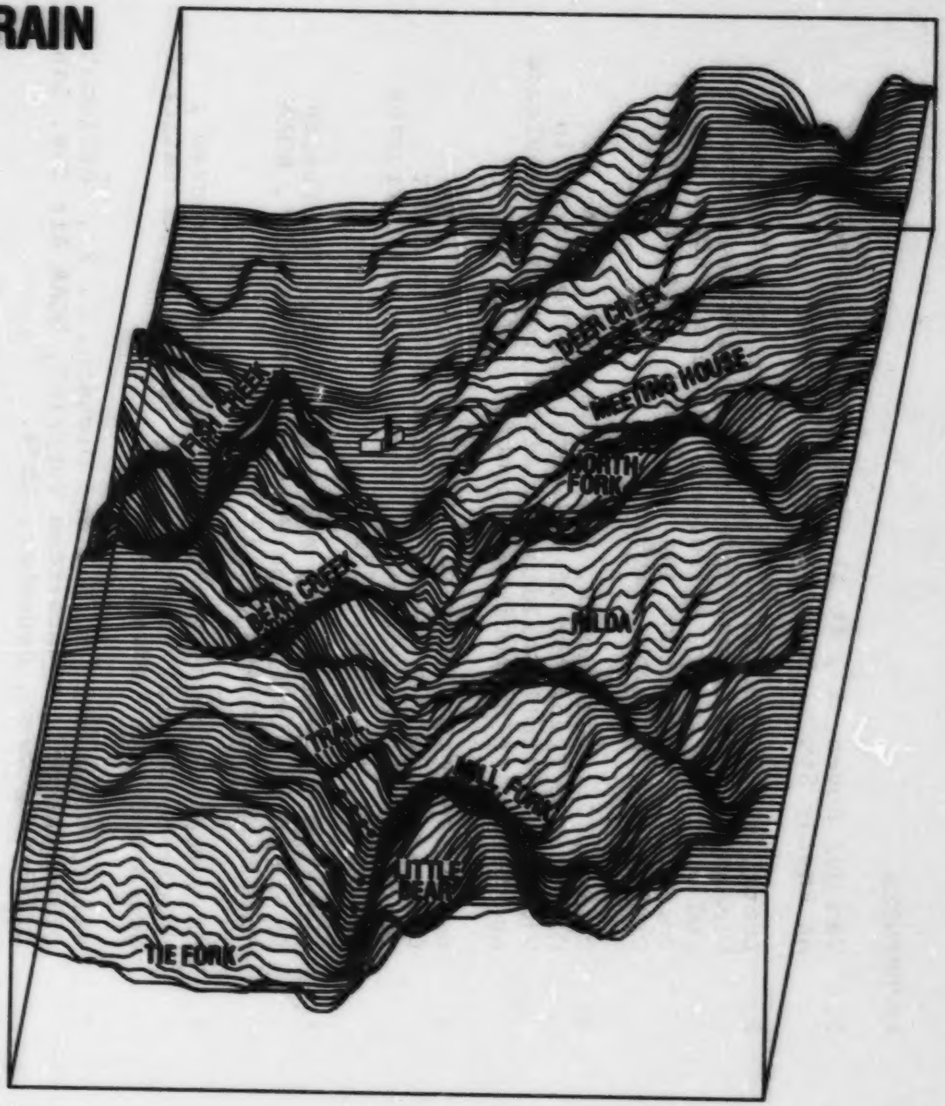
DEER CREEK
MEETING HOUSE
NORTH FORK
FISH CREEK
BEAR CREEK
HILDA
TRAIL
MILL FORK
LITTLE BEAR
TIE FORK

Figure 2

COMPARISON OF MEASUREMENTS WITH CALCULATIONS

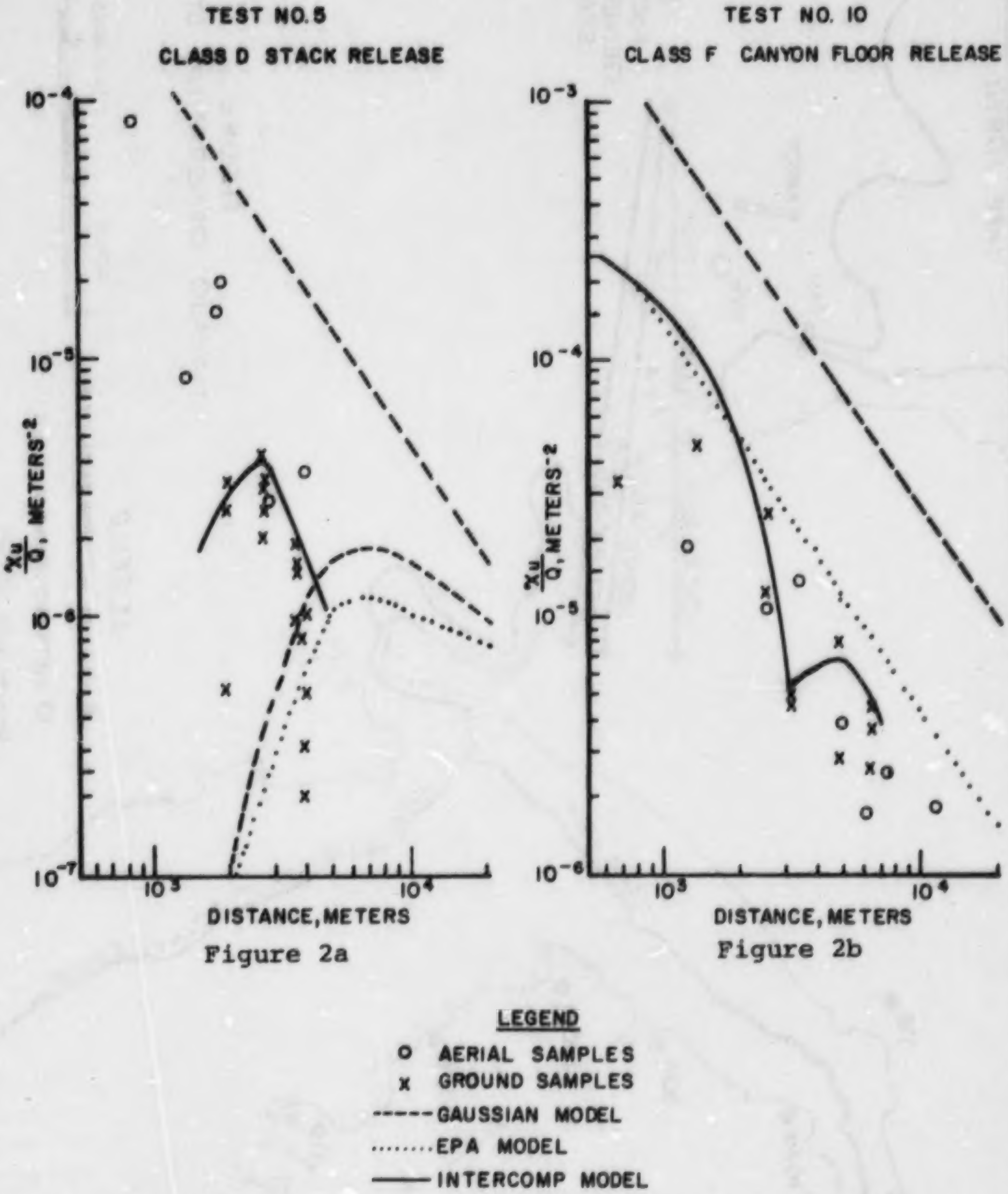

Figure 2a

Figure 2b

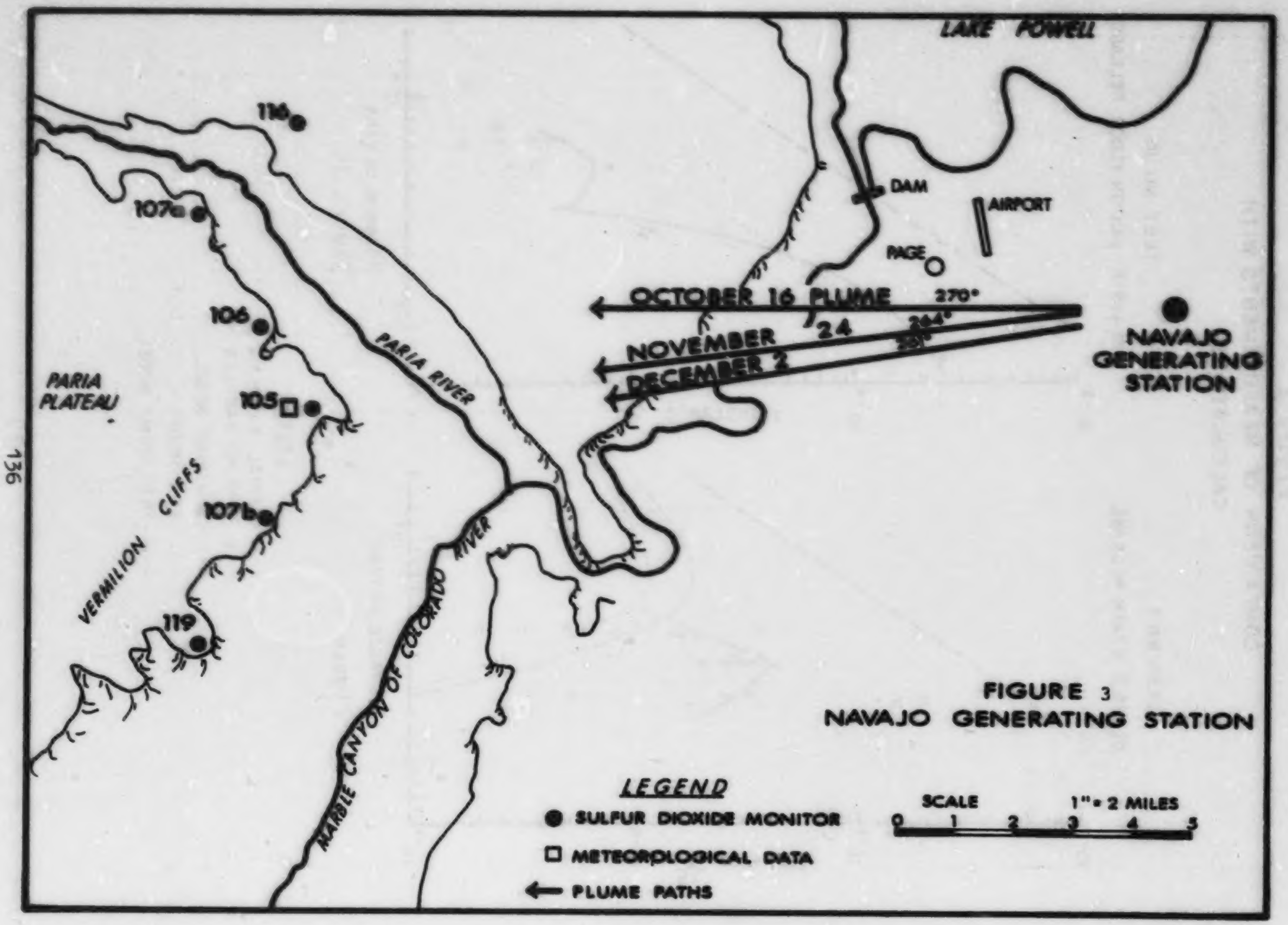
LAKE POWELL
DAM
AIRPORT
PAGE
OCTOBER 16 PLUME
270°
NOVEMBER 24
264°
DECEMBER 2
NAVAJO GENERATING STATION
116
107a
106
105
107b
119
PARIA PLATEAU
VERMILION CLIFFS
PARIA RIVER
MARBLE CANYON OF COLORADO RIVER
LEGEND
● SULFUR DIOXIDE MONITOR
☐ METEOROLOGICAL DATA
← PLUME PATHS
SCALE
1" = 2 MILES
0
1
2
3
4
5

FIGURE 3
NAVAJO GENERATING STATION

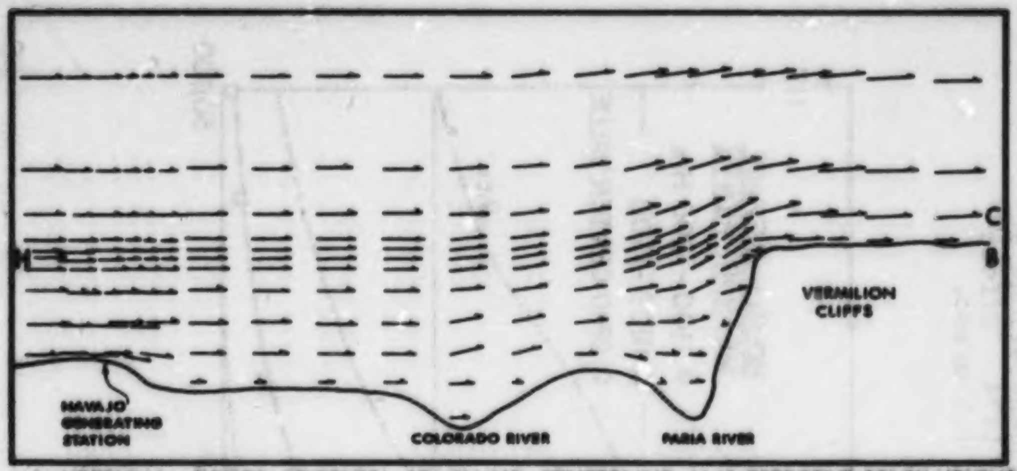
H
C
B
VERMILION CLIFFS
NAVAJO GENERATING STATION
COLORADO RIVER
PARIA RIVER

A. VERTICAL CROSS-SECTION AT PLUME CENTERLINE, H IS EFFECTIVE STACK HEIGHT V/H 10:1

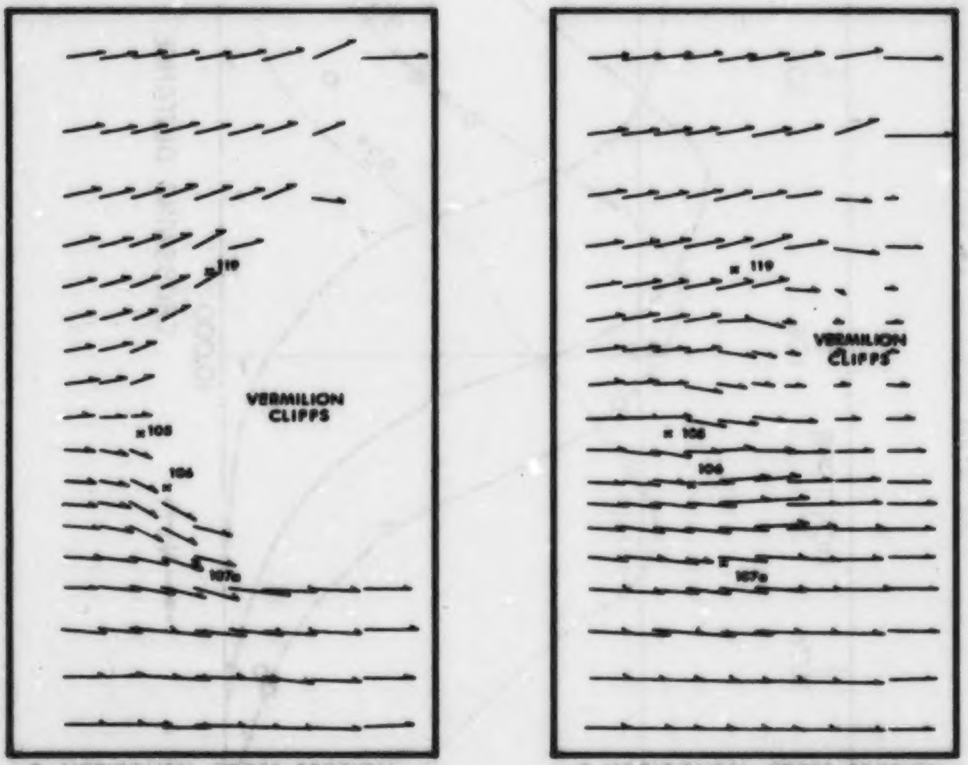
119
VERMILION CLIFFS
108
106
107a
119
VERMILION CLIFFS
108
106
107a

B. HORIZONTAL CROSS-SECTION BELOW CLIFF TOP V/H 1:1

C. HORIZONTAL CROSS-SECTION ABOVE CLIFF TOP V/H 1:1

FIGURE 4: MODEL DERIVED WIND FLOW, OCT.16, 1974
F STABILITY; 1.5 M/SEC.

SCALE

WINDSPEED, M/SEC.

Figure 5 - Comparison of Calculated and Measured Concentrations at Vermillion Cliffs Monitors - October 16, 1974. Effect of Wind Direction all for F Stability at 1.5 m/sec.

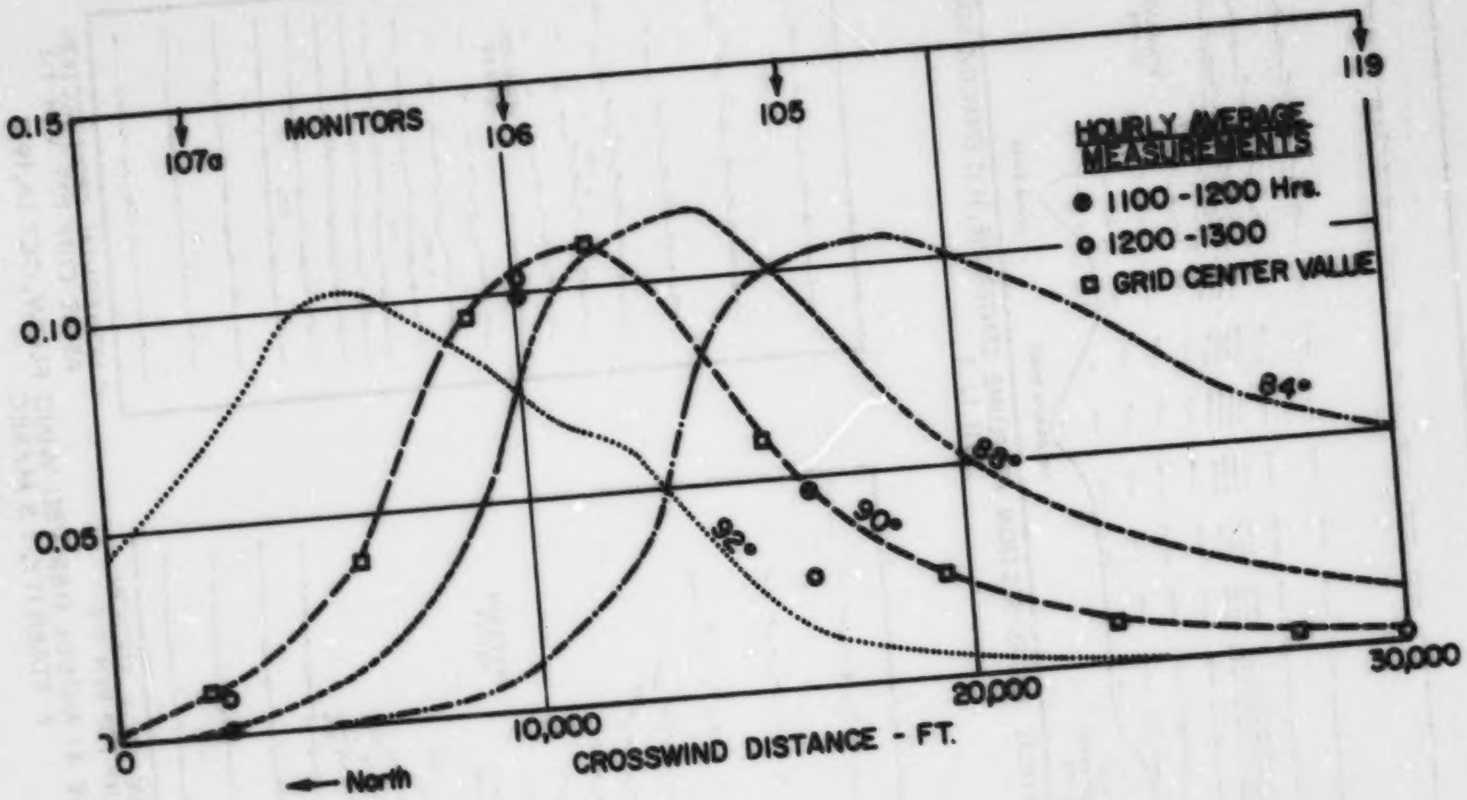

Figure 6. Distribution of ground level samplers and terrain heights for Tests 1-7.

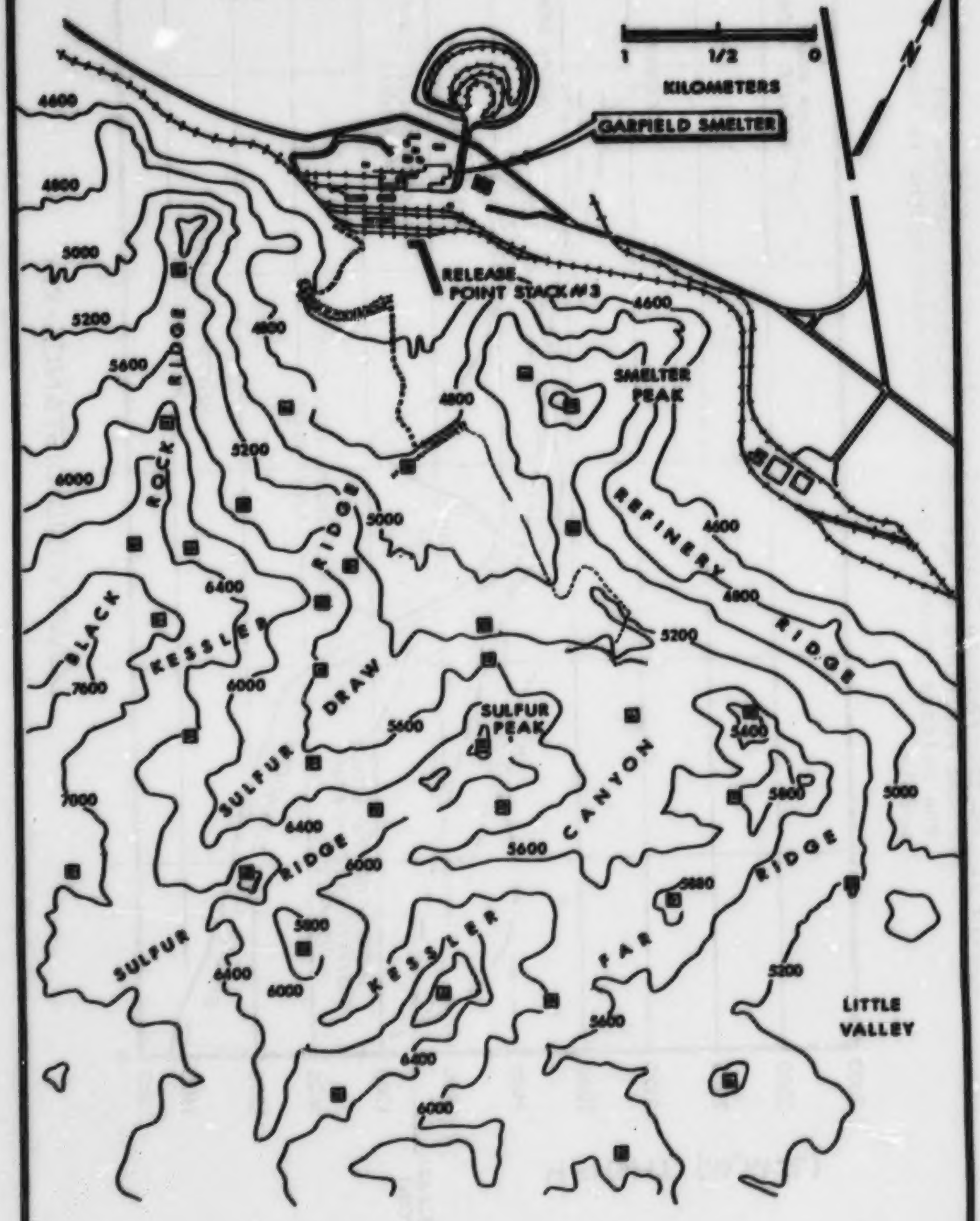
1
1/2
0
KILOMETERS
N
GARFIELD SMELTER
RELEASE POINT STACK #3
4600
4800
5000
5200
5600
6000
ROCK RIDGE
4800
5200
4800
5000
RIDGE
4600
SMELTER PEAK
REFINERY RIDGE
4600
4800
5200
BLACK
KESSLER
6400
7600
6000
DRAW
SULFUR
5600
SULFUR PEAK
CANYON
5600
5800
5000
7000
6400
RIDGE
6000
5600
5880
RIDGE
SULFUR
5800
6400
6000
KESSLER
FAR
5200
LITTLE VALLEY
5600
6400
6000

Figure 7. Height-Downwind Distance Depictions of the Mean Plume Positions as Measured by Helicopter Samples (H). The release point is the effective stack height in the models.

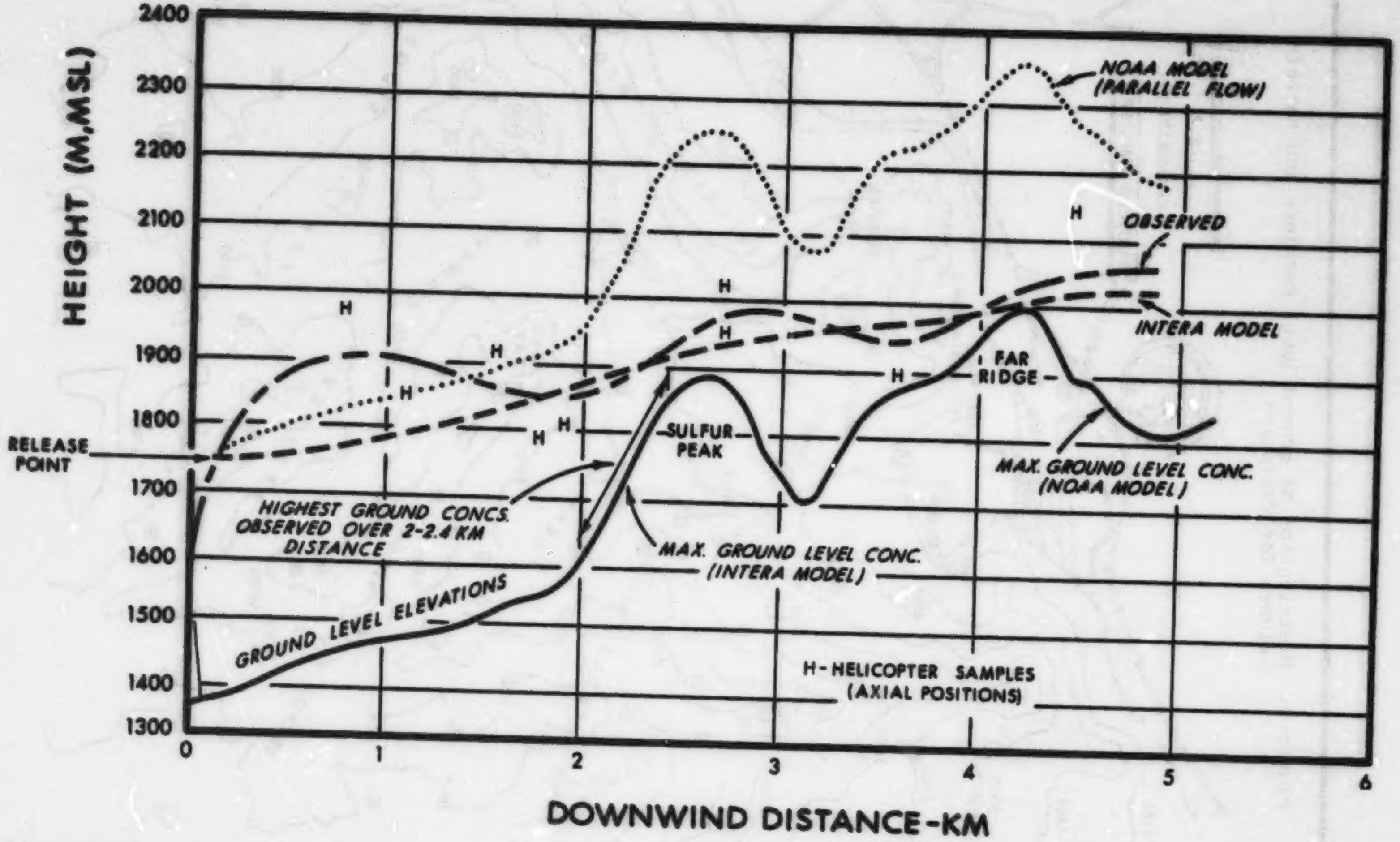

Figure 8a - Test 2
(INTERA MODEL RESULTS
STANDARD WIND PROFILE)

All Concentrations in 10^{-7} g/m^3

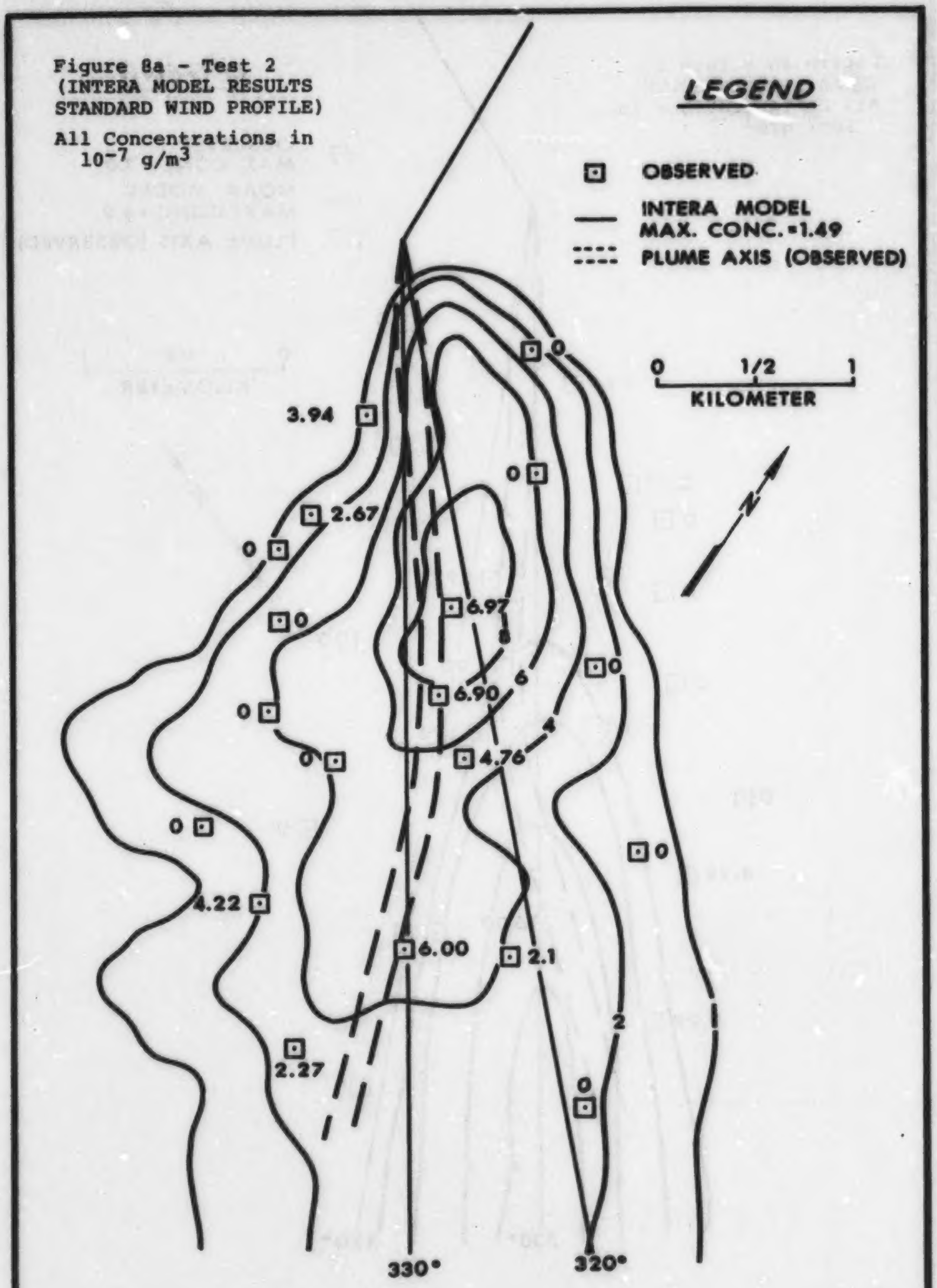
LEGEND
⊡ OBSERVED
INTERA MODEL
MAX. CONC.=1.49
PLUME AXIS (OBSERVED)
0 1/2 1
KILOMETER
N
3.94
2.67
0
0
0
0
0
0
0
0
0
0
0
6.97
8
6
4
2
6.90
4.76
4.22
6.00
2.1
2.27
330°
320°

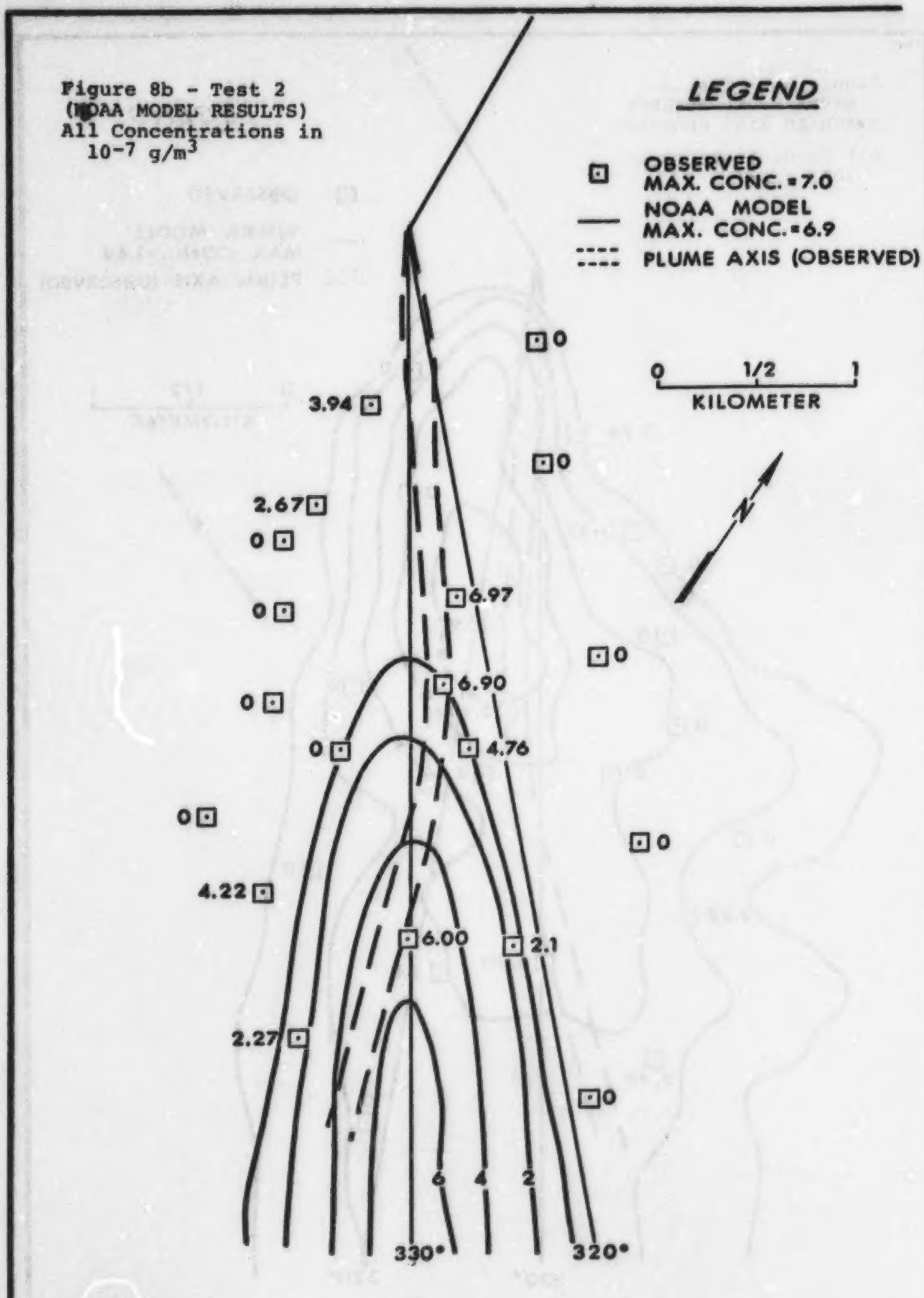
Figure 8b - Test 2
(NOAA MODEL RESULTS)
All Concentrations in
10^{-7} g/m^3

LEGEND
OBSERVED
MAX. CONC. = 7.0
NOAA MODEL
MAX. CONC. = 6.9
PLUME AXIS (OBSERVED)
0
1/2
1
KILOMETER
N
0
3.94
0
2.67
0
0
6.97
0
6.90
0
0
4.76
0
0
4.22
6.00
2.1
2.27
0
6
4
2
330°
320°

7TH INTERNATIONAL TECHNICAL MEETING
ON AIR POLLUTION MODELING AND ITS APPLICATION

THE APPLICATION OF DISPERSION MODELS IN A FJORD VALLEY AREA OF NORWAY

BJARNE SIVERTSEN
Norwegian Institute for Air Research

SEPTEMBER 7-10, 1976
AIRLIE VIRGINIA
UNITED STATES OF AMERICA

ABSTRACT

Different air pollution dispersion models have been applied to a non stationary meteorological situation governed by land/sea breeze and mountain valley wind. One important aim has been to find a model suited for calculating the diurnal variation and the occurrence and magnitude of the maximum concentration in the populated valley area. Concentrations of nitrogen oxides (NO plus NO_2) have been used in the validation of the models.

The calculations demonstrates the importance of a proper windfield simulation in areas with complex topography. Straight lined trajectories applied to quasistationary gaussian type dispersion models does not reflect the diurnal concentration pattern observed in the test area. Calculations performed in selected test periods show that the use of non stationary finite difference models improves the calculations considerably.

INTRODUCTION

Throughout the last few years several air pollution studies have been carried out in Nedre Telemark; a relatively highly industrialized area about 150 km southwest of Oslo. The existing industry consists of a fertilizer factory, chemical plants, smelters, paper industry and a cement plant. At present new petrochemical industry is being built in the area, while old industries are reducing the emissions.

To estimate the effect of these changes, and to supply authorities and area planners with adequate informations in the decision making process, several air pollution models have been applied to the area. The diurnal variation of the wind during nice summer days have a strong impact on air pollution in the populated areas during the transition period between the valley wind in the early morning and the sea breeze later in the day. The onset of sea breeze brings the air pollutants accumulated over the fjord basin back inland into the valley, causing a peak load of air pollution. The aim of this work has been to find a model that will predict concentrations during these situations.

THE AREA

The Nedre Telemark area consists of a mixture of uncultivated land, farming districts, scattered housing, suburban and urban areas and a few industrial sites. A large portion of the air pollutants emitted in the area originates from the industrial complex at Herøya (H in Fig. 1). This industrial site is located at the lower end of a bended 4-5 km wide river valley, which continue into the 8 km long Frierfjord. The rather flat valley-fjord system is surrounded by 100-200 m high hillsides and by higher mountains on a larger scale. The main part of the population live at the valley bottom. The area covered by the model calculations extend about 30 km northwards from the coastline and is about 15 km wide.

EMISSION INVENTORY

Emission inventories have been established for different air pollutants in the area. The emission from home heating and traffic have been based on: emission factors, population distribution, oil consumption and traffic density. Emissions from industrial areas have been estimated from information about average emissions and oil consumption figures supplied by the industry. The study was focused on nitrogen oxides (NO_2+NO). As shown in Figure 2 a main part of the nitrogen oxides are emitted from the industrial area H (Fig. 1).

TEST PERIOD

The summer of 1975 has been selected as test period for the models applied to the Nedre Telemark area. One of the aims of this study has been to find a model which can be used for calculating the maximum air pollution load in the valley during summer conditions. This usually means non stationary wind regimes caused by land/sea breeze and mountain/valley wind systems.

For testing long term average concentration dist[illegible]ions the month of July 1975 has been selected. For more detailed studies data from two "summerdays"; 11 June and 18 July 1975 have been used.

METEOROLOGICAL AND AIR QUALITY DATA

The following meteorological data were collected in the area during the summer 1975:

- wind speed and direction at 8 locations
- surface temperature at 6 locations
- temperature aloft (air plane soundings) at 3 locations
- vertical temperature profiles (radiosonde) at one location
- vertical wind profiles (pilot balloons) at 2 locations

Timelapse photography of plumes was done occasionally. Nitrogen oxides (NO_2 and NO) were measured continuously at 2 stations and NO_2 at 2 stations. Measurements of nitrogen oxides were also taken with a suitable equipped semimobile station on different locations during a few case studies.

THE MODELS

Two different types of models, a multiple source Gaussian model and a finite difference transport model has been applied to the test area.
A combination of the two model-types for different type of sources, and two different integration methods used in the transport model entail that 4 dispersion models have been tested. A trajectory type puff model is being developed for the area, but no results from this model is yet ready for presentation.

A multiple source Gaussian-model

A multiple source gaussian type model (1) has been applied to the area for calculating long time average concentration distributions and short term variations of the ground level concentration.

Area sources are treated as virtual point sources, with specification of width and height (sylindrical) and dispersion parameters as input. The dispersion conditions (stability category) is determined from measurements of temperature variation with height. The dispersion parameters are given as $\sigma = a \cdot x^p$ (2). Plume rise is calculated for point sources by Holland's, Stümke's or Briggs' equations, depending upon the amount of heat emitted (3).

A finite difference transport model "UPSTREAM"

The 3-dimensional model for calculating air pollution transport in Oslo (4) has been adapted to the Nedre Telemark area (5). The background for calculating the concentration (c) of an air pollution component is the law of mass conservation:

$$\frac{\partial c}{\partial t} + \nabla \cdot (\mathbb{V} c) = K_H \, \nabla_H{}^2 c + \frac{\partial}{\partial z} K \frac{\partial c}{\partial z} + Q + R \qquad (1)$$

where $\mathbb{V}$ is mean wind vector, Q the source strength rate, R the chemical reaction rate and K the eddy diffusion coefficients. In these calculations the diffusivity has been neglected, and the equation has been integrated vertically to become:

$$\frac{\partial \bar{c}}{\partial t} = -\overline{\nabla \cdot (\mathbb{V}_h \bar{c})} - \frac{wc}{h} + Q + R \qquad (2)$$

where $\mathbb{V}_h$ is the horizontal wind component, w is the vertical wind and h is the height of a well mixed boundary layer. The wind field is calculated from the non divergent stream function ψ:

$$V = \mathbb{k} \times \nabla_h \psi \qquad (3)$$

Observed winds at the boundary are used to estimate the stream functions in the area.
Terrain effects can be taken into account to a certain degree by determining the stream function in the area from:

$$\nabla^2 (\psi \cdot (H-Z) = 0$$

where H is the mixing height and Z the height of topography. The "UPSTREAM" finite difference approximation is used for space integration in this model. This approximation lead to "pseudodiffusion" and a smoothing of strong concentration gradients especially when the wind direction is not parallel to the grid axis. It is assumed in the calculation of the vertical average concentration that the pollution is kept below the height of h = 200 m.

Combined "UPSTREAM" and gauss-model

Calculations have also been carried out with a combined model, in which the dispersion of pollutants from area sources and small point sources have been calculated based upon the finite difference upstream model and the largest point sources have been treated by a gaussian type dispersion model.

The non homogeneous wind field applied to the area sources has been determined by the stream function. A 50 m high well mixed boundary layer has been assumed in this part of the model. Wind speed and direction at the large point sources has been calculated from the analyzed wind field (stream function) and applied as straightlined trajectories to a quasi stationary gaussian dispersion model. Concentrations from the two parts of the model have been added at each gridpoint and at specified receptor points.

A finite difference model "MOMENT"

Equation 2 has also been solved with a numerical integration method that reduces "pseudodiffusion" compared to that introduced in the "UPSTREAM" integration method. The numerical integration method is based upon a material conserving computation procedure involving the zeroth, first and second moments of the concentration distribution within each grid element (6, 7).

In this paper homogeneous wind fields estimated from the analyzed wind pattern, have been applied to the model referred to as "MOMENT". Nonhomogeneous winds, calculated from the stream function have also been tested, but is not presented here. The height of a well mixed boundary layer has in these model calculations been assumed equal to 200 m.

REPRESENTATIVITY OF WIND DATA

Representative wind observations as input to the gaussian type plume models is of great importance. When large gradients in the emission patterns exist, particularly in uneven terrain, an improper selection of wind data might result in large errors in the calculated concentrations. Joint frequency distributions of wind and stability have been established at several stations in the area. The multiple source gaussian type dispersion model has been used to compute monthly concentration distributions.

The patterns of NO_x-concentrations computed for July 1975 are based on data from two different stations; A and H. The concentration patterns in Figure 3 clearly demonstrate the importance of a proper choice of wind data.

The calculated average concentration of NO_x for July 1975 is compared to measured average concentrations at two receptor points:

Receptor point	A	B
Measured NO_x (μg NO_2/m^3)	∿ 50	195
Calculated NO_x Gauss. wind A	58	81
Calculated NO_x Gauss. wind H	12	35

We see that by applying wind observations from station H, which is in the area of the largest emissions, the monthly average concentration at both receptor points is underestimated. By using wind observations from station A, however, the calculated average concentrations will be closer to the observed ones. At B the average concentrations are still underestimated.

The cumulative frequency distributions in Figure 4, show that the model too often calculate low concentrations compared to the measurements. In a few cases the model calculates very high concentrations that are not observed.

A regression analysis of the relation between observed and calculated (gaussmodel) one hour average concentrations throughout one month (July) show no correlation between the two sets of data. Therefore it must be concluded that the dispersion of air pollution in the area during a typical summer month is governed by processes which are not simulated by gaussian type dispersion models. This conclusion is corroborated by the following discussion of typical meteorological features in the area.

Meteorological features during the summer

Most obvious is the strong diurnal variation of the wind field during the summer. Figure 5 illustrates the high frequency of down valley flow in the early morning and up valley wind in the afternoon. This channelled flow is a result of a combination of land/sea breeze and mountain/valley wind. The phenomenon has been investigated through the summers of 1974 and 1975 (8).

The principal results of this investigation can be summarized very briefly:

- in about 15% of the time during the summer pure thermally driven mesoscale circulations occur without significant synoptic scale wind. The diurnal changes and vertical dimensions of such a system is shown in Figure 6.
- in these situations a "stagnation" period during transition from land breeze to sea breeze occur over the fjord basin in the morning. The occurrence and length of this period is, however, to a large extent dependent of the speed and direction of the synoptic wind.
- diurnal variations of the local winds in the valley characterized by down and up valley winds (also influenced by large scale winds) occur more than 50% of the days during the summer (up valley afternoon winds occur about 70% of the time).
- observations have shown that air pollutants emitted in the valley are first transported very slowly by the land breeze into the fjord basin of Frierfjorden, while the onset of the sea breeze brings the polluted air back inland.
- in the valley a peak concentration is often observed as the sea breeze frong passes the monitoring station.

To calculate the transport and dispersion of air pollutants during these meteorological conditions it seems necessary to use a non stationary dispersion model. The channelled wind flow in the bended valley-fjord system indicate that wind analysis have to be based on observations from several stations and that straight-lined trajectories not simulate the wind pattern in the area adequately.

Estimated wind flow

Figure 7 shows the result of streamfunction analysis for 3 hours during one of the test periods. Assuming the quasi-stationary stream to be nondivergent and that the vorticity is negligible the stream function is evaluated from measured winds along the boundary of the area.

A northerly flow is simulated at 0600 hrs out the valley. At 0800 hrs the wind is turning. A very weak flow is calculated in the northern part of the area, while the onset of a southeasterly sea breeze is already working in the southern coastal areas. At 1000 hrs a southeasterly sea breeze is simulated throughout the test area.

Other methods for analysing the wind field as input to the transport models have been tested. Improvements of the applied method might be introduced, if the rate of land heating (and cooling) in the different areas could be properly simulated. This in turn can imply corrections in the wind field with respect to a divergent part of the velocity. Measurements indicate that it should be possible to estimate this wind component from a simplified quasi-stationary dynamic balance.

APPLICATION OF DIFFERENT MODELS ON SELECTED TEST PERIODS

As one purpose of this work has been to obtain a model which can predict the peak concentrations that occur in the valley during a typical summer day, observed and calculated concentrations at station B will be presented for two such days of 1975.

11 June 1975

Observed and calculated 1-hour average concentrations of NO_x (as µg NO_2/m^3) are presented in Figure 8 for 24 hours of 11 June 1975. A maximum NO_x-concentration is observed at station B in the valley at 1100 hrs. This peak is connected to onset of the sea breeze. The lower maxima later in the afternoon is caused by direct influence of the main sources in the area.

As seen from the graphs the gaussian type model does not at all reflect the morning peak. The plumes causing rise in observed NO_x-concentrations at receptor point B in the afternoon is fairly well reflected by the gaussian model.

The improvement in calculating the morning maximum, by utilizing time dependent finite difference models is clearly demonstrated. The air pollutants accumulated over the fjord during the near calm period, are brought back into the valley by the sea breeze. In this situation the peak concentration is overestimated at the receptor point in both the finite difference models and the combined model. The upstream model which uses the nonhomogeneous wind field from stream function analysis, also overestimate the afternoon concentrations. Corrections of the wind field at these hours might bring further improvements to this part of the calculation.

18 July 1975

The graphs in Figure 9 again illustrate the applicability of numerical transport models for computing the concentrations in the valley.

The observed morning maximum at station B is not computed by the gaussian model. The gaussian plumes affect the receptor point in the afternoon, but the plumes seem to be too narrow and concentrated.

The finite difference models fairly well reflects the observed variations in NO_x-concentrations. The combined model in this case underestimates the concentrations. The "upstream" model for area sources added to a trajectory-puff model for the point sources (in stead of the straight-lined gauss-model) would have improved the results in this case. Such a model is at present being developed for the area.

The concentrations at a more remote receptor point; S, not directly influenced by emissions from H, is fairly well estimated by the transport models (Fig. 10). The upstream model will at this receptor point overestimate the concentrations, probably due to "pseudodiffusion", and improper wind field estimation.

MODEL COMPARISON

A regression analysis show that there is no correlation between NO_x-concentrations calculated from the gaussian model and observed values (Fig. 11). The correlation coefficients are, however, increased to .68 and .82 by applying the numerical transport models. The best correlation is obtained with the model "MOMENT", but this underestimates the average concentration at receptor point B. The average concentrations and the coefficients of the linear regression line:

$$C_{obs} = a \cdot C_{calc} + b$$

is given for the test periods in the following table.

Calculated:	Average NO_x-conc.	a	b
Model: Gaussian	57	0.03	171
UPSTREAM	164	1.19	-13
UPSTREAM + GAUSS	113	1.99	-42
MOMENT	105	1.69	-45
Observed	173	1.00	

For average conditions it is seen that the calculated concentrations from the "UPSTREAM" model is closest to the observed values, while the model "MOMENT" best explain the variations in the concentrations in the valley. About 67% of the variance is explained by this model.

Spatial distribution of the NO_x-concentrations

In Figure 12 the spatial distribution of NO_x is presented based upon calculations with the two transport models. The effect of pseudodiffusion in the "UPSTREAM" model can be seen. A rather well defined sea breeze of about 4-5 m/s from southeast was observed at 1400 hrs on 11 June 1975. In this case the model "MOMENT" seem to simulate the distribution somewhat better than "UPSTREAM". In the near calm situations this is not necessarily the case.

SUMMARY AND DISCUSSIONS

The model area presented in this paper has a rather complex topography. The meteorological conditions during which the models have been tested are changing in time and space. Application of dispersion models to these problems are usually not straight forward.

The calculations demonstrates the importance of a proper wind field representation in areas with uneven topography. Straight lined trajectories applied to quasi-stationary gaussian type dispersion models does not reflect the observed diurnal concentration pattern of the test area. The applied non-stationary transport models, which have the ability of moving the mass along with the everchanging wind speed and direction improve the calculations considerably.
It is believed that further improvements can be achieved by a better simulation of the wind field, taking into account differential heating of the surface layer. A model extension

from the two-dimensional vertical integrated type used in this paper to a multilayer three dimensional model is also believed to improve the calculations. Puff-trajectory type models for calculating the dispersion from large point sources might improve the calculations, but a good wind field simulation will again be the critical point.

ACKNOWLEDGEMENT

The author is indepted to Knut E. Grønskei for valuable discussions and suggestions.

REFERENCES

(1) Schjoldager, J. Program "Kilder". Beregning av spredning fra punktkilder og volumkilder. Programbeskrivelse og brukerveiledning. NILU TN 2/75 (1974).

(2) Singer, I.A., Smith, M. Atmospheric Dispersion at Brookhaven National Laboratory. Air & Water Poll. Int. J. 10, 125-135 (1966).

(3) Sivertsen, B. Plume Rise Calculation. NILU TN 80/74 (1974).

(4) Grønskei, K.E. A three-dimensional transport model for air pollution in urban area with application to SO_2-concentration in Oslo. NILU OR 41/72 (1972).

(5) Grønskei, K.E. Regnemaskinprogrammet HNTEL. En beskrivelse av programmet som beregner arealkildenes bidrag til luftforurensningene. NILU TN 15/75 (1975).

(6) Egan, B.A., Mahoney, J.R. Numerical Modeling of Advection and Diffusion of Urban Area Source Pollutants. J. Appl. Met. 11, 312-322 (1972).

(7) Pedersen, L.B., Prahm, L.P. En numerisk metode til løsning af adveksjonsligningen $\frac{\partial c}{\partial t} = -\mathbf{V}\cdot\nabla c$. Meteorologisk Institutt, Danmark, Rapport Juni 1973 (1973).

(8) Sivertsen, B. Land-sea breeze studies in Telemark 1974/75. NILU TN 13/75 (1975).

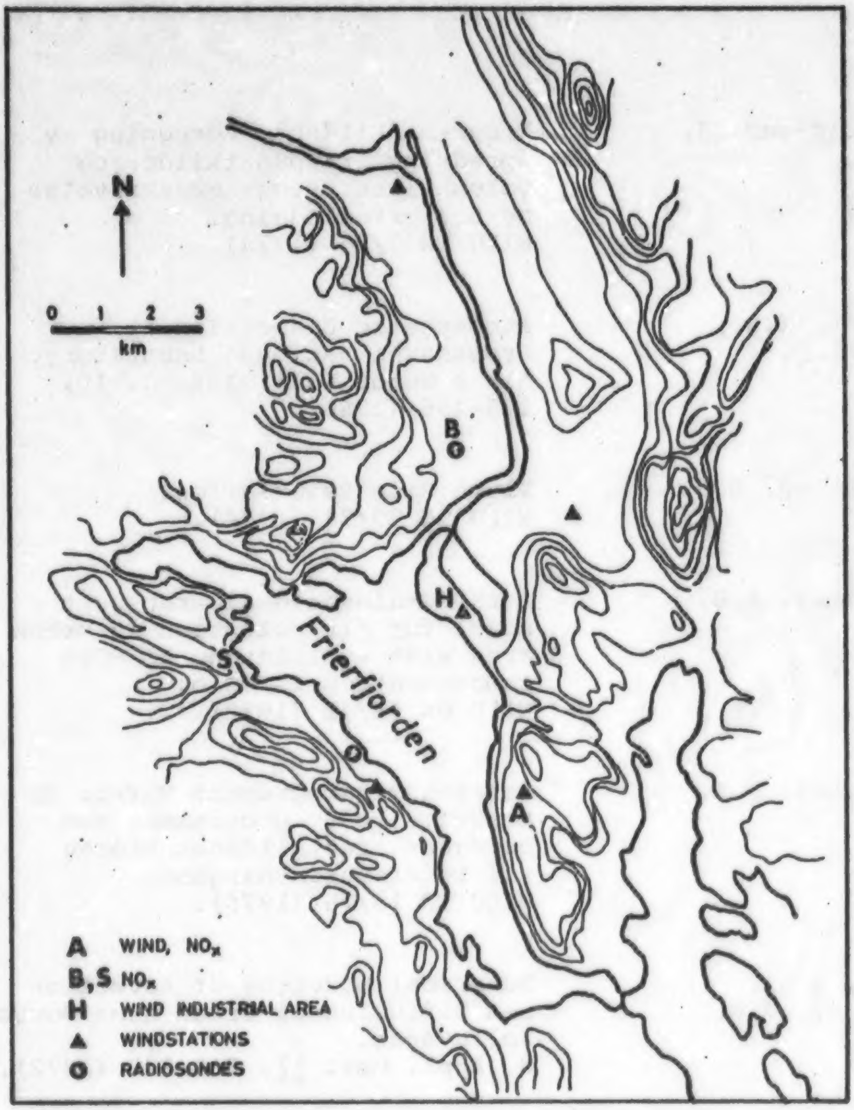
N
0 1 2 3
km
B
H
S
A
Frierfjorden
A WIND, NOx
B,S NOx
H WIND INDUSTRIAL AREA
▲ WINDSTATIONS
O RADIOSONDES

Figure 1: Topographical map of the test area. Stations referred to in the text are indicated.

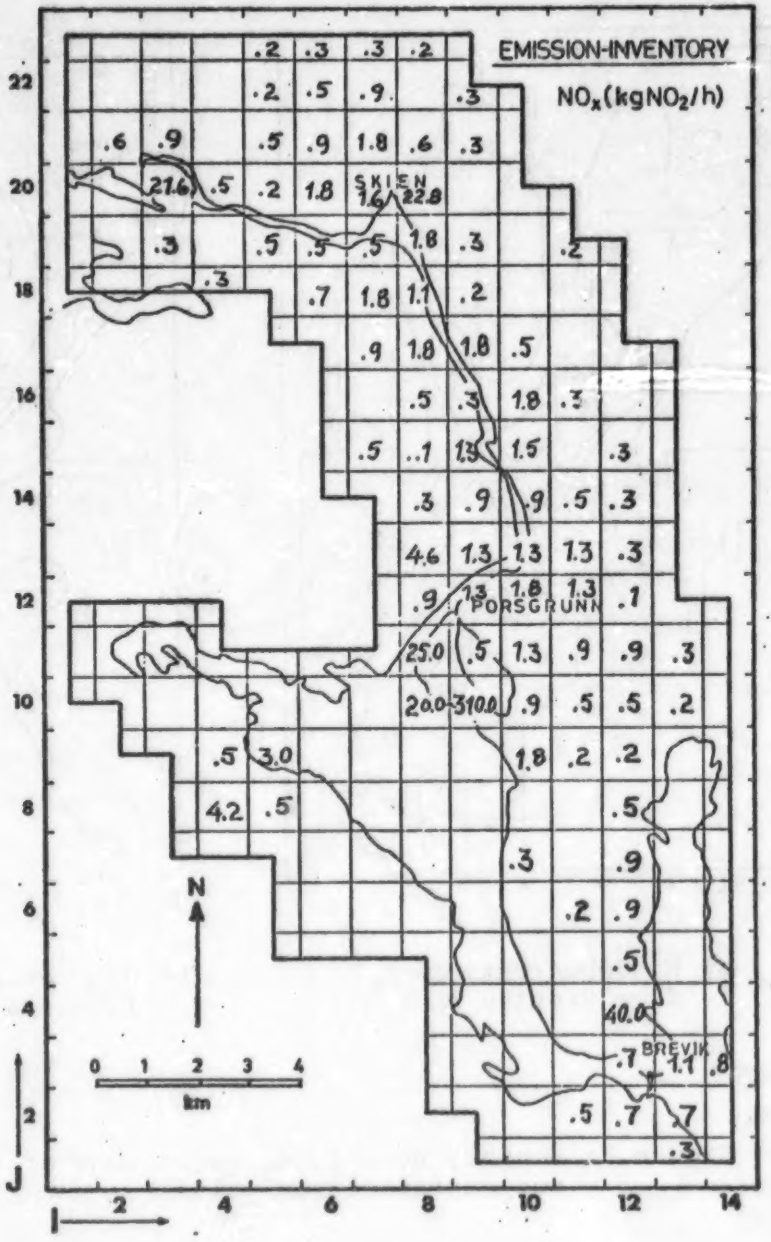

EMISSION-INVENTORY
NOx(kgNO2/h)
SKIEN
PORSGRUNN
BREVIK
N
0 1 2 3 4
km
J
I
22
20
18
16
14
12
10
8
6
4
2
2
4
6
8
10
12
14
21.6
22.8
25.0
20.0
310.0
40.0

Figure 2: The average emissions of nitrogen oxides (as kg NO_2/h) for each square kilometer of the area.

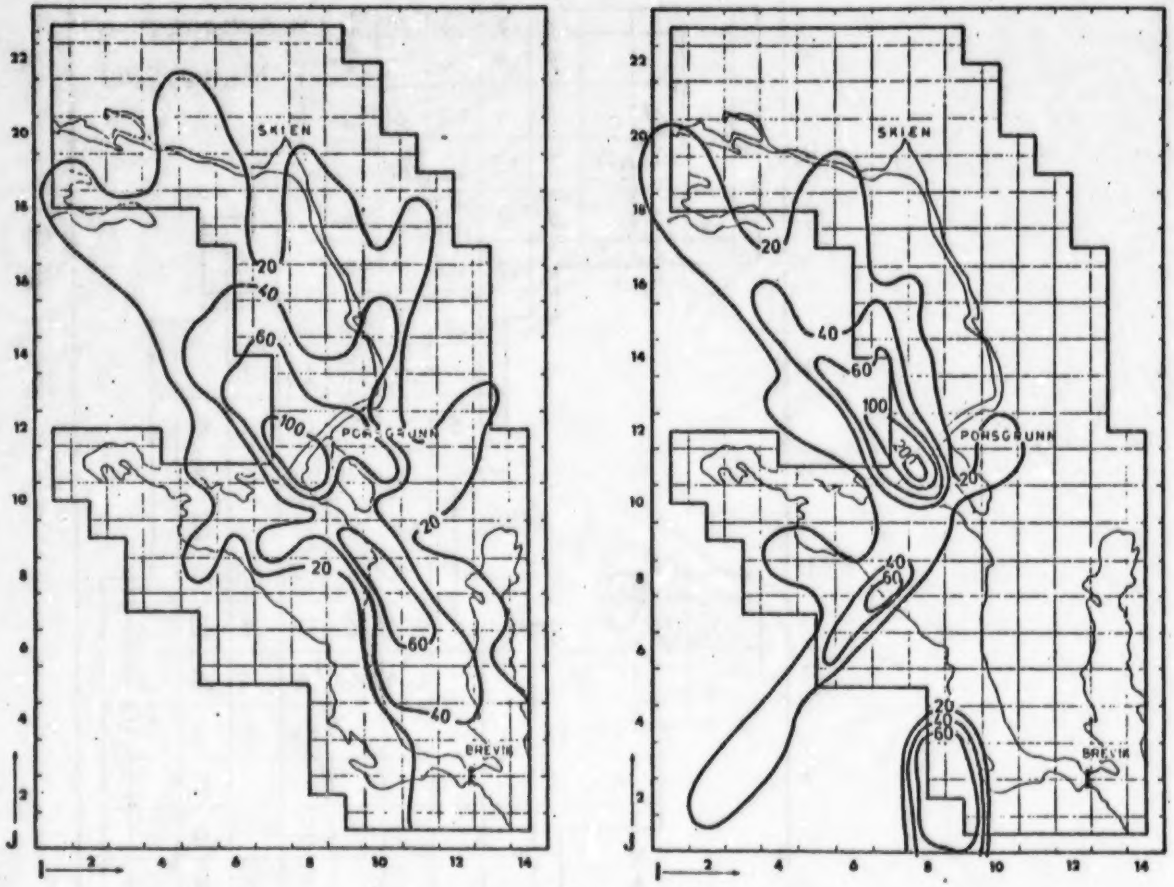
SKIEN
PORSGRUNN
BREVIK
20
40
60
100
200
J
I
2
4
6
8
10
12
14
16
18
20
22

a) Windobservations
from station A

b) Wind observations
from station H.

Figure 3: Monthly average distributions of the NO_x
concentration (July 1975).

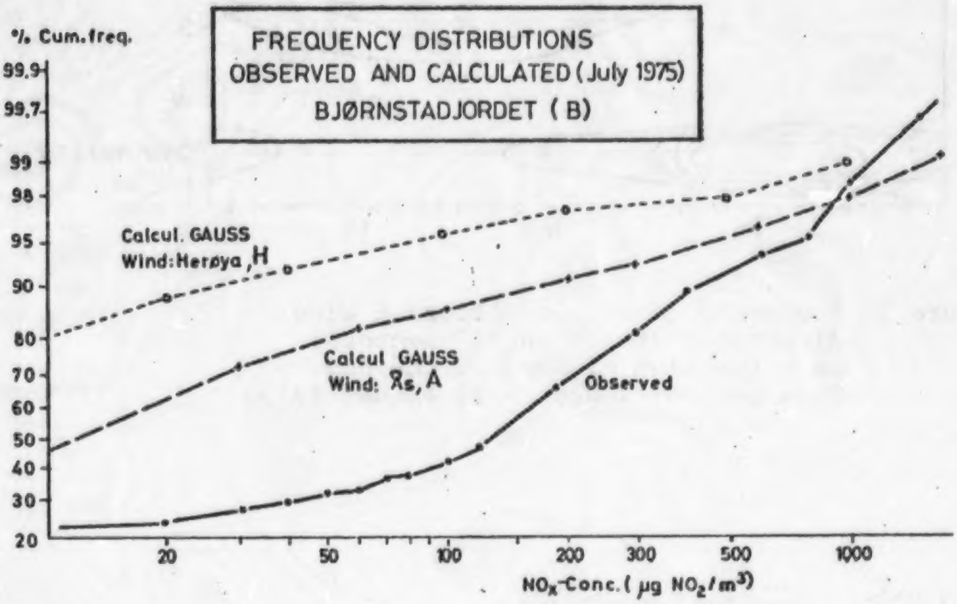

Figure 4: Cumulative frequency distributions of observed and calculated 1-hour average concentrations of nitrogen oxides at station B, based on data from July 1975.

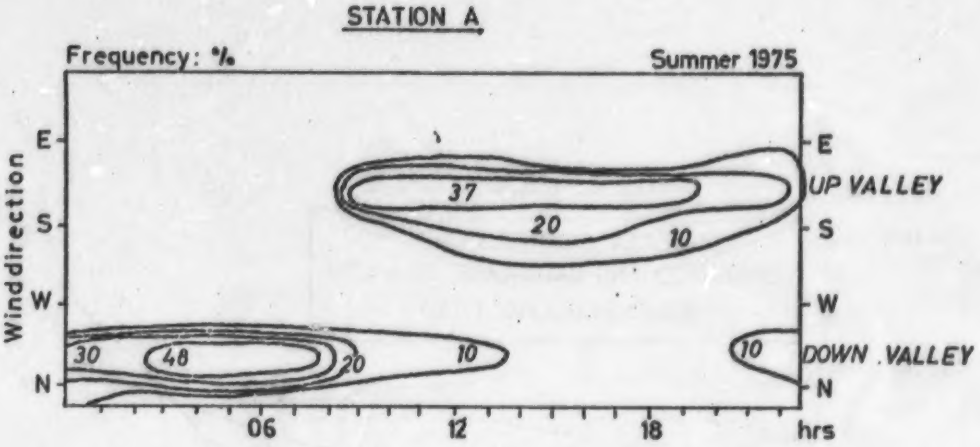

Figure 5: Frequency (in %) of different wind directions (based on 30°-sectors) as a function of hour of the day. Data period: 1 June - 31 August 1975.

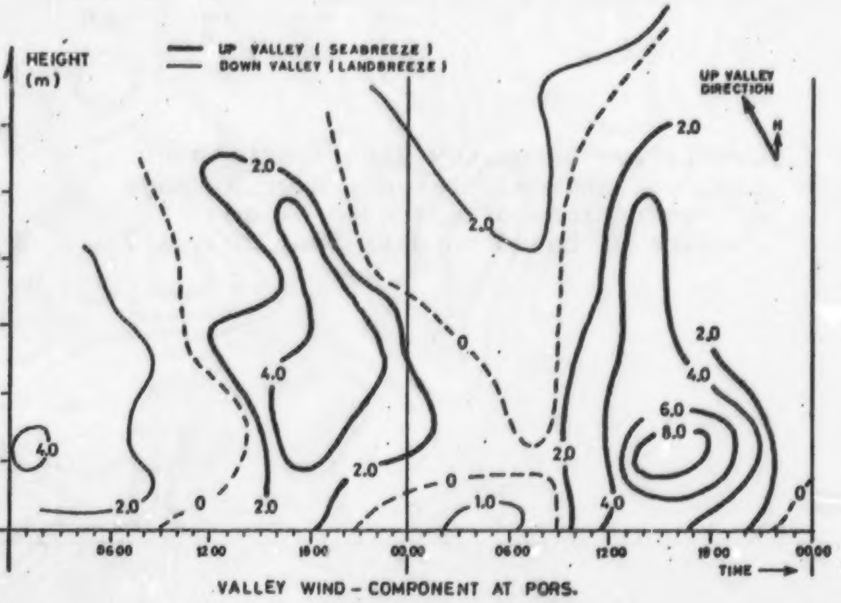

Figure 6: Up and down valley wind component as a function of height above ground and hour of the day on 10 and 11 June 1975. Measured in the valley near station B.

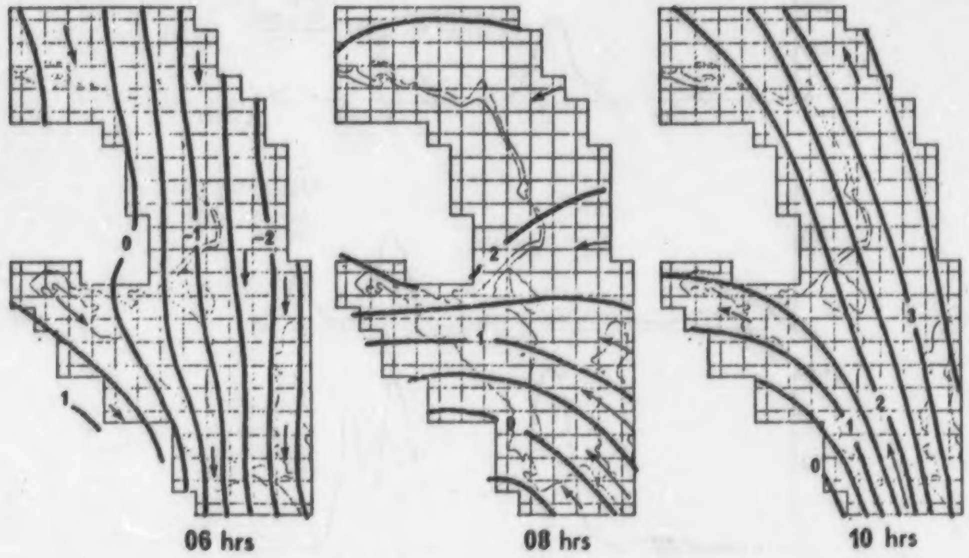

06 hrs

08 hrs

10 hrs

Figure 7: Estimated stream lines at three hours on 11 June 1975, based on the stream function evaluated from measured wind along the boundary.

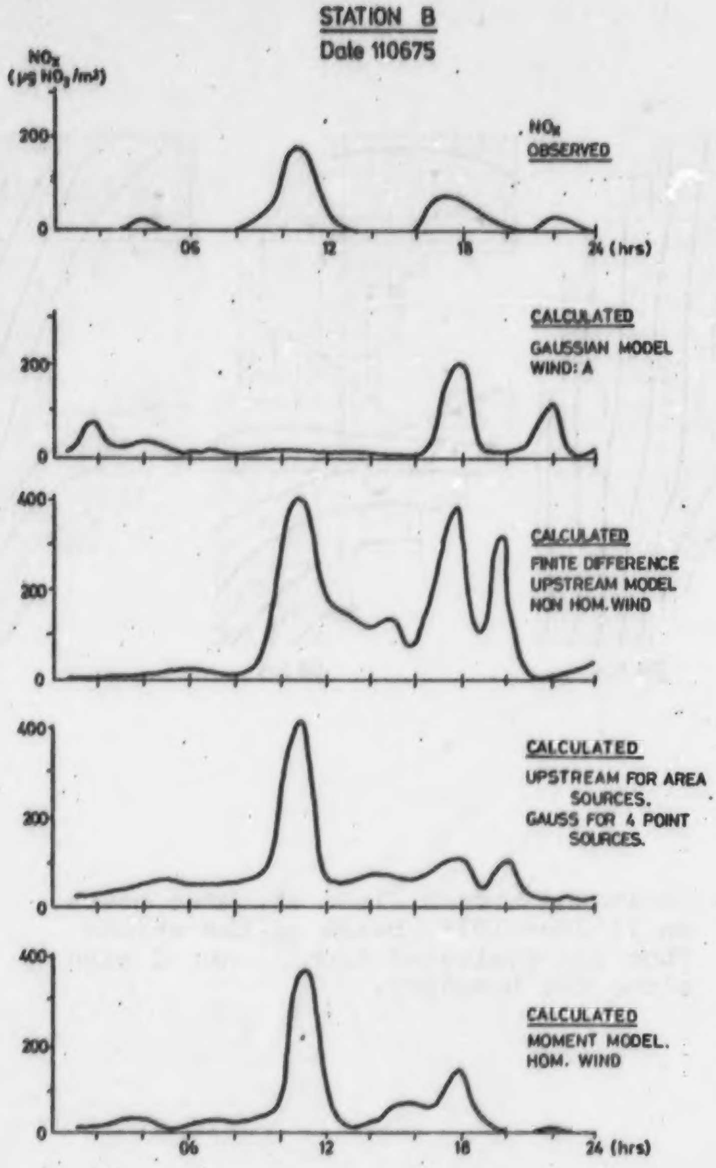

Figure 8: The diurnal variation of the observed and calculated NO_x-concentration at station B on 11 June 1975.

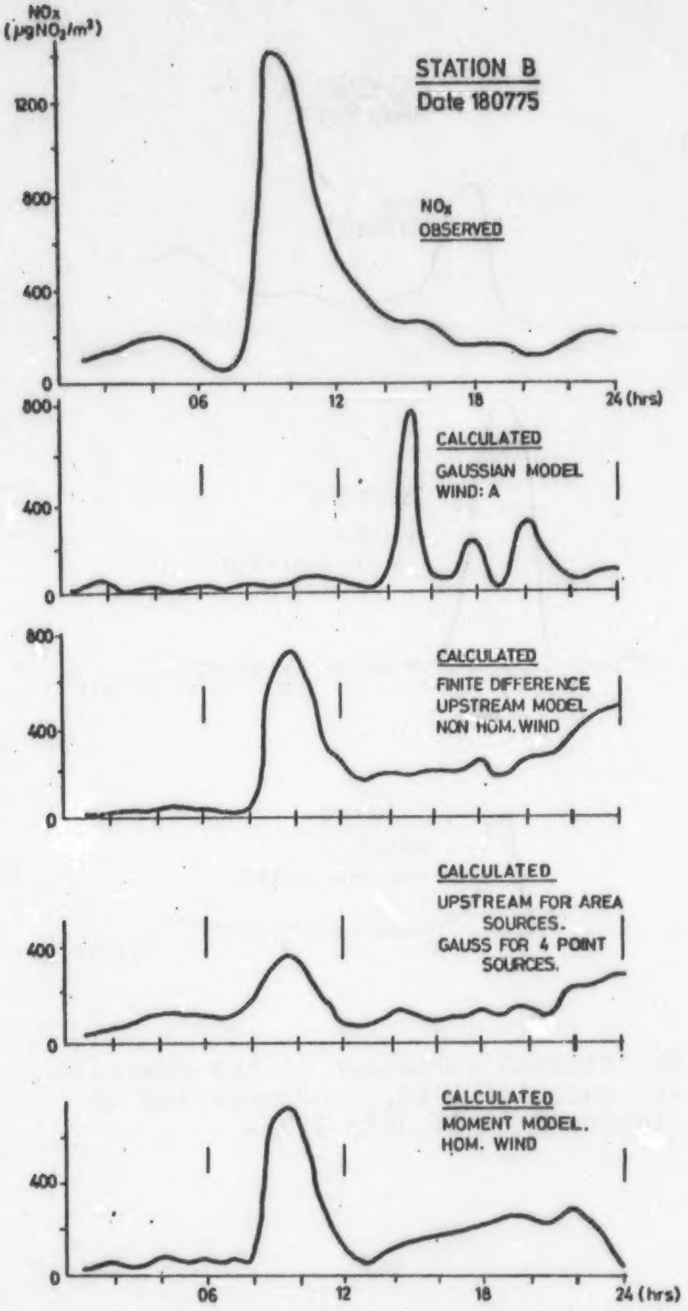

Figure 9: The diurnal variation of the observed and calculated NO_x-concentration at station B on 18 July 1975.

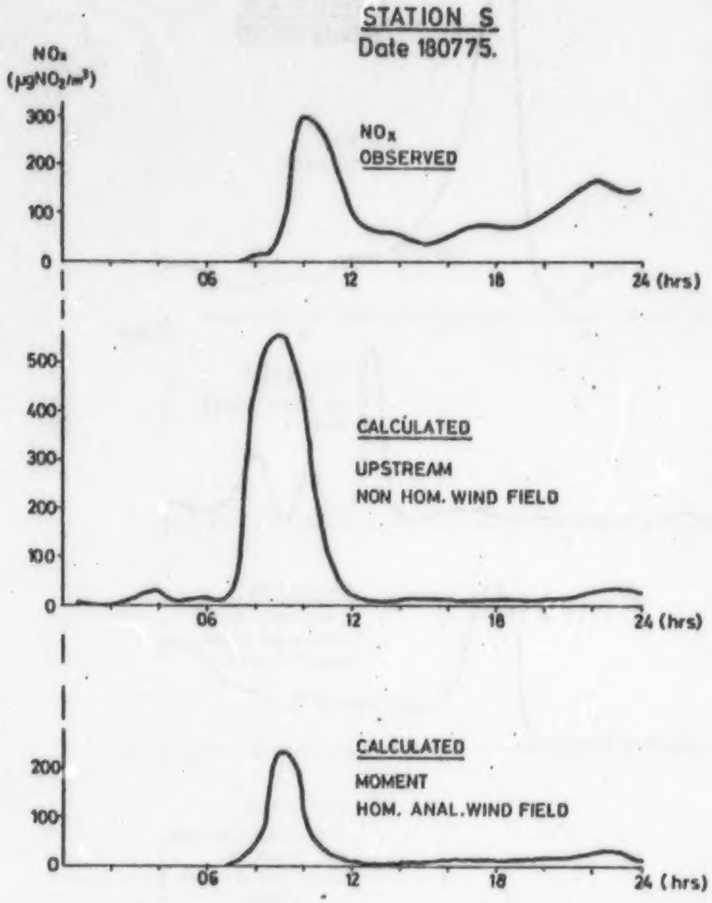

Figure 10: The diurnal variation of the observed and calculated NO_x-concentration at station S on 18 July 1975.

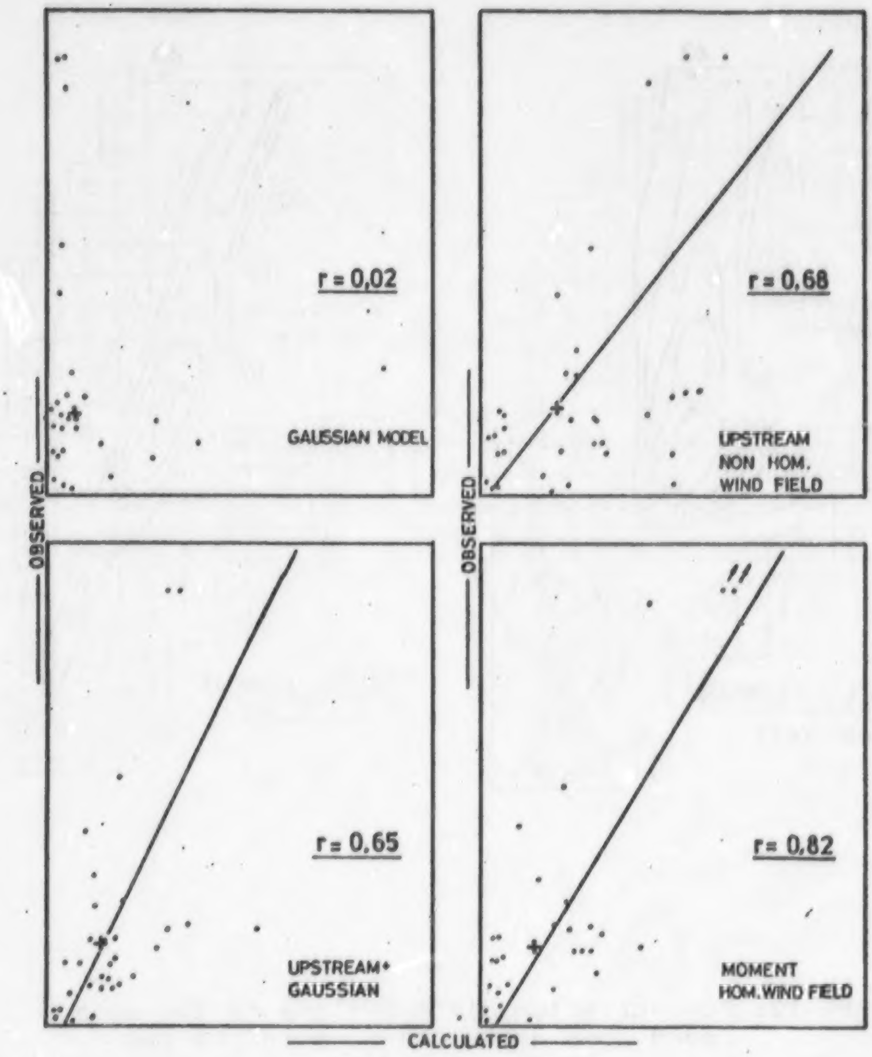

Figure 11: Correlation between observed and calculated 1-hour average concentration of NO_x at station B for selected test periods.

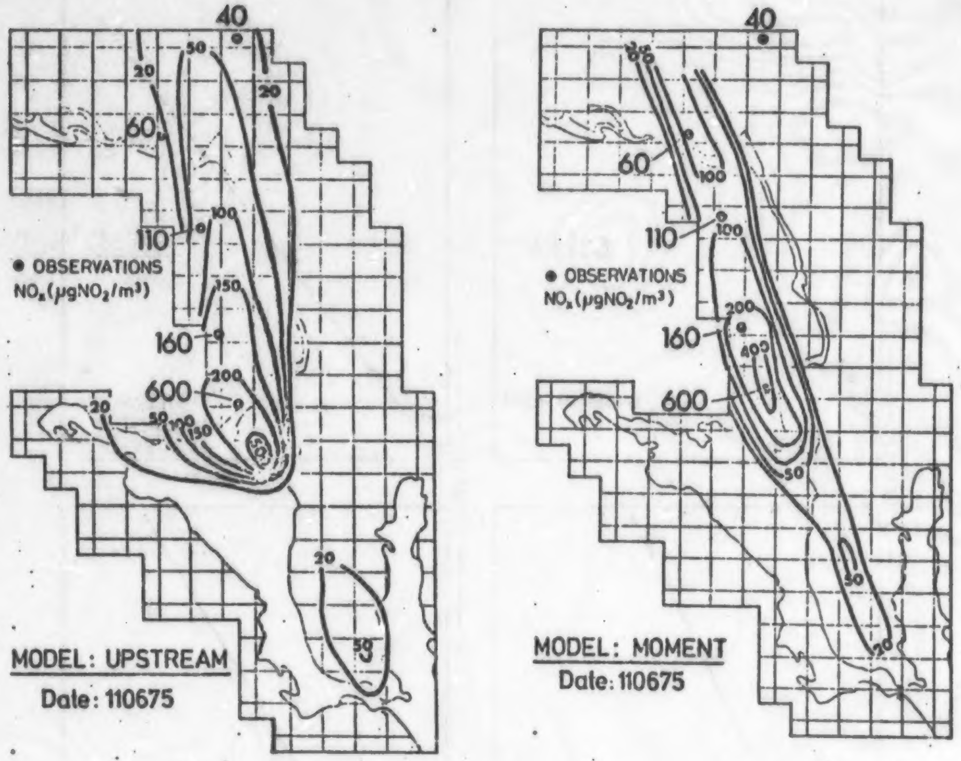
40
50
20
20
60
110
100
150
160
200
600
20
50
100
150
20
50
• OBSERVATIONS
NOx (μgNO2/m³)
MODEL: UPSTREAM
Date: 110675
40
60
100
110
100
200
160
400
600
50
50
20
• OBSERVATIONS
NOx (μgNO2/m³)
MODEL: MOMENT
Date: 110675

Figure 12: Concentration distributions in the area based upon calculations with the two transport models. Observations taken with a semimobile station are indicated. The distributions refer to data collected at 1400 hrs on 11 June 1975.

7th International Technical Meeting
on Air Pollution Modeling and its Application

The validation of the Gaussian dispersion model for long-term average ground level concentrations in the Rijnmond region.

F.T.M. Nieuwstadt, **Royal Netherlands Meteorological Institute, de Bilt**

C.M. Verheul, **Shell InternationalePetroleum Maatschappij B.V., The Hague**

J. Addicks, **Provinciale Waterstaat in Zuid-Holland, The Hague**

September 7 - 10, 1976
Airlie Virginia
United States of America

Abstract

The well-known Gaussian plume model has been used to calculate the concentration of SO_2 averaged over 3 months in the heavily industrialized Rijnmond region. The number of point sources taken into account was 87 and the number of area sources with the dimensions of 1 × 1 km was 491. The area sources represent the emissions of agricultural and domestic heating and the emissions of the ships in the port of Rotterdam. The concentration measurements at about 120 points in the region have been used in this validation.

The validation has been performed for two time periods: 1st quarter and 3rd quarter of 1973.

From the results of the validation in the 1st quarter a correlation coefficient followed between the measured and calculated concentrations at the measuring points of about 0.9.

During the validation in the 1st quarter an investigation was made into the influence of a change of dispersion coefficients for the low sources and the area sources. The influence of the mixing height, deposition and decay on the calculated concentrations was also investigated.

The most important conclusion from the validation results for this period is that the dispersion coefficients for low sources should be corrected for the surface roughness in the area.

The correlation coefficient between the measured and calculated concentrations at the measuring points for the 3rd quarter amounted to 0.8.

During the validation for this period an investigation has been made into the influence of a change of dispersion parameters and the plume rise formula of the point sources on the calculated concentrations.

The contribution of the very high sources to the calculated concentrations has also been investigated.

The most important conclusion from the validation results for this period is that the combined contribution of the very high sources to the calculated concentrations at ground level is more sensitive to a change in the dispersion parameters than the total contribution of the other point sources.

Taking the results of this validation into account, a recommendation has been prepared for a national air pollution model in the Netherlands for the calculation of long-term averaged concentrations.

I. Introduction.

Calculations of the dispersion of air pollution in the Netherlands have mainly been performed with the well-known Gaussian plume model. Several institutes have an air pollution model in operational use primarily for planning purposes.
The results of a validation calculation have been reported for two of these models: Huisman and Verheul (1974) with the "Stacmap" model of Shell Internationale Petroleum Maatschappij, and Nieuwstadt and van Dop (1975) with the "Luvolong" model of Royal Netherlands Meteorological Institute.

Most of the models mentioned above used different "input" parameters. From a comparison of these models it was found that the results (especially the calculation results for a single point source) are heavily influenced by the choice of these "input" parameters. These discrepancies obscured in the first place the discussions between the model users: for instance, firms which applied for a license to use a stack of which the dimensions were based on model calculations, and governmental authorities which were to issue the license, had to make a decision based on model results.

A working group was formed in 1972. In it were represented all the institutes (governmental and industrial) which had developed air pollution models or used an operational version of an air pollution model. The main objective of this group was the construction of a national air pollution model. It was decided that this national air pollution model would be used for the calculation of a long-term (seasonally, annually) averaged concentration based on the Gaussian plume model. In this model only "one" set of input parameters was to be utilized, so that discussions of the type mentioned above would no longer occur.

In order to recommend a physically sound set of parameters for this national model a validation of the Gaussian plume model was performed in cooperation between governmental and industrial institutes.
The results of this validation are discussed in this paper.

The working group has recently published a report on different arpects of the Gaussian plume model. In this report a proposal for a national air pollution model has been included (Kleine Commissie TNO, 1976).

The recommendation for the national air pollution model has been appended to this paper.

II. The air pollution model.

The Gaussian plume model for the calculation of long-term averaged (seasonally, annually) ground level concentrations (Calder, K.L., 1971) has been used as the dispersion model.

Two computer versions of this model were employed in this validation study: Stacmap and Luvolong (see chapter I.) These versions differed from each other in some details which can be found for Stacmap in Huisman and Verheul (1974) and for Luvolong in Nieuwstadt and van Dop (1975) and in Nieuwstadt (1974). Prior to the validation study both versions were run in a calculation for a test case. Identical input parameters were taken.
From these calculations it was found that the results of the two versions were interchangeable.

During the validation study an investigation was made into the sensitivity of the model results to some input parameters. A short description is therefore given of the input parameters. The details of how these model parameters are incorporated in both programs can be found in the above references.

a) Dispersion coefficients.

A distinction was made between the dispersion coefficients for low sources (area sources and low point sources) and high point sources.

Several sets of dispersion coefficients have been used in this validation: for the area sources Pasquill-Gifford (Turner,1969) and Fortak (Dreyhaupt, 1973); for the low point sources Pasquill-Gifford and Klug (1969); for the high point sources Singer and Smith (1969) and Klug (1969).

b) Distribution of stability, wind speed and wind direction classes.

As stability class definition a modified form of the definition of Pasquill classes (Nieuwstadt, 1974) was used. The definition of the wind speed and wind direction classes has been given in Nieuwstadt et al. (1975).

The distribution function has been constructed from the meteorological data during the validation period, which were collected at Zestienhoven Airport, situated in this region. (see figure 1).

Periods with wind speeds below 0.5 m/s, variable winds and periods with fog (about 8% of the time of the 1st quarter) were not included in the calculation of this distribution function, since the model cannot cope with these situations.

As hourly averaged concentration measurements were available (see chapter IV), an analysis could be made of the measured concentration averaged over the whole validation period and over the period for which the distribution function was calculated. The results of this investigation showed that concentrations averaged over the period for which the distribution function was calculated are at most 10% lower than the concentrations averaged over the whole validation period. It may therefore be expected that with the calculated distribution function a representative concentration averaged over the validation period can be calculated.

c) Transport velocity.

The calculation method for the transport velocity depends on the choice of the dispersion coefficients (Nieuwstadt, 1975).

In all cases use has been made of a dependence of the wind speed on height following a power law. The exponent of the power law is chosen as a function of stability class. (Nieuwstadt et al., 1975 Huisman et al., 1974).

d) Plume rise.

Various plume rise formulas have been used in this validation: the neutral formula of Briggs (1971), Concawe, Brummage (1968) and the K.S.L.A.[x)] formula (Huisman, 1974).

The formula of Briggs has been slightly modified. It has been found that for low wind speeds this formula seems to give unrealistically high plume rises. An upperbound has therefore been imposed on the neutral formula of Briggs, which is based on the fact that, averaged over a long period of time, the atmosphere may be considered to be slightly stable (temperature gradient $dT/dz \sim -0.6.10^{-2}\ {}^{o}C/m$). The stable plume rise formula of Briggs, in which the temperature gradient mentioned above has been substituted, has consequently been used for this upperbound.

With this modification it has been found that the quotient of the plume rises following the formulas of Concawe and Briggs will vary between 0.7 and 1.0, the plume rise of Briggs being slightly higher than the plume rise of Concawe, which in turn is slightly higher than the results of the K.S.L.A. formula.

[x)] Royal Dutch/Shell Laboratory, Amsterdam.

e) Area source description.

For the description of the dispersion from an area source the virtual point source model has been chosen. For this virtual point source model the normal equations for the point source are slightly modified in order to take into account the initial lateral and vertical dispersion inside the area source (Nieuwstadt, 1974; Turner, 1969).

Since the virtual point source leads to unacceptable results for the concentration inside the area source itself, it is required that an area source is completely located within a calculation grid square. For the concentrations inside an area source an interpolation between the results at the neighboring grid points is used.

f) Mixing height.

In the basic version the models are run with one fixed mixing height for each stability class. For these mixing heights the values of Klug (1969) have been chosen.

A separate study, however, has been made of the influence of the mixing height on the model results.

With the well-known model of Summers (1969) the minimum mixing height during the night can be calculated. Assuming a nightly heat output in the validation region of 100 W/m^2, it has been found that the height of the mixing layer during the night amounts to L_{NIGHT} = 150 m ± 70 m (average and standard deviation of this mixing height over the validation period).

A maximum mixing height can be calculated each day during the validation period with the method of Holsworth (1967). For this validation period L_{MAX} = 1200 m ± 1000 m (average and standard deviation of this mixing height over the validation period) has been found.

Interpolation by means of a sinus function between the daily maximum value of the mixing height and the value of the nightly mixing height then gives a value of the mixing layer for each time of the day. Next a distribution of mixing heights for each stability class and wind speed class can be constructed. This distribution function of mixing heights is then used in the model.

g) Deposition and decay.

The basic version of the model is run without taking into account the influence of removal processes. In order to estimate their effect a separate study of the influence of these processes on the calculated concentrations has been made.

Deposition was taken into account by using the deposition model described in Slade (1968). For the deposition velocity which enters into this model the value of 1 cm/s has been chosen, independent of stability and wind speed.

The effect of decay (including the effects of washout and rainout) has been modeled by applying an exponential damping term to the concentration formula. The half-life $\Lambda\left[s^{-1}\right]$ which enters into this damping term has been chosen for wet conditions: $(2\ \text{hours})^{-1}$ and for dry conditions: $(2\ \text{days})^{-1}$. In the 1st quarter of this validation 30% of the time wet weather conditions occurred (rain, snow).
From this result an effective half-life Λ_e has been constructed, as shown in table I.

III. Emission.

1. Validation area

The validation area is shown in figure 1. It is the Rijnmond region, including heavy industry, the port of Rotterdam, the cities of Rotterdam, Delft and The Hague and hothouse cultivation of fruit, vegetables and flowers in the Westland area and north of Rotterdam.

2. Components

The validation study was made for SO_2 only. For this component the most accurate set of emission data could be obtained by calculation from fuel consumption and sulfur content. In addition more measuring data were available for SO_2 than for any other component (see chapter IV). SO_2 can thus be considered to be the most suitable component for a validation.

3. Types of sources

A distinction was made between emissions in individual point sources and area sources.

- Individual stacks were used when they could be identified and emission data were quantifiable.
- Area sources were employed for the remainder of the emissions. On most occasions 1 km^2 sources were used, except when the actual area source was significantly smaller.
  The minimum size applied was 500 × 500 m.

4. Inventory

Two sets of emission data were used in the study: 1st and 3rd quarter of 1973.

a) 1st quarter of 1973

Individual stacks (see figure 1)

Emission data on the individual stacks in the area were obtained by means of an enquiry made among more than 60 affiliated industrial concerns by Stichting Europoort/Botlek Belangen, the coordinating body of industry in the region. Power station and other significant point source emissions in the area were collected in the same enquiry. The data obtained consisted of quarterly averaged SO_2 emissions together with stack dimensions, flue gas quantities and temperatures. In this way all data required on the 87 individual stacks emitting SO_2 were available for the validation study.

The emission data for the point sources are schematically shown in table II.

Area sources

For each square kilometer the average emission of SO_2 was determined. Depending on the type of emitter, an average effective source height was estimated on the basis of actual source height and plume rise estimates, which were always found to be small.

Groups of sources (see figure 1)

- Domestic heating in the Rotterdam and The Hague agglomerations.
- Hothouse cultivation in the Westland and the rest of the region.
- Shipping in main waterways and inland harbors and tanker emissions in the Europoort harbors.

Data on domestic and hothouse emissions were derived from a detailed study on SO_2 emissions in 1970/71, performed by Provincial Authority in Zuid-Holland (Provinciale Waterstaat in Zuid-Holland).
From detailed maps and local inspection the number of houses was estimated in each square kilometer within an urban area.
From data supplied by natural gas distributors it was possible to find the average domestic heating requirement for the first quarter as a percentage of annual consumption. From these results and the fraction of the houses which did not use gas for heating, the consumption of oil for domestic heating could be deduced. This procedure was chosen because oil consumption in the first quarter could not be directly estimated. From the sulfur content of the oil the annual SO_2 emission could then be calculated (the contribution to SO_2 emission by heating with natural gas is negligible).

In hothouse areas the fraction of the area which consisted of heated hothouses was estimated from the map by means of a planimeter and from results of local inspection. Heat requirement for hothouses per m^2 surface and sulfur content of fuel used, resulted in SO_2 emissions.

The 1970/71 data were updated to 1973 taking into account:
- new areas and extension of existing ones
- switch from fuel oil to natural gas, mainly in hothouse areas

From detailed natural gas consumption data it could be assessed that in the 1st quarter of 1973 the heat requirement expressed as a percentage of the year's total consumption was:

domestic: 38%
hothouse: 45%.

Shipping emission data are based on the results of a study by Stichting Europoort/Botlek Belangen. Information on ship traffic, including size, power installed, sulfur content and consumption of fuel and traveling times formed the basis of the data. A special category was introduced for the large tankers in the main harbors of Europoort.

b) 3rd quarter of 1973

Individual stacks

The 1st quarter data were used unchanged for the 3rd quarter. Although differences occurred in reality, a check on part of the sources revealed that they were too small to justify a separate enquiry.

Area sources

- Domestic heating. Although some emission will have taken place, the contribution to the immissions could be ignored.
- Hothouse. A significant contribution was expected from the Westland area only. From heat requirement estimates, as described in the emission inventory for the 1st quarter, it could be assessed that 8% of the year's total fuel consumption was burnt in the 3rd quarter.
- Shipping. 1st quarter data were used unchanged.

On the whole the 3rd quarter emission inventory can be expected to be inferior to the 1st quarter data, but certainly good enough for the validation study.

The contribution of road traffic to SO_2 emissions was not taken into account. At the time of the study no good inventory was readily available. Recent estimates by the Provincial Authority in Zuid-Holland show that a minor contribution to the immission by this kind of source may be expected.

IV. Immission data.

1. Concentration measurements.

During both validation periods the SO_2 concentration was measured at 124 measuring points. This large number of measuring points made a detailed validation possible.

Two measuring methods were used. The first method consists in collecting 24-hourly averaged samples, which were chemically analysed by means of the H_2O_2 method (OECD, 1964).
The second method consists in collecting 1-hourly averaged samples by a PW-9700 Philips SO_2 monitor, which makes use of a coulometric principle to measure the SO_2 content of the sample (Brouwer et al., 1971).

The results of 31 measuring points based on the latter method were available. These measuring points form the Rijnmond measuring network.

After inspection of the measuring data the results of three measuring points were found to be suspect in both validation periods and were further excluded from the validation calculations.

For the remaining measuring points an average for both validation periods was calculated.

2. Immission pattern for the 1st quarter of 1973.

In figure 2 the pattern is shown of the concentration averaged over the 1st quarter of 1973. This figure also shows the location of the measuring points which were used in the validation calculations of this period.

A high immission level is found in the Westland area, mainly due to the emissions of the hothouses.

3. Immission pattern for the 3rd quarter of 1973.

In figure 3 the pattern is shown of the concentration averaged over the 3rd quarter of 1973, together with the location of the measuring points which were used for the validation calculations of this period.

It is clear from a comparison with figure 2 that in the 3rd quarter the results of fewer measuring points have been taken into account. The results of the measuring points in the urban agglomeration of The Hague and in the

Westland area have been omitted for reasons to be discussed in the next chapter. It was found that the results of the Rijnmond measuring network for this period were significantly lower than comparable results from the 24-hour measuring equipment (figure 5).
Although no definite cause for this behavior could be indicated, it was nevertheless considered justifiable to exclude the results of the Rijnmond network from the validation calculations for this period.

The overall immission in the 3rd quarter is considerably lower than the immission in the 1st quarter. This is due to the fact that in the 3rd quarter the emission of the hothouses is greatly reduced compared to their emission in the 1st quarter. In the 3rd quarter the contribution to the immission by domestic heating is also negligible, compared to its contribution in the 1st quarter (see chapter III).

V. Results.

A. Validation in the 1st quarter of 1973.

It has been found that in this quarter, which falls in the winter season, the largest contribution to the concentration in almost all the receptor points is caused by the area sources. This validation therefore can be considered to be a validation for the area source model and its parameters.

1. Dispersion coefficients for low sources.

In table III the results are given for this validation for different parameters. Beside the model parameters for the area sources, the model parameters for the point sources have also been varied simultaneously. Since the contribution to the concentrations by the point sources is relatively small, the influence of a parameter change for the point sources may be ignored compared to the influence of a parameter change for the area sources.

The results in table III have been calculated from the calculated χ_c and observed χ_o concentrations averaged over the validation period for the receptor points, as discussed in chapter IV. From these concentration values in the receptor points the mean (m) and the standard deviation (s) of the observed χ_o and the calculated concentration χ_c and of the absolute and relative difference $\chi_o - \chi_c$ and $(\chi_o - \chi_c)/\chi_o$ has been calculated.
The correlation coefficient between χ_o and χ_c over all receptor points has also been calculated.

From table III it follows that with the Pasquill-Gifford coefficients the calculated concentrations are higher than the observed concentrations, whereas for the Fortak coefficients the opposite occurs.
This is because the Pasquill-Gifford coefficients are lower than the Fortak coefficients.

This difference between the two dispersion coefficients results in the first place from the difference in terrain roughness. The coefficients of Pasquill-Gifford are partly based on the results of the prairie-grass experiments, which took place in a terrain of small surface roughness (Cramer, 1959). The coefficients of Fortak are based on the results of McElroy and Pooler in St. Louis (McElroy, 1969), i.e. they are coefficients for an area with large surface roughness.

The dependence of the dispersion coefficients on the surface roughness for ground level sources can be described by the results of the Lagrangian similarity theory for neutral conditions (Pasquill, 1974).

$$\frac{\sigma_z}{x} = \frac{1.3\,k^2}{\ln\left(\frac{c\sigma_z}{1.3\,z_o}\right) - 1}$$

where x $[\mathrm{m}]$ is the distance and z_o $[\mathrm{m}]$ the roughness length of the terrain and where k and c are chosen as 0.4 and 0.6 respectively. Assuming a representative roughness for the Pasquill-Gifford coefficients of $z_o = 1$ cm and a representative roughness for the validation area of $z_o = 30$ cm, it is possible to calculate from this equation the quotient $\sigma_z(z_o = 30\ \mathrm{cm})/\sigma_z(z_o = 1\ \mathrm{cm})$ as a function of distance. This quotient ranges between 2.4 (x = 100 m), 1.8 (x = 1000 m) and 1.5 (x = 10000 m).

From these results it is concluded that the Pasquill-Gifford coefficients, multiplied by a constant factor of 1.8, form a set of dispersion coefficients which is more representative of the roughness of the area.
Although it is shown above that this coefficient should be a function of distance, a constant coefficient has been chosen for reasons of simplicity. The results obtained with these dispersion coefficients are also shown in table III. It follows that the difference between the calculated and the observed concentrations has decreased compared to the results obtained with the two original coefficients. In a scatter diagram (figure 4) the results obtained with the last set of dispersion coefficients have also been shown.

Because of the large number of effects that are involved in the dispersion of air pollutants and the resultant large amount of scatter in the results, it is difficult to draw definite conclusions.
However, it has been demonstrated that it is important to incorporate the effects of roughness in the dispersion coefficients for area sources and low point sources.

2. Background concentration

It has been attempted to calculate the background concentration in several ways (for example following the method described in Nieuwstadt, 1975). These estimates amount to a background concentration ranging from 10 to 30 $\mu g/m^3$.

Because of the uncertainty in this determined background concentration and in view of the fact that all the important sources in the neighborhood of the validation area have been taken into account, the contribution of the background concentrations to the calculated concentrations has been ignored.

3. Mixing height

As described in chapter II, the basic version of the model is run with one fixed mixing height for each stability class.

A comparison is made between the results of this basic version and the results of two other cases, I: no mixing height, II: a more detailed description of the mixing height as described in chapter II.

The results calculated from an average over a number of receptor points are shown in table IV. For both cases the relative concentration change with respect to the results of the basic version has been given for two different kinds of sources (point and area sources) as a function of distance.

If no mixing height is used (case I), the results of the area sources do not change appreciably. This is due to the fact that in the basic version the mixing height is too high to influence the dispersion of the area sources, which mainly occurs near the ground. The concentrations contributed by the point sources drop considerably for this case, because the dispersion of the plumes is no longer vertically restricted.

The results for case II show that the concentration contributed by area sources will increase. This is because on average the mixing height for this case is lower than the mixing height in the basic version.
For the point sources the results are only very slightly influenced.
This is probably caused by the balancing of two counteracting effects:
a) an increase in the contribution to the total concentration by the low point sources, because of the on average lower mixing height;
b) a decrease in the contribution by the high point sources, because some of these sources emit above the mixing height when it is low, and therefore do no contribute to the concentration at ground level.

4. Decay and deposition.

The influence of decay has been described by an effective half-life (chapter II). In table V the relative decrease is given of the concentration calculated with decay with respect to the concentration calculated with the basic version in which no decay is used. The results are not dependent on the kind of source. From the results shown in this table it may be concluded that the influence of the decay is negligible.

The influence of deposition on the concentration has been compared to the results of the basic version in which no deposition is applied. In table VI the relative concentration decrease is shown as a function of distance for two kinds of sources. The immissions of the area sources are heavily influenced by deposition. The point sources are less affected, because at first the plumes of the point sources are well above the ground, so that no deposition can take place. Later the pollution of the point sources extends over a large layer above the surface, and since deposition operates only at ground level the concentration depletion will then be relatively slow.

B. Validation in the 3rd quarter of 1973.

The model has been applied for this quarter, which falls in the summer season, in order to investigate the performance of the model for point sources. As has been discussed in chapter IV,the contribution from the area sources may then be expected to be very low. However, it was found that in the agglomeration of The Hague and in the Westland area the contribution of the area sources to the total immission in this quarter was not negligible. It was therefore decided not to take into account the measuring points in these areas for the validation results.

1. Dispersion coefficients for point sources.

In table VII the results have been given for this validation. These results have been calculated in the same way as the results for the validation of the 1st quarter shown in table III.

The results have been presented for two cases, for which the dispersion coefficients and the plume rise of the point sources have been varied. The influence of the change of dispersion parameters, which is applied simultaneously to the area sources, may be ignored.

In the first case the dispersion coefficients of Pasquill and of Singer and Smith were used. The coefficients of Pasquill were applied to sources with a physical stack height of less than 50 m and the coefficients of Singer and Smith to sources with a higher physical stack height. For sources with a heat output of less than 11 Mw the plume rise formula of Concawe was chosen and for higher heat outputs the formula of Briggs.

In the second case the coefficients of Klug are used for all the point sources together with the plume rise formula of K.S.L.A.

From the results in table VII it may be concluded, that taking into account the scatter of the model results, there is no significant difference between the results obtained with the two sets of parameters.

In figure 5 a scatter diagram is given of the results obtained with the set of parameters described above as the first case. In this figure the results of the Rijnmond network measuring points have been shown separately, for reasons discussed in chapter IV.

2. The contribution to the concentration by the very high point sources.

The very high point sources are tentatively defined as sources which have at least a physical stack height of 150 m and which have under normal conditions an effective stack height of around 400 m. In this validation only 4 stacks of the 87 point sources taken into account fall into this category. These 4 stacks are responsible for 64% of the emission of all point sources (table II).

It has been investigated how the contribution by these very high sources depends on the choice of dispersion coefficients. The other point sources have been calculated with one set of parameters described as the first case in the preceding section.

The mean (m) and standard deviation (s) over all receptor points of the relative contribution by the very high point sources is given in table VIII.

It follows from these results that the contribution of these very high sources is highly sensitive to a change in the dispersion parameters. This is caused by the fact that these very high sources have a large emission and therefore a change in the parameters for these sources may have a considerable effect on the total calculated concentration.

It is obvious that the Pasquill stability category, which is based on a description of the stability near ground level,will not be suitable as a stability class definition for these very high sources. Nor is it clear which dispersion parameters should be used for these sources,mainly because of the lack of experimental data, although from the validation results it could be concluded that the use of the Singer and Smith coefficients will probably seriously overestimate the contribution of the very high sources.
For some other recent investigations into the contribution by very high sources reference may be made to Clarke et al. (1976).

It must therefore be concluded that these sources and their contribution to the concentration should be carefully handled in a calculation with the Gaussian plume model for long-term averages and cannot yet be covered by a standardized calculation method.

VI. Summary and conclusions

A detailed and extensive validation of the long-term averaged Gaussian plume model has been performed in the Rijnmond region (Netherlands) for the component SO_2 and for the time periods 1st and 3rd quarter of 1973. An investigation has been made into the effects on the calculated concentrations of a variation of some model parameters: dispersion coefficients, plume rise formula, mixing height, deposition and decay.

The comparison between the calculated and measured concentrations for both quarters is shown in figure 4 and 5. The regression coefficients are about 0.9 for the 1st quarter and 0.8 for the 3rd quarter.

From the validation results of the 1st quarter it could be concluded that the effect of roughness should be included in the dispersion parameters for the low point sources and for area sources.

Other conclusions from these results are:
- the influence on the calculated concentration by a variation of the imposed mixing height depends on the source configuration;
- the influence of decay on the calculated results is small;
- the influence of deposition on the calculated concentration is substantial only for the area sources.

From the validation results of the 3rd quarter it could be concluded that results are relatively insensitive to a change in the dispersion parameters. This is probably caused by the fact that in the Rijnmond region, which can be considered as a complex source region (many sources of different dimensions), the effects of the parameter change on the concentration contribution by different sources will cancel each other out.

Another important conclusion from the results of this period is that the contribution of the very high sources is very sensitive to a change in the dispersion parameters; application of the dispersion coefficients of Singer and Smith will probably seriously overestimate the immission of the very high sources.

The results of this validation have led to a proposal for a Dutch National Air Pollution model. This proposal is included in this paper as an appendix.

Acknowledgements

The Stichting Europoort/Botlek Belangen made available the emission registration of the point sources.

The first author is indebted to the Director in chief of the Royal Netherlands Meteorological Institute,Dr. H.C. Bijvoet,for his permission to undertake this study.

Mr. C.A. Engeldal has contributed greatly to this validation by performing all the validation calculations.

The third author wishes to thank Mr. H.F. Kooij for his work on the emission registration of the area sources.

References.

Briggs, G.A.	Some recent analyses of plume rise observations. Proc. of the Second International Clean Air Congress (1971) p. 1029-1032
Brouwer, H.J. *de Veer, S.M.* *Zeedijk, H.*	The measuring network for SO_2 concentrations in the Rijnmond region. (in Dutch) Philips Technisch Tijdschrift, Vol.32, Nr. 2 (1971) p. 29-41
Brummage, K.G.	The calculation of atmospheric dispersion from a stack. Atm. Env. Vol. 2, (1968) p. 197-224
Calder, K.L.	A climatological model for multiple source urban air pollution. NATO-CCMS, Proc. 2nd Meeting on Air Pollution Modeling, (1971) p. I-1 - I-33
Clarke, A.J. *Spurr, G.*	Routine sulfur dioxide surveys around large modern power stations. Atm. Env. Vol. 10, Nr. 4 (1976) p. 265-268
Cramer, H.E.	A brief survey of the meteorological aspects of atmospheric pollution. B.A.M.S. Vol. 40, Nr. 4 (1959) p. 165
Dreyhaupt, F.J.	Praktische Anwendung der Ausbreitungrechnung zur Normierung von Schutzabstände zwischen emittierenden Industrie und Wohngebieten. VDI-Berichten Nr. 200 (1973)
Huisman, M.L. *Verheul, C.M.*	"Stacmap" Air Pollution Dispersion Model. (in Dutch) KIVI 1974 Koninklijk Instituut van Ingenieurs Prinsessegracht 23, Den Haag
Kleine Commissie TNO	Models for the dispersion of air pollution. (in Dutch) Staatsuitgeverij, Den Haag, 1976
Klug, W.	Ein Verfahren zur Bestimmung der Ausbreitungsbedingungen aus synoptischen Beobachtungen. Staub 29 (1969) Nr. 4
McElroy	A comparative study of urban and rural dispersion. Journal of Appl. Met., Vol. 8, Feb. 1969, p.19
Nieuwstadt, F.T.M. *van Dop, H.*	Validation of a multiple source diffusion model based on the Gaussian plume model. NATO-CCMS, Proc. 6th Meeting on Air Pollution Modeling (1975)
Nieuwstadt, F.T.M.	The Gaussian plume model. (in Dutch) KNMI WR 74-15 (1974)

OECD	Methods of measuring air pollution. OECD publ. (1964)
Pasquill, F.	Atmospheric diffusion. 2nd edition, J. Wiley (1974)
Provinciale Waterstaat in Zuid-Holland	Small SO_2 sources in South-Holland (1970-71) (in Dutch) Provinciale Waterstaat in Zuid-Holland Koningskade 2 Den Haag
Slade, D.H. (ed.)	Meteorology and atomic energy. U.S. Atomic Energy Commission
Summers	Unpublished Ph. D. Thesis University of Montreal (1964) Also discussed in Oke, T.R., Review of urban climatology 1968-1973, WMO-Technical Note No.134
Turner, D.B.	Workbook of atmospheric dispersion estimates. U.S. Dept, of Health, Education and Welfare, No. 999-AD-26 (1969)
Smith, M.E. *Singer, I.A.*	Atmospheric dispersion at Brookhaven National Laboratory. Int. J. Air and Water Poll. (1966) Vol. 10, p. 125-135

TABLE I

Effective half-life $\Lambda_e \left[s^{-1}\right]$ as a function of stability and wind speed classes.

Dry atmospheric conditions $\Lambda_d = 5.8.10^{-6}$ (2 days)$^{-1}$

Wet atmospheric conditions $\Lambda_w = 1.4.10^{-4}$ (2 hours)$^{-1}$

(wet conditions are assumed to occur only in stability class D)

Effective half-life $\Lambda_e = -\frac{U}{x} \ln(\alpha e^{-\Lambda_w x/U} + (1 - \alpha) e^{-\Lambda_d x/U})$

α = fraction of the time that wet conditions occur

x = the distance from the source (assumed to be 10^4 m)

Stability class	Wind speed class	$\Lambda_e \left[s^{-1}\right]$
A	all	$5.8.10^{-6}$
B	all	$5.8.10^{-6}$
C	all	$5.8.10^{-6}$
D	1: 0.5 - 2.5 m/s	$3.4.10^{-5}$
	2: 3 - 5.5 m/s	$4.2.10^{-5}$
	3: > 6 m/s	$4.3.10^{-5}$
E	all	$5.8.10^{-6}$
F	all	$5.8.10^{-6}$

TABLE II

SO_2 emissions of individual stacks, distinguished by construction height and heat output, 1st quarter of 1973.

In each block are indicated:

(number of stacks)
total SO_2 emission in kg/s

Q_H [MW] / h, [m]	≤ 1.0	1.0-10.0	10.1-20.0	20.1-50.0	50.1-100.0	> 100.0	sub-total →
≤ 25.0	(8) 0.0340	(5) 0.0750					(13) 0.1090
25.1-50.0	(11) 0.0502	(6) 0.0868	(1) 0.0072	(1) 0.0370			(19) 0.1812
50.1-75.0	(1) 0.0200	(10) 0.1505					(11) 0.1705
75.1 - 100.0		(11) 0.2668	(9) 0.7513	(4) 0.3203			(24) 1.3384
100.1 - 149.9		(10) 0.5690	(1) 0.0056	(4) 0.3051	(1) 0.0834		(16) 0.9631
≥ 150.0			(1) 0.3655	(1) 0.6510		(2) 3.8773	(4) 4.8938
sub-total ↓	(20) 0.1042	(42) 1.1481	(12) 1.1296	(10) 1.3134	(1) 0.0834	(2) 3.8773	TOTAL (87) 7.656

TABLE III

Validation results for the 1st quarter.

χ_c = calculated concentration in $\mu g/m^3$ at the receptor point } averaged over the validation period.
χ_o = observed concentration in $\mu g/m^3$ at the receptor point }

m,s = mean and standard deviation over all receptor points

r = correlation coefficient between χ_c and χ_o over all receptor points

n = number of receptor points

Area sources	Point sources		χ_o		χ_c		$\chi_o-\chi_c$		$(\chi_o-\chi_c)/\chi_o$		r	n
disp. coeff.	disp.coeff.	plume rise	m	s	m	s	m	s	m	s		
I Pasquill	Singer/Smith Pasquill	Briggs Concawe	96.6	44.8	129.1	77.0	-32.5	44.1	-0.32	0.45	0.87	121
II Fortak	Klug	K.S.L.A.	96.6	44.8	74.7	31.4	21.9	22.3	0.19	0.23	0.89	121
III Pasquill (multiplied by 1.8)	Singer/Smith Pasquill	Briggs Concawe	96.6	44.8	107.5	58.9	-10.9	30.0	-0.11	0.36	0.87	121

TABLE IV

Influence of the mixing height.
Relative concentration change in % with respect to the results of the basic version (one mixing height for each stability class).

Case I: no mixing layer.

Case II: simulation of the mixing layer (described in chapter II)

distance from the source in km	area sources		point sources	
	I	II	I	II
0 - 15	0	16	-32	-5
15 - 30	-9	73	-67	-5

TABLE V

Influence of decay.
Relative concentration decrease in % with respect to the results of the basic version (no decay).

distance in km.	relative concentration decrease in %
0 - 10	3
10 - 20	9
20 - 30	20

TABLE VI

Influence of deposition.

Relative concentration decrease in % with respect to the results of the basic version (no deposition).

distance in km	relative concentration decrease in %	
	area sources	point sources
0 - 10	10	2
10 - 20	31	7
20 - 30	45	11

TABLE VII

Validation results for the 3rd quarter.
(for notation see table III)

Area sources	Point sources		χ_o		χ_c		$\chi_o-\chi_c$		$(\chi_o-\chi_c)/\chi_o$		r	n
disp.coeff.	disp.coeff.	plume rise	m	s	m	s	m	s	m	s		
I.Pasquill (multiplied by 1.8)	Singer/Smith Pasquill	Briggs Concawe	39.1	16.1	42.4	23.8	-3.3	14.7	-0.10	0.43	0.80	70
II Fortak	Klug	K.S.L.A.	39.1	16.1	32.9	14.3	6.2	10.0	0.11	0.35	0.79	70

TABLE VIII

Relative contribution of the very high sources in % to the total concentration at each receptor point.
The point sources have been calculated with dispersion coefficients of Singer /Smith and Pasquill and with the plume rise formula of Briggs and Concawe.
The area sources have been calculated with the coefficients of Pasquill (multiplied by a factor of 1.8).

m = the mean of the relative contribution over all receptor points.
s = the standard deviation of the relative contribution over all receptor points.

dispersion coefficient used for very high sources	relative contribution in %	
	m	s
Singer/Smith	35	11
Pasquill	15	8

Legends to the figures

figure 1 SO_2 emission configuration in the 1st quarter of 1973

Domestic heating:	D1 + D2 :	0.10 kg/s
	D3 :	0.15 kg/s
Hothouses:	H1 :	2.10 kg/s
	H2 + H3 :	0.28 kg/s
Industry:		7.66 kg/s
Shipping:		0.38 kg/s
	total	10.67 kg/s = 922 t/day

figure 2 Pattern of measured SO_2 concentrations ($\mu gr/m^3$) averaged over the 1st quarter of 1973. The dots indicate the measuring points on which the pattern is based.

figure 3 Pattern of measured SO_2 concentrations ($\mu gr/m^3$)averaged over the 3rd quarter of 1973. The dots indicate the measuring points on which the pattern is based.

figure 4 Scatter diagram of observed concentrations χ_o and calculated concentrations χ_c at the measuring points. Each point is an average over the 1st quarter of 1973. The parameter used for the calculated results are indicated as case III in table III. The solid line is the linear regression line.

figure 5 Scatter diagram of observed concentrations χ_o and calculated concentrations χ_c at the measuring points.Each point is an average over the 3rd quarter of 1973. The parameters used for the calculated results are indicated as case I in table VII. The solid line is the linear regression. The crosses indicate the measured and calculated results for the Rijnmond network, which have not been taken into account for the validation in the 3rd quarter.

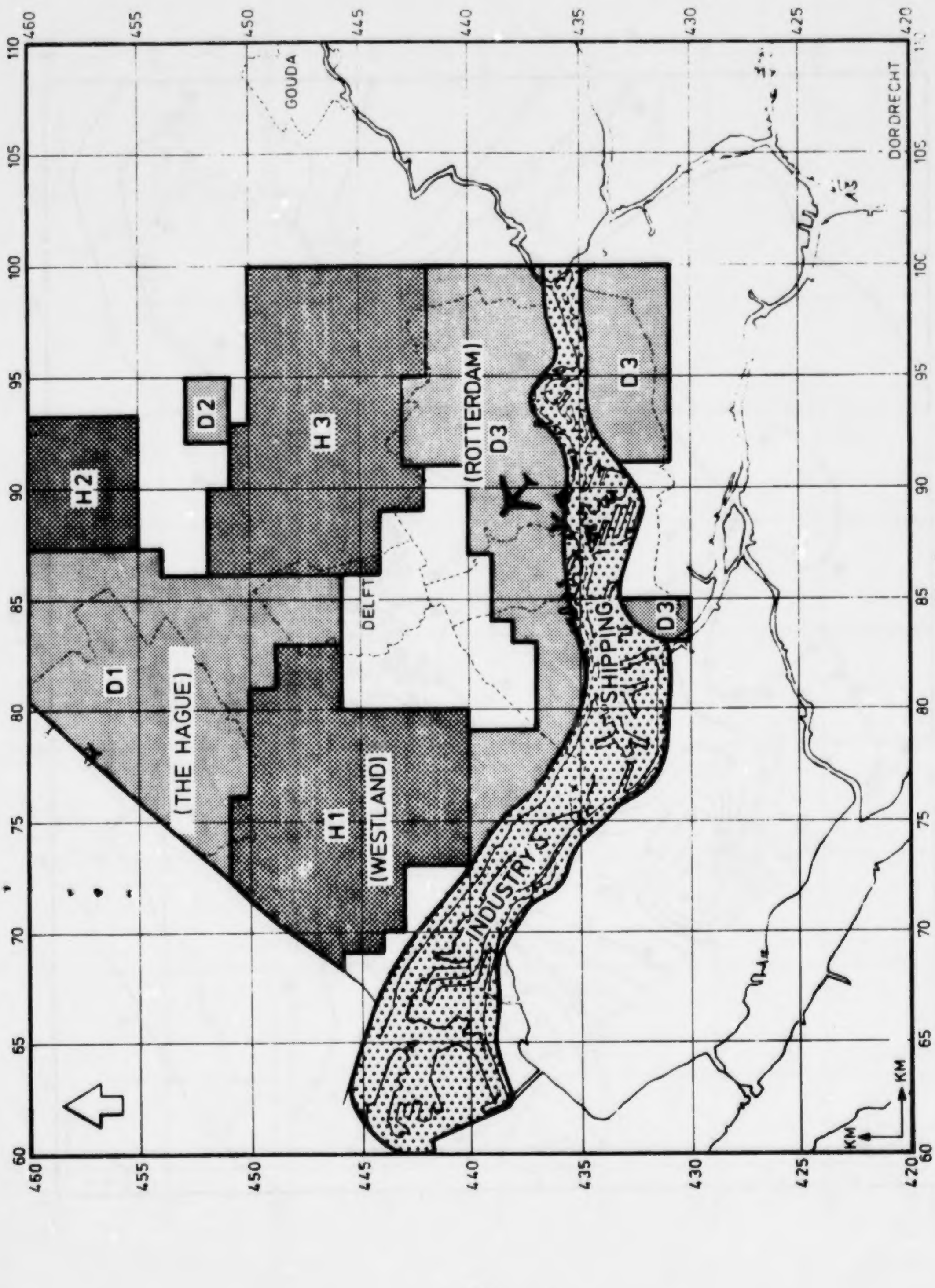
H1
H2
H3
D1
D2
D3
D3
D3
(THE HAGUE)
(WESTLAND)
(ROTTERDAM)
DELFT
GOUDA
DORDRECHT
INDUSTRY
SHIPPING
KM
KM
60
65
70
75
80
85
90
95
100
105
110
420
425
430
435
440
445
450
455
460

Fig.1

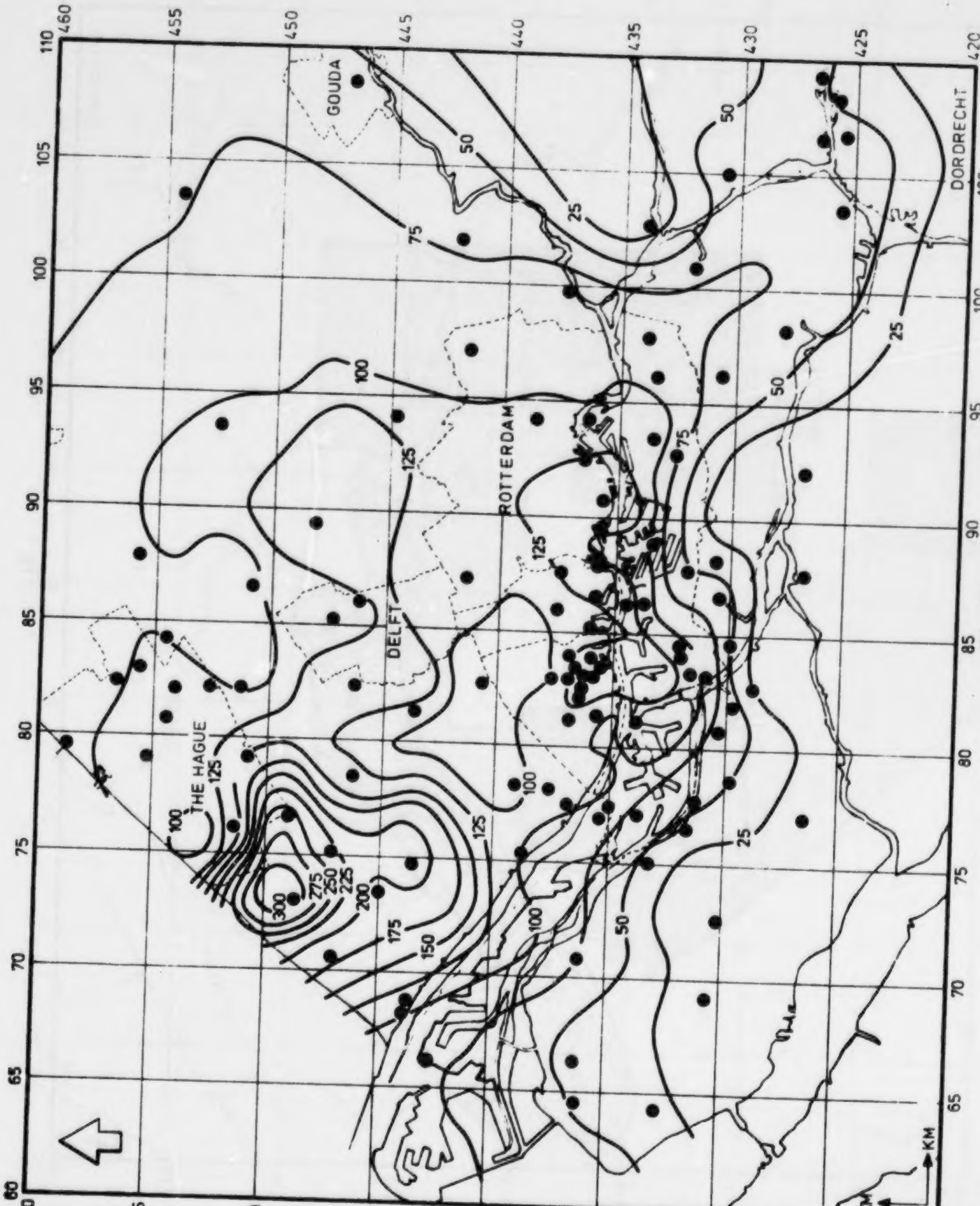

THE HAGUE
DELFT
ROTTERDAM
GOUDA
DORDRECHT
300
275
250
225
200
175
150
125
100
75
50
25
KM
KM
60
65
70
75
80
85
90
95
100
105
110
420
425
430
435
440
445
450
455
460

Fig. 2

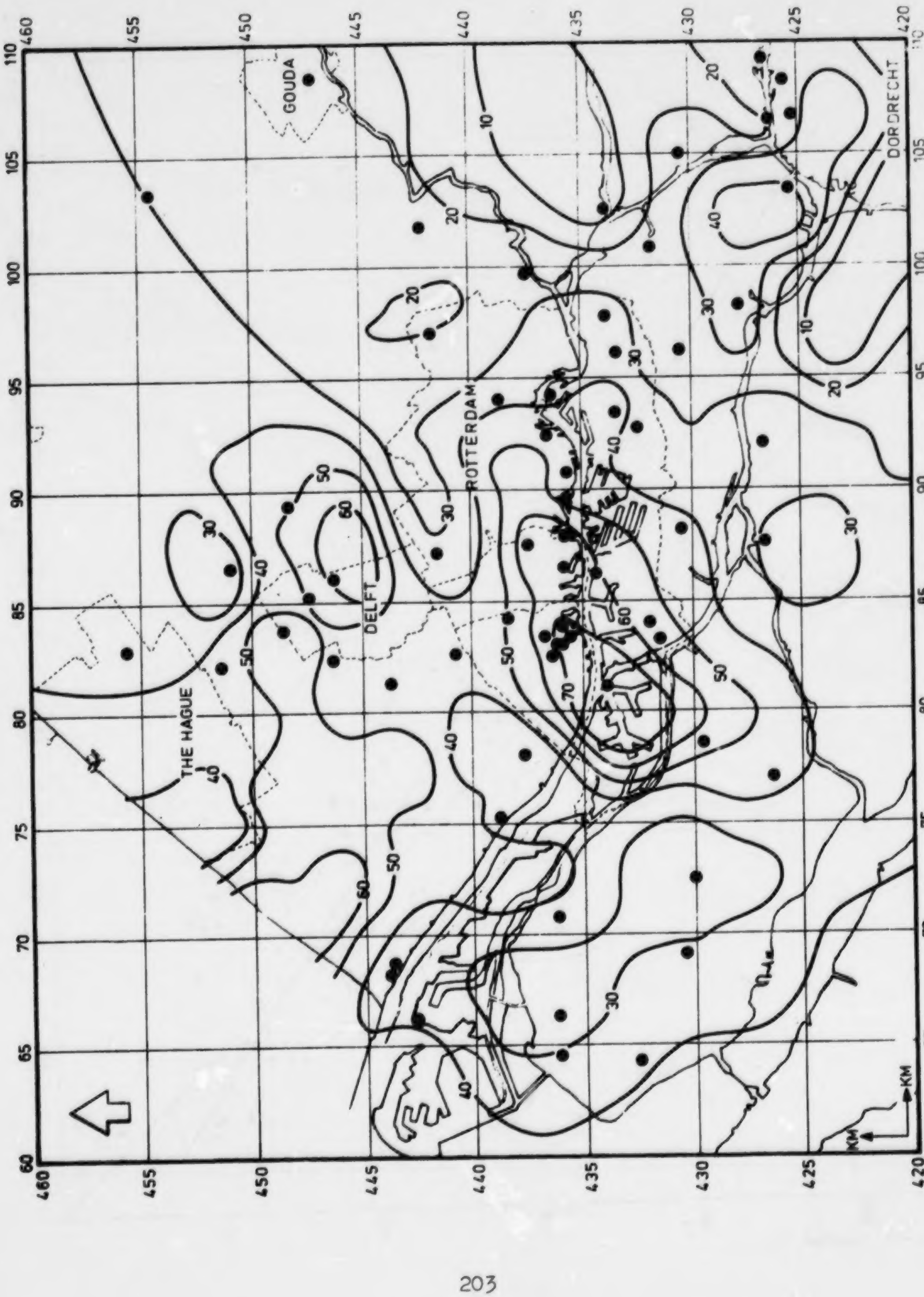
THE HAGUE
DELFT
ROTTERDAM
GOUDA
DORDRECHT
KM
KM
60
65
70
75
80
85
90
95
100
105
110
420
425
430
435
440
445
450
455
460
10
20
30
40
50
60
70

Fig. 3

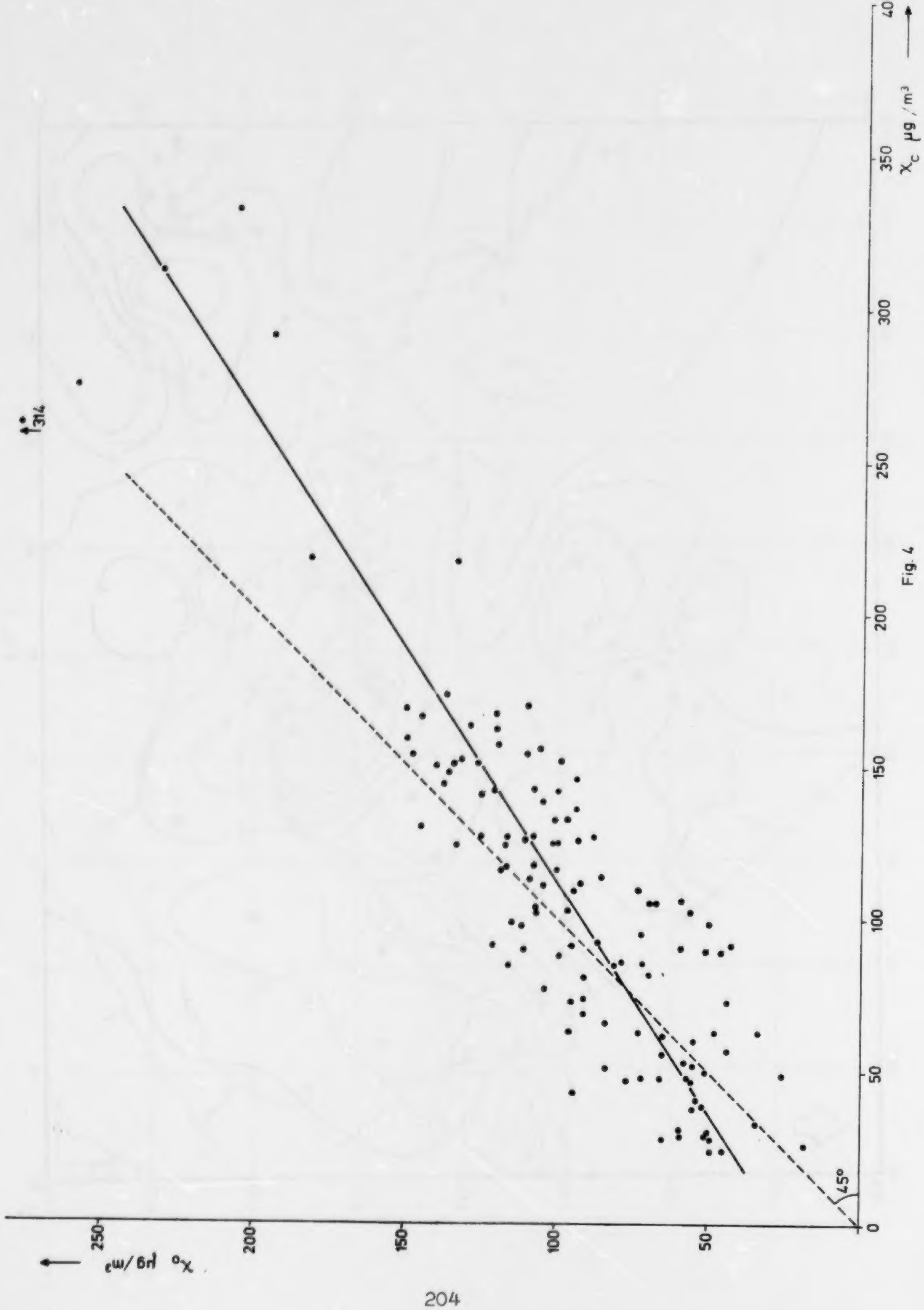

χo μg/m³
250
200
150
100
50
0
50
100
150
200
250
300
350
400
χc μg/m³
45°
314

Fig. 4

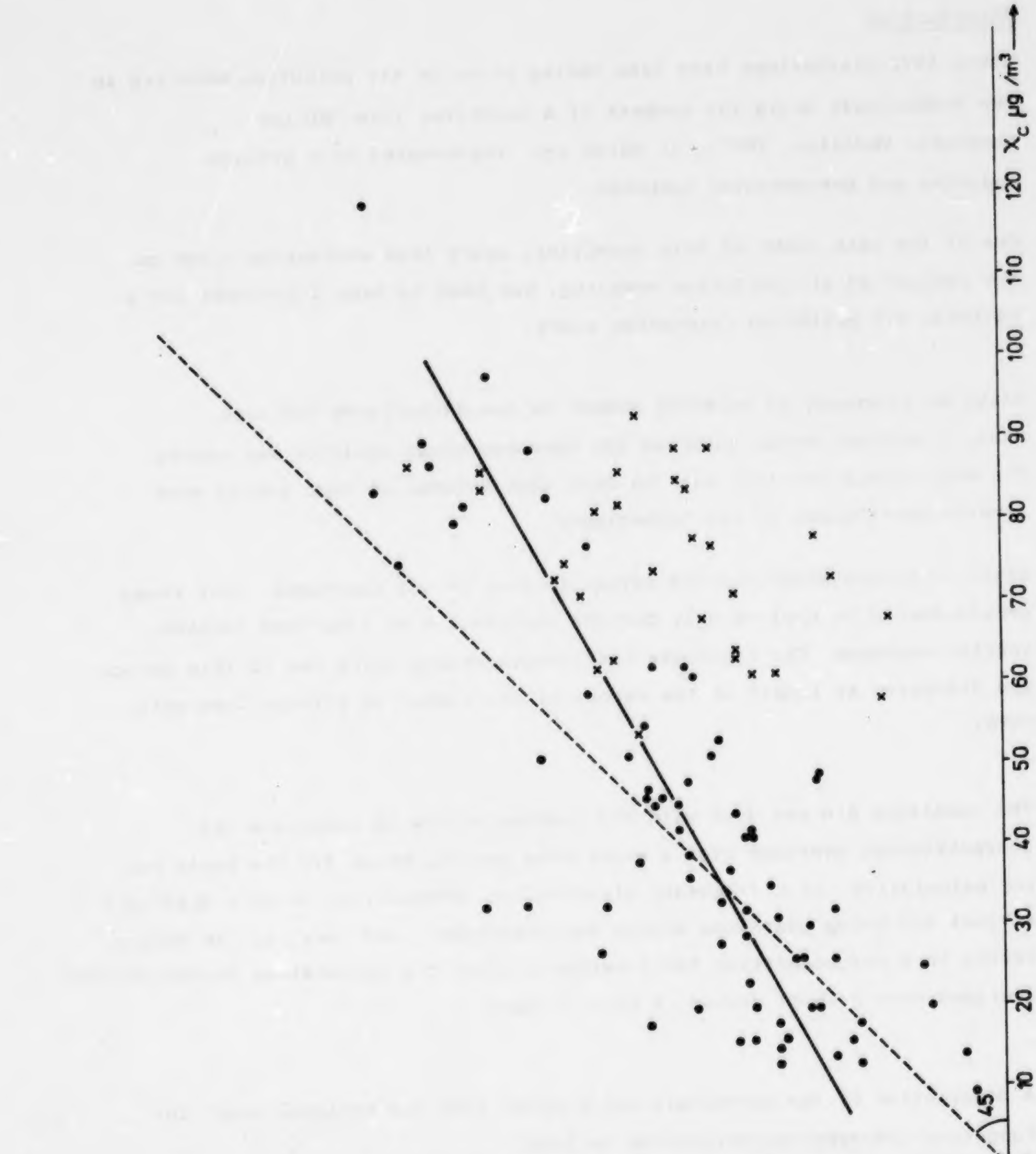

Fig.5

APPENDIX

Recommendation for the parameters in the long-term averaged Gaussian plume model.

I. *Introduction*

Since 1972 discussions have been taking place on air pollution modeling in the Netherlands among the members of a committee (the "Kleine Commissie Modellen, TNO"), in which are represented both private industry and governmental agencies.

One of the main tasks of this committee, apart from exchanging views on the subject of air pollution modeling, has been to make a proposal for a national air pollution dispersion model.

After an inventory of existing models in the Netherlands had been made, a national model based on the Gaussian plume equation was chosen. The main reason for this was the fact that several of such models were already operational in the Netherlands.

After various discussions and investigations it was concluded that these models should be applied only for the calculation of long-term (season, yearly) averages. The arguments and investigations which led to this choice are discussed at length in the report of the committee (Kleine Commissie, 1976).

The committee did not deal with the problem of how to calculate the concentrations averaged over a short time period, which are the basis for the calculation of a frequency distribution. Discussions on this difficult subject are being continued within the committee, and may, in the future, result in a recommendation for a national model for calculating concentrations averaged over a short period (1 hour, 1 day).

A description of the parameters which enter into the national model for long-term averaged concentrations follows.
They have been chosen partly on a basis of the results of an extensive validation of the model (Nieuwstadt et al., 1976), and partly on theoretical grounds.

It should be mentioned separately that for the *very* high sources (physical stack height $\geqq$ 150 m and effective stack height > approx. 400 m) no definite recommendation could be made.

In the following sections the equations are given for the long-term Gaussian plume model and for the parameters which enter into the model.

These directives form an interrelated entity. It is not advisable to use individual parameters of this recommendation in combination with other parameters.
The arguments behind the choice of these parameters are extensively discussed in the report of the "Kleine Commissie" (1976).

II. Recommended parameters

2.1 The long-term Gaussian model.

The concentration averaged over a long period (season, year) $\bar{C}\left[g/m^3\right]$ at ground level, as a result of a source at the location: (0,0,H), is described by

$$\bar{C}(x,y) = \sum_S \sum_N \left\{ \frac{2Q}{\sqrt{2\pi}\, u_N \sigma_{z_S}} \cdot f(\theta,S,N)\, \frac{n}{2\pi r} \cdot C_{L_S} \cdot \exp\left(-\frac{H^2_{S,N}}{2\sigma^2_{z_S}}\right) \right\}$$

In this equation $r\left[m\right]$ is the horizontal distance from the source: $r = \sqrt{x^2 + y^2}$. The source has an emission $Q\left[g/s\right]$.

The concentration is given in a sector $2\pi/n$ in width around the direction $\theta + 180^\circ$ (θ indicates the wind direction class, defined as a sector also $2\pi/n$ in width around θ).
The vertical dispersion coefficient $\sigma_z\left[m\right]$ is classified according to stability classes (S).
The transport velocity of the plume $u\left[m/s\right]$, calculated from the wind speed, is subdivided into wind speed classes (N). $H\left[m\right]$ is the effective source height, which follows from the physical stack height $h\left[m\right]$ and the plume rise $\Delta h\left[m\right]$. The function $f(\theta,S,N)$ gives the distribution over the wind speed, wind direction and stability classes. The coefficient C_{L_S} describes the influence exerted on the ground level concentration by the mixing height (2.8).

For a discussion on the derivation of this equation and the underlying assumptions see the literature, e.g. Calder (1971), Pasquill (1974).

2.2 Stability classes (S).

To determine the stability class the KNMI scheme, which is a modification of the Pasquill stability class definition, is chosen. The stability class is defined from the amount of clouds (in eighths), the wind speed at a height of 10 m (in knots, 1 knot = ½ m/s), the time of the day and the season (see figure A).

The dispersion coefficients for high sources are classified after the stability class definition by Singer and Smith (1966).
A tentative relation between the stability classes after the KNMI definition and after the Singer and Smith definition is

KNMI		Singer and Smith
A	→	B_2
B	→	B_2
C	→	B_1
D ($u \leqq 5.5$ m/s)	→	B_1
D ($u > 5.5$ m/s)	→	C
E	→	D
F	→	D

where u is the wind speed at a height of 10 m.

2.3 The distribution function of wind direction classes, stability classes and wind speed classes $f(\theta,S,N)$.

The distribution function consists of a frequency distribution over 6 stability classes S (2.2), 3 wind speed classes N and 12 wind direction classes θ of the size of $2\pi/n = 30^\circ$ ($345^\circ - 015^\circ$, $015^\circ - 045^\circ$ etc.).

After an investigation it was found that for planning purposes it was sufficient to perform the calculations with the distribution function of only two meteorological stations: the distribution function of the Schiphol meteorological station for the north and west of the Netherlands (which is the area near the coast), and the distribution function of the Eindhoven station for the eastern and southern interior regions of the country. Both distribution functions are given in figures B and C.

For more specific calculations, for instance a validation of the model against measured concentrations, the distribution function of the most representative meteorological station should be used.

For the 3 wind speed classes the representative wind velocity at a height of 10 m is defined as

Wind speed class	Wind speed limits	Representative wind speed
1	1-5 kts (0.5-2.5 m/s)	1.45 m/s
2	6-11 kts (3-5.5 m/s)	4.0 m/s
3	$\geqq$ 12 kts ($\geqq$ 6 m/s)	8.0 m/s

2.4 Dispersion coefficients (σ_z).

The dispersion coefficients are a function of the height above the earth's surface, because the turbulence on which the dispersion coefficients depend is a function of the height above the surface. The recommendation for the dispersion coefficients is therefore subdivided according to the effective source height H.

a) Low sources ($H \leqq 10$ m) and area sources.

σ_z according to Pasquill (1974).

$\sigma_z = ar^b \times C_{z_0}$ (σ_z and r in m)

Stability class	a	b
A	0.28	0.90
B	0.23	0.85
C	0.22	0.80
D	0.20	0.76
E	0.15	0.73
F	0.12	0.67

The coefficient C_{z_0} describes the effect of the surface roughness on the dispersion coefficient. The roughness of the area where the source is situated is characterized by the roughness length $z_0[m]$ (Pasquill, 1974).

For $z_0 = 0.10$ m it follows that $C_{z_0} = 1$. For other values of z_0 the coefficient C_{z_0} (derived from Figure 6.13 (d) from Pasquill, 1974) becomes

$$C_{z_0} = (10\ z_0)^{0.53}\ r^{-0.22}$$

$z_o[m]$ is the roughness length and $r[m]$ the horizontal distance from the source (2.1).

Some representative values for z_o are

	z_o
flat country (e.g. polder landscape with a few trees)	approx. 0.03 m
agricultural land (e.g. airfield, arable land, polder with many trees)	approx. 0.10 m
cultivated land (e.g. hothouse area, open area with much vegetation, scattered houses)	approx. 0.30 m
residential area (e.g. area with many but low buildings, wooded area, industrial area with not too high obstacles)	approx. 1.00 m
urban area (e.g. a big city with high buildings, industrial area with high obstacles)	approx. 3.00 m

b) High sources ($100 \leqq H <$ circa 400 m).

σ_z according to Singer and Smith (1966)

$\sigma_z = ar^b$ (σ_z and r in m).

Stability class	a	b
B_2	0.411	0.907
B_1	0.326	0.859
C	0.223	0.776
D	0.062	0.709

c) Sources with an effective height 10 m < H < 100 m.

The σ_z is determined for each value of r by means of a linear interpolation:

$$\sigma_z = \sigma_z(a)(100-H)/90 + \sigma_z(b)(H-10)/90$$

where $\sigma_z(a)$ is the σ_z as calculated according to a) and $\sigma_z(b)$ is the σ_z as calculated according to b).

d) *very* high sources ($h \geqq 150$ m and $H >$ approx. 400 m).

For these sources no reliable values of σ_z could be estimated. The immissions of these sources must be calculated separately in consultation with specialists, in order to take into account the most recent information on the dispersion from these sources.

2.5 Plume rise (Δh)

The plume rise is calculated with formulas of Briggs (1970)

$$\Delta h = 109\, Q_H^{3/4}/u \qquad Q_H < 6 \text{ MW}$$

$$\Delta h = 143\, Q_H^{3/5}/u \qquad Q_H \geqq 6 \text{ MW}$$

The Q_H is the heat output of the sources in MW. The u is the wind velocity at the top of the stack (h) (calculated by means of the equation given in 2.7).

An upper limit to the plume rise is set by the equation

$$\Delta h = 115 (Q_H/u)^{1/3}$$

This equation results from the plume rise formula of Briggs (1970) for stable conditions, with the temperature gradient parameter s equal to 1.4 10^{-4}.

The Q_H is calculated with respect to an average air temperature of 15° C.

2.6 Transport velocity (u).

The transport velocity of the plume must be representative of the entire layer in which the diffusion takes place. This velocity is calculated from the representative wind speed at a height of 10 m (u_{10}) for each wind speed class N (2.3). From the wind speed u_{10} the wind velocity u(z) at an arbitrary altitude z can be calculated by means of the equation given in 2.7.

In the calculation of the transport velocity a classification is applied after the effective source height, analogous to the classification of the dispersion coefficients (2.4).

a) Point sources ($H \leqq 10$ m): the wind velocity at a height of 10 m: u_{10}.

Area sources: the wind velocity at the effective source height H (with a minimum of H = 10 m): u(H)

b)(100 m < H <approx. 400 m).
I. $H \leqq \frac{1}{2}L$ $\quad u = u(H)$ $\quad$ if $0.62\,\sigma_z \leqq H$
$u = u(0.62\sigma_z)$ $\quad$ if $H \leqq 0.62\,\sigma_z \leqq \frac{1}{2}L$
$u = u(\frac{1}{2}L)$ $\quad$ if $0.62\,\sigma_z > \frac{1}{2}L$
II. $H > \frac{1}{2}L$ $\quad u = u(H)$
in the case of $L \leqq H \leqq 3/2\, L$: $u = u(L)$

The σ_z is calculated according to 2.4 b. The mixing height L is discussed in 2.8.

c) $(10 \leqq H \leqq 100$ m).

For all distances the transport velocity u is determined by a linear interpolation.

$$u = u(a)(100 - H)/90 + u(b)(H - 10)/90$$

where u(a) is the transport velocity as calculated according to a) and where u(b) is the transport velocity as calculated according to b), with σ_z following from 2.4 b and with H chosen as equal to 100 m.

2.7 Wind profile according to a power law.

The wind speed at an arbitrary height z[m] is calculated from the wind speed at a height of 10 m: u_{10} by means of the equation

$$u(z) = u_{10}\,(z/10)^p$$

The exponent p is a function of the stability class.

Stability class according to Pasquill	p
A	0.10
B	0.10
C	0.16
D	0.16
E	0.30
F	0.30

2.8 Mixing height.

The mixing height sets a limit to the vertical dispersion.
For each stability class one fixed mixing height is chosen.

Stability class according to Pasquill	L(in m)
A	1500
B	1500
C	1000
D	500
E	200
F	200

The influence of the mixing height on the ground level concentration is determined by the coefficient C_{L_S} (2.1).

	C_{L_S}
$0 < \sigma_z/L \leqq 0.6\sqrt{1-H/L}$	1
$0.6\sqrt{1-H/L} < \sigma_z/L < 0.9$	$1+\left[\exp\left\{-\frac{(2L-H)^2}{2\sigma_z^2}\right\}+\exp\left\{-\frac{(2L+H)^2}{2\sigma_z^2}\right\}\right]\Big/\exp\left\{-H^2/2\sigma_z^2\right\}$
$\sigma_z/L > 0.9$	$\frac{1}{L}\,\frac{\sqrt{2\pi}\,\sigma_z}{2\exp(-H^2/2\sigma_z^2)}$

This last factor leads to the uniform vertical distribution of the concentration in the mixing layer. In the evaluation of C_{L_S} the σ_z is calculated according to 2.4 a, b, or c.

When $h > L$ holds good, it is assumed that the plume is above the mixing layer and for that reason will not contribute to the concentration at ground level.

It is also assumed that for $H > 3/2\ L$ the plume will break through the inversion capping the mixing layer and will not contribute to the ground level concentration either. When $L \leqq H \leqq 3/2\ L$, the effective source height H is set equal to the height of the mixing layer L.

2.9 Area sources.

An area source is for practical reasons subdivided into squares with a side of 1 km.

To calculate the dispersion from an area source the virtual point source equation is used. The virtual point source is situated in the middle of each square of the area source. The ground level concentration from each virtual point source is calculated with the equation

$$\overline{C}=\sum_{S}\sum_{N}\left\{\frac{Q\ f(\theta,N,S)}{u_N\left(\sqrt{\frac{\pi}{2}}\,\sigma_{z_S}\,\frac{2\pi r}{n}+\frac{A}{K}\right)}\,C_{L_S}\,\exp\left(-\frac{H_{S,N}^2}{2\sigma_{z_S}^2}\right)\right\}$$

For an explanation of most of the parameters used in this equation see section 2.1.

The emission Q is the total emission $[g/s]$ of the area source square. The initial vertical dispersion inside the area source is simulated by adding a virtual distance $r_o[m]$ to the horizontal distance $r[m]$ in the evaluation of σ_z: $\sigma_z(r + r_o)$.

The virtual distance r_o is determined from the equation $\sigma_z(r_o) = H$, where H is the effective source height of the area source and where the σ_z for each stability class is calculated according to 2.4 a, b, or c, the roughness correction included.

The initial horizontal mixing inside the area source is described by the term A/K in the denominator of the above equation. The $A[m^2]$ is the area of the area source.

The factor K is a function of the size of the area source square. For a square of 1 × 1 km K can be chosen as equal to 50.

The virtual point source model should not be used for calculating the ground level concentration inside the area source square.

References.

Briggs, G.A.	Some recent analyses of plume rise observation. Proc. 2nd International Clean Air Congress, 6-11 dec. 1970, Academic Press, N.Y. (1971), p. 1029-1032.
Calder, K.L.	A climatological model for multiple source urban air pollution. Proc. 2nd Meeting on Air Pollution Modeling, NATO-CCMS, Nr. 5,(1971)
Kleine Commissie TNO	Air Pollution Dispersion Models.(In Dutch), Staatsuitgeverij, The Hague, Netherlands.(1976)
Nieuwstadt, F.T.M. *Verheul, C.M.* *Addicks, J.*	The validation of the Gaussian dispersion model for long-term average ground level concentrations in the Rijnmond region, NATO-CCMS, 7th International Meeting on Air Pollution Modeling (1976).
Pasquill, F.	Atmospheric diffusion. 2nd ed., John Wiley & Sons (1974).
Singer, I.A. *Smith, M.E.*	Atmospheric dispersion at Brookhaven National Laboratory. Int. J. of Air & Water Poll. 10 (1966)

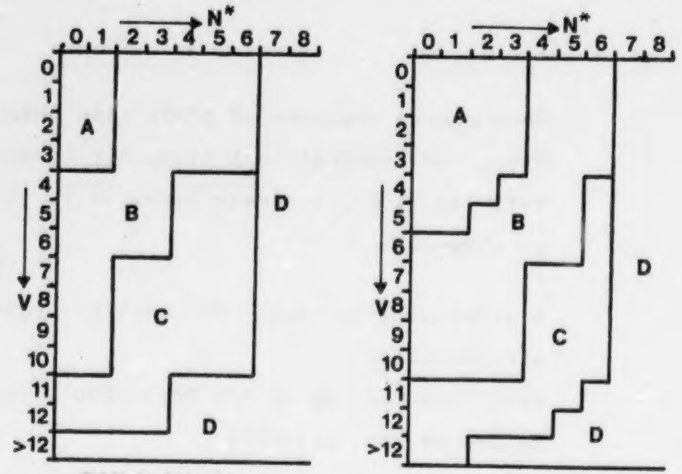

DAY (winter) DAY (spring)

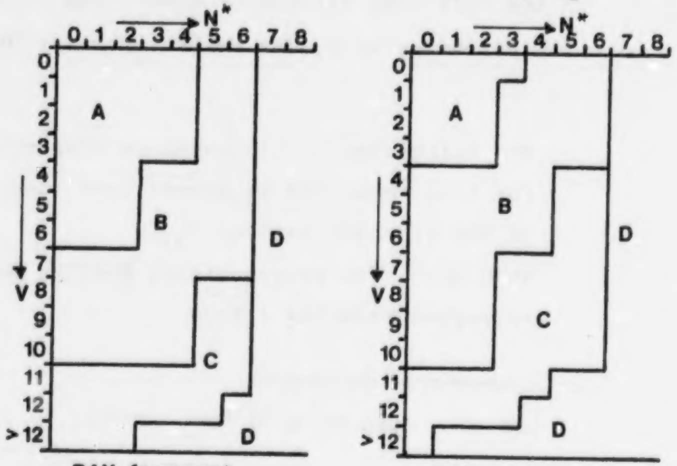

DAY (summer) DAY (fall)

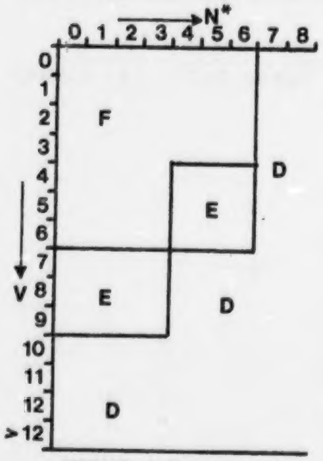

NIGHT (all seasons)

(hours in GMT)

		DAY	NIGHT
WINTER	december	9–15	16–8
	january	9–16	17–8
	february	9–16	17–8
SPRING	march	8–17	18–7
	april	7–18	19–6
	may	6–19	20–5
SUMMER	june	5–20	21–4
	july	6–18	19–5
	august	6–18	19–5
FALL	september	7–17	18–6
	october	8–16	17–7
	november	9–15	16–8

V= windspeed in knots (1 knot≅½ m/s)
N*= cloudiness of the sky in eights

FIGURE A. STABILITY CLASS DEFINITION

Average yearly climatology of Schiphol

indicated: number of hourly observations in wind speed class N,

wind direction class θ and stability class S

total number of observations: 179112

S ⟶	A	A	B	B	C	C	C	D	D	D	E	E	F	F
N ⟶	1	2	1	2	1	2	3	1	2	3	1	2	1	2
θ ↓														
0	170	30	234	533	40	470	352	1075	2761	2984	175	601	1260	271
1	153	26	161	624	25	483	630	744	2082	2872	99	536	689	181
2	200	44	206	1209	45	688	1214	986	3514	5616	93	909	866	345
3	279	42	239	990	40	461	441	1168	3641	3497	133	1310	1022	372
4	202	19	211	553	34	300	147	1028	2490	1372	145	620	879	221
5	195	27	217	521	48	367	101	1350	4070	3123	212	984	984	318
6	223	28	302	514	55	491	117	1766	5586	5617	319	973	1284	338
7	166	23	218	465	42	593	164	1476	6356	11480	240	1112	822	304
8	180	29	226	487	33	584	555	1507	4456	13153	259	780	1093	266
9	186	30	258	757	32	780	536	1286	3661	9744	169	520	809	174
10	146	24	196	575	36	572	285	989	2584	6063	148	397	664	125
11	165	36	208	535	46	571	309	1082	2817	4539	160	495	983	169

Wind speed class N : 1 0,5 - 2,5 m/s (1 - 5 kts)
2 3,0 - 5,5 m/s (6 - 11 kts)
3 6,0 m/s (12 kts)

Stability class S ; A, B, C (unstable) D (neutral) E,F (stable)

Wind direction class θ:

North = 000°

θ	
0	345° - 015°
1	015° - 045°
2	045° - 075°
3	075° - 105°
4	105° - 135°
5	135° - 165°
6	165° - 195°
7	195° - 225°
8	225° - 255°
9	255° - 285°
10	285° - 315°
11	315° - 345°

FIGURE B.

Average yearly climatology of Eindhoven

indicated: number of hourly observations in wind speed class N,
wind direction class θ and stability class S
total number of observations: 167547

S ⟶	A	A	B	B	C	C	C	D	D	D	E	E	F	F
N ⟶	1	2	1	2	1	2	3	1	2	3	1	2	1	2
θ ↓														
0	265	27	350	549	54	532	172	1159	2112	1465	137	405	1009	219
1	310	35	428	794	78	530	225	1699	2621	1300	179	665	1520	321
2	343	66	370	1295	71	622	543	1296	3222	2076	144	1142	1607	471
3	310	41	295	1070	65	516	487	994	2322	1936	118	902	1010	316
4	283	27	323	667	66	442	234	1321	2574	1578	285	721	1269	328
5	277	29	341	336	73	304	38	1670	2657	1049	291	581	1304	259
6	203	19	321	391	62	489	81	1902	4195	3562	335	705	1273	235
7	173	16	386	504	70	713	172	2078	6726	10621	347	1046	1217	363
8	166	31	326	706	88	1044	293	2051	7614	14283	275	1037	865	264
9	109	26	303	423	53	754	142	1755	4883	7796	272	646	834	225
10	118	20	247	380	63	542	122	1214	2947	3756	164	352	759	155
11	142	22	261	419	55	539	154	1138	2473	2412	163	279	909	136

Wind speed class N : 1 0,5 - 2,5 m/s (1 - 5 kts)
2 3,0 - 5,5 m/s (6 -11 kts)
3 ≥ 6,0 m/s (≥ 12 kts)

Stability class S : A,B,C (unstable) D (neutral) E,F (stable)

Wind direction class θ : 0 345° - 015°
1 015° - 045°
2 045° - 075°
3 075° - 105°
4 105° - 135°
5 135° - 165°
6 165° - 195°
7 195° - 225°
8 225° - 255°
9 255° - 285°
10 285° - 315°
11 315° - 345°

North = 000°

FIGURE C.

7th International Technical Meeting on Air Pollution Modeling and It's Application

A DUAL TRACER STUDY FOR THE VALIDATION OF MODELS WITH RESPECT TO HIGH AND LOW ALTITUDE SOURCES

by

J.H. Overton, Jr.
Northrop Services, Inc.
Research Triangle Park, NC

B.K. Lamb and F.H. Shair
Department of Chemical Engineering
California Institute of Technology
Pasadena, California 91125

W.E. Wilson, Jr.
Environmental Protection Agency
Research Triangle Park, NC

September 7-10, 1976
Airlie, Virginia
United States of America

The Regional Air Pollution Study (RAPS) in St. Louis has as its overall goal the development of improved air quality models and the creation of a data base for evaluation and validation of models. The Midwest Interstate Sulfur Transport and Transformation Study (Project MISTT) is concerned with the dispersion of sulfur pollutants from energy-producing sources. The Industrial Environmental Research Laboratory is interested in determining the relative contribution of high-altitude, rural sources (new power plants with tall stacks located outside cities) compared to low-altitude, urban sources (industrial boilers with short stacks located within urban areas). To meet these three needs, an experimental field study was planned.

Recent investigations have shown that gaseous tracers, suitable for electron capture detection, may permit detailed transport and dispersion data to be obtained more rapidly and cheaply than by other techniques.[1,2,3,4] To obtain information on the dispersion of pollutants from low-altitude and high-altitude sources under identical meteorological conditions, it was decided to attempt a dual tracer study. One tracer (SF_6) would be added to high-altitude sources and a second (CF_3Br) to low altitude sources.

The study was conducted during the summer of 1975 by personnel from the California Institute of Technology. A description of the experiment and a complete data set are available.[1] Persons wishing to use this data set to evaluate models may obtain the report from EPA.*

The purposes of this paper are (1) to discuss the results of a tracer study performed to obtain specific transport and dispersion data from low and high altitude sources and (2) to compare the results with values calculated from an existing air quality model.

The Experiments

Tracers were released from high-altitude rural and low-altitude urban points. The initial goal of the tracer program was to release SF_6 through one of the five outer lying power plants surrounding St. Louis. However, because of the strike occurring at the Union Electric Company during the time specified for the field studies, the elevated rural source was simulated by releasing SF_6 at the top of the KETC-TV tower. The daytime low-altitude releases were made from RAMS Site No. 111. The nighttime low-altitude urban release was made from the parking lot of Webster College. The height and location of the tracer releases, as well as the release rates, are given in Table 1. The locations are shown on the map in Figure 1.

Sequential air samplers were located throughout the St. Louis region at 21 Regional Air Monitoring System (RAMS) stations. The air samplers (made by Developmental Science, Incorporated) permitted the collection of hourly averaged air samples each hour for 12 consecutive hours.

Automobile traverses were made by having a passenger in each of three cars take grab samples in 30 cm^3 plastic syringes. Generally, samples were collected every 0.1, 0.2, 0.3, 0.4, or 0.5

---

*W.E. Wilson, Environmental Protection Agency, MD-57, Research Triangle Park, NC 27711

TABLE 1

TRACER RELEASE INFORMATION

Date	Test	Height and Location of SF_6 Release	Release Period (CDT)	Release Rate GRAMS/SECOND	Height and Location of CF_3 Br Release	Release Period (CDT)	Release Rate GRAMS/SECOND
8/8/75	(1)	100 feet from RAMS Site No. 111	11:00am until 3:00pm	9.6	30 feet from RAMS Site No. 111	11:00am until 3:00pm	7.0
8/9/75	(2)	1000 feet from KETC-TV Tower	10:30am until 3:00pm	9.2	100 feet from RAMS Site No. 111	10:40am until 3:00pm	8.1
8/11/75	(3)	1000 feet from KETC-TV Tower	10:40am until 3:00pm	6.1	100 feet from RAMS Site No. 111	10:00am until noon	7.9
8/12-13/75	(4)	20 feet from parking lot of Webster College	8:40pm until 3:00am	6.2	- - -	- - -	---
8/15/75	(5)	100 feet from RAMS Site No. 111	8:35am until 2:25pm	7.1	20 feet from RAMS Site No. 111	9:30am until 1:30pm	

TABLE 2. COMPARISON OF CALCULATED AND MEASURED CONCENTRATIONS OF SF_6 (ppt)

	Test #1 (8/8/75) Time of Day - CDT				Test #3 (8/11/75) Time of Day - CDT			
Station Number	11-12	12-1	1-2	2-3	11-12	12-1	1-2	2-3
101	0	2/0	0	-	0/1	2/7	0/1	0
102	-	6/0	0	0	0	0/17	26/17	8/4
103	-	0	0	0	0	0/4	0	0
104	0	0	0	0	0	0/0	0	0
105	4/0	0	5/0	-	0/1	0/1	0	0
106	12/279	13/206	4/79	0/32	0/8	27/26	6/11	7/1
109	5/0	-	1/0	-				
110	0	2/0	0	0				
112	6/9	36/65	63/172	46/189				
113	0	-	1/0	2/0	0	0	9/6	7/21
114	0	0	0	0	5/0	0	7/12	13/29
115	0	0	0	-	0	0	0/3	0
116	0	0	0	-	0	0	0	0
117	0	0	0	0				
118	0	0	4/0	0	0	0	0	0
119	0	0	0	0	6/15	22/18	18/22	44/18
120	-	-	-	-	0	0	0	0
121	0	0	0/2		0	0	0	0

Single entry: Both calculated and experimental concentrations are the same. Double entry: Experimental/calculated stations not included either had faulty data, no sample taken or a value of zero.

miles, depending upon the distance from the release point and the steadiness of the wind. The total traverse distance and length of time were recorded. Since the car speed was constant, the times at which the samples were taken can be computed.

Both tracers, SF_6 and $CBrF_3$, were analyzed using electron capture gas ch. 'graphy. Analytical and operating details for the electron capture chromatography detection of SF_6 are described elsewhere.[2] Calibration of all the chromatographs was accomplished by means of a well-mixed exponential dilution system. Concentrations down to 10^{-12} part SF_6/part air can be detected at a signal-to-noise ratio of better than 3 to 1. In the case of $CBrF_3$, the detection limit is approximately 1×10^{-9} part $CBrF_3$/part air. The chromatogram peaks were integrated with an Autolab System I electronic digital integrator (Spectra-Physics, Santa Clara, California). Twelve gas chromagraphs and two digital integrators were set up. Approximately 100 SF_6 samples or 40 $CBrF_3$ samples could be analyzed per hour of operation. The uncertainty of the test data was approximately ±8%.

Experimental Results

The results of the five days of experiments are illustrated with data from experiments 1 and 3. Hourly-averaged concentrations (ppt) taken at RAMS stations are given in Table 2. Plots of concentrations versus distance along traverses are given in Figures 2, 3, 5, and 6. The simulated values are given along with the experimental data and will be discussed later.

Experiment No. 1: August 8, 1975 - Daytime Releases from 30 Feet and 100 Feet above Ground

During Experiment No. 1, SF_6 was continuously released from 11:00 am until 3:00 pm from a point 100 feet above ground level at RAMS 111 at a rate of 9.6 grams/second. $CBrF_3$ was continuously released from 11:00 am until 3:00 pm at a point 30 feet above ground level from RAMS 111 at a rate of 7.0 grams/second. The purpose of Experiment 1 was to characterize dispersion from low urban sources and to test the differences in dispersion between two such sources, one at 100 feet and one at 30 feet.

Between 11:56 am and 2:32 pm, twelve automobile traverses were conducted; the SF_6 plume was clearly identified in nine traverses. The relationship between six of the traverses (7 through 12) and the source location is illustrated in Figure 1. Traverses 7, 8 and 9 are along Highway 40. The segment of highway along which data was observed was from 7 to 10 miles from the source. The wind, from the southeast, makes an angle of about 45° with the traverses. Traverses 10, 11 and 12 were on Highway 44. The detectable data was on a segment that approximates a circular arc of radius 6 miles from the source.

Graphs of SF_6 concentration versus distance along a traverse are shown in Figure 2 for 7, 8 and 9, and Figure 3 for 10,11 and 12. $CBrF_3$ was not detected.

Experiment No. 3: August 11, 1975 - Daytime Releases from 100 Feet and 1000 Feet above Ground

On the day of Experiment 3, SF_6 was released continuously from 10:40 am until 3:00 pm at a rate of 6.1 grams/second. The KETC-TV tower was used to provide a release point 1000 feet above the ground. $CBrF_3$ was continuously released from 10:00 am until noon at a rate of 7.9 grams/second. This tracer was released at 100 feet above the ground from RAMS 111. The purpose of Experiment 3 was to provide a comparison between dispersion from high, rural sources and low, urban sources.

Eleven automobile traverses were taken from 10:58 am to 2:26 pm; SF_6 was detected in seven traverses. A map of the source location and highways over which traverses 3 through 8 were carried out is shown in Figure 4. Traverses 3, 4 and 5 are along Highway 40. The segment of highway along which data was observed is from 15 to 23 miles away from the source and makes an angle of about 60° with the wind direction. Samples for traverses 6, 7 and 8 were collected along a segment of Highway 44 which ranged from 10 to 20 miles from the release point. The angle between the wind vector and the road varied from 45° to about 90°. Graphs of the data are found in Figure 5 for traverses 3, 4 and 5 and in Figure 6 for 6, 7 and 8.

$CBrF_3$ was found in three traverses, each within 1.5 miles of the source at RAMS 111. Figure 7 illustrates the relationship between the traverses and the source as well as how the $CBrF_3$ was distributed along the traverses. Figure 8 is a plot of the concentrations on an absolute scale.

Simulation of Tracer Experiment Model

The model used was developed at IBM for EPA by C.C. Shir and L.J. Shieh. It is essentially the same model discussed by these authors in Reference 5. EPA's model differs somewhat from the journal version; it is described in Reference 6.

While this is essentially an Eulerian grid model, it does accommodate point source plumes. This model was chosen for two reasons. It will be used for modeling the St. Louis area as part of the RAPS study. Therefore it was of interest to know how well it would handle a point source plume. This model had been modified for the St. Louis area, was available in an operational computer code, and could be readily modified for use with the tracer data set.

The model grid (see Figure 1) covers an area 60 km in the north-south direction and 40 km in the east-west direction and is centered at RAMS station 101. This grid is divided into 1200 grid elements, each element having an area of 1 or 2 square kilometers depending on the elements location. The smaller elements are located in the center urban region while the larger ones are on the outer suburban region.

An abbreviated description of the model is taken from the computer program reference manual (Reference 6):

The governing equation in the atmosphere, based on the mass conservation law, is

$$\frac{\partial C}{\partial t} + \nabla \cdot \underset{\rightarrow}{V} C = K_H \nabla_H^2 C + \frac{\partial}{\partial z} K \frac{\partial C}{\partial z} + Q, \qquad (1)$$

where C is the mean concentration, $\underset{\rightarrow}{V} = (U,V,W)$ is the mean wind vector, Q is the source strength rate, K_H is the horizontal eddy diffusivity, ∇_H^2 is the horizontal Laplacian operator, and K is the vertical eddy diffusivity. Point sources are handled by utilizing a Lagrangian plume trajectory.

$\underset{\rightarrow}{V}$ is determined from the hourly-averaged surface wind speeds and directions that are recorded at the 25 RAMS stations. Values above the ground are computed using a power law formula. The vertical diffusivity, K, depends on atmospheric stability, wind speed, surface roughness and the height of the boundary layer. The mixing height, H, is determined from sounding taken twice during the day. For the present study values were available from soundings taken at approximately the center of the grid (Upper Air Network station 141, see Figure 1.) at about 10 am and 3 pm. The mixing heights used by the program were obtained by a linear interpolation between the two times. More precise definitions of how $\underset{\rightarrow}{V}$, K, K_H and z_o are computed can be found in References 5 and 6. They are computed once for each hour of simulated time (i.e., $\underset{\rightarrow}{V}$ is based on hourly averages).

Equation (1) is solved numerically using a second-order central finite-difference scheme. The time step is variable depending on an internally set accuracy requirement and in our simulations varied from two to four minutes.

Results of Simulations

The results of simulating tracer Experiments 1 and 3 are shown with the experimental data in Table 2 and Figures 2, 3, 5, 6, and 8. For Experiment 1 (source 100 feet high) both the hourly averages and the traverse data show essentially no agreement as far as the values of the concentration are concerned. The simulated values are much larger than the experimental. Much better agreement is obtained with the position of the concentration peaks along the traverses (Figures 2 and 3).

For Experiment 3, the results of the SF_6, 1000 ft. source height release, are given in Table 2 and Figures 5 and 6. Unlike the case for Experiment 1, the simulated concentration peaks are not all too large but are bigger or smaller than the experimental peaks depending on the particular traverse.

Figure 8 illustrates the results of simulating the $CBrF_3$ release in Experiment 3. Here the simulated values are consistantly much less than the experimental data; however, the locations of the experimental and simulated data along the traverses agree.

Only a modest attempt has been made so far to explain the differences between the simulated and experimental data by perturbing some of the input parameters. Source locations, stack height and mixing height were chosen because they could be varied without changing the program. The source location was changed by ± 1 km perpendicular to the approximate wind direction and ± 1 km along the wind direction. Stack and mixing heights were altered by ± 10%. In no case did the changes cause significantly better agreement. There is reasonable agreement in position and width of the plumes. Therefore, further investigations should be directed toward K, the vertical eddy diffusivity.

LITERATURE CITED

1. Shair, F.H., B.K. Lamb, J.H. Overton, and W.E. Wilson, Jr. A Dual Tracer Study of Validation of Models with Respect to High and Low Altitude Sources. EPA-600/3-77-000.

2. Drivas, P.J. (1974) "Investigation of Atmospheric Dispersion Problems by Means of a Tracer Technique," Ph.D. Thesis, California Institute of Technology, Pasadena, California 91125.

3. Drivas, P.J. and F.H. Shair (1974). "A Tracer Study of Pollutant Transport and Dispersion in the Los Angeles Area," Atmos. Environ., 8, 1155-1163.

4. Drivas, P.J. and F.H. Shair (1975). "The Chemistry, Dispersion, and Transport of Air Pollutants Emitted from Fossil Fuel Power Plants in California: Plume Tracer (SF_6) Measurement and Analysis," Final Report for California Air Resources Board Contract No. ARB 3-915, 1709 11th Street, Sacramento, California.

5. Shir, C.C. and L.J. Shieh. "A Generalized Urban Air Pollution Model and Its Application to the Study of SO_2 Distribution in the St. Louis Metropolitan Area." J. Appl. Meteor., 13, 185-204.

6. Shir, C.C. and L.J. Shieh. Development of Urban Air Quality Simulation Model Compatible with Compatible RAPS Data. EPA Contract No. 68-02-1833, May 1975.

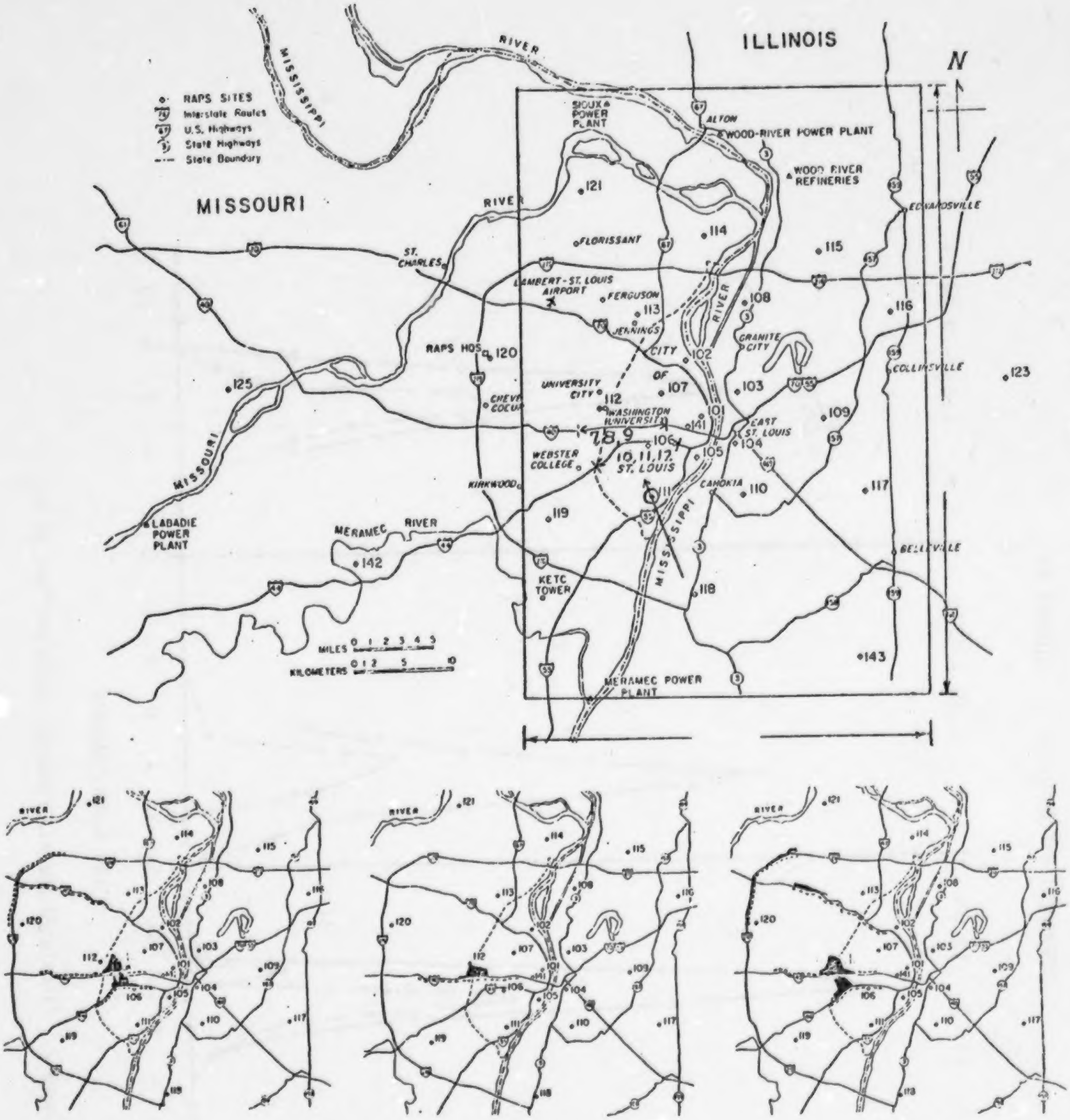
ILLINOIS
MISSOURI
N
RAPS SITES
Interstate Routes
U.S. Highways
State Highways
State Boundary
MISSISSIPPI
RIVER
MISSOURI
MERAMEC RIVER
SIOUX POWER PLANT
ALTON
WOOD-RIVER POWER PLANT
WOOD RIVER REFINERIES
EDWARDSVILLE
ST. CHARLES
FLORISSANT
LAMBERT - ST. LOUIS AIRPORT
FERGUSON
JENNINGS
GRANITE CITY
RAPS HQS
UNIVERSITY CITY
CITY OF
WASHINGTON UNIVERSITY
COLLINSVILLE
CHEVY CHASE
EAST ST. LOUIS
WEBSTER COLLEGE
ST. LOUIS
CAHOKIA
KIRKWOOD
BELLEVILLE
LABADIE POWER PLANT
KETC TOWER
MERAMEC POWER PLANT
MILES 0 1 2 3 4 5
KILOMETERS 0 1 2 5 10
7,8,9
10,11,12
101
102
103
104
105
106
107
108
109
110
111
112
113
114
115
116
117
118
119
120
121
123
125
141
142
143

AUTO TRAVERSES
- > 1 12:00-12:10 p.m. CDT
- -> 4 12:30-12:40 p.m. CDT
- ► 7 11:58-12:08 p.m. CDT
- ► 10 11:56-12:02 p.m. CDT
- * RELEASE POINT

MAX. [SF$_6$] = 156 ppt.

AUTO TRAVERSE:
- -> 8 1:32-1:42 p.m. CDT
- * RELEASE POINT

MAX. [SF$_6$] = 104 ppt.

AUTO TRAVERSES:
- > 3 2:00-2:10 p.m. CDT
- -> 6 2:21-2:32 p.m. CDT
- ► 9 1:58-2:08 p.m. CDT
- ► 12 1:53-2:00 p.m. CDT
- * RELEASE POINT

MAX. [SF$_6$] = 166 ppt.

Figure 1. Location of source and traverses for experiment 1, St. Louis, 8/8/75.

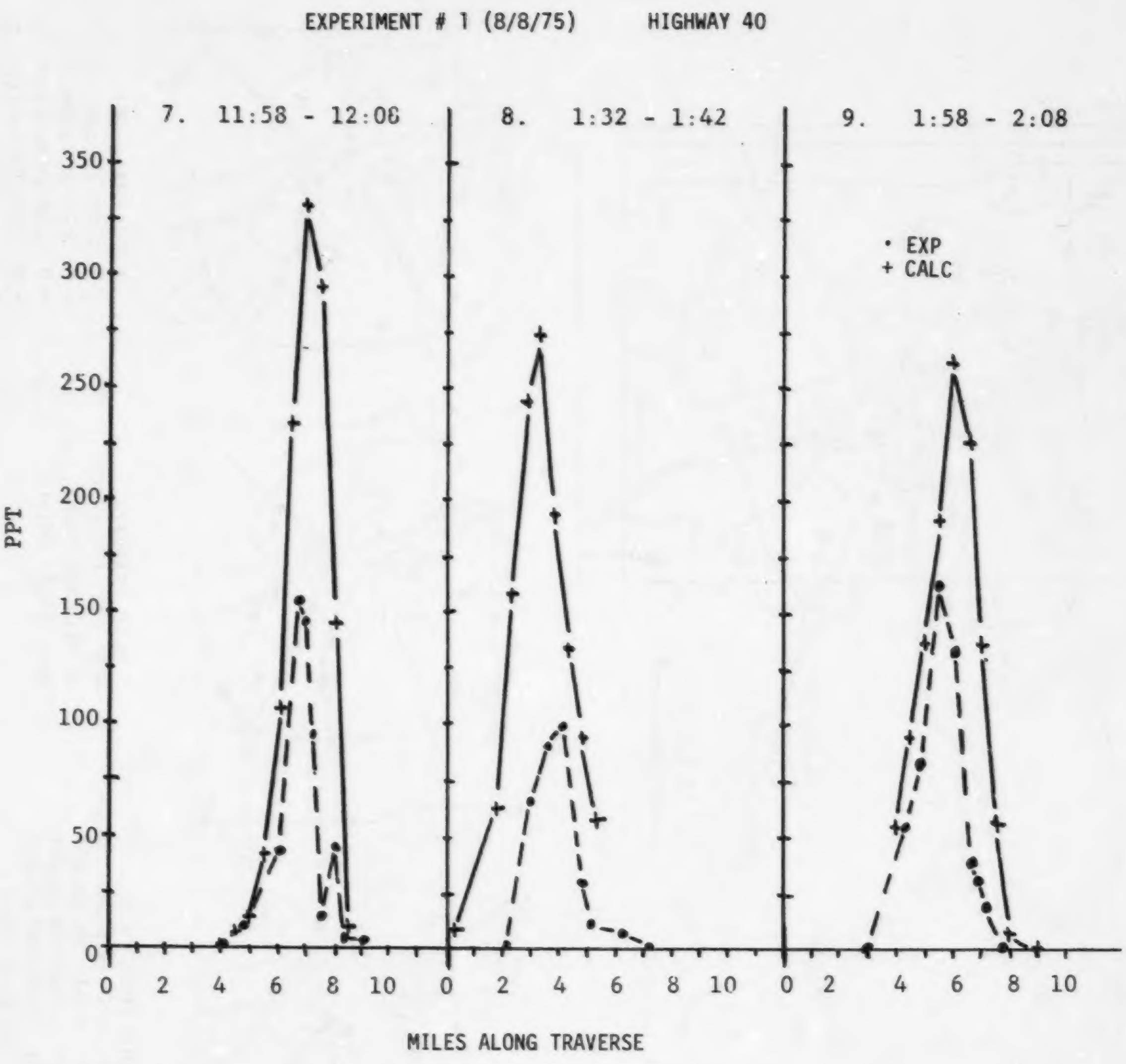

Figure 2. Calculated and experimental concentrations of SF_6.

EXPERIMENT # 1 (8/8/75), HIGHWAY 44

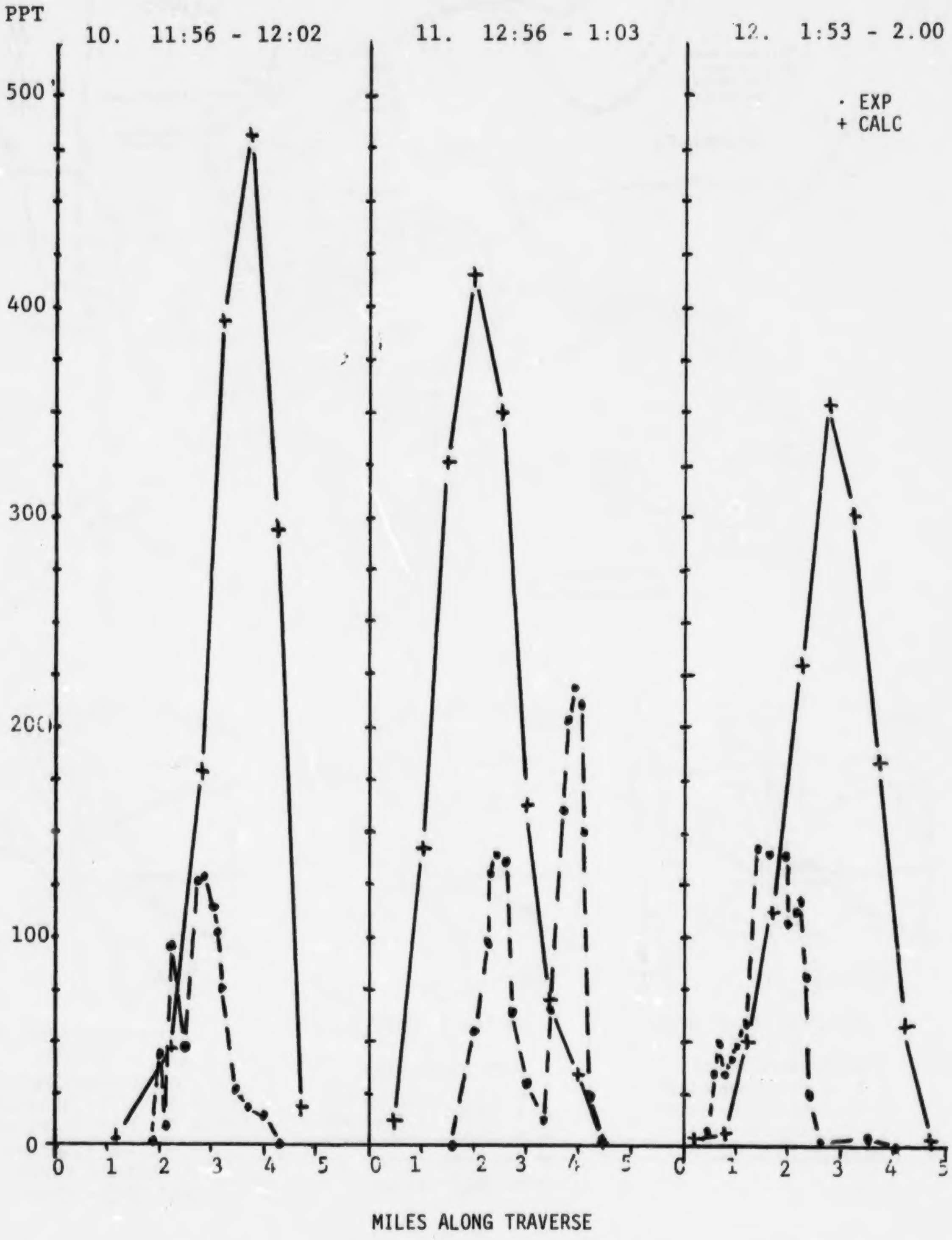

Figure 3. Calculated and experimental Concentrations of SF_6.

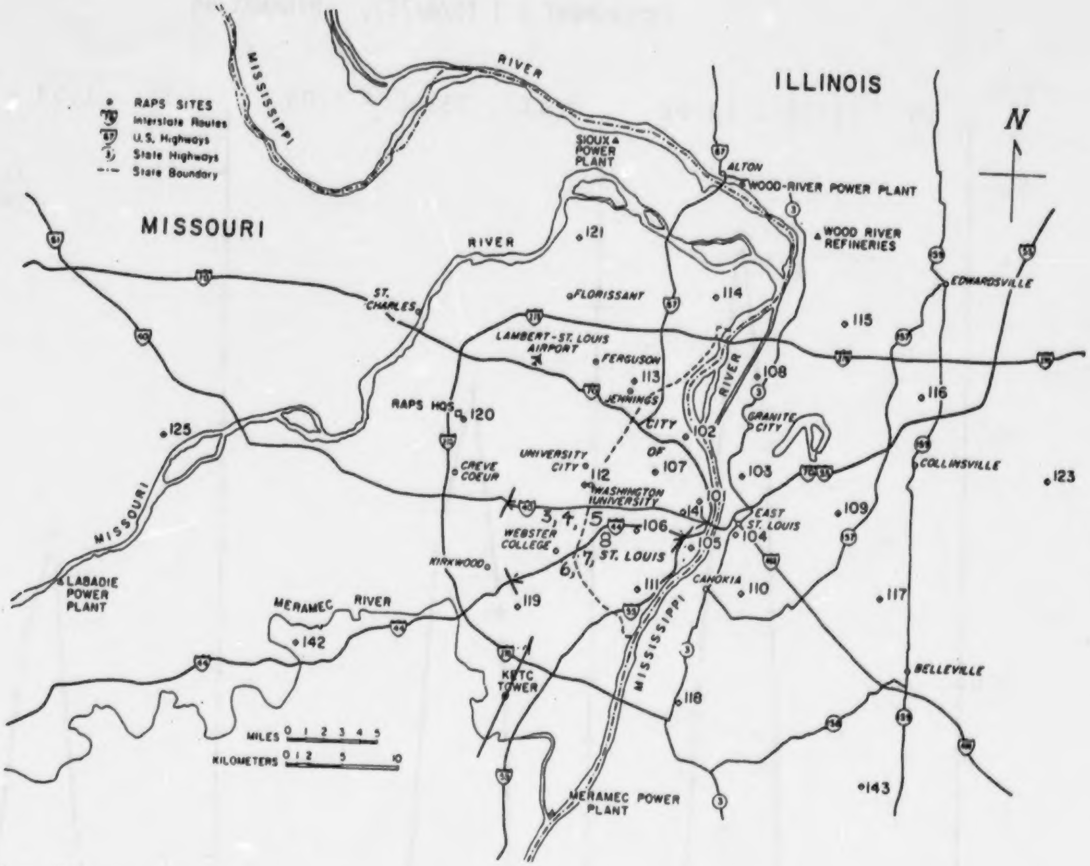
RAPS SITES
Interstate Routes
U.S. Highways
State Highways
State Boundary
MISSOURI
ILLINOIS
N
MISSISSIPPI
RIVER
MISSOURI
MERAMEC RIVER
SIOUX POWER PLANT
ALTON
WOOD-RIVER POWER PLANT
WOOD RIVER REFINERIES
EDWARDSVILLE
ST. CHARLES
FLORISSANT
LAMBERT-ST. LOUIS AIRPORT
FERGUSON
JENNINGS
CITY OF ST. LOUIS
GRANITE CITY
COLLINSVILLE
RAPS HQS
UNIVERSITY CITY
CREVE COEUR
WASHINGTON UNIVERSITY
WEBSTER COLLEGE
KIRKWOOD
EAST ST. LOUIS
CANOKIA
BELLEVILLE
KETC TOWER
LABADIE POWER PLANT
MERAMEC POWER PLANT
3, 4, 5
8
7
6
101
102
103
104
105
106
107
108
109
110
111
112
113
114
115
116
117
118
119
120
121
123
125
141
142
143
MILES 0 1 2 3 4 5
KILOMETERS 0 1 2 5 10

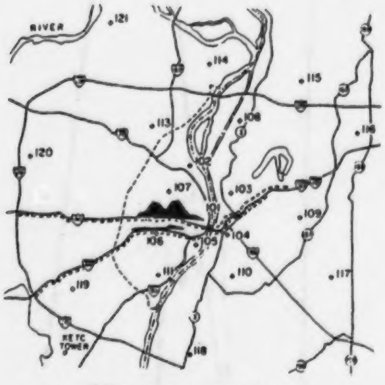

ST. LOUIS TEST NO.3
8/11/75
AUTO TRAVERSES:
▻ 3 12:15 - 12:39 p.m. CDT
► 6 11:56 - 12:20 p.m. CDT
✱ RELEASE POINT
MAX. $[SF_6]$ = 74 ppt.

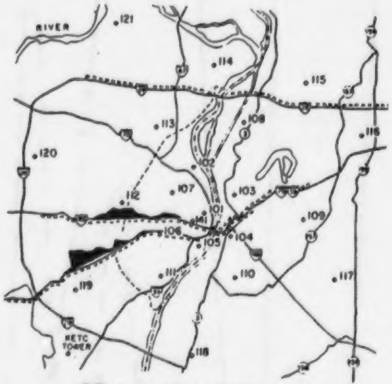

ST. LOUIS TEST NO.3
8/11/75
AUTO TRAVERSES:
> 1 12:30 - 1:00 p.m. CDT
▻ 4 12:56 - 1:20 p.m. CDT
► 7 12:58 - 1:24 p.m. CDT
✱ RELEASE POINT
MAX. $[SF_6]$ = 69 ppt.

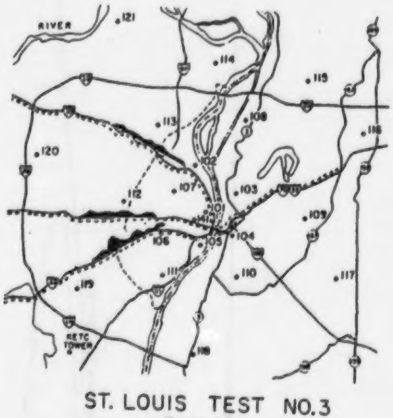

ST. LOUIS TEST NO.3
8/11/75
AUTO TRAVERSES:
> 2 1:45 - 2:26 p.m. CDT
▻ 5 1:42 - 2:08 p.m. CDT
► 8 1:56 - 2:18 p.m. CDT
✱ RELEASE POINT
MAX. $[SF_6]$ = 52 ppt.

Figure 4. Location of source and traverses 3-8 for experiment 3, St. Louis, 8/11/75.

EXPERIMENT #3 (8/11/75), HIGHWAY 40

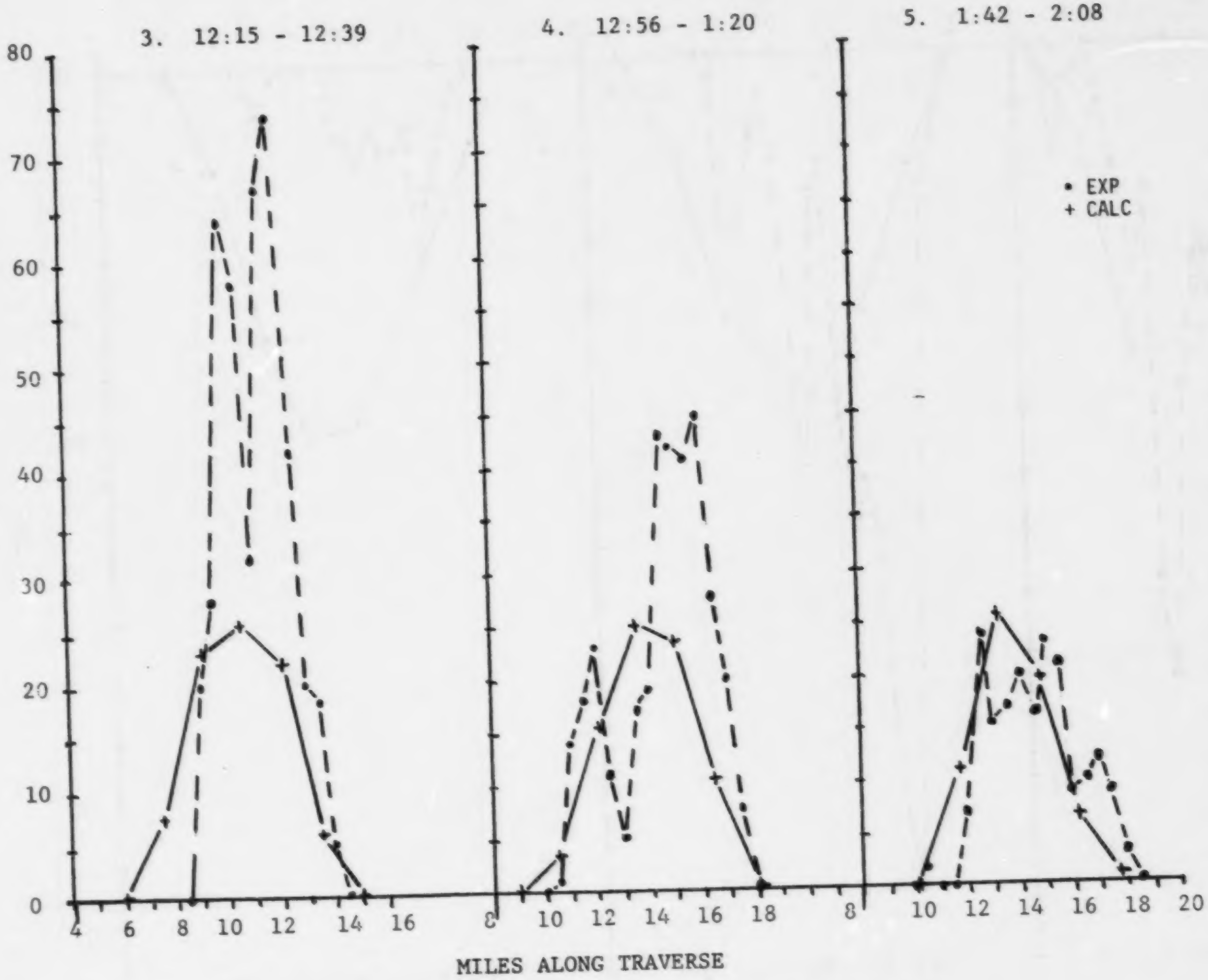

Figure 5. Calculated and experimental concentrations of SF_6.

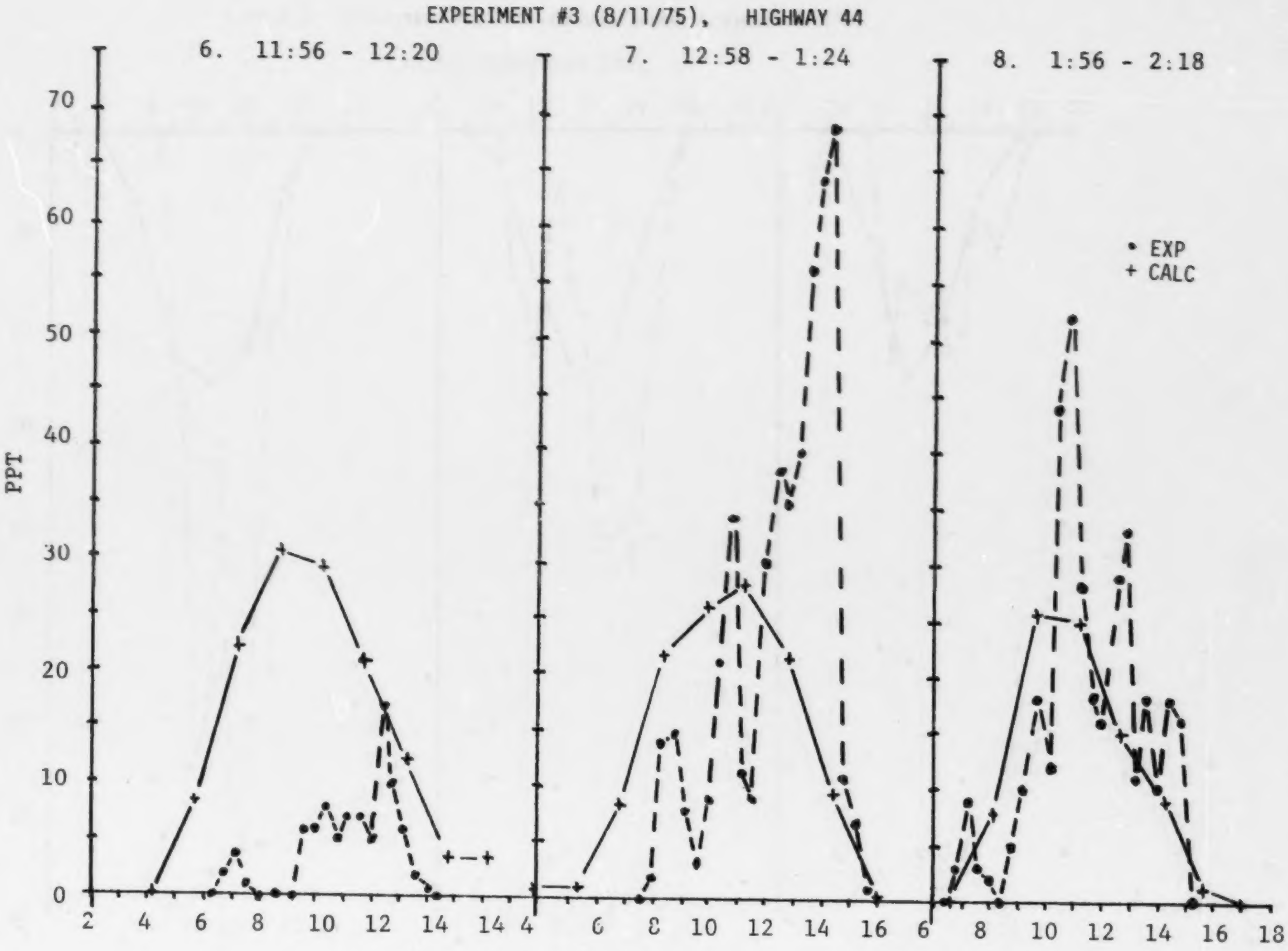

Figure 6. Calculated and experimental concentrations of SF_6.

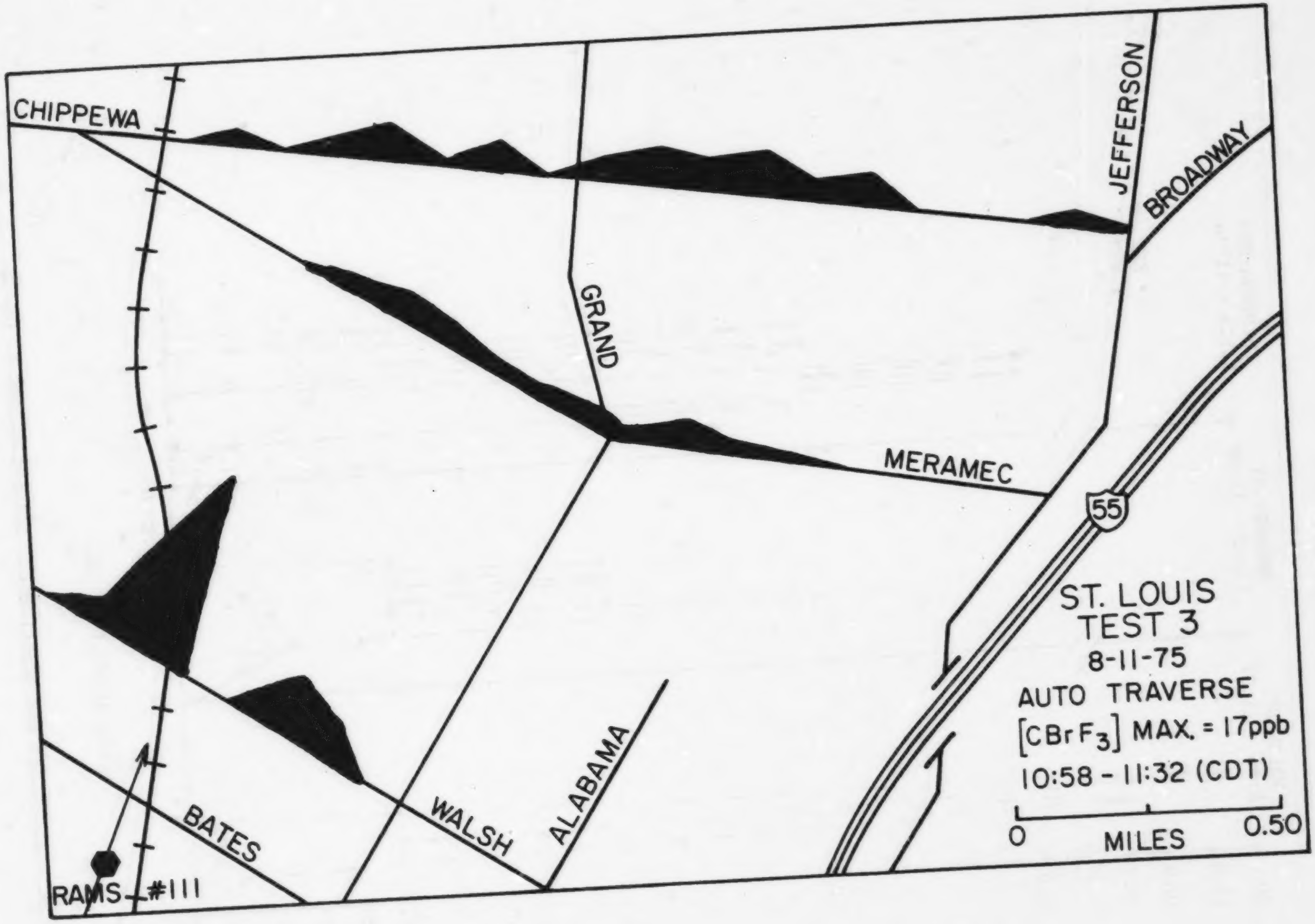
CHIPPEWA
JEFFERSON
BROADWAY
GRAND
MERAMEC
55
ST. LOUIS
TEST 3
8-11-75
AUTO TRAVERSE
[CBrF3] MAX. = 17ppb
10:58 - 11:32 (CDT)
0
MILES
0.50
ALABAMA
WALSH
BATES
RAMS #111

Figure 7. Location of source and $CBrF_3$ concentration profiles.

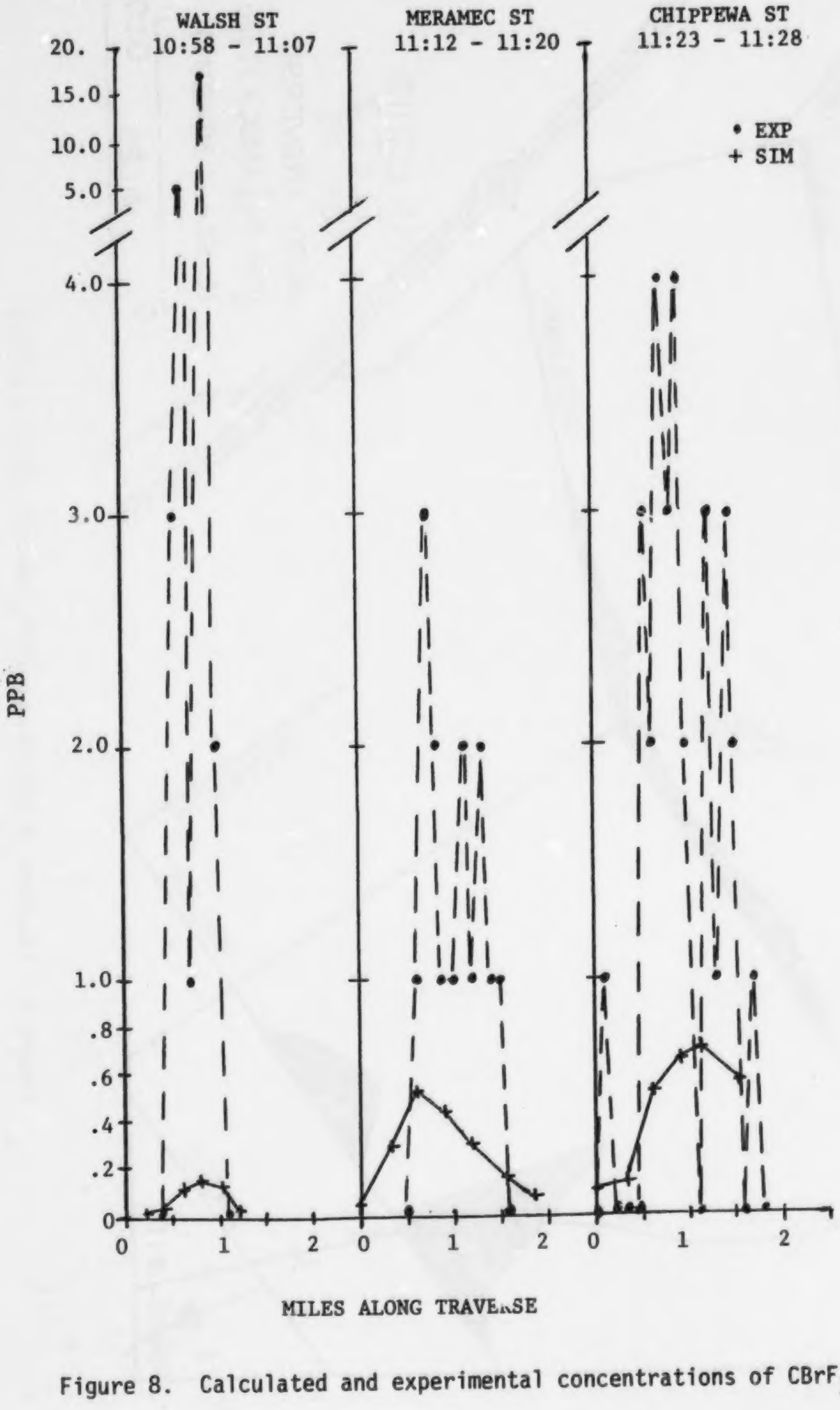

Figure 8. Calculated and experimental concentrations of $CBrF_3$.

7th International Technical Meeting
on Air Pollution Modeling and its Application

VALIDATION OF THE IMMISSION FREQUENCY DISTRIBUTION MODEL IN THE REGION OF ANTWERPEN, BELGIUM

by

J.G. KRETZSCHMAR, G. DE BAERE and J. VANDERVEE
Nuclear Energy Centre, Mol, B-2400 Belgium

September 7 - 10, 1976
Airlie Virginia
United States of America

1. INTRODUCTION

The evaluation of the impact of new or existing sources upon the levels of air pollution due to a specific component in a given region is only possible by means of some kind of mathematical model. Due to its particular structure and vocation the Belgian Nuclear Energy Centre (SCK/CEN) has been involved in this field since many years and practical engineering studies have been carried out for private companies as well as for different central and regional ministries.

The actual model is the so-called IFDM or Immission Frequency Distribution Model. It is a bi-Gaussian dispersion model calculating complete frequency distributions of short term levels (e.g. daily averages) over a given period in whatever point of a complex region influenced by point and/or area sources of the pollutant under investigation.

It is quite clear that the results of whatever kind of mathematical simulation are questionable, unless one has some rigorous way to validate the model by comparing measured and calculated patterns, distributions and individual immission levels due to (almost) completely specified air pollution situations from the present or the past. Validation procedures are therefore not new as they are inherent to mathematical models. A complete survey of the litt. wasn't made but the papers cited in reference [7], [9], [15], [18], [21 to 32] and [35 to 42] show that there is no universally accepted validation procedure. In this context it must be pointed out that the objectives of the specific model will greatly influence the validation procedure anyway.

The purpose of this paper is to discuss the preliminary results of some possible tests on the validity of the IFDM in the region of Antwerpen (Fig. 1a and 1b). The reason for choosing Antwerpen as test-city is double. First of all it is one of the largest belgian agglomerations and a very important harbour and industrial area and secondly it is possibly the only region where emission, meteorological and immission data of the required kind are available and this for several consecutive years.

It must be emphasized that the results of the reported preliminary tests are uncorrected. The main objective of the study is not to demonstrate the model's superiority but to pinpoint the weak points in the model and in its input data in order to have good information for further optimisation of the model. The usefulness of certain validation procedures as a function of the objectives of the model has been evaluated at the same time.

2. THE IMMISSION FREQUENCY DISTRIBUTION MODEL (IFDM)

2.1. General description

The IFDM, like many other operational models for off-line air-pollution studies (AQDM, CDM, SCIM, KILDER,...), is a numerical model based on the bi-Gaussian dispersion formula [4]. The model is source-oriented. The most important characteristics relating to the practical application of the bi-Gaussian dispersion formula are as follows.

Sulphur dioxide, the pollutant under investigation, is passive and completely reflected at the earth surface as well as at the top of the inversion layer. Both perfect reflectors are taken into account by using virtuel sources as described in [6, 19].

The dispersion coefficients $\sigma_y(x)$ and $\sigma_z(x)$ are given by

$$\sigma_y(x) = Ax^a$$
$$\sigma_z(x) = Bx^b$$

with A, B, a, b constants depending upon the stability of the air in the friction layer and x the upwind distance between receptor point and source [4]. For current practical use in the flat region of the Nuclear Energy Centre seven different stability categories suffices to specify the possible atmospheric conditions [6,11]. Those seven categories , E_1, E_2 ... E_7, are based on the ratio between the vertical gradient of the mean potential temperature between 114 m and 8 m, and the square of the average windspeed at 69 m (taken as reference height on the meteorological tower of the SCK/CEN). The corresponding values of A, a, B and b are given in Table 1.

Table 1 Dispersion coefficients used at the SCK/CEN, Mol [6,11]

Stability categorie	A	a	B	b
E_1	0.235	0.796	0.311	0.711
E_2	0.297	0.796	0.382	0.711
E_3	0.418	0.796	0.520	0.711
E_4	0.586	0.796	0.700	0.711
E_5	0.826	0.796	0.950	0.711
E_6	0.946	0.796	1.321	0.711
E_7	1.043	0.698	0.819	0.669

The average wind direction during the time of observation is parallel with the x-axis and is supposed to remain constant in time and space over the region during the averaging time of 1 hour used for the computations of the individual concentration levels. The values of the dispersion coefficients are averages over the same interval.

The average windspeed $\bar{u}(h)$ at a height h is derived from the average windspeed $\bar{u}(h_0)$ measured at reference height h_0 by using the exponential law for the wind profile. In the application of the basic bi-Gaussian dispersion formula several possibilities exist for the definition of transport speed in the denominator of that formula [2, 3, 4, 5, 8, 10, 14, 16, 18, 20, 21, 34, 42]. In the actual validation study the average windspeed at the effective height $\bar{u}(h_e)$ of the point and area sources has been used by applying the previously mentioned exponential wind profile law.

Real (industrial) stacks with geometrical or physical height h_g are replaced by fictitious point sources of the same strength at an effective height $h_e = h_g + \Delta h$ by using Stümke's second plume rise formula [1, 42].

Area sources for SO_2 are simulated by circular areas of constant emission density (= constant population density) at an effective height h_e metres above ground-level. Based on the same basic formulas as for the industrial point sources the following empirical formulas have been derived for the computation of the concentration level caused by a circular area :

$$C(r_1) = F\left[(A_{1i} + B_{1i}\sqrt{r_1} + C_{1i}\, r_1) + h_e(A_{2i} + B_{2i}\sqrt{r_1} + C_{2i}\, r_1)\right]/\bar{u}(69)$$

for receptor points inside the circular area and

$$C(r_1, r_2) = F\left[B_{1i} + B_{2i}\, h_e)(\sqrt{r_2} - \sqrt{r_1}) + (C_{1i} + C_{2i}\, h_e)(r_2 - r_1)\right]/\bar{u}(69)$$

for receptor points outside the area.

The coefficients A_{ji}, B_{ji} and C_{ji} are functions of the stability class E_i, while F takes the physical temperature and the real population density into account, as both factors determine the actual emissions caused by home heating.
The variables r_1 and r_2 are the upwind distances between the receptor point and the nearest, respectively the farthest point of the boundary of the circular area of constant emission density influencing the specified receptor point under the given wind direction. The windspeed $\bar{u}(69)$ is the hourly average at 69 m above ground-level and is measured or calculated as described before.

2.2. Practical organisation of the model

The following steps are typical for the IFDM-procedure used for SO_2-studies :

- a regular grid with maximum 16 × 21 meshes of m × n km^2 is superimposed upon the region under investigation. Although m and n are freely choosen, a routine run will have m = n = 1 km ;
- for each of the possible combinations of seven stability classes (Table 1), four wind speed categories and a number of different wind directions (depending upon the available meteorological observations e.g. 18 classes if the resolution is twenty degrees) a standard pollution map for that combination is obtained by computing the hourly average concentration in each grid point due to the combined effect of all the point sources in- or outside the region. For the same combinations and a standard indoor - outdoor temperature difference a similar set of pollution maps is obtained for the SO_2 area sources ;
- background levels are introduced as a fixed value for each wind direction category If no sufficient information is available, the background is supposed to be constant ;
- for the specified reference period (e.g. one year) the actual meteorological data, obtained in the region by means of a meteorological tower, are used to select hour by hour the appropriate standard pollution maps for the point- and the area sources respectively. The latter is corrected for the real indoor - outdoor temperature difference and added to the former. This gives the computed immission situation in the different grid points for that specific hour. If no local meteorological observations of the required type are available a representative set of another comparable region could be used ;
- for each grid point one finally obtains the arithmetic mean, the maximum concentration and the distribution of the hourly averages for the specified period. Distributions of the daily averages is only a question of combining successive hourly values ;
- spatial distributions of the measured and the calculated values for the average and the extreme levels, as well as for whatever percentile of the cumulative frequency distributions, are possible by means of some plotting subroutines.

3. THE VALIDATION PROCEDURE

The main objective of the IFDM, namely the evaluation of the impact of new or existing sources upon the actual air-pollution levels due to a specific component in a given region, automatically implies the use of air quality standards for the specific pollutant and region under investigation. As most air quality standards specify an average level over a given period (e.g. arithmetic- or geometric mean for one year), as well as certain short term levels not to be exceeded more than a predetermined number of times during that same period (e.g. the 95- or 98-percentile of the distribution of the hourly or daily averages during that same year) it is obvious that off-line impact models will have to generate data of this kind, and that validation procedures will have to compare calculated and measured values of long term averages and cumulative frequency distributions of the individual short term averages. The necessity of this approach, together with the fundamental requirement of repeating this test over several different years, was clearly demonstrated by H. Fortak et al. in ref. [38].

Although a positive result for those tests is a necessary condition for the validity of an impact model, it must be pointed out that it is not a sufficient condition in our opinion. Without having reached that goal, we feel that a complete set of statistical tests as described by Olsson et al. in [27] would form the minimum validation procedure approach if it is repeated over several different years. The preliminary results for Antwerpen have to be situated in this context, as some examples for the comparison of cumulative frequency distributions, time series and regression and correlation analysis will be discussed.

In order to minimize the probability of biasing the conclusions of the tests, three different years (1971-1972-1973) and six different measuring stations were used. Station ZR806, ZR808 and ZR814 are highly influenced by area sources, ZR812 to a large extent by industrial sources and ZR818 and 820 almost entirely by the latter (Fig. 1b and 2). One station, namely ZR812 has been analysed for two consecutive years.

4. INPUT DATA FOR THE PRELIMINARY TEST ON ANTWERPEN

The available input data for the SO_2-test were :

- hourly averages for windspeed, wind direction and temperature at two levels (51 m, 154 m) on the meteorological tower in Zwijndrecht (Fig. 1b). Wind directions are given with intervals of 20 degrees. Those data are obtained by the N.V. Vinçotte, Brussels and are available in the SCK/CEN air pollution data bank ;
- yearly averages for the industrial SO_2-emissions of approximately 150 stacks (inventory by the Stadslaboratorium Antwerpen) ;
- detailed information on the population density (NIS*, Brussels) and a yearly SO_2-emission estimated on ≈ 14 000 ton SO_2 for a population of ≈ 800 000.

---

*Nationaal Instituut voor Statistiek, Brussel

This figure is based on the yearly amounts of gasoil and coal sold for home heating purposes in Belgium ;

- daily averages of the SO_2 concentrations in the monitoring stations of the national network for sulphuroxides and standard smoke (ZR-network, IHE*-KMI** Brussels).

Variable input parameters of the model were choosen as follows :

m_i = 0.28 as exponent for the wind profile for all stability classes E_i (i = 1, 2...7), H = 550 m as height of the inversion layer and a uniform background pollution of 20 μg SO_2/m^3 due to distant and/or unknown sources. As the region of Antwerpen is flat no topographic corrections were necessary.

As standard meteorological conditions all possible combinations of seven stability categories, four wind speed classes and 18 wind directions were used.

For the comparison between measured and calculated daily averages,or sets of daily averages, only those days with simultaneously available measured and calculated SO_2-levels were used. To calculate a daily average SO_2-level at least 23 valid hourly averages for the meteorological parameters must be available. This rather severe criterion, and the fact that also some measured daily averages were missing, resulted in 250 to 300 comparable days for a year.

5. COMPARISON OF MEASURED AND CALCULATED CUMULATIVE FREQUENCY DISTRIBUTIONS

Figures 3a to 5b give the comparison between measured and calculated cumulative frequency distributions for seven different station-year combinations. On each figure are indicated the number of the station, the year, the averaging time for the individual concentrations and the number of valid days used for the comparison. The comparison between the calculated and measured values for some commonly used statistical parameters is given in Table 2, together with the ratios between calculated and measured value for each of the parameters. Those ratios vary between 0.5 and 1.7, with an average of 0.9. The largest deviations occur at the lower and upper end of the distributions in stations ZR818 and ZR820, two stations which are mainly influenced by industrial SO_2 (point)sources (Fig. 1b + Fig. 2).

As well on the figures, as in Table 2, it is striking that the calculated values are almost systematically too low and that the characteristics of station ZR820 are quite different from those of the other stations.

Due to its specific position (Figure 1b) it was possible to analyse the individual daily averages in station ZR820 as a function of the average wind sector over 24 hours. It was noticed that for winds from the sector north to east-south-east

---

* Instituut voor Hygiëne en Epidemiologie

** Koninklijk Meteorologisch Instituut

Table 2 : Comparison between measured and calculated statistical parameters for daily averages over periods of one year in different ZR-stations in the region of Antwerpen

		$X_{.50}(\mu g/m^3)$			$\bar{X}(\mu g/m^3)$			$X_{.95}(\mu g/m^3)$			max. $(\mu g/m^3)$			
year	station	m	c	c/m	m	c	c/m	m	c	c/m	m	c	c/m	Figure
1971	ZR 806	151	106	0.70	162	117	0.72	300	242	0.81	435	358	0.82	3a
1971	ZR 812	83	74	0.89	103	84	0.82	213	163	0.77	414	288	0.70	3b
1972	ZR 812	83	86	1.04	104	102	0.98	260	227	0.87	417	272	0.65	4a
1972	ZR 814	145	132	0.91	155	142	0.92	304	266	0.98	389	512	1.32	4b
1972	ZR 818	108	91	0.84	116	101	0.87	239	229	0.96	319	531	1.67	4c
1973	ZR 808	142	133	0.94	164	147	0.90	340	331	0.97	557	525	0.94	5a
1973	ZR 820	75	35	0.47	88	82	0.93	194	278	1.43	354	358	1.01	5b

with m : measured value

c : calculated value by means of the IFDM

$\bar{X}$: yearly average

$X_{.50}, X_{.95}$: 50- and 95-percentile of the distribution of the daily averages during the [illegible]fied year.

max. : maximum daily average during the specified year the calculated concentrations were always too high, while for the other sectors they were practically always too low. This could mean that the influence of some nearby industrial sources is overestimated, while the background or distant industrial and domestic sources are underestimated. A similar analysis in the other stations seems to confirm this conclusion.

The general underestimation in the other stations is partly due to the same incomplete knowledge of the background and the unknown influence of distant sources, especially in the direction of the other important industrial areas in Belgium and in the vicinity of its borders (Fig. 1a). A second important factor is the estimated 14 000 ton SO_2/year for the area sources in the region of Antwerpen (Fig. 1b). An increase of 30 % in those emissions improves the agreement between calculated and measured cumulative frequency distributions very much. This increase is not so dramatic if one realizes that there is more than a factor two difference in the actually available data for non-industrial SO_2-emissions in Belgium. The emission inventory of the national R&D programme Air will certainly give more precise and reliable data in the near future. It must also be emphasized that the national ZR-network measures total acidity (OCDE-procedure) and not specifically SO_2. Some measurements by other organizations seem to indicate that the actual ZR-measurements in Antwerpen are upper bounds. The belgian automatic monitoring network, starting at the end of 1976, will give interesting information in this field (Ministry of Public Health).

As mentioned in paragraph 2 all calculations are based on average windspeeds $\bar{u}(h_e)$ at the effective height of the fictitious point sources replacing the industrial and domestic sources. Some supplementary calculations using the average windspeed $\bar{u}(h_g)$ at the top of the industrial stacks instead of at the effective plume height resulted in a net increase of the arithmetic averages with 10 % to 20 %, an increase of 20 % to 35 % for the 95-percentiles and 30 % to 55 % for the maximum values. This shows the importance of the choice of the windspeed level and the exponent of the wind profile.

6. TIME SERIES ANALYSIS

Although from the point of view of air quality standards a good correspondence between measured and calculated cumulative frequency distributions is a necessary condition for an acceptable impact model, it is not always a sufficient condition to obtain a reliable simulation of the actual situations. A further step in this direction is the analysis of measured and calculated concentration patterns as a function of time in different points of the region under investigation, in order to determine if certain well-known cycles, such as the seasonal trend for

SO_2 in urban areas, are reproduced in a reasonable way.

Figures 6a to 6g demonstrate this test for the seven station-year combinations of Table 2. Those figures readily show that :

- the seasonal trend in the measured time pattern is well reproduced in the calculated pattern, especially in the stations mainly influenced by the area sources (ZR806, ZR808 and ZR814 to a lesser extent) ;
- certain peak values are simultaneously appearing in both patterns while others fail. More station-year combinations will be required to find out if this is due to meteorological effects, local emission variations or interferences ;
- for ZR812 and ZR818 a set of not measured peaks was calculated in the period July-September. As this is a non-heating period there seems to be an over-estimation of the industrial sources in the region. This could be due to the model but also to its input. July and August are the warmest months and also the main vacation months in Belgium. It is thus realistic to suppose that even the industrial emmissions are lower than the yearly average during that period ;
- the special character of ZR820 (Figure 1b and 5b) is due to the superposition of too high peaks, coming from the local industry, upon a too constant background, due to unknown distant sources. Another important factor to be analysed here is the possible influence of the river separating the measuring station and the industrial complexes around the docks on the right river bank.

7. CORRELATION AND REGRESSION ANALYSES

Correlation and regression analyses are one step further in the direction of the analysis of the individual couples of measured and calculated daily averages in a given receptor point, although the properties of the collective of all the individual elements for a given period (e.g. one year) are strongly influencing the end result.

For the actual linear regression analysis the same data sets as before were used and the main results are given in Table 3. The linear correlation coefficient varies between 0.45 and 0.73. Taking into account the size n of the populations it is obvious that all the r-values are highly significant. The value of the slope of the different regression lines is significant for the previously mentioned general tendency towards underestimation of the measured levels.

A better illustration of the practical meaning and consequences of the numerical

Table 3 : Characteristic parameters for the linear regression analysis on the measured and calculated daily averages in the different stations

station	year	n	r	a	b	fig.
ZR 806	1971	279	0.57	0.49	37	7a
ZR 812	1971	279	0.55	0.35	47	7b
ZR 812	1972	241	0.51	0.42	58	7c
ZR 814	1972	248	0.53	0.45	71	7d
ZR 818	1972	248	0.46	0.52	40	7e
ZR 808	1973	294	0.73	0.67	37	7f
ZR 820	1973	295	0.45	1.02	-8	7g

with n : number of simultaneously measured and calculated daily averages

r : linear correlation coefficient

a,b : slope and intercept of the regression equation $y = ax+b$ with y the calculated daily average and x the corresponding measured concentration.

values summarized in Table 3 is given by the plots reproduced on Figure 7a to Figure 7g. The dispersion of the individual couples of the simultaneously measured and calculated daily averages is obvious. Another important phenomenon is the difference between two successive years in the same station ZR812 (Figure 7b and 7c).

The regression subroutine also gives the possibility to automatically identify the days with a difference between calculated and measured concentration level larger than a predetermined value (absolute or relative with respect to the measured concentration level). An analysis in the different stations of all the calculated values outside the interval determined by the corresponding measured value plus or minus 50 % showed once again that overestimation predominantly occurred for wind direction pointing from the industrial zone on the right bank of the Schelde towards the station under investigation, and that underestimation was associated quite frequently with winds blowing from the sectors where no local sources were identified.

8. CONCLUSIONS

The impact of new or existing sources upon the levels of air pollution in a given region must be studied as a function of air quality criteria or standards and this in its specific context. This means with emission, immission and meteorological data that are representative for the region under investigation. In the actual state of the art bi-Gaussian models seem to be acceptable tools for those off-line studies as has been demonstrated by means of the validation tests on the Immission Frequency Distribution Model but further improvement of the models, their input and their validation procedures is possible.

The preliminary tests on three consecutive years of SO_2 in the region of Antwerpen were quite satisfying and new information, obtained in the different projects of the National R&D Programme Air, will improve our understanding of air pollution simulation models. Some of the most important needs could be summarized as follows.

For the meteorological parameters a better knowledge of the height of the mixing layer as a function of the stability classes,and possibly other parameters, is required. The same holds for the exponent of the wind profile and the exact specification of the different wind speeds appearing in the bi-Gaussian dispersion formula. The influence of persistent precipitation and large water surfaces has not been solved. Last but not least the wind direction over a complex region such as Antwerpen is certainly not constant,while four classes of windspeed for the practical calculations is possibly not enough for the required resolution in time and space.

On the local source side a better specification for the total amounts and their variability will certainly improve things. Information on the background or the influence of distant (unknown) sources as a function of the meteorological parameters,or their combinations, is a must. We hope that pollution roses on the existing large amount of 24 h-averages, together with the 30 minute information of the automatic monitoring network, will be of great help in this field. For the plume rise calculations different plume rise formulas could be introduced as a function of the specific source [34,40].

Validation procedures must be standardized as a function of the objectives of the models.They should use several different mathematical techniques and this on different levels in the time and space scale. It must be emphasized in this context that the data obtained in the study described in this paper will have to pass some further tests based on pollution roses, error analysis and spatial distributions.

9. ACKNOWLEDGEMENT

Thanks are due to all the members of the "Mathematical Modeling Group of the SCK/CEN" as the reported results were obtained by their combined efforts. Mrs. Steylemans and Mr. Van Tongerloo were responsible for having this paper ready in due time.

The Interministerial Commission for Science Policy is acknowledged for its support in the framework of the national R&D programme Air.

REFERENCES

[1] **H. STÜMKE**
Vorschlag einer empirischen Formel für die Schörnsteinüberhöhung
Staub, Bd. 23, No. 12, 1963

[2] **F. WIPPERMANN**
Diagramme zur Beurteilung der Eignung von Schornsteinhöhen für die Luftreinhaltung
Staub, Bd. 23, No. 7, 1963

[3] **U. HÖGSTRÖM**
A statistical approach to the air pollution problem of chimney emission
Atm. Env., Vol. 2, pp. 251-271, 1968

[4] **D.B. TURNER**
Workbook of atmospheric dispersion estimates
U.S. Department of Health, Education and Welfare
Public Health Service Publication No 999-AP-26, 1969

[5] Air Quality Display Model
Air Pollution Technical Publications of the U.S. Env. Prot. Agency, APTD-1341, 1969

[6] **H. BULTYNCK et al.**
Atmospheric dilution factors and calculation of doses in the environment of SCK/CEN Mol for short and long duration stack discharges
BLG 446, 1970

[7] **H.G. FORTAK**
Numerical simulation of temporal and spatial distributions of urban air pollution concentration
Proceedings of Symposium on multiple-source urban diffusion models
EPA Air Pollution Control Office Publication, AP-086, 1970

[8] **G. MANIER**
Eine neue Methode zur Bestimmung von Schornsteinmindesthöhen
VDI-Berichte No. 149, 1970

[9] **R.C. KOCH et al.**
Validation and sensivity analysis of the Gaussian plume multiple-source urban diffusion model
NTIS, PB 206 951, 1971

[10] **J.M. LEAVITT et al.**
Meteorological program for limiting power plant stack emissions
JAPCA, Vol. 21, No. 7, 1971

[11] **H. BULTYNCK et al.**
Evaluation of atmospheric dilution factors for effluents diffused from an elevated continuous point source
Tellus XXIV, No. 5, 1972

[12] **A. DEROUANE et al.**
Luchtverontreiniging door zwaveloxyde en rook in België van 1 april 1969 tot 31 maart 1970
KMI-Brussel, Publicaties, serie A, nr. 74, 1972

[13] **A. DEROUANE et al.**
Luchtverontreiniging door zwaveloxyde en rook in België van 1 april 1970 tot 31 maart 1971
KMI-Brussel, Publicaties, serie A,nr. 82, 1972

[14] **T.L. MONTGOMERY et al.**
Results of recent TVA investigations of plume rise
JAPCA, Vol. 22, No. 10, 1972

[15] **D.B. TURNER**
Air quality frequency distributions from dispersion models compared with measurements
Symposium on Statisticals Aspects of Air Quality Data, Chapel Hill,N.C., 1972

[16] **A.D. BUSSE et al.**
User's guide for the CDM
EPA-R4-73-024, 1973

[17] **A. DEROUANE et al.**
Luchtverontreiniging door zwaveloxyde en rook in België van 1 april 1971 tot 31 maart 1972
KMI-Brussel, Publicaties, serie A, nr. 84, 1973

[18] **R.C. KOCH et al.**
Evaluation of the multiple-source Gaussian plume diffusion model
Geomet. report No. EF-186, 1973

[19] **M. LEGRAND**
Modèle climatologique de la pollution de l'air par les oxydes de soufre
Proceeding of the third international clean air congress, Düsseldorf 1973

[20] **T.L. MONTGOMERY et al.**
A simplified technique used to evaluate atmospheric dispersion of emissions from large power plants
JAPCA, Vol. 23, No. 5, 1973

[21] **H. BRESSER et al.**
Dispersion model used in the Cologne region
Proceeding of the fourth meeting of the expert panel on air pollution modeling, NATO-CCMS, No. 30, 1973

[22] **F.A. GIFFORD**
The simple ATDL urban air pollution model
Proceedings of the fourth meeting of the expert panel on air pollution modeling, NATO-CCMS, No. 30, 1973

[23] **B. BRINGFELT et al.**
A numerical air-pollution dispersion model for central Stockholm
Atm. Env. 8, 1974

[24] **H. FORTAK**
Potential applications of mathematical-meteorological diffusion models to the solution of problems of air quality maintenance
Proceeding to the fifth meeting of the expert panel on air pollution modeling, NATO-CCMS, No. 35, 1974

[25] **D.G. FOX**
Considerations of the US regional air pollution study
idem

[26] **L. KROPP**
Use of dispersion models during planning phases of industrial and domestic regions
idem

[27] **L.E. OLSSON et al.**
Validation of urban air pollution dispersion models
idem

[28] **E. RUNCA**
An introduction to the Venice air pollution project
idem

[29] **L. SHENFELD**
The utilization of an urban air pollution model in air management
idem

[30] **H.H. SLATER** et al.
Application of implemetation planning program modeling analysis to the New Jersey, New York, Connecticut Interstate AQRC
idem

[31] **H.H. SLATER**
Application of a multiple source urban model
idem

[32] **J. STROTT** et al.
Application of the AQDM model and the ATDL model and comparison of the results
idem

[33] **A. DEROUANE** et al.
Luchtverontreiniging door zwaveloxyde en rook in België van 1 april 1972 tot 31 maart 1973
KMI-Brussel, Publicaties serie A, nr. 88, 1975

[34] **E. VERMAAS** et al.
Handleiding voor het computerprogramma van het Gaussische pluimmodel
KNMI, WR 75-7, De Bilt 1975

[35] **A. BRAIG**
Results of the revised ATDL-model compared with the results of the AQDM- and CDM models
Proceedings of the sixth international technical meeting on air pollution modeling and its application, NATO-CCMS No. 42, 1975

[36] **B. BRINGFELT**
The state of air pollution modeling and model applications in Sweden
idem

[37] **C.E. CANTONI**
Preliminary report about a diffusion model for Milano
idem

[38] **H. FORTAK** et al.
Further investigations of the ambient air-quality situation in the Unter-Main region making use of Fortak's dispersion model
idem

[39] **R.F. LEE** et al.
Validation of a single source dispersion model
idem

[40] **E.T.M. NIEUWSTADT** et al.
Validation of a multiple source diffusion model based on the Gaussian plume model
idem

[41] **E. RUNCA** et al.
Simulation of SO_2-dispersion in the Venetian area
idem

[42] **J.G. KRETZSCHMAR** et al.
Evaluation of the impact of new or existing sources upon the levels of air pollution by means of the Immission Frequency Distribution Model
Proceeding of the IMC Symposium on Systems and Models in Aur and Water Pollutio
London 22-24 September 1976.

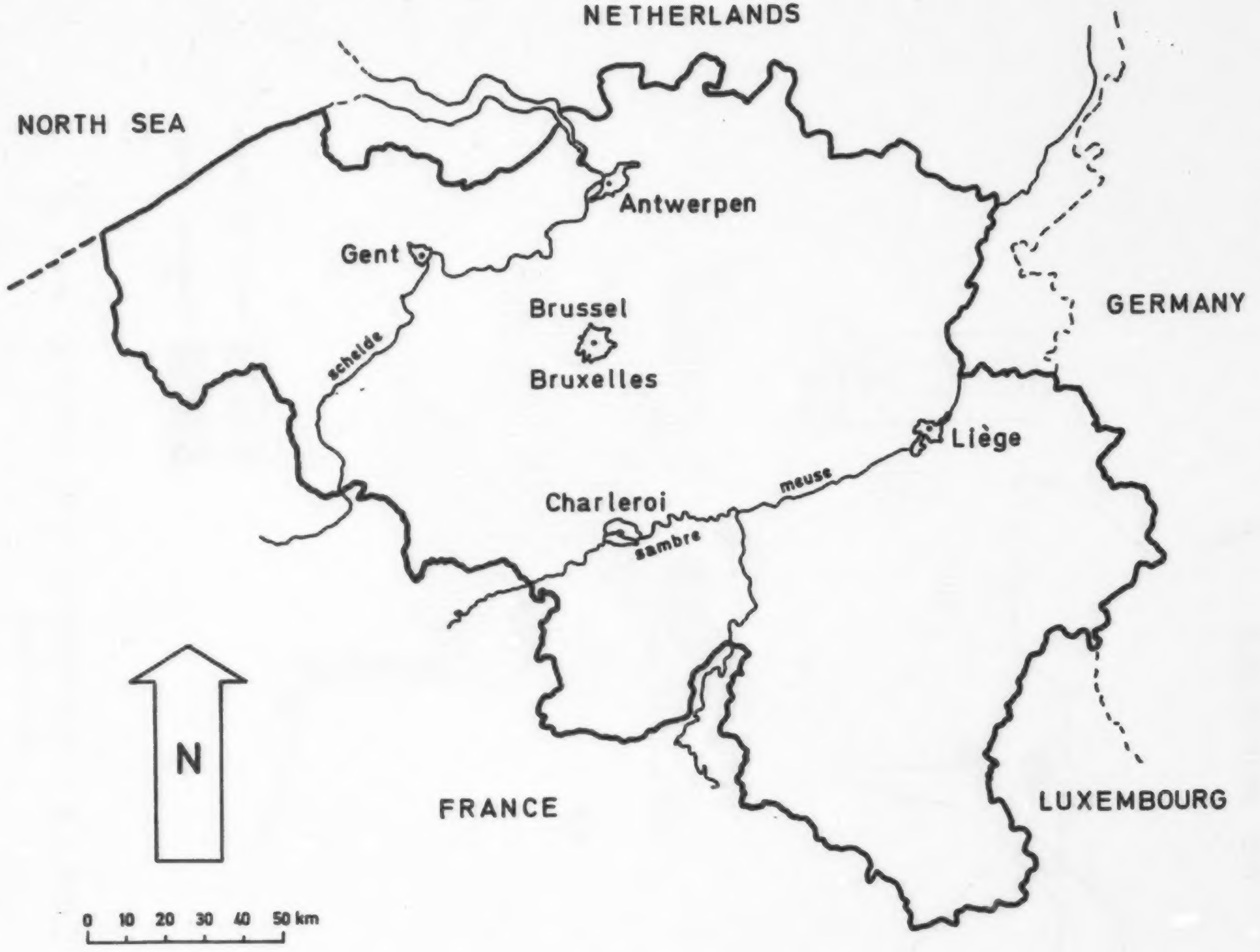
NETHERLANDS
NORTH SEA
Antwerpen
Gent
Brussel
Bruxelles
GERMANY
scheldt
Liège
meuse
Charleroi
sambre
N
FRANCE
LUXEMBOURG
0 10 20 30 40 50 km

Figure 1a : Location of the largest agglomerations and industrial areas in Belgium.

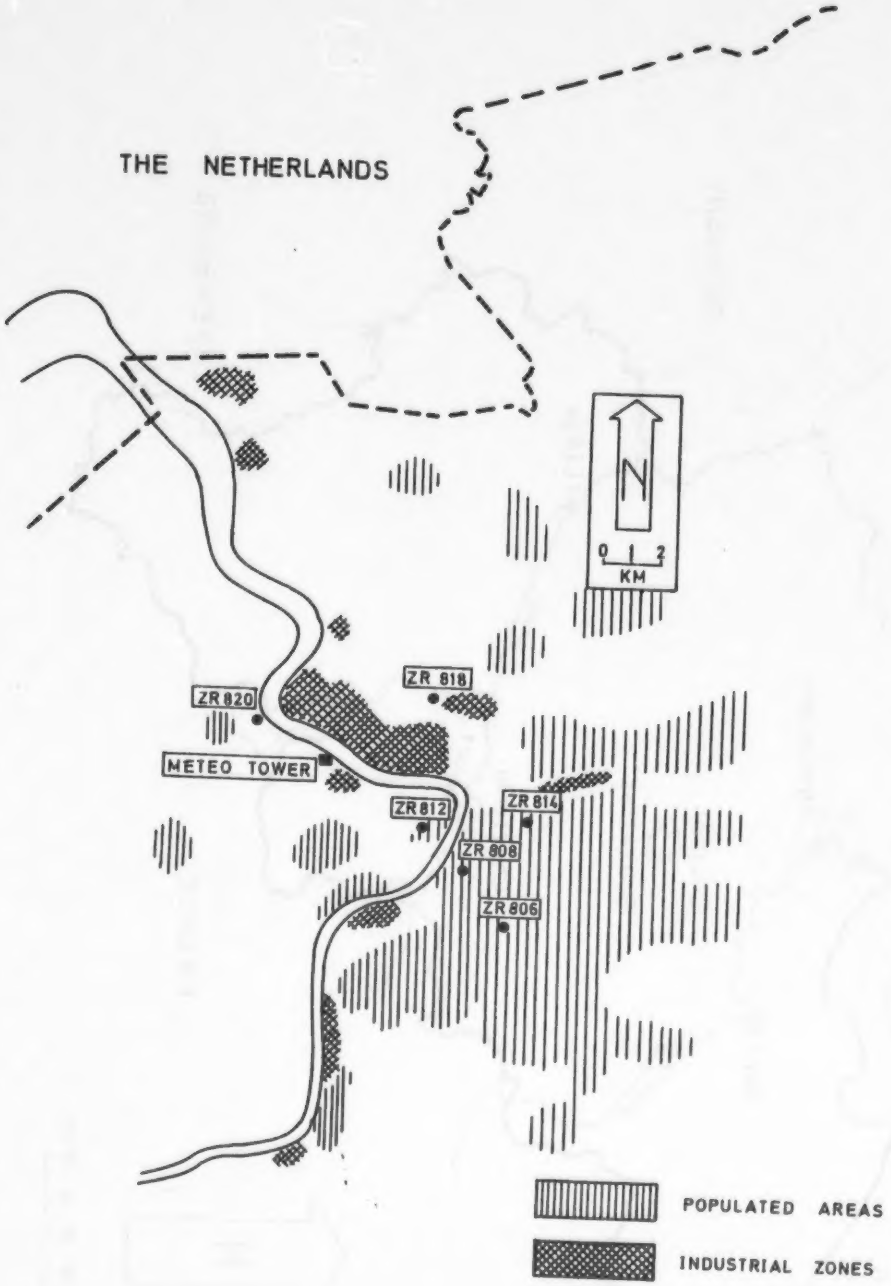
THE NETHERLANDS
N
0 1 2
KM
ZR 818
ZR 820
METEO TOWER
ZR 812
ZR 814
ZR 808
ZR 806
POPULATED AREAS
INDUSTRIAL ZONES

Figure 1b : Agglomeration and industrial area of Antwerpen.

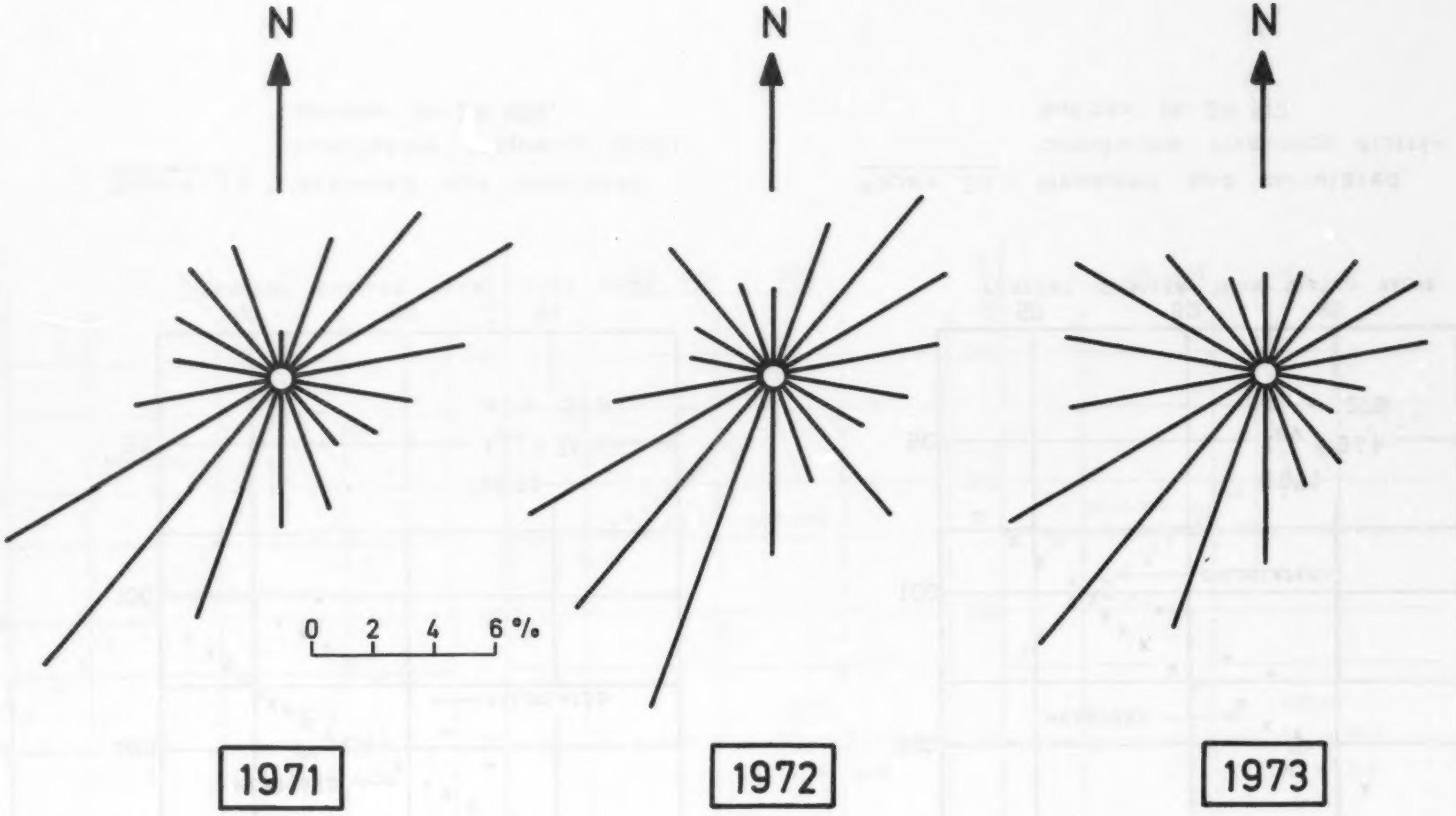

Figure 2 : Relative frequency of the different wind directions ($t_{av} = 1\,h$) for 1971, 1972 and 1973 at a height of 51 m on the meteorological tower in Zwijndrecht (see figure 1 b).

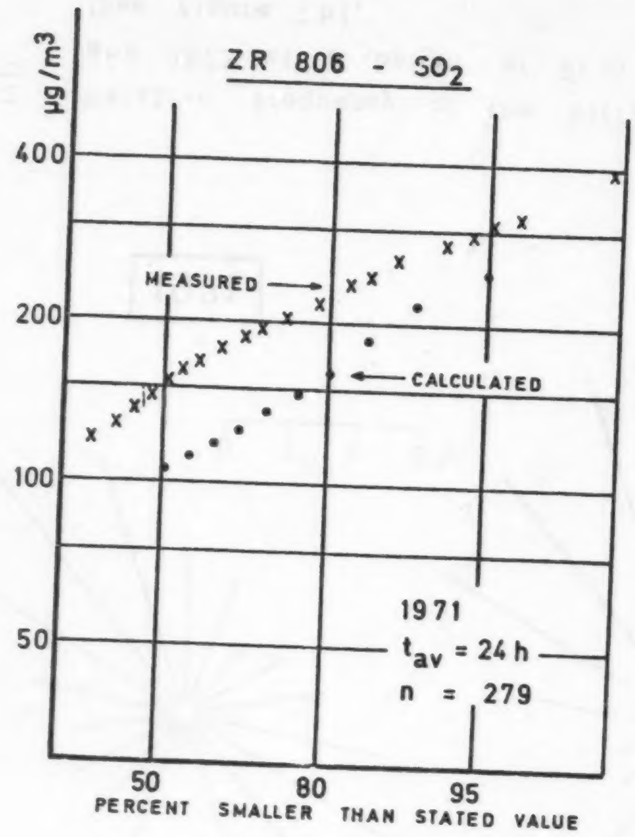

Figure 3a : Measured and calculated cumulative frequency distributions in ZR 806.

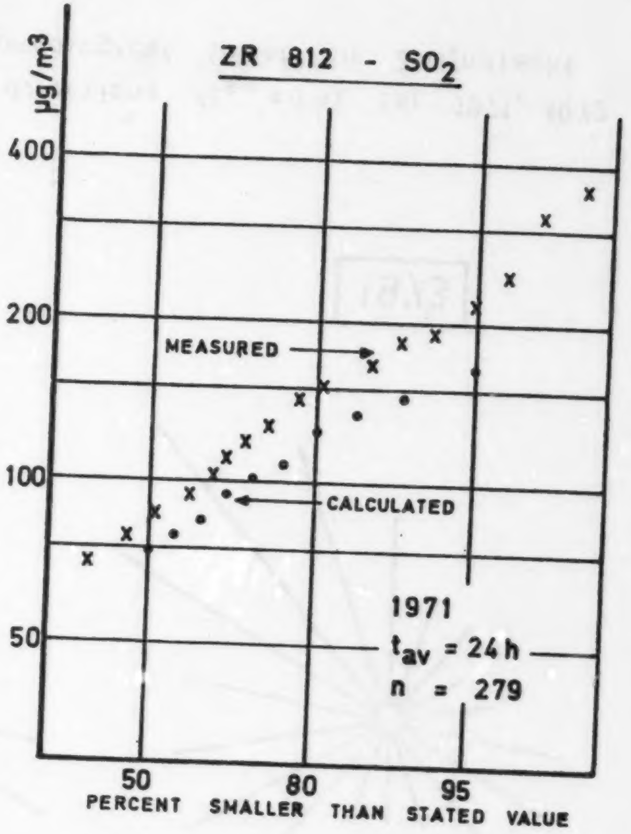

Figure 3b : Measured and calculated cumulative frequency distributions in ZR 812.

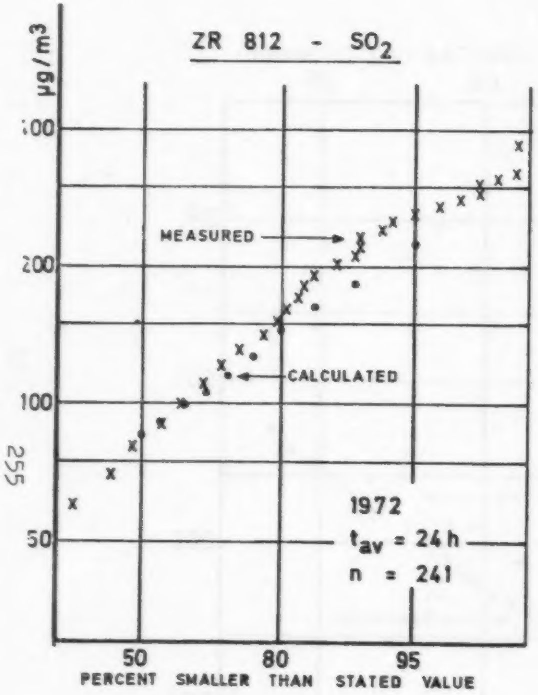

Figure 4a: Measured and calculated cumulative frequency distributions in ZR 812.

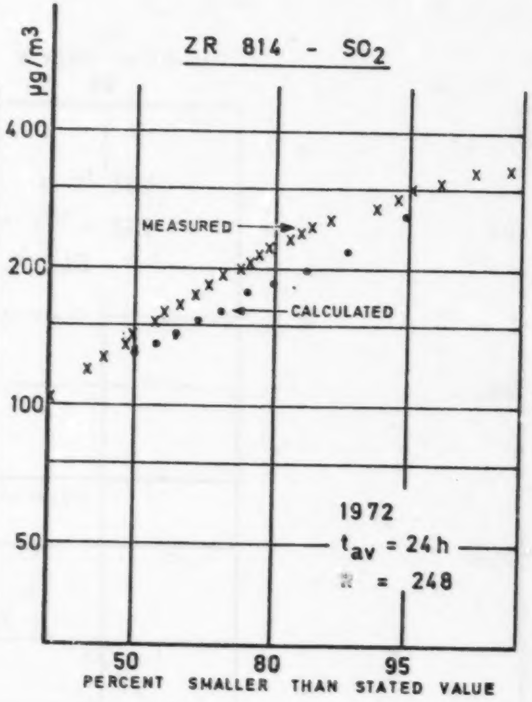

Figure 4b: Measured and calculated cumulative frequency distributions in ZR 814.

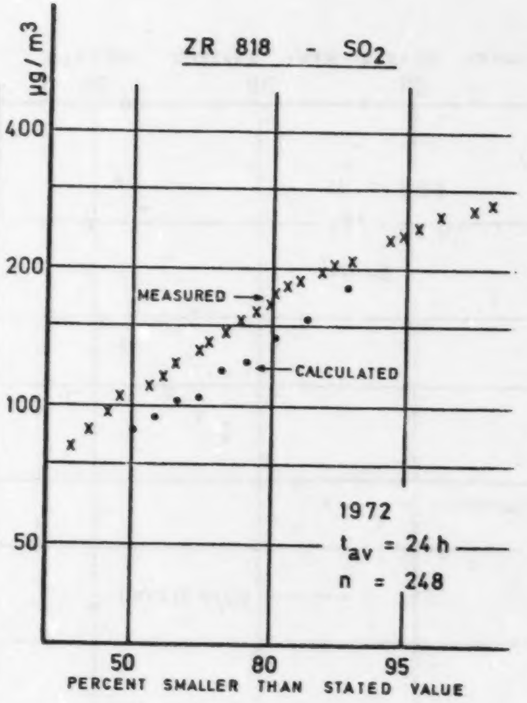

Figure 4c: Measured and calculated cumulative frequency distributions in ZR 818.

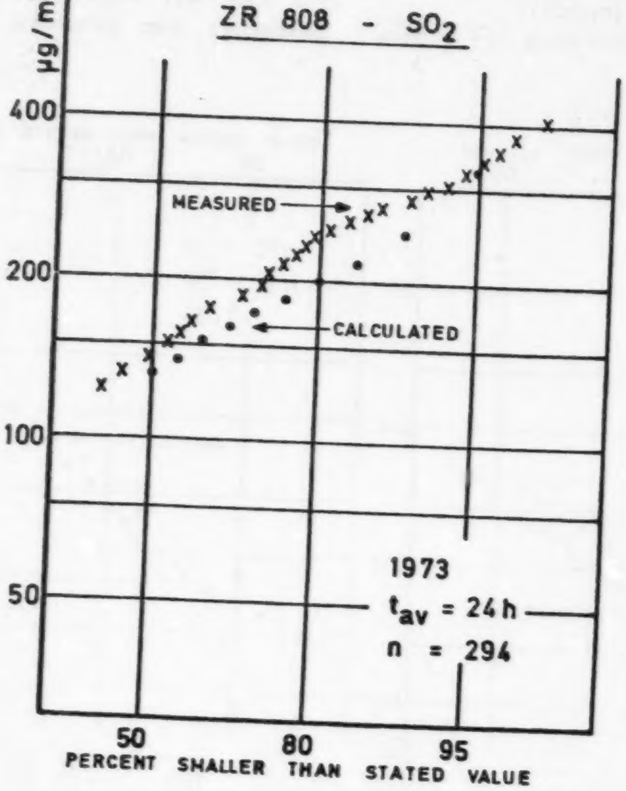

Figure 5a : Measured and calculated cumulative frequency distributions in ZR 808.

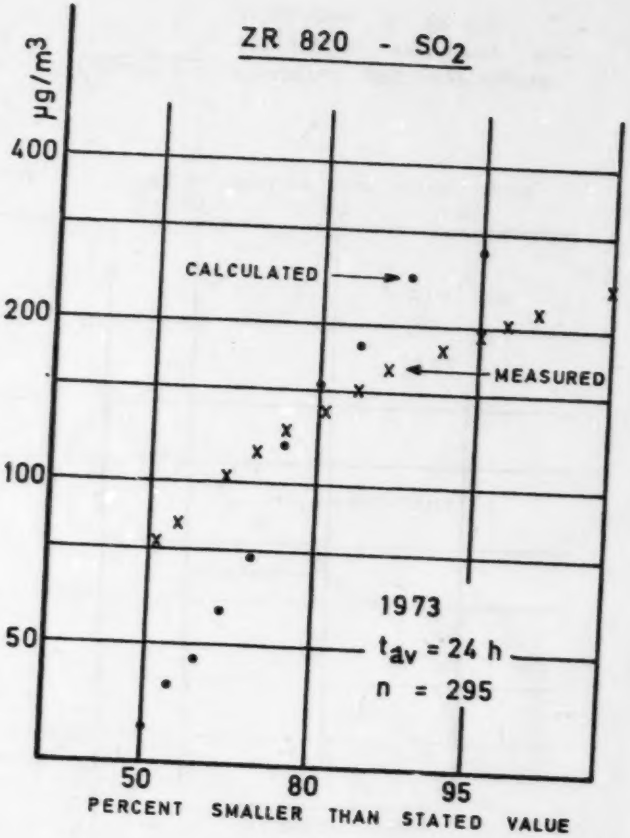

Figure 5b : Measured and calculated cumulative frequency distributions in ZR 820.

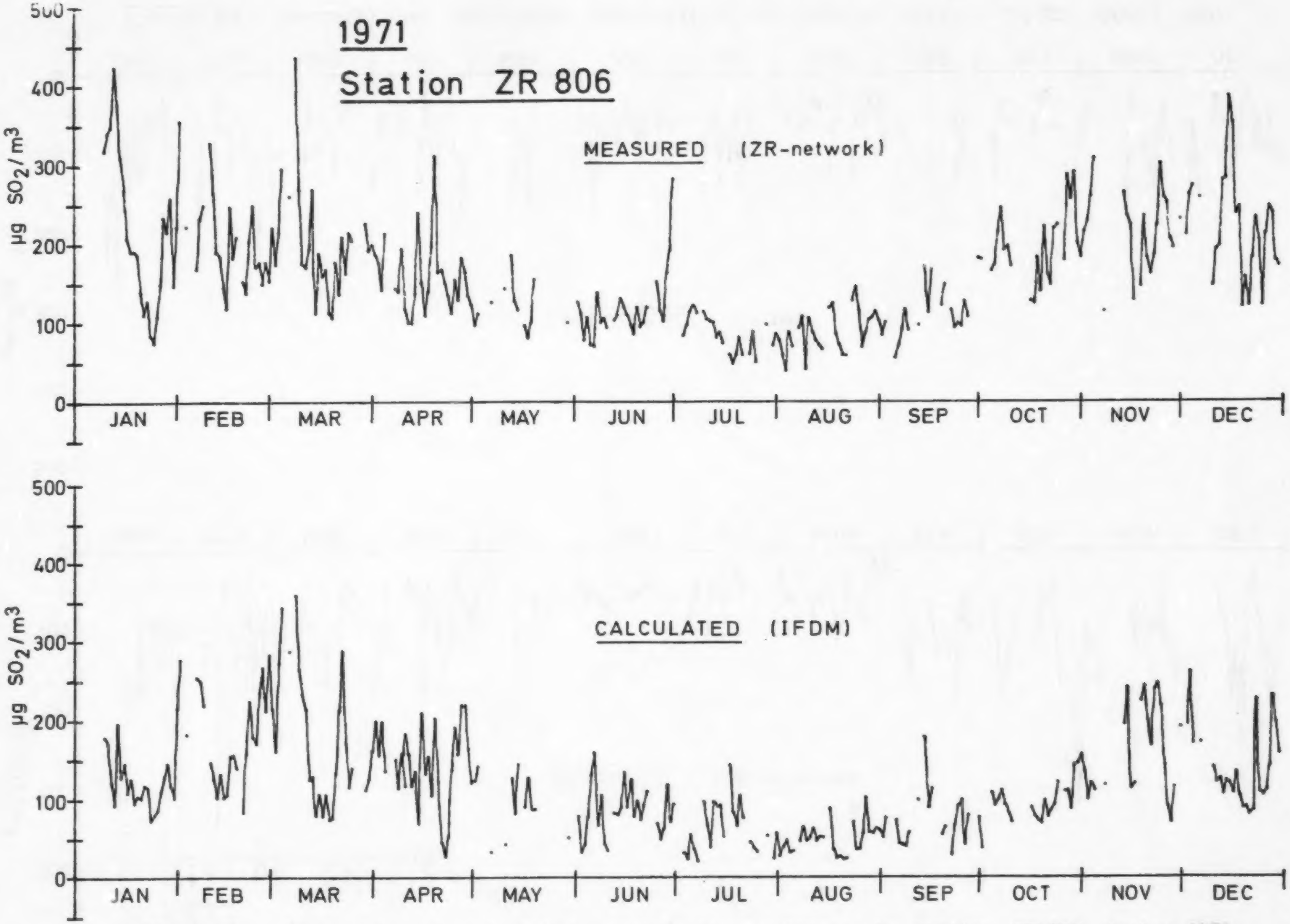

Figure 6a : Measured and calculated concentration patterns in station ZR 806 during 1971.

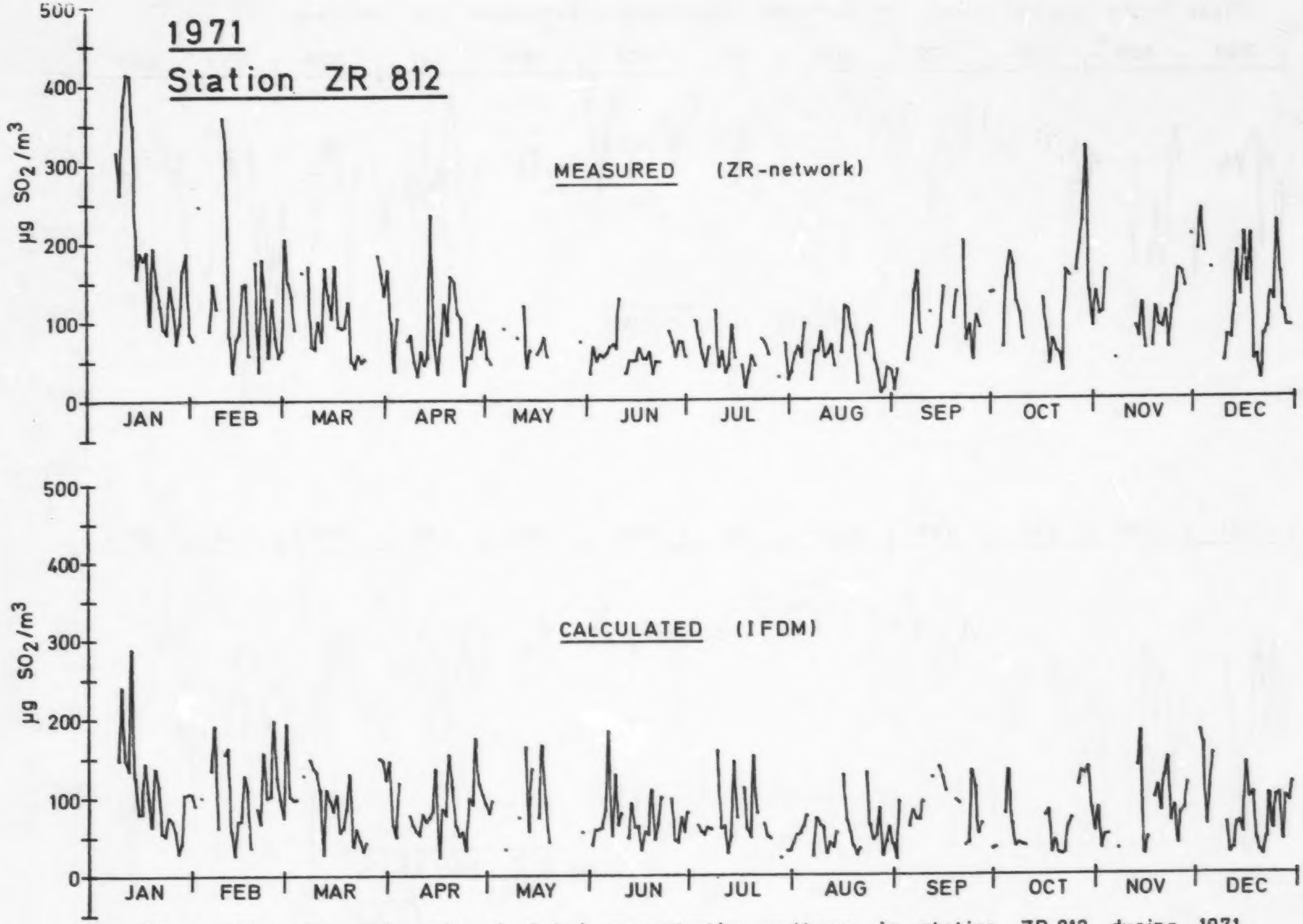

Figure 6b : Measured and calculated concentration patterns in station ZR 812 during 1971.

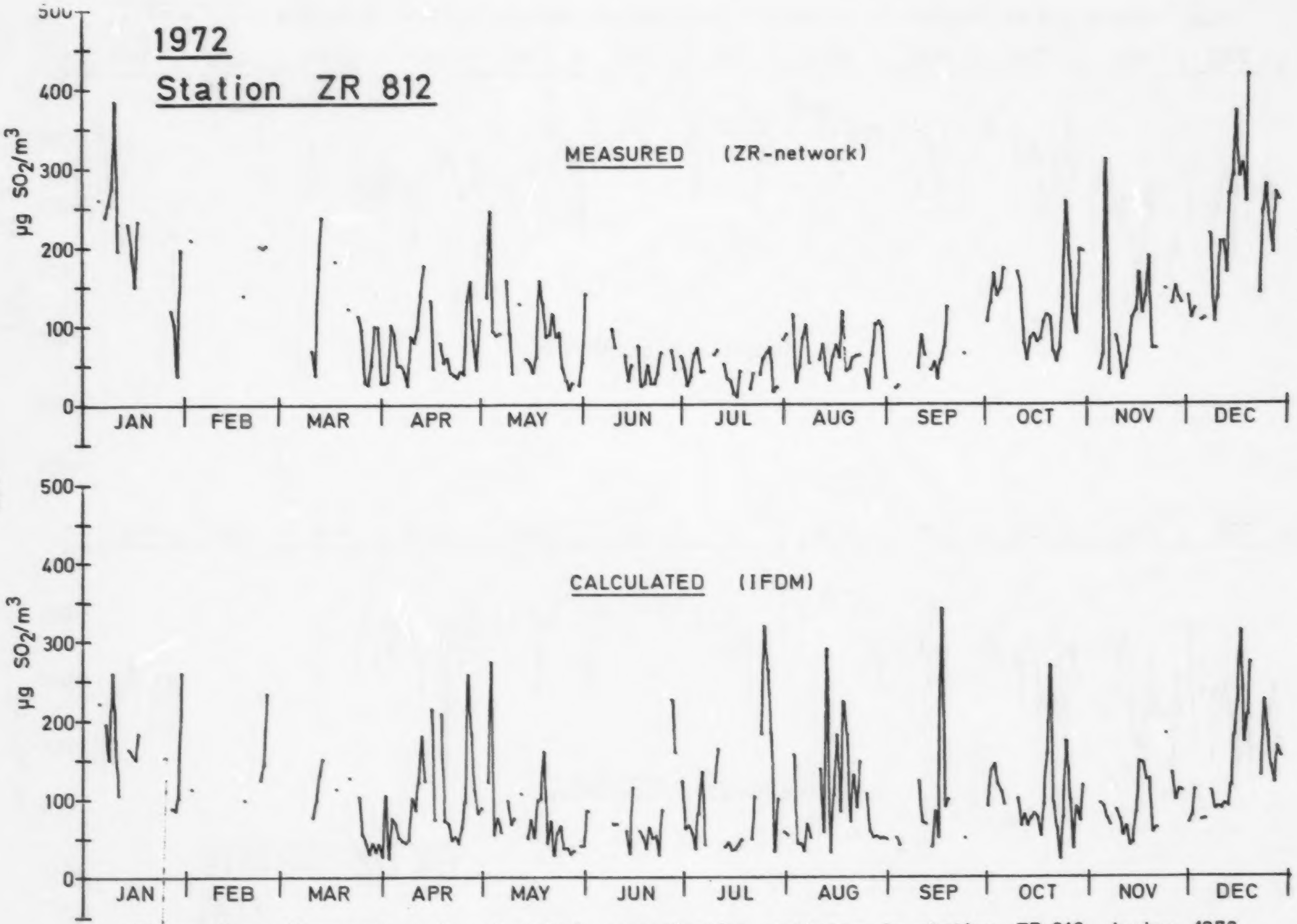

Figure 6 c : Measured and calculated concentration patterns in station ZR 812 during 1972.

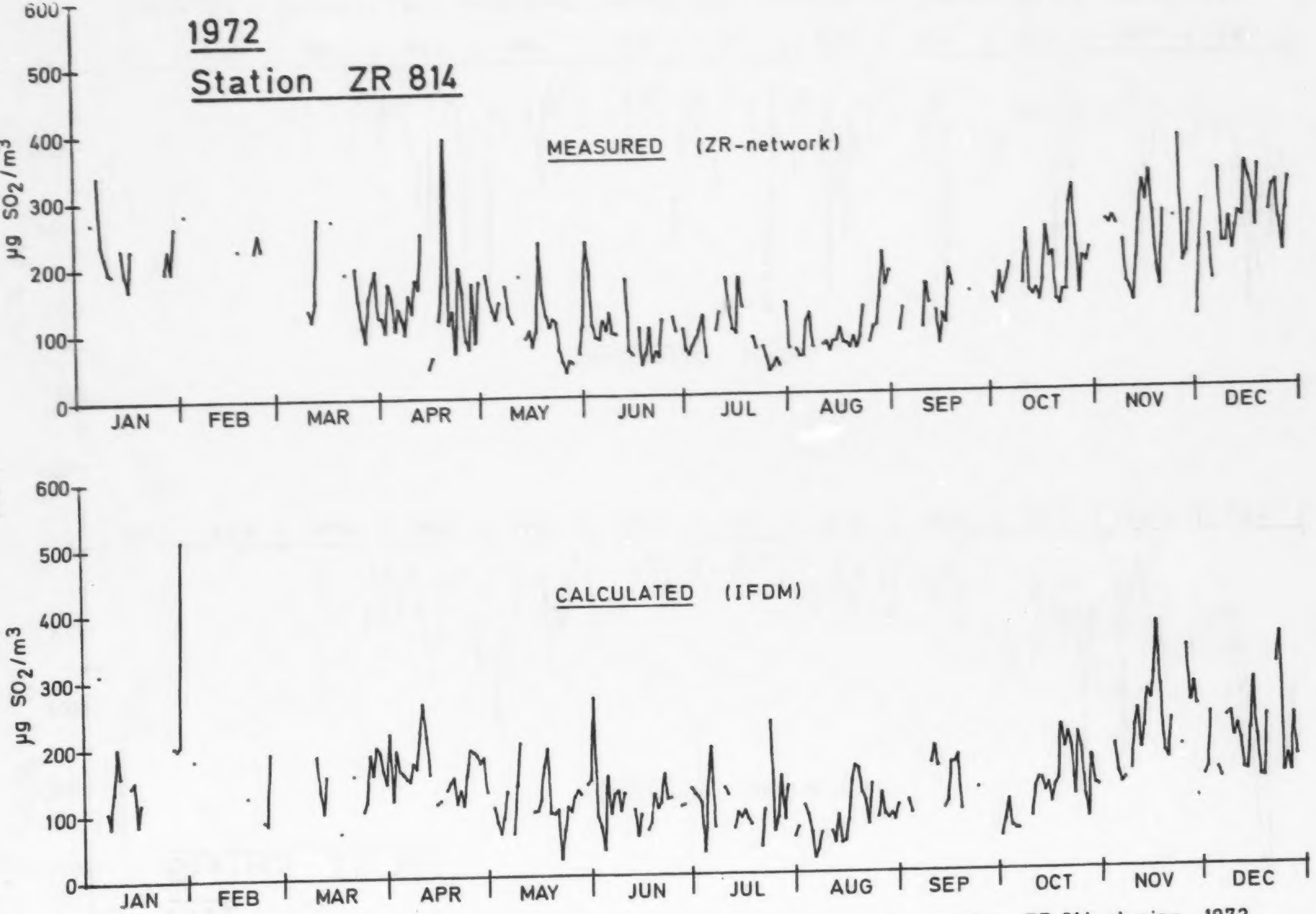

Figure 6d : Measured and calculated concentration patterns in station ZR 814 during 1972.

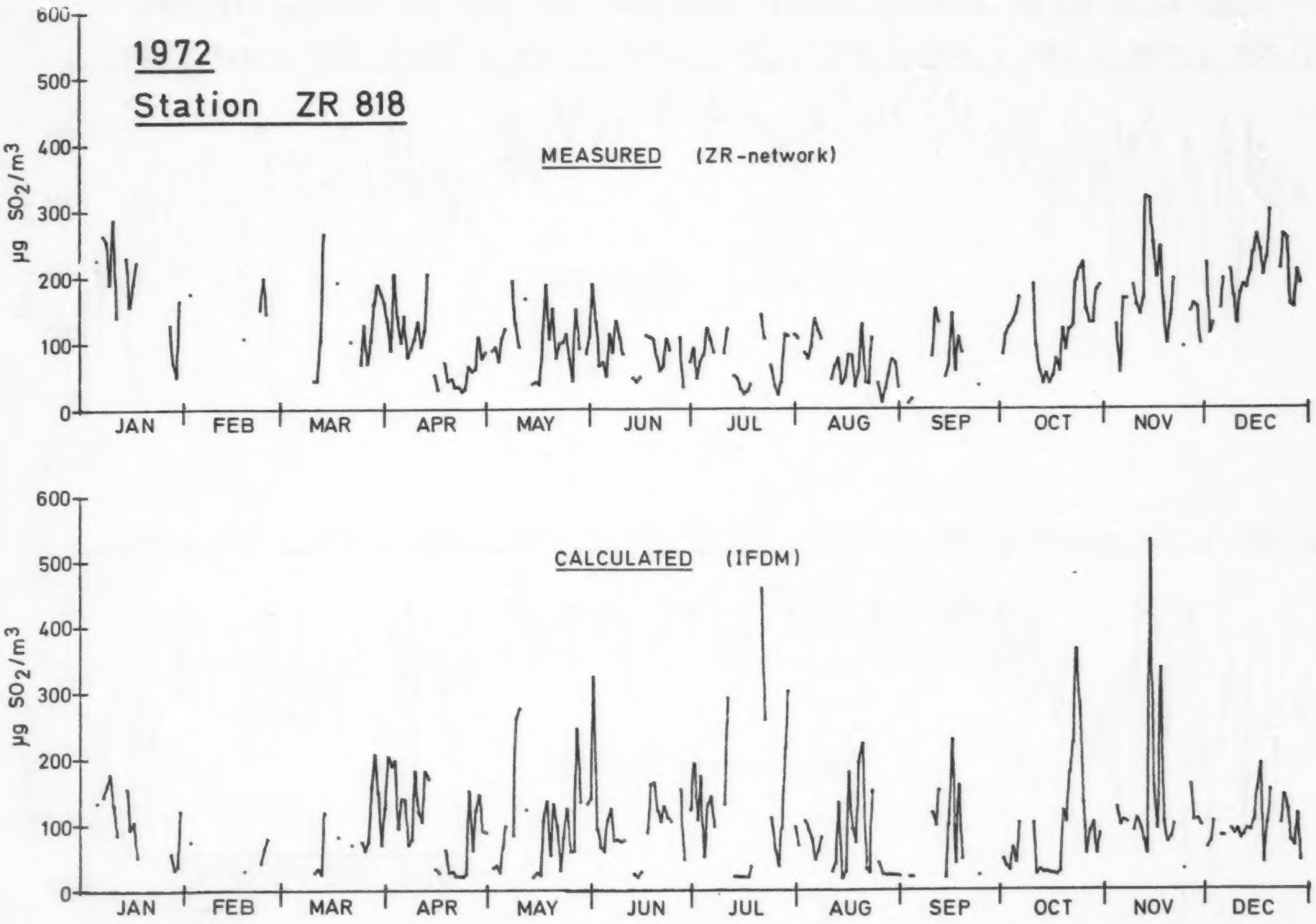

Figure 6e: Measured and calculated concentration patterns in station ZR 818 during 1972.

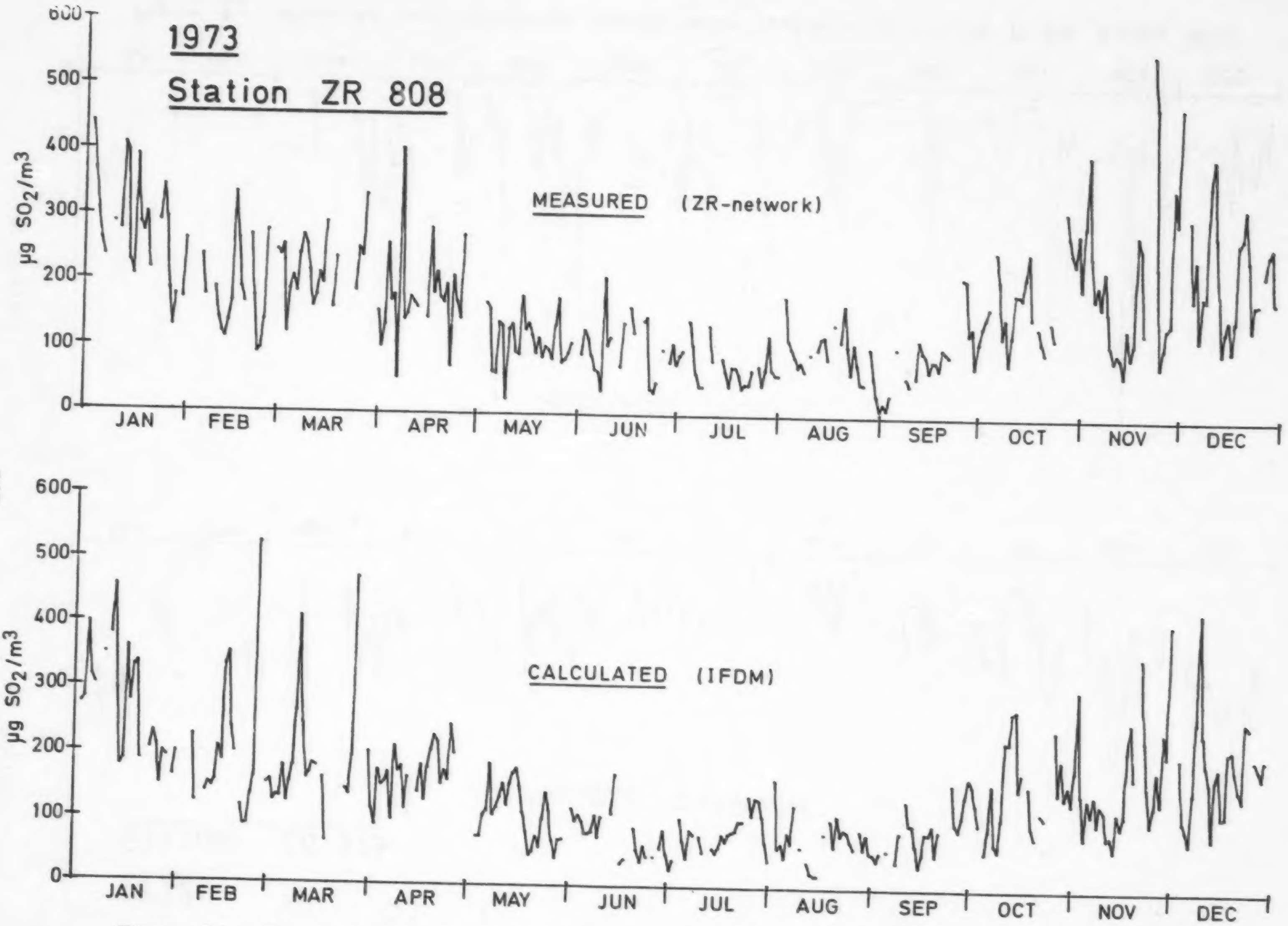

Figure 6f : Measured and calculated concentration patterns in station ZR 808 during 1973.

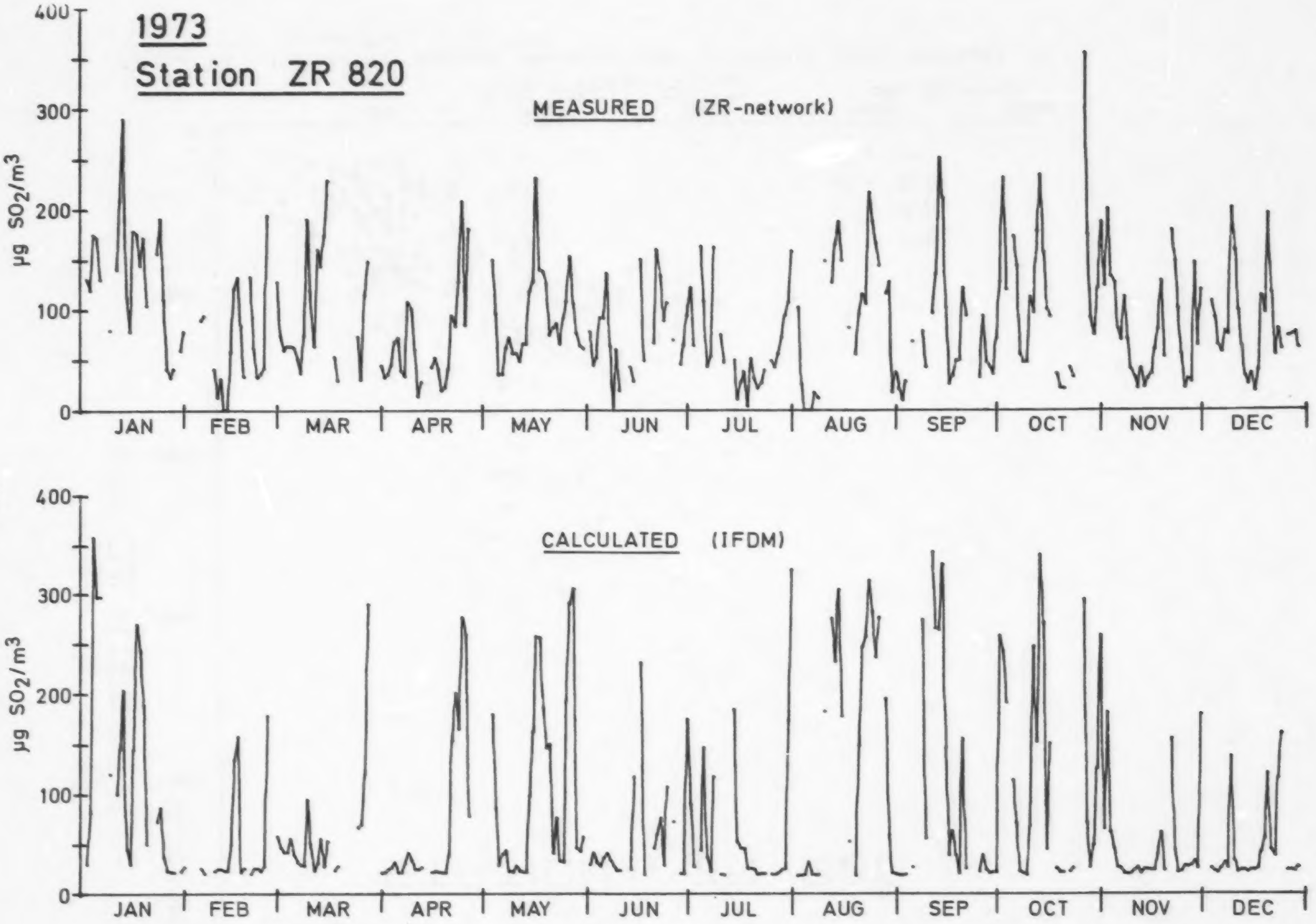

Figure 6g : Measured and calculated concentration patterns in station ZR 820 during 1973.

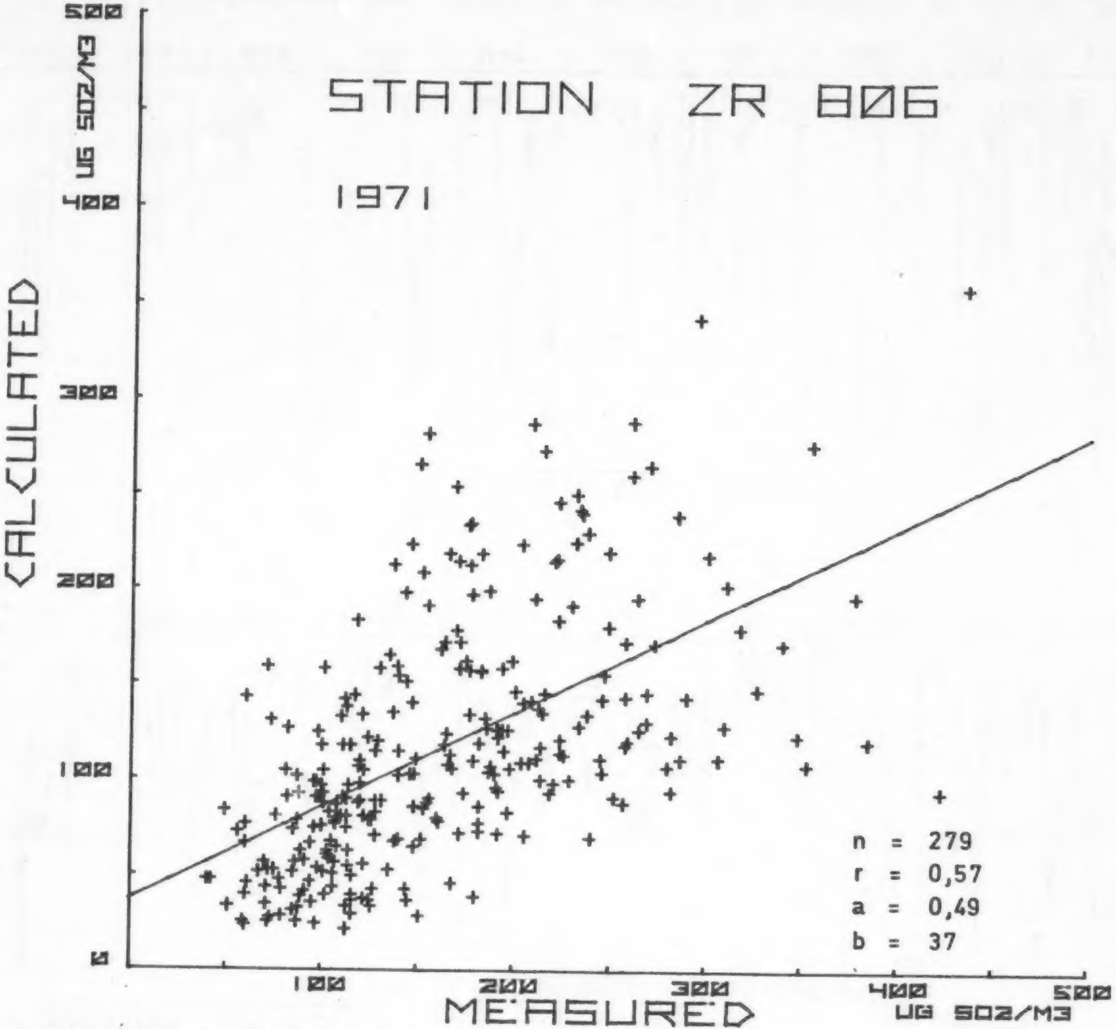

Figure 7a : Correlation between measured and calculated daily averages in station 806 during 1971

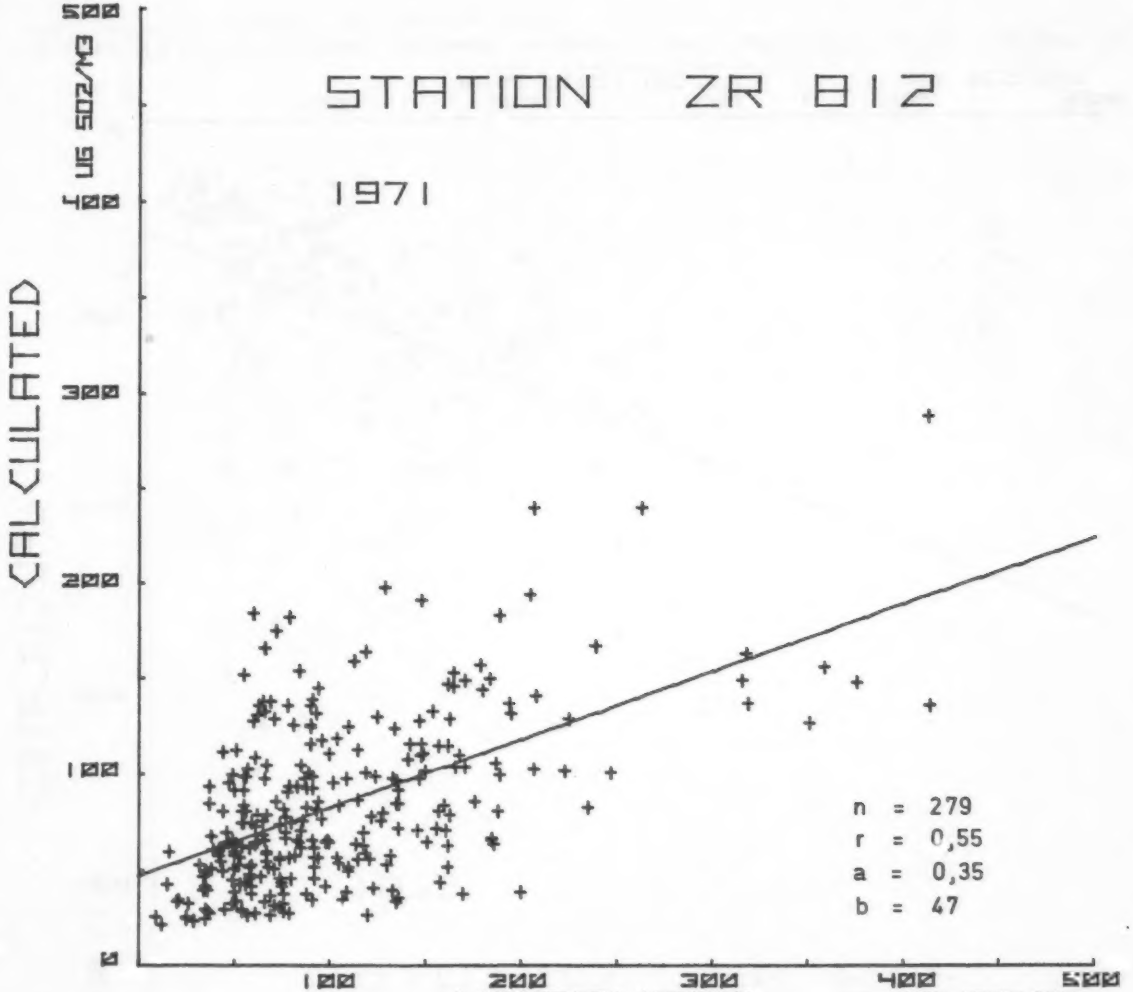

Figure 7b : Correlation between measured and calculated daily averages in station 812 during 1971

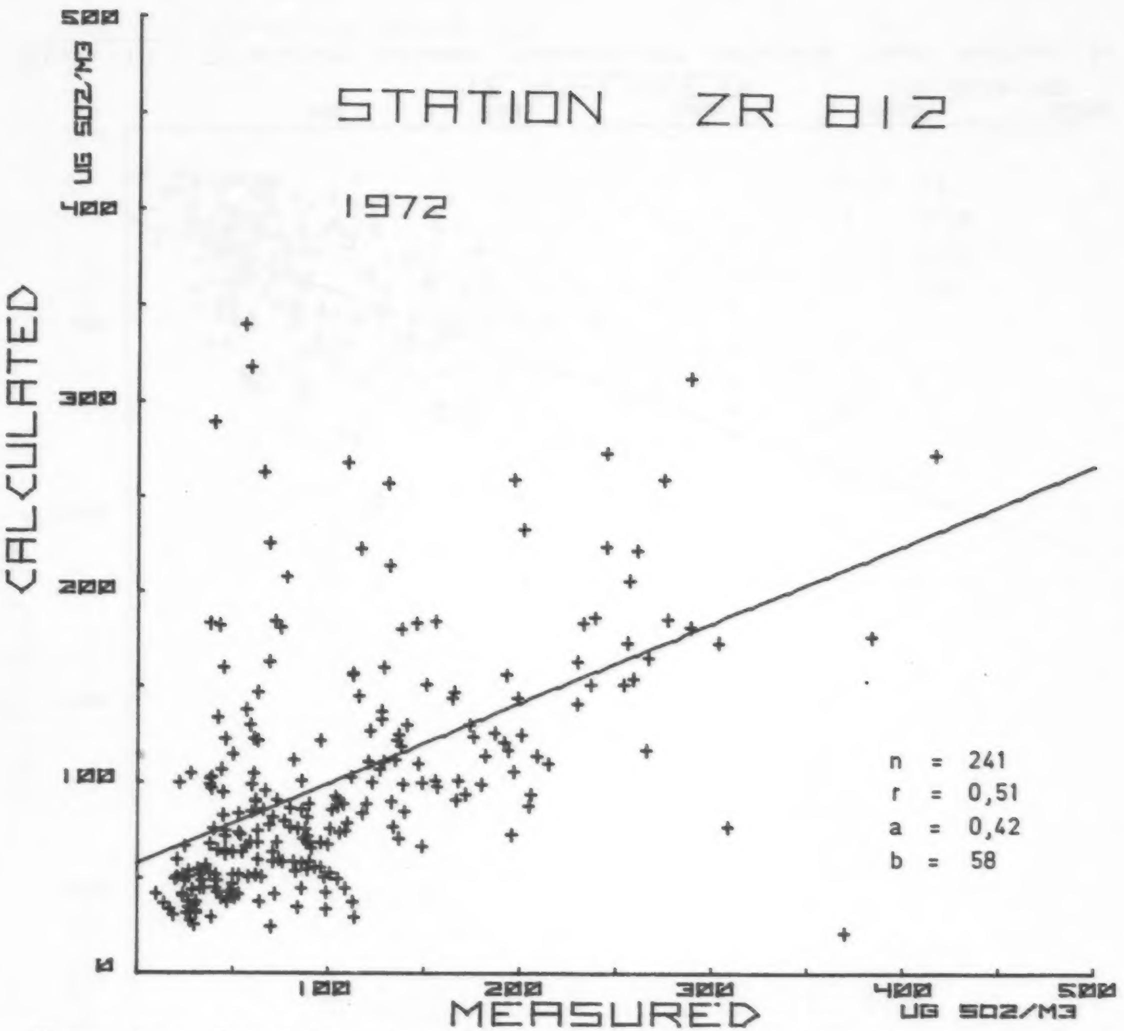

Figure 7c : Correlation between measured and calculated daily averages in station 812 during 1972

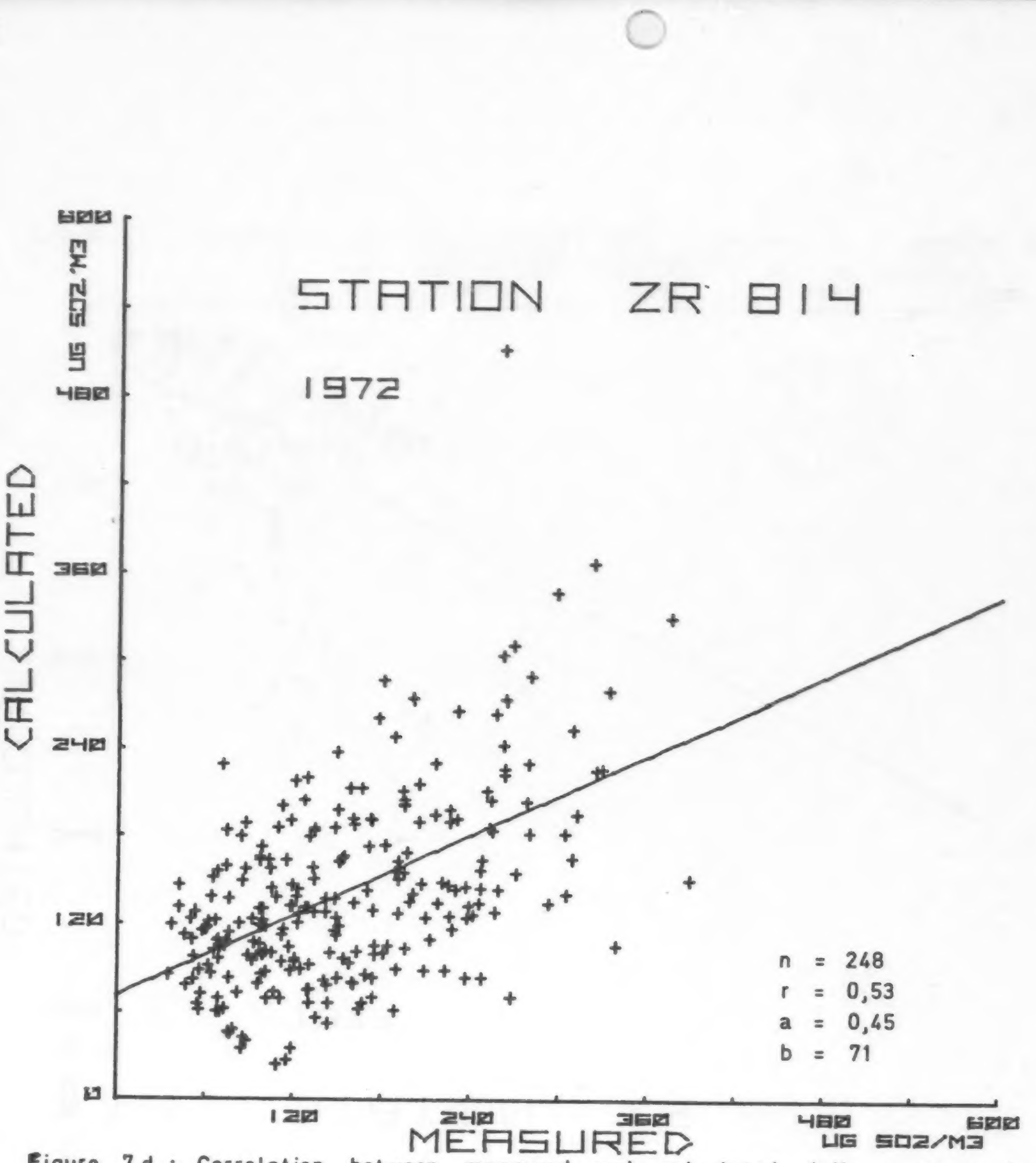

Figure 7 d : Correlation between measured and calculated daily averages in station 814 during 1972

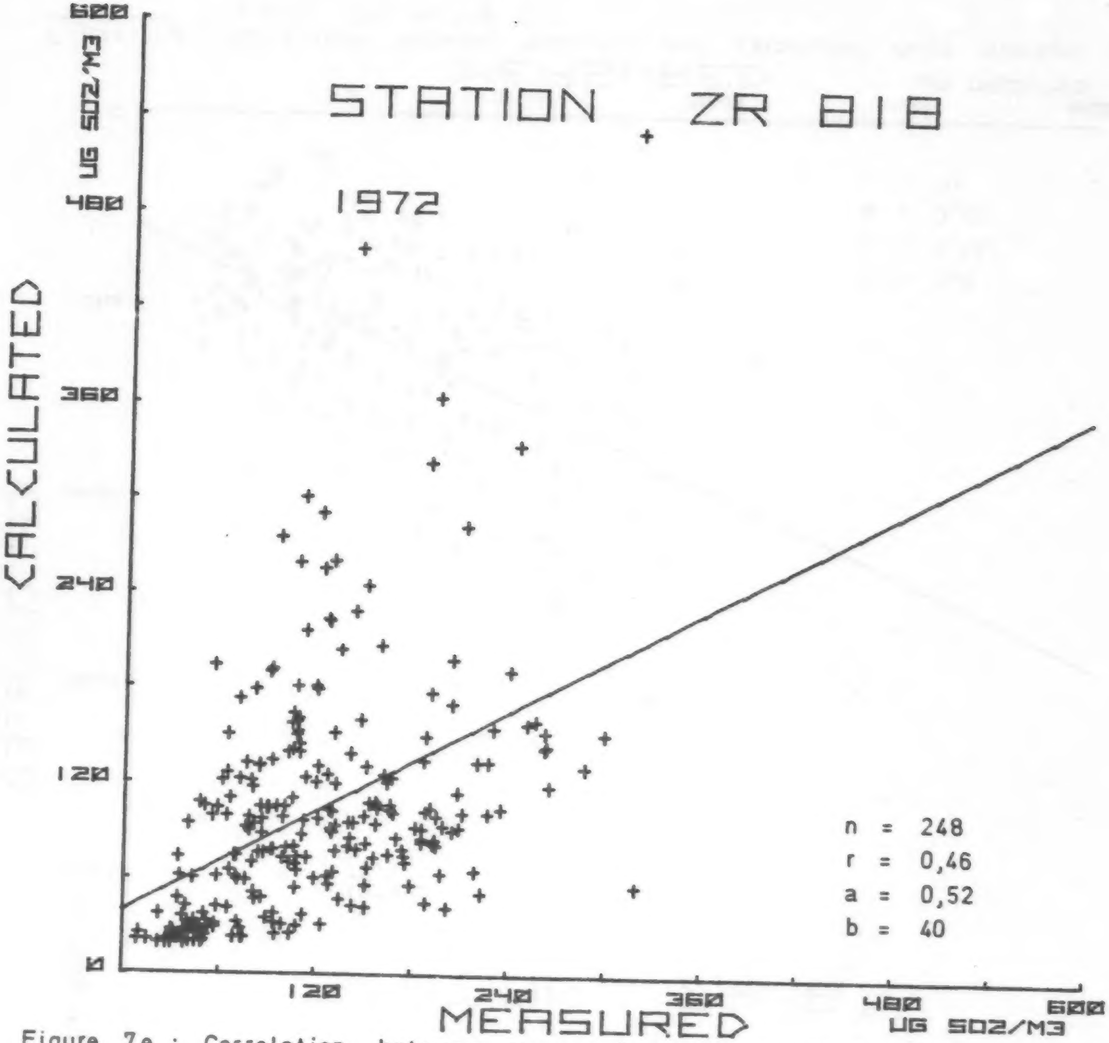

Figure 7e : Correlation between measured and calculated daily averages in

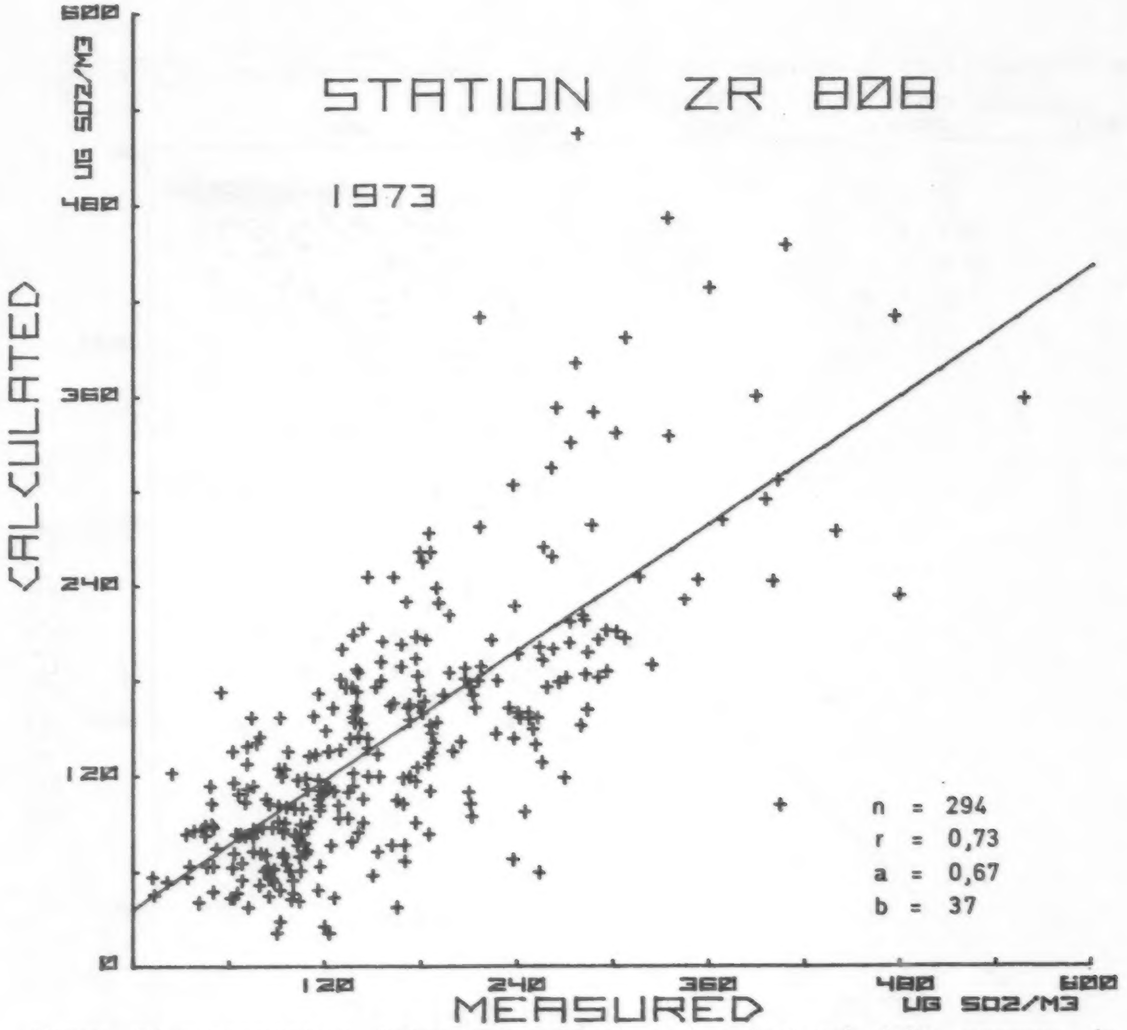

Figure 7f : Correlation between measured and calculated daily averages in station 808 during 1973

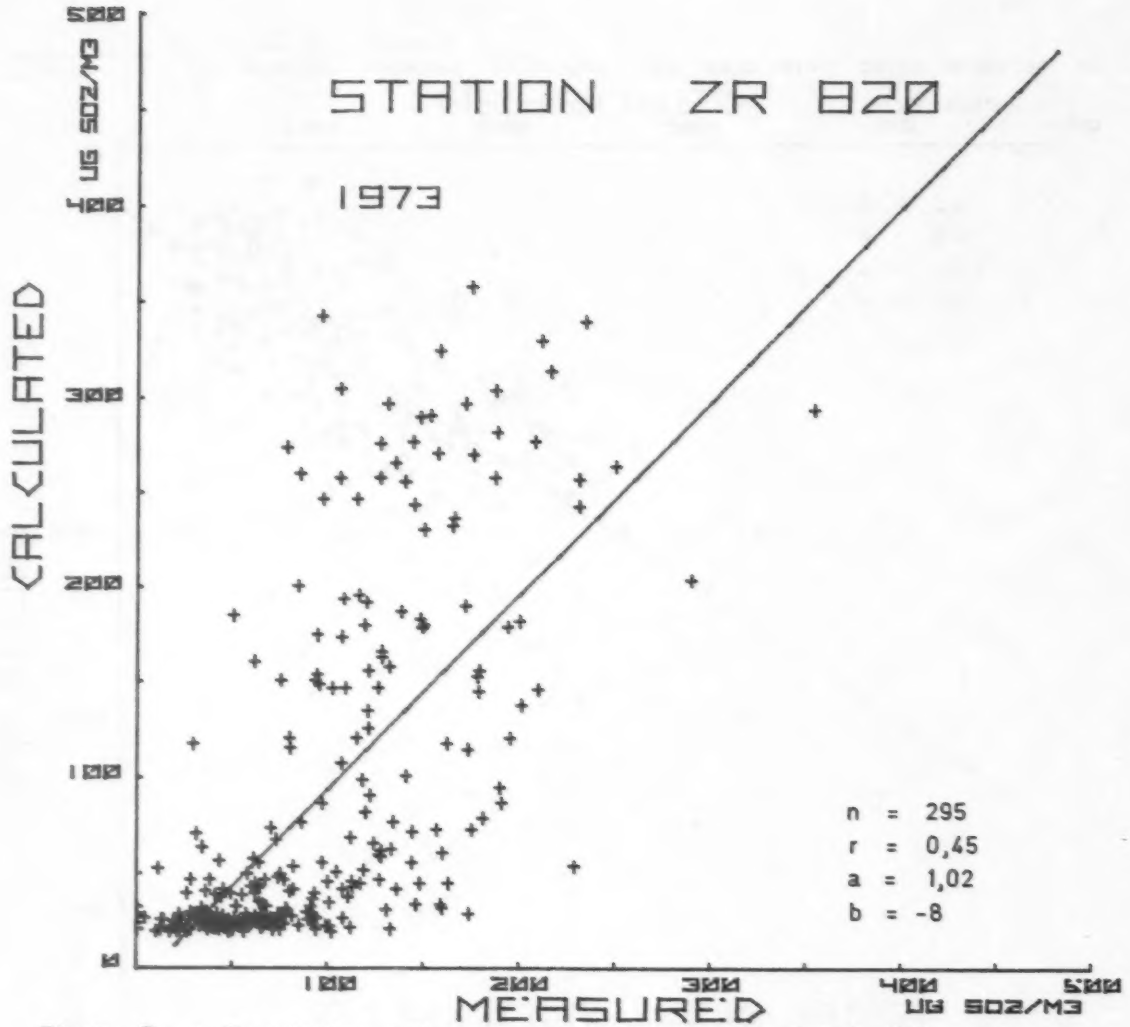

Figure 7g : Correlation between measured and calculated daily averages in station 820 during 1973

NATO/CCMS MEETING, AIRLIE, VIRGINIA

Discussion Report for Topic 1:
Examples of Model Validation and Model Application

September 8, 1976

Bruce A. Egan, Rapporteur

Paper 5: Diffusion Model Comparisons to Measured Data in Complex Terrain.
G. Hoffnagle.

The presentation was prefaced with a hypothesis that wind flow calculations need to be made prior to calculations of ground level concentrations in rough terrain. The paper summarized comparisons of model predictions and observations at the Huntington Canyon and the Garfield smelter sites in Utah and the Navajo power plant site in Arizona. The paper concludes that a numerical model incorporating terrain lifting effects provided more accurate and realistic estimates and patterns of ground level concentrations. The gaussian models used for comparison appear to overpredict concentrations under stable atmospheric conditions and underpredict under unstable conditions.

Discussion subsequent to the presentation brought out the following points: (1) The model does not include 'blocking' effects per se for very stable conditions but model parameters can be adjusted to force the flow around the terrain object. (2) The model is a steady state model for the prediction of one-hourly averaged concentrations. (3) Surface roughness effects can be included by changing the wind profile. Diffusivity levels are a function of local wind speed. (4) The model is based on potential flow considerations and does not include locally generated circulations. (5) Validation work to date on terrain models has been primarily concerned with comparisons of concentration levels. Very little work has been concerned with verifying hypothesized flow fields.

Discussion closed on the topic of gaussian versus numerical models. A question of fairness to more general gaussian models was raised on the basis that knowledge of flow fields was not included in the computations. It is not the gaussian plume form that is a problem but rather that the flow field cannot be ignored in either numerical or gaussian models. It would be possible to produce more realistic results with modified gaussian models if proper accounting for terrain effects on plume elevation and distortion are included, e.g. by coupling with a potential flow model. The Session Chairman pointed out that the EPA model referred to for stable conditions was originally developed for purposes of calculating 24-hour average concentrations, and not one-hour values and expressed an opinion that potential-flow type models would find increased acceptance in the future but that we were far from having a model applicable to a large number of situations of interest in rough terrain.

Paper 6: The Use And Validation of Dispersion Models in a Fjord Valley Area of Norway. B. Sivertsen.

In his presentation, Dr. Sivertsen compared air quality model predictions of different models to observed data for a meteorological flow situation involving diurnal land/sea breezes and mountain-valley winds. The models utilized included (a) a multiple source gaussian type model, (b) a vertically integrated finite-difference transport model utilizing a two-dimensional flow field calculated from a stream function, (c) a combination of the gaussian and finite difference model utilizing gaussian "puffs" and (d) a finite difference model utilizing the 'moment method' to suppress numerical pseudo diffusion. The results demonstrated the importance of including wind field variations into the model. The straight-line flow gaussian model showed the poorest agreement. Among the numerical models, the moment method resulted in the highest correlation coefficient and a concentration pattern in best agreement with the observed data. The upstream finite difference model matched the average conditions more accurately. Suggested improvements to the simulations included the development of more accurate wind fields, accounting for differential heating of the surface layer and extending the grid simulation to include multi-layers in the vertical. In the limited discussion period Sivertsen clarified the fact that the numerical models had only one layer in the vertical and that horizontal wind flow variations and temporal variations were important elements in the calculations.

Paper 7: The Validation of a Gaussian Plume Model for Long-Term Averaged Concentrations in the Rijnmond Area. F. Nieuwstadt.

The presentation described a model validation program performed utilizing data collected at about 120 locations for three-month winter and summer seasons. The results indicated that for the winter months an increase of the Pasquill dispersion coefficients to account for urban roughness effects would improve the model accuracy for area-source concentrations. For the summer months, the large elevated sources had a major impact and the model results were shown to be quite sensitive to the plume rise and dispersion rate assumptions. Discussion of the paper resulted in the following comments and information: (1) The correction factors to be applied to the winter season results were independent of stability-class; (2) background concentrations were estimated to be about 20% of the calculated values in the summer and contributed about 10% in the winter. Effect of uncertainties in background would add to the scatter in the results but would not alter the conclusions of the study. (3) Sensitivity tests of the model did not show significantly different results when compared with observed data for different plume rise formulae - although the impact of individual sources is sensitive to differences among alternative equations. (4) Background estimates were determined from upwind-downwind type analyses of ambient air quality data.

Paper 8: A Dual Tracer Study for the Validation of Models with Respect to High and Low Altitude Sources. W.E. Wilson.

Results of a study using simultaneous releases of tracers from near and well above the ground were presented. Air quality samples were collected during automobile traverses. Observed data were compared with predictions using the Shir-Shieh numerical model. Wilson concluded that the data analysis did not provide grounds for use of the model.

In the discussion of the paper, questions were asked about the extent that the measurements covered the area and whether some of the discrepancies in the model predictions could be associated with large spatial gradients of the ground level concentration pattern and differences in the time scales of the measurements and predicted levels. Meteorological inputs to the model were inversion height, ground level wind speed and a tower temperature difference measurement. The sampling time of the concentration measurements was estimated to be of order a few seconds. The "K-theory" numerical model used had a time step which was hypothesized to be much larger than the sampling time. Suggestions made to improve the model comparisons included incorporation of more extensive meteorological data - since the numerical model can accommodate these, and to calculate concentrations at specific monitoring locations rather than computing grid-cell-averaged values. Alternatively, the measurements could be spatially averaged for comparative purposes. The possibility that pseudo-diffusive effects may be contributing to the discrepancies also needs to be explored.

Paper 9: Validation of The "Immission Frequency Distribution Model" in The Region of Antwerpen. J.G. Kretzchmar.

The author presented comparisons of frequency distributions of observed and predicted air quality concentrations for six stations in the region of Antwerpen. The model utilizes twenty-degree sectors, seven stability classifications and plume rise formulae after Stümke. Emissions were corrected on an hour-by-hour basis to include effects of temperature, wind speed, and precipitation on heating needs. Correlation coefficients were found to be in range of 0.5 to 0.98. Suggested improvements to the model included a better treatment of background contributions and improved estimation of wind speed at plume height. Improved validation procedures making more extensive use of spatial distributions of concentrations were being investigated.

In the discussion period, it was stated that the log-normal frequency distribution provided a good fit to both the observed data and the calculated concentration distributions. Calms (defined as cases where the wind speed was less than one meter per second) were not included in the analyses because of wind direction uncertainties.

7 th NATO/CCMS
International Technical Meeting
on Air Pollution Modeling

TOPIC II
INTERREGIONAL AND REGIONAL MODELS

7th International Technical Meeting
on Air Pollution Modeling and its Application

Preliminary Results of the Application of a Statistical Model on Interregional Transport of SO_2

B. Dietzer
Institut für Meteorologie
Technische Hochschule Darmstadt

September 7 - 10, 1976
Airlie Virginia
United States of America

1. Introduction

A Dutch - German project was initiated to investigate the interregional transport of SO_2 from the Ruhr area into the Netherlands. In the region between Ruhr area and the Netherlands a network of about 31 stations was set up, which measures hourly averages of the SO_2 surface concentrations.

As until now no emission inventory was available, it is tried, to describe the SO_2 patterns with a statistical model.

2. Model

The used model is based on the description of the observed patterns of SO_2 concentrations with a set of eigenvectors, which vary only in space, and their associated time dependent eigencoefficients. In the meteorological literature it was used several times, for example by Peterson, to calculate SO_2 over Metropolitan St. Louis in 1970 and 1972. Thus, the model will be described briefly.

At m stations we have observed SO_2 concentrations. Every station measures synchronously at n times. Then we can set up a $m \times n$ matrix P, which contains the n observations at m stations.

The matrix P can be expressed in terms of the $m \times m$ eigenvectormatrix Y and their associated coefficients Q, which is a $m \times n$ matrix.

$$P = Y \cdot Q \qquad (1)$$

We get the eigenvectors, if we solve the following eigenvalue problem

$$A \cdot Y = Y \cdot D \qquad (2)$$

where D is the $m \times m$ diagonal matrix of the eigenvalues, and

$$A = P \cdot P^T \tag{3}$$

is a symmetric $m \times m$ matrix, which contains the observed measurements.

If we have computed the eigenvectors with a given numerical method, we can calculate the eigencoefficients after the expression

$$Q = Y^T \cdot P \tag{4}$$

As the observed measurements are correlated among each other, it can be shown, that only with k eigenvectors ($k < m$) the observed pattern can be described well. The fraction of the total variance of the observed data field G, explained by the k eigenvectors, depends on the magnitude of its corresponding eigenvalues λ_i as follows :

$$G = \frac{\sum_{i=1}^{k} \lambda_i}{\sum_{i=1}^{m} \lambda_i} \tag{5}$$

Therefore we can compute the observed patterns with fewer than $n \cdot m$ values, that is with $n \cdot k$ values, if G is large enough.

If the eigencoefficients, which vary only in time, are correlated with meteorological variables, then it is possible to calculate the eigencoefficients from given or forecasted meteorological data. Together with the eigenvectors the concentrationfield can be computed.

3. Data

From the 31 SO_2 - stations, 17 were selected, which are considered not to be influenced mainly by local sources. Their position is given in Fig. 1.

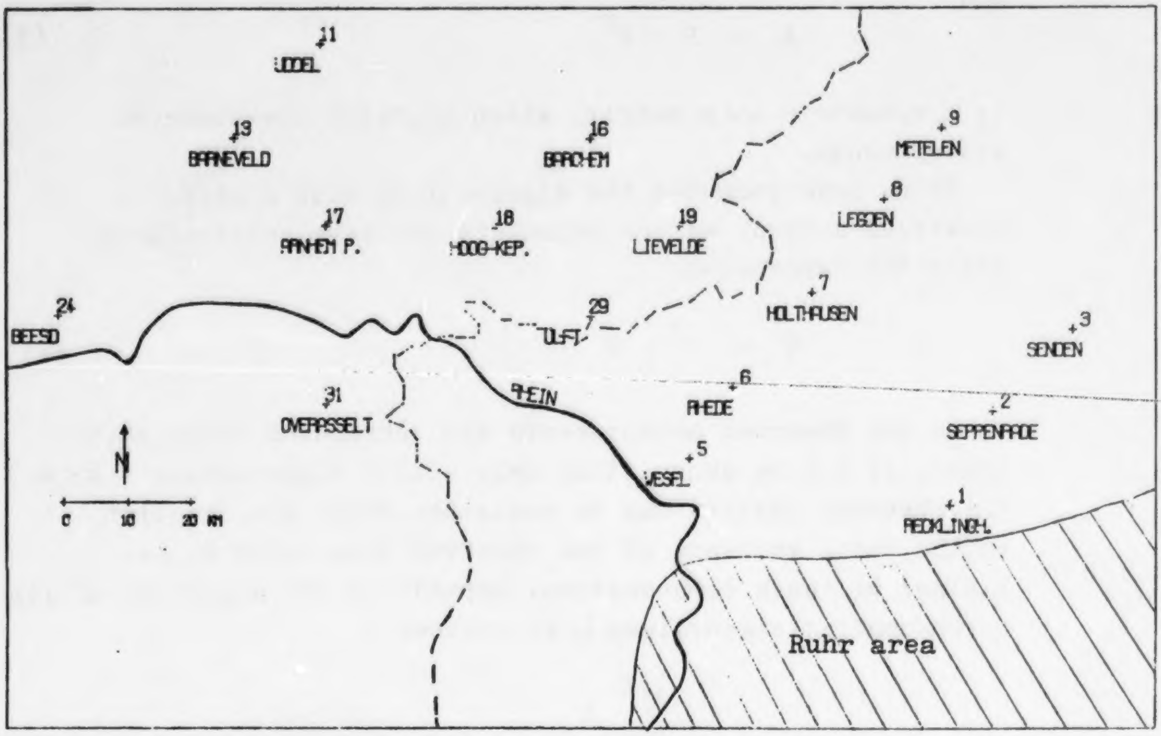
11
UDDEL
13
BARNEVELD
16
BARCHEM
9
METELEN
8
LEGDEN
17
ARNHEM P.
18
HOOG-KEP.
19
LIEVELDE
24
BEESD
29
ULFT
7
HOLTHAUSEN
3
SENDEN
31
OVERASSELT
RHEIN
6
RHEDE
2
SEPPENRADE
N
5
WESEL
1
RECKLINGH.
0
10
20 KM
Ruhr area

Fig. 1 Position of the used SO_2 stations.

At these stations hourly averaged SO_2 ground concentrations were available from May 1974 to October 1975. For the first calculations seven days were selected, at which measurements of the temperature gradient in the lower atmosphere were also available.

Altogether we have for this period 168 measured SO_2 concentrations at each of the 17 stations. It was necessary to correct the SO_2 measurements. A subjective method was used, drawing concentration isolines and fitting them by hand.

4. Calculation of the eigenvectors

With these SO_2 concentrations the matrix A was built up, and the eigenvectors and their associated coefficients were computed.

The cumulative percentage variance explained by the first seven eigenvectors, computed after formula (5), is shown in Table 1.

Correlating the calculated values from one to seven eigenvectors with the observed measurements, we get the mean correlation coefficient, which is also presented in Table 1.

It is seen, that with the first five eigenvectors we can explain 96 percent of the measured SO_2 concentrations.

Table 1. Cumulative percentage variance explained by the first seven eigenvectors and mean corr. coeff. between observed and computed SO_2 concentrations.

Eigenvector	1	2	3	4	5	6	7
Explained percentage	83.	88.	93.	95.	96.	97.	98.
Mean corr. coeff.	0.69	0.72	0.87	0.91	0.92	0.94	0.95

5. Correlation with meteorological variables

Now the time dependent eigencoefficients were correlated with meteorological variables, such as wind direction, wind speed,temperature,thermal stability and so on.

The highest correlation was found between the wind direction of the surface wind, expressed by a sinus function and using a phase shift for the wind direction. But also wind speed was found to be well correlated with the eigencoefficients.

Unfortunately data for thermal stability and temperature were only available for 35 hours of the total 168 hours. The highest correlation coefficient was found for the mean temperature gradient between 0 and 200 meters, and the height of the lowest temperature inversion.

The diurnal and seasonal variation of the SO_2 concentrations were best expressed by trigonometrical functions, containing the hour or month of the time, at which the concentrations were measured.

6. The regression equations

With the chosen independent variables, regression equations were computed for the first five eigencoefficients. For the whole period of seven days only the four independent variables wind direction, wind speed, hour and month of the measuring date were used.

For the period, during which data of the thermal stratification were available, five additional independent variables could be added to the regression equations : the averaged temperature gradient between 0 and 200 meters, the height and the thickness of the lowest temperature inversion, the temperature and the wet bulb temperature at ground.

To check the influence of these thermal variables, for the same period, the regression equations were also calculated without these variables.

In Table 2, we find the multiple correlation coefficient of the regression equations and percentage of variance explained by the used meteorological variables for the first five eigencoefficients.

In the first case, for the whole considered period, we have for the higher eigencoefficients a percentage of explained variance of about 60 percent, not a very high value.

If only the cases are considered, for which data of the thermal stratification were available, we find higher multiple correlation coefficients, especially for the 4 th and 5 th eigencoefficient.

Using the stratification data in the regression for the eigencoefficients, this yields a higher multiple correlation coefficient for all five eigencoefficients. The percentage of explained variance was about 80 percent, varying from 89 percent for the 1 st and 4 th, to 70 percent for the 2 nd eigencoefficient.

Now we can compute the SO_2 concentrations from the independent variables using the regression equations. Then we can compute the correlation coefficient between observed and calculated values and the mean ratio of calculated and observed concentrations. The values are shown in Table 3.

Table 2. Multiple correlation coefficient (MCC) and percentage of variance (VAR) explained by the used meteorological variables for three types of regression equations, for the first five eigencoefficients.

case 1 : regression using wind direction and speed, hour and month of the date.
The whole period of seven days : n = 168

case 2 : regression using the same variables as in case 1. Only hours, at which thermal data were available : n = 35.

case 3 : regression using wind direction and speed hour and month of the date, temperature gradient between 0 and 200 m, height and thickness of the lowest inversion, temperature and wet bulb temperature at ground. The same hours as in case 2 : n = 35.

Eigencoefficients		1	2	3	4	5
case 1	MCC	0.90	0.72	0.80	0.75	0.73
	VAR	81.	52.	65.	56.	53.
case 2	MCC	0.92	0.79	0.81	0.89	0.85
	VAR	84.	62.	65.	79.	73.
case 3	MCC	0.94	0.84	0.85	0.95	0.92
	VAR	89.	70.	73.	89.	84.

Table 3. Correlation coefficient r and mean ratio S between calculated and observed SO_2 concentrations for the three cases of Table 2.

	r	S
case 1	0.66	1.65
case 2	0.72	1.53
case 3	0.78	1.39

The calculated values are well correlated with the observed concentrations. The ratio between calculated and observed values indicates a mean overestimation by the computed values. But a direct comparison of observed and calculated data, given in Table 4 for case 3, shows, that only the lower concentrations are overestimated, the higher are underestimated. In this case 3, fifty-six percent of the observed - calculated cases agree. The skill score is 0.39.

Table 4. Comparison of observed and calculated values of SO_2 in µgr/m^3 for case 3

calculated concentrations	observed concentrations: 0- 50	50-100	100-150	150-200	200-250	250-300	>300	total
0- 50	155	29	0	0	0	0	0	184
50-100	62	117	33	4	0	0	0	216
100-150	6	41	46	24	5	1	0	123
150-200	0	7	9	12	10	4	0	42
200-250	0	0	5	4	5	2	4	20
250-300	0	0	0	1	1	2	3	7
> 300	0	0	0	0	0	1	2	3
total	223	194	93	45	21	10	9	595

The Figure 2 shows a situation with high SO_2 concentrations. The first pattern describes the observed concentration field, indicating a SO_2 transport with south-easterly winds from the Ruhr area into the Netherlands.

The patterns below, show the computed concentrations, first without the stratification data, and then using them. The high concentrations are found to be underestimated, but in the case with stratification data the calculated concentrations are higher, than in the case without.

A situation with low SO_2 concentrations and westerly winds is given in Figure 3.

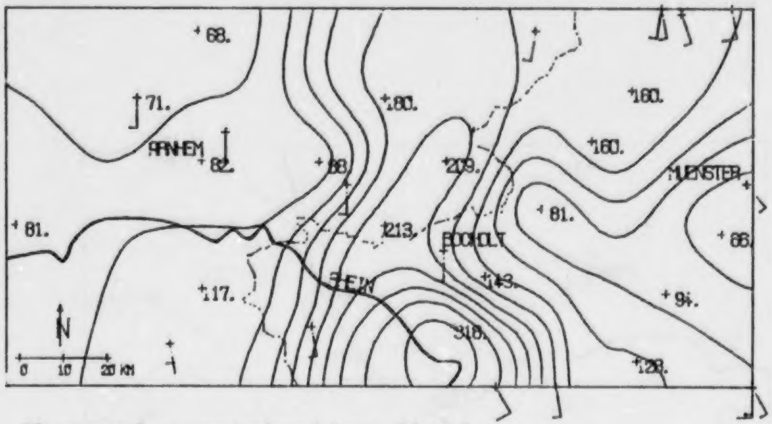
68.
71.
ARNHEM
82.
88.
180.
160.
160.
209.
MUENSTER
81.
81.
213.
BOCHOLT
86.
RHEIN
143.
117.
94.
N
318.
0
10
20 KM
128.

Observed concentration field

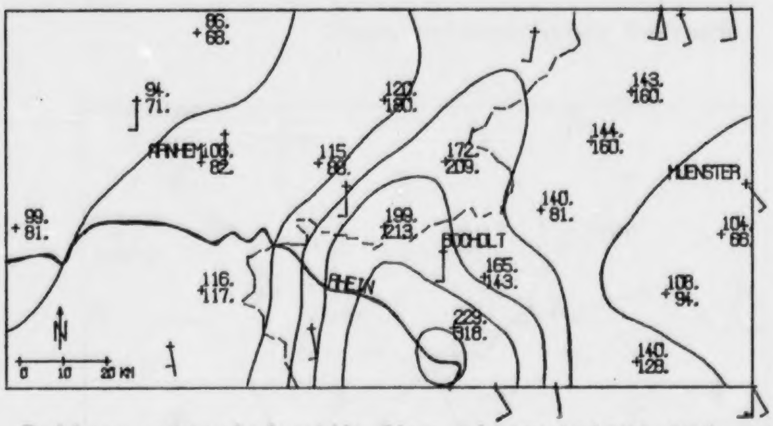
86.
68.
94.
71.
120.
180.
143.
160.
144.
160.
ARNHEM
108.
82.
115.
88.
172.
209.
MUENSTER
140.
81.
99.
81.
199.
213.
BOCHOLT
104.
86.
165.
143.
116.
117.
RHEIN
108.
94.
N
229.
318.
0
10
20 KM
140.
128.

Pattern computed with five eigenvectors and eigencoefficients, using wind and time as independent variables.

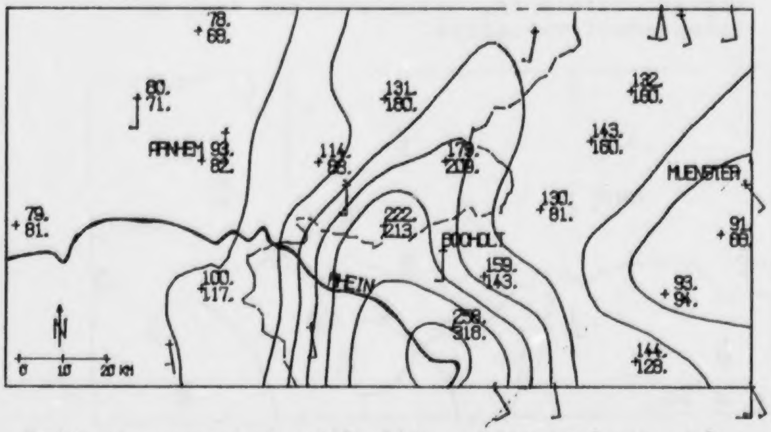
78.
68.
80.
71.
131.
180.
132.
160.
143.
160.
ARNHEM
93.
82.
114.
88.
179.
209.
MUENSTER
130.
81.
79.
81.
222.
213.
BOCHOLT
91.
86.
159.
143.
100.
117.
RHEIN
93.
94.
N
258.
318.
0
10
20 KM
144.
128.

Pattern computed with five eigenvectors and eigencoefficients, using additionally stratification data as independent variables.

Figure 2. SO_2 concentrations $\left[\mu gr/m^3\right]$ 23rd February 1975, 11 MEZ

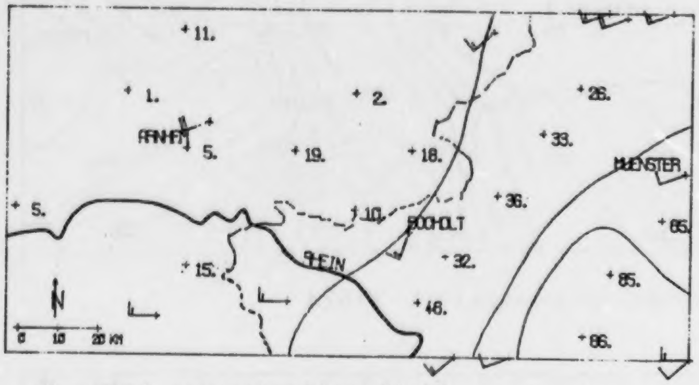
11.
1.
2.
26.
ARNHEM
5.
19.
18.
33.
MUENSTER
5.
10.
BOCHOLT
36.
65.
15.
RHEIN
32.
85.
N
46.
0 10 20 KM
86.

Observed concentration field

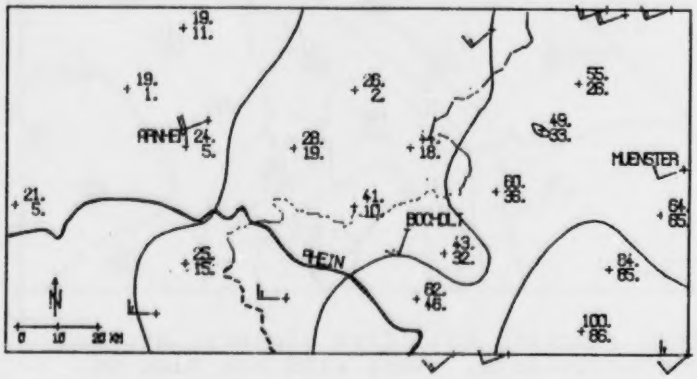
19.
11.
19.
1.
26.
2.
55.
26.
ARNHEM
24.
5.
28.
19.
18.
48.
33.
MUENSTER
21.
5.
41.
10.
60.
36.
BOCHOLT
64.
65.
25.
15.
RHEIN
43.
32.
84.
85.
N
62.
46.
0 10 20 KM
100.
86.

Pattern computed with five eigenvectors and eigencoefficients, using wind and time as independent variables.

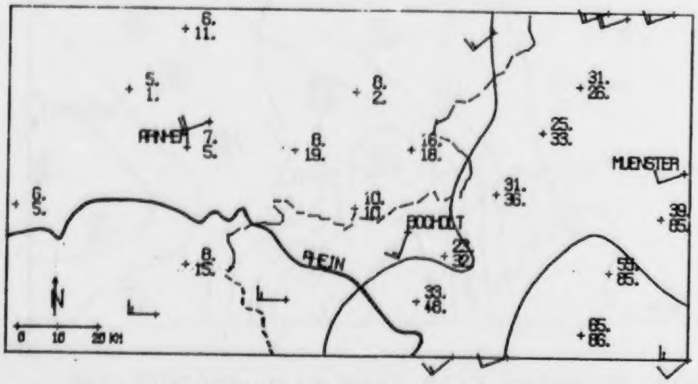
6.
11.
5.
1.
8.
2.
31.
26.
ARNHEM
7.
5.
8.
19.
16.
18.
25.
33.
MUENSTER
6.
5.
10.
10.
31.
36.
BOCHOLT
39.
65.
8.
15.
RHEIN
23.
32.
59.
85.
N
33.
46.
0 10 20 KM
65.
86.

Pattern computed with five eigenvectors and eigencoefficients, using additionally stratification data as independent variables.

Figure 3. SO_2 concentrations $\left[\mu gr/m^3\right]$ 4th July 1974, 12 MEZ

7. Computing the whole period

In a second computation, the model was applied to a larger number of measurements. For all hours during May 1974 to October 1975, at which all the 17 stations had measured, the eigenvectors and eigencoefficients were computed, after the procedure given before. Data from 2461 hours were used. The observed concentrations were taken uncorrected into the calculations.

The cumulative percentage variance explained by the first seven eigenvectors is shown in Table 5. The mean correlation coefficient of the observed data and calculated values from up to seven eigenvectors is also given.

Table 5. Cumulative percentage variance explained by the first seven eigenvectors and mean corr. coeff. between observed and computed SO_2 concentrations.

Eigenvector	1	2	3	4	5	6	7
Explained percentage	67.	76.	81.	84.	87.	89.	91.
Mean corr. coeff.	0.62	0.68	0.73	0.76	0.79	0.85	0.86

The values are about 10 percent lower, than the values from the first period.

Then the regression equations for the eigencoefficients were computed, but using as independent values only wind direction, wind speed, hour and month of the measuring date. The multiple correlation coefficients and the percentage of variance explained by the independent variables are quite low, as we see in Table 6.

With the regression equations for the first five eigencoefficients and the chosen independent variables, the concentrations of the whole period from May 1974 to October 1975 were computed and compared with the observed values, if available. The correlation coefficient was found to be 0.41. Correlating

Table 6. Multiple correlation coefficient (MCC) and percentage of variance (VAR) explained by the used meteorological variables for the first seven eigencoefficients.

Eigencoefficients	1	2	3	4	5	6	7
MCC	0.83	0.71	0.55	0.49	0.57	0.49	0.36
VAR	69.	50.	30.	24.	33.	24.	13.

Table 7. Mean concentrations of SO_2 during the period from 1.5.74 to 31.10.75.
Calculated values using five eigenvectors and their associated coefficients, which are computed from wind speed, wind direction, hour and month of the measuring date.

station	mean value SO_2 [μgr/m^3]		ratio $\overline{S}_{cal}/\overline{S}_{obs}$	corr. coeff.	number of values
	observed	calcul.			
Recklinghausen	70.84	74.17	1.05	0.46	11.276
Seppenrade	47.68	49.84	1.05	0.50	11.627
Senden	38.55	38.12	0.99	0.47	11.765
Wesel	42.86	51.81	1.21	0.61	11.638
Rhede	32.43	38.67	1.19	0.53	11.905
Holthausen	30.31	35.41	1.17	0.56	11.700
Legden	27.45	33.50	1.22	0.51	11.293
Metelen	30.36	33.92	1.12	0.53	11.711
Uddel	20.19	18.10	0.90	0.16	9.285
Barneveld	13.47	13.94	1.03	0.39	9.738
Barchem	15.92	25.56	1.61	0.19	8.758
Arnhem-P.	18.06	17.70	0.98	0.13	9.029
Hoog-Keppel	13.22	16.70	1.26	0.38	10.141
Lievelde	23.80	25.16	1.06	0.42	9.041
Beesd	19.05	20.23	1.06	0.38	9.251
Ulft	20.04	27.87	1.39	0.46	10.192
Overasselt	20.72	18.72	0.90	0.35	9.602

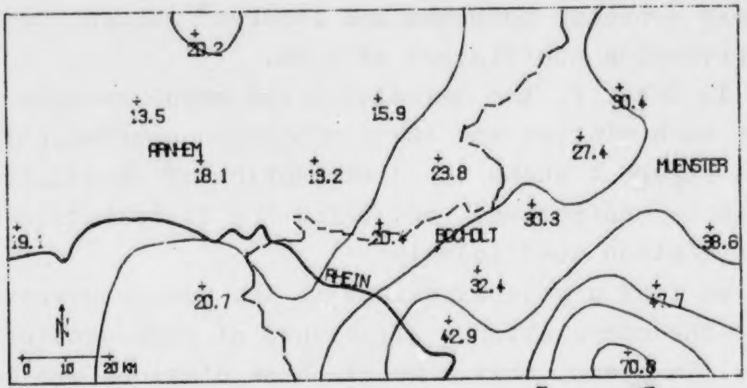
29.2
13.5
15.9
30.4
ARNHEM
18.1
19.2
23.8
27.4
MUENSTER
30.3
19.1
20.4
BOCHOLT
38.6
RHEIN
32.4
20.7
47.7
42.9
70.8
N
0
10
20 KM

Observed mean SO_2 concentrations $[\mu gr/m^3]$ from May 1974 to October 1975.

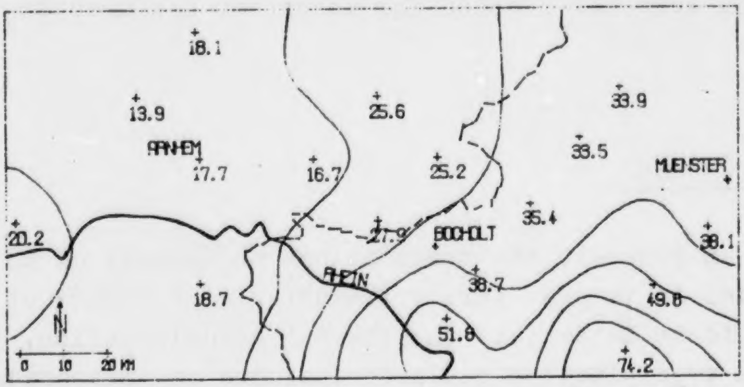
18.1
13.9
25.6
33.9
ARNHEM
17.7
16.7
25.2
33.5
MUENSTER
35.4
20.2
27.9
BOCHOLT
38.1
RHEIN
38.7
18.7
49.8
51.8
74.2
N
0
10
20 KM

Calculated mean SO_2 concentrations $[\mu gr/m^3]$ from May 1974 to October 1975.

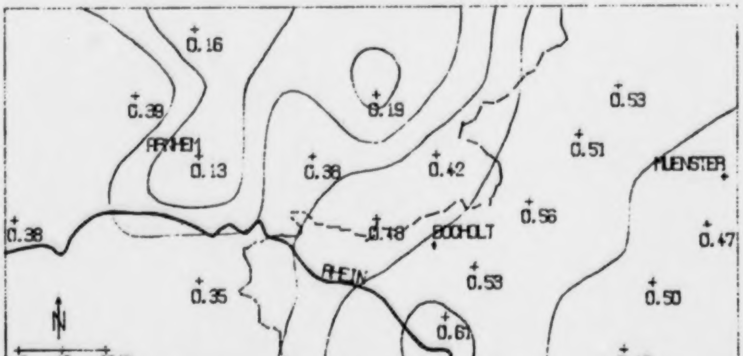
0.16
0.39
0.19
0.53
ARNHEM
0.13
0.38
0.42
0.51
MUENSTER
0.56
0.38
0.48
BOCHOLT
0.47
RHEIN
0.53
0.35
0.50
0.67
0.46
N
0
10
20 KM

Mean correlation coefficient between observed and calculated SO_2 concentration from May 1974 to October 1975.

Figure 4.

daily averaged computed and observed values, we found a correlation coefficient of 0.54.

In Table 7, the calculated and measured mean concentrations for each station and the correlation coefficient are listed. The Figure 4 shows the distribution of calculated and measured mean concentrations, and below the distribution of the correlation coefficients.

We find a good agreement in the mean concentration values. But the correlation coefficients at some stations are very low. It seems, that some of these stations are more influenced by local SO_2 - sources, than by the SO_2 - transport from the Ruhr area. It shall be mentioned once more, that the used data were not checked for incorrect measured SO_2 concentrations.

8. Summary

In general, the computations encourages us to work with the model in future. Surely the calculated values of large periods would be better, if the thermal stratification, temperature and precipitation could be included as independent variables in the regression equations for the eigencoefficients. Furthermore corrected concentration values should be used.

References

CLARKE J.C. and PETERSON J.T. (1973) An empirical model using eigenvectors to calculate the temporal and spatial variations of St. Louis heat island. J.appl.Met.12,195-210.

KUTZBACH J.E. (1967) Empirical eigenvectors of sea-level pressure, surface temperature and precipitation complexes over North America. J.appl.Met. 6,791-802.

PETERSON J.T. (1970) Distribution of sulfur dioxide over metropolitan St. Louis, as described by empirical eigenvectors, and its relation to meteorological parameters. Atmos.Envir. 4,501-518.

PETERSON J.T. (1972) Calculations of sulfur dioxide concentrations over metropolitan St. Louis. Atmos.Envir. 6,433-442.

STIDD C.K. (1967) The use of eigenvectors for climatic estimates. J.appl.Met. 6,1033-1038.

STANFORD RESEARCH INSTITUTE
Menlo Park, California 94025 · U.S.A.

NATO/CCMS Air Pollution Pilot Study:
7th International Technical Meeting
on Air Pollution Modeling and its Application

THE EUROPEAN REGIONAL MODEL OF AIR POLLUTION (EURMAP) AND ITS APPLICATION TO TRANSFRONTIER AIR POLLUTION

Warren B. Johnson
Daniel E. Wolf
Robert L. Mancuso

Stanford Research Institute
Menlo Park, California, USA

September 7-10, 1976
Airlie, Virginia
United States of America

ABSTRACT

This paper reports on progress to date of an ongoing effort to develop, evaluate, and apply a European Regional Model of Air Pollution (EURMAP). This model is designed to be capable of calculating long-term (monthly, seasonal, and/or annual) averages of the contributions from SO_2 in individual emittor countries to concentrations, dry deposition, and wet deposition in receptor countires. The model covers all of Western and Central Europe, a geographical area 2100 km x 2250 km in size.

An innovative trajectory-type approach is used, which involves the tracking of pollutant "puffs" released from each emissions cell in an extensive grid. Meteorological data in the form of wind and precipitation values from some 45 upper-air and 536 surface stations are input at 6-hourly intervals for use in the calculations of puff transport and wet deposition. A wet deposition coefficient is used that depends upon precipitation rate. Because of the need for computational economy, the current basic version of EURMAP is quite simplified, involving, for example, constant emission rates and mixing depth. Refinements are planned at a later date as appropriate.

For demonstration purposes, the model has been used to calculate preliminary maps of concentration, dry deposition, and wet deposition patterns resulting from SO_2 emissions in each of thirteen countries in Western and Central Europe, taken both individually and together. These results have also been used to prepare preliminary tables of the percent contributions of emittor countries to concentrations, dry deposition and wet deposition in receptor countries, as well as in receptor regions of the Federal Republic of Germany (FRG). The quantitative data in the figures and tables are the results of preliminary computations which are not definitive.

Although EURMAP has not yet been thoroughly evaluated against observations, the preliminary results are of a form that in its final version should eventually prove useful in the development of international air pollution control agreements.

FOREWORD

This study is being conducted under a contract from the Federal Environmental Office (Umweltbundesamt) of the Federal Republic of Germany (FRG), under the direction of Dr. D. Jost of that office and Dr. E. Weber of the Federal Ministry of the Interior (FRG). We wish to acknowledge with thanks the assistance of Dr. Jost, Dr. Weber, and Dr. B. Ottar of the Norwegian Institute of Air Research in furnishing valuable technical information necessary for this project.

CONTENTS

ABSTRACT ii

FOREWORD iv

I INTRODUCTION. 1

  A. Nature of the Problem, and Related Studies 1

  B. Objectives of this Study 2

II DESCRIPTION OF EURMAP DESIGN AND APPLICATION 3

  A. Model Rationale and Design Goals 3

  B. Pollutant Emissions. 5

  C. Pollutant Transport. 5

  D. Pollutant Diffusion. 12

  E. Pollutant Transformations. 13

  F. Pollutant Removal. 13

    1. Wet Deposition. 14
    2. Dry Deposition. 18

  G. Calculation of Monthly-Mean Concentration and Deposition Distributions. 19

III RESULTS FROM PRELIMINARY EURMAP COMPUTER RUNS 23

IV ADDITIONAL MODELING WORK PLANNED. 30

REFERENCES 31

APPENDICES

A MAPS OF CONCENTRATION PATTERNS RESULTING FROM SO_2 EMISSIONS IN THIRTEEN INDIVIDUAL COUNTRIES IN WESTERN AND CENTRAL EUROPE DURING JULY 1973 . . . . A-1

B MAPS OF DRY DEPOSITION PATTERNS RESULTING FROM SO_2 EMISSIONS IN THIRTEEN INDIVIDUAL COUNTRIES IN WESTERN AND CENTRAL EUROPE DURING JULY 1973 . . . . B-1

C MAPS OF WET DEPOSITION PATTERNS RESULTING FROM SO_2 EMISSIONS IN THIRTEEN INDIVIDUAL COUNTRIES IN WESTERN AND CENTRAL EUROPE DURING JULY 1973 . . . . C-1

dry deposition, and wet deposition in receptor countries. This approach complements the OECD work, which has emphasized short-term case studies.

B. Objectives of this Study

The overall objectives of this study are to develop, evaluate, and apply an accurate and practical quantitative technique for assessing the current and future effects of air pollution emissions in each country in Central and Western Europe on long-term air quality in each of the other countries. In furtherance of this general objective, the following tasks are geing undertaken:

(1) Extension of the geographical coverage of a preliminary air budget model (Johnson et al., 1974) to include all of Central and Western Europe.

(2) Modification of the preliminary model to calculate air pollution concentration fields instead of transborder fluxes.

(3) Incorporation of $SO_2/SO_4^=$ chemical transformations.

(4) Evaluation of the modified model by comparing calculated values with observed data.

(5) Refinement of the individual model elements dealing with pollutant emissions, transport, transformations, and removal processes, as required on the basis of the results from the model evaluation tests.

(6) Adaptation of the model to enable it to handle carbon monoxide and nitrogen oxides, in addition to sulfur dioxide and sulfates.

(7) Application of the completed model to its intended use in assessing transfrontier air pollution effects in Central and Western Europe.

This progress report describes preliminary results from the first two tasks listed above.

II DESCRIPTION OF EURMAP DESIGN AND APPLICATION

A. Model Rationale and Design Goals

In the design and development of any air quality simulation model, there are usually two conflicting goals: maximum realism and accuracy on the one hand, and minimum computing requirements on the other. The achievement of better realism and accuracy usually requires more detailed and sophisticated formulations, which in turn requires more computer time and memory capacity.

In designing EURMAP, it was clear from the outset that the computing requirements could become severe, for two reasons:

- The model must treat a very large geographical area (2100 km N-S by 2250 km E-W), as illustrated in Figure 1, and
- The model must compute monthly and annual mean concentration and deposition fields, and thus must cover long periods of time.

Accordingly, as a first step, we set out to design a very simple model--one that would have minimum computing requirements (and thus be practical and economical to use), while at the same offering reasonable realism in simulating the most important processes involved in the transfrontier air pollution problem.

The result of this effort is the current basic version of EURMAP, which is described in the following sections. Updated versions of this basic model as well as of the parameters used will be developed as the work progresses and as the need for improvements becomes clearly evident through the evaluation process. In this regard, the basic version of EURMAP is expected to serve as a useful standard by which to make cost/benefit comparisons with future model versions.

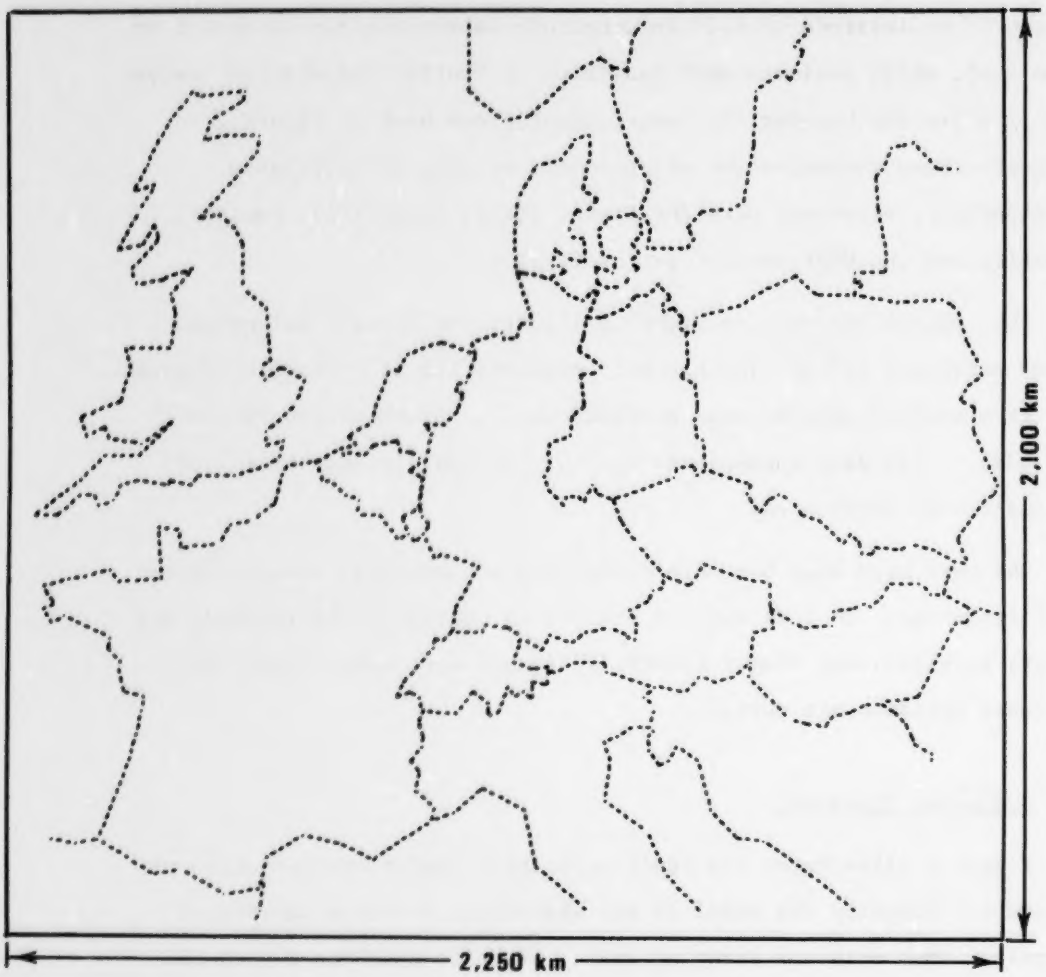
2,100 km
2,250 km

FIGURE 1 GEOGRAPHICAL AREA COVERED IN EURMAP APPLICATION

B. Pollutant Emissions

The SO_2 emissions inventory used in this study was taken from that developed by Rystad et al. (1974) as part of the OECD-sponsored LRTAP (Long Range Transport of Air Pollutants) project. As shown in Figure 2, annual total SO_2 emissions data for 1973 were available for an array of cells 0.5° in latitude by 1.0° in longitude (approximately 55 km N-S by 70 km E-W), which includes most countries in Central and Western Europe. Table 1 gives the key for the letter identifiers used in Figure 2 to designate those countries for which emissions data are available. Unfortunately, emissions data for Spain, Italy, Yugoslavia, Rumania, Bulgaria, and the USSR are not yet available.

The contour analysis in Figure 3 illustrates the general nature of the emissions field. The highest emissions lie in a broad band extending from Central England east-southeastward to Southwestern Poland (Silesia). This area encompasses most of the heavily industrialized regions in the study area.

The base maps used here are sinusoidal projections, referenced to 16° E longitude. On this type of projection, parallels of latitude are linear, parallel, and evenly spaced, while all meridians except the reference meridian are curved.

C. Pollutant Transport

Figure 4 illustrates the basic principles behind the operation of the model.* Normally the model is run separately for each country of interest. Thus only the array of emissions cells associated with the particular country of interest is used at any one time.

For each of these cells, the annual-average emissions are divided into discrete 12-hour-average emission increments, or "puffs," which are released at 12-hour intervals and tracked at 3-hour time steps until

---

* The basic concept is similar in principle to that developed by Start and Wendell (1974) in their MESODIF model, except that MESODIF is designed to be used with only one or a few point sources.

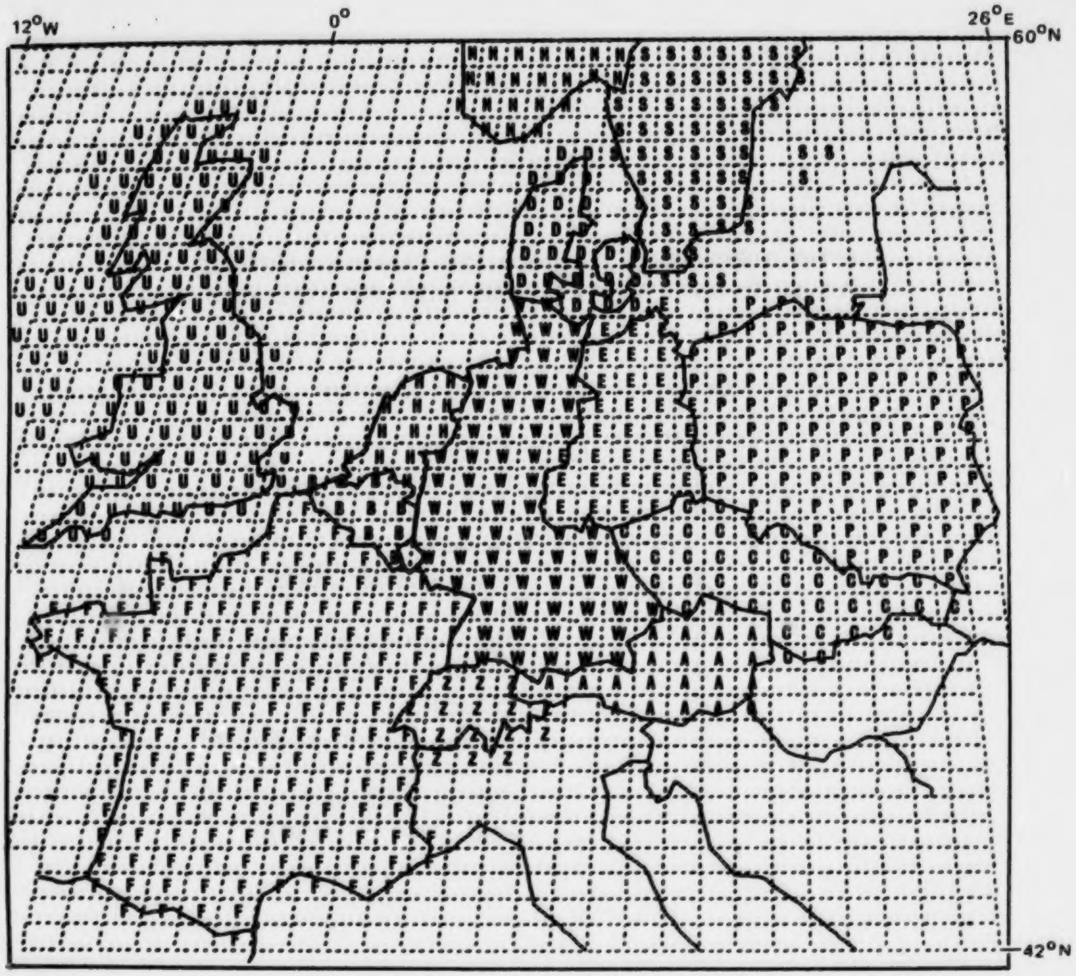

FIGURE 2 EMISSIONS DATA GRID USED IN THE MODEL RUNS; LETTERS REPRESENT COUNTRIES (SEE TEXT) FOR WHICH 1973 SO_2 DATA WERE AVAILABLE FROM RYSTAD ET AL. (1974)

Table 1

LETTER IDENTIFIERS USED FOR THE VARIOUS COUNTRIES FOR WHICH 1973 SO_2 EMISSIONS DATA ARE AVAILABLE

Letter	Country
A	Austria
B	Belgium/Luxembourg
C	Czechoslovakia
D	Denmark
E	East Germany (GDR)
F	France
H	The Netherlands (Holland)
N	Norway (South of 60° N)
P	Poland
S	Sweden (South of 60° N)
Z	Switzerland
U	United Kingdom
W	West Germany (FRG)

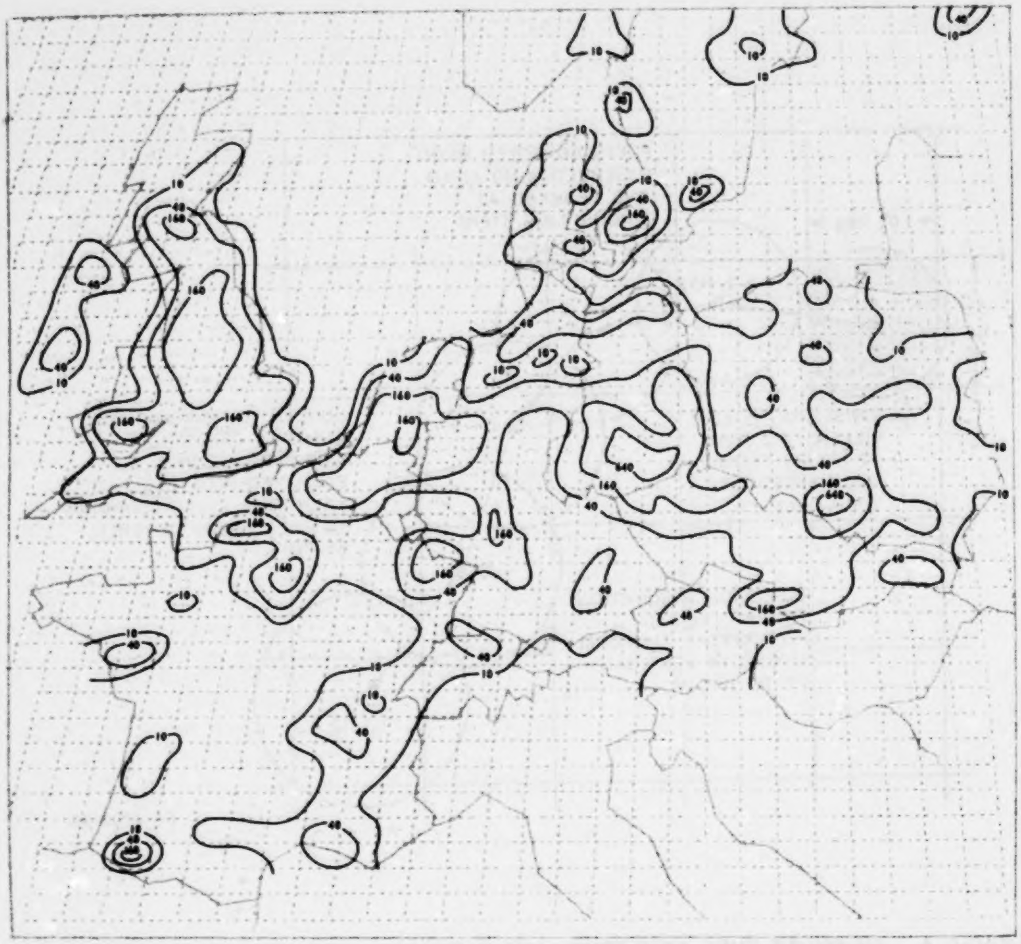

FIGURE 3   SPATIAL DISTRIBUTION OF 1973 SO_2 EMISSIONS (KILOTONS/YR) BASED UPON GRIDDED DATA FROM RYSTAD ET AL. (1974)

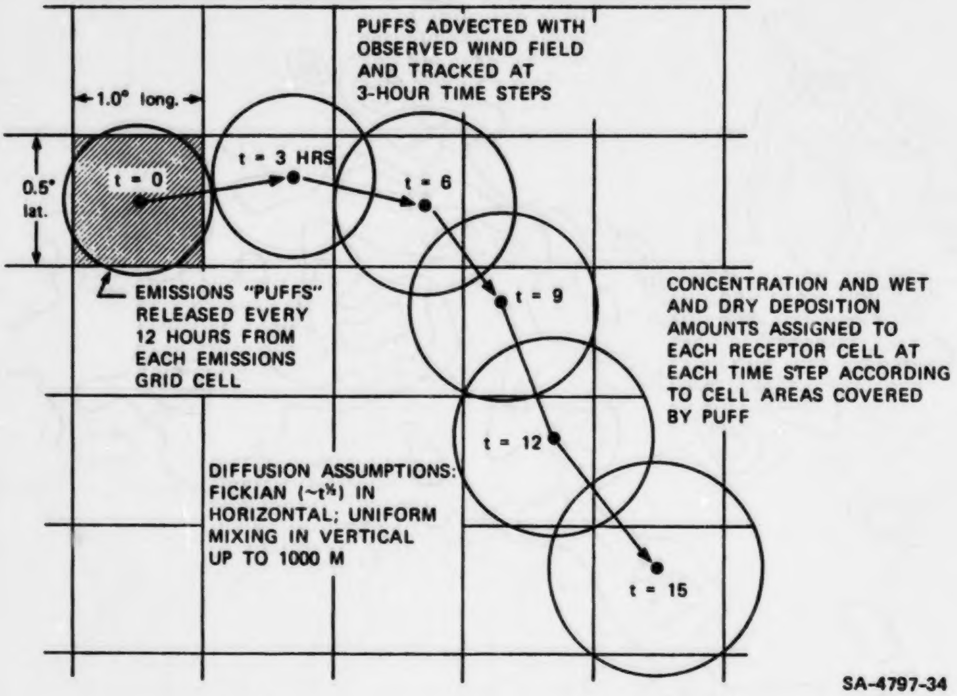
PUFFS ADVECTED WITH OBSERVED WIND FIELD AND TRACKED AT 3-HOUR TIME STEPS
1.0° long.
0.5° lat.
t = 0
t = 3 HRS
t = 6
t = 9
t = 12
t = 15
EMISSIONS "PUFFS" RELEASED EVERY 12 HOURS FROM EACH EMISSIONS GRID CELL
CONCENTRATION AND WET AND DRY DEPOSITION AMOUNTS ASSIGNED TO EACH RECEPTOR CELL AT EACH TIME STEP ACCORDING TO CELL AREAS COVERED BY PUFF
DIFFUSION ASSUMPTIONS: FICKIAN (~t^½) IN HORIZONTAL; UNIFORM MIXING IN VERTICAL UP TO 1000 M
SA-4797-34

FIGURE 4 EMISSIONS PUFF ADVECTION AND DIFFUSION SCHEME USED IN EURMAP

either they move outside the overall study region (see Figure 1) or their concentration drops to an insignificant level. The reason for selecting the 12-hour intervals is that these intervals correspond to the frequency at which most synoptic upper-air wind observations are available. Thus, during the course of a year, 730 puffs are released and tracked for each of the cells. The largest country, France, contains 146 emissions cells; thus for France 106,580 puffs would be tracked during the course of a year.

The individual puffs are transported according to the wind field applicable at that time, as interpolated objectively from the available upper-air wind observations at 850 mb (approximately 1500 m above sea level) for the year 1973. Although we recognize that significant vertical wind shears occur between the surface and the 1500-m level, especially in winter and at night, we feel that the use of a single wind to represent the transport within this layer is justified as a first approximation.

To account in an approximate fashion for surface-friction effects that cause wind shear in the boundary layer, the 850-mb winds have been adjusted as follows to give a more representative layer average:

$$\overline{U} = 0.75\ U_{(850\ \mathrm{mb})} \qquad (1)$$

$$\overline{\theta} = \theta_{(850\ \mathrm{mb})} - 15^{\circ} \qquad (2)$$

where $\overline{U}$ and $\overline{\theta}$ are the adjusted layer-average wind speed and direction, respectively. At a later stage in the work, it may be appropriate to develop a more realistic way of obtaining layer-average transport winds through the inclusion of wind data from lower levels.

Figure 5 shows the locations of the upper-air meteorological sounding stations for which 850-mb wind data were used in this study. Only about 45 of these stations report regularly.

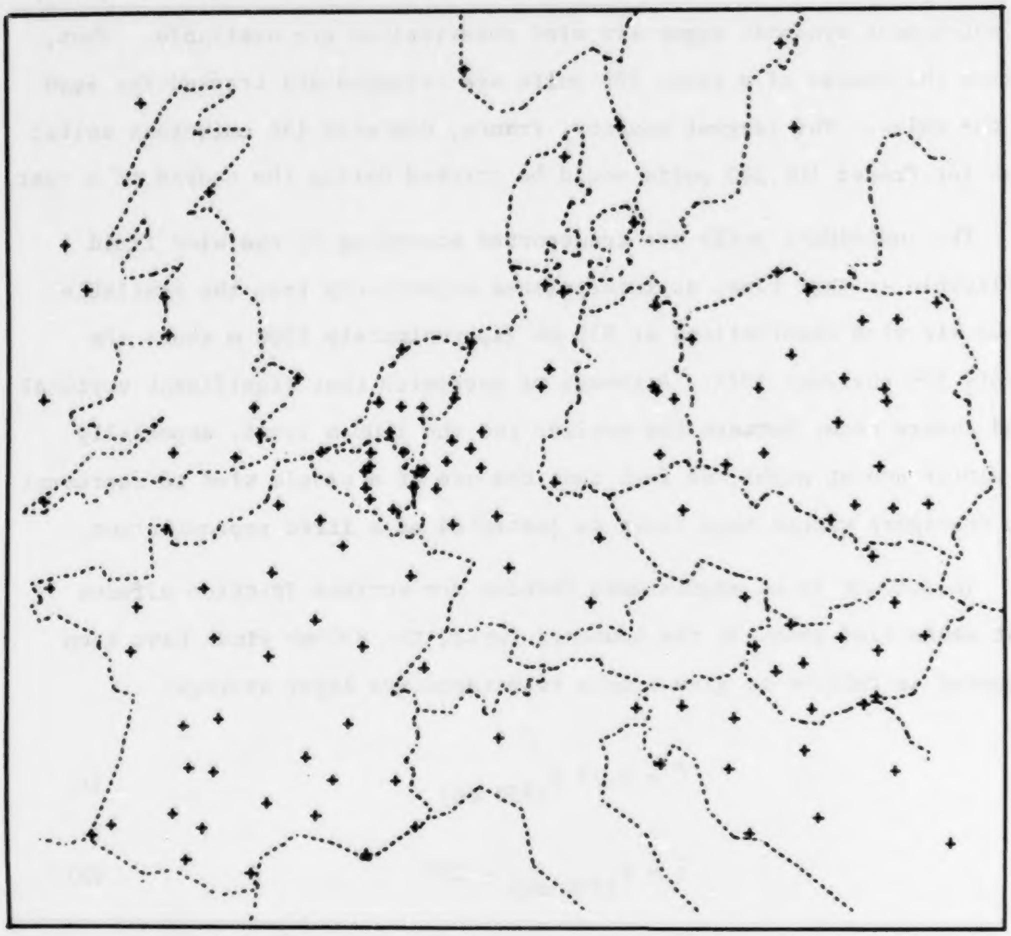

FIGURE 5 LOCATIONS OF UPPER-AIR METEOROLOGICAL STATIONS FOR WHICH JULY 1973 WIND DATA WERE USED (Not all stations report continuously)

D. Pollutant Diffusion

The variation in pollutant concentration (C) in a puff as a function of time (t) as the puff moves with the wind may be written as follows:

$$\frac{dC}{dt} = \frac{MK}{\pi H(r_o^2 + Kt)^2} - k_d C - k_w C, \qquad (3)$$

where M = pollutant mass emitted

H = height of the mixed volume ≡ 1000 m

r_o = initial puff radius

K = horizontal eddy diffusivity

$\equiv 10^8$ cm^2 sec^{-1} = 36 km^2 hr^{-1}

k_d = dry deposition coefficient

k_w = wet deposition coefficient

Here the first term on the right represents the pollutant diffusion process, while the last two terms represent removal processes by dry and wet deposition, respectively.

Since diffusion on the regional scale is clearly less important than the transport and removal processes, a very simple treatment of diffusion is used in the current version of EURMAP. Upon release, each puff is assumed to immediately diffuse vertically to give a uniform concentration in the layer between the surface and the 1000-m level.* The initial lateral extent of the puff is approximated by a disk whose diameter (about 60 km) is adjusted such that the cross-sectional area of the disk is the same as that for the emissions cell. Fickian diffusion is then assumed during the transport of the puff, as indicated in Equation (3) above.

---

* Model refinements are planned that will make the mixing depth dependent upon (at least) geographical location and season. In the meantime, aircraft measurements reported by Jost (1973, 1974) indicate that an average mixing depth value of 1000 m is reasonable.

E. Pollutant Transformations

The current basic version of EURMAP does not include the chemical conversion of SO_2 to sulfates and other sulfur compounds, although this important (and complex) process clearly plays a significant role in the long-range fate and effects of sulfur air pollution. As discussed in Section I, we plan as our next task to incorporate into the model a chemical transformations mechanism that will allow differentiation between sulfur species. As a first step, we will probably consider a simple, first-order $SO_2/SO_4^{=}$ conversion formulation, as is used in several other models (e.g., Rao et al., 1976). This, in turn, will be improved at a later stage if shown to be necessary.

In the meantime, the current version of the model simply considers "sulfur compounds" or "$SO_2/SO_4^{=}$" as a single class, with a mass equivalent to that of SO_2, as if the pollutant material had remained in that form.

F. Pollutant Removal

The conversion of SO_2 to sulfate aerosol and other compounds, and the subsequent removal of these sulfur compounds from the air by means of cloud droplets (rainout), falling precipitation (washout), and vegetation and soil uptake and other chemical reactions at the surface (dry deposition) together constitute one of the most complex problem areas in the field of air pollution. Recognizing that SO_2 removal by dry and wet processes is particularly significant over the relatively long transport distances involved in our study, we have attempted to include these deposition effects in the model in a simplified, but hopefully realistic, manner. However, determining the best way to model these removal processes is not a straightforward task, since the current state of knowledge is far from complete, and new results tend to emphasize the large number of variables that enter into the problem.

As an example, studies by Weber (1970a, 1970b, 1971) and Gartrell (1964) show that the half-life of SO_2 in urban areas or near large sources may be as short as 20 or 30 min under certain conditions, while others have estimated SO_2 half-lives to be as long as a week. These results indicate that SO_2 residence time is at least a function of concentration, meteorological conditions (humidity, clouds, rain, fog), and the presence of catalysts and other compounds, such as ammonia (Weber, 1971).

1. Wet Deposition

For the purpose of calculating the SO_2/sulfate removal by wet deposition, daily total precipitation observations during 1973 at a total of about 536 stations are input to the model. The locations of these stations are plotted in Figure 6. Interpolated precipitation values are used to calculate the SO_2 mass removed from each puff at each location on the grid during each three-hour time step.

The pollutant removal by wet deposition is taken to be a function of precipitation rate and is calculated assuming that the following relationship holds:

$$C/C_o = \exp(-k_w t) \qquad (4)$$

where k_w = wet deposition coefficient = λR

C = SO_2 concentration at time t

C_o = initial SO_2 concentration

λ = washout/rainout coefficient

$[hr^{-1}(mm\ hr^{-1})^{-1}$, or $mm^{-1}]$

R = precipitation rate (mm hr^{-1} of water) occurring over a given period of time t (hr).

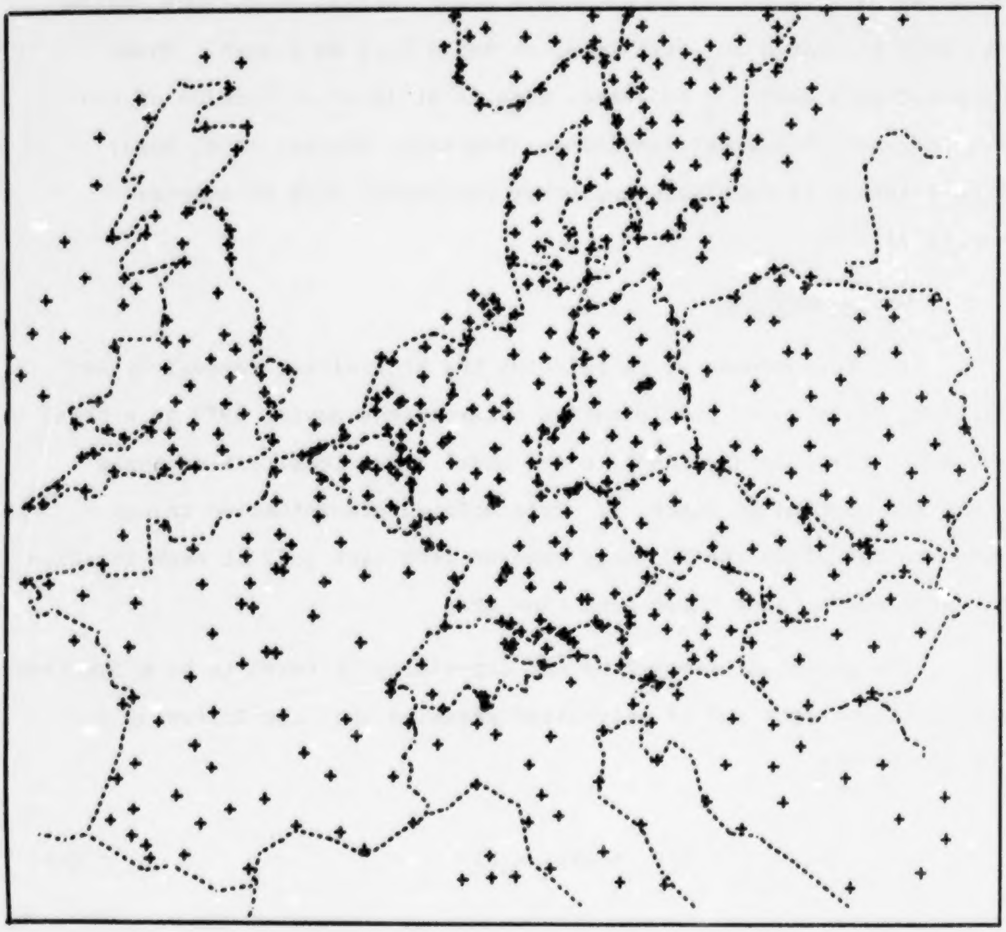

FIGURE 6 LOCATIONS OF SURFACE METEOROLOGICAL STATIONS FOR WHICH JULY 1973 PRECIPITATION DATA WERE USED

This equation may be obtained as a result of integrating the wet-deposition term in Equation (3).

A review of recent field, laboratory, and theoretical studies was conducted to find an appropriate value for the wet deposition coefficient, k_w. Some of the studies reviewed did not report results directly in the form of values of k_w, but these have been calculated or estimated on the basis of the information given. A summary of these results is given in Table 2. The values derived from the available information and used in this study are enclosed by the boxes on the bottom line of the table.

As indicated, some investigators have considered SO_2 and $SO_4^=$ separately, while others have lumped the two species together, as we have done in our study so far. Most of the investigators have taken the wet deposition coefficient to be a function of precipitation type (snow or rain); notable exceptions are Hogstrom (1974) and Ottar (1975), as indicated. Some of the only field data available on the dependence of the wet deposition coefficient on precipitation rate have been reported by Hogstrom.

It is clear that there is a wide range in the available coefficient values, with those of Hales et al. (1970) considerably lower than the others. The values from Summers and Hitchon (1973) may well be overestimates, since they apply principally to convective rains. The laboratory (rain chamber) results of Bielke and Georgii (1968) might also be high, in view of the rather high pollutant concentrations (800 $\mu g/m^3$) used in their experiments. On the other hand, the latter data could be underestimates of the total wet deposition rate, since they do not include rainout effects, while Summers and Hitchon indicate that their results represent mainly rainout processes.

Table 2

SUMMARY OF VALUES OF THE WET DEPOSITION COEFFICIENT (k_w) DERIVED OR USED BY VARIOUS INVESTIGATORS

Investigator	Pollutant Considered	k_w (hr^{-1})	
		Snow	Rain
Bielke and Georgii (1968)	SO_2	------	0.9-2.8
Dana et al. (1975)	$SO_4^=$	------	0.058
Hales et al. (1970)	SO_2	0.0014	0.072
Hogstrom (1974)	$SO_2 + SO_4^=$	0.53-2.5*	
Ottar (1975)	SO_2	0.36	
Summers and Hitchon (1973)	SO_2	0.16	1.8
Johnson, et al. (1974, 1976+)	$SO_2 + SO_4^=$	$\boxed{0.10^*}$	$\boxed{1.0^*}$

*For precipitation rate of 1 mm/hr.

+Current study.

For lack of better estimates, we have used the following values for our initial model runs:

(STILL PRELIMINARY)

	λ (mm^{-1})
Summer	1.0
Winter	0.1
Spring and Fall	0.5

The low winter value reflects the nonconvective nature of much of the precipitation, and the fact that some of the precipitation will be in the form of snow. The intermediate spring and fall value reflects the varied precipitation types which occur during those seasons. The deposition coefficient could be made dependent upon precipitation type, rather than season. This is a refinement that can be easily incorporated at a later date.

The computer program keeps track of each puff's location and duration of exposure to the variable precipitation intensity, calculates the pollutant mass removed during each time step, and assigns this amount to the appropriate cell (geographical location) in the receptor grid. The precipitation rate is calculated by dividing the observed values of accumulated precipitation by the number of hours in the accumulation period. This infers an assumption that the precipitation was uniform during this period.

2. Dry Deposition

To calculate pollutant removal by dry deposition processes, we have used the relation,

$$C/C_o = \exp(-k_d t), \qquad (5)$$

which is identical to the previous equation for wet deposition, except that k_d represents the dry deposition coefficient, in units of hr^{-1}. Again, we have surveyed the literature in an attempt to arrive at a best estimate for the value of this coefficient; the results are summarized in Table 3. Again, there is considerable scatter in the available values. An additional complication is that some of the investigators lumped dry and wet deposition and treated both with a single removal coefficient, as indicated in the table.

A value of 0.010 hr^{-1} (enclosed in the box on the bottom line of Table 3) was used in the original study (Johnson et al., 1974). Since this value is not inconsistent with the coefficients used by the other investigators, it has been retained for the current EURMAP runs. It was derived originally by resorting to estimates by Kellogg et al. (1972) that the average annual ratio of dry to wet deposition over the Northern Hemisphere is approximately 0.3. On the basis of an annual washout/rainout coefficient of 0.5 mm^{-1} calculated from the average of the seasonal values used, and taking into account the annual average precipitation intensity in Western and Central Europe of about 750 mm yr^{-1}, we have arrived at an estimate of about 0.01 hr^{-1} for the value of the dry deposition coefficient. This preliminary value is subject to change as the model validation work proceeds and better information becomes available.

Based on the assumed value of this coefficient, the model removes an appropriate fraction of the pollution in each puff at each time step, and assigns it as dry deposition to the appropriate cell (geographical location) in the receptor grid.

G. Calculation of Monthly-Mean Concentration and Deposition Distributions

EURMAP is designed to calculate long-term (monthly, seasonal, and/or annual) mean distributions of $SO_2/SO_4^=$ concentration, dry deposition, and wet deposition over all of Western and Central Europe, resulting from SO_2 emissions from each of the 13 countries in this area taken individually.

Table 3

SUMMARY OF VALUES OF THE DRY DEPOSITION COEFFICIENT (k_d) DERIVED OR USED BY VARIOUS INVESTIGATORS

Investigator	k_d (hr^{-1})		
	SO_2	$SO_4^=$	$SO_2 + SO_4^=$
Eliassen and Saltbones (1975)	0.036*	0.014*	-----
Powell and Alkezweeny (1976)	0.020	0.002	-----
Prahm et al. (1976)	0.072*	0.014*	-----
Johnson et al. (1974, 1976+)	-----	-----	$\boxed{0.010}$

*Includes wet deposition, in addition to dry.

+Current study.

Accordingly, each computer run of EURMAP involves reading in long sequences of surface and upper-air meteorological data at 6-hourly intervals. Each of the SO_2 puffs released at 12-hourly intervals from each of the emissions cells for the country of interest is moved every three hours in accordance with the interpolated field of observed winds applicable for that time.

Values of concentration, dry deposition, and wet deposition are summed up at each 3-hourly time step over the 41 x 44 grid of receptor cells illustrated in Figure 7. (Each cell is 50 km on a side.) This is carried out by adding the contributions of each of the puffs at each of the receptor cells.

Concentrations are assigned to cells around the location of the puff at the beginning of the time step. Deposition amounts are evenly divided between the cells at the starting location and those at the ending location of the puff for each time step. Both for concentration and deposition, pollutant amounts are assigned to the cell containing the center of the puff and to the eight surrounding cells in amounts proportional to the area of the puff relative to the area of the central cell.

Long-term mean concentration distributions are obtained simply by averaging the concentrations assigned to each cell at each time step over the total period (number of time steps) of interest. Corresponding deposition distributions are obtained by totalling all amounts deposited in each cell during the period of interest.

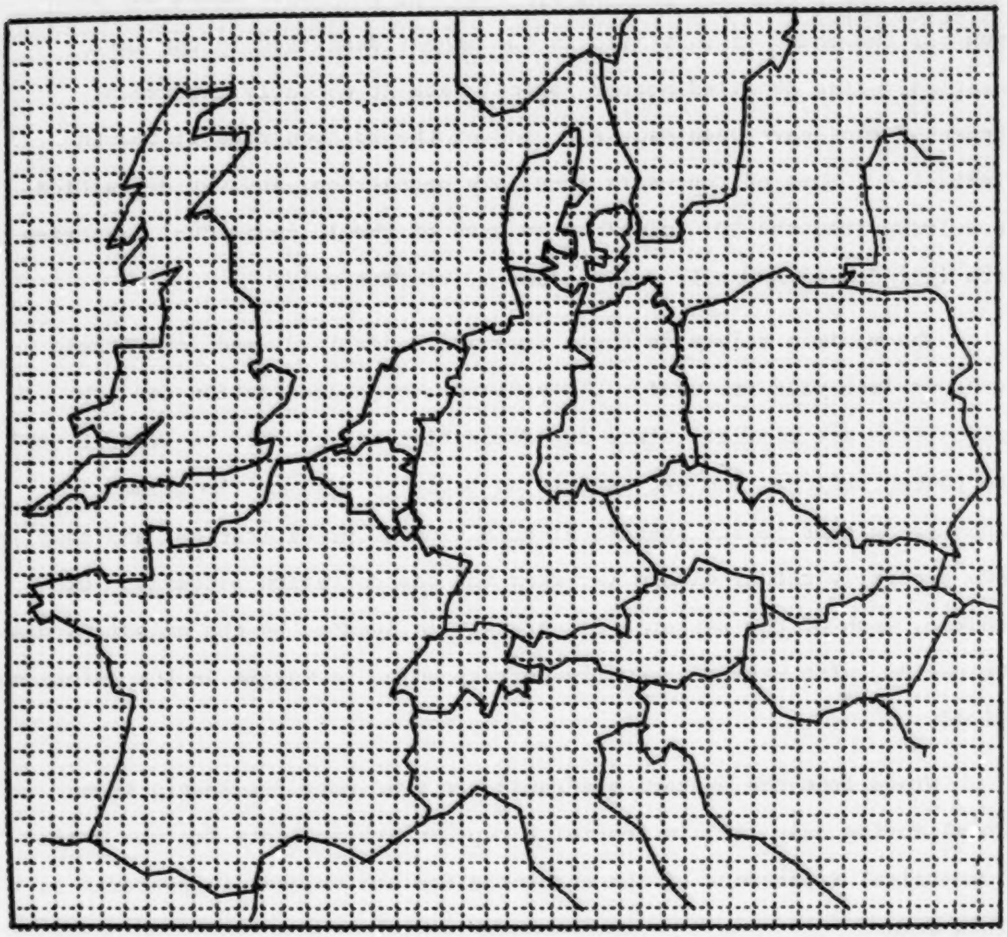

FIGURE 7 RECEPTOR GRID OF 41 x 44 CELLS WITH DIMENSIONS OF 50 KM ON A SIDE

III RESULTS FROM PRELIMINARY EURMAP COMPUTER RUNS

For the purpose of preliminary testing, the basic model has been run for the month of July 1973 in the manner described in the last section, using detailed meteorological data at 6-hourly intervals. Separate runs have been made for each of the 13 countries listed in Table 1.* Maps of concentrations, dry deposition, and wet deposition resulting from the SO_2 emissions in each of the 13 individual countries are included in Appendices A, B, and C, respectively.

The maximum values on these maps are underlined, and logarithmic contour intervals are used. The patterns for concentration and dry deposition are similar, since dry deposition is taken to be proportional to concentration. The wet deposition patterns reflect the normal inhomogeneities in the spatial distribution of precipitation, and thus are generally rather dissimilar from the concentration patterns. Of course, each of the patterns is strongly influenced by the emissions distribution, with maxima generally corresponding to maxima in the emissions field.

Winds from the eastern quadrants occurred more frequently than usual during July 1973 in Central Europe, which accounts for the rather symmetrical appearance of the concentration and deposition patterns in this area.

The results from the individual runs have also been combined into three maps showing the total concentration, dry deposition, and wet deposition distributions resulting from SO_2 emissions from all 13 countries taken together (Figures 8, 9, and 10). These patterns show a broad band of high values corresponding to the heavily industrialized region extending from Central England east-southeastward to Southern Poland.

---

* For convenience, Luxembourg has been combined with Belgium and denoted simply as "Belgium."

At this stage it should be emphasized that EURMAP has not yet been thoroughly evaluated against observations, and thus the uncertainties associated with these calculations are unknown. Thus, caution should be exercised in drawing any conclusions from these results.

On the basis, however, that preliminary comparisons with observations and the results of other models (e.g., Bolin and Persson, 1975) indicate that the calculated values appear to be reasonable, and to demonstrate how EURMAP can be applied in a practical sense, we have carried the work one step further. Tables 4 and 5 list the contributions of each of the emittor countries to wet deposition, dry deposition, and concentrations in each of the receptor countries (Table 4) and in each of the receptor regions (states) in the FRG (Table 5). Because of the reason mentioned previously, the dry deposition and concentration percentages are virtually identical, but the wet deposition values are frequently significantly different. For example, Table 4 shows that during July 1973, approximately 24 percent of the wet deposition occurring in Denmark resulted from SO_2 emissions in the United Kingdom, while only 12 percent of the dry deposition and concentration came from the same source. Such differences are rather more pronounced in Table 5, since the receptor areas are smaller.

After the model has been thoroughly evaluated and refined as necessary, information in the form shown in Tables 4 and 5 should be useful in the management of air quality on an international basis in Western and Central Europe. Using information on planned or potential future changes in the emissions distribution over the region, EURMAP could also be used at some later stage to prepare air quality projections for future years.

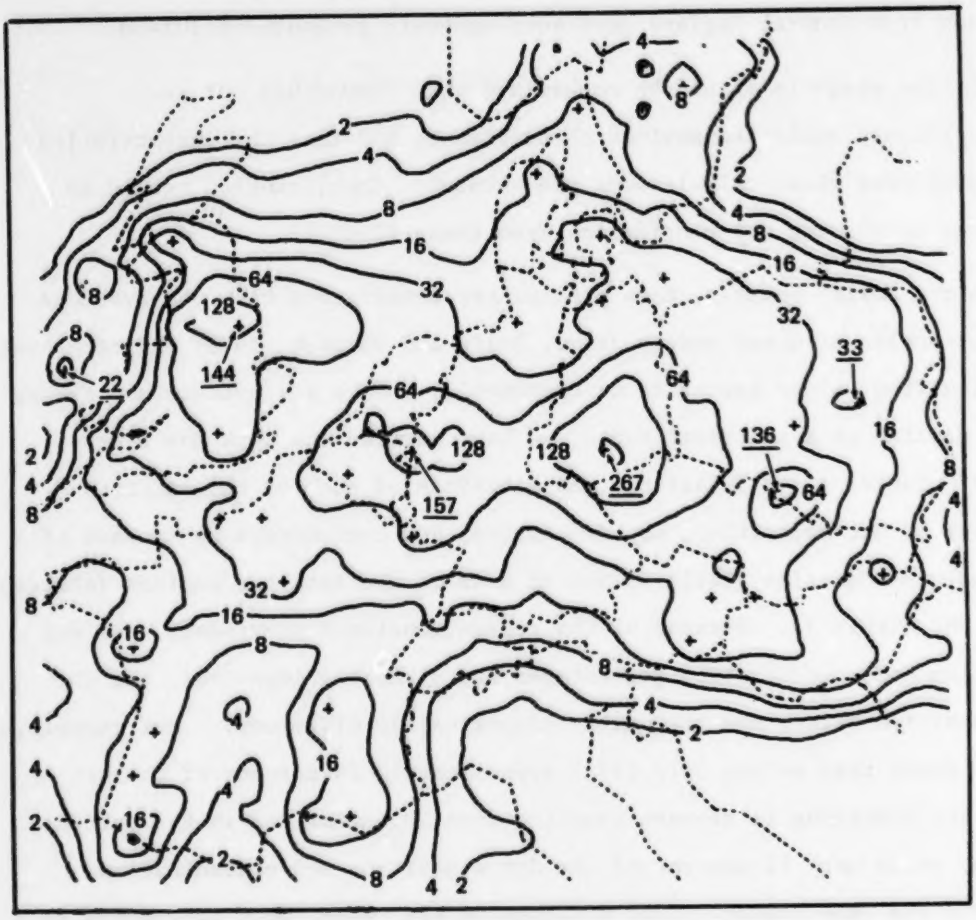
4
8
2
4
8
16
32
64
128
144
8
8
22
2
4
8
64
128
157
128
267
64
33
136
64
16
2
4
8
16
4
4
32
16
16
8
8
4
2
4
4
16
4
2
16
2
8
4
2

FIGURE 8 CONCENTRATION OF SULFUR COMPOUNDS (IN TERMS OF EQUIVALENT WEIGHT OF SO_2, 10^{-6} g m^{-3}) FROM EMISSIONS IN WESTERN AND CENTRAL EUROPE (13 COUNTRIES) DURING JULY 1973

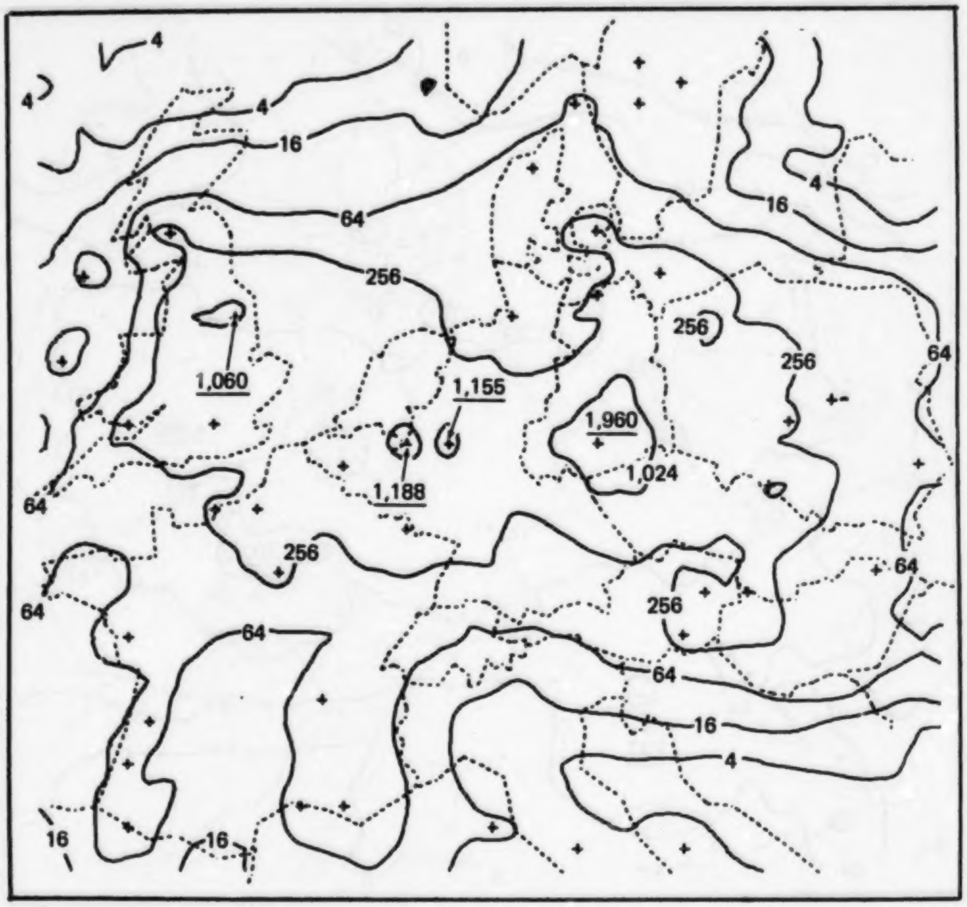
4
4
4
16
64
256
16
4
256
1,060
1,155
256
64
1,960
1,188
1,024
64
256
64
64
256
64
64
16
4
16
16

FIGURE 9 DRY DEPOSITION OF SULFUR COMPOUNDS (IN TERMS OF EQUIVALENT WEIGHT OF SO_2, 10^{-3} g m^{-2}) FROM EMISSIONS IN WESTERN AND CENTRAL EUROPE (13 COUNTRIES) DURING JULY 1973

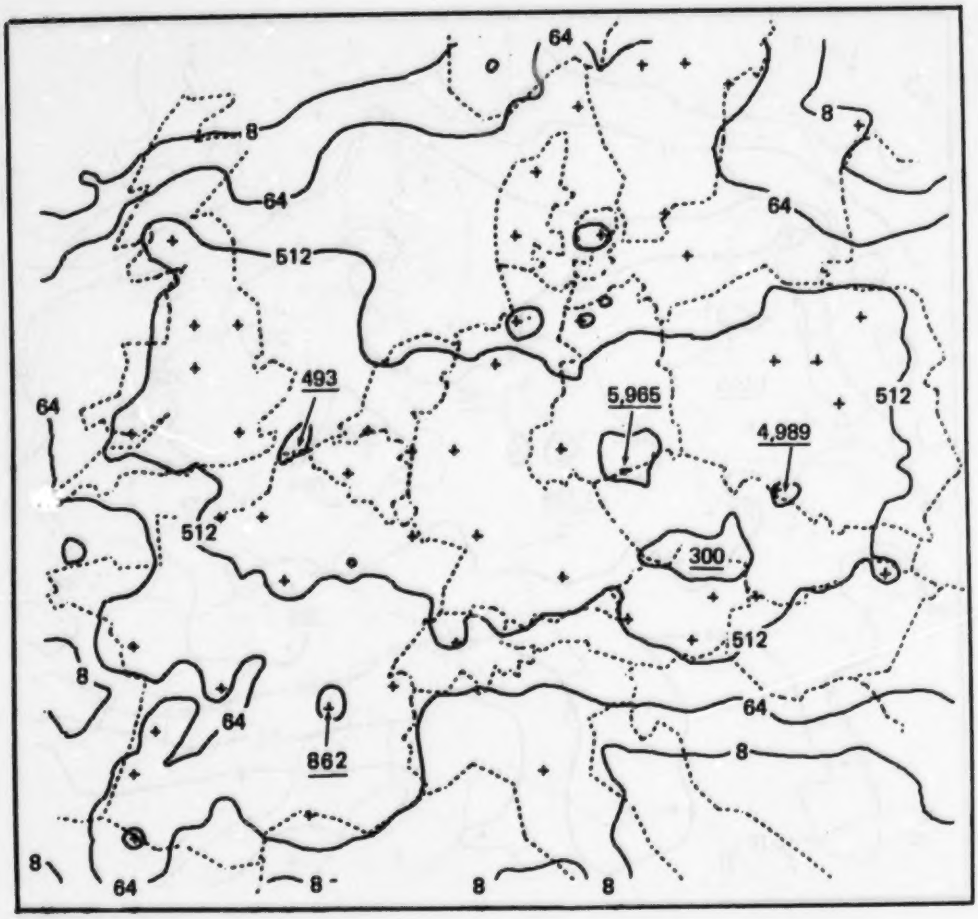
64
8
8
64
64
512
493
5,965
4,989
512
64
512
300
512
8
64
64
862
8
8
64
8
8
8

FIGURE 10 WET DEPOSITION OF SULFUR COMPOUNDS (IN TERMS OF EQUIVALENT WEIGHT OF SO_2, 10^{-3} g m^{-2}) FROM EMISSIONS IN WESTERN AND CENTRAL EUROPE (13 COUNTRIES) DURING JULY 1973

Table 4

PERCENT CONTRIBUTIONS TO SULFUR WET DEPOSITION (TOP), DRY DEPOSITION (MIDDLE), AND CONCENTRATIONS (BOTTOM) WITHIN RECEPTOR COUNTRIES FROM SO_2 EMISSIONS IN EMITTOR COUNTRIES

(Monthly average EURMAP results for July 1973)

.... PERCENT CONTRIBUTIONS TO SULFUR WET DEPOSITIONS WITHIN RECEPTOR COUNTRIES ....

EMITTOR COUNTRY	FRG	GDR	FRANCE	POLAND	CZECH	DENMARK	HOLLAND	BELGIUM	U. K.	S.NORWAY	S.SWEDEN	AUSTRIA	SWITZ
W. GERMANY (FRG)	44.9	8.2	11.6	2.4	3.8	8.2	13.4	21.6	.1	0.0	.8	20.2	5.4
E. GERMANY (GDR)	20.3	83.1	1.6	30.9	20.8	.3	1.0	3.7	0.0	.0	.3	2.1	.0
FRANCE	9.6	.4	76.6	.1	.2	.1	3.9	22.3	1.3	0.0	.0	7.3	43.1
POLAND	.8	2.4	.0	49.6	11.7	.6	.0	0.0	0.0	0.0	.2	9.2	0.0
CZECHOSLOVAKIA	3.7	2.2	.2	15.3	59.7	0.0	.0	.2	0.0	0.0	0.0	20.1	.0
DENMARK	.6	.1	.0	.2	.0	54.7	3.1	.0	.0	1.6	13.6	.0	0.0
HOLLAND	9.3	1.9	.6	.7	.3	4.7	55.7	3.5	1.5	0.0	.4	.6	.0
BELGIUM	8.3	1.5	6.8	.3	.7	.1	14.7	47.2	1.0	0.0	.0	3.1	.3
U. K.	1.5	.2	.9	.0	.0	24.2	7.7	1.2	96.1	12.0	15.8	.0	.0
S. NORWAY	.0	0.0	0.0	0.0	0.0	.1	0.0	0.0	.0	82.6	4.5	0.0	0.0
S. SWEDEN	.1	.0	.0	.1	.0	7.0	.4	.0	.0	3.8	64.4	.0	0.0
AUSTRIA	.7	.0	.2	.3	2.8	0.0	0.0	.1	0.0	0.0	0.0	35.2	.2
SWITZERLAND	.3	0.0	1.5	0.0	.0	0.0	0.0	0.0	0.0	0.0	0.0	2.1	51.0
TOTAL	100.0	100.0	100.0	100.0	100.0	100.0	100.0	100.0	100.0	100.0	100.0	100.0	100.0

.... PERCENT CONTRIBUTIONS TO SULFUR DRY DEPOSITIONS WITHIN RECEPTOR COUNTRIES ....

EMITTOR COUNTRY	FRG	GDR	FRANCE	POLAND	CZECH	DENMARK	HOLLAND	BELGIUM	U. K.	S.NORWAY	S.SWEDEN	AUSTRIA	SWITZ
W. GERMANY (FRG)	47.1	6.5	10.0	3.2	2.2	17.3	19.0	19.9	.2	.0	3.1	14.4	6.6
E. GERMANY (GDR)	22.5	84.2	.2	36.9	21.8	1.7	.6	1.5	0.0	.1	1.6	2.0	.0
FRANCE	7.0	.2	74.2	.2	.1	.0	10.1	21.9	1.3	0.0	.0	3.6	49.1
POLAND	.6	2.0	.0	44.4	18.9	.2	.0	0.0	0.0	0.0	.3	13.2	0.0
CZECHOSLOVAKIA	5.3	5.2	.0	12.8	54.0	0.0	.0	.1	0.0	0.0	0.0	24.1	.0
DENMARK	.6	.3	.0	.8	.0	53.9	.8	.1	.0	1.3	19.6	.0	0.0
HOLLAND	6.6	.9	1.1	.9	.1	7.0	48.0	6.2	.9	.0	1.5	.3	.0
BELGIUM	7.6	.6	9.5	.5	.3	.1	17.5	49.1	1.1	.0	.0	1.7	.2
U. K.	.5	.1	3.0	.1	.0	11.6	3.9	1.2	96.4	13.8	8.5	.0	.0
S. NORWAY	.0	0.0	0.0	0.0	0.0	.1	0.0	0.0	.0	72.3	4.5	0.0	0.0
S. SWEDEN	.1	.0	.0	.2	.0	7.9	.1	.0	.0	12.6	60.8	.0	0.0
AUSTRIA	2.0	.0	.4	.1	2.6	0.0	0.0	.1	0.0	0.0	0.0	39.7	.4
SWITZERLAND	.1	0.0	1.5	0.0	.0	0.0	0.0	0.0	0.0	0.0	0.0	.9	43.6
TOTAL	100.0	100.0	100.0	100.0	100.0	100.0	100.0	100.0	100.0	100.0	100.0	100.0	100.0

.... PERCENT CONTRIBUTIONS TO SULFUR CONCENTRATIONS WITHIN RECEPTOR COUNTRIES ....

EMITTOR COUNTRY	FRG	GDR	FRANCE	POLAND	CZECH	DENMARK	HOLLAND	BELGIUM	U. K.	S.NORWAY	S.SWEDEN	AUSTRIA	SWITZ
W. GERMANY (FRG)	47.1	6.5	10.0	3.2	2.2	17.2	18.9	19.8	.2	.0	3.2	14.4	6.6
E. GERMANY (GDR)	22.5	84.2	.2	36.9	21.8	1.7	.6	1.5	0.0	.1	1.6	2.0	.0
FRANCE	7.0	.2	74.4	.2	.1	.0	10.1	21.8	1.3	0.0	.0	3.6	49.1
POLAND	.6	2.0	.0	44.4	18.8	.2	.0	0.0	0.0	0.0	.3	13.2	0.0
CZECHOSLOVAKIA	5.3	5.2	.0	12.8	54.0	0.0	.0	.1	0.0	0.0	0.0	24.1	.0
DENMARK	.6	.3	.0	.8	.0	53.8	.8	.1	.0	1.3	19.6	.0	0.0
HOLLAND	6.6	.9	1.1	.9	.1	6.9	48.1	6.2	.9	.0	1.5	.3	.0
BELGIUM	7.6	.6	9.4	.5	.3	.1	17.5	49.2	1.1	.0	.0	1.7	.2
U. K.	.5	.1	2.9	.1	.0	11.9	3.9	1.2	96.4	13.5	8.5	.0	.0
S. NORWAY	.0	0.0	0.0	0.0	0.0	.1	0.0	0.0	.0	73.0	4.5	0.0	0.0
S. SWEDEN	.1	.0	.0	.2	.0	7.9	.1	.0	.0	12.2	60.8	.0	0.0
AUSTRIA	2.0	.0	.4	.1	2.6	0.0	0.0	.1	0.0	0.0	0.0	39.7	.4
SWITZERLAND	.1	0.0	1.5	0.0	.0	0.0	0.0	0.0	0.0	0.0	0.0	.9	43.7
TOTAL	100.0	100.0	100.0	100.0	100.0	100.0	100.0	100.0	100.0	100.0	100.0	100.0	100.0

Table 5

PERCENT CONTRIBUTIONS TO SULFUR WET DEPOSITION (TOP), DRY DEPOSITION (MIDDLE), AND CONCENTRATIONS (BOTTOM) WITHIN RECEPTOR REGIONS OF THE FRG FROM SO_2 EMISSIONS IN EMITTOR COUNTRIES

(Monthly average EURMAP results for July 1973)

.... PERCENT CONTRIBUTIONS TO SULFUR WET DEPOSITIONS WITHIN RECEPTOR REGIONS IN THE FRG ....

EMITTOR COUNTRY	SCHLESWIG HOLSTEIN	HAMBURG	BREMEN	LOWER SAXONY	NORTHRHINE-WESTPHALIA	WEST BERLIN	RHINELAND-PALATINATE	HESSEN	SAARLAND	BADEN-WURTTENBERG	BAVARIA
W. GERMANY (FRG)	78.0	49.1	63.9	44.5	53.8	5.1	37.8	43.9	31.2	37.5	45.3
E. GERMANY (GDR)	1.3	4.9	.9	9.9	7.0	40.9	29.8	32.5	21.6	26.8	23.6
FRANCE	.4	4.0	1.5	2.7	5.1	.1	10.9	4.3	35.5	24.4	6.7
POLAND	.5	.1	.0	.4	.1	2.2	.2	.9	.0	.7	2.5
CZECHOSLOVAKIA	0.0	0.0	0.0	.0	.4	.0	3.6	2.8	2.6	4.5	11.0
DENMARK	2.2	.6	.4	1.8	.6	.0	.6	.5	.3	.2	.1
HOLLAND	14.5	35.2	27.7	30.3	16.8	1.0	3.7	4.3	.8	.8	1.4
BELGIUM	.4	2.1	1.6	5.3	12.7	.6	12.7	10.3	7.3	2.5	7.2
U. K.	2.3	3.8	3.9	4.7	3.4	.0	.1	.2	.0	.0	.0
S. NORWAY	.0	0.0	0.0	.0	0.0	0.0	0.0	0.0	0.0	0.0	0.0
S. SWEDEN	.3	.1	.1	.4	.1	.0	.0	.0	.0	.0	.0
AUSTRIA	0.0	0.0	0.0	0.0	.0	0.0	.5	.1	.6	1.1	2.1
SWITZERLAND	0.0	0.0	0.0	0.0	0.0	0.0	.0	0.0	.0	1.6	.1
TOTAL	100.0	100.0	100.0	100.0	100.0	100.0	100.0	100.0	100.0	100.0	100.0

.... PERCENT CONTRIBUTIONS TO SULFUR DRY DEPOSITIONS WITHIN RECEPTOR REGIONS IN THE FRG ....

EMITTOR COUNTRY	SCHLESWIG HOLSTEIN	HAMBURG	BREMEN	LOWER SAXONY	NORTHRHINE-WESTPHALIA	WEST BERLIN	RHINELAND-PALATINATE	HESSEN	SAARLAND	BADEN-WURTTENBERG	BAVARIA
W. GERMANY (FRG)	69.5	62.3	73.5	45.5	56.2	3.5	48.9	36.8	46.8	50.7	37.9
E. GERMANY (GDR)	7.6	20.3	3.0	28.2	12.4	91.6	22.6	43.2	9.4	9.9	22.8
FRANCE	.2	1.5	1.3	2.3	5.5	.1	9.4	2.0	33.8	25.6	3.0
POLAND	.3	.4	.1	.5	.1	1.8	.2	1.0	.0	.3	1.7
CZECHOSLOVAKIA	0.0	0.0	0.0	.9	1.1	2.0	3.6	7.0	1.5	2.7	20.5
DENMARK	9.4	1.9	1.3	1.4	.4	.0	.3	.2	.1	.1	.0
HOLLAND	10.3	9.7	15.8	15.3	11.2	.8	1.8	2.4	.8	1.4	1.3
BELGIUM	1.0	2.9	3.5	4.5	12.1	.1	11.4	6.3	5.3	3.6	4.9
U. K.	.9	.7	1.4	1.2	.9	.0	.0	.1	.0	.0	.0
S. NORWAY	.0	0.0	0.0	.0	0.0	0.0	0.0	0.0	0.0	0.0	0.0
S. SWEDEN	.7	.3	.2	.2	.0	.0	.0	.0	.0	.0	.0
AUSTRIA	0.0	0.0	0.0	0.0	.0	0.0	1.7	.9	2.2	4.3	7.9
SWITZERLAND	0.0	0.0	0.0	0.0	0.0	0.0	.0	0.0	.0	1.5	.1
TOTAL	100.0	100.0	100.0	100.0	100.0	100.0	100.0	100.0	100.0	100.0	100.0

.... PERCENT CONTRIBUTIONS TO SULFUR CONCENTRATIONS WITHIN RECEPTOR REGIONS IN THE FRG ....

EMITTOR COUNTRY	SCHLESWIG HOLSTEIN	HAMBURG	BREMEN	LOWER SAXONY	NORTHRHINE-WESTPHALIA	WEST BERLIN	RHINELAND-PALATINATE	HESSEN	SAARLAND	BADEN-WURTTENBERG	BAVARIA
W. GERMANY (FRG)	69.6	62.3	73.6	45.5	56.2	3.5	49.9	36.8	46.8	50.7	37.9
E. GERMANY (GDR)	7.6	20.3	3.0	28.2	12.4	91.6	22.5	43.2	9.4	9.8	22.8
FRANCE	.2	1.5	1.3	2.3	5.5	.1	9.4	2.0	33.8	25.7	2.9
POLAND	.3	.4	.1	.5	.1	1.6	.2	1.0	.0	.3	1.7
CZECHOSLOVAKIA	0.0	0.0	0.0	.9	1.1	2.0	3.6	7.0	1.5	2.7	20.5
DENMARK	9.4	1.9	1.3	1.4	.4	.0	.3	.2	.1	.1	.0
HOLLAND	10.2	9.6	15.7	15.3	11.2	.8	1.8	2.4	.8	1.3	1.3
BELGIUM	1.0	2.9	3.5	4.5	[illegible]	.1	11.4	6.3	5.3	3.6	4.9
U. K.	.9	.7	1.4	1.2	.9	.0	.0	.1	.0	.0	.0
S. NORWAY	.0	0.0	0.0	.0	0.0	0.0	0.0	0.0	0.0	0.0	0.0
S. SWEDEN	.7	.3	.2	.2	.0	.0	.0	.0	.0	.0	.0
AUSTRIA	0.0	0.0	0.0	0.0	.0	0.0	1.7	.9	2.2	4.3	7.8
SWITZERLAND	0.0	0.0	0.0	0.0	0.0	0.0	.0	0.0	.0	1.5	.1
TOTAL	100.0	100.0	100.0	100.0	100.0	100.0	100.0	100.0	100.0	100.0	100.0

IV ADDITIONAL MODELING WORK PLANNED

As indicated in Section I, this project is in its early stages, and much work remains to be accomplished before the project objectives can be achieved. Our work plans include the following:

- Include a chemical transformations model element for $SO_2/SO_4^=$ conversion
- Treat SO_2 and $SO_4^=$ deposition separately
- Evaluate EURMAP using available observations
- Consider adding meteorological refinements:
    - Better layer-average transport wind
    - Multiple vertical layers
    - Variable mixing depth in space and time
- Consider adding emissions refinements:
    - Diurnal variations
    - Seasonal variations
    - Variable emissions heights
- Extend model runs to one year
- Apply to additional pollutants (CO and NO_x)
- Apply EURMAP to current and future assessments of air quality in Western and Central Europe.

REFERENCES

Bielke, S., and H.W. Georgii, 1968: Investigation on the incorporation of sulfur dioxide into fog- and rain-droplets. Tellus, 20, No. 3, 435-441.

Bolin, B., and C. Persson, 1975: Regional dispersion and deposition of atmospheric pollutants with particular application to sulfur pollution over Western Europe. Tellus, 27, No. 3, 281-310.

Dana, M.T., J.M. Hales, and M.A Wolf, 1975: Rain scavenging of SO_2 and sulfate from power plant plumes. J. Geophys. Research, 80, No. 30, 4119-4129.

Eliassen, A., and J. Saltbones, 1975: Decay and transformation rates of SO_2, as estimated from emission data.trajectories and measured air concentrations. Atmospheric Environment, 9, 425-429.

Gartrell, F.E., L.F. Thomas, and S.B. Carpenter, 1963: Atmospheric oxidation of SO_2 in coal burning power plant plumes. J. Amer. Ind. Hyg. Assoc., 24, 113.

Hales, J.M., J.M. Thorp, and M.A. Wolf, 1970: Precipitation scavenging (1970). Proc. of Symposium, June 1970, Richland, Washington, U.S.A. U.S. Atomic Energy Commission, Division of Technical Information.

Hogstrom, U., 1974: Wet fallout of sulfurous pollutants emitted from a city during rain or snow. Atmospheric Environment, 8, 1291-1303.

Johnson, W.B., D.E. Wolfe, and R.L. Mancuso, 1974: Feasibility of the air quality budget concept. Stanford Res. Inst. No. 3038 - 6 final report for the Federal Republic of Germany, 49 p.

Jost, D., 1973: Zur Husbreitung von Luftbeimengungen über Industriegebieten. Annalen der Meteorologie, 6, 151-156.

Jost, D., 1974: Aerological studies on the atmospheric sulf budget. Tellus, 26, No. 1-2, 206-212.

Kellogg, W.W., R.D. Cadle, E.R. Allen, A.L. Lazrus, and E.A. Martell, 1972: The sulfur cycle. Science, 175, 587-596.

Ottar, B., 1975: The deposition and distribution in European countries of pollutants from distant and local sources (draft). Final report for the OECD project, LRTAP, coordinated by the Norwegian Institute for Air Research.

Powell, D.C., and A.J. Alkezweeny, 1976: Estimation of transformation rate of SO_2 to SO_4 from atmospheric concentration data. Batelle, Pacific Northwest Labs. paper BNWL-SA-5739 submitted to Atmospheric Environment March 1976.

Prahm, L.P., U. Torp, and R.M. Stern, 1976: Deposition and transfromation rates of sulphur oxides during atmospheric transport over the Atlantic. Tellus, 28, No. 4.

Rao, K.S., I. Thomson, and B.A. Egan, 1976: Regional transport model of atmospheric sulfates. Proc. of Annual Meeting of APCA, June 1976, Portland, OR., Paper No. 76-34.3.

Rystad, B., S. Stromsoe, E. Amble, and T. Knudsen, 1974: The LTRAP emission survey. Norwegian Inst. for Air Research, Norway, 19p.

Appendix A

MAPS OF CONCENTRATION PATTERNS RESULTING FROM SO_2 EMISSIONS IN THIRTEEN INDIVIDUAL COUNTRIES IN WESTERN AND CENTRAL EUROPE DURING JULY 1973

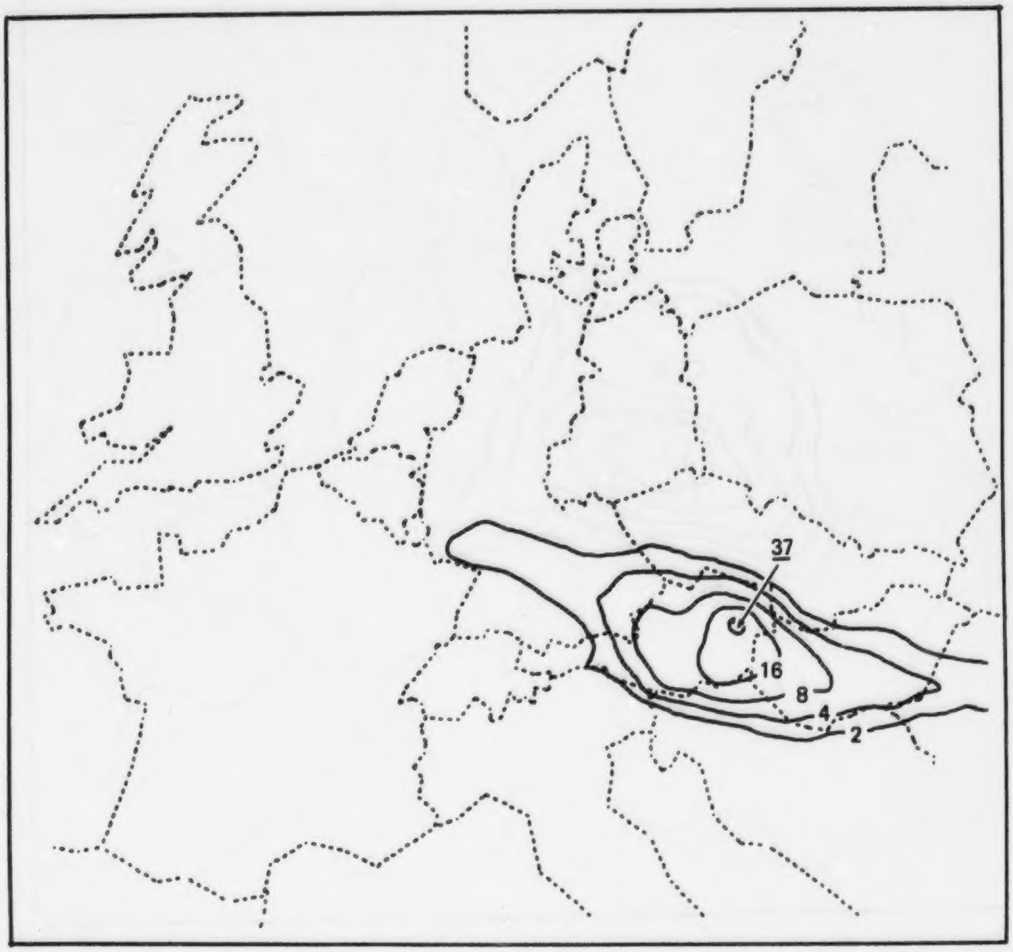

FIGURE A-1 CONCENTRATION OF SULFUR COMPOUNDS (IN TERMS OF EQUIVALENT WEIGHT OF SO_2, 10^{-6} g m^{-3}) FROM EMISSIONS IN AUSTRIA DURING JULY 1973

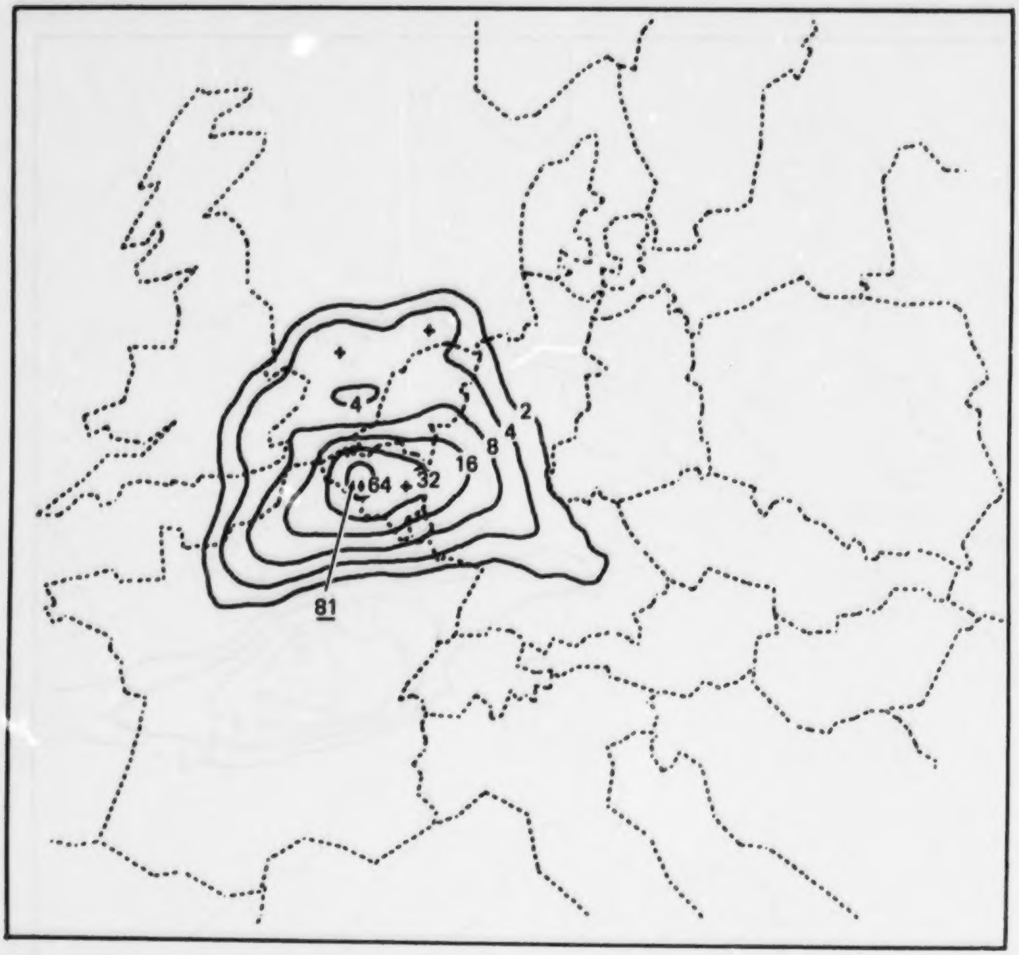

FIGURE A-2 CONCENTRATION OF SULFUR COMPOUNDS (IN TERMS OF EQUIVALENT WEIGHT OF SO_2, 10^{-6} g m^{-3}) FROM EMISSIONS IN BELGIUM DURING JULY 1973

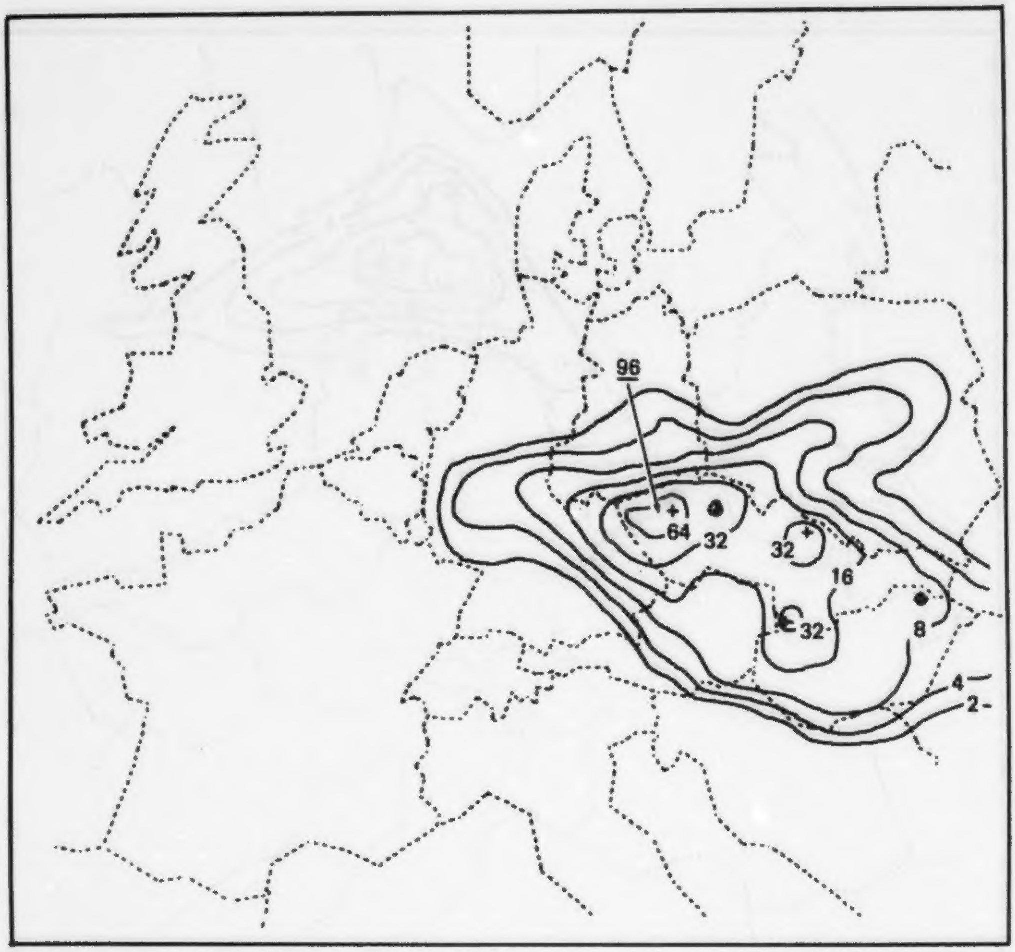
96
64
32
32
16
32
8
4
2

FIGURE A-3 CONCENTRATION OF SULFUR COMPOUNDS (IN TERMS OF EQUIVALENT WEIGHT OF SO_2, 10^{-6} g m^{-3}) FROM EMISSIONS IN CZECHOSLOVAKIA DURING JULY 1973

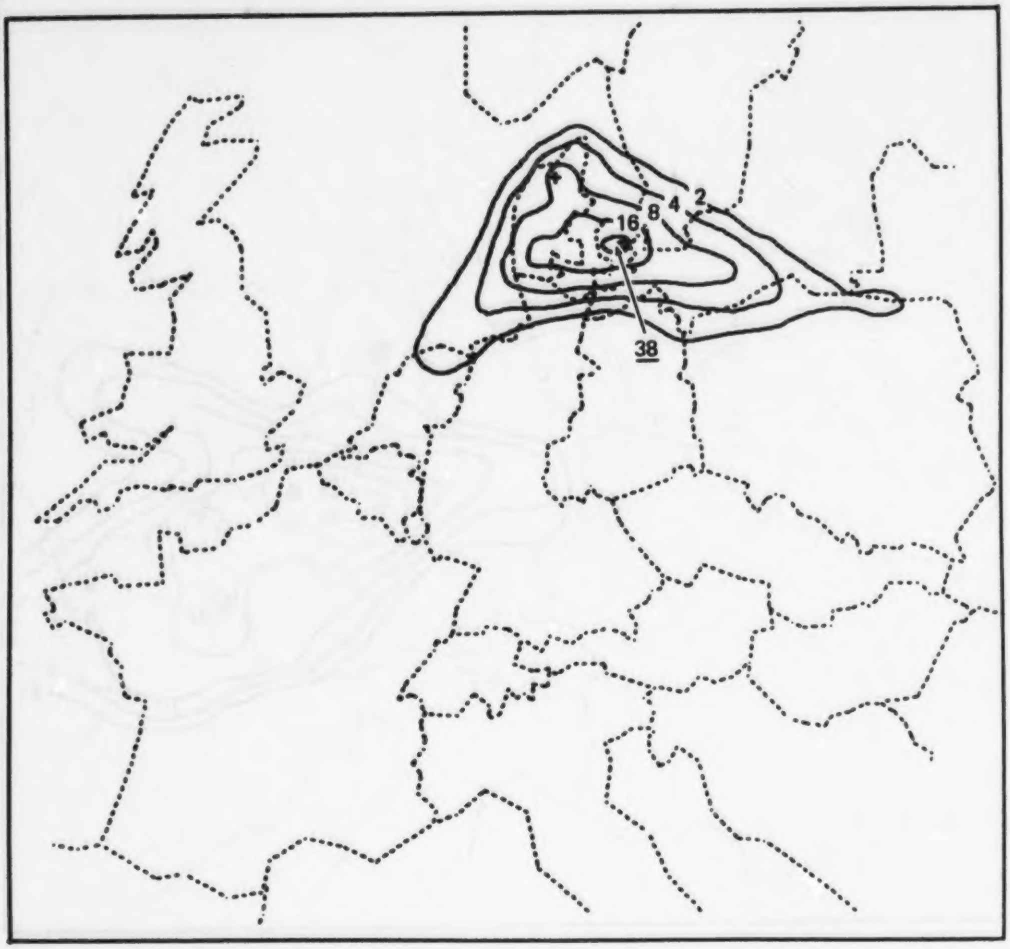

FIGURE A-4 CONCENTRATION OF SULFUR COMPOUNDS (IN TERMS OF EQUIVALENT WEIGHT OF SO2, 10^{-6} g m^{-3}) FROM EMISSIONS IN DENMARK DURING JULY 1973

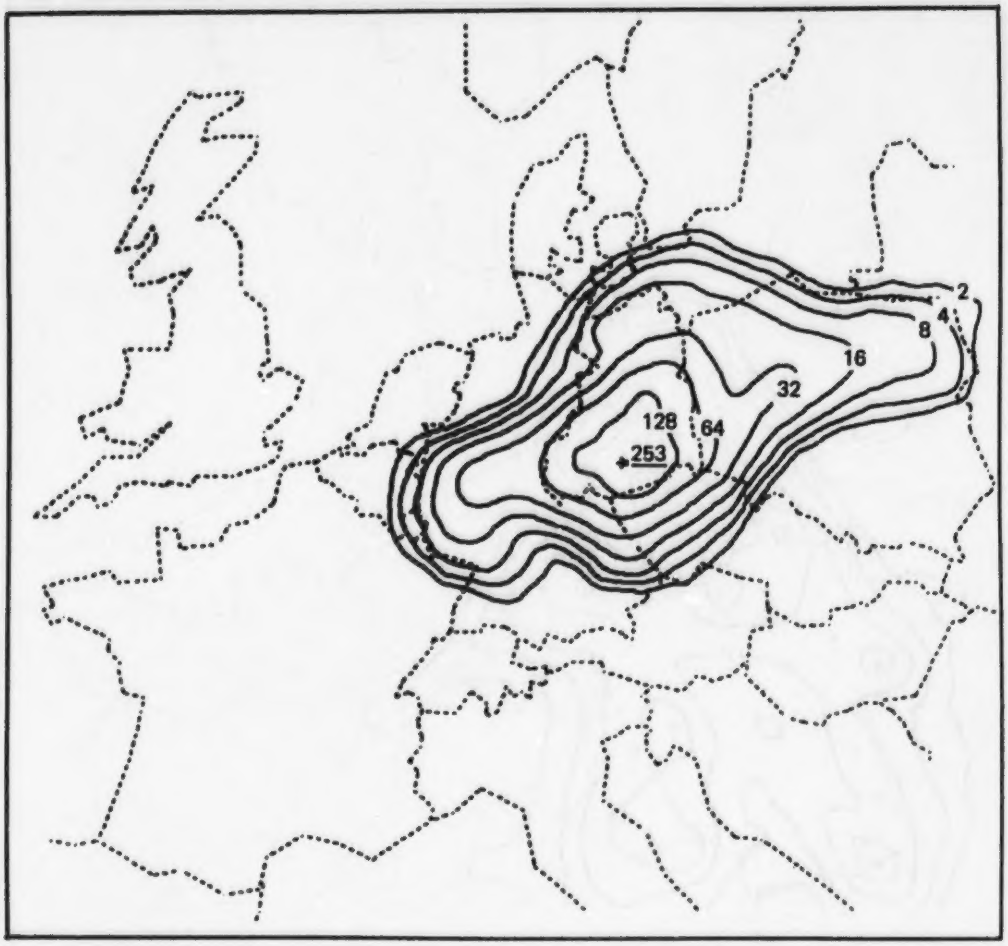
2
4
8
16
32
64
128
253

FIGURE A-5 CONCENTRATION OF SULFUR COMPOUNDS (IN TERMS OF EQUIVALENT WEIGHT OF SO_2, 10^{-6} g m^{-3}) FROM EMISSIONS IN EAST GERMANY DURING JULY 1973

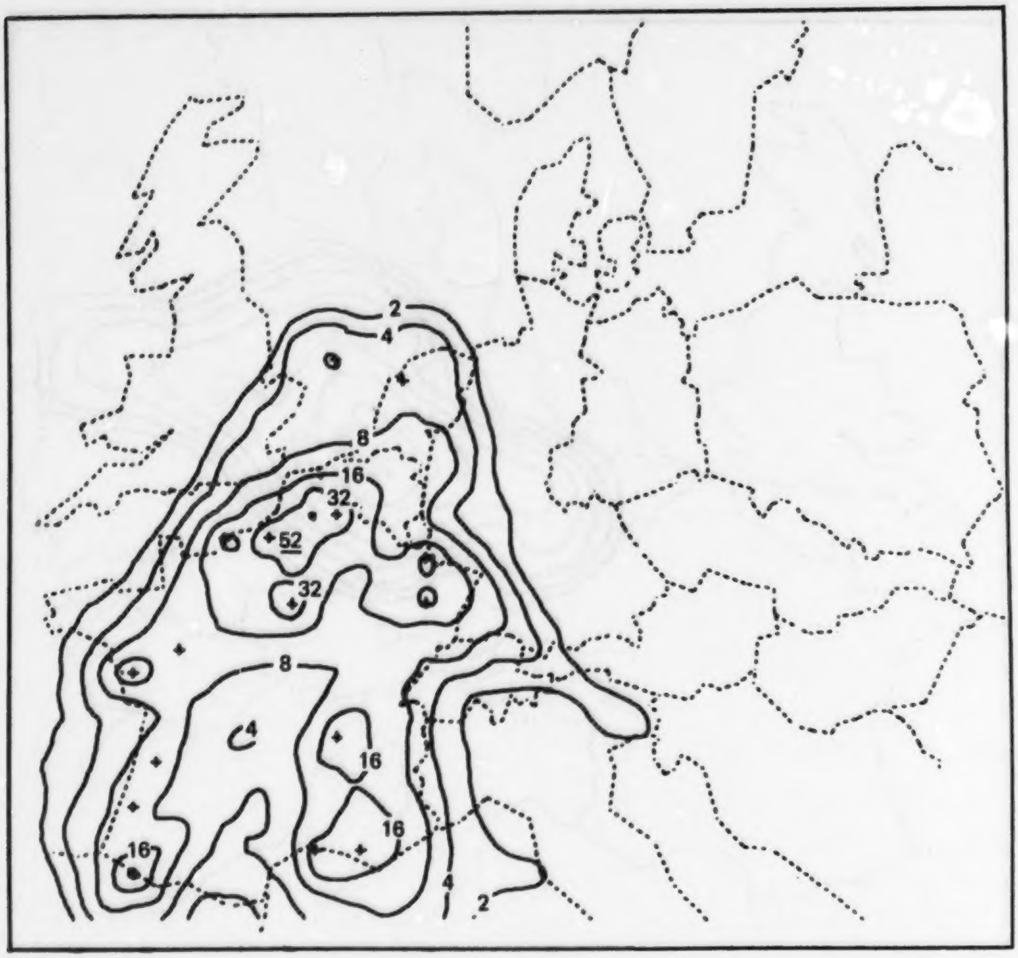
2
4
8
16
32
52
32
8
4
16
16
16
4
2

FIGURE A-6 CONCENTRATION OF SULFUR COMPOUNDS (IN TERMS OF EQUIVALENT WEIGHT OF SO_2, 10^{-6} g m^{-3}) FROM EMISSIONS IN FRANCE DURING JULY 1973

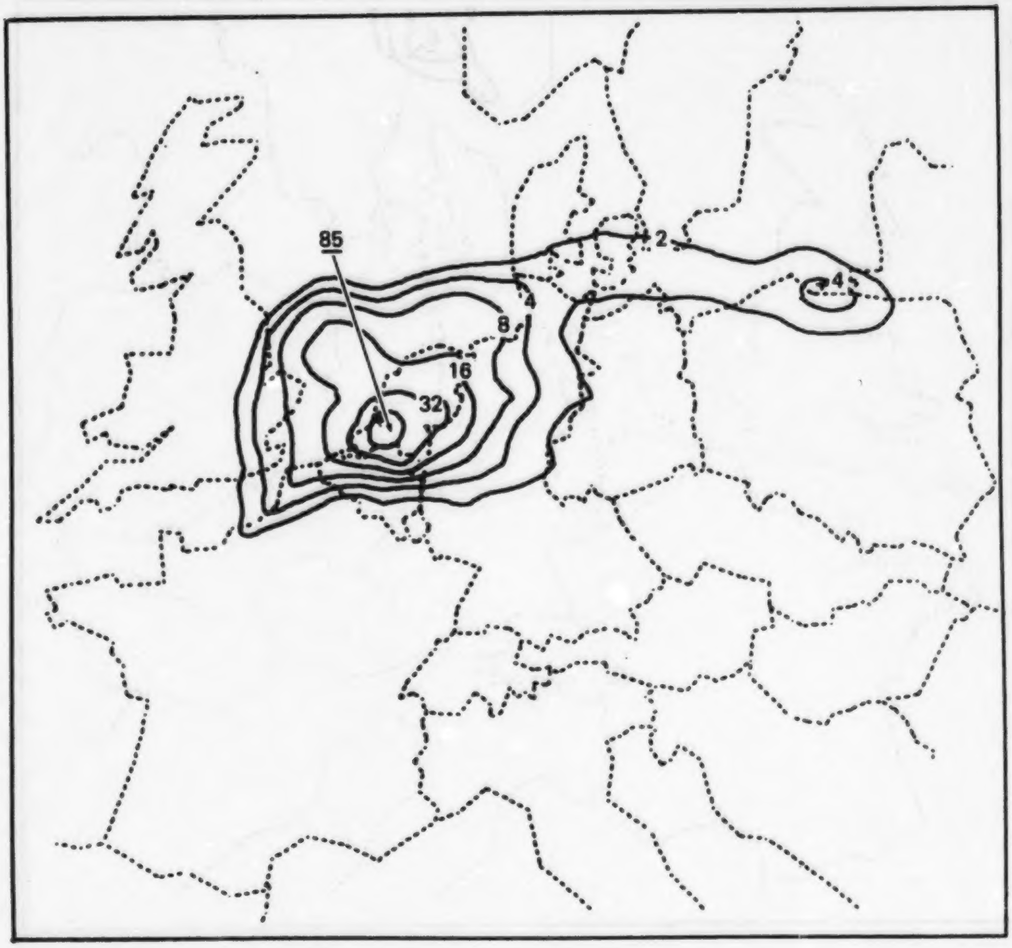

FIGURE A-7 CONCENTRATION OF SULFUR COMPOUNDS (IN TERMS OF EQUIVALENT WEIGHT OF SO_2, 10^{-6} g m^{-3}) FROM EMISSIONS IN THE NETHERLANDS DURING JULY 1973

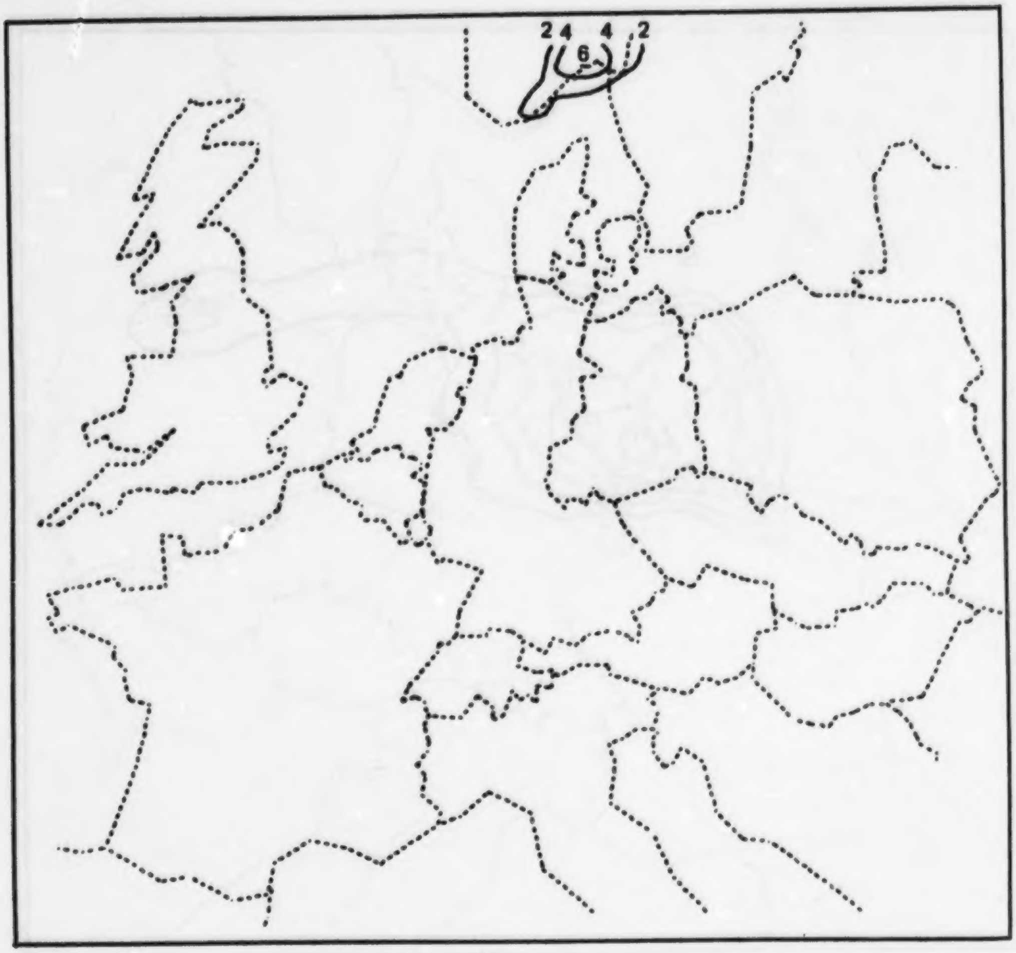

FIGURE A-8 CONCENTRATION OF SULFUR COMPOUNDS (IN TERMS OF EQUIVALENT WEIGHT OF SO_2, 10^{-6} g m^{-3}) FROM EMISSIONS IN NORWAY (SOUTH OF 60°N) DURING JULY 1973

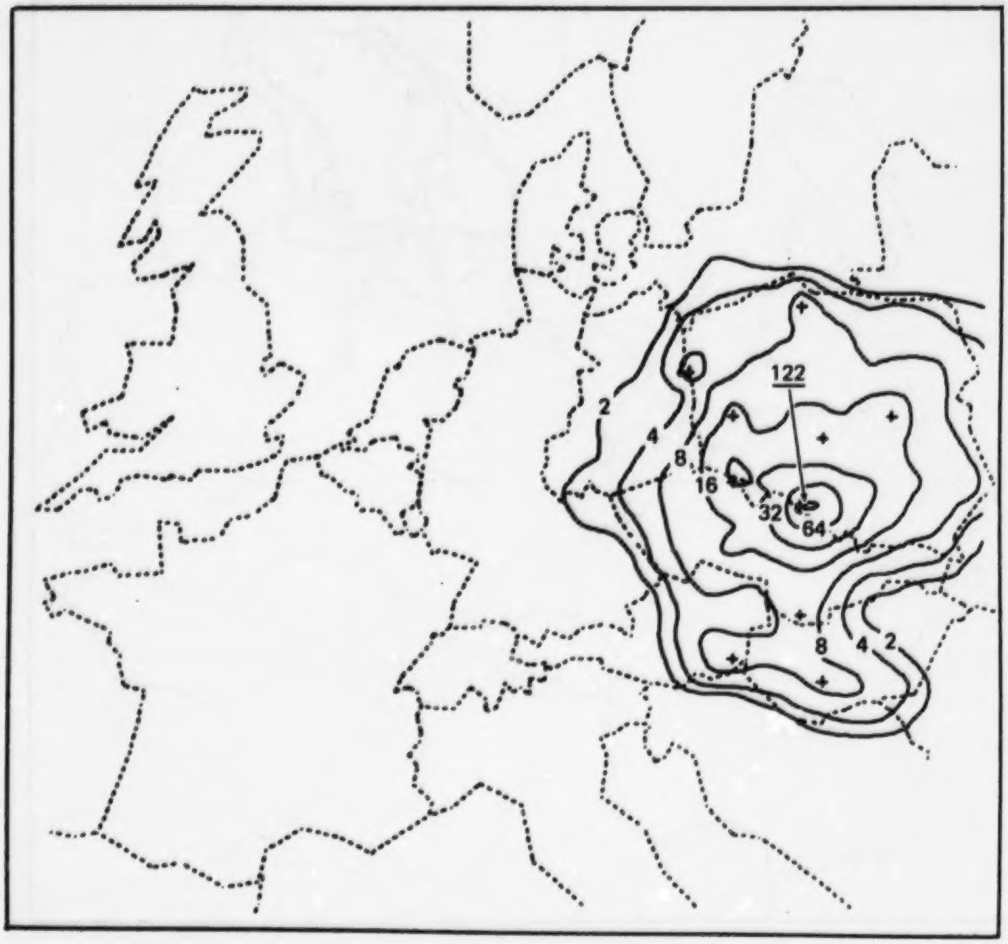
122
2
4
8
16
32
64
8
4
2

FIGURE A-9 CONCENTRATION OF SULFUR COMPOUNDS (IN TERMS OF EQUIVALENT WEIGHT OF SO_2, 10^{-6} g m^{-3}) FROM EMISSIONS IN POLAND DURING JULY 1973

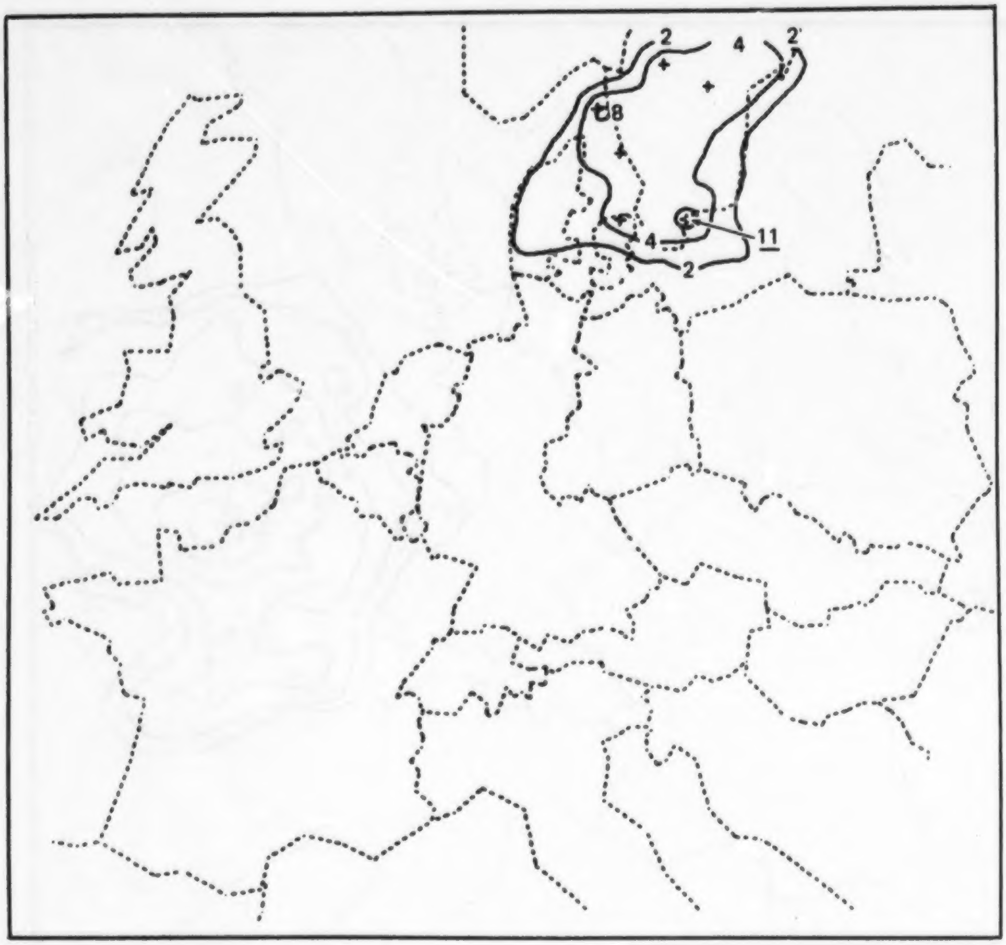

FIGURE A-10 CONCENTRATION OF SULFUR COMPOUNDS (IN TERMS OF EQUIVALENT WEIGHT OF SO_2, 10^{-6} g m^{-3}) FROM EMISSIONS IN SWEDEN (SOUTH OF 60°N) DURING JULY 1973

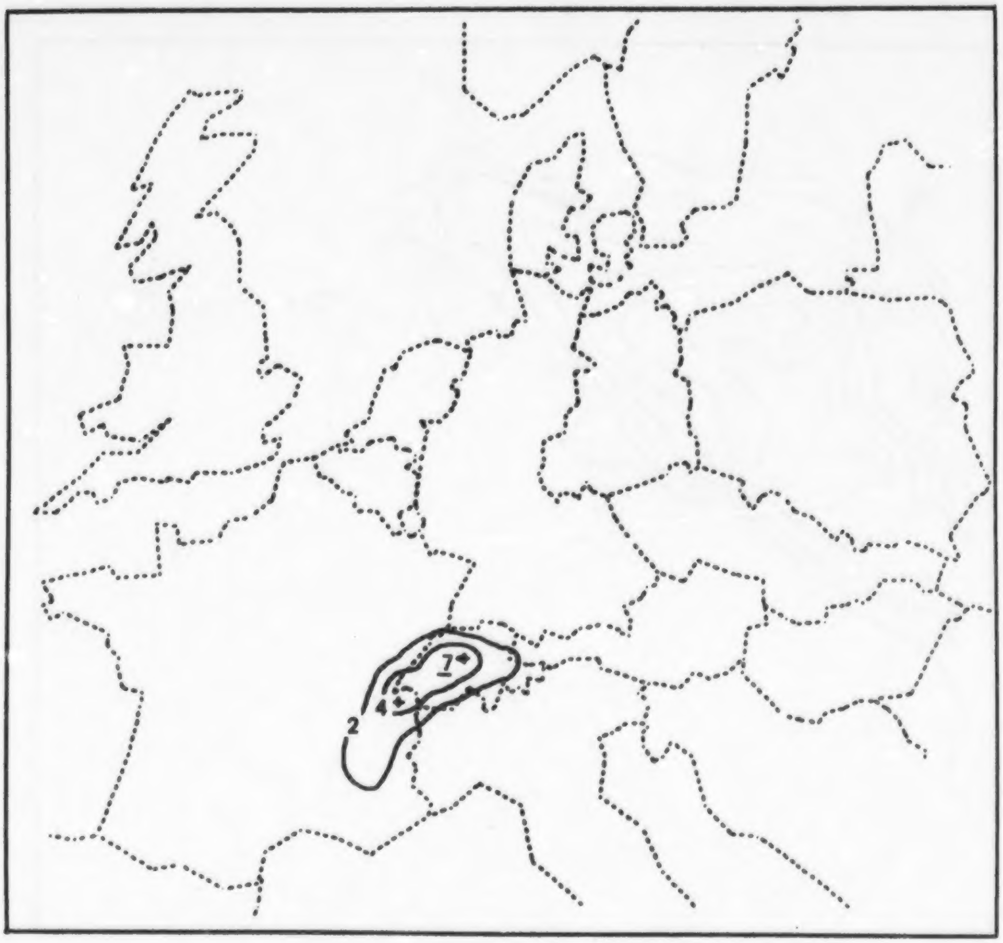

FIGURE A-11 CONCENTRATION OF SULFUR COMPOUNDS (IN TERMS OF EQUIVALENT WEIGHT OF SO_2, 10^{-6} g m^{-3}) FROM EMISSIONS IN SWITZERLAND DURING JULY 1973

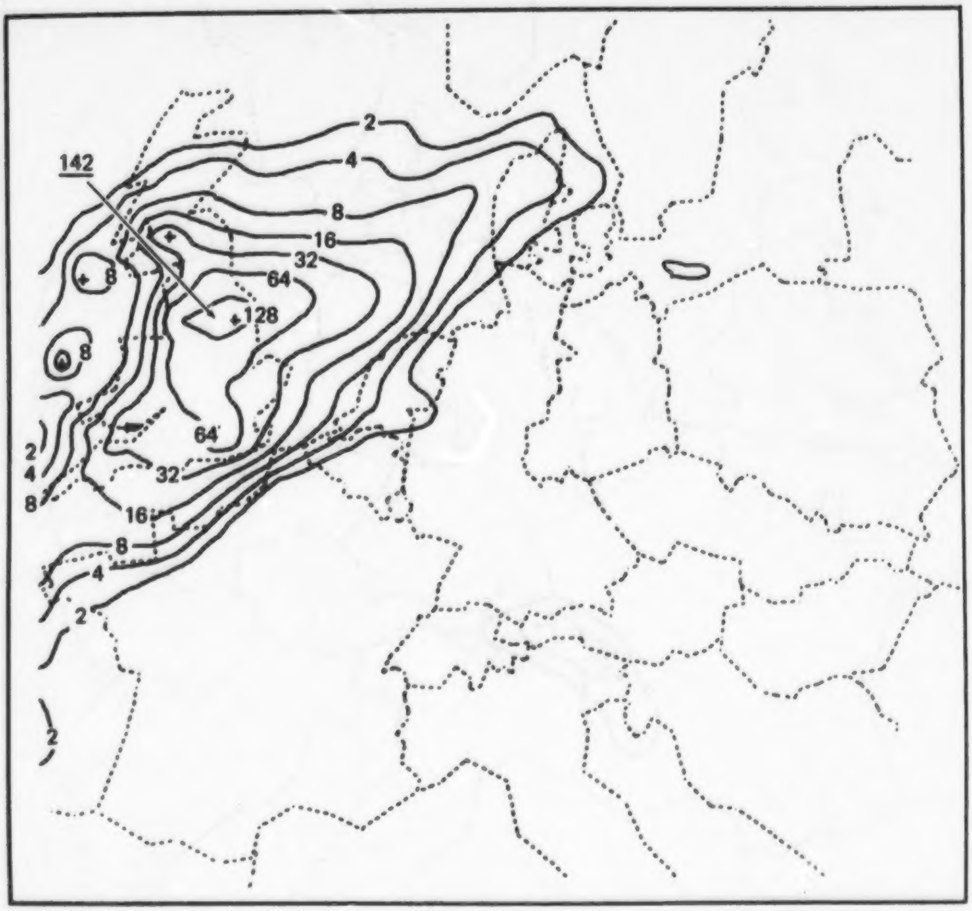
142
2
4
8
16
32
64
+128
8
8
64
2
4
8
32
16
8
4
2
2

FIGURE A-12 CONCENTRATION OF SULFUR COMPOUNDS (IN TERMS OF EQUIVALENT WEIGHT OF SO_2, 10^{-6} $g\ m^{-3}$) FROM EMISSIONS IN THE UNITED KINGDOM DURING JULY 1973

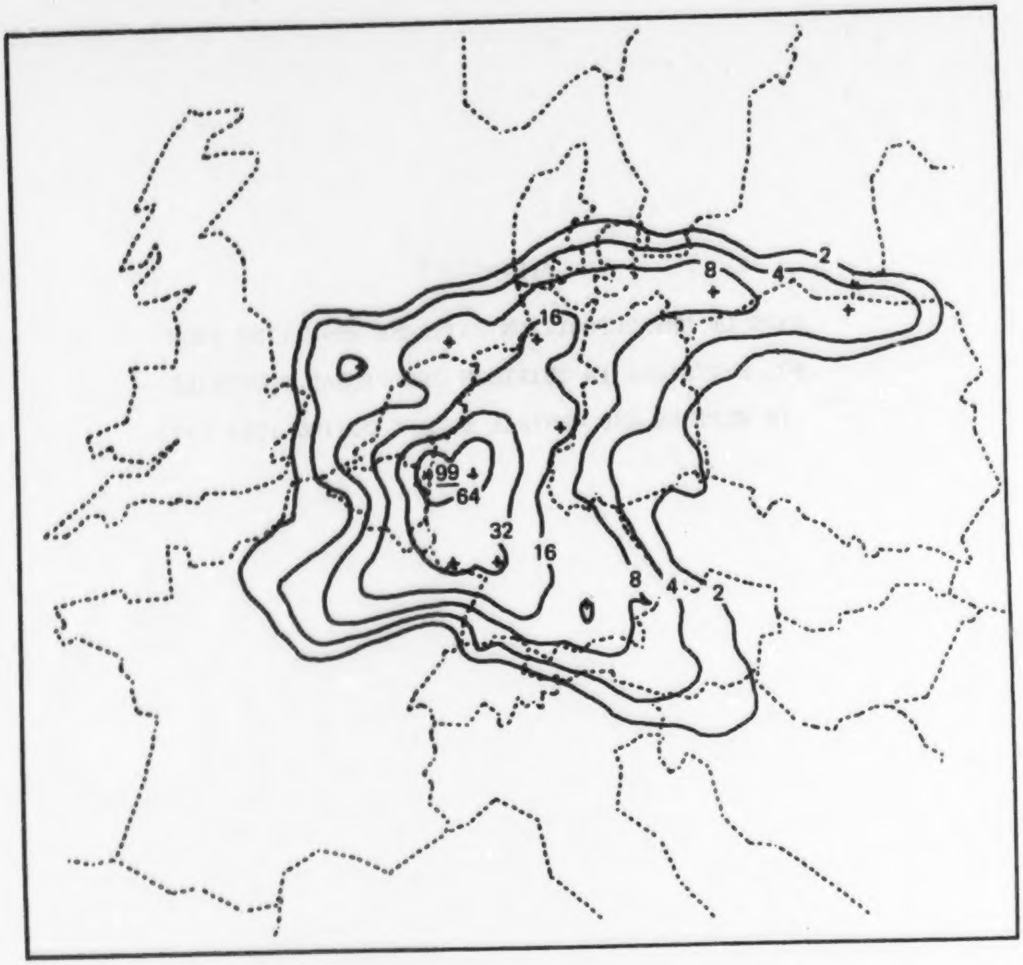
2
4
8
16
99
64
32
16
8
4
2

FIGURE A-13 CONCENTRATION OF SULFUR COMPOUNDS (IN TERMS OF EQUIVALENT WEIGHT OF SO_2, 10^{-6} g m^{-3}) FROM EMISSIONS IN WEST GERMANY DURING JULY 1973

Appendix B

MAPS OF DRY DEPOSITION PATTERNS RESULTING FROM SO_2 EMISSIONS IN THIRTEEN INDIVIDUAL COUNTRIES IN WESTERN AND CENTRAL EUROPE DURING JULY 1973

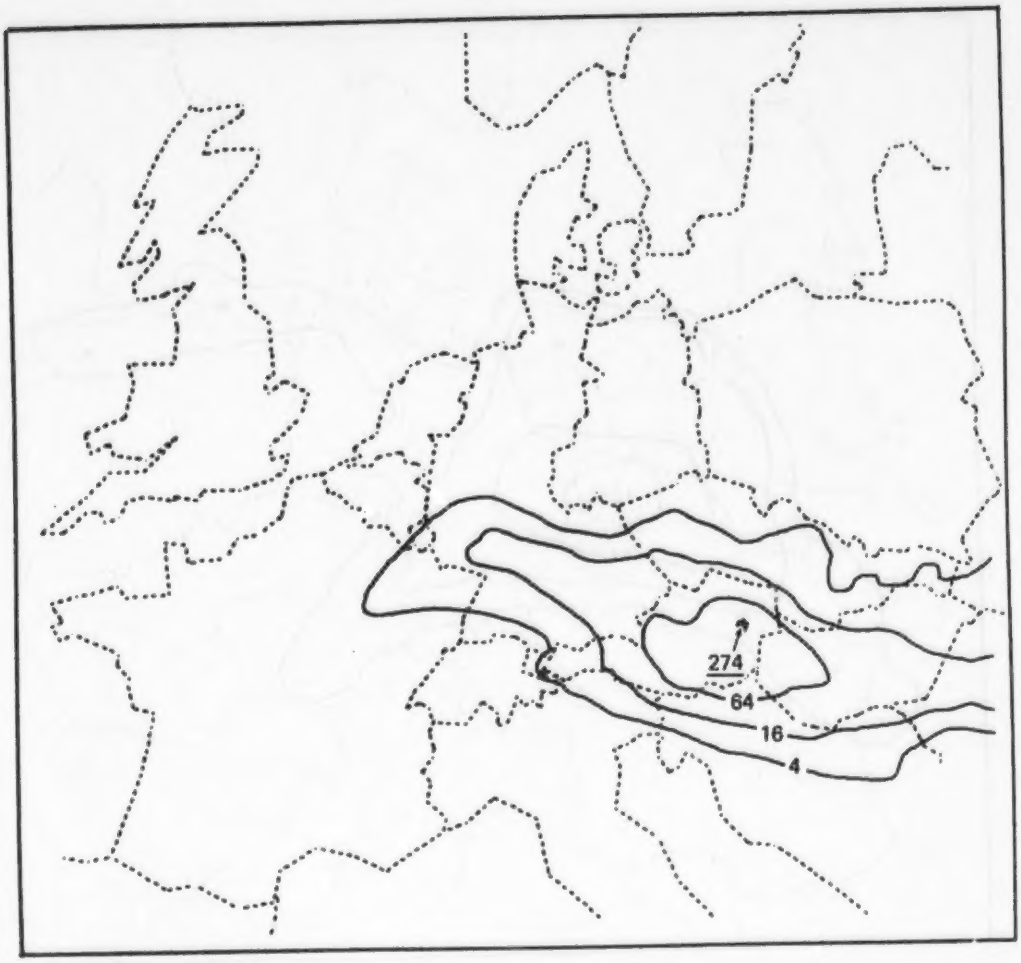

FIGURE B-1 DRY DEPOSITION OF SULFUR COMPOUNDS (IN TERMS OF EQUIVALENT WEIGHT OF SO_2, 10^{-3} g m^{-2}) FROM EMISSIONS IN AUSTRIA DURING JULY 1973

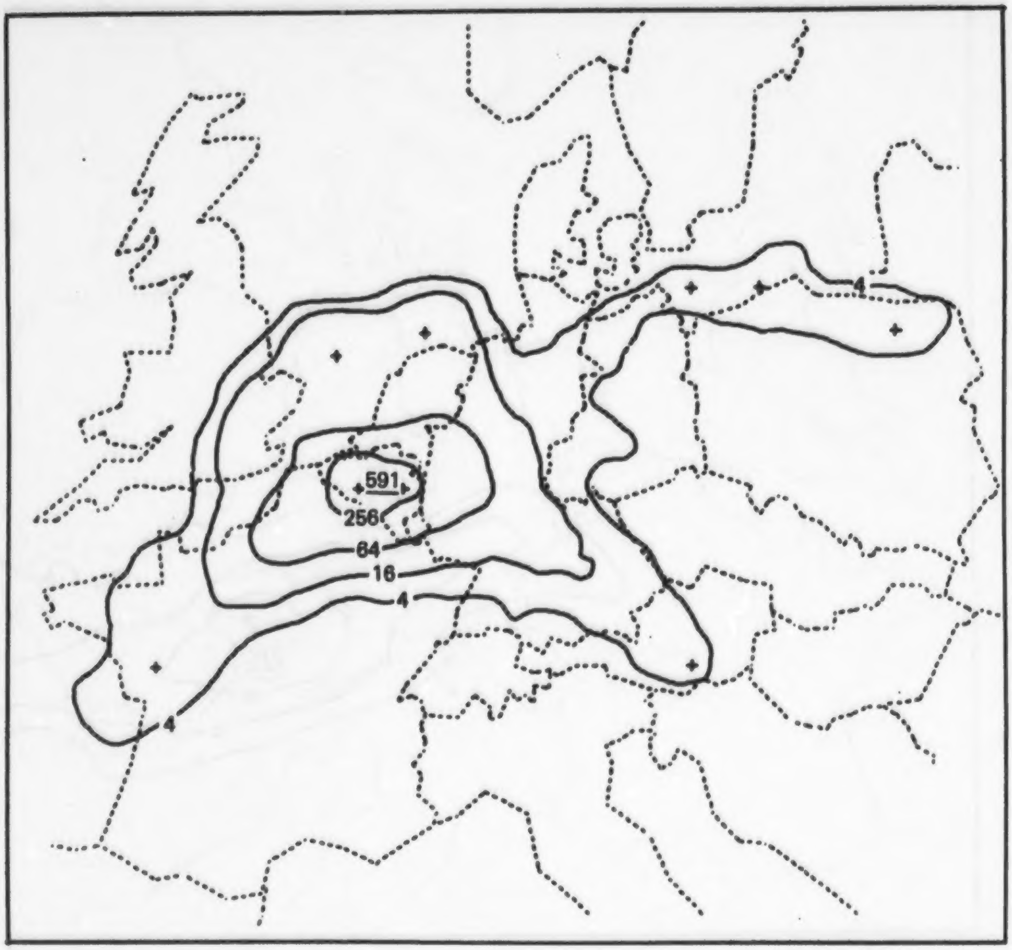
591
256
64
16
4
4
4

FIGURE B-2 DRY DEPOSITION OF SULFUR COMPOUNDS (IN TERMS OF EQUIVALENT WEIGHT OF SO_2, 10^{-3} g m^{-2}) FROM EMISSIONS IN BELGIUM DURING JULY 1973

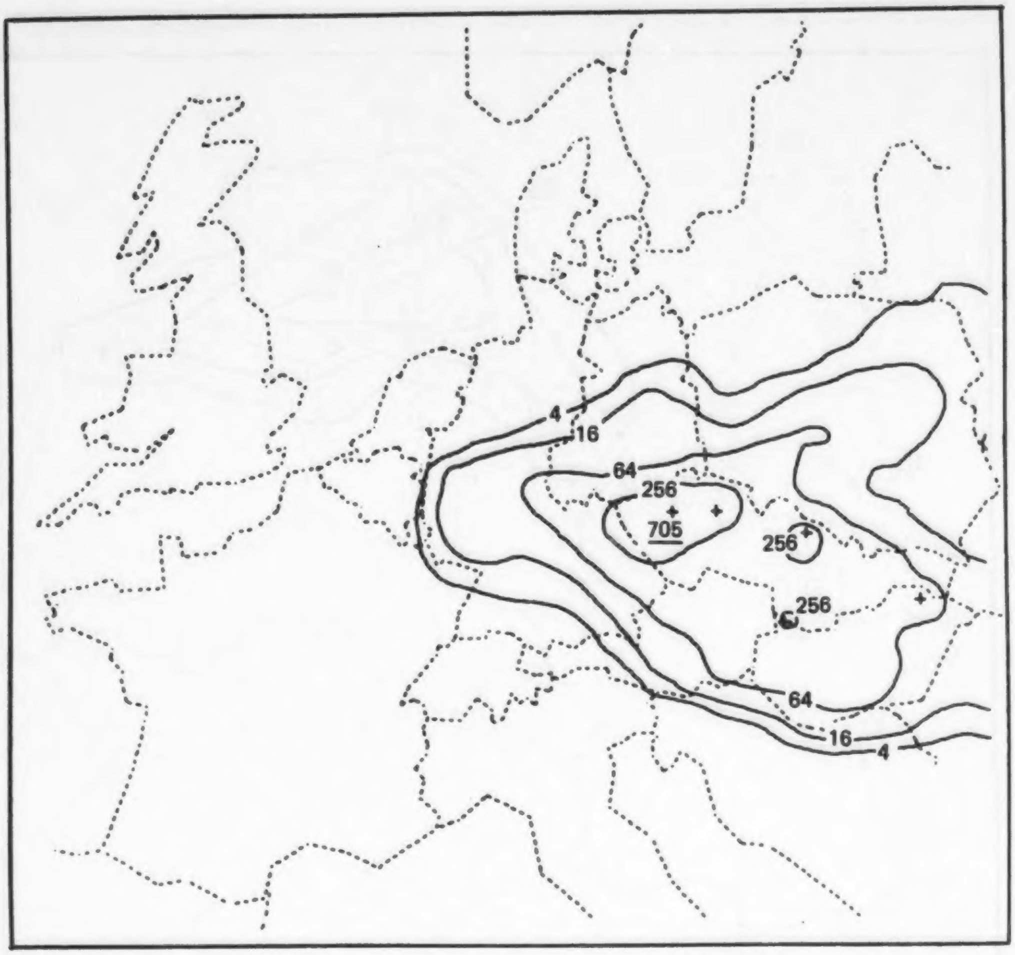
4
16
64
256
705
256
256
64
16
4

FIGURE B-3 DRY DEPOSITION OF SULFUR COMPOUNDS (IN TERMS OF EQUIVALENT WEIGHT OF SO_2, 10^{-3} g m^{-2}) FROM EMISSIONS IN CZECHOSLOVAKIA DURING JULY 1973

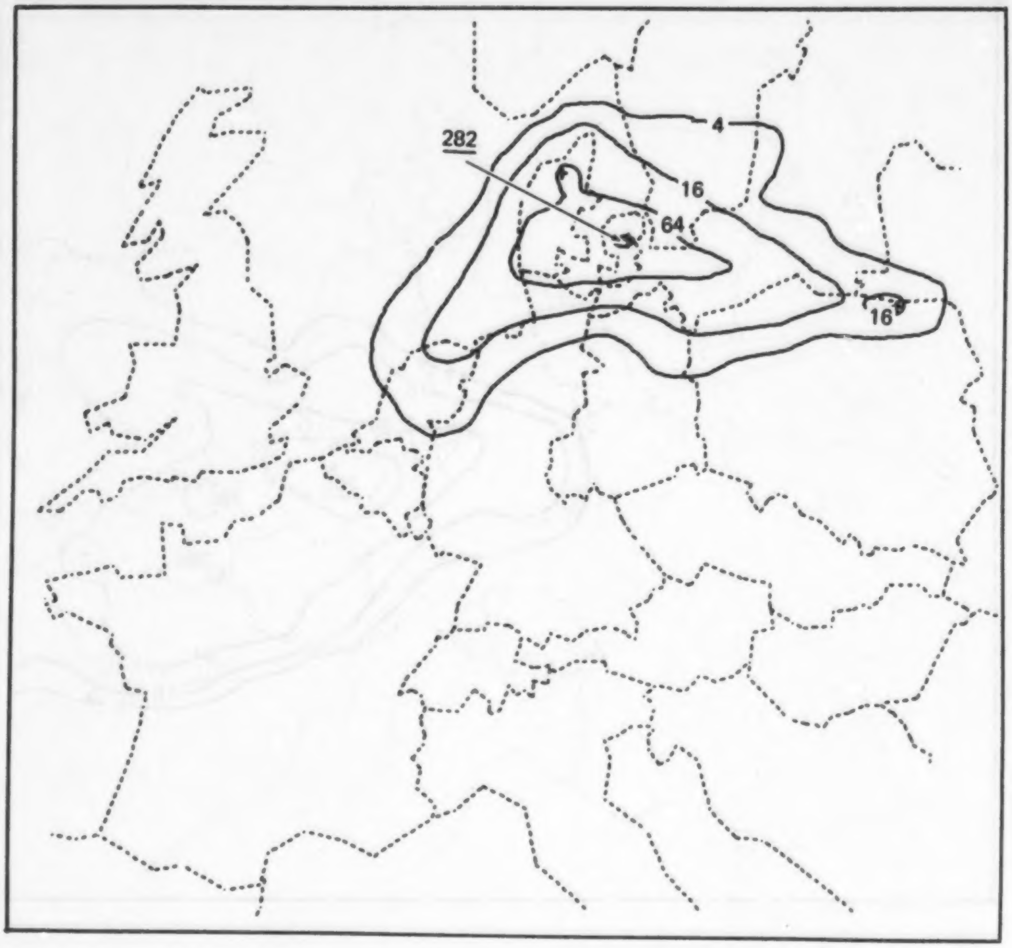

FIGURE B-4 DRY DEPOSITION OF SULFUR COMPOUNDS (IN TERMS OF EQUIVALENT WEIGHT OF SO_2, 10^{-3} g m^{-2}) FROM EMISSIONS IN DENMARK DURING JULY 1973

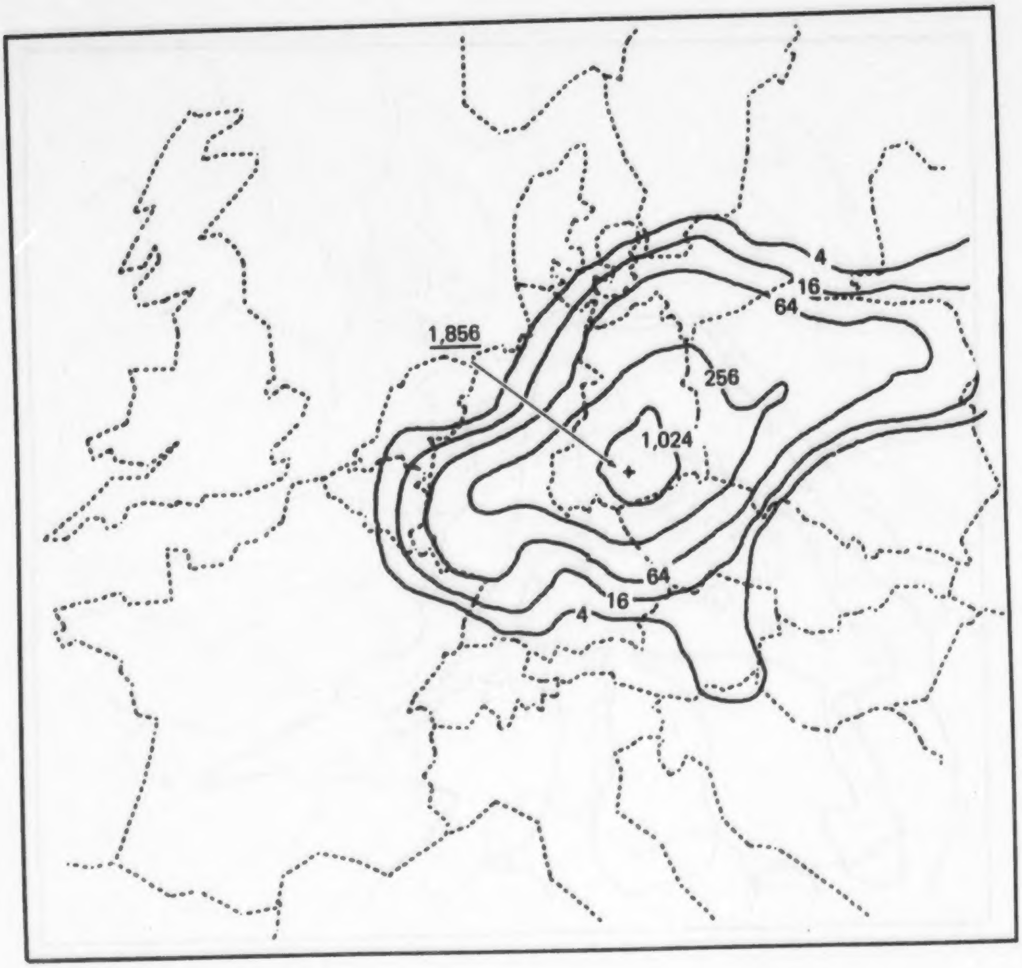
1,856
1,024
256
64
16
4
4
16
64

FIGURE B-5 DRY DEPOSITION OF SULFUR COMPOUNDS (IN TERMS OF EQUIVALENT WEIGHT OF SO_2, 10^{-3} g m^{-2}) FROM EMISSIONS IN EAST GERMANY DURING JULY 1973

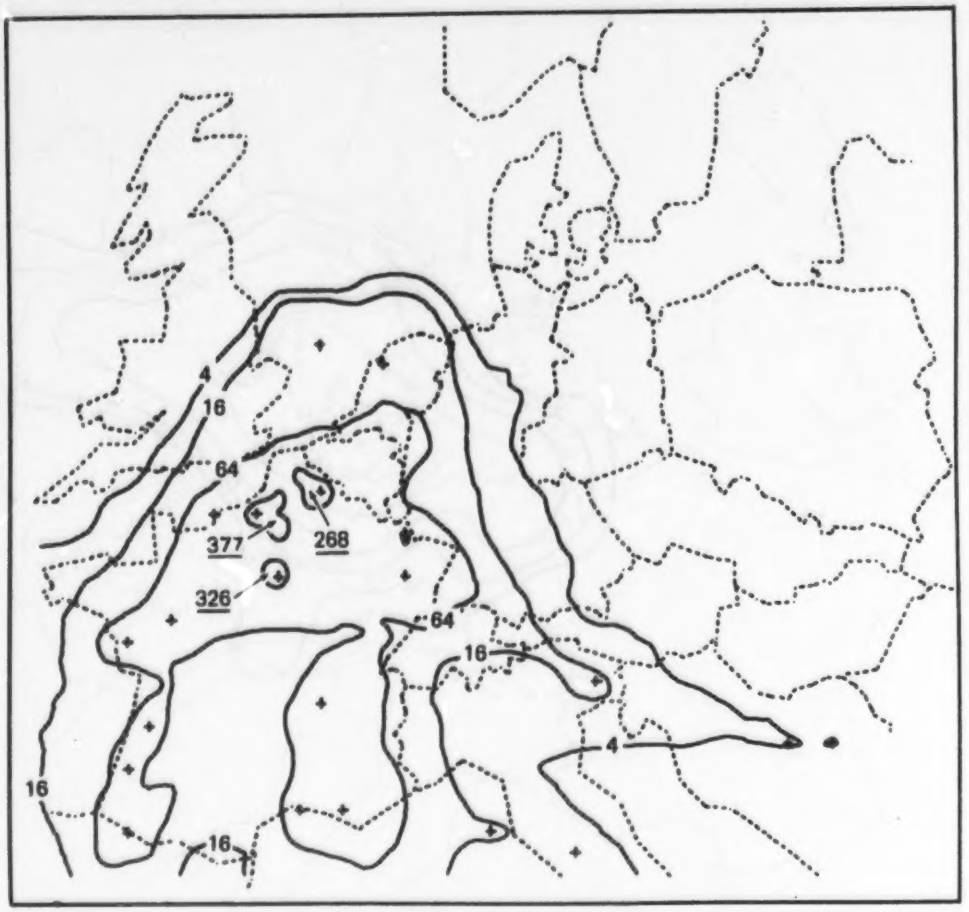
4
16
64
377
268
326
64
16
4
16
16

FIGURE B-6 DRY DEPOSITION OF SULFUR COMPOUNDS (IN TERMS OF EQUIVALENT WEIGHT OF SO_2, 10^{-3} g m^{-2}) FROM EMISSIONS IN FRANCE DURING JULY 1973

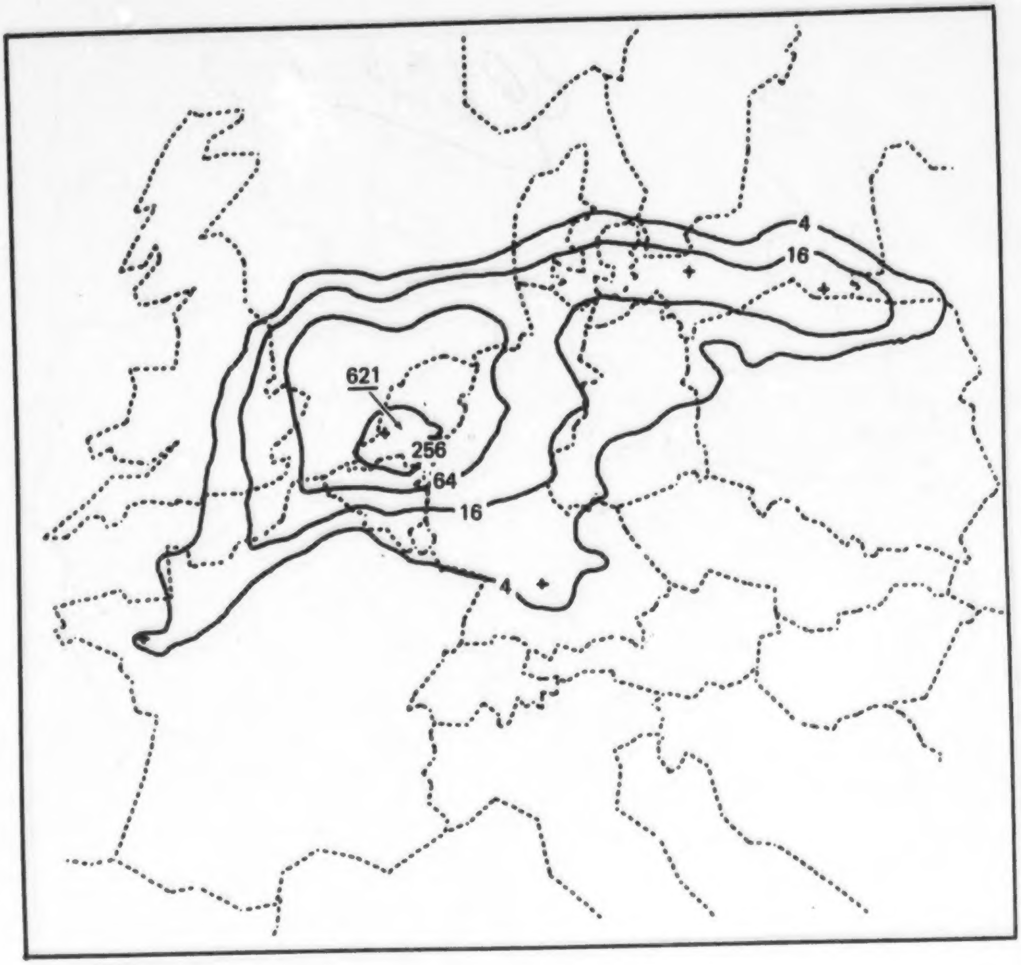
4
16
621
256
64
16
4

FIGURE B-7 DRY DEPOSITION OF SULFUR COMPOUNDS (IN TERMS OF EQUIVALENT WEIGHT OF SO_2, 10^{-3} g m^{-2}) FROM EMISSIONS IN THE NETHERLANDS DURING JULY 1973

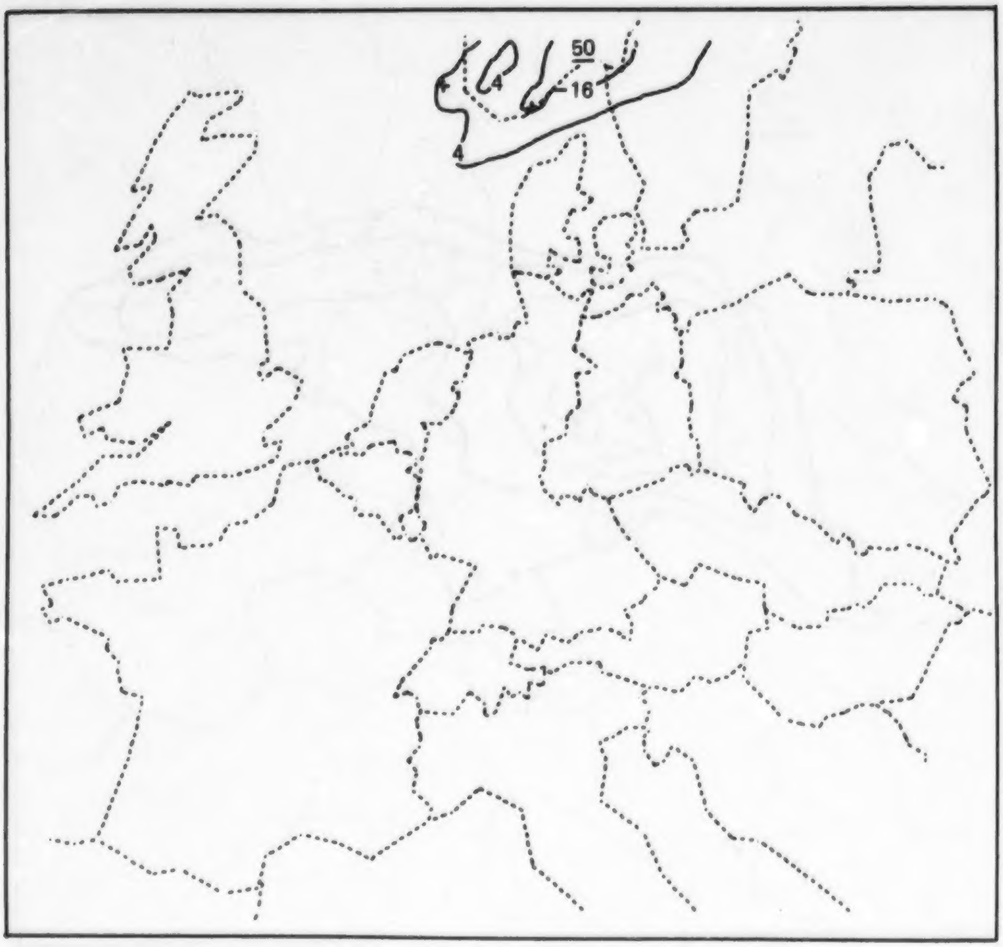

FIGURE B-8 DRY DEPOSITION OF SULFUR COMPOUNDS (IN TERMS OF EQUIVALENT WEIGHT OF SO_2, 10^{-3} g m^{-2}) FROM EMISSIONS IN NORWAY (SOUTH OF 60°N) DURING JULY 1973

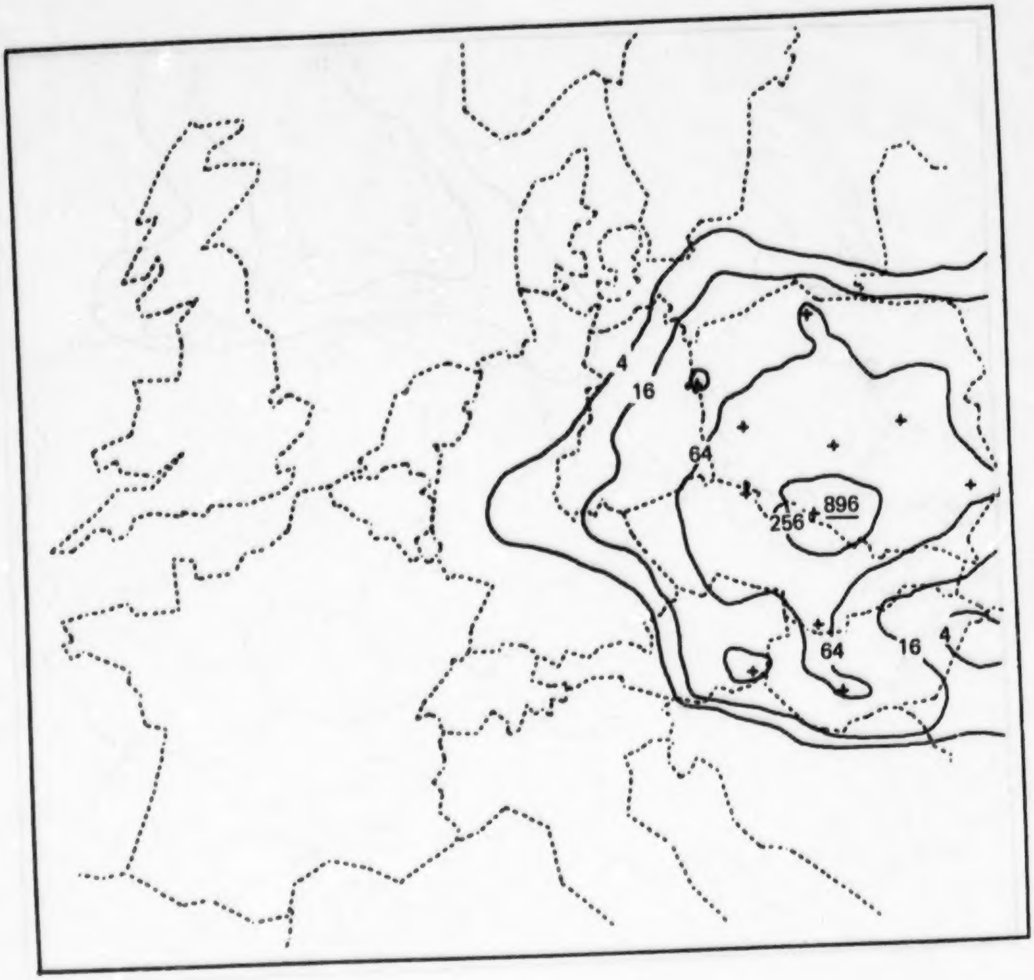
4
16
64
256
896
64
16
4

FIGURE B-9 DRY DEPOSITION OF SULFUR COMPOUNDS (IN TERMS OF EQUIVALENT WEIGHT OF SO_2, 10^{-3} g m^{-2}) FROM EMISSIONS IN POLAND DURING JULY 1973

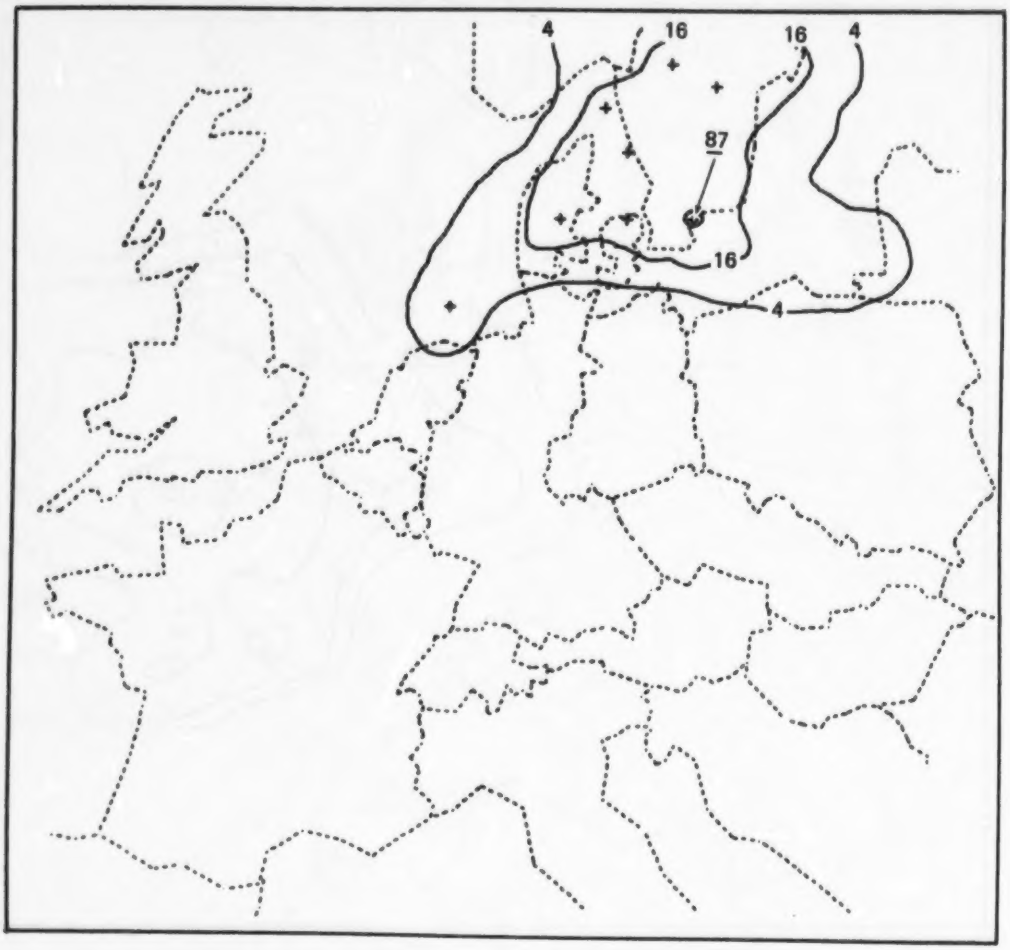

FIGURE B-10 DRY DEPOSITION OF SLUFUR COMPOUNDS (IN TERMS OF EQUIVALENT WEIGHT OF SO_2, 10^{-3} g m^{-2}) FROM EMISSIONS IN SWEDEN (SOUTH OF 60^{0}N) DURING JULY 1973

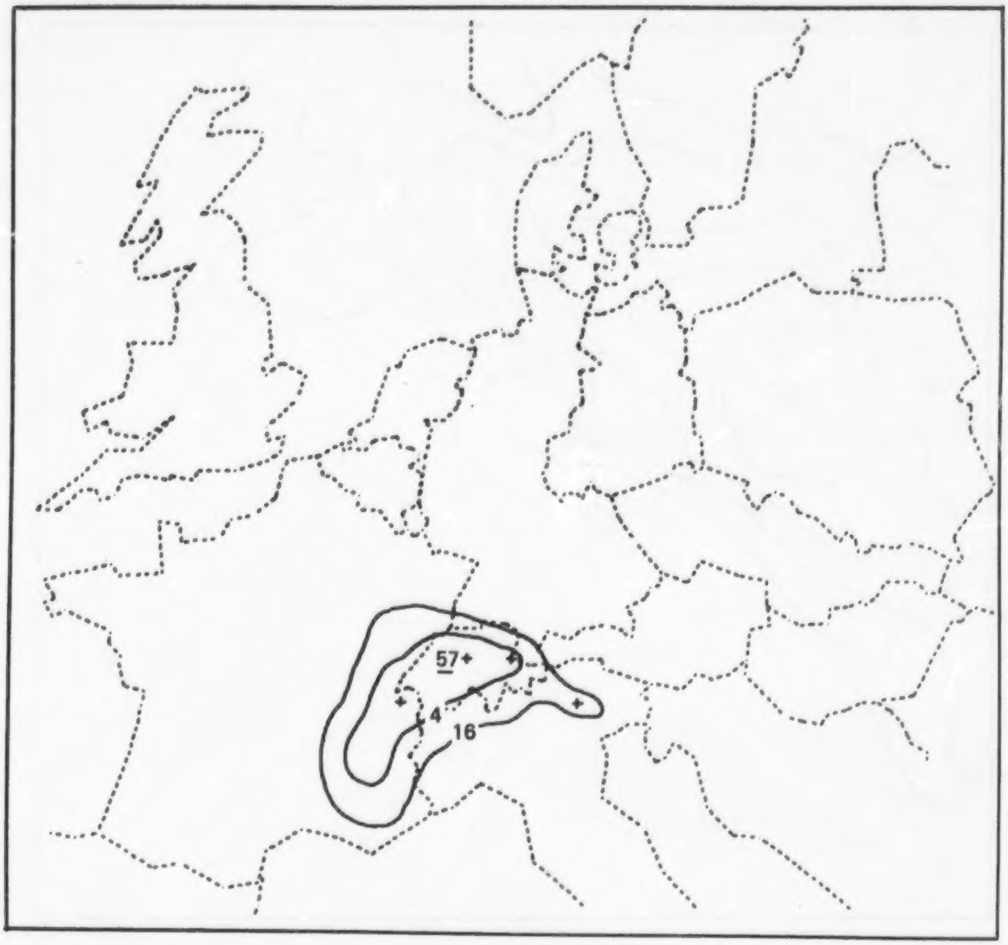

FIGURE B-11 DRY DEPOSITION OF SULFUR COMPOUNDS (IN TERMS OF EQUIVALENT WEIGHT OF SO_2, 10^{-3} g m-2) FROM EMISSIONS IN SWITZERLAND DURING JULY 1973

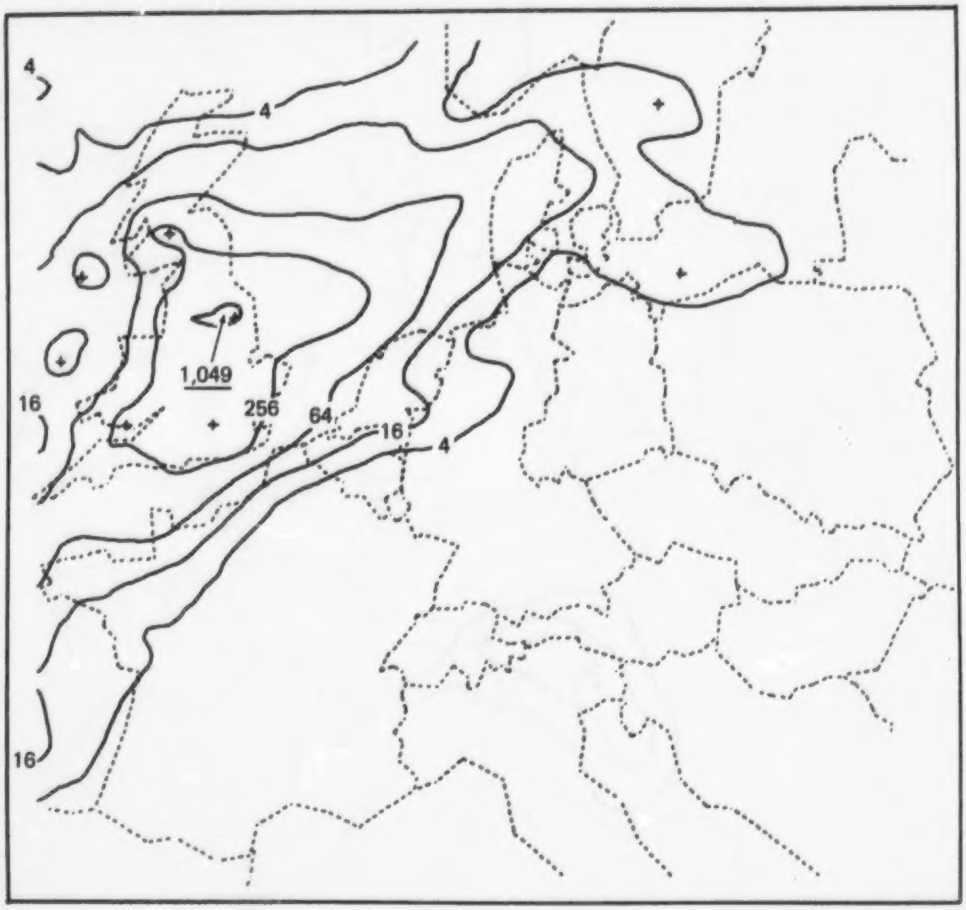
4
4
16
1,049
256
64
16
4
16

FIGURE B-12 DRY DEPOSITION OF SULFUR COMPOUNDS (IN TERMS OF EQUIVALENT WEIGHT OF SO_2, 10^{-3} g m^{-2}) FROM EMISSIONS IN THE UNITED KINGDOM DURING JULY 1973

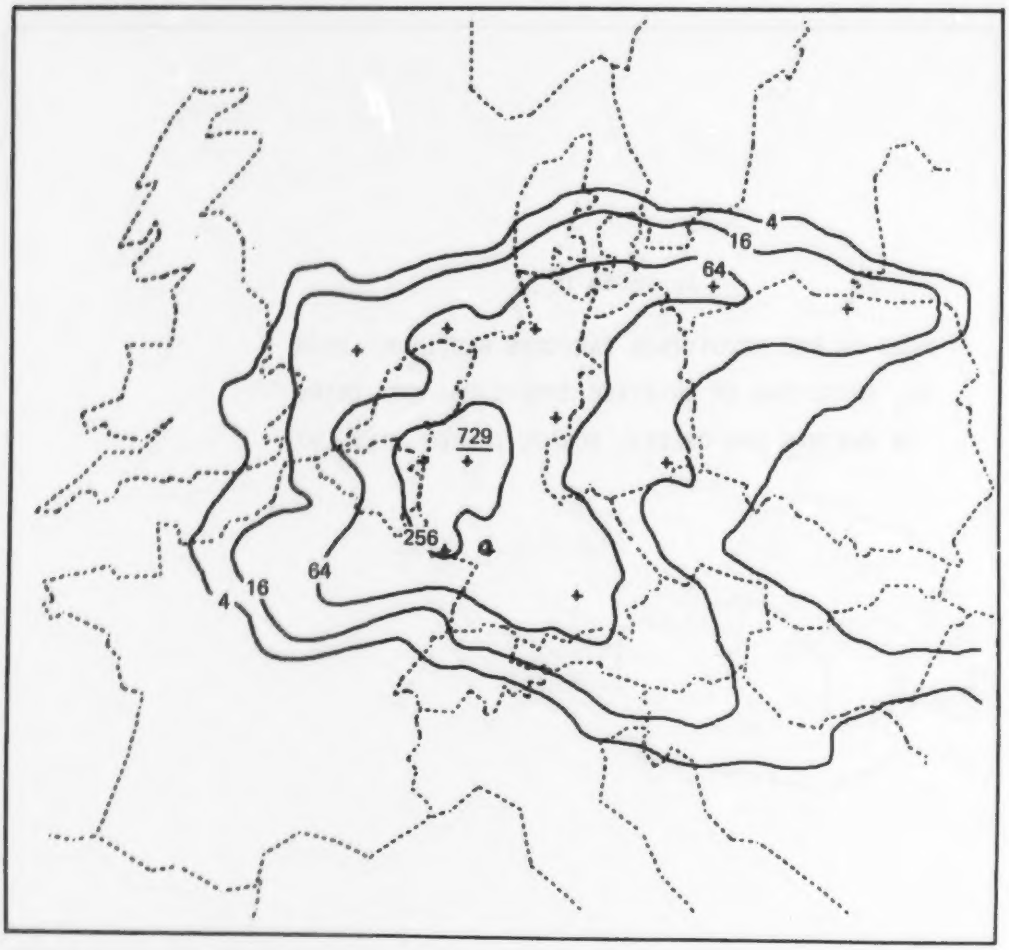

4
16
64
729
256
64
16
4

FIGURE B-13 DRY DEPOSITION OF SULFUR COMPOUNDS (IN TERMS OF EQUIVALENT WEIGHT OF SO_2, 10^{-3} g m^{-2}) FROM EMISSIONS IN WEST GERMANY DURING JULY 1973

Appendix C

MAPS OF WET DEPOSITION PATTERNS RESULTING FROM SO_2 EMISSIONS IN THIRTEEN INDIVIDUAL COUNTRIES IN WESTERN AND CENTRAL EUROPE DURING JULY 1973

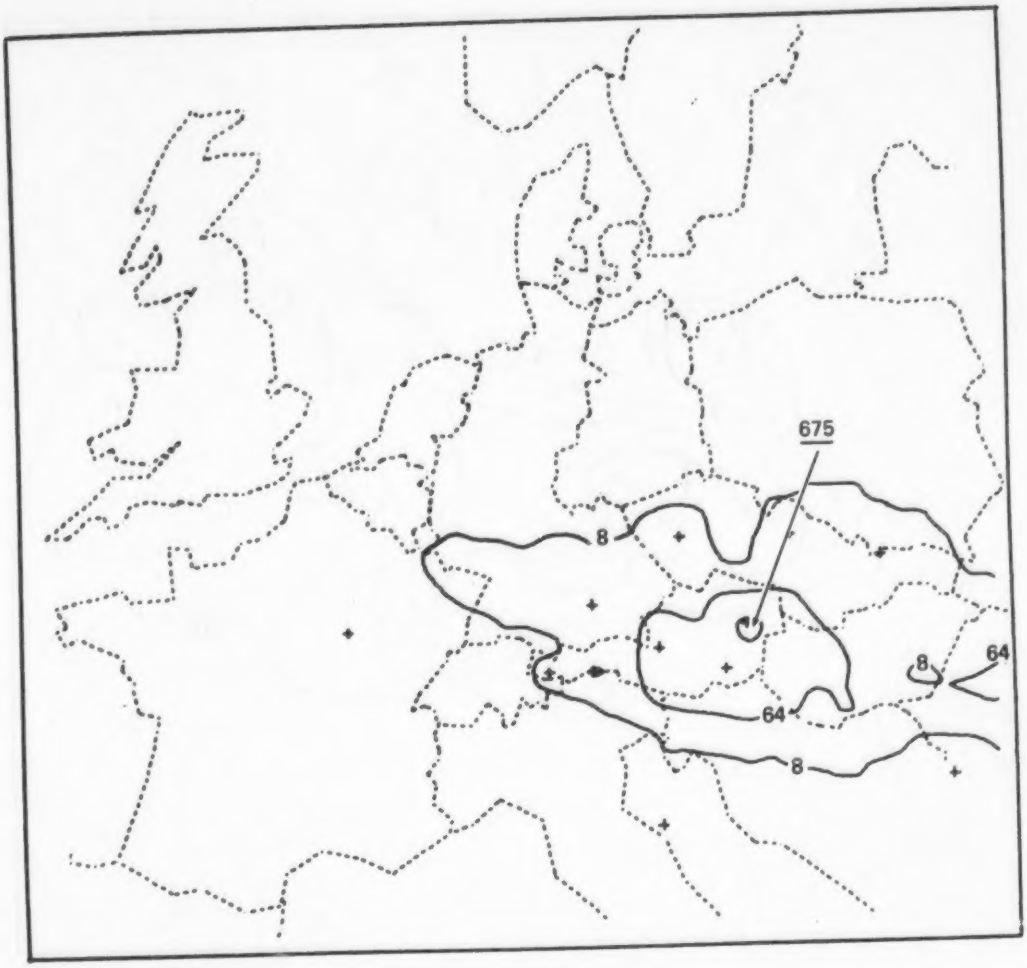

FIGURE C-1 WET DEPOSITION OF SULFUR COMPOUNDS (IN TERMS OF EQUIVALENT WEIGHT OF SO_2, 10^{-3} g m^{-2}) FROM EMISSIONS IN AUSTRIA DURING JULY 1973

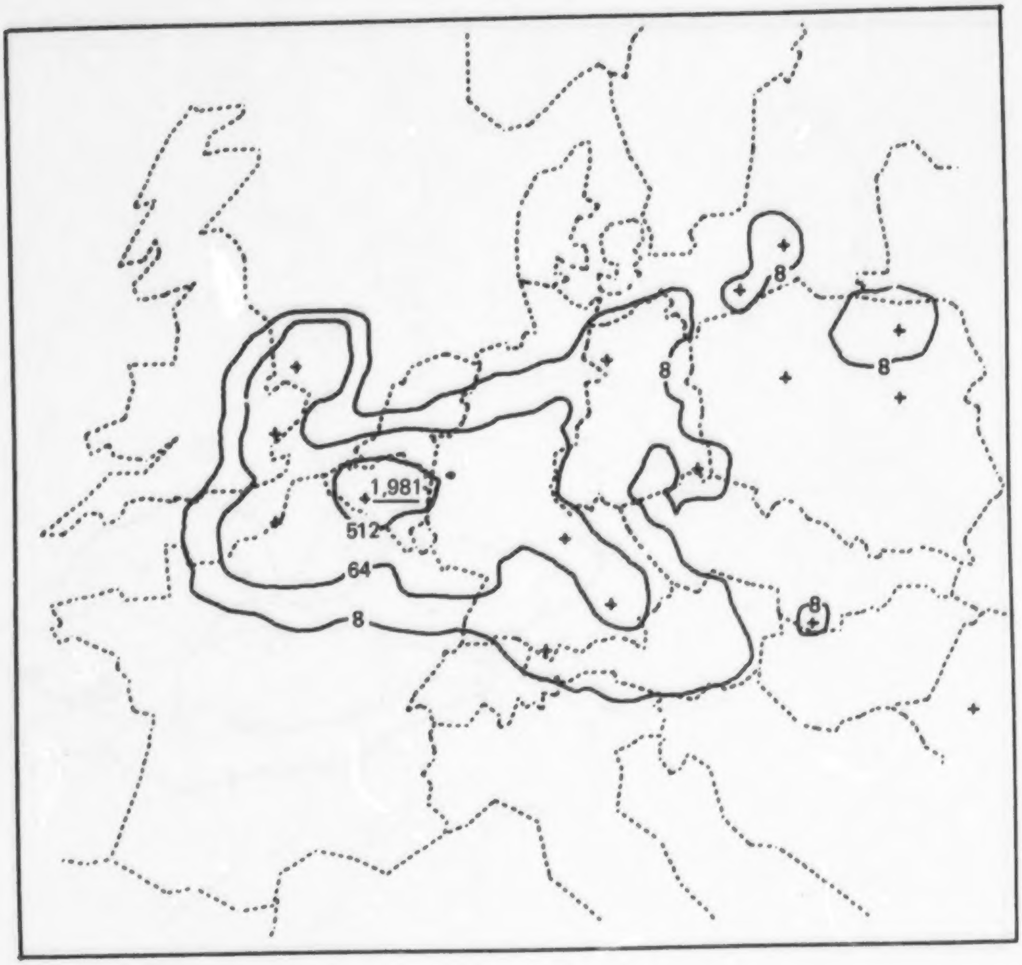
8
8
8
8
1,981
512
64
8
8

FIGURE C-2 WET DEPOSITION OF SULFUR COMPOUNDS (IN TERMS OF EQUIVALENT WEIGHT OF SO_2, 10^{-3} g m^{-2}) FROM EMISSIONS IN BELGIUM DURING JULY 1973

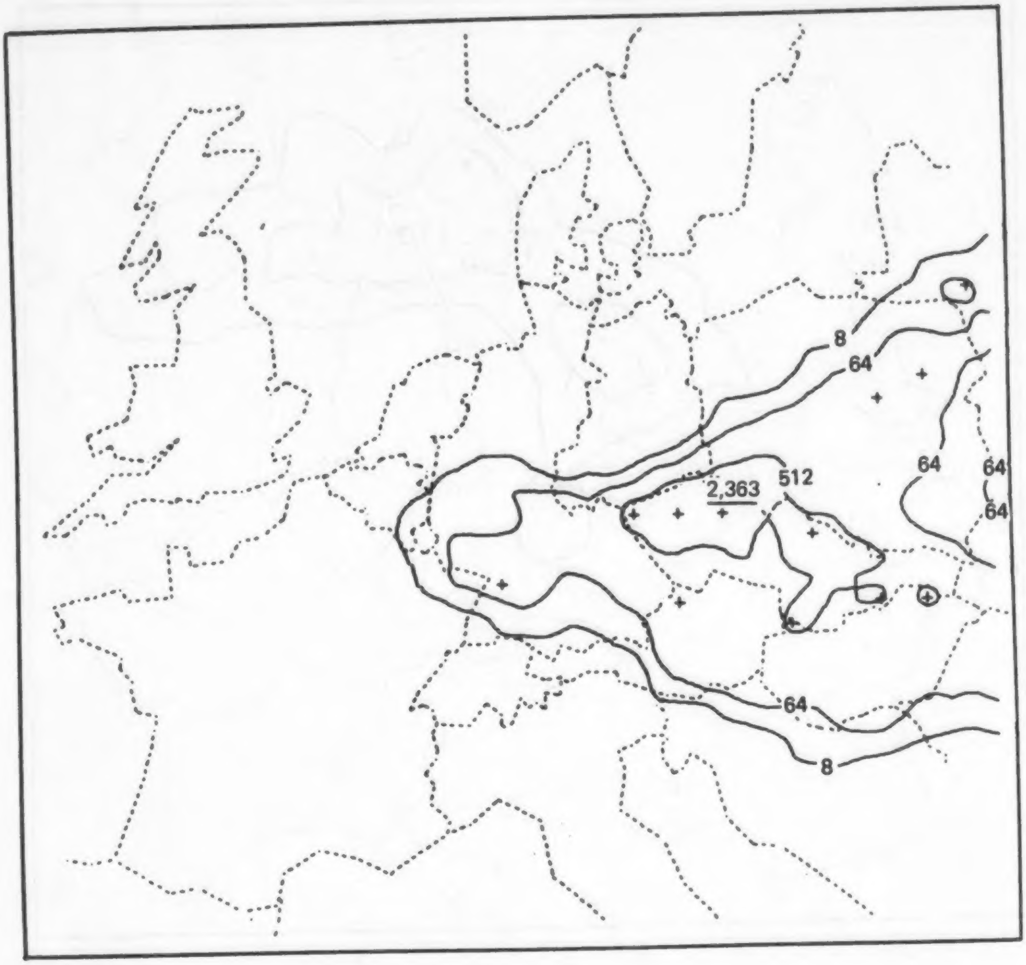
8
64
64
64
64
2,363
512
64
8

FIGURE C-3 WET DEPOSITION OF SULFUR COMPOUNDS (IN TERMS OF EQUIVALENT WEIGHT OF SO_2, 10^{-3} g m^{-2}) FROM EMISSIONS IN CZECHOSLOVAKIA DURING JULY 1973

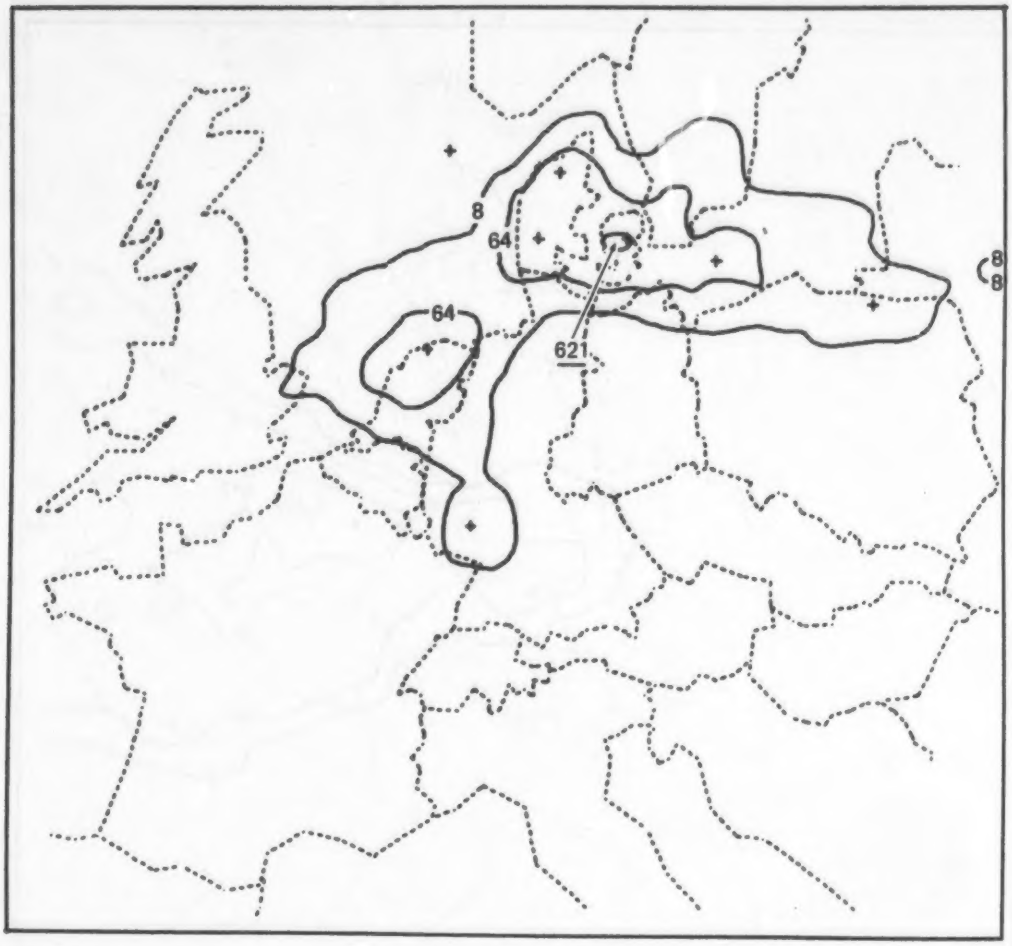

FIGURE C-4 WET DEPOSITION OF SULFUR COMPOUNDS (IN TERMS OF EQUIVALENT WEIGHT OF SO_2, 10^{-3} g m^{-2}) FROM EMISSIONS IN DENMARK DURING JULY 1973

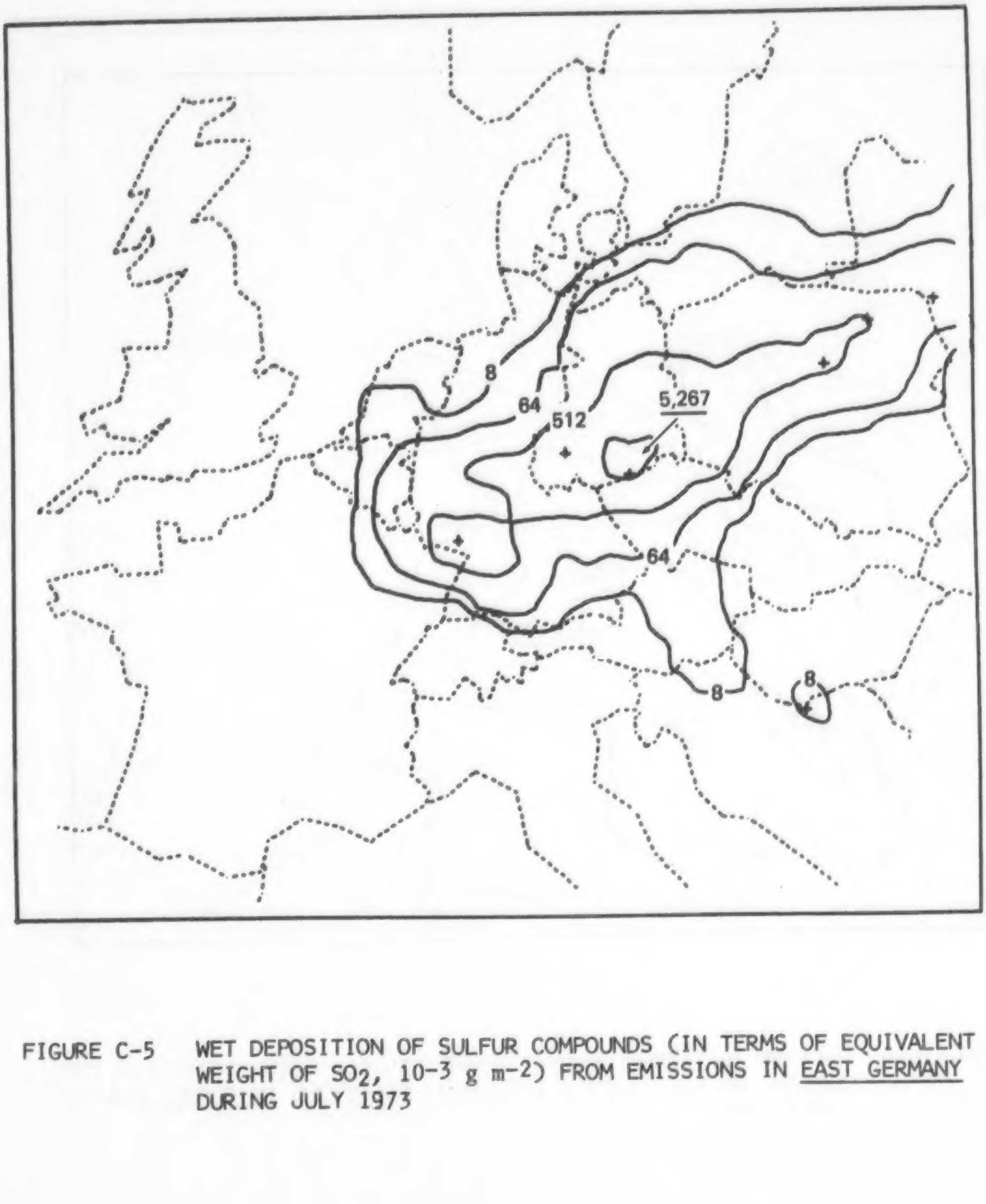
8
64
512
5,267
64
8
8

FIGURE C-5 WET DEPOSITION OF SULFUR COMPOUNDS (IN TERMS OF EQUIVALENT WEIGHT OF SO_2, 10^{-3} g m^{-2}) FROM EMISSIONS IN EAST GERMANY DURING JULY 1973

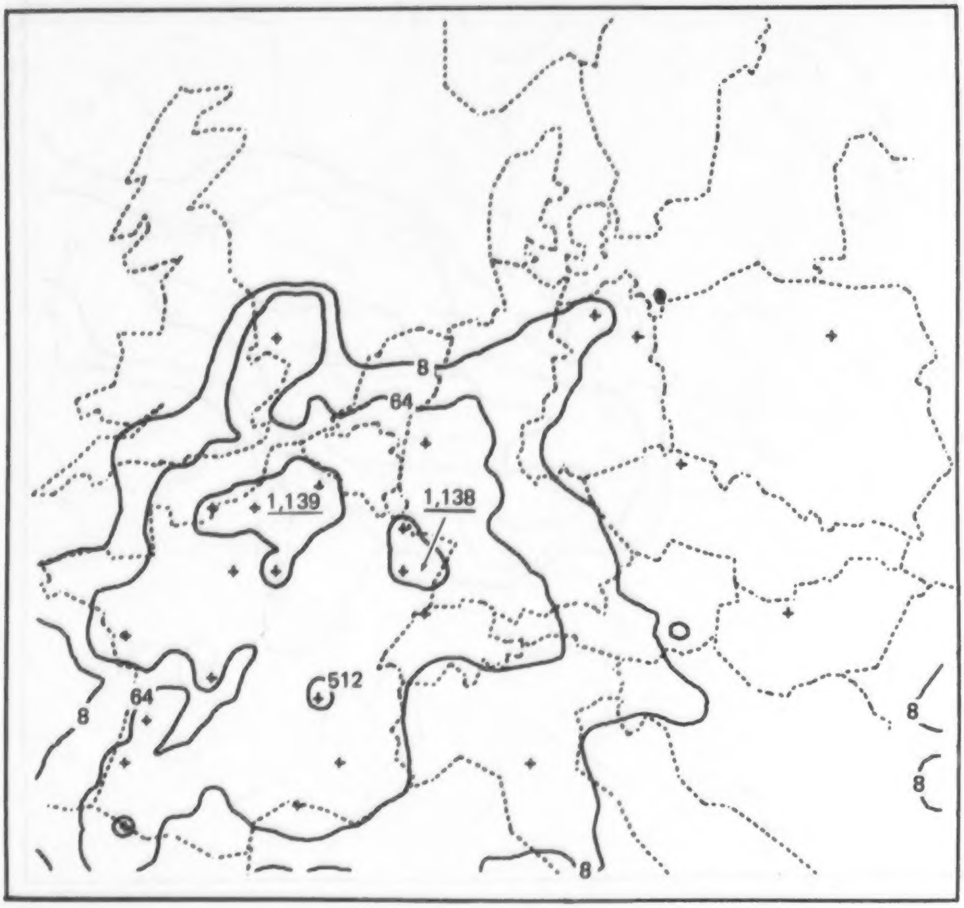
8
64
1,139
1,138
512
64
8
8
8
8

FIGURE C-6 WET DEPOSITION OF SULFUR COMPOUNDS (IN TERMS OF EQUIVALENT WEIGHT OF SO_2, 10^{-3} g m^{-2}) FROM EMISSIONS IN FRANCE DURING JULY 1973

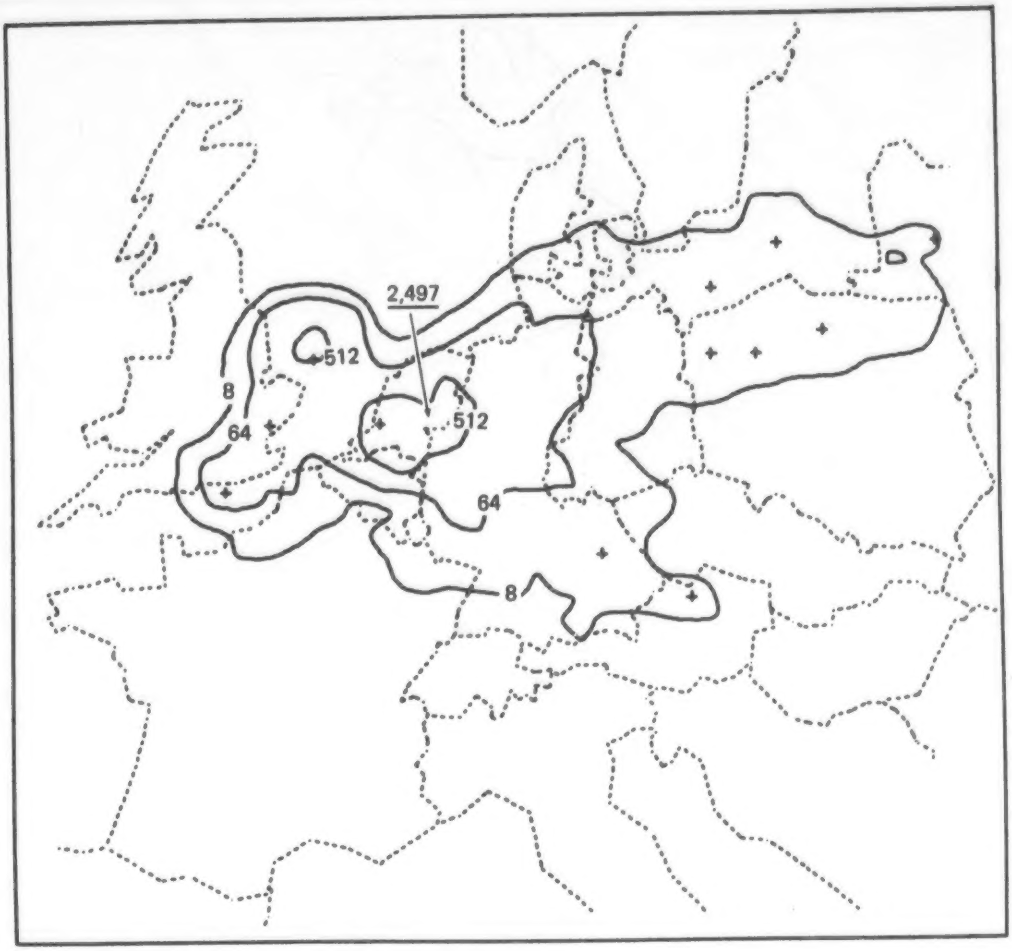
2,497
512
512
8
64
64
8

FIGURE C-7 WET DEPOSITION OF SULFUR COMPOUNDS (IN TERMS OF EQUIVALENT WEIGHT OF SO_2, 10^{-3} g m^{-2}) FROM EMISSIONS IN THE NETHERLANDS DURING JULY 1973

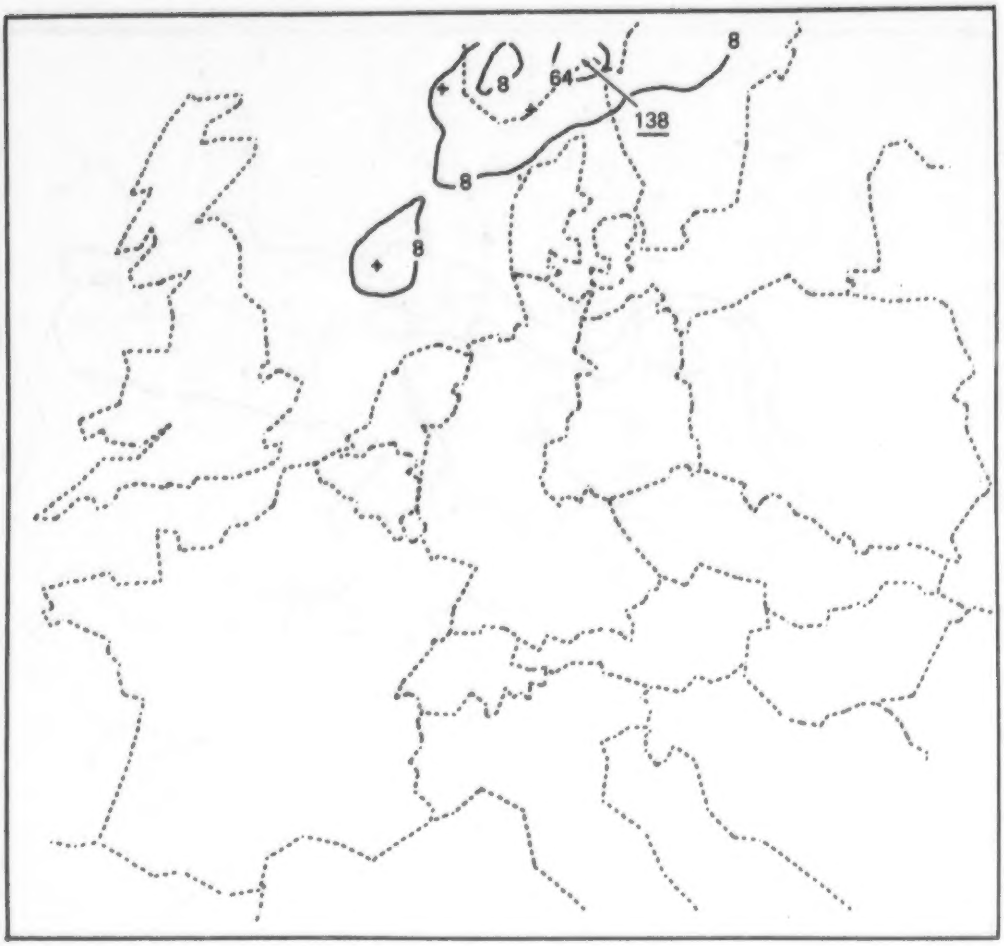

FIGURE C-8 WET DEPOSITION OF SULFUR COMPOUNDS (IN TERMS OF EQUIVALENT WEIGHT OF SO_2, 10-3 g m-2) FROM EMISSIONS IN NORWAY (SOUTH OF 60°N) DURING JULY 1973

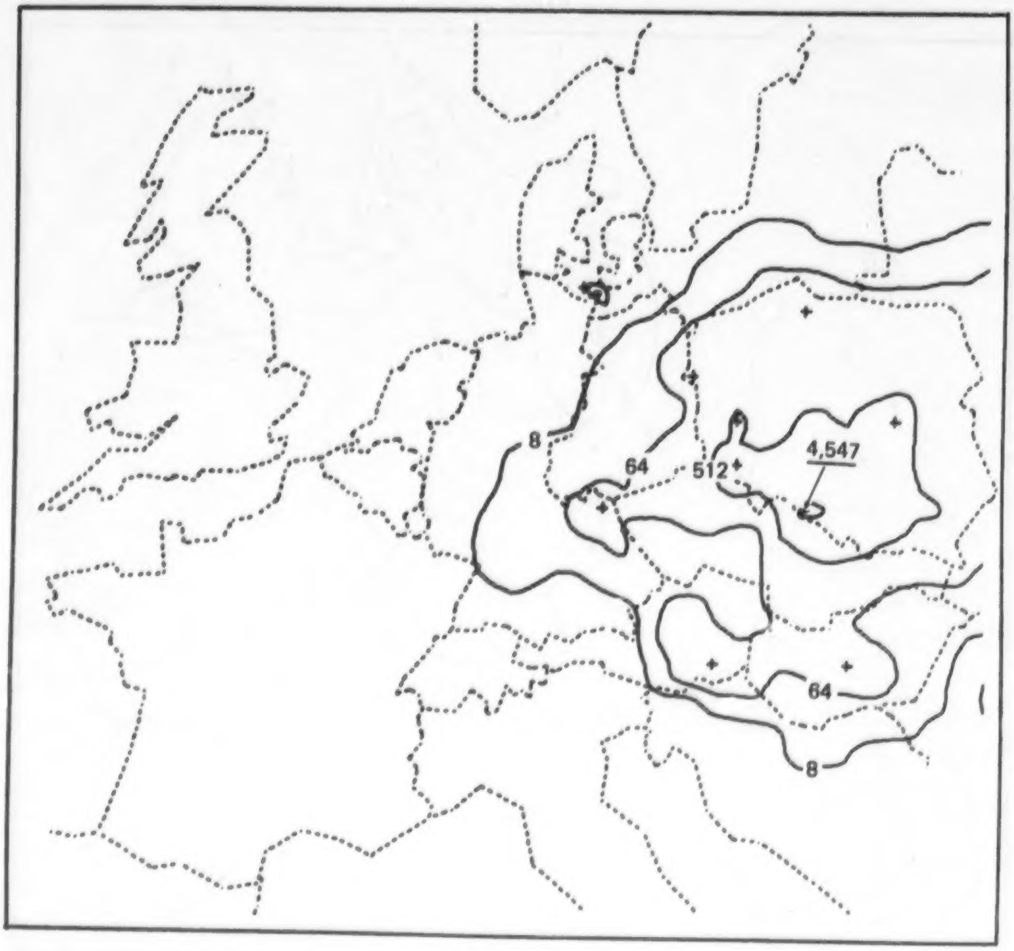
8
64
512
4,547
64
8

FIGURE C-9 WET DEPOSITION OF SULFUR COMPOUNDS (IN TERMS OF EQUIVALENT WEIGHT OF SO_2, 10^{-3} g m^{-2}) FROM EMISSIONS IN POLAND DURING JULY 1973

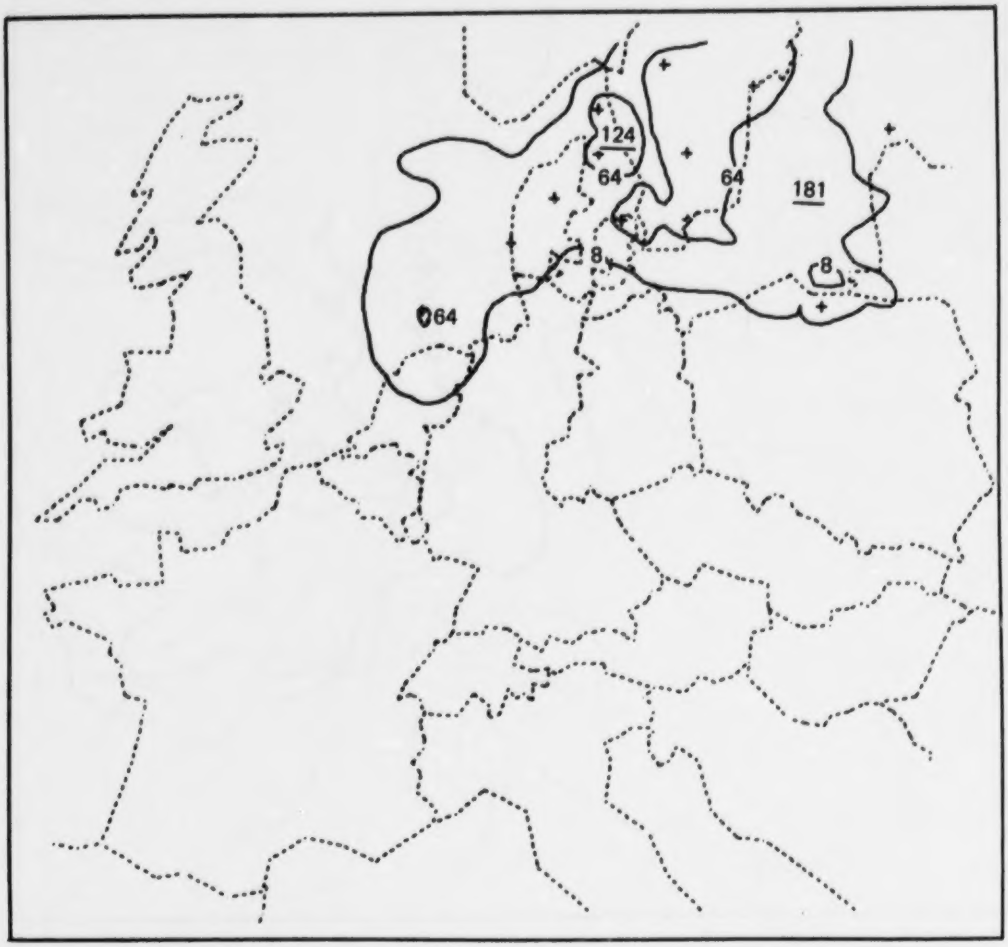
124
64
64
181
8
8
64

FIGURE C-10 WET DEPOSITION OF SULFUR COMPOUNDS (IN TERMS OF EQUIVALENT WEIGHT OF SO_2, 10^{-3} g m^{-2}) FROM EMISSIONS IN SWEDEN (SOUTH OF 60°N) DURING JULY 1973

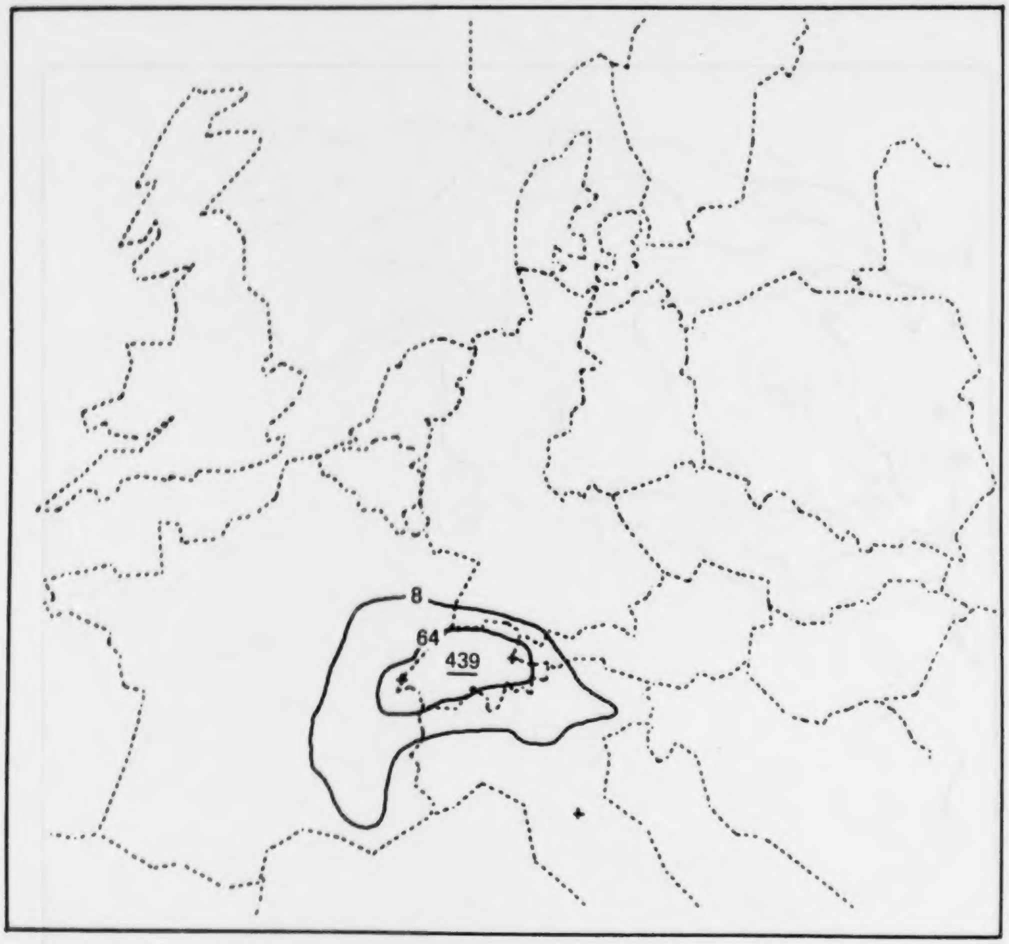

FIGURE C-11 WET DEPOSITION OF SULFUR COMPOUNDS (IN TERMS OF EQUIVALENT WEIGHT OF SO_2, 10^{-3} g m^{-2}) FROM EMISSIONS IN SWITZERLAND DURING JULY 1973

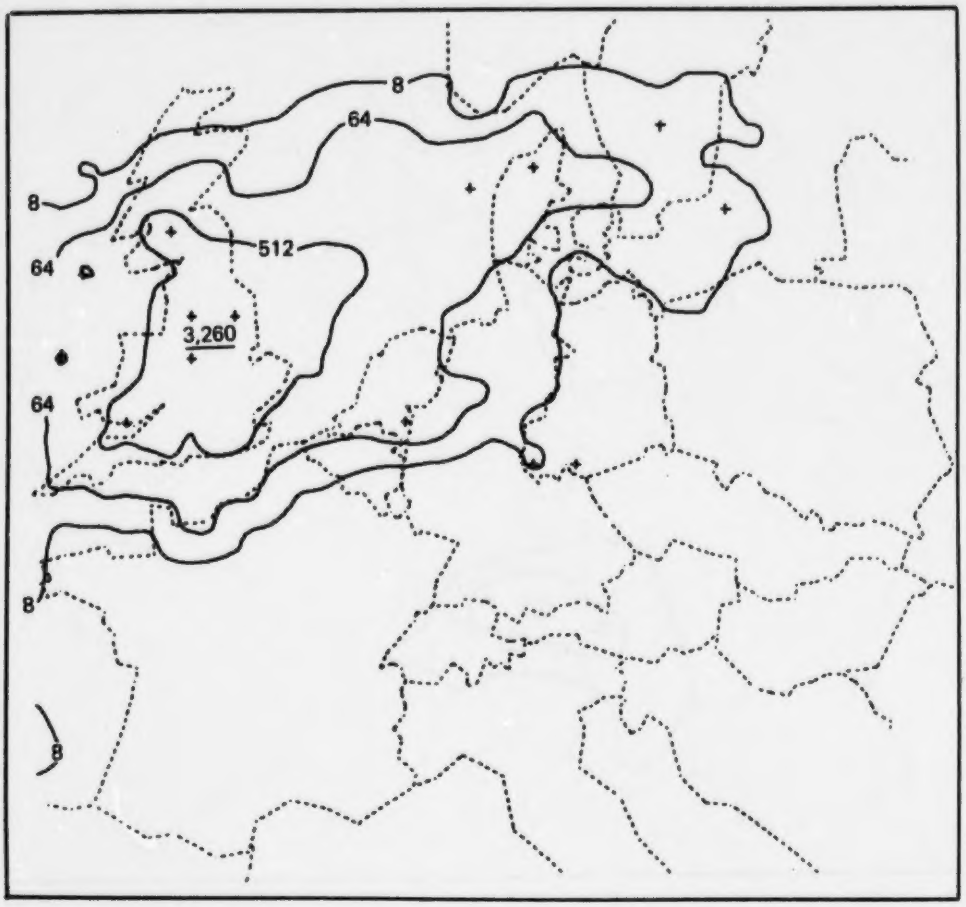
8
64
8
64
512
3,260
64
64
8
8

FIGURE C-12 WET DEPOSITION OF SULFUR COMPOUNDS (IN TERMS OF EQUIVALENT WEIGHT OF SO_2, 10^{-3} g m^{-2}) FROM EMISSIONS IN THE UNITED KINGDOM DURING JULY 1973

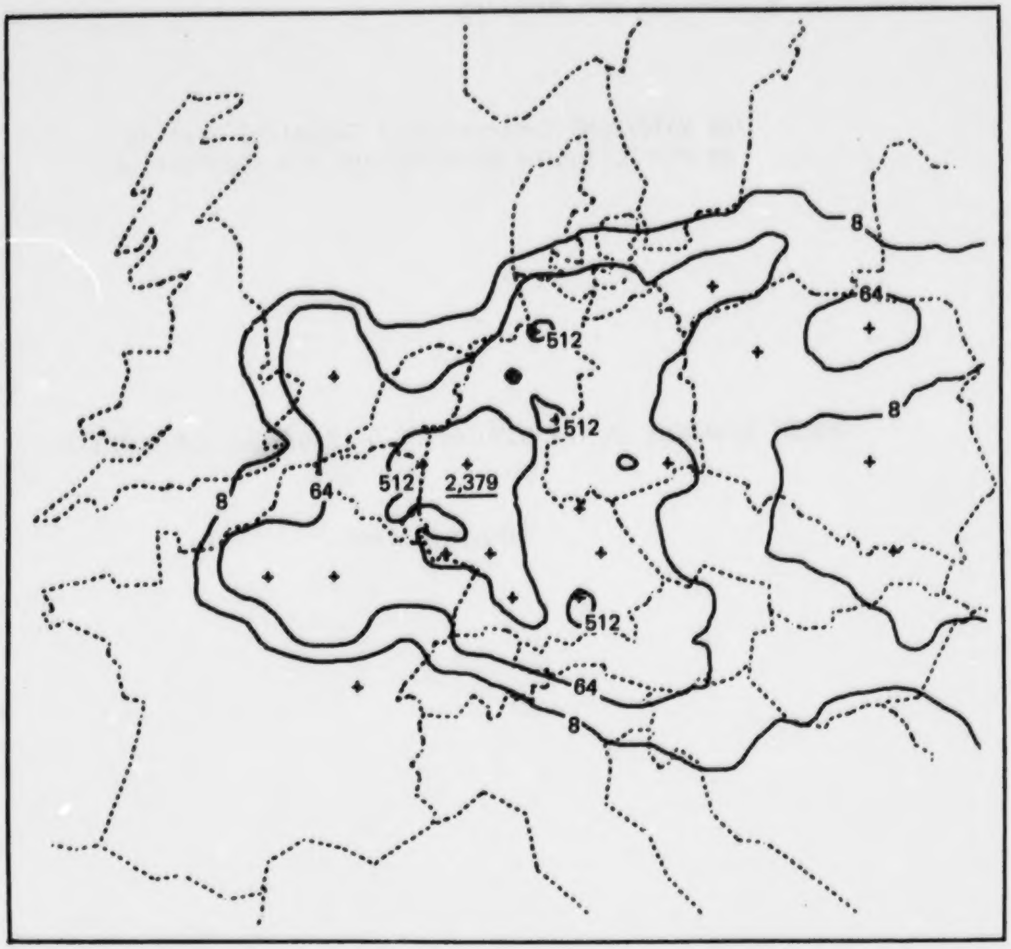
8
64
512
512
8
512
2,379
64
8
512
64
8

FIGURE C-13 WET DEPOSITION OF SULFUR COMPOUNDS (IN TERMS OF EQUIVALENT WEIGHT OF SO_2, 10^{-3} g m^{-2}) FROM EMISSIONS IN WEST GERMANY DURING JULY 1973

NATO/CCMS
Air Pollution Pilot Study
Assessment Methodology and Modeling

7th NATO/CCMS International Technical Meeting
on Air Pollution Modeling and its Application

RECENT ADVANCES IN THE SIMULATION OF REGIONAL AIR QUALITY

Joseph B. Knox

September 7-10, 1976

Airlie, Virginia, U.S.A.

UCRL-78176

RECENT ADVANCES IN THE SIMULATION OF REGIONAL AIR QUALITY*

Joseph B. Knox

Atmospheric and Geophysical Sciences Division
Physics Department
Lawrence Livermore Laboratory, University of California
Livermore, California 94550

August 1976

ABSTRACT

For the past several years the ERDA, NSF, and more recently the EPA has sponsored research at LLL for development, validation, and application of regional air quality models for passive and reactive pollutants emitted from distributed sources or multiple point sources. Although the motivation of the research is agency dependent, the basic capability required is a rational framework of relating distributed and complex sources to the temporal spatial pollutant distributions that evolve through transport-diffusion, chemical transformation, and deposition (or surface absorption) in regions of about 10^4 km^2 including effects of complex terrain.

Models developed to date that are subject to on-going validation include the following:

1. A two dimensional (MACAW) and a three dimensional (MATHEW) mass-consistent atmospheric flux and wind field models, respectively, have been developed to provide air pollution models with dynamically consistent input data. Using observed inversion height and wind field information, these diagnostic models use techniques of variational calculus to adjust observed

---

*The work was performed under the auspices of the U. S. Energy Research and Development Administration under contract No. W-7405-Eng-48.

fluxes or windfields so that they satisfy the continuity equation and appropriate boundary conditions associated with complex terrain and inversion configuration. The models simulate conditions wherein the inversion is below major topographic features with the result that the horizontal flow fields are molded around obstacles.

2. A hybrid Lagrangian-Eulerian atmospheric transport-diffusion code has been developed for calculating the three dimensional pollutant distribution for transient regional flows. This model (ADPIC) has been validated against both closed-form analytic solutions and several full scale regional tracer experiments performed at ERDA sites.

3. An operational regional photochemical-pollutant simulation model (LIRAQ-2) has been developed for the San Francisco Bay Area that treats the evolution of 15 active chemical species on a 20 by 20 grid with variable grid size of 1, 2, or 5 kilometers on a side. A brief synopsis of the model formulation, submodel structure, and validation results is provided.

Current development efforts:

1. The LIRAQ-2 model is being extended to St. Louis with the inclusion of simple sulfur chemistry and is to be tested against air quality measurements acquired by the EPA-RAPS.

2. A three dimensional coupled transport-kinetic model is being developed for isolated strong point-sources of hydrocarbons, NO_x, and SO_2 that play an important role in the generation of significant concentrations of oxidant in non-urban areas, and also on the air quality in downwind urban areas.

1. Introduction

It is the intent of this paper to summarize recent advances in the simulation of regional air quality or pollutant distributions. We focus on the development, validation, and application of regional models for both passive and reactive pollutants emitted from distributed sources and/or multiple point sources. The emerging capability is a rational framework for relating distributed-complex emissions to temporal-spatial pollutant distributions evolving from transport-diffusion, chemical transformation, and deposition in regions of up to 10^4 km^2 including effects of complex terrain. Models developed during the past several years that are and have been subject to an on-going validation program include (a) regional mass-consistent wind field modeling (MATHEW), (b) a 3-dimensional Lagrangian-Eulerian transport-diffusion model (ADPIC), and (c) an operational regional passive or photochemical-pollutant simulation model (LIRAQ) for the San Francisco Bay Area. Select research-application highlights are presented herein; the bibliography cites full references on model structure, validation, and code documentation (for LIRAQ only).

2. MATHEW

The MATHEW model provides a three dimensional, time-averaged wind field suitable for calculating the regional advective-transport of pollutants including the effects of complex terrain.[1] The model is diagnostic in nature and is based on the variational method of objective analysis which adjusts observations of the horizontal wind to the grid of an air quality model so that the adjusted wind field satisfies the equation of continuity. The techniques use the Euler-Lagrange equations for the velocity potential and the equation of continuity such that the best least squares fit (to the observations) is achieved and the adjusted field is non-divergent. In addition, the adjusted wind field satisfies the variable lower boundary condition prescribed by terrain; lateral and upper boundary conditions are open and are satisfied by the velocity potential equal zero. In operation, MATHEW is an advanced interpolation scheme for providing estimates of the three dimensional wind vector; most important the interpolation scheme includes the influence of topography in shaping the terrain controlled flow. At the same time, the MATHEW adjusted wind field is mass consistent so that concentration predictions driven by input from MATHEW are not flawed by inconsistent data. With the current implementation of this model adjusted three dimensional winds can be obtained on a grid of 30 to 40,000 grid points in a few minutes of CDC 7600 time with the residual divergence being of the order of 10^{-10} $\sec^{-1}$. Initial interpolation of wind fields to grid points gives residual divergences of seven orders of magnitude higher which are clearly not suitable for air quality calculations involving grid type models. It is our experience that the mean wind field input to regional grid air quality models must be mass consistent to the extent provided by MATHEW in order for regional transport to be appropriately calculated. Illustrations of this capability are contained in Figure 1, (showing the surface wind observations on the lower Hudson near Indian Point as obtained by Prof. Davidson[2]); Figure 2 showing the interpolated horizontal wind field at 1200 EST at a height of 90m above reference level; Figure 3, showing the adjusted mass consistent horizontal winds at 90m above reference level.[3]

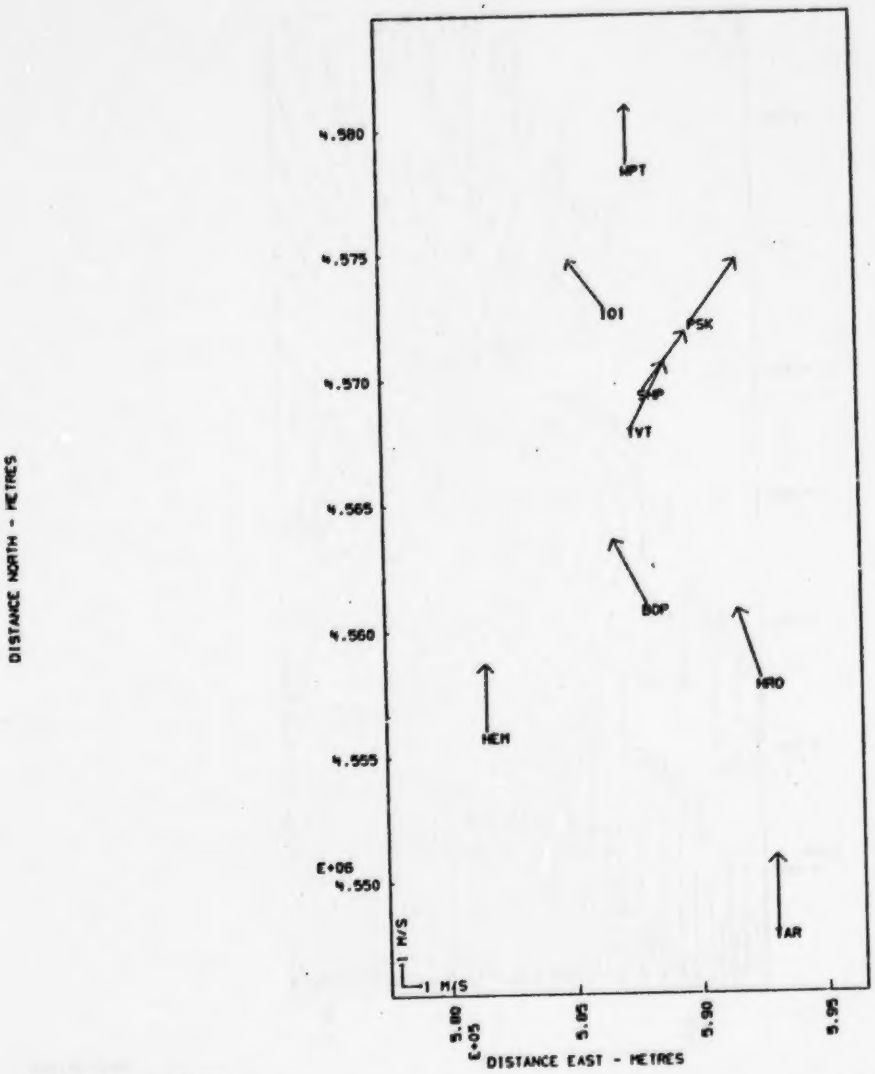

ADJUSTED TO 50. METRES
ABOVE TOPOGRAPHY USING
POWER LAW EXPONENT OF 0.12

GRID ORIGIN
X: 577500. UTM
Y: 4545500. UTM
Z: 45. MASL

Wind Measurement at 1200 EST

FIGURE 1.

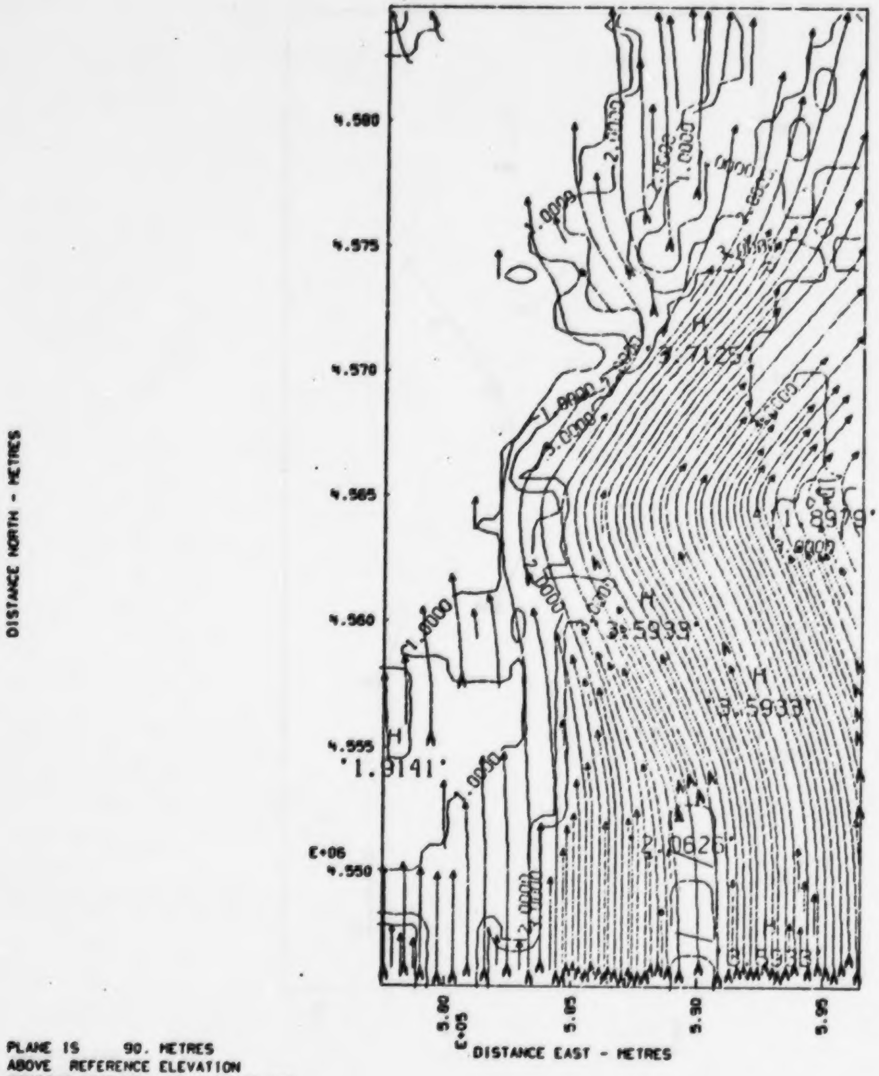

PLANE IS 90. METRES
ABOVE REFERENCE ELEVATION
CONTOUR INTERVAL IS 1.0E+00 M/S
SCALE IS 1.0E+00 M/S

GRID ORIGIN
X: 577500. UTM
Y: 4545500. UTM
Z: 45. MASL

Interpolated Horizontal Winds at 1200 EST

FIGURE 2.

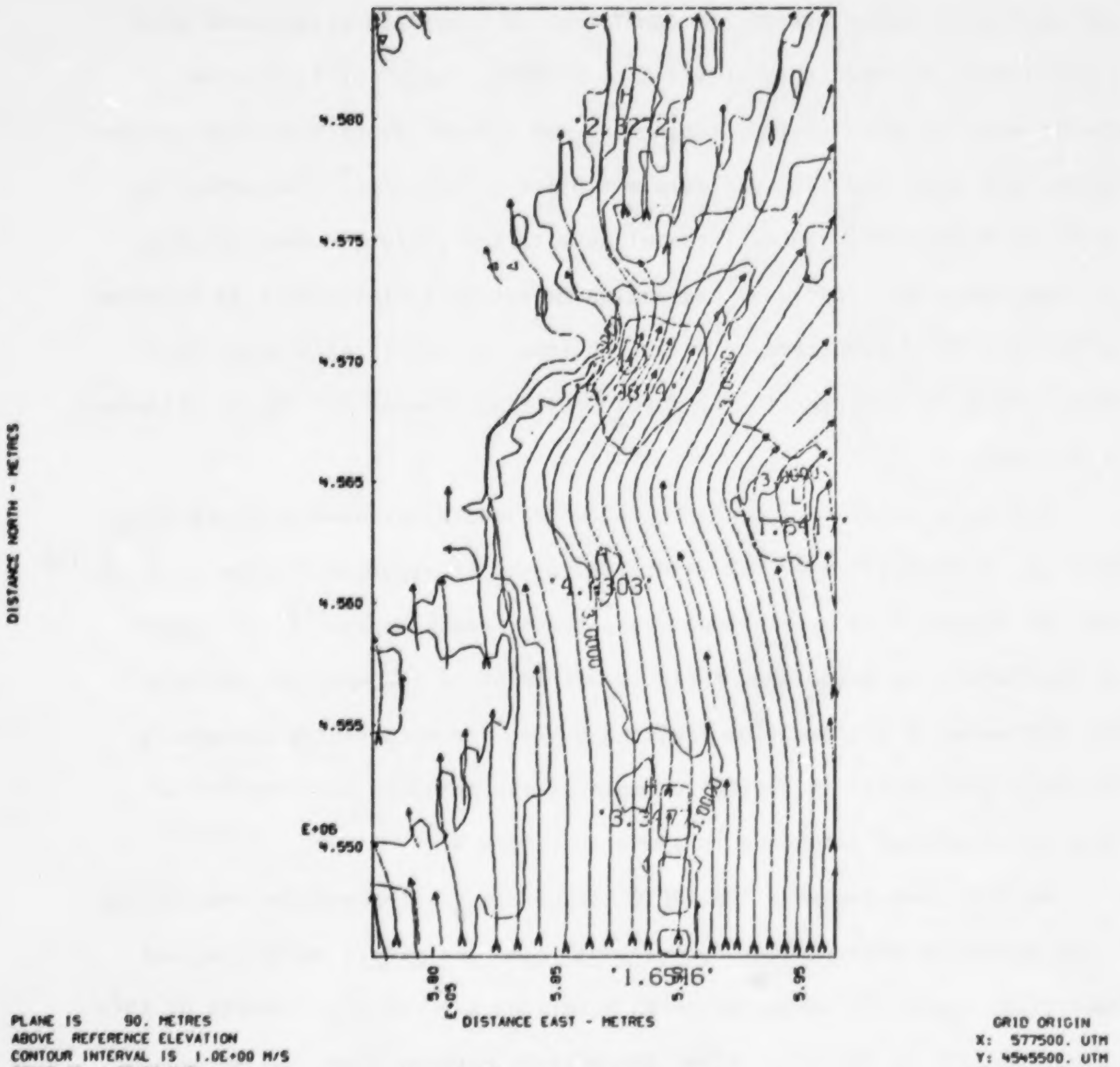

Adjusted Horizontal Winds
at 1200 EST
FIGURE 3.

3. ADPIC (Atmospheric Diffusion Particle-in-Cell)

ADPIC is a numerical, three-dimensional, Cartesian, particle diffusion code[4,5] for calculating the time-dependent (regional) distribution of air pollutants under prescribed conditions of speed and directional wind shear (input to ADPIC grid provided by MATHEW); "calm" or light wind conditions, variable surface roughness, wet and dry deposition, radioactive decay, and space and time variable diffusion parameters.* The method is based on the particle-in-cell technique with the pollutant concentration represented statistically by Lagrangian marker-particles within an Eulerian grid. The chief advantage of this technique is that it eliminates fictitious diffusion inherent in the purely Eulerian schemes (or finite difference solutions).

Extensive verification of the ADPIC framework has been achieved using both (a) closed-form analytic solutions to the transport-diffusion equation,[4] and (b) several full or regional-scale tracer experiments.[6] In regard to the former, we found that ADPIC is within 5% of the analytic solution for diffusion in uniform flow fields and also for wind fields containing vertical wind shear. A typical example of the analytic verification of this calculational technique is shown in Figure 4.

We have also compared the ADPIC calculations with Gaussian results for plume depletion factors over agricultural land for simple meteorological conditions (under which the Gaussian solutions are valid). Results of this comparison are in Table 1. Other comparisons between these two methods of estimating air concentrations and ground deposition have been similar to those shown here when the meteorological input data were simple, i.e., single point measurements of wind direction and speed.

---

*Emission sources may be either single or multiple point sources of either a continuous or instantaneous nature.

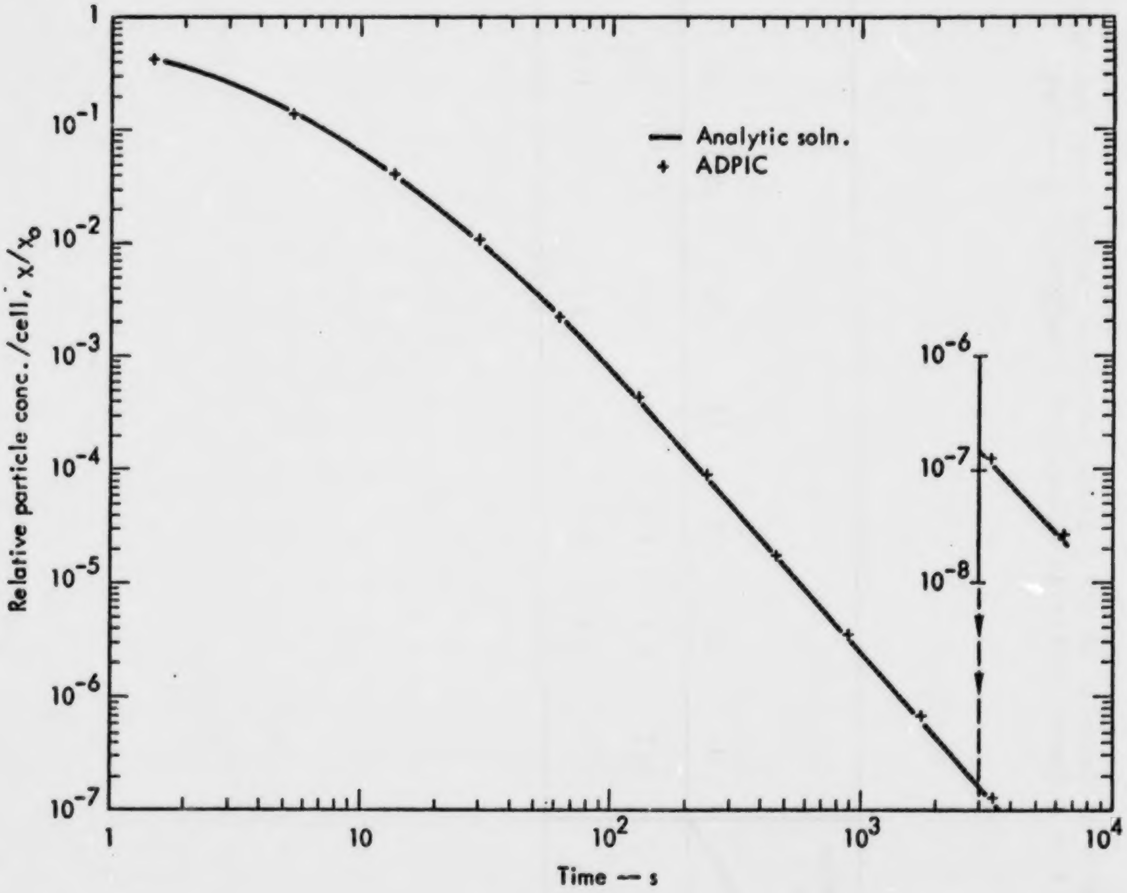

Relative cloud center concentrations, puff diffusion in simple shear flow.

FIGURE 4.

TABLE 1. Ratio of Gaussian to ADPIC plume depletion factors over agricultural land for 0.3 μm diameter particles released at a height of 10 metres.

Stability Category \ Distance km	1	2	5	10	15	20	25	30	35
F	1.1	1.1	1.1	1.0	1.0	1.0	1.0	.92	.94
B	1.1	1.1	1.1	1.1	1.1	1.1	1.1	1.1	1.1

The MATHEW/ADPIC computer codes have been verified against several regional field tracer studies.[7] These studies included Methyl-Iodine tracer studies at the Idaho National Engineering Laboratory (INEL), Idaho Falls, Idaho and ^{41}Ar plumes at Savannah River Plant (SRP), South Carolina. The agreement between measurements (made in two and three dimensions) and calculations have been remarkably consistent; 60 percent of the time calculated concentrations are within a factor of two. In these studies measurements were taken at distances of 4 to 80 km from the source and included high volume surface samplers for the Methyl-Iodine and surface and airborne measurements of gamma energy from ^{41}Ar. Recently we conducted another series of ^{41}Ar tracer experiments coinciding with simultaneous releases of SF_6 at SRP in conjunction with the Savannah River Laboratory (SRL) personnel. Although a detailed comparison of measurements and calculations has not been completed, preliminary results indicate that the MATHEW-ADPIC computer codes were able to successfully calculate concentrations during a 180 degree shift in wind direction for a SF_6 plume released for a period of four hours and then shut off.

The utility of ADPIC for calculating regional temporal-spatial pollutant distributions is illustrated for the Indian Point operating releases during a typical fall day with diurnally-reversing boundary layer flows (Figures 5 to 12). These figures show the projection of the marker-particles for selected times onto the horizontal plane, with the Hudson River in background display, during the diurnal cycles.[3]

In this example, ADPIC modeled the transport and diffusion of the total pollutant plume by generating ∿90,000 tracer particles for the typical 24 hour period of which a maximum of 20,000 resided simultaneously within the

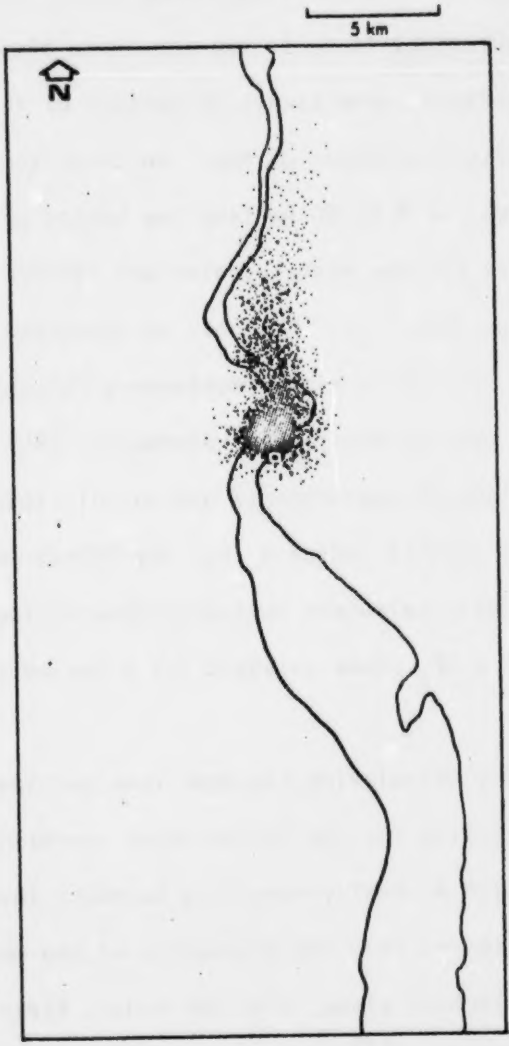

FIGURE 5. ADPIC Particle Distribution, Hudson River Valley, 2000 EST.

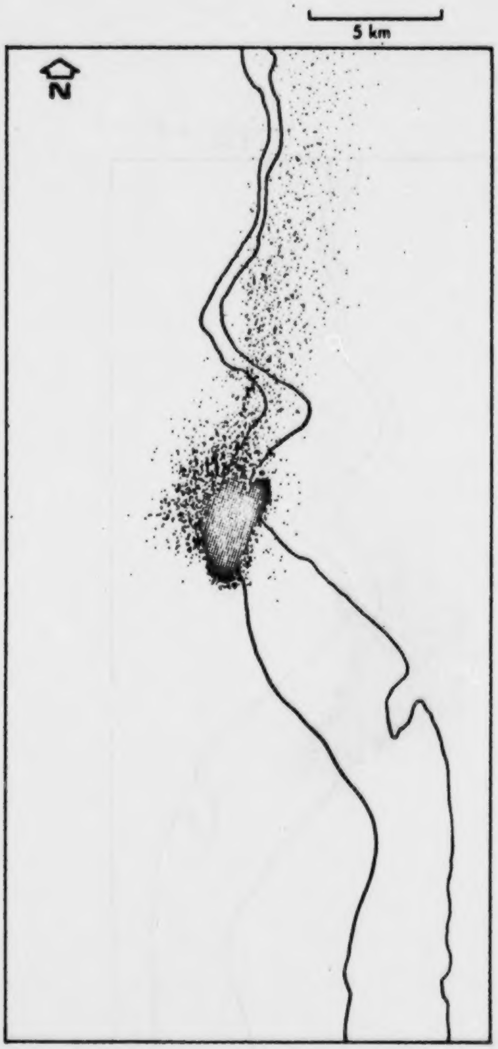

FIGURE 6. ADPIC particle distribution, Hudson River Valley, 2200 EST.

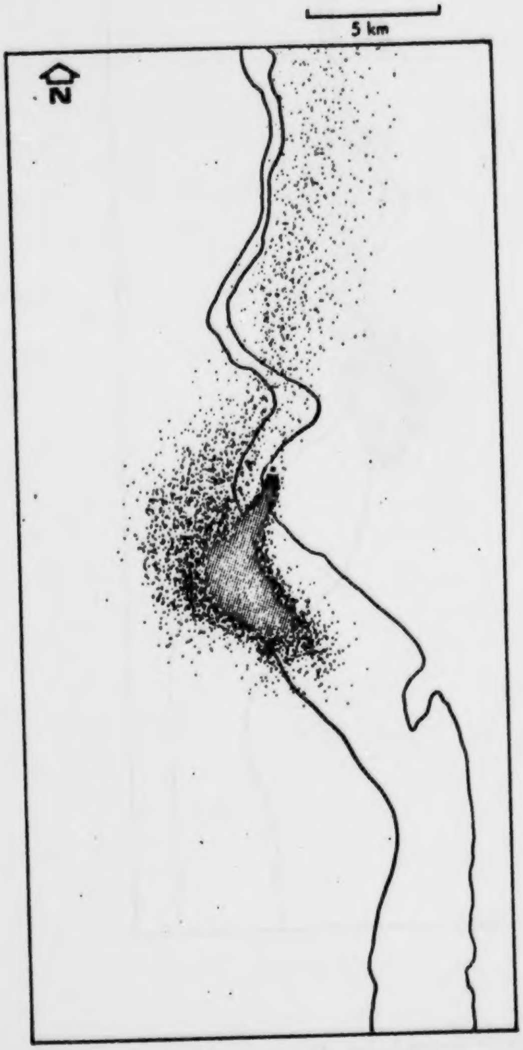

FIGURE 7. ADPIC particle distribution, Hudson River Valley, 2300 EST.

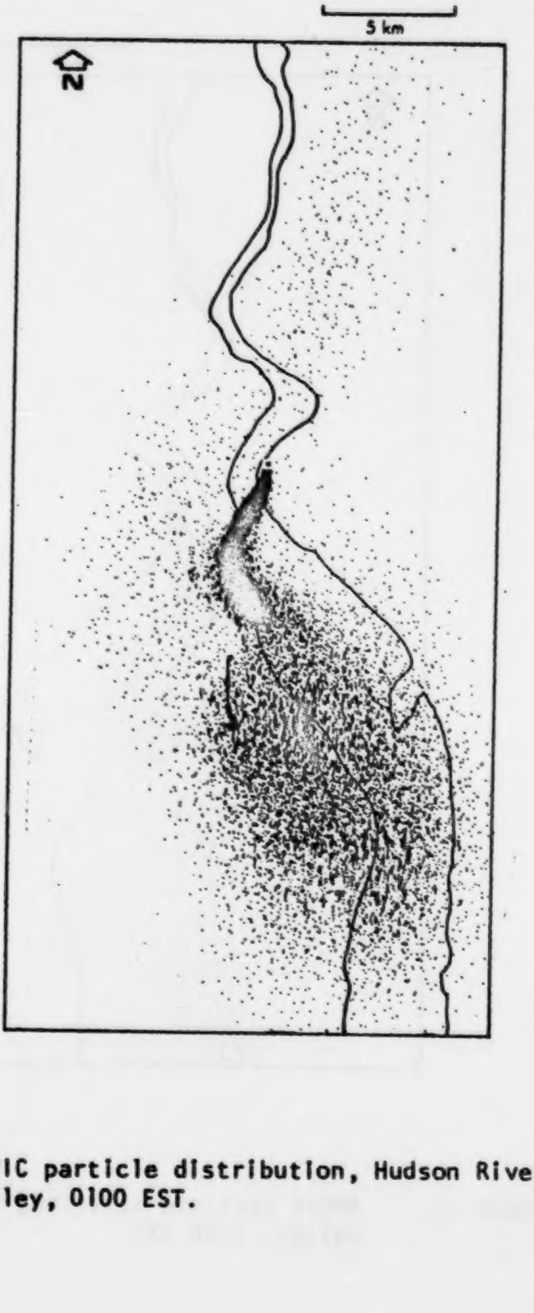

FIGURE 8. ADPIC particle distribution, Hudson River Valley, 0100 EST.

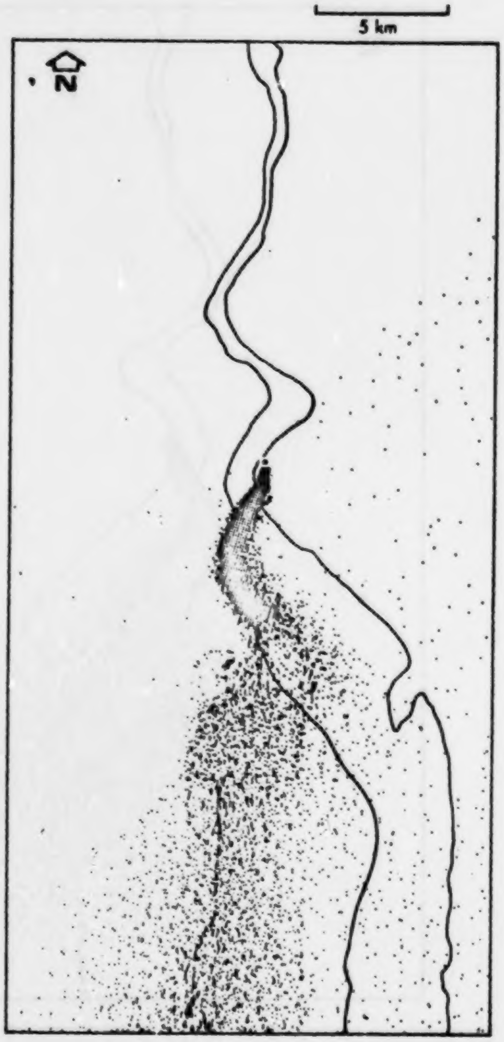

FIGURE 9. ADPIC particle distribution, Hudson River Valley, 0700 EST.

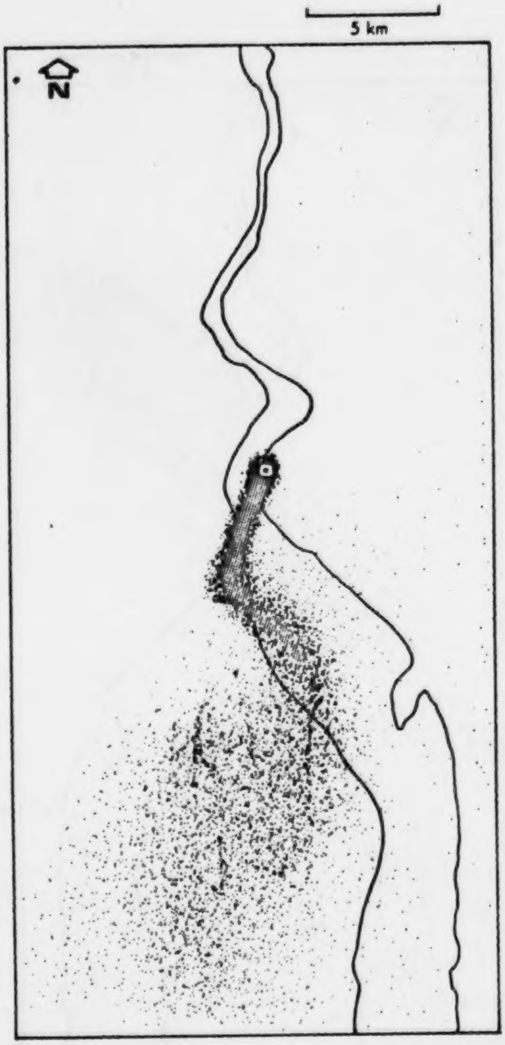

FIGURE 10. ADPIC particle distribution, Hudson River Valley, 1100 EST.

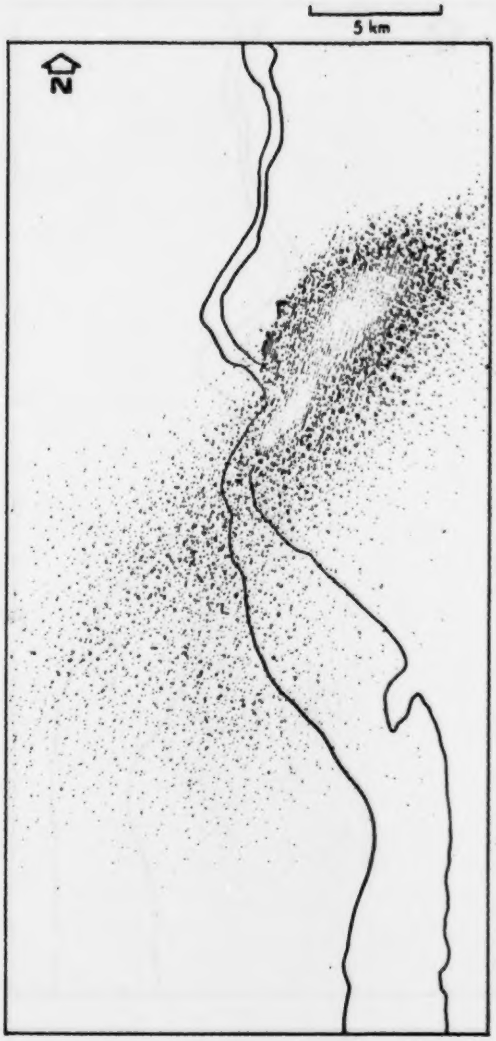

FIGURE 11. ADPIC particle distribution, Hudson River Valley, 1200 EST.

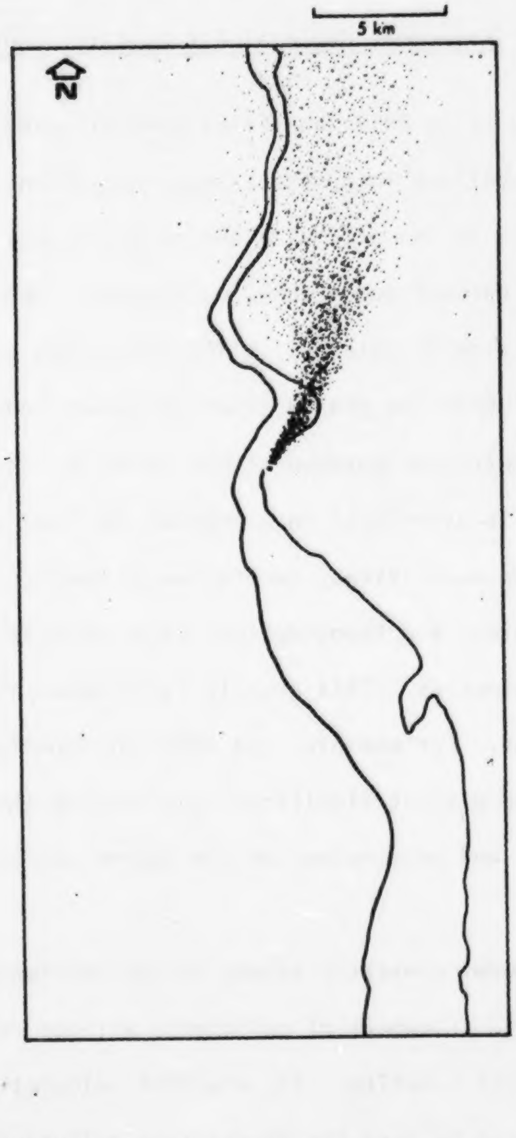

FIGURE 12. ADPIC particle distribution, Hudson River Valley, 1700 EST.

grid, the rest being either deposited, radioactively decayed, or carried out of the grid by transport-diffusion. Concurrently, the particle-in-cell approach of ADPIC allowed separate treatment of radioactive decay and deposition of the individual isotope species.

4. LIRAQ (Livermore Regional Air Quality) Model

LIRAQ is an Eulerian (fixed spatial grid) multicell regional air-quality model the incorporates mass-consistent advection, eddy diffusion appropriate to the grid size, and photochemical kinetics. Using as input data the regional topography, meteorology, and pollutant source inventory for the region of interest, LIRAQ calculates the time and spatial distributions of both the ground-level pollutant concentrations as well as the mean concentration between ground level and the base of the inversion layer. The model is structured in a modular fashion, with a module (submodel) for each of the major steps, generation of mass-consistent wind fields from meteorological and topographical data, such as pollutant transport, and chemical kinetics. This greatly facilitates the model adaptation to new regions. For example, the chemical kinetics submodel can be revised or expanded without significantly affecting the transport submodel, or the topography and meteorology of one region can be readily replaced by those of another.

The model presently exists in two versions. LIRAQ-1 is designed to focus on the transport of pollutants without representing extremely detailed photochemical kinetics. Its explicit calculational technique for physical transport can be used for nonreactive pollutants (such as CO) or can be coupled to relatively simple, nonstiff reaction sets for reactive pollutants.

LIRAQ-2 has been designed to treat rather complex chemical reation sets (15 active species and 50 reactions) in detail. It uses a modified Gear package to solve the large sets of coupled ordinary differential equations with a high-order, implicit method,[8,9] and thus, is able to handle very stiff reaction sets.

These two air quality models were developed to provide the co-investigating agency, the BAAPCD, an operational regional photochemical-pollutant simulation model oriented toward land-use planning, such as the determination of the impact on air quality of new towns, shopping centers, regional population growth patterns, short-term control strategies, and other developments and regulations of similar scale.

The Eulerian multicell grid as applied to the San Francisco Bay Area is shown in Figure 13 with two different spatial resolutions (1 km and 5 km). Calculations of the full region at 1 km resolution is not feasible at this time for detailed chemistry on the CDC 7600 without exceeding high speed memory.

The "raw data" processed by the LIRAQ submodels for subsequent input to the main program are listed in Table 2.

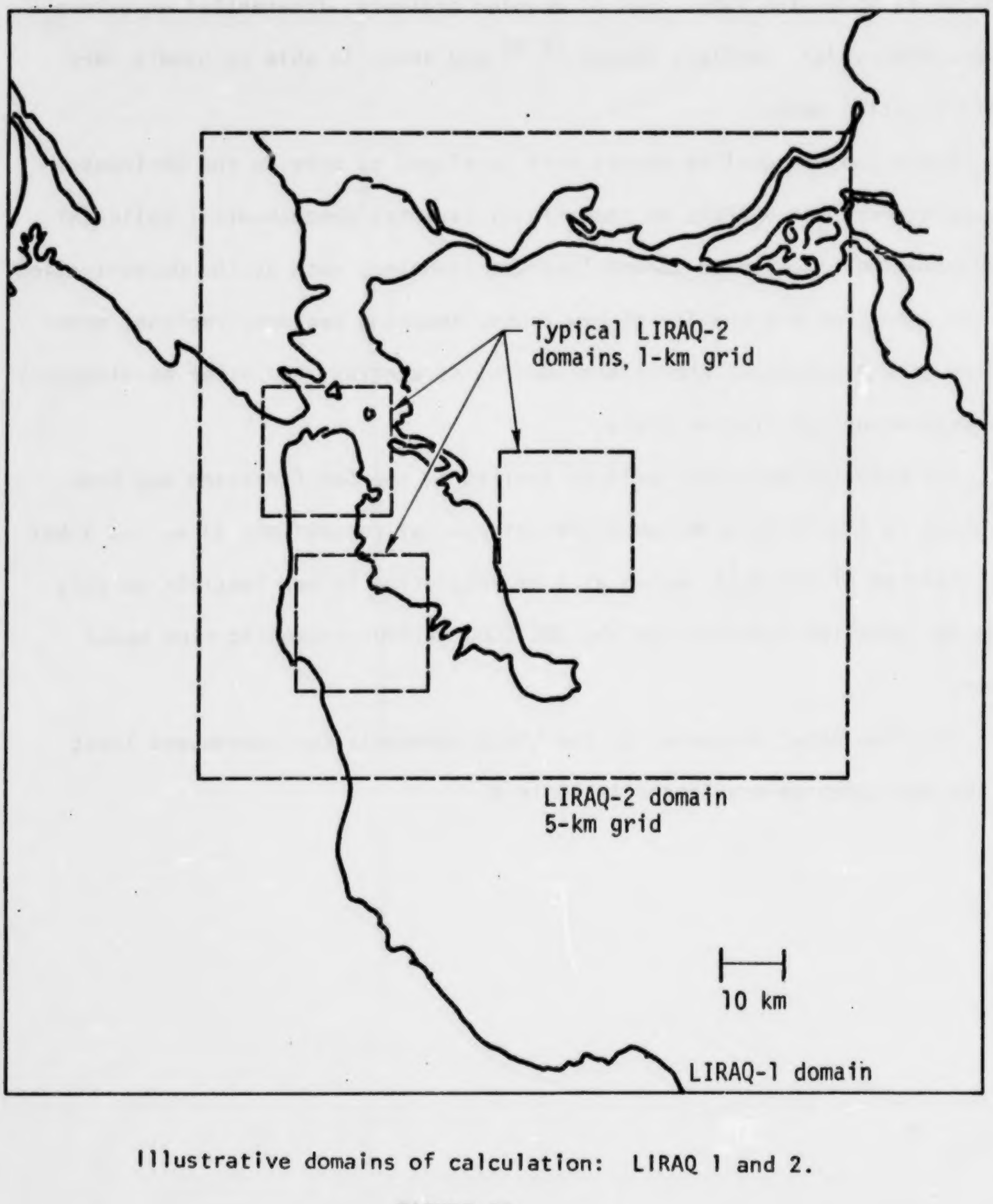
Typical LIRAQ-2
domains, 1-km grid
LIRAQ-2 domain
5-km grid
10 km
LIRAQ-1 domain

Illustrative domains of calculation: LIRAQ 1 and 2.

FIGURE 13.

TABLE 2. LIRAQ Data Bases.

Geographic and topographic features of the region of interest.

Observations of species concentrations.

Meteorological observations, e.g.,

- Wind fields for transport.
- Inversion heights.
- Surface transport.
- Water-vapor and temperature fields.
- Cloud cover which will affect photodissociations rates.

Source inventories, which consist of:

- Mobile, hourly.
- Population, by census, daily.
- Point, by grid square.
- Airport, time-independent.

The pre-processing submodels and the main-code structure, including the Executive Routines are shown in Figures 14 and 15.

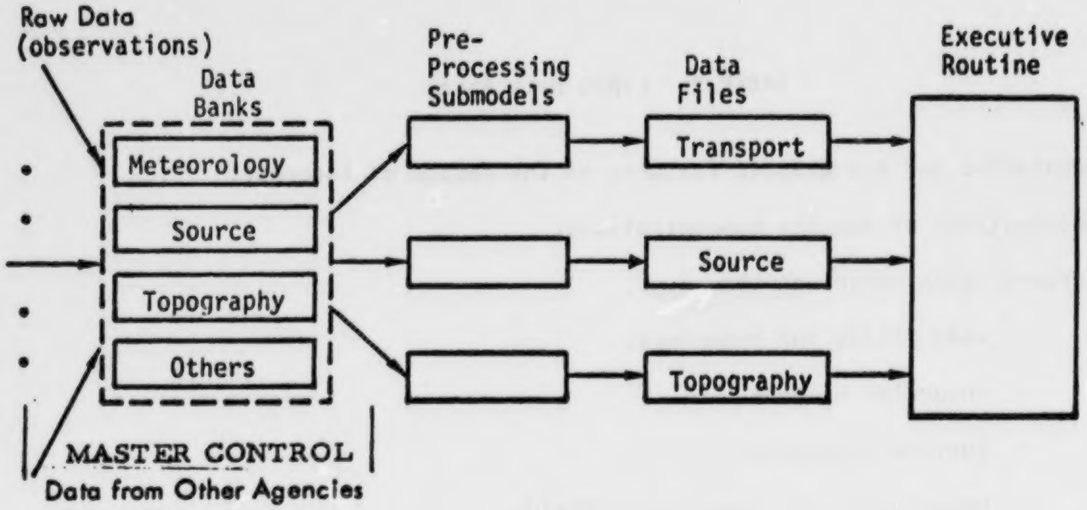
Raw Data
(observations)
Data
Banks
Meteorology
Source
Topography
Others
MASTER CONTROL
Data from Other Agencies
Pre-
Processing
Submodels
Data
Files
Transport
Source
Topography
Executive
Routine

FIGURE 14. Pre-processing submodels present tabulated or raw observational data in a form usable by the operational model.

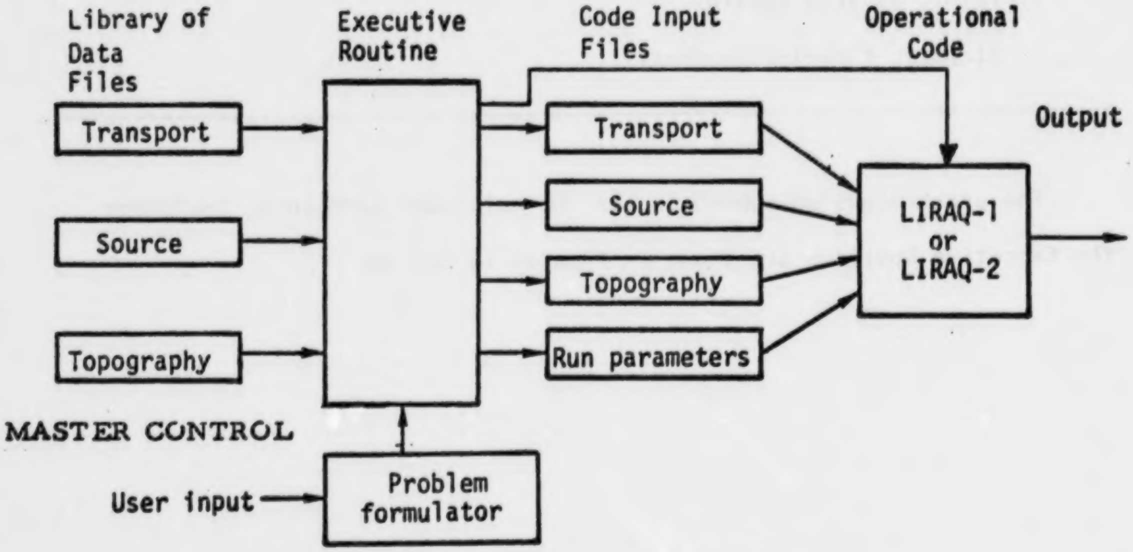
Library of
Data
Files
Transport
Source
Topography
Executive
Routine
Code Input
Files
Transport
Source
Topography
Run parameters
Operational
Code
LIRAQ-1
or
LIRAQ-2
Output
MASTER CONTROL
User input
Problem
formulator

FIGURE 15. An executive routine modifies the necessary data files as required by the user through the problem formulator, obtains run parameters and options, and then executes the desired operational code.

A 24-hour simulation problem (LIRAQ-2) using a 20 x 20 mesh presently takes approximately an hour of 7600 time. This time is not uniformly distributed (Fig. 16).

a. For example, it requires about 11 minutes to run a 12-hour problem from 6:00 a.m. (approximately 30 minutes after sunrise) to 6:00 p.m. (approximately 30 minutes before sunset). Sunrise (i.e., sunrise until 10 minutes after sunrise) requires approximately 4 minutes, and similar time is taken at sunset. This is due to the effects of rapidly varying photodissociation coefficients and species.

b. Meteorological updates, which result in discontinuity in transport coefficients, cause a slowing of the code at the time of their occurrence.

SAMPLE RESULTS (Figures 17-24)

Figures 17-20 are contour plots of ozone concentration calculated by the LIRAQ-2 photochemical model for various times of day, for a high oxidant day in the San Francisco Bay Area. The (a) plots correspond to vertical average concentrations, the (b) plots to concentrations at ground level. These plots constitute a series of snapshots giving the spatial variation of ozone at specific times of the day.

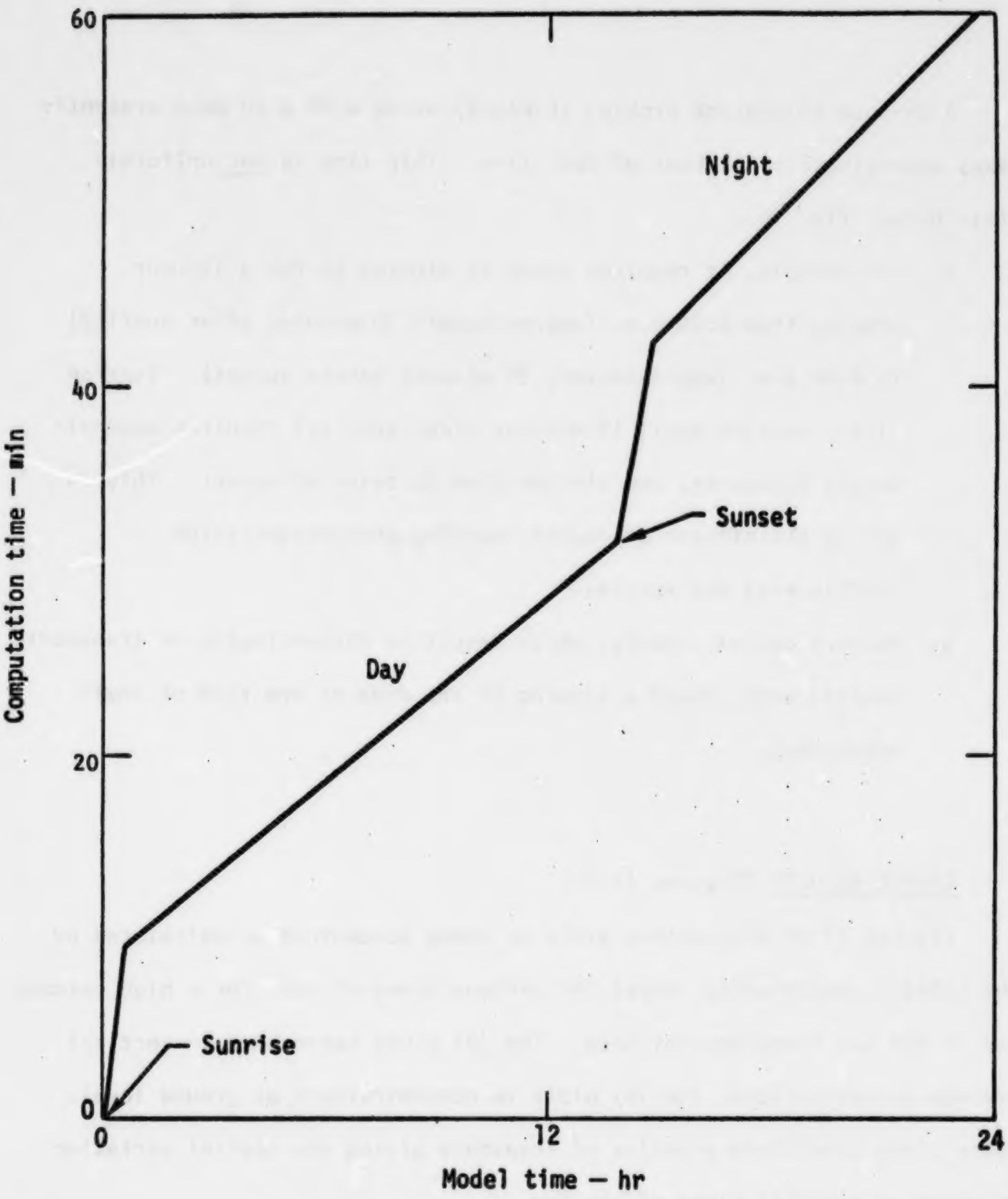

FIGURE 16. A 24-hour simulation requires approximately 60 minutes of computer time, unequally distributed through the period of simulation.

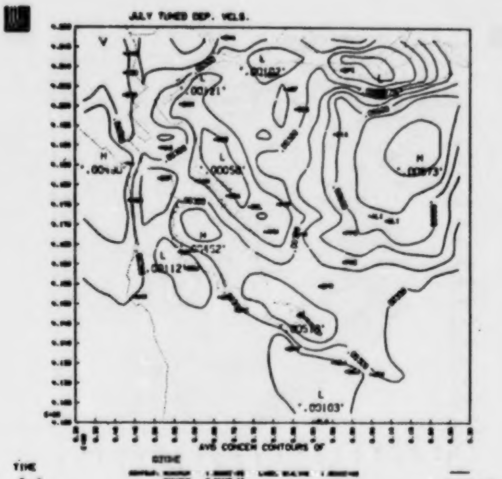
JULY TUNED DEP. VELS.
L
'.00102'
L
'.00121'
H
'.00440'
L
'.00058'
H
'.00873'
H
'.00452'
L
'.00112'
'.00518'
L
'.00103'
AVG CONCEN CONTOURS OF
OZONE
TIME
0: 0.

FIGURE 17a.

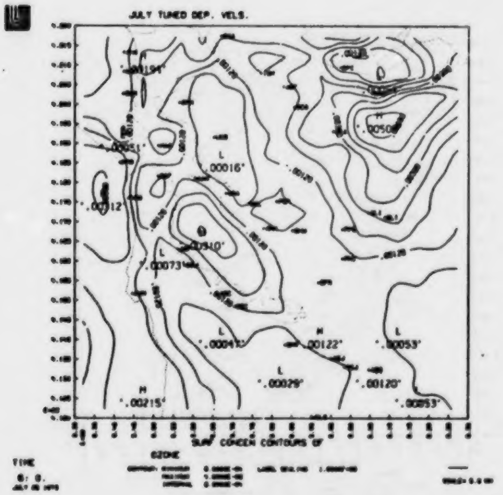
JULY TUNED DEP. VELS.
'.00194'
'.00051'
L
.00016'
H
'.00508'
'.00112'
'.00310'
L
'.00073'
L
'.00041'
H
.00122'
L
'.00053'
L
'.00029'
'.00120'
H
'.00215'
'.00053'
SURF CONCEN CONTOURS OF
OZONE
TIME
0: 0.

FIGURE 17b

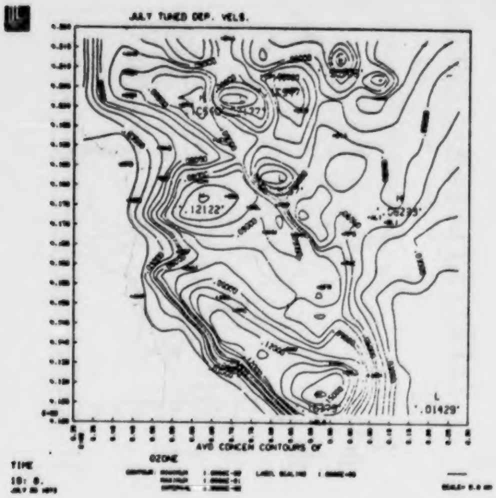
JULY TUNED DEP. VELS.
H
.12122
L
.01429
H
AVG CONCEN CONTOURS OF
OZONE
TIME
10: 0.

FIGURE 18a.

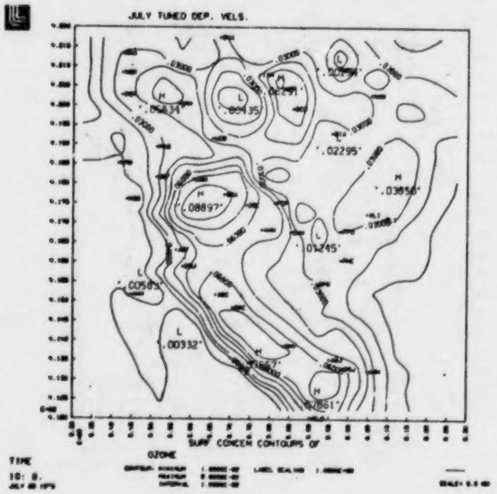
JULY TUNED DEP. VELS.
H
.05634
L
.00435
L
.02295
H
.08897
H
.03650
L
.01245
L
.00583
L
.00332
H
.07861
SURF CONCEN CONTOURS OF
OZONE
TIME
10: 0.

FIGURE 18b.

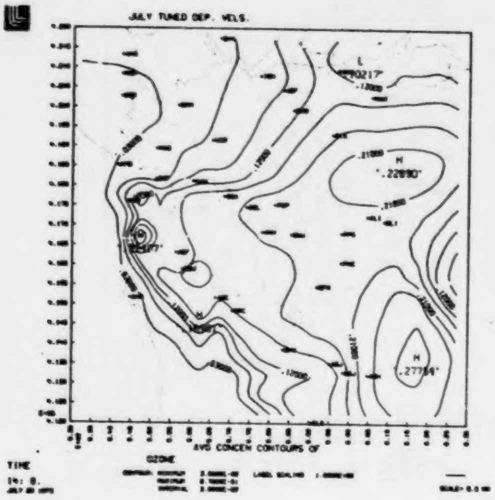
JULY TUNED DEP. VELS.
L
.00217
.12000
.21000
H
.22890
H
.27759
AVG CONCEN CONTOURS OF
OZONE
TIME
14: 0.

FIGURE 19a.

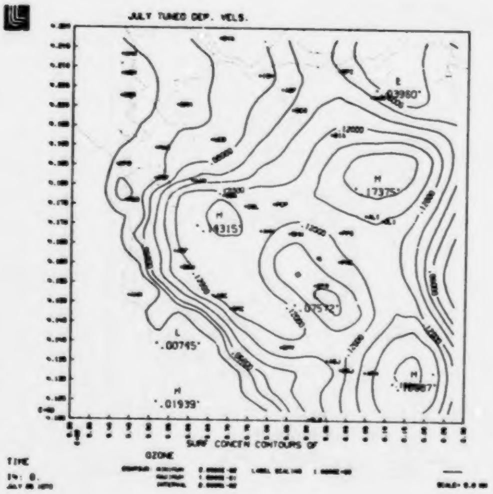
JULY TUNED DEP. VELS.
L
.03960
.12000
H
.17375
H
.14315
.07572
L
.00745
H
.01939
SURF CONCEN CONTOURS OF
OZONE
TIME
14: 0.

FIGURE 19b.

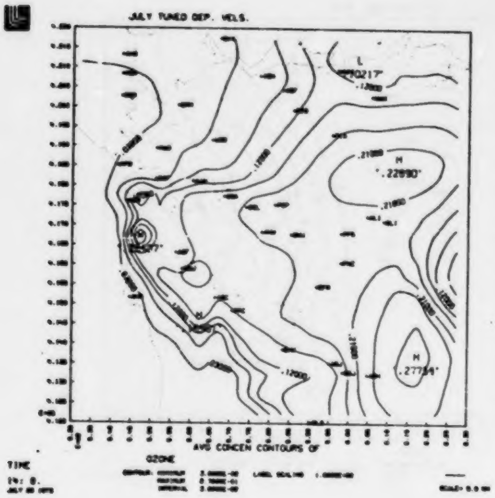
JULY TUNED DEP. VELS.
L
.00217
.12000
.21000
H
.22890
.21000
.12000
.12000
.21000
.12000
H
.27734
AVG CONCEN CONTOURS OF
OZONE
TIME
14: 0.

FIGURE 19a.

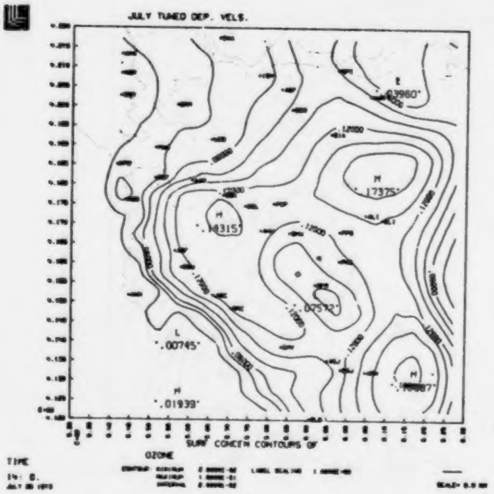
JULY TUNED DEP. VELS.
L
.03960
.12000
H
.17375
.12000
H
.10315
.12000
.07572
.12000
L
.00745
H
.01939
H
SURF CONCEN CONTOURS OF
OZONE
TIME
14: 0.

FIGURE 19b.

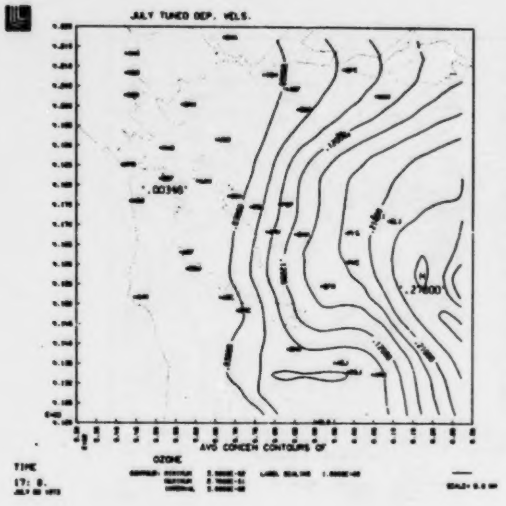

FIGURE 20a.

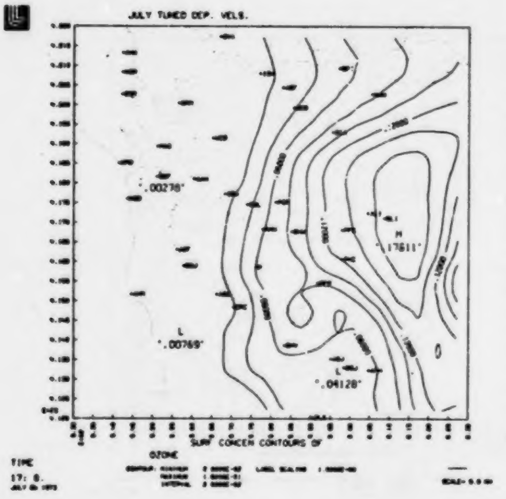

FIGURE 20b.

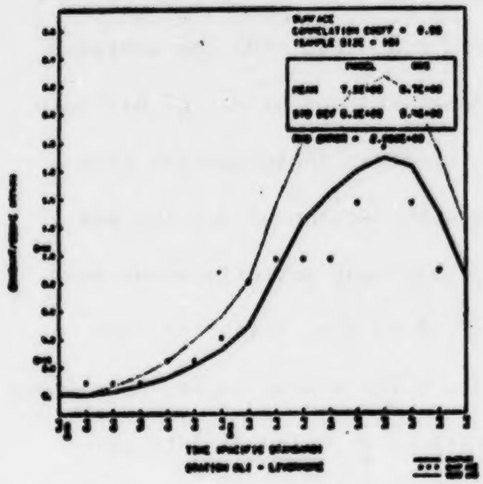

FIGURE 21

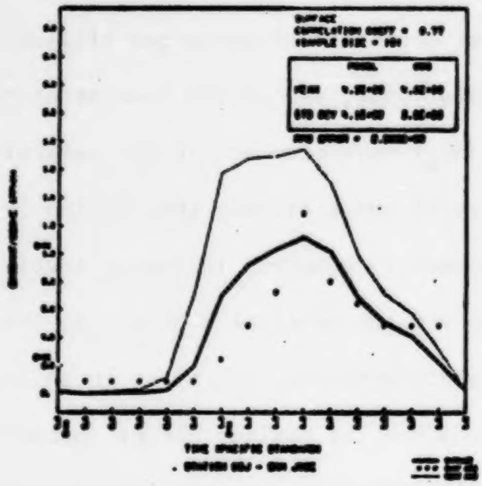

FIGURE 22

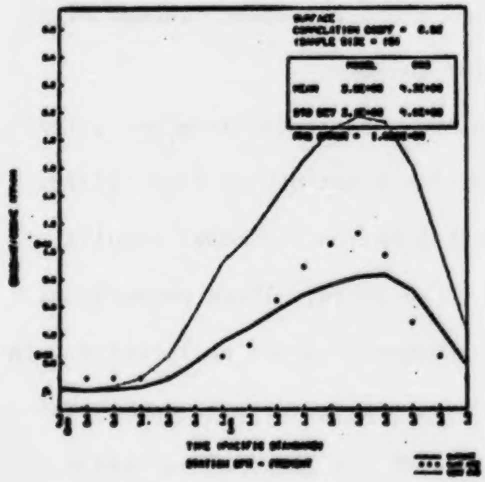

FIGURE 23.

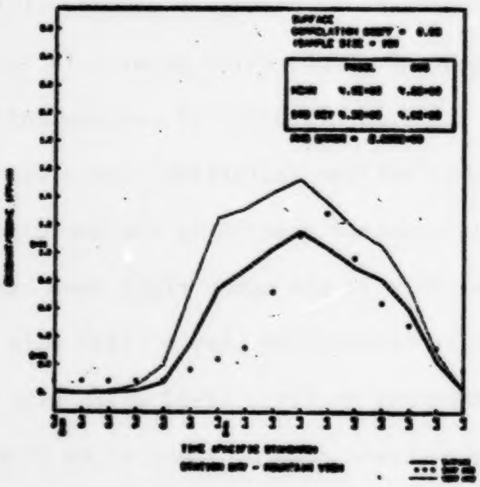

FIGURE 24.

At 6:00 a.m. (Figure 17) is seen a relatively quiescent condition, following the hours of darkness, concentrations of ozone being quite low, of the order of parts per billion. At 10:00 a.m. (Fig. 18) the various stationary and mobile sources of hydrocarbons (HC) and oxides of nitrogen (NO_x) have been active for several hours, injecting these species into a still comparatively thin mixing layer. Here the action of the sun has begun to generate increased levels of ozone and weak westerly winds have moved the material somewhat to the east. By 2:00 p.m. (Fig. 19), the photochemistry, operating in an increasingly thick mixing layer, has almost reached its maximum effect (ozone concentrations of 0.1-0.3 parts per million) and advection has carried significant amounts of ozone to the east. At 5:00 p.m. (Fig. 20) the sun is low in the sky and further photochemical production of ozone has virtually ceased. The winds from the west have become quite strong, cleaning out the region along the coast, though high concentrations still persist in the interior valleys.

Time histories of surface and average ozone concentrations and actual observations (asterisks) are given for specific locations in Figs. 21-24. Information describing the correlation of observation and model results appears in the upper right hand corner of these plots. These comparisons with observation play a vital role in the process of model calibration. In contrast to Figs. 17-20 which give instantaneous pictures over some broad geographic domain, these plots give a picture of the temporal variation of ozone at specific points within our region of interest. In these plots can be clearly seen the process of ozone buildup through combined action of HC and NO_x with sunlight and advective transport and the later "cleaning out" due to advection.

Full documentation of the LIRAQ models is contained in the Project Final Report[10] and User's Guide.[11]

The LIRAQ model for the San Francisco Bay Area was developed by LLL in cooperation with the Bay Area Air Pollution Control District (BAAPCD) and the NASA Ames Research Center. The effort, supported by the Research Applied to National Needs (RANN) program of the National Science Foundation models to be used by the BAAPCD in land-use planning studies, such as the determination of the impact on air quality of new towns or shopping centers, regional population growth patterns, and short-term control strategies.

To facilitate access to the model by BAAPCD, the LIRAQ codes' associated files have been transferred to computers at Lawrence Berkeley Laboratory, where BAAPCD personnel may run problems from their offices in San Francisco via telephone-line links.

5. Present Extensions of LIRAQ

The Environmental Protection Agency (EPA) has entered into an interagency agreement with LLL to adapt the LIRAQ model for use in the St. Louis, Missouri area as part of its Regional Air Pollution Study (RAPS) program. Under this agreement data concerning St. Louis topography, emission inventory, and meteorological data will be made available. For treating St. Louis, a simple system of sulfur chemical reactions is being included in the model. LIRAQ, already partially validated in the San Francisco Bay Area, will be validated for four days of RAPS data in St. Louis. Proper arrangements, procedures, and user's guides will be made available to EPA personnel to enable them to operate this model at Lawrence Berkeley Laboratory Computer Center.

The following reactions converting SO_2 to sulphate have been incorporated into the LIRAQ-2 code:

REACTION	k
$RO_2 + SO_2 \rightarrow SO_4^= + RO$	2×10^{-15} cm^3/sec
$RO + SO_2 \rightarrow SO_4^= + HO_2$	4×10^{-13} cm^3/sec
$HO_2 + SO_2 \rightarrow SO_4^= + HO$	9×10^{-16} cm^3/sec
$HO + SO_2 \rightarrow SO_4^= + HO_2$	6×10^{-13} cm^3/sec

Also, deposition velocities of 1 cm/sec for SO_2 and 0.5 cm/sec for $SO_4^=$ are assigned. This reaction set is based on the assumptions that any intermediate products (e.g. SO_3, HSO_3) will be converted to $SO_4^=$ rapidly and that the actual products of the $HO + SO_2$ reaction will have approximately the same effect as the assumed products. During model tests on a 5 km grid covering the San Francisco Bay Area, these reactions had very little effect on any of the calculated radical concentrations.

To improve the running characteristics of the code when sulfur compounds are included, the species HO_2, RO_2, RCO_3, and N_2O_5 have been placed in steady state; these are in addition to O, NO_3, HO, and RO, which have always been so treated. Also, RNO_2 has been deleted from the system. Assuming that HO_2 was in steady state had nearly a 1% effect on some species concentrations (notably H_2O_2 and HO_2). The other changes (including adding SO_2 reactions) caused lesser changes in the concentrations of the species present in the earlier versions of the code. In order to make doubly sure that the above changes did not adversely affect the LIRAQ-2 predictions, the July verification problem carried out as part of the NSF project was rerun and effects on the station records were found to be negligible.

The LIRAQ-2 model has been used to simulate sulfur compound concentrations in the Bay Area. The code predicts the correct range of concentrations, based on data concerning sulfur compounds available in the NSF data base. However, the concentrations are not well correlated with observed station data. This is not unreasonable given the use of 5 km resolution and three hour meteorology in a 2-D Eulerian model when the species considered is emitted from a mixture of surface and elevated point sources located near the observing stations, many of which have variable emissions on a day to day basis. It is also worth noting that almost all of the BAAPCD stations which monitor sulfur are intentionally located so as to maximize the effect of nearby point sources, not to determine kilometer average concentrations.

REFERENCES

1. Sherman, C. A., "A Mass-Consistent Model for Wind Fields over Complex Terrain," Lawrence Livermore Laboratory Report UCRL-76171, Rev. 1, October 1975 (submitted to Journal of Applied Meteorology).

2. Preliminary Safety Analysis Report for Indian Point Nuclear Generating Unit No. 3, Consolidated Edison Company of New York, 1973.

3. Lange, R., M. H. Dickerson, K. R. Peterson, C. A. Sherman, and T. J. Sullivan, "Particle-in-Cell Vs. Gaussian Calculations of Concentration and Deposition out to 70 Km for Two Sites," Lawrence Livermore Laboratory (report in preparation, August 1976).

4. Lange, R., "ADPIC - A Three-Dimensional Computer Code for the Study of Pollutant Dispersal and Deposition Under Complex Conditions," Lawrence Livermore Laboratory Report UCRL-51462, 1973.

5. Lange, R., and J. B. Knox, "Adaption of a Three-Dimensional Atmospheric Transport and Diffusion Model to Rainout Assessments," Lawrence Livermore Laboratory Report UCRL-75731, 1974.

6. Gudiksen, P. H., K. R. Peterson, R. Lange, J. B. Knox, "Plume Depletion Following Postulated Plutonium Dioxide Releases from Mixed-Oxide Fuel-Fabrication Plants," Lawrence Livermore Laboratory Report UCRL-51781, 1975, submitted to Health Physics.

7. Lange, R., "ADPIC - A Three-Dimensional Transport-Diffusion Model for the Dispersal of Atmospheric Pollutants and Its Validation Against Regional Tracer Studies," Lawrence Livermore Laboratory Report UCRL-76170, Rev. 1 (October 10, 1975), submitted to Journal of Applied Meteorology.

8. Gear, C. W., "Numerical Initial Value Problems in Ordinary Differential Equations," (Prentice-Hall, Engelwood Cliffs, N.J., 1971).

9. Hindmarsh, A. C., "GEAR: Ordinary Differential Equation System Solver," Lawrence Livermore Laboratory, Computer Documentation Report UCID-30001, Rev. 1 (1972).

10. MacCracken, M. C., and G. D. Sauter (editors), "Development of an Air Pollution Model for the San Francisco Bay Area, Final Report to the National Science Foundation," Volumes 1 and 2, Lawrence Livermore Laboratory Reports UCRL-51920, Vol. 1 and Vol. 2, 1975.

11. MacCracken, M. C., (principal investigator), "User's Guide to the LIRAQ Model: An Air Pollution Model for the San Francisco Bay Area," Lawrence Livermore Laboratory Report UCRL-51983, 1975.

Rapporteur's Report on the First Three Papers of Topic #2 - "Interregional and Regional Models"

Chairman: M. Kwizak

Rapporteur: H. E. Turner

Discussion of Paper #1 given by B. Dietzer, FRG

J. Kretzschmar - Do I understand correctly that your model is developed by taking a certain data set and looking for the best fit?

B. Dietzer - Yes, but the observations are first splitup into space - and time - dependent parts. Only the time-varying eigenvalues and their associated coefficients are correlated with meteorological values.

L. Shenfeld - Would your model not be affected by changes in source emissions during model development?

B. Dietzer - Yes, but no such changes occurred.

Discussion of Paper #2 given by W. Johnson, USA

W. Veigele - Puff-model results are generally dependent upon the inter-puff time interval. Have you considered the sensitivity of your results to the rather large 12-hour time interval used?

W. Johnson - Yes, this has been looked into, but we are saved by the fact that the dependence is smoothed by calculating a 30-day average.

B. Sivertsen - Have you considered the inclusion of SO_2/SO_4 transformation on your calculations since it ought to be important on this time scale? Also, are you aware of the OECD report on a 2-layer model, as you propose, tried by the Norwegian Institute for Air Research?

W. Johnson - We have not included SO_2/SO_4 transformation, but plan to try a linear, first-order decay term. We are aware of the OECD report and it was partly on the basis of that work that we decided to stay with a single layer for the time being.

T. Schneider - Observations indicate, however, that pollution travels in distinct layers.

W. Johnson - The need to have emissions and transport at the right height is most important on the first 300-400 km and we plan to investigate this.

J. Knox - Our work suggests that the number of layers which should be considered depends upon the particular day and arbitrary choices can cause difficulties.

D. Fox - We have had some experience with a similar but simpler model. Have you looked at the sensitivity of the model to the deposition parameters used?

W. Johnson - Yes, to some degree, but the values are not defined well enough as yet to look at this in detail.

Discussion of Paper #3 given by J. Knox, USA

H. Schultz - How do you determine your diffusion coefficients?

J. Knox - It depends upon the particular case. For example, in the Savannah case, turbulence instrumentation was available with a readout every 15 minutes.

E. Runca - How many tracer particles are used in the APDIC simulation?

J. Knox - 90,000 particles/24 hour period. The model cancarry 5 species from a single source or 1 species from each of 5 different sources.

R. Porter - What class of computer do you use?

J. Knox - We use a CDC7600. Running times are 2-4 minutes per data set for MATHEW, 6 minutes for one APDIC simulation, and one hour/24 hour period for LIRAC-2 with 15 species.

SUMMARY

The chairman opened the session by noting the appropriateness of the topic to the current concern for alternative fuels, and to the need for research into the effects of such alternatives upon air pollutant receptors (e.g. potential for and areal extent of acidification of soil and water). The importance of regional and interregional transport is only now being recognized as evidenced by the recent organization of major interregional deposition studies. There will be a strong need to exchange and syntheize the resulting data.

The first three papers of the session concerned two interregional models (one causal and one correlative) applied to SO_2 transport and three regional models, one for each of three-dimensional windfield, pollutant distribution under the influence of transient regional flow and photochemical pollutant simulation. Discussion of these papers was, for the most part, concerned with the appropriate parameterization of scavenging processes, the need for inclusion of chemical transformation in the models, and the cost/benefit on terms of computer running time.

The relative infancy of the field of interregional modeling coupled with its importance as stressed by the Chairman, and because of the fact that relevant supporting data is now becoming available, all stress the need for continued consideration of this topic at future technical meetings.

7th International Technical Meeting
on Air Pollution Modeling and its Application

MODELING MOUNTAIN AIR QUALITY

Douglas G. Fox and Michael A. Fosberg
USDA/FS Rocky Mountain Forest and Range Experiment Station
Fort Collins, Colorado 80521

September 7 - 10, 1976
Airlie, Virginia
United States of America

ABSTRACT

There are increasing needs for methods to determine the air pollution potential of mountainous lands. In the United States, and most other temperate latitude countries, mountainous areas are relatively undeveloped except for forest related industry, mineral extraction and recreational use. Recent years have shown tremendously increasing markets for all of these activities but in particular for the last two. This paper presents a sequence of modeling techniques that have been designed for use by managers responsible for mountainous lands. The modeling package includes three fundamental, somewhat complex, components which are used to calculate simple indices useful to planners and managers in assessing their air quality problems.

The component models include: a model to estimate the surface temperature in complex topography; a model of the surface wind field, using surface temperature, roughness and a larger scale prevailing wind; and a model to calculate the dispersion of pollution by these winds. Currently the temperature modeling is done using statistical-climatological techniques although some research to incorporate components of a dynamic surface energy balance will be presented. The winds model is a single layer model which calculates the wind as a combination of potential flow with corrections due

to vorticity and modifications by friction and surface heating. Finally, dispersion from point sources is handled using a unique adaptation of the Gaussian diffusion concept which will be described in detail. Dispersion from non-point sources is handled using conventional techniques.

The major point of this paper, however, will be to present a means of providing the relatively complicated output from this modeling sequence in terms that can be readily understood by the general public and that are compatible with other information being used for planning. To this end, use is made of the proposed Ψ (Pollutant Standards Index) and a recently developed air pollution potential index.

INTRODUCTION

Rural and wildland of the United States are being confronted with increasing pressures for development. A principle mineral resource of our country, low sulfur coal, is our most reasonable alternative to supply electricity for the present generation, and is found in close proximity to uniquely beautiful National Park and National Forest lands. The mobility and living standard of our population has continued to increase demands for greater amounts and greater diversity of outdoor recreational facilities. The Rocky Mountain National Park in Northern Colorado, for example, received about 3,000,000 visitors in the summer of 1976. Moreover, the realizable size of our world is shrinking so rapidly and the economic and sociological pressures are increasing such that these issues must be viewed with an international perspective.

Among the problems facing managers responsible for our Federal wildlands are preservation of the current air and water quality in these areas. There are two major assaults on air quality, one from upwind, namely the visitation by urban air on our rural areas, and the other internally, that is, polluting activities on the lands themselves. Generally, nonurban recreational lands are located in regions with harsh climates and in mountainous physiography. Meteorological conditions resulting from complex terrain lead to some severe air pollution potentials in confined valleys because of local inversions. Sufficient meteorological air quality data are not readily available to intelligently assess that potential in rural areas. Since these mountain wildlands will be developed, methods capable of dealing with large areas at minimal cost are required to establish air quality constraints and land use plans within economic and social functions of an area.

These are the challenges faced in trying to provide some air quality information to aid land managers. Clearly, modeling the meteorology and the air quality is the only reasonable approach to provide the needed data. This paper first discusses some of the manager's needs for, and concerns about air quality. Secondly, it details the development of an air quality assessment methodology. Models and methodologies discussed here are designed to suit systems requirements of land managers and land use planners.

LAND MANAGERS NEEDS FOR AIR QUALITY DATA

Nature, lesislative actions, and administrative goals establish the general framework in which a land manager must work. Natural requirements deal with the biology and physics of the ecosystem. The land manager has an impressive list of responsibilities but his overriding concern must be with the preservation or improvement of the natural system. There are certainly differences between a National Park Naturalist's concern for the most minute details of the preservation of a natural ecosystem for posterity and the forester's concern with optimal use of a forest for timber production, recreation, water yield for downstream use, etc. Both managers must ensure that the air quality is commensurate with his particular needs. Specific requirements for the naturalist might suggest that since we don't know enough about sulfur metabolism in living systems, any elevation of sulfur concentration in the air might be deleterious to the natural ecosystem. Specific requirements for the forester might suggest that if sulfur concentrations are maintained below levels of known effects or damage to trees the effects of a little sulfur in areas with sulfur deficient soils might be positive. It is clear, however, that as a minimum the manager desires air at the primary standard for SO_2 (80 ug/m^3 in the U.S.) as a yearly average. There is a great deal more research that needs to be done concerning pollution effects on vegetation, particularly in the area where low levels are maintained over long periods of time and in effects of climatic conditions on SO_2 metabolism and the resulting vegetation response.

Legislative and administrative requirements to preserve air quality have not been a major concern to land managers until very recently. In isolated cases, there has been some concern that a particular activity might lead to violation of the ambient air quality standards, but this has been rare. There has been more than casual interest in problems of smoke generated by forest fires. Fire is a major tool used by the land manager for removal of residues from timber harvests and other thinning operations. Smoke generated as a result of residue reduction is the major source of pollution in many rural areas and in some urban areas. Problems associated with residue burning have caused the U.S. Forest Service to establish some elaborate control practices through burning schedules or in extreme cases, use of expensive disposal techniques other than burning. However, by far the largest impact on the wildland manager will come as a result of currently proposed amendments to the Clean Air Act of 1969. At issue is whether the Government has a right to enforce a policy of no significant deterioration in areas where air quality currently is well above agerage. Of particular concern is whether to maintain the existing air quality by not allowing, or placing limitations on, construction of new direct and indirect sources or by limiting certain polluting activities, or to utilize the resources of these areas for national well being at the cost of deteriorating air quality.

In response to a U.S. Supreme Court decision, the EPA has established a three level classification system wherein a Class I area may sustain only minimal increases in concentration, a Class II area can accommodate limited and orderly development, and a Class III area allows pollution up to the NAAQS standards. Since the question of public health is not involved, a great deal of controversy has been associated with the nondegradation issue resulting in the amendments currently (September 1976) under consideration by the Congress. These amendments require that much Federally owned land come under mandatory classification as either Class I or Class II areas. Implications for the land manager of this classification include a need to assess the current air quality of his region of responsibility and a need to include air quality considerations in all future plans for the region.

The remaining sections detail a proposed methodology to deal with this problem.

MOUNTAIN METEOROLOGY

The major stumbling block toward providing an assessment of air quality in the mountains is the fantastic complexity of the meteorology influencing diffusion in this type of environment. A variety of slopes, aspects, elevation and surface conditions are manifested within very small geographic areas giving rise to highly diverse microclimates. Temperatures for exmple, may vary 10's of degrees in less than a mile. Similarly, sheltering and diverting of winds can cause extreme wind variations within rather short distances. The procedures outlined in this paper are designed to exploit what we might term the stationary patterns of meteorological variables resulting from the fixed forcing of the terrain. Certainly, extremely complicated conditions occur in the mountains as a local response to larger scale synoptic forcing. It is, however, our purpose to characterize general climatic features which will predominate as longer averages are considered. The two major elements of the climate for this purpose are surface temperature and winds. Clearly these are not unrelated phenomena.

Perhaps the first major difficulty in doing an analysis of mountain meteorology is the severe lack of available data. National Weather Service meteorological stations are generally located only at airports in major population centers. This problem has been somewhat mitigated, however, by the development of an extensive network of data collection over rural wildlands. A number of Federal, State and private forest managers take meteorological observations which are not readily available through the Weather Service. These data are now archived on the Computer Oriented Meteorological Data Library (COMED) (Furman and Brink,

1975) by the U.S. Forest Service. This Library adds some 2000 once per day observations to the NWS network and is almost the only data available in wildland areas. The advantage of these data is that they are dispersed over mountainous lands with a mean separation of approximately 10 km. Unfortunately the data are collected only once per day during the summer season. Research is currently underway to extend the value of this data resource by using statistical techniques through time series analysis to develop temporal variations around the once a day measurement.

These types of procedures are also being applied to develop spatial variability of meteorological parameters over a mountain valley complex. Temperature is perhaps the most reasonable variable with which to expect success. In addition, temperature is the most important variable in determining the two most critical dispersion parameters, namely wind speed and stability. A recent study (Furman, 1976) suggests that all of the variability due to elevation and aspect in a mountain temperature signal is contained in the deterministic (mean) component. This lends support to efforts to model the temperature variability as a physical process. Efforts are underway to simulate the various elements in a surface energy balance. The surface temperature can be calculated from heat flux in turn estimated from an energy balance at the surface. Mountain conditions lead to an extremely complex radiation component consisting of direct solar and indirect long wave energy being differentially reflected and absorbed over the area. While these methods are quickly becoming available, at the present time it is necessary to utilize rather conventional statistics to generate temperature fields from existing data. When the data are not available general climatological approximations such as contained in Baker (1944) are utilized.

A second element of mountain meteorological data needed to analyze air pollution is, of course, the wind field. The essence of our analysis is a wind model (Fosberg, Marlatt and Krupnak, 1976) which integrates various elements of a potential flow with the vorticity generated by differential values of surface roughness and surface temperature and incorporates these as corrections to an overall boundary layer flow (i.e. Mesoscale and LFM scales of resolution; Sommers, 1976). This model has undergone extensive testing for validation and we expect that the model is accurate to within 2. mps and 22° (RMS error) when used under the proper conditions; namely without violating any of the assumptions. Generally the model is operated using terrain data read from computer tapes made up of the digital 1:250,000 U.S. Geological Survey topographic maps. Surface roughness is grossly determined based upon land use categories available from these same U.S.G.S maps. Surface temperature required by the wind model is determined from a combination of the statistical and physical techniques mentioned above.

TOPOGRAPHIC AIR POLLUTION ANALYSIS SYSTEM (TAPAS)

We have proposed (Fosberg & Fox, 1976) a set of indices that should be useful to land use planners and others responsible for assessing the air pollution potential of mountainous lands. Basically these indices are composite indicators of the diffusion process as applied within the confines of complex terrain. It has been established after many field experiments that plumes emitted from complex topographic situations disperse at rates different from that which the classical Pasquill-

Gifford stability classes would predict. Approaches have been suggested which range from an independent classification of diffusion parameters to prescriptions for changing the stability class when under mountain conditions. Strong sentiment toward abandoning the Gaussian formulation in favor of a more complex diffusion calculation has often been expressed. Clearly, for cases where pollution disperses over multiple mountain-valley scales the Gaussian concept loses its value. Serious concerns over impaction and transport around topography suggest the need for a detailed solution of the fundamental mass conservation equation which properly includes effects of advection and turbulent diffusion. Within the planning context of this discussion however, the need for information about long range (i.e. multiple valley) transport is usually limited to a determination of the trajectory and the overall stability in the area. We are making such calculations by using the wind field developed in our WINDS model to provide boundary conditions for a diffusion equation solution based upon earlier work by Reiquam (1970) and Egan and Mahoney (1972).

A relatively larger number of land use planning applications, however, need not abandon the Gaussian model concept. In order to apply the concept to mountain conditions we have suggested a non-turbulent dispersion correction (Fosberg, Fox, Howard and Cohen, 1976) based on including the mass divergence of the wind in the classical Gaussian model. The resulting equation for concentration becomes

$$\chi = \frac{Q}{\sqrt{2}\ \pi \sigma_y \sigma_z u} \exp \left[- \frac{1}{2} \left(\frac{y}{\sigma_y} \right)^2 + \left(\frac{z}{\sigma_z} \right)^2 \right] \exp (- \delta \Delta t)$$

where Q = emission rate

u = mean wind speed

σ_y, σ_z = standard deviations from Turner (1969)

δ = mass divergence

Δt = time interval over which δ is constant.

In order to provide readily useful planning information we have defined a mixing volume index (Fosberg and Fox, 1976) as

$$I(x,y,z) = \frac{\chi(x,y,z)}{Q} 10^6 = \frac{\exp}{\sqrt{2}\,\pi \sigma_y \sigma_z u} \left[-\frac{1}{2} \left(\frac{y^2}{\sigma_y{}^2} + \frac{z^2}{\sigma_z{}^2} \right) - \delta \Delta t \right] \times 10^6$$

where the 10^6 is a scaling factor such that the Index values range in extremely stable conditions up to 1000 while in practice they rarely exceed 100. This mixing volume index with dimensions sec/m^{-3} represents the diffusion potential of an area. In application we calculate $I(X,o,o) = I$ for each cell in which a wind and a divergence is calculated by the WINDS model.

The recently proposed PSI index (Thom & Ott, 1976) is designed to standardize comparison of pollution levels from location to location and pollutant to pollutant. The index is basically a piecewise linear fitting of the standards to a reference value. The general equation is simply

$$\Psi = a + b \frac{\chi}{\chi_s}$$

where a, b are constant determined by which segment is being fitted, χ is the ambient concentration and χ_s is the standard. For most planning applications and for most pollutants, $a = 0$ and $b = 100$; namely, the desired air quality is within the ambient air quality standard and the index assumes values in the range of 0-100. A combination of the mixing volume index, I and Ψ leads us to a third and most useful index which we call the Pollution Index, or Π matrix

$$\Pi = \Sigma\, n_i Q_i = \left(\frac{\Psi - a}{b}\right) \frac{X_s}{I}\, 10^6$$

Fig. 1 illustrates a rather complete set of programs which come under the general title of Topographic Air Pollution Analysis System (TAPAS) which couple the wind model, the temperature model and the various diffusion indices along with the appropriate peripheal information such as topography, surface roughness, stabilities, emission rate etc. The basic output of this system is the pollution index on a grid basis. In an interactive mode, the planner is able to calculate acceptable numbers of various sources which can be accommodated within each cell. Moreover, the Π matrix provides a single value per cell which can be easily interfaced as the "air pollution" input to more general planning models using linear programming concepts to consider economic, social, biological and physical constraints.

Baker, Federick S., 1944. Mountain Climates of the Western United States. Ecol. Monogrm. 14:223-258

Egan, Bruce A. and James R. Mahoney, 1972. Numerical Modeling of Advection and Diffusion of Urban Area Source Pollutants. J. Applied Meteor. 11:312-332

Fosberg, Michael A. and Douglas G. Fox, 1976. Use of Air Quality Indices in Mountain Land Use Planning. (Manuscript submitted to Atmospheric Environment.)

Fosberg, Michael A., Douglas G. Fox, E. A. Howard and Jack Cohen, 1976. Non-Turbulent Dispersion Processes in Complex Terrain. Atmospheric Environment (in press)

Fosberg, Michael A., William E. Marlatt and Lawrence Krupnak, 1976. Estimating Airflow Patterns over Complex Terrain. USDA Forest Service Research Paper RM 162, 16 pp.

Furman, R. William, 1976. Time Series Analysis of Daily Maximum Temperatures on a Mountain Slope. (Manuscript submitted to J. Applied Meteor.)

Furman, R. William and Glen E. Brink, 1975. The National Fire Weather Data Library: What it is and how to use it. USDA Forest Service, General Tech. Report RM-19 8 pp.

Reiquam, H., 1970. Atmospheric Transport and Accumulation Model for Airsheds. Atmospheric Environment 4:233-247.

Sommers, William T., 1976. On the Relationship between LFM Predictions, On Site Rawinsonde Observations and Surface Flow in Mountainous Terrain. Paper presented at Sixth Conf. on Weather Forecasting and Analysis, May 10-13, Albany, N.Y. Abstract in Bull. American Meteor. Soc. 57:170

Thom, Gary C. and Wayne R. Ott, 1976. A Proposed Uniform Air Pollution Index. Atmospheric Environment 10:261-264.

Turner, D. Bruce, 1970. Workbook of Atmospheric Dispersion Estimates. Environmental Protection Agency 84 pp.

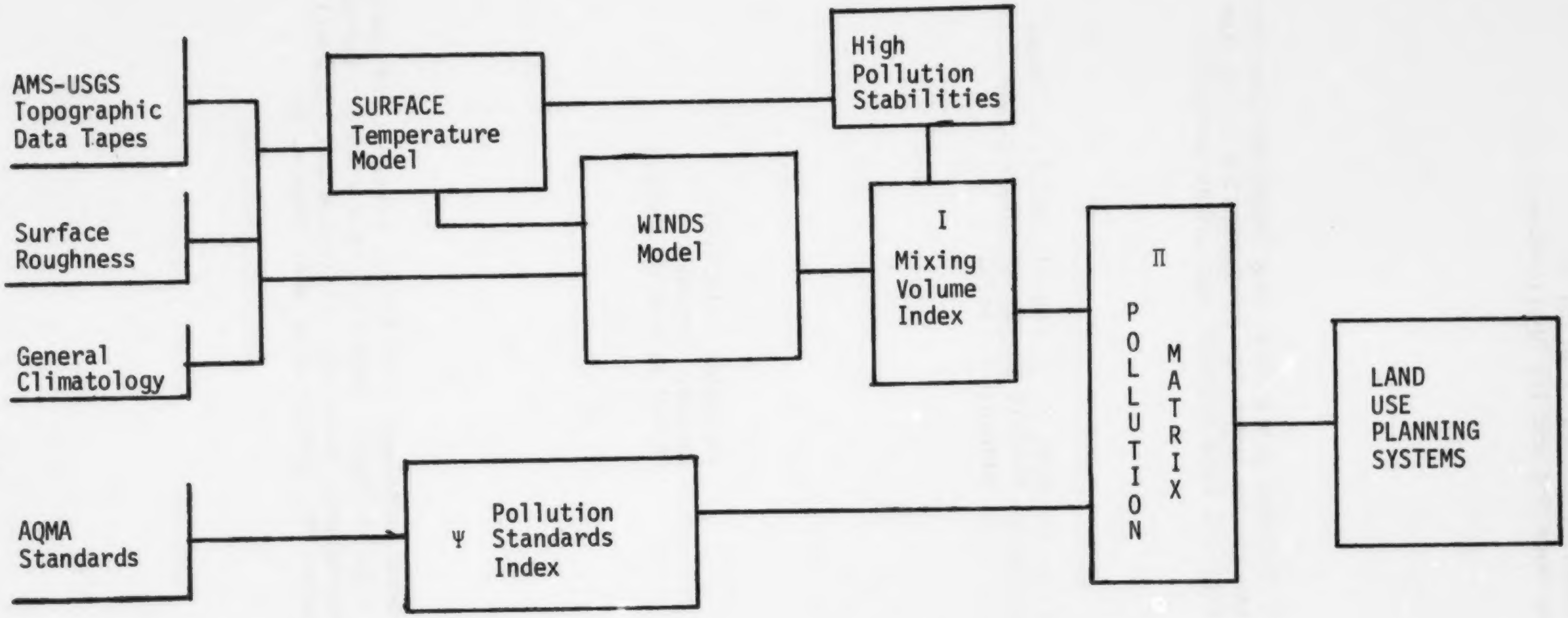

Topographic Air Pollution Analysis System (TAPAS)

AMS-USGS Topographic Data Tapes
Surface Roughness
General Climatology
AQMA Standards
SURFACE Temperature Model
WINDS Model
High Pollution Stabilities
I Mixing Volume Index
Ψ Pollution Standards Index
Π POLLUTION MATRIX
LAND USE PLANNING SYSTEMS

Figure 1 - The conceptual outline of TAPAS, a combination of complex data files and sophisticated computer simulation models which provide a useful, simply applied index of the air pollution carrying capacity of mountain lands.

7th International Technical Meeting on
Air Pollution Modeling and Its Application

A REGIONAL SCALE MODEL FOR COMPUTING DEPOSITION AND GROUND LEVEL AIR CONCENTRATION OF SO_2 AND SULFATES FROM ELEVATED AND GROUND SOURCES*

L. L. Wendell, D. C. Powell, and R. L. Drake
Battelle, Pacific Northwest Laboratories
Richland, Washington 99352

September 7-10, 1976
Airlie, Virginia
United States of America

---

*This paper is based on work performed under Energy Research and Development Administration Contract E(45-1)-1830). Reprinted from Preprint Volume of the Third Symposium on Atmospheric Turbulence Diffusion and Air Quality, October 19-22, 1976, Raleigh, NC, published by AMS, Boston, MA.

A REGIONAL SCALE MODEL FOR COMPUTING DEPOSITION AND GROUND LEVEL AIR CONCENTRATION OF SO_2 AND SULFATES FROM ELEVATED AND GROUND SOURCES*

L. L. Wendell, D. C. Powell, and R. L. Drake

Pacific Northwest Laboratories
Battelle Memorial Institute
Richland, Washington 99352

1. INTRODUCTION

As the demand for energy requires increased use of sulfur-bearing fuels, concern has been growing about the environmental impact of the SO_2-sulfate cycle. The National Academy of Sciences (NAS, 1975) has prepared a comprehensive review addressing primarily the sulfate question. Also, the Environmental Protection Agency (EPA, 1975) has prepared a position paper regarding their concerns about regulating atmospheric sulphates. Studies cited in both of these documents have indicated that the oxidation products of SO_2, including sulfuric acid and suspended sulfate particulates are more toxic than the parent compound. Since the removal rates for the very small sulfate particles are somewhat less than for SO_2 gas, the sulfates can be transported to greater distances than the SO_2 (NAS, 1975; EPA, 1975). This has shifted attention from local pollution problems to regional scale power plant pollution. One of the critical needs, for the development of reasonable control strategies, is the development of regional scale models to estimate long-range transport phenomena for sulfates, as well as the local concentrations.

The regional scale sulfur pollution problem in Europe has been addressed in a modeling effort reported by Bolin (1975). In the northeastern United States work on various phases of regional scale modeling of power plant pollution has begun at several laboratories. Reports of this work appear in this preprint document of the symposium proceedings. The model reported in this paper is designed to use time- and space-varying gridded wind and precipitation data, along with source locations and source strengths, to compute average air concentrations and deposited amounts of SO_2 and sulfate. The model simulates transport and dispersion, chemical transformation, and wet and dry removal. In this first version of the model the simulations of the transformation and removal processes are of a simple linear nature. They do, however, allow some investigation of the sensitivity of the overall process to its interacting parts.

The analysis reported in this paper was designed to test the sensitivity of the model results to wet removal by real-time and time-averaged precipitation. Previous investigators have treated the phenomenon of wet removal as constant in time and space (Bolin, 1975) or as proportional to the climatological rainfall rate (Heffter and Ferber, 1975). One can argue that from a statistical point of view that over a long enough period of time the differences in wet deposition due to the intermittency of real-time precipitation would average out. This argument, however, assumes little or no correlation between the air flow and precipitation patterns. The cyclical nature of the frontal storms through the middle latitudes indicates such a correlation is possible and makes the problem worthy of closer examination. The model described in this paper has been designed with this examination in mind.

2. TRANSPORT AND DISPERSION

The transport of material in this model is purely kinematic and is accomplished using similar techniques as developed for mesoscale purposes (Wendell, 1972). The model is designed to accept a time series of gridded winds, assumed to be representative of the layer carrying the contaminant. The gridded wind fields for this work are currently generated from 12-hourly radiosonde data. The model approximates a continuous plume centerline by a series of particles released from selected source locations, at 1-hr intervals, into wind fields obtained by hourly interpolation between the 12-hourly observations. An example of the result of this procedure is displayed graphically in Figure 1. The positions of the particle are computed on an hourly basis.

The plumes depicted in Figure 1 are analogous to a satellite picture 12 and 24 hr after release. Despite the fact that this type of representation only approximates what is happening in the atmosphere, it provides some interesting depictions of plume stretching and overlapping in a time- and space-varying flow on this scale.

Dispersion of the mass of material associated with each particle is allowed to develop in a Gaussian fashion. The plume widths shown in Figure 1 are determined by assuming the plume edges to be $2\sigma_y$ from the centerlines, making a

---

* This paper is based on work performed under Energy Research and Development Administration Contract E(45-1)-1830.

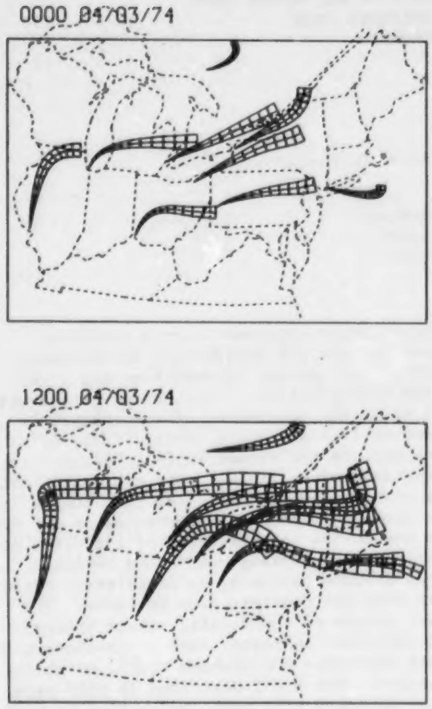

Figure 1. Twelve-hourly plume plots from nine sites with continuous releases beginning at 1200 GMT April 2, 1974. The lines perpendicular to the centerlines indicate plume segments generated during 1 hr of release time.

total width of $4\sigma_y$. The variable σ_y is approximated with the form

$$\sigma_y = as^b \tag{1}$$

where s is distance traveled by the particle of concern and the values of a and b are selected according to stability class to reproduce the Pasquill-Gifford curves (Slade, 1968). Vertical dispersion is accounted for by approximating σ_z according to stability class and travel distance as shown in Table 1.

The average surface air concentrations and the deposition quantities are calculated by sampling the approximated plumes over a network of grid squares, approximately 34 × 34 km. The model has been constructed with the option of neglecting horizontal diffusion about the plume centerline. This is an assumption made by others in long-term assessment models on a similar spatial scale (Bolin, 1975; Sheih, 1976). Preliminary tests comparing runs with and without horizontal plume diffusion indicate that the extra expense (factor of 4) is probably not justified for long-term assessments.

Table 1

Suggested Expressions for σ_z as Functions of Distance (s) in Meters

Stability	σ_z
A	$0.20s/(1 + 2\cdot10^{-5}\ s)$
B	$0.12s/(1 + 2\cdot10^{-5}\ s)$
C	$0.08s/(1 + 2\cdot10^{-4}\ s + 4\cdot10^{-10}\ s^2)^{1/2}$
D	$0.06s/(1 + 1.5\cdot10^{-3}\ s + 4\cdot10^{-10}\ s^2)^{1/2}$
E	$0.03s/(1 + 3\cdot10^{-4}\ s)$
F	$0.02s/(1 + 3\cdot10^{-4}\ s)$.

3. TRANSFORMATION AND REMOVAL

The chemical transformation of SO_2 to the various forms of sulfate in the atmosphere and the removal processes, both wet and dry, are extremely complex and are receiving intensive study (EPA, 1975; NAS, 1975). However, for the initial purposes of this model, transformation and removal processes were approximated in a simple manner. A set of differential equations was written describing the conservation of mass of SO_2 and sulfate in an air parcel. The following assumptions are incorporated into the set of equations:

1. The chemical conversion of SO_2 to sulfate is first order.
2. The transformation and removal rates are independent of atmospheric concentrations.

The following definitions are employed:

$X(t)$ = mass of SO_2 in an air parcel.

$Y(t)$ = mass of sulfate in an air parcel.

$D_x(t)$ = mass of SO_2 deposited from the air parcel.

$D_y(t)$ = mass of sulfate deposited from the air parcel.

k_x = coefficient of dry deposition of SO_2 (hr^{-1}).

ℓ_x = coefficient of wet deposition of SO_2 (hr^{-1}).

k_y = coefficient of dry deposition of sulfate (hr^{-1}).

ℓ_y = coefficient of wet deposition of sulfate (hr^{-1}).

k_{xy} = transformation rate of SO_2 to sulfate (hr^{-1}).

With these definitions the equations for the conservation of mass may be written:

$$\frac{dX}{dt} = -\left(k_x + \ell_x + k_{xy}\right) X \tag{2}$$

$$\frac{dY}{dt} = -\left(k_y + \ell_y\right) Y + \frac{3}{2} k_{xy} X \qquad (3)$$

$$\frac{dD_x}{dt} = \left(k_x + \ell_x\right) X \qquad (4)$$

$$\frac{dD_y}{dt} = \left(k_y + \ell_y\right) Y \quad . \qquad (5)$$

The 3/2 factor in (3) accounts for the different masses associated with equimolar quantities of sulfate ion ($SO_4^{=}$) and SO_2. Assuming the initial conditions

$$X(0) = X_o$$

$$Y(0) = D_x(0) = D_y(0) = 0 \quad ,$$

the solutions to (2) through (5) are

$$X(t) = X(t_o)\, A \qquad (6)$$

$$Y(t) = Y(t_o)\, B + T_{xy}\, X(t_o)\left[B-A\right] \qquad (7)$$

$$D_x(t) = T_x\, X(t_o)\, \left[1-A\right] \qquad (8)$$

$$D_y(t) = Y(t_o)\, \left[1-B\right]$$

$$+ T_{xy}\, X(t_o)\, \left[1-B\right] - T_y\, \left[1-A\right] \qquad (9)$$

where

$$A = \exp\left[-\left(k_x + \ell_x + k_{xy}\right)\left(t - t_o\right)\right]$$

$$B = \exp\left[-\left(k_y + \ell_y\right)\left(t - t_o\right)\right]$$

$$T_x = \frac{k_x + \ell_x}{k_x + \ell_x + k_{xy}}$$

$$T_y = \frac{k_y + \ell_y}{k_x + \ell_x + k_{xy}}$$

$$T_{xy} = \frac{3}{2}\ \frac{k_{xy}}{k_x + \ell_x + k_{xy} - k_y - \ell_y} \quad .$$

The solutions (6) through (9) are evaluated, in the model, for each plume segment at each time step, usually $(t - t_o) = 1$ hr, in the advection-sampling process.

The rates of dry removal k_x and k_y were formulated by dividing a deposition velocity v_d by a length Δz that is characteristic of the vertical distribution. Thus

$$k_{x,y} = \frac{(v_d)_{x,y}}{\Delta z}$$

The subscripts in this notation indicate that the formalism may be applied to either of the two removal rates. In the early part of the trajectory of a plume segment, Δz is from the Gaussian assumption:

$$\Delta z = (\Pi/2)^{1/2}\sigma_z \quad .$$

When the pollutants become evenly distributed throughout the mixed layer, Δz is taken to be equal to the depth of this layer.

The rates of wet removal ℓ_x and ℓ_y were formulated as follows:

$$\ell_{x,y} = \frac{P}{d}\, C_{x,y}$$

where P is the hourly precipitation rate (m hr^{-1}), d is a characteristic drop size diameter, and C is a collection efficiency. The model has three options for the specification of the hourly precipitation:

1. Unchanging in time and uniform in space, one value specified over the whole grid for a complete run (a specification of zero would mean running the model for transformation and dry removal only).
2. Unchanging in time but varies in space, the climatological average is specified in each square of the sampling grid.
3. Changing in time and space, the hourly average values determined for each grid square (Wendell and Hane, 1976) are read into the model for each hour of the advection-sampling process.

An example of the effects of the real-time precipitation data is shown in Figure 2. For the purposes of this graphical display any portion of the plume center encountering a precipitation rate, in a grid square, greater than 0.25 mm hr^{-1} was immediately dropped. The plume plots of Figure 2 correspond to those shown in Figure 1 which were produced by running the model in a day mode. The numbers indicating precipitation represent hourly values for the hour ending at the time shown at the top of each plot. Blank portions in plumes in areas with no indication of precipitation depict encounters with precipitation between plot times.

Under the conditions and assumptions described above, the model was prepared for a sensitivity analysis to examine the effects of the use of real time precipitation data.

4. SENSITIVITY ANALYSIS

4.1 Definition of Removal Modes

The model was run with three removal alternatives for purposes of comparison. First the dry removal process was modeled exclusively. Second, both dry and wet removal were included; wet removal being modeled as the result of time-averaged precipitation. For this process the precipitation rate used in each grid square was the time-averaged amount occurring during the specified

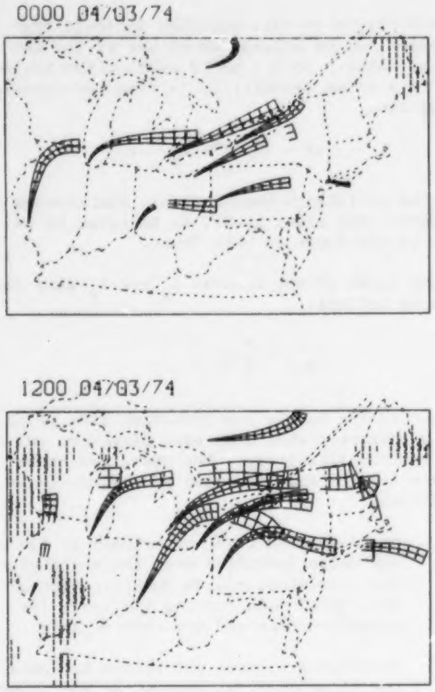

Figure 2. Same plume plots as in Figure 1 except that hourly precipitation is allowed to eliminate those portions of the plumes encountered. The numbers on the plots indicate hourly precipitation amounts according to the following code; 1:0.01-0.10 in, 2:0.11-0.20 in, 3:0.21-0.30 in, etc.

18-day interval. Third, a real-time precipitation was substituted for the time-averaged values. In this process new rainfall rates for each grid square were entered hourly into the computation process. By comparison of the concentration and deposition patterns predicted by these last two processes, it is possible to assess the effects of the correlation between wind and precipitation patterns and also the effects of locally heavy precipitation through a densely polluted layer.

4.2 Description of Data and Parameters

The meteorological data used for this test included a set of 12 hourly gridded wind fields from 1200 GMT April 2, 1974, through 1200 GMT April 20, 1974. The gridded winds were obtained through a random to grid interpolation of radiosonde winds averaged through a layer from 100 m to 1000 m. Hourly precipitation data from 777 reporting stations were gridded from this same period for the precipitation scavenging calculations.

Since our main concern for this test was the effect of real-time versus average precipitation, the parameters were kept as simple as possible. A neutral stability class was maintained for the diffusion calculations throughout the period. The growth of σ_z was not limited by a varying mixing depth.

The continuous release was prescribed to be from a single location just east of St. Louis, Missouri at a rate of 100,000 tons/year. The effective release height was held at 400 m above the surface for the entire period.

For the purpose of this test, the values assigned to the parameters were as follows:

$$k_{xy} = 0.05 \text{ hr}^{-1}$$

$$(v_d)_x = 1 \text{ cm sec}^{-1}$$

$$(v_d)_y = 0.1 \text{ cm sec}^{-1}$$

$$C_x = 1.0$$

$$C_y = 0.1$$

$$d = 2 \text{ mm}$$

The last three parameters result in wet removal constants as follows:

$$\ell_x = \frac{P}{2} \text{ hr}^{-1}$$

$$\ell_y = \frac{P}{20} \text{ hr}^{-1}$$

For the relatively light rainfall rate of 0.1 mm hr^{-1}, $\ell_x = .05 \text{ hr}^{-1}$ and $\ell_y = 0.005 \text{ hr}^{-1}$. For a moderate rain of 5 mm hr^{-1}, $\ell_x = 2.5 \text{ hr}^{-1}$ and $\ell_y = 0.25 \text{ hr}^{-1}$.

During the 18-day period of the test, six frontal storms passed through the area covered by the computational grid with precipitation amounts varying from light (<2.5 mm hr^{-1}) to heavy (>25 mm hr^{-1}) and a high degree of spatial variability. However, when the rainfall was averaged in each grid square for the entire period the resulting pattern was comparatively uniform.

4.3 Test Results - Total Budget

To show the effects of real-time versus average precipitation on the model results, the total SO_2-sulfate budgets at the end of the 18-day test are presented for the three modes of removal in Table 1. The fractions of the total SO_2 released which remain in the air as SO_2 and sulfate at the end of the period are presented only to show the complete budget. These fractions will decrease as the duration of the release increases.

The quantities of interest are the amounts removed and the amounts escaping the computational grid. Note that amounts removed in the form of SO_2 and sulfate reflect the larger removal parameters for SO_2 than for sulfate. The difference in removal rates also appears in the amounts which escape the grid; 4-5 times more of the SO_2 released escaped the grid as sulfate than as SO_2.

In comparing the results for the three modes of removal we find some distinct differences. The case with no precipitation was included to serve as a reference when comparing the two modes of wet

Table 1

Fate of SO_2 Released for 18 Days from a 400 m Effective Height (%)

Precip. cond.	Left in air over grid		Deposited on surface of grid		Transported beyond grid		Total
	SO_2	Sulfate	SO_2	Sulfate	SO_2	Sulfate	
Dry	2.7	7.7	33.6	4.6	10.7	41.3	100.0
18-day average	1.4	3.7	62.3	7.8	4.1	20.7	100.0
Real time	2.0	6.1	50.0	8.8	5.1	28.0	100.0
Real time - average	+0.6	+2.4	-12.3	+1.0	+1.0	+7.3	0.0

removal. It is apparent that using the 18-day average precipitation rate continuously in each grid square produces a significantly higher removal of SO_2 than applying the precipitation rates as actually measured during the period. When both modes of wet removal for SO_2 are compared to the dry removal the increase affected by the real-time precipitation is about 50% while that affected by the 18-day average is about 90%. This over-removal by the average precipitation is reflected in the fact that 35% more sulfate escaped the grid when real-time precipitation was used. That more SO_2 is available for transformation in the real-time precipitation case is also evident from the higher removal of sulfate than for the average precipitation case.

4.4 Test Results - Spatial Distribution

Maps were produced for the three modes of removal which displayed the spatial distribution of the average air concentrations for SO_2 and sulfate as well as the deposited amounts of each. The major points from those maps (not shown here) are:

- The highest 18-day average air concentrations for SO_2 were on the order of 1 $\mu g\ m^{-3}$ within 50-100 km of the source, dropping off rapidly with distance. There was no significant difference in the spatial variability between the three removal modes.

- The highest 18-day average air concentrations for sulfate were on the order of 0.3 $\mu g\ m^{-3}$ within 50-200 km of the source depending on the removal mode. The sulfate patterns contrasted sharply with the SO_2 patterns in that the concentrations dropped off much more slowly with distance from the source and showed a greater variation in distribution with removal mode.

- The patterns for the SO_2 deposited over the 18-day period were similar to the patterns for the SO_2 average air concentrations, with major amounts deposited within 100-2-0 km of the source. Deposited amounts near the source were on the order of 10,000 $\mu g\ m^{-2}$ for the dry removal mode and 30,000 $\mu g\ m^{-2}$ for the two modes including wet removal. Again the patterns for all three modes were very similar with deposited amounts dropping to less than 100 $\mu g\ m^{-2}$ beyond a 1000 km radius from the source.

The patterns of deposited sulfate for the three modes of removal are shown in Figures 3a through 3c. The pattern for the dry mode shown in Figure 3a is similar to the pattern for the average air concentration of sulfate and should reflect the major paths of the material over the area during the period. The second mode of removal including precipitation scavenging on a continuous basis with the 18-day average rainfall rate is shown in Figure 3b. The pattern for this case is very similar to the one for the dry mode, except for the amplification which reflects the 70% increase shown for the total budget in Table 1. There are additional amounts shown deposited in New England which would be expected from the pattern on the air concentration map.

The pattern of sulfate deposition produced using the removal mode, including real-time precipitation, is shown in Figure 3c. The pattern for the lower half of the grid is recognizable from the patterns of the first two removal modes but the pattern in the upper half of the grid has some striking differences. In the northwestern portion of the grid the major difference is the order of magnitude greater deposit in west central Wisconsin. The other major difference in pattern is in the New York, New Jersey and New England area. For the real-time precipitation mode there is an order of magnitude more sulfate deposited in the New York and New Jersey but significantly less in the New England states.

Probably the most striking feature of the sulfate deposition, for the parameters used, is that the 1000 $\mu g\ m^{-2}$ being deposited 1500 miles from the source is of the same order of magnitude as the amount being deposited no more than 50-100 km from the source.

5. DISCUSSION AND RECOMMENDATIONS

Considering the complexities of the problem and the crude parameterizations in the model during this single sensitivity analysis, a fair degree of caution must be exercised in drawing

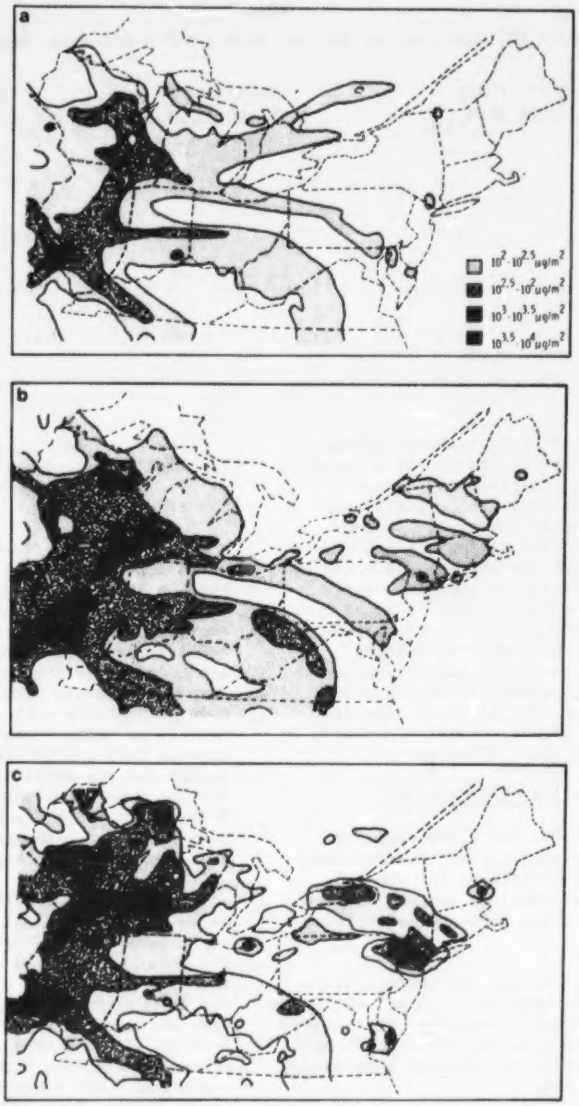
a
10^{2}-$10^{2.5}$ µg/m^{2}
$10^{2.5}$-10^{2} µg/m^{2}
10^{3}-$10^{3.5}$ µg/m^{2}
$10^{3.5}$-10^{4} µg/m^{2}
b
c

Figure 3. Sulfate deposition in µg m^{-2} for a) dry removal only, b) wet and dry removal using average precipitation, c) wet and dry removal using real-time precipitation.

conclusions from the results. In this test we have considered the case of a single source which emits 100,000 tons of SO_2 per year under the conditions including a slow to average rate of conversion and removal efficiencies about an order of magnitude greater for SO_2 than for sulfate. Under these conditions and simplifying assumptions with respect to stability conditions and mixing depth, the model has produced results for an 18-day period from which we made the following observations:

- A single plant of this size in the designated area does not add a significant amount of SO_2 or sulfate to the background level of average air concentration beyond the immediate vicinity of the source.
- Almost 60% of the SO_2 emitted was deposited within the northeastern United States as SO_2 or sulfate.
- About 33% of the SO_2 emitted leaves the northeastern United States in the form of sulfate to be deposited elsewhere.
- The use of time-average precipitation in the model causes a significant over-removal of SO_2, primarily near the source. This allows less sulfate to be removed at more distant locations within the computational grid or to escape the grid altogether.

The major conclusion with regard to the use of real time or average precipitation is that the most significant discrepancy appears in the spatial distribution of sulfate deposition. This discrepancy cannot be corrected by a simple change in magnitude of the washout coefficient. Whether the spatial discrepancy in pattern would cancel out over a long-term assessment run is still subject to determining a distinct correlation between flow and precipitation patterns. The case we have selected is typical of meterorological conditions in the spring. More cases should be examined during other seasons of the year and for longer periods of time.

As we pointed out, the results obtained in this test depend on the parameterizations of the transformation and removal processes. Because of the wide range and the uncertainty of the results obtained by different investigators, it would be worthwhile to conduct further sensitivity analyses with various combinations of parameters as well as perform validations with experimental data.

The model described in this paper is presently in the form of a vehicle to be improved upon. It contains many of the essential elements, in varying degrees of approximation, needed to begin validation and assessment exercises. The approach in this effort has been to maintain a balance between development and application. Validation efforts, assessment exercises and comparisons with other models should suggest the priority of necessary improvement. These efforts are being undertaken, in coordination with other investigators, in an attempt to develop tools for assessing the impact of power plant pollution.

6. REFERENCES

Bolin, B, and C. Persson, 1975: Regional Dispersion and Deposition of Atmospheric Pollutants with Particular Application to Sulfur Pollution over Western Europe. *Tellus XVII*, 3, 281-310.

E.P.A., 1975: *Position Paper on Regulation of Atmospheric Sulfates*, U. S. Environmental Protection Agency, Office of Air and Waste Management, Office of Air Quality Planning and Standards, Research Triangle Park, NC 27711, Publication number EPA-450/2-75-007, September 1975.

Heffter, J. L., and G. A. Ferber, 1975: A Regional Continental Scale Transport, Diffusion and Deposition Model, Part II: Diffusion-Deposition Models. *NOAA Tech. memo*, ERL ARL-50.

N.A.S., 1975: *Air Quality and Stationary Source Emission Control*. Commission on Natural Resources, National Academy of Sciences, Washington, D.C. Prepared for Committee on Public Works, United States Senate, Washington, D.C., March 1, 1975.

Sheih, J., 1976: Application of a Lagrangian Statistical Trajectory Model to the Simulation of Sulphur Pollution over North Eastern United States. Appearing in the proceeding of the *Third Symposium on Atmospheric Turbulence, Diffusion, and Air Quality*, October 1976.

Slade, D. H., 1968: *Meteorology and Atomic Energy*, U. S. Atomic Energy Commission, Div. of Technical Information, available as TID-24190 from the National Technical Information Service, U. S. Department of Commerce, Springfield, VA 22151, p. 404.

Wendell, L. L., 1972: Mesoscale Wind Fields and Transport Estimates Determined from a Network of Wind Towers. *Mon. Wea. Rev.*, Vol. 100, 565-578, July 1972.

7th International Technical Meeting on
Air Pollution Modeling and its Application

ANALYTICAL-NUMERICAL MODEL FOR MESOSCALE TRANSPORT, TRANSFORMATION AND REMOVAL OF AIR POLLUTANTS

N. V. Gillani and R. B. Husar
Air Pollution Research Laboratory
Department of Mechanical Engineering
Washington University
St. Louis, Missouri 63130

September 7 - 10, 1976
Airlie, Virginia
United States of America

1. INTRODUCTION

The formation of harmful secondary pollution depends on the rate of primary-to-secondary conversion as well as on the atmospheric residence time of the primary pollutant. Such secondary formation becomes increasingly significant for plume transport beyond the mesoscale range. Recent plume mapping experiments from airborne sampling platforms have successfully measured significant contributions to ambient pollutant levels, both primary and secondary, at distances in excess of 100 km from isolated single power plant sources (Brown et al., 1972; unpublished data of Project MISTT 1976, EPA), from the St. Louis urban area (Breeding et al., 1975; White et al., 1976), and from the industrial regions of Britain (Smith & Jeffrey, 1975). The fate of the primary emissions within the mesoscale range of approximately 1 - 100 km is of significant importance in determining their availability for long range transport and transformation.

In this paper, a rather simple, three-dimensional model is presented for application to isolated single plumes (point source or area source) over a mesoscale distance under well-defined and reasonably steady meteorological conditions. The model is based on eddy diffusion, the vertical component of which is considered variable with height within the daytime mixing layer. The model also includes the role of pollutant transformations, such that conversion rates are allowed to change with the age of the polluted air mass which characterizes the chemical composition. The effect of ground removal of the pollutant by dry deposition is also included explicitly in the model. The solution of the model is carried out by a combined analytical-numerical technique, and results are presented for elevated as well as ground-based plumes.

The model is formulated in dimensionless form, and the appropriate dimensionless system parameters characterizing source elevation, plume dispersion, and pollutant transformation and ground removal are identified and their roles are discussed. The sensitivity of the model to these parameters is viewed in the light of field data of both gaseous and particulate sulfur obtained from aircraft sampling performed in the St. Louis region as part of Project MISTT (Midwest Interstate Sulfur Transformation and Transport) sponsored by the U.S. Environmental Protection Agency. The model is applied to observed data for a power plant plume and plumes from the St. Louis urban-industrial complex, and quantitative information pertinent to the overall kinetics of the conversion and removal processes over the mesoscale range is extracted.

2. FIELD OBSERVATIONS

Project MISTT is a plume mapping program which has been conducted in St. Louis during the summer since 1973. Its objectives include a quantitative assessment of the transport, transformation and removal of SO_2 from isolated large urban and power plant plumes. The schematic drawing in Figure 1 shows the two principal sampling components of the field experiments prior to 1976 (Husar et al., 1976a). A single-engine instrumented aircraft continuously monitors levels of SO_2 and particulate sulfur, as well as NO, NO_x, ozone, size-segregated aerosol parameters

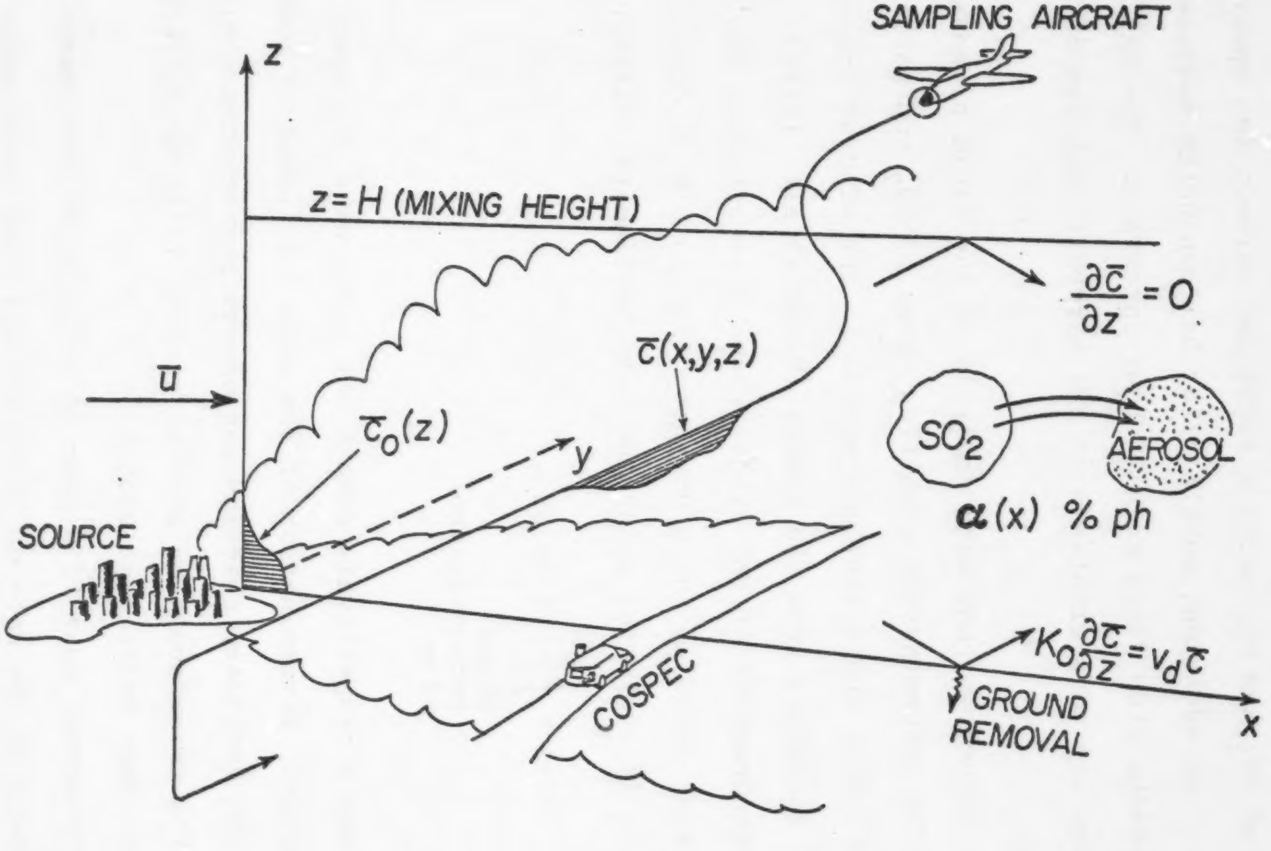
SAMPLING AIRCRAFT
z
z= H (MIXING HEIGHT)
$\frac{\partial \overline{c}}{\partial z} = 0$
$\overline{u}$
$\overline{c}(x,y,z)$
$\overline{c}_0(z)$
y
SO₂
AEROSOL
$\alpha(x)$ % ph
SOURCE
$K_0 \frac{\partial \overline{c}}{\partial z} = v_d \overline{c}$
COSPEC
GROUND
REMOVAL
x

Figure 1. *Schematic drawing to illustrate the plume mapping program and model development.*

and several meteorological parameters. The ground van measures ground level SO_x and NO_x, as well as the integrated overhead burdens of SO_2 and NO_2 using a Barringer correlation spectrometer (COSPEC). In addition, mobile pilot balloon units measure the instantaneous wind field at half-hour intervals. The balloon launchings are co-ordinated with the aircraft sampling in space and time.

The experiment and data analysis of the field program are designed to determine the mass flow rates of SO_2 and particulate sulfur at plume cross-sections normal to the wind at increasing downwind distances from the source (Husar et al., 1976a). From direct measurements of the excess plume concentration field c, and the wind field u, the plume mass flow rate Q at downwind distance x is evaluated using the mass continuity relation

$$Q(x) = \iint\limits_{\substack{\text{plume}\\ \text{cross-section}\\ \text{at } x}} c.u \, dy \, dz \ , \qquad (1)$$

where y and z respectively denote the cross-wind and vertical co-ordinates. Determination of the mass flow rates of both the primary and secondary reaction components permits the estimation of both the transformation and the removal rates by performing the sulfur mass balance at each x.

The observed mass flow rate of airborne $SO_2(Q)$, normalized with respect to the rate of emission (Q_o) from broad urban-industrial sources near the ground is shown plotted in Figure 2 as a function of plume transport time. As the data indicate, depletion of SO_2 takes place in these plumes at a rate greater

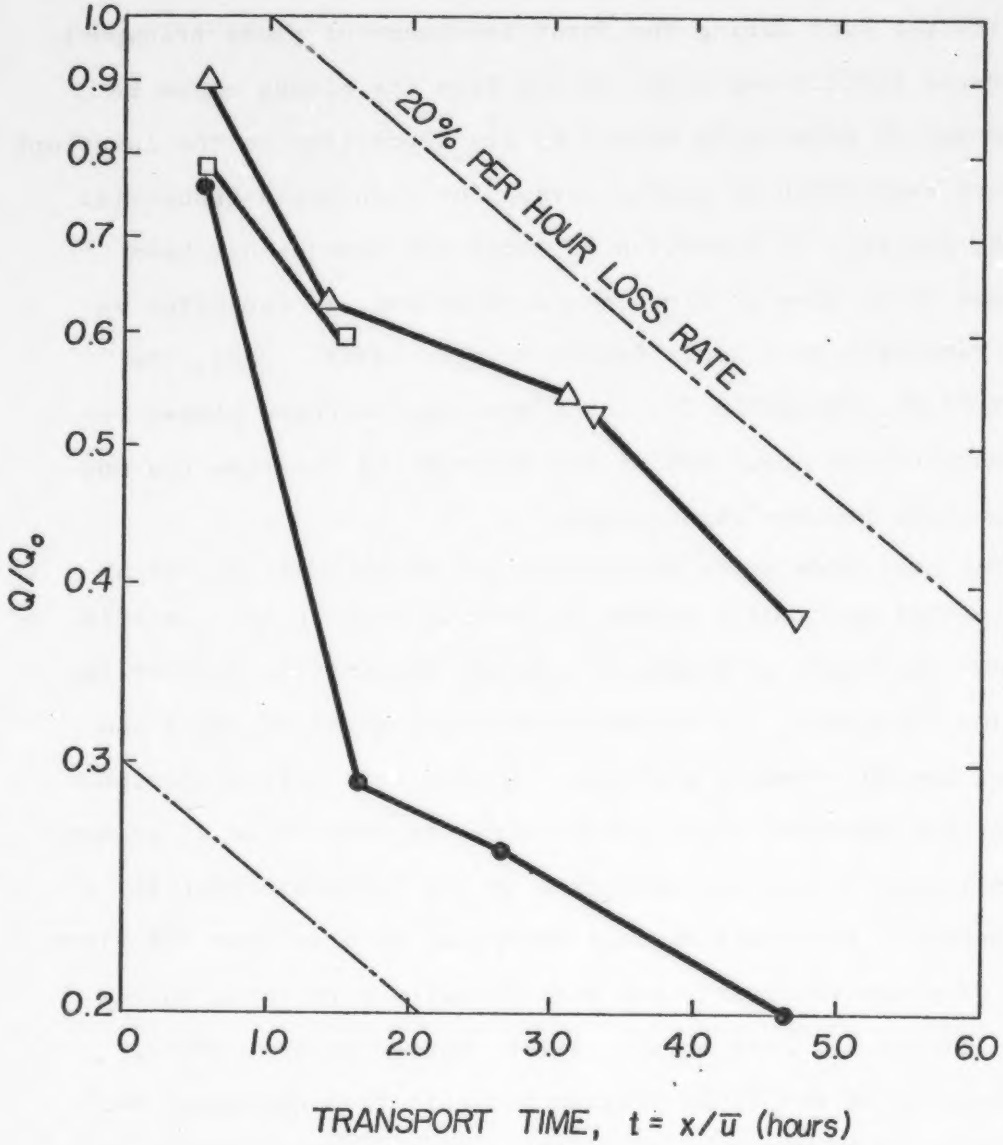

Figure 2. *SO$_2$ depletion data for St. Louis urban-industrial plumes:*
∇ = urban plume, 9/6/1973, NE wind;
Δ = plume of Wood River Petroleum refinery complex and sources south of it, 8/12/1974, S wind;
□ = Wood River refinery complex, 8/15/1974, SE wind;
● = Wood River refinery complex, 7/29/1975, SE wind.

Data for 7/29/75 are based on COSPEC measurements made by Environmental Measurements, Inc. All other data are based on aircraft measurements by Meteorology Research, Inc. (MRI) than 20% per hour during the first few hours of plume transport. This rapid initial depletion of SO_2 from the plumes close to the ground is presumably mostly by dry deposition to the luxuriant Missouri vegetation on summer days. For such urban-industrial plumes, the rate of formation of secondary aerosol has been observed to be slow at first and considerably faster after an aging time of 1 to 2 hours (White et al., 1976). Thus, the amount of SO_2 available for transformation in these plumes has been depleted to about 60% of the emission by the time the conversion rate becomes significant.

The mass flow rates of gaseous and particulate sulfur in the elevated plume of a modern coal-fired power plant (Labadie, 2200 MW) are shown in Figure 9. During the initial hour or two of plume transport, the effect of ground removal is small and much of the SO_2 remains airborne. During this initial period, most of the measured particulate sulfur appears to be of primary origin (directly emitted or formed in the immediate vicinity of the source). Secondary aerosol formation is slow over the first 30 km of plume transport, and significantly more rapid thereafter (Figure 9; Husar et al., 1976b; Whitby et al., 1976).

Results of the field program indicate that the model must be capable of handling source configurations corresponding to broad low-level emissions as well as elevated power-plant emissions. Furthermore, it should be capable of simulating pollutant transformation at rates variable with the age of the polluted air mass. It is also desirable that the effects of turbulent pollutant dispersion, transformation and removal be parametrized such that the various complex contributing factors are lumped into overall parameters. Such overall rate constants may be applied directly at the grid level in synoptic scale transport models currently being developed.

3. MATHEMATICAL MODEL

3.1 The Basic Equation

For the transport of a gaseous pollutant over a homogeneous flat surface under steady meteorological conditions, the principle of conservation of mass may be expressed in the following form of the eddy diffusion equation:

$$\bar{u} \frac{\partial \bar{c}}{\partial x} = \frac{\partial}{\partial y}\left(K_y \frac{\partial \bar{c}}{\partial y}\right) + \frac{\partial}{\partial z}\left(K_z \frac{\partial \bar{c}}{\partial z}\right) + R \qquad (2)$$

A horizontal wind of mean speed $\bar{u}$ in the direction of the x-coordinate is assumed. K_y and K_z denote the mass eddy exchange coefficients in the y and z directions, respectively, and R denotes pollutant sources and sinks such as the chemical transformation process. As is customary, horizontal diffusion in the direction of advection is neglected.

The applicability of steady eddy diffusion models is generally limited within certain time and length scales based on the structure of atmospheric turbulence, on wind conditions, and on the diurnal cycle of atmospheric stability. For best results, such models may be applied approximately in the range of 1 - 100 km from the source under fairly steady wind conditions and near neutral stability. All the field data reported here were collected during such quasi-steady meteorological conditions in the daytime, and within well-defined mixing layers. The eddy diffusion model is a semi-empirical formulation in that values of $\bar{u}$, K_y and K_z within the mixing region must be empirically determined, based on averaging times which are large enough to include the effect of much of the turbulent fluctuations.

Under typical daytime convective conditions over the contiguous U.S., the existence of a finite mixing layer of height H ranging upto 3 km is known to be common. As shown in Figure 3, the transition from a convectively well-mixed atmosphere to a relatively stable atmosphere at the top of the mixing layer is generally quite well-defined during midday hours. At the interface, an effective barrier to vertical mass dispersion confines pollutant transport within the mixing layer.

Within the mixing layer, characteristic vertical profiles exist for temperature, wind speed, wind direction, shear stress, heat flux, r.m.s. turbulent velocity and the scale of turbulence. Of these, the profiles of the mean temperature and wind field are well understood, but those of vertical turbulent components contributing to K_z are still under investigation. In the mesoscale study of pollutant dispersion, the vertical profile of K_z is of very significant importance in making reliable estimates of ground uptake, for example, because vertical dispersion is responsible for pollutant delivery to and from the ground. The model developed here is applicable to arbitrary vertical profiles of K_z. The following functional form of K_z is used in the model calculations:

$$K_z = K_M \cdot f(x) \cdot g(z) , \qquad (3)$$

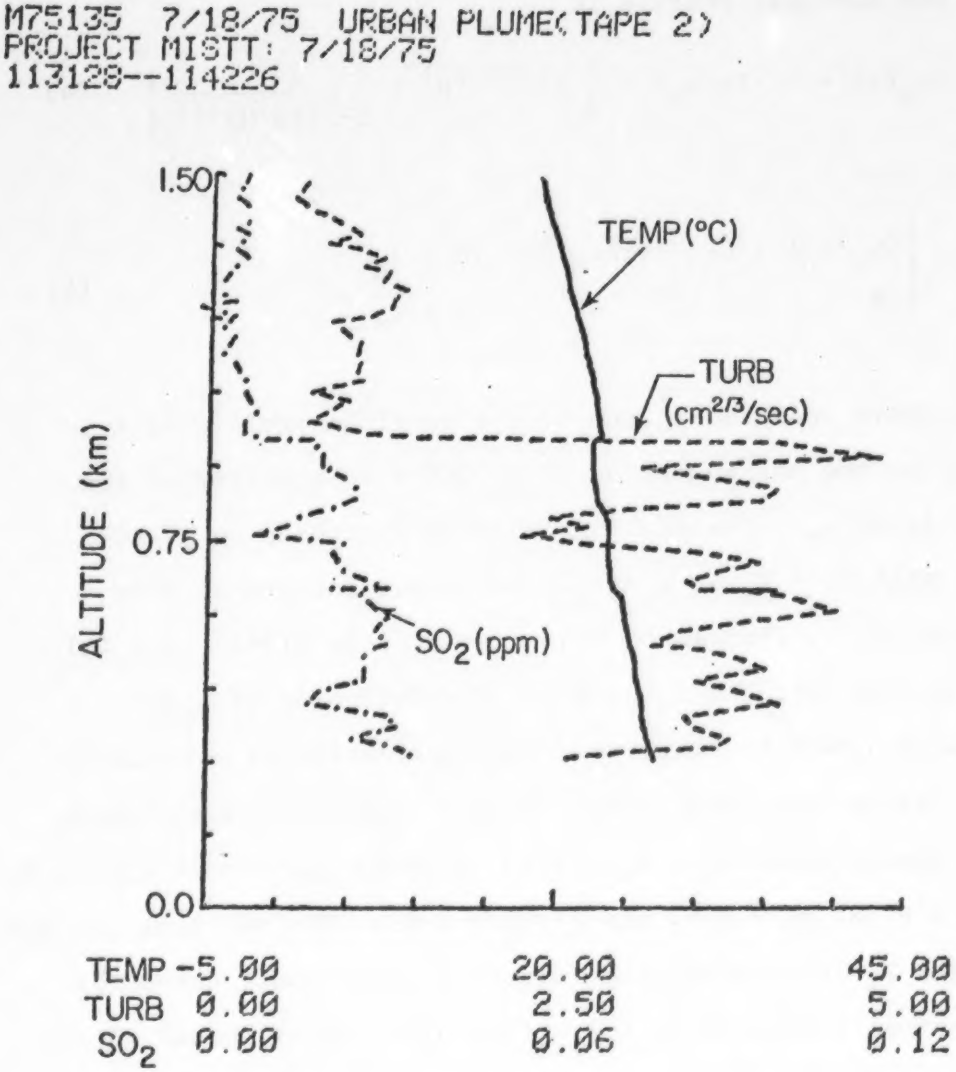

Figure 3. Typical vertical profiles in the midday mixing layer. Note the sharp decrease in turbulence at the top of the mixing layer (~ 1 km), and the associated stable temperature lapse rate (kink) and decrease in SO_2 level. Data based on aircraft measurements by MRI.

where the vertical profile is

$$g(z) = a_o(z) + b \cdot (z/z_M) \cdot \left\{ e^{1-(z/z_M)} + \frac{1}{1+16(z/H)^{1.6}} \right\}, \quad (4)$$

and

$$a_o(z) = \begin{cases} (K_o/K_M) \cdot [1 - (z/z_M)] \ , & z \leq z_M \\ 0 \ , & z \geq z_M \end{cases} \quad (5)$$

In the above analytical form of the vertical profile of K_z, K_M denotes the maximum value of K_z which is attained at the height level z_M. The scaling factor b is chosen so as to ensure that $K_z = K_M$ at $z = z_M$. The above analytical form (equation 4) is similar to that used by Shir (1973) if $a_o(z)$ is chosen as zero and z_M as H/4. The insertion of $a_o(z)$ is made in order to facilitate the application of a realistic ground removal boundary condition at a reference height close to the ground where $K_z = K_o$. g(z) is shown plotted in Figure 4, with b = 0.73, $z_M = H/4$, and $K_o/K_M = 0.01$. The vertical profile shown for K_z is also closely related to that constructed for near-neutral stability by Smith (Pasquill, 1975), based on the formula

$$K_z = (\varepsilon^{1/3} \lambda_m{}^{4/3})/15 \ , \quad (6)$$

which uses the turbulence statistics ε(turbulent energy dissipation rate) and λ_m (wavelength at which maximum energy occurs in the vertical velocity spectrum). In the laboratory simulation studies of Willis and Deardorff (1974) and the field studies of Arnold and Rowland (1976), the peak value of vertical turbulent

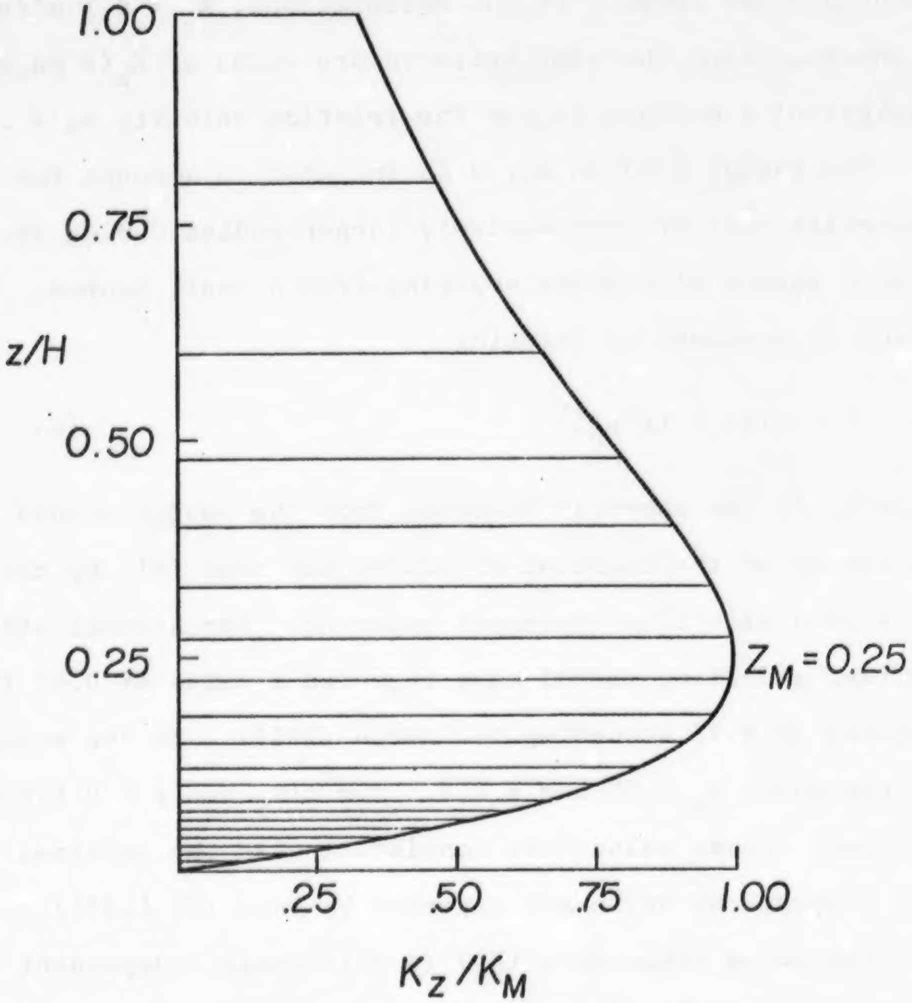

Figure 4. Height-dependence of the vertical eddy exchange coefficient, K_z, for $z_M/H = 0.25$ The lines indicate the finite difference spacing used in the model solution.

dispersion was observed to occur more nearly in the middle altitudes of the mixing layer ($z_m \sim H/2$).

The value of K_M depends on atmospheric stability. Under near-neutral conditions, values of K_M were chosen as shown in Table 1, with higher values corresponding to the stronger measured lapse rates. In the calculations, $K_o = 0.1\ m^2/sec$ is chosen, being the similarity theory value of $K_z (= \kappa u_* z)$ at a height of 1 m above ground for friction velocity $u_* = .25$ m/sec.

The factor f(x) in Eq. 3 is included to account for the dispersive role of progressively larger eddies during the initial spread of a plume emerging from a small source. This effect is achieved by choosing

$$f(x) = (x/x_r)^{\gamma} , \qquad (6)$$

where x_r is the shortest distance from the source within which the action of the spectrum of eddies has been felt by the plume, and γ is a stability-dependent exponent. For neutral stability, Islitzer and Slade (1968) have reported a value of 0.42 for γ, compared to 0.75 according to Sutton (1953). In the model calculations, $x_r = 3H$ and $\gamma = 0.5$ for $x \leq x_r$ and $\gamma = 0$ for $x > x_r$ are used. These values are consistent with the vertical spread data computed by Smith and reported by Pasquill (1975).

Crosswind dispersion (K_y) is relatively independent with height in the bulk of the mixing layer (see, for example, Pasquill, 1975). Consequently, K_y is chosen as

$$K_y = K_H \cdot (x/x_r)^{\gamma} \qquad (7)$$

where K_H is the scale of horizontal eddy diffusion. The value of K_H is chosen as 10 K_M in the model calculations. Varying the magnitude of K_H does not effect the total plume mass flow rate or the ground uptake.

Model solution is greatly simplified if the ratio $(K_y/\bar{u})$ is independent of height. Consequently, a constant wind speed is assumed in the model. Its value at each downwind section is determined by averaging the measured wind profiles over the height attained by the plume.

The rate of primary pollutant loss by transformation processes is assumed to be pseudo-first order.

Thus, $$R = -\alpha\bar{c} , \tag{8}$$

where α is an overall rate constant representing the combined effects of all factors influencing the transformation rate. In the oxidation of SO_2 to sulfates, humidity and the presence of ammonia and ozone, for example, are believed to be factors in the transformation process. Since ozone itself is a secondary pollutant whose concentration generally changes with x within the plume, it follows that α must be free to vary with plume transport time, or $\alpha = \alpha(x)$. Assuming the validity of Taylor's (1938) translation hypothesis $t \rightarrow x/\bar{u}$, where t is the transport time of a given parcel of emissions within an air mass, α may be expressed as a function of the age of the polluted air mass, i.e.

$$\alpha = \alpha(t) . \tag{9}$$

Implicit in this functional form of the overall rate parameter is the dependence of gas-to-particle conversions on the changing plume geometry and chemical composition, and the characteristics of the background air.

3.2 Boundary Conditions

The source is treated as a vertical area source, symmetric laterially about the plane y = o. Source emission may be distributed arbitrarily in the vertical direction as $\bar{c}_o(z)$ (see Figure 1). Hence

$$\int_o^H \bar{c}_o(z)\, dz = \frac{Q_o}{2b\bar{u}} \quad , \quad |y| \leq b \qquad (10)$$

where Q_o is the source emission rate, and b is the lateral half-width of the source.

In the cross-wind direction,

$$\bar{c} \rightarrow o \text{ as } y \rightarrow \pm \infty \qquad (11)$$

The vertical boundary condition at z = H is that $(\partial\bar{c}/\partial z) = 0$. For low ambient ground level concentrations of SO_2, it has been shown (Hill, 1971) that the vegetation uptake rate F is proportional to the concentration, i.e.

$$F = v_d\bar{c} \text{ at } z = z_{ref} \; ,$$

where v_d is the proportionality constant (the so-called deposition velocity), and z_{ref} is a reference height near the ground, commonly taken at 1 to 2m. Conceptually, it is more convenient to substitute $v_d = (1/r)$, where r is the total resistance to vertical mass transfer below z_{ref}. r is made up of two series resistances, viz. the aerodynamic resistance r_a, and the surface resistance r_s. It has been observed in experiments conducted under Project MISTT that in summer as well as in winter, the surface resistance accounts for about 85% of the total resistance (Dannevik et al., 1976). Since the vertical mass flux to the ground is also equal to $K_o \frac{\partial \bar{c}}{\partial z}$, it follows that the ground boundary condition is

$$K_o \frac{\partial \bar{c}}{\partial z} = v_d \bar{c} \quad \text{at} \quad z = 0 \tag{12}$$

3.3 Non-dimensionalization

Identification of the appropriate system parameters is made possible by non-dimensionalization of the model. As part of the non-dimensionalization procedure, the following mathematical transformations are applied to $\bar{c}$ and x in order to simplify the model:

$$X = \frac{\bar{c}\; e^{\int \alpha(t)dt}}{(Q_o/\bar{u}H^2)} \quad , \text{ and} \tag{13}$$

$$X = \frac{1}{Pe} \int \left(\frac{x}{x_r} \right)^{\gamma} \cdot d(x/H) \ . \tag{14}$$

In the above expressions, $t = x/\bar{u}$ is the transport time, and

$Pe = \frac{\bar{u}H}{K_M}$ is a Peclét number of turbulent mass transport.

The other dimensionless lengths are

$$Y = \frac{y}{H} \ , \ B = \frac{b}{H} \ , \text{ and } Z = \frac{z}{H} \ .$$

An additional dimensionless parameter related to the ground boundary condition is also identified as:

$Sh = \frac{v_d H}{K_o}$, a Sherwood number of turbulent surface mass transfer.

The model may now be expressed in the following simplified, dimensionless form:

$$\frac{\partial \chi}{\partial X} = \frac{K_H}{K_M} \frac{\partial^2 \chi}{\partial Y^2} + \frac{\partial}{\partial Z} \left(g(Z) \frac{\partial \chi}{\partial z} \right) ; \qquad (15)$$

$$\int_o^1 \chi_o (Z)\, dZ = \frac{1}{2B} \quad , |Y| \leq B$$

$$\chi \rightarrow 0 \text{ as } Y \rightarrow \pm \infty$$

$$\frac{\partial \chi}{\partial Z} = 0 \text{ at } Z = 1, \text{ and } \frac{\partial \chi}{\partial Z} = Sh \;.\; \chi \text{ at } Z = 0.$$

The two system parameters specifically identified in the above formulation are the Peclet and Sherwood numbers. Pe may be interpreted as a net downwind transport parameter, with $\bar{u}H$ representing an advection ventilation function of the mixing layer. A high value of Pe generally results in a higher rate of pollutant dilution. Use of the Peclet number in the co-ordinate transformation of Eq. 14 provides a convenient reduction of the downwind distance co-ordinate with respect to the prevalent meteorological conditions. The Sherwood number is a dimensionless mass transfer coefficient between the air and the ground. It is the appropriate measure of the efficiency of ground removal. In addition to Pe and Sh, it may be recalled that the quantity α appears in the dimensionless model implicitly through the transformation of Eq. 13, and governs the role of the conversion process.

The normalized airborne mass flow rate of the primary pollutant is given by:

$$\frac{Q(X)}{Q_o} = e^{-\int \alpha(t)dt} \int_0^1 \int_{-\infty}^{\infty} \chi(X,Y,Z)\ dYdZ \qquad (16)$$

3.4 Model Solution

An analytical solution of the model for the case in which K_z and χ_o are constant with height has been presented previously (Gillani & Husar, 1975). The mathematical solution of the present more general model is performed by an analytical-numerical method. First, as a result of choosing $K_y/\bar{u}$ to be independent of height, it is possible to express the solution by the following separation of variables:

$$\chi(X,Y,Z) = \eta(X,Y)\ .\ \zeta(X,Z)\ . \qquad (17)$$

$\eta(X,Y)$ may be determined analytically as

$$\eta(X,Y) = \frac{1}{4B}\left[\mathrm{erf}\left(\frac{Y+B}{2\sigma}\right) - \mathrm{erf}\left(\frac{Y-B}{2\sigma}\right)\right], \qquad (18)$$

where $\sigma = \sqrt{(K_H/K_M)\ .\ X}$

The factor $\zeta(X,Z)$ is a solution of the following two-dimensional problem:

$$\frac{\partial\zeta}{\partial X} = \frac{\partial}{\partial Z}\left(g(Z)\frac{\partial\zeta}{\partial Z}\right), \quad 0<Z<1 \qquad (19)$$

$$\frac{\partial\zeta}{\partial Z} = 0 \text{ at } Z = 1\ , \quad \frac{\partial\zeta}{\partial Z} = Sh.\zeta \text{ at } Z = 0\ .$$

The solution of (19) is performed at each X by approximating the right hand side by finite differences between N grid lines stratifying the mixing layer. Figure 4 shows the grid lines (N = 21) of the non-uniform mesh used in the solution of pollutant dispersion from a source near ground level. The finite difference equations at the grid nodes along the vertical plane at a given X are obtained as:

$$\frac{\partial \zeta_1}{\partial X} = \frac{2}{Z_2 - Z_1} \left[g_{1+1/2} \frac{\zeta_2 - \zeta_1}{Z_2 - Z_1} - g_1 . Sh . \zeta_1 \right] \text{ at } Z = Z_1 = 0$$

$$\frac{\partial \zeta_i}{\partial X} = \frac{2}{Z_{i+1} - Z_{i-1}} \left[g_{i+1/2} \frac{\zeta_{i+1} - \zeta_i}{Z_{i+1} - Z_i} - g_{i-1/2} \frac{\zeta_i - \zeta_{i-1}}{Z_i - Z_{i-1}} \right], \; i = 2, 3, .. (N-1)$$

$$\frac{\partial \zeta_N}{\partial X} = \frac{2}{Z_N - Z_{N-1}} \left[- g_{N-1/2} \frac{\zeta_N - \zeta_{N-1}}{Z_N - Z_{N-1}} \right] \text{ at } Z = Z_N = 1 .$$

In the above equations, the subscript i refers to the value of the variable at the node of the i th grid line above the ground. i = 1 corresponds to Z = 0, and i = N to the top of the mixing layer at Z = 1. The subscript i + 1/2 refers to the value of the variable at the mid point between nodes i and i + 1. The equations for i = 1 and i = N include the boundary conditions at the ground and the mixing layer top, respectively. The above set of N simultaneous first-order differential equations at each X are integrated numerically by means of Hammings modified predictor-corrector method (Ralston & Wilf, 1960) using the subprogram DHPCL, which is part of the IBM-supplied Scientific Subroutine Package. All computations and graphics are performed on a PDP-11/40 minicomputer system. For greater accuracy, a finer grid spacing must be used, possibly requiring the use of a larger and faster computer.

4. MODEL RESULTS AND COMPARISON WITH DATA

The main objective of the data analysis is to compare the observed change in the mass flow rates of gaseous and particulate sulfur with model calculations in order to extract those values of the transformation and removal rate parameters which provide the best fit. In order to perform such a mass balance of the sulfur compounds in the plume, the change of Q/Q_o for SO_2 with increasing dimensionless distance X for given transformation rates α , and given values of the ground removal rate parameter Sh, was investigated. We wish to re-emphasize at this point that it is the Sherwood number ($Sh=v_d H/K_o$) which determines the overall ground removal rate from a plume rather than the deposition velocity v_d by itself. Both the experimental program and the model development have been conducted with the goal of estimating such overall removal rate parameters which can be used in long range transport models. Following the determination of Sh from the comparison of model and measured data, the value of v_d may be obtained if H and K_o are known. Thus, in general, the accuracy of inferred values of v_d is less than that of Sh itself.

Model calculations of χ and Q/Q_o were performed using the analytical expression of K_z(equation 4) with $Z_M=0.25$, for two different source configurations - a broad diffuse source near ground, and an elevated power-plant source. The ground source provides the proper conditions for investigating the practical range of Sh, because the conversion process is slow in the initial stages of plume transport (White et al., 1976), and in the absence of rain, dry deposition is believed to be the predominant mode of scavenging of SO_2 from plumes emitted from large sources close to the ground (Bolin & Persson, 1974). Figure 5 shows a plot of calculated Q/Q_o versus X for Sh values ranging between 50 and 500, and $\alpha = 0$. The source is chosen such that the effective emission distribution is uniform from $Z = 0$ to $Z = 0.02$, and then falls off linearly to zero at $Z = 0.06$. For $H = 1000m$, for example, half of the emission of SO_2 from such a source is uniformly distributed over the lowest 20m above ground, and the other half comes from effective heights between 20 and 60m. Such a distribution of emissions is typical for an urban area or a large petroleum refinery complex. Varying the width of the source has effect on the dimensionless concentration χ but not on Q/Q_o. Source widths of 20 km for the St. Louis urban area, and 1 km for the Wood River petroleum refinery complex in Alton, Illinois, just to the northeast of St. Louis, are used.

The critical role of Sh in governing the rate of surface removal for emissions from such a near-ground source is evident. The removal rate is greater for larger values of Sh, and SO_2 depletion is particularly rapid close to the source. The experimental points shown in Figure 5 are the same data presented in Figure 2. Table 1 gives more detailed information concerning measured inputs to the model. From measured values of $\bar{u}$ and H, and values of K_M assumed as shown, values of Pe, and hence of X, are obtained. The measured values of the airborne SO_2 mass flow rates are also listed in Table 1. By comparing each data point with the corresponding model curves, the applicable value of Sh is inferred, as shown in Table 1.

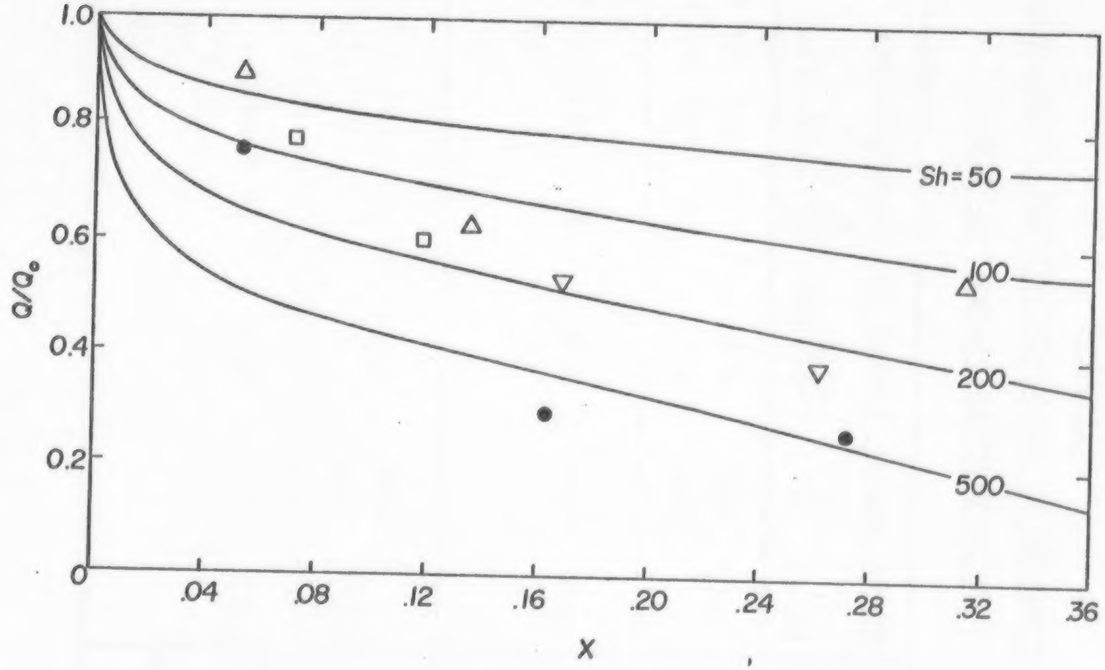

Figure 5. Role of Sherwood number, $Sh = v_d H/K_o$, in the ground removal of SO_2 emission from a source near ground level. $\hat{X}$ is the dimensionless downwind co-ordinate. Experimental data (same as in Figure 2) are for mass flow rates of SO_2 in St. Louis urban-industrial plumes.

TABLE 1

COMPARISON OF URBAN-INDUSTRIAL PLUME DATA WITH DISPERSION-REMOVAL MODEL

Plume Identification	Method of Measurements	Model Inputs (Based on Measurements)								Values Derived From Model Comparison	
		$\bar{U}$ (m/s)	H (m)	$-\Delta T/\Delta z$ (°C/100M)	K_M (m^2/s)	Pe	x (km)	X	Q/Q_o	Sh	V_d (cm/s)
Urban Plume 9/6/73	Aircraft Sampling	3.0	900	0.8	12	225	35	0.168	0.53	190	2.1
			1000	1.0	16	188	50	0.261	0.38	260	2.6
Wood River Refinery Complex and sources south of it 8/12/74	Aircraft Sampling	4.3	700	0.9	14	215	9	0.055	0.90	40	0.6
							21	0.135	0.63	140	2.0
							48	0.314	0.54	110	1.6
Wood River Refinery Complex 8/15/74	Aircraft Sampling	4.5	600	0.9	14	193	9	0.072	0.78	80	1.0
			800			257	25	0.118	0.60	170	2.1
Wood River Refinery Complex 7/29/74	Correlation Spectrometer in Mobile Ground Van	6.0	750	1.0	16	281	12	0.053	0.76	105	1.4
							35	0.163	0.29	570	7.6
							58	0.272	0.26	460	6.1
							100	0.471	0.19	290	3.8

Values of Sh for the aircraft data range between 40 and 260, with the highest values corresponding to slowest transport speed ($\bar{u}$ = 3 m/sec). For K_o = 0.1 m^2/sec, the corresponding values of v_d range between 0.6 and 2.6 cm/sec. These values of v_d are in general agreement with values reported elsewhere (Hill, 1971; Owers & Powell, 1974). A much more rapid removal rate is implied by the COSPEC data. An important feature of Figure 5 with respect to data interpretation is that data collected at different times under widely varying environmental conditions can be directly plotted and compared on the same graph. This is owing to the fact that the meteorological variables are included in the dimensionless distance X, and that Sh is an overall ground removal parameter including the effects of pollutant diffusion to the ground as well as the surface sorption characteristics.

Figure 6 shows sample results of model calculations of χ for a low level source such as the Wood River petroleum refinery complex. The dimensionless concentration isopleths and vertical profiles within the mixing layer corresponding to realistic values of Pe(= 500) and Sh(= 200) show clearly the error which would be made by box model assumptions in a mesoscale range. The role of finite, height-dependent vertical mixing is to introduce a surface layer of relatively high resistance to vertical mass transfer between the bulk mixing layer and the ground. The resulting impedance to pollutant delivery to or from the ground has an important effect on pollutant removal as well as transformation. For ground level emissions, the surface layer impedance has the effect of maintaining ground concentration at a high level for

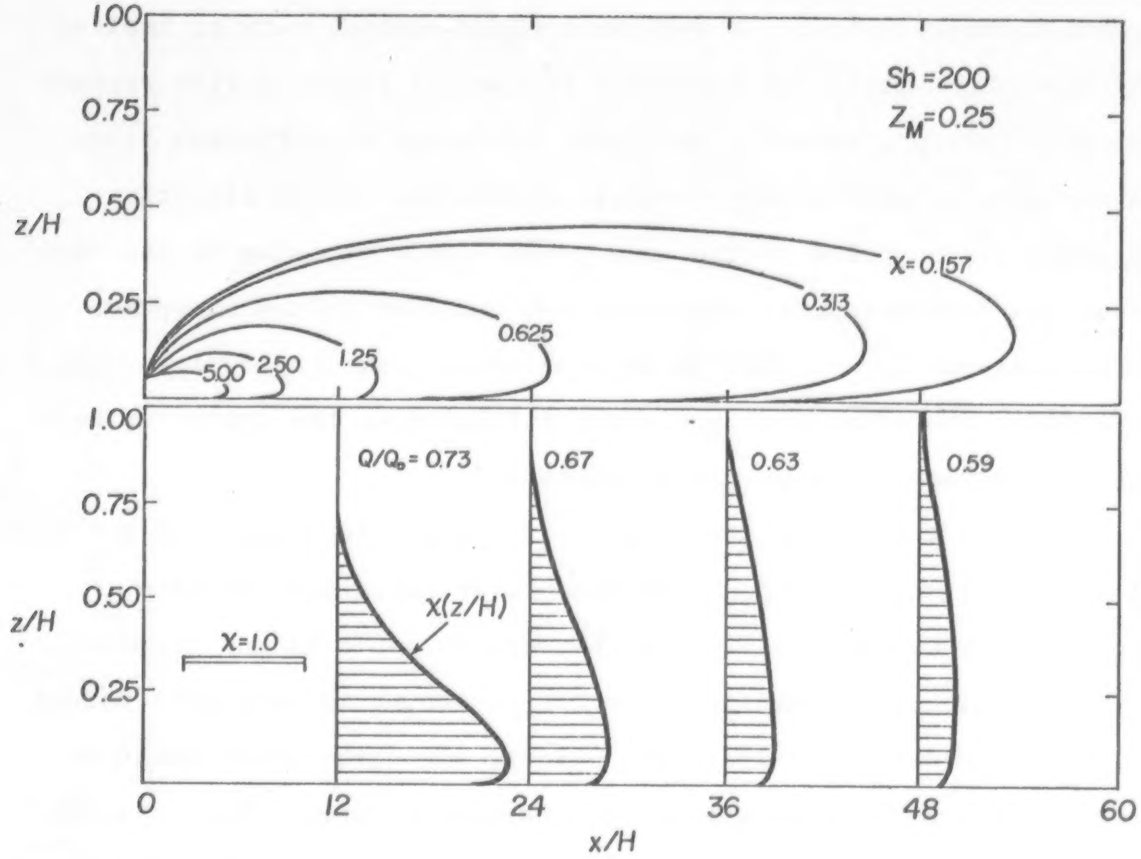

Figure 6. Dimensionless concentration isopleths and vertical profiles of SO_2 for ground source.

relatively long downwind distances. As a result, ground uptake is quite rapid and the amount of SO_2 available for conversion to aerosol is greatly reduced. For elevated emissions, the surface layer impedance retards pollutant delivery to the ground, and surface uptake is slow. Consequently, pollutant residence in the air is longer than in the case of a box model, and the amount of sulfate formation is greater.

The vertical dispersion shown in Figure 6 is based on the modified Shir model for K_z used in the calculations. Field observations under meteorological conditions corresponding to values of Pe = 500 generally reveal a more rapid vertical mixing of the pollutant within the mixing layer. Consequently, calculations were also made using $Z_M = 0.5$ in the expression of K_z. The resulting vertical profile of K_z is shown in Figure 7, and the corresponding concentration isopleths for the ground source are shown in Figure 8. This new K_z profile shows slightly lower values of K_z in the lower levels, but substantially higher values in the upper levels of the mixing layer. As a result, the vertical dispersion is even slower in the first 30-50 km, but once the pollutant reaches the middle levels of the mixing layer, it is carried upwards much more rapidly than in the previous case, and the plume becomes well-mixed throughout the mixing layer in a shorter net distance.

Measured and calculated mass flow rates of sulfur compounds in the plume of a modern coal-fired power plant (Labadie, stack height approximately 200m) are shown in Figure 9. The flow rates are normalized with respect to the emission rate of total sulfur, $(Q_o)_{TS}$. Measured data show that SO_2 depletion from the plume

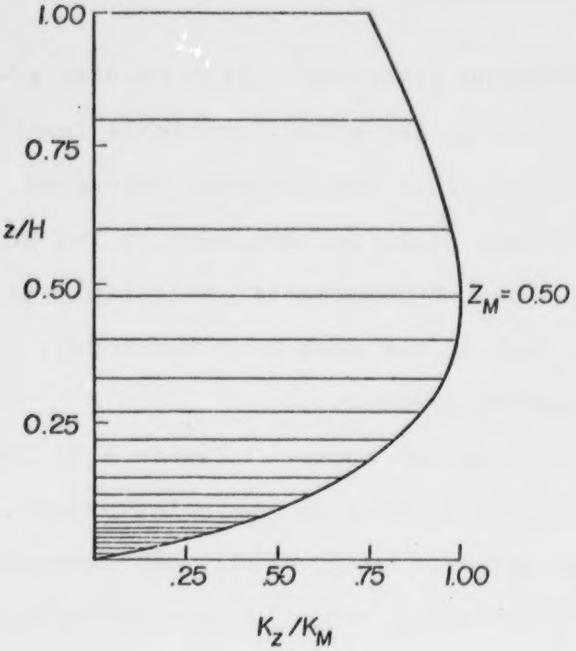

Figure 7. Vertical profile of K_z/K_M for $z_M/H = 0.50$.

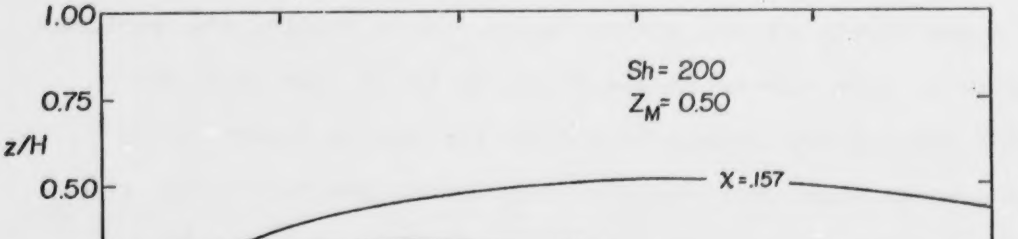

Figure 8. Dimensionless concentration isopleths of SO_2 for a ground source, with K_z based on $z_M/H = 0.50$.

in 50 km is slow compared to that observed in the urban-industrial plumes. This is owing to the absence of ground removal before plume touchdown on the ground. Measured flow rates of particulate sulfur indicate the conversion of about 7% of sulfur from gaseous to aerosol phase in about 3 hours of transport at a relative humidity of about 70%. Most of this conversion took place in the last hour. Model calculations were performed for an effective stack height of 300m (= 0.3H), with Pe=500 based on observed values of the meteorological quantities, and Sh=200 based on the results of ground removal from the urban-industrial plumes. The choice of the conversion rate $\alpha(t)$ used in the model and shown in the lower portion of Figure 9(b), was made to match the observed amount of particulate sulfur formation with the amount of SO_2 conversion according to the model. The sharp increase of particulate sulfur level during the third hour of transport is corroborated by the observed increase of the aerosol concentration in the 0.1 to 1.0 μm subrange (Whitby et al., 1976), of the light scattering coefficient, and of aerosol charge content (Husar et al., 1976b).

5. SUMMARY AND CONCLUSIONS

A three-dimensional mesoscale eddy diffusion model incorporating the effects of primary pollutant transformation as well as ground removal is developed. The transformation rate is allowed to be dependent on the age of the polluted air mass. Ground removal is described in terms of an overall removal rate parameter, the dimensionless Sherwood number. A meteorological transport parameter, the dimensionless Peclet number, is also identified.

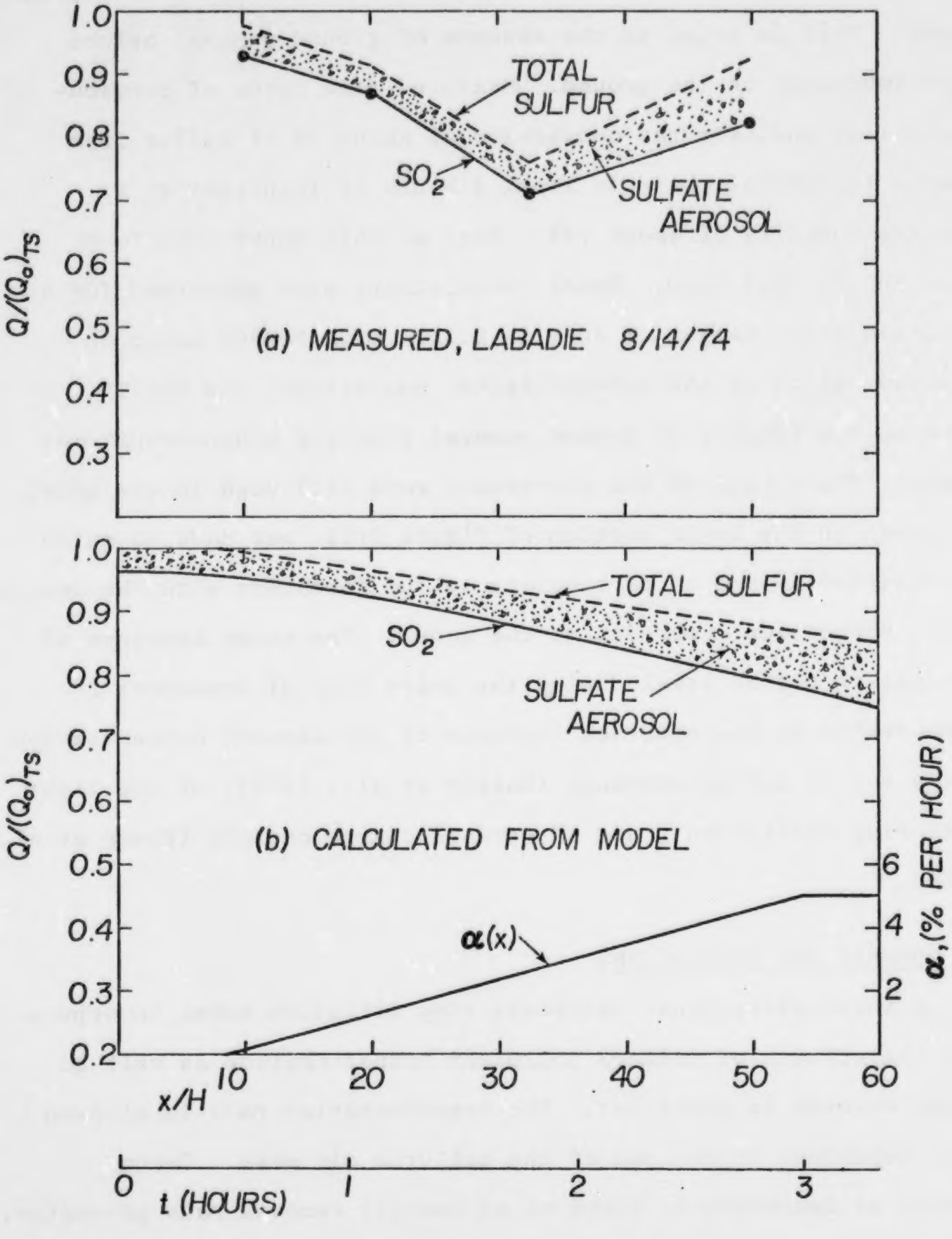

Figure 9. Mass flow rates of gaseous and particulate sulfur as fractions of total sulfur emission $(Q_o)_{TS}$ for the Labadie power plant plume on 8/14/1974. Data based on aircraft measurements by MRI.

Vertical eddy diffusion within the confines of a mixing layer is modeled as a height-dependent phenomenon. Results of plume mapping experiments conducted as part of EPA's Project MISTT are presented in the reduced form of mass flow rates of SO_2 as well as particulate sulfur. Field data are compared with model calculations to extract estimates of overall SO_2 ground removal rates from broad urban-industrial plumes originating near ground level, and of SO_2-to-sulfate conversion rates in an elevated power plant plume.

The comparison of model results and aircraft data from St. Louis shows that ground removal from plumes of near-ground emissions is initially quite rapid and corresponds to values of Sherwood number, $Sh=v_dH/K_o$, ranging between 40 and 260 on summer days. In the elevated plume, ground removal is less important up to 50 km, and the rate of SO_2 conversion to sulfate aerosol depends on the age of the polluted air mass. The transformation rate rose to about 5% per hour after three hours of transport time from a much slower initial rate.

A net effect of the dispersion, transformation and ground removal parameters is that the mesoscale fate of atmospheric pollutants with pseudo-first order gas-to-particle conversions is such that more of the primary emissions as well as their secondary products become available for long range transport in the case of elevated power-plant sources than for broad, low-level area sources.

ACKNOWLEDGEMENT

The work reported here was conducted as part of Project MISTT sponsored under EPA Grant No. 803896. We wish to thank all other participants of the program, especially W.E. wilson for his direction.

REFERENCES

Arnold, A. and J.R. Rowland, 1976: Fine scale observations of free convection in the atmospheric boundary layer. Preprint, Third Symposium Atmospheric Turbulence, Diffusion and Air Quality, Raleigh, N.C. (October).

Bolin, B. and C. Persson, 1974: Regional dispersion and deposition of atmospheric pollutants. Tech. Rept. AC-28, Dept. of Meteorology, Univ. of Stockholm.

Breeding, R.J. et al., 1975: The urban plume as seen at 80 and 120 km by five different sensors. J. Appl. Meteor. 14, 204-216.

Dannevik, W.P. et al., 1976: SO_2 deposition measurements in the St. Louis region. Third Symp. on Atm. Turb., Diff. and Air Quality, Raleigh, N.C. (October).

Hill, A.C., 1971: Vegetation: A sink for atmospheric pollutants. J.A.P.C.A. 21 (6), 341.

Gillani, N.V. and R.B. Husar, 1975: Mathematical modeling of air pollution: A parametric study. Proc. 2nd Federal Conf. on the Great Lakes, Argonne, Illinois. (March).

Husar, R.B. et al., 1976a: Pollutant flow rate measurement in large plumes: sulfur budget in power plant and area source plumes in the St. Louis region. Proc. 171st National ACS Meeting, Div. Environ. Chem., New York. (April).

———1976b: Particulate sulfur formation in power plant, urban and regional plumes. Symp. Aerosol Sci. & Tech., 82nd National Meeting of AIChE, Atlantic City, N.J. (Sept.)

Islitzer, N.F. and D.H. Slade, 1968: Meteorology and Atomic Energy, Ch. 4.

Owers, M.J. and A.W. Powell, 1974: Deposition velocity of SO_2 on land and water surfaces. Atmos. Environ. 8: 63.

Pasquill, F., 1975: Ch. 1 in Lectures on Air Pollution and Environmental Impact Analyses, AMS.

Ralston, A. and H.S. Wilf, 1960: Mathematical Methods for Digital Computers, Wiley, N.Y., 95-109.

Shir, C.C., 1973: A preliminary numerical study of atmospheric turbulent flows. J. Atmos. Sci. 30, 1327-1338.

Smith, F.B. and G.H. Jeffrey, 1975: Airborne transport of SO_2 from the U.K., Atmos. Environ. 9, 643-659.

Sutton, O.G., 1953: Micrometeorology, McGraw-Hill, N.Y.

Taylor, G.I., 1938: The spectrum of turbulence. Proc. Roy. Soc., A164, 476-490.

White, W.H. et al., April 1976: Formation of ozone and light scattering aerosols in the St. Louis urban plume. Proc. 171st National ACS Meeting, New York.

Whitby, K.T. et al., 1976: Aerosol formation in a coal-fired power plant plume. Proc. 171st National ACS Meeting, Div. Environ. Chem., New York.

Willis, G.E. and J.W. Deardorff, 1974: A laboratory model of unstable planetary boundary layer. J. Atmos. Sci., 31, 1297-1307.

7th International Technical Meeting on
Air Pollution Modeling and its Application

NATO/CCMS

A Study of Long Range Transport from Visibility Observations, Trajectory Analysis and Local Air Pollution Monitoring Data

R. B. Husar, N. V. Gillani,
J. D. Husar and D. E. Patterson
Air Pollution Research Laboratory
Department of Mechanical Engineering
Washington University
St. Louis, Missouri 63130

September 7 - 10, 1976
Airlie, Virginia
United States of America

INTRODUCTION

In recent years, the recognition of long range transport of air pollution in the U.S. has led to an increasing level of activity in modeling the atmospheric transport and fate of pollutants on the macroscale. It is extremely difficult to understand events on this scale. There are complex interactions between the synoptic air flow and the dynamic boundary layer within which pollutants are emitted from many widely-dispersed sources at different height levels. Little is known about the changing distribution of pollutants on this scale. Satellite studies have revealed the existence of haziness on the scale of an entire synoptic air mass (Lyons, 1975), and the suspended particulate content of such hazy air masses has been observed to be substantially greater than longer-term averages at given locations (Hall et al., 1973).

Long range transport can lead to an exposure of large receptor areas to polluted hazy air masses, whose major constituents are secondary pollutants such as ozone and light scattering aerosols (White et al., 1976). When the secondary products of emissions from many sources accumulate in a given air mass during a stagnant synoptic meteorological condition, large hazy 'blobs'* may develop. The spatial and temporal scales and pollutant variability within such air masses are not known, mainly because of the lack of suitable large-scale air quality network data. An attractive qualitative surrogate for fine particulate pollution data in studying the spatial extent and temporal behavior of large hazy air masses in the U.S. is the surface visibility observation data collected by the National Weather Service network of monitoring stations. In this paper, we report a case study of an air pollution episode over the eastern half of the U.S. which lasted nearly two weeks during June, July 1975. The method of analysis is based principally on inspection of computer plots of the national visibility data, of hand-plots of the sparser ozone and sulfate aerosol data in the eastern U.S., of synoptic weather maps, and of computed air parcel trajectories. In addition, local measurements of air pollution parameters in St. Louis and other cities are also used.

---

*According to The Random House Dictionary, Random House, New York (1966) "blob - an object, esp. a large one, having no distinct shape or definition". In the context of this report, "blob" is used synonymously with "hazy air mass".

DATA BASE FOR THE ANALYSIS

The following three sources of data have been utilized in this work.

(a) U.S. Weather Service network (Service A):

Values of ground level visual range, surface wind and other weather parameters are recorded every hour at several hundred stations distributed over the U.S. The data from about 300 of these stations (Fig. 1a) are available on magnetic tapes supplied by the National Climatic Center, NOAA. The high spatial density of this network permits the meaningful use of computer contour plotting techniques. Using the visibility data, the spatial extent, the temporal evolution and the transport of hazy 'blobs' may be followed for several days by inspection of chronological

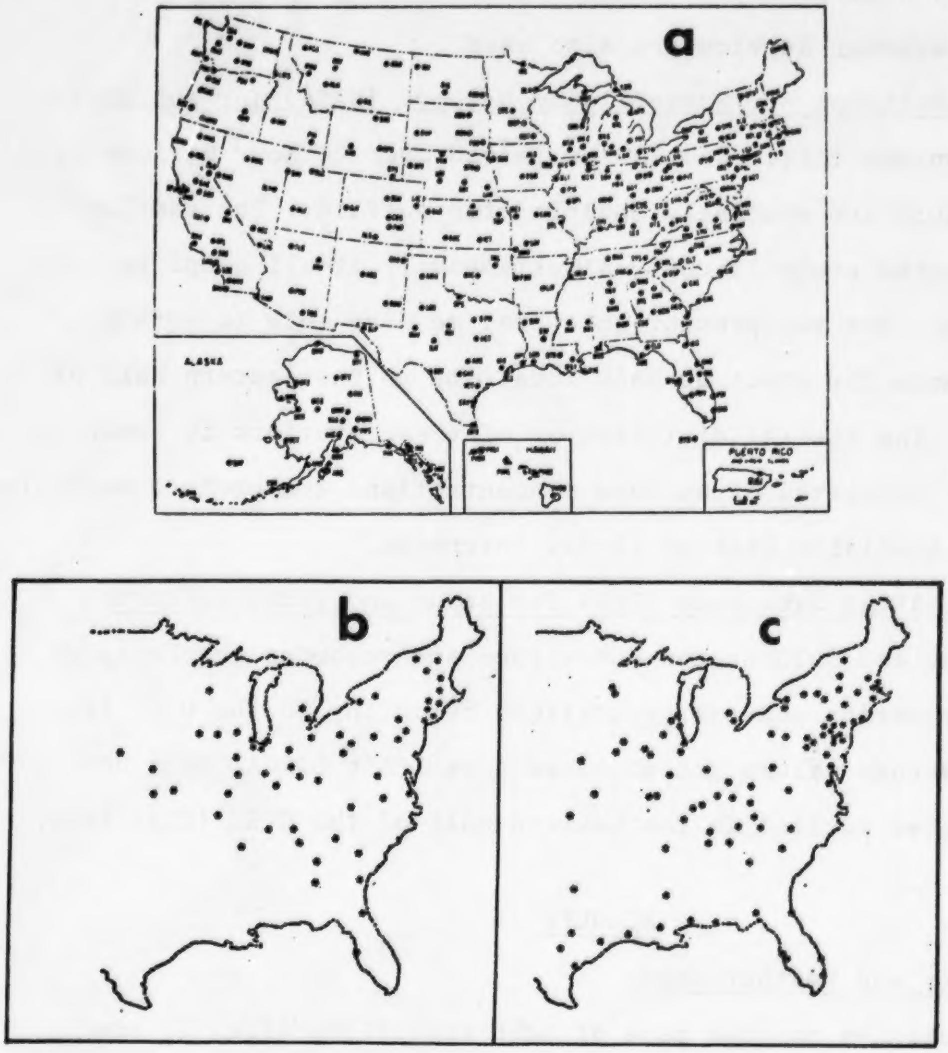
a
ALASKA
HAWAII
PUERTO RICO
b
c

Figure 1. Geographical distribution and density of network stations where data utilized in this paper were recorded: a) National Weather Service Network for visibility; b) National Air Surveillance Network for sulfate; c) EPA/SAROAD network for ozone.

visibility contour maps. Daily weather maps prepared by the National Weather Service are also used.

(b) The National Air Surveillance Network (NASN) for sulfate:

Hi-volume filter samples collected over 24 hour periods by this network are routinely analyzed for sulfate. The samples are collected every 12 days, simultaneously at all sampling locations. For the present analysis, we were able to obtain sulfate data for about 60 NASN locations in the eastern half of the U.S. The spatial distribution of these stations is shown in Fig. 1b. Isopleths of sulfate concentrations are plotted manually from the available data at 12-day intervals.

(c) The SAROAD data base (EPA) for ozone and total oxidant:

Ozone and oxidant concentrations are recorded regularly at local aerometric monitoring stations reporting to the U.S. EPA. Hourly average values are obtained from EPA's SAROAD data bank for 89 sites located in the eastern half of the U.S. (Fig. 1c).

RESULTS

Visibility and Weather Maps:

Successive contour maps of noon visibility (Fig. 2) are plotted for every second day from June 25 through July 5, 1975. Noon visibilities were chosen to minimize the effect of the early morning ground fog on the visibility contours. For inland stations, the noon relative humidity ranged between 50% and 80%. The visibilities used have not been corrected for relative humidity effects. The different shaded regions in the figure correspond to different observed visual ranges V(m), or equivalently, to different levels of light extinction coefficient $b_{ext}(m^{-1})$. The two quantities are related by (Middleton, 1952):

$$b_{ext} = \frac{3.912}{V} .$$

Inspection of the sequence of maps reveals that multi-state regions are covered with a haze layer in which the noon visibility is less than 10 km ($b_{ext} \gtrsim 4 \times 10^{-4} m^{-1}$). From long-range air parcel trajectory calculations and surface wind information, it was determined that the air mass of June 25, within which the visibility was less than 10 km, was of maritime origin in the Gulf of Mexico. This air mass had been transported in a northerly flow across Louisiana, Arkansas, Illinois and Indiana. Between June 25 and 27, a NNE trajectory prevailed in the southern states, but relative stagnation prevailed in the Great Lakes region. In the region of stagnation, the air mass became increasingly hazy, presumably as a result of accumulating pollution from this high-emission-density region of northeastern U.S.

The daily weather maps for the period June 29 through July 4, 1975 are shown in Fig. 3. A major feature of the weather system during that period was the tropical storm "Amy", moving up off the nortneast coast. By its presence, the tropical storm provided a barrier against large scale eastward motion. From the northwest, a front was approaching the Great Lakes. Between June 28 and 30, as the storm advanced north, an easterly flow developed inland, causing the hazy air mass to drift slowly westward, passing over St. Louis, MO on June 28-29, and continuing across Missouri and Kansas (June 30). Midday visibilities over eastern Missouri deteriorated to about 4 km at the peak of the

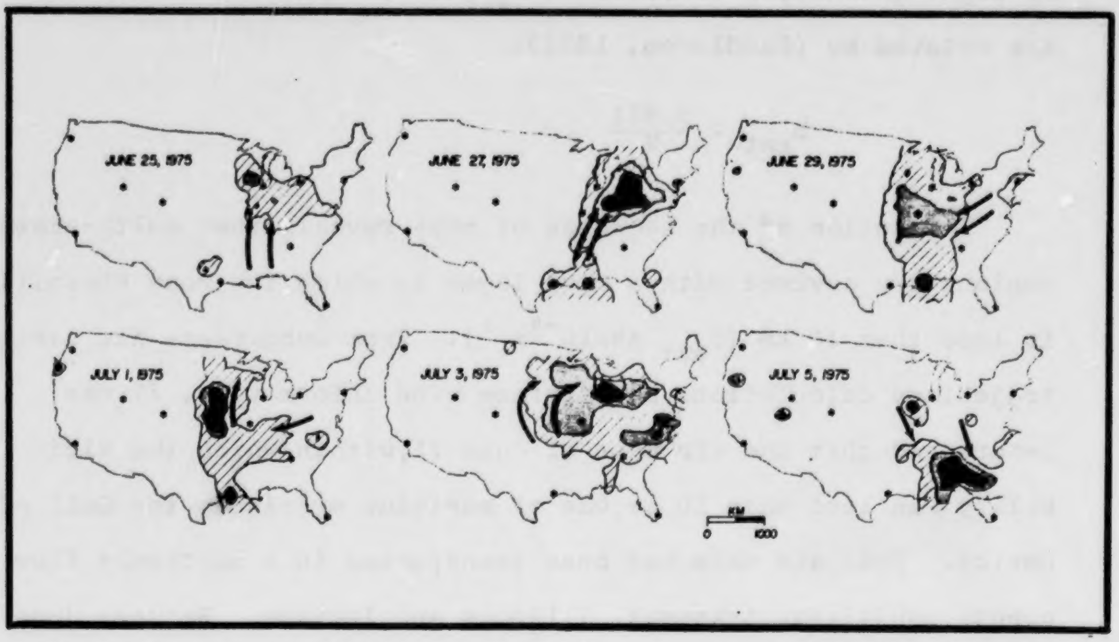
JUNE 25, 1975
JUNE 27, 1975
JUNE 29, 1975
JULY 1, 1975
JULY 3, 1975
JULY 5, 1975
KM
0
1000

Figure 2. Sequential contour plots of noon visibility at ground level for the period June 25 to July 5, 1975. Contours are for b_{ext} = 4,6,8($10^{-4}m^{-1}$), corresponding to approximate visual ranges of 6.5-10 km (light shade), 5-6.5 km (medium shade), and <5 km (black).

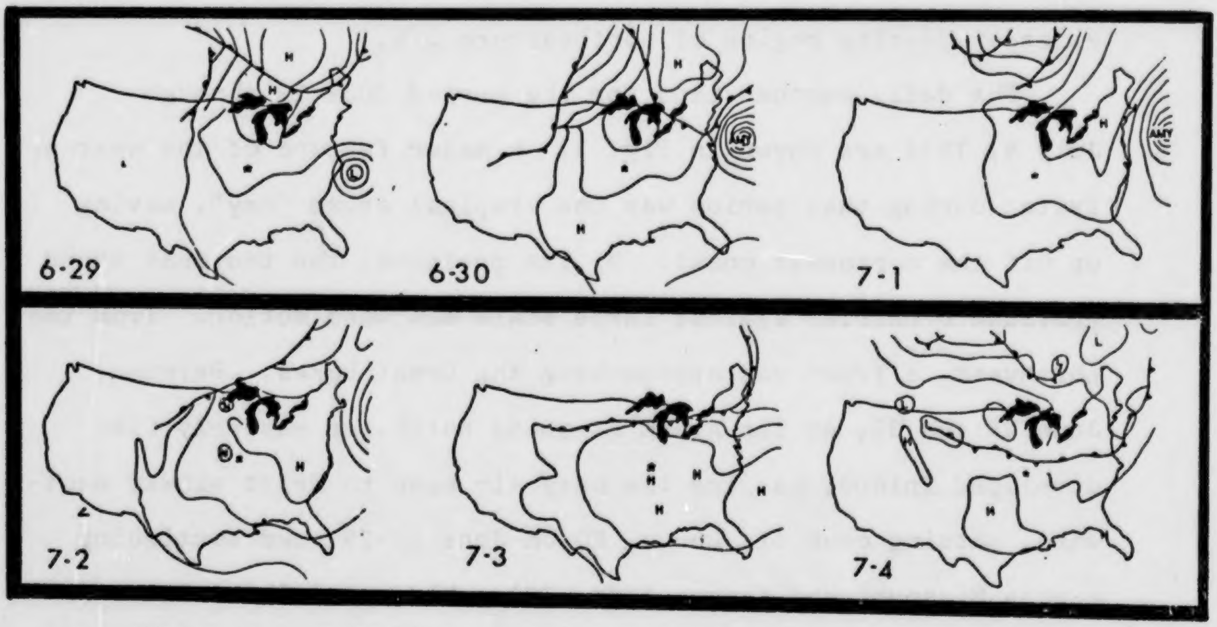
H
L
AMY
6-29
6-30
7-1
7-2
7-3
7-4

Figure 3. Daily U.S. weather maps, June 29 - July 4, 1975.

episode. Weather satellite pictures of the area on June 30 revealed the presence of the hazy air mass in the same region as that obtained by visibility contour plotting (Lyons and Husar, 1976). The surface wind pattern at noon (1700 GMT) of June 30 is shown in Figure 4. Observe the clockwise circulation associated with the high pressure region below the front. From June 30 to July 2, the hazy air mass moved in this circulating wind pattern up and around to the southern Great Lakes region. In the meantime, pollutant emissions continued into this high pressure region. By July 3, the Canadian front had itself reached the southern Great Lakes, and it formed the northern border of a massive hazy blob occupying most of midwestern and northeastern U.S. Once again, the visibility deteriorated to about 4 km near St. Louis, MO. In the next two days, the cold front rapidly advanced southward, passing over St. Louis on July 4 and continuing on. As the front advanced, the hazy blob was pushed ahead of it. By July 5, the blob was in southeastern U.S., and the visibility was less than 6 km over Atlanta, GA, Birmingham, AL, and Tallahassee, FL. The long range motion of the hazy air parcel from the Great Lakes to southeastern U.S. between July 3 and 5 was confirmed by air trajectory analysis.

Sulfate and Ozone Maps:

There exists a strong correlation between aerosol mass concentration in the size range of 0.1 to 1 μm diameter and the extinction of light by scattering (Charlson, 1969; Hidy et al., 1974). Furthermore, measurements in and near St. Louis, MO have shown that sulfates often account for 50% or more of the aerosol mass in this size range (Charlson et al., 1974). The significance of the use of visibility data as a surrogate for atmospheric pollution may thus be checked by direct comparison of the visibility maps with corresponding maps for sulfate. NASN sulfate data were available for June 23 and July 5, 1975. These are shown plotted in Figure 5 in the form of contours over the eastern half of the U.S. The contours are hand-plotted because the density of data points was judged too sparse to justify computer plots. Direct comparison of visibility and sulfate maps for the two days clearly shows a substantial positive correlation between the two. Sulfate concentrations in excess of 30 $\mu g/m^3$ are seen to coincide with regions of lowest visibility.

During the period considered in the present case study, insolation was generally above seasonal norms. Under similar conditions, high rural ozone levels have been observed in conjunction with high concentrations of light scattering aerosols (White et al., 1976). In order to examine the correlation between ozone and visibility reduction on a synoptic scale, contour plots were also prepared (by hand) for ozone for the period June 25 through July 5, 1975 (Figure 6). Ozone values shown are daily maximum levels which are attained in the early afternoon. The plots show that the U.S. standard concentration for ozone (0.08 ppm) was exceeded over large areas of the eastern U.S. on all days of the air pollution episode. Comparison of the maps for visibility and ozone (Figures 2 and 6, respectively) reveals that the geographical location of high ozone concentrations roughly corresponds to the areas of low visibility (and high sulfate). As may be anticipated, however, the correlation with

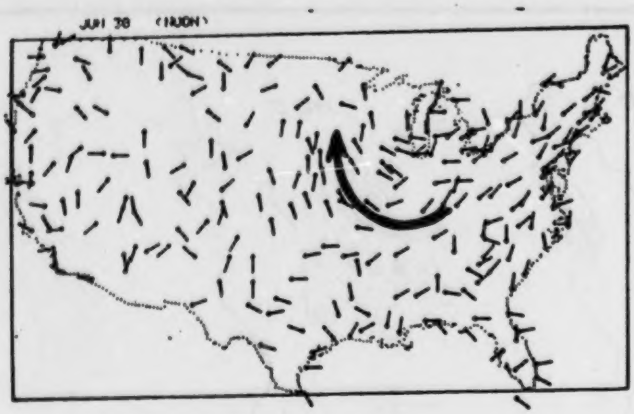

Figure 4. Surface wind directions at National Weather Service stations for 1700 GMT, June 30, 1975.

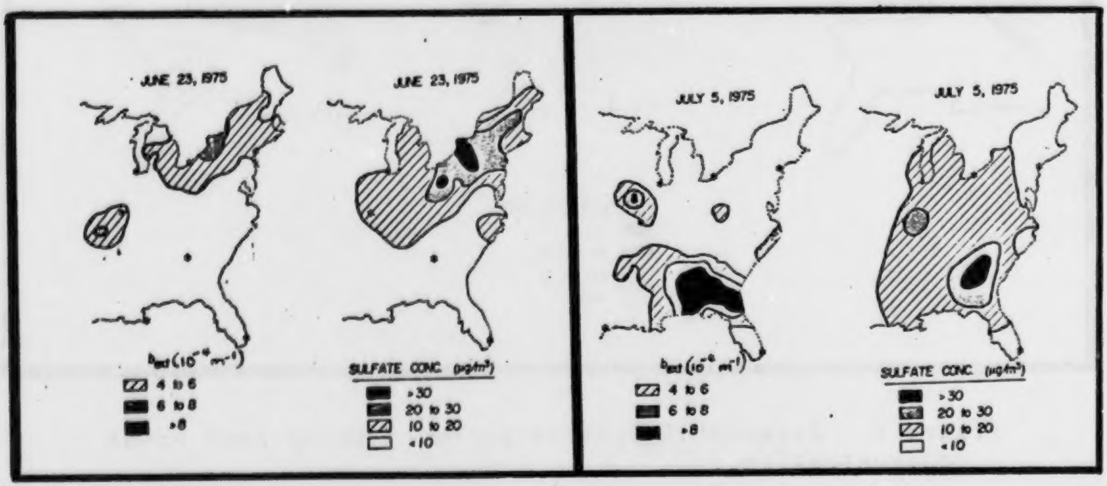
JUNE 23, 1975
JUNE 23, 1975
JULY 5, 1975
JULY 5, 1975
b_ext (10^-4 m^-1)
4 to 6
6 to 8
>8
SULFATE CONC. (μg/m³)
>30
20 to 30
10 to 20
<10

Figure 5, Comparison of contour plots of noon visibility reduction (b_{ext}, $10^{-4}m^{-1}$) and sulfate concentration for 6/23 and 7/5/1975.

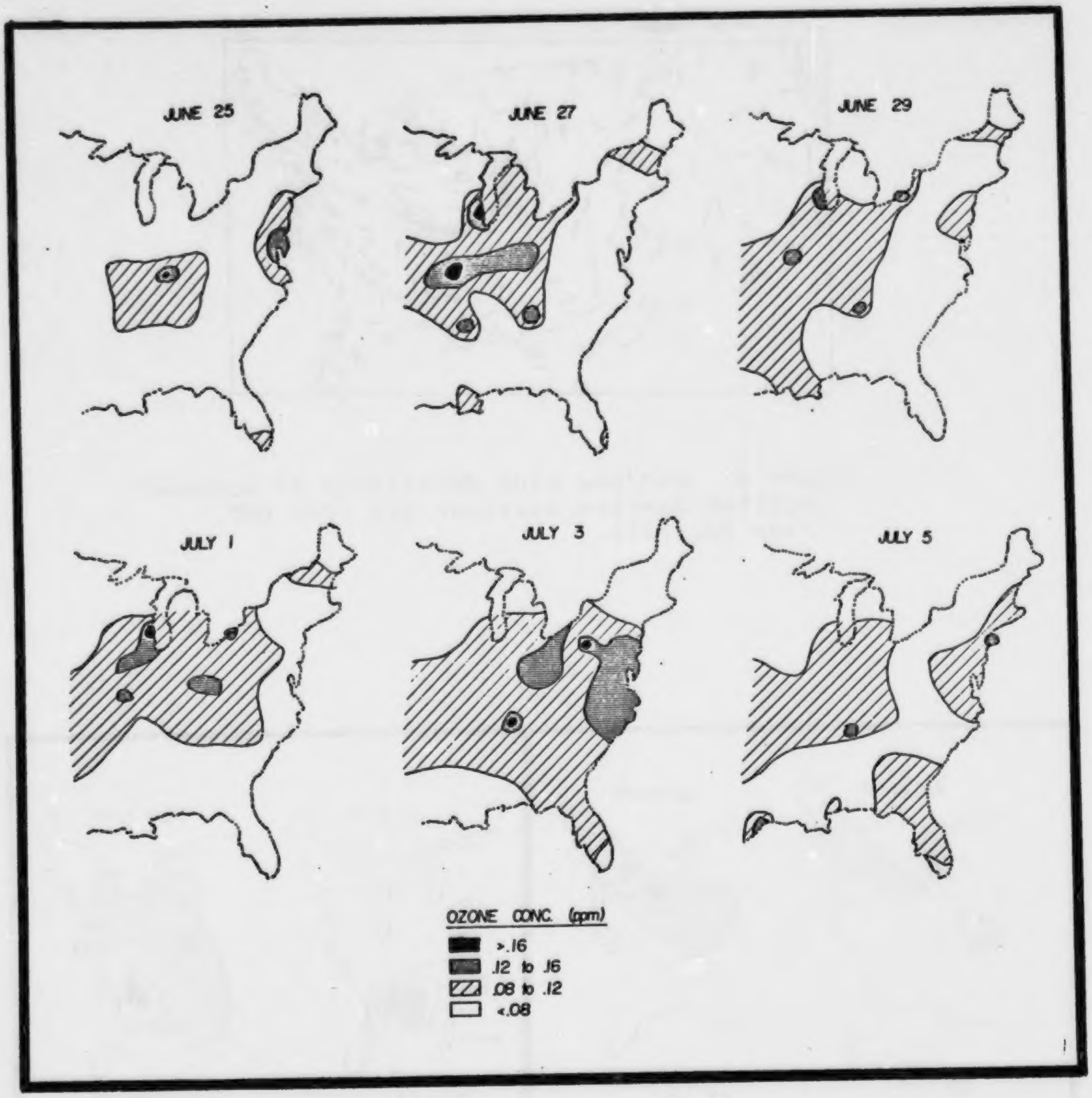
JUNE 25
JUNE 27
JUNE 29
JULY 1
JULY 3
JULY 5
OZONE CONC. (ppm)
>.16
.12 to .16
.08 to .12
<.08

Figure 6. Sequential contour plots of daily peak ozone concentration.

haziness (low visibility) is much better for sulfates than for ozone.

Local Air Pollution Data (St. Louis, MO):

Data for ozone and light extinction coefficient for St. Louis, MO are shown in Figure 7 for the entire summer of 1975. The surface ozone data exhibit the typical diurnal pattern consisting of near-zero readings during the night and early morning, and peaks in the early afternoon followed by a drop during the evening hours. The two passages of the hazy blob over St. Louis are confirmed by the elevated peaks for both ozone and b_{ext} during the periods June 27-29 and July 2-4. The peaks of b_{ext} are also seen to lag behind those for ozone, suggesting a possible role of ozone as precursor to secondary aerosol formation.

The two episodes of air pollution in St. Louis during the period of the case study are also evidenced by the data of light scattering coefficient (b_{scat}) measured locally using integrating nephelometers (Figure 8a). The data were collected at three widely-spaced local air monitoring stations. One of the stations is situated in the city (station 4), one on the outskirts of the city (station 9), and one at a background location (station 6) about 40 km to the west of the city. The data from all three stations reveal a common temporal pattern of atmospheric fine particulate loading, thus confirming that the major changes in the light scattering coefficients during the entire period occurred over a spatial scale substantially greater than that of the St. Louis metropolitan area. These data also indicate that the increase in the light scattering aerosol concentrations during this period were the result of external inflow rather than of

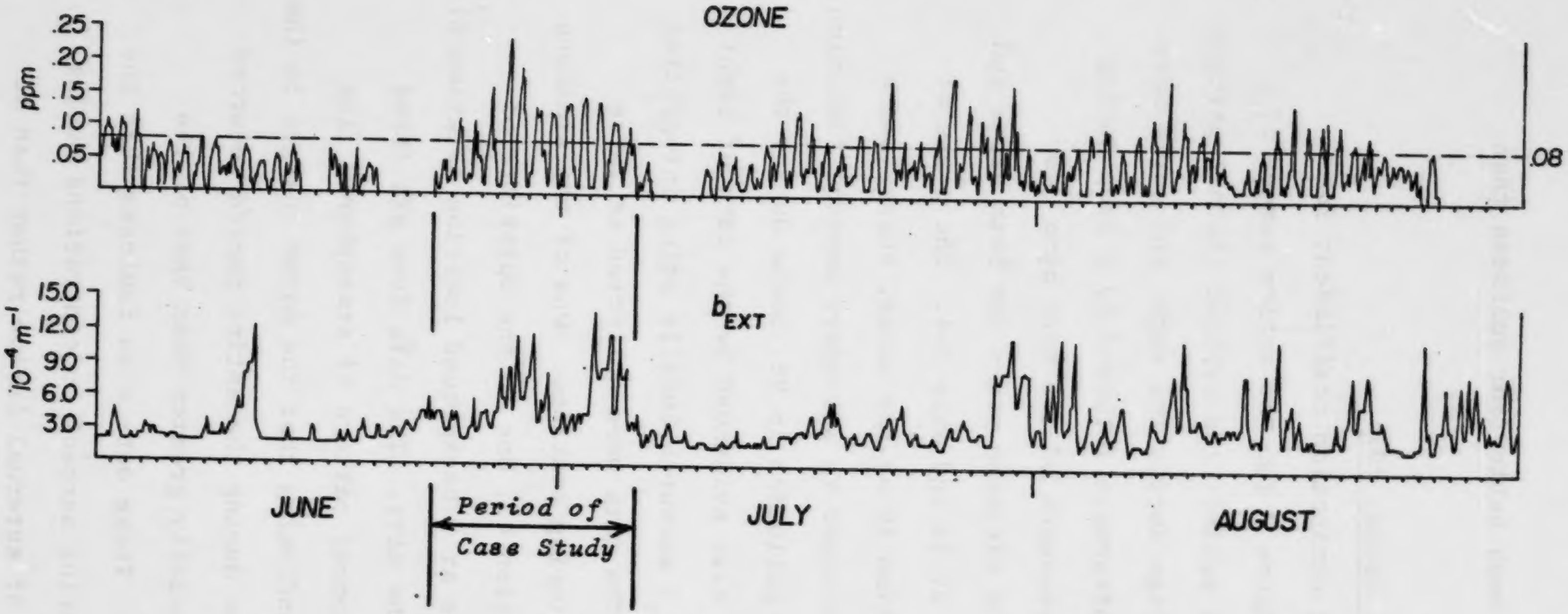

Figure 7. Comparison of long-term observations of ozone and light extinction coefficient at an air monitoring station in St. Louis, MO.

local source contributions. Figure 8b shows the temporal variations of the light extinction coefficient computed based on observed visibility ranges at the major airports of St. Louis, MO and Springfield, IL. The two observation sites are about 150 km apart. Both traces reveal the two passages of the blob whose spatial scale is larger than the separation of the sites. The time offset of the two traces is much smaller than the temporal scale of each blob passage over the region, and is due to the separation of the sites. Comparison of Figures 8a and b reveals a close correlation between the actual measured light scattering coefficient (b_{scat}) and the light extinction coefficient (b_{ext}) inferred from visibility data. This correlation demonstrates the utility of visibility observations as a qualitative surrogate for aerosol concentration of the atmosphere.

The daily average sulfate concentrations using Hi-Volume filters were measured before, during, and after the passage of the hazy air mass over St. Louis, MO. Hi-Volume filter samples, collected every six days by the St. Louis County Department of Health, were analyzed for particulate sulfur using flash volatilization-flame photometric detection method (Husar et al., 1975). An increase from 9.2 μgm^{-3} on June 23 to 32.7 μgm^{-3} on June 29 is shown in Fig. 8a. The sulfate content then dropped to 8.0 μgm^{-3} on July 5 after the passage of the Canadian front. Sulfate accounted for 19% of total aerosol mass before, 34% during, and 15% after the passage of the hazy air mass. The daily average sulfate concentrations were compared to daily average b_{ext} (uncorrected for relative humidity effects) for the entire summer (June, July, August 1975). The correlation coefficient was found

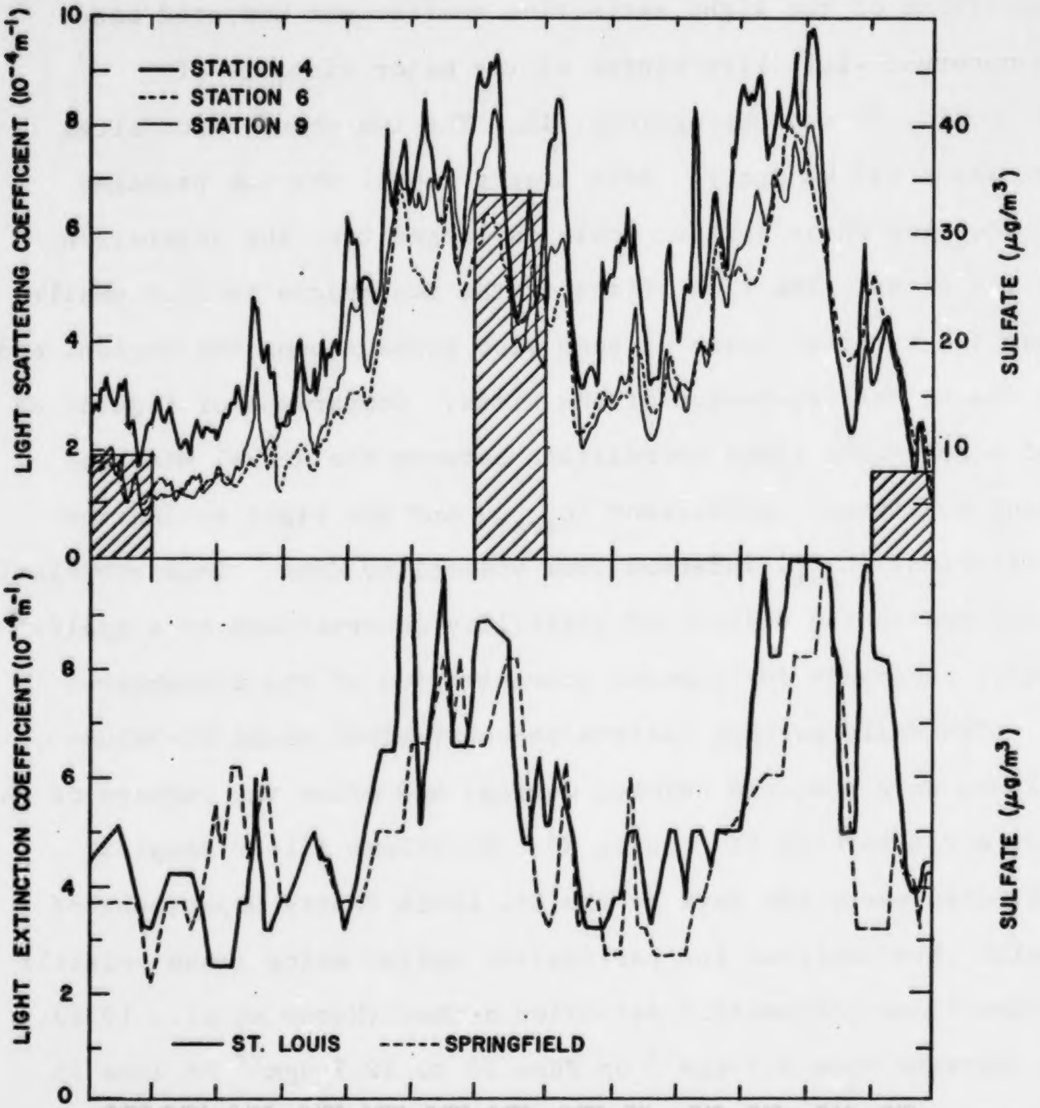

Figure 8. a) Light scattering coefficient, b_{scat}, recorded by nephelometers at three stations of the St. Louis City/County air monitoring network. Similar b_{scat} records (not shown here) were also recorded at the other stations in the network;
b) Light extinction coefficients, b_{ext}, determined from visibility observations at St. Louis Lambert Airport and Springfield, IL Airport (150 km apart).

to be r = 0.7 and the regression equation for sixteen points was $b_{ext}[10^{-4}m^{-1}] = 3.24 + 0.11\ SO_4^{--}[\mu gm^{-3}]$. These results tend to suggest that a substantial fraction of the haze aerosol, particularly during the passage of "blobs", was associated with sulfates.

Effect of Relative Humidity:

As stated earlier, no corrections have been made to the visibility data for the contribution of relative humidity. However, the plots correspond to visibility observations at noon when the reduction of visibility due to fog or "water haze" is minimal. To investigate the effects of geographical location as well as relative humidity on local visibility observations, all hourly data for visibility and relative humidity for the entire period of June, July and August of 1975 were plotted for four widely-spaced stations, as shown in Figure 9. For all four stations, the reduction of visibility is small for increasing R.H. up to about 75%. For higher values of R.H., there is a sharp reduction of visibility. The role of atmospheric moisture content in visibility reduction may be factored out from the consideration of geographical variation of seasonal visibility by comparing b_{ext} for the four sites for a common R.H. range, for example, 60-70% (common at noon). In this range of R.H., it is clear that Huntington, W.VA has much more haze during the summer months than San Antonio, TX. The distribution of haziness over the entire U.S., seasonally averaged for the summer months, and considering only those local observations which correspond to R.H. in the range 60-70%, is shown in Figure 10. These data often correspond to local midday conditions. The lowest

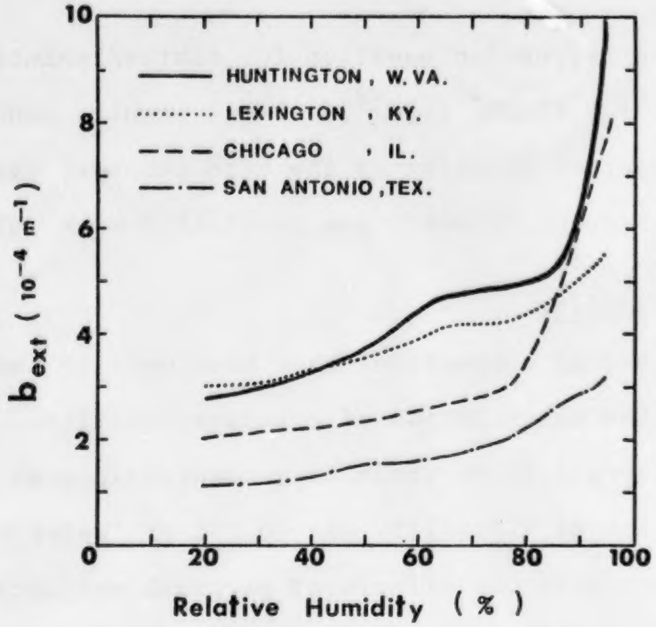

Figure 9. Light extinction coefficient in four U.S. cities for different ranges of relative humidity during Summer 1975. b_{ext} is determined by averaging all observations (for entire summer) which are in given RH ranges (e.g. 40-50%, and so on).

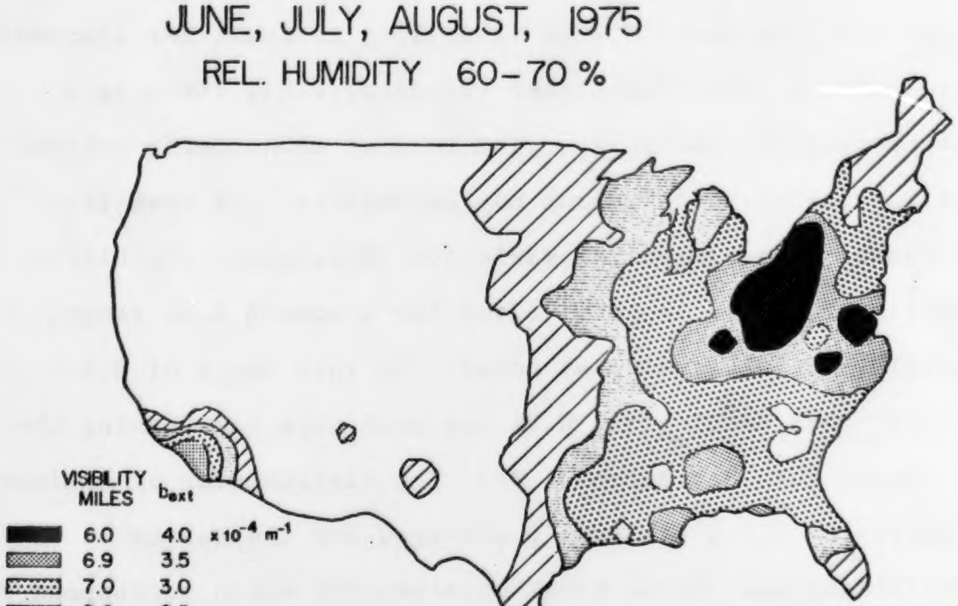
JUNE, JULY, AUGUST, 1975
REL. HUMIDITY 60-70 %
VISIBILITY MILES
b_{ext}
6.0 4.0 $\times 10^{-4}\,m^{-1}$
6.9 3.5
7.0 3.0
9.6 2.5
12.0 2.0
>16.0 <1.5

Figure 10. Geographical variation of b_{ext} for RH = 60-70% during Summer 1975.

visibilities are observed to be in the northeastern section of the U.S., with the worst conditions prevailing in the region of the Ohio River valley. This is also roughly the region of highest emission density of SO_2 in the U.S., indicating the possible dominance of aerosols of anthropogenic origin in causing visibility reduction at R.H. below about 70%.

CONCLUSION

This brief analysis of national visibility data, synoptic weather maps, air parcel trajectories and national as well as local air quality data, points out two intriguing phenomena. Multi-state scale haziness may be caused by the accumulation in the atmosphere of pollutant emissions from one region and its subsequent transport over a long range. Secondly, a major fraction of the pollutant content of such large hazy air masses is constituted of secondary ozone and aerosols, mainly sulfates. Evidently, the role of meteorology is important in the occurrence of such regional scale pollution episodes lasting many days, even weeks. A much more intriguing question may be raised concerning the possibility of synergism between the ozone and sulfate contents of such polluted air masses. What is the role of such interactions in the origin and spread of such large scale air pollution episodes? The task of the long-range transport modeler in simulating large scale air pollution episodes is obviously extremely difficult, and it is important for him to utilize all available tools and data to understand first at least the gross features of the large polluted air masses.

ACKNOWLEDGEMENT

The research was supported by the U.S. Environmental Protection Agency under Grant No. R803896. We are indebted to C.C. Paley, P.N. Turcu, W. Biel, W.E. Wilson and D.A. Pecsok for their help during various stages of the work.

REFERENCES

Charlson, R.J., 1969: Atmospheric visibility related to aerosol mass concentration. Environ. Sci. Technol., 3 (10), 913-918 (October).

Charlson, R.J., 1974: Sulfuric Acid and Ammonium Sulfate Aerosols: Optical Detection in the St. Louis Region. Science, 184, 156.

Hall, F. P. et al., 1973: Long-range transport of air pollution: A case study, August 1970. Monthly Weather Rev., 101(5), 404-411.

Hidy, G. M. et al., 1974: Characterization of aerosols in California, Final Report IV, California Air Resources Board..

Husar, J. D. et al., 1975: Determination of submicrogram amounts of atmospheric particulate sulfur. Anal. Chem. 47, 2062.

Lyons, W. A., 1975: Satellite detection of air pollutants, in Remote Sensing Energy-Related Studies, John Wiley & Sons, N.Y., 263-290.

Lyons, W. A. and R. B. Husar. SMS/GOES visible images detect synoptic scale air pollution episode, (to be published).

Middleton, W.E.K., 1952: Vision through the atmosphere. pp. 60-82, Univ. of Toronto Press, Toronto.

White, W. H. et al., Formation and transport of secondary air pollutants: ozone and aerosols in the St. Louis urban plume. Science (in print).

NATO/CCMS 7th International Technical Meeting

Topic 2: Paper 4-6; Rapporteur's Report - A. Keddie

Paper 4 (D.G. Fox)

In presenting his paper, Dr. Fox began by stating that his work was primarily application orientated using modeling techniques to assist the Forest Service in assessing the impact of mineral extraction and recreation developments in relatively undeveloped, mountainous areas. With effects on vegetation his main concern, the component models deal with surface temperature, surface wind fields and, finally, the calculation of pollutant dispersion in complex terrain. Main output is in the form of current and projective pollution index values which can be readily understood by the public, and which are compatible with other information used by planners. During discussion, it was pointed out that the most severe effects (greatest index values) were generally to be found in the lee of the mountains, although this pattern could be modified by, e.g., upwind flow on the mountainsides.

Paper 5 (L. L. Wendell)

The model presented computes the regional distribution of SO_2 and SO_4 from time changing wind field and precipitation data in a grid system. Advection, chemical transformation and removal by wet and dry deposition were taken into account. A transformation rate of 5% per hour was assumed and the lateral spread of each plume was assumed to be Gaussian, although plume meandering was found to be more important. Calculated SO_2 and SO_4 patterns for an 18-day period in April, 1974, for north eastern USA were presented. It was shown that the calculated total removal using averaged precipitation rates for each grid square was greater than for hourly precipitation rates but the latter did produce significantly greater deposition in local areas. Mass balance calculations, e.g., in terms of the percentages deposited had been included. The intention was to repeat the work for a complete year's data.

Paper 6.1 (N. V. Gillani)

A single-plume dispersion model including the observed effects of removal and a time-dependent transformation rate was presented. It was stressed that the rate of removal by dry deposition is more strongly dependnt on the ratio of the deposition velocity to the surface vertical diffusivity than on the deposition velocity itself. This point had also been made by Fisher and Scriven in their study of mesoscale transport over England. The model's application to plume travel distances of up to 50 km was given, and it was demonstrated that for power plants there was little loss and little conversion within the first 50 km, a figure of 20% being quoted.

Paper 6.2 (N. V. Gillani)

In this paper was proposed the idea of using surface visibility, as defined by the U.S. National Weather Service, as a means of identifying and tracking the transport of polluted air masses from one locality to another. A case study of two sequential air pollution episodes in St. Louis during the summer of 1975 was presented. It was postulated that these episodes were due to the movement of the same air mass across St. Louis at two different times before finally being swept northwards by a cold Canadian front. During these episodes, midday visibility was reduced to less than 3 miles, while the 24-hour average particulate SO_4 concentration almost tripled

Ozone levels were also high. Although local emissions could not be entirely ruled out as the source of the high SO_4 values observed in the St. Louis area, surface winds and U. S. Air Force trajectories strongly supported the hypothesis that accumulation within the one slowly moving air mass was largely responsible.

TOPIC III

SENSITIVITY ANALYSIS AND DISPERSION UNDER LOW WIND SPEEDS

7th International Technical Meeting on Air Pollution Modeling
and its Application

Sensitivity Analysis of the Single Source (CRSTER) Model

Warren P. Freas and Russell F. Lee*

Monitoring and Data Analysis Division
U. S. Environmental Protection Agency

September 7-10, 1976
Airlie, Virginia
United States of America

---

*On assignment from National Oceanic and Atmospheric Administration, U. S. Department of Commerce

SENSITIVITY ANALYSIS OF THE SINGLE SOURCE (CRSTER) MODEL

by

Warren P. Freas and Russell F. Lee*
Monitoring and Data Analysis Division
Environmental Protection Agency
Research Triangle Park, N. C. 27711

Abstract

The Single Source (CRSTER) Model has been used extensively by EPA to estimate the air quality impact of fossil fueled steam-electric power plants and selected industrial emission sources. The purpose of this paper is to describe a sensitivity analysis of this dispersion model.

For the purposes of numerical simulations, model sensitivity is defined as "the incremental change in the calculated concentration resulting from the incremental change in input." The two aspects of model sensitivity are the sensitivity of the model calculated concentrations to (1) variations in the magnitude of each of the input variables and (2) the collective variations in all the input variables. Because of the complex interactions of the meteorological and source variables found in this particular model, only the first aspect of model sensitivity is addressed; that is, variations in the magnitude of the input variables related to both the source and the meteorology.

The results of the analysis are presented in tables, input/output response graphs, and cumulative frequency distribution plots. Primary emphasis is placed on the maximum 24-hour concentration of SO_2. This averaging time is the critical one for which power plants must meet primary National Ambient Air Quality Standards (NAAQS).

As a result of this analysis it can be concluded that: (1) the sensitivity of model estimates to accuracy in the input parameters varies from source to source; (2) accuracy in the source parameters becomes more critical as the stack becomes shorter; (3) errors in individual meteorological parameters, with the exception of stability class, result in somewhat smaller errors in estimated concentrations than errors in source parameters; and (4) the cumulative errors in meteorological parameters which result from the use of data from an unrepresentative site, can cause substantial errors in estimated concentrations.

---

*On assignment from National Oceanic and Atmospheric Administration, U. S. Department of Commerce

SENSITIVITY ANALYSIS OF THE SINGLE SOURCE MODEL

Introduction

The purpose of this paper is to describe a sensitivity analysis of the Single Source (CRSTER) Model,[1] a model which has been used extensively by EPA to estimate the air quality impact of fossil fueled steam-electric power plants and selected industrial emission sources.

The question of model "validity" or "reasonableness" is addressed in some recent validation studies of the model for selected power plants.[2,3] A sensitivity analysis of the model provides the natural complement to these validation studies. Whereas a validation study assesses the impact of model formulation on calculated concentrations, a sensitivity analysis takes the model formulation as given and examines the impact of errors in the input data on the model calculated concentrations. The objective of a sensitivity analysis, therefore, is to identify the critical model input parameters--those variables which have the greatest influence on model predictions. Knowing the critical model parameters assists the model user in assigning proper priorities in the data collection and quality assurance procedures and in understanding the complex interactions within the model.

In order to complement the model validation studies, a case study approach is selected which models the same three Ohio power plants, Muskingum River, Philo, and J. M. Stuart.

Model Description

The dispersion model is a Gaussian plume model which calculates hourly and daily SO_2 concentrations for an array of 180 receptor locations, calculates maximum daily SO_2 concentrations for a year, and identifies the meteorological conditions associated with these maxima.

A ground plane displacement procedure is used in the model to simulate the effect of elevated terrain in the vicinity of the plant sites. This procedure consists of adjusting (decreasing) the height of each plume by an amount equal to the difference in elevation between the plant site and the average surrounding terrain.

An annual average SO_2 source strength and monthly variation factors must be specified.

Meteorological inputs to the model consist of hourly surface observations of wind speed, wind direction sector, temperature, total cloud cover, and twice daily mixing heights. The data are input into a preprocessor program which in turn writes a tape containing hourly values of stability index, mixing height, temperature, wind speed, flow vector (wind direction plus 180°), and randomized flow vector. The randomized flow vector is equal to the flow vector minus four degrees plus a random number between 0 and 9 degrees. The preprocessor output tape is read by the Single Source Model which performs the actual concentration calculations.

Plant Descriptions

The physical characteristics of each plant listed in Table 1 are those reported in the 1973 Federal Power Commission (FPC) Form 67, "Steam-Electric Plant Air and Water Quality Control Data for the year ended December 31, 1973."

Some of the stack heights listed below for the Philo and Muskingum plants differ from those reported in the referenced validation study.[3] It has been determined that modifications/replacement of some of the stacks at these plants are not reported in the 1973 FPC data. The stack heights listed in the validation study represent the current plant configuration (these values were obtained directly from the utility), whereas the stack heights in the present analysis reflect plant configuration prior to 1973.

Source Data

The source strength and monthly variation factors are calculated from data contained in the 1973 FPC Form 67. The data used in the calculations consists of the monthly fuel consumption and average sulfur content data. The values for the source strengths and monthly variation factors are listed for each plant in Table 2.

The adjustments for elevated terrain in the vicinity of each plant are those used in previous modeling studies of these plants.[4] The terrain adjustments, which represent the difference in elevation between the plant sites and the average of the surrounding terrain, are forty-nine meters for Muskingum River, thirty meters for Philo, and sixty-seven meters for Stuart.

TABLE 1. PLANT CHARACTERISTICS

Characteristic		Plant							
		Muskingum River				Philo			Stuart
		Stack 1	Stack 2	Stack 3	Stack 5	Stack 4	Stack 5	Stack 6	Stack 1-3
Stack	Height (m)	91	91	131	251	46	46	55	244
	Diameter (m)	4.5	4.5	4.8	6.7	5.7	4.5	2.6	6.0
	Velocity (m/s)	13.4	13.4	22.3	16.8	6.3	10.1	28.9	23.2
	Temperature (°K)	430	430	416	428	458	458	430	375
Number of Boilers per stack		1	1	2	1	2	2	1	1

Source: 1973 FPC Form 67

TABLE 2. PLANT EMISSIONS DATA

<table>
<tr><th rowspan="3">Source Parameter</th><th colspan="10">PLANT</th></tr>
<tr><th colspan="4">Muskingum River</th><th colspan="3">Philo</th><th colspan="3">Stuart</th></tr>
<tr><th>Stack 1</th><th>Stack 2</th><th>Stack 3</th><th>Stack 5</th><th>Stack 4</th><th>Stack 5</th><th>Stack 6</th><th>Stack 1</th><th>Stack 2</th><th>Stack 3</th></tr>
<tr><td>Source Strength (g /s)</td><td>1446</td><td>1414</td><td>2952</td><td>4025</td><td>586</td><td>566</td><td>601</td><td>1381</td><td>1261</td><td>1559</td></tr>
<tr><td>Monthly factors:</td><td colspan="4">All Stacks</td><td colspan="3">All Stacks</td><td colspan="3">All Stacks</td></tr>
<tr><td>Jan.-June</td><td colspan="4">1.04 .99 .92 .89 1.04 .96</td><td colspan="3">.92 1.09 .86 .87 1.06 1.08</td><td colspan="3">.92 .95 .79 .79 .79 1.07</td></tr>
<tr><td>July-Dec.</td><td colspan="4">1.06 1.03 1.13 .74 1.19 1.04</td><td colspan="3">.97 1.02 .98 1.08 1.10 .96</td><td colspan="3">1.11 1.17 1.06 1.17 1.10 1.12</td></tr>
</table>

Source: 1973 FPC Form 67

Meteorological Data

The sources for the meteorological data used in this analysis are listed below.

Table 3. METEOROLOGICAL STATIONS

Plant	Surface Observations Airport	Upper Air Data Airport	Year
Muskingum	Huntington, W. Va.	Huntington, W. Va.	1964
Philo	Columbus, Ohio	Dayton, Ohio	1964
J. M. Stuart	Cincinnati, Ohio	Dayton, Ohio	1964

Methodology

Model sensitivity is defined as the partial derivative of the calculated concentration with respect to the parameter, p, evaluated at some value for p. That is,

$$\left.\frac{\partial \chi}{\partial p}\right|_{p = p_o}$$

For the purposes of numerical simulations, model sensitivity may be defined as "the incremental change in the calculated concentration resulting from the incremental change in input." These two definitions suggest the general approaches available for conducting a sensitivity analysis, analytical and numerical. Either method may be used to investigate both aspects of model sensitivity: the sensitivity of model predictions to (1) variations in the magnitude of each of the input variables and (2) the collective variations in all the input variables.

Because of the complex interactions of the meteorological and source variables found in this particular model, it is not possible, nor desirable, to examine the model sensitivities analytically. Analyses of this type have been performed for other Gaussian models, however.[5,6,7] This analysis concentrates on the first aspect of model sensitivity; that is, variations in the magnitude of the input variables related to both the source and the meteorology.

Source Related Parameters

The source related parameters examined in this analysis include:

1. Stack height (m)
2. Stack gas temperature (°C)
3. Stack gas exit velocity (m/s)
4. Stack diameter (m)
5. Emission rate (g/s)
6. Terrain adjustment (m)
7. Monthly variation factors

For the first six source-related parameters, systematic changes are introduced in each of the individual model parameters. Conceptually, this approach can be viewed as simulating events such as consistent instrument or technician bias. The actual numerical procedure consists of varying each of the initial source parameter values by factors of ±5, ±10 and ±25 percent of the initial value while holding all the other parameter values constant. For the seventh parameter, the monthly variation factors, only the effect of no monthly variation (i.e. a constant emission rate for the year) is simulated. Interactions from changes in combinations of these parameters are not examined. In the analysis of the source parameters, computational savings are achieved by limiting the model calculations to the meteorology for the "worst 20 days" of the year.* These days are chosen on the basis of the calculated daily maximum 24-hour average concentrations from the "base case" simulations.

Meteorological Parameters

The meteorological parameters included in the analysis are:

1. mixing heights (m)
2. wind speeds (m/s)
3. ambient temperature (°C)
4. stability class
5. randomized flow vector
6. surface/upper air data sets

---

*The phrase "worst 20 days" is used throughout this report to denote those days used in the source parameter analysis. The distribution of daily maximum 24-hour concentrations is examined for a "clean break" occurring near the top 20 days. The actual number of days selected varies from 22 days at Philo to 26 days at Stuart.

The analysis methodology for the first four meteorological parameters parallels that used for the source parameters. Systematic variations introduced in each of the meteorological parameters simulate the effect of errors resulting from factors such as observer and instrument bias or consistent trends in the meteorological variables. These variations are applied to each parameter individually; the effect of interaction is not examined.

In contrast to the analysis of the source parameters which uses only the meteorology from the "worst 20 days" in the simulations, the simulation procedure for the meteorological variables uses all 366 days of the year. This latter procedure eliminates the possibility of having the actual model calculated maximum concentration not fall on one of the "worst 20 days" due to the variations introduced in the meteorology related variables. The values of the parameters, wind speed, mixing height, and ambient temperature are biased by factors of ±5, ±10, and ±25 percent. Stability is biased by ±1 class, with the added restriction that stability class cannot be less than 1 or greater than 7.

The simulation procedures developed for the randomized flow vector include: (1) substituting a new random number generator (Univac's RANDU) and nine different starting numbers, and (2) eliminating the random number generator, i.e. using the average flow vector.

In an effort to assess the effect of changes in all of the meteorological variables, simulations are conducted for each plant using the surface/upper air data sets from the other two plants. The advantages of this ad hoc procedure over explicit numerical methods are (1) ease of operation, (2) minimal additional computer requirements, and (3) and identification of the effects of using different upper air and surface wind stations. With this procedure, however, it is not possible to explicitly identify the range of variation in each of the input variables.

Results

The results of the sensitivity analysis for the Single Source Model for the three Ohio plants are presented in tables, input/output response graphs, and cumulative frequency distribution plots. Primary emphasis is placed on the maximum 24-hour concentration of SO_2 in the graphical presentation of the results. This averaging time is the critical one for which power plants must meet primary National Ambient Air Quality Standards (NAAQS). The effects on the 1-hour and annual average concentrations are noted in the tables, however.

To provide a basis for comparison, the results from the base case simulations are summarized in Figure 1, the cumulative frequency distributions for the model calculated maximum 24-hour concentrations. As modeled, the Muskingum River plant has two short 91 meter stacks, one 131 meter stack, and one 251 meter stack. Unstable conditions are associated with the base case maximum 24-hour concentration at this plant. The three short stacks and elevated terrain considerations at the Philo plant yield a base case maximum 24-hour concentration which is associated with near neutral stability and persistent wind direction, about 11 hours with the winds within ±10 degrees of direction. At Stuart, a plant with three tall stacks (244 meters), the base case maximum 24-hour concentration is associated with unstable, light wind conditions with some limited mixing.

Source Related Parameters

The results of the sensitivity analysis for the source related parameters are summarized for all three plants in Tables 4 and 5 and input/output response curves, Figures 2 and 3. Apparent discontinuities in these response curves arise whenever, as the parameter values vary from their initial levels, the day associated with the maximum 24-hour concentration changes. Naturally, the meteorological conditions for this new maximum day differ somewhat from the original maximum day, thus producing a slightly different response.

An examination of the tables and graphs reveals, that for the Muskingum River and Philo plants, the maximum 24-hour concentrations are quite sensitive to changes in the values of the stack parameters, i.e. a unit change in the value of an individual stack parameter yields at least a unit change in the maximum 24-hour concentration. At the Stuart plant, however, a unit change in the value of any of the stack parameters yields less than a unit change in the maximum 24-hour concentration.

TABLE 4 PERCENTAGE CHANGE FROM BASE CASE MAXIMUM 24-HOUR CONCENTRATIONS DUE TO VARIATIONS IN SOURCE RELATED PARAMETERS

Percent error in value / Parameter	Muskingum River			Philo			Stuart		
	5	10	25	5	10	25	5	10	25
Stack height (m)	-2	-5	-11	-6	-12	-27	-2	-5	-11
Stack temp (°C)	-4	-8	-17	-4	-8	-18	-2	-4	-7
Exit velocity (m/s)	-5	-9	-19	-6	-10	-23	-2	-3	-7
Stack diameter(m)	-9	-17	-30	-11	-20	-41	-3	-7	-15
Terrain ADJ (m)	1	3	12	5	9	24	1	1	3
Emissions (g/s)	5	10	25	5	10	25	5	10	25

Percent error in value / Parameter	Muskingum River			Philo			Stuart		
	-5	-10	-25	-5	-10	-25	-5	-10	-25
Stack height (m)	3	7	32	6	12	33	3	5	14
Stack temp (°C)	5	10	32	5	10	32	2	5	16
Exit velocity (m/s)	5	10	28	6	12	36	2	4	11
Stack diameter(m)	10	20	58	12	24	88	4	8	23
Terrain ADJ (m)	-1	-2	-5	-4	-8	-20	-1	-1	-3
Emissions (g/s)	-5	-10	-25	-5	-10	-25	-5	-10	-25

TABLE 5. GREATEST PERCENTAGE CHANGE FROM BASE CASE CONCENTRATIONS DUE TO VARIATIONS IN SELECTED INPUT PARAMETERS

SIMULATION	MUSKINGUM RIVER			PHILO			STUART		
	Annual Mean	Max 24-hr	Max 1-hr	Annual Mean	Max 24-hr	Max 1-hr	Annual Mean	Max 24-hr	Max 1-hr
No Monthly Variation in Emissions	-0.1	4.2	-5.4	0.2	-4.5	-2.3	-3.8	-6.5	-10.0
Urban Mixing Heights	6.2	11.4	9.8	3.4	0.0	-0.3	4.4	-2.4	0.0
No Randomized Flow Vector	7.1	7.0	1.4	32.3	10.2	8.2	0.6	-3.1	0.4
New Random Number Generator (RANDU)	-3.2	13.7	1.1	10.3	0.8	8.2	-8.3	-13.0	-6.6
New Surface/ Upper Air Data	20.7	11.6	5.1	33.5	-28.4	4.4	-33.2	35.0	-14.6

The data reveal that, for variations in stack diameter, the percentage change in the maximum 24-hour concentration is about double that found for exit gas velocity. The relationship between exit velocity and stack diameter is found in the model expression for volumetric flow rate:

$$VF = \alpha V_s D^2$$

Where α is a constant term, V_s is the stack gas exit velocity, and D is the stack diameter. Given this relationship and remembering the analytical definition of model sensitivity, i.e., the partial derivative of concentration with respect to the given parameter, one expects the sensitivity of the model calculated concentrations to variations in stack diameters to be twice that of stack gas exit velocity.

Except for the Philo plant, maximum 24-hour concentrations are not sensitive to variations in the value of the terrain adjustment, because the amount of the adjustment is quite small relative to the height of the stacks.

From the formulation of the model, we know that a unit change in emissions results in a unit change in the model calculated concentrations. Also, maximum concentrations occur on the same day as the base case maximum concentrations, only the concentration changes.

The seasonal factors simulate the effect of monthly variations in the emissions rate resulting from either differing load factors or varying sulfur content of the fuel. The effect of changing these factors, therefore, is to change the yearly distribution of emissions.

The effect of uniform emissions throughout the year, i.e. no seasonal variation, is shown in Table 5.

Meteorological Parameters

Tables 5 through 9 and Figures 4 through 8 summarize the sensitivity analysis results for the meteorological parameters.

The maximum 24-hour concentrations are very insensitive to variations in mixing heights at the Muskingum River and Philo plants. Using urban mixing heights rather than the base case rural mixing heights, the calculated maximum 24-hour concentration is unchanged at Philo, decreases by 2 percent at Stuart, and increases by 11 percent at Muskingum River as compared with the base case (Table 5).

At the Muskingum River and Philo plants, increasing the average wind speed produces higher 24-hour concentrations. However, at the Stuart plant which has three tall stacks, increasing (decreasing) the average wind speed decreases (increases) the maximum 24-hour concentration, i.e., the reverse of the relationship at the other two plants (Figure 5). The maximum concentration from a point source is affected by the wind speed in two ways, higher wind speeds dilute the plume and also reduce the plume rise, reducing the distance to the highest concentration. These two effects combine to produce the higher concentration at some critical wind speed. Thus, the maximum concentrations may either increase or decrease when wind speed increases.

TABLE 6 PERCENTAGE CHANGE IN BASE CASE MAXIMUM 24-HOUR CONCENTRATIONS DUE TO VARIATION IN METEOROLOGICAL PARAMETERS

Percent error in value / Parameter	Muskingum River			Philo			Stuart		
	5	10	25	5	10	25	5	10	25
Mixing height (m)	0	0	0	0	0	0	-3	-5	-11
Wind speed (m/s)	3	5	9	4	7	21	-2	-3	-9
Ambient temp (°C)	1	2	6	1	2	6	1	2	5
Stability class*	—	—	-43	—	—	-48	—	—	-47

*Biased by +1 Stability Class

Percent error in value / Parameter	Muskingum River			Philo			Stuart		
	-5	-10	-25	-5	-10	-25	-5	-10	-25
Mixing Height (m)	0	0	1	0	0	0	3	6	20
Wind speed (m/s)	-3	-7	-8	-4	-9	-24	2	5	12
Ambient temp (°C)	-1	-2	-6	-1	-2	-5	-1	-2	-3
Stability Class*	—	—	123	—	—	91	—	—	41

*Biased by -1 Stability Class

TABLE 7 ANNUAL MEAN CONCENTRATIONS PERCENTAGE CHANGE FROM BASE CASE

Surface/Upper Air Data Set	Muskingum River	Philo	Stuart
Huntington/Huntington	-	3.3	10.7
Columbus/Dayton	-20.7	-	-33.2
Cincinnati/Dayton	9.7	33.6	-

TABLE 8 YEARLY MAXIMUM 24-HOUR CONCENTRATIONS PERCENTAGE CHANGE FROM BASE CASE

Surface/Upper Air Data Set	Muskingum River	Philo	Stuart
Huntington/Huntington	-	-28.4	-19.4
Columbus/Dayton	47.8	-	36.0
Cincinnati/Dayton	11.6	-5.8	-

TABLE 9 YEARLY MAXIMUM 1-HOUR CONCENTRATIONS PERCENTAGE CHANGE FROM BASE CASE

Surface/Upper Air Data Set	Muskingum River	Philo	Stuart
Huntington/Huntington	-	1.9	-2.1
Columbus/Dayton	5.1	-	-14.6
Cincinnati/Dayton	1.4	4.3	-

Because the ambient temperatures are significantly lower than the stack gas temperatures, for a fixed change in ambient temperature there is small percentage change in plume buoyancy and thus a small percentage change in plume rise. Understandably, for the range of values considered in the analysis, the calculated maximum 24-hour concentrations are insensitive to variations in ambient temperature.

Lowering the stabilities by one class (one step more unstable) yields higher concentrations and raising stability by one class lowers concentrations. As Table 6 illustrates, the 24-hour concentrations are very sensitive to a bias of one stability class.

Using a different randum number generator (RANDU) and nine different starting numbers, the greatest change from the base case maximum 24-hour concentration is +14% at Muskingum River, +0.8% at Philo, and -13% at Stuart (Table 5).

When the average flow vector is used in place of the randomized flow vector, the model calculated maximum 24-hour concentrations are 7% higher at Muskingum River, 10% higher at Philo, and 3% lower at Stuart (Table 5). Thus, the inclusion of the randomized flow vector in the model can either decrease or increase the calculated 24-hour concentrations. For example, when the wind blows directly toward the receptor, concentrations will always decrease when the randomized flow vector is added. However, if the wind blows 10° to the left of the receptor, the addition of the randomized flow vector can either decrease or increase the concentrations.

The sensitivity of the model calculated concentrations to the selection of individual surface/upper air data sets is determined by running the model for each plant with the meteorological data sets from the other two plants. Because two of these data sets share a common upper air station, it is also possible to factor out the effect of different surface wind stations on calculated concentrations.

The surface/upper air stations associated with each plant are Huntington/Huntington (HTG/HTG) at Muskingum River, Columbus/Dayton (CM/DAY) at Philo, and Cincinnati/Dayton (CVG/DAY) at Stuart.

Cumulative frequency distributions of the daily maximum 24-hour concentrations for all three data sets at each plant are presented in Figures 6 through 8. The shapes of all the distributions are quite similar except for some divergence at the upper percentile values.

Table 10 ranks the model calculated concentrations for the three averaging times from each of the meteorological data set simulations.

Table 10. MODEL CALCULATED CONCENTRATION RANKINGS

Surface/ Upper Air	Muskingum River			Philo			Stuart		
	Annual Avg.	Max. 24-hr.	Max. 1-hr.	Annual Avg.	Max. 24-hr.	Max. 1-hr.	Annual Avg.	Max. 24-hr.	Max. 1-hr.
HTG/HTG	2	3	2	1	3	2	2	3	3
CMH/Day	3	1	3	3	1	3	3	1	1
CVG/Day	1	2	1	2	2	1	1	2	2

For all three plants, the highest 24-hour concentration and the lowest annual average are associated with the CMH/DAY data sets.

Comparing the results from the CMH/DAY and CVG/DAY data sets indicates that the Columbus surface wind data always give the maximum 24-hour concentration and the lowest annual average concentration. The maximum 24-hour concentration is a result of a single day with extremely strong wind persistence, about 11 hours with the winds within ±10 degrees of direction.

A further examination of the concentration rankings reveals that the HTG/HTG data always give the lowest value for the maximum 24-hour concentration. This appears to be due to a greater degree of fluctuations of the wind direction from hour to hour in the Huntington data.

Conclusions

As a result of this analysis it can be concluded that: (1) the sensitivity of model estimates to errors in the input parameters varies from source to source; (2) errors in the source parameters become more critical as the stack becomes shorter; (3) errors in individual meteorological parameters, with the exception of stability class, result in somewhat smaller errors in estimated concentrations than errors in source parameters; and (4) the cumulative errors in meteorological parameters which result from the use of data from an unrepresentative site, can cause substantial errors in estimated concentrations.

REFERENCES

1. Hrenko, J., D. B. Turner and J. Zimmerman. "Interim User's Guide to a Computation Technique to Estimate Maximum 24-hour Concentrations from Single-Sources," unpublished manuscript, U. S. Environmental Protection Agency (1972).

2. Mills, M. T. and F. A. Record, "Comprehensive Analysis of Time-Concentration Relationships and the Validation of a Single Source Dispersion Model," Publication No. EPA 450/3-75-083, prepared by GCA/Technology Division under Contract No. 68-02-1376, Environmental Protection Agency, Research Triangle Park, N.C. (1975).

3. Mills, M. T. and R. W. Stern, "Model Validation and Time-Concentration Analysis of Three Power Plants," Publication No. EPA 450/3-76-002, prepared by GCA/Technology Division under Contract No. 68-02-1376, Environmental Protection Agency, Research Triangle Park, N.C. (1975).

4. Morgenstern, Paul, "Summary Report on Modeling Analysis of Power Plants for Compliance Extensions in 51 Air Quality Control Regions," Publication No. EPA 450/3-75-060, prepared by Walden Research Division of Abcor, Inc. under Contract No. 68-02-0049, Environmental Protection Agency, Research Triangle Park, N.C. (1973).

5. Roth, P. M., et. al., "An Examination of the Accuracy and Adequacy of Air Quality Models and Monitoring Data for Use in Assessing the Impact of EPA Significant Deterioration Regulations on Energy Developments," prepared by Systems Applications, Inc. for Greenfield, Attaway, and Tyler, Inc. under Prime Contract to Office of General Council, American Petroleum Institute, Washington, D.C. (1975).

6. Thayer, S. D. and R. C. Koch, "Sensitivity Analysis of the Multiple-Source Gaussian Plume Urban Diffusion Model," Proceedings of the Conference on Urban Environment and Second Conference on Biometeorology, Philadelphia, Pa. (1972).

7. Hilst, G. R., "The Sensitivities of Air Quality Predictions to Input Errors and Uncertainties," Proceedings of the Symposium on Multiple Source Urban Diffusion Models, Environmental Protection Agency, Research Triangle Park, N.C. (1970).

LIST OF FIGURES

1. Cumulative frequency distributions for model calculated max 24-hour concentrations at all three plants--base case.

2. Sensitivity of the yearly max 24-hour concentration to changes in stack gas exit velocity.

3. Sensitivity of the yearly max 24-hour concentration to changes in stack height and terrain adjustment.

4. Sensitivity of the yearly max 24-hour concentration to changes in mixing height.

5. Sensitivity of the yearly max 24-hour concentration to changes in wind speed.

6. Cumulative frequency distributions of daily max 24-hour concentrations at Muskingum River--three meterological data sets.

7. Cumulative frequency distributions of daily max 24-hour concentrations at Philo--three meteorological data sets.

8. Cumulative frequency distributions of daily max 24-hour concentrations at Stuart--three meteorological data sets.

FIGURE 1. CUMULATIVE FREQUENCY DISTRIBUTIONS FOR MODEL CALCULATED MAX 24-HOUR CONCENTRATIONS AT ALL THREE PLANTS - BASE CASE

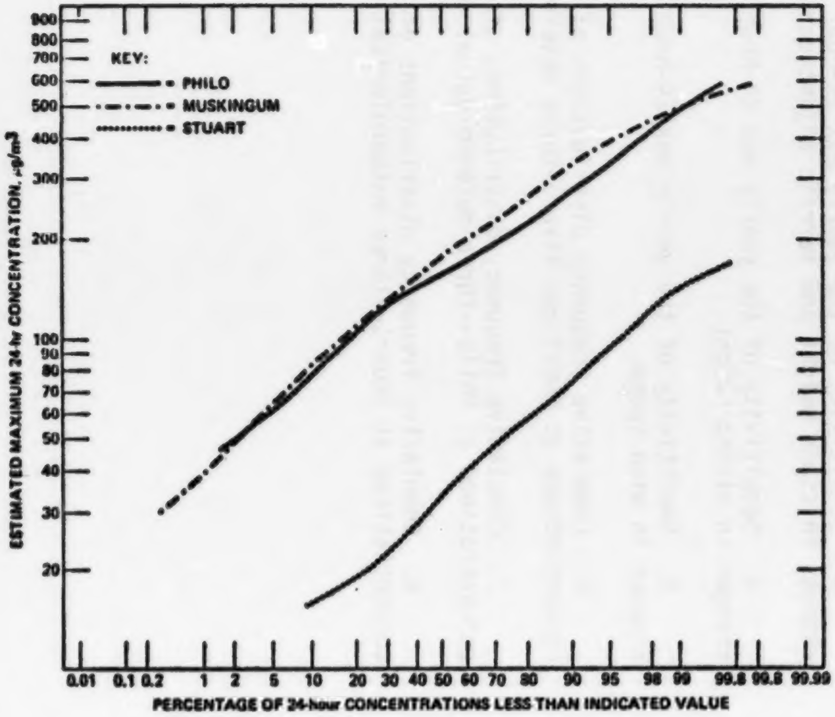

FIGURE 2. SENSITIVITY OF THE YEARLY MAX 24-HOUR CONCENTRATION TO CHANGES IN STACK GAS EXIT VELOCITY

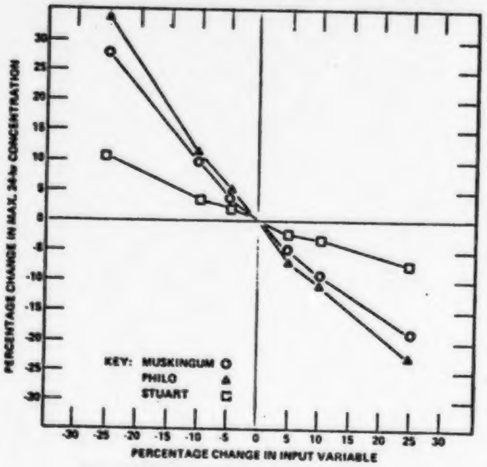

FIGURE 3. SENSITIVITY OF THE YEARLY MAX 24-HOUR CONCENTRATION TO CHANGES IN STACK HEIGHT AND TERRAIN ADJUSTMENT

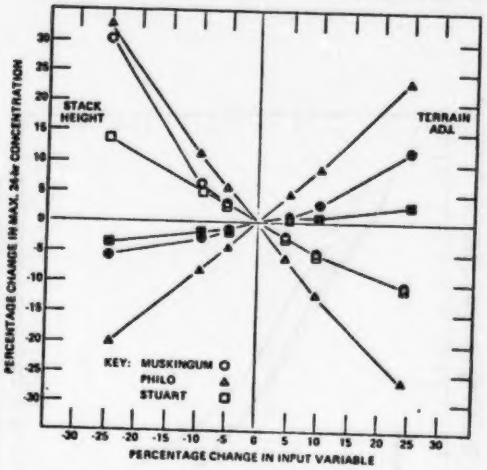

FIGURE 4. SENSITIVITY OF THE YEARLY MAX 24-HOUR CONCENTRATION TO CHANGES IN MIXING HEIGHT

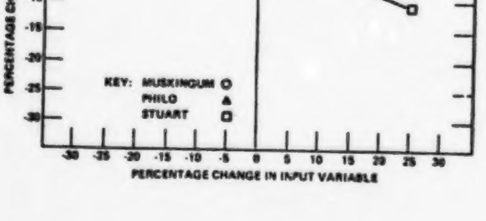

FIGURE 5. SENSITIVITY OF THE YEARLY MAX 24-HOUR CONCENTRATION TO CHANGES IN WIND SPEED

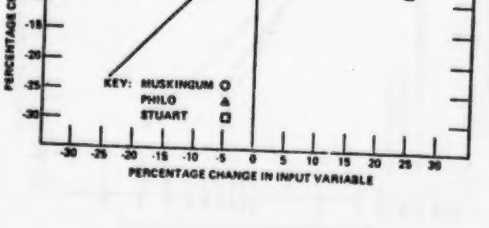

FIGURE 6. CUMULATIVE FREQUENCY DISTRIBUTIONS OF DAILY MAX 24-HOUR CONCENTRATIONS AT MUSKINGUM RIVER - THREE METEOROLOGICAL DATA SETS

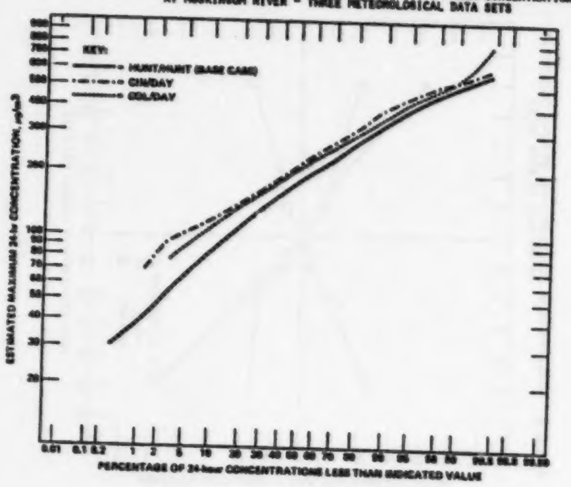

FIGURE 7. CUMULATIVE FREQUENCY DISTRIBUTIONS OF DAILY MAX 24-HOUR CONCENTRATIONS AT PHILO - THREE METEOROLOGICAL DATA SETS

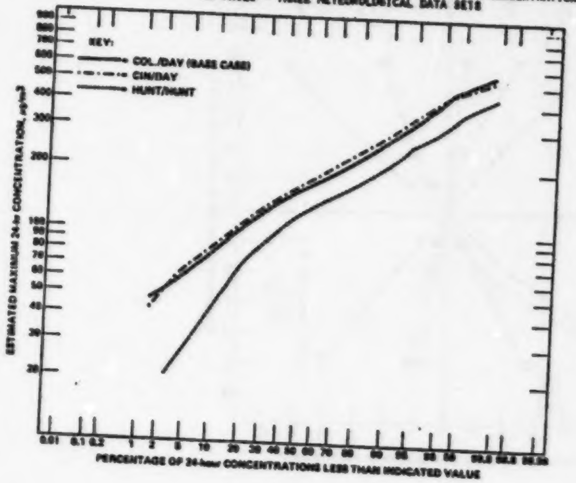

FIGURE 8. CUMULATIVE FREQUENCY DISTRIBUTIONS OF DAILY MAX 24-HOUR CONCENTRATIONS AT STUART - THREE METEOROLOGICAL DATA SETS

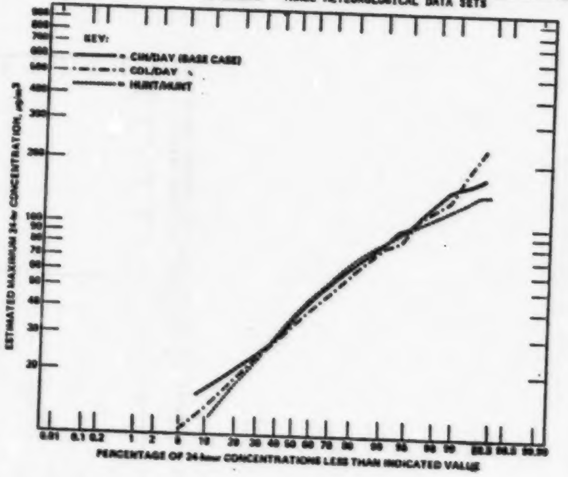

CONCENTRATION AND INDEX SENSITIVITY OF A GAUSSIAN PLUME MODEL*

William J. Veigele
and
Reed L. Clayson

9 September 1976
Airlie, Virginia
U.S.A.

7th International Technical Meeting on Air Pollution Modeling
and its Application

---

*The work reported in this paper was sponsored in part by a grant from the U.S. Federal Highway Administration and in cooperation with the Colorado Department of Highways. The contents of this paper reflect the views of the contractor, who was responsible for the facts and the accuracy of the data and forms presented herein. The contents do not necessarily reflect the official views or policies of the Colorado Department of Highways or the Federal Highway Administration. This paper does not constitute a standard, specification, or regulation. The sponsoring agencies have not reviewed this paper.

CONCENTRATION AND INDEX SENSITIVITY OF A GAUSSIAN PLUME MODEL

1. INTRODUCTION

Land planners need convenient and comprehensive tools to assist them in evaluating the impact on air quality of proposed alternative land use plans, and public support of efforts to attain improved air quality is essential. For these reasons, it is necessary to develop and present air quality information in a manner which the specialists can use and the public can understand and use as a basis for decision. In the Pikes Peak area of Colorado, a fast growing area of the United States, we have found computer modeling to be an effective method for obtaining air quality information and presenting it for public consideration. Its effectiveness is enhanced by the use of an air quality index which helps planners make judgements and each individual grasp how he is likely to be affected by the air quality resulting from various growth and development alternatives.

This is a unique application of an index. Usually an index is used to give information about present air quality that is obtained from measurements. In our application we form an index from model predictions of future air quality.

This paper summarizes a study which helped define how well the air quality model and associated pollution index performed their intended function and informed land planners of how much detail they need for input data to the model to achieve desired accuracy.

2. ADVANTAGES AND DISADVANTAGES OF AN AIR QUALITY INDEX

Various air pollutants may be measured or predicted by modeling at many places in an urban area. This results in much data which the specialist, such as a land planner, needs to do his job. The mass of information may frustrate the citizen, however, because of his lack of familiarity with the meaning of the data. What the citizen needs is a simple single-valued representation of the complex air pollution situation. This is an air quality index.

Such an index has also been found useful for the land planner because it provides him with a single quantity to use as a criterion for judging the overall effect on air quality of future land development. This index allows him to make rapid evaluations of alternative land use plans.

The specialist must be aware, though, of the complexity that is hidden by a simple index. He must use the index only as a first approximation and guide to the influence on air quality of land development, and he must explore in greater detail candidate plans which he may have selected on the basis of the index.

3. CHARACTERISTICS OF THE COLAIR MODEL AND INDEX

The air quality model used in our study is a short- and long-term, steady state, nonreacting pollutant, Gaussian plume model built around the well-known formulation shown in Figure 1. The model simulates area, line, and point sources. It accepts area source inputs from the Projective Land Use Model (PLUM), which is maintained and used by the local Pikes Peak Area Council of Governments. It accepts line source inputs from the DOT-FHWA highway battery traffic simulations. Point sources are obtained from a local inventory of major emitters.

Our validation study showed that the model's outputs agree quite well with the observed data for the area, which consisted primarily of particulate readings from 10 stations.

Figure 2 shows the level of agreement. It is interesting to note that the model's outputs helped identify a poorly located monitoring station, represented by $\boxed{x}$ in the figure. The station was subsequently moved.

Outputs such as that illustrated in Figure 3 helped citizens and planners obtain some idea of the average and expected maximum levels of each pollutant. However, because of the mass of such information produced when several alternatives are considered, an air quality index was added to the model to simplify visualization of future air quality.

Federal primary and secondary ambient standards were established to protect the health and welfare of people. When compared by pollutant, these standards describe relative effects. A simple and direct index for relating given concentrations to relative effects then can be given by C_i/S_i, where C_i is the concentration and S_i is the ambient standard for the i th pollutant. This gives a simple factor by which the concentration of a pollutant exceeds or is less than that concentration considered harmful to health or prejudicial to welfare, if S_i is the primary or secondary standard, respectively.

This concept may be extended to consider a number of noninteracting pollutants simultaneously by writing the index as shown in Eq. (1) of Figure 4, where p is the total number of pollutants considered. A convenient scale or range of values can be established by adding undetermined constants to give the index illustrated in Eq. (2) and evaluating the constants by setting $C_i = S_i$ and $C_i = B_i$ where B_i is a lower limit, say the national or regional background concentration. This is equivalent to the Oak Ridge Index.

We further generalized Eq. (2) to calculate it at a receptor point, j, in each PLUM zone. The index for a PLUM zone was then given by Eq. (3) of Figure 4, where q is the number of receptors in the zone.

BASIC MODEL FORMULATION

$$\overline{\chi}(x, \psi) = \sum_{s} \sum_{v} \frac{2Qf(\psi, s, v)}{\sqrt{2\pi}\ \ \sigma_z\ \overline{v}\left(\frac{2\pi x}{16}\right)} e^{\left(-H^2/2\sigma_z^2\right)}$$

where $\overline{\chi}$ = mean concentration at distance x in direction ψ,

s = stability class,

v = wind speed class.

$f(\psi, s, v)$ = frequency of wind occurrence in direction ψ, stability class, s, and speed class, v,

Q = source emission rate,

σ_z = vertical dispersion coefficient at distance x,

$\overline{v}$ = mean wind speed in speed class v, and

H = mean effective source height calculated from the Briggs equation.

KAPPA SYSTEMS, INC.

Figure 1

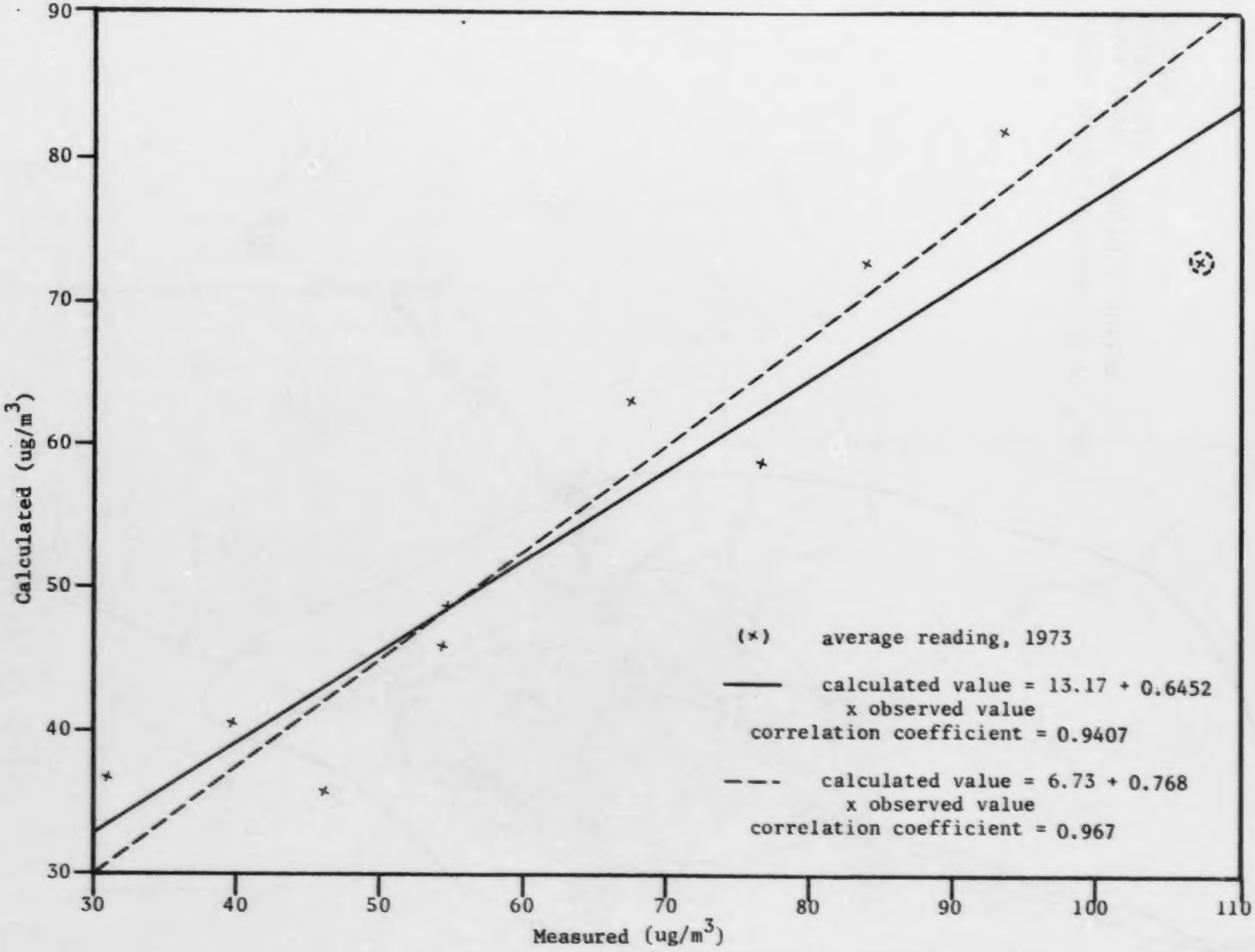
Calculated (ug/m³)
90
80
70
60
50
40
30
30
40
50
60
70
80
90
100
110
Measured (ug/m³)
(×) average reading, 1973
calculated value = 13.17 + 0.6452 x observed value
correlation coefficient = 0.9407
calculated value = 6.73 + 0.768 x observed value
correlation coefficient = 0.967

Figure 2

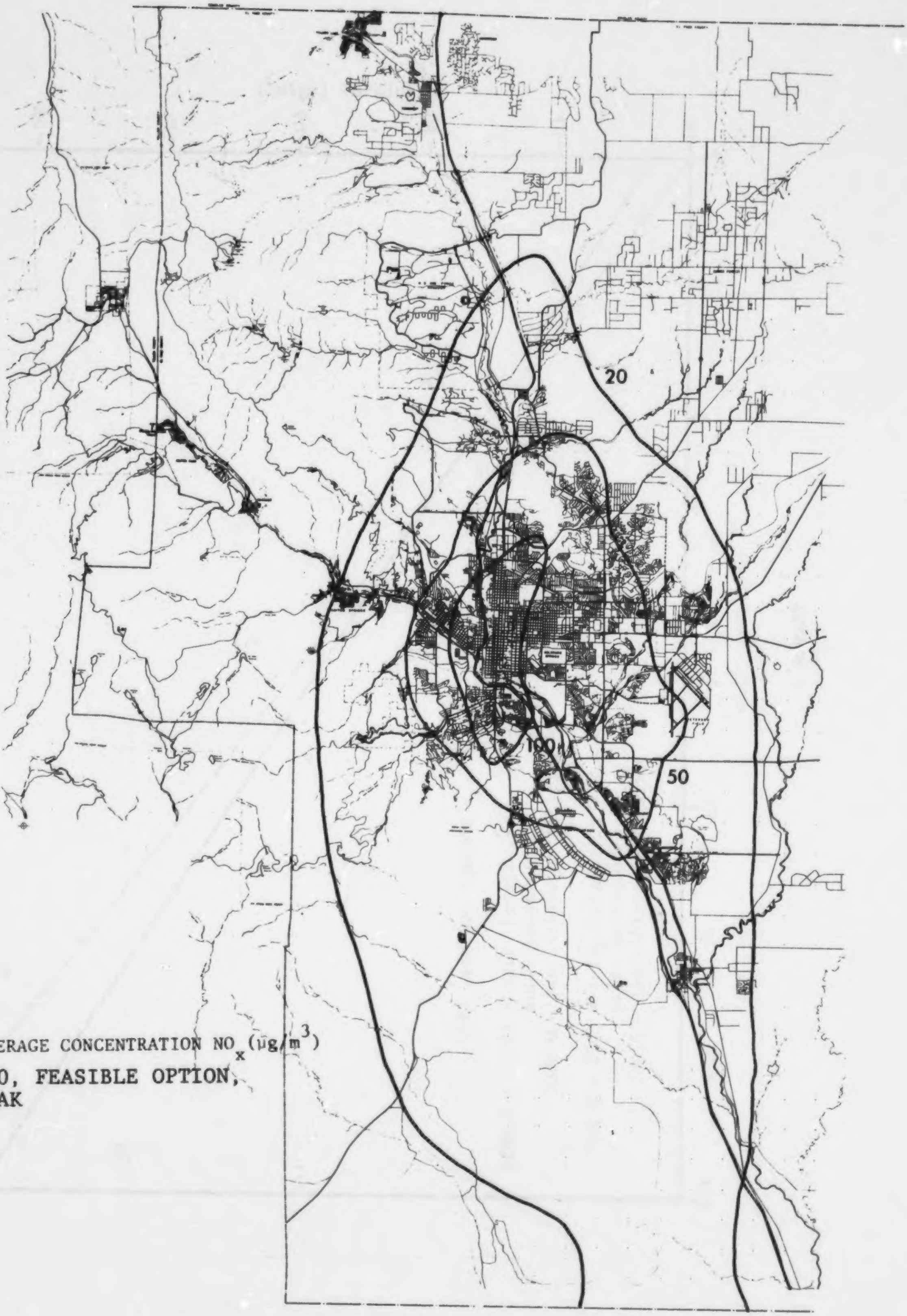

ANNUAL AVERAGE CONCENTRATION NO_x ($\mu g/m^3$)

YEAR 2000, FEASIBLE OPTION,
PIKES PEAK
REGION

Figure 3

INDEX FORMULATION

$$I_o = \sum_{i=1}^{p} \left(C_i / S_i \right) \qquad (1)$$

$$I = a \left[\sum_{i=1}^{p} \left(C_i / S_i \right) \right]^n \qquad (2)$$

$$I_z = (1/q) \sum_{j=1}^{q} a \left[\sum_{i=1}^{p} \left(C_{ij} / S_i \right) \right]^n \qquad (3)$$

KAPPA SYSTEMS, INC.

Figure 4

However, the PLUM zones are of various sizes and shapes, as shown in Figure 5. They represent neighborhoods, and the population and employment within each zone tend to be uniformly distributed. If we examine an extreme case, say Zone 32, and if the receptor grid places receptors as shown in Figure 6, we see that some of the receptors located just outside the zone tell us something about air quality in part of the zone. Also, a receptor located near the centroid of a zone is more representative of the air quality of the zone than is one located near the edge.

With this in mind, we used a probabilistic procedure in calculating the zonal index. The centroid of each zone was found, and it was assumed that pollutant concentrations that contribute significantly to the zonal index are from receptors that are within a circle of radius 2R, where $R = \sqrt{\pi/A}$ and A is the area of the zone. It was further assumed that the influence of each of these receptors varies with the distance, r_j, from the centroid as given in Eq. (1) of Figure 7, where $P(r_j)$ is the probability that the concentration at the receptor j will influence the zone of interest and A is a normalizing constant. This leads to the working equation given as Eq. (2) in Figure 7.

The zonal index proved useful because people could associate air quality with places where they lived or worked. However, we were also interested in predicting how population would be affected by alternative growth strategies, so we extended the index to include the number of people who should be associated with each receptor. It was assumed that the population and employment density within each zone was uniform, and both population and employment were considered in defining an average population for each zone. The distance of a receptor from the centroid was used in the allocation of population to receptors as described in the determination of a zonal index, and we could then predict what fraction of the population of each zone should be assigned the air quality index associated with each nearby receptor. From these data, we could determine an average population exposure and a cumulative exposure distribution. We could then compare alternative growth and development strategies on several bases, such as average regional air quality, average exposure, and number of percentage of people exposed to more than a given cumulative pollution level.

4. APPLICATIONS OF THE COLAIR MODEL AND INDEX

Predicted air quality concentrations and indices were used for evaluating a series of future community growth options. A refined growth plan was evolved, based in part upon public response to the data developed by the air quality model. The model has also been used for other planning activities.

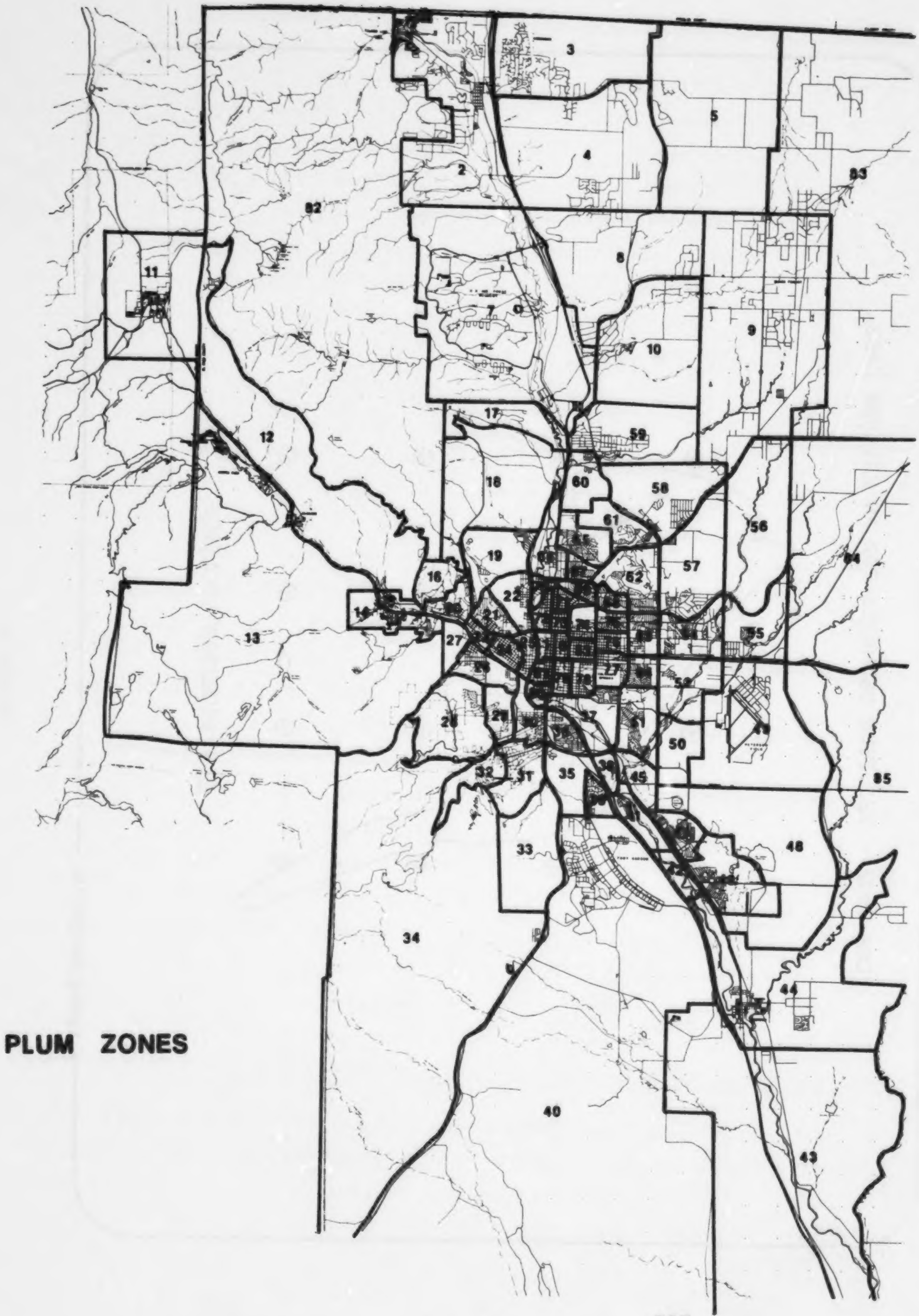
PLUM ZONES
3
5
4
2
83
82
11
8
7
10
9
17
59
12
18
60
58
61
56
19
57
62
84
16
14
22
55
13
27
28
26
29
27
50
85
32
31
35
38
45
33
48
34
44
40
43

Figure 5

PLUM ZONE - RECEPTOR GEOMETRY FOR AN EXTREME CASE

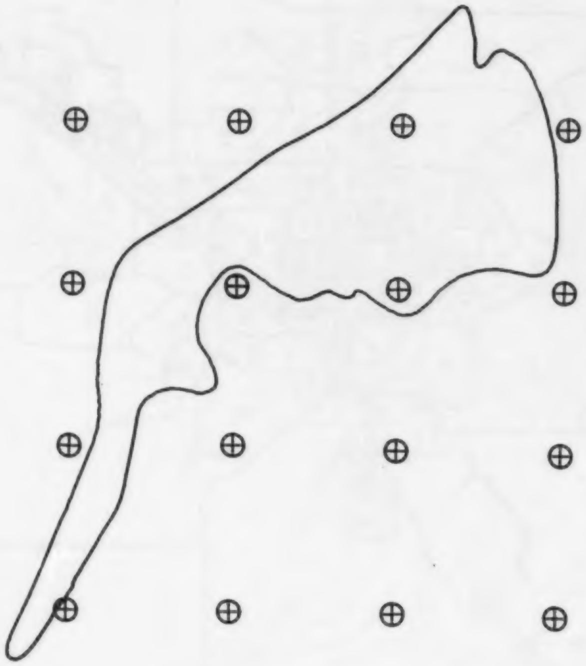

⊕ = RECEPTOR LOCATION

KAPPA SYSTEMS, INC.

Figure 6

PROBABILISTIC FORMULATION OF ZONAL INDEX

$$P(r_j) = Ae^{-r_j^2/R^2} \qquad (1)$$

$$I_p = \sum_{j=1}^{q} P(r_j) \quad a\left[\sum_{i=1}^{p}\left(C_{ij}/S_i\right)\right]^n$$

$$= \frac{\sum_{j=1}^{q}\left\{ e^{-r_j^2/R^2} \quad a\left[\sum_{i=1}^{p}\left(C_{ij}/S_i\right)\right]^n \right\}}{\sum_{j=1}^{q} e^{-r_j^2/R^2}} \qquad (2)$$

Figure 7

5. SENSITIVITY OF CONCENTRATIONS AND INDICES

If a computer model is used frequently, it is important to know how detailed and accurate the input data should be because time to maintain the data base, time to prepare input data, and time to run the model on a computer are all functions of the detail of the input data. The important question arises, "How detailed must the input data be to achieve a desired accuracy in the output?" Or one could ask a corollary question, "How sensitive is the output to uncertainties in input data?"

To answer these questions, we performed a series of sensitivity analyses. We were interested in the sensitivity of the individual pollutant concentrations and the index values to errors in input variables.

We started with a base case defined as the "no error" case, which was a detailed prediction of air quality for the year 2000, and sequentially introduced data aggregations or errors in input parameters. For convenience, we call all of these input variations errors. Some errors are likely to be random, and others systematic. We introduced the errors shown in Figure 8. Generally, we evaluated the resulting errors in concentrations of each pollutant, and zonal index, by averaging over 315 receptor points in our grid.

An example of errors in concentrations from errors in input data is the following. Eighty-one PLUM zones are presently used as area sources in the model. Sensitivity to the number of area sources was tested by aggregating these 81 zones into 15 superzones that are commonly used by the local planning agency. Results are shown by pollutant in Figure 9. Except for particulate matter, the average errors introduced by the aggregation are quite small. This is because CO, HC, and NO_x are mostly from point and line sources. Thus, the planner can exercise less care in preparing area source inventories of pollutants other than TSP.

Figure 10 illustrates model sensitivity to other errors, using the zonal pollution index as the criterion. To see how the zonal pollution index tends to average errors in pollutant concentrations, we refer to the case of random errors in source strength shown in Figure 11. We assumed that there would be many sources with small errors in strength and fewer sources with large positive or negative errors. Therefore, the errors were introduced to the sources by selecting each source randomly and assigning an error to it by using a random number generator and comparing each number with a normal distribution of errors. A standard deviation of the distribution of $\sigma = 0.5$ was selected arbitrarily.

Results indicate errors of about 20-30% in concentrations of HC, NO_x, and TSP but only about 10% in the zonal index. The error in CO is low because there are many sources well distributed.

ERRORS INTRODUCED IN SENSITIVITY TEST

RANDOM ERRORS IN SOURCE STRENGTH

SYSTEMATIC ERRORS IN WIND SPEED

SYSTEMATIC ERRORS IN EFFECTIVE STACK HEIGHT

SYSTEMATIC ERRORS IN VERTICAL DIFFUSION STANDARD DEVIATION

SYSTEMATIC ERRORS IN SOURCE LOCATION

SEQUENTIAL AVERAGING OF POINT SOURCES INTO AREA SOURCES

AGGREGATION OF AREA SOURCES INTO LARGER AREAS

AGGREGATION OF LINE SOURCES INTO AREA SOURCES

Figure 8

ERRORS IN CONCENTRATIONS (%) PRODUCED BY REAGGREGATION OF AREA SOURCES INTO SUPERZONES

CO	0.3
HC	0.4
NO_X	2.1
TSP	7.3

KAPPA SYSTEMS, INC.

Figure 9

SENSITIVITY OF ZONAL POLLUTION INDEX TO INPUT ERRORS

CASE	DESCRIPTION OF INPUT ERROR	PERCENT ERROR IN ZONAL INDEX
1	Random Error ($\sigma = 0.5$) in Source Strength	9.9
2	+50% Error in Wind Speed	30.7
3	-50% Error in Point Source Stack Height	10.5
4	-10% Error in Point Source Stack Height	3.6
5	+10% Error in Point Source Stack Height	0.7
6	+50% Error in Point Source Stack Height	4.1
7	-10% Error in Vertical Diffusion Coefficient (σ_z)	6.7
8	+10% Error in Vertical Diffusion Coefficient (σ_z)	5.5
9	5% Error in Vertical Source Location	81.35*
10	Conversion of Point Sources to Area Sources ($<$ 50 tons/year)	1.4
11	Aggregation of Area Sources into "Superzones"	N/A
12	Conversion of Small ($<$ 15,000 VM/day) Line Sources to Area Sources	1.3

*Based on NO_x concentrations only, with "background" excluded; all other cases based on combined carbon monoxide, hydrocarbon, nitrogen oxide, and particulate matter concentrations.

KAPPA SYSTEMS, INC.

Figure 10

ERRORS (%) IN CONCENTRATIONS AND ZONAL POLLUTION INDEX PRODUCED BY RANDOM ERRORS IN SOURCE STRENGTHS

CO	1.9
HC	29.6
NO_X	23.3
TSP	21.9
ARITHMETIC MEAN	19.2
GEOMETRIC MEAN	13.0
ZONAL POLLUTION INDEX	9.9

KAPPA SYSTEMS, INC.

Figure 11

Whereas the average concentration and zonal index are area-weighed, the population exposure index is weighted by population. Figure 12 is a cumulative distribution chart of the population exposure. For example, one might use this chart to find what percent of the population would be exposed to over-standard conditions under each land use alternative. Recalling that an index of over 100 is equivalent to exposure to over-standard pollution, and considering an index of say 60, this chart shows that, for the base case, about 40% of the population is predicted to be exposed to an index of at least 60.

If we introduce a 50% error in wind speed into our model one sees that the estimate of the fraction of the population exposed to an index of at least 60 drops to 20%. This means that an error of 50% in wind speed causes the planner to think that only half as many people will be exposed to this pollution level. Therefore, care should be exercised in obtaining wind speed input data as in a single source model.

Note that aggregation of small line sources (less than 15,000 vehicles per day) into area sources causes little error in the population exposure index. Therefore small line sources need not be inventoried carefully.

Figures 13 and 14 show similar distributions for errors in stack height and diffusion standard deviation.

The model also outputs distribution functions such as these for the population in each PLUM zone or for arbitrary groupings of PLUM zones or superzones. As one might expect, the effects on the population exposure index of some types of errors appear more pronounced when these more detailed outputs are compared.

We made a limited cost-effectiveness comparison to evaluate the amount of time to be saved if input data were prepared in less detail. Assumptions used in formulating this test included the following: the program already exists, 20 runs are to be made, and assembly of a data base for each case is required. The results are summarized in Figure 15, which shows, for example, that if line sources are aggregated into areas instead of being inventoried in detail the error in zonal pollution index is 1.4% but the total cost of doing these 20 cases is reduced by 19.2%.

6. CONCLUSIONS

To us, the most striking result of the analysis was the relative insensitivity of the pollution concentrations and pollution indices to almost all types of errors in input data of the magnitudes tested. This insensitivity would appear to apply to all cases in which there is no single, dominant emitter as in Colorado Springs, and in which many receptor points are employed in the prediction of air quality. This may not be true for restricted geographical areas in the region under particular meteorological conditions, or for short averaging times.

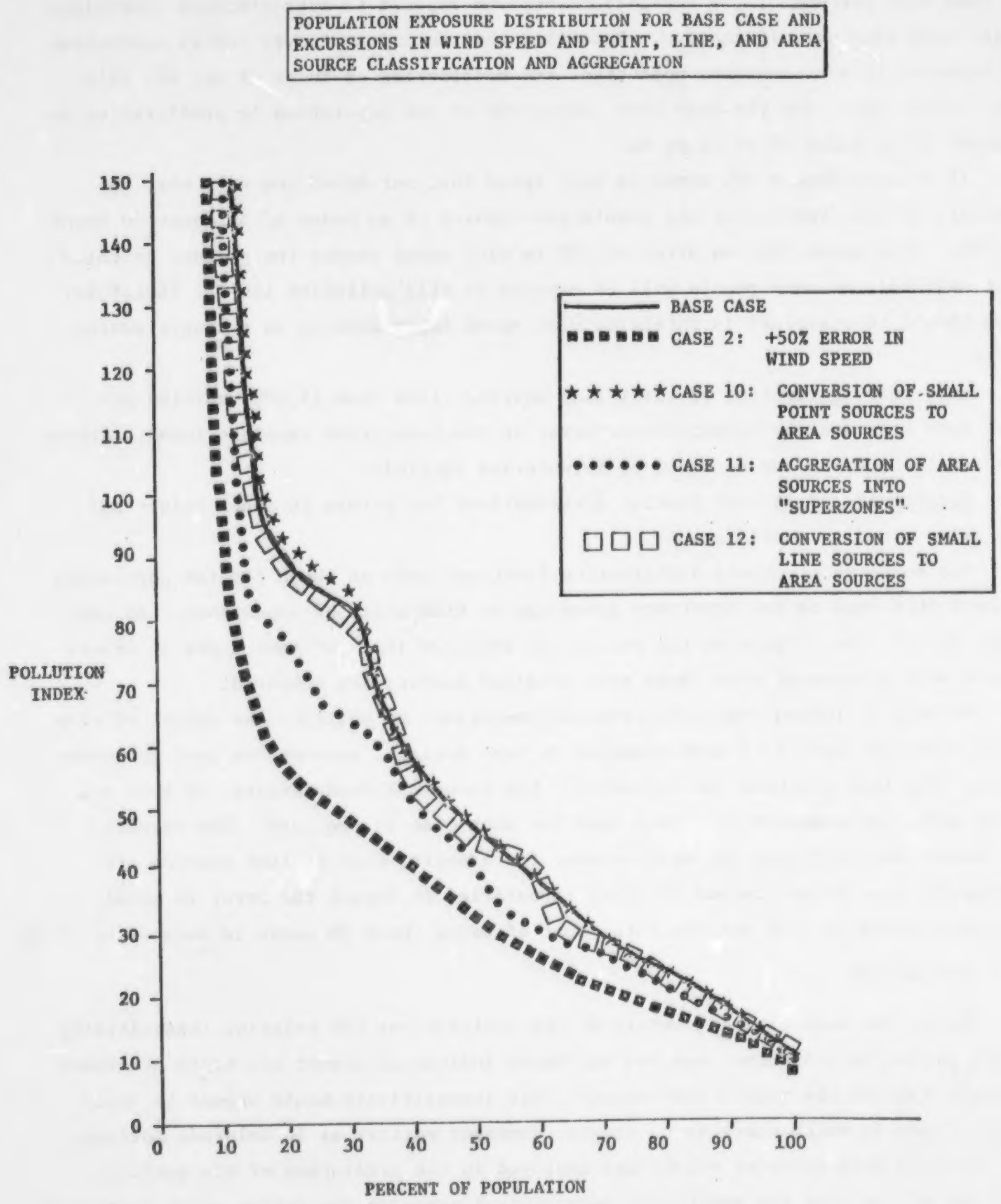
POPULATION EXPOSURE DISTRIBUTION FOR BASE CASE AND EXCURSIONS IN WIND SPEED AND POINT, LINE, AND AREA SOURCE CLASSIFICATION AND AGGREGATION
BASE CASE
■■■■■■ CASE 2: +50% ERROR IN WIND SPEED
★★★★★ CASE 10: CONVERSION OF SMALL POINT SOURCES TO AREA SOURCES
●●●●●● CASE 11: AGGREGATION OF AREA SOURCES INTO "SUPERZONES"
□□□ CASE 12: CONVERSION OF SMALL LINE SOURCES TO AREA SOURCES
POLLUTION INDEX
150
140
130
120
110
100
90
80
70
60
50
40
30
20
10
0
0
10
20
30
40
50
60
70
80
90
100
PERCENT OF POPULATION

Figure 12

POPULATION EXPOSURE DISTRIBUTIONS FOR BASE CASE AND EXCURSIONS IN POINT SOURCE STACK HEIGHT

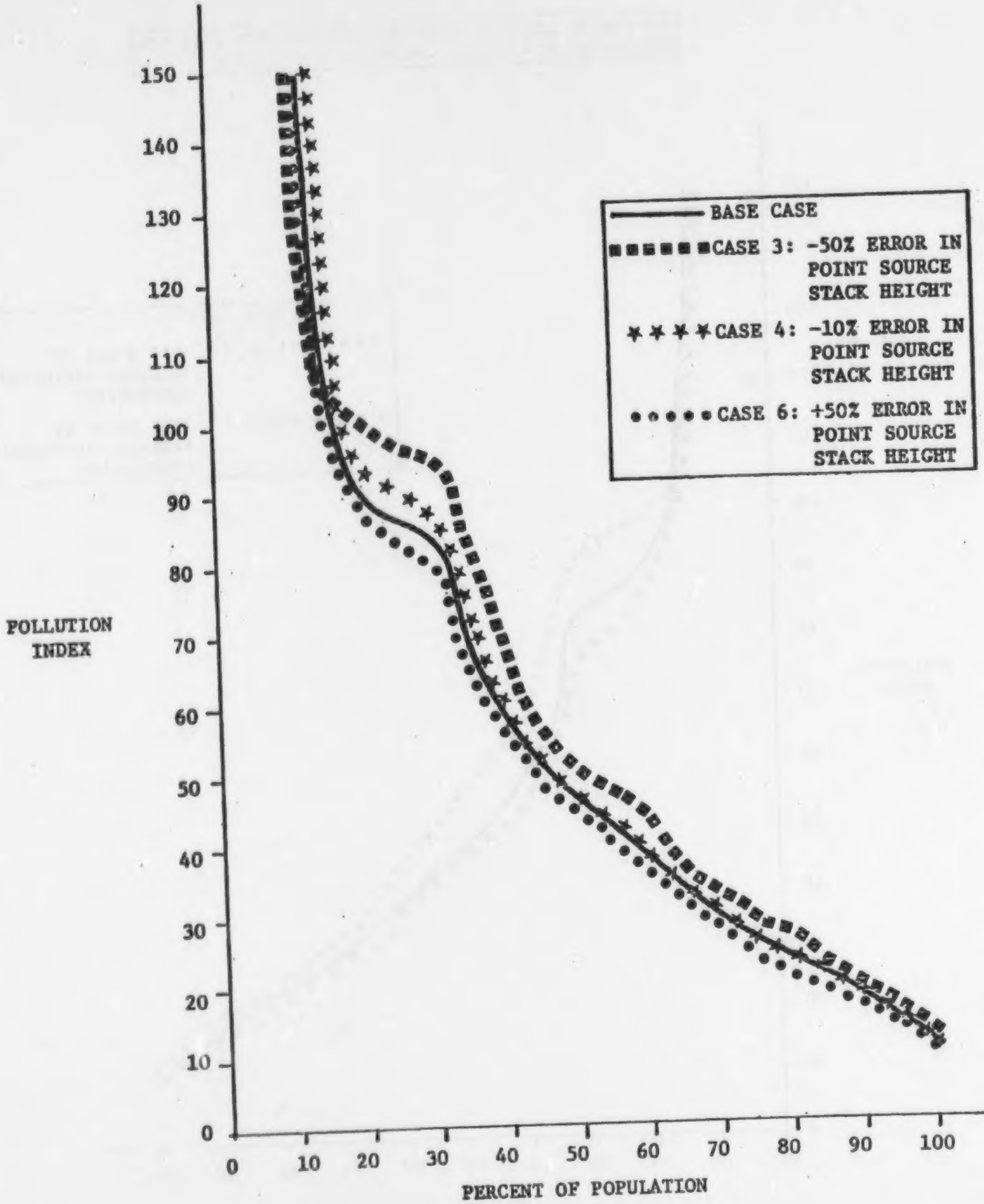

Figure 13

POPULATION EXPOSURE DISTRIBUTIONS FOR BASE CASE AND EXCURSIONS IN VERTICAL DIFFUSION COEFFICIENT

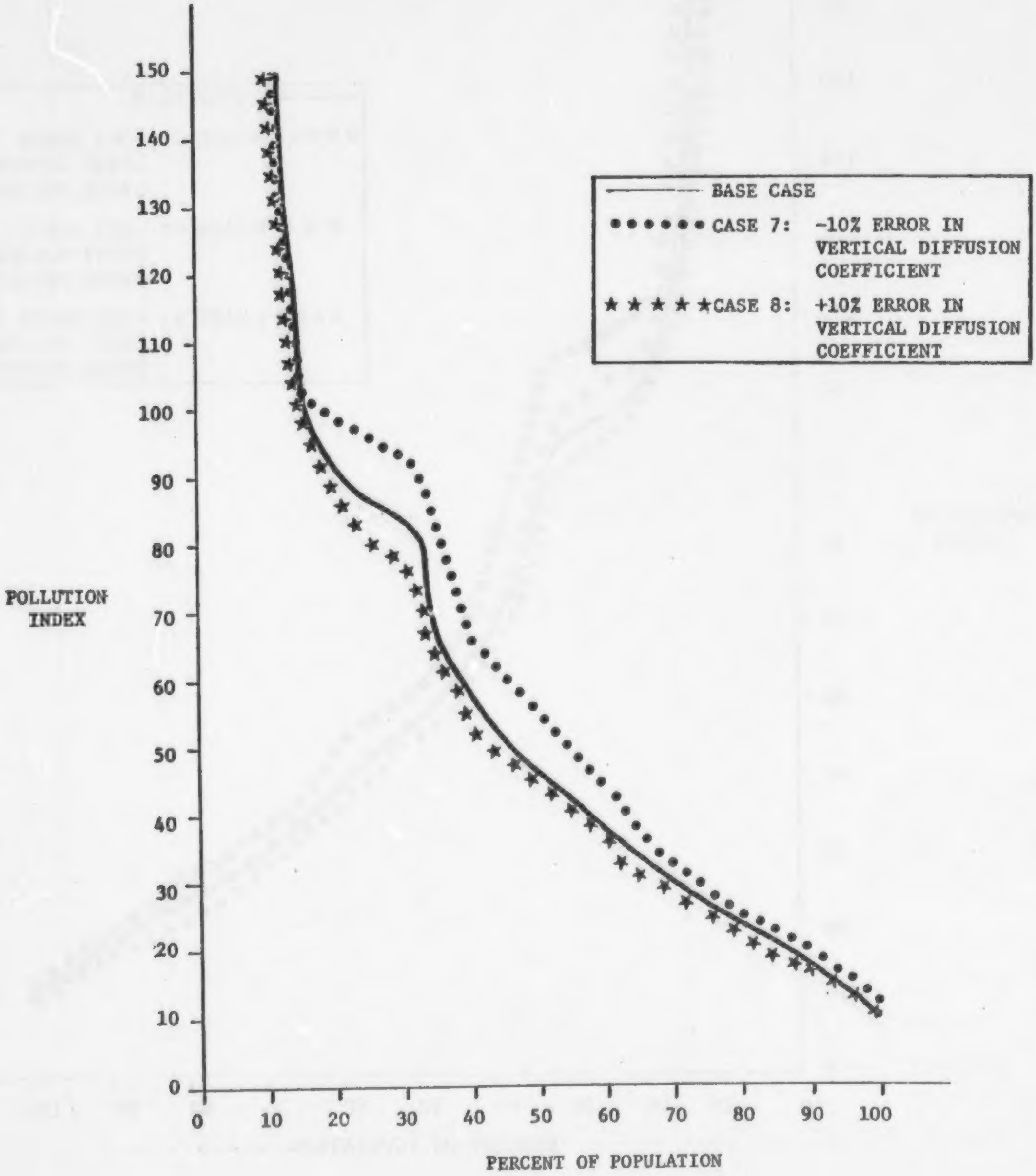

Figure 14

	PERCENT SAVINGS	ZONAL POLLUTION INDEX PERCENT ERROR
AGGREGATE AREA SOURCES (CASE 11)	8.9	1.3
AGGREGATE LINE SOURCES (CASE 12)	19.2	1.4
AGGREGATE POINT SOURCES (CASE 10)	9.3	2.5
AGGREGATE ALL SOURCES	37.4	-

Figure 15

Given this degree of insensitivity of the Gaussian model to errors in input data, concern over minor uncertainties in input data is not warranted. Therefore, significant savings in data preparation time and in computer processing time are possible. It also was shown that a zonal pollution index and a population exposure index are useful tools for land planning for air quality and for evaluating the sensitivity of a dispersion model.

7th International Technical Meeting
on Air Pollution Modeling and its Application

AN AIR QUALITY DISPERSION MODEL APPLICABLE TO CALM CONDITIONS

by

Robert J. Yamartino Jr.
Energy and Environmental Systems Division

Argonne National Laboratory
9700 South Cass Avenue
Argonne, Illinois 60439

September 7 - 10, 1976
Airlie Virginia
United States of America

AN AIR QUALITY DISPERSION MODEL APPLICABLE TO CALM CONDITIONS*

R. J. Yamartino

ARGONNE NATIONAL LABORATORY, Argonne, IL 60439

1. Introduction

Most solutions, both analytic and numerical, to the differential equation for atmospheric diffusion ignore diffusion in the downwind direction. This fact gives rise to the term u^{-1} in the expression for the concentration and renders these solutions unreliable for wind speeds (u) below about 1m/sec. This loss of predictive capability is unfortunate, as severe pollution episodes can occur during calm periods or periods of low winds when the wind direction becomes indeterminate.

An analysis[1] of the climatology near Chicago shows that such calm periods are not infrequent. Table 1 gives the percent probability of recording low hourly average wind speeds and reveals that during the summer months, calm conditions occur at night in excess of 40% of the time. Though these calm periods at Argonne persisted on the average for less than two hours (~1.8 hours) and never for more than 12 hours in the 15 year period considered, a calm ($u \leq 0.5$ mph) of seven hours duration is expected to occur once per year. Hence, from the point of view of compliance with ambient air standards, these infrequent, long-persistence calms may be of great importance.

Analytic solutions to the differential equation,

$$\frac{\partial C}{\partial t} = - \nabla \cdot (C\underset{\sim}{u}) + \nabla \cdot (D\nabla C) \quad ,$$

describing the space-time dependence of a pollutant concentration C and including the downwind diffusion term $D_x \frac{\partial^2 C}{\partial x^2}$, were first given by Roberts[2] (1923). His solutions, while well behaved at u = 0, were restricted to the case of constant diffusivities (i.e., molecular diffusion). More recently, Beryland et. al.[3] solved the time independent equation for u = 0 in cylindrical coordinates. Though their solution exhibits interesting properties, it is not clear how to make a smooth transition from their solution to traditional finite wind speed solutions as u is increased. Nunge[4] has also obtained solutions to the time dependent problem, though not in a form suitable for straightforward evaluation of the time averaging integral.

---

*Work supported by the U.S. Air Force Civil Engineering Center.

In this paper we begin with a Gaussian puff solution to the diffusion equation and obtain a closed form expression for the observed time-averaged concentration due to a steady-state source. The solution, valid for all wind speeds, is in a form compatible at finite wind speeds with the steady-state Gaussian plume formulation. Mathematical details of the model development are presented in section 2.

In section 3 we describe the procedure for setting the dispersion parameters and relate their values to existing experimentally determined quantities.

Special cases of model application under calm conditions are treated in sect. 4 and include: an approximate procedure for treating extended sources, effects of an inversion lid, line sources, and extended periods of calm.

Model limitations and possible improvements are discussed in sect. 5.

Table 1. Percentage of the Time that Hourly Average Wind Speeds (at 19') are Below a Given Value

Time Period	$u \leq 3$ mph (1.34 m/sec)	$u \leq 0.5$ mph (0.22 m/sec)
All months		
All day	17.3	3.1
0700-1800 CST	9.8	1.2
1900-0600 CST	24.9	5.0
July - September		
All day	27.7	5.2
0700-1800 CST	14.0	1.4
1900-0600 CST	41.4	8.9

2. Model Development

In the interest of achieving maximal compatibility at finite u with the steady-state Gaussian plume formulation, let us consider the dispersion of a Gaussian puff[5] of pollutant

$$C(x,y,z,t) = \frac{q}{(2\pi)^{3/2}\,\sigma_X(T)\;\sigma_Y(T)\;\sigma_Z(T)}\,e^{-1/2\left\{\frac{(X-uT)^2}{\sigma_X^2\,(T)} + \frac{Y^2}{\sigma_Y^2\,(T)} + \frac{Z^2}{\sigma_Z^2\,(T)}\right\}}$$

where u = wind speed　　$X = x - x'$

(x,y,z,t) = receptor coordinates　　$Y = y - y'$

(x', y', z', t') = source coordinates　　$Z = z - z'$

and q = pollutant mass　　$T - t - t'$

This expression explicitly satisfies mass conservation and for $\sigma_X(T) = \sigma_Y(T) = a_h T^{b_h}$ and $\sigma_Z(T) = a_v\, T^{b_v}$ satisfies the differential equation for diffusion with $D_X = D_Y = b_h\, a_h^2\, T^{2b_h - 1}$ and $D_Z = b_v\, a_v^2\, T^{2b_v - 1}$.

In order to obtain the time averaged concentration one would observe in the case of continuous pollutant emission at rate Q, we must integrate over source time and average over receptor time. Fortunately, the integrand is only a function of $T = t - t'$, so that the two-dimensional integral may always be reduced to a sum of at most three one-dimensional integrals. Ignoring momentarily the case $b_v \neq b_h$ (i.e., $b \equiv b_h = b_v$) and introducing the new variable $\phi = \phi\,(T) = \left(\frac{t_d}{T} - \eta\right)$ and additional parameters $t_d \equiv (R/a_h)^{1/b}$, $\varepsilon \equiv \frac{ut_d}{R}$, $\eta \equiv \varepsilon\,\frac{X}{R}$ where $R \equiv \sqrt{X^2 + Y^2 + Z'^2}$ and $Z' \equiv \frac{a_h}{a_v} Z$, we find that the time average concentration, $\overline{C}\,(x,y,z)$, for the case of both source and receptor being turned on at time zero and off at time τ is just

$$\overline{C}\,(x,y,z) = \frac{Q\,t_d^{1-3b}}{(2\pi)^{3/2}\,a_h^2\,a_v}\int_{\phi_\tau}^{\infty} d\phi\;(\phi-\phi_\tau)\;(\phi+\eta)^{3b-3}\;e^{-1/2\{\phi^2-\eta^2+\varepsilon^2\}\;(\phi+\eta)^{2b-2}} \qquad (1)$$

where $\phi_\tau \equiv \phi(\tau)$. Combining the results of solving the above integral exactly for u = o and approximately for all u by setting b = 1 in the integrand, we obtain the approximate solution.

$$\overline{C}\,(x,y,z) = \frac{Q\Gamma\left(\frac{3b-1}{2b}\right)}{(2\pi)^{3/2}\, a_h^2\, a_v\, (2b)} \left(\frac{2a_h^2}{R^2}\right)^{\frac{3b-1}{2b}} e^{-\frac{\varepsilon^2}{2}\,(1-X^2/R^2)}\, f(\phi_\tau/\sqrt{2}) \qquad (2)$$

where $f(\xi) \equiv e^{-\xi^2} - \sqrt{\pi}\;\xi \operatorname{erfc} \xi$.

A somewhat better approximation is obtained by noting that for b = 1 the integrand takes on its maximal value at $\phi = \frac{\phi_\tau}{2} + \sqrt{1 + \frac{\phi_\tau^2}{4}}$. Assuming that most of the contribution to the integral comes from this ϕ region, the last two terms in the solution become

$$e^{-\frac{\varepsilon^2\alpha^2}{2}\,(1-X^2/R^2)}\quad \alpha f\,(\alpha\phi_\tau/\sqrt{2})\ ,\quad \text{where } \alpha \equiv \left[\eta + \frac{\phi_\tau}{2} + \sqrt{1 + \frac{\phi_\tau^2}{4}}\right]^{b-1}.$$

Though this modification to the original solution (eq. 2) falls short of providing an exact analytic solution, it does enable one to get back to the Gaussian plume expression

$$\overline{C}\,(x,y,z) = \frac{Q}{2\pi\,\sigma_Y\,\sigma_Z\,u}\; e^{-1/2\left\{\frac{Y^2}{\sigma_Y^2} + \frac{Z^2}{\sigma_Z^2}\right\}}.$$

with $\sigma_y = a_h\left(\frac{X}{u}\right)^b$ and $\sigma_Z = a_v\left(\frac{X}{u}\right)^b$

in the limit when conditions appropriate to the Gaussian plume approach (i.e., $R/u \ll t_d$, $X \simeq R$, and $\tau \to \infty$) pertain.

In spite of this formal advantage offered by the modified solution, numerical results have proven quite insensitive to the change so that in practice the original solution (eq. 2) has been used.

This method of considering where the integrand takes on its maximum value can also be employed to estimate the reduced concentration one would observe when monitoring a pollutant with a slow decay or loss rate $\lambda << 1/\tau$. The approximate result is that the concentration is reduced by the factor $e^{-\lambda T_R}$ where the effective residence time T_R is given as

$$T_R \approx \left[\frac{1}{2} \left(\frac{Xu}{R^2} + \frac{1}{\tau} \right) + \frac{1}{t_d} \sqrt{1 + \frac{\phi_\tau^2}{4}} \right]^{-1}$$

For $R/u << t_d$, $R/u << \tau$ and $X \approx R$ the above expression reduces to $T_R \approx X/u$ for $X > 0$, while in the zero wind speed limit with $\tau >> t_d$, the residence time becomes $T_R \approx t_d$ as expected.

Finally, let us consider removal of the restriction $b_v = b_h$ $(\equiv b)$. Though brute force attempts at dealing with this appear fruitless, one might ask whether there exists a transformation of the form $Z' = KZ^p$ which will enable us to satisfy the mass conservation condition

$$\frac{1}{\sqrt{2\pi\, a_v\, T^{b_v}}} \int_{-\infty}^{\infty} dZ \quad e^{-\frac{1}{2}\left\{ \frac{Z'^2}{a_h^2\, T^{2b}} \right\}} = 1$$

for all T? Evaluation of the above integral leads immediately to the solution

$$K = \sqrt{2}\; a_h \left[\frac{\Gamma\left(\frac{1}{2p}\right)}{\sqrt{2\pi}\; a_v\; p} \right]^p \qquad \text{where } p = b/b_v$$

Incorporating this change into equation (1) leads to a slightly modified solution

$$\overline{C}(x,y,z) = \frac{Q\,\Gamma\left(\frac{3\bar{b}-1}{2b}\right)}{(2\pi)^{3/2}\,a_h^2\,a_v\,(2b)}\left(\frac{2a_h^2}{R^2}\right)^{\frac{3\bar{b}-1}{2\bar{b}}} e^{-\frac{\varepsilon^2}{2}(1-X^2/R^2)}\, f(\phi_\tau/\sqrt{2}) \qquad (3)$$

where $\bar{b} \equiv \dfrac{2b + b_v}{3}$ and $Z' = KZ^p$ throughout.

Thus, we have achieved a situation where the form $\sigma_Z = a_v T^{b_v}$ appears in the expression for the axial concentration (i.e., $Z = 0$) without sacrificing explicit mass conservation. What is lost however is the explicit Gaussian form in the Z direction, that is

$$\ln\left[\frac{C(Z)}{C(0)}\right] \sim Z^{2p} \text{ with } p \neq 1.$$

That this is not a serious loss can be argued by noting that experimental[6] measurements of vertical plume profiles have indicated that $2p \approx 1.5 \pm 0.3$, while transverse plume profiles[7] fit with

$$\ln\left[\frac{C(Y)}{C(0)}\right] \sim Y^r$$ have yielded values of r ranging from 1.5 to 2.7.

Comparison of the slopes of the time dependent dispersion coefficients, $\sigma_Y(T)$ and $\sigma_Z(T)$, presented in either the Nashville[8] or St Louis[9] studies strongly suggests the need for allowing the slope parameters b_v and b_h to be different. In the next section we present the coefficients resulting from a best fit to Gaussian plume predicted concentrations. It was found that the additional degree of freedom (i.e., $b_v \neq b_h \equiv b$) did not lead to improved results and was therefore deleted. This apparent contradiction might be due to the fact that our results pertain to constant radiation class and not constant stability class. In addition, the explicit Gaussian dependences in the Gaussian plume model strongly bias against $b_v \neq b_h$ in this treatment.

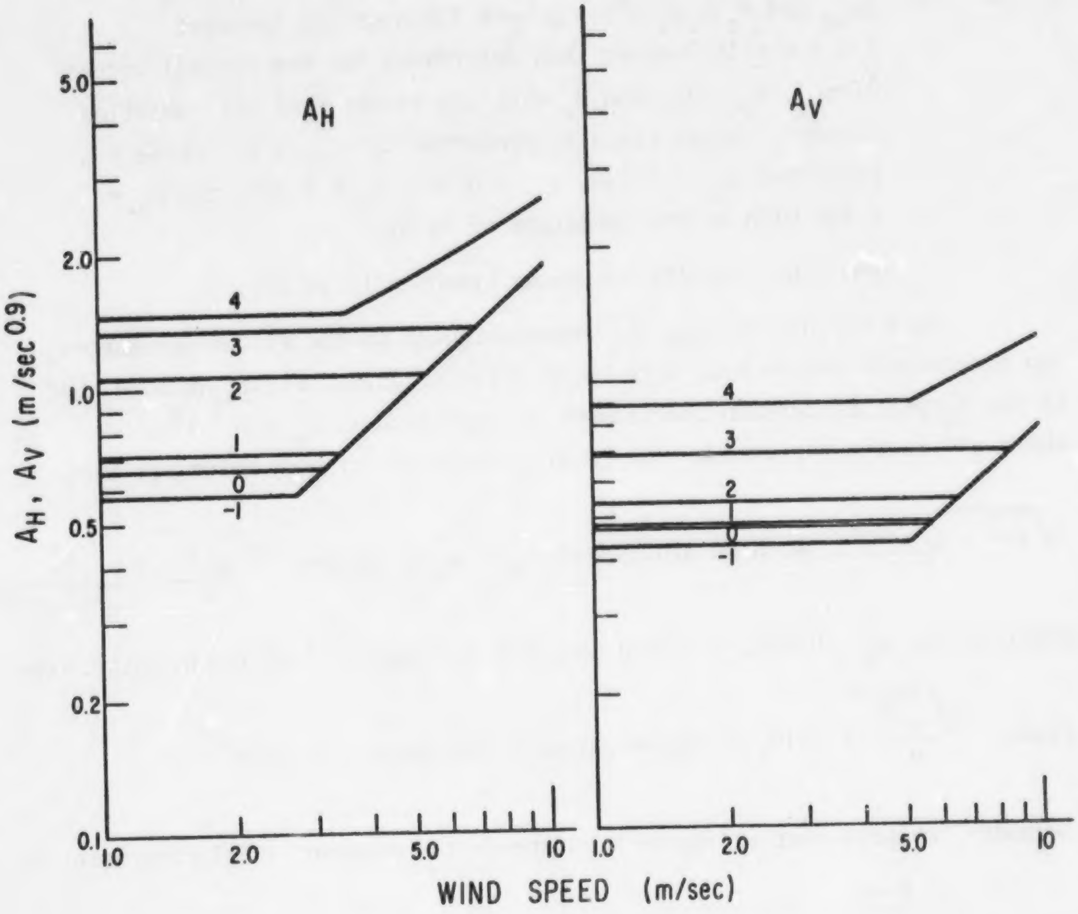

fig. 1 Horizontal and vertical dispersion coefficients as a function of wind speed. The curves are numbered according to radiation class.

iii) To avoid the sudden transition from the low to high wind speed solutions, a constant $d_h(d_v)$ was added to the high wind speed parameterization of $a_h(a_v)$ so that the value of $a_h(a_v)$ now becomes the greater of a_{hc} and $d_h + a_h' u^b$ (a_{vc} and $d_v + a_v' u^b$). A best fit over the interval $1.5 \leq u \leq 16.2$ m/sec then determines the new optimal values of a_{hc}, a_{vc}, d_h, and d_v with the result that all radiation classes, except class 4, preferred $d_h = d_v = 0$. Class 4 preferred $a_{hc} = 1.462$, $a_{vc} = 0.893$, $d_h = 0.728$, and $d_v = 0.459$ with an RMS deviation of 28.4%.

The final results are shown graphically in Fig. 1.

As a way of checking the reasonableness of the fitted parameters, two comparisons can be made with other existing data. First, we note that if the lateral dispersion coefficient is expressed as $\sigma_h^2 = \overline{v'^2}\, T^2$, where $\overline{v'^2}$ is the variance of the lateral component of eddy velocity, then

$\sqrt{\overline{v'^2}} = a_h/\tau^{1-b}$. At high wind speeds $a_h = a_h' u^b$ so that $\sqrt{\frac{\overline{v'^2}}{u}} = \frac{a_h'}{u^{1-b}\,\tau^{1-b}}$.

Substituting $a_h' = 0.233$, $\tau = 3600$ sec, $b = 0.9$, and $u^{0.1}$ of order unity, one finds $\sqrt{\frac{\overline{v'^2}}{u}} = 0.10$, in agreement with the canonical value[12].

Secondly, we note that at finite wind speeds the downwind axial concentration falls as $x^{\frac{2-4b}{b}}$. For $b = 0.9$ this exponent is -1.78; in reasonable agreement with observed values[12] near -1.75.

4. Special Cases of Model Application at Zero Wind Speed

Up to this point we have dealt with a model capable of describing both finite wind and zero wind situations. However, now that the parameters a_h, a_v, and b have been determined, we ignore further consideration of finite wind and deal with special applications at u = o, where equation (2) simplifies to:

$$\overline{C}(x,y,z) = \frac{Q\,\Gamma\left(\frac{3b-1}{2b}\right)}{2(2\pi)^{3/2}\, a_h^2\, a_v b} \left(\frac{2a_h^2}{R^2}\right)^{\frac{3b-1}{2b}} f(\phi_\tau/\sqrt{2}) \qquad (4)$$

where $\phi_\tau = t_d/\tau$ for u = o.

A. Source Averaging

Equation (4) gives the time(τ) averaged concentration $\overline{C}$ measured by a receptor at (x,y,z) due to a point source of strength Q at (x', y', z'). In many cases one is far enough from the source that a point approximation is sufficient, but what of cases when one is near to or perhaps even inside a spatially diffuse source? For $u \neq 0$ it is possible to simulate the effect of an area source by replacing it with a point source located a specific distance upwind. However, when u = o, the pseudo point source concept breaks down, and the actual integration over source coordinates must be dealt with. For simplicity, let us consider the case of a source with a Gaussian spatial strength specified by the quantities σ_{xs}, σ_{ys}, and σ_{zs}. In principle, one could numerically carry out the triple integral;

$$\overline{\overline{C}}(x,y,z) = \frac{1}{(2\pi)^{3/2}\sigma_{xs}\sigma_{ys}\sigma_{zs}} \iiint_{-\infty}^{+\infty} dx_s dy_s dz_s\, \overline{C}(X-x_s,\ Y-y_s,\ Z'-z_s')\, e^{-\frac{1}{2}\left\{\frac{x_s^2}{\sigma_{xs}^2}+\frac{y_s^2}{\sigma_{ys}^2}+\frac{z_s^2}{\sigma_{zs}^2}\right\}}$$

however, the computation effort would be prohibitive considering the number of source-receptor combinations in many applications.

Hence a numerical approximation to the above integral must be found. The first approximation we make is to pull the term $f(\phi_\tau/\sqrt{2})$ outside of the integral and set $\phi_\tau = 0$ when the receptor is inside the 1σ ellipsoidal surface of the source or $\bar{\phi}_\tau = \frac{\left(R_{MOD}/a_h\right)^{1/b}}{\tau}$ for receptors outside the 1σ surface, where

$$R^2_{MOD} \equiv (|x - x'| - \sigma_{xs})^2 + (|y - y'| - \sigma_{ys})^2 + \left(\frac{a_h}{a_v}\right)^2 (|z - z'| - \sigma_{zs})^2$$

and x', y', z' are now the coordinates of the source center.

This is a reasonable approximation since for source-receptor distances small enough to require source integration, the diffusion time, $t_d = (R/a_h)^{1/b}$, is much less than the averaging time τ (= 1 hour). Hence $\phi_\tau << 1$ anywhere of interest and $f(\phi_\tau/\sqrt{2}) \approx 1 - \sqrt{\frac{\pi}{2}}\,\phi_\tau \approx 1$ to first order.

Thus, ignoring constants, the problem reduces to consideration of the integral

$$I = \left(\frac{a_v}{a_h}\right) \iiint_{-\infty}^{+\infty} \frac{dx_s dy_s dz'_s \quad e^{-\frac{1}{2}\left\{\frac{x_s^2}{\sigma_{xs}^2} + \frac{y_s^2}{\sigma_{ys}^2} + \frac{z_s'^2}{\sigma_{zs}'^2}\right\}}}{\left[(X-x_s)^2 + (Y-y_s)^2 + (Z'-z_s)^2\right]^p} \quad ,$$

where $\sigma'_{zs} = \left(\frac{a_h}{a_v}\right)\sigma_{zs}$ and $p = \frac{3b-1}{2b}$,

which can be shifted to spherical coordinates to eliminate the singularity, for p in the range of physical interest.

The integral was then evaluated to ~ 2% accuracy via an unweighted Monte Carlo procedure for 1000 cases involving a variety of source shapes and source-receptor configurations.

Source shape was determined by selecting random values of σ_{xs},σ_{ys}, and σ_{zs} in the interval from 0.1 to 3.0 (arbitrary units), thus permitting source aspect ratios as high as 30. Receptor location was then chosen randomly in the interval $o \leq X \leq 5\,\sigma_{xs}$, $o \leq Y \leq 5\,\sigma_{ys}$, and $o \leq Z \leq 5\,\sigma_{zs}$. It was found that the source integration could be approximated to within ~ 5% (RMS) by simply replacing R by R* where $R^{*2} \equiv X^{*2} + Y^{*2} + Z'^{*2}$ and

$$X^* = G\left(\left|\frac{X}{\sigma_{xs}}\right|\right) \quad |X| + q_4\,(\sigma_{xs}^2 + \sigma_{ys}^2 + \sigma_{zs}'^2)^{1/2} + q_5\,(\sigma_{xs}\,\sigma_{ys}\,\sigma'_{zs})^{1/3}$$

$$+ q_6 (\sigma_{ys}^2 + \sigma'^2_{zs})^{1/2} + q_7 \sigma_{ys} \left[\frac{X^2}{X^2 + q_8 \sigma_{ys}^2} \right] + q_7 \sigma'_{zs} \left[\frac{Z'^2}{X^2 + q_8 \sigma'^2_{zs}} \right]$$

$$+ q_9 \sigma_{xs} \left[\frac{Y^2 + Z'^2}{Y^2 + Z'^2 + q_{10} \sigma_{xs}^2} \right]$$

with $G(s) \equiv \left[1.0 - e^{-\theta(s)} (1.0 + \theta(s)) \right]^2$, $\theta(s) = q_1 s + q_2 s^2 + q_3 s^3$

for $0 \leq s \leq 5$, and $G(s) \equiv 1.0$ for $s > 5$.

Y^* and Z'^* then follow trivially from symmetry considerations.

The coefficients $q_1 - q_{10}$ below are given as the optimal set by MINUIT[13] and are sensitive only to the value of b.

$q_1 = 1.495$

$q_2 = -7.44 \times 10^{-2}$

$q_3 = -7.0 \times 10^{-3}$

$q_4 = 1.47 \times 10^{-3}$

$q_5 = 0.282$

$q_6 = 0.1626$

$q_7 = -0.4889$

$q_8 = 23.686$

$q_9 = 0.4318$

$q_{10} = 0.8757$

B. Two-Dimensional Dispersion

The effect of an inversion lid at height z=L can be computed by two techniques, both of which assume 100% reflection of the pollutant from the ground and from the lid. The first method involves simply representing each reflection by an appropriate "image" source and then summing the series. Unfortunately, for distances far from the source, this infinite series converges very slowly. Hence, let us consider the case of a uniform z distribution of pollutant with no further z diffusion. The average concentration seen by a receptor is just

$$\overline{C}(x,y,z) = \frac{Q}{2\pi L \tau a_h^2} \int_0^{\tau} \frac{dT(\tau - T)}{T^{2b}} \; e^{-\frac{1}{2} \left\{ \frac{(X-uT)^2 + Y^2}{a_h^2 T^{2b}} \right\}}$$

which for u = 0 can be integrated exactly and yields

$$\overline{C}(x,y,z) = \frac{Q}{2\pi L a_h^2 (2b)} \left(\frac{2a_h^2}{R^2} \right)^{\frac{2b-1}{2b}} F(b,\phi_\tau')$$

where

$$\phi_\tau' \equiv \left(\frac{1}{2} \right)^{1/2b} \frac{t_d}{\tau} \quad \text{and where}$$

F may be expressed in terms of incomplete Gamma functions as

$$F(b,\phi_\tau') = \Gamma\left(\frac{2b-1}{2b} , \phi_\tau'^{2b} \right) - \phi_\tau' \, \Gamma\left(\frac{b-1}{b} , \phi_\tau'^{2b} \right) .$$

Inspection of the series and asymptotic expansions[14] for the incomplete Gamma function suggests the more economical approximation

$$F(b,\phi_\tau') \approx \frac{\Gamma\left(\frac{2b-1}{2b} \right) e^{-\phi_\tau'^2}}{1.0 + f(\phi_\tau') + 2b \, \Gamma\left(\frac{2b-1}{2b} \right) \phi_\tau'^{2b+1}}$$

where $f(\phi_\tau')$ is a polynomial of order $< 2b + 1$ and where $f(0) = 0$. Choosing $f(\phi_\tau') = 6.1978 \, \phi_\tau' + 0.91880 \, \phi_\tau'^2$ for $b = 0.90$, one obtains an approximation for F good to ~ 2% over all ϕ_τ'.

C. Line Sources

The prediction of concentrations one will observe from line source emissions is usually complicated by the variable specifying the orientation of the line with respect to the wind direction. Fortunately, when u = 0 such problems disappear and the line source can simply be thought of as a high aspect-ratio volume source. Non-uniformities in source strength as a function position along the line can be accommodated by merely breaking the line into smaller line source segments. Such non-uniformities arise, for example, when considering accelerating aircraft, but even in the absence of this problem, some segmenting would have to be done in light of the fact that the volume source considered in Section 4A has a Gaussian profile in all three directions. A question arises of how well a sum of uniformly spaced Gaussians having the same σ, approximates a uniform distribution? It can be shown that for a given segment length, ℓ, the optimal value of σ is just $\sigma = \ell/2.30$.

The problem of arbitrary line source orientation is accommodated by a shift to a set of rotated coordinates (ρ_x, ρ_y, ρ_z) where the line source direction defines the ρ_x axis and the ρ_y axis has lies in the x,y plane. In this frame the receptor coordinates are

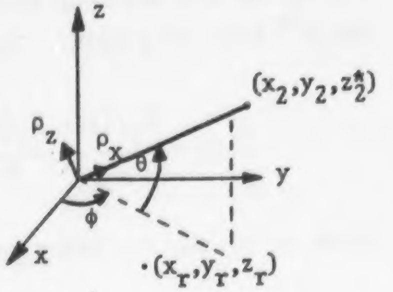

$$\rho_{xr} = x_r \cos\theta \cos\phi + y_r \cos\theta \sin\phi + z_r^* \sin\theta$$

$$\rho_{yr} = -x_r \sin\phi + y_r \cos\phi$$

$$\rho_{zr} = -x_r \sin\theta \cos\phi - y_r \sin\theta \sin\phi + z_r^* \cos\theta$$

where $\sin\theta \equiv z_2^*/d$, $\cos\phi \equiv \dfrac{x_2}{d\cos\theta}$, and $d^2 = x_2^2 + y_2^2 + z_2^{*2}$

and where

$$z_2^* = \left(\frac{a_h}{a_v}\right) z_2 \text{ and } z_r^* = \left(\frac{a_h}{a_v}\right) z_r$$

are the appropriately scaled z coordinates, d is the line source length, and (x_2,y_2,z_2^*) are the coordinates of the second end of the line.

Hence at any point ℓ along the source line, the appropriate source-receptor distance is just

$$R = \left[(\rho_{xr} - \ell)^2 + \rho_{yr}^2 + \rho_{zr}^2\right]^{1/2}$$

Source receptor coupling constants are then calculated (as in Section 4A) for each of the source segments. For source segments near ground level, a multiplicative factor of 2 is used to correctly account for the first ground reflection term. However, for elevated source segements and higher order reflections, each line segment is approximated by a point source located at the center of the segment. This point approximation to a line segment is also used whenever the particular line segment satisfies the criteria for a uniform vertical pollutant distribution (Section 4B).

D. Extended Periods of Calm

The formulae developed so far pertain to the time averaged receptor concentration, $\overline{C}(\tau)$, observed when both source and receptor are turned on at time zero and off at τ. Hence, for an n hour calm, the n hour time average, $\overline{C}(n)$, is obtained by setting τ=n hours. However, this is not equivalent to asking for the one hour receptor average, $\overline{C}_n(1)$, that one would observe during the n^{th} hour of a calm. The relationship between these two quantities is just

$$\overline{C}(n) = \frac{\overline{C}_1(1) + \overline{C}_2(1) + \ldots . \overline{C}_n(1)}{n}$$

hence we obtain the relation

$$\overline{C}_n(1) = n\overline{C}(n) - (n - 1)\ \overline{C}(n - 1)$$

which enables us to compute $\overline{C}_n(1)$ without further model development.

5. Discussion

Starting with the Gaussian puff solution to the diffusion equation, we have obtained an approximate, analytic solution for the time averaged pollutant concentration resulting from a continuous source of strength Q. Most of the deficiencies attributed to the Gaussian plume model, such as the inability to incorporate terrain and the assumption of a wind speed independent of height, also apply to this model, with the exception that the achievement of steady-state conditions is not explicitly required, though it has been incorporated to the extent that steady-state, one hour average dispersion coefficients have been used to determine the parameters of the model. The main virtue of this model is that it extends the usefulness of the much maligned, yet extensively utilized Gaussian plume formalism.

This model incurs an additional limitation due to the dispersion coefficients being parameterized as a simple power law in T. The statistical treatment introduced by Taylor[15] suggests that the dispersion (σ) grows as T for small T and as $\sqrt{T}$ for large T. Thus, the model's parameters are necessarily optimized for some limited range of diffusion times or source-receptor distances. One possible remedy would be to adopt a form having the proper asymptotic properties, such as:

$$\sigma = \frac{aT}{1 + \alpha \sqrt{T}}$$

as suggested by Draxler.[16] Though this particular form appears to lead to intractable integrals, a related form:

$$\sigma = \frac{aT}{\sqrt{1 + \alpha^2 T}}$$

appears promising.

Finally we note that the close relationship between the parameters a_h and a_v and the r.m.s. eddy velocity suggests that it should be possible to express these parameters as a simple function of the sum of the mechanical and thermal turbulent energies and thus as a function of meteorological measurables (e.g., wind speed, sensible heat flux, surface roughness). Such a representation would be extremely useful and the results of Section 3 suggest some rather simple relationships.

REFERENCES

1. H. Moses and M. A. Bogner, *Fifteen-Year Climatological Summary, January 1, 1950 - December 31, 1964*, Argonne National Laboratory, ANL-7084 (1967).

2. O. F. T. Roberts, *The Theoretical Scattering of Smoke in a Turbulent Atmosphere*, Proc. Roy. Soc., A, 104, 640 (1923).

3. M. E. Berlyand, O. I. Kurenbin, and I. M. Zrajevsky, *Theory of Tracer Distribution Near the Ground*, J. Geophys. Res., 75, 18, 3657 (1970).

4. R. J. Nunge, *Application of an Analytical Solution For Unsteady, Advective - Diffusion to Dispersion in the Atmosphere - I-II*, Atmos. Environ., 8, 969 (1974).

5. D. M. Rote, J. W. Gudenas and L. A. Conley, *Studies of the Argonne Integrated-Puff Model*, ANL/ES-9 (1971).

6. W. P. Elliott, *The Vertical Diffusion of a Gas from a Continuous Source*, Int. J. Air & Water Poll., 4, 33 (1961).

7. W. D. Crozier and B. K. Seely, *Concentration Distributions in Aerosol Plumes Three to Twenty-two Miles from a Point Source*, Trans. Amer. Geophys. Union, 36, 42 (1955).

8. D. B. Turner, *A Diffusion Model for an Urban Area*, J. Appl. Meteorol., 3, 83 (1964).

9. J. L. McElroy and F. Pooler Jr., *St. Louis Dispersion Study Vol. II Analysis*, U.S. Dept. of Health, Education, and Welfare, NAPCA AP-53 (1968).

10. D. B. Turner, *Workbook of Atmospheric Dispersion Estimates*, U.S. Dept. of Health, Education, and Welfare, PB-191 482 (1970).

11. D. B. Turner, *St. Louis Study*, private communication (1970).

12. F. Pasquill, *Atmospheric Diffusion*, 2nd Edition, Halsted Press, New York (1974).

13. F. James and M. Roos, *MINUIT*, CERN D506, D516, MINUIT is a minimization program which utilizes Monte Carlo search, the Simplex method of Nelder and Mead, and the Davidon variable metric method (1971).

14. M. Abramowitz and I. A. Stegun, *Handbook of Mathematical Functions*, Applied Math Series, Vol. 55, National Bureau of Standards (1964).

15. G. I. Taylor, *Diffusion by Continuous Movements*, Proc. London Math. Soc., Ser. 2, 20, 196 (1921).

16. R. R. Draxler, *Determination of Atmospheric Diffusion Parameters*, Atmos. Environ., 10, 99 (1976).

7th International Technical Meeting
on Air Pollution Modeling and its Application

The Role of Turbulent Diffusion in the Direction of the Mean Wind in a Numerical AQSM

by Dipl.Met. Klaus Herrmann
Institut für Meteorologie
Technische Hochschule Darmstadt

September 7 - 10, 1976
Airlie Virginia
United States of America

The Role of Turbulent Diffusion in the Direction of the Mean Wind in a numerical AQSM

by Klaus Herrmann

1. Introduction

The diffusion in the mean wind direction (x-direction) can be ignored in a large number of applications of numerical AQSMs,because the advection dominates the transport along the x-axis.As a lower limit of the wind speed,for which this assumption is justified,1m/sec is the mostly mentioned value;due to the lack of knowledge of the effect,which the omitted diffusion term has on the concentration field,this limit is more influenced by the fact,that routine measurements do not differenciate for wind speeds below 0.5m/sec,so that all low wind situations are put into wind speed class 1.

This paper deals with effects,which the diffusion in x-direction has on the concentration field.This is achieved by simulating the transport by advection and diffusion along the three axes x,y,and z with a numerical model and relating the results to that case,in which the x-diffusion term has not been taken into account.We are aware,that this method can only give a first qualitative insight into the problem, because the input data of the model are wind speed and the three diffusion coefficients KX,KY,and KZ for the x,y,and z-direction;as mentioned above,the wind speed is normally only available on a very rough scale,while at the present time knowledge of the coefficients KY and KZ is poor and that of KX nearly nonexistent.So the used parameter set is more or less an arbitrarily one,especially the values for KX.

To cover the whole range of the problem,three aspects have been investigated.The first gives an introduction in the qualitative role of the x-diffusion,if an advection exists.Some important details can be described in a rather abstract form,but this is not leading to quantitative results,because the effect of KX-diffusion shows high spatial variability and strong dependance on the whole ensemble of the other parameters.

In the second part the influence of single parameters,such as wind speed, diffusion coefficients,source height,and mixing height,on the changes of the concentraion field are studied.

Thirdly some realistic combinations of the parameters were related from a scheme of stability classes;that gives estimations of the values for various stabilities.By doing so an important result follows:If the wind speed reaches values of 1 Kt. or higher,the advection dominates the corresponding diffusion in such a way,that only unrealistic high values of KX can change the concentration field considerably. Therefore the interest can turn to extremely low wind speed situations, especially connected with low level inversions. The model can be reduced for these cases to a very simple form, including only parameters such as horizontal source distance, mixing height, time, and horizontal mixing coefficient. If a realistic estimation of the latter parameter can be reached, the simulation of inversion situations is neither a mathematical problem nor expensive, compared to the simulation of normal situations.

2. The Diffusion Model

The model is based on the often used box model, where the mass is equally distributed in each of the small volumes, which fill up the area of interest from the ground to the mixing height. The change of concentration in a box during a time interval Δt is given by the sum of the mass fluxes over its boundaries. These fluxes can be advection in all directions, diffusion in all directions, fall out, rain out, wash out, and so on, in principle, every transport effect one can imagine. Looking for the effect of KX-diffusion, only the advection in x-direction and the three diffusion terms are taken into account. The following parameter names are used:

x,y,z	cartesian coordinates (m)
u	wind speed (m/sec)
KX,KY,KZ	diffusion coefficients (m^2/sec)
ZMIX	mixing height (m)
DX,DY,DZ	length, width, and depth of a box (m)
i,j,k	index to sign the position of a box
ℓ,m,n	total number of boxes in x,y,z-direction
iq,jq,kq	index of the source box
s	concentration (g/m^3)
C	standardized concentration (sec)
VOL	volume of a box (m^3)
Q	standardized source strength (g/m^3sec)
QP	strength of a point source (g/sec)
DT,Δt	time step (sec)

With this nomenclature the corresponding diffusion equation for one single point source of strength QP is

$$(1) \quad \frac{\partial s}{\partial t} = -u \cdot \frac{\partial s}{\partial x} + KX \cdot \frac{\partial^2 s}{\partial x^2} + KY \cdot \frac{\partial^2 s}{\partial y^2} + KZ \cdot \frac{\partial^2 s}{\partial z^2} + QP(x_o, y_o, z_o)/VOL$$

Due to the lack of more realistic data, mentioned in the introduction, the meteorological parameters are taken as constant with height. Because the source strength is not of interest for our special problem, it should be eliminated by using a standardized concentration C with

$$(2a) \quad C = \frac{s}{QP} \cdot VOL$$

which leads to the diffusion equation

$$(2) \quad \frac{\partial C}{\partial t} = -u \cdot \frac{\partial C}{\partial x} + KX \cdot \frac{\partial^2 C}{\partial x^2} + KY \cdot \frac{\partial^2 C}{\partial y^2} + KZ \cdot \frac{\partial^2 C}{\partial z^2} + 1$$

Corresponding to the box scheme, figured in 1, the discrete equation for the change of concentration in box i,j,k during time interval Δt is:

$$(3a) \quad \Delta C_{ijk}/\Delta t = u/DX \cdot (C_{i-1} - C_i) + KX/DX^2 \cdot (C_{i-1} - C_i) + KX/DX^2 \cdot (C_{i+1} - C_i) +$$
$$KY/DY^2 \cdot (C_{j-1} - C_j) + KY/DY^2 \cdot (C_{j+1} - C_j) +$$
$$KZ/DZ^2 \cdot (C_{k-1} - C_k) + KZ/DZ^2 \cdot (C_{k+1} - C_k) + 1$$

or using short forms for the fluxes:

$$(3b) \quad \Delta C/\Delta t = fu + fx_1 + fx_2 + fy_1 + fy_2 + fz_1 + fz_2 + fq$$

The sequence of the terms corresponds directly to that in equation (3a). The boundary conditions are the following:

1. no sedimentation or transport through the ground
   $k=1 \rightarrow fz_1=0$

   no transport throughout the mixing height
   $k=n \rightarrow fz_2=0$

2. no background concentration
   $i=1 \rightarrow fu=-u/DX \cdot C_1$

3. no transport through the lateral boundaries
   $j=1 \rightarrow fy_1=0$; $j=m \rightarrow fy_2=0$

This condition is unrealistic,as long as no real border like hills etc. stops the lateral transport.To avoid consequences for the concentration field it is necessary to chose m so large,that with $C_1 = C_m = 0$ the condition is fulfilled in every case.

4. no diffusion across the upwind boundary
   $i=1 \rightarrow fx_1=0$

   With $C_1=0$ this condition can be met,what can be obtained by a great iq,so that the upwind transport cannot reach the upwind boundary.

5. estimation of the diffusion across the downwind boundary
   $i=\ell \rightarrow fx_2=-fx_1$ or $C_\ell - C_{\ell+1} = C_{\ell-1} - C_\ell$

   which means the use of $\Delta C/\Delta x$ at the position $\ell-1$ instead of position ℓ.In reality we find

   $$|C_{\ell-1} - C_\ell| > |C_\ell - C_{\ell+1}|$$

   so that the above form gives an overestimation of the turbulent transport across the downwind boundary.This can be noted as a defect of the mass flux

$$(4) \quad BIL = \sum_{j=1}^{m} \sum_{k=1}^{n} C \cdot u/DX$$

which should have the exact value of the source flux.Therefore this is a method to find out those receptor points downwind from the source,which are not influenced by the boundary condition.It is necessary to enlarge the number of boxes in x-direction,so that the concentration field of interest is based on conserved mass flux.

To avoid numerical instability one has to respect an upper limit for the time interval.Using the box scheme,the physical reason for this wellknown fact can be described by the balance between the mass,that is just inside a box,and the mass,that is transported outside the box in the following time interval.All fluxes together cannot transport more mass out of the box than it contains;therefore negative concentration values are marking numerical instability.The estimations

$$|C_{i-1} - C_i| < C_i \ , \quad |C_{i+1} - C_i| < C_i \ , \quad |C_{j-1} - C_j| < C_j \quad \text{and so on}$$

mark the case of highest possible transport out of the box.Using these estimations in equation (3a),we get a description of the extreme form of the balance between the masses,which are contained in a box,and the mass fluxes.This form should not occur during the whole running forward in time.Therefore the time step DT,which avoids numerical instability,is given by:

$$(5) \quad DT^{-1} > u/DX + 2 \cdot KX/DX^2 + 2 \cdot KY/DY^2 + 2 \cdot KZ/DZ^2$$

This relates the meteorological transport parameters to the corresponding grid lengths and can be used for every transport simulation,taking into account the transport terms,which are just of interest.If vertical profiles are used,the maximum values for u,KX,KY,and KZ give the limit of DT.

Another problem corresponds with the position of the source.The source flux is taken into account in the equation for one box,which has a volume of DX·DY·DZ and therefore seems to have a lot of possible positions for the source inside.But one has to postulate a certain source position,given by the upwind boundary of the box for the x-direction and the mid position for the y- and z-direction,to make the calculated concentration field independent on the chosen grid length.The discrete field C(i,j,k) should approach the continuous field C(x,y,z) the better the smaller the grids are;this can only be met,if the source position is exactly determined in the mentioned way,and if the receptor points are fixed in the mid position of the boxes.

In the first part of this paper,where transport situations including advection are of interest,only steady state cases are treated.These are reached after short forward march in time,marked by $\Delta C/\Delta t=0$ in the whole field and the fulfilling of mass conservation (4).For KX=0 these steady state concentration fields are equal to the corresponding Gauß-distributions,because the meteorological parameters are constant with height.Note,that for this comparison (which gives the chance to check on numerical diffusion) the standard deviations are given by:

$$(6a) \quad \sigma_y = \sqrt{2 \cdot KY \cdot x/u} \qquad \sigma_z = \sqrt{2 \cdot KZ \cdot x/u}$$

The reflection at ground and mixing height demands a description of the vertical distribution,which includes an infinite number of virtual sources,caused by double reflection,so that the Gauß-concentration is given by:

$$(6) \quad s = \frac{QP}{2\pi u \cdot \sigma_y \cdot \sigma_z} \cdot \exp(-y^2/2\sigma_y^2) \cdot F(x,z,H)$$

$$(6b) \quad F(x,z,H) = \exp\left(-\frac{(z-H)^2}{2\sigma_z^2}\right) + \exp\left(-\frac{(z+H)^2}{2\sigma_z^2}\right) + \sum_{k=1}^{\infty} \exp\left(-\frac{z(k)^2}{2\sigma_z^2}\right)$$

with $z(k)=2k \cdot ZMIX \pm z \pm H$ (all combinations of signs must be taken into account).

At last, the fact of equally distributed mass in the boxes has to be considered by calculating a mean value of the Gauß-distribution over the range of a box:

$$(7) \quad C(i,j,k) = \frac{1}{VOL} \cdot \int_X \int_Y \int_Z C(x_i, y_j, z_k) \cdot dx \cdot dy \cdot dz$$

On the other hand this correspondence could have been reached by using a more detailed box scheme for the numerical model, so that the continuous concentration distribution is better approached. By this way, an important problem corresponding to the application of AQSMs becomes evident. Both methods give the same results if the basic assumptions are the same. But if the models are applied to a certain emission inventory considerable differences will appear:

The users of the Gauß-formula have to assume well defined values for the distance from the source to the receptor, for the source height and the height of the receptor, and for the wind direction, so that to each receptor one exact concentration value is attached. Furthermore, this value is treated as representative for the environment, without any respect to the concentration values at other points inside the grid, which can differ considerably from the receptor value.

In contrast the box model gives a rather smoothed concentration distribution, as it has been mentioned above. Depending on the intensity of the smoothing effect, which itself depends on the grid length, important details of the concentration distribution could be neglected. If, for example the vertical diffusion exceeds a certain strength, the highest concentration value will appear in the source box and the strength and position of the maximum is described not very detailed. The form of the concentration distribution then differs considerably from that, given by the Gauß-formula.

Therefore the chosen grid length has an important effect on the calculations. In this paper DX=DY=1km has been used, because this is the often used grid length for emission inventories. But these values give, of course, a strong smoothing effect and there is no chance to decide, how realistic this is.

Therefore one should remember this fact, when concentration distributions will appear, which are considerably different from that, one would have expected from the Gauß-formula. The KX-diffusion has been studied in its extreme form, to be on the safe side with the results.

Figure 1: The box scheme, on which the diffusion model, given by equation (3), is based. The x-axis has the direction of the mean wind. The source box has the index combination (iq,jq,kq); the position of the source is marked by *. The notations of the fluxes across the boundaries of the box (i,j,k) correspond to the short form of the discrete diffusion equation (3b).

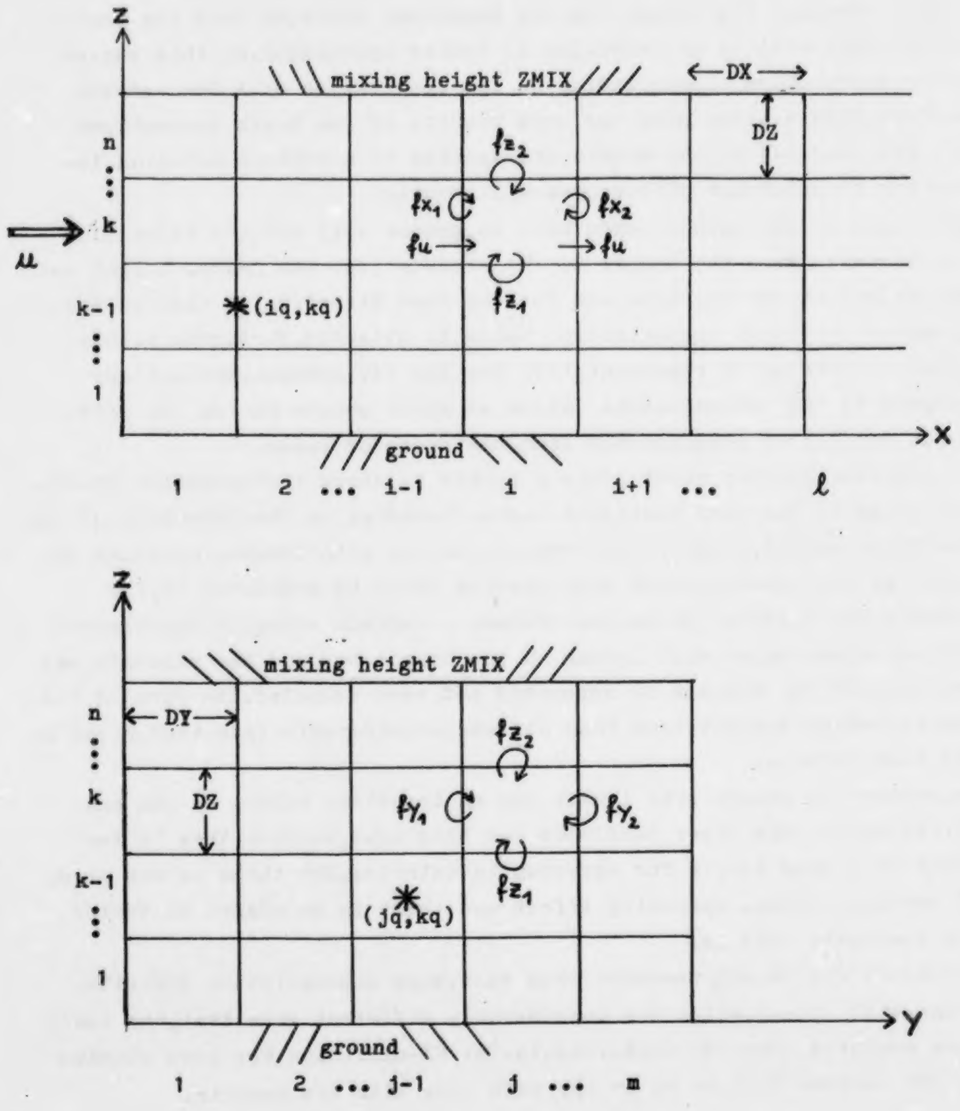
z
mixing height ZMIX
←DX→
DZ
n
k
k-1
1
u
f_{z_2}
f_{x_1}
f_{x_2}
f_u
f_u
f_{z_1}
*(iq,kq)
ground
x
1
2 ... i-1
i
i+1 ...
ℓ
z
mixing height ZMIX
n
←DY→
DZ
k
k-1
1
f_{z_2}
f_{y_1}
f_{y_2}
f_{z_1}
(jq,kq)
ground
y
1
2 ... j-1
j ... m

3. The Role of the X-Diffusion if Advection Exists

In this section those cases are treated,for which the advection and the KX-diffusion together determine the transport along the x-axis.As it has been mentioned before the effect of an added diffusion term on the concentration field shows a high spatial variability and is furtheron strongly determined by the other parameters;the single transport term cannot be treated isolated from all the other mechanisms.Therefore it is impossible to give a simple quantitative description of the problem, because a great number of various conditions,given by the parameter set u,KX,KY,KZ,H,and ZMIX,must be taken into account.For the sake of brevity the description has to be restricted to the important part of the concentration field between ground and source height.

3.1 Some Qualitative Aspects

In order to get an impression of the processes,the following idea can be used:The transport along the x-axis is determined by the advection and the diffusion term.Because the advection is the dominating part,the effect of KX should be treated relative to the advection.Adding both terms and transforming them into a fictive advection,the diffusion can be expressed as a defect Δu of the wind speed u:

$$(8a) \quad - u \cdot \frac{\partial C}{\partial x} + KX \cdot \frac{\partial^2 C}{\partial x^2} = - (u + \Delta u) \cdot \frac{\partial C}{\partial x}$$

what gives an equation for the defect Δu:

$$(8b) \quad \Delta u = - KX \cdot \frac{\partial^2 C}{\partial x^2} \Big/ \frac{\partial C}{\partial x} = - KX \cdot \frac{C''}{C'}$$

or if the descrete scheme of the diffusion equation is used:

$$(8c) \quad \Delta u = - KX/DX \cdot \left[1 + (C_{i+1} - C_i)/(C_{i-1} - C_i) \right]$$

(Note,that the box model uses a non centered $\Delta C/\Delta x$ for the advection term).

This form is very useful to give a qualitative description of the effect, the added diffusion term has on the concentration field.The importance of KX corresponds with the changes C' and C'' of the concentration field along the x-axis.It is a well known fact,that marked changes of concentration distributions appear only near the source,while going downwind, C'' disappeares and C' tends to a nearly constant value.Following from that,the role of the KX-diffusion is restricted to positions nearby the source.

Here the effect is a smoothing one,meaning that mass is transported from the maximum to lower values.The intensity of this transport depends on the intensity of the concentration changes along the x-axis, which again strongly depend on all the other parameters.This makes evident the spatial variability of the KX-diffusion effect and the strong influence of the other parameters.It seems to be suggestive to estimate C'' and C' from wellknown concentration distributions (for the case KX=0,for example,where the special Gauß-formula (6) can be used) and to determine then the changes of the concentration field from Δu. This has been done without much success,because the changes of the wind field are not directly correlated to the changes of the concentration field.So the Δu-method can only be used to give a rough qualitative insight into the role of the KX-diffusion,as it has been given before. If however the quantitative aspects are of interest,one has to calculate the concentration fields for KX=0 and KX>0 and to compare them;an example is given in figure 2,where some onedimensional distributions C(x) and C(z) for a constant parameter set with u=1m/sec and KX=$1000m^2$/sec are shown.The value for KX has been chosen so extremely large to get a pronounced difference between the two cases.Note,that the direction of the smoothing transport is not restricted to the x-direction; mass is diffused from the maximum to positions nearer to the source and to greater lateral and vertical positions.Later on,we will see,that other forms of the smoothing transport can appear;sometimes all the boxes of the center line between ground and source loose mass to positions aside and above.These various forms result from the interdependence of all transport terms and therefore the whole parameter set plays an important role,to which the interest is spend in the following section.

But before discussing this another fact should be added.Caused by the KX-diffusion,material is transported against the wind,which gives a concentration distribution upwind from the source.These values have not been inserted into the figure,because they are very low,compared to the downwind concentrations.The same effect results from all the other examples,which have been evaluated;the upwind transport can therefore be neglected in all cases,when advection exists.

Figure 2: Example for the role of the KX-diffusion. For the cases KX=0 (index 0) and $KX=1000m^2/sec$ (index 1) the distributions of the normalized concentration have been compared. The figures 2a-2c give the center line concentration (y=0) for the heights z=125m (source height), z=75m, and z=25m as a function of the horizontal source distance x, while the figures 2d-2f show the vertical distributions C(z) at a fixed downwind position x (10km) for the lateral distances y=0, y=1km, and y=2km. (Note, that the vertical coordinate axis is marked with k, which gives the index of the vertical box distribution).
The meteorological parameters are: wind speed u=1m/sec, diffusion coefficients $KY=10m^2/sec$ and $KZ=1m^2/sec$, mixing height ZMIX=500m. The grid distances are DX=DY=1km and DZ=50m. The figures can be found on the following two pages.

3.2 The influence of single parameters

To save clarity and due to the spatial variability of the KX-diffusion effect, in this section only the ground level concentration distribution of the center line is taken into account; the effect on the other receptor points is a corresponding one in such a way, that the mass distribution is balanced and the mass, which is lost in one box, is distributed to the environment, where a higher concentration results. To look into the influence of single parameters, concentration fields have been calculated, based on a constant set of the other parameters and various values of that one, which is just of special interest. The results are given in figure 3 for u, KX, KY, KZ, and H. The following facts can be noticed:
a) wind speed u (m/sec)
By decreasing the advection an increase of the KX-effect and a maximum nearer to the source results. The relative differences between the cases KX=0 and KX>0 correspond to the concentration distribution, as it has been mentioned before. For a wind speed less than 0.5m/sec the advection no longer dominates the x-transport. This can be seen from the strong increase of the differences; then the transport situation is no longer from the advective type and the x-diffusion becomes rather important.
b) diffusion coefficient KX (m^2/sec)
The influence of the diffusion coefficient KX is much smaller than that of the wind speed. Note again, that large values have been chosen, to get pronounced effects. The change of concentration shows a nearly linear dependence on KX, which could have been expected from the Δu-formula.

(2a) C(X): Y=0KM Z=H=125M

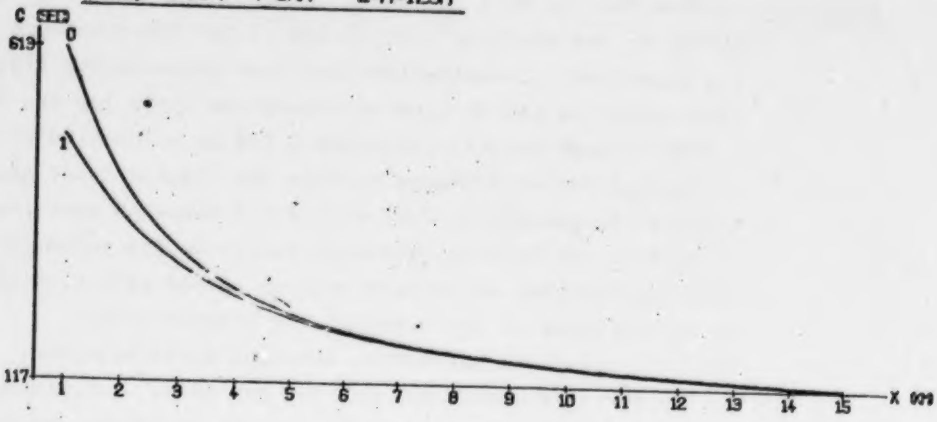

(b) C(X): Y=0KM Z=75M

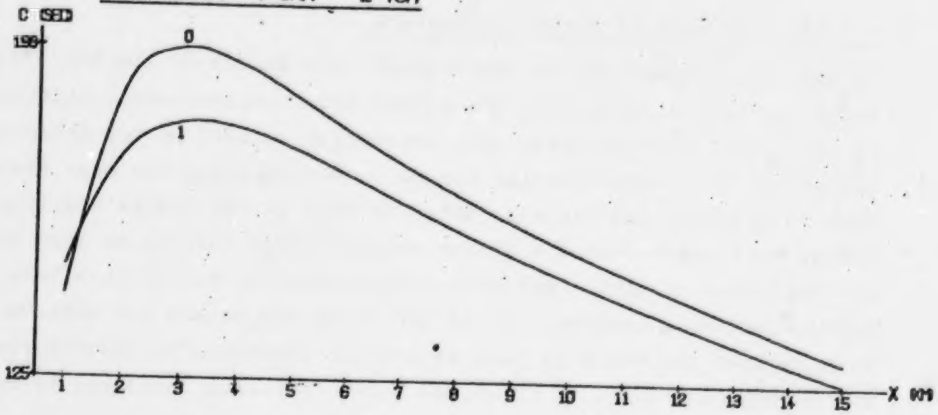

(c) C(X): Y=0KM Z=25M

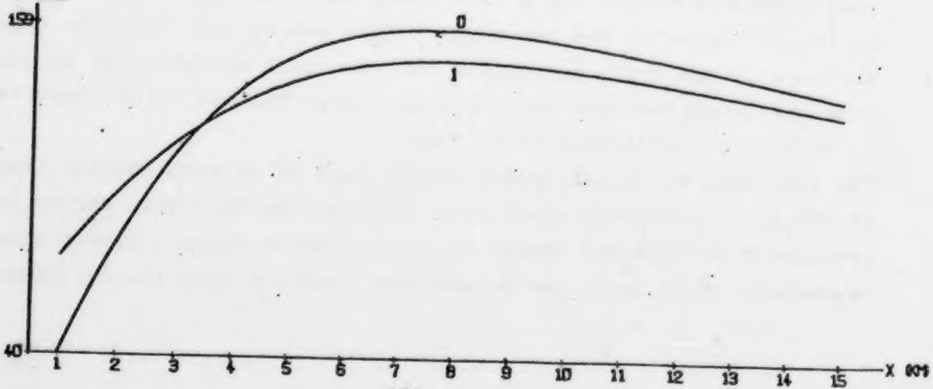

(d) C(Z): X=10KM Y=2KM

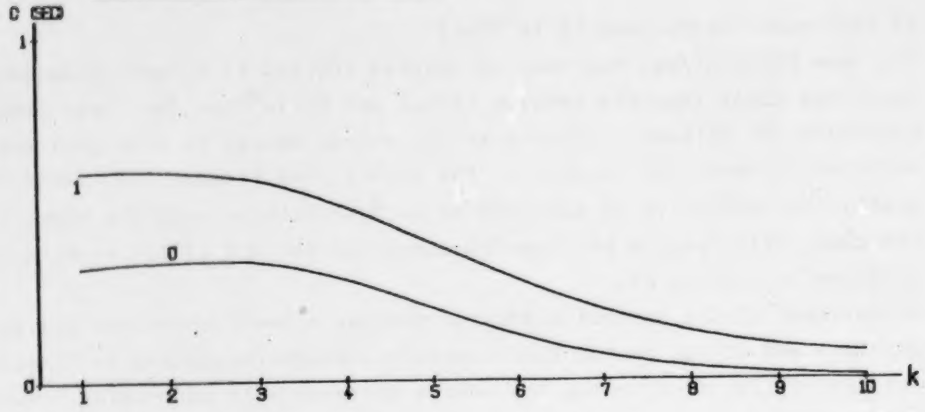

(e) C(Z): X=10KM Y=1KM

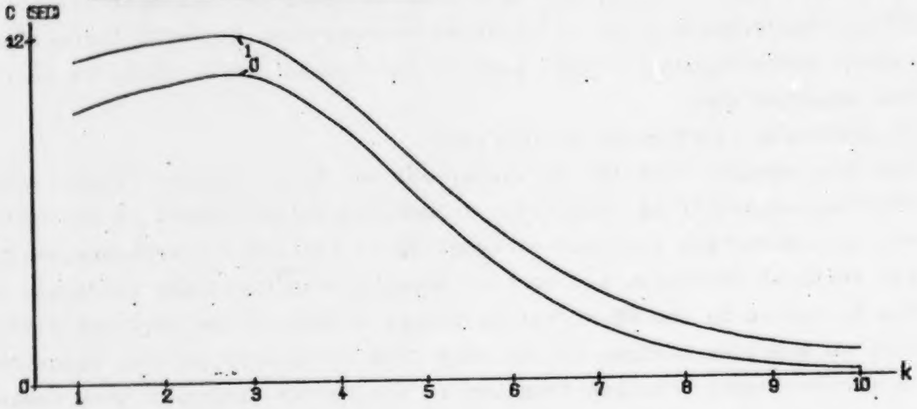

(f) C(Z): X=10KM Y=0KM

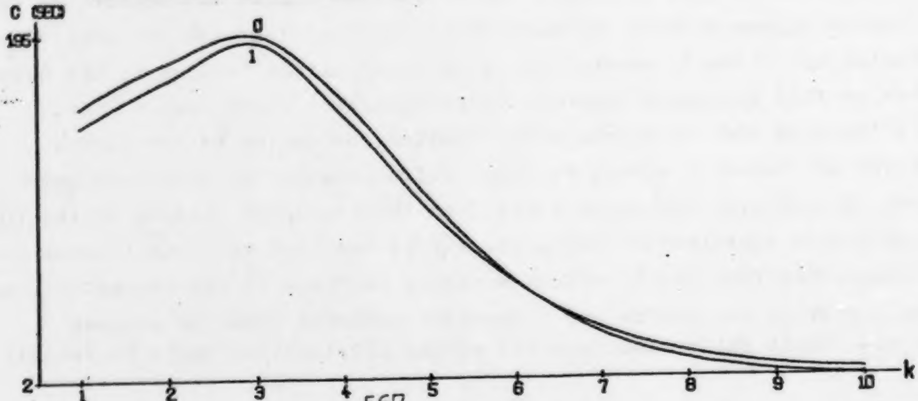

c) diffusion coefficient KY (m^2/sec)

The case KY=0.1m^2/sec has been calculated too,but it is not shown,because one finds identity between KY=0.1 and KY=1m^2/sec;for these small KY-values the lateral diffusion is not strong enough to transport any material to boxes not located on the center line,because only positions nearby the source are of interest here.(Take into account the special box model effect,which has been discussed at the end of the model description in section 2).

An increase of the lateral diffusion implies a decrease of the maximum distance and of the center line concentration.Corresponding to that,the relative differences nearby the source increase with increasing lateral diffusion.The upper limit of this rule is reached with a value of some hundred m^2/sec for KY;then the lateral transport is so strong,that a pronounced maximum no longer appears and the concentration distribution is rather smoothed with its largest value in the source box; for this single position the KX-effect is again the stronger the larger KY is chosen,but now the differences decrease rapidly with increasing source distance,because this part of the concentration field is just the smoothed one.

d) diffusion coefficient KZ (m^2/sec)

For this special case the parameter set has to be changed (ZMIX=1000m, DZ=100m and,resulting from these values,the source height is H=150m),to restrict numerical labour.Corresponding to the great importance,which the vertical diffusion has on the concentration field,the influence of the KZ-values on the KX-effect is rather strong.If the vertical diffusion is weak,the maximum is far away from the source and the concentration considerably changes from box to box.The KX-diffusion then causes an increase of the concentrations nearby the source.With increasing vertical diffusion the maximum is located nearer to the source and a part of the KX-diffusion is now based on that part of the concentration field,we find downwind from the maximum,and a mixed form of the KX-effect results with increased concentrations nearby the source and decreased values a short distance downwind.If,at last,the vertical diffusion is extremely strong,indicated by a maximum located in the source box,we find decreased concentrations along the whole center line.

If the grid size is chosen more detailed,the maxima of the cases, which are based on strong vertical diffusion,will be described more detailed.Then,of course,we would find the strongest changes of the concentration distribution along the x-axis combined with the largest KZ-values.Then from the KX-effect a strong increase of the concentrations very near to the source and a decrease downwind from the maximum would result.But obviously,these strong fluctuations would be restricted to a very short distance compared with the grid length.If we will apply the model to an emission inventory,we will not be interested in such small scale variations but in the change of the concentration values at receptor points,which are representative for their environment.Therefore it is more realistic to base this study on a grid length of 1km,so that the resulting KX-effect corresponds to a scale,which would be used in practice.

Due to this special fact the KX-effect is increased with decreasing vertical diffusion.

e) source height H (m)

The role of the source height in a AQSM is well known.Its importance on the KX-effect can be directly related to the corresponding concentration distribution.For lower sources we find negative differences,because we are downwind from the maximum,while with increasing source height the mixed forms with increased concentrations nearby the source and decreased values downwind from the maximum occur.But note, that the relative differences for the higher sources are too much pronounced,which is caused by the small concentration values the differences are related to.

d) mixing height ZMIX (m)

If a mixing depth of a few hundred meters is used,the double reflection is already effective nearby the source,which gives a very smoothed concentration distribution and an unimportant role of the KX-diffusion. For ZMIX=200m for example,all differences are less than 1%.With increasing mixing height the reflection at the upper limit looses its influence on the concentration field near the ground,so that for ZMIX > 500m the KX-diffusion does not depend on the mixing height.

In conclusion the following facts should be noted:

The most important effect on the role of the KX-diffusion is exerted by the wind speed;for values of 0.5m/sec or less the advection can no longer be treated as the dominating transport along the x-axis,while for values of 1m/sec the influence of the diffusion term is relatively poor,we then find a transport situation from the advective type.

Compared to that,the influence of the other parameters is much smaller. Strong lateral diffusion,expressed by KX and KY,intensifies the influence of the added diffusion,while strong vertical mixing effects reduce it considerably.

Figure 3: The influence of the parameters wind speed u, diffusion coefficients KX, KY, KZ, and the source height H on the effect, which the x-diffusion has on the concentration field. (ground level concentration of the center line).

The upper part of each figure shows the distribution of the normalized concentration along the x-axis, while in the lower part the relative differences between the case $KX > 0$ and the case $KX=0$ are given. The curves are marked with the corresponding value of the parameter, which is just of special interest. The parameter and the corresponding dimension can be obtained from the head line.

The parameter set, which has been used for this study, is:

$u = 1 m/sec$; $KX = 1000 m^2/sec$; $KY = 10 m^2/sec$;

$KZ = 5 m^2/sec$; $ZMIX = 500 m$; $H = 125 m$;

$DX = DY = 1 km$; $DZ = 50 m$.

For the figure 3d (vertical diffusion) the parameter set has to be changed, to restrict numerical labour:

$ZMIX = 1000 m$; $DZ = 100 m$; $H = 150 m$.

Find the figures on the following 5 pages.

3.3 Realistic Combinations of the Parameters

In reality all parameters together depend on atmospheric stability, so that only certain combinations can appear, meaning that a combination of high lateral diffusion with a low vertical one is rather unrealistic. To find out some of these realistic parameter sets and to look into their comprehensive effect on the KX-diffusion, one has to go back to one of the diffusion class schemes, because at this time no other method of estimating the meteorological parameters as a function of stability exists. In practice the Klug (1) classification has been used to determine mean values for KY and KZ, combined with a certain value for ZMIX and a range of the wind speeds, which can occur in a special diffusion class. Because the diffusion coefficients change with source distance, a mean value for the range $0 < x \leq 20 km$ has been used. With

$\sigma = \sqrt{2 \cdot K \cdot x/u}$ and $\sigma_z \leq ZMIX$

the following combinations of the parameters have been calculated:

(3a) PARAMETER : U (M/SEC)

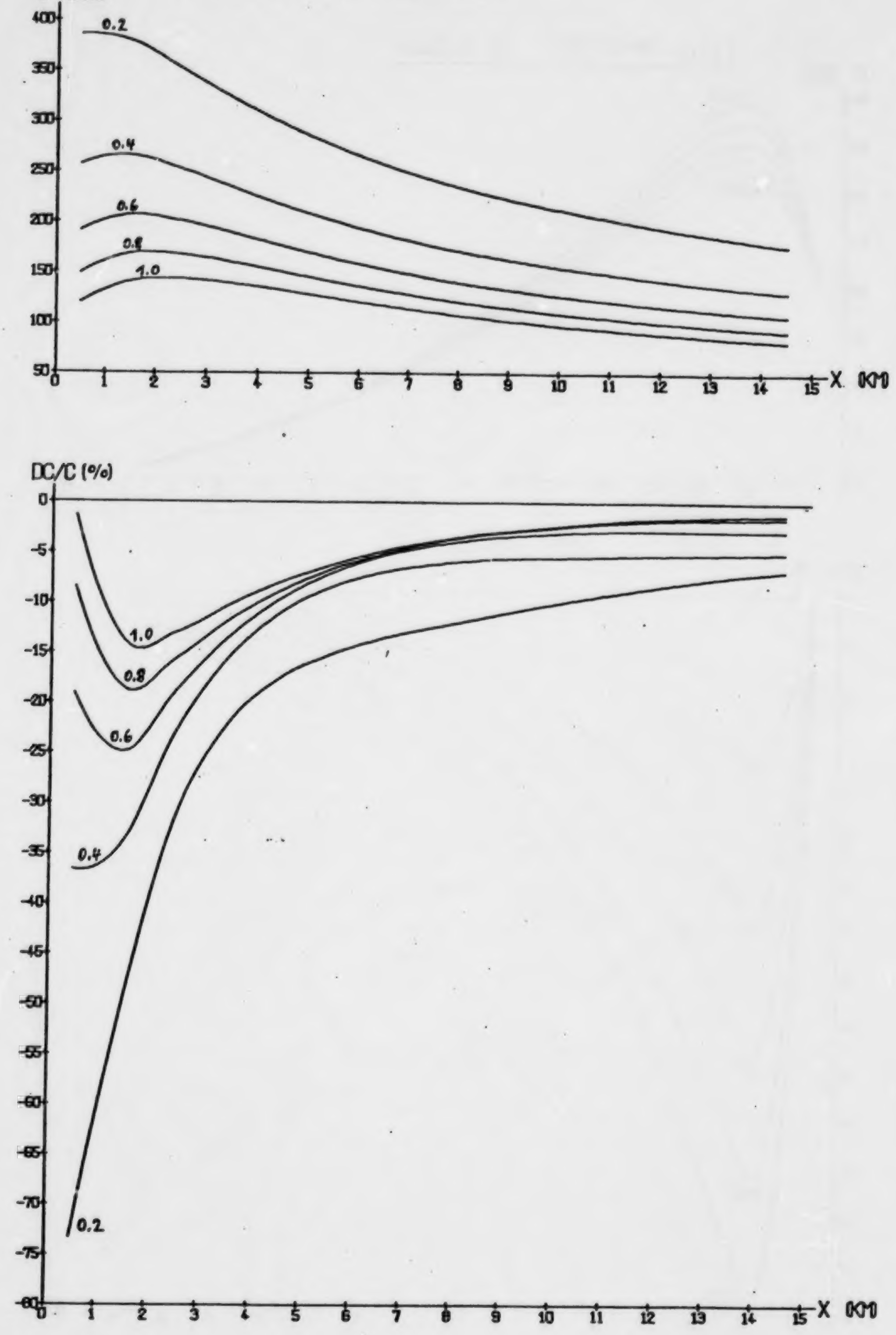

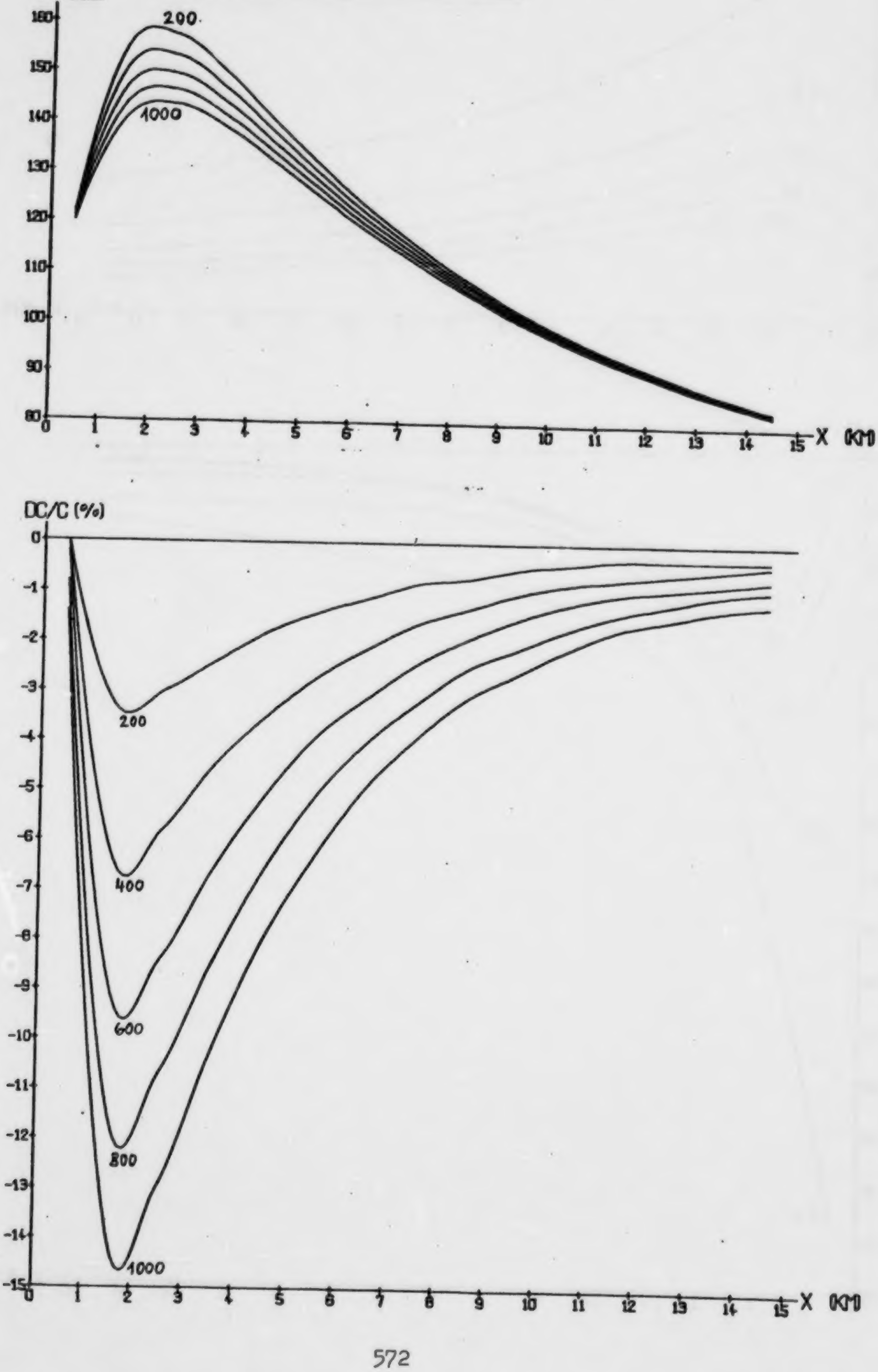

(3b) PARAMETER : KX (M²/SEC)

(3c) PARAMETER: KY (M^2/SEC)

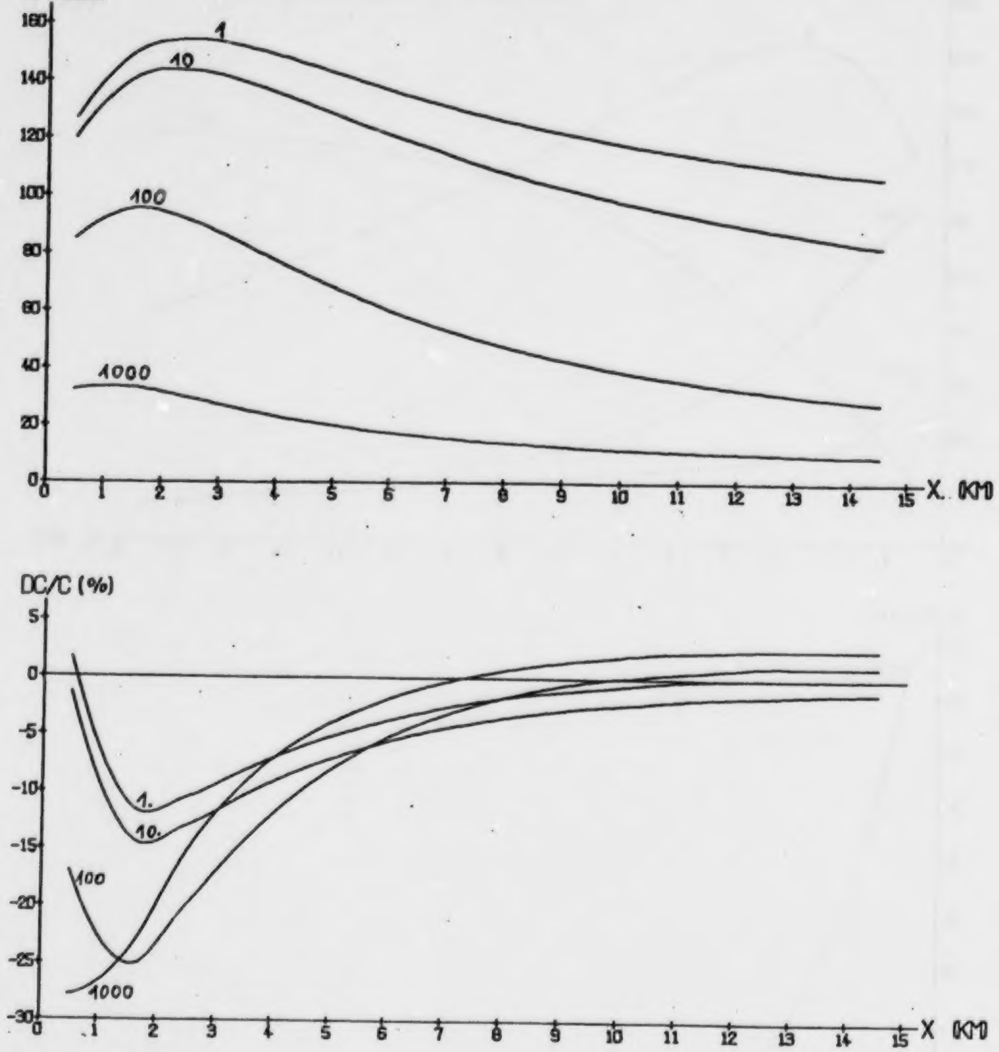

(3d) PARAMETER: KZ (M²/SEC).

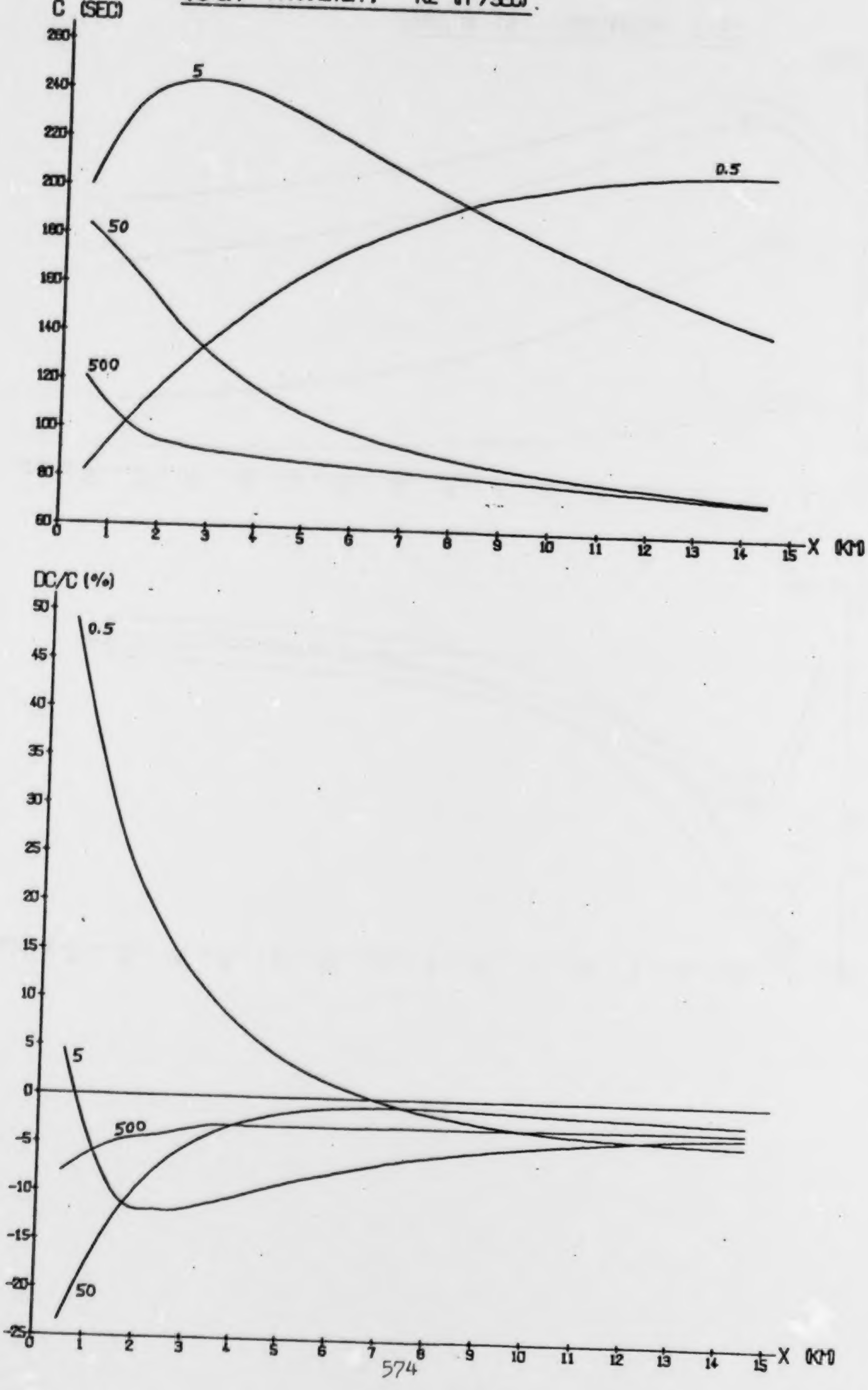

(3e) PARAMETER: H (M)

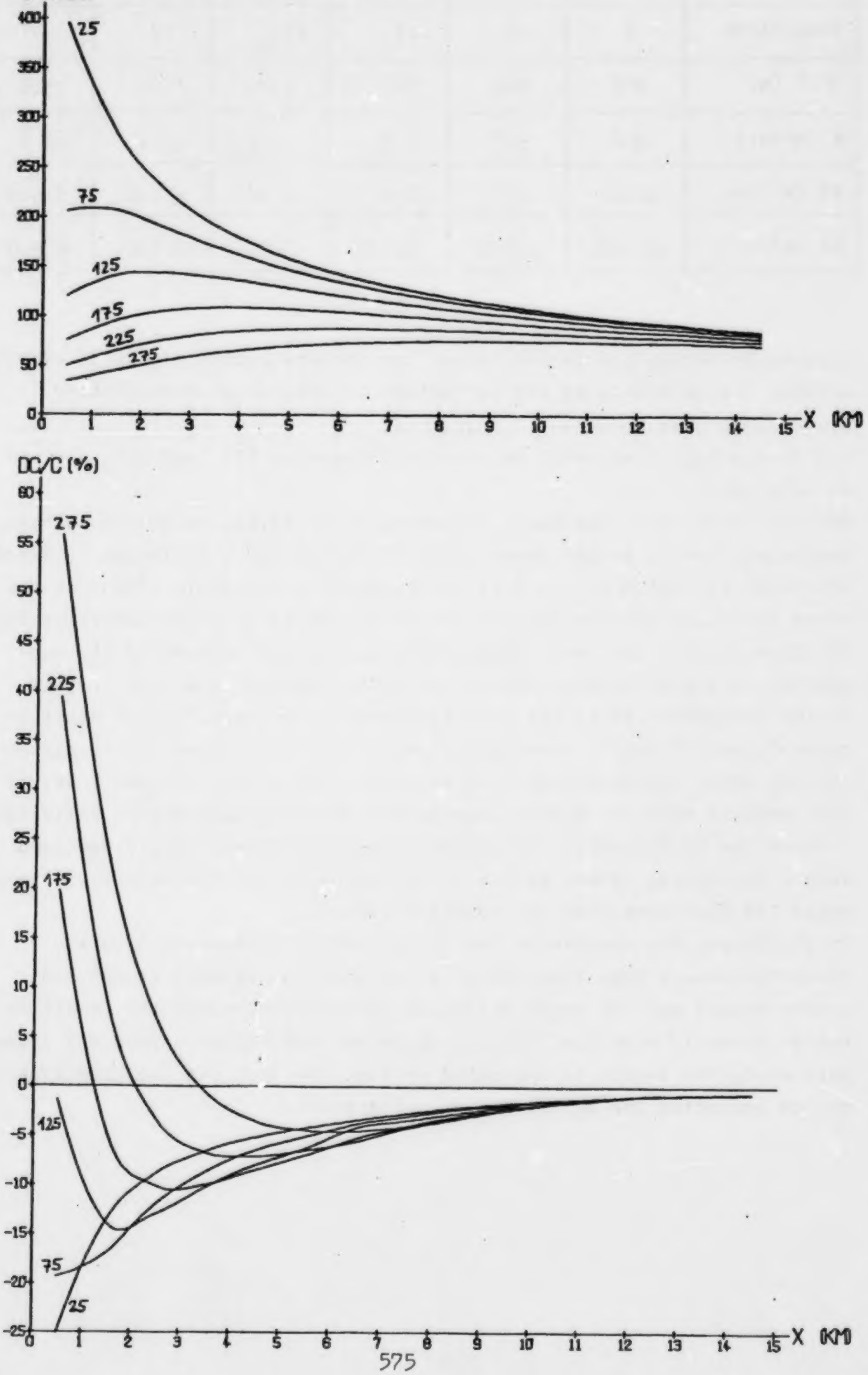

stability	extr.stab.	stable	neutral	sl.unst.	unstable	ex.unstab.
Klug-class	I	II	III_1	III_2	IV	V
ZMIX (m)	200	200	500	1000	1500	1500
u (m/sec)	≤ 2	≤ 3	≥ 3	≥ 2	≤ 4	≤ 3
KY (m^2/sec)	≤ 0.5	≤ 3	≥ 6	≥ 20	≤ 200	≤ 600
KZ (m^2/sec)	≤ 0.06	≤ 0.3	≥ 1.5	≥ 6	≤ 120	≤ 300

This rough estimation is sufficient for the evaluation of the KX-effect, because the influence of the parameters is only pronounced,if they are changed over an order of magnitude.

Due to the high wind speed values the categories III_1 and III_2 are not of interest.

For the other cases the above combinations of KY,KZ,and ZMIX have been used,completed by a wind speed value of 1m/sec and a diffusion coefficient KX=1000m^2/sec,which should give the heighest conceivable effect of the added diffusion term as long as the situation is from the advective type. The KX-diffusion does not cause rather pronounced changes of the concentration fields between ground and source height in any of the diffusion categories.As it has been mentioned in section 3.2,the unstable cases (class IV and V) are combined with smoothed concentration distributions and a corresponding weak KX-effect.The stable classes I and II are combined with low mixing heights and the resulting double reflection reduces the KX-diffusion effect.Additional,low KY-values are combined with a decreasing effect of the KX-diffusion on the concentration field while low KZ-values give the opposite effect.

In conclusion the changes of the concentration field,caused by the KX-diffusion,are less than 10% at every position between ground and source height and for every diffusion category.Therefore the result is rather clear:If wind speed values of 1m/sec and higher appear,the transport along the x-axis is dominated by the advection and the KX-diffusion can be neglected for all diffusion categories.

4. Transport without Advection

As we have seen,the transport is no longer from the advective type,if the wind speed decreases to values less than 0.5m/sec.Then the diffusion plays a rather dominant role.These cases do not appear very often under normal climatological conditions,but their importance is evident, especially if they are combined with a low level inversion during winter. Therefore these cases have been treated in a special way,ignoring now the advection.Note,that $\bar{u}=0$ does not mean a situation without any wind during the whole time,but low wind speeds coming from various directions; these situations are from the diffusive type.Taking a homogenious diffusion coefficient K for the horizontal diffusion,the lateral transport is a symmetrical one and we can use a cylindric coordinate system,what gives the diffusion equation:

$$(9) \qquad \frac{\partial C}{\partial t} = K\cdot\left(\frac{\partial^2 C}{\partial r^2} + \frac{1}{r}\cdot\frac{\partial C}{\partial r}\right) + KZ\cdot\frac{\partial^2 C}{\partial z^2} + 1$$

where again the concentration C is normalized by the source strength.

It is realistic to use low mixing heights for the simulation of inversions.For these cases after a very short time the vertical diffusion leads to concentrations constant with height,because the lateral and the vertical transport effects are now of the same order of magnitude, while in contrast the vertical distance is much smaller than the lateral.Following from this the vertical diffusion can be assumed to be so intensive,that the material is distributed homogenious between the ground and the inversion.

Due to this fact the numerical solution is very simple and should be prefered to the mathematical solution,which contains the infinite number of virtual sources,caused by the double reflection,and is therefore rather complicated.

The numerical scheme is based on a cylindric box system,which is given in figure 4.Each box fills the whole distance between ground and inversion,so that its depth is equal to ZMIX.The descrete scheme is:

$$(10) \qquad \Delta C_i/\Delta t = K/DR^2\cdot\left[(C_{i-1} - C_i)\cdot\frac{2i-3}{2i-2} + (C_{i+1} - C_i)\cdot\frac{2i-1}{2i-2}\right]$$

The following condition for the time step has to be met:

$$(10a) \qquad \Delta t < DR^2/(4\cdot K)$$

The resulting model does no longer include the vertical coordinate z and the source height;all sources below the inversion are summarized to one source strength Q,which is related to the volume of the box and therefore has the dimension g/m^{3}sec.

Note,that this method is not equivalent to the use of a simple two dimensional diffusion equation for horizontal transport;what has been done is,to restrict the details of the discrete scheme, according to the fact of homogenious vertical concentration distribution.

The mixing height does not appear in the discrete scheme;it determines the box volume and is included in the normalized concentration;its influence on the concentration field is therefore a linear one.

Figure 4: The cylindric box system for the simple low wind model.

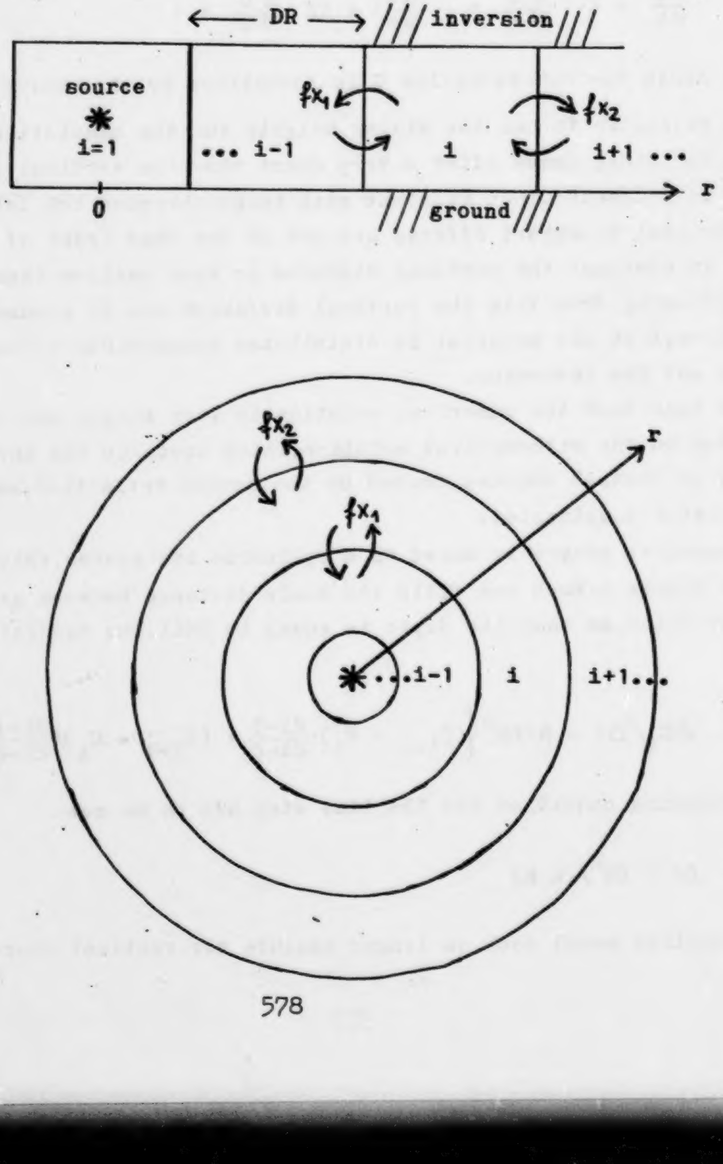

The concentration distributions C(r,t),resulting from this method, seem to depend on the chosen box width;but the source term Q contains all sources inside the box and depends on the grid length in the same way.Therefore the grid system can be chosen arbitrarily;for the given examples a distance of DR=1km has been chosen.

Figure 5 shows,how the concentration in the center box depends on the time.In the beginning of the inversion situation the concentration increases rapidly,while the transport to larger distances is small. After a certain time interval,which length depends on the strength of the lateral diffusion,the concentration tends to a constant value (the steady state case is reached),corresponding with a lateral transport, which is now strong enough to diffuse the born material to greater distances.The time dependent distribution of the center box concentration is of special interest,if an inversion situation occures,because the largest concentration value,which could appear,if the inversion is a very persistent one,is included.

The lateral diffusion coefficient is the most important parameter. Decreasing it,the concentration is strongly increased.Note,that in the figure a concentration $\hat{C}$ has been used,which is the normalized concentration multiplied by the value of K.This has been done to be in the same order of magnitude with the four examples.From this,one can see,that the concentration is increased by nearly a factor 10,if the diffusion coefficient is reduced to 1/10.

If the estimation of this parameter will be possible in practice,this simple method should give a sufficient description of the air pollution situation,which is caused by low wind combined with a low level inversion.

Figure 5: The concentration of the center box as a function of time for various lateral diffusion coefficients K;the curves are marked with the corresponding values of K in the dimension m^2/sec.$\hat{C}$ means the product of the normalized concentration with the K-value;this has been done to be in the same order of magnitude with the four examples.

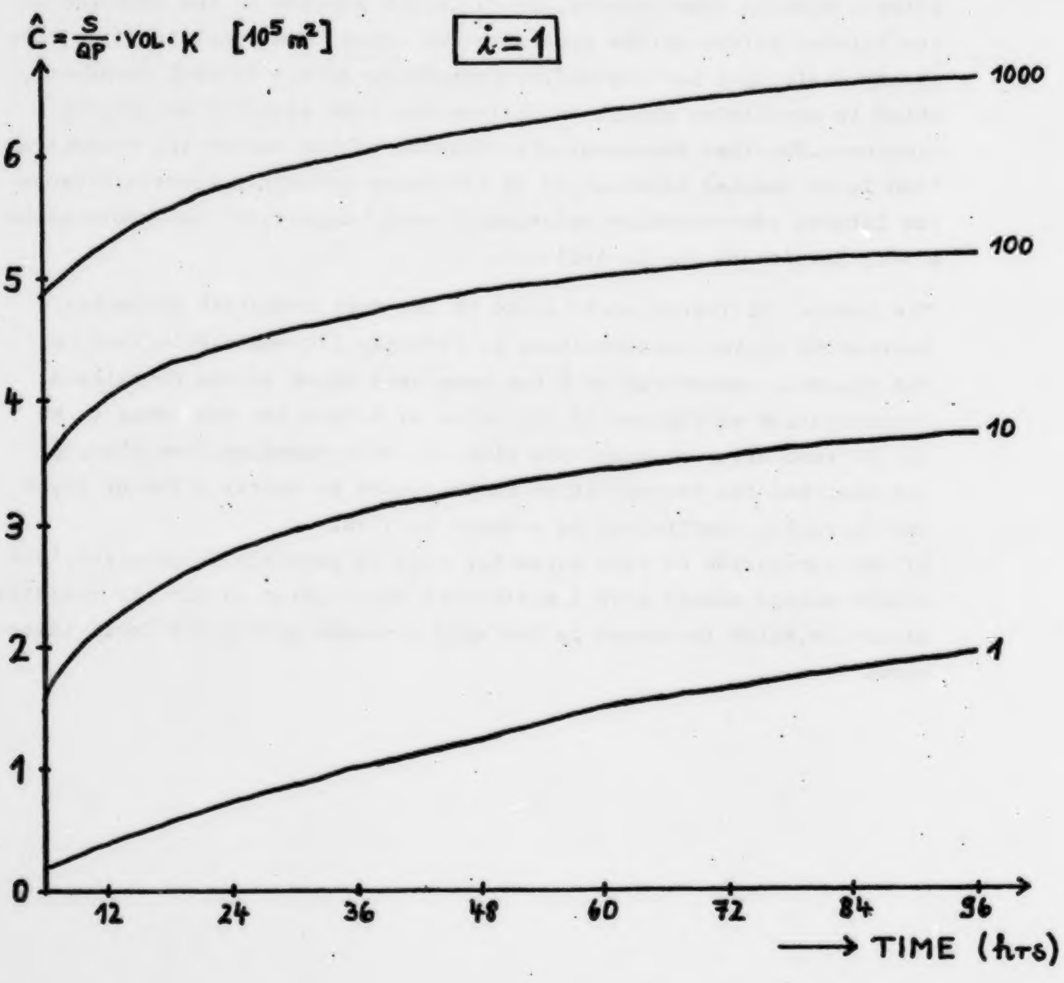

References

(1) W. Klug — Ein Verfahren zur Bestimmung der Ausbreitungsbedingungen aus synoptischen Beobachtungen
in: Staub,Reinhaltung der Luft 29 (1969), Nr.4 (April)

(2) K. Ragland — Multiple Box Model for Dispersion of Air Pollutants from Area Sources
in: Atmospheric Environment 7 , 1017 - 1032

(3) K. Ragland — Point Source Atmospheric Diffusion Model with Variable Wind and Diffusivity Profiles
in: Atmospheric Environment 9 , 175 - 189

7th NATO/CCMS
International Technical Meeting
on Air Pollution Modeling

Influences of Model Parameters and Sensitivity to Their Variation within the Immissions Forecasting

by

L. Kropp and H. Bresser
Technischer Überwachungsverein Rheinland e.V.,
Köln

Airlie House,
Airlie, Virginia, USA
September 7.-10.1976

Abstract

INFLUENCES OF MODEL PARAMETERS AND SENSITIVITY TO THEIR VARIATION WITHIN THE IMMISSION FORECASTING.

L. Kropp, H. Bresser TÜV Rheinland e.V.

Air pollution forecasts are generally subject to the model applied, its parameters and the restrictions to this model. This paper shall give a review and summary of the influences of the parameters and the sensibility to their variation.

The influence of different diffusion parameters, effective source height, meteorologic data (requirements of accuracy), mixing and inversion height, source data and their exactness, source dimension and chemical or physical processes was investigated quantitatively.

The most critical influencing is given by the diffusion parameters. It can be stated that there are available different sets of diffusion parameters from different experiments which lead to a consistent result i.e. immission value calculations.

Another critical parameter for air pollution modeling and forecasting is the effective source height. A slight change of this value within a certain region of height shows remarkable changes of the calculated ground level concentrations.

The primary aim of the investigations was to find or develop a model with applicable parameters that can be standardized and used within the German licensing procedure.

Beyond this scope of work these investigations and results show the way to define the procedure to be followed and to get more accurate air quality and diffusion models and parameters.

TECHNISCHER ÜBERWACHUNGS-VEREIN RHEINLAND E.V.

Influences of Model Parameters and Sensitivity to their Variation within the Immission Forecasting *)

Introduction

Air pollution model verification and forecasts ought not be dependant on the model used. However, reality shows a more or less strong influence of the model and parameters used.

This paper summarises results of an investigation concerning gaussian plume model calculation and the sensitivity to the variation of model parameters like

- diffusion parameters
- turbulence classification
- wind speed and direction classification
- effective source height
- accuracy of source data including the description of area sources
- mixing height
- meteorological conditions.

Far more parameters influence the results, of course. Within the accuracy of the model they are of lower importance, however.

Model input data

Model calculations have generally been performed for source heights of 10 and 100 m in this investigation being representive for sources of residential combustion and industrial stacks.

---

*) This paper presents results of an investigation on behalf of the German Federal Ministry of the Interior, a comprehensive report of which was completed early in 1976. / 1 /

Different sets of diffusion parameters have been used; they are those of

- Mc Elroy and Pooler / 2 /
- Singer and Smith / 3 /
- Klug / 4 /
- Pasquill and Gifford / 5 /
- Polster and Vogt / 6 /.

The turbulence situation of the lower atmosphere was described by the classification of

- Turner / 7 /
- Klug and Manier / 8 /
- Polster and Vogt / 9 /.

The effective source height was calculated using the formula of Moses and Carson / 10 /.

The meteorologic situation was described by 36 sectors of wind direction, 10 representative wind speeds and up to 6 turbulence classes.

The results are given either as average values or as values for percentages of excess frequencies or as probability distributions of concentrations at ground level.

Results

Diffusion parameters

The ground level concentrations for a source height of 10 m calculated with 4 sets of diffusion parameters are shown in fig. 1 (average values) and fig. 2 (5 % excess frequency values). The parameters of Mc Elroy and Pooler and those of Polster and Vogt show quite similar average immission values in shape and size. The concentrations calculated with the parameters of Pasquill and Gifford and those of Klug are higher by a factor of 4 and less smoothed. This situation of more smoothed concentration distribution is to be seen more clearly in the display of the 5 % excess frequency values.

Fig. 3 gives a display of ground level concentrations for different distances from the source. The dependencies are given for unstable, neutral and stable turbulence situations. In every case using Klug's diffusion parameters the concentrations are the highest ones. The lowest ones are calculated with the parameters of Polster and Vogt (or Mc Elroy and Pooler for the stable condition. The differences are up to a factor of 50 independant of the distance. Though the parameters of Polster and Vogt and Mc Elroy and Pooler are derived from different experiments the calculations lead to very similar results.

Calculations for a source height of 100 m are shown in figs. 4 and 5. The same conclusion as above can be derived for the parameters of Polster and Vogt and those of Singer and Smith (quite equivalent results).

It can be stated, therefore, that two equivalent sets of diffusion parameters are available - except only some necessary changes or revision of the σ_y values of Polster and Vogt for the very unstable turbulence condition.

Turbulence classification

A comparison of calculations using Polster and Vogt's diffusion parameters in connection with their turbulence classification on the one hand and the turbulence classification of Klug and Manier on the other hand shows no significant changes in the results of ground level concentration (average and 5 % excess probability values). See fig. 6.

A comparison between calculations using Turner's and the above mentioned system is still outstanding.

Nevertheless it can be stated already that turbulence classifications and diffusion parameters should correspond to each other. At least a thorough prior check is necessary.

Wind directions classification

Calculations have been performed for wind directions sectors of 10 deg. width each being divided into subsectors of 1, 1.25, 1.67, 2.5 or 5 degrees with constant wind frequency. The results from these calculations taking into account the absolute values of concentrations show that a resolution of 2 deg. is sufficient to get consistent results. (see fig. 7)

Wind speed classification

A comparison of calculations based on 9 or 5 wind speed classes give rise to the conclusion of sufficient confidential results within the present accuracy of the model if only 5 representative wind speeds are concidered (see fig. 8).

Mixing height

The influence of the mixing height depends of course on the source height. Concentration calculations have been performed for mixing heights of 500, 1000, 1500 m and infinite height (see fig. 9). The average values at 10 000 m distance from the source differed from each other by less than 20 % for low sources and less than 10 % for high sources. The concentration of 5 % excess probability differed by less than 10 % for high sources and nearly a factor of 2 for low sources and large distances (10 000 m).

The effect due to the mixing height is of lower importance even in those cases of deviations of a factor of 2 because of the very low absolute concentrations.

Meteorological conditions at different places

Very often an immissions forecast is necessary at places where complete three-dimensional sets of meteorological observations are not available. In addition to the results presented at the 1975 meeting at Frankfurt it can be stated that transformations of meteorological data from one station to another one are acceptable within certain limits.

The data of Düsseldorf and Münster have been transferred to Köln by adapting the wind direction frequencies only. The calculations for the Düsseldorf data at the Köln area show deviations of approximately 10 % or less. (The distance of these stations is about 60 km). This is valid for different directions and distances of 200 to 10 000 m and the calculations of average or 5 % excess probability values.

A transformation of the meteorological data of Münster to Köln was not successful as deviations rose to factors of 2 or even 4 in certain directions (see fig. 10). (distance of the stations is ca. 400 km)

Source dimensions

Calculations have been performed for area sources of 500 m x 500 m and 100 m x 500 m. The area sources were simulated by point sources. The calculated concentration (for 5 % excess probability) using 100 and 20 point sources each being representative for an area source of 50 m x 50 m should stand for the "ideal resolution". Using less or more point sources the deviation of calculated from the "real" ones at more than 200 m distance was a factor of 150 or less (see fig. 11). A resolution of 20 % is necessary for calculations up to distances of 2000m, i.e. the dimension of the area source represented by a point source should not exceed 20 % of the distance between source and immission point. Beyond 2000 m distance more simple approximations can be used.

Source data

A variation of several source data results in a change of concentration as follows:

low source height (10 m)

dates varied by 10 %	effect on concentration at 200 m distance (average value)	(5 % excess value)
emission amount	10 %	10 %
source height	-3.8 %	-4.7 %
exhaust gas	-1.4 %	-1.9 %
temperature	-1.5 %	-1.9 %
exit velocity	-0.1 %	-0.1 %

high source (100 m)

dates varied by 10 %	effect on concentration at maximum point (average value)	(5 % excess value)
emission amount	10 %	10 %
source height	-68 %	-90 %
exhaust gas	-4.1 %	-6.8 %
temperature	-4.3 %	-6.8 %
exit velocity	-0.2 %	-1.1 %

especially the variation of exit velocity is of very low influence.

Variing the geometrical height from 70 to 150 m the average concentration values and those of 5 % excess probability change as follows:

height (m)	immission relative to that for height 100 m (average value)	(5 % excess value)
70	5.7	5.7
80	3.8	4.1
90	2.2	2.6
100	1.0	1.0

110	0.86	0.78
120	0.74	0.69
130	0.61	0.60
150	0.48	0.43

Conclusion

The aforementioned results are a very short summary of the conclusions to be deducted from the investigations / 1 /. It can be said generally that there are two different sets of diffusion parameters deducted from different experiments which lead to consistent results of immission concentration calculations.

The most critical parameters for gaussian plume model calculations are the diffusion parameters. According to priority considerations critical and important parameters are

- effective source height
- turbulence classification
- description and handling of area sources
- meteorological data (wind speed and direction) resolution
- source data resolution
- mixing height influences
- chemical and physical processes.

Further investigations should be performed as follows:

- dependancies of diffusion parameters on roughness of the ground and from the height. Especially the parameters of Polster and Vogt for high sources and extremely unstable turbulence situations are necessary to be revised.

- check of calculations against measurements with regard to the verification of the Gauss model taking into account different sets of parameters and the plume rise.
- experiencing the influence of low wind speed and inversion layers
- development of models for complex topography
- investigation on influences of chemical and physical deposition and changes

References

/ 1 / TÜV Rheinland e.V. Köln
Standardisierung und Weiterentwicklung der Ausbreitungsrechnung (Standardising and Further Development of Diffusion Calculations)
Final Report on behalf of the Federal Minister of the Interior (1976)

/ 2 / McElroy, J. L., F. Pooler
St. Louis Dispersion Study, Vol. II - Analysis
Arlington, Virginia 1968
= National Air Pollution Control Administration
Publ. No. AP-53

/ 3 / Singer, I. A., M. E. Smith
Atmospheric Dispersion at Brookhaven National Laboratory
Int. I. Air Water Pollution Bd 10 (1966), S. 125

/ 4 / Klug, W.
Ein Verfahren zur Bestimmung der Ausbreitungsbedingungen aus synoptischen Beobachtungen
Staub-Reinhalt. Luft 29, 143 (1969)

/ 5 / Gifford, F.A.
Atmospheric Dispersion Calculations Using the Generalized Gaussian Plume Model.
Nuclear Safety 1 (3) März 1960 S. 56
" " 2 (3) Dez. 1960 S. 56

Use of Routine Meteorological Observations for Estimating Atmospheric Dispersion.
Nuclear Safety 2 (4) Juni 1961 S. 47

/ 6 / Vogt, K.J., H. Geiß
Kurzzeit- und Langzeitausbreitungsfaktoren zur Berechnung der Umweltbelastung durch Abluftfahnen
KFA Jülich ZAbt. Strahlenschutz ZST-Bericht Nr. 198
Sept. 1974
mit Ergänzung "private Mitteilung" über Parameter zu
H = 100 m

/ 7 / B. Turner
A Diffusion Model for an Urban Area
J. Appl. Met. 3 (1964) 83

/ 8 / Manier, G.
Vergleich zwischen Ausbreitungsklassen und Temperaturgradienten - TH Darmstadt Sektion Meteorologie
1. Teilbericht zu dem Forschungsvorhaben "Festlegung und Vorhersage der Ausbreitungsbedingungen in der Bundesrepublik Deutschland" des Bundesministers des Innern
- UB II 2-320-01-38/73 -

/ 9 / private information

/ 10 / Moses, H., G. H. Strom, J. E. Carson
Effects of Meteorological and Energineering Factors on Stack Plume Rise
Nucl. Safety 6, 1

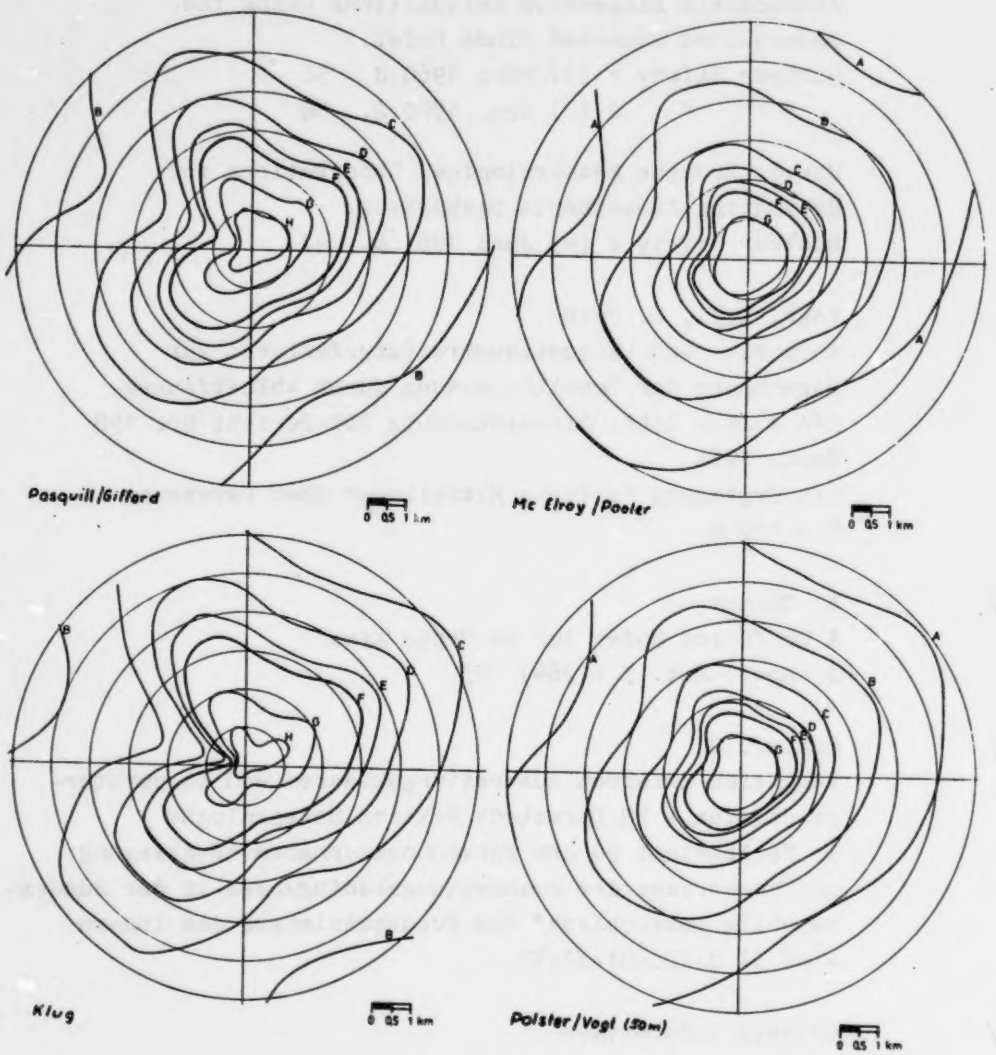

Fig. 1: Isoplethes of groundlevel concentration (averages in mg/m^3) for low source and different sets of diffusion parameters

$A = 1 \cdot 10^{-4}$	$E = 8 \cdot 10^{-4}$
$B = 2 \cdot 10^{-4}$	$F = 1 \cdot 10^{-3}$
$C = 4 \cdot 10^{-4}$	$G = 2 \cdot 10^{-3}$
$D = 6 \cdot 10^{-4}$	$H = 4 \cdot 10^{-3}$

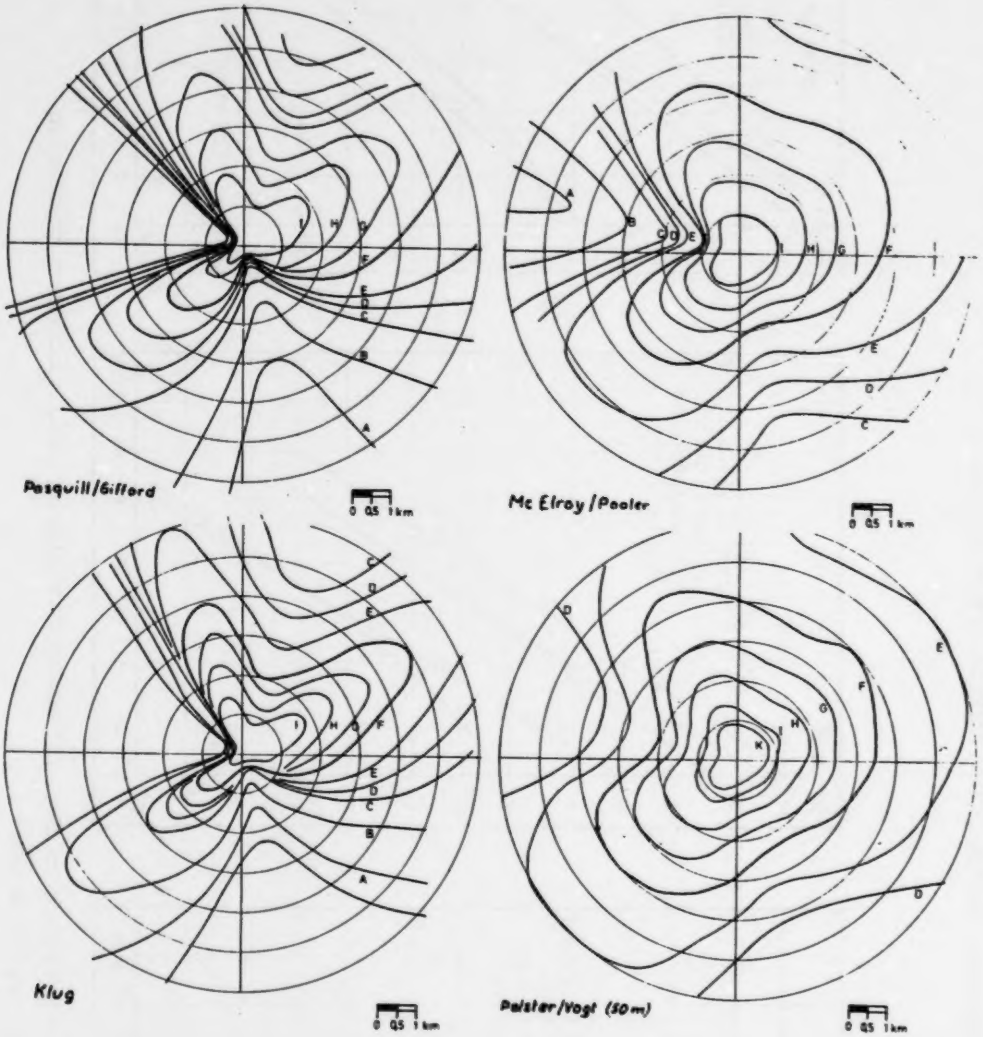
Pasquill/Gifford

Mc Elroy/Pooler

Klug

Polster/Vogt (50m)

fig. 2: Isoplethes of ground level concentrations (95 percentile in mg/m^3) for low source and different sets of diffusion parameters

A = 10^{-7}
B = 10^{-6}
C = 10^{-5}
D = $2 \cdot 10^{-5}$
E = $4 \cdot 10^{-5}$
F = $1 \cdot 10^{-4}$
G = $2 \cdot 10^{-4}$
H = $4 \cdot 10^{-4}$
I = $1 \cdot 10^{-3}$
K = $2 \cdot 10^{-3}$

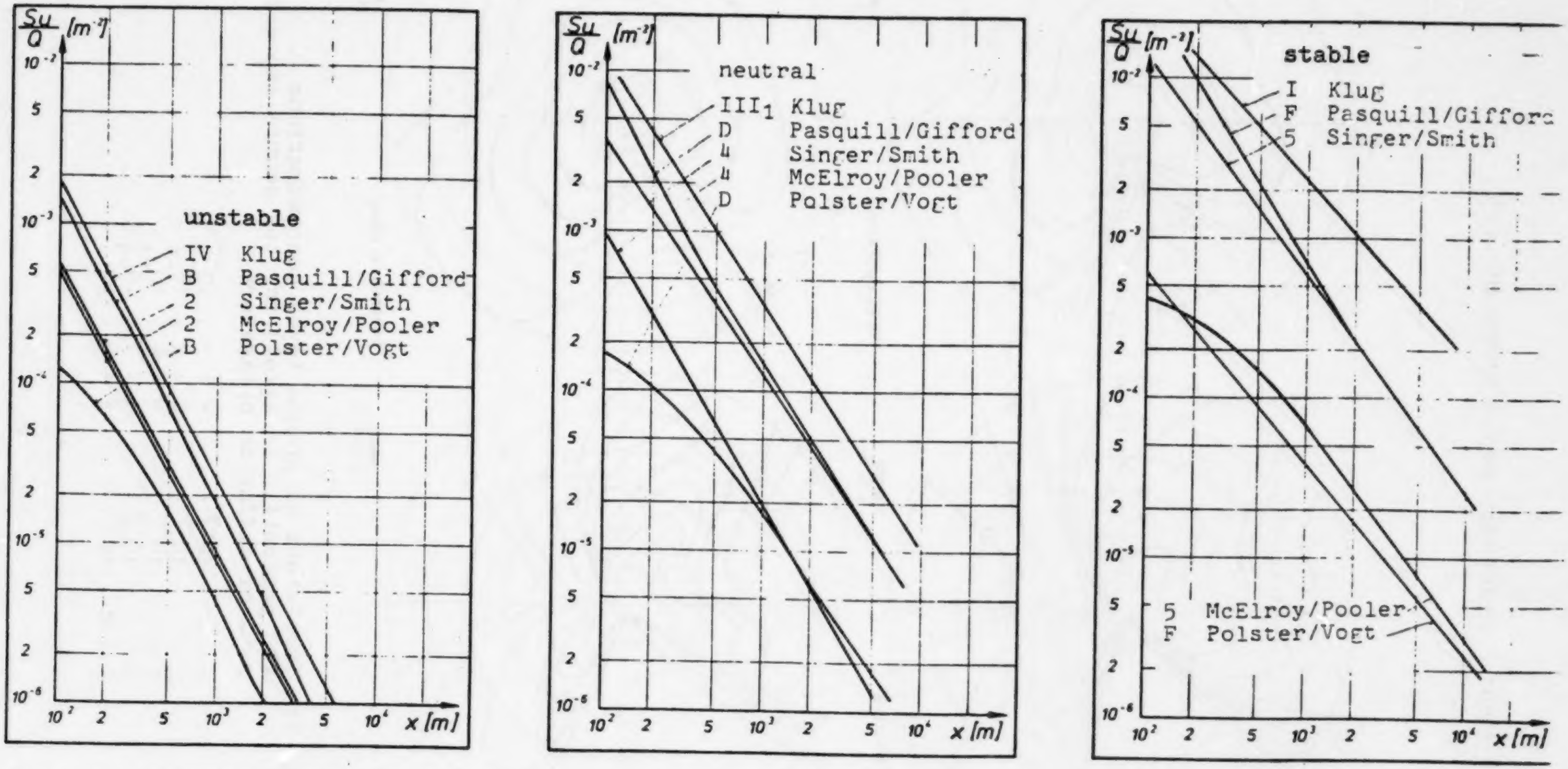

fig. 3: ground level concentration for different turbulence conditions and diffusion parameters σ_y, σ_z, $h = 0$ m

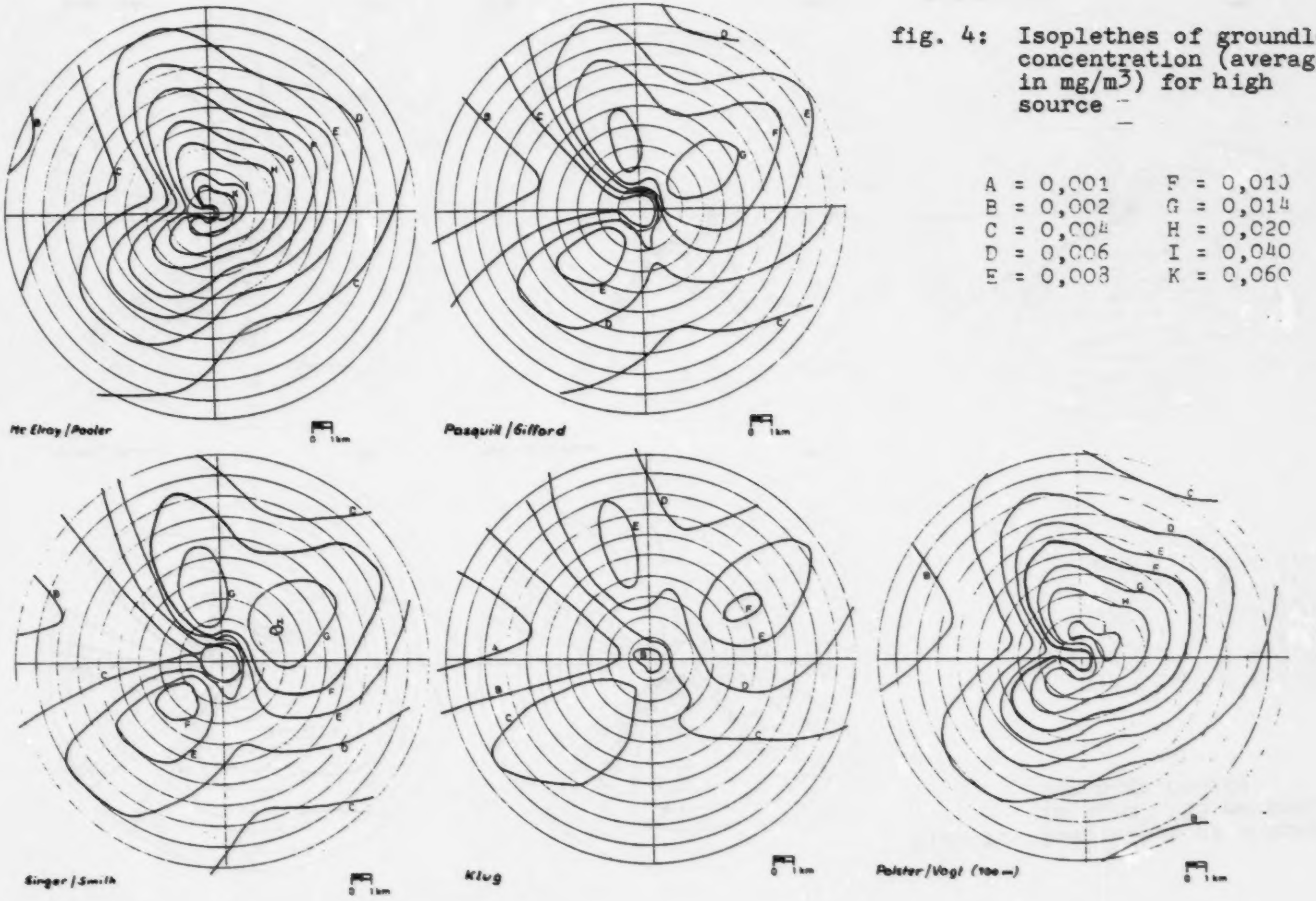

fig. 4: Isoplethes of groundlevel concentration (averages in mg/m^3) for high source

A = 0,001
B = 0,002
C = 0,004
D = 0,006
E = 0,008
F = 0,010
G = 0,014
H = 0,020
I = 0,040
K = 0,060

Fig. 5: Isoplethes of concentration in mg/m^3 (95 percentiles) for high source

A = 10^{-7}
B = 10^{-6}
C = 10^{-5}
D = 10^{-4}
E = 0,001
I = 0,002

G = 0,004
H = 0,006
I = 0,008
K = 0,01
L = 0,02
M = 0,04

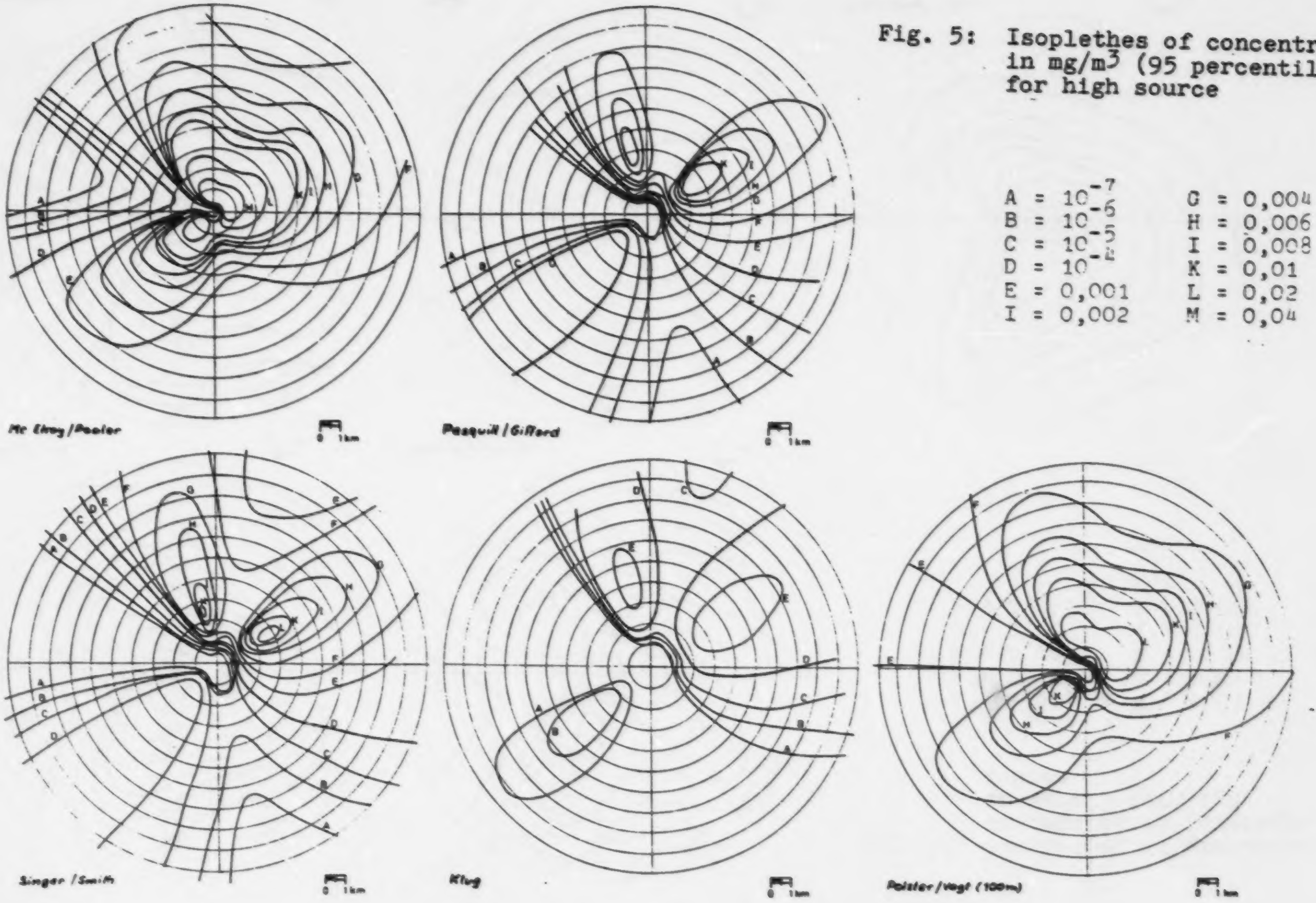

fig. 6: Comparison of concentrations ($\bar{S}$ - average, S_{95} - 95 percentiles) using turbulence classes of Polster/Vogt and Klug/Manier, parameter of Polster/Vogt, Düsseldorf

PV - Polster/Vogt KM - Klug/Manier

---

low source

$\bar{S}$ [10^{-6} mg/m^3]

distance	direction ENE		SSE		WSW		NNW	
m	PV	KM	PV	KM	PV	KM	PV	KM
250	603	608	282	288	461	458	573	568
500	201	214	101	112	193	200	215	221
1000	62	68	32	36	70	72	72	75
2000	19	20	10	11	23	24	23	24
3000	9	10	5	5	12	12	12	12

S_{95} [10^{-6} mg/m^3]

distance	direction ENE		SSE		WSW		NNW	
m	PV	KM	PV	KM	PV	KM	PV	KM
250	3900	3790	2200	2180	3700	3530	4160	3990
500	1310	1230	660	645	1510	1380	1560	1430
1000	360	332	150	142	440	380	450	401
2000	90	88	30	26	100	88	120	99
3000	40	41	10	8	40	38	50	45

high source

$\bar{S}$ [10^{-5} mg/m^3]

distance	direction ENE		SSE		WSW		NNW	
m	PV	KM	PV	KM	PV	KM	PV	KM
1000	549	572	212	218	271	290	398	421
2000	403	381	154	139	206	195	303	294
3500	210	199	81	75	113	109	164	160
5000	127	123	50	48	72	71	103	102
10000	45	45	19	19	30	30	39	40

S_{95} [10^{-5} mg/m^3]

distance	direction NNE		SSE		WSW		NNW	
m	PV	KM	PV	KM	PV	KM	PV	KM
1000	4550	4660	326	305	1200	1500	3370	3680
2000	3200	3020	472	598	985	1030	2230	2210
3500	1520	1480	225	387	705	797	1070	1220
5000	904	923	133	223	447	543	747	798
10000	315	340	100	109	173	180	275	309

Fig. 7: comparison of 95 percentiles for different wind direction resolutions (high source, meteorological data of Köln)

direction NW (300°)

distance	wind direction resolution				
m	5°	$2,5^{\circ}$	$1,67^{\circ}$	$1,25^{\circ}$	1°
1000	$0,127 \cdot 10^{-2}$	$0,139 \cdot 10^{-2}$	$0,133 \cdot 10^{-2}$	$0,140 \cdot 10^{-2}$	$0,138 \cdot 10^{-2}$
3500	$0,150 \cdot 10^{-1}$	$0,143 \cdot 10^{-1}$	$0,142 \cdot 10^{-1}$	$0,143 \cdot 10^{-1}$	$0,146 \cdot 10^{-1}$
10000	$0,129 \cdot 10^{-1}$	$0,908 \cdot 10^{-2}$	$0,993 \cdot 10^{-2}$	$0,975 \cdot 10^{-2}$	$0,913 \cdot 10^{-2}$

direction N

distance					
m	5°	$2,5^{\circ}$	$1,67^{\circ}$	$1,25^{\circ}$	1°
1000	$0,205 \cdot 10^{-3}$	$0,187 \cdot 10^{-3}$	$0,199 \cdot 10^{-3}$	$0,186 \cdot 10^{-3}$	$0,163 \cdot 10^{-3}$
3500	$0,206 \cdot 10^{-3}$	$0,987 \cdot 10^{-3}$	$0,151 \cdot 10^{-2}$	$0,139 \cdot 10^{-2}$	$0,124 \cdot 10^{-2}$
10000	$0,155 \cdot 10^{-3}$	$0,395 \cdot 10^{-3}$	$0,249 \cdot 10^{-3}$	$0,287 \cdot 10^{-3}$	$0,265 \cdot 10^{-3}$

direction W

distance					
m	5°	$2,5^{\circ}$	$1,67^{\circ}$	$1,25^{\circ}$	1°
1000	$0,163 \cdot 10^{-5}$	$0,150 \cdot 10^{-5}$	$0,181 \cdot 10^{-5}$	$0,181 \cdot 10^{-5}$	$0,173 \cdot 10^{-5}$
3500	$0,515 \cdot 10^{-4}$	$0,461 \cdot 10^{-4}$	$0,584 \cdot 10^{-4}$	$0,599 \cdot 10^{-4}$	$0,592 \cdot 10^{-4}$
10000	$0,341 \cdot 10^{-4}$	$0,547 \cdot 10^{-4}$	$0,891 \cdot 10^{-5}$	$0,101 \cdot 10^{-4}$	$0,791 \cdot 10^{-5}$

fig. 8: comparison of mean values and 95 percentiles for different numbers of representative wind speeds

low source

distance [m]	mean value [mg/m³]		95- percentiles [mg/m³]	
	9 steps	5 steps	9 steps	5 steps
200	$0,148 \cdot 10^{-2}$	$0,150 \cdot 10^{-2}$	$0,806 \cdot 10^{-2}$	$0,844 \cdot 10^{-2}$
500	$0,477 \cdot 10^{-3}$	$0,483 \cdot 10^{-3}$	$0,297 \cdot 10^{-2}$	$0,288 \cdot 10^{-2}$
1000	$0,167 \cdot 10^{-3}$	$0,170 \cdot 10^{-3}$	$0,959 \cdot 10^{-3}$	$0,966 \cdot 10^{-3}$
2000	$0,559 \cdot 10^{-4}$	$0,568 \cdot 10^{-4}$	$0,278 \cdot 10^{-3}$	$0,290 \cdot 10^{-3}$
3500	$0,229 \cdot 10^{-4}$	$0,234 \cdot 10^{-4}$	$0,101 \cdot 10^{-3}$	$0,106 \cdot 10^{-3}$
5000	$0,129 \cdot 10^{-4}$	$0,132 \cdot 10^{-4}$	$0,546 \cdot 10^{-4}$	$0,562 \cdot 10^{-4}$
7500	$0,676 \cdot 10^{-5}$	$0,688 \cdot 10^{-5}$	$0,272 \cdot 10^{-4}$	$0,288 \cdot 10^{-4}$
10000	$0,426 \cdot 10^{-5}$	$0,434 \cdot 10^{-5}$	$0,154 \cdot 10^{-4}$	$0,160 \cdot 10^{-4}$

high source

distance [m]	mean value [mg/m³]		95- percentiles [mg/m³]	
	9 steps	5 steps	9 steps	5 steps
200	$< 10^{-6}$	$< 10^{-6}$	$< 10^{-6}$	$< 10^{-6}$
500	$0,269 \cdot 10^{-3}$	$0,262 \cdot 10^{-3}$	$< 10^{-6}$	$< 10^{-6}$
1000	$0,114 \cdot 10^{-2}$	$0,116 \cdot 10^{-2}$	$0,138 \cdot 10^{-2}$	$0,144 \cdot 10^{-2}$
2000	$0,211 \cdot 10^{-2}$	$0,210 \cdot 10^{-2}$	$0,137 \cdot 10^{-1}$	$0,140 \cdot 10^{-1}$
3500	$0,231 \cdot 10^{-2}$	$0,230 \cdot 10^{-2}$	$0,146 \cdot 10^{-1}$	$0,136 \cdot 10^{-1}$
5000	$0,209 \cdot 10^{-2}$	$0,208 \cdot 10^{-2}$	$0,128 \cdot 10^{-1}$	$0,130 \cdot 10^{-1}$
7500	$0,174 \cdot 10^{-2}$	$0,174 \cdot 10^{-2}$	$0,123 \cdot 10^{-1}$	$0,118 \cdot 10^{-1}$
10000	$0,145 \cdot 10^{-2}$	$0,146 \cdot 10^{-2}$	$0,913 \cdot 10^{-2}$	$0,934 \cdot 10^{-2}$

fig. 9: Influence of mixing height on mean values $\overline{S}$ and 95 percentiles S_{95}; direction WNW (300°) met. data of Köln.

---

high source (H = 100 m, Q = 247 kg/h, T_s = 140° C, R = 176000 Nm^3/h, V_s = 10 m/s)

distance / m /	$\overline{S}$ / mg/m³ / H_M / m /				S_{95} / mg/m³ / H_M / m /			
	500	1000	1500	∞	500	1000	1500	∞
500	$0{,}269\cdot10^{-3}$	$0{,}269\cdot10^{-3}$	$0{,}269\cdot10^{-3}$	$0{,}269\cdot10^{-3}$	-	-	-	-
1000	$0{,}114\cdot10^{-2}$	$0{,}114\cdot10^{-2}$	$0{,}114\cdot10^{-2}$	$0{,}114\cdot10^{-2}$	$0{,}141\cdot10^{-2}$	$0{,}141\cdot10^{-2}$	$0{,}141\cdot10^{-2}$	$0{,}141\cdot10^{-2}$
2000	$0{,}215\cdot10^{-2}$	$0{,}211\cdot10^{-2}$	$0{,}211\cdot10^{-2}$	$0{,}211\cdot10^{-2}$	$0{,}145\cdot10^{-1}$	$0{,}144\cdot10^{-1}$	$0{,}144\cdot10^{-1}$	$0{,}144\cdot10^{-1}$
3500	$0{,}239\cdot10^{-2}$	$0{,}232\cdot10^{-2}$	$0{,}231\cdot10^{-2}$	$0{,}231\cdot10^{-2}$	$0{,}156\cdot10^{-1}$	$0{,}148\cdot10^{-1}$	$0{,}147\cdot10^{-1}$	$0{,}146\cdot10^{-1}$
5000	$0{,}219\cdot10^{-2}$	$0{,}210\cdot10^{-2}$	$0{,}209\cdot10^{-2}$	$0{,}209\cdot10^{-2}$	$0{,}140\cdot10^{-1}$	$0{,}131\cdot10^{-1}$	$0{,}128\cdot10^{-1}$	$0{,}123\cdot10^{-1}$
10000	$0{,}156\cdot10^{-2}$	$0{,}147\cdot10^{-2}$	$0{,}146\cdot10^{-2}$	$0{,}145\cdot10^{-2}$	$0{,}113\cdot10^{-1}$	$0{,}985\cdot10^{-2}$	$0{,}948\cdot10^{-2}$	$0{,}913\cdot10^{-2}$

low source (H = 10 m, Q = 0,342 kg/h, T_s = 250° C, R = 295 Nm^3/h, V_s = 2 m/s)

distance m	$\overline{S}$/ mg/m³ / H_M m				S_{95} / mg/m³ / H_M m			
	500	1000	1500	∞	500	1000	1500	∞
200	$0{,}148\cdot10^{-2}$	$0{,}148\cdot10^{-2}$	$0{,}148\cdot10^{-2}$	$0{,}148\cdot10^{-2}$	$0{,}806\cdot10^{-2}$	$0{,}806\cdot10^{-2}$	$0{,}806\cdot10^{-2}$	$0{,}806\cdot10^{-2}$
500	$0{,}477\cdot10^{-3}$	$0{,}477\cdot10^{-3}$	$0{,}477\cdot10^{-3}$	$0{,}477\cdot10^{-3}$	$0{,}297\cdot10^{-2}$	$0{,}297\cdot10^{-2}$	$0{,}297\cdot10^{-2}$	$0{,}297\cdot10^{-2}$
1000	$0{,}167\cdot10^{-3}$	$0{,}167\cdot10^{-3}$	$0{,}167\cdot10^{-3}$	$0{,}167\cdot10^{-3}$	$0{,}959\cdot10^{-3}$	$0{,}959\cdot10^{-3}$	$0{,}959\cdot10^{-3}$	$0{,}959\cdot10^{-3}$
2000	$0{,}570\cdot10^{-4}$	$0{,}560\cdot10^{-4}$	$0{,}559\cdot10^{-4}$	$0{,}559\cdot10^{-4}$	$0{,}294\cdot10^{-3}$	$0{,}278\cdot10^{-3}$	$0{,}278\cdot10^{-3}$	$0{,}278\cdot10^{-3}$
3500	$0{,}244\cdot10^{-4}$	$0{,}232\cdot10^{-4}$	$0{,}230\cdot10^{-4}$	$0{,}229\cdot10^{-4}$	$0{,}122\cdot10^{-3}$	$0{,}101\cdot10^{-3}$	$0{,}101\cdot10^{-3}$	$0{,}101\cdot10^{-3}$
5000	$0{,}144\cdot10^{-4}$	$0{,}133\cdot10^{-4}$	$0{,}131\cdot10^{-4}$	$0{,}129\cdot10^{-4}$	$0{,}755\cdot10^{-4}$	$0{,}570\cdot10^{-4}$	$0{,}550\ 10^{-4}$	$0{,}546\cdot10^{-4}$
10000	$0{,}540\cdot10^{-5}$	$0{,}459\cdot10^{-5}$	$0{,}441\cdot10^{-5}$	$0{,}426\cdot10^{-4}$	$0{,}312\cdot10^{-4}$	$0{,}206\cdot10^{-4}$	$0{,}177\cdot10^{-4}$	$0{,}154\cdot10^{-4}$

fig. 10: Comparison of mean values $\bar{S}$ and 95 percentiles for different meteorological data transferred to Köln place

K data of Köln

D → K data of Düsseldorf transferred to Köln

M → K data of Münster transferred to Köln

	distance / m /	$\bar{S}^K$ / mg/m^3 /	$\frac{\bar{S}^{D \to K}}{\bar{S}_K}$	$\frac{\bar{S}^{M \to K}}{\bar{S}_K}$	S_{95}^K / mg/m^3 /	$\frac{S_{95}^{D \to K}}{S_{95}^K}$	$\frac{S_{95}^{M \to K}}{S_{95}^K}$
N	200	$0,71 \cdot 10^{-3}$	0,90	1,19	$0,36 \cdot 10^{-2}$	0,89	1,34
	500	$0,17 \cdot 10^{-3}$	0,91	1,29	$0,93 \cdot 10^{-3}$	0,90	1,20
	1000	$0,55 \cdot 10^{-4}$	0,92	1,39	$0,28 \cdot 10^{-3}$	0,89	1,09
	2000	$0,18 \cdot 10^{-4}$	0,93	1,46	$0,74 \cdot 10^{-4}$	0,89	0,95
	3500	$0,71 \cdot 10^{-5}$	0,94	1,53	$0,24 \cdot 10^{-4}$	0,91	0,84
	5000	$0,39 \cdot 10^{-5}$	0,94	1,56	$0,10 \cdot 10^{-4}$	0,89	0,77
	7500	$0,20 \cdot 10^{-5}$	0,94	1,60	$0,37 \cdot 10^{-5}$	0,90	0,74
	10000	$0,13 \cdot 10^{-5}$	0,94	1,63	$0,17 \cdot 10^{-5}$	0,91	0,65
O	200	$0,63 \cdot 10^{-3}$	0,94	1,46	$0,33 \cdot 10^{-2}$	0,93	1,41
	500	$0,16 \cdot 10^{-3}$	0,94	1,71	$0,91 \cdot 10^{-3}$	0,92	1,55
	1000	$0,50 \cdot 10^{-4}$	0,95	1,90	$0,28 \cdot 10^{-3}$	0,91	1,67
	2000	$0,16 \cdot 10^{-4}$	0,96	2,08	$0,81 \cdot 10^{-4}$	0,91	1,94
	3500	$0,61 \cdot 10^{-5}$	0,96	2,22	$0,29 \cdot 10^{-4}$	0,91	2,21
	5000	$0,34 \cdot 10^{-5}$	0,97	2,30	$0,14 \cdot 10^{-4}$	0,90	2,57
	7500	$0,17 \cdot 10^{-5}$	0,97	2,39	$0,55 \cdot 10^{-5}$	0,89	3,31
	10000	$0,11 \cdot 10^{-5}$	0,97	2,46	$0,26 \cdot 10^{-5}$	0,92	4,24
S	200	$0,47 \cdot 10^{-3}$	0,93	1,02	$0,28 \cdot 10^{-2}$	0,93	1,02
	500	$0,12 \cdot 10^{-3}$	0,92	1,03	$0,51 \cdot 10^{-3}$	0,91	0,95
	1000	$0,39 \cdot 10^{-4}$	0,93	1,04	$0,86 \cdot 10^{-4}$	0,93	0,91
	2000	$0,12 \cdot 10^{-4}$	0,93	1,05	$0,11 \cdot 10^{-4}$	0,94	0,88
	3500	$0,49 \cdot 10^{-5}$	0,93	1,05	$0,12 \cdot 10^{-5}$	0,97	0,83
	5000	$0,27 \cdot 10^{-5}$	0,93	1,05	$0,25 \cdot 10^{-6}$	1,01	0,84
	7500	$0,14 \cdot 10^{-5}$	0,94	1,06	$0,29 \cdot 10^{-7}$	1,05	0,79
	10000	$0,88 \cdot 10^{-6}$	0,94	1,06	$0,52 \cdot 10^{-8}$	1,08	0,70
WNW	200	$0,15 \cdot 10^{-2}$	1,09	0,96	$0,81 \cdot 10^{-2}$	1,19	0,93
	500	$0,48 \cdot 10^{-3}$	1,12	0,89	$0,30 \cdot 10^{-2}$	1,11	0,81
	1000	$0,17 \cdot 10^{-3}$	1,13	0,85	$0,96 \cdot 10^{-3}$	1,07	0,72
	2000	$0,56 \cdot 10^{-4}$	1,13	0,82	$0,28 \cdot 10^{-3}$	1,06	0,76
	3500	$0,23 \cdot 10^{-4}$	1,13	0,80	$0,10 \cdot 10^{-3}$	1,01	0,78
	5000	$0,13 \cdot 10^{-4}$	1,13	0,79	$0,55 \cdot 10^{-4}$	1,02	0,77
	7500	$0,68 \cdot 10^{-5}$	1,13	0,78	$0,27 \cdot 10^{-4}$	0,98	0,72
	10000	$0,43 \cdot 10^{-5}$	1,13	0,77	$0,15 \cdot 10^{-4}$	0,98	0,73

Fig. 11 Maximum of deviation between calculated concentrations for an area source represented by N point sources and concentration for an area source repr. by 100 or 20 point sources

$$\text{deviation} = \frac{\text{conc (N sources)}}{\text{conc (100 or 20 sources)}}$$

A area source 500 x 500 m

N	corresponding area element m	distance (m) 200	500	1000	2000	3500	5000	10000
1	500 x 500	153	44	54	15	15	6,2	5,5
4	250 x 250	73	23	10,4	2,9	4,4	2,4	3,8
9	167 x 167	63	2,9	4,4	1	5,0	2,6	3,4
25	100 x 100	31	1	1,3	1	2,4	1	1
49	71 x 71	2,1	1	1	1	1	1	1
100	50 x 50	1	1	1	1	1	1	1

B area source 100 (W-O) x 500 (N-S) m

B1 directions W, O, WNW (300°)

N	corresponding area element	distance (m) 200	500	1000	2000	3500	5000	10000
1	500 x 100	88	45	41	15	11	10	1
2	250 x 100	67	33	27	12	22	10	1
5	100 x 100	1	1	2,2	1,0	1	1	1
20	50 x 50	1	1	1,7	1	1	1	1

B2 directions N, S

N	corresponding area element	distance (m) 200	500	1000	2000	3500	5000	10000
1	500 x 100	49	33	16	2,5	1	1,3	1
2	250 x 100	95	57	16	1	1	3,2	1
5	100 x 100	67	4,1	6,1	1	1	1	1
20	50 x 50	2,8	1	1	1	1	1	1

Rapporteur Summary Report

Topic 3

Session on Sensitivity Analysis and Dispersion Under Low Wind Speeds

Rapporteur: Richard Porter

1. R.F. Lee: - "Sensitivity of the Single Source (CUSTER) Model"

Hoffnagle: We have found 20 to 25 percent variation in the observed maximum values by using meteorology of successive years. In five years of data, only two gave nearly the same maximum concentrations.

Egan: We found similar results with a similar model, but the maxims were found to occur with persistent winds.

Lee: We do see the maximus occur with persistent winds, but unstable cases also give maximums.

Keddie: Have you looked at other sets of vertical and horizontal standard deviations?

Lee: We have a contractor report on that due soon.

Fanaki: Why did the change in the wind speed effect the tall stack more than the short stack?

Freas: For each stack and set of stack parameters, there is a critical wind speed for which the concentration is maximum. Below this wind speed the higher plume rise causes lower concentration. Above the critical wind speed increased dilution causes lower concentrations. The effect of change in wind speed will be different for each stack according to how in relation to the critical wind speed the wind speed is varied.

2. W. J. Veigele - "Concentration and Index Sensitivity of Gaussian Plume Model"

Fox: Could you describe the Council of Regional Planners to our members from other countries?

Veigele: Representatives of local city and county governments in a region meet together as a regional planning body. The purpose is to plan for orderly growth in the region with a minimum of pollution impact from that growth.

Slater: A comment. The EPA and the Council of Environmental Quality have proposed a pollution index scheme. A question. Why is the sensitivity of the index so low for CO?

Veigele: There is a large number of CO sources. Random errors introduced to a large number of sources tend to cancel. Pollutants that have fewer sources show larger impact from introduction of random errors.

Hilst: The annual average concentrations are nearly uniform. Would your methods be applicable in an area such as New York City where the concentration gradient is very large?

Veigele: A more sophisticated model and techniques would be advised.

3. R. J. Yamartino - "An Air Quality Dispersion Model Applicable to Calm Conditions"

Fortak: There is a problem with this model under light and variable winds that circulate the plume repeatedly around the source.

Yamartino: Some wind flux is accounted for in the model, but circulating winds would be a problem.

Johnson: The light and variable wind is a problem in daytime. The model applies better in the light persistent wind conditions found at night.

Cramer: We have modeled calm winds with a strong inversion We use a 1/2 m/sec wind speed. By determining the wind flow pattern, we had a good match with observed data.

4. K. Herrmann - "The Role of Turbulent Diffusion in the Direction of the Mean Wind in Numerical Model"

Calder: What was the basis of the Ky and Kz values from Klug stability?

Herrmann: $\sigma = \sqrt{2K \frac{X}{\mu}}$ based on release from a point source.

Fortak: In this case the Ky values are very critical.

5. L. Kropp - "Influences of Model Parameters and Sensibility to their Variation within the Immissions Forecasting"

Klug: What was the averaging time for the 95 percentile number?

Kropp: 1 hour.

Fortak: It is not appropriate to apply the steady Gaussian plume model in a study to determine time dependent functions.

Cramer: I believe that because the critical values usually come with meteorology that is persistent, we do not have a problem with steady state model.

Kropp: Area sources in this study were simulated with a point source at the area centroid. We found this to be better than the virtual point source method.

PROCEEDINGS OF THE SEVENTH INTERNATIONAL TECHNICAL MEETING ON AIR POLLUTION MODELING AND ITS APPLICATION

7 - 10 September 1976

AIRLIE HOUSE, VIRGINIA
United States of America

A Report of the Air Pollution Pilot Study

NATO Committee on the Challenges to Modern Society

1976

TOPIC IV

NUMERICAL GRIDS AND PHYSICAL MODELING

7th International Technical Meeting
on Air Pollution Modeling and its Application

Dispersion of Roof-Top Emissions from Isolated Buildings -- A Wind Tunnel Study

Roger S. Thompson
Meteorology and Assessment Division
Environmental Sciences Research Laboratory
Environmental Protection Agency

and

David J. Lombardi
Northrop Services Inc.

Research Triangle Park, NC
United States of America

September 7 - 10, 1976
Airlie Virginia
United States of America

Dispersion of Roof-Top Emissions from Isolated Buildings -- A Wind Tunnel Study

Roger S. Thompson
Meteorology and Assessment Division
Environmental Sciences Research Laboratory
Environmental Protection Agency

and

David J. Lombardi
Northrop Services Inc.

Work Performed In

Fluid Modeling Facility
Meteorology and Assessment Division
Environmental Protection Agency
Research Triangle Park, NC 27711
United States of America

ABSTRACT

A fluid modeling study of the dispersion of roof-top emissions from rectangular buidings was performed in the meteorological wind tunnel of the EPA Fluid Modeling Facility. The basic building shape was a 0.18 meter cube, but variations included buildings two times as wide and two and three times as high. Each building was placed in a 1.8 meter, simulated, neutral atmospheric boundary layer. Low momentum, nonbuoyant emissions were released through an opening at the roof center. Photographs of flow visualization experiments are provided for a qualitative evaluation of the building wakes. Concentration measurements at ground-level and aloft are presented for each case at downwind distances within 20 building heights. Concentrations are presented in a nondimensional form for ease in application to full scale situations. The orientation of the wind to the building was found to significantly affect ground-level concentrations near the building. A 45° orientation of the cubical building increased the maximum ground-level concentration by a factor of 6 over that observed for a perpendicular orientation.

INTRODUCTION

Because fluid modeling can accurately reflect the complex nature of turbulent air flow near structures, it is uniquely suited to the study of the dispersion of matter released from a building's roof-top. In such studies, two distinct phenomena have been observed downwind of an isolated, blunt structure. One is the development of an aerodynamic cavity of high turbulence and reverse flow caused by separation of the air flow over the building roof. The other is the confinement of roof-top emissions to the wake or dispersion envelopes, which are determined by the shape of the building and by the approaching wind field.

The dispersion of roof-top emissions was modeled by Halitsky (1968) in a study of the concentration fields at and near rectangular buildings placed at various orientations to the wind. He used an approach flow of uniform mean velocity and low turbulence and an emission source located at the center of the roof. Although effluent momentum was varied, all emissions were nonbuoyant. In another study, Yang and Meroney (1970) considered low momentum releases from all faces of a cubical structure and modeled both neutral and stratified boundary layers. Robins (1975) presented some maximum ground-level concentrations measured in a wind tunnel study of releases from a cubical building under conditions quite similar to those in the study reported here.

The present study, which was performed in the Environmental Protection Agency's Fluid Modeling Facility, extends previous work by analyzing concentration fields downwind of four different shapes of rectangular buildings. Block-shaped model buildings were placed in a simulated, neutral atmospheric boundary layer to determine the influence of the wind field and building geometry on the dispersion of roof-top emissions. Only simple building shapes were used with no other buildings, trees, or hills located nearby. Air containing a low percentage of methane as a tracer was released from the center of the roof to model a low momentum, nonbuoyant effluent. Ground-level and vertical concentration profiles were determined downwind by measuring tracer levels in samples taken at various positions.

This paper is a condensed version of the project report (Thompson and Lombardi, 1976) and contains selected flow visualization photographs and concentration profiles from that document. Some of the statements made here are based on observations of the visualization experiments and the concentration profiles contained in that report.

EXPERIMENTAL TECHNIQUES

The experiment was performed in EPA's Meteorological Wind Tunnel (Snyder, 1974; Snyder et al., 1976). This low speed, open circuit wind tunnel has an 18 meter (m) long, 2.1 m high, and 3.7 m wide test section in which atmospheric boundary layer airflow can be simulated. Based on the procedure developed by Counihan (1969), vortex generating fins measuring 1.8 m in height were used to produce a boundary layer height, δ, of 1.8 m. Two-dimensional roughness slats were mounted on the tunnel floor to maintain an equilibrium boundary layer over the test section.

A dimensionless ratio of interest in modeling dispersion near buildings is the building Reynolds number, $Re = HU_H/\nu$ (where H is the building height, U_H is the mean wind speed at z = H with no building present, and ν is the kinematic viscosity of air). Ideally, the model Reynolds number and the full-scale Reynolds number should match but the full-scale number is generally orders of magnitude larger than that which can be obtained in wind tunnel studies. Golden (1961) showed that concentration fields near building models are invariant with the Reynolds number provided the building Reynolds number is greater than 11,000. In this study, the minimum Reynolds number for any case was 17,500.

Eight combinations of building shape and orientation to the wind were studied (Table 1 and Figure 1). The most extensive measurements were taken for Case 1, a cubical building (H = 0.18 m) facing perpendicular to the wind. An additional run, Case 8, was a repeat of Case 1 with the mean tunnel speed twice that for Case 1 and was performed to verify that the dispersion was indeed independent of the building Reynolds number. For all cases, the model building was well within the boundary layer.

Smoke produced by an oil-fog generator was released from the model building so the qualitative features of the dispersion could be visualized. Based on these observations of plume trajectories, sampling positions for quantitative measurements were established.

For the quantitative experiments, a 4.8 percent by volume mixture of methane-in-air was used as the tracer. The effluent rate, monitored through rotameters, was held at 4.0 liters per minute throughout the experiment. With the source diameter, D, of 0.0254 m, the effluent velocity, w, was 0.13 meters per second (m/sec). Thus, the ratio of effluent velocity to local velocity, w/U_H, was much less than 1.0 for all cases (see Table 1) providing assurance that momentum effects were negligible. Buoyancy resulting from the use of hydrocarbon tracer was also negligible; the ratio of stack density to ambient density, ρ_s/ρ_a, was 0.98 for all cases.

Samples were drawn through a 0.002-m-diameter sampling probe and passed through a flame ionization detector to determine tracer concentrations. The ambient hydrocarbon background level was measured before and after each run and used to correct the raw data.

EXPERIMENTAL RESULTS

Velocity and turbulence measurements were made to evaluate how well the model flow represented the atmospheric boundary layer. Measurements were also made at several positions downwind of the building. The mean free-stream speed was 2 m/sec.

Profiles of the mean velocity measured over the release point with the building removed and at two locations downwind of the building are shown in Figure 2. The mean velocity profiles are conveniently approximated by a one-seventh power law in the approach to the cubical building (x = 0) and the far-wake region of the building (x = 10H). A one-seventh power law profile is typical of flow over flat rural topography (Davenport, 1963). Although hot-film anemometer measurements are unreliable near the building where turbulence levels are high and flow reversals may occur, severe distortion of the mean velocity profile caused by the building can be observed in the profile at x = 2H.

Longitudinal turbulence intensities were also comparable to field observations made in a neutral atmosphere. The maximum local turbulence intensity in the approach flow, $\sqrt{u'^2} / U = 0.24$, occurred at ground level and the intensity subsequently decreased to wind-tunnel background turbulence levels as the height increased. Approach flow turbulence (x = 0), shown in Figure 3, was not unlike the field data reported by Harris (1968) in tendency and magnitude. A previous study (Huber and Snyder, 1976) using this same boundary layer examined dispersion from short stacks. Analysis of the lateral and vertical spreading of the plume from an isolated stack in their study showed the dispersion to be representative of Pasquill-Gifford category "C" -- that is, slightly unstable -- for a model scale on the order of 1:100. In the wake of the cubical building (x = 2H), the local turbulence intensity measurements from the present study were unreliable but showed the profile to be erratic and the turbulence to be of large magnitude. The presence of the building, however, did not seem to disturb the flow above approximately the 1.5H ($z = 0.15\delta$) level for this approach flow.

All measured concentrations, C, were made nondimensional with the source emission rate, Q, according to the corresponding building height, H, and mean wind speed at that height, U_H;

$$\chi = \frac{CU_H H^2}{Q}$$

This should be kept in mind when comparing values for different building heights. To avoid interference with the surface roughness slats, a height of z = 0.0025 m was taken as "ground level" for concentration measurements. Coordinates (x, y, z) are defined in Figure 1.

Of the building shapes considered, a cubical building was the most elementary. Figure 4 demonstrates the behavior of a roof-centered effluent release from a cubical model when the wind was perpendicular to a side (Case 1). Reverse flow just above the top of the cube caused the advection of some of the effluent to the upwind edge of the roof. The height of the dispersion envelope as determined by smoke visualization was approximately 1.5H over the building and approximately 2.0H at a downwind distance of 5H. Vertical concentration profiles (Figure 5) indicate similar envelope heights. The maximum concentration for the vertical profile at a downwind distance of $x = 2H$ occurred at an elevation of $z = H$. At distances farther downwind, the peak value moved closer to the ground, as indicated by each profile.

A longitudinal ground-level profile along the plume centerline (Figure 6) indicated a maximum ground-level concentration of $\chi = 0.43$ at a distance of $x = 5H$. This result is close to the value of $\chi = 0.31$ reported by Robins (1975) for a model study that, except for a somewhat higher effluent momentum, was essentially the same as the study of the cube reported here.

A different wind direction produces a significant change in the way the roof-top emissions disperse. When a corner of the cube was pointed into the wind (Case 2, Figure 7), flow reversals atop the building did not occur as in Case 1. Emissions were swept directly over the downwind building corner with no reverse flow over the building roof and more smoke reached ground level immediately downwind of the building than was observed for Case 1. Ground-level concentrations were much higher for Case 2 than for Case 1 for distances up to about x = 5H, but were nearly equal by the time they reached x = 10H (Figure 6). Also with this building orientation, the dispersion envelope did not extend far above the building, nor did it grow rapidly with increasing downwind distance. The vertical concentration profiles illustrate the differing characteristics (Figure 8).

For cases in which cubical buildings are oriented at other angles to the mean flow, emissions may be expected to produce concentration levels that are between those of Case 1 and Case 2. Case 9 was such a configuration with the building rotated to an angle, Θ, of 22.5°. The plume for this case was found to be slightly skewed about the line ($y = 0$). The longitudinal concentration profile (Figure 6) and the vertical profile (Figure 8) were taken directly downwind of the release. In Figure 6, the concentration levels near the building for Case 9 fell between those of Cases 1 and 2. Farther downwind, concentrations for all three cases approached the same levels. The vertical profile of Case 9 was similar to that of Case 2.

Case 8, which was a repeat of Case 1 at twice the freestream velocity, was performed to verify that the dispersion was independent of the Reynolds number. A longitudinal, ground-level concentration profile (Figure 9) and a vertical profile at x = 5H (Figure 5) are practically identical to the corresponding profiles for Case 1. The close agreement of these profiles indicates that the dispersion field did not change substantially with a doubling of the building Reynolds number.

A model building having a width twice the other dimensions, Case 3, produced an envelope of slightly greater vertical extent than for Case 1. The vertical profile at x = 5H (Figure 8) was similar in shape to that for Case 1. However, concentrations below the building height (z = H) were lower by approximately 20 percent. This effect can be attributed in part to the more lateral spreading of the plume in Case 3. Moreover, the ground-level concentrations along the plume centerline (Figure 9) were lower by about 30 percent at locations far from the building ($x > 5H$). The maximum ground-level value, however, was about the same as for Case 1, but it occurred closer to the building.

Case 4, a model building whose length in the direction of the wind was twice its other dimensions, exhibited a similar vertical limit on the envelope. The vertical profile for Case 4 (Figure 8) was also similar to that for Case 1, and the ground-level concentrations along plume centerline were only slightly lower than for Case 1 (Figure 9).

The building whose height was twice its other dimensions, Case 5, had an envelope directly over the building (Figure 10) that was similar to that of Case 1, but its height did not increase downwind of the building. Also illustrated by Figure 10 is the fact that little of the smoke reached the ground immediately downwind of the building. When this building was rotated to 45° (Case 6), however, a considerable amount of the smoke reached the ground. Case 7 involved the use of a building three times as high as the building used in Case 1. Ground-level concentrations near the building for Cases 5 and 7 were not high enough above background levels to obtain reliable measurements.

Vertical profiles for Cases 5 and 6 are shown in Figure 11. Rotating this taller building 45° from the perpendicular shifted the peak of the profile from the building roof level to the ground. The vertical profile for Case 7 at $x/H = 1.66$ is included in Figure 11 for comparison.

CONCLUDING REMARKS

Smoke visualization and measured concentration profiles have been presented for generalized building shapes and wind directions. The situation was simplified in that the source was positioned at the roof center and the effluent was nonbuoyant and had negligible momentum. Considering the cubical building model, Case 1, as the basis for comparison, some general observations can be made:

1. A change in the direction of the approaching wind significantly altered the shape and size of the aerodynamic cavity and the dispersion envelope. These changes resulted in different dispersion patterns and ground-level concentrations. A wind direction of 45° increased the maximum ground-level concentration by a factor of six.

2. Doubling the width of the building reduced by about 20 percent the concentrations below the building height ($z = H$) at a downwind distance of $x = 5H$. The ground-level maximum was approximately the same as that for the cube, but occurred nearer the building.

3. Doubling the length of the building in the direction of the wind had little effect on the concentrations.

4. Doubling or tripling the height of the building elevated the plume and lowered the ground-level concentrations. The shape of the dispersion envelope immediately over the building was similar for all three heights tested. Changing the wind direction from the perpendicular for the cases involving taller buildings increased the ground-level concentrations near the building.

The concentration measurements as presented should be of use to numerical modelers in developing schemes for predicting concentrations near roof-top incinerators, roof exhausts, and other similar pollutant sources. For full-scale situations that are reasonably similar to those of the block models of this study, the χ values of the figures can be applied directly to predict concentrations.

REFERENCES

Counihan, J. (1969): An Improved Method of Simulating an Atmospheric Boundary Layer in a Wind Tunnel, Atm. Env. 3, 197-214.

Davenport, A.G. (1963): The Relationship of Wind Structure to Wind Loading. Paper 2, Proc. of Conf. on "Wind Effects on Buildings and Structures", Nat. Phys. Lab., June, 1963, HMSO, London, 1965 p. 54-102.

Golden, J. (1961): Scale Model Techniques. M.S. Thesis, College of Engr., NYU, May.

Halitsky, J. (1968): Gas Diffusion Near Building, in Meteorology and Atomic Energy, 1968, edited by David H. Slade, pp. 221-255.

Harris, R.I. (1968): Measurement of Wind Structure at Heights up to 598 ft. above Ground Level, Symp. Wind Effects on Buildings and Structures, Loughborough Univ. Tech. (Dept. of Transport Technology).

Huber, A.H. and W.H. Snyder (1976): Building Wake Effects on Short Stack Effluents. To be published in the preprint volume of the American Meteorological Society 3rd Symposium on Atmospheric Turbulence, Diffusion and Air Quality. Raleigh, N.C., October 19-22, 1976.

Robins, A. (1975): Experimental Model Techniques for the Investigation of the Dispersion of Chimney Plumes. Proc. Instn. Mech. Engrs. 189. 44-54.

Snyder, W.H. (1974): Fluid Modeling Program of the Meteorology Laboratory, U.S. Environmental Protection Agency. Chapter 31 of Proceedings of the Fifth Meeting of the Expert Panel on Air Pollution Modeling. NATO-CCMS, N. 35.

Snyder, W.H., R.S. Thompson, and R.E. Lawson, Jr. (1976): The EPA Meteorological Wind Tunnel: Design, Construction, and Operating Details, Environmental Protection Agency, Research Triangle Park, N.C. (In preparation).

Thompson, R.S. and D.J. Lombardi (1976): Dispersion of Roof-Top Emissions from Isolated Buildings -- A Wind Tunnel Study, Environmental Protection Agency, Research Triangle Park, N.C. (Project report in preparation).

Yang, B.T. and R.N. Meroney (1970): Gaseous Dispersion Into Stratified Building Wakes. FDDL Technical Report, CSU, CER70-71BTY RNM-8.

Table 1. GEOMETRY AND DEFINING PARAMETERS FOR EACH CASE

	Shape, m[a]			Parameter[b]				
Case	L	W	H	θ, degrees	H/δ	U_H, m/sec	w/U_H	$Re = \frac{U_H H}{\nu}$
1	0.18	0.18	0.18	0	0.1	1.46	0.090	17,500
2	0.18	0.18	0.18	45	0.1	1.46	0.090	17,500
3	0.18	0.36	0.18	0	0.1	1.46	0.090	17,500
4	0.36	0.18	0.18	0	0.1	1.46	0.090	17,500
5	0.18	0.18	0.36	0	0.2	1.62	0.081	38,900
6	0.18	0.18	0.36	45	0.2	1.62	0.081	38,900
7	0.18	0.18	0.54	0	0.3	1.70	0.078	61,000
8	0.18	0.18	0.18	0	0.1	2.92	0.045	35,000
9	0.18	0.18	0..18	22.5	0.1	1.46	0.090	17,500

[a] L = length, W = width, H = height.

[b] θ = building orientation to wind, H/δ = ratio of building height to boundary layer height, U_H = mean wind speed at building height, w/U_H = ratio of effluent velocity to local velocity, Re = Reynolds number.

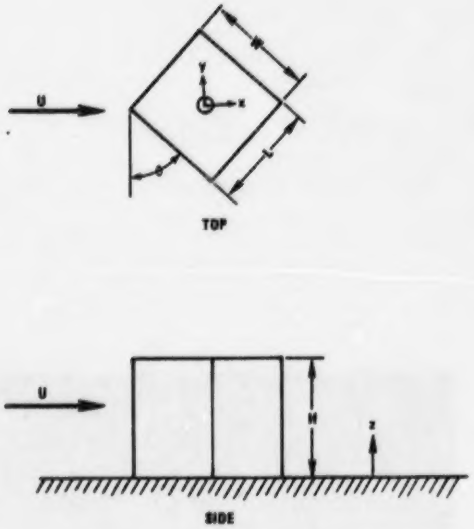

Figure 1. Top and side views of building model.

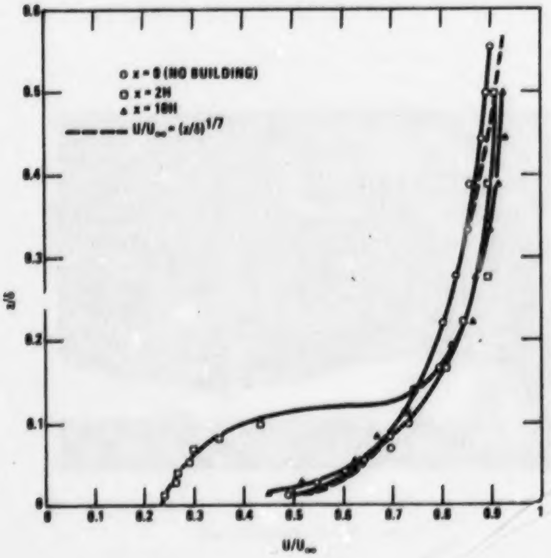

Figure 2. Mean velocity profiles at location of cubical model without model in position (x = 0) and downwind of the model (x = 2H, 10H).

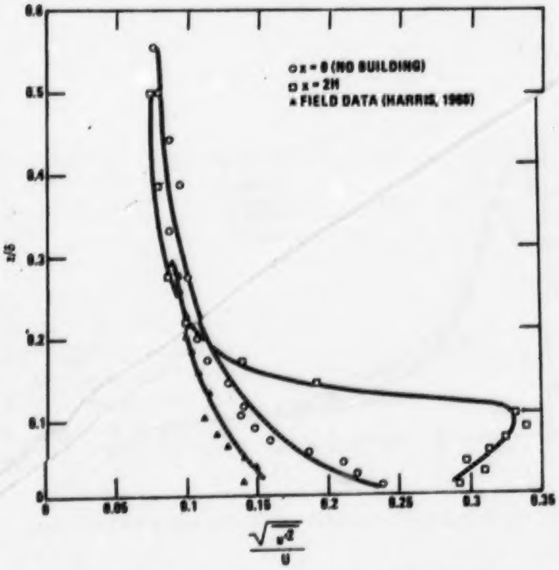

Figure 3. Local turbulence intensity at location of cubical model without model in position (x = 0) and downwind of the model (x = 2H).

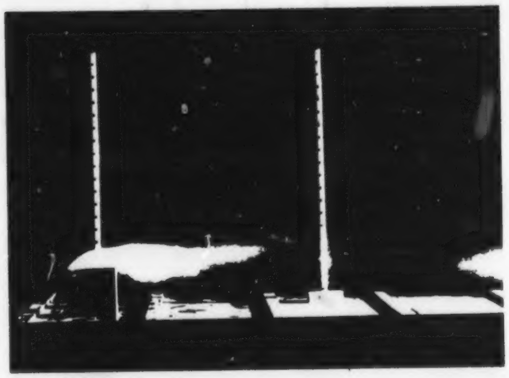

Figure 4. Flow visualization of Case 1.

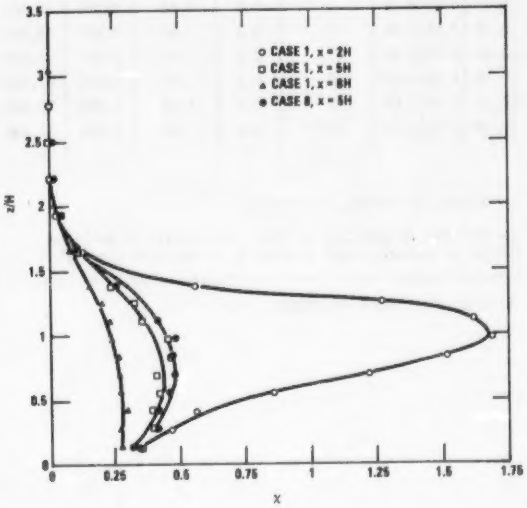

Figure 5. Vertical concentration profiles for Cases 1 and 8. (y = 0.)

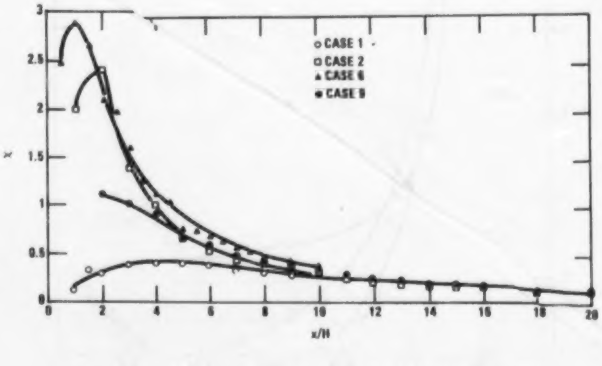

Figure 6. Ground-level concentrations for Cases 1, 2, 6, and 9. (y = 0; z = 0.025 m.)

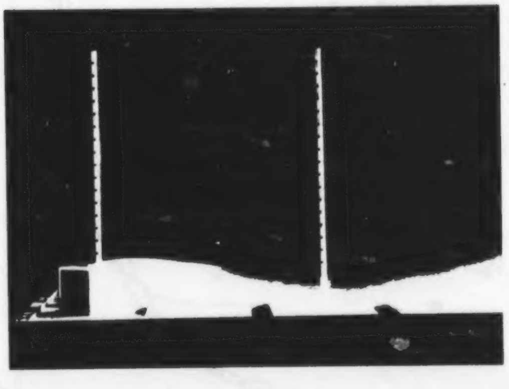

Figure 7. Flow visualization of Case 2.

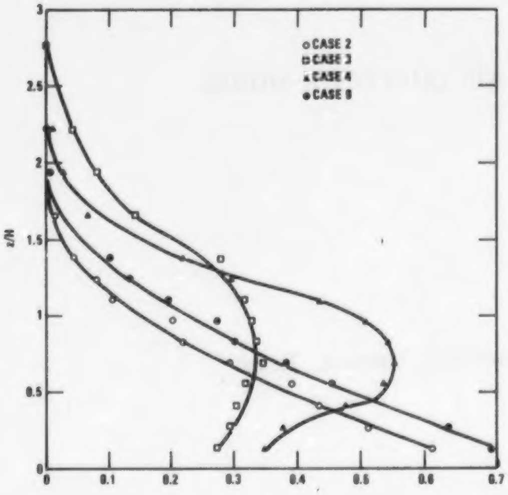

Figure 8. Vertical concentration profiles for Cases 2, 3, 4, and 9 at x = 5H (x = 0.09 m.)

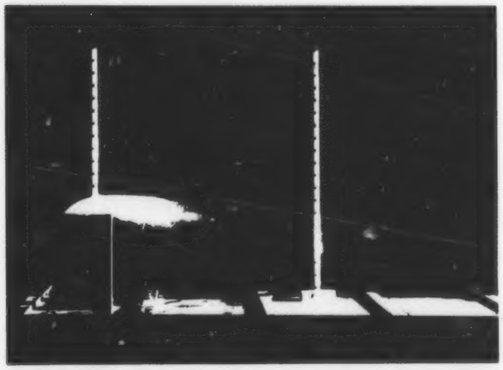

Figure 10. Flow visualization of Case 5.

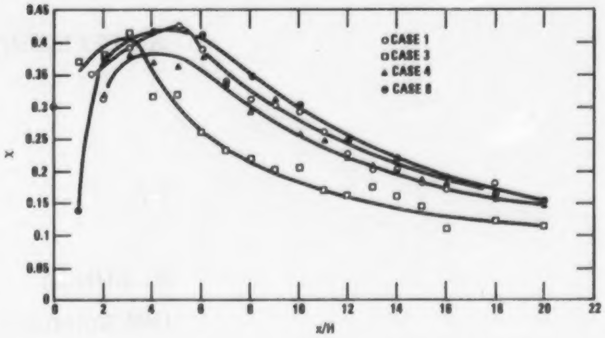

Figure 9. Ground-level concentrations for Cases 1, 3, 4, and 8. (y = 0; z = 0.025 m.)

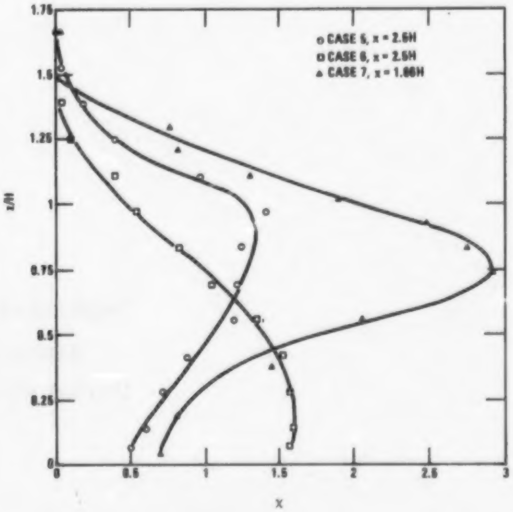

Figure 11. Vertical concentration profiles for Cases 5, 6, and 7. (x = 0.9 m.)

7th International Technical Meeting
on Air Pollution Modeling and its Application

AN EFFICIENT AIR QUALITY K-MODEL

by

E. RUNCA
IBM Scientific Center, Venice, Italy

September 7-10, 1976
Airlie Virginia
United States of America

AN EFFICIENT AIR QUALITY K-MODEL

by E.RUNCA - IBM Italy - Venice Scientific Center

Abstract

An air quality model based on the numerical integration of the time dependent tridimensional convection diffusion equation, written according to the k-theory, is developed. The finite difference scheme proposed for the integration of the model equation is based on the method of fractional steps. The convection and diffusion steps are treated with Carlson's and Crank-Nicolson's scheme respectively. This algorithm, which is unconditionally stable, shows a great flexibility. Furthermore, a numerical investigation on the two-dimensional case describing horizontal advection and vertical diffusion of an atmospheric pollutant downwind from a line-source has proved that the proposed scheme, although of first order accuracy, is in practice substantially more accurate than other difference schemes of first and second order, to which it was compared. A new method has been developed for computing accurately the concentration distribution close to the sources without being forced to place the source ina grid point. The sensitivity of the model to variations of emission height, wind field, diffusion coefficients and of inversion layer height is analyzed in detail.

Introduction

The control of air quality requires the definition of a model which relates the concentrations of air pollutants to the rate of emissions as well as to the meteorological conditions and local effects due to the geography of the area and the position of the sources. The models can be divided into three categories:

- Gaussian models
- Stochastic models
- K-models

The Gaussian models are based on a semiempirical formulation that Sutton (24) proposed by developing Taylor's statistical concepts. Even if this formulation has strong limitations it proved satisfactory (4), (8), (12), (17), (20), (25) for some applications and mainly for the simulation of long term average concentration.

The stochastic models avoid the problems related to the description of the turbulent diffusion in the atmospheric boundary layer as well as the problems related to the inventory of the emissions. They depend on the availability of historical series of air pollutant concentrations and meteorological data. Since only in the last few years measurements of air pollutants concentrations and meteorological data have been taken extensively these models have not yet been fully investigated. Larsen's (11) pioneering work and the more recent applications (5) seem very promising, showing that stochastic models might provide a valid tool for the prediction of air quality trends both on a short and a long term basis.

Gaussian and stochastic models meet most of the users' needs but they give a poor analysis of the influence of the spatial and temporal variation of the parameters affecting dispersion on the air pollutants concentration.

The K-models (14), (22), (23), which are based on the numerical integration of the diffusion convection equation, provide some results in this direction. The use of a K-model requires generally a consistent amount of computer time and memory, in addition to a tridimensional representation of the wind field and the dispersion coefficients so that its implementation is not an easy task. The application field of a k-model deserves some consideration.

It is obvious that the use of a k-model as a tool for the forecast in real time of an alert situation is still quite expensive and too little rewarding, as the validity of the results given by the model depends greatly upon the exactness of the input data which should consist of the prediction of the local meteorological situation and emission rates. Therefore a k-model must be seen mainly as a tool for analyzing the problem. From this point of view its use can be very rewarding as it can identify better than the previous models the influence of meteorological factors and local effects on the pollution pattern.Thus, it can be applied to investigate to a high degree of detail the impact of new sources, which is a main problem in developing new areas.

In addition to the above mentioned difficulties, setting up a k-model requires the definition of an algorithm for the numerical integration of the diffusion convection equation. Next chapters will describe a numerical scheme which has been devised for an efficient and correct treatment of advection and diffusion of air pollutants.

Equation and numerical scheme

Under the assumption that the flow is non-divergent and that molecular diffusion is negligible if compared with turbulent diffusion, the atmospheric convection diffusion equation can be written:

$$\frac{\partial c}{\partial t} + u\frac{\partial c}{\partial x} + v\frac{\partial c}{\partial y} + w\frac{\partial c}{\partial z} = \frac{\partial}{\partial x}\left(K_x\frac{\partial c}{\partial x}\right) + \frac{\partial}{\partial y}\left(K_y\frac{\partial c}{\partial y}\right) + \frac{\partial}{\partial z}\left(K_z\frac{\partial c}{\partial z}\right) \qquad (1)$$

where C is the average concentration, u, v, and w are the average wind components along the x, y and z directions respectively, and k_x, k_y and k_z represent the eddy diffusion coefficients.

Concentration and velocity in equation (1) are considered as averaged over a time interval which is large if compared with the dominant time scale of turbulent fluctuations, but small in comparison to the time scale for variation in the mean concentration.

Since analytic solutions of equation (1) are not known for arbitrary function of wind speed and diffusion coefficients, numerical techniques have been used to solve equation (1).

According to equation (1), the concentration of an air particle changes as it is advected along a wind trajectory as a result of the action of a diffusion process described by the right-hand terms. It is well known that solving the advection part of equation (1) with a conventional finite difference scheme leads to the introduction of large numerical diffusion errors which can be of the same order of magnitude as the calculated quantity (3), (16). This pseudo diffusion originates since the air particles are not moved correctly along the wind trajectories (i.e. the travel distance per time step is not equal to the mesh spacing) so that the pollutant is spread numerically upwind and downwind of its real location. In order to limit such a pseudo-diffusion, considerable efforts have been made in the last few years to develop new techniques. Egan and Mahoney (7) proposed a method which involves the zeroth, first and second moment of the concentration distribution within each grid element. Mixed Eulerian Lagrangian schemes have also been proposed as the particle in cell method (23), (10), which can be also referred as the MOC (Method of Characteristics) (9), and the method devised by Runca and Sardei (18). Lately some scientists have shown the convenience of treating advection and diffusion of air pollutants by Galerkin Technique (6), (13).

Yet, the methods above recalled present some unsatisfactory features, which depending on the method, are the constraint of the stability condition and/or a high complexity in programming. Therefore it was looked for a numerical scheme free from the constraint of the stability condition, simple as to programming and requiring a limited amount of computer time and memory.

The above goals are met by the scheme described below and presented in a previous paper by Sardei and Runca (19). This scheme is based on the method of fractional steps which has been widely used to integrate atmospheric diffusion convection equation (2), (22).

Recently it has been shown(19) that by virtue of the sequential treatment of convection and diffusion by the fractional step procedure the difference operator for the diffusion is made to conform closely to the path of the air particle trajectories.

For sake of simplicity the proposed algorithm will be discussed for the two dimensional case of equation (1) which is assumed (1), (18), (21) to describe pollutant diffusion downwind from a line source. In the case of diffusion downwind from a line source and with sufficiently high wind velocity, equation (1) is reduced to:

$$\frac{\partial c}{\partial t} + u(z)\frac{\partial c}{\partial x} = \frac{\partial}{\partial z}\left(K_z(z)\frac{\partial c}{\partial z}\right) \tag{2}$$

with the following typical initial and boundary conditions:

$$c(x,z,0) = 0 \tag{3}$$

$$c(0,z,t) = \frac{Q}{u(h)}\,\delta(z-h), \quad t>0 \tag{4}$$

$$K_z\frac{\partial c}{\partial z} = 0 \qquad z=0,\,H \tag{5}$$

where h and H are the elevation of the source and the inversion layer base respectively, Q is the emission rate and S is the Dirac's-function. Moreover it is assumed that wind and vertical k coefficient depend only on z. The relation (5) implies the assumption that both ground and inversion layer base fully reflect the diffusing material.

Fractional step procedure

According to the method of fractional steps, the concentration field at the time t +Δ t is obtained from that at the time t by separating the contribution due to advection and diffusion terms of equation (2) as follows:

In the first step the advection equation:

$$\frac{\partial c}{\partial t} + u(z)\frac{\partial c}{\partial x} = 0 \tag{6}$$

is solved in the whole x-z integration region over the time interval Δ t with the concentration field at the time t as initial condition and the relation (4) as boundary condition.

The diffusion equation:

$$\frac{\partial c}{\partial t} = \frac{\partial}{\partial z}\left(K_z(z)\frac{\partial c}{\partial z}\right) \tag{7}$$

is solved in the second step over the same time interval. Here the initial condition is provided by the concentration field obtained from the first step and the boundary by the relation (5). The solution of (7) is an approximation of the concentration field at the time t +Δt.

It is well known that the truncation error associated with the upwind finite difference approximation reduces to zero for $u\Delta t = \Delta x$. Since the stability condition requires $u\Delta t \leqslant \Delta x$ the truncation error can be reduced to zero only where u is maximum. It is obvious that truncation errors should be zero at least at source height where the largest concentration gradients occur.

A solution to this problem is provided by the method described by Carlson ([15]) which is illustrated in Fig.1.

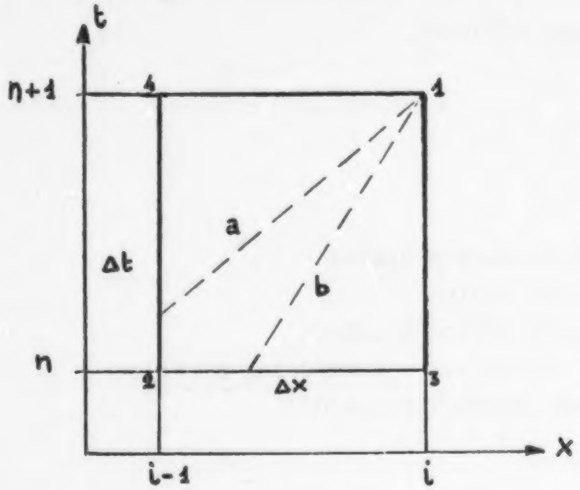

Fig.1 Grid element in the (x,t) plane to illustrate Carlson's scheme. The dashed lines are trajectories corresponding to $u\Delta t/\Delta x \geqslant 1$ (a) and $u\Delta t/\Delta x \leqslant 1$ (b).

According to Carlson's scheme the approximation to equation (6) is:

$$C_i^{n+1} = C_i^n - \frac{u\Delta t}{\Delta x}\left(C_i^n - C_{i-1}^n\right) \quad \text{for} \quad \frac{u\Delta t}{\Delta x} \leqslant 1 \tag{8}$$

$$C_i^{n+1} = C_{i-1}^{n+1} - \frac{\Delta x}{u\Delta t}\left(C_{i-1}^{n+1} - C_{i-1}^n\right) \quad \text{for} \quad \frac{u\Delta t}{\Delta x} \geqslant 1 \tag{9}$$

The use of equation (9) in place of equation (8) for $u\Delta t \geqslant \Delta x$ makes the Carlson's scheme unconditionally stable and allows the reduction to zero of the truncation error at source height by choosing

$$\Delta x = u(h)\,\Delta t \tag{10}$$

Numerical approximation to equation (7) with the method devised by Crank Nicolson [15], leads finally to the following algorithm:

Advection step

$$C^{*}_{i,k} = C^{n}_{i,k} - \frac{u_k \Delta t}{\Delta x}\left(C^{n}_{i,k} - C^{n}_{i-1,k}\right) \qquad \text{for } \frac{u_k \Delta t}{\Delta x} \leqslant 1 \tag{11}$$

$$C^{*}_{i,k} = C^{*}_{i-1,k} - \frac{\Delta x}{u_k \Delta t}\left(C^{*}_{i-1,k} - C^{n}_{i-1,k}\right) \qquad \text{for } \frac{u_k \Delta t}{\Delta x} \geqslant 1 \tag{12}$$

Diffusion step

$$C^{n+1}_{i,k} = C^{*}_{i,k} + \frac{1}{2}\left(D_z\left[C^{n+1}_{i,k}\right] + D_z\left[C^{*}_{i,k}\right]\right) \tag{13}$$

where:

$$D_z\left[C_{i,k}\right] = \frac{\Delta t}{\Delta Z^2}\left[K_{k+1/2}\,C_{i,k+1} - \left(K_{k+1/2} + K_{k-1/2}\right)C_{i,k} + K_{k-1/2}\,C_{i,k-1}\right] \tag{14}$$

is the standard difference operator for centered diffusion.

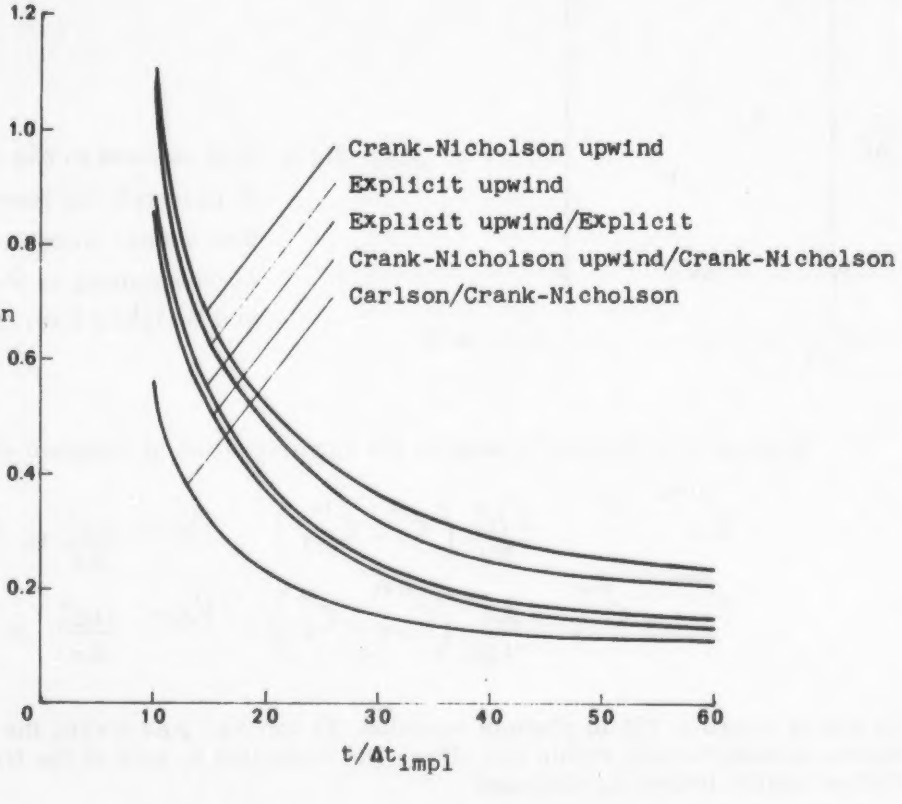

Fig.2 **Time evolution of the root mean square errors ε_{mean} as reported in ref. [19]. ε_{mean} is normalized to the average concentration of the reference solution.**

The accuracy of the proposed scheme was tested by comparison, jointly to four other schemes of first or second order, with a reference solution in the paper by Sardei and Runca (19) from which the plots of Fig.2 are taken. The reference solution was obtained with a standard finite difference scheme second order in time by using an extremely fine grid and a very small interval. The plots show the root mean square deviation of the concentration from the corresponding values of the reference solution for the tested schemes.

The good results achieved by the application of equations (11)-(14) depend in addition to the reduction of the truncation error at source location, upon the method of fractional steps.
This appears from the following considerations.

For $u_k \Delta t = \Delta x$ equations (11)-(14) give:

$$C^{n+1}_{i,k} = C^{n}_{i-1,k} + \frac{1}{2}\left(D_z\left[C^{n+1}_{i,k}\right] + D_z\left[C^{n}_{i-1,k}\right]\right) \qquad (15)$$

whereas the corresponding approximation to equation (2) by the direct scheme (i.e. the scheme obtained by using the same finite difference operators but without splitting) is:

$$C^{n+1}_{i,k} = C^{n}_{i-1,k} + \frac{1}{2}\left(D_z\left[C^{n+1}_{i,k}\right] + D_z\left[C^{n}_{i,k}\right]\right) \qquad (16)$$

The comparison of equation (15) with equation (16) shows that the latter approximates the diffusion operator (see Fig.1) along x = const and the former along the trajectory segment $\Delta x = u_k \Delta t$. By virtue of relation (10) equation (15) holds at source height, so that the transport as well as diffusion are properly described in the region of maximum concentration gradient.

In addition to the previous consideration it should be noted that the Carlson Crank Nicolson scheme calculates the new concentration values by utilizing the three "most relevant" points of the mesh, i.e. points (see Fig.1) 1,2,3 or 1,2,4 depending on whether the trajectory through point 1 intersects Δx or Δt.

In the tridimensional case the benefits which derive from the fractional steps procedure are enhanced. In fact, as the procedure requires inversion of much smaller matrices, a substantial saving in computer time is obtained as well as a simplification in programming the computer code.

Examples of the fractional step method applied to the numerical solution of the time dependent three dimensional atmospheric diffusion convection equation are provided by Shir and Shieh (22) and Bankoff and Hanzevack (2). They both use an implicit formulation for the vertical terms of equation (1) in order to allow for a variability of the vertical grid spacing, while the remaining terms are solved by an explicit formulation so that the time step and the horizontal grid spacing must respect the stability condition. The extension of the Carlson/Crank Nicolson scheme to the three dimensional case eliminates the constraints of the stability condition, thus allowing a great flexibility in the design of the mesh and in the choice of the time step.

As in the vertical the advection is usually negligible compared to diffusion owing to the small vertical component of the wind velocity and assuming that the horizontal diffusion coefficients are constant , equation (1) can be written:

$$\frac{\partial c}{\partial t} + u\frac{\partial c}{\partial x} + v\frac{\partial c}{\partial y} = K_x\frac{\partial^2 c}{\partial x^2} + K_y\frac{\partial^2 c}{\partial y^2} + \frac{\partial}{\partial z}\left(K_z\frac{\partial c}{\partial z}\right) \tag{17}$$

The extension of the algorithm represented by the relations (11)-(14) to equation (17) is straigthforward and leads to the following sets of finite difference equations:

$$\overset{*}{C}_{ijk} = \overset{n}{C}_{ijk} - \frac{u_{ijk}\Delta t}{\Delta x}\left(\overset{n}{C}_{ijk} - \overset{n}{C}_{i-1jk}\right) \qquad \text{for } \frac{u_{ijk}\Delta t}{\Delta x} \leqslant 1 \tag{18}$$

$$\overset{*}{C}_{ijk} = \overset{*}{C}_{i-1,jk} - \frac{\Delta x}{u_{ijk}\Delta t}\left(\overset{*}{C}_{i-1,jk} - \overset{n}{C}_{i-1,jk}\right) \qquad \text{for } \frac{u_{ijk}\Delta t}{\Delta x} \geqslant 1 \tag{19}$$

$$\overset{**}{C}_{ijk} = \overset{*}{C}_{ijk} - \frac{v_{ijk}\Delta t}{\Delta y}\left(\overset{*}{C}_{ijk} - \overset{*}{C}_{ij-1k}\right) \qquad \text{for } \frac{v_{ijk}\Delta t}{\Delta y} \leqslant 1 \tag{20}$$

$$\overset{**}{C}_{ijk} = \overset{**}{C}_{ij-1,k} - \frac{\Delta y}{v_{ijk}\Delta t}\left(\overset{**}{C}_{ij-1,k} - \overset{*}{C}_{ij-1k}\right) \qquad \text{for } \frac{v_{ijk}\Delta t}{\Delta y} \geqslant 1 \tag{21}$$

$$\overset{***}{C}_{ijk} = \overset{**}{C}_{ijk} + \frac{1}{2}\left(D_x\left[\overset{**}{C}_{ijk}\right] + D_x\left[\overset{***}{C}_{ijk}\right]\right) \tag{22}$$

$$\overset{****}{C}_{ijk} = \overset{***}{C}_{ijk} + \frac{1}{2}\left(D_y\left[\overset{***}{C}_{ijk}\right] + D_y\left[\overset{****}{C}_{ijk}\right]\right) \tag{23}$$

$$\overset{n+1}{C}_{ijk} = \overset{****}{C}_{ijk} + \frac{1}{2}\left(D_z\left[\overset{****}{C}_{ijk}\right] + D_z\left[\overset{n+1}{C}_{ijk}\right]\right) \tag{24}$$

where D_x , D_y and D_z are the standard difference operator for centered diffusion as defined by relation (14) .

Point source model

The application of the numerical scheme described by equations (18) - (24) requires the definition of the initial and boundary conditions which, under the assumption that the lateral grid boundaries are located at a considerable distance from the source, can be written:

$$C(x,y,z,0) = 0 \qquad (25)$$

$$C(x,y,z,t) = 0 \qquad x=0, x_{max};\ y=0, y_{max} \qquad (26)$$

$$K_z \frac{\partial c}{\partial z} = 0 \qquad z=0, H \qquad (27)$$

$$\int_{S_R} \vec{V} \times C \vec{ds} = Q \qquad R \to 0,\ t>0 \qquad (28)$$

where S_r is the surface of the sphere of radius R centered at the source location (x_s, y_s, z_s).

The numerical treatment of condition (28) and the problems connected with the approximation of the Dirac's function are discussed in a paper to be published by Runca and Sardei. Below it is only outlined how the method which has been devised allows a correct solution close to the source, which, moreover can be located anywhere within the grid without the restriction of being coincident with a grid point.

Under the hypothesis of linearity and assuming for semplicity, that the emission rate is constant the concentration field at a certain instant of time $T = n\Delta t$ can be approximated by the superposition of the contributions due to n puffs of intensity $Q\Delta t$ released at the instants $0, \Delta t, 2\Delta t, \ldots\ldots (n-1)\Delta t$.

The numerical calculation of the contribution of a puff at the time Δt after being released is a very delicate matter as the concentration gradient tends to infinity at the source location. This problem has been usually overcome by assuming that the puff distributes instantaneously and uniformly within a cell volume. The numerical errors introduced by this arbitrary approximation can result very large close to the source, thus causing a distortion of the concentration field which may mask completely the real behaviour of the phenomenon. A correct treatment of the problem has been devised as follows.

Let's first examine the case of an integration time step so small that the dispersion of the puff can be considered affected, during its first interval of life Δt, only by the values assumed by the wind and the diffusion coefficients at the source location. In this case the distribution of a puff at time Δt after its release can be approximated by the equation[24]:

$$C_{\Delta t}(x,y,z,\Delta t) = \frac{Q\Delta t}{8(\pi\Delta t)^{3/2}(K_{x_s}K_{y_s}K_{z_s})^{1/2}} \exp\left\{-\frac{(x-u\Delta t-x_s)^2}{4K_{x_s}\Delta t} - \frac{(y-v\Delta t-y_s)^2}{4K_{y_s}\Delta t} - \frac{(z-z_s)^2}{4K_{z_s}\Delta t}\right\} \qquad (29)$$

Therefore, the values provided by equation (29) at the grid points are a correct approximation of the contribution given to the concentration field by a puff during its first interval of life Δt.
In order to verify the condition

$$\iiint C_{\Delta t}\, dx dy dz = Q \Delta t \tag{30}$$

which expresses the conservation of the mass emitted in the region, the values computed by equation (29) must be normalized after being multiplied by $Q\Delta t$ to the value

$$\sum_{ijk} \left(C_{ijk}\right)_{\Delta t} \Delta x_i \Delta y_i \Delta z_k \tag{31}$$

In practice under the hypothesis of a sufficiently small time step, the numerical integration proceeds as follows:

$t = \Delta t$ the concentration field $C_{\Delta t}$ is provided by the normalized values of equation (29)

$t = 2\Delta t$ the concentration field $C_{\Delta t}$ is assumed as initial condition and it is transformed according to the set of equations (18)-(24), thus obtaining $C'_{2\Delta t}$. Finally $C_{2\Delta t}$ is computed by the relation: $C_{2\Delta t} = C'_{2\Delta t} + C_{\Delta t}$

" " "

$t = n\Delta t$ proceeding as above it is obtained $C_{n\Delta t} = C'_{n\Delta t} + C_{\Delta t}$

It should be noted that $C_{\Delta t}$ is constant only under the hypothesis that emission rate, wind field and dispersion coefficients are constant. Generally it has to be recalculated at every time step.

For a time step not sufficiently small $C_{\Delta t}$ cannot be computed by equation (29), as the puff dispersion is affected by the wind and dispersion coefficients distribution. Nevertheless, as the puff in its first interval of life distributes in a limited region around the source, $C_{\Delta t}$ can be equally computed with accuracy by defining a smaller time step submultiple of the original time step, i.e. $\Delta\tau = \Delta t/m$ and by reducing proportionally the original grid dimensions so that the region close to the source is described very accurately. As $\Delta\tau$ can now be assumed sufficiently small, equation (29) is used to estimate the normalized $C_{\Delta\tau}$ (after noting that the puff intensity is $Q\Delta t$). Then the concentration field $C_{\Delta\tau}$ is transformed by applying (m-1) times the set of equations (18)-(24). The obtained concentration distribution is a correct approximation of the contribution given by a puff during its first interval of life Δt. As it has been computed on the grid compressed on the source, only the concentration values which correspond to the original location of the grid points can be considered and used to approximate $C_{\Delta t}$.

These values after being multiplied by $Q\Delta t$ must be normalized, as previously done to the quantity expressed by relation (31) in order to assure the conservation of mass. From here on the numerical integration proceeds as described in the case of a small Δt. It is obvious that the use of a larger time step is convenient if the emission rate, wind and diffusion coefficients have a time scale variation which is large with respect to the integration time step.

In Fig.3 the concentration profile at ground level and in the vertical (one Km far from the source) are shown as computed by the proposed method and the method which assumes an instantaneous and uniform diffusion in a cell volume. As indicated by the figure the latter approximation introduces errors which reduce far from the source (see profile at ground level) but distort the vertical distribution, thus making problematic the use of the model for a tridimensional analysis of the pollutant distribution. The correct shape of the vertical profile, even in a region very close to the source, is simulated correctly by the proposed method.

For the plots of Fig. 3 as well as for the remaining ones, which will be shown, the wind and vertical diffusion coefficient have been expressed by the laws:

$$u = u_R \left(\frac{z}{z_R}\right)^{\alpha} \tag{32}$$

$$K_z = K_{z_R}\left(\frac{z}{z_R}\right)^{1-\alpha} \tag{33}$$

In addition to that, for all the computations, Δt was chosen according to the relation:

$$\Delta t = \frac{\Delta x}{u(z_s)} \tag{34}$$

All the plots represent steady state solutions obtained by using an integration time substep $\Delta\tau = \Delta t/4$; only in Fig. 4 the dashed lines were obtained by computing $C_{\Delta t}$ directly by equation (29). Finally all the values, if not differently indicated, are expressed in units of the international metric system.

Concentration profiles at ground level are plotted in Fig.4 for the case of $C_{\Delta t}$ estimated directly by equation (29) and $C_{\Delta t}$ estimated by integrating over the time interval Δt with a substep $\Delta\tau = \Delta t/4$. As a consequence of the variation with height of K_z expressed by equation (33), the former approximation causes a too rapid dispersion of the pollutant to the ground.

In order to test the sensitivity of the designed algorithm to the variations of the parameters affecting dispersion, many numerical experiments have been performed. Some comprehensive results are shown in Figs.5-7 where ground level concentration profiles are represented after a relaxation time such that the situation can be considered steady.

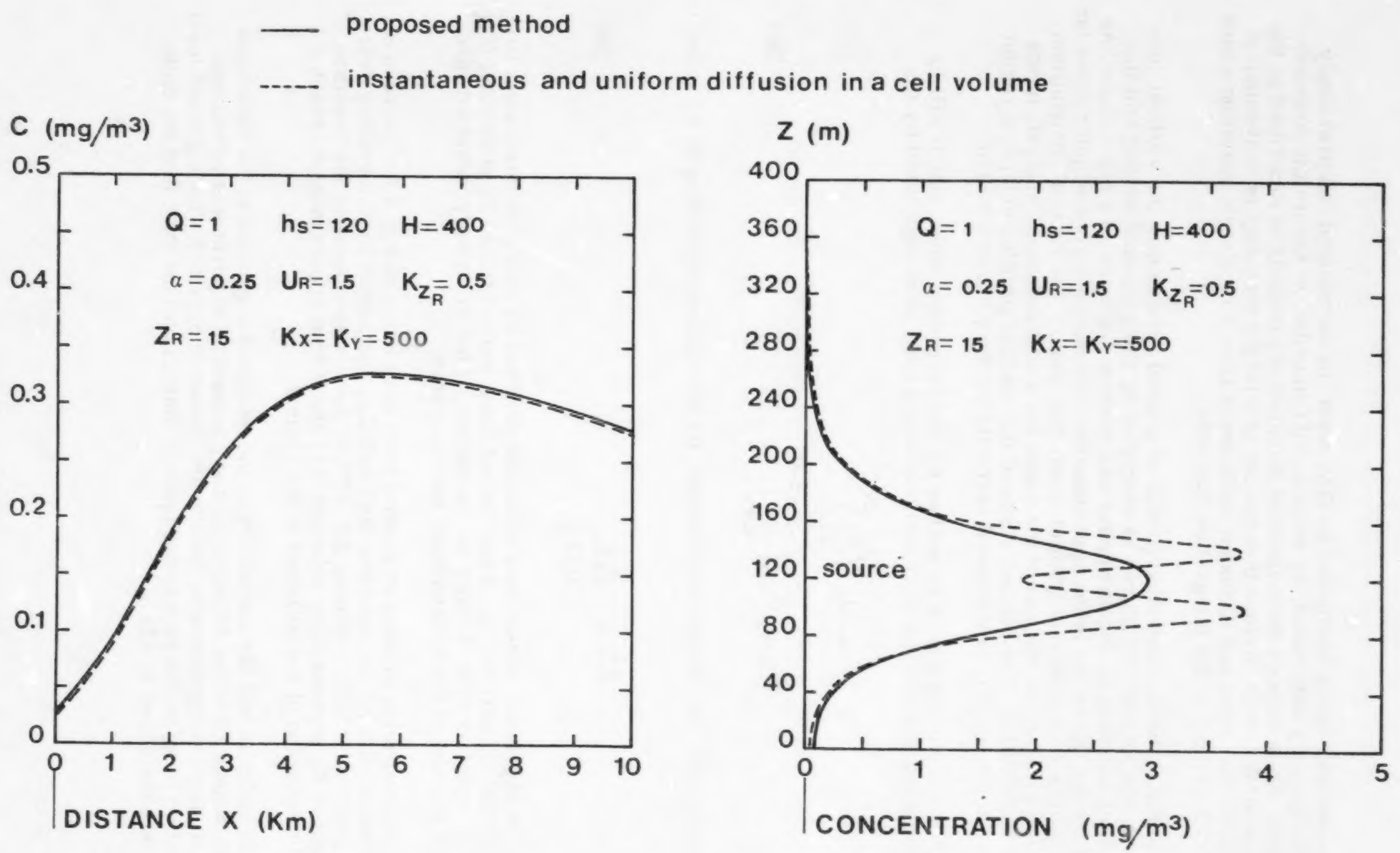

Fig.3 Concentration profiles at ground level (left hand side) and in the vertical one Km far from the source (right hand side) for $\Delta x = \Delta y = 500$ and $\Delta z = 20$.

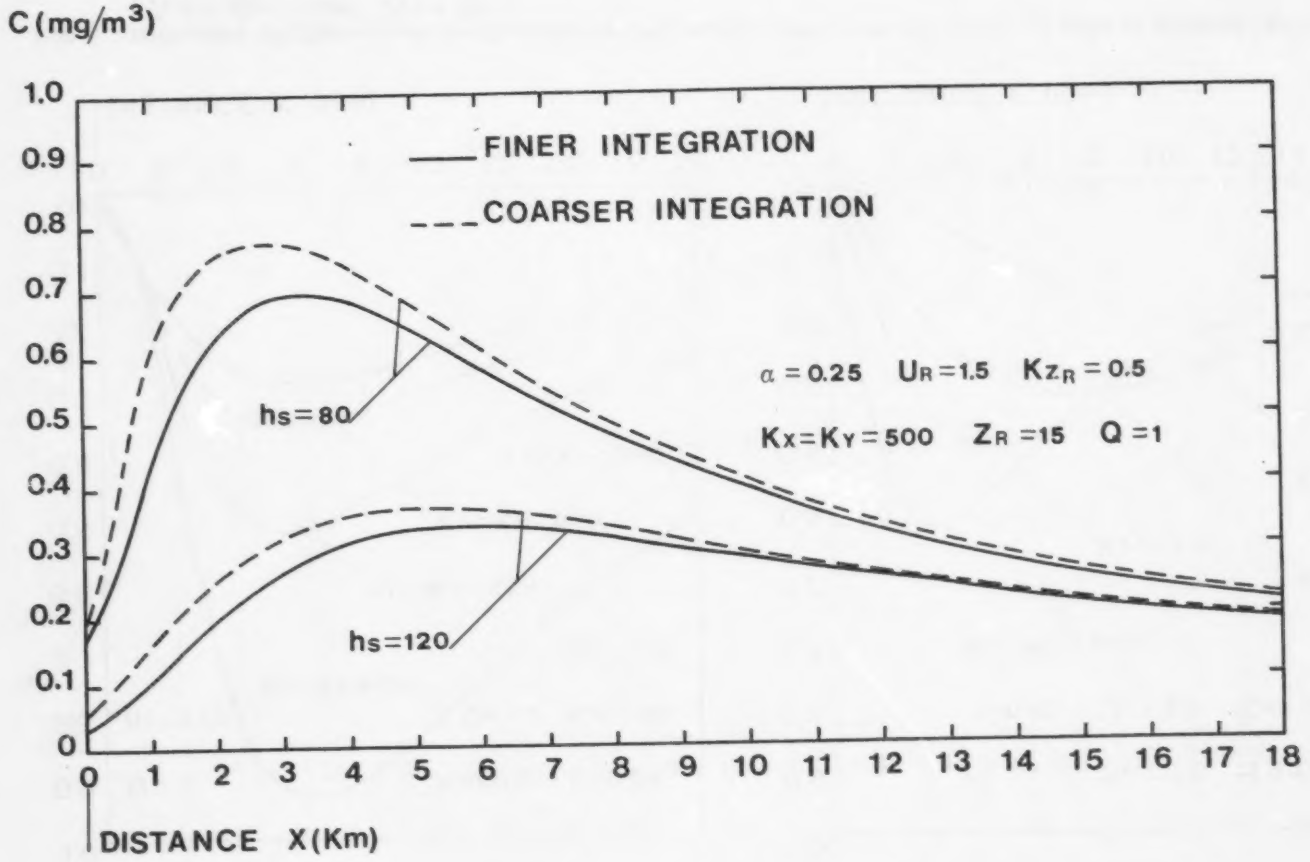

Fig.4 Influence of the approximation of the puff distribution in its first interval of life Δt on the steady state concentration profiles at ground level for two different stack heights. ($\Delta x = \Delta y = 1000$, $\Delta z = 20$).

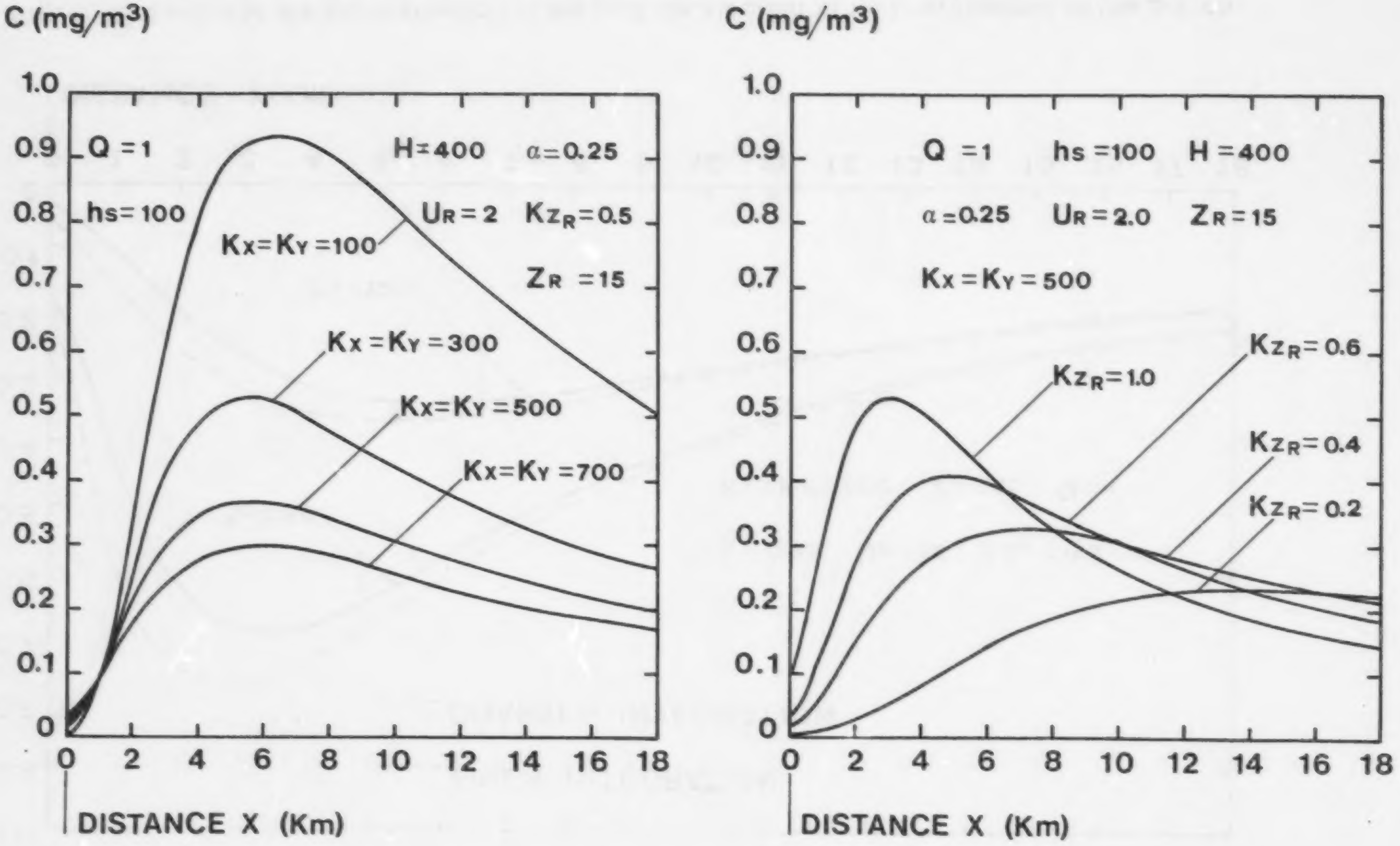

Fig.5 Influence of dispersion coefficients on the steady state concentration profile at ground level ($\Delta x = \Delta y = 1000$, $\Delta z = 20$) .

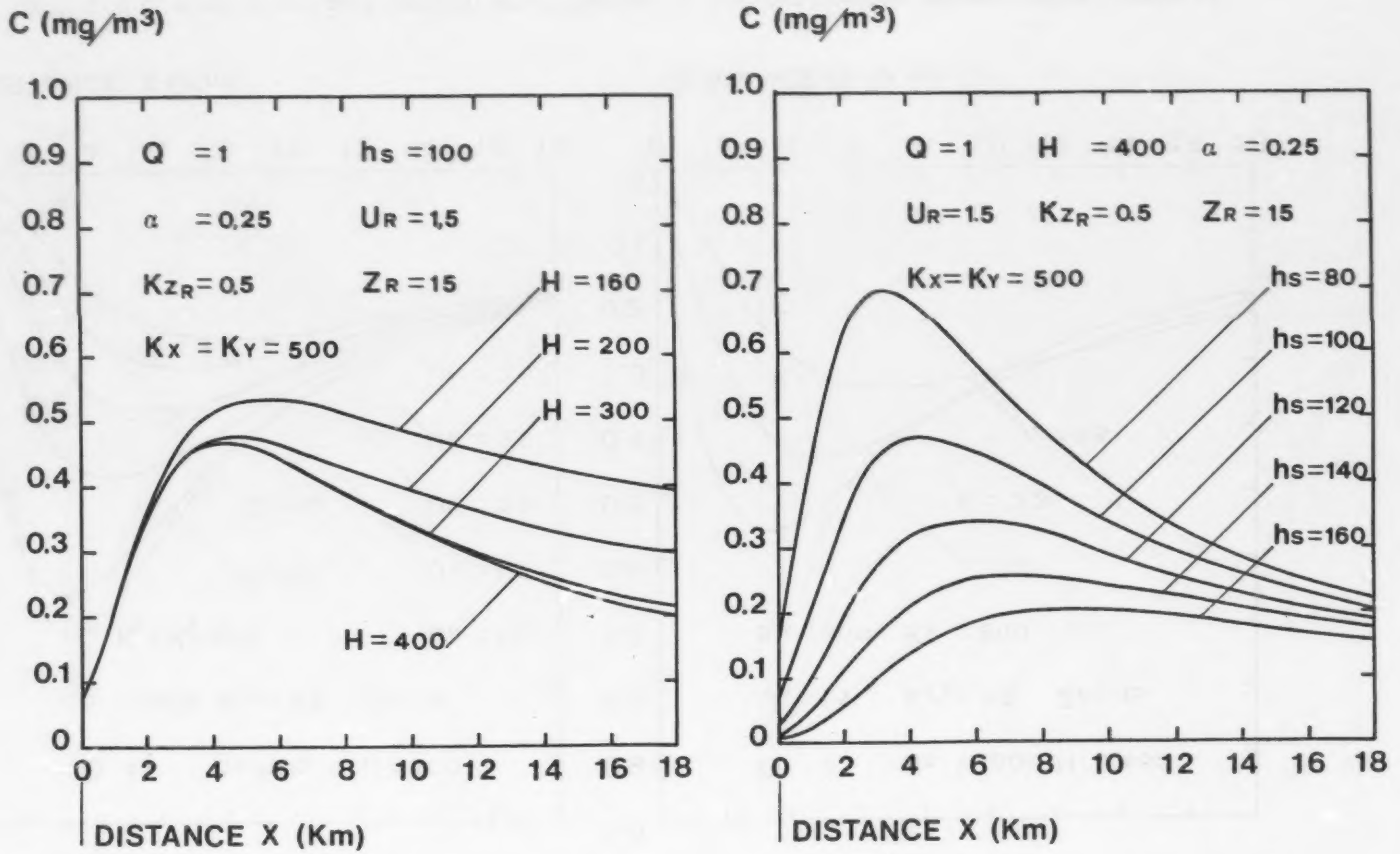

Fig.6 Influence of inversion layer and source heights on the steady state concentration profile at ground level ($\Delta x = \Delta y = 1000$, $\Delta z = 20$) .

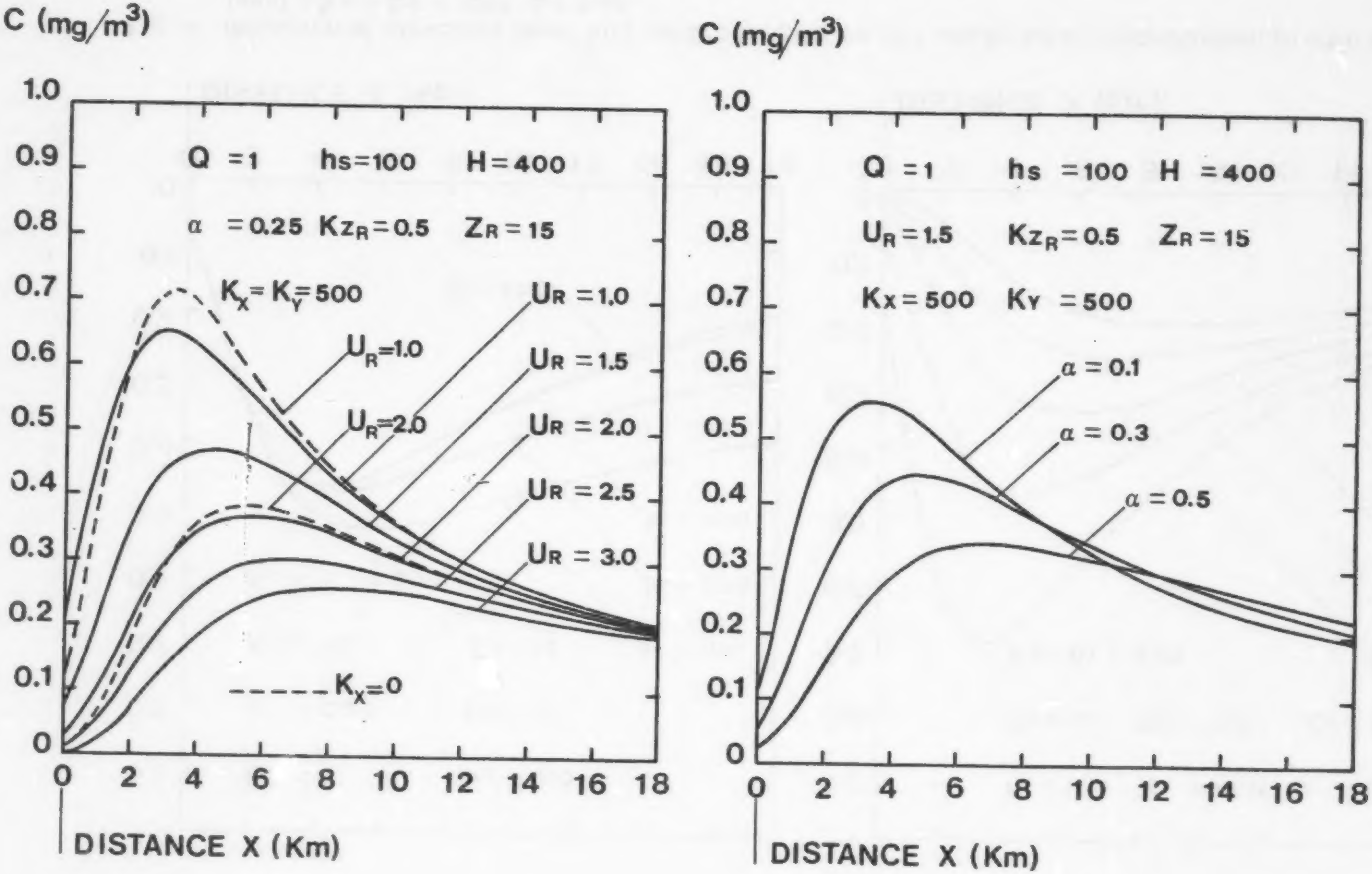

Fig.7 Influence of wind speed and vertical stratification on the steady state concentration profile at ground level ($\Delta x = \Delta y = 1000$, $\Delta z = 20$) .

The plots have been obtained by using a time step which, as defined by relation (34), was ranging from 207s to 622s. The pattern shown by the figures agrees with the physical interpretation which is given so far of the phenomenon.

It is remarkable the small influence of the term representing the horizontal diffusion (see Fig.7) even if the wind speed is lower than 2 m/s at the reference level. In practice such a term can be neglected except that in very low wind speed situations, with a noticeable saving of computer time as the corresponding finite difference equation is not executed. In the same way the finite difference equations corresponding to the transport terms are not executed if the related wind component is zero.

Substantially the implemented algorithm allows to take into account only the terms which contribute to the evolution of the phenomenon.

Multiple point sources model

In addition to the benefits above discussed the proposed algorithm has a fundamental advantage, as for its application the source is not required to be located in a grid point. The misplacement of the source introduces large errors which are illustrated in Figs. 8-9 by comparison of exact numerical solutions (solid line) with the solutions (dashed lines) obtained by moving the source to the closest grid point. The exact numerical solution was computed by placing a grid point in the source location.

The dots describe the numerical solution obtained without moving the source. All the tests performed showed that the solutions computed by the proposed method; i.e. leaving the source in its real location, were practically identical to the corresponding exact numerical solutions. Even if the source was located asymmetrically in the cell the accuracy didn't decrease , as shown in Fig. 9. This result shows, as it could be expected, that the accuracy with which the puff distribution is represented, at the end of its first interval of life, depends only upon the grid spacing and time step, and not upon the source location.

From the above discussion the proposed method proved very appropriate for the case of multiple point sources, as the deformations of the concentration field shown by Figs. 8-9 were eliminated. Unfortunately the method might require too much computer time if the number of point sources were very large, and for every source the puff distribution had to be computed by using a substep $\Delta\tau$. The optimization of the proposed algorithm for the treatment of a very large number of point sources is a problem which the author will investigate under the light of practical applications.

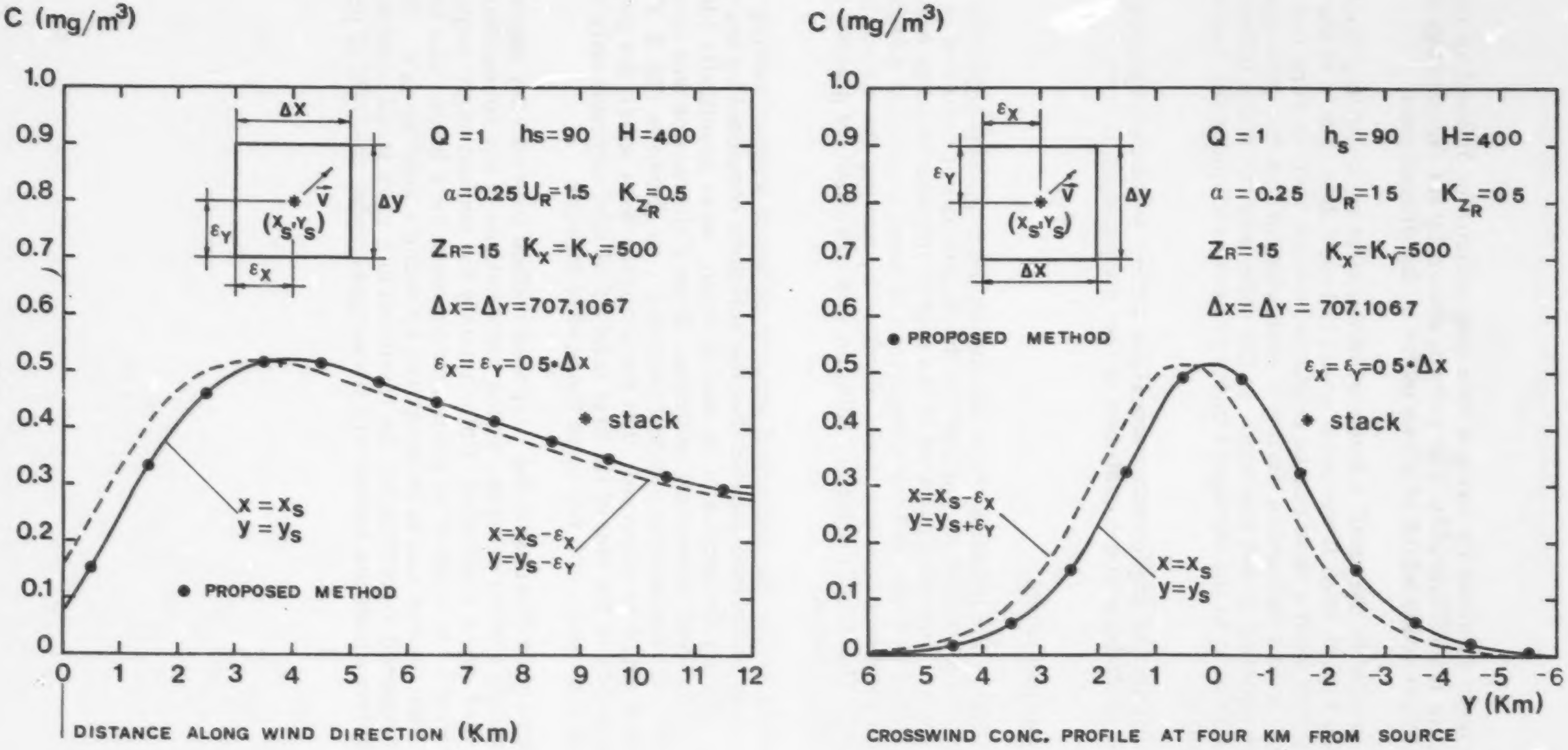

Fig.8 Comparison between the solutions obtained by: a) placing a grid point in the source location (solid line);
b) moving the source to the closest grid point (dashed line);
c) without moving the source from its real location (dots).

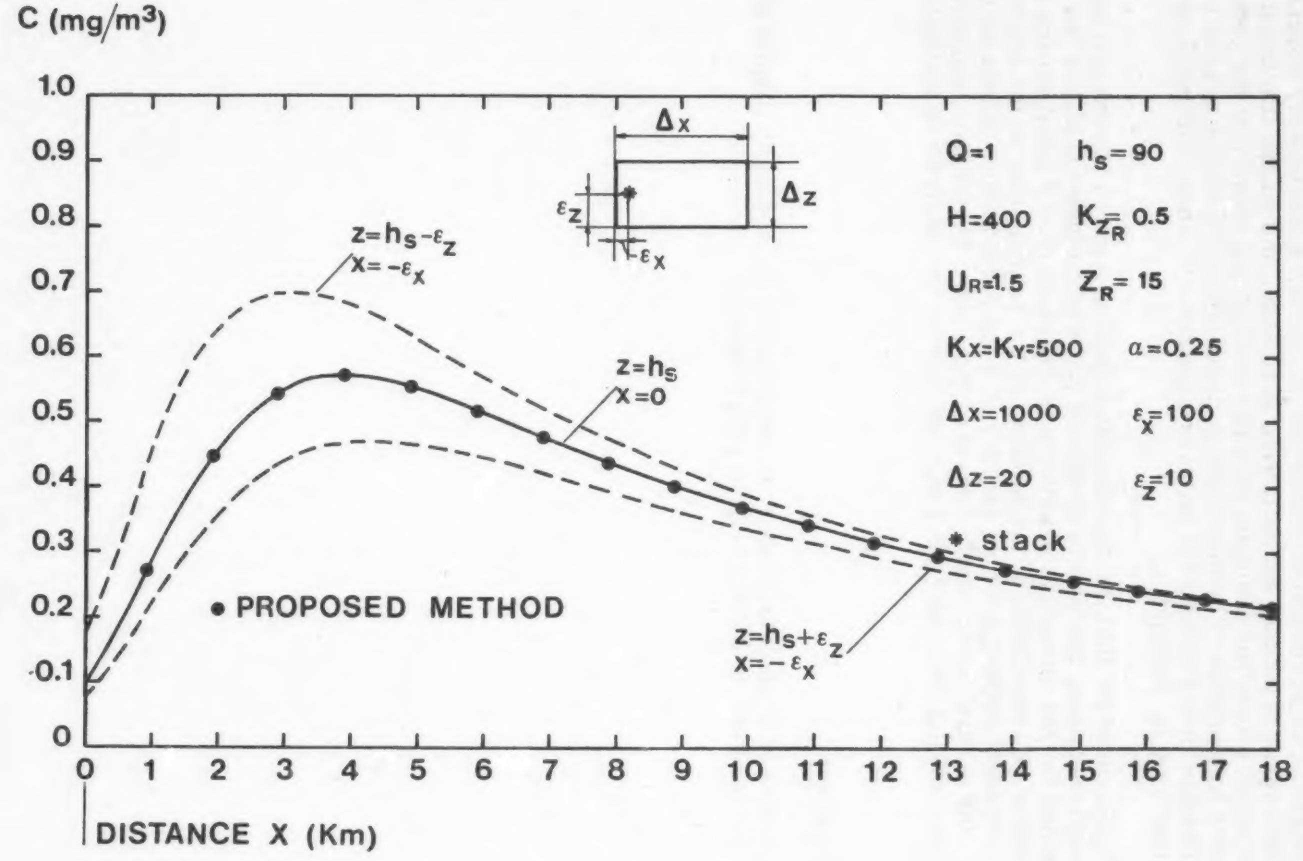

Fig. 9 Same as in Fig. 8 but for misplacement in the vertical .

Conclusions

Carlson's and Crank Nicolson scheme have been combined according to the method of the fractional steps for the treatment of transport and diffusion terms of equation (1) respectively. The good accuracy of the devised scheme depends on the exact Lagrangian advection at source height, which ensures very accurate resolution in the region of largest concentration gradients, and on the fractional step procedure which makes the diffusion operator conforming closely to the path of the air pollutants trajectories. The algorithm is unconditionally stable, easy to be coded and very flexible in overriding the terms of equation (1) whose influence on the concentration field is negligible.

The assumption that the concentration field at a given instant can be computed by superimposing the effects of emitted puffs of intensity $Q\Delta t$ has led to a correct method for the numerical simulation of diffusion from a point source and for an accurate representation of the solution in the region close to the source. Since the proposed method does not require that the point source is located in a grid point, the errors due to misplacement of the source have been completely eliminated, thus making the model very appropriate for the analysis of multiple point sources.

Acknowledgements

The author wishes to thank Francesco Sardei for the many helpful discussions and Sandro Boscolo for his help in programming.

REFERENCES

1 Allen L.H. (1975) Line-source carbon dioxide release. III: Prediction by a two-dimensional numerical diffusion model. Boundary-Layer Meteorology 8, 39-79.

2 Bankoff S.G. and Hanzevack E.L. (1975) The adaptive-filtering transport model for prediction and control of pollutant concentration in an urban airshed. Atmospheric Environment 9, 793-808.

3 Bella D.A. and Grenney W.J. (1970) Finite-difference convection errors J. Sanit.Engin. Division, ASCE, Vol.96,No.SA6, 1361-1375.

4 Calder K.L. (1971) A climatological model for multiple source urban air pollution. Proceedings of the 2ˆ meeting of the expert panel on air pollution modelling - NATO/CCMS, Air Pollution, No.5.

5 Chock D.P., Terrel T.R and Levitt S.B. (1975) Time-series analysis of Riverside, California air quality data. Atmospheric Environment 9,978-989.

6 Christensen O. and Prahm L.P. (1976) A pseudospectral model for dispersion of atmospheric pollutants. I: numerical tests. Report Danish Meteorological Institute, Copenhagen.

7 Egan B.A. and Mahoney J.R. (1972) Numerical modelling of advection and diffusion of urban area source pollutants. J.Appl.Met. 11, 312-322.

8 Fortak H.G. (1970) Numerical simulation of temporal and spatial distributions of urban air pollution concentration. Proceedings of Symposium on multiple source urban diffusion models. Publication No.AP-86, EPA Research Triangle Park, N.Carolina.

9 Garden Jr.A.O., Peaceman D.W. and Pozzi Jr.A.L. (1964) Numerical calculation of multidimensional miscible displacement by the method of characteristics. Society of Petroleum Engineers Journal, March 1964.

10 Lange R. (1973) ADPIC - A three dimensional computer code for the study of pollutant dispersal and deposition under complex conditions. Report UCRL-51462 Lawrence Livermore Laboratory, Ca.

11 Larsen R.I. (1969) A new mathematical model of air pollutant concentration averaging time and frequency. Journal of the Air Pollution Control Association 19(1), 24-30.

12 Martin D.O. (1971) An urban diffusion model for estimating long term average values of air quality - Journal of Air Pollution Control Association 21, 16-19.

13 Melli P. (1976) An application of the Galerkin method to the Eulerian-Lagrangian treatment of time dependent advection and diffusion of air pollutants. Proceedings of the International Conference in Finite Elements for Water Resources, Princeton, July 12-16.

14 Randerson D. (1970) A numerical experiment in simulating the transport of sulfur dioxide through the atmosphere. Atmospheric Environment,4, 615-632.

15 Richtmyer R.D. and Morton K.W. (1967) Difference methods for initial value problems. Interscience, New York.

16 Roberts K.V. and Weiss N.O. (1966) Convective difference schemes. Mathematics of Computation 20, 272-299.

17 Runca E.,Melli P. and Zannetti P. (1976) Computation of long term average SO_2 concentration in the Venetian Area. Applied Mathematical Modelling 1, 9-15.

18 Runca E. and Sardei F. (1975) Numerical treatment of time dependent advection and diffusion of air pollutants. Atmospheric Environment 9, 69-80.

19 Sardei F. and Runca E. (1975) An efficient scheme for solving time dependent problems of air pollution advection and diffusion. Proceedings of the Seminar on Air Pollution Modelling, IBM Italy, Venice Scientific Center.

20 Shieh L.J. et al. (1972) Air quality diffusion model; application to New York City. Journal of IBM Res. and Development, 16, 162-170.

21 Shir C.C. (1972) Numerical investigations of the atmospheric dispersion of stack effluents. IBM J.Res.Development 16, 171-179.

22 Shir C.C. and Shieh L.J. (1973) A generalized urban air pollution model and its application to the study of SO_2 distribution in the St.Louis metropolitan area. Technical Report RJ 1277, IBM San José Research Center, California.

23 Sklarew R.C.,Fabrick A.J. and Prager J.E. (1971) A particle-in-cell method for numerical solution of the atmospheric diffusion equation, and application to air pollution problems. Report 3SR - 844, Systems,Science and Software, La Jolla, California.

24 Sutton O.G. (1953) Micrometeorology. Mc.Graw-Hill, New York.

25 Turner D.B. (1964) A diffusion model for an urban area. Journal of Applied Meteorology, 3, 83-91.

26 Yanenko N.N. (1971) The method of fractional steps, Springer, Berlin.

7th International Technical Meeting
on Air Pollution Modeling and its Application

FURTHER DEVELOPMENTS IN THE APPLICATION OF SHIR'S MODEL TO THE VENICE AREA

G.L.Marziano, A.Sutera, L.Gianolio, M.Ciprian
"G.DONEGANI" RESEARCH INSTITUTE, MONTEDISON S.p.A.
NOVARA, ITALY

September 7 - 10, 1976
Airlie Virginia
United States of America

INDEX

Page

Abstract 1

1. Introduction 2

2. Foreward 5

3. The air quality simulation model 7

3.1 The model equations 7

3.2 The physisical parameters of the model 8

3.3 The numerical solution 10

4. The input data for the application to the Venice area 11

4.1 Geographical data and numerical grid determination 11

4.2 Source emission data 11

4.3 Meteorological data 12

5. Results 15

6. Analysis of the results 18

7. Conclusions 23

8. References 24

Abstract

In this paper an application to the area of Venice (Italy) of the air quality simulation model developed by Shir and Shieh is presented. Two different periods of the year (winter and summer) have been chosen for the simulation, so that different meteorogical and emission situations might be considered.

The model results are analysed by comparison with experimental data. It appears that the model gives as good results in Venice as were obtained in St. Louis , by Shir and Shieh, provided equally accurate values of input parameters are supplied. The most critical of these parameters turned out to be the wind field, that in our simulations is obtained by simplified interpolation between geostrophic and surface wind data.

1. Introduction

In recent years the simulation of the dispersion of pollutants in the atmosphere has been approached in many different ways. The aim of this simulation is to study the relationship between air quality and emitting sources as a function of meteorogical and surface conditions.

In general we can assume that this relationship is governed by the principle of mass conservation, that in differential form can be written as follows:

$$\frac{d}{dt} c = F \tag{1.1}$$

where c is the concentration of the pollutant in the atmosphere and F is the total balance of emitting sources, while $\frac{d}{dt}$ is the usual Euler time derivative.

Equation (1.1) is valid for instantaneous values of the involved parameters. The term on the right hand side of the equation is generally assumed as the sum of two different contributions: F_s, that accounts for the pollutant emissions from sources located in the volume element to which the balance is extended, and F_r, that accounts for the disappearance of pollutant due to possible chemical transformations into other chemical species. Expliciting the Eulero's time derivative, and accounting for the continuity constraint ($\vec{\nabla} \cdot \vec{u} = 0$), equation (1.1) transforms into the following:

$$(1.2) \qquad \frac{\partial c}{\partial t} + \underrightarrow{\nabla} \cdot (\underrightarrow{u}\, c) = F$$

still relating instantaneous quantities ($\underrightarrow{u}$ represents the wind vector). Equation (1.2) must obviously hold also when average is made over a sufficiently short time that the time derivative itself doesn't loose sense.
So, letting $u = \bar{u} + u'$ and $c = \bar{c} + c'$ and averaging according to Reynold's Axioms, equation (1.2) becomes:

$$(1.3) \qquad \frac{\partial \bar{c}}{\partial t} + \underrightarrow{\nabla} \cdot (\underrightarrow{\bar{u}} \cdot \bar{c}) = - \underrightarrow{\nabla} \cdot (\underrightarrow{\overline{u'c'}}) + \bar{F}$$

where the overbars denote mean values and the primes characterize instantaneous deviations from the mean: equation (1.3) represents the well known so-called "diffusion equation". In this equation two terms appear, that in equation (1.1) were hidden: the advection term (second term on the left) that accounts for the trasport of pollutants due to the mean air motion, and the turbulent transport term (first term on the right), that accounts for the spread of pollutants due to the eddy fluctuations.
The required relationship between air quality and emitting sources would imply the solution of equation (1.3), provided the source emissions, the meteorogical variables, the turbulent transport mechanism, which depends also on the surface conditions, and the transformation rate of the pollutants are given as imput parameters: this is practically impossible.

As a matter of fact, in order to specify the input parameters with the required details, one should know the urban air motions very closely.
It appears, from the previous discussion, that the problem is not soluble without drastic assumptions about the atmospheric motions in the area of interest.
Various approaches have been attempted, based either on statistical theory or on phenomenological considerations or even on arbitrary assumptions. Correspondingly, various air quality simulation models have been developed.

2. Foreward

As the problem of air pollution becomes more and more important, the application of air quality simulation models for practical purposes becomes, at least from an industrial point of view, almost as interesting as the development of new, more sophisticated ones. Moreover, problems which arise in the practical application of the models can give many helpful suggestions about how to make models fit in the best way the users' needs.

For our interest was mainly concerned with the possibility of an optimal control of emitting sources in the industrial and urban area of Venice using an air quality simulation model, our work has not been devoted to the development of a new model, but to the application and verification of an already existing model whose characteristics might match the requirements of this kind of problem.

Moreover our aim was to better understand the relationships between the air quality and the relevant parameters in the considered area, determining also the degree of accuracy to which each of them had to be known in order to get satisfactory results: for this reason also a study on the model sensivity to errors in some input parameters has been attempted.

The model we have chosen for the present study is the one developed by Shir and Shieh and already applied to

the St. Louis (Missouri) metropolitan area.
The reason of our choice principally stands on the two following considerations:

1) Shir and Shieh's model is a dynamical model, that is, it is able to account for short range temporal variations of the input parameters; moreover it is designed to face with non uniform surface conditions and space variations of the meteorological parameters both in the horizontal and in the vertical.
2) It can simulate both large industrial emissions (point sources) and urban residential emissions (area sources).

In our application we have considered two different periods of the year: a winter period and a summer one. In this way we could test the model in almost all the principal meteorological situations which, according to our feelings, happen in the area of Venice. Moreover, in the summer time it was possible to set to zero the emissions due to residential heatings, for which it is very difficult to get accurate values, eliminating a possible large source of error. The winter period chosen for our simulation was the one going from the 15th to the 28th February 1975; the summer period was the one going from the 28th of July to the 10th of August 1975.

3. The air quality simulation model

3.1 The model equations

As previously mentioned, the air quality simulation model we used is the one developed by C.C. Shir and L.J. Shieh [1]. Fundamentally it is based on the assumption that the concentration C of pollutant gas, which is function of time and space, is solution of the differential equation:

$$\frac{\partial c}{\partial t} + \vec{V} \cdot \vec{\nabla} C = K_H \nabla^2_H C + \frac{\partial}{\partial z} \left(K \frac{\partial c}{\partial z} \right) + Q + R \qquad (3.1)$$

where:

$\vec{V}$: wind velocity (which cartesian components are U, V, W), that is considered function of space and time.

$\vec{\nabla}$: gradient operator $\left(\frac{\partial}{\partial x} \vec{i} + \frac{\partial}{\partial y} \vec{j} + \frac{\partial}{\partial z} \vec{k}\right)$

K_H : horizontal turbulent diffusion coefficient.

K : vertical turbulent diffusion coefficient, which is assumed function of z and of the atmospheric conditions.

$\nabla^2_H C$: $\frac{\partial^2 C}{\partial x^2} + \frac{\partial^2 C}{\partial y^2}$: horizontal laplacian of C

Q : emitting sources intensity

R : chemical reaction rate

In equation (3.1) the term $\vec{V}\vec{\nabla}C$ represents the advection, while the first two terms on the right hand side represent the turbulent diffusion in the horizoltal and the vertical respectively. It's worthy to note that the equation is of turbulent type, which means that the concentration C (x, y, z, t) is not to be considered an instantaneous value, but a value averaged on a time interval sufficiently large to eliminate the rapid oscillations of the corresponding instantaneous variable and small enough that the temporal derivative itself doesn't loose sense.

The boundary conditions are:

$$K \frac{\partial C}{\partial z} = 0 \qquad \text{at } z = 0 \text{ and } z = H$$

$$(3.2) \qquad \frac{\partial^2 C}{\partial x^2} = 0 \qquad \text{at } x = 0 \text{ and } x = x_{max}$$

$$\frac{\partial^2 C}{\partial y^2} = 0 \qquad \text{at } y = 0 \text{ and } y = y_{max}$$

where H is the mixing height, which is assumed dependent of time, according to the meteorogical conditions.

3.2 The physical parameters of the model

The integration of equation (3.1) requires that values for H, $\vec{V}$, K_H, Q, R are supplied as functions of time.

- The chemical reaction rate R is assumed proportional to C according to equation:

(3.3) $$R = -k_a C$$

with $k_a = 10^{-4} \sec^{-1}$, when the pollutant is SO_2.

- K is assumed depending on height (z), surface roughness and meteorological conditions (expecially stability, which is considered a continuous function of wind speed and insolation - the latter related to sky cover and time of the day, once the place and the season are specified -).
- $\vec{V}$ is interpolated, at ground level, using data obtained at meteorological stations. Its variation with height is assumed a power law of the type

(3.4) $$|\vec{V}| = |\vec{V}_g| (z/z_g)^p$$

where p is computed using two values of upper wind according to the relation:

(3.5) $$p = \ln (|\vec{V}_2| / |\vec{V}_1|) / \ln(z_2/z_1)$$

and the subscript g refers to ground level (z_g is assumed equal to 10 m). Also the variation with height of the wind direction is accounted for.

- K_H is assumed related to K according to the formula

(3.6) $$K_H = 100\, K_{max} \cdot \frac{z}{z_s} \exp [-0.004\, (z - z_s)]$$

with the constraint that K_H be not less than 100 and not larger than 500 m^2/sec.

For fuller details refer to the paper by Shir and Shieh (1974).

3.3 The numerical solution

The differential equation (3.1) is integrated using a finite difference scheme. More precisely, the advection and horizontal diffusion terms are approximated by second order central difference, and the Crank-Nicholson formula was used for the vertical diffusion term; furthermore, a time splitting method was applied in the discretization of the advective part of the concentration equation.

4. The input data for the application to the Venice area

4.1 Geographical data and numerical grid determination

A reactangular areá of 22.5 x 30 kilometers, with longer side parallel to the North-South direction and shorter side parallel to the East-West direction, including the urban and industrial areas of Venice, Mestre and Porto Marghera (see fig. 1), was chosen. It was then divided into 30x40 square grids of 750 m side each, that was the base of the numerical solution of equation (3.1).
As to the vertical grids, fourteen of them where considered, with size increasing with height from 20 to 140 meters at maximum. As the top of the model is assumed variable with the mixing height, ranging from 500 to 1000 m, the last five grids' sizes were assumed variable with time according to the meteorological conditions.
For each surface grid a value of surface roughness was determined according to its morphological characteristics as they could be desumed from the map of the considered area.

4.2 Source emission data

From the urban characteristics, as they could be determined from the map, the 24 hr average values of area source emissions were computed for each grid, starting from the value of global fuel consumption in the whole area. A diurnal pattern of area source emissions was assigned, in the lack of any information about it, based on reasonable assumptions on the way in which residential heating plants are operated.

In the considered area 60 stacks of industrial plants were located. For some of them it was possible to get hourly averaged SO_2 emission values, for some other only longer term (up to one day) average values, and for the remaining ones just an yearly average value.

For the summer period, the source emission data were collected in the same way as for the winter period: however, as residential heatings are not operated in this season, the values of area source emissions were set to zero.

4.3 Meteorological data

As to the meteorological conditions, values of surface wind speed and direction every half an hour were given by two meteorological stations located within the considered area: these values were used to get hourly average values of wind speed and direction which then were interpolated to get corresponding values at every surface grid. In the lack of experimental observations, the upper wind values at 70 and 200 m were calculated from the value of geostrophic wind desumed from meteorological charts, using the so called "Taylor's spiral" formula.

As values of geostrophic wind were supplied every twelve hours, the intermediate values were determined by linear interpolation, so that hourly values of upper wind could be obtained.

The mixing height at every hour of simulated time was computed using the following formula:

$$H = \left(\alpha_o + \frac{3}{4}\pi\right)\sqrt{\frac{2K}{f}} \qquad (4.1)$$

where α_o depends on stability and surface roughness, f is Corioli's parameter and K is the value of eddy diffusivity assumed constant in Taylor's spiral formula.

At one of the two forementioned meteorological stations (Tessera Airport), among other variables, also the sky cover, the temperature and the pressure were determined. The first one was supplied every hour to the model, to allow computation of continuous stability class in the way explained in the paper by Shir and Shieh.

There are, especially in winter, two particular meteorological situations, which origin in the area of interest a kind of local circulation for which the assumptions made before about upper wind values and mixing height become completely unreasonable: they are the fog and the bora wind.

When there is fog, synoptic conditions are such that a strong low inversion is present over the area: in such situation it is reasonable to assume that the height of the mixing layer coincides with the height of the fog stratus; in the lack of better information about the height of the fog stratus, an average value of 200 meters was assigned to the mixing height when fog was present: moreover no variation of wind speed was assumed with height.

When bora wind blows one may assume that the wind speed is constant up to roughly 800 meters: so, when the surface wind speed at ground level was greater than 6 m/sec and its direction was comprised between 0 and 90 degrees, a uniform wind field in the whole area was assumed and the mixing height was set up to 800 meters.

In figures 2 and 3 the wind roses for the two considered periods are presented. As it can be seen, both in winter and in summer there is a large percentage of calm cases. In winter most of the calm cases correspond to the presence of fog; when wind blows, its prevailing directions, from the north and north east sectors, are the directions of the bora wind. For the summer period the prevailing wind system is the sea breeze, characterized by a large percentage of calm, during the night, and by a wind blowing from the south and south east sectors during the day (as it can be seen, the nocturnal land breeze is much weaker, as shown by the percentage of cases of wind blowing from the north and north west sectors).

5. Results

With the data described in the previous paragraph, the air quality simulation model computed the hourly average of surface concentration of SO_2 at every point of the numerical grid. The SO_2 concentration was also measured at monitoring stations located over the area. As generally the monitoring stations are not exactly located at grid points, the values computed by the model at each station were obtained by bi-linear interpolation of the four grid points among which the station falls. Comparison was made between the computed and the detected values. This comparison is obviously not so meaningful, as it is made between local values and values which should be considered as averages made over a relatively large volume: however, keeping in mind this fact, it still can give a reasonable evaluation of the accuracy of the model.

In figure 4 the diagrams of one hour average concentrations computed by the model and detected at 20 monitoring stations for all the 14 days of the considered winter period are presented: the same diagrams related to the 14 days of the considered summer period are reported in figure 9. It must be considered that, as concentrations lower than 4 of the arbitrary units reported on the diagrams are not meaningful, whether they are computed or detected, values lower than 4 have been set equal to 4.

As it can be seen, the model simulates, on the average, the concentration patterns both in the case of high and low concentrations. However it does not follow the sharp variations of the detected concentration both because of the rather high uncertainty in the input data (as will be shown in the next paragraph) and because of the fact, already explained, that the model gives volume averages, while the monitoring stations detect local values, which can be influenced by local factors that are accounted for by the model only on an average base.

Moreover, one has to consider that not all the stations were working properly during the whole considered periods: see for example stations 3T and 21T that in the winter period gave satisfactory results, while in the summer period did not work at all.

In figures 5÷7 the comparison between observed and computed 24 hr averages of concentration at the same twenty stations is presented, for the winter period: the corresponding diagrams for the summer period are reported in figures 10÷11 (stations 3T and 21T are not reported as no observed values were available from them). As it can be observed, the points do not generally lie so distant from the diagonal, showing a sufficiently good correlation between computed and observed data. As previously mentioned, for some stations which appear quite bad in these diagrams the doubt arises that they were not working so properly.

In figures 8 and 12 the comparison between the 14 days' average computed and detected concentrations at the twenty stations is presented, for the winter and summer period respectively. Again, a good correlation between computation and observation appears.

In figures 13 and 14 are shown the 24 hours average concentration isopleths computed for two characteristic days in winter and in summer.

6. Analysis of the results

The results exposed in the previous paragraph were subjected to linear regression analysis, in order to get, for each of the two considered periods, the correlation coefficient between computed and observed concentrations at every monitoring station, and the parameters of the regression line.

These values were computed for both one hour and 24 hours averages, using linear scale and logarithmic scale as well: they are shown in tables 1 - 2.

Also the parameters computed using the total sample (all the stations together) are reported.

Using the total sample of 24 hours averages also other parameters, which can help to evaluate the model performance, were computed: they are the average value and the standard deviation of the ratio between computed and observed concentrations (which is related to the relative error) and of the absolute error (difference between computed and observed concentration), and the normalised root mean square error (root mean square error divided by the standard deviation of the observed values). These parameters are reported in table 3.

For the period averages (which are plotted, in logarithmic scale, in figures 8 and 12 for the winter and the summer periods respectively) the correlation coefficients and the parameters of the regression line are reported in table 4: as already apparent from the figures, the correlation between computed and observed values is very good, especially using logarithmic scale.

As to the values reported in table 3, they suggest that the model tends to under estimate the higher concentrations, while probably over estimates the very low ones: this is very well explained by the grid structure of the model, which obviously tends to smooth the concentration gradients. Due to the fact that the ratio between computed and observed concentrations cannot be less than 0 (no negative values of concentration are meaningful), it turns out that the distribution of this ratio is not exactly normal.

In the hypothesis that for the allowed values the distribution be not far from normal, one can use the properties of this distribution just cutting off the queue under 0.

It follows that in the 65% of the cases, for the winter simulation, and in the 55 % for the summer simulation, the computed 24 hours average concentrations are comprised between .5 and 2 times the observed ones.

The above results show that the model did not give a very precise evaluation of the real situation occurred in the considered area.

Moreover the summer results appear less satisfactory than the winter ones. However one has to consider that the data used in the simulation were affected by a rather large error. The point sources, for example, were known with a rather large approximation, as to their 1 hr average value: this value, actually, was likely to be different from the used one by a percentage that could raise, in some cases, to as much as 40%; the wind direction, then, was known to a 45 degrees approximation (45 degreees = 1 octant of the wind rose). Other input parameters (the area sources, the mixing height, the upper wind values) could be even more imprecise, as they had to be computed in an approximate way, in the lack of any experimental information.

While in winter a very important role could be played by the residential emissions, in summer this source of error is not present: it must be considered, however, that the area sources have also a smoothing effect on the concentration distribution, so that in summer, when they are not active, much more important become the meteorological parameters, as wind speed and direction, due to the higher concentration gradients. Moreover, in summer, due to the presence of sea breeze, the wind field is probably more complicated than it was assumed in the present study.

To test how much an error in the input parameters could influence the accuracy of the results given by the model, four other simulations were performed, for the same 15th-28th February and 28th July-10th August periods, with input data modified in the following manner:

a) in the first one, only the point sources were modified, giving them a decrement variable, from source to source, from 2% to a maximum of 40%: the average reduction of the point sources emission was round 10÷15 per cent

b) in the second one, again only the point sources were modified, increasing them by the same percentage by which they were decreased in a)

c) in the third one the wind direction was modified by -22 degrees

d) in the fourth one the wind direction was modified by +23 degrees

For every station the minimum and maximum one hour average concentration values were determined among the five values computed in the original simulation and in the four above described. In this way, to every observed value an interval of computed values was associated: from this interval, the value closest to the observed one was chosen and the regression analysis previously described was again performed.

The results are reported in tables 5-8. Comparing these values with the corresponding ones reported in tables 1-4, a very significant improvement of the performance of the model appears. Reasoning in the same way shown previously, from the values in table 7 it is possible to deduce that the percentage of cases for which the concentration computed by the model is comprised between .5 and 2 times the observed one raises to 71 % for the winter simulation and to 68% for the summer one. This result is not far from the one obtained by Shir in St. Louis. It is worthy to note that the results shown in tables 5-8 cannot be considered the ones that would be obtained if the point source emissions and the wind direction at ground level were known exactly; however it must be considered that not all of the error sources previously listed were accounted for in the analysis performed and that no error was supposed to affect the detected values, which is clearly not true. So it is likely that an even better result could be obtained going into

deeper detail in the analysis of the accuracy of the input data. In particular we feel that a very important role could be played, for the winter simulation, by a more accurate determination of the spatial and temporal distribution of the area sources [6] and, for the summer period, by a detailed knowledge of the upper wind field.

7. Conclusion

An application to the area of Venice (Italy) of the air quality simulation model developed by Shir and Shieh was made for the periods 15th÷28th February and 28th July÷10th August 1975. The results obtained were quite satisfactory in view of the rather large errors affecting the input data. A rough approximation of the extent to which a reasonable error in some of the input parameters could affect the model accuracy was given, showing that an increase of the precision just of point source emission values and surface wind direction is likely to increase the correlation coefficient by more than 20% as well as the percentage of cases in which the computed values are of the same order of the detected ones. Of course some part of the model inaccuracy cannot be explained by the error affecting the input data: this is due to the approximations used in the model and is unavoidable, unless the model itself is properly changed. However a precise evaluation of the inaccuracy due only to the model is very difficult to obtain and must be the object of further investigation.

8. References

1) C.C. Shir, L.J. Shieh: A generalized urban air pollution model and its application to the study of SO_2 distributions in the St. Louis metropolitan area. Journ. of Applied Meteorology 13, 2 (1974), pp. 185-204.

2) J.E. Fromm: Numerical solution of the Navier-Stokes equations at high Reynolds numbers and the problem of discretization of convective derivates. IBM Research Report.

3) L. Collatz: The numerical treatment of differential equations (Springer 1960).

4) R. Holton: An introduction to dynamic meteorology, Academic Press, 1972

5) G.J. Haltiner and F.L. Martin: Dynamical and physical meteorology, Mc Graw-Hill, 1957.

6) L.J. Shieh, C.C. Shir: Analysis of input parameters and results of urban air pollution computation, in press.

TABLE 1 - ANALYSIS OF COMPUTED VS. OBSERVED 1 HR AVERAGE CONCENTRATIONS

Station N°	WINTER SIMULATION						SUMMER SIMULATION					
	Corr.Coeff.		Constant		Slope		Corr.coeff.		Constant		Slope	
	Lin. scale	Log. scale	Lin. scale	Log. scale	Lin. scale	Log. scale	Lin. scale	Log. scale	Lin. scale	Log. scale	Lin. scale	Log. scale
1E	0.073	0.036	41.8	1.50	0.042	0.028	0.257	0.314	14.5	0.67	0.261	0.372
3E	0.178	0.154	54.2	1.60	0.065	0.063	0.185	0.368	37.9	1.26	0.025	0.162
5E	0.587	0.588	19.2	0.51	0.703	0.654	0.212	0.391	25.7	0.72	0.495	0.565
6E	0.130	0.203	144.5	1.77	0.151	0.196	0.325	0.107	46.7	1.61	0.151	0.050
12E	0.285	0.427	39.0	1.08	0.215	0.324	0.305	0.370	26.2	0.99	0.499	0.400
13E	0.291	0.322	43.0	0.64	0.238	0.521	0.151	0.114	15.5	0.96	0.090	0.101
16E	0.315	0.129	39.4	1.36	0.213	0.111	0.253	0.450	13.8	0.67	0.120	0.372
17E	0.073	0.126	32.4	1.23	0.042	0.112	0.168	0.323	9.2	0.61	0.103	0.264
19E	0.584	0.498	7.6	0.43	0.570	0.514	0.279	0.306	5.8	0.34	0.922	0.777
2T	0.224	0.236	39.5	1.16	0.085	0.222	0.501	0.468	12.5	0.63	0.368	0.453
3T	0.326	0.282	19.8	0.66	0.254	0.390	-	-	-	-	-	-
16T	0.369	0.576	15.1	0.28	0.187	0.588	0.101	0.146	8.2	0.62	0.133	0.163
18T	0.345	0.455	19.2	0.11	0.161	0.679	0.188	0.335	8.4	0.52	0.058	0.251
19T	0.286	0.289	6.0	0.56	0.057	0.180	0.027	0.108	4.3	0.59	0.003	0.029
21T	0.501	0.554	12.8	0.27	0.411	0.613	-	-	-	-	-	-
22T	0.654	0.591	1.3	-0.08	0.599	0.788	0.212	0.159	5.1	0.60	0.354	0.190
25T	0.295	0.501	6.9	0.17	0.142	0.472	0.039	0.153	8.5	0.64	0.013	0.149
26T	0.533	0.562	4.0	0.19	0.384	0.567	0.497	0.388	2.7	0.45	0.222	0.251
28T	0.503	0.309	6.1	0.52	0.504	0.339	0.314	0.288	3.5	0.47	0.183	0.216
29T	0.272	0.424	56.5	1.14	0.177	0.357	0.357	0.373	33.6	0.88	0.476	0.450
Total sample	0.383	0.489	24.5	0.52	0.313	0.534	0.278	0.428	17.3	0.58	0.119	0.428

TABLE 2 - ANALYSIS OF COMPUTED VS. OBSERVED 24 HR AVERAGE CONCENTRATIONS

Station N°	WINTER SIMULATION						SUMMER SIMULATION					
	Corr.coeff.		Constant		Slope		Corr.coeff.		Constant		Slope	
	Lin. scale	Log. scale	Lin. scale	Log. scale	Lin. scale	Log. scale	Lin. scale	Log. scale	Lin. scale	Log. scale	Lin. scale	Log. scale
1E	-0.104	-0.279	48.1	1.83	-0.045	-0.164	0.279	0.215	13.6	0.83	0.314	0.204
3E	0.304	0.184	50.2	1.61	0.117	0.055	0.356	0.584	37.3	1.27	0.029	0.155
5E	0.889	0.659	1.6	0.40	1.326	0.755	0.434	0.524	18.3	0.63	1.137	0.673
6E	0.251	0.344	93.2	0.93	0.600	0.614	0.402	0.330	47.3	1.48	0.140	0.133
12E	0.254	0.389	41.9	1.19	0.162	0.256	-0.064	0.235	33.1	1.16	-0.077	0.191
13E	0.577	0.615	-11.7	-1.54	0.898	1.724	-0.031	-0.093	18.4	1.19	-0.019	-0.090
16E	0.362	0.080	31.1	1.43	0.321	0.073	0.145	0.426	13.9	0.48	0.113	0.557
17E	0.049	0.022	33.9	1.40	0.020	0.016	-0.041	0.094	11.1	0.79	-0.025	0.060
19E	0.833	0.738	-1.2	0.04	0.935	0.866	0.413	0.535	-9.9	-1.75	4.279	4.073
2T	0.550	0.305	21.5	0.53	0.311	0.586	0.504	0.655	12.1	0.39	0.389	0.655
3T	0.444	0.410	0.0	-0.42	0.590	1.042	-	-	-	-	-	-
16T	0.695	0.783	3.6	0.02	0.364	0.744	0.272	0.283	5.4	0.53	0.323	0.245
18T	0.662	0.619	3.4	-0.43	0.333	0.962	0.077	0.286	8.9	0.57	0.029	0.205
19T	0.386	0.469	6.5	0.54	0.048	0.193	0.262	0.261	3.8	0.56	0.032	0.057
21T	0.764	0.612	-1.9	0.14	0.783	0.711	-	-	-	-	-	-
22T	0.846	0.722	-7.4	-0.30	0.870	0.955	0.328	0.327	2.1	0.37	0.751	0.479
25T	0.540	0.630	2.5	0.06	0.224	0.542	0.088	0.457	7.4	0.45	0.035	0.330
26T	0.748	0.691	1.3	0.09	0.481	0.644	0.723	0.618	1.3	0.32	0.312	0.371
28T	0.650	0.301	-3.2	0.47	0.901	0.358	0.762	0.689	-0.6	0.10	0.510	0.582
29T	0.345	0.407	54.9	1.25	0.198	0.295	0.499	0.659	27.9	0.17	0.611	0.956
Total sample	0.561	0.584	6.8	0.24	0.600	0.702	0.444	0.556	14.4	0.36	0.215	0.615

TABLE 3 - STATISTICS ON 24 HR AVERAGE CONCENTRATIONS (TOTAL SAMPLE)

	RATIO C_c/C_o		ABSOLUTE ERROR		Normalised root mean sqare err.
	Average value	Standard deviation	Average value	Standard deviation	
Winter simulation	0.881	0.970	-16.98	38.05	1.06
Summer simulation	1.228	1.237	-5.27	32.36	0.91

TABLE 4 - ANALYSIS OF COMPUTED VS. OBSERVED 14 DAYS AVERAGE CONCENTRATIONS

	CORR.COEFF.		CONSTANT		SLOPE	
	Lin. scale	Log. scale	Lin. scale	Log. scale	Lin. scale	Log. scale
Winter simulation	0.738	0.748	-14.8	-0.25	0.963	1.021
Summer simulation	0.587	0.677	11.6	0.14	0.325	0.825

TABLE 5 - ANALYSIS OF COMPUTED VS. OBSERVED 1 HR AVERAGE CONCENTRATIONS (MODIFIED DATA)

Station N°	WINTER SIMULATION						SUMMER SIMULATION					
	Corr.coeff.		Constant		Slope		Corr.coeff.		Constant		Slope	
	Lin. scale	Log. scale	Lin. scale	Log. scale	Lin. scale	Log. scale	Lin. scale	Log. scale	Lin. scale	Log. scale	Lin. scale	Log. scale
1E	0.276	0.268	34.8	1.24	0.149	0.191	0.552	0.569	8.5	0.38	0.479	0.624
3E	0.338	0.388	47.6	1.44	0.115	0.156	0.350	0.602	38.8	1.12	0.044	0.263
5E	0.686	0.706	15.6	0.43	0.745	0.734	0.315	0.559	16.4	0.46	0.584	0.731
6E	0.401	0.455	99.0	1.35	0.359	0.377	0.593	0.377	38.0	1.41	0.278	0.172
12E	0.545	0.688	29.8	0.83	0.358	0.495	0.445	0.464	18.7	0.81	0.591	0.496
13E	0.490	0.458	32.3	0.40	0.346	0.667	0.482	0.427	10.6	0.66	0.285	0.366
16E	0.539	0.351	25.5	1.05	0.351	0.293	0.523	0.687	10.7	0.44	0.249	0.574
17E	0.225	0.321	28.6	1.00	0.118	0.271	0.398	0.547	6.8	0.42	0.222	0.441
19E	0.711	0.620	4.7	0.31	0.659	0.624	0.341	0.372	4.0	0.24	0.865	0.818
2T	0.439	0.447	35.5	0.95	0.162	0.370	0.749	0.684	9.1	0.49	0.515	0.596
3T	0.549	0.435	12.5	0.39	0.434	0.590	-	-	-	-	-	-
16T	0.456	0.620	14.9	0.28	0.226	0.621	0.301	0.331	5.3	0.46	0.314	0.345
18T	0.410	0.449	19.4	0.23	0.198	0.643	0.431	0.592	7.1	0.33	0.122	0.452
19T	0.393	0.342	6.0	0.54	0.089	0.232	0.143	0.218	4.3	0.56	0.021	0.074
21T	0.629	0.669	10.7	0.17	0.484	0.721	-	-	-	-	-	-
22T	0.741	0.656	-0.3	-0.15	0.673	0.867	0.351	0.329	3.5	0.46	0.469	0.353
25T	0.384	0.549	7.0	0.13	0.190	0.549	0.130	0.300	7.6	0.55	0.036	0.252
26T	0.639	0.619	2.7	0.12	0.479	0.648	0.617	0.528	1.4	0.32	0.344	0.385
28T	0.598	0.415	4.6	0.42	0.573	0.446	0.445	0.390	3.0	0.41	0.259	0.310
29T	0.492	0.696	45.2	0.85	0.287	0.523	0.499	0.521	25.2	0.74	0.565	0.545
Total sample	0.514	0.590	20.1	0.41	0.369	0.617	0.415	0.583	14.8	0.42	0.160	0.561

TABLE 6 - ANALYSIS OF COMPUTED VS. OBSERVED 24 HR AVERAGE CONCENTRATIONS (MODIFIED DATA)

Station N°	WINTER SIMULATION						SUMMER SIMULATION					
	Corr.coeff.		Constant		Slope		Corr.coeff.		Constant		Slope	
	Lin. scale	Log. scale	Lin. scale	Log. scale	Lin. scale	Log. scale	Lin. scale	Log. scale	Lin. scale	Log. scale	Lin. scale	Log. scale
1E	0.273	0.122	38.1	1.47	0.103	0.060	0.600	0.532	6.1	0.48	0.636	0.521
3E	0.491	0.495	42.2	1.44	0.184	0.155	0.633	0.843	36.7	1.11	0.061	0.268
5E	0.917	0.756	1.5	0.35	1.244	0.804	0.593	0.737	8.0	0.27	1.309	0.947
6E	0.435	0.511	56.2	0.66	0.733	0.723	0.719	0.595	37.9	1.27	0.279	0.265
12E	0.608	0.666	32.2	0.95	0.314	0.411	0.267	0.429	22.8	0.93	0.252	0.355
13E	0.695	0.665	-12.9	-1.35	0.892	1.634	0.324	0.229	13.0	0.86	0.194	0.202
16E	0.547	0.282	16.4	1.14	0.468	0.238	0.406	0.601	9.8	0.28	0.290	0.728
17E	0.297	0.256	29.0	1.17	0.112	0.172	0.296	0.452	7.8	0.55	0.156	0.301
19E	0.881	0.772	-3.2	-0.01	0.986	0.917	0.430	0.554	-8.2	-1.62	3.452	3.757
2T	0.711	0.475	19.0	0.31	0.368	0.737	0.711	0.751	10.1	0.41	0.477	0.662
3T	0.619	0.477	-11.7	-0.69	0.848	1.236	-	-	-	-	-	-
16T	0.740	0.832	5.6	0.04	0.368	0.760	0.528	0.504	3.0	0.41	0.475	0.390
18T	0.637	0.581	7.1	-0.16	0.332	0.853	0.358	0.556	7.1	0.43	0.112	0.355
19T	0.462	0.458	7.0	0.57	0.068	0.214	0.485	0.385	3.3	0.51	0.080	0.117
21T	0.826	0.730	-1.7	0.04	0.799	0.819	-	-	-	-	-	-
22T	0.870	0.754	-7.9	-0.34	0.910	1.008	0.430	0.474	1.0	0.21	0.793	0.650
25T	0.576	0.662	3.6	0.04	0.252	0.609	0.311	0.628	5.9	0.34	0.114	0.457
26T	0.809	0.715	-0.2	0.03	0.588	0.720	0.777	0.667	0.1	0.23	0.425	0.465
28T	0.690	0.398	-3.3	0.38	0.904	0.456	0.797	0.740	-1.1	0.01	0.578	0.699
29T	0.652	0.688	42.1	0.98	0.330	0.446	0.631	0.741	22.0	0.21	0.631	0.926
Total sample	0.652	0.655	5.8	0.19	0.602	0.750	0.577	0.676	12.0	0.23	0.259	0.728

TABLE 7 - STATISTICS ON 24 HR AVERAGE CONCENTRATIONS (TOTAL SAMPLE) (MODIFIED DATA)

	RATIO C_c/C_o		ABSOLUTE ERROR		Normalised root mean sqare err.
	Average value	Standard deviation	Average value	Standard deviation	
Winter simulation	0.826	0.745	-17.91	31.58	0.92
Summer simulation	1.040	0.853	-6.60	29.83	0.85

TABLE 8 - ANALYSIS OF COMPUTED VS. OBSERVED 14 DAYS AVERAGE CONCENTRATIONS (MODIFIED DATA)

	CORR.COEFF.		CONSTANT		SLOPE	
	Lin. scale	Log. scale	Lin. scale	Log. scale	Lin. scale	Log. scale
Winter simulation	0.774	0.782	-9.8	-0.20	0.865	1.008
Summer simulation	0.697	0.762	9.3	0.04	0.364	0.909

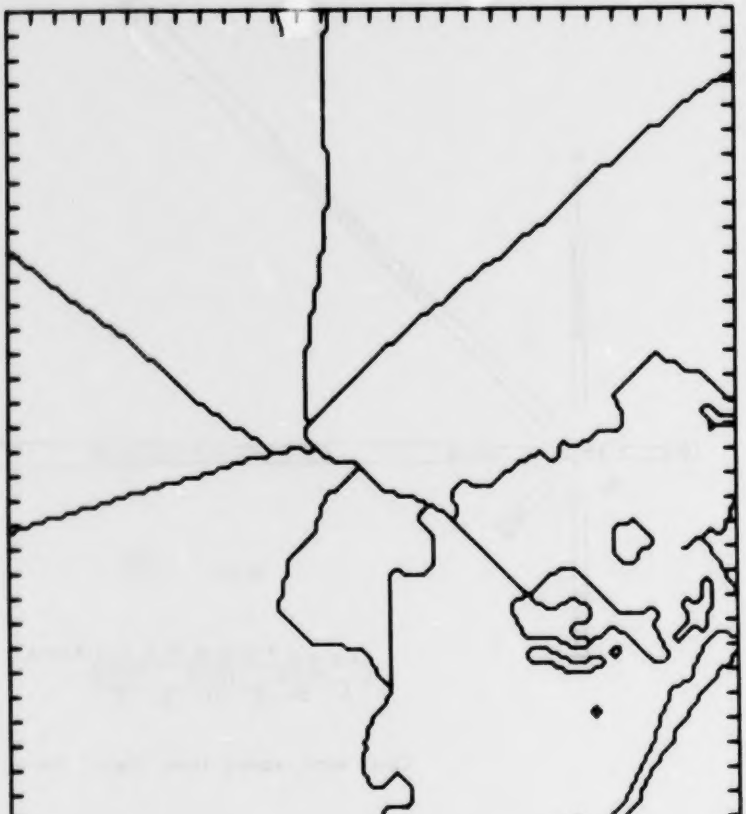

FIG. 1— MAP OF THE AREA OF VENICE

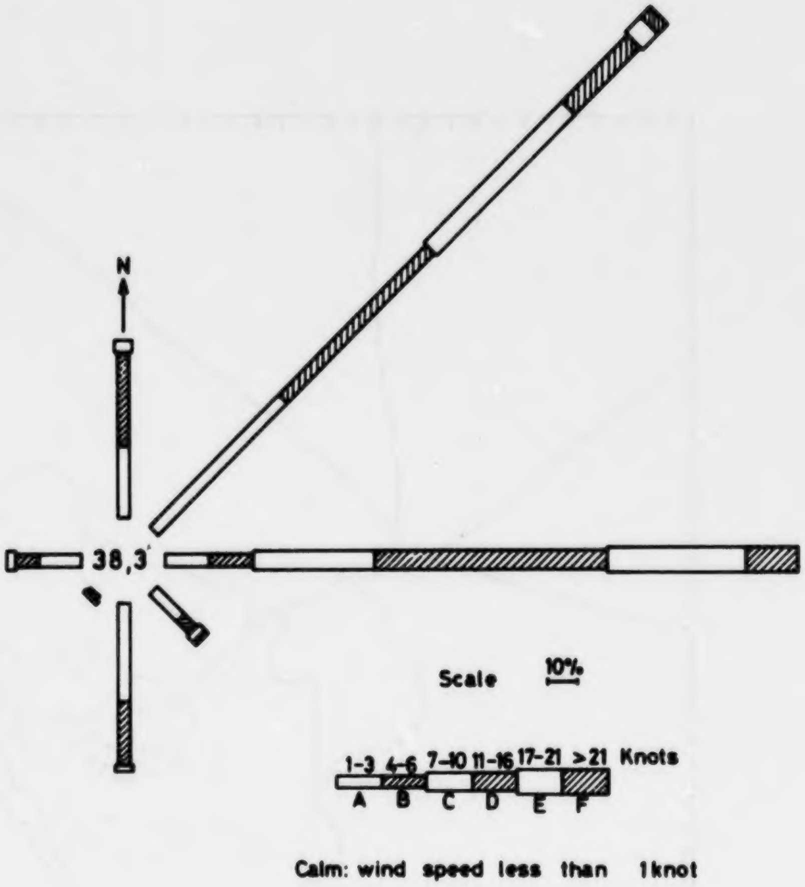

FIG. 2-WIND ROSE FOR THE WINTER PERIOD

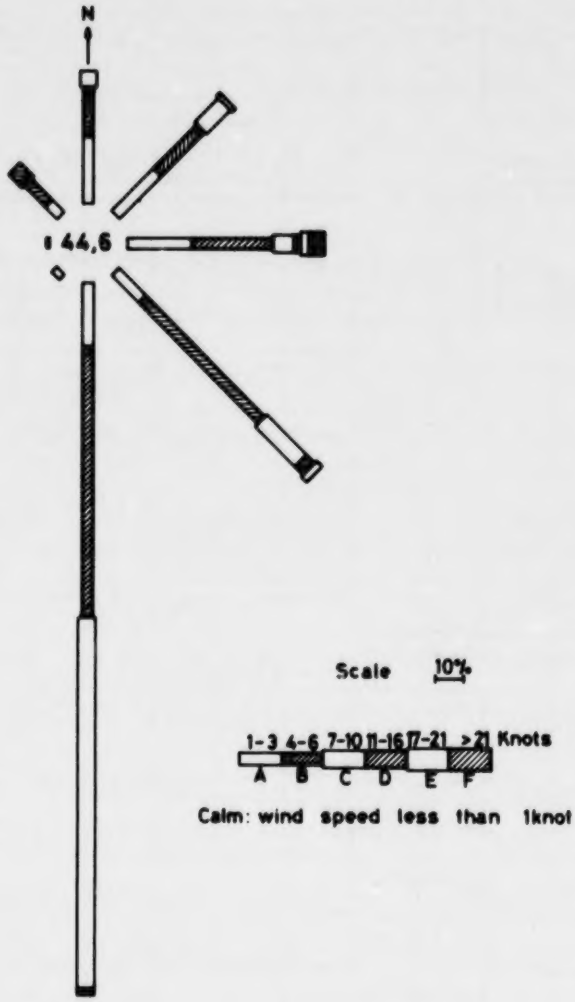

FIG. 3-WIND ROSE FOR THE SUMMER PERIOD

FIG. 4 — WINTER SIMULATION — COMPARISON OF 1 HR AVERAGE COMPUTED AND OBSERVED SO_2 CONCENTRATIONS (ARBITRARY UNITS)

——— COMPUTED ; - - - - - OBSERVED

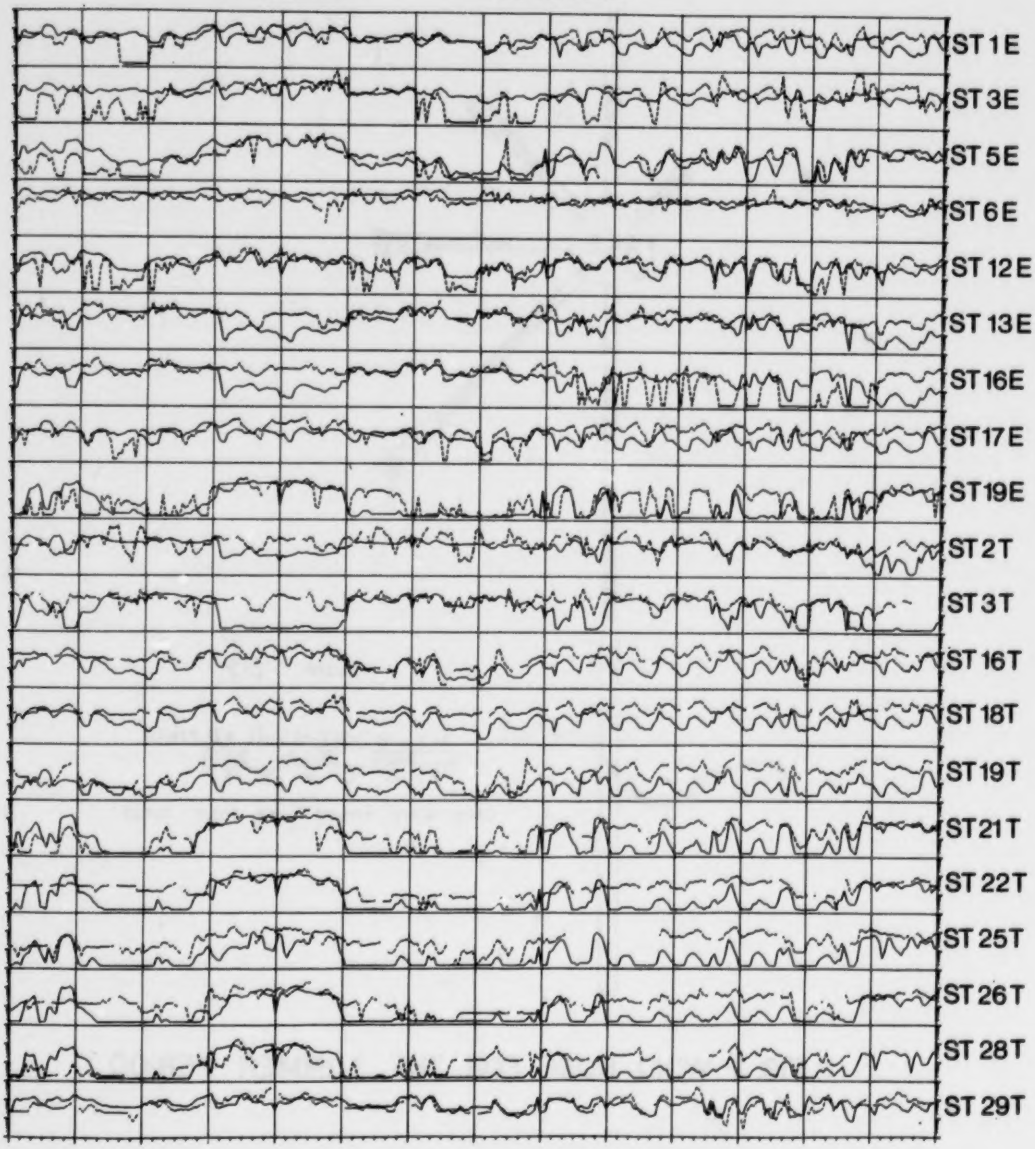

FIG. 5 - WINTER SIMULATION - COMPARISON OF 24HR AVERAGE COMPUTED AND OBSERVED SO_2 CONCENTRATIONS (ARBITRARY UNITS)

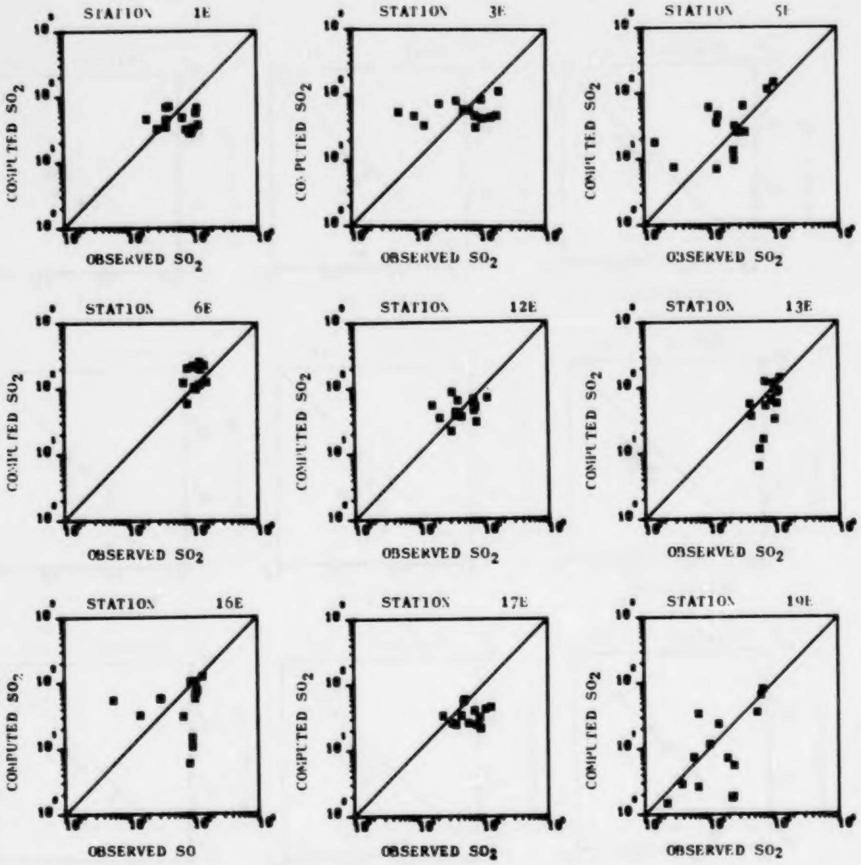

FIG. 6 - WINTER SIMULATION - COMPARISON OF 24HR AVERAGE COMPUTED AND OBSERVED SO_2 CONCENTRATIONS (ARBITRARY UNITS)

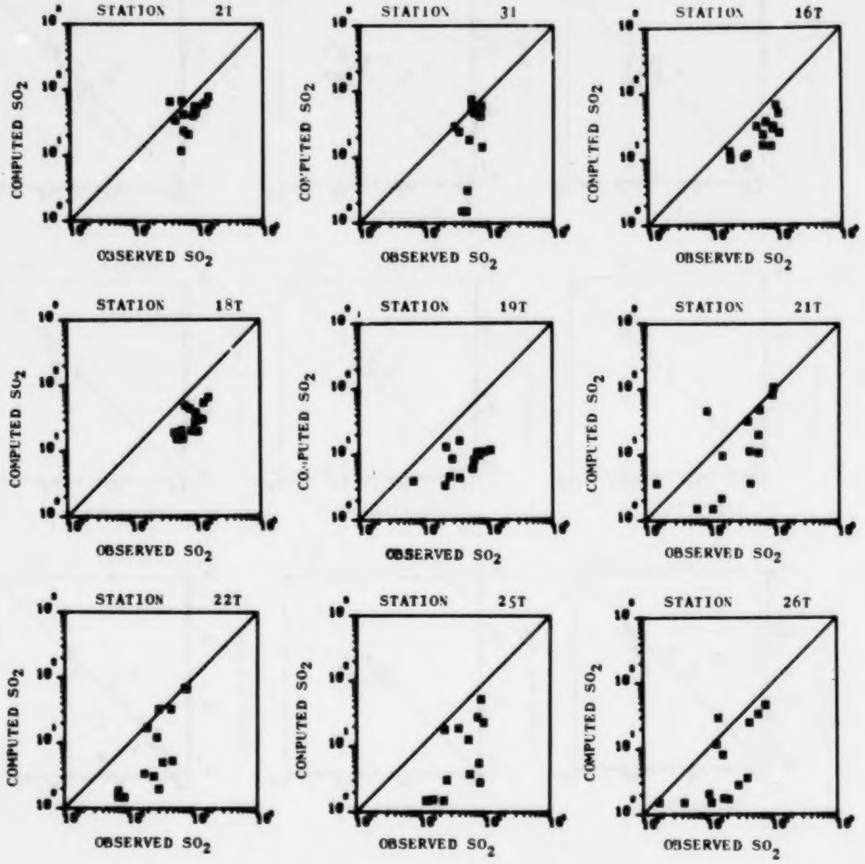

FIG. 7 - WINTER SIMULATION-COMPARISON OF 24 HR AVERAGE COMPUTED AND OBSERVED SO_2 CONCENTRATIONS (ARBITRARY UNITS).

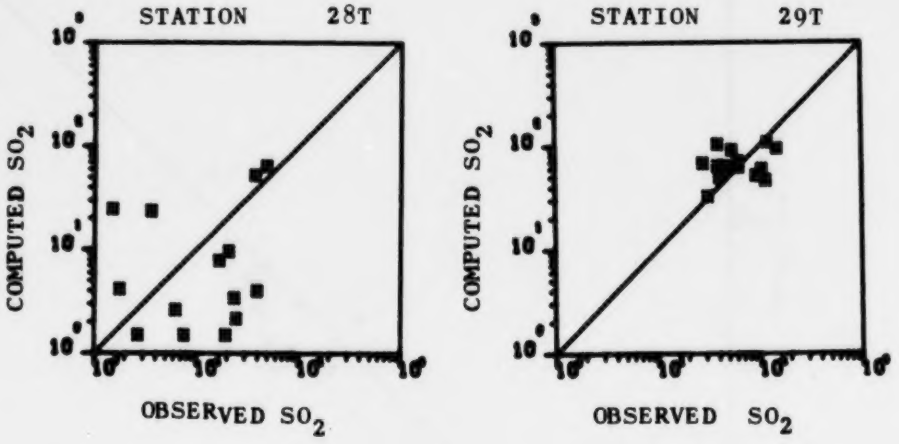

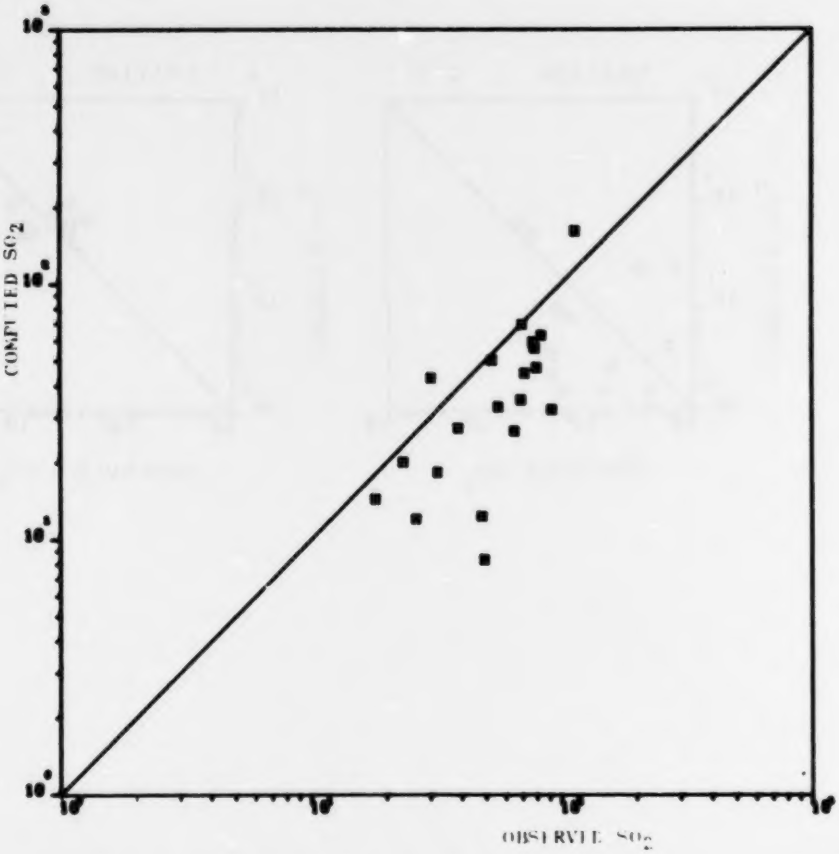

FIG. 8 - WINTER SIMULATION - COMPARISON OF 14 DAYS AVERAGE COMPUTED AND OBSERVED SO_2 CONCENTRATIONS (ARBITRARY UNITS)

FIG. 9 —SUMMER SIMULATION—COMPARISON OF 1 HR AVERAGE COMPUTED AND OBSERVED SO_2 CONCENTRATIONS (ARBITRARY UNITS)

——— COMPUTED ; -------- OBSERVED

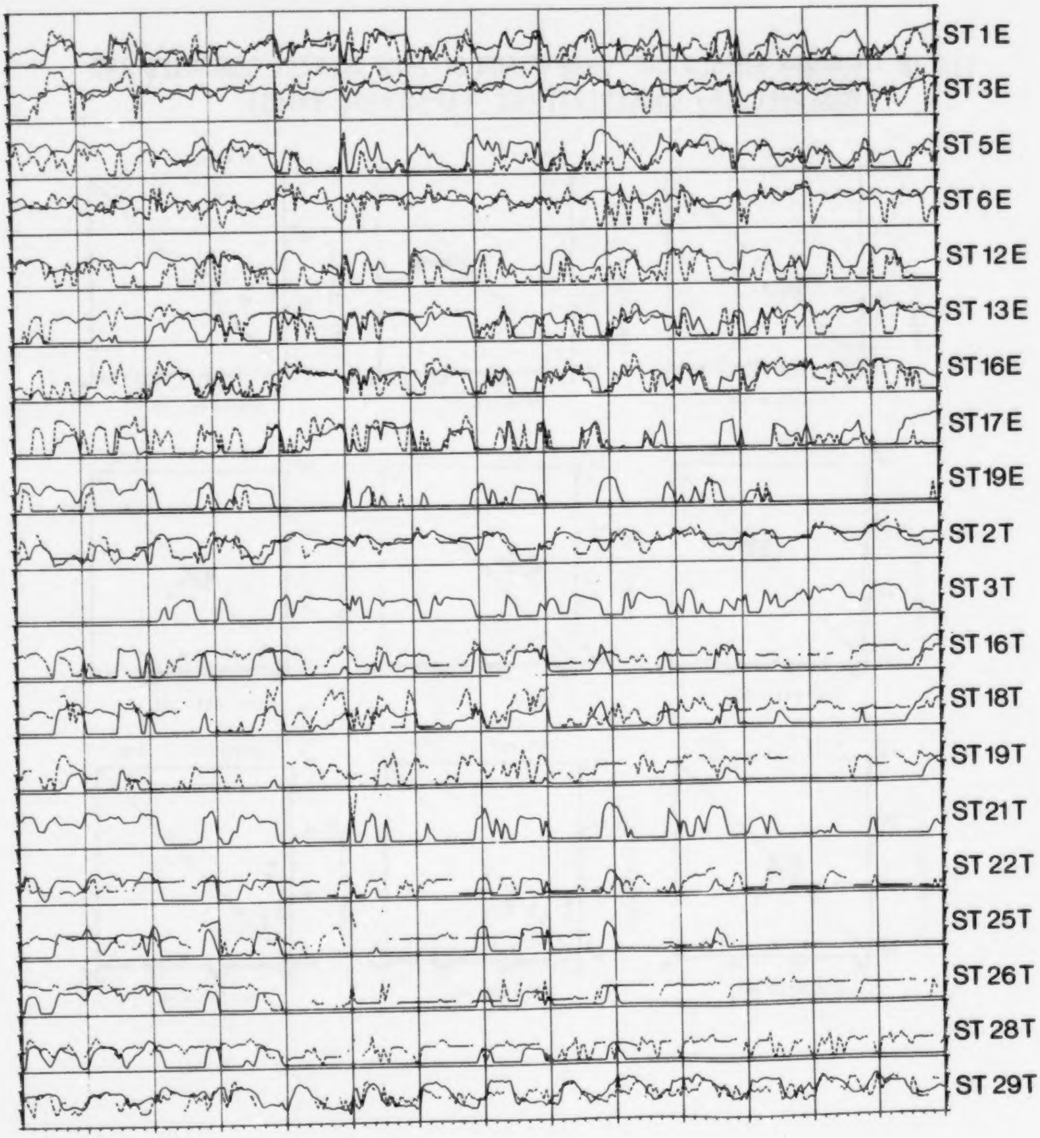

FIG. 10 - SUMMER SIMULATION-COMPARISON OF 24HR AVERAGE COMPUTED AND OBSERVED SO_2 CONCENTRATIONS (ARBITRARY UNITS)

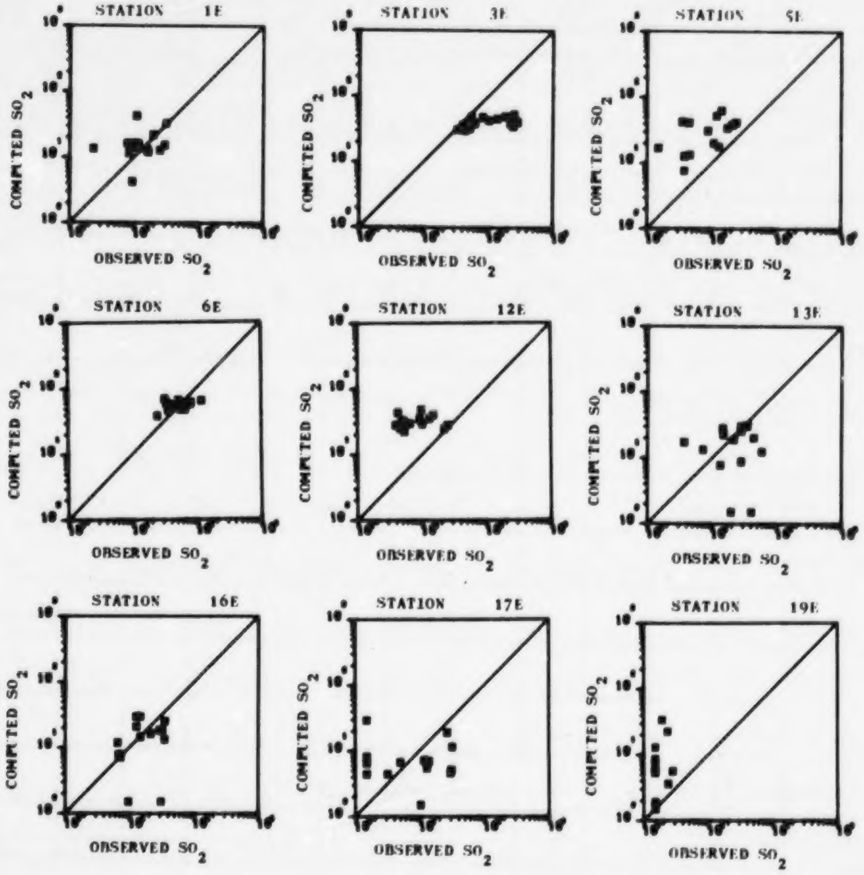

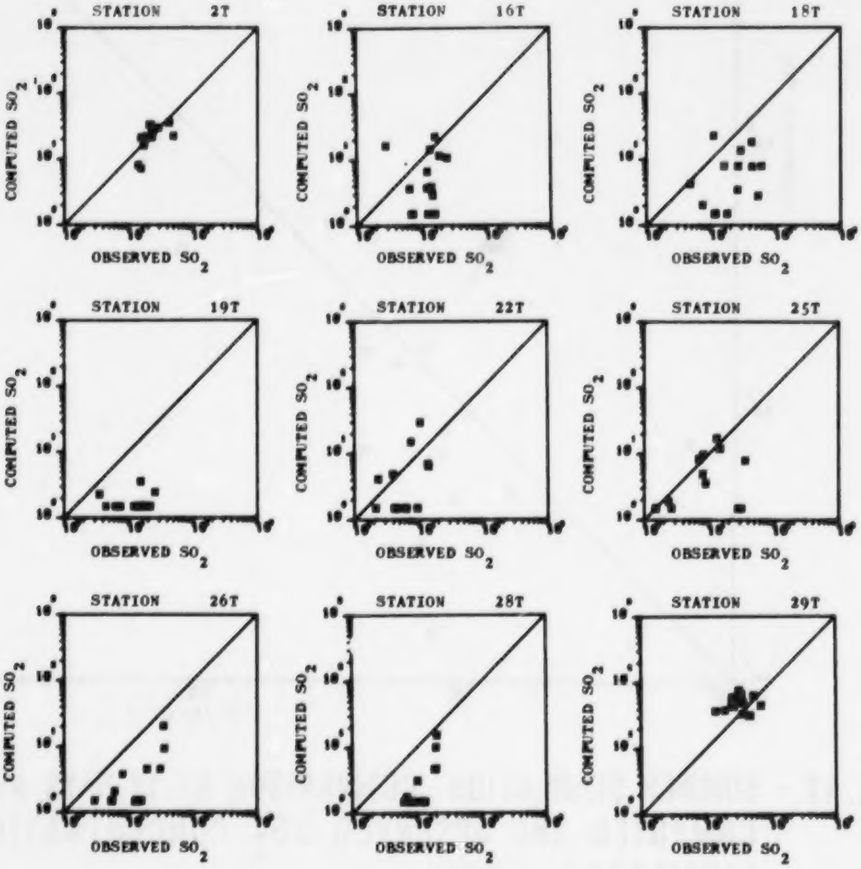

FIG. 11 - SUMMER SIMULATION - COMPARISON OF 24HR AVERAGE COMPUTED AND OBSERVED SO_2 CONCENTRATIONS (ARBITRARY UNITS)

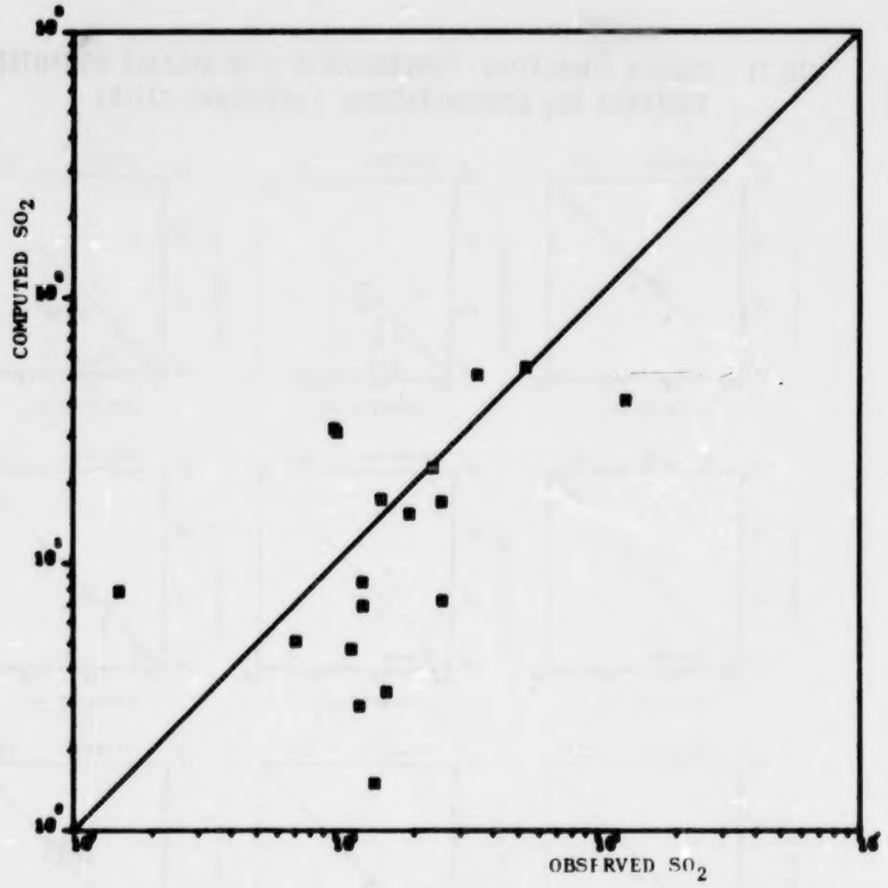

FIG. 12 - SUMMER SIMULATION - COMPARISON OF 14 DAYS AVERAGE COMPUTED AND OBSERVED SO_2 CONCENTRATIONS (ARBITRARY UNITS)

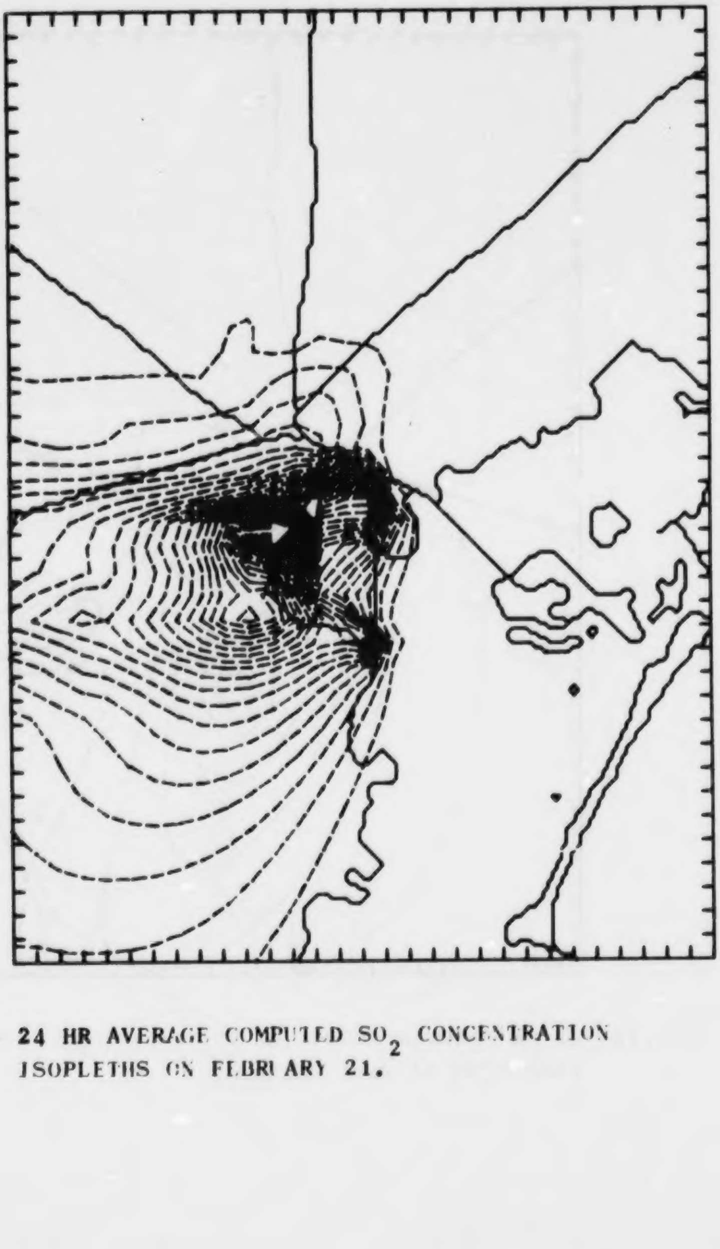

FIG. 13- 24 HR AVERAGE COMPUTED SO_2 CONCENTRATION ISOPLETHS ON FEBRUARY 21.

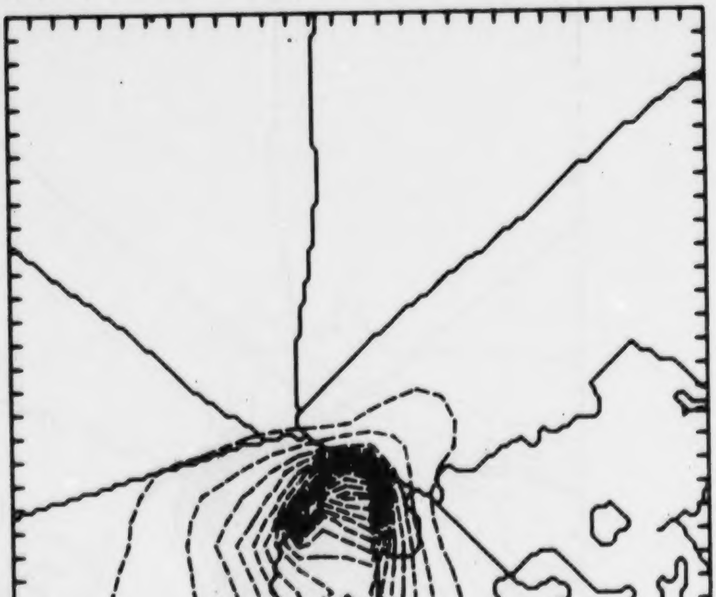

FIG. 14- 24 HR AVERAGE COMPUTED SO_2 CONCENTRATION ISOPLETHS ON AUGUST 3.

7th International Technical Meeting
on Air Pollution Modeling and its Application

A Three-Dimensional Advective-Diffusive Model for Long Range Sulfate Transport and Transformation

B. A. Egan, K. S. Rao, A. Bass

Environmental Research & Technology, Inc.
696 Virginia Road, Concord, Massachusetts 01742

September 7-10, 1976
Airlie Virginia
United States of America

A Three-Dimensional Advective-Diffusive Model for Long Range Sulfate Transport and Transformation

B. A. Egan, K. S. Rao,* A. Bass

Environmental Research & Technology, Inc.
696 Virginia Road, Concord, Massachusetts 01742

INTRODUCTION

There is a recent increase of concern that sulfates in the atmosphere may have been contributing to the health hazards of air pollution, adverse ecological effects due to increased acidity in lakes, corrosion and degradation of materials and a general reduction of visibility. As more information has been developed on the mechanisms for formation of sulfates in the atmosphere it has become apparent that many other pollutants such as nitrates and trace metals may be involved in the mechanisms of sulfate production. The concern over sulfates introduces a number of issues of concern to air quality modelers which differ from those which have been historically addressed when identifying air pollution control measures. Specifically, current studies in the United States and Europe indicate that the exposure to sulfate particulates resulting from anthropogenic SO_2 emissions covers large regions extending for hundreds of kilometers downwind from major urban sources. It appears that the relatively slow chemical transformations of SO_2 to sulfates causes the major impact of sources to be far downwind. Predicting sulfate levels then becomes a long range transport problem involving consideration of meteorological flow conditions over scales of hundreds of kilometers, a detailed knowledge of the various sources of emissions of sulfur oxides and other pollutants over the region, and an understanding of the potentially very complicated chemical interactions. Strategies for the control of sulfates must then transcend regional approaches limited by political boundaries and may involve control of sources far removed from the geographical regions to be protected. Specific control measures to be addressed include the effects of increased use of tall stacks, industrial planning on a continental scale and possible use of temporal controls involving the impact of one region's emissions on the air quality of another region. A large scale Sulfate Regional Experiment (SURE) program has been proposed to further our understanding of the production and dispersion of atmospheric sulfates. This paper addresses one aspect of a design study for SURE: the development/adaptation of a numerical grid model for the calculation of SO_2 and $SO_4^=$ over large regional scales. The modeling effort was directed toward providing guidance in the design of the field program. Data from the experimental program will be used to test a number of cause and effect hypotheses associated with sulfate air quality levels (Hidy, et. al., 1976) and will be used to develop a mathematical model for use in defining control strategies.

---

*Present Affiliation: NOAA - ARL Atmospheric Turbulence and Diffusion Laboratory, P.O. Box E, Oak Ridge, TN 37830.

MODEL DESCRIPTION AND FORMULATIONS

The three-dimensional grid cell numerical model utilized for this first-phase effort is an adaptation of the advection-diffusion transport model of Egan and Mahoney (1972). The model essentially solves the mass conservation (tracer) equation which includes terms describing the horizontal advection transport, turbulent diffusion, emission, chemical transformation, and deposition processes. The model was set up to solve the following mass conservation equations for two species in a non-divergent flow field:

$$\frac{\partial C_1}{\partial t} = - U \frac{\partial C_1}{\partial x} - V \frac{\partial C_1}{\partial y} + \frac{\partial}{\partial z} (K \frac{\partial C_1}{\partial z}) + \frac{Q}{h_i} - k_t C_1 \qquad (1)$$

$$\frac{\partial C_2}{\partial t} = - U \frac{\partial C_2}{\partial x} - V \frac{\partial C_2}{\partial y} + \frac{\partial}{\partial z} (K \frac{\partial C_2}{\partial z}) + \frac{3}{2} k_t C_2 \qquad (2)$$

where subscripts 1 and 2 denote SO_2 and $SO_4^=$ species respectively, C is the concentration, K is the vertical eddy diffusivity, Q is the SO_2 area-emission rate in the grid cell of height h_i, and k_t is the transformation rate of SO_2 to $SO_4^=$. The factor of 3/2 in (2) enters from the ratio from molecular weights of $SO_4^=$ to SO_2.

The deposition of the species at the earth's surface is described by the boundary condition:

$$[K \frac{\partial C}{\partial z}]_{z=0} = (1 - r) \overline{K} C_o/\overline{h} \qquad (3)$$

where r is a reflection coefficient defined by

$$r = 1 - V_d \overline{h}/\overline{K}, \quad 0 \leq r \leq 1 \qquad (4)$$

In Eqs. (3) and (4), $\overline{h}$ and $\overline{K}$ are the mean depth and the mean eddy diffusivity of the lowest two vertical layers, C_o is the ground-level concentration, and V_d is the deposition velocity of the pollutant. The latter is dependent upon the type of pollutant material, the type of deposition substrate, and the meteorological conditions. Lateral spread of emissions from a grid element by horizontal diffusion was considered to be negligible compared to the horizontal transport by mean wind and vertical turbulent diffusion. In effect, the 'narrow plume hypothesis' of Calder (1969) was adopted. Therefore, the governing equations of the model do not include the horizontal diffusion terms although these could be readily added.

The computational scheme employed is based on a forward time step-explicit computational scheme which conserves not only the pollutant mass in each cell but also the first and second moments of the mass distribution within each cell. Conserving these statistical features of the mass distribution results in a suppression of the pseudo-diffusive errors which are common to conventional finite difference procedures used for the solution of the advective terms. This is important because uncontrolled numerical pseudo-diffusion effects are largest when large grid cell spacing is to be utilized and can result in significant errors when spatially and temporally varying meteorological input data are utilized. Numerical diffusion effects will also propagate to produce significant errors in the chemical reactive terms since, for first order reactions, production or loss terms are proportional to concentration levels.

APPLICATION OF THE MODEL

The region selected for the test of the model had dimensions of 2080 km (east-west) x 1360 km (north-south) in the eastern United States and southern Canada and is shown in Figure 1. The region is divided into 26 x 17 cells having dimensions of 80 x 80 km. To accomplish the turbulent diffusion calculations the model has three levels in the vertical, having depths of 0-300 m, 300-700 m and 700-1500 m. Emission rates for SO_2 were developed for each of these 1326 grid elements by analysis of the NEDS emission inventory data. The emissions were classified by the effective height of emission, season, and species and stored on a computer disk for link-up with a computer program. For a given 80 x 80 km region, the emissions were allocated to the three layers, depending upon the effective effluent release height for elevated point sources, defined as the stack height plus plume rise. The plume rise for each major source was computed using emission data and a nominal windspeed of 5 m per second with Briggs' plume rise formula for near-neutral stability conditions (Briggs 1969). All ground-level point and area source emissions are introduced into the lowest layer to the ground; thus this model is particularly suited to investigate the effects of tall stacks on atmospheric concentration levels of SO_x pollutants. Values of the deposition velocities for SO_2 and $SO_4^=$ used were 1.3 cm per second and 0.1 cm per second, respectively. These values appear to be in the general range of experimentally determined rates. The top boundary of the computational grid was assumed to be perfectly reflecting (r=1).

For purposes of testing the model, data available for an October 2-5, 1974 "episode" were utilized. SO_2 and $SO_4^=$ data were obtained from sampling stations which were part of the AIRMAP system operated by Environmental Research & Technology, Inc. Locations of the monitoring points are also shown in Figure 1.

For the duration of the episode, the observed mean wind speed and direction at each 1000 ft. level above the mean sea level, at 12-hour intervals, were available from the National Weather Service radiosonde data. These data were plotted as U and V isotachs over the horizontal grid region for each of the three grid levels. These winds were corrected for the local topography and interpolated in the program to calculate the U and V components at the center of each grid cell. The mean wind field was assumed to be two-dimensional. The three air layers are vertically displaced parallel to the local topography such that each of the layers has uniform thickness over the entire region.

The model has the capability of incorporating temporally and spatially varying mixing depths (H) input data. In the present study observed mixing depth data for the episode period modeled were not readily available, and a constant value of mixing depths of 1500 m was assumed.

The profile of the vertical eddy diffusivity (K) used in equations (1) and (2) was developed to have the correct asymptotic behavior for regions of the atmosphere very near the surface and the region very near the assumed inversion height. At intermediate levels the profile was assigned values to agree with Mack et. al., (1972) and Pasquill (1975). In the present study, neutral conditions were assumed for simplicity and the K-profile is specified and extrapolated above the surface layer ($\delta \approx 100$m) as shown in Figure 2 where it is also compared nondimensionally with the neutral K-profiles from other investigatious. From this profile discrete values of K are specified for each of the three vertical layers. The convergence and stability of the numerical solution are determined by the following criteria:

$$U \frac{\Delta t}{\Delta x} \leq 1 \qquad \text{for advection}$$

$$K_i \frac{\Delta t}{h_i^2} < 0.5 \qquad \text{for eddy diffusion}$$

For the grid system utilized, the latter is the more stringent of the two criteria and therefore is a necessary and sufficient condition for numerical stability. It determines the maximum time step (Δt) that can be specified for the integration. For the K values specified in the present grid, it was possible to use Δt = 1-hour. For each time step, a grid comprised of 26 x 17 x 3 cells is swept twice to solve the two coupled tracer equations by calculating the three moments for each species. New wind inputs are specified every 12 hours. In spite of the complexity of the program, the computing times for a 24-hour integration are very reasonable (under five minutes in the present study).

NUMERICAL MODEL RESULTS

The tracer equations were integrated with respect to time over a 24-hour period (October 3, 1974) selected for modeling. Two computer runs are made with k_t = 1 percent per hour and k_t = 2 percent per hour; for both runs, the deposition velocities specified are V_{d_1} = 1.3 cm/sec and V_{d_2} = 0.1 cm/sec. By summation of the values for each time step the 24-hour average concentrations of SO_2 and $SO_4^=$ in each grid cell can be obtained. The calculated concentrations in level 1 were then compared with the ground-level concentrations observed at ERT's AIRMAP Network receptors for this sampling period. The available $SO_4^=$ data from filter analyses are plotted against the predicted $SO_4^=$ concentrations for two different values of the transformation rate as shown in Figure 3. The plot shows a good correlation between predictions and observations, and suggests a value of k_t = 1 to 2 percent per hour as appropriate for the model. A similar plot for the ground-level SO_2 concentrations is shown in Figure 4. Here also the agreement between observations and predictions is satisfactory but indicates more scatter than the $SO_4^=$ data. This may be a result of the fact that SO_2 levels are expected to have a higher spatial variability in the near field of sources (because the maximum impact is more local) and thus are not well modeled by large grid cell representations. The comparatively small change between the predicted SO_2 concentrations for the two transformation rates indicates that the chemical sink term in Eq. (1) is not important.

For k_t = 1 percent per hour, the isopleths of the predicted daily average $SO_4^=$ and SO_2 concentrations over the horizontal grid region in level 1 are shown in Figures 5 and 6, respectively. Analysis of the model results indicates that the SO_2 levels show a higher spatial variability than the $SO_4^=$ values and are more directly correlated with the SO_2 emission inventory than are the sulfate values. Similar isopleths for vertical levels 2 and 3 are shown in Figures 7 to 10. The results suggest that the mid-level emissions strongly influence the estimated ground-level $SO_4^=$ concentrations. It appears that intensive contributions to the latter occur from sources within an influence zone of 100-300 km, which supports the regional scale model treatment of the atmospheric sulfate transport.

CONCLUSIONS

Models for long range transport of pollutants need to be able to treat both temporally and spatially variable meteorological conditions. Numerical simulation models based on "K theory" provide one approach. Our results with such a model show that advective transport and chemical transformation rates are dominant factors in predicting ground-level sulfate concentrations. In this study we have only performed preliminary tests of this model. For assessing alternative sulfate control strategies, further developments will be required in the areas of better definition of emissions inventories, meteorological transport fields, and reactive chemistry transformation rates as a function of meteorological conditions and other atmospheric constituents. Comprehensive data from field measurement studies will be essential to further develop and verify long range transport models for atmospheric sulfates.

ACKNOWLEDGEMENTS

The work reported in this paper is part of the Sulfate Regional Experiment (SURE) Design Project sponsored by the Electric Power Research Institute (EPRI). The authors wish to acknowledge the assistance of Mrs. C. Ingersoll and Messrs. I. Thomson and D. McNaughton in the preparation of inputs to the model.

REFERENCES

1. Hidy, G., et al, 1976: Design of the Sulfate Regional Experiment (SURE). Prepared for Electric Power Research Institute, Palo Alto, California.

2. Egan, B. A. and J. R. Mahoney, 1972: Applications of a numerical air pollution transport model to dispersion in the atmospheric boundary layer, J. Appl. Meteorol., 11, pp. 1023-1039.

3. Calder, K. L., 1969: A Narrow Plume Simplification for Multiple Urban Source Models. Unpubl. ms., Environmental Protection Agency, Research Triangle Park, N.C. 11 pp.

4. Briggs, G. A., 1969: Plume Rise, TID-25075, Clearinghouse for FSTI, Springfield, VA 22151, 82 pp.

5. Mack, E. J. et al, 1972: A Field Investigation and Numerical Simulation of Coastal Fog, Tech. Report, CAL NO. CJ-5055-M-1, CALSPAN, Buffalo, NY.

6. Pasquill, F., 1975: The Dispersion of Materials in the Atmospheric Boundary Layer - The Basis for Generalization, Workshop Lectures on Air Pollution and Environmental Impact Analysis, D. A. Haugen, Coordinator, Am. Meteorolog. Soc., Boston, MA pp. 1-35.

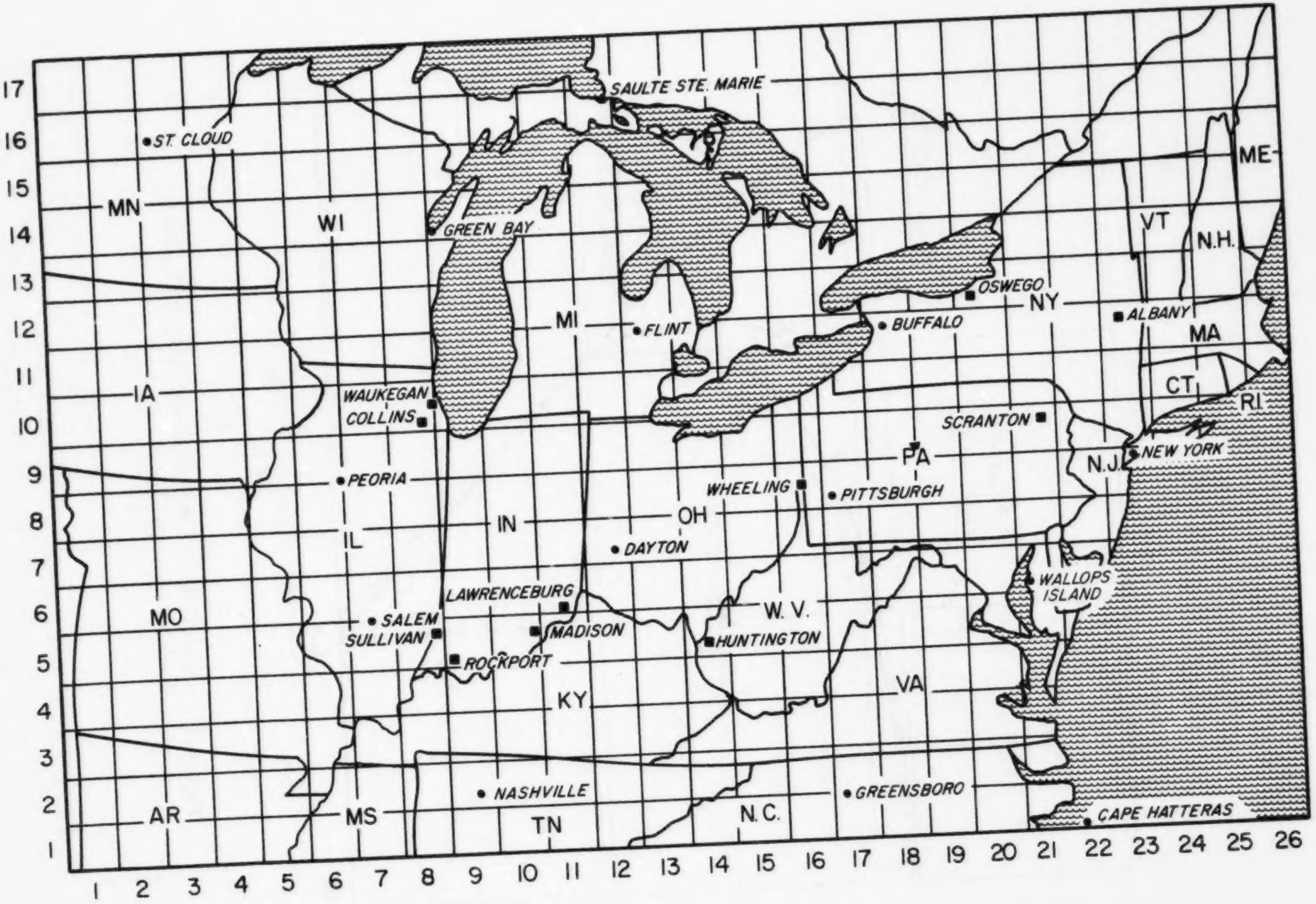
SAULTE STE. MARIE
ST. CLOUD
MN
WI
GREEN BAY
ME
VT
N.H.
OSWEGO
NY
ALBANY
MA
MI
FLINT
BUFFALO
IA
WAUKEGAN
COLLINS
CT
RI
SCRANTON
PA
N.J.
NEW YORK
PEORIA
WHEELING
PITTSBURGH
IN
OH
IL
DAYTON
WALLOPS ISLAND
LAWRENCEBURG
W. V.
MO
SALEM
SULLIVAN
MADISON
HUNTINGTON
ROCKPORT
VA
KY
NASHVILLE
GREENSBORO
AR
MS
TN
N.C.
CAPE HATTERAS
1
2
3
4
5
6
7
8
9
10
11
12
13
14
15
16
17
18
19
20
21
22
23
24
25
26

Figure 1 Computational Grid Plan and Monitoring Data Locations (Indicated by Squares).

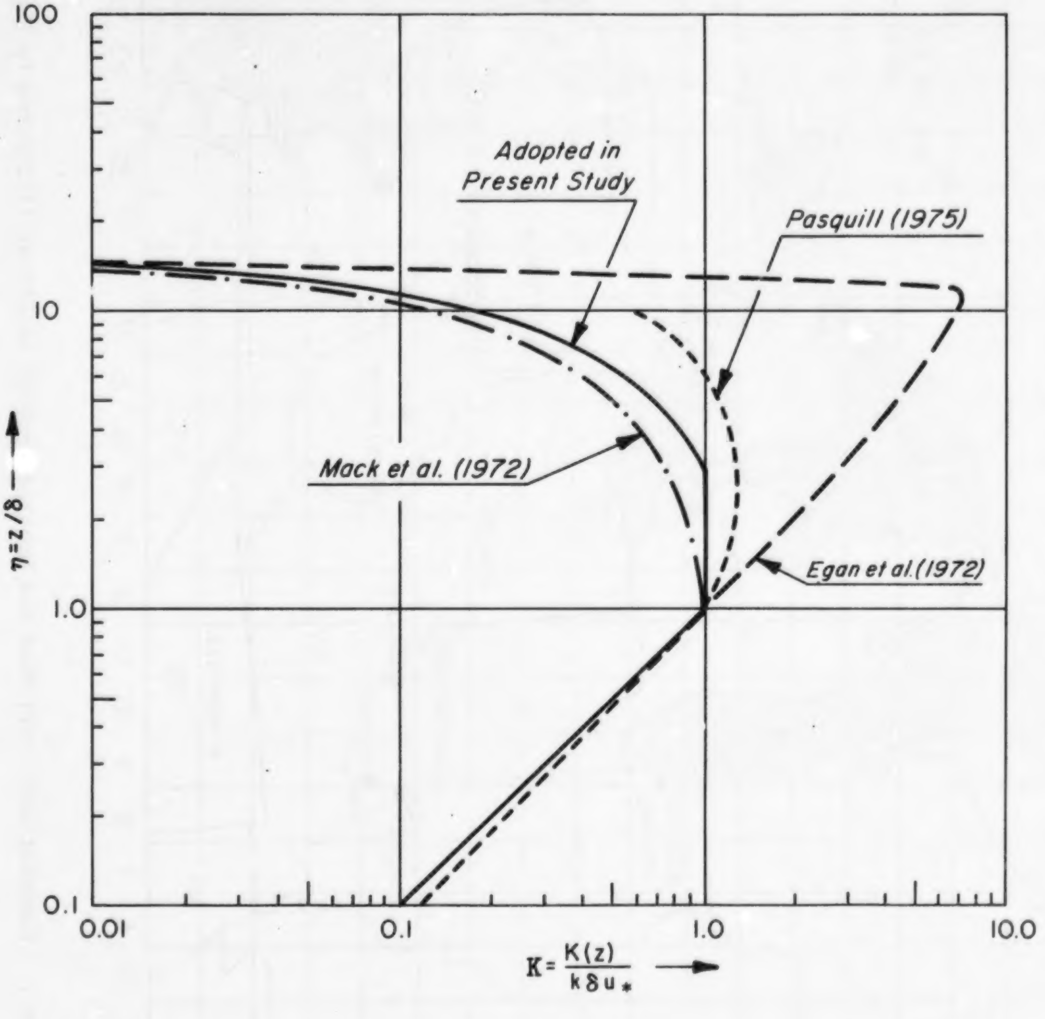

Figure 2 Comparison of Nondimensional Eddy Diffusivity Profiles (Neutral Case).

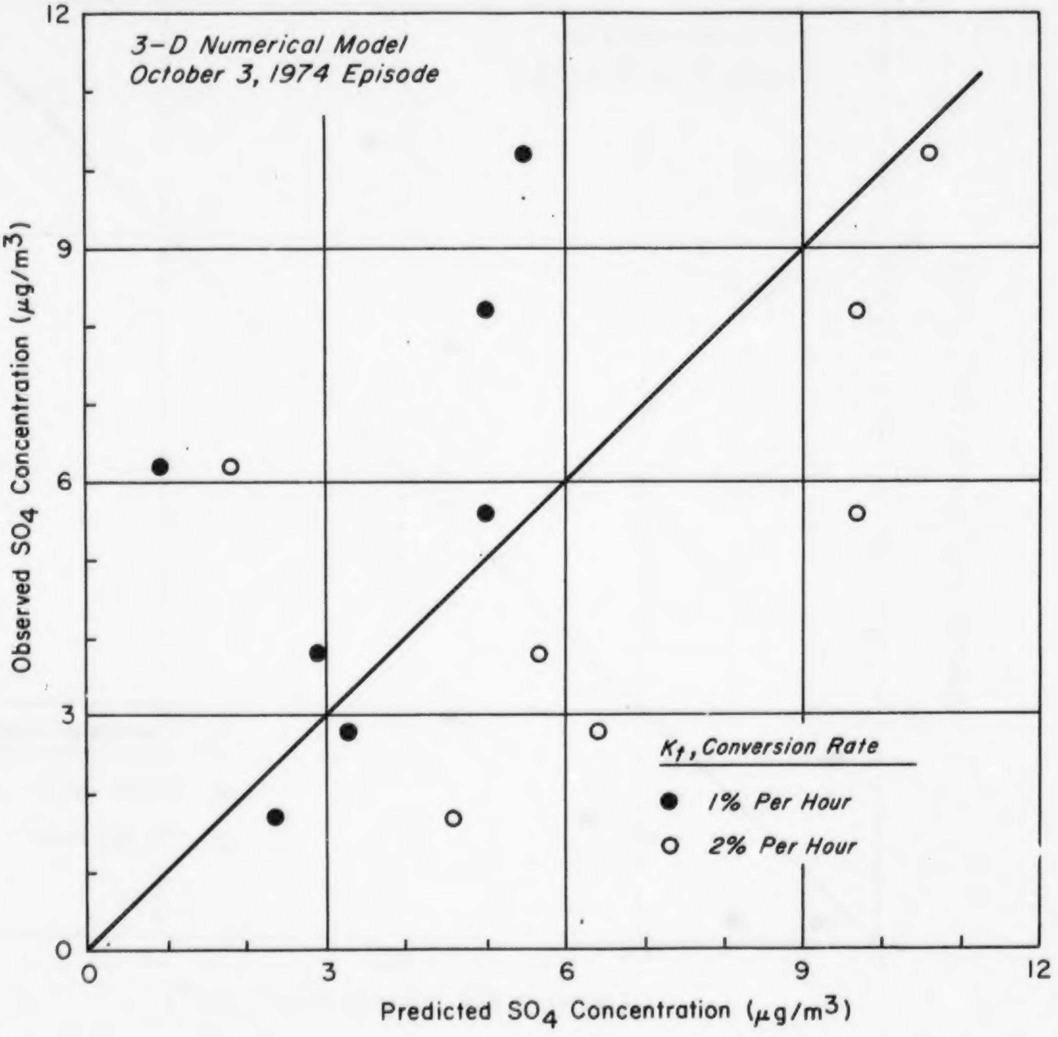

Figure 3 Comparison of Predicted to Observed Ground-Level $SO_4^=$ Concentrations

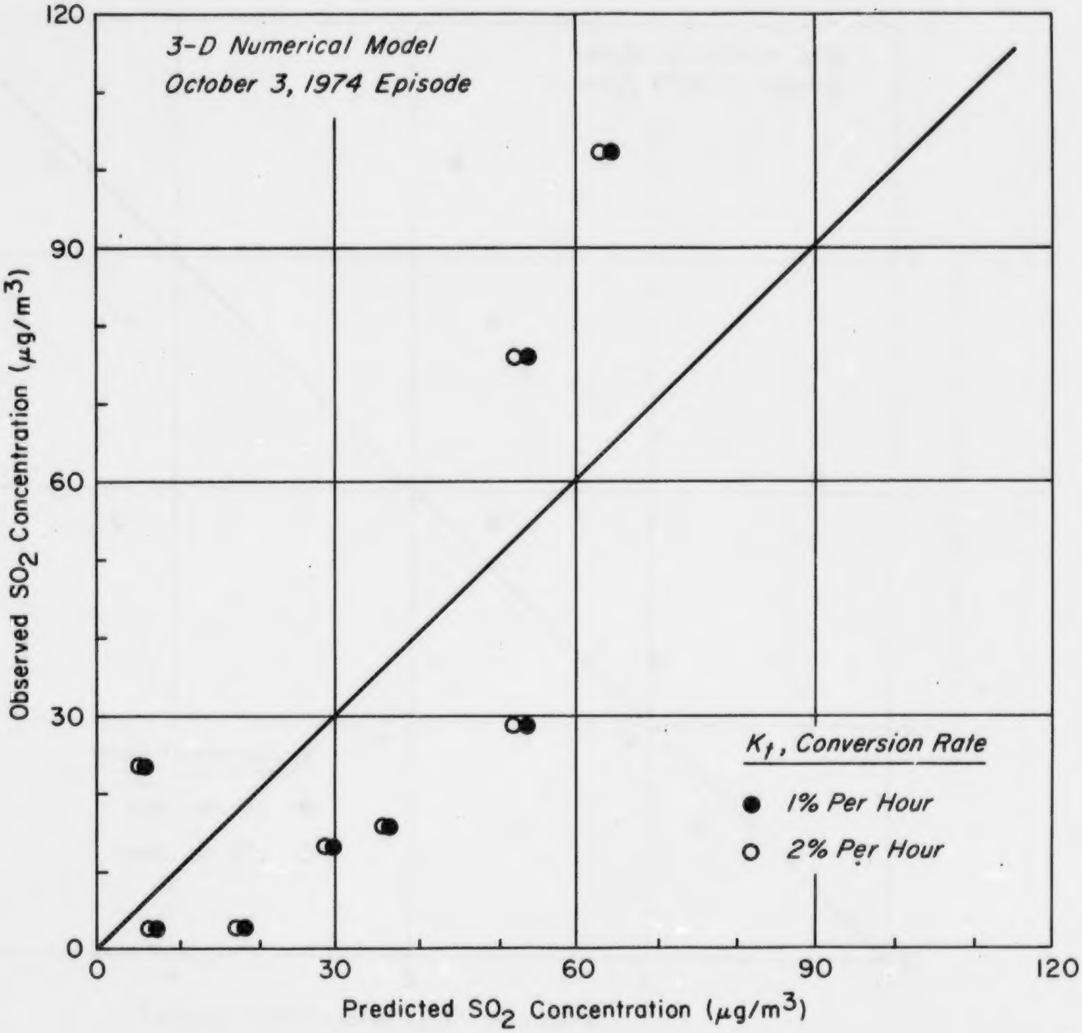

Figure 4 Comparison of Predicted to Observed Ground-Level SO_2 Concentrations

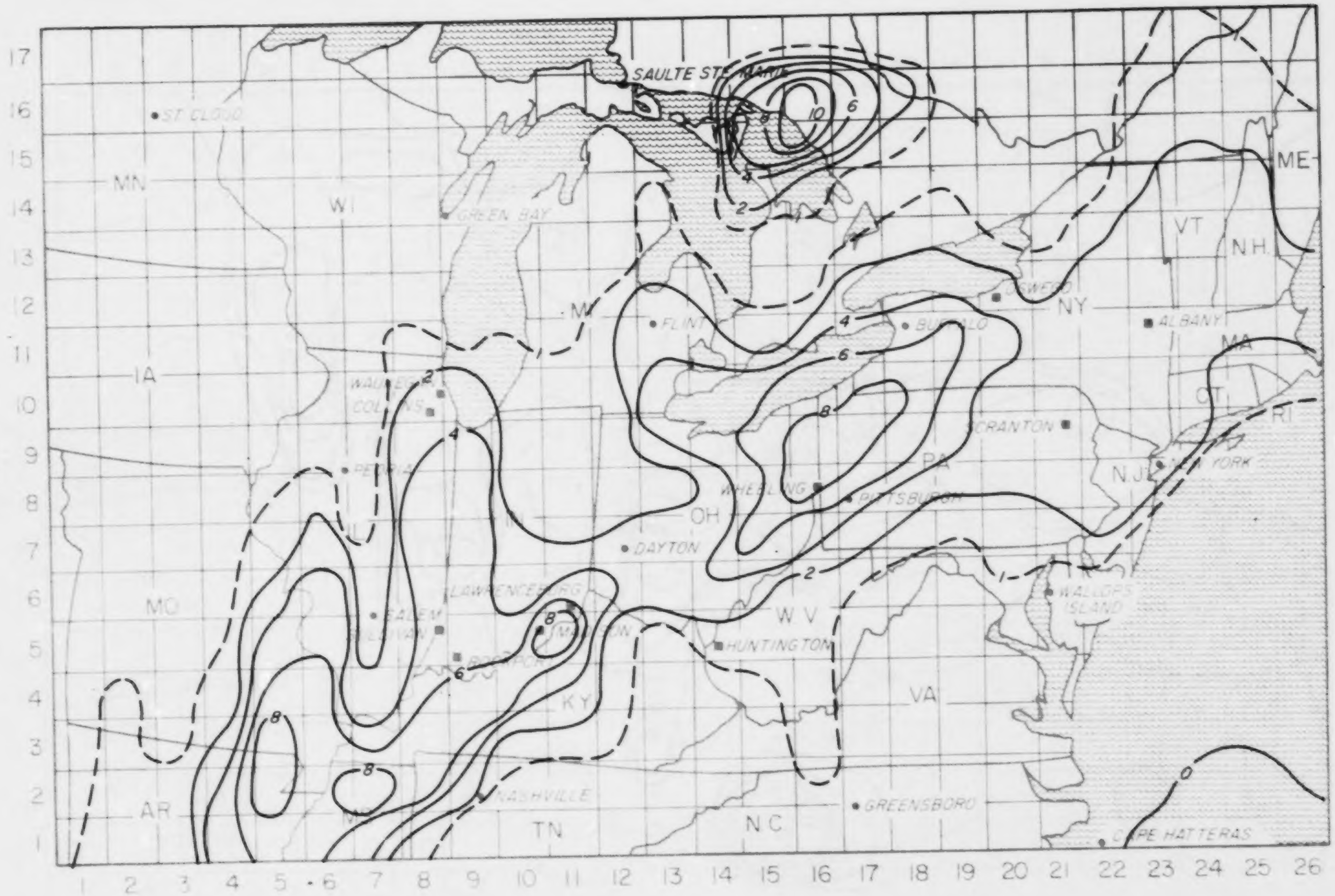
SAULTE STE MARIE
ST CLOUD
GREEN BAY
FLINT
BUFFALO
OSWEGO
ALBANY
WAUKEGAN
COLLINS
SCRANTON
NEW YORK
PEORIA
WHEELING
PITTSBURGH
DAYTON
LAWRENCEBURG
SALEM
SULLIVAN
MADISON
HUNTINGTON
WALLOPS ISLAND
NASHVILLE
GREENSBORO
CAPE HATTERAS
MN
WI
MI
IA
IL
IN
OH
PA
NY
VT
NH
ME
MA
CT
RI
NJ
MO
KY
WV
VA
AR
TN
NC
MS
0
2
4
6
8
10
1
2
3
4
5
6
7
8
9
10
11
12
13
14
15
16
17
18
19
20
21
22
23
24
25
26

Figure 5 Isopleths of $SO_4^=$ Concentrations ($\mu g/m^3$) in the Lowest Grid Level Calculated for October 3, 1974

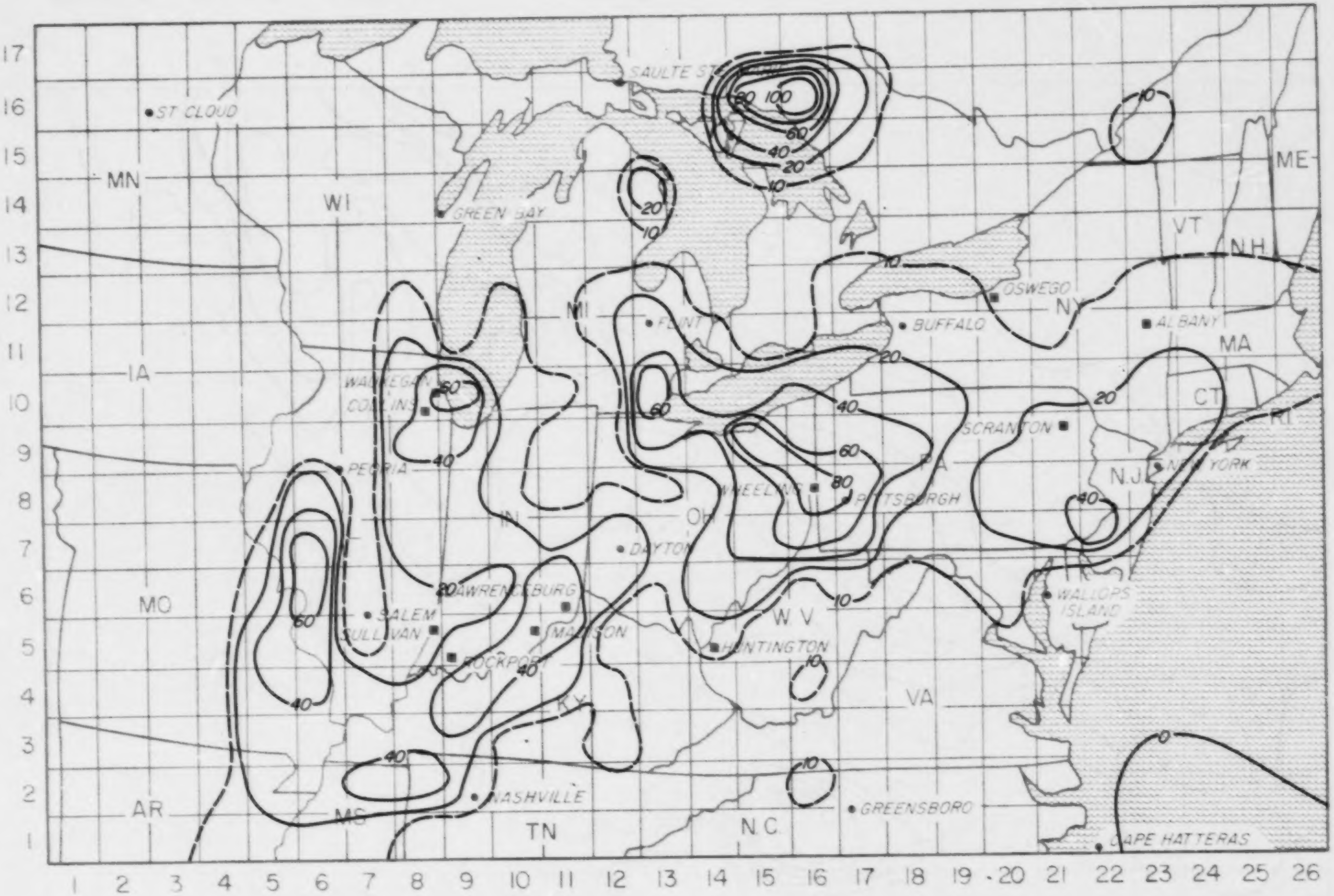
ST CLOUD
SAULTE STE MARIE
GREEN BAY
MN
WI
IA
MO
AR
MS
TN
KY
IN
OH
MI
W V
VA
N.C
PA
NY
VT
NH
ME
MA
CT
RI
N.J.
FLINT
BUFFALO
OSWEGO
ALBANY
SCRANTON
NEW YORK
WAUKEGAN
COLLINS
PEORIA
SALEM
SULLIVAN
LAWRENCEBURG
MADISON
ROCKPORT
DAYTON
WHEELING
PITTSBURGH
HUNTINGTON
WALLOPS ISLAND
NASHVILLE
GREENSBORO
CAPE HATTERAS
100
80
60
40
20
10
0
1 2 3 4 5 6 7 8 9 10 11 12 13 14 15 16 17 18 19 20 21 22 23 24 25 26
1 2 3 4 5 6 7 8 9 10 11 12 13 14 15 16 17

Figure 6 Isopleths of SO_2 Concentrations ($\mu g/m^3$) in the Lowest Grid Level Calculated for October 3, 1974

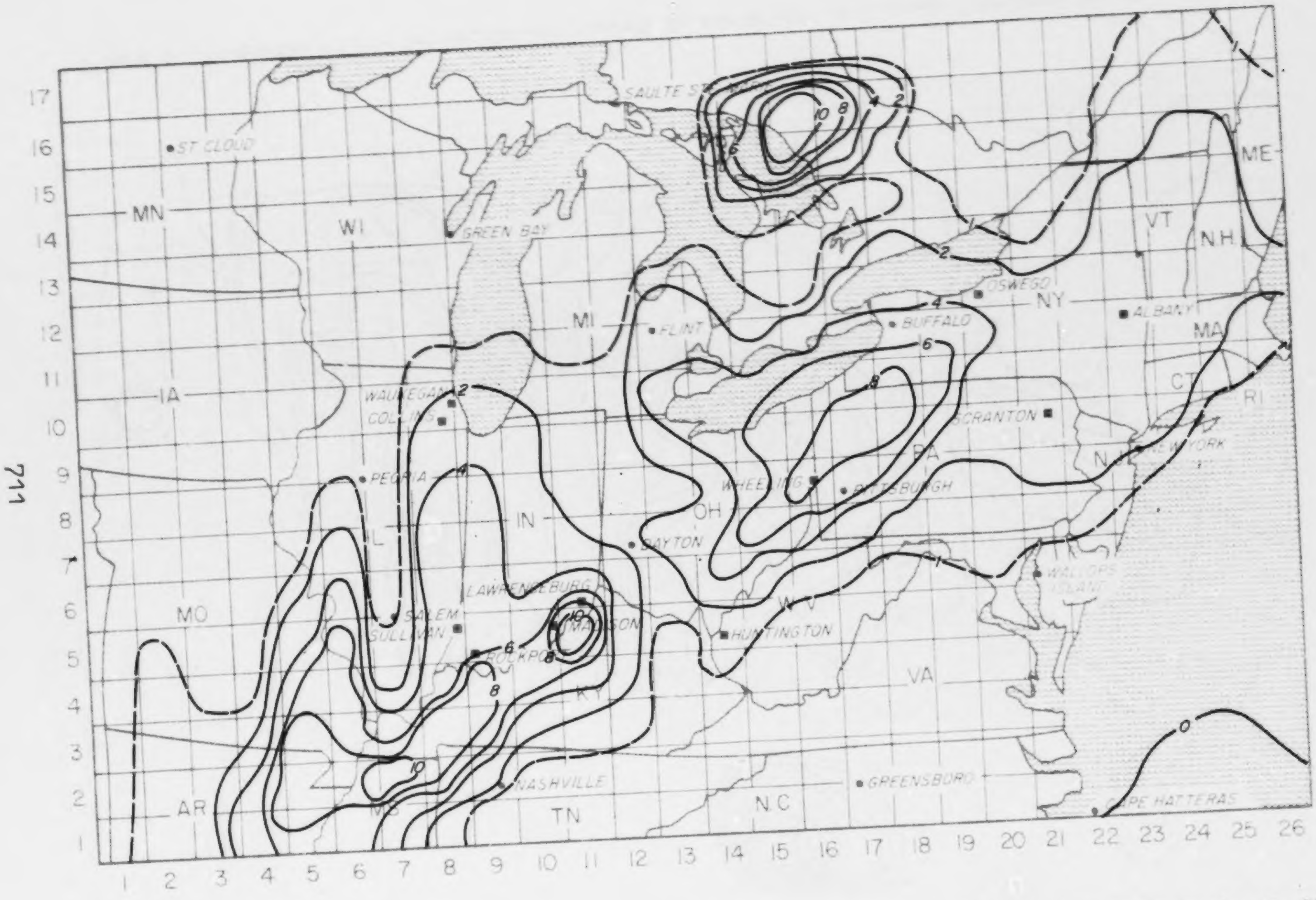
ST CLOUD
SAULTE ST
GREEN BAY
FLINT
BUFFALO
OSWEGO
ALBANY
WAUKEGAN
COLLINS
SCRANTON
NEW YORK
PEORIA
WHEELING
PITTSBURGH
DAYTON
WALLOPS ISLAND
LAWRENCEBURG
SALEM
SULLIVAN
MADISON
ROCKPORT
HUNTINGTON
NASHVILLE
GREENSBORO
CAPE HATTERAS
MN
WI
MI
IA
IL
IN
OH
PA
NY
VT
NH
ME
MA
CT
RI
NJ
MO
KY
WV
VA
AR
MS
TN
NC
1
2
4
6
8
10
0
1 2 3 4 5 6 7 8 9 10 11 12 13 14 15 16 17 18 19 20 21 22 23 24 25 26
1 2 3 4 5 6 7 8 9 10 11 12 13 14 15 16 17

Figure 7 Isopleths of $SO_4^{=}$ Concentrations ($\mu g/m^3$) in the Middle Grid Level Calculated for October 3, 1974

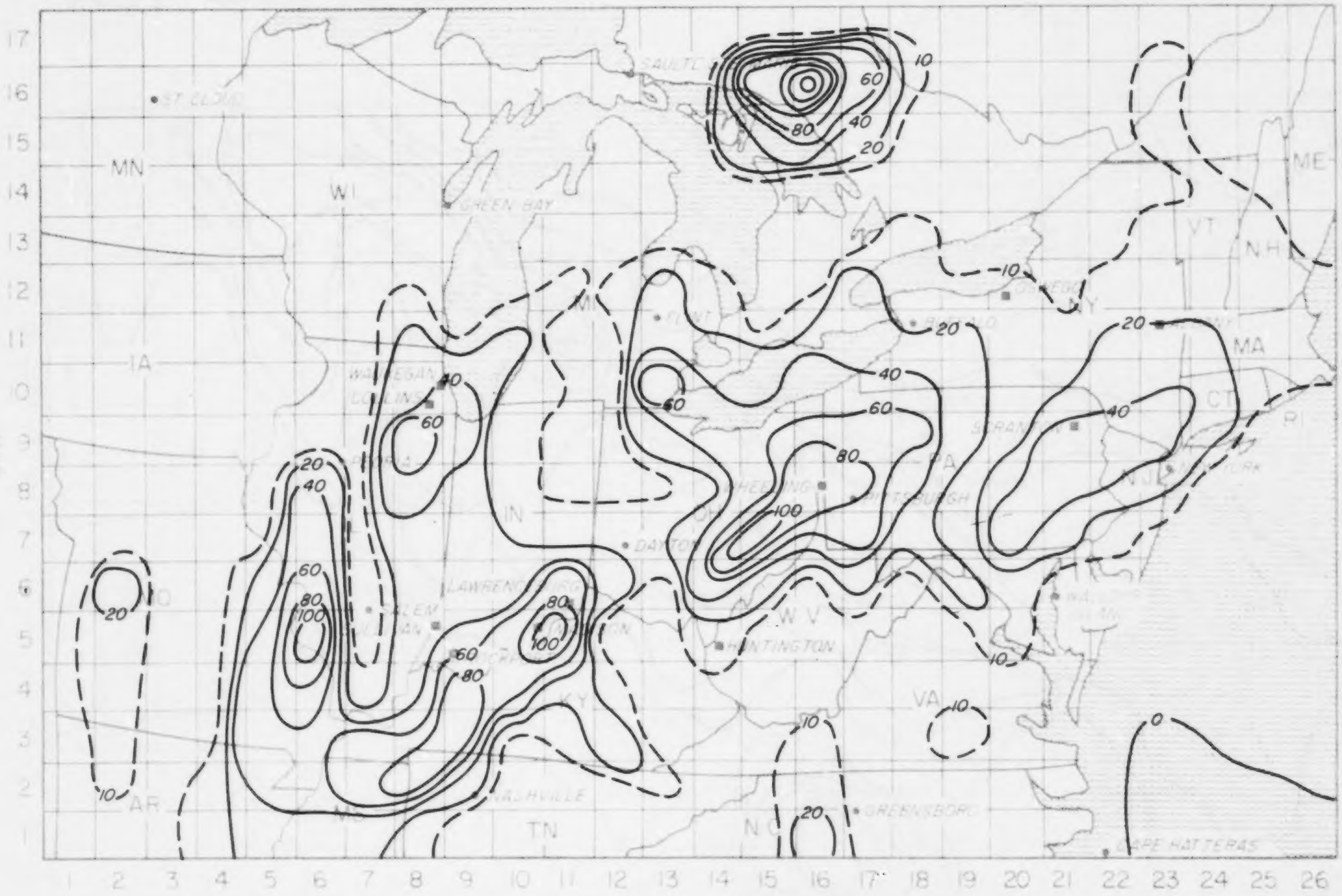
MN
WI
IA
MI
IN
MO
AR
TN
KY
OH
W V
VA
N C
PA
NY
VT
N.H
ME
MA
CT
RI
NJ
ST. CLOUD
GREEN BAY
SAULT
WAUKEGAN
COLLINS
PEORIA
LAWRENCEBURG
DAYTON
FLINT
WHEELING
PITTSBURGH
HUNTINGTON
BUFFALO
SCRANTON
NEW YORK
GREENSBORO
NASHVILLE
CAPE HATTERAS
10
20
40
60
80
100
0
1 2 3 4 5 6 7 8 9 10 11 12 13 14 15 16 17 18 19 20 21 22 23 24 25 26
1 2 3 4 5 6 7 8 9 10 11 12 13 14 15 16 17

Figure 8 Isopleths of SO_2 Concentrations ($\mu g/m^3$) in the Middle Grid Level Calculated for October 3, 1974

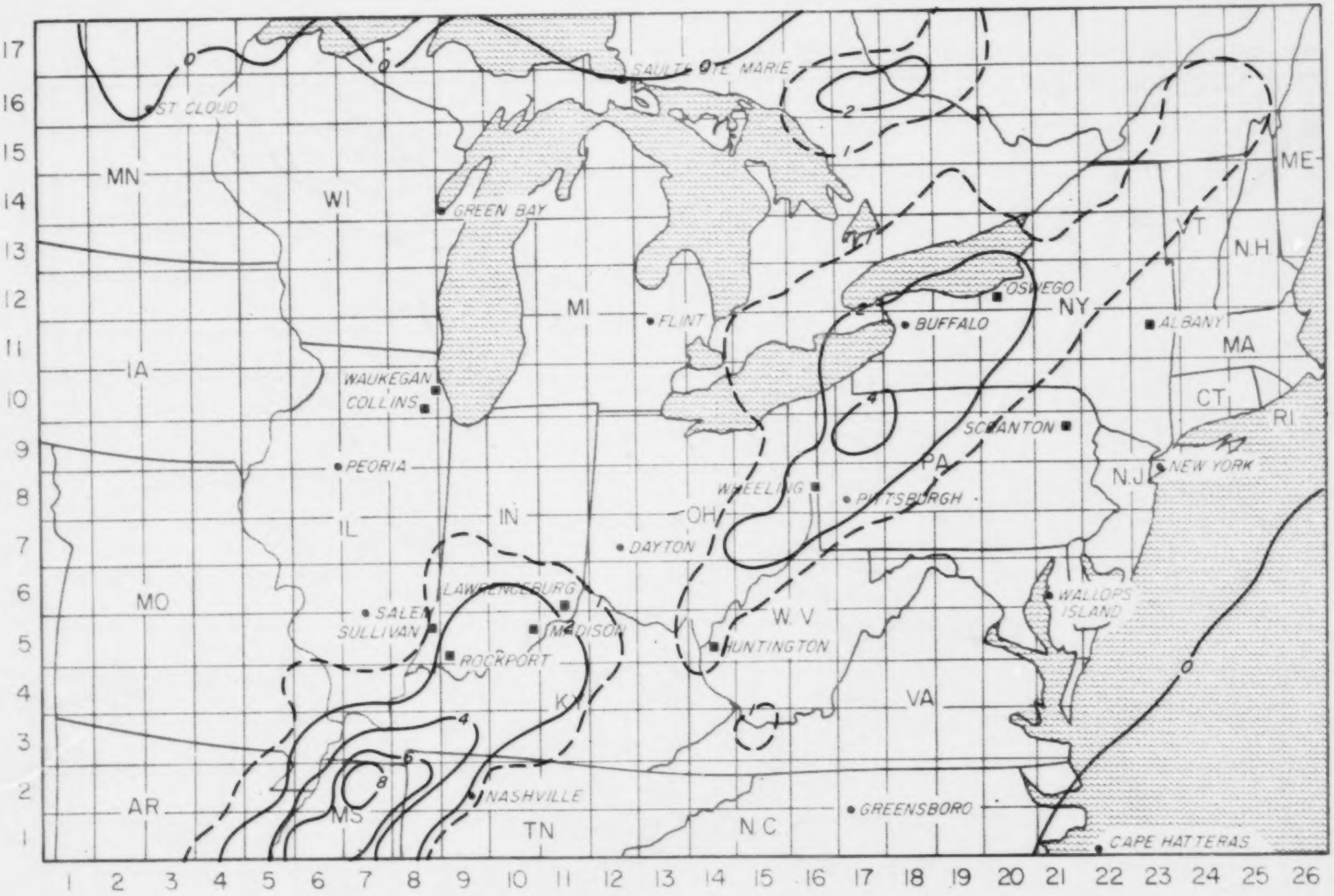
ST CLOUD
SAULT STE MARIE
GREEN BAY
FLINT
WAUKEGAN
COLLINS
PEORIA
DAYTON
WHEELING
PITTSBURGH
BUFFALO
OSWEGO
ALBANY
SCRANTON
NEW YORK
LAWRENCEBURG
SALEM
SULLIVAN
MADISON
ROCKPORT
HUNTINGTON
WALLOPS ISLAND
NASHVILLE
GREENSBORO
CAPE HATTERAS
MN
WI
IA
MI
IL
IN
OH
MO
KY
W.V
VA
PA
NY
N.J
VT
N.H
ME
MA
CT
RI
AR
MS
TN
N.C
0
1
2
4
6
8
17
16
15
14
13
12
11
10
9
8
7
6
5
4
3
2
1
1 2 3 4 5 6 7 8 9 10 11 12 13 14 15 16 17 18 19 20 21 22 23 24 25 26

Figure 9 Isopleths of $SO_4^=$ Concentrations ($\mu g/m^3$) in the Highest Grid Level Calculated for October 3, 1974

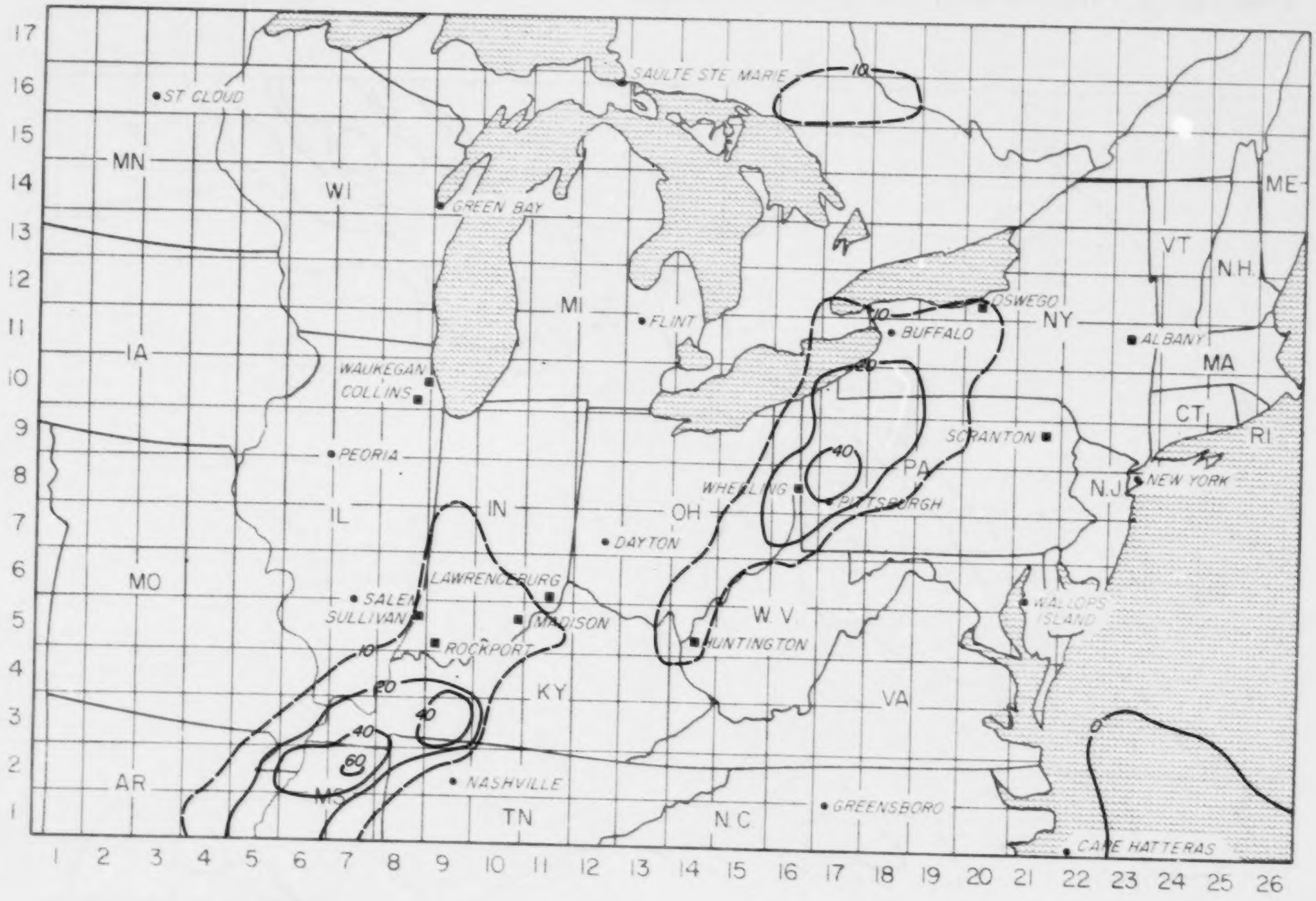
ST CLOUD
SAULTE STE MARIE
GREEN BAY
WAUKEGAN
COLLINS
PEORIA
FLINT
DAYTON
SALEM
SULLIVAN
LAWRENCEBURG
MADISON
ROCKPORT
NASHVILLE
WHEELING
PITTSBURGH
HUNTINGTON
BUFFALO
OSWEGO
SCRANTON
ALBANY
NEW YORK
WALLOPS ISLAND
GREENSBORO
CAPE HATTERAS
MN
WI
IA
IL
MO
AR
MI
IN
OH
KY
TN
MS
W.V.
VA
N.C.
PA
NY
N.J.
VT
N.H.
ME
MA
CT
RI
10
20
40
60
0
1
2
3
4
5
6
7
8
9
10
11
12
13
14
15
16
17
18
19
20
21
22
23
24
25
26

Figure 10 Isopleths of SO_2 Concentrations ($\mu g/m^3$) in the Highest Grid Level Calculated for October 3, 1974

An empirical equation for simulating maximum concentration values occuring at buildings projecting into the path of a plume in the immediate vicinity of an emission source

J. Giebel
Landesanstalt für Immissions- und Bodennutzungsschutz,
Essen, FRG

When a heating plant or another source with smaller emissions is planned in the immediate vicinity of higher buildings the question arises: Must the stack of the source be higher than the surrounding buildings or not. To answer this question we compared simulated concentrations with ambient air quality standards. For distances more than 5o m concentrations were simulated with an equation of the Gaussian-type using the standard deviations of Pasquill and Turner,[1].D.
For distances less than 5o m we used a formula found in Stern's book "Air Pollution" [5]. But this formula gives only an estimate of the short period maximum concentration in the path of the plume. There was however a demand for knowing maximum concentrations averaged over a period of half an hour or so to be able to compare the simulated concentrations with the ambient air quality standards. Because of that and since there was not much confidence in the Gaussian type model when used for distances less than 1oo m, concentrations occurring at buildings projecting

into the path of a plume, coming from a gasfired heating plant, were measured /‾4_7. Picture No 1 shows the site where the measurements were taken. On the left side is the heating plant. The stack height is 9,5 m, extending 1,5 m above the flat roof of the heating plant.

At a distance of 38 m a building lies with a height of 24 m. 2o to about 7o m from the source is a building 31 m high. Measurements were taken at distances of 2o, 29, 4o and 49 m. The heights of the sampling points over the ground ranged from about 13 to 21 m. The distance of the sampling points to the building wall was 1 m.

Carbon dioxide and nitrogen oxides were measured; nitrogen oxides at the sampling points No 1, 2, 3 and 4 and carbon dioxide at the sampling points No 4, 5 and 6. The sampling time was 2o minutes. With the exception of nitrogen oxides at sampling point No 4 measurements were taken once an hour at each sampling point. The measurements were carried out from December to April. Beside the concentration measurements the emissions were measured, but not continually. Meteorological measurements were carried out, too. 3 m above the top of the heating plant wind direction and wind speed were measured. The maximum capacity of the gasfired heating plant was 3.2 Gcal/h, but the capacity used while measuring was only about o,8 Gcal/h.

The velocity with which the flue then came out of the stack was 2.3 m/s, the volume flux o,35 m^3/s and the temperature of the flue at the end of the stack 15o° C.

The introduction of buildings into a flow field causes a change in the velocity and pressure fields. The new fields are aerodynamically distorted. In the distorted region turbulence is high. The measurements show that very well. Short period concentrations were up to 9 times higher than the values averaged over 2o minutes. Picture No. 2 shows the distributions of the maximum values measured at 2.5 per cent of the time when the wind was blowing out of a sector of 45° from the stack to the sampling point. On the x-axis the concentration is given, on the y-axis the number of maximum concentration values for each sampling point, the sampling time being 2o minutes. In the squares the wind speed is given. It is mostly 1 or 2 m/s.

As was expected, the largest concentration values were measured at the source distance of 2o m, this being the shortest distance. At the sampling point in the corner of the building relatively few high values were found. The sampling points No 4 and 5 at the distance of 49 m gave concentrations as high as at the distance of 4o m at sampling point No 6. That is probably because the building wall causes the flue to turn into the direction of these sampling points No 4 and 5. The maximum values were mainly measured in the morning, the evening and in the night. The atmosphere was nearly always in a stable equilibrium; the wind speed was 1.5 m/s on the average. At this low wind speed mechanical turbulence is weak. The turbulent region is not so well developed. The influence of the local peculiarities of the building configuration on the wind field is weakened. When the maximum values were measured, the capacity of the heating plant was about o,8 Gcal/h. The emission of Nitrogen oxides was 24 mg/s.

The new equation was developed on the basis of the maximum concentrations measured at the sampling points No 1,2 and 6. It is given in picture No. 3

In the equation

S = concentration in mg/m^3

Q = emission in mg/s

u = wind speed in m/s

x = distance to the source along the path of the plume in m.

The equation simulates maximum concentration values that occur at objects projecting into the path of the plume in the immediate vicinity of a source; the source distance ranging perhaps from 1o to 8o m. The concentrations are to be expected in 2.5% of the time when the wind blows out of a sector of 45° from the source to the sampling point. The sampling time is 2o minutes.

The equation was compared with other formulas. The results are to be seen on picture No.3.

The"Stern-formula", referred to in the beginning, gives an estimate of the short period maximum in the path of the plume. The equation is based on the model given by scorer and Barret. It is developed especially for a 5 m/s wind and gives results which are in approximate agreement with the minimum dilution values obtained by Halitsky with wind tunnel experiments on a building of complicated shape.

Used for a 1 m/s wind the formula gives values which at a source distance of 2o m are about 4 times and at a source distance of 5o m 3 times larger than the concentrations calculated with the new equation. But the results of the "Stern-equation" are short period maximum concentrations wheras the results of the new equation are related to a sampling time of 2o minutes.

And as is known, the shorter the sampling time, the larger the maximum concentration. In the case of a Gaussian distribution at the plume axis the factor 4 is expected when the sampling times differ by about the factor 16 [1]. The two formulas then would give the same results when the Stern formula was related to a sampling time of about 9o seconds.

Comparisons with diffusion models of the Gaussian-type show the following results:
With the standard deviations of Mc Elroy and Pooler, Class V, stable equilibrium [13], the Gaussian model gives values which at a source distance of 100m are lower by about a factor 1,5. At this distance the validity range of the two formulas over-lap. But with the standard deviation of Pasquill and Turner Class D, neutral equilibrium [6], the Gaussian formula gives values which are larger by about the factor 25.
Mc. Elroy and Pooler obtained their standard deviations in St. Louis. The heights of the sources were low. The topography is similar to that where the measurements for the new equation were taken. The Pasquill Turner standard deviations on the contrary, come from relatively uncomplicated terrain in open country. That is presumably the reason for giving much larger results.

The comparisons with the "Stern-formula" and the equation of the Gaussian type with the standard deviations of Mc Elroy and Pooler suggest that the developed equation is not only valid for the building configuration where the measurements were carried out. I think therefore it can be used at other sites when source height, source distance and wind speed are similar.

1) Bringfelt, B. et al:
A Numerical Air Pollution Dispersion
Model for Central Stockholm
Atm, Environment, 8 (1974), S. 131/148.

2) Csanady, G.T.:
Turbulent Diffusion in the Environment
Dordrecht/Holland 1973

3) McElroy, J.L.:
A Comparative Study of Urban and Rural Dispersion
J. Appl. Meteorol., 8 (1969), S. 19/31

4) Emissions- und Immissionsmessungen am
St. Elisabeth-Hospital, Beckum, im Winterhalbjahr 72/73.
Interner Bericht der Ruhrgas AG, Berichts-Nr. LuK 2/74
Dorsten

5) Air Pollution, Bd. 1,
Air Pollution and Its Effects
Hrsg. A. C. Stern, 2. Auflage, Academic Press, New York 1968

6) VDI 2289, Blatt 2 (Entwurf)
Ausbreitung luftfremder Stoffe in der Atmosphäre
Schornsteinhöhen unter Berücksichtigung der Bebauung
und des Bewuchses
Hrsg. VDI-Kommission Reinhaltung der Luft
Beuth Vertrieb Köln-Berlin

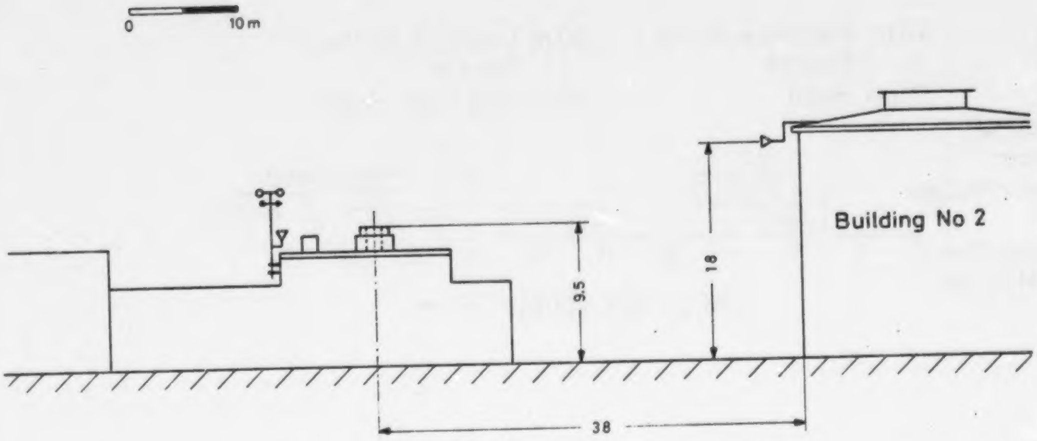
0
10 m
Building No 2
9.5
18
38

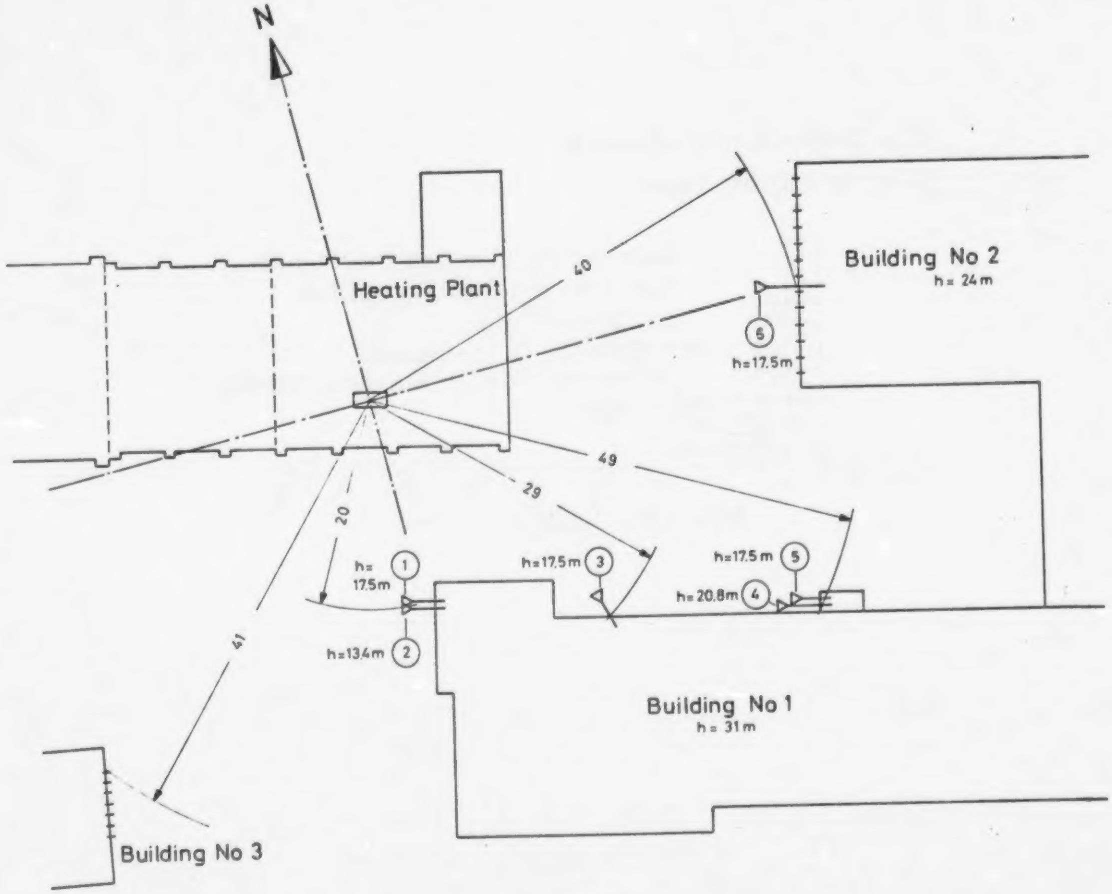
N
Heating Plant
Building No 2
h= 24m
40
6
h=17.5m
49
29
20
h= 17.5m
1
2
h=13.4m
h=17.5m
3
h=17.5m
5
h=20.8m
4
Building No 1
h= 31m
41
Building No 3

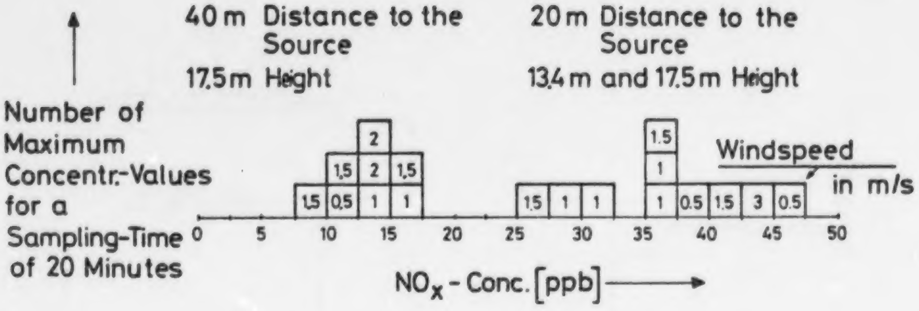
40m Distance to the Source
17.5m Height
20m Distance to the Source
13.4m and 17.5m Height
Number of Maximum Concentr.-Values for a Sampling-Time of 20 Minutes
Windspeed in m/s
1.5
0.5
1
2
1.5
2
1
1.5
1
1.5
1
1
1
1
1.5
0.5
1.5
3
0.5
0
5
10
15
20
25
30
35
40
45
50
NOx - Conc. [ppb]

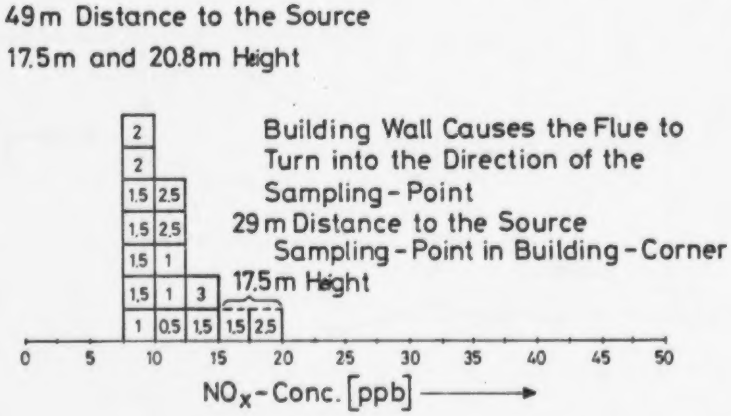
49m Distance to the Source
17.5m and 20.8m Height
Building Wall Causes the Flue to Turn into the Direction of the Sampling-Point
29m Distance to the Source
Sampling-Point in Building-Corner
17.5m Height
2
2
1.5
1.5
1.5
1.5
1
2.5
2.5
1
1
0.5
3
1.5
1.5
2.5
0
5
10
15
20
25
30
35
40
45
50
NOx - Conc. [ppb]

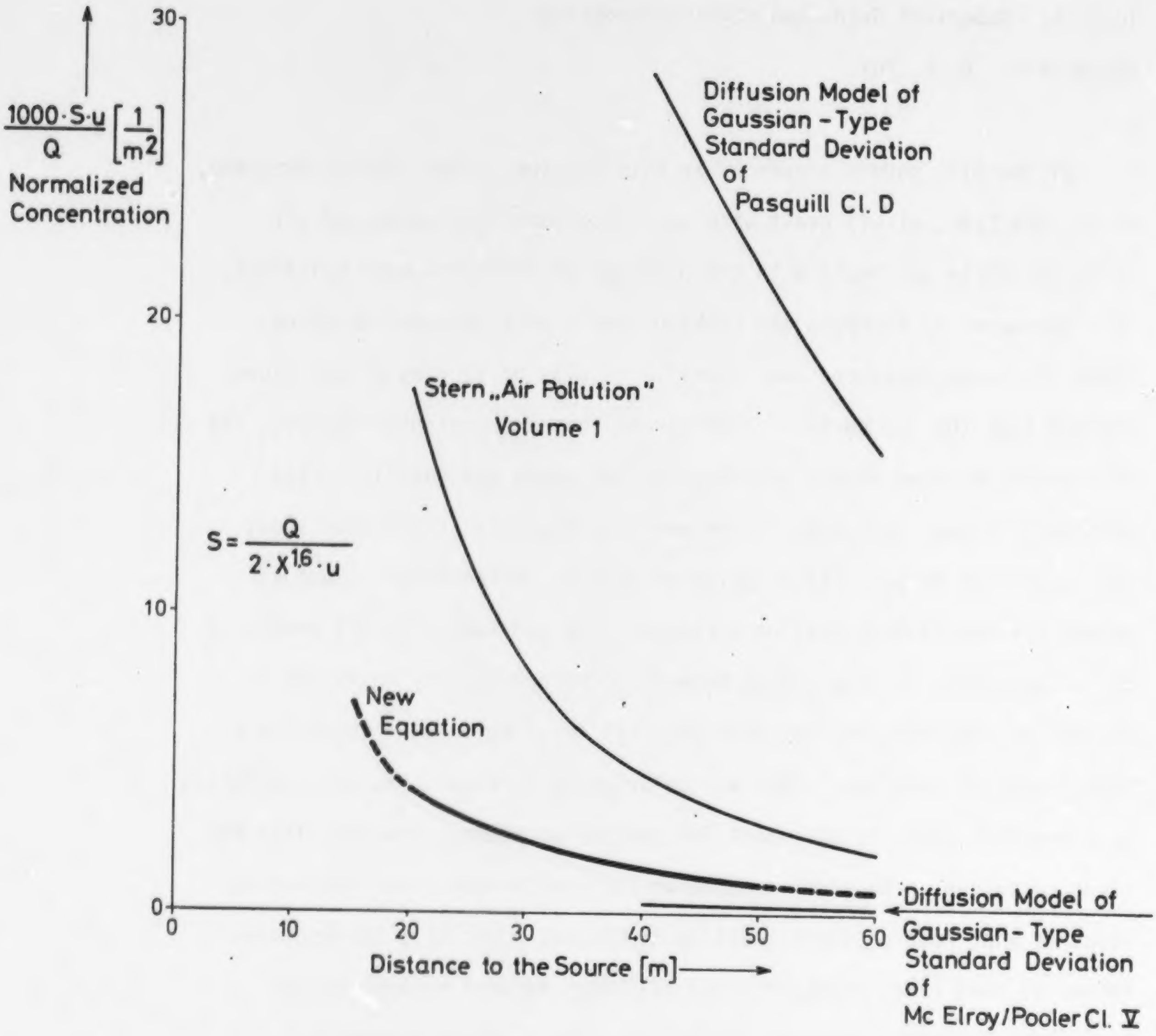
1000·S·u / Q [1/m²]
Normalized Concentration
30
20
10
0
0
10
20
30
40
50
60
Distance to the Source [m]
Diffusion Model of Gaussian-Type Standard Deviation of Pasquill Cl. D
Stern „Air Pollution" Volume 1
S = Q / 2·X^1.6·u
New Equation
Diffusion Model of Gaussian-Type Standard Deviation of Mc Elroy/Pooler Cl. V

Topic 4: Numerical Grids and Physical Modeling

Rapporteur: D. G. Fox

Of the five papers presented in this session, three (Runca, Marziano, et al, and Egan, et al) dealt with grid type numerical models of air pollution while two dealt with the problems of diffusion near buildings, only the paper by Thompson and Lombardi dealt with physical modeling. Since the paper presented some specific results of studies of the plume emitted from the top surface of different shaped rectangular objects, the discussion centered around specifics of the shape and details of the particular plumes observed. There was no substantive discussion about the usefulness or validity of physical models. While Fanaki (Canada) raised the question of scaling a buoyant flow and Keddie (U.K.) mentioned the relationship of time scales between model and reality there was no discussion regarding how and when physical modeling is more appropriate than numerical modeling. This was unfortunate because certainly simulation by a physical model is essential for certain problems. However, like any other technique, a physical simulation has limitations. An interesting point is what role physical modeling techniques might play in resolving issues of long range transport, and pollutant removal by dry and wet processes, two major concerns in air pollution modeling currently.

The paper by Giebel reported interesting results from experimental investigations of dispersion in the immediate vicinity of buildings. This work generated a new empirical formulation for calculating concentrations near buildings which it was suggested might be somewhat more general than would be expected because a reasonable comparison with the McElroy-Pooler diffusion coefficients determined in urban area was approached in the limit.

The main body of the session was devoted to grid models. Dr. Runca discussed the commonly recognized incompatability between a relatively large grid volume and a point source. Runca used techniques of subgrid discretization in space and time and the exact difference equation for Gaussian dispersion to show that it is no longer necessary to locate either single point or multiple point sources at grid points to achieve accurate results. Marziano, et al, discussed the application of a rather complex grid model based upon the "IBM model" of Shir and Runca to Venice. The results as calculated were rather similar to other studies of the accuracy of grid models done for St. Louis and reported at the Roskilde, Denmark, export meeting in 1974. The Venice work, however, represented a vastly improved data set. While discussion of Runca and Marziano was limited because of time, a number of interesting questions came to mind associated with these model results. The problem of data requirements remains a major issue. Is the improvement in accuracy possible with a complete three dimensional grid model worth the effort and expense of the needed data? It is obvious that models such as these will not be routinely used until our need for information is sufficiently precise to warrant large expenses for data collections. Furthermore, the models have shown some improvement particularly through Runca's work in resolving plumes but, as Wilson suggested, some further improvement is necessary before these models achieve general acceptance. In fact, Wilson's (USA) paper in Topic 1 discussing a comparison of diffusion experiments with a grid model illustrate the point well. A great deal of data are required to operate a grid model and its operation is somewhat sophisticated. Most of us who support the grid model approach would argue that Wilson's application of the model was too casual--he did not pay enough attention to significant details of the interaction between raw data and model filtered data to allow a reasonable comparison, but there also are challenges to the grid models to provide for simpler applications. A separate concept which might warrant consideration is the application of a reversed version of Runca's to allow analysis of concentration at a receptor. One of the rationalities grid modelers have used has been that averages over the volume of a grid cannot be compared with a point measurement at a receptor. Perhaps a time history of back trajectories could be calculated using Runca's type algorithims to generate a point comparison. I look forward to continuing discussion in future meetings on grid model development since it holds great promise for the complex applications of the future.

Egan, et al, applied a somewhat simpler grid model to deal with regional dispersion problems and also to assess the transformation of SO_2 to SO_4 on such a scale. Questions following his presentation concerned the vertical mixing rate data used and some other technical model points. Of significance was a preceived (by the Rapporteur) concern on the part of the group implying a need to compare this Eulerian calculation with Lagrangian techniques. Johnson (USA), for example, questioned computing time requirements between this code and his. This type of discussion seems somewhat moot since these models do different things. It seems to me that we would do well to concentrate more seriously on selecting and designing the proper model to do the required job. To answer a "Lagrangian" question, one uses a Lagrangian concept and vice versa. More attention should continue to go toward stating - up front - the assumptions and limitations of models and to considerations of the goals of the models. It should also be realized that Eulerian models are of greatest applicability when global applications--those asking what the effect on point A by forces applied at either a single or set of other points separated from point A--are under consideration.

7 th NATO/CCMS
International Technical Meeting
on Air Pollution Modeling

TOPIC V

TALL STACK PLUME,
INCLUDING SULPHATE TRANSFORMATION
AND REMOVAL PROCESSES

Seventh International Technical Meeting on Air
Pollution Modeling and its Application

IMPROVED TECHNIQUES FOR MODELING THE DISPERSION OF TALL STACK PLUMES

HARRISON E. CRAMER

H. E. CRAMER COMPANY, INC.
University of Utah Research Park
P. O. Box 8049
Salt Lake City, Utah 84108

7-10 September 1976
Arlie, Virginia
United States of America

TABLE OF CONTENTS

Section	Title	Page
	ABSTRACT	ii
1	INTRODUCTION	1
2	PLUME RISE EQUATIONS AND MODEL FORMULAS	4
	2.1 Plume Rise Equations	4
	2.2 Short-Term Dispersion Model Formulas	7
	2.3 Long-Term Dispersion Model Formulas	11
	2.4 Application of the Models in Complex Terrain	12
	2.5 Specifications of Model Input Parameters	18
3	DISCUSSION OF THE MAXIMUM GROUND-LEVEL CONCENTRATIONS PRODUCED BY TALL STACK PLUMES	25
4	COMPARISON OF TALL-STACK DISPERSION MODEL CALCULATIONS WITH MEASUREMENTS	31
	4.1 Comparison of Calculated and Observed SO_2 Concentrations Produced by Major Sources in Allegheny County, Pennsylvania	32
	4.2 Comparison of Calculated and Observed SO_2 Concentrations Produced by Tall-Stack Emissions from the ASARCO Copper Smelter in Tacoma, Washington	33
	4.3 Comparison of Calculated and Observed Plume Characteristics for Two Electrical Generating Plants in Marshall County, West Virginia	35
	ACKNOWLEDGMENTS	44
	REFERENCES	45

ABSTRACT

This paper describes a comprehensive set of generalized dispersion formulas for calculating the air quality impact of the plumes discharged from tall stacks located in either flat or complex terrain. The Briggs plume rise equations, with a restriction on plume rise for stack Froude numbers greater than about 3 when the mean wind speed at stack height approaches or exceeds the stack exit velocity, are used to calculate plume stabilization height, stabilization distance and the plume diameter at stabilization. For plumes that stabilize within the surface mixing layer, an improved Gaussian plume model is used to calculate downwind lateral and vertical plume dimensions, axial and ground-level concentrations and other dispersion parameters. The vertical term of the Gaussian model contains the vertical intensity of turbulence at plume stabilization height, a rectilinear expansion law, a virtual distance expression to adjust for the vertical plume dimension at stabilization and multiple reflection terms that limit the plume to the surface mixing layer. Variations in terrain height are accounted for by assuming that the plume axis is at a fixed elevation above mean sea level (the plume stabilization height) and defining ground level to be the elevation above mean sea level of each point of interest. The lateral term contains the lateral turbulent intensity at plume stabilization height and a virtual distance expression to adjust for the lateral plume dimension at stabilization. To calculate seasonal or annual average concentrations, the vertical term is substituted in a conventional sector model similar to Calder's Climatological Dispersion Model. These improved techniques have been incorporated in computer programs and have been used to model tall stack emissions from single sources and source complexes in both flat and complex terrain. Results of selected applications are presented in the form of comparisons of model estimates with aircraft measurements of plume characteristics and with air quality observations.

SECTION 1
INTRODUCTION

In the use of atmospheric dispersion models to estimate the impact of pollutant emissions on ambient air quality, one of the most pressing requirements is that of accurately calculating the ground-level concentrations produced by tall stack plumes. The procedures most frequently used to make these calculations are those described in the Turner (1969) Workbook in which the dispersion parameters σ_y and σ_z are defined by the Pasquill-Gifford curves. As the proponent of similar parameters (Cramer, 1957; 1959), I have been acutely aware, as have others, of their many questionable features, especially with respect to tall stack applications. Pasquill (1976) has recently pointed out these features and has suggested certain interim changes in the Workbook parameters and procedures as well as identifying important knowledge gaps that need to be filled before other revisions can be made. My colleagues and I have been working for many years on the development of improved Gaussian modeling techniques and their application to a wide variety of practical problems including the effects of pollutant emissions on ambient air quality. During the past several years, we have devoted much of our attention to the tall stack dispersion problem and have developed and tested improved modeling techniques that we believe provide at least interim resolution of many of the questionable features identified by Pasquill (1976). The purpose of this paper is to describe these improved techniques and to present the results of selected applications that demonstrate their potential usefulness in estimating the impact of tall stack emissions on ambient air quality.

There are several basic concepts that are important to an understanding of the tall stack dispersion modeling techniques described below. The meteorological inputs to the models are directly related to the vertical profiles of wind speed, wind direction, air temperature, humidity and the lateral and vertical intensities of turbulence within a reference mesoscale air volume containing the source and the points at which concentration calculations are to be made. The reference volume extends vertically from the earth's surface through the surface mixing layer beyond the highest level that will be intersected by the plume at the horizontal extremities of the reference volume. The horizontal dimensions of the reference air volume must be large enough to contain significant ground-level concentrations. Typical vertical dimensions are thus of the order of 1 kilometer and typical horizontal dimensions vary from 10 to 100 kilometers. The vertical profiles of the basic meteorological parameters mentioned above are assumed to be known from actual measurements or are specified on some other basis. A single profile representative of the reference volume is usually assigned each meteorological parameter on an hour-by-hour basis. A calculation grid is also specified and the coordinates and elevations of all grid points as well as the stack must be known. Universal Transverse Mercator (UTM) coordinates are used to define the location of the stack and grid points and elevations are usually referenced to mean sea level.

The basic dispersion model calculation is intended to define the lateral and vertical plume dimensions, the spatial coordinates of the plume and the concentration field within the plume for an averaging time of the order of the time required for plume stabilization (2 to 10 minutes). This is accomplished by first using plume rise equations to calculate the stabilization height, distance from the stack to stabilization and the lateral and vertical plume dimensions at stabilization. The next step is to substitute these values in a short-term Gaussian dispersion model that provides for the effects of the plume dimensions at stabilization, multiple reflection from elevated stable layers that may be present and the ground surface, and the effects of differences in terrain elevation. The ground-level concentrations thus calculated are assumed to be for a 10-minute averaging time. Concentrations for a 1-hour averaging time are obtained by increasing the lateral plume dimensions according to a power law $\left(\sigma_y \propto t^{1/5}\right)$ or by using 1-hour values of the lateral and vertical dispersion parameters in the short-term dispersion model. For averaging times longer than 1 hour, new hourly meteorological inputs are used in the model or, if the meteorological conditions are assumed to be persistent, the lateral plume dimensions are increased by a means of the one-fifth power law. With suitable modifications, the above techniques have been incorporated in a long-term sector model, similar to Calder's (1971) Climatological Dispersion Model, for calculating seasonal and annual ground-level concentrations. The plume-rise equations, dispersion-model formulas, and the specification of source and meteorological input parameters are described below.

SECTION 2

PLUME RISE EQUATIONS AND MODEL FORMULAS

2.1 PLUME RISE EQUATIONS

The plume rise equations are based on the expressions developed by Briggs (1971) and include a semi-empirical correction factor to account for stack downwash. For an adiabatic or unstable atmosphere, the buoyant rise Δh_N is given by

$$\Delta h_N = \left[\frac{1}{\bar{u}\{h\}} \left(\frac{3F}{2\gamma_1^{\,2}} \right)^{1/3} (10h)^{2/3} \right] f \tag{1}$$

where the expression in the brackets is from Briggs (1971) and f is the semi-empirical correction factor used to correct for stack downwash. The other parameters appearing in the above expression are

$\bar{u}\{h\}$ = mean wind speed at the stack height h

γ_1 = adiabatic entrainment coefficient ~0.6 (Briggs, 1972)

F = initial buoyancy flux

$$= \frac{gV}{\pi} \left(1 - \frac{T_a}{T_s} \right) \tag{2}$$

V = volumetric emission rate of the stack

$= \pi r^2 w$

r = inner radius of stack

w = stack exit velocity

g = acceleration due to gravity

T_a = ambient air temperature (^{o}K)

T_s = stack exit temperature (^{o}K)

The factor f in Equation (1) used to account for downwash in the lee of the stack when the wind speed at stack height approaches or exceeds the stack exit velocity is defined (Cramer et al., 1975) by the expression

$$f = \left\{ \begin{array}{ll} 1 & \bar{u}\{h\} \leq w/1.5 \\ \left(\frac{3w - 3\bar{u}\{h\}}{w}\right) & ; \; w/1.5 < \bar{u}\{h\} < w \\ 0 & ; \; \bar{u}\{h\} \geq w \end{array} \right\} \qquad (3)$$

Briggs (1969), Fay, et al., (1970) and others have pointed out that their plume rise equations may not apply when the ratio of the stack exit velocity and the mean wind speed $(w/\bar{u}\{h\})$ is less than 1.5 to 1.2 for stack Froude numbers greater than unity. From an analysis of the Bringfelt (1968) plume-rise data, we have concluded that Equation (3) generally applies to stacks with Froude numbers greater than 3.0 where the Froude number is defined by $w^2/2gr\left(\frac{T_s - T_a}{T_a}\right)$. We have found no evidence of stack downwash effects for Froude numbers less than 1.0

In Equation (1), which is one of several different forms of the Briggs (1971) adiabatic rise formula, the plume rise increases with stack height and the final plume rise is attained at a distance of ten stack heights (10h). Both Moore (1974) and Briggs (1974) have found that Equation (1) fits the available plume rise data as well as other, more complicated expressions. In addition, we believe Equation (1) provides the best estimates of plume rise from very tall stacks (h > 100 meters) under neutral and unstable conditions.

Plume rise under stable conditions is given by the Briggs (1971) formula

$$\Delta h_S = \left\{ \begin{array}{ll} \left[\dfrac{6F}{\bar{u}\{h\} \gamma_2^{\,2} S} \right]^{1/3} & ; \ \pi \bar{u}\{h\} S^{-1/2} < 10h \\ \\ \left[\dfrac{3F}{\bar{u}\{h\} \gamma_2^{\,2} S} \left(1 - \cos \left(\dfrac{10 S^{1/2} h}{\bar{u}\{h\}} \right) \right) \right]^{1/3} & ; \ \pi \bar{u}\{h\} S^{-1/2} \geq 10h \end{array} \right\} f \qquad (4)$$

where

γ_2 = stable entrainment coefficient ~0.66 (Briggs, 1972)

$S = \dfrac{g}{T_a} \dfrac{\partial \theta}{\partial z}$

$\dfrac{\partial \theta}{\partial z}$ = vertical potential temperature gradient

The above expression restricts the calculated rise Δh_S as the vertical potential temperature gradient $\frac{\partial \theta}{\partial z}$ approaches zero (neutral stratification) so that it cannot exceed the calculated rise Δh_N for neutral and unstable stratification. Briggs (1972) recommends a procedure of this type.

Following the suggestion made by Briggs (1972), which is based on visual observations of plume behavior, the standard deviations of the lateral and vertical concentration distributions at the point of plume stabilization are given by

$$\sigma_{yR} = \sigma_{zR} = \frac{0.5 \, \Delta h}{2.15} \qquad (5)$$

Alternatively, use of the values given above for entrainment coefficients γ_1 and γ_2 would change the numerator in Equation (5) from 0.5 Δh to 0.6 Δh (adiabatic formula) and 0.66 Δh (stable formula) and thus increase both σ_{yR} and σ_{zR} by approximately 20 to 30 percent. It follows from Equations (1) and (4) that the downwind distance to stabilization x_R is given by

$$x_R = \left\{ \begin{array}{ll} 10h & ; \ \frac{\partial\theta}{\partial z} \le 0 \\ \pi\,\bar{u}\{h\}\,S^{-1/2} & ; \ \frac{\partial\theta}{\partial z} > 0 \text{ and } \pi\,\bar{u}\{h\}\,S^{-1/2} < 10h \\ 10h & ; \ \frac{\partial\theta}{\partial z} > 0 \text{ and } \pi\,\bar{u}\{h\}\,S^{-1/2} \ge 10h \end{array} \right\} \qquad (6)$$

2.2 SHORT-TERM DISPERSION MODEL FORMULAS

The concentration produced at downwind distance x, crosswind distance y and height z by a continuous elevated source is given by

$$\chi\{x, y, z\} = \frac{Q}{2\pi\,\bar{u}\{H\}\,\sigma_y\,\sigma_z} \exp\left[-\frac{1}{2}\left(\frac{y}{\sigma_y}\right)^2\right] V \qquad (7)$$

where

$$V = \left\{ \exp\left[-\frac{1}{2}\left(\frac{H - z}{\sigma_z}\right)^2\right] + \exp\left[-\frac{1}{2}\left(\frac{H + z}{\sigma_z}\right)^2\right] \right. \qquad (8)$$

(Equation (8) continued on
following page.)

(Equation (8) continued.)

$$+ \sum_{i=1}^{\infty} \left[\exp\left[-\frac{1}{2} \left(\frac{2i\,H_m + H + z}{\sigma_z} \right)^2 \right] + \exp\left[-\frac{1}{2} \left(\frac{2i\,H_m + H - z}{\sigma_z} \right)^2 \right] \right. \tag{8}$$

$$\left. + \exp\left[-\frac{1}{2} \left(\frac{2i\,H_m - H + z}{\sigma_z} \right)^2 \right] + \exp\left[-\frac{1}{2} \left(\frac{2i\,H_m - H - z}{\sigma_z} \right)^2 \right] \right] \Bigg\}$$

and

Q = pollutant emission rate

$\bar{u}\{H\}$ = mean wind speed at the plume stabilization height H

σ_y, σ_z = standard deviation of the lateral, vertical concentration distribution

H_m = depth of the surface mixing layer

H = plume stabilization height

As shown by Equation (8), the method of image sources is used to account for multiple reflections at the surface and the top of the mixing layer. At long downwind distances, Equation (8) changes the form of the vertical concentration distribution from Gaussian to rectangular.

Following the derivation of Cramer, et al. (1972), the standard deviation of the lateral concentration distribution is given by

$$\sigma_y\{x\} = \sigma'_A \, x_{ry} \left[\frac{x + x_y - x_{ry}\,(1-\alpha)}{\alpha x_{ry}} \right]^{\alpha} \tag{9}$$

$$x_y = \begin{cases} \dfrac{\sigma_{yR}}{\sigma'_A} - x_R & ; \dfrac{\sigma_{yR}}{\sigma'_A} \leq x_{ry} \\ \alpha x_{ry} \left(\dfrac{\sigma_{yR}}{x_{ry}\, \sigma'_A} \right)^{1/\alpha} - x_R + x_{ry}(1-\alpha) & ; \dfrac{\sigma_{yR}}{\sigma'_A} > x_{ry} \end{cases} \qquad (10)$$

where

σ'_A = standard deviation of the wind-azimuth angle in radians (lateral turbulent intensity) at the plume stabilization height H

x_{ry} = distance over which rectilinear lateral plume expansion occurs downwind from an ideal point source (~ 50m)

σ_{yR} = standard deviation of the lateral concentration distribution at downwind distance x_R

α = lateral diffusion coefficient (~ 0.9)

It should be noted that the virtual distance x_y is not permitted to be less than zero.

The standard deviation of the vertical concentration distribution σ_z is given by the expression

$$\sigma_z\{x\} = \sigma'_E(x + x_z) \qquad (11)$$

$$x_z = \begin{cases} \dfrac{\sigma_{zR}}{\sigma'_E} - x_R & ; \dfrac{\sigma_{zR}}{\sigma'_E} \geq x_R \\ 0 & ; \dfrac{\sigma_{zR}}{\sigma'_E} < x_R \end{cases} \qquad (12)$$

where

σ'_E = standard deviation of the wind elevation angle in radians (vertical turbulent intensity) at the plume stabilization height H

σ_{zR} = standard deviation of the vertical concentration distribution at downwind distance x_R

As in the case of Equation (7), the virtual distance x_z is not permitted to be less than zero. According to Equation (11), rectilinear vertical plume growth is assumed for all stabilities. We have found this to be a very good approximation, especially for elevated sources, in combination with the multiple reflection term given by Equation (8) which restricts the plume to the surface mixing layer. Yamamoto and Yokoyama (1974) and others have found a linear relationship between σ_z and downwind distance for all stabilities. The σ_z values obtained from Equation (11), using values for σ'_E appropriate for the Pasquill stability categories, will in general be smaller than the corresponding values indicated by the Pasquill-Gifford curves for the A and B categories and will be larger than indicated by the Pasquill-Gifford curves for the D, E and F categories at the longer downwind distances, without taking into account the restriction on vertical plume expansion imposed by Equation (3). Also, in comparing σ_z values obtained from Equation (11) with the Pasquill-Gifford σ_z curves, it must be recognized that typical vertical plume dimensions σ_{zR} at the plume stabilization distance, as shown by Equation (5), range from 25 to 50 meters for a stack height of 100 meters. The portions of the Pasquill-Gifford σ_z curves for σ_z less than 25 to 50 meters are thus generally inapplicable to tall stack plumes.

In the model calculations, the observed mean wind speed $\bar{u}_R$ is adjusted from the measurement height z_R to the stack height h for plume rise calculations and to the stabilization height H for the concentration calculations by a wind-profile exponent law

$$\bar{u}\{h\} = \bar{u}\{z_R\}\left(\frac{h}{z_R}\right)^p$$

$$\bar{u}\{H\} = \bar{u}\{z_R\}\left(\frac{H}{z_R}\right)^p \qquad (13)$$

The exponent p, which is assigned on the basis of atmospheric stability, ranges from about 0.1 for very unstable conditions to about 0.4 for very stable conditions.

2.3 LONG-TERM DISPERSION MODEL FORMULAS

In the long-term model, which is similar in form to the Calder (1971) Climatological Dispersion Model, a continuous source of pollutants is divided into sectors of equal angular width corresponding to the class intervals of the seasonal and annual frequency distributions of wind direction. For a single source, the mean seasonal concentration at radial distance r and angle θ is given by

$$\chi_\ell\{r,\theta\} = \frac{2Q}{\sqrt{2}\,\pi\, r\, \Delta\theta'} \sum_{i,j,k} \left[\frac{f_{i,j,k,\ell}}{\bar{u}_i\{H_{i,k,\ell}\}\,\sigma_{z;i,k,\ell}}\right] S\{\theta\}\, V_{i,k,\ell} \qquad (14)$$

where

$f_{i,j,k,\ell}$ = frequency of occurrence of the i^{th} wind-speed category, j^{th} wind-direction category and k^{th} stability or time-of-day category for the ℓ^{th} season

$\Delta\theta'$ = sector width in radians

$S\{\theta\}$ = a smoothing function

$$S\{\theta\} = \begin{cases} \dfrac{\Delta\theta' - \left|\theta'_j - \theta'\right|}{\Delta\theta'} & ; \left|\theta'_j - \theta'\right| \leq \Delta\theta' \\ 0 & ; \left|\theta'_j - \theta'\right| > \Delta\theta' \end{cases} \quad (15)$$

where

θ'_j = angle measured in radians from north to the centerline of the j^{th} wind-direction sector

θ' = angle measured in radians from north to the point (r,θ)

The remaining terms are identical to those defined for the short-term model except that the i subscript refers to the wind-speed category, the j subscript refers to the wind-direction category, the k subscript refers to the stability category and the ℓ subscript refers to the season. The mean annual concentration at the point (r,θ) is obtained by averaging the seasonal concentrations.

2.4 APPLICATION OF THE MODELS IN COMPLEX TERRAIN

We have developed the procedures described below for applying the short-term and long-term concentration models to tall stack emissions in regions of complex terrain. These procedures contain a number of simplifying assumptions that have thus far served very well in numerous applications for which measurements of plume characteristics and ground-level concentration were available for comparison with model predictions (see Section 4). As new information becomes available on the behavior of tall stack plumes in complex terrain, the incorporation of any necessary revisions should not prove difficult because of the very flexible nature of the model framework.

The simplifying assumptions made for complex terrain applications are:

(1) The top of the surface mixing layer extends over the calculation grid at a constant elevation above mean sea level.

(2) Buoyant tall stack plumes that stabilize above the top of the surface mixing layer $(H > H_m)$ do not contribute to the ground-level concentration at any point, including points on elevated terrain above the top of the mixing layer.

(3) The axis of a plume contained in the surface mixing layer remains at the plume stabilization height as the plume mixes to the ground.

(4) The wind speed and direction at any given height above mean sea level are constant over the calculation grid.

(5) In the case of plumes initially contained within the surface mixing layer that pass over elevated terrain points that are within the surface mixing layer, the mixing depth is not permitted to fall below a specified minimum value; the specification of a minimum effective mixing depth is necessary to preclude physically unrealistic effects resulting from forcing the plume into highly compressed layers.

(6) A stack plume that intersects a terrain elevation greater than the plume stabilization height follows the terrain.

In order to determine whether a stabilized plume is contained within the surface mixing layer, it is necessary to calculate the mixing depth $H_m^*\{z_s\}$ at the source from the relationship

$$H_m^*\{z_s\} = \left(H_m + z_a - z_s\right) \tag{16}$$

where

H_m = the depth of the surface mixing layer measured at a point (airport) with elevation z_a above mean sea level

z_s = the height above mean sea level of the source (stack base)

Equation (16) is represented schematically in Figure 1. In accord with assumption (1), the top of the surface mixing layer is shown at a constant elevation above mean sea level. If the height of the stabilized plume above the base of the stack $H \leq H_m^*\{z_s\}$, the plume is defined to be contained within the surface mixing layer.

The height H_o of the stabilized plume above mean sea level is given by the sum of the height H of the stabilized plume above the base of the stack and the elevation z_s of the base of the stack. At any elevation z above mean sea level, the effective height $H'\{z\}$ of the plume centerline above the terrain is then given by

$$H'\{z\} = \begin{Bmatrix} H_o - z & ; & H_o - z \geq 0 \\ 0 & ; & H_o - z < 0 \end{Bmatrix} \tag{17}$$

The effective mixing depth $H_m'\{z\}$ for a point at elevation z above mean sea level is defined by

$$H_m'\{z\} = \begin{Bmatrix} H_m & ; & z \geq z_a \\ H_m + z_a - z & ; & z < z_a \end{Bmatrix} \tag{18}$$

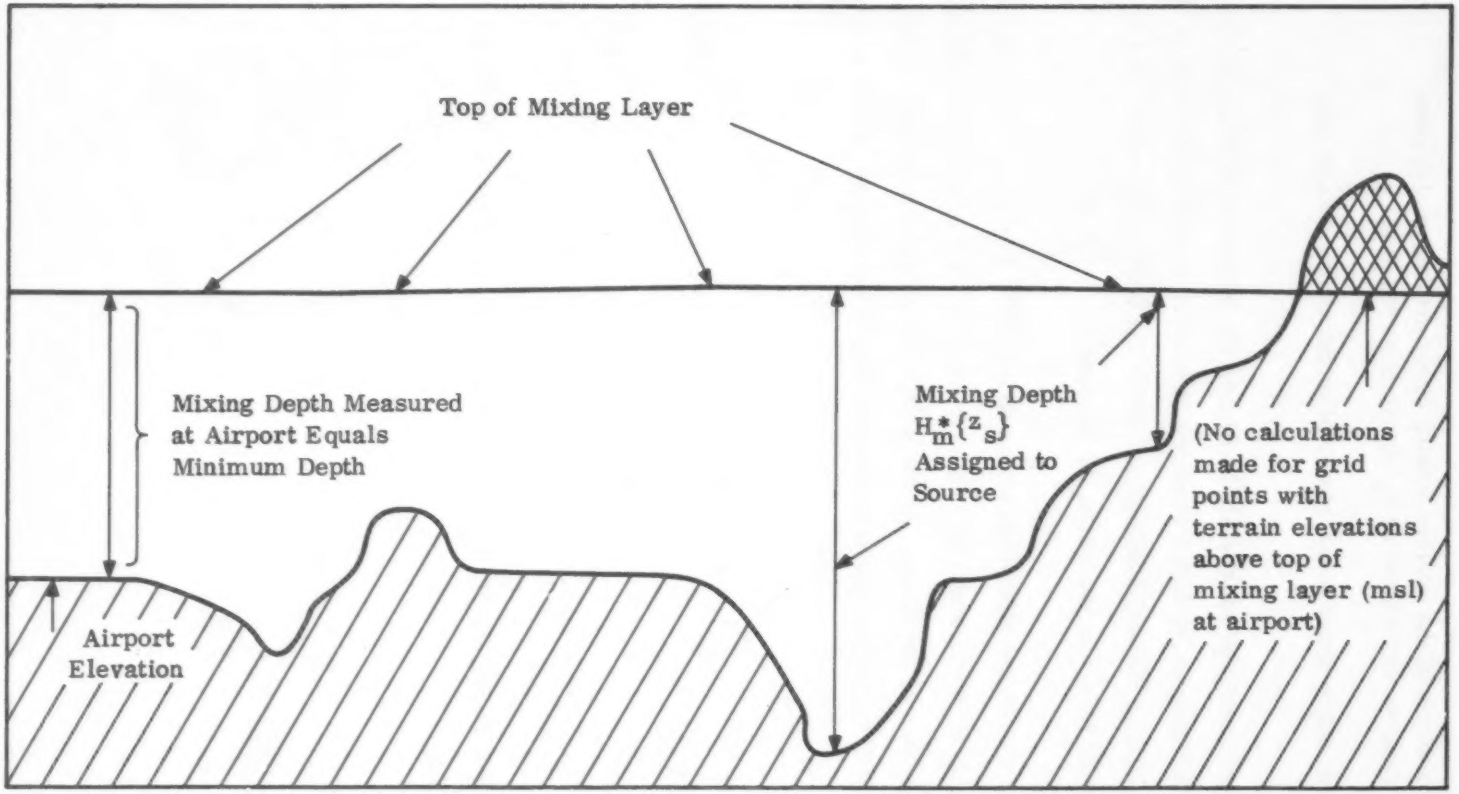
Top of Mixing Layer
Mixing Depth Measured at Airport Equals Minimum Depth
Mixing Depth $H_m^*\{z_s\}$ Assigned to Source
(No calculations made for grid points with terrain elevations above top of mixing layer (msl) at airport)
Airport Elevation

Figure 1. Mixing depth $H_m^*\{z_s\}$ used to determine whether a stabilized plume is contained within the surface mixing layer.

Figure 2 illustrates the application of Equation (18). For grid points at elevations below the airport elevation, the effective mixing depth $H'_m\{z\}$ is allowed to increase in a manner consistent with Figure 1. However, in order to prevent a physically unrealistic compression of plumes as they pass over elevated terrain, the effective mixing depth is not permitted to be less than the mixing depth measured at the airport. It should be noted that the concentration is set equal to zero for grid points above the actual top of the mixing layer (see Figure 1).

The terrain adjustment procedures also assume that the mean wind speed at any given height above sea level is constant. Thus, the wind speed $\bar{u}_R$ measured at height z_R above the surface at a point with elevation z_a above mean sea level is adjusted to the stack height for the plume-rise calculations by the relationship

$$\bar{u}\{h\} = \begin{cases} \bar{u}_R \left(\dfrac{h_o - z_a}{z_R}\right)^p & ; \quad h_o \geq z_a + z_R \\ \\ \bar{u}_R & ; \quad h_o < z_a + z_R \end{cases} \tag{19}$$

where h_o is the height above mean sea level of the top of the stack. Similarly, the wind speed $\bar{u}\{H\}$ used in the concentration calculations is given by

$$\bar{u}\{H\} = \begin{cases} \bar{u}_R \left(\dfrac{H_o - z_a}{z_R}\right)^p & ; \quad H_o \geq z_a + z_R \\ \\ \bar{u}_R & ; \quad H_o < z_a + z_R \end{cases} \tag{20}$$

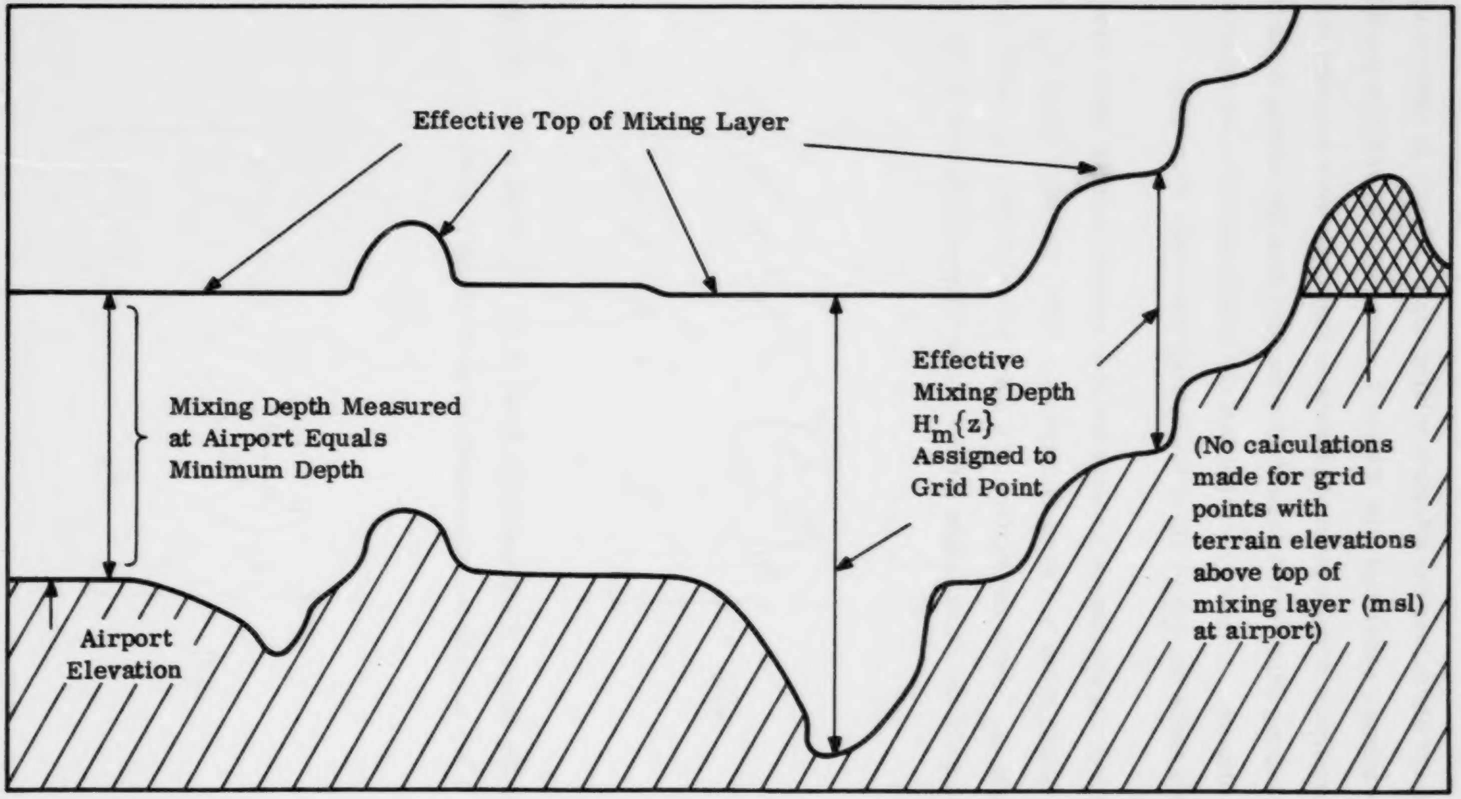
Effective Top of Mixing Layer
Mixing Depth Measured at Airport Equals Minimum Depth
Effective Mixing Depth $H'_m\{z\}$ Assigned to Grid Point
(No calculations made for grid points with terrain elevations above top of mixing layer (msl) at airport)
Airport Elevation

Figure 2. Effective mixing depth $H'_m\{z\}$ assigned to grid points for the concentration calculations.

As noted previously, the terrain-adjustment procedures outlined above provide a very simple representation of plume behavior in complex terrain that is not at present well understood. Because the model assumptions are generally conservative, it is possible that concentrations calculated for elevated terrain, especially elevated terrain near a source, exceed the concentrations that actually occur. It should also be noted that the procedures described above differ from previous "terrain-intersection" models in that terrain intersection is only permitted for a plume contained within a mixing layer. That is, terrain intersection is permitted for all stability categories, but only for a plume contained within the surface mixing layer. We recognize that, for plumes in stable layers above the surface mixing layer which approach closely to elevated terrain, there are high concentration gradients in the vicinity of the plume-terrain interface. However, we do not know of any reliable method for calculating the concentration at the interface under these stable conditions. Also, we do not know of any measurements that support high (axial) concentration estimates at the terrain interface under these conditions.

2.5 SPECIFICATIONS OF MODEL INPUT PARAMETERS

The following stack parameters and emissions data are required by both the short-term and long-term dispersion models:

- Stack height (m)
- Stack diameter (m)
- Elevation of stack base above mean sea level (m)
- Stack X and Y UTM coordinates (m)
- Stack exit temperature (^{o}K)
- Stack exit velocity (m/sec)

- Density of stack effluent (g/m^3)
- Pollutant emission rate (g/sec)

The first four stack parameters are fixed. The last four parameters dealing with emissions are variable and the values assigned vary according to the data available and the purposes of the calculations.

Because the ground-level concentration calculations will normally be made on a calculation grid, it is necessary to specify the overall dimensions of the grid, the location of each grid point in terms of UTM or other suitable coordinates, and the elevation above mean sea level of each grid point.

The meteorological inputs required by the short-term and long-term models are shown in Tables 1 and 2 respectively. Except for σ'_A, σ'_E representative hourly values of all of these inputs can be obtained directly from surface and upper-air measurements, from statistical analysis and climatological summaries such as those available from the National Climatic Center, or by using estimation procedures based on existing knowledge of meteorological structures for various stabilities, surface roughnesses and synoptic scale circulations. Assignment of representative values for σ'_A and σ'_E is more difficult because direct measurements of these quantities are not usually made. However, the extreme range of possible values for σ'_E and, over short averaging times (3 to 10 minutes), for σ'_A is relatively small (0.02 to 0.20 for σ'_E and 0.02 to 0.40 for σ'_A). Also, the height dependence of σ'_A in all stabilities is approximately given by a simple power law of the form

$$\sigma'_A\{z\} = \sigma'_A\{z_R\}\left(\frac{z}{z_R}\right)^{-p} \tag{28}$$

TABLE 1

HOURLY METEOROLOGICAL INPUTS REQUIRED BY THE SHORT-TERM CONCENTRATION MODEL

Parameters	Definition
$\bar{u}_R$	Mean wind speed at height z_R
θ	Mean wind direction at height z_R or z_H
p	Wind-profile exponent
σ'_A	Wind azimuth-angle standard deviation in radians
σ'_E	Wind elevation-angle standard deviation in radians
T_a	Ambient air temperature (^oK)
H_m	Depth of surface mixing layer
$\frac{\partial\theta}{\partial z}$	Vertical potential temperature gradient

TABLE 2

METEOROLOGICAL INPUTS REQUIRED BY THE LONG-TERM CONCENTRATION MODEL

Parameter	Definition
$f_{i,j,k,\ell}$	Frequency distribution of wind-speed and wind-direction categories by stability categories for the ℓ^{th} season
$p_{k,i}$	Wind-profile exponents for each stability category and i^{th} wind-speed category
$\sigma'_{E;i,k}$	Standard deviation of the wind elevation angle in radians for the i^{th} wind-speed category, k^{th} stability category and ℓ^{th} season
$T_{a;k,\ell}$	Ambient air temperature for the k^{th} stability category and ℓ^{th} season
$\left(\frac{\partial\theta}{\partial z}\right)_{i,k}$	Vertical potential temperature gradient for the i^{th} wind-speed category and k^{th} stability category
$H_{m;i,k,\ell}$	Median surface mixing depth for the i^{th} wind-speed category, k^{th} stability or category and ℓ^{th} season
$\bar{u}\{z_R\}_i$	Mean wind speed at height z_R for the i^{th} wind-speed category

where p is the power-law exponent on wind speed (Swanson and Cramer, 1965). The height dependence of σ'_E is a function of stability and is approximately described by the following simple power laws

$$\sigma'_E\{z\} = \left\{ \begin{array}{ll} \sigma'_E\{z_R\}\left(\dfrac{z}{z_R}\right)^{0.33\,p} & ;\ \text{unstable} \\ \\ \sigma'_E\{z_R\}\left(\dfrac{z}{z_R}\right)^{0} & ;\ \text{neutral} \\ \\ \sigma'_E\{z_R\}\left(\dfrac{z}{z_R}\right)^{-(p+0.1)} & ;\ \text{stable} \end{array} \right] \qquad (29)$$

A procedure for estimating 10-minute values of σ'_A and σ'_E based on bivane measurements made at Cape Kennedy at a reference height of 18 meters and using the above power-law expressions is described by Dumbauld, et al. (1970). Extensions of the 10-minute values of σ'_A to 1-hour can be made by means of a $t^{1/5}$ or $t^{2/5}$ law (Osipov, 1972 and others) or from hourly wind-direction range observations if they are available.

For general purposes, we have found the hourly values of σ'_E and σ'_A shown in Table 3 for the various Pasquill stability categories to be useful in tall-stack dispersion model calculations (Cramer, et al., 1975). The σ'_E entries in the table are based in part on the bivane measurements at 92 meters made by Luna and Church (1971) and are also approximately equal to the σ'_E values implicit in the vertical expansion curves presented by Pasquill (1961) at a distance of 100 meters $\left(\sigma'_E = \dfrac{\sigma_z\{100\text{m}\}}{100}\right)$. In order to adjust for the effects of surface roughness elements and heat sources, the rural σ'_E values for the stability category one step

TABLE 3

HOURLY VALUES OF σ'_E AND σ'_A BY PASQUILL STABILITY CATEGORY FOR TALL-STACK DISPERSION CALCULATIONS IN RURAL AND URBAN AREAS (FROM CRAMER *ET AL.*, 1975)

Pasquill Stability Category	σ'_E (radians)		σ'_A (radians)	
	Rural	Urban	Rural	Urban
A	0.1745	0.1745	0.2495	0.2495
B	0.1080	0.1745	0.1544	0.2495
C	0.0735	0.1080	0.1051	0.1544
D	0.0465	0.0735	0.0665	0.1051
E	0.0350	0.0465	0.0501	0.0665
F	0.0235	--	0.0336	--

more unstable are recommended for urban areas. Also, the Pasquill E and F stability categories have been combined for urban areas as suggested by Calder (1971) because the effects of surface roughness and heat sources are generally incompatible with the minimal turbulent mixing associated with the Pasquill F stability category. The measurements of Luna and Church (1971) also show an approximate equivalence between σ'_A and σ'_E for a 10-minute averaging time for all stability categories. The hourly σ'_A values in Table 1 assume σ'_A and σ'_E to be equivalent for a 10-minute averaging time at heights on the order of 100 meters and use the $t^{1/5}$ law (Osipov, 1972 and others) to extend σ'_A to longer averaging times. That is, the hourly σ'_A for a given stability category is 1.43 ($6^{1/5}$) times the corresponding σ'_E value. A $t^{2/5}$ law could be used for the A and B categories. However, in our experience, these categories are generally not associated with high 3-hour and 24-hour ground-level concentrations produced by tall stack emissions.

SECTION 3

DISCUSSION OF THE MAXIMUM GROUND-LEVEL CONCENTRATIONS PRODUCED BY TALL STACK PLUMES

In the case of buoyant plumes emitted from tall stacks located in flat terrain, the highest persistent ground-level concentrations are generally expected to occur under the critical wind-speed, limited-mixing condition. A simplified expression for the maximum ground-level concentration under the critical wind-speed condition can be derived as follows. If the mixing depth H_m is much larger than the plume stabilization height H, the ground-level concentration obtained from Equation (7) is

$$\chi\{x, o, o\} = \frac{Q}{\pi \sigma_y \sigma_z \bar{u}\{H\}} \exp\left[-\frac{1}{2}\left(\frac{H}{\sigma_z}\right)^2\right] \tag{21}$$

Neglecting the effects of the plume dimensions at stabilization and setting the lateral and vertical dispersion coefficients α and β equal to unity, Equations (8) and (21) simplify to

$$\sigma_y = \sigma'_A x \tag{22}$$

$$\sigma_z = \sigma'_E x \tag{23}$$

By substituting Equations (22) and (23) in Equation (20) the distance to the maximum ground-level concentration is given by

$$x_{\max} = H/\sqrt{2}\,\sigma'_{E} \tag{24}$$

and the maximum ground-level concentration is given by

$$\chi_{\max} = \frac{2Q}{\pi e\,\bar{u}\{H\}\,H^{2}}\left(\frac{\sigma'_{E}}{\sigma'_{A}}\right) \tag{25}$$

Equation (25) is similar in form to the well known O. G. Sutton expression for a continuous elevated point source except that H is the sum of the actual stack height and the buoyant rise. If the Briggs adiabatic plume rise expression given in Equation (1) with the factor f set to unity is substituted in Equation (25), the mean wind speed that maximizes Equation (25) is

$$\bar{u}_{c}\{H\} = \left(\frac{150\,F}{\gamma_{\prime}^{2}\,h}\right)^{1/3} \tag{26}$$

where $\bar{u}_{c}\{H\}$ is the critical wind speed. The maximum ground-level concentration for the critical wind-speed condition is then

$$\chi_{\max}\{\bar{u}_{c}\} = \frac{Q}{2\pi e\,\bar{u}_{c}\{H\}\,h^{2}}\left(\frac{\sigma'_{E}}{\sigma'_{A}}\right) \tag{27}$$

The ratio $(\sigma'_{E}/\sigma'_{A})$ is approximately unity in all stabilities at heights of the order of 100 meters if low-frequency fluctuations in σ'_{A} (see Panofsky, 1973, p. 257, and others) are neglected. Thus, the maximum ground-level concentrations for averaging times of the order of ten minutes produced by tall stack plumes in flat terrain are basically a function of only the stack height and the heat content. This result has also been obtained by Csanady (1973), Pasquill (1974) and others.

The maximum ground-level concentration given by Equation (27) holds approximately for a wide range of mean wind speeds. For example, Figure 3 shows a plot of the normalized maximum ground-level concentrations versus the normalized mean wind speed at plume stabilization height. Departures of the mean wind speed from the critical wind speed by a factor of two result in decreases in the maximum ground-level concentration of about 10 percent or less. The figure also shows that the effect of reducing the value of the lateral dispersion coefficient α to 0.9 from 1.0 is also small.

The effects of the presence of an elevated inversion above the plume stabilization height on the maximum ground-level concentration of a buoyant stack plume are shown in Figure 4. The value of unity for the ratio H/H_m, which results in a doubling of the maximum ground-level concentration, holds strictly for an ideal point source (plume dimensions at stabilization were neglected in constructing the figure). If the plume dimensions at stabilization are taken into account ($\sigma_{zR} = 0.5\ \Delta h$), the maximum effect of an elevated inversion is given by the curve for $H/H_m = 0.8$ which shows an increase of about 35 percent in the maximum ground-level concentration due to reflection from an elevated inversion layer located at a height of about 2.5 times the stack height (since $H = 2h$ for the critical wind-speed condition). In this case, the top of the plume ($H + 2.15\ \sigma_{zR}$) is just touching the base of the elevated inversion. If half the stabilized plume is assumed to be in the inversion ($H = H_m$) and thus precluded from mixing to the ground, there is no increase in the maximum ground-level concentration given by Equation (27).

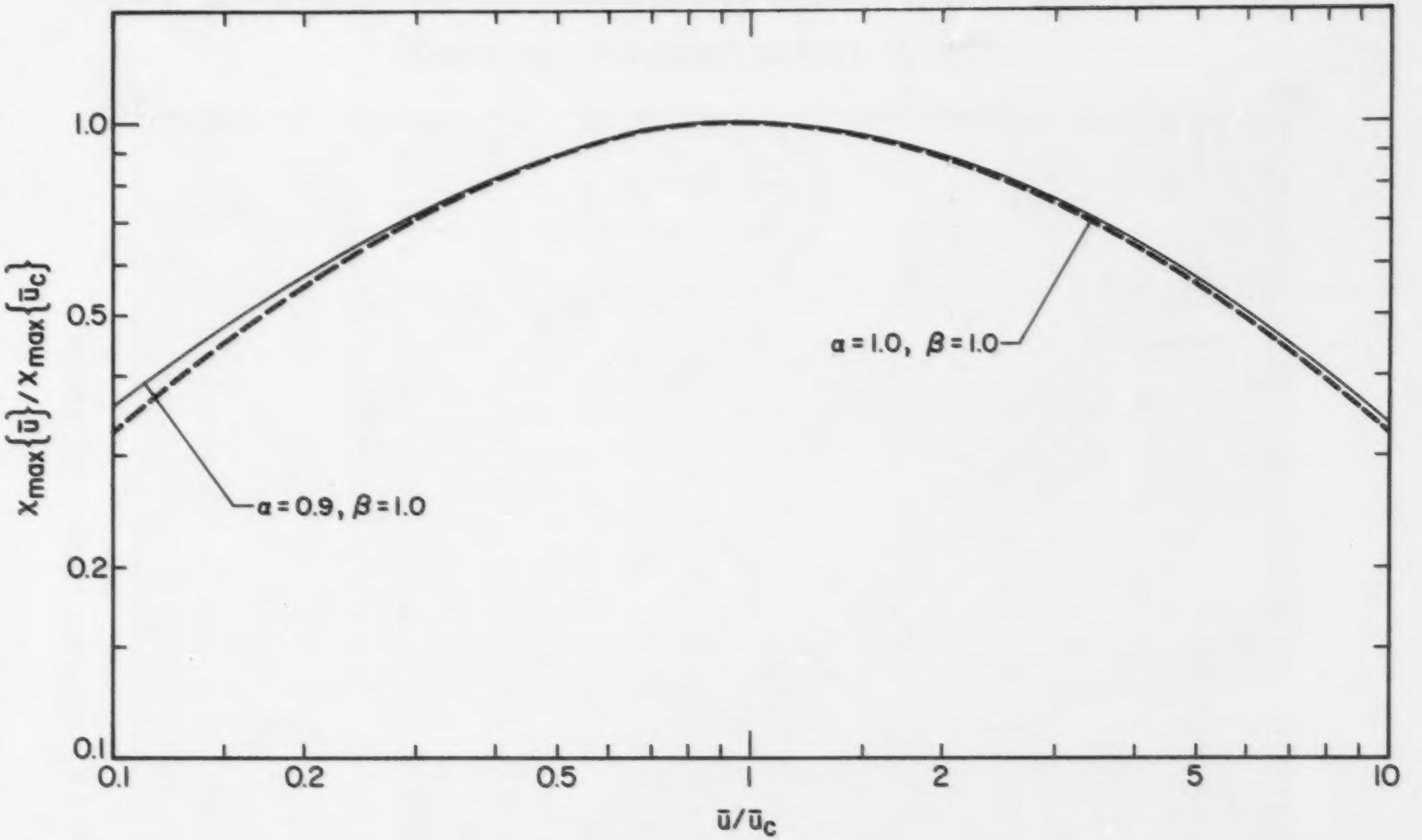

Figure 3. Dependence of the maximum ground-level concentration on the departures of the mean wind speed from the critical mean wind speed.

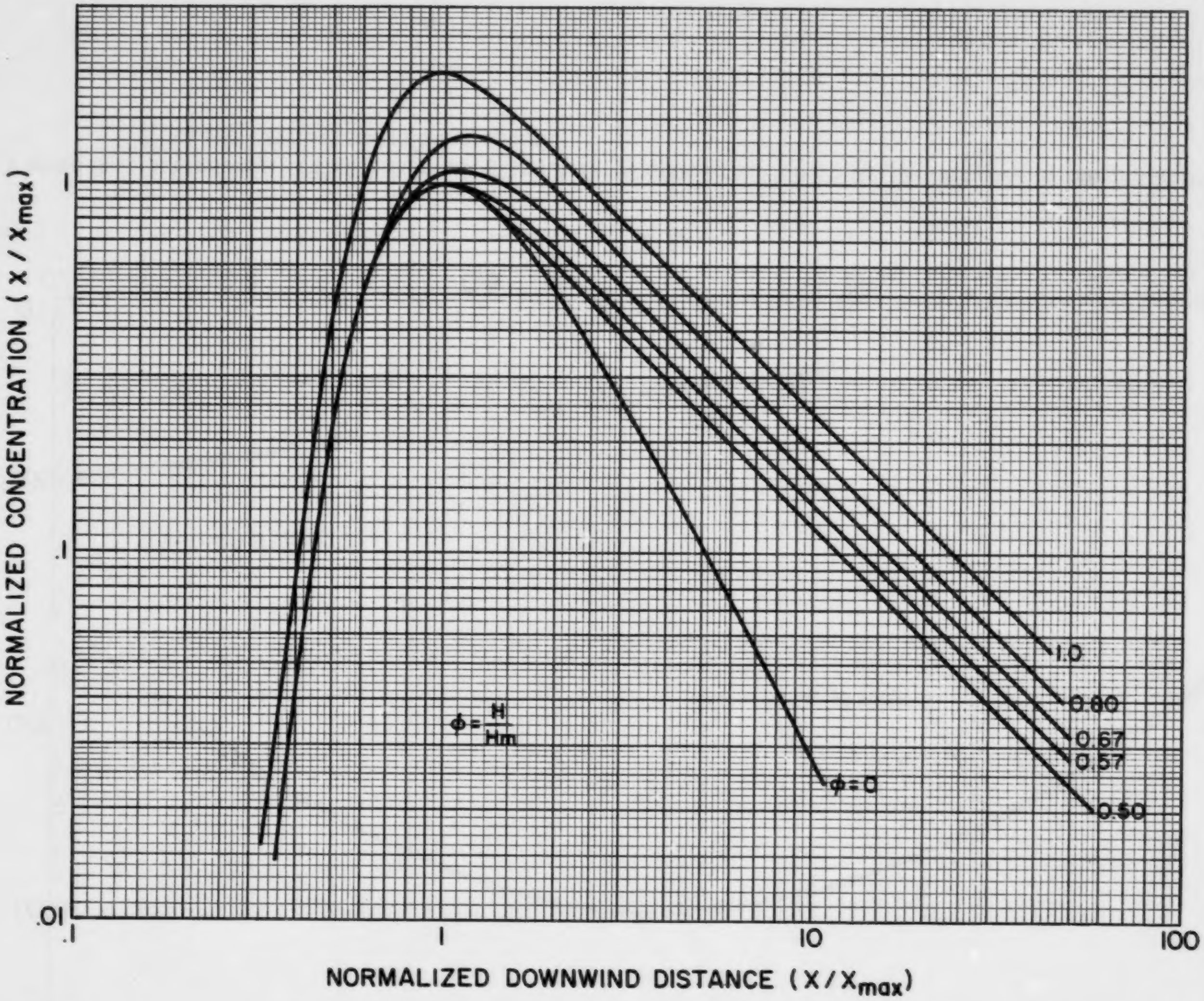

Figure 4. Dependence of ground-level concentration on the ratio of the plume stabilization height H to the depth of the surface mixing layer H_m.

For tall stacks located in complex terrain, the conditions leading to maximum ground-level concentrations are uniquely related to the source parameters (stack height, stack exit velocity, plume heat content, etc.), terrain heights and meteorological factors. In general, the maximum concentration on elevated terrain points that are lower than the top of the stack increases as the mean wind speed increases and, in the limit, can exceed the critical wind-speed concentration by an order of magnitude (see Section 4). Very large increases in the maximum ground-level concentration above the critical wind-speed concentration also occur in flat terrain for stacks with high Froude numbers and low exit velocities as the result of stack downwash.

SECTION 4

COMPARISON OF TALL-STACK DISPERSION MODEL CALCULATIONS WITH MEASUREMENTS

We have used the tall-stack dispersion modeling techniques described above in a number of studies of the impact on ambient air quality of SO_2 emissions from tall stacks located in various types of terrain. In most of these studies, air quality observations and/or aircraft observations of plume characteristics were available to check the results of the model calculations. Also, in most of these studies, concurrent emissions data and meteorological data were available and were used to calculate the requisite model input parameters without any adjustments. As might be expected, the best overall agreement between calculated and observed concentrations has generally been obtained for annual average and 24-hour average SO_2 concentrations. Good agreement between calculated and observed hourly SO_2 ground-level concentrations is difficult to achieve for many reasons. A major difficulty arises from the fact that wind direction observations are inherently too coarse to allow sufficiently accurate calculations of hourly plume trajectories. Hourly angular plume widths are typically only a few degrees and observed hourly mean wind directions are usually reported only to the nearest 10 degrees. The fact that these observations are generally taken near the surface rather than at plume stabilization height further compounds the problem. In some cases, the density of the SO_2 monitoring network is such that the position of the plume centerline at the ground can be fixed within the 1 or 2 degree accuracy required for satisfactory comparisons of calculated and observed values.

To demonstrate the performance of our tall-stack dispersion models in estimating air quality impacts, there are presented below summary descriptions of the pertinent results from three air quality studies that my colleagues and I have conducted in the past several years for the U. S. Environmental Protection Agency. The three studies are identified as follows:

- Short-term and long-term ground-level SO_2 concentrations produced by the major stationary SO_2 sources located in and adjacent to Allegheny County, Pennsylvania (Cramer, Geary and Bowers, 1975)

- Short-term ground-level SO_2 concentrations produced by emissions from the ASARCO copper smelter in Tacoma, Washington (Cramer, Bowers and Geary, 1976)

- Short-term plume characteristics (plume stabilization heights and axial concentrations and short-term ground-level concentrations on elevated terrain) for the plumes from two coal-fired power plants located in complex terrain (Bowers and Cramer, 1976)

Other, similar studies that have recently been completed but are not described here include model calculations of the air quality impact of SO_2 emissions from two large electrical generating plants respectively located in very complex terrain in southern Nevada and central Utah. In both studies, very close agreement has been obtained between calculated and observed long-term and short-term ground-level SO_2 concentrations.

4.1 COMPARISON OF CALCULATED AND OBSERVED SO_2 CONCENTRATIONS PRODUCED BY MAJOR SOURCES IN ALLEGHENY COUNTY, PENNSYLVANIA

The short-term and long-term dispersion modeling techniques described above were used to calculate the ground-level concentrations in Allegheny County produced by SO_2 emissions from 107 major stationary sources located within or adjacent to Allegheny County. Concurrent emissions data and meteorological data for 1973 were substituted in computer programs containing the dispersion models and calculations made of the 1973 annual average concentrations as well as the 3-hour and 24-hour concentrations for three selected 24-hour periods during 1973 when high SO_2 concentrations were measured by the Allegheny County SO_2 monitors. Stack heights of individual sources ranged from about 30 meters to 100 meters. The terrain in Allegheny County is moderately complex with maximum differences in elevation of about 150 meters. A summary of the calculated and observed 1973 SO_2 ground-level concentrations at various monitor locations is given in Table 4. The calculated concentrations, which do not include any background SO_2, were obtained by direct substitution of the emissions data and meteorological data in the dispersion models without any adjustments. The mean ratios given in the table show that, on the average, the calculated maximum 3-hour, 24-hour and annual average concentrations at the monitors were within 10 to 20 percent of the observed concentrations. As explained in the report describing this study (Cramer, Geary and Bowers, 1975), the correspondence between the calculated and observed 3-hour and 24-hour maximums at individual monitors can be significantly improved if reasonable adjustments are made in the hourly wind direction data which in most cases were obtained by averaging the hourly surface observations from the Greater Pittsburgh and Allegheny County Airports.

4.2 COMPARISON OF CALCULATED AND OBSERVED SO_2 CONCENTRATIONS PRODUCED BY TALL-STACK EMISSIONS FROM THE ASARCO COPPER SMELTER IN TACOMA, WASHINGTON

The ASARCO copper smelter in Tacoma, Washington is one of the largest copper smelters in the United States. The smelter is located near the tip of the Tacoma peninsula and is surrounded by water on three sides. The land surfaces in the vicinity of the smelter range vary from relatively smooth tidal flats and beaches to rugged hills that extend 150 meters above mean sea level. The smel-

TABLE 4

COMPARISON OF CALCULATED AND OBSERVED 1973 GROUND-LEVEL SO_2 CONCENTRATIONS IN ALLEGHENY COUNTY*

Case	Monitor Location	SO_2 Concentrations ($\mu g/m^3$)		Calculated Concentration / Observed Concentration
		Calculated	Observed	
(a) 3-Hour Maximum Concentration				
4 January 1973	Logans Ferry	2207	1880	1.17
18 January 1973	Glassport	375	300	1.25
18 January 1973	Liberty Borough	717	1305	0.55
13 July 1973	Glassport	496	395	1.26
13 July 1973	Liberty Borough	1204	820	1.47
			Mean Ratio	1.14
(b) 24-Hour Average Concentration				
4 January 1973	Logans Ferry	979	891	1.10
18 January 1973	Glassport	186	153	1.22
18 January 1973	Liberty Borough	268	647	0.41
13 July 1973	Glassport	101	139	0.73
13 July 1973	Liberty Borough	258	361	0.71
			Mean Ratio	0.83
(c) Annual Average Concentration				
1973	Glassport	80	79	1.01
1973	Liberty Borough	116	139	0.83
1973	Hazelwood	86	92	0.93
			Mean Ratio	0.92

*Based on data given by Cramer, Geary and Bowers (1975).

ter uses a Supplementary Control System (SCS) to reduce the SO_2 emission rate from the main 172-meter stack during periods when meteorological conditions are conducive to high ground-level concentrations.

The SO_2 monitoring networks operated by the ASARCO smelter and the Puget Sound Air Pollution Control Agency (PSAPCA) are sufficiently dense such that the ASARCO plume was simultaneously detected by two or more SO_2 monitors during a number of the cases that we studied. This made it possible to fix the location of the plume centerline within 1 or 2 degrees. As pointed out in our report on the ASARCO smelter (Cramer, Bowers and Geary, 1976), the hourly concentration calculated at a fixed receptor point is very sensitive to small uncertainties in the mean wind direction used to calculate the plume trajectory. Table 5 shows a comparison of calculated and observed hourly SO_2 concentrations for the cases when the observed concentrations at the monitors exceeded the PSAPCA hourly ambient air quality standard of 0.25 parts per million (ppm). The hours listed in Table 5 include only those hours when the ASARCO plume was simultaneously detected by two or more SO_2 monitors so that the plume centerline could be accurately positioned. As shown by the mean ratios at the bottom of the table, the average ratio of the calculated and observed concentrations is approximately unity. We believe that uncertainties in the ASARCO hourly SO_2 emission rates, which vary over a wide range due to the smelter's SCS activities, are the major cause of large differences between the calculated and observed concentrations for the individual cases.

4.3 COMPARISON OF CALCULATED AND OBSERVED PLUME CHARACTERISTICS FOR TWO ELECTRICAL GENERATING PLANTS IN MARSHALL COUNTY, WEST VIRGINIA

The Kammer and Mitchell Power Plants are located on the east side of the Ohio River Valley in Marshall County, West Virginia. The valley width varies from 1 to 2 kilometers, and terrain elevations on both sides of the river range from 100 to over 200 meters above the valley floor. The Mitchell Power Plant has a single

TABLE 5

COMPARISON OF CALCULATED AND OBSERVED SO_2 CONCENTRATIONS FOR CRITICAL WIND-SPEED AND LIMITED-MIXING CASES WHEN THE OBSERVED HOURLY CONCENTRATION EXCEEDED 0.25 PPM (FROM CRAMER, BOWERS AND GEARY, 1976)

Case No.	Monitor	Observed Concentration* (ppm)	Calculated Concentration (ppm)	Calc. Conc. / Observed Conc. **
2	N26th and Pearl	(1.23)	0.88	(0.72)
	Reservoir	0.27	0.04	0.15
	Highlands	0.73	0.44	0.60
3	N26th and Pearl	0.40 (0.46)	0.25	0.63 (0.54)
4	N26th and Pearl	0.56 (0.68)	0.61	1.09 (0.90)
	Reservoir	0.62	0.64	1.03
6	N26th and Pearl	0.30 (0.22)	0.30	1.00 (1.36)
	N26th and Pearl	0.26 (0.26)	0.23	0.88 (0.88)
7	N26th and Pearl	0.60 (0.46)	0.26	0.43 (0.57)
8	N26th and Pearl	0.32 (0.21)	0.44	1.38 (2.10)
	Reservoir	0.37	0.39	1.05
9	N26th and Pearl	0.37 (0.67)	0.64	1.73 (0.96)
	N26th and Pearl	0.31 (0.21)	0.11	0.35 (0.52)
10	N26th and Pearl	0.25 (0.25)	0.34	1.36 (1.36)
12	McMicken Heights	0.50	0.52	1.04
13	Meeker	0.28	0.28	1.00
	Meeker-Brown	0.31	0.35	1.13
	Meeker	0.38	0.42	1.11
	Meeker-Brown	0.42	0.50	1.19
	Meeker	0.59	0.56	0.95
	Meeker-Brown	0.49	0.53	1.08

TABLE 5 (Continued)

Case No.	Monitor	Observed Concentration* (ppm)	Calculated Concentration (ppm)	Calc. Conc.** / Observed Conc.
14	McMicken Heights	0.30	0.09	0.33
	Tukwila	0.41	0.10	0.24
19	N26th and Pearl	0.42 (0.35)	0.87	2.07 (2.49)
	Reservoir	0.50	1.00	2.00
	N26th and Pearl	0.27 (0.17)	0.10	0.37 (0.59)
			Mean Ratio	0.97 (1.00)

*Numbers enclosed by parentheses are concentrations measured by the ASARCO SO_2 monitor at N26th and Pearl.

**Numbers enclosed by parentheses are the ratios of calculated and observed concentrations for the ASARCO monitor at N26th and Pearl.

365-meter stack that is one of the tallest in the United States. The Kammer Power Plant has two 183-meter stacks that extend to about the same height as the terrain on either side of the river valley. The heat content of the Kammer No. 1 stack is about double that of the Kammer No. 2 stack. During the period August-September 1975, the Environmental Monitoring and Support Laboratory (Las Vegas, Nevada) of the U. S. Environmental Protection Agency made airborne measurements of SO_2 concentrations downwind from the two power plants. We used concurrent meteorological and emissions data with our short-term dispersion model to calculate the plume characteristics for comparison with the EMSL measurements. The following discussion is principally taken from a paper by Bowers and Cramer (1976).

The observed plume rise for each stack was determined for each trial by subtracting the stack height from the height of the corresponding maximum observed SO_2 concentration at the closest downwind distance at which aircraft measurements were made. This measurement distance was always greater than the calculated plume stabilization distance and was also frequently at a distance where the plume from the Kammer No. 2 stack was significantly affected by reflection from the ground. In these cases, the height of the maximum observed SO_2 concentration for the Kammer No. 2 plume should be lower than the plume stabilization height because reflection from the ground decreases the height of the maximum concentration and eventually brings it to the ground surface (see Dumbauld and Bowers, 1976). Reflection from the bases of elevated inversions at the top of the surface mixing layer also affected the observed SO_2 concentrations in some of the trials, but this effect was generally small in comparison with the effect of ground reflection. Interaction of the Kammer No. 1 and No. 2 plumes additionally affected the observed maximum concentrations and introduced other uncertainties in the determination of the observed plume rises from the aircraft measurements.

Table 6 shows the observed plume rises determined from the aircraft measurements and the corresponding calculated plume rises. For the reasons given above, we believe that the observed plume rises for the Kammer No. 2 stack generally underestimate the actual plume rises and have indicated this qualification by quotation marks. In Trials 10 and 11, the heat contents and SO_2 emissions for both Kammer plumes were nearly identical and the aircraft observations for each trial showed a single merged plume. The predicted plume rises in Table 6 are in good agreement with the observations for Mitchell and Kammer No. 1. In every case, the plume rise calculated for Kammer No. 2 exceeds the "observed" plume rise. As explained above, this result was expected because of the interaction of this plume with the terrain at the distance of the aircraft measurements.

Table 7 presents the calculated and observed axial SO_2 concentrations. Heights 1 and 2 in the table are the heights of the two highest measured concentrations and refer either to the two Kammer plumes individually, or to a single merged Kammer plume and the Mitchell plume. Downwind Distance 1 in the table varies from about 3.7 to 11 kilometers and Downwind Distance 2 varies from about 7.4 to 18.5 kilometers. As discussed above, the heights of the two highest observed concentrations do not necessarily correspond to the actual plume stabilization heights because of the effects of reflection and interaction of superposed plumes. The calculated axial concentrations are the concentrations calculated by means of the short-term dispersion model equations at the heights of the highest concentrations measured by EMSL, using the Briggs plume rise formulas to obtain plume stabilization heights. The calculated axial concentrations thus include the effects of reflection and the combined contributions of the two Kammer plumes plus, where appropriate, the contribution of the Mitchell plume.

Table 7 shows that the model estimates of axial concentrations are, on the average, approximately 21 percent larger than the observed axial concentrations at Downwind Distance 1. This could be due to the fact that the observed concentrations have not been adequately adjusted for the response time of the SO_2 instrument in the helicopter(see Johnson, et al., 1976). Also, the Mitchell plume bifurcated during

TABLE 6

CALCULATED AND OBSERVED PLUME RISES FOR THE MITCHELL AND KAMMER POWER PLANTS (FROM BOWERS AND CRAMER, 1976)

Trial Number	Mitchell Plume Rise (m)			Kammer No. 1 Plume Rise (m)			Kammer No. 2 Plume Rise (m)		
	O	C	C/O	O	C	C/O	"O"	C	C/"O"
1	186	176	0.95	---	---	---	---	---	---
3	338	270	0.80	412	486	1.18	230	391	1.70
5	---	---	---	839	602	0.72	382	478	1.25
6	---	---	---	291	262	0.90	---	---	---
7	---	---	---	412	420	1.02	230	319	1.39
8	369	347	0.94	534	668	1.25	458	534	1.17
10	---	---	---	321	324	1.01	321	337	1.05
11	348	345	0.99	412	413	1.00	412	427	1.04
12	217	253	1.17	351	386	1.10	---	---	---
13	308	308	1.00	229	245	1.07	---	---	---
15	400	401	1.00	473	316	0.67	229	241	1.05
16	140	200	1.43	214	172	0.80	---	---	---
	Mean Ratio		1.04	Mean Ratio		0.97	Mean Ratio		1.24

O = Observed Plume Rise
C = Calculated Plume Rise
O/C = Ratio of Calculated and Observed Plume Rise

TABLE 7

CALCULATED AND OBSERVED AXIAL SO_2 CONCENTRATIONS (FROM BOWERS AND CRAMER, 1976)

Trial	Axial SO_2 Concentration (ppm)											
	Downwind Distance 1						Downwind Distance 2					
	Height 1			Height 2			Height 1			Height 2		
	O	C	C/O	O	C	C/O	O	C	C/O	O	C	C/O
3	0.71	0.67	0.94	0.68	0.75	1.10	0.26	0.17	0.65	0.28	0.17	0.61
5	0.25	0.33	1.32	--	--	--	--	--	--	--	--	--
6	0.99	1.48	1.49	--	--	--	0.60	0.52	0.87	--	--	--
7	0.51	0.53	1.04	--	--	--	--	--	--	--	--	--
12	0.50	0.62	1.24	1.17	1.47	1.26	--	--	--	--	--	--
13	1.86	2.35	1.26	--	--	--	0.87	0.65	0.75	1.15	0.69	0.60
	Mean Ratio		1.22	Mean Ratio		1.18	Mean Ratio		0.75	Mean Ratio		0.61

O = Observed Concentration
C = Calculated Concentration
O/C = Ratio of Calculated and Observed Concentration

several trials, and the model would be expected to overpredict axial concentrations within several kilometers of the stack under these conditions. At Downwind Distance 2, the calculated axial concentrations are all less than the observed concentrations. The fact that no SO_2 background is included in the calculated values partially accounts for this result. However, the possibility that the model overestimates lateral plume growth cannot be excluded.

During Trial 3, the Kammer plumes were observed intersecting a hill about 3.7 kilometers west of the plant and during Trial 17 the Kammer plumes were observed impacting on a hill about 2.8 kilometers northeast of the plant. On both occasions, the EMSL helicopter made a number of passes through the plumes at a height of 15 to 30 meters above ground level. Table 8 lists the observed maximum SO_2 concentrations and the maximum ground-level SO_2 concentrations calculated with and without the terrain-adjustment procedures described in Section 2. Table 6 shows that the 10-minute concentrations calculated by including terrain effects are in good agreement with the observed concentrations. If it is assumed that the plume axes are terrain following (i.e., no terrain adjustments are required), the calculated concentrations are substantially lower than the observed concentrations.

TABLE 8

MAXIMUM OBSERVED AND CALCULATED GROUND-LEVEL SO_2 CONCENTRATIONS (FROM BOWERS AND CRAMER, 1976)

Trial	Terrain Height (m above MSL)	Observed Conc. (ppm)	Calculated Concentration (ppm)		$\frac{\text{Calculated Concentration}}{\text{Observed Concentration}}$	
			With terrain adjustments	Without terrain adjustments	With terrain adjustments	Without terrain adjustments
3	442	0.52	0.76	0.35	1.46	0.67
17	274	0.15	0.14	0.02	0.93	0.13
				Mean Ratio	1.20	0.40

ACKNOWLEDGMENTS

The dispersion modeling techniques described in this paper have been jointly developed by myself and my colleagues, especially Mr. R. K. Dumbauld and Mr. J. F. Bowers. I am additionally indebted to Mr. Bowers for assisting me in the preparation of much of the material presented in this paper.

REFERENCES

Bowers, J. F. and H. E. Cramer, 1976: Comparison of calculated and observed characteristics of plumes from two coal-fired power plants located in complex terrain. Preprint of a paper to be presented at the Third Symposium on Atmospheric Turbulence, Diffusion and Air Quality, Raleigh, North Carolina, October 19-22, 1976.

Briggs, G. A., 1969: Plume Rise. Available as TID-25075 from Clearinghouse for Federal Scientific and Technical Information, Springfield, Va., 80.

Briggs, G. A., 1971: Some recent analyses of plume rise observations. In Proceedings of the Second International Clean Air Congress, Academic Press, New York.

Briggs, G. A., 1972: Chimney plumes in neutral and stable surroundings. Atm. Env., 6(7), 507-510.

Briggs, G. A., 1974: Private communication with R. K. Dumbauld, H. E. Cramer Company, Inc.

Bringfelt, B., 1968: Plume rise measurements at industrial chimneys. Atmospheric Environment, 2(6), 575-598.

Calder, K. L., 1971: A climatological model for multiple source urban air pollution. Proc. 2nd Meeting of the Expert Panel on Air Pollution Modeling, NATO Committee on the Challenges of Modern Society, Paris, France, July 1971, 33.

Cramer, H. E., 1957: A practical method for estimating the dispersal of atmospheric contaminants. Proceedings of the First National Conference on Applied Meteorology, Ann Arbor, Mich.

Cramer, H. E., 1959: Engineering estimates of atmospheric dispersal capacity. J. Ind. Hyg. Assoc., 20, 183-189.

Cramer, H. E., et al., 1972: Development of dosage models and concepts. GCA Technical Report TR-70-15-G, Final Report under Contract No. DAAD09-67-C-0020(R), U. S. Army Deseret Test Center, Fort Douglas, Utah, 367.

REFERENCES (Continued)

Cramer, H. E., H. V. Geary and J. F. Bowers, 1975: Diffusion-model calculations of long-term and short-term ground-level SO_2 concentrations in Allegheny County, Pennsylvania. H. E. Cramer Company Technical Report TR-75-102-01 prepared for the U. S. Environmental Protection Agency, Region III, Philadelphia, Pennsylvania. EPA Report 903/9-75-018. NTIS Accession No. PB-245262/AS.

Cramer, H. E., J. F. Bowers and H. V. Geary, 1976: Assessment of the air quality impact of SO_2 emissions from the ASARCO-Tacoma smelter. EPA Report No. EPA 910/9-76-028. U. S. Environmental Protection Agency, Region X, Seattle, Washington.

Csanady, G. T., 1973: Effect of plume rise on ground-level pollution. Atmospheric Environment, 7, 1-16.

Dumbauld, R. K., et al., 1970: Handbook for estimating toxic fuel hazards. Final Report under Contract No. NAS8-21453, NASA Rpt. No. CR-61326.

Dumbauld, R. K. and J. F. Bowers, 1976: Discussion of the paper "A point source atmospheric diffusion model." Atmospheric Environment, 10, 418.

Fay, J. A., M. Escudier and D. P. Hoult, 1970: A correlation of field observations of plume rise. Journal of the Air Pollution Control Association, 20(6), 391-397.

Johnson, F. G., R. B. Evans and T. M. Zeller, 1976: Airborne measurements of power plant plumes in West Virginia, 1975. EPA Draft Report. U. S. Environmental Protection Agency, Las Vegas, Nevada.

Luna, R. E. and H. W. Church, 1971: A comparison of turbulence intensity and stability ratio measurements to Pasquill turbulence types. Paper presented at a Conference on Air Pollution Meteorology, Raleigh, N. C., 5-9 April 1971.

Moore, D. J., 1974: A comparison of the trajectories of rising buoyant plumes with theoretical/empirical models. Atmospheric Environment, 8, 441-457.

Osipov, Y. S., 1972: Diffusion from a point source of finite time of action. In AICE Survey of USSR Air Pollution Literature - Volume XII, distributed by the National Technical Information Service, Springfield, Virginia.

REFERENCES (Continued)

Panofsky, H. B., 1973: The boundary layer above 30 meters (Part III). Boundary-Layer Meteorology, 4, 251-274.

Pasquill, F., 1961: The estimation of the dispersion of windborne material. Met. Mag., 90, 33-49.

Pasquill, F., 1974: Atmospheric Diffusion (Second Edition). Ellis Horwood Limited, Sussex, England, 429.

Pasquill, F., 1976: Atmospheric dispersion parameters in Gaussian plume modeling, Part II. EPA-600/4-76-030 6, Research Triangle Park, North Carolina.

Swanson, R. N. and H. E. Cramer, 1965: A study of lateral and longitudinal intensities of turbulence. J. Appl. Met., 4, 409-417.

Turner, D. B., 1969: Workbook of Atmospheric Dispersion Estimates. PHS Pulbication No. 999-AP-26, U. S. Dept. of Health, Education and Welfare, National Air Pollution Control Administration, Cincinnati, Ohio.

Yamamoto, S. and O. Yokoyama, 1974: A practical method for estimating the dispersion of plumes. Paper No. 142 presented at the 15th National Air Pollution Research Conference, Chiba, Japan, November 6-8, 1974.

7th International Technical Meeting
on Air Pollution Modeling and its Application

Plume Dispersion from the Sudbury Tall Stack

by

F.H. Fanaki and H.E. Turner
Atmospheric Environment Service
Toronto, Canada

September 7 - 10, 1976

Airlie Virginia

United States of America

Plume Dispersion from the Sudbury Tall Stack

by

F.H. Fanaki and H.E. Turner

Abstract

Increasing consideration is being given to the tall stack as a technique for maintaining air quality at ground level. This, in turn, has focussed attention on the difficulties associated with the estimation of the plume rise and dispersion to be expected from such structures, in particular, the specification of appropriate plume rise formulas, stability categories and associated plume diffusion parameters. In this paper, the problem is discussed in terms of the results from a field study of plume dispersion from a 381 meter smelter stack where experimental observations are compared with simple theoretical models.

Plume Dispersion from the Sudbury Tall Stack

1. Introduction

Over the past decade, increasing consideration has been given to the tall stack as a technique for maintaining air quality at ground level. This, in turn, has focussed attention on the difficulties associated with the estimation of the plume behaviour to be expected from such structures under various meteorological conditions. To a large extent, the problem arises because of a lack of experimental observations and an inadequate understanding of the relevant atmospheric structure and processes above the better-researched surface boundary layer. As a consequence, the application of existing prediction formulas often requires questionable extrapolations for height-dependent parameters and relationships. There is, therefore, a strong need to establish a relevant data base from the appropriate height in the planetary boundary layer in order to validate aspects of pollutant dispersion from tall stacks.

In 1973, the Atmospheric Environment Service of Environment Canada and the Air Resources Branch of the Ontario Ministry of the Environment initiated a joint program to investigate plume dispersion from the 381 meter smelter stack of the International Nickel Company of Canada (INCO) at Sudbury, Ontario. Associated field studies were carried out in June and October, 1973, March and September, 1974, and June, 1975, with a further one planned for September of this year. Each of these studies included one or more of the measurement programs listed in Table I below.

Table I

Measurement Programs During The Sudbury Tall Stack Field Studies

Measurement	Technique
Emissions	In-stack traversing probes
Plume-rise	Photography
Pollutant-concentration distributions	Ground-based lidar Ground-based correlation spectrometer Airborne _in situ_ sensor Ground-based mobile _in situ_ sensor
SO_2 oxidation	Airborne filter pack
Wind and temperature profiles	Radiosonde, tethersonde, minisonde, pilot balloon

This paper is concerned with the measurement of plume-rise and plume dispersion coefficients as detected by photography and airborne _in situ_ sensing and a comparison of the observations with predictions calculated on the basis of concurrent meteorological measurements.

2. Source Description

The INCO Copper Cliff smelter complex is located in the west end of the city of Sudbury which lies on the Precambrian Shield in the border zone between what is generally considered Southern and Northeastern Ontario (Figure 1). The surface features of the Sudbury area owe their form and structure to continental glaciation which left behind a complex of rock outcropping, broken hills, river valleys, small lakes and intermittent soil pockets. The relief is modest, however, with gentle slopes and altitudes confined between 250 and 500 meters MSL.

Emissions to the atmosphere from the Copper Cliff plant originate from the pyrometallurgical production of nickel and copper from sulphidic ore concentrates. The 381 meter smelter stack (Figure 2) commenced operation in August 1972 and, during the study reported here, it possessed the emission characterisics given in Table II. The annual average SO_2 emission was equivalent to approximately 3700 metric tons/day.

3. Measurement and Analysis Procedures

The technique of photographing the INCO plume in order to measure its rise has been described previously by Fanaki and Lesins (1975) the theoretical principle followed in the analysis of these photographs was discussed in detail by Halitsky (1961). Due to the uncertainty of the azimuthal position of the plume at any instant and to the randomness of the plume height, many photographs were required in order to average out deviations from the mean. In this study the plume was photographed every 30 seconds over a period of at least 30 minutes. By superimposing several photographs and tracing the plume outlines a time-mean path of the plume was obtained. The observations of the rise of the plume are the outcome of three field studies conducted during the months of June 1973, October 1973 and September 1974. The range of the meteorological conditions at the plume level are summarized in Table III.

Table II

Characteristics of the INCO 381 Stack

Parameter	Magnitude
Height	381 m
Inside diameter	13.7 m
Exit velocity	20 m sec^{-1}
Stack gas temperature at stack exit	$182^{o}C$
SO_2 emission rate	35.8 kg sec^{-1}
Mean heat flux	8×10^{7} cal sec^{-1}

Table III

Meteorological Conditions at the Plume Level During the Study Period

Date	Mean Wind Speed ($m\ sec^{-1}$)	Average Air Temperature (K)	Potential Temperature Gradient (K/m)
June 1973	2.7 to 10.4	280 to 289	-.0033 to .0057
Oct. 1973	4.2 to 18.8	271 to 287	.0007 to .0161
Sept. 1974	1.6 to 17.5	267 to 282	-.0018 to .0098

The plume from the INCO stack is buoyant and rises to several hundred meters. Its trajectory during ascent under steady winds is similar to the one described by Scorer (1968). Some additional characteristics were recorded and described in detail by Fanaki (1975).

It appears that the INCO plume never levels off and therefore the final rise of the plume is assumed to be reached when its rate of rise is minimum (see Montgomery _et al_, 1971).

Airborne measurements of SO_2 concentrations in the plume were limited to the June and October field studies of 1973. Observations were carried out from a twin-engine Piper Apache aircraft instrumented with a Sign-X SO_2 Monitor (Model 6600 A). The sampling probe was mounted in the aircraft nose in place of the headlight and extended several inches beyond the aircraft skin. Sensitivity of the measuring system covered the range 0.02 to 50 ppm SO_2 and the system response time was 3 seconds. The aircraft was also equipped with a precision pressure-height transducer.

Individual flights were planned to last about two hours in order to minimize the influence of temporal variations in meteorological parameters. During the June period, horizontal transects perpendicular to the plume were flown at several heights for each of a series of downwind distances. These distances generally included at least one in the 2-10 km range, one in the 10-20 km range and one as far downwind as the plume maintained adequate definition (> 125 km in one case). Traverses were carried out at an air speed of 40 meters/second and visual navigation was used to establish the geographical location of traverse end-points with respect to a pre-selected grid of distinctly identifiable ground features. A total of 14 useful flights were obtained during the June study.

The flight plan was modified during the October period because of a requirement to gain some information on peak/mean concentration ratios in the plume. As a consequence, the several plume transects at each downwind distance were flown at a fixed height which corresponded closely to the height of maximum concentration. Downwind distances of approximately 5, 15 and 30 km were used in each case and, again, a total of 14 useful flights were obtained for this period.

For each downwind distance, horizontal and vertical dispersion coefficients were approximated by the second moments of the vertically and horizontally integrated crosswind concentration distributions, respectively.

4. Observations

4.1 Plume Rise

There are numerous formulas for modeling the rise of a buoyant plume (see Briggs, 1969). These formulas, however, were derived for relatively short stacks. In order to model the rise of the INCO tall stack plume, these widely used formulas require re-evaluation. In this study the most commonly used formulas, namely Briggs (1969 , 1971 and 1972), TVA 1971 and 1972 (see Montgomery _et al_., 1971 and 1972), Holland (1953), CONCAWE (see Brummage, 1968) and Moses and Carson (1967) were selected to examine their predictive capability in determining the rise of INCO plume. This was done by comparing the observed plume rise with the predicted value and the results are shown in Figures (3-8). It can be seen by the scatter of the points in the figures that none of the models are good predictors for the measured values. CONCAWE and Moses and Carson's formulas significantly under-predict the rise of the plume which in turn will lead to overestimates of the maximum ground-level pollutant concentration. The predictive capability of the remaining formulas depends on the wind speed. Table IV shows the mean values of the ratio of the observed plume rise to the predicted value of the plume rise for different ranges of wind speed. With all the formulas except Briggs', the fit becomes steadily worse with increase in the wind speed. By comparison, Briggs' model appears to perform best but the correlation is still low when one considers the strong dependence of predicted concentrations upon assumed plume rise.

Table IV

Ratios of Observed to Predicted Plume Rise
for Different Wind Speed Ranges

Wind Speed Range ($m\ sec^{-1}$)	Ratios of Observed to Predicted Plume Rise			
	Briggs	TVA (1971)	TVA (1972)	Holland
$U<3$	1.26	1.01	0.95	0.75
$3\leq U<5$	1.09	0.93	0.75	0.63
$5\leq U<7$	1.22	1.29	0.94	0.88
$7\leq U<9$	1.45	1.78	1.29	1.39
$9\leq U$	1.28	1.87	1.36	1.74

4.2 Dispersion Coefficients

In all instances in this sub-section, the observed plume behaviour from the tall stack is either classified according to or discussed in relation to the predictions of classical Gaussian plume theory. In particular, the observations are stratified into stability categories determined by applying the algorithm of Turner (1964) to the hourly observations from the Sudbury airport (20 km to the northeast of the stack) and comparisons are made with calculations based on Pasquill-Gifford dispersion parameters as given by Turner (1967). This was done in order to provide a convenient and well-known reference framework for discussion of the idiosyncrasies of tall stack plume behaviour and not because of any preconceived notion that the theory ought to apply. This latter point is well-demonstrated in Figure 9. Here, the temperature profiles measured during the June study are averaged for stability categories 2-3, 4, 5-6 and shown relative to the stack height and the range of observed plume heights. It will be noted that the significant changes in the average lapse rate with stability are limited to heights of the order of stack top while, on the average, the plume centreline resides in a region of slight stability independent of the category. The situation is further complicated by the fact that tall stack plumes exist at a height where important atmospheric structure is advected and is thus not predictable from local surface observations.

The June measurements of the horizontal dispersion coefficient (σ_y) are presented in Figure 10 where three observations may be made. First, these data are generally large and, for all observed stability categories, compare with Pasquill-Gifford values for plume growth under unstable conditions. Secondly, there is no apparent relationship between the measured coefficients and their corresponding stability classes. Finally, it should be noted that the early morning cases (marked with a star on Figure 10) tend to lie either at the top or the bottom of the data distribution. In the former case, the results reflect increased horizontal plume growth due to vertical wind shear (see Figure 11) which is more prevalent, of course, under the stable conditions associated with that time of day. That such apparent plume growth may be attributed to shear is supported by the horizontal dispersion coefficient data from the October study as shown in Figure 12. Although the first two points made above for the June data also hold for this figure, the early morning cases do not lie near the top of the distribution here since the measurement technique (fixed height traverses) was not sensitive to the effect of vertical wind shear.

In Figure 10, the early morning data that lie below the F stability curve represent one interesting special case where the plume dispersed under conditions of an isothermal temperature gradient, strong steady wind and no vertical shear in wind direction. Plume tracking was limited to 125 km for logistical reasons only and the plume displayed virtually no vertical growth to that point. No horizontal plume growth was evident between 1 and 30 km but a small increase occurred beyond this distance due to a slight decrease in the steadiness of the wind.

Figure 13 compares the June data for the vertical dispersion coefficient (σ_z) with the corresponsing Pasquill-Gifford curves. Here, the data show somewhat better agreement with the predictions although the observations are compressed towards the stable curves. A separation between the stable and unstable values is evident but the neutral values tend to be uniformly spread between the C and F curves. No σ_z data was collected during the October study.

Since the Pasquill-Gifford curves generally underestimate observed σ_y and overestimate σ_z for the Sudbury data, it is of interest to examine the resulting impact upon Gaussian theory predictions for spatial SO_2 concentrations. Calculated concentration values were obtained by using the steady-state Gaussian formula, plume height equal to the mean of actual heights (average traverse height, weighted by horizontally-integrated concentrations) measured by aircraft within 30 km of the stack and wind speed equal to the mean speed measured by pilot balloon through the plume's vertical extent during each particular flight. Because of limited ground-level data (June only), these calculations were also compared with plume centreline concentrations. It should be noted, however, that the experimental values of plume centreline concentration are estimated by the maximum concentration encountered by the aircraft at the particular downwind distance. The relationship between this value and true maximum concentration, either instantaneous or time-averaged, is not clear but would be expected to deteriorate under unstable conditions. On the otherhand, ground-level observations correspond to measurements averaged over 20 minutes to half an hour.

The comparison between measured and calculated centreline concentrations for June are shown in Figure 14. The agreement here for all stabilities is suprisingly fair (except for one unstable case) with perhaps a slight shift of the experimental data towards the stable curves and with the special ultra-stable case clearly evident at the top of the figure. The agreement is not so good, however, for the October data as illustrated in Figure 15. Here there is a larger spread of neutral experimental values while unstable values are much larger than predicted. At least part of the spread of the neutral data may be understood by noting the preponderance of early morning cases amongst the larger values. On the other hand, the differences in the magnitudes of the experimental values for unstable conditions between Figures 14 and 15 may reflect a difficulty with attempting to predict instability for tall stack plumes or may just be a product of the experimental technique for estimating the centreline concentrations.

During the June study, there were 12 occasions on which simultaneous aircraft and ground-level observations were made.

The ratio of observed to predicted concentration at the surface is given in Figure 16 as a function of downwind distance. On seven occasions, the predictions were within a factor of about 2 while a further two occasions were underestimated by a factor of 4. Of the remaining three data points, drastic underestimates were produced because of strong looping in one case and because of limited mixing (warm front aloft) in the remaining two.

5. Concluding Remarks

It is apparent from the observations presented in this paper that there are several aspects of plume dispersion from the Sudbury tall stack which require detailed study before a satisfactory predictive model can be derived. For example, a theoretical approach to plume-rise estimation should take into account the three-dimensional behaviour (billowing) of the plume. This problem is further complicated by the frequent occurrence of bifurcation and vertical wind shear. In the area of transport and diffusion, there is also a need to understand the impact of wind shear and to parameterize horizontal plume growth in terms other than hydrostatic stability. In addition, better criteria are required to determine the onset of looping which, together with limited mixing, have been observed to produce the highest ground-level concentrations. These problems are the subjects of current and future studies at Sudbury.

References

Briggs, G.A. 1969,"Plume Rise". AEC Critical Review Series TID-25075, 81 pp, National Technical Information Service.

Briggs, G.A. 1971, "Some Recent Analyses of Plume Rise Observation" Proc. Second International Clean Air Congress, Academic Press, 1029-1032.

Briggs, G.A. 1972, "Discussion on Chimney Plumes in Neutral and Stable Surroundings". Atmos. Environment 6, 507-510.

Brummage, K.G. 1968, "The calculation of Atmospheric Dispersion from a Stack" Atmos. Envir. 2, 197.

Fanaki, F.H. and Lesins, G. 1975, "Photographic Measurement of Smoke Plume Heights from Industrial Stacks". Journal of the SMPTE 84, 77-81.

Fanaki, F.H. 1975, "Experimental Observations of a Bifurcated Buoyant Plume". Boundary-Layer Meteorology 9. 480-495.

Holland, J.Z. 1953, A Meteorological Survey of the Oak Ridge Area. U.S. Atomic Energy Commission Report ORO - 99, 554.

Montgomery, T.L., Carpenter, S.B., Colbaugh, W.C. and Thomas, F.W. 1971, "Full-Scale Study of Plume Rise at Large Electric Generating Stations - Bull Run Supplement. Air Quality Branch, TVA, Muscle Shoals, Ala. 58 pp.

Montgomery, T.L., Carpenter, S.B., Colbaugh, W.C. and Thomas, F.W. 1972, "Results of Recent TVA Investigations of Plume Rise. J. Air Pollution Control Assoc., 22, 779-784.

Moses, H. and Carson, J.E. 1967, "Stack Design Parameters Influencing Plume Rise". Paper presented at the 60th Annual Meeting of the Air Pollution Control Association, Cleveland, Ohio. Paper 67-84.

Scorer, R.S. 1968. "Air Pollution", Pergamon Press, London.

Turner, D.B., 1964. "A diffusion model for an urban area" Journ. Appl. Met. 3, 83-91.

Turner, D.B., 1967. "Workbook of Atmospheric Dispersion Estimates", Public Health Service Publication 999-AP-26, U.S. Dept. of Health, Education and Welfare.

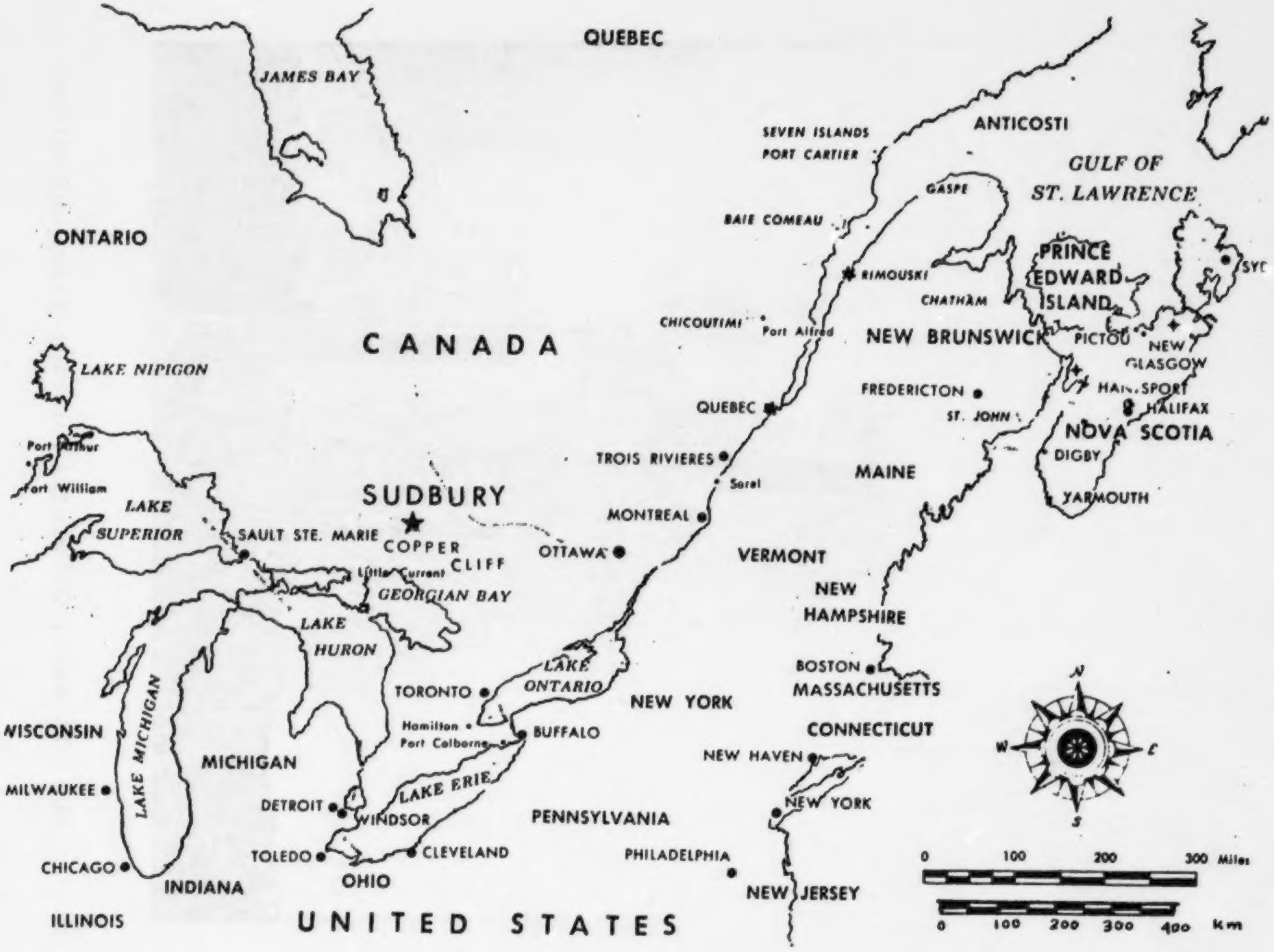
QUEBEC
JAMES BAY
ONTARIO
CANADA
LAKE NIPIGON
Port Arthur
Port William
LAKE SUPERIOR
SAULT STE. MARIE
SUDBURY
COPPER CLIFF
Little Current
GEORGIAN BAY
LAKE HURON
LAKE MICHIGAN
WISCONSIN
MILWAUKEE
CHICAGO
ILLINOIS
INDIANA
MICHIGAN
DETROIT
WINDSOR
TOLEDO
OHIO
CLEVELAND
LAKE ERIE
Hamilton
Port Colborne
BUFFALO
TORONTO
LAKE ONTARIO
OTTAWA
MONTREAL
Sorel
TROIS RIVIERES
QUEBEC
CHICOUTIMI
Port Alfred
BAIE COMEAU
SEVEN ISLANDS
PORT CARTIER
RIMOUSKI
GASPE
ANTICOSTI
GULF OF ST. LAWRENCE
PRINCE EDWARD ISLAND
CHATHAM
NEW BRUNSWICK
FREDERICTON
ST. JOHN
PICTOU
NEW GLASGOW
HANTSPORT
HALIFAX
NOVA SCOTIA
DIGBY
YARMOUTH
SYD
MAINE
VERMONT
NEW HAMPSHIRE
BOSTON
MASSACHUSETTS
CONNECTICUT
NEW YORK
NEW HAVEN
NEW YORK
PENNSYLVANIA
PHILADELPHIA
NEW JERSEY
UNITED STATES
N
E
S
W
0
100
200
300 Miles
0
100
200
300
400 km

Figure 1: Map of Eastern Canada showing the location of Sudbury

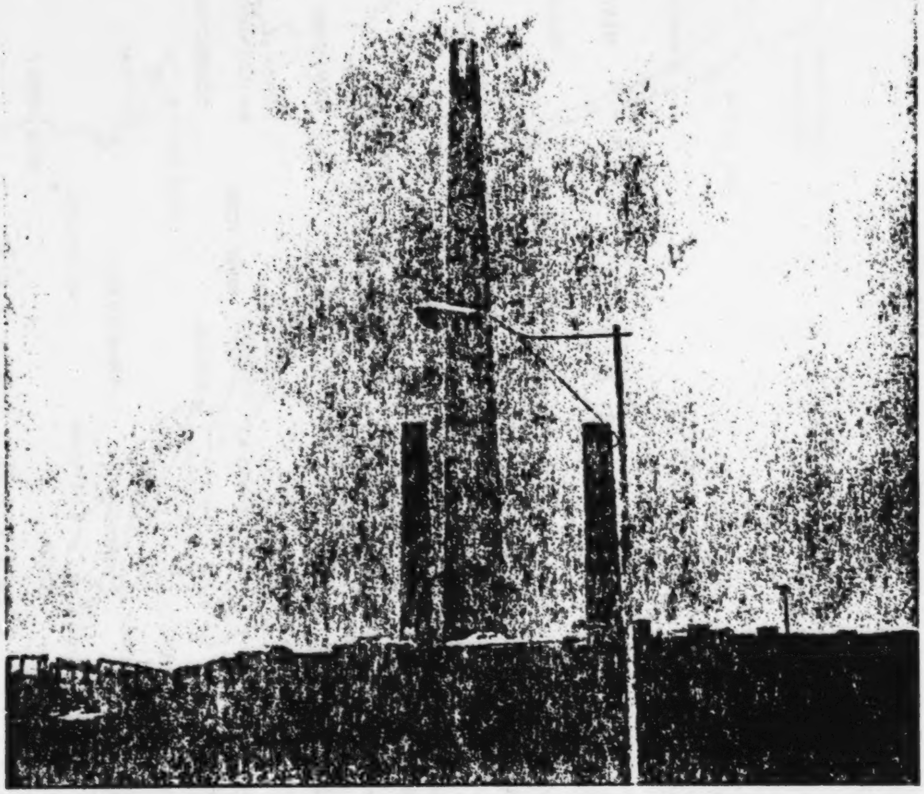

Figure 2: The 381 meter INCO stack during plant operation

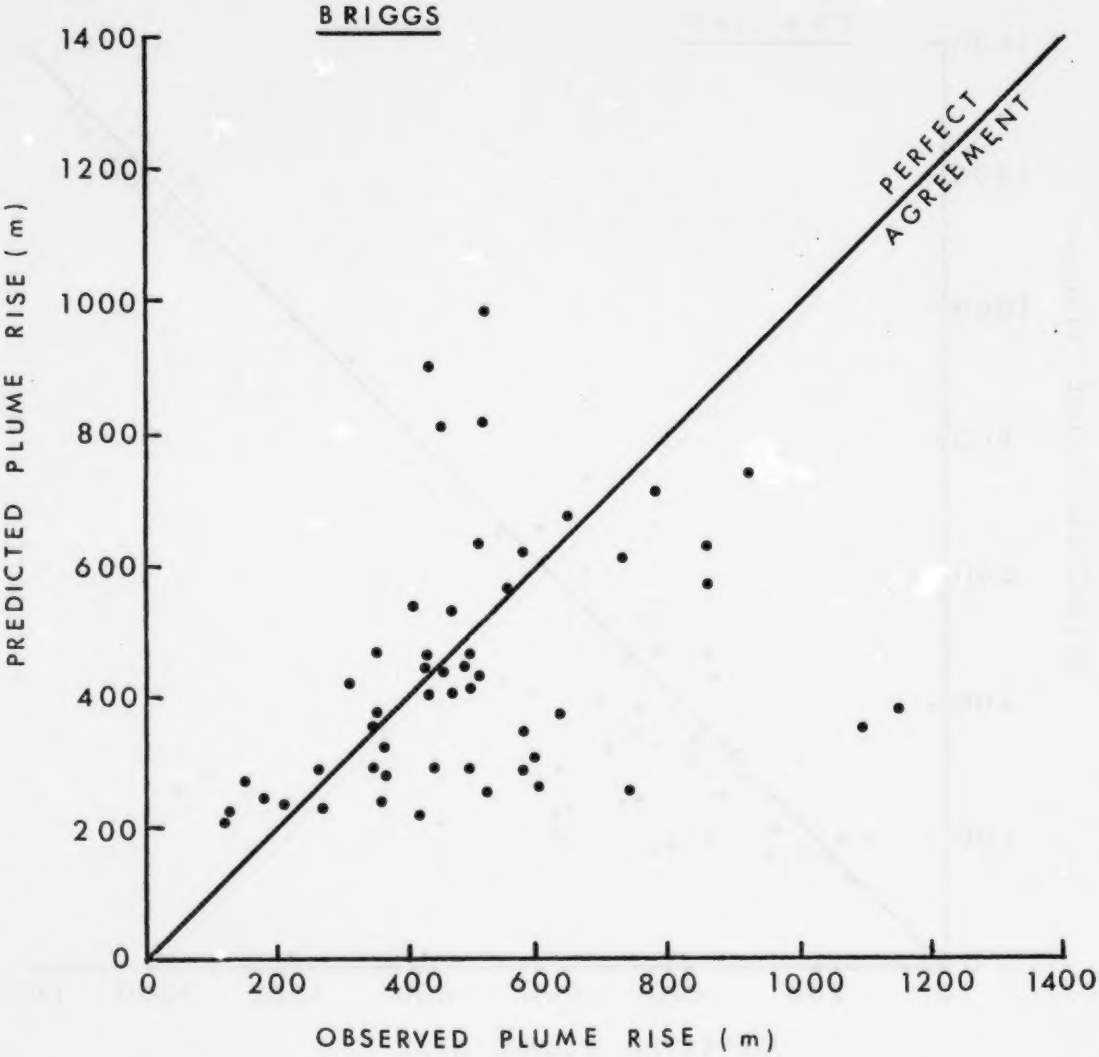

Figure 3: Comparison of predicted versus observed plume rise. Solid line represents perfect agreement.

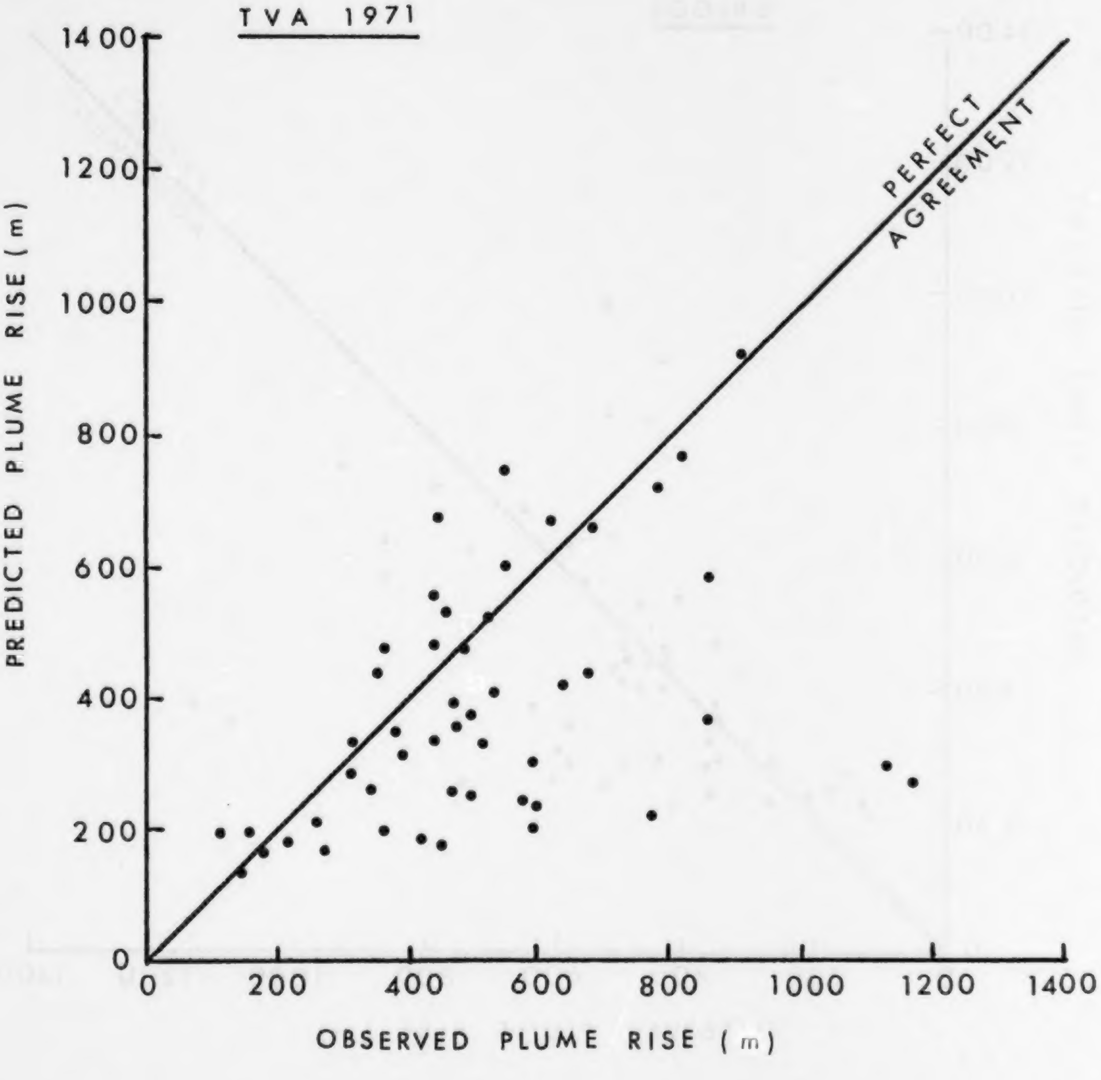

Figure 4: Comparison of predicted versus observed plume rise. Solid line represents perfect agreement.

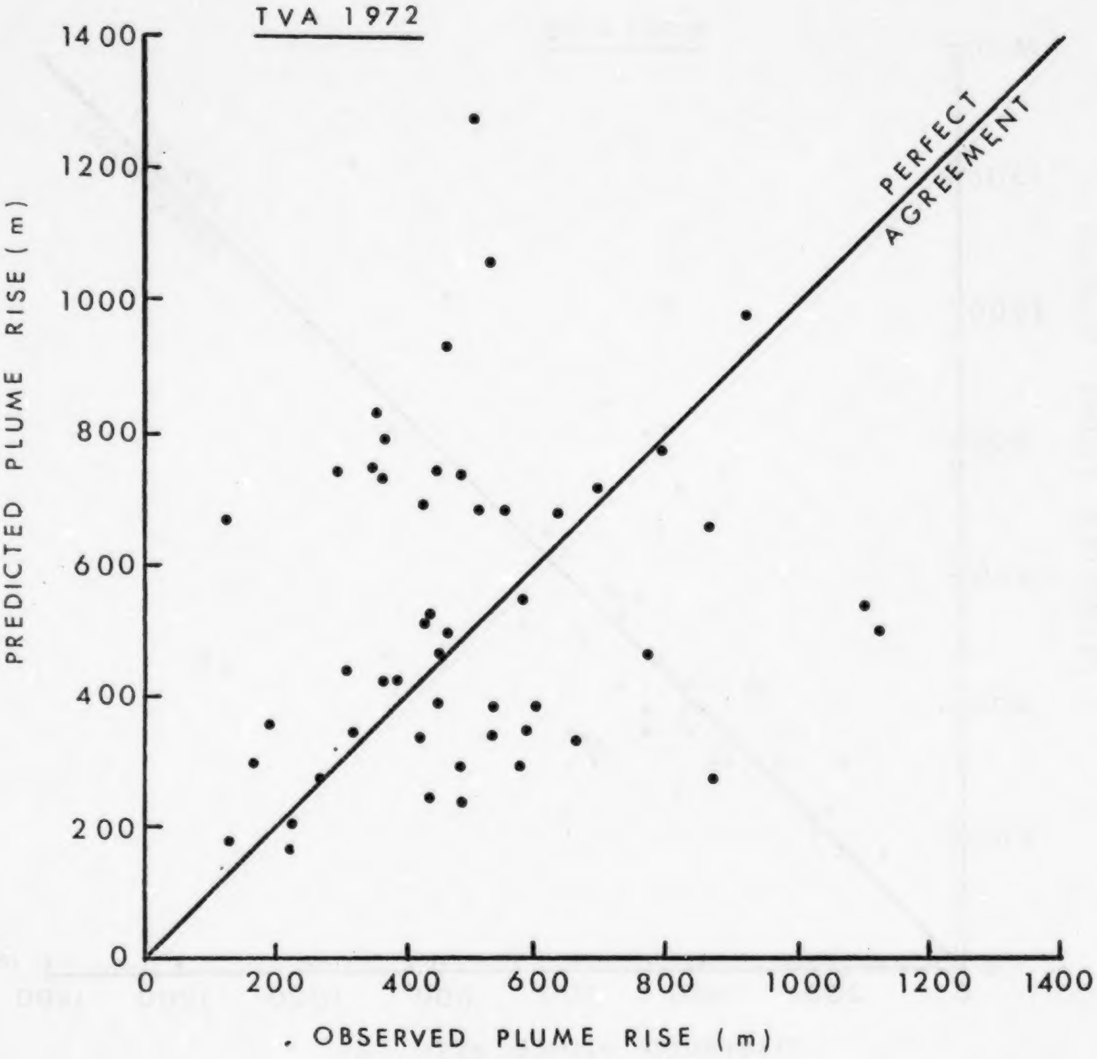

Figure 5: Comparison of predicted versus observed plume rise. Solid line represents perfect agreement.

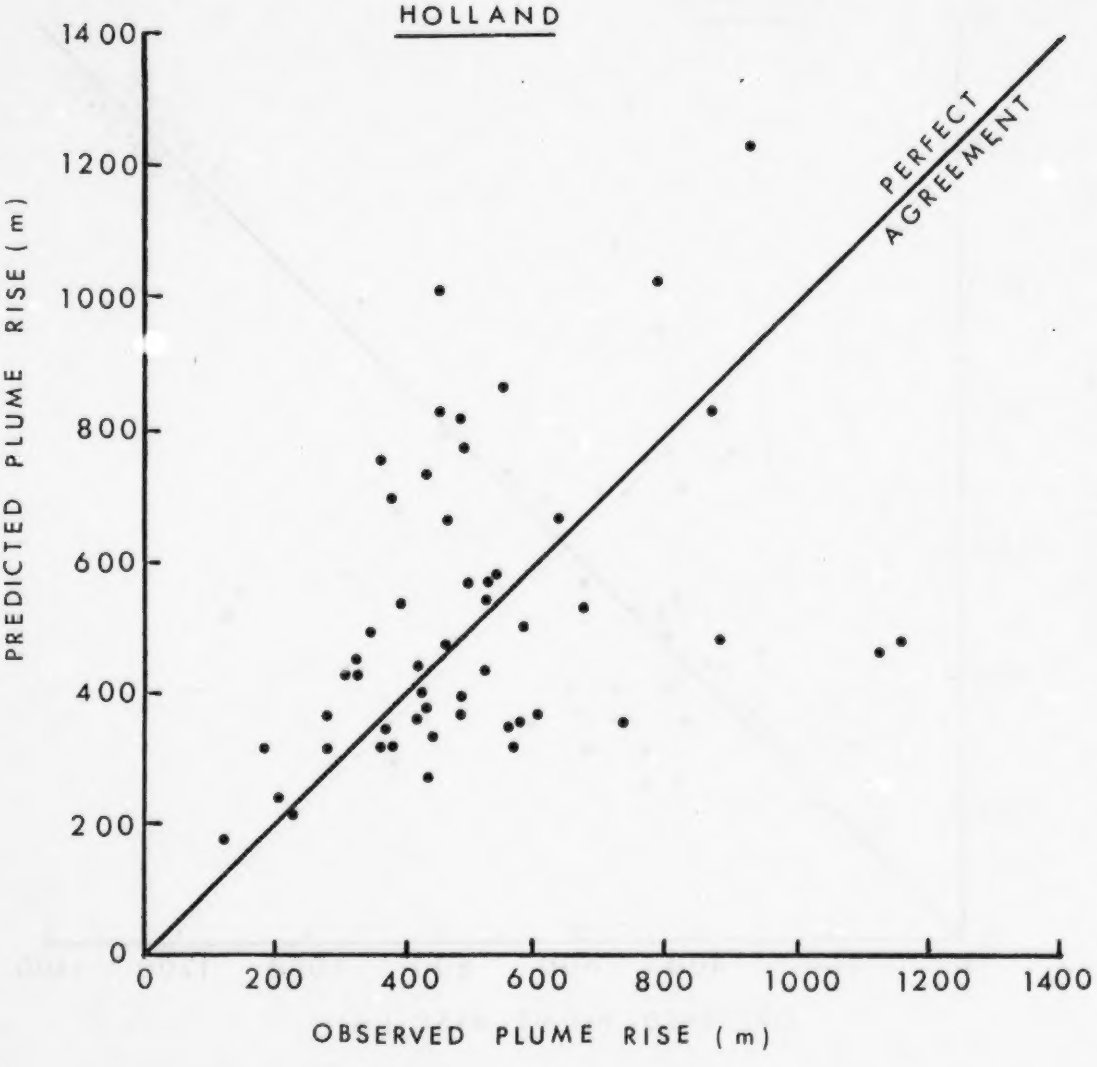

Figure 6: Comparison of predicted versus observed plume rise. Solid line represents perfect agreement.

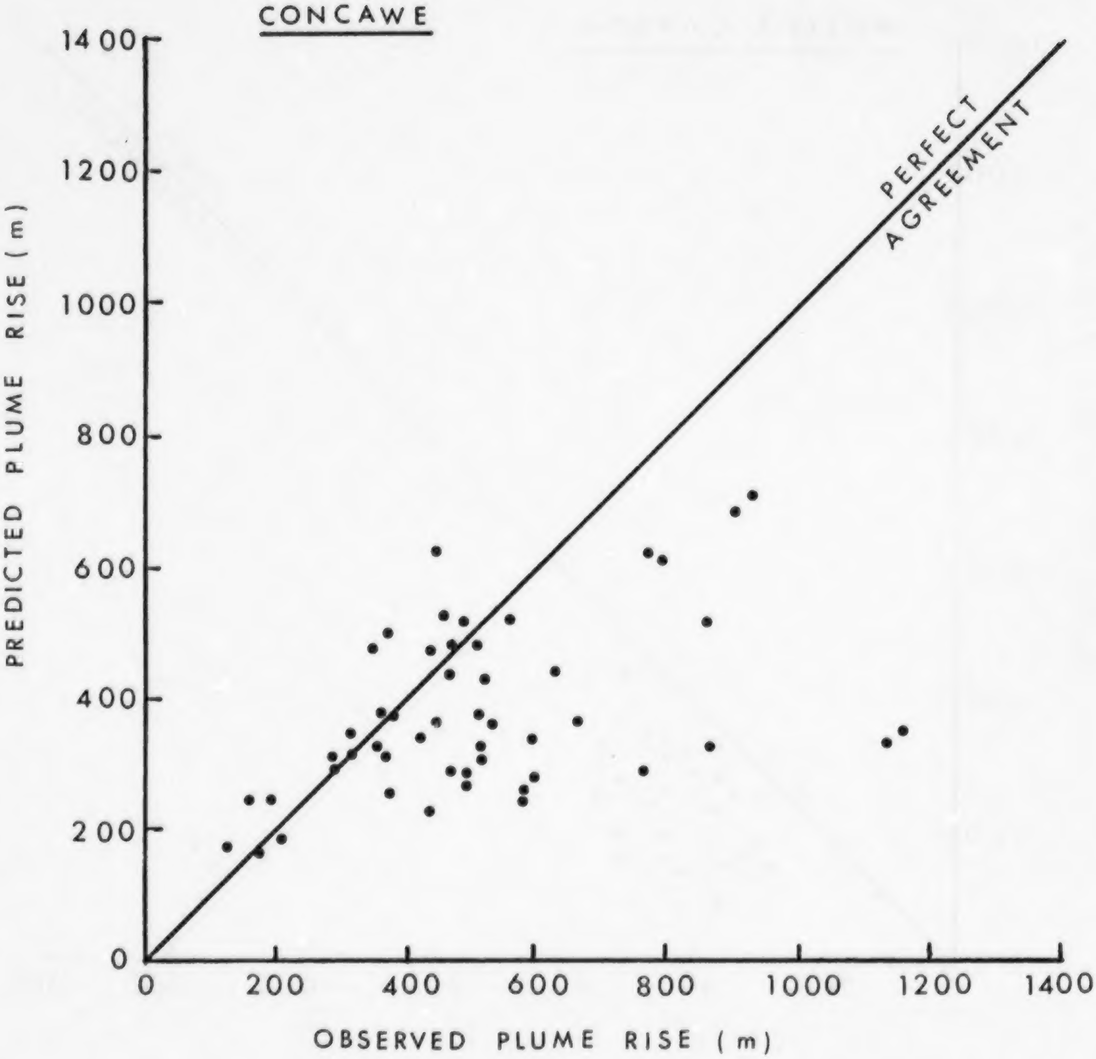

Figure 7: Comparison of predicted versus observed plume rise. Solid line represents perfect agreement.

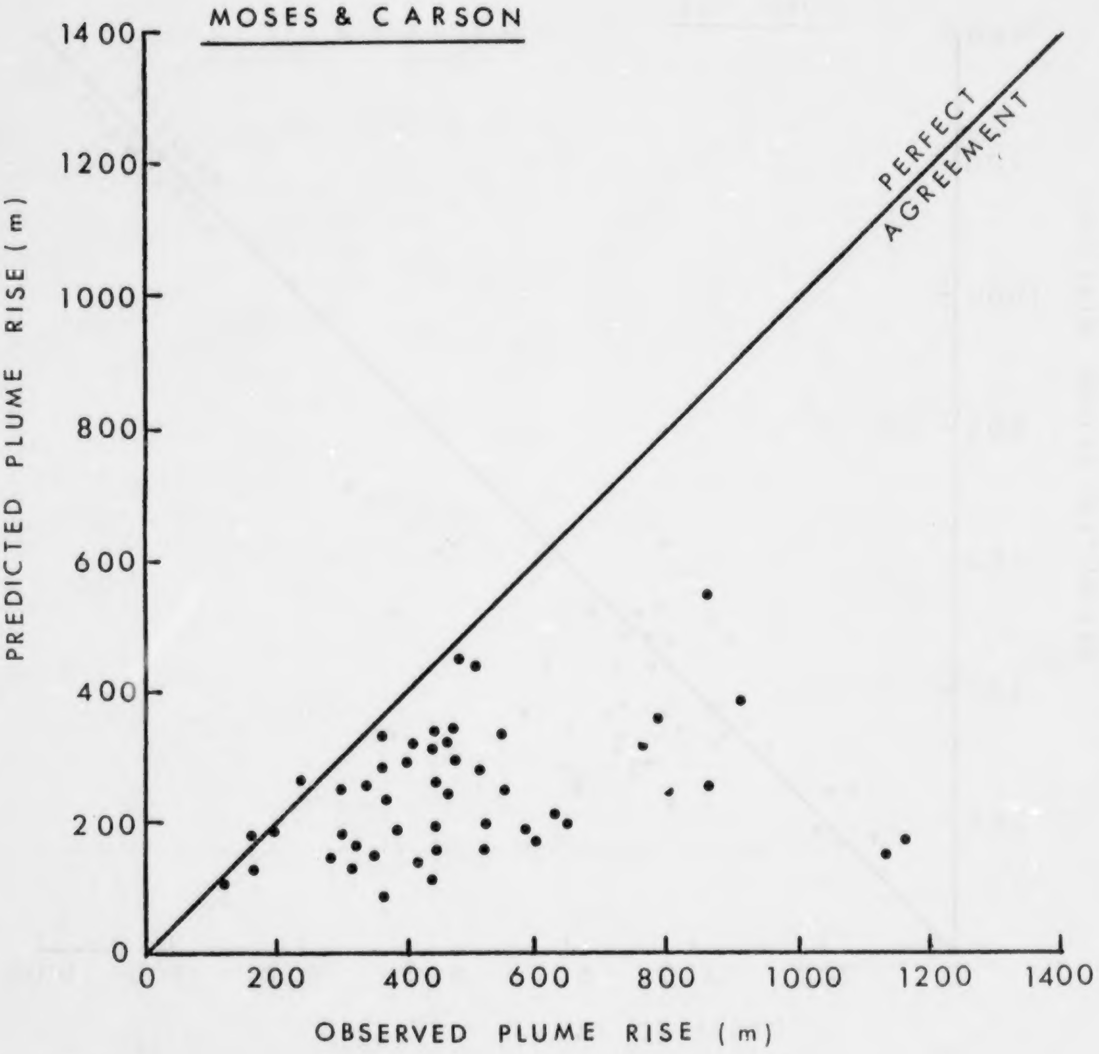

Figure 8: Comparison of predicted versus observed plume rise. Solid line represents perfect agreement.

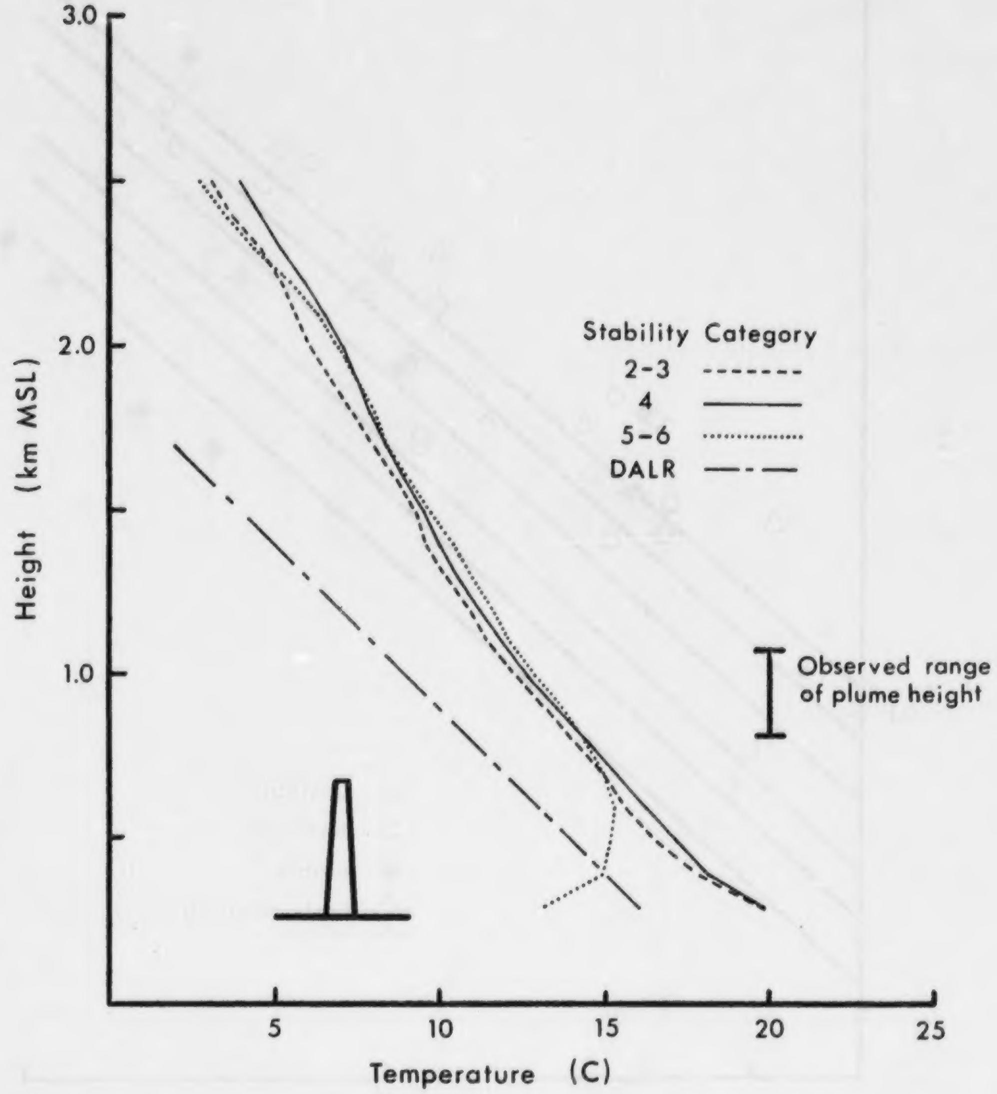

Figure 9: Variation of the average temperature profile with stability category for the Sudbury Study of June, 1973.

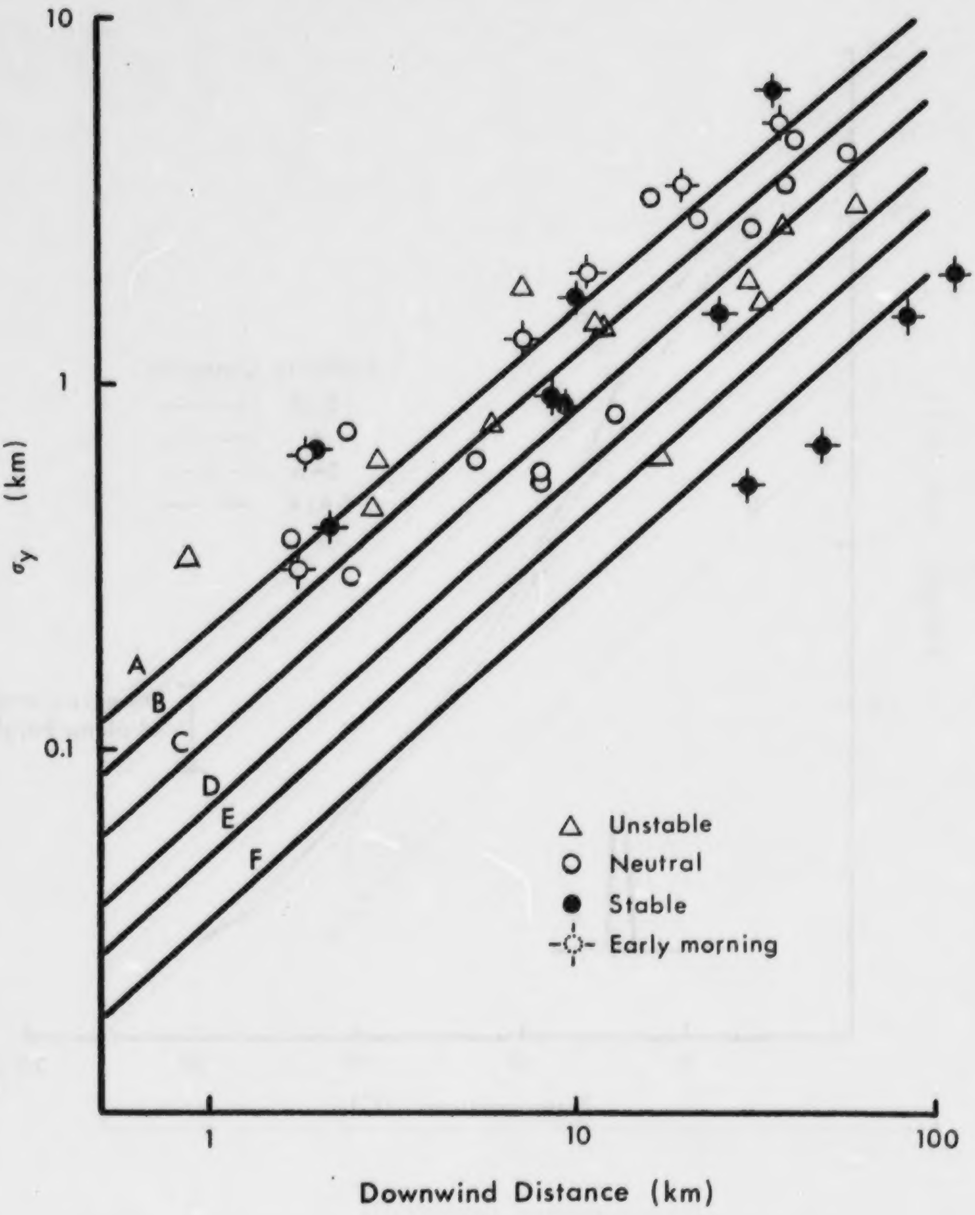

Figure 10: Comparison of observed horizontal dispersion coefficients with Pasquill-Gifford predictions for the Sudbury Study of June, 1973.

Figure 11: Example of a measured plume outline (0.1 ppm contour) under the influence of strong directional wind shear as shown by the concurrent wind profiles (Sudbury, June/73).

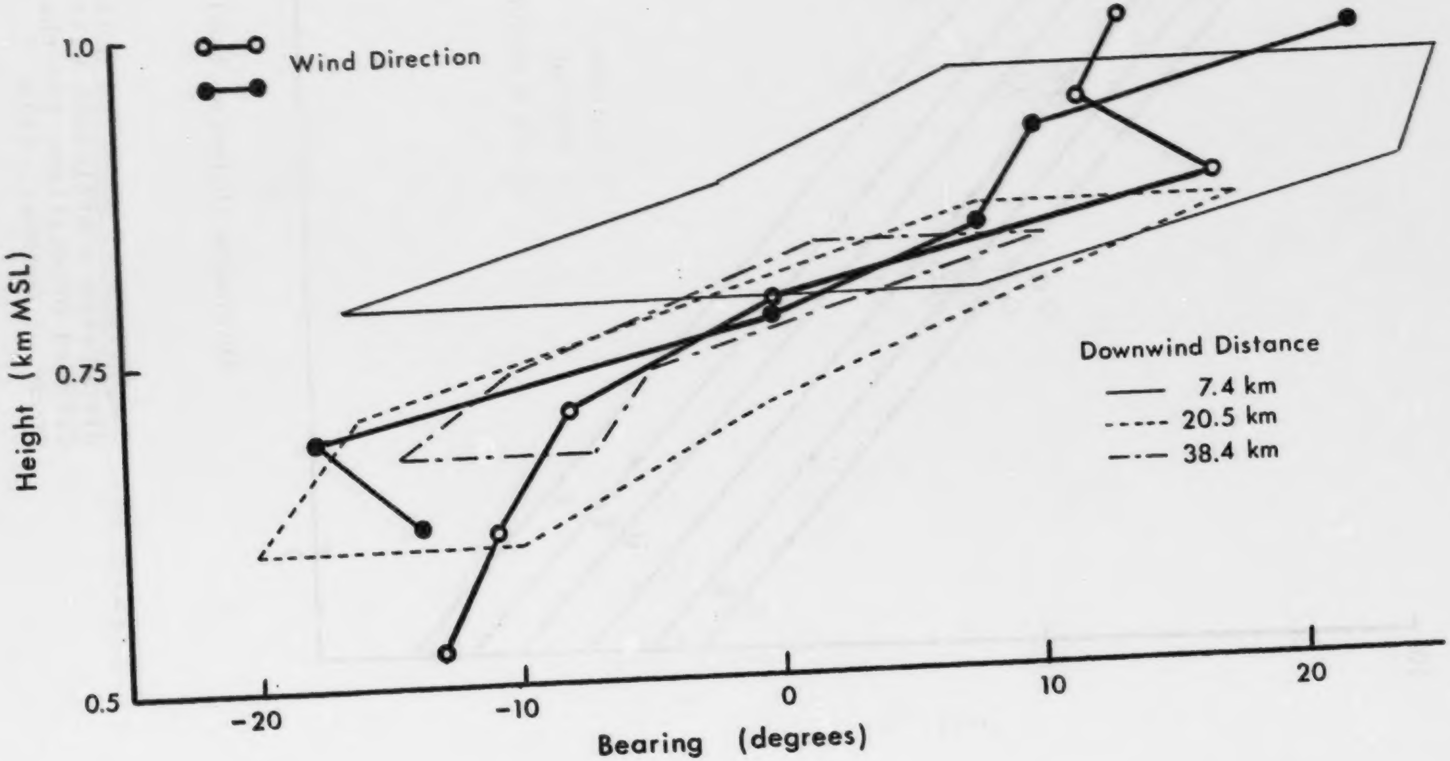

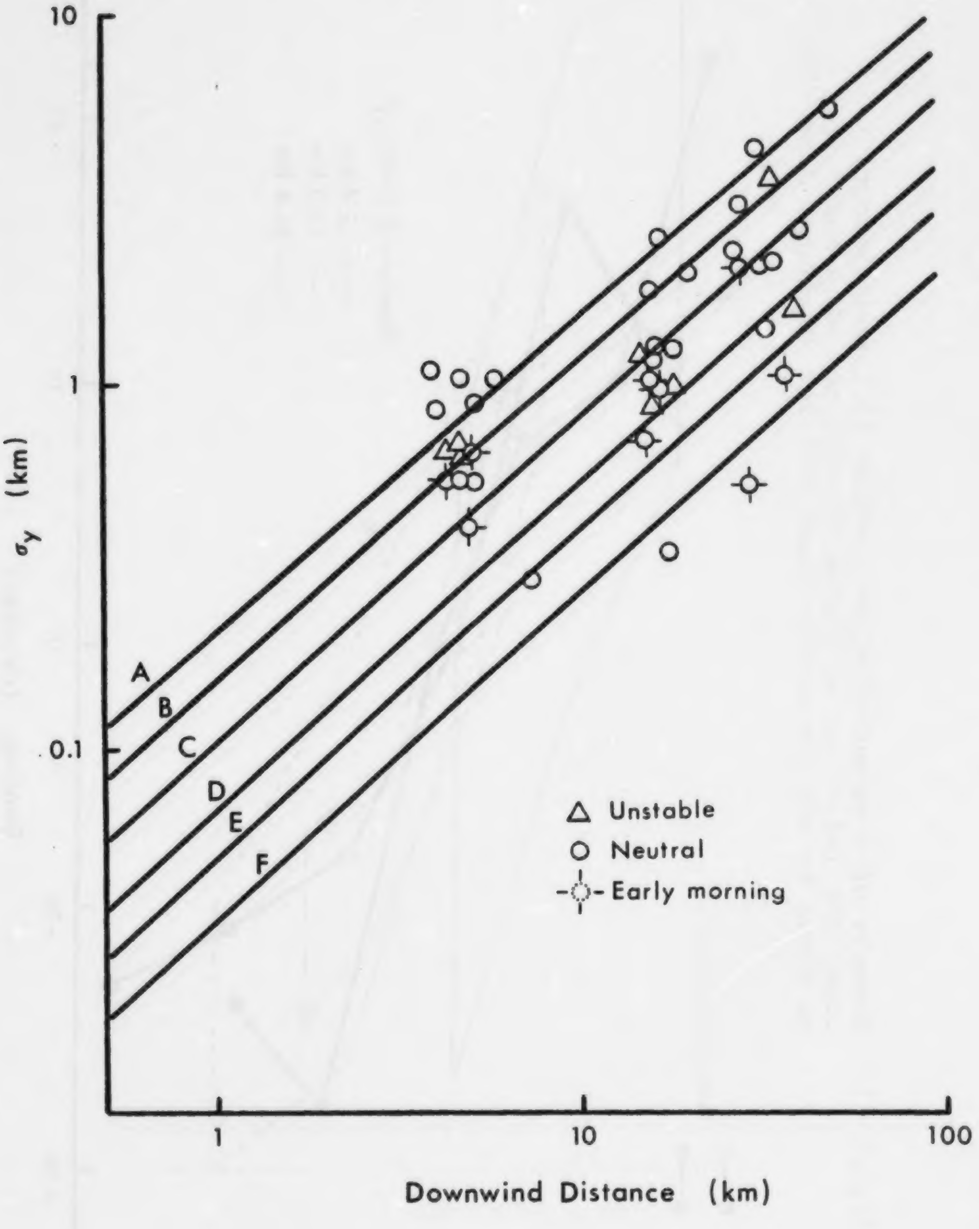

Figure 12: Comparison of observed horizontal dispersion coefficient with Pasquill-Gifford predictions for the Sudbury Study of October, 1973.

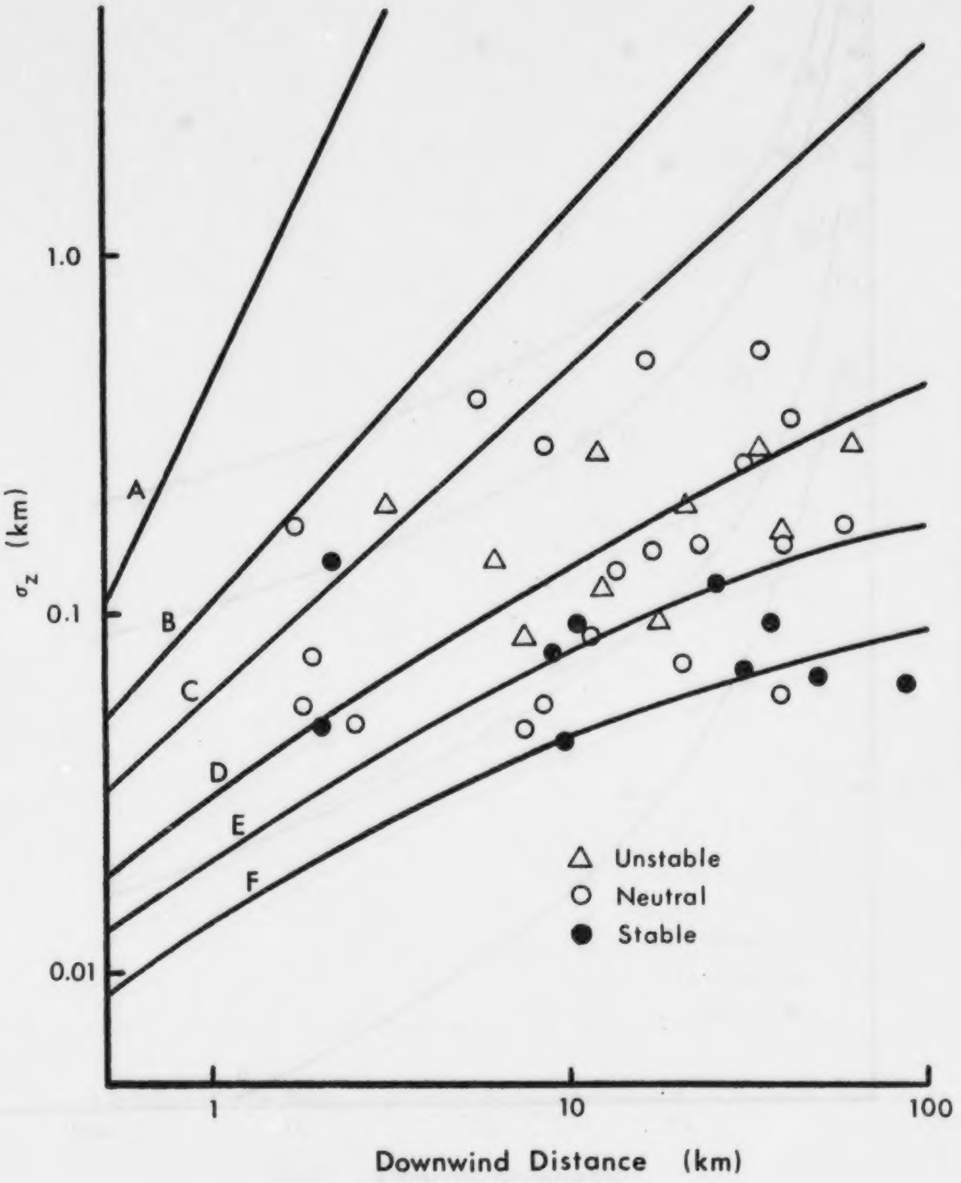

Figure 13: Comparison of observed vertical dispersion coefficient with Pasquill-Gifford predictions for the Sudbury Study of June, 1973.

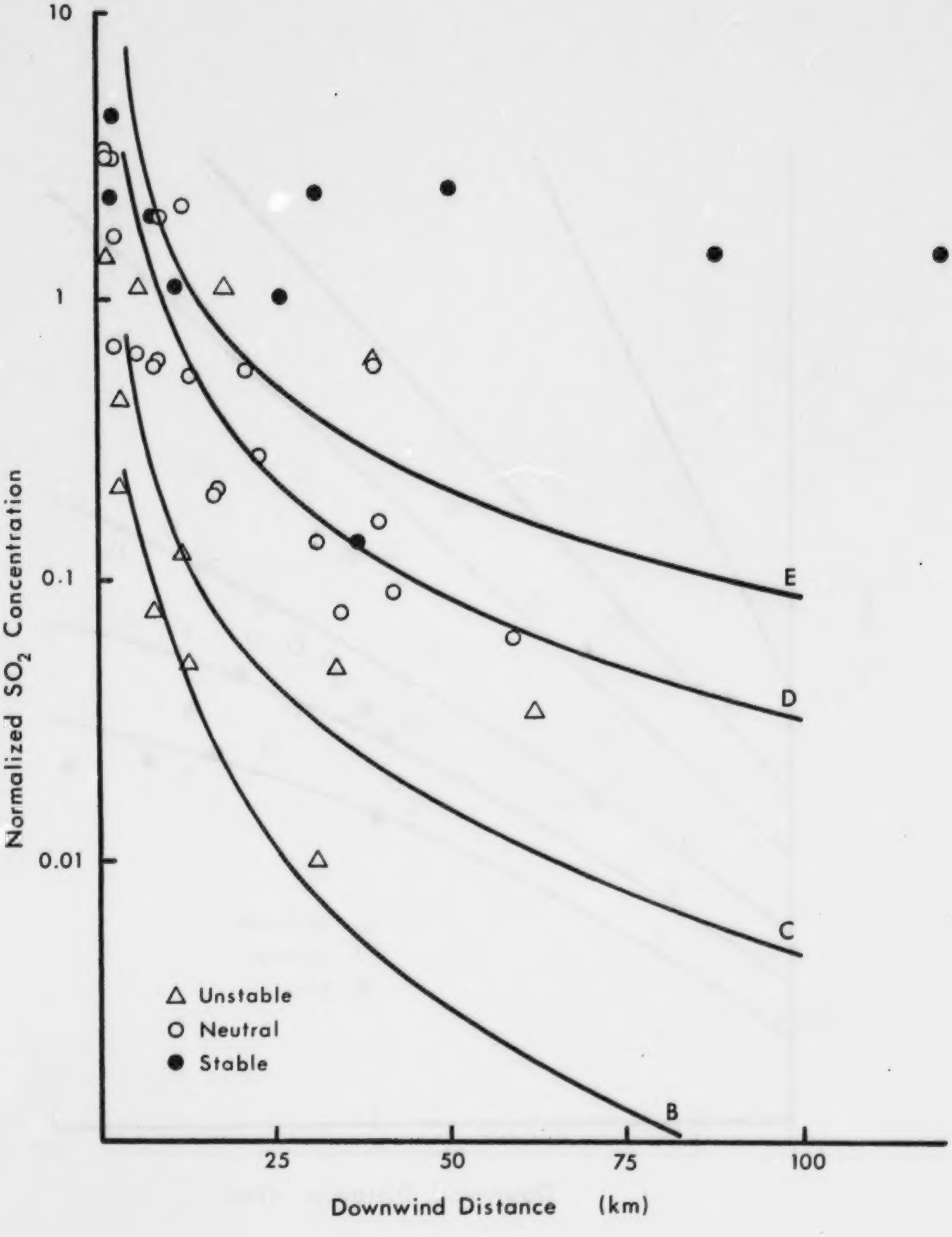

Figure 14: Comparison of observed centerline concentrations (normalized by wind speed and source strength) of SO_2 at plume height with Gaussian theory predictions for the Sudbury Study of June, 1973.

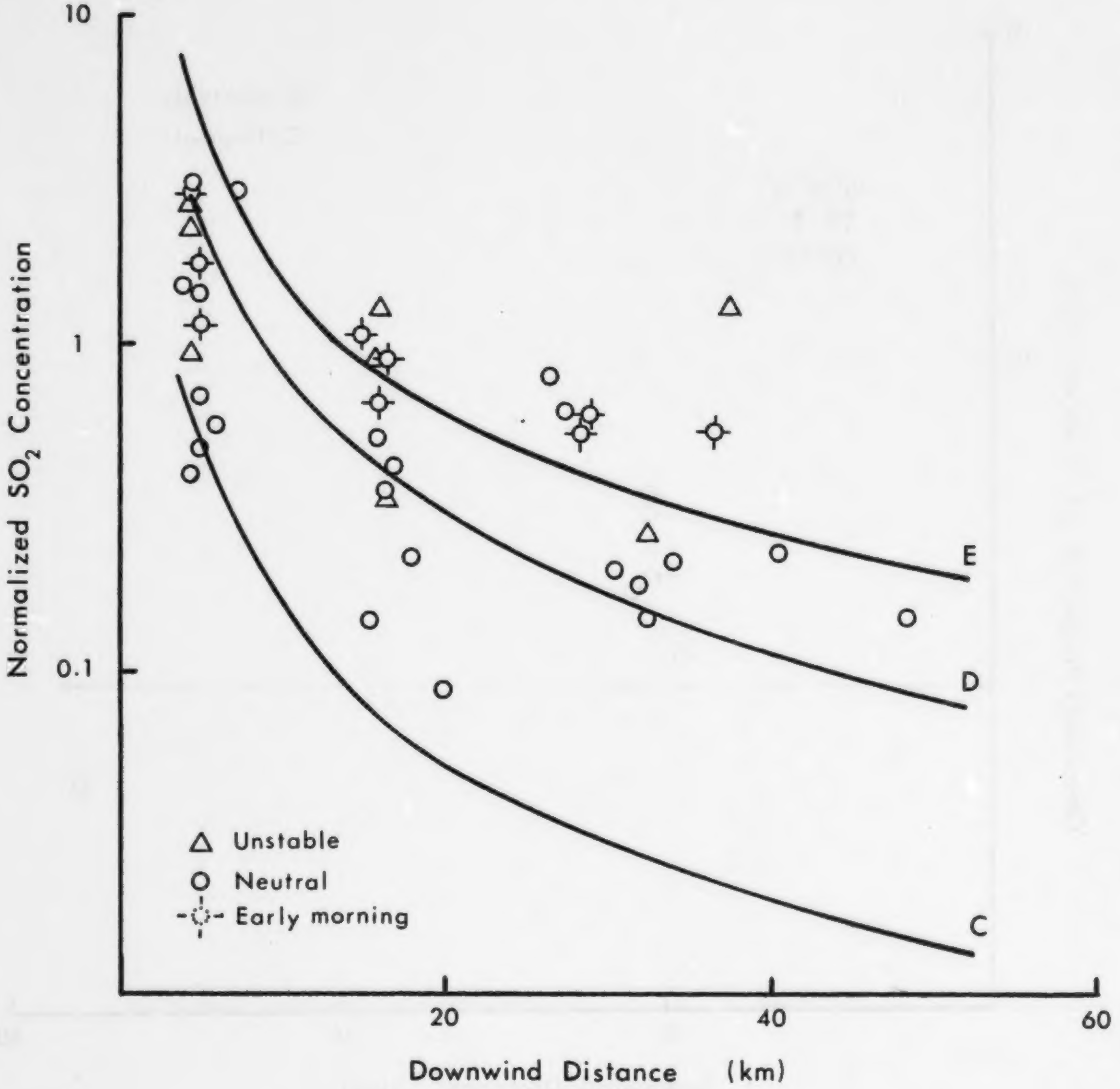

Figure 15: Comparison of observed centerline concentrations (normalized by wind speed and source strength) of SO_2 at plume height with Gaussian theory predictions for the Sudbury Study of October, 1973.

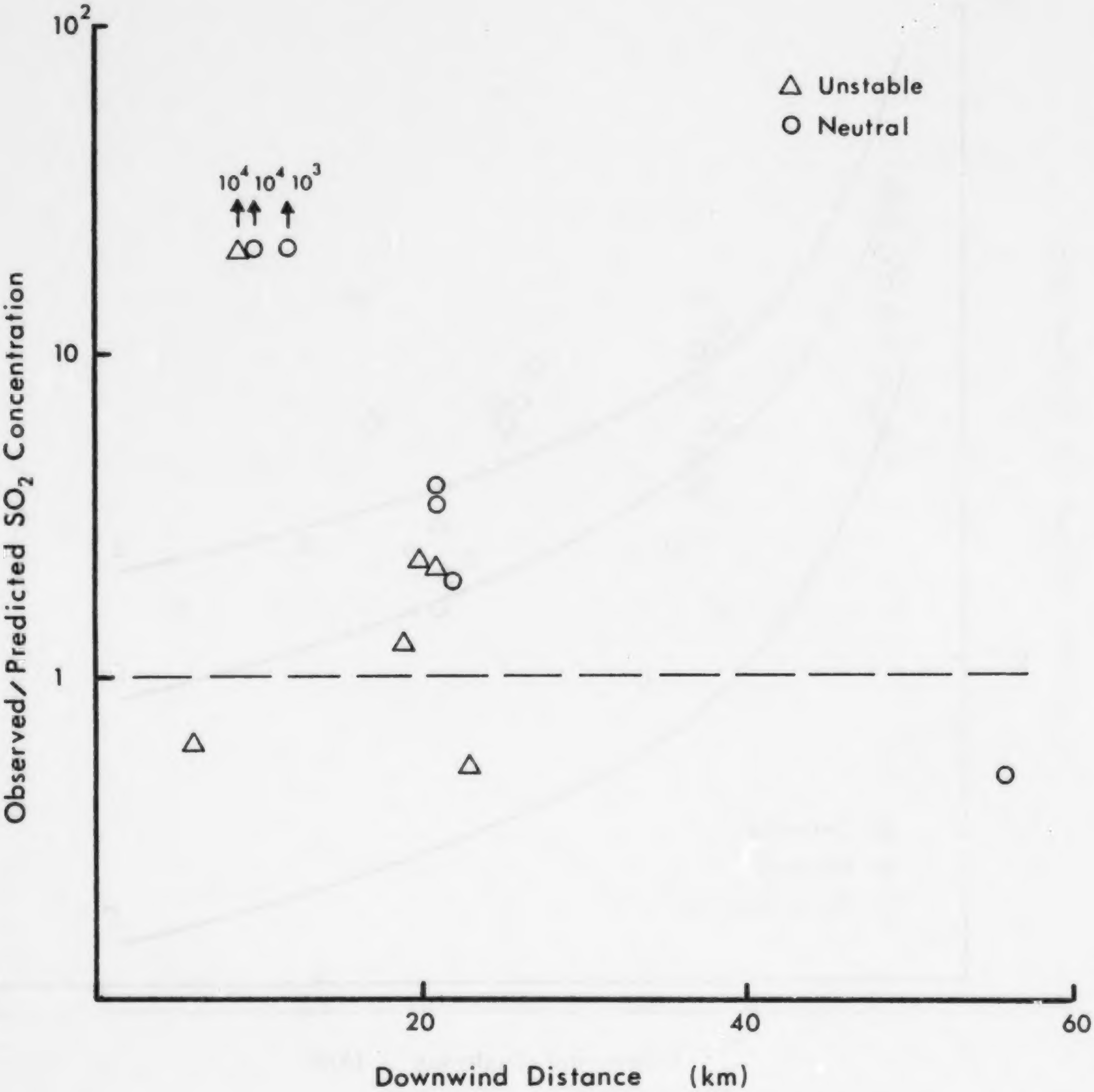

Figure 16: Ratio of observed to predicted SO_2 concentrations at ground level for the Sudbury Study of June, 1973.

7th International Technical Meeting
on Air Pollution Modeling and its Application

A COMPARISON OF "STAR" STABILITY PREDICTIONS, MEASURED LAPSE-RATE STABILITY CLASSIFICATIONS AND OBSERVED TALL STACK PLUME DISPERSION PARAMETERS

by

R.V. PORTELLI

Atmospheric Environment Service
Toronto, Ontario

September 7 - 10, 1976
Airlie, Virginia
United States of America

1. INTRODUCTION

Today, individuals involved in the air pollution field (air pollution meteorologists, environmental engineers, etc.) are often required to make estimates of dispersion of airborne pollutants from various sources. The most widely accepted method to-date has been the use of the Gaussian plume model (Gifford, 1961; Turner, 1970) which is given below with all symbols having their common meaning:

$$X = \frac{Q}{2\pi\sigma_y\sigma_z U} \exp\left[-\frac{1}{2}\left(\frac{y}{\sigma_y}\right)^2\right] \left\{ \exp\left[-\frac{1}{2}\left(\frac{z-H}{\sigma_y}\right)^2\right] + \exp\left[-\frac{1}{2}\left(\frac{z+H}{\sigma_z}\right)^2\right] \right\} \quad (1)$$

The major difficulty in applying this model and the various other models which basically rely on equation 1, is the determination of σ_y and σ_z, the dispersion coefficients (or standard deviations of plume concentration in the horizontal and vertical, respectively). Ideally, one would like to have on-site long-term records of wind fluctuations, at plume height, from which σ_y and σ_z could be directly obtained. However, such data are generally not available and in situ measurements at the appropriate height in the atmosphere present technical difficulties, especially for tall stacks.

To approximate the dispersion climatology of an area where detailed wind measurements are not available, the system devised by Pasquill (1961) and modified by Gifford (1961) and Turner (1961) is frequently employed. Pasquill suggested estimates of the cross-wind and vertical spread of a plume in the atmospheric surface layer for six stability categories; these stability classes being defined qualitatively in terms of wind speed and a radiation balance. Gifford (1961) transformed the values of plume width and height into the dispersion coefficients, σ_y and σ_z, respectively. Turner (1961, 1964) introduced an additional, extremely stable class and made completely objective the stability classification through the introduction of a net radiation index which is defined in terms of the solar elevation and cloud cover, i.e., in terms of routine surface weather observations only. This system is commonly referred to as the Pasquill-Turner stability classification scheme and is the basis of the so-called 'Star Program' which is used in the United States by the National Climatic Center and in Canada by the Atmospheric Environment Service of Environment Canada to produce synthetic stability classifications in attempting to approximate dispersion climatology.

Although originally developed for the atmospheric surface layer, this stability classification scheme is often used for elevated sources. When dealing with plume dispersion from tall stacks, application of this scheme requires rather questionable extrapolations of height-dependent parameters. In this paper, field measurements of vertical thermal stability and tall stack plume dispersion parameters are compared with Star predictions. The observations were obtained during two field programs, June 1973 and September 1974, initiated jointly by the Atmospheric Environment Service of Environment Canada and the Air Resources Branch of the Ontario Ministry of the Environment to investigate plume dispersion from the 381 m smelter stack of the International Nickel Company (INCO) of Canada at Sudbury, Ontario. The present study utilizes the meteorological measurements (minisonde and radiosonde), photographic plume-rise observations and aircraft plume sampling data taken during these field programs (Turner 1973, 1975).

2. METHODS AND SOURCES OF DATA

During the Sudbury field studies of June 12-22, 1973 and September 17-27, 1974 vertical temperature profiles were obtained from radiosonde and minisonde (Turner and Markes, 1974) ascents, generally for the period between early morning (~0530 HRS) and late afternoon (~1800 HRS). Quasi-simultaneous balloon releases were made from a fixed (base) station located 0.9 km from the tall stack and a mobile station located 12-24 km downwind. Using the relationships given by USAEC (1972), shown in Table 1, stability categories were derived from the observed temperature lapse-rates in the lowest air layer above the ground and in the layer which contained the plume. This was done so that Star predictions could be compared with low-level stabilities - where the stability classification scheme is intended to apply - and with plume-level stabilities. The lapse-rate in the lowest layer was computed from the surface temperature and the first observed temperature aloft.

Table 1

STABILITY CLASSES ACCORDING TO USAEC (1972)

Pasquill Stability Class	Average Vertical Temperature Gradient $\Delta T/\Delta Z$ ($^oC/100m$)
A	$\Delta T/\Delta Z \leq -1.9$
B	$-1.9 < \Delta T/\Delta Z \leq -1.7$
C	$-1.7 < \Delta T/\Delta Z \leq -1.5$
D	$-1.5 < \Delta T/\Delta Z \leq -0.5$
E	$-0.5 < \Delta T/\Delta Z \leq 1.5$
F	$1.5 < \Delta T/\Delta Z \leq 4.0$
G	$4.0 < \Delta T/\Delta Z$

To determine the lapse-rate in the layer containing the plume the following approach was used. For each day of field observations, the vertical temperature profiles were plotted in chronological sequence - Figure 1 exhibits a sample set of afternoon profiles. The plume photographic records (see Fanaki, 1975 for details of photographic techniques) were then examined to obtain estimates of plume depth. Time lapse photography provided one frame every 30 seconds and up to 30 or 40 frames were taken for each observation. The plume outline on each photograph was traced and composite figures of 6 to 10 superimposed traces provided a time-mean path of the plume, as a function of height and horizontal downwind distance from the source. The depth of the plume was determined from these figures (which afford a 3 to 5 minute average plume) at the furthest downwind distance recorded, generally about 2 to 7 km. The plume depths were plotted, in proper time sequence, with the temperature profiles as indicated in Figure 1. Although the times of plume observations and temperature profiles did not always coincide it was possible to make a reasonable estimate of the layer which would contain the plume at the time of each profile. The lapse-rate in the layer was computed from the closest temperature observation to the upper-level and the (interpolated) temperature at 381 m - see circled temperatures in Figure 1. All photographs indicated that the plume remained above 381 m for the distances recorded.

For cases when plume observations were not available, the upper-level was taken as 1000 m unless the base of an isothermal or inversion layer extended lower, in which event the height of the base was used (the lowest observed base above 381 m

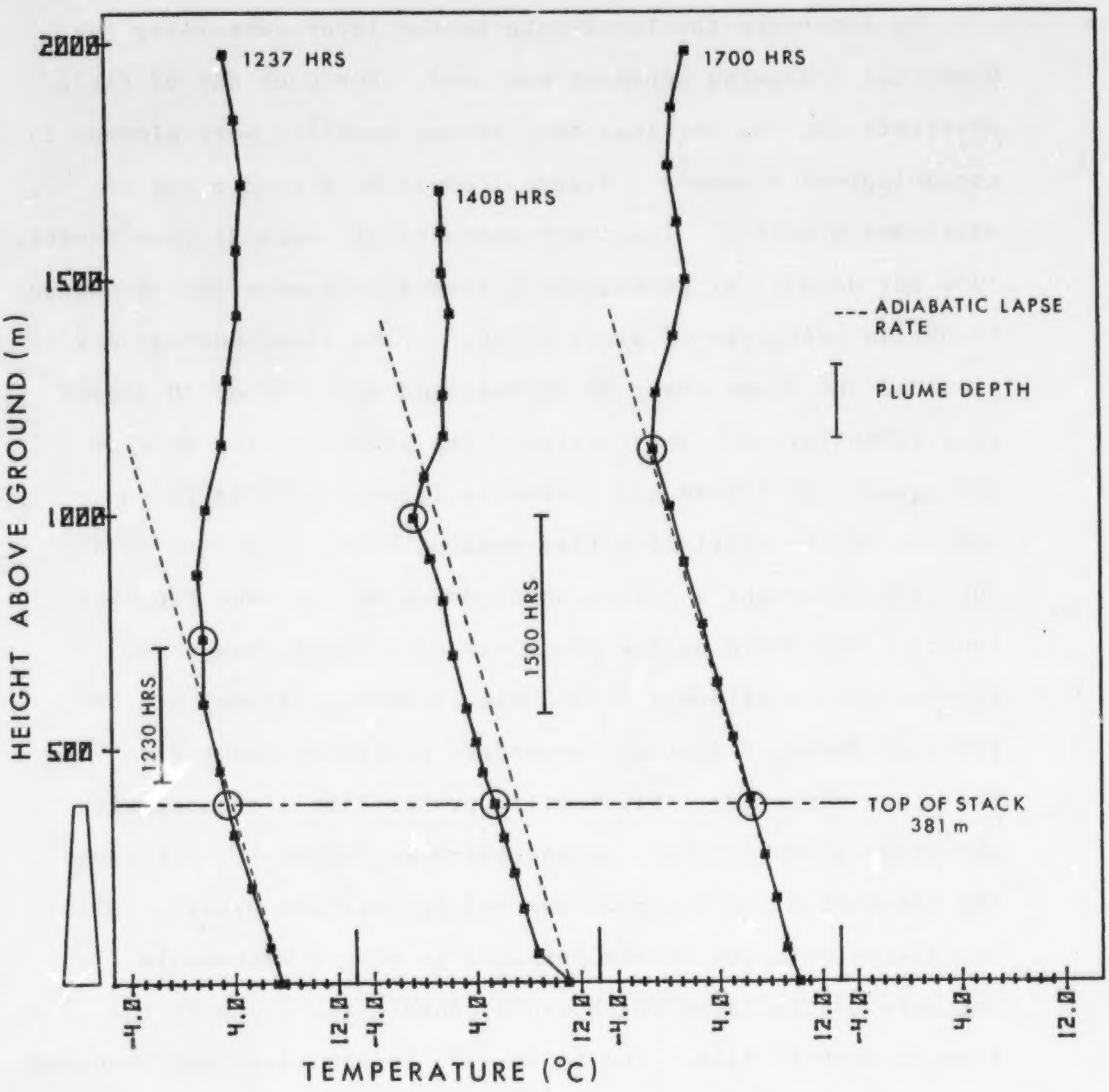

Figure 1. Temperature profiles(minisonde) and plume depth estimates - Sept. 17,1974. (Circles denote temperatures used to compute plume-level lapse-rates).

was at about 600 m and a corresponding plume observation indicated the plume was contained).

Based on standard surface observations from the local weather station, estimates of stability were made using the Star Program for times corresponding to those of the vertical temperature profiles discussed above. Actual comparisons of Star-predicted stability classes were made separately with the low-level and plume-level lapse-rate stability classifications, on an hour-by hour basis. Descriptive statistics on the performance of the Star program were computed for each data set - June '73 and September '74.

During the Sudbury '73 study, aircraft-based measurements of SO_2 concentrations in the tall stack plume were carried out (Turner, 1973). For each of 14 flights (taking roughly 3 hours per flight) the aircraft flew horizontally through the plume at several levels in the vertical at a number of downwind distances to about 40 or 50 km. Dispersion coefficients, σ_y and σ_z, were computed, for each flight at every downwind point where the aircraft traversed the plume by taking the second moment of the horizontal and vertical distributions of SO_2, respectively (Fanaki & Turner, 1976). For the purpose of this study, the vertical dispersion coefficients were transformed into stability classes using Turner's (1970) nomogram of σ_z versus downwind distance and these were averaged to afford a mean stability class for each flight. Comparisons were made then on a flight-by-flight basis of these stabilities and those obtained from Star predictions and plume-level lapse-rate classifications.

3. DISCUSSION OF RESULTS

The histograms of Figure 2 exhibit the frequency distributions of stability classes obtained from Star predictions, low-level and plume-level temperature lapse-rate obsevations. In all three data sets for Sudbury '73 and Sudbury '74, class D occurred most frequently. For the two studies, the plume-level frequency of class D (~90%) is much greater than that at low-level (~40%), as expected. However, Star D predictions (~70%) compare better at plume-level than at low-level. A significant number (~50%) of low-level observations fell into the unstable regime (classes A,B,C) while at plume-level no unstable cases were found. Obviously, solar heating produces a great deal of thermal instability at low-levels whereas at heights above 381 m such conditions would not be anticipated. Star prediction of unstable conditions (~22%) underestimates at low-level and overestimates at plume-level, whereas for stable conditions (classes E,F,G) the prediction is reasonably close for both. A peculiarity of the low-level distributions is the pronounced dip for classes B and C which appears to reflect the narrow ranges of temperature gradient assigned to these classes (see Table 1).

Probably the most striking feature of Figure 2 is how remarkably similar the Sudbury '73 distributions of each data type are to those of Sudbury '74. Since the two studies were carried out in the same locality and roughly during the same season (early-late summer), this type of result shows promise at least for empirical adjustments to Star predictions and possibly for more fundamental modifications to the Pasquill-Turner stability classification scheme to suit local conditions and thereby better its performance.

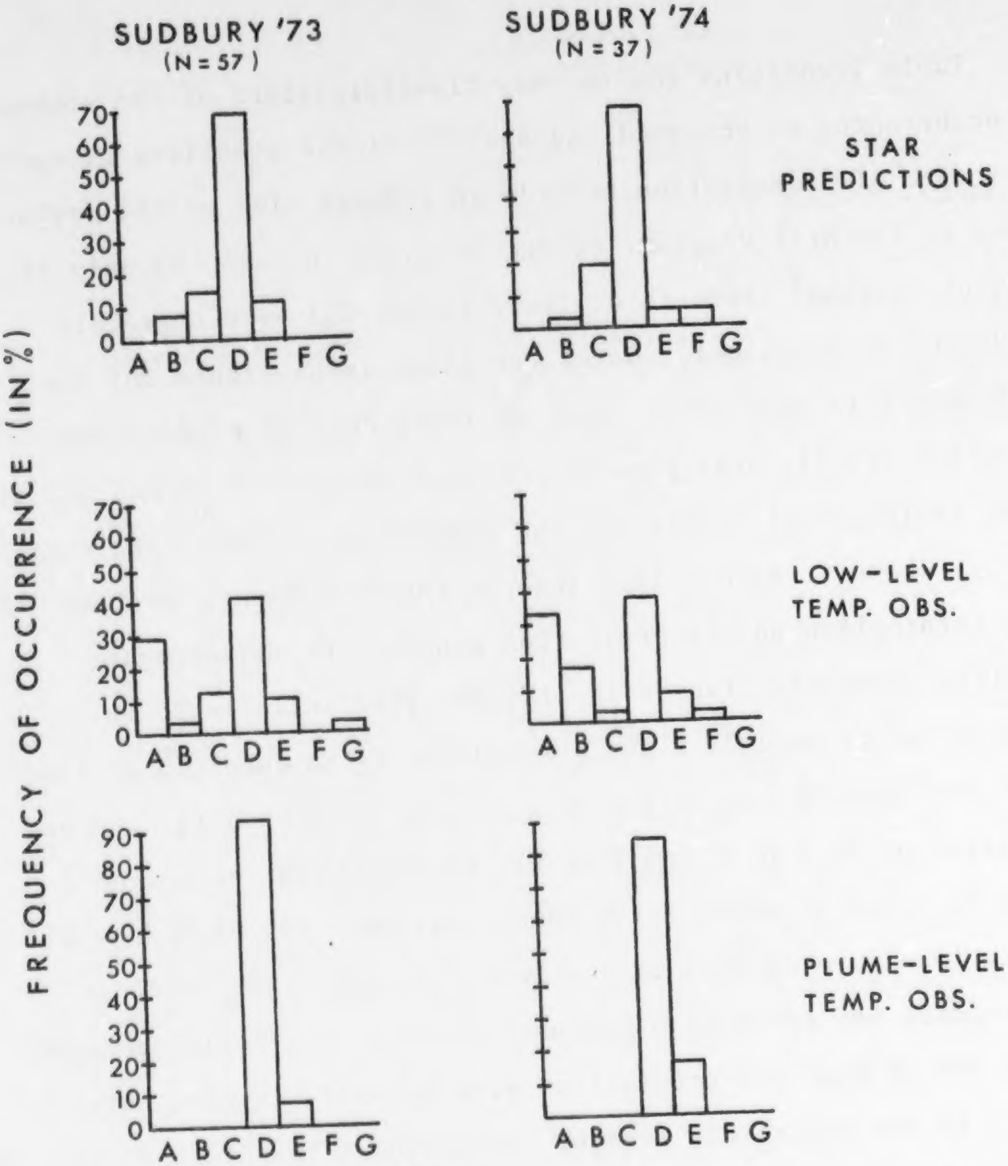

Figure 2. Frequency distributions of stability classes obtained from Star predictions, low-level and plume-level temperature lapse-rate observations

Table 2 contains the two-way classifications of the number of occurrences of observed and Star-predicted stability classes. This type of presentation affords an indepth view of the performance of the Star Program. Of the 57 cases in June '73 only 21 (sum of diagonal elements of Table 2a) or 37% were correctly predicted at low-level, whereas at plume-level (Table 2b) the performance is much better with 36 (63%) correct predictions. In September '74, Star predictions were correct in 38 and 62% of cases at low-level (Table 2c) and plume-level (Table 2d), respectively, which is almost identical to the performance in June '73.

Information on the prediction scheme's performance for specific stability classes is also revealed in Table 2. For example, there were 23 class D measurements in June '73 at low-level of which 18 (or 78%) were correctly predicted (1 case was predicted as B, 2 as C and 2 as E). However, Star estimated D class to occur 39 times which means that only 46% of Star's D predictions were correct at low-level. On the other hand, at plume-level 68% of class D measurements were correctly predicted while 92% of Star's D predictions were actually correct. With regard to the relatively greater spread about the diagonal in the low-level data as compared to the plume-level data, it should be clear that the degree of spread indicates the variability of the prediction scheme.

Figure 3 illustrates the degree of spread of Star predictions in terms of stability class deviations. Along the ordinate is the frequency of occurrence and along the abscissa is the number of stability class deviations (negitive values indicate less stable predictions than observed, 0 indicates correct predictions, and positive values indicate more stable predictions than observed).

Table 2. Two-way classifications of the number of occurrences of observed and Star-predicted stability classes.

a) Star vs low-level obs.-1973

		STAR							
		A	B	C	D	E	F	G	TOT
	A		2	4	10	1			17
	B			1	1				2
O	C		1	1	5				7
B	D		1	2	18	2			23
S	E				4	2			6
	F								0
	G				1	1			2
	TOT	0	4	8	39	6	0	0	57

b) Star vs plume-level obs.-1973

		STAR							
		A	B	C	D	E	F	G	TOT
	A								0
	B								0
O	C								0
B	D		3	8	36	6			53
S	E		1		3				4
	F								0
	G								0
	TOT	0	4	8	39	6	0	0	57

c) Star vs low-level obs.-1974

		STAR							
		A	B	C	D	E	F	G	TOT
	A			5	7				12
	B		1	1	4				6
O	C			1					1
B	D				12	2			14
S	E				1		2		3
	F				1				1
	G								0
	TOT	0	1	7	25	2	2	0	37

d) Star vs plume-level obs.-1974

		STAR							
		A	B	C	D	E	F	G	TOT
	A								0
	B								0
O	C								0
B	D		1	5	22	1	2		31
S	E			2	3	1			6
	F								0
	G								0
	TOT	0	1	7	25	2	2	0	37

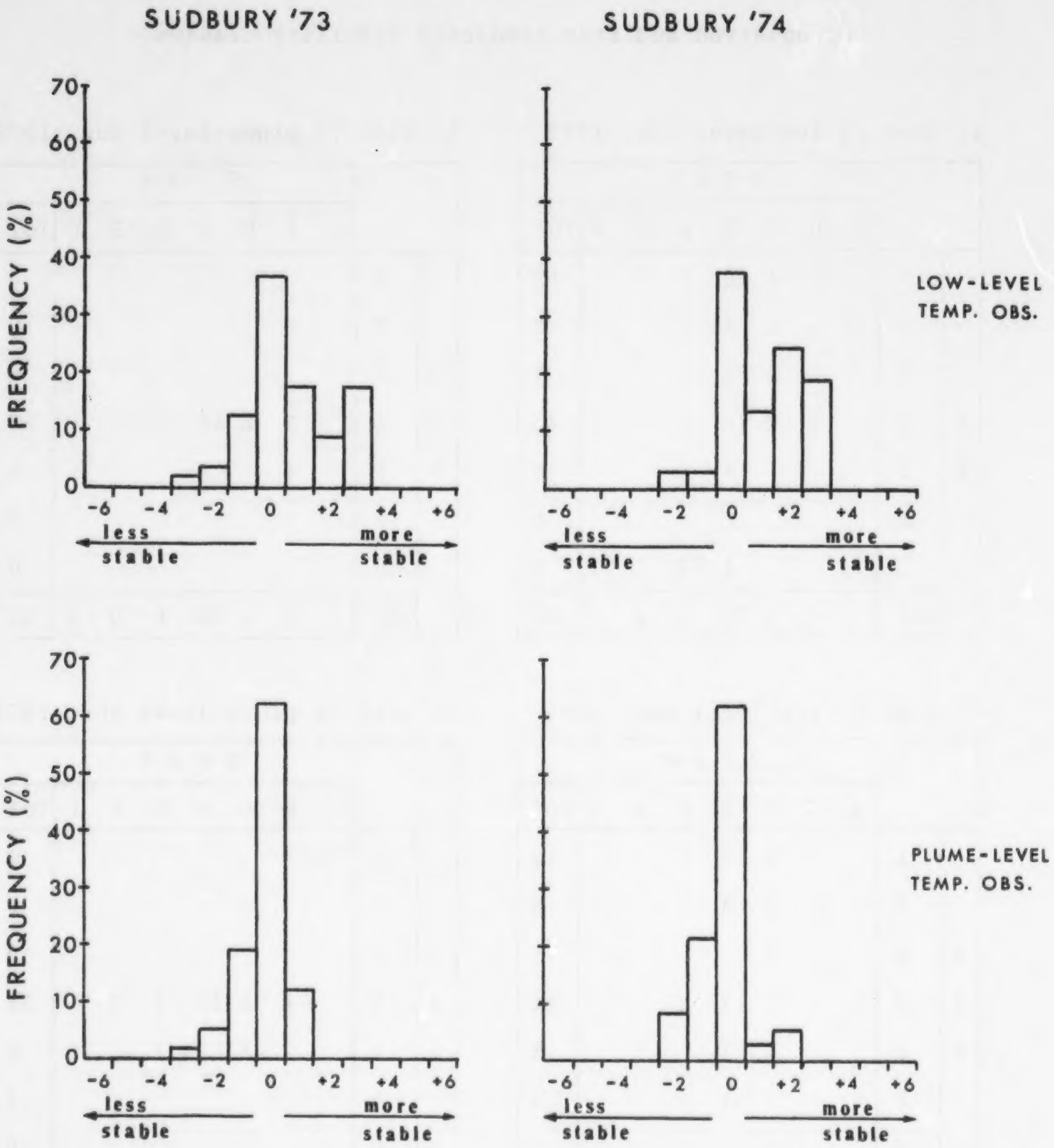

Figure 3. Spread of Star predictions in terms of stability class deviations

In general, the low-level distribution patterns for Sudbury '73 and '74 are quite similar as are those at plume-level, which further emphasize the agreement between the data sets of the two studies. The histograms also point out, that when the prediction scheme did not select the correct stability class at low-level, there was a strong tendency to predict a more stable class than a less stable class; the reverse holding true at plume-level, albeit the tedency is not as pronounced.

Although the Pasquill-Turner stability classification scheme was developed for low-level application, Figure 3 suggests that it performs better at plume-level during the summer season in the Sudbury area. This attributed in part to the fact that the stability at plume-level is generally near-neutral and that the prediction scheme tends to favour class D, as shown in a study by Portelli (1976) for several Canadian locations. Nevertheless, dispersion estimates for the INCO tall stack plume require stability data at plume-level and if this scheme can provide such stability predictions with the accuracy suggested in Figue 3 (over 60% correct), then it can be a very useful tool.

In Table 3 are the results of the analysis of the June '73 aircraft plume sampling data which are compared to Star predictions and plume level lapse-rate observations for corresponding times. Of the 14 aircraft observations, the majority fell into class D, as did those of the Star predictions and plume-level lapse-rates. This demonstrates further that the plume dispersion from the tall stack was principally governed by a near-neutral atmosphere. Senshu et al. (1974) compared σ_z values from their experiments of smoke diffusion from a tall stack to Pasquill stability classes and also found the representative stability to be near-neutral. However, their data showed that Pasquill's classification scheme corresponds well to the lapse-rate at low-levels but it does not always represent the stability above 200 m above ground.

Table 3. Stability classifications as determined from aircraft plume observations,plume-level lapse-rate measurements and Star predictions.

Flight No.	Date	Time (hrs)	Aircraft Obs.	Plume-level Obs.	Star Prediction
1	Jun 12	0600-0900	F	E	C
2	"	1400-1700	E	D	D
3	" 13	0500-0900	D	D	D
4	"	1300-1400	D	D	C
5	" 14	0500-0900	F	E	D
6	"	1400-1700	D	D	D
7	" 15	1200-1400	C	D	D
8	" 16	1700-2000	C	D	D
9	" 17	1000-1400	D	D	C
10	"	1700-1900	D	D	D
11	" 19	0500-0700	D	D	D
12	" 20	1600-2000	D	D	D
13	" 21	0900-1200	D	D	D
14	" 22	0600-0800	E	D	D

The degree of agreement between the data sets presented in Table 3 is summarized in Table 4. The stability classifications from aircraft observations and plume-level lapse-rate measurements compare very well being within ±1 class in all cases. The comparison of Star predictions and plume-level temperature observations shows greater complete agreement (10/14)

Table 4. Degree of Agreement Between Stability Classifications from Aircraft Plume Observations(S1), Plume-Level Lapse-Rate Observations(S2) and Star Predictions(S3).

Degree of Agreement	S1 vs S2	S2 vs S3	S1 vs S3
Complete	8/14	10/14	6/14
Within ±1 class	14/14	13/14	12/14
Within ±2 classes		14/14	13/14
Within ±3 classes			14/14

than the foregoing, whereas the comparison of aircraft observations and Star predictions indicates somewhat less complete agreement (6/14) and greater spread. Nevertheless, the agreement is considered reasonably good since 12/14 (85%) are within ±1 class.

Although there were only 14 aircraft observations, the results suggest that realistic estimates of the vertical spread of the INCO tall stack plume may be obtained by using the Pasquill-Turner classification scheme and the nomogram of σ_z versus downwind distance (Turner, 1970).

4. CONCLUSIONS

The results obtained in this study from the analysis of the Sudbury experimental data indicate that the Star Program performs better in predicting plume-level stability than low-level stability - contrary to what one might expect. The correct stability class, as determined by plume-level lapse-rate measurements, was predicted in over 60% of the cases. Also, stability classifications derived from aircraft plume observations were found to compare well with lapse-rate classifications and Star predictions; the tall stack plume generally residing in a near-neutral atmosphere.

These findings suggest that Star stability predictions may be used to make reasonable estimates of vertical spread of the INCO tall stack plume. Furthermore, the repetative nature of the data distributions for the two field studies implies that the possibility exists for improving performance by empirically adjusting Star predictions, if not by fundamental modifications to the Pasquill-Turner classification scheme.

In conclusion, it must be stated that although these results shed a favourable light on the Star Program for use in predicting plume dispersion from the tall stack, they are based on a limited amount of data. Their representativeness, particularly for seasons of the year other than summer, can only be substantiated by longer term experimental data.

5. ACKNOWLEDGEMENTS

I would like to thank Drs. H. E. Turner and F. H. Fanaki for the helpful discussions held on the Sudbury data and Ms. A. M. Malkiewicz for her assistance in the analysis of the data.

6. REFERENCES

Fanaki, F.H. and G. Lesins, 1975: Photographic Measurements of Smoke Plume Heights From Industrial Stacks. J. of Soc. of Motion Picture and Television Engineers, Vol 85, pp77-81.

___________ and H.E. Turner, 1976: Plume Dispersion From the Sudbury Tall Stack. Paper for presentation at 7th International Tech. Meeting on Air Pollution Modeling and its Apllication, Sept. 7-10,1976, Airlie, Virginia, U.S.A.

Gifford, F.A., 1961: Use of Routine Meteorological Observations for Estimating Atmospheric Dispersion. Nuclear Safety, 2, pp 47-51.

Pasquill, F., 1961: The Estimation of the Dispersion of Windborne Material. Meteor. Mag., 90, pp 33-49.

Portelli, R.V., 1976: A Comparative Study of Experimentally Measured Atmospheric Stability and 'Star Program' Predictions. Paper to be presented at the 3rd Symposium on Atmospheric Turbulence, Diffusion and Air Quality, Oct 19-22, 1976, Raleigh, N.C., U.S.A.

Senshu, T., S. Yoshida and N. Nakamura, 1974: A Model of the Boundary Layer for the Prediction of Atmospheric Pollution. Proc. Symposium on Atmospheric Diffusion and Air Pollution, Sept. 9-13, 1974, Santa Barbara, Calif., pp 180-183.

Turner, D.B., 1961: Relationships Between 24-Hour Mean Air Quality Measurements and Meteorological Factors in Nashville, Tennesse. J. APCA, Vol 11, No. 10, pp 483-489.

__________, 1964: A Diffusion Model For An Urban Area. J. Appl. Meteor., 3, pp 83-91.

__________,1970: Workbook of Atmospheric Dispersion Estimates. U. S. Environmental Protection Agency, Office of Air Programs Publication AP-26, Revised 1970.

Turner, H.E., 1973: Preliminary Report on the Sudbury Dispersion Study of June 1973. Report ARQT-10-73, Atmospheric Environment Service, Environment Canada, Downsview, Ontario.

__________, 1975: Preliminary Report on the Sudbury Dispersion Study of September 1974. Report ARQT-6-75, Atmospheric Environment Service, Environment Canada, Downsview, Ontario.

__________ and J. Markes, 1974: A Minisonde System for Atmospheric Profiles. Report ARQT-1-74, Atmos. Env. Service, Downsview, Ontario.

USAEC, 1972: Regulatory Guide 1.23. On-site Meteorology Programs.

7th International Technical Meeting
on Air Pollution Modeling and its Application

Mathematical Modelling of Chemical Reactions in a Plume

M. Lusis
Atmospheric Environment Service
4905 Dufferin Street
Downsview, Ontario
Canada

September 7 - 10, 1976
Airlie Virginia
United States of America

INTRODUCTION

The treatment of point sources of reacting contaminants was identified by Seinfeld et al. (1973) as one of the important unsolved problems in urban airshed modelling. Sulphur dioxide, for example, which is converted to sulfuric acid and sulfates in the atmosphere, is emitted largely from industrial and generating station chimneys. In many areas, a significant fraction of the smog-precursor nitrogen oxides also comes from these sources. Indeed, Hilst (1974) has pointed out that almost all of man's contributions to atmospheric pollution ultimately emanate from essentially point sources.

By now it has become clear that the effect of chemical reactions on the concentration of reactive air pollutants cannot be included in mathematical models in any simple way-for example, in the form of exponential decay terms. The interaction of chemical reactions and atmospheric dispersion must be more realistically considered. In the following sections we focus attention on plumes from point sources, and present some mathematical models which we have developed for treating chemical changes and dispersion in such emissions. It is hoped that the methods discussed will be useful to other modellers for estimating concentration changes which take place due to chemical reactions before the effluent plume has touched ground.

(1) Gaussian Plume with Slow Chemical Reactions

The first model is based on the ideas of Friedlander and Seinfeld (1969), and is of special interest to the case of SO_2 oxidation in plumes (see below). It is assumed that when chemical reactions take place, the concentration C of any reacting constituent is given by the gaussian equation:

$$C = \frac{Q}{2\pi\sigma_y\sigma_z U} \exp\left[-\frac{1}{2}\left(\frac{y^2}{\sigma_y^2} + \frac{z^2}{\sigma_z^2}\right)\right] \qquad (1)$$

where all the terms have their usual meaning, except that the "emission rate" Q is now a function of plume age t. From mass conservation considerations, the variation of Q with t must be related to the reaction rate r by the equation:

$$\frac{1}{U}\frac{dQ}{dt} = \int_{-\infty}^{\infty}\int_{-\infty}^{\infty} r\, dy\, dz \qquad (2)$$

Thus, given an expression for r in terms of the concentrations of the reactive constituents, Equations (1) and (2) may be used to compute the variation of Q with plume age, and hence the extent of concentration changes due to chemical reactions.

The use of Equation (1) for reacting constituents, with variable Q, is reasonable provided the fractional rate of change of concentration due to chemical reactions is small compared with the fractional rate of expansion of the plume

(Freidlander and Seinfeld, 1969). For example, supposing we take σ_y as a characteristic dimension of the plume, and stipulate that the effects of chemical reaction must be less than one-tenth the effects of dispersion, that is,

$$\left| \frac{1}{Q}\frac{dQ}{dt} \Big/ \frac{1}{\sigma_y}\frac{d\sigma_y}{dt} \right| < 0.1 \tag{3}$$

If σ_y is given by an expression of the form

$$\sigma_y = a\,t^b \tag{4}$$

one can easily show that the following must be true:

$$\left| \frac{1}{Q}\frac{dQ}{dt} \right| < \frac{0.1\,b}{t} \tag{5}$$

Since b generally has values ranging from about 0.71 to 0.91, depending on atmospheric stability (ASME, 1973), the above rough calculations suggest that the present model should be satisfactory if the oxidation rate at plume age t hr is less than about $7t^{-1}$ percent per hr. It is interesting to note that, with some exceptions, field observations on SO_2 oxidation in plumes would seem to satisfy this condition, at least for plume ages less than about one or two hours (Gartrell et al., 1963; Stephens and McCaldin, 1971; Newman et al., 1975; Lusis and Wiebe, 1976; Whitby et al., 1976).

In Appendix A an example is given of the use of Equations (1) and (2) to predict conversion rates of SO_2 to sulfates in the plume of a nickel smelter stack. In this case an expression for reaction rate r proposed by Freiberg (1974,1975) is used in the calculations.

(2) The Elliptical Ring Plume Approximation

Recently Freiberg (1976) has published the results of some theoretical calculations on oxidation and dispersion of SO_2 in stack plumes. He used a gaussian plume model, the plume being divided into a number of concentric elliptical rings, within each of which the concentration was assumed to be uniform. Since no communication of pollutants was allowed between rings, concentration changes in the plume due to chemical reactions were in effect assumed to be very small compared to those due to dispersion - i.e., Freiberg was considering essentially the same problem as was treated in Section (1) above.

In this section we take an approach similar to that of Freiberg, with the important difference that turbulent exchange between adjacent rings in the plume is taken into account. This results in a fairly general set of equations for concentrations of reacting pollutants in a plume, which can be used irregardless of whether the reaction rate is fast or slow, and includes chemical interactions of pollutants emitted at the chimney with those entrained into the plume from the ambient air (e.g. nitrogen oxides and ambient ozone).

As in the previous section, the present model applies to a plume in which an inert pollutant would be distributed in a gaussian manner. Divide the plume into a series of N elliptical rings (see Figure 1) such that, for an inert pollutant, each ring contains the same amount of pollutant. The concentration is assumed to be uniform within each ring. (The reader is referred to Freiberg's 1976 paper for a detailed discussion of the elliptical ring concept.) Designating the inner ring as 1, the next ring as 2,etc., the area of any ring i can be shown to be (Freiberg, 1976):

$$A_i = 2\pi\sigma_y\sigma_z \ln\left(\frac{N-i+1}{N-i}\right) \qquad (6)$$

where as before σ_y and σ_z are the horizontal and vertical dispersion coefficients.

The rate of turbulent exchange of pollutants between adjacent rings can be related to the overall dispersion of the plume as follows (consider for the moment non-reactive pollutants):

Let K_i be a mass interchange coefficient per unit length of plume, such that the mass transferred by eddy diffusion from ring i to ring (i+1) per unit time is equal to $K_i(C_i - C_{(i+1)})$, where C_i is the concentration of pollutant in ring i.

As the plume is diluted by ambient air, the boundaries of the elliptical rings will expand. As the outer boundary of ring i expands, for example, ring i will "entrain" some of the contents of its adjacent ring, (i+1). Similarly, the outer ring, N, will entrain some ambient air. For a unit length of plume, the rate at which volume flows from ring (i+1) to ring i due to expansion, at plume age t, is

$$\frac{d}{dt}\left(\sum_{m=1}^{i} A_m\right)$$

and the mass flow rate is just $C_{(i+1)}$ times this.

Each ring by definition contains a constant amount of mass. Thus, the net rate of change of mass in each ring caused by these processes must be zero. For example, equating the rate at which mass is lost by turbulent diffusion from ring 1 to ring 2, to the rate at which the contents of ring 2 are entrained by the expanding boundary of ring 1 gives, per unit length of plume:

$$K_1(C_1 - C_2) = C_2 \frac{d}{dt}(A_1) \qquad (7)$$

Since, for the same amount of mass in every ring, the concentration is inversely proportional to the area, this gives the following expression for K_1:

$$K_1 = \frac{A_1}{A_2 - A_1} \frac{d}{dt}(A_1) \qquad (8)$$

Continuing this process from the centre of the plume outwards, the coefficient K_i for eddy exchange between rings i and (i+1) can be shown to be:

$$K_i = \frac{A_i}{A_{(i+1)} - A_i} \frac{d}{dt}\left(\sum_{m=1}^{i} A_m\right) \qquad (9)$$

Since we are carrying out a discrete approximation to concentrations in a gaussian plume, and all the mass of the emitted pollutant is contained in the N elliptical rings, then by definition K_N must be equal to zero (i.e. no transport outside of the last ring). Also, in the present calculations we arbitrarily set the area of the final ring, A_N, to be twice that of ring (N-1):

$$A_N = 2A_{(N-1)} \qquad (10)$$

It is important to note that A_i and K_i are only functions of the total number of rings N chosen in the gaussian plume approximation and the rate of plume dispersion-see Equations (6) and (9). They do not depend on any chemical changes which may be taking place in the plume, and should be the same for reactive and unreactive pollutants.

Consider now the case of chemically reactive pollutants. A mass balance, per unit length of plume, for ring i and reactive species B, for example, gives:

$$\begin{aligned} \frac{d}{dt}\left(C_{B_i}A_i\right) = {} & -K_i\left(C_{B_i} - C_{B(i+1)}\right) + K_{(i-1)}\left(C_{B(i-1)} - C_{B_i}\right) \\ & + C_{B(i+1)}\frac{d}{dt}\left(\sum_{m=1}^{i} A_m\right) - C_{B_i}\frac{d}{dt}\left(\sum_{m=1}^{i-1} A_m\right) \qquad (11) \\ & + r_{B_i}A_i \end{aligned}$$

where the term on the left hand side of Equation (11) represents the net rate of change of mass of B in ring i; the first two terms on the right hand side are the rate of eddy diffusion from ring i to (i+1) and from ring (i-1) to i respectively; the next two terms are the rate of influx of mass from ring (i+1) to i, and efflux from i to (i-1), respectively due to expanding ring boundaries; and the final term on the right hand side represents the rate of production of B in ring i by chemical reactions (r_B is the net rate of formation of B per unit volume of plume).

For purposes of computation, it is useful to write Equation (11) in the following form:

$$\frac{d}{dt}(C_{B_i}) = \lambda\left(\alpha_i C_{B(i-1)} + \beta_i C_{B_i} + \gamma_i C_{B(i+1)}\right) + r_{Bi} \qquad (12)$$

$$i = 1, 2, \ldots N$$

Equation (12) results after some algebraic manipulation making use of the expressions for K_i and A_i, and noting that:

$$\frac{d}{dt}\left(\sum_{m=1}^{i} A_m\right) = \left(\sum_{m=1}^{i} A_m\right)\frac{d}{dt}\ln \sigma_y \sigma_z \qquad (13)$$

It is of the same form as mass balance equations for reactive pollutants in a multiple-cell trajectory model of the type discussed by Eschenroeder and Martinez (1971), only the meaning of the coefficients of C_B is of course different. The coefficient λ incorporates the effects of dispersion, and is given by:

$$\lambda = \frac{d}{dt}\ln \sigma_y \sigma_z \qquad (14)$$

The coefficients α, β and γ depend only on the particular cell being considered (i) and the total number of cells involved

(N), and are given by:

$$\alpha_i = \frac{1}{A_i} \frac{A_{(i-1)}}{A_i - A_{(i-1)}} \left(\sum_{m=1}^{i-1} A_m \right) \tag{15}$$

$$\gamma_i = \frac{1}{A_i} \frac{A_{(i+1)}}{A_{(i+1)} - A_i} \left(\sum_{m=1}^{i} A_m \right) \tag{16}$$

$$\beta_i = -(\alpha_i + \gamma_i) \tag{17}$$

The values of A_i can be calculated from Equation (6), remembering that for the next-to-outside cell (N-1), $A_{(i+1)}$ is given by Equation (10).

Special consideration must be given to the inner and outside rings (i=1 and N respectively). Using methods similar to those above, it can be shown that β_1 and α_N are given by Equations (17) and (15) respectively, while

$$\alpha_1=0 \tag{18}$$

$$\gamma_1=\frac{A_2}{A_2-A_1} \tag{19}$$

$$\beta_N = -\alpha_N - \frac{1}{A_N}\left(\sum_{m=1}^{N} A_m\right) \tag{20}$$

$$\gamma_N = 0 \tag{21}$$

Furthermore, for ring N the term r_{Bi} must be replaced by:

$$r_{B_i} = r_{B_N} + \frac{C_B^o \lambda}{A_N}\left(\sum_{m=1}^{N} A_m\right) \tag{22}$$

The second term on the right hand side of Equation (22) represents the effects of entrained ambient air, where the concentration of species B is C_B^o.

In summary, Equations (12) and (14)-(22) involve a discrete approximation to dispersion and chemical reactions in a plume which, for inert pollutants, gives a gaussian concentration distribution. Reactive pollutants which may be entrained from the ambient air are taken into account through the C_B^o terms, while chemical reactions enter through the r_B terms. The form of the latter will of course depend on the type of reactions being considered.

In Appendix B an example is given of the use of Equations (12) and (14)-(22) to predict conversion of NO to NO_2 by entrained ambient O_3 in the plume of a power plant chimney.

Acknowledgement

I am grateful to several of my colleagues, especially Drs. H.E. Turner and L. Barrie, for discussions of the work reported above; also, to Dr. C.R. Phillips at the University of Toronto and Mr. O. Melo of Ontario Hydro. I would like to thank Ontario Hydro for making available their data from the Nanticoke Study.

References

ASME, Air Pollution Control Division (1973). Recommended Guide for the Prediction of the Dispersion of Airborne Effluents (2nd Ed.). American Society of Mechanical Engineers, New York.

Eschenroeder, A.Q. and Martinez, J.R. (1971). Concepts and Applications of Photochemical Smog Models. General Research Corp. Technical Memorandum 1516, Santa Barbara, California.

Freiberg, J. (1974). Effects of Relative Humidity and Temperature on Iron-Catalyzed Oxidation of SO_2 in Atmospheric Aerosols. Environ. Sci. Technol. 8, 731-734.

Freiberg, J. (1975). The Mechanism of Iron Catalyzed Oxidation of SO_2 in Oxygenated Solutions. Atm. Env. 9, 661-672.

Freiberg, J. (1976). The Iron Catalyzed Oxidation of SO_2 to Acid Sulphate Mist in Dispersing Plumes. Atm. Env. 10, 121-130.

Freidlander, S.K. and Seinfeld, J.H. (1969). A Dynamic Model of Photochemical Smog. Environ. Sci. Technol. 3, 1175-1181.

Gartrell, F.E., Thomas, F.W. and Carpenter, S.B. (1963). Atmospheric Oxidation of SO_2 in Coal-Burning Power Plant Plumes. Am. Ind. Hyg. Assoc. J. 24, 113-120.

Hilst, G.R. (1974). Dynamics and Kinetics in Environmental Problems-Are They Separable? Proc. Symp. on Chemical Aspects of Air Quality Modeling, University of North Carolina, April 17-19, 1974.

Leighton, P.A. (1961). Photochemistry of Air Pollution. Academic Press, New York.

Lusis, M.A. and Wiebe, H.A. (1976). The Rate of Oxidation of Sulfur Dioxide in the Plume of a Nickel Smelter Stack. To be published in Atm. Env.

Lusis, M.A., Wiebe, H.A. Anlauf, K.G. Stevens, R.D.S. and Sanderson, H.P. (1974) The Rate of Oxidation of Sulfur Dioxide to Sulfuric Acid and Sulfates in the Plume of the INCO Superstack at Sudbury, Ontario - September 17-26, 1974, Atmospheric Chemistry, Criteria and Standards Division, Atmospheric Environment Service, Downsview, Ontario.

Melo, O. and Stevens, R.D.S. (1976). An Airborne Investigation of the Nanticoke Generating Station's Plume. Given at an Ontario Ministry of the Environment Seminar, Feb. 5, 1976.

Mozzon, D., Ontario Ministry of the Environment, private communication.

Newman, L., Forrest, J. and Manowitz, B. (1975). The Application of an Isotopic Ratio Technique to a Study of the Atmospheric Oxidation of Sulfur Dioxide in the Plume from an Oil-Fired Power Plant. Atm. Env. 9, 959-968.

Newman, L., Forrest, J. and Manowitz, B. (1975). The Application of an Isotopic Ration Technique to a Study of the Atmospheric Oxidation of Sulfur Dioxide in the Plume from a Coal Fired Power Plant. Atm. Env. 9, 969-977.

Seinfeld, J.H., Hecht, T.A. and Roth, P.M. (1973). Existing Needs in the Experimental and Observational Study of Atmospheric Chemical Reactions. Environmental Protection Agency Report EPA-R4-73-031.

Steiner, J. (1974). INCO's Superstack Emissions. Given at an Ontario Ministry of the Environment Seminar Entitled "Emissions from Smelter Operations and Their Effect on The Environment", February 21, 1974.

Stephens, N.T. and McCaldin, R.O. (1971). Attenuation of Power Station Plumes as Determined by Instrumented Air-Craft. Environ. Sci. Technol. 5, 615-621.

Whitby, K.T., Cantrell, B.K., Husar, R.B., Gillani, N.V., Anderson, J.A., Blumenthal, D.L. and Wilson, W.E. (1976). Aerosol Formation in a Coal Fired Power Plant Plume. 171st National Meeting of the Amer. Chem. Soc., New York, April 4-9.

Appendix A: Conversion of SO_2 to sulfates in dispersing plumes.

During September 1974 and June 1975, field measurements of SO_2 oxidation rates were made in the plume of the INCO nickel smelter stack at Sudbury, Canada (Lusis and Wiebe,1976). Sulfur trioxide makes up about 1% of the total sulfur effluent from this point source and the plume also contains about 3.5% by volume water (Steiner, 1974), so that an acid mist forms within a few feet of the stack. Iron is the most predominant emitted metal capable of catalyzing oxidation of SO_2 in solution. It is therefore reasonable to adopt Freiberg's kinetic model for the iron-catalyzed oxidation of SO_2 in plumes (Freiberg, 1974, 1975) to illustrate the use of Equations (1) and (2), and to see if the observed SO_2 oxidation rates can be predicted theoretically.

According to this model, the local rate of SO_2 conversion to sulfate at any point in the plume is given by:

$$r = - K_o \beta_s^2 K_s^2 \left[\frac{\beta_n K_n \lambda_a}{2(1-RH) K_w} \right]^3 C_s^2 C_c C_n^3 \qquad \text{(A1)}$$

where subscripts s, c and n on concentration C refer to sulphur dioxide, catalyst (Fe^{3+}), and ambient ammonia respectively. RH is the relative humidity, and the K's and β's are rate, equilibrium and Ostwald constants. For the present calculations, λ_a is taken to be the vapor pressure lowering coefficient of sulfuric acid, and can be obtained from standard sources of physical data. The reader is referred to Freiberg's original papers for a full discussion of the meaning of the terms in Equation (A1).

Following Freiberg (1976), we assume that C_n is constant throughout the plume, and equal to 6×10^{-7} moles m^{-3}. Then Equation (A1) may be written:

$$r = -\frac{k}{(1-RH)^3} C_c C_s^2 \qquad \text{(A2)}$$

where

$$k = K_o \beta_s^2 K_s^2 \left[\frac{\beta_n K_n \lambda_a}{2 K_w}\right]^3 C_n^3 \qquad \text{(A3)}$$

The concentration distribution of both SO_2 and Fe^{3+} catalyst is given by Equation (1). If Q_c is the emission rate of catalyst (which is not a function of plume age) and Q_s is that for SO_2, then substitution of Equations (1) and (A2) into Equation (2), followed by integration of the exponential terms, gives:

$$\frac{dQ_s}{dt} = -\frac{k}{12(1-RH)^3} \frac{Q_c}{(\pi \sigma_y \sigma_z U)^2} Q_s^2 \qquad \text{(A4)}$$

By integrating Equation (9), the fraction of SO_2 remaining in the plume at plume age t_2, $(Q_s/Q_s^o)_2$, can be related to the fraction remaining at t_1, $(Q_s/Q_s^o)_1$:

$$\left(\frac{Q_s^o}{Q_s}\right)_2 - \left(\frac{Q_s^o}{Q_s}\right)_1 = \frac{k Q_c Q_s^o}{12(1-RH)^3 (\pi U)^2} \int_{t_1}^{t_2} \frac{dt}{(\sigma_y \sigma_z)^2} \qquad \text{(A5)}$$

where Q_s^o is the emission rate of SO_2 at the stack.

The predictions of Equation (A5) can be compared with the results of field measurements in the INCO plume. During the September 1974 study a detailed stack emission rate measurement was made (Mozzon, 1976), giving iron and SO_2 emission rates (g moles min^{-1}) of about 85 and 35000 respectively. Following Freiberg (1976), we assume that about 8% of the emitted iron is soluble and catalytically active. With the exception of λ_a and C_n, the values of the parameters necessary for calculating k at different temperatures were taken from Freiberg's paper (1974), using extrapolation where necessary. Some plume concentration profile measurements had been made during the September 1974 study (Lusis et al., 1974), from which it was possible to estimate representative values of (σ_y σ_z) as a function of plume age. With the units of t in minutes, the product (σ_y σ_z) (m^2) over the study period could be estimated from

$$(\sigma_y \sigma_z) = 10^4 t \qquad \text{(A6)}$$

the deviation between predicted values and those calculated from individual plume profile experiments usually being less than 40%.

During the field studies at Sudbury, samples were collected at various distances from the chimney (Lusis and Wiebe, 1976). The percentage of sulfur in the form of sulfate at the different sampling points, as well as the relevant meterological parameters, are given in Tables 1 and 2 of the above reference. Using the percent converted at the closest-in location as a starting point, conversions at the farther-out locations were predicted with Equation (A5). The results for September 1974 are given in Table A1.

The results shown in Table A1 indicate very low predicted conversion rates, which is in qualitative agreement with the observations, since a representative value for the INCO plume was found to be about 1% hr^{-1} (Lusis and Wiebe, 1976). Thus, under the conditions of the present study, iron is predicted to have a much less important catalytic role than under those obtaining during the program of Gartrell et al. (See Freiberg, 1976). On the other hand, the model predicts significant oxidation rates only within the first few minutes of plume age, and for low temperatures and/or high relative humidities. However, the experimental data suggested that the conversion rate is independent of plume age, and no temperature or humidity effects could be found (Lusis and Wiebe, 1976).

The major source of error in the predicted values may be Freiberg's kinetic model, which probably does not apply in a quantitiative way for the high pollutant concentrations and the range of relative humidities encountered in the Sudbury study. This cannot be a definite conclusion, however, because of the uncertainties in several model input parameters on which the predicitions are quite sensitive, most importantly the background ammonia concentration C_n (which was not measured during the study period) and the dispersion coefficients (σ_y σ_z).

Table A1 : Comparison of predicted and observed conversion of SO_2 to sulfate

Date Sept.	Temp. C	Rel. humidity %	Plume age min.	% Sulfur as sulfate	
				Observed	Predicted
17	1	40-60	18	1.2	-
			38	1.1	1.2
			107	1.3	1.2
18	0	50-80	18	1.2	-
			56	1.1	1.3
			250	3.2	1.3
21	1	70	7	1.5	-
			110	2.3	2.0
			300	4.3	2.0
22	-5	50-70	3	0.7	-
			67	3.3	6.6
			167	2.8	6.7
25	3	90	2	1.5	-
			38	3.3	5.3
			120	6.5	5.4
26	3	70-80	17	0.9	-
			117	3.9	0.9
	6	80-90	3	1.2	-
			53	7.0	1.9

Appendix B: Conversion of NO to NO_2 by entrained ambient O_3 in the plume of a power plant chimney.

During November of 1975 the Ontario Ministry of the Environment and Ontario Hydro carried out a joint study concerned with dispersion and chemical reactions in the plume of the 200 m Nanticoke Generating Station Stack, on the north shore of Lake Erie (Melo and Stevens, 1976). The Nanticoke area is relatively free of other sources of primary pollutants. High ozone concentrations are occasionally observed, probably due to O_3 generated from photochemical reactions on a regional scale.

One day of particular interest was November 17, on which the plume was trapped in a stable layer aloft, and profile measurements of NO_x, NO and O_3 were made as far as 93 km down wind of the chimney. Simultaneous measurements were made of wind speed and air temperature as a function of height.

In the calculations, the only reactions occuring in the plume which involve nitrogen oxides and ozone were assumed to be:

$$NO_2 + h\nu \xrightarrow{k_1} NO + O$$

$$O + O_2 + M \xrightarrow{k_2} O_3 + M$$

$$NO + O_3 \xrightarrow{k_3} NO_2 + O_2$$

Hydrocarbons are expected to play a negligible role in the NO_x-O_3 cycle, because of the absence of local sources of these pollutants at Nanticoke, while reactions involving SO_2 were assumed to be relatively unimportant.

Assuming a pseudosteady state for oxygen atoms, the following rate equations result:

$$r_{NO_2} = -r_{NO} = -r_{O_3} = -k_1 C_{NO_2} + k_3 C_{O_3} C_{NO} \qquad (B1)$$

Values of k_1 and k_3 were taken from Leighton (1961). For the solar zenith angle and metorological conditions obtaining during the November 17 study, these rate constants were estimated to be 0.1 min^{-1} and 22 ppm^{-1} min^{-1} respectively.

The wind speed was 800 m min^{-1} at plume height, and the NO_x emission rate during the sampling period was 90 kg min^{-1}. From plume cross-wind measurements at different downwind locations, the dependence of $\sigma_y \sigma_z$ (m^2) on plume age t (min) was estimated to be:

$$(\sigma_y \sigma_z) = 2.1 \times 10^3 \, t^{0.47} \qquad (B2)$$

With these input parameters and an ambient O_3 level of 0.105 ppm (measured during the flight), calculations were made to determine the ratio NO/NO_x at various downwind locations. Integration was started at a plume age of 3.4 min, where the NO/NO_x ratio was 0.94 (measured). At this initial point the NO and NO_2 profiles were calculated using the NO_x emission rate given above, and the O_3 concentration in the plume was assumed to be zero.

A ten-ring plume model was used, with integration over time increments of 0.5 min. (Up to 30 rings, and smaller time increments, did not change the results significantly.) The method of Pade approximants suggested by Eschenroeder and Martinez (1971) was employed to integrate Equation (12).

Figure 2 shows a comparison of the ratio (NO/NO_x) in the plume calculated by the present methods (the solid curve) and measured during crosswind traverses at or near the plume centre-line. It can be seen that the model gives a fairly good representation of NO oxidation by entrained ambient O_3. The predicted rate of NO conversion to NO_2 is initially rapid, then levels off downwind to give a (NO/NO_x) ratio which is in good agreement with the measured values. It should be noted that during the study period, there were actually two chimneys in operation at the generating station. The effect of these two sources could be seen in the NO_x profiles measured downwind (two peaks being usually apparent), although in the modelling calculations only one source of NO_x was assumed.

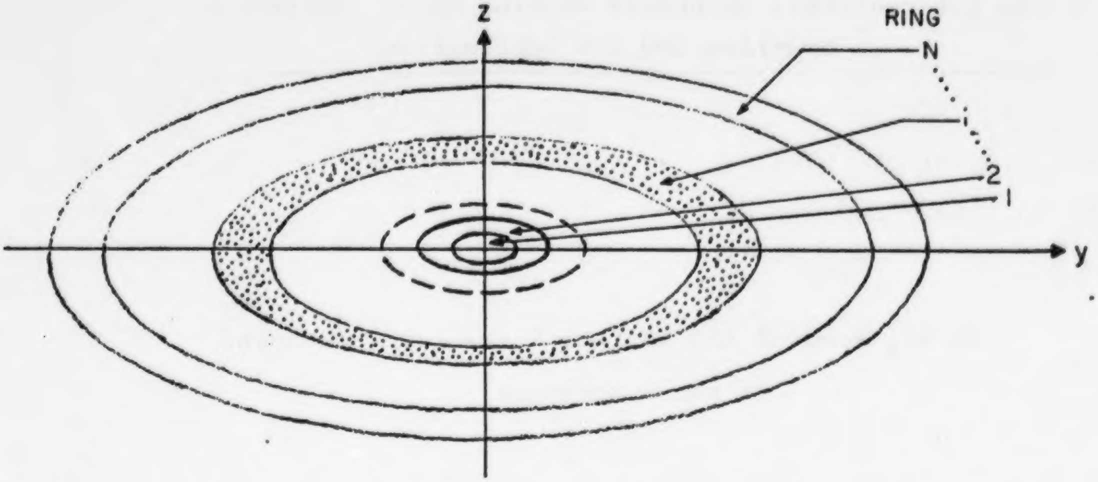

Figure 1 : Cross-section of plume showing elliptic rings.

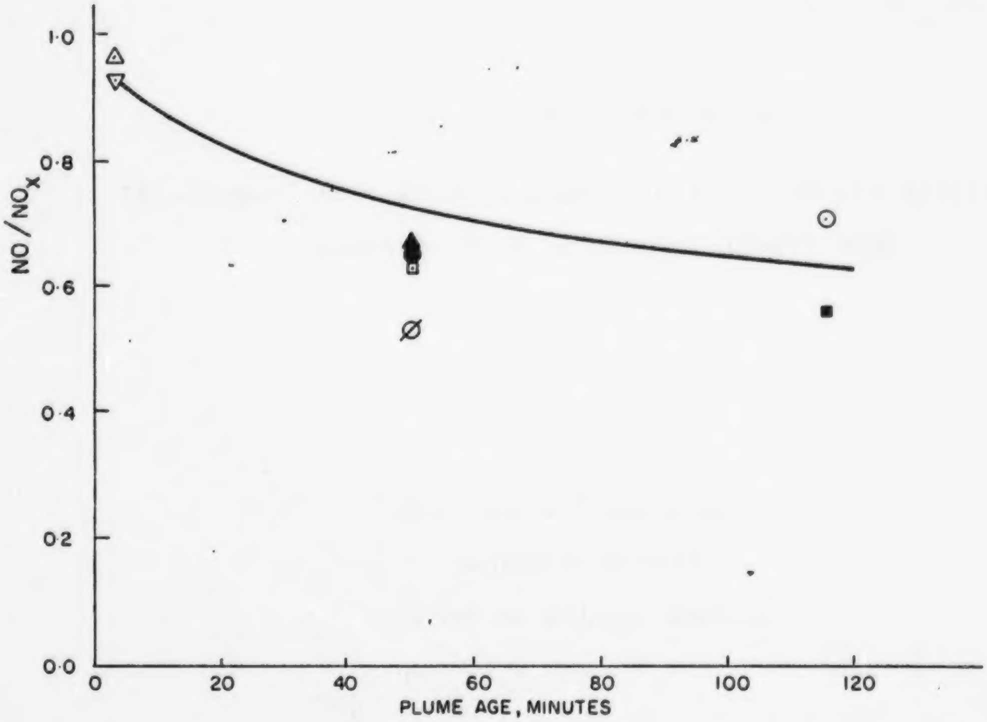

Figure 2 : Comparison of observed and predicted conversion of NO to NO_2 in Nanticoke plume.

7th International Technical Meeting on Air Pollution
Modeling and its Application

On SO_2-Removal and Sulfate Formation Processes in the Atmosphere

Results presented within the Framework of EUCO - COST (European Cooperation and Coordination in the Field of Scientific and Technical Research) COST project 61a

D. R. KALTHOFF

Institut für Meteorologie und Geophysik, Feldbergstr. 47
6000 Frankfurt/Main 1, F. R. Germany

September 7 - 10, 1976
Airlie Virginia
United States of America

ON SO_2-REMOVAL AND SULFATE FORMATION PROCESSES IN THE ATMOSPHERE

INTRODUCTION

To introduce experimental data into diffusion models, space and time scales are important considerations.
Dealing with the classical problem, the emission of a pollutant and it's concentration prediction down wind from a source the dependance of most meteorological and physico-chemical parameters on travel distance has to be taken into account. Not only meteorological "steady-state" and homogeneous turbulence conditions are no longer valid the larger the travel-distance become, but also the physico chemical behaviour of the considered pollutant may have greater impact on it's statistic. Most pollutant are not chemically inert. Consequently with increasing travel distance - or travel time - their conversion and removal rates become more important in diffusion models.
With changing meteorological conditions - e.g.changing of solar irradiation temperature humidity, cloud and fog formation - removal and conversion processes of the considered pollutant may change or even, since one pollutant can undergo several chemical processes in a real atmosphere, different mechanisms may be realistic at the same time, depending on the physic chemical condition. So the assumption implicit in most diffusion models that all the pollution remains in the atmosphere (perfect reflection at the interface, no precipitation scavinging, no chemical reaction) is unrealistic in order to

estimate regional and global budgets of our pollution.

For sulfurdioxide, one of the major components in air-chemistry, such conversion and removal mechanisms were not well known. There was a great lack of knowledge about which mechanisms were realistic for the atmosphere.

The European Cooperation and Coordination in the Field of Scientific and Technical Research (EUCO - COST), which is organized by the Commission of the European Communities, therefore launched a program - named COST 61a - with the aim to push the research into the physico-chemical behaviour of Sulfurdioxide in the atmosphere.Eleven European Common Market member and non-member countries signed an agreement in November 1972 and since then a considerable progress within participating research projects was made.
The results presented in this paper are strongly confined to those, achieved within COST 61a projects.

Sulfurdioxide can be removed from the atmosphere either by chemical reactions or by absorption on various surfaces.

1. CHEMICAL REACTIONS

Chemical reactions of SO_2 in the atmosphere can be subdivided in

1.1 homogeneous gas phase oxidations, which include direct oxidation of SO_2 by oxidizing trace gases (O_3, NO_2), and

ON SO_2-REMOVAL AND SULFATE FORMATION PROCESSES IN THE ATMOSPHERE

INTRODUCTION

To introduce experimental data into diffusion models, space and time scales are important considerations.
Dealing with the classical problem, the emission of a pollutant and it's concentration prediction down wind from a source the dependance of most meteorological and physico-chemical parameters on travel distance has to be taken into account. Not only meteorological "steady-state" and homogeneous turbulence conditions are no longer valid the larger the travel-distance become, but also the physico chemical behaviour of the considered pollutant may have greater impact on it's statistic. Most pollutant are not chemically inert. Consequently with increasing travel distance - or travel time - their conversion and removal rates become more important in diffusion models.
With changing meteorological conditions - e.g.changing of solar irradiation temperature humidity, cloud and fog formation - removal and conversion processes of the considered pollutant may change or even, since one pollutant can undergo several chemical processes in a real atmosphere, different mechanisms may be realistic at the same time, depending on the physic chemical condition. So the assumption implicit in most diffusion models that all the pollution remains in the atmosphere (perfect reflection at the interface, no precipitation scavinging, no chemical reaction) is unrealistic in order to

photochemically induced reactions and

1.2 heterogeneous gasphase oxidation.

Here absorption of SO_2 on aerosolparticles, dust or water droplets, followed by oxidation is involved.

1.1.1 Several various photochemical mechanisms fo SO_2 oxidation were suggested. It was concluded that only the following processes are the most important:

1. Oxidation of SO_2 by free radical intermediates
2. Oxidation of SO_2 by Ozone-Olefin reaction intermediates . The term"dark reaction" is often used, since this reactiontype is not confined to periods of high irradiation intensity.

The direct Oxidation of SO_2 by even high concentrations of O_3 and NO_2 can be completely neglected as a sink for SO_2 under atmospheric conditions as well as the direct oxidation of excited SO_2 (Singlet or Triplet-state).

It now seems to be well established, that the atmospheric oxidation of hydrocarbons and SO_2, which in polluted air leads to photochemical smog formation, proceeds by a radical chain process-production and depletion of radicals within a set of processes- where the chain determinating step is the formation of Sulfurtrioxide (SO_3) and its reaction with water vapour to form sulfuric acid aerosols (H_2SO_4). All efforts of laboratory simulation experiments are done to provide reaction rate constants which are necessary for model calculations. The free radicals involved are (OH),

(O_2H) and their corresponding organic radicals RO, RO_2, where R represents a hydrocarbon fragment.

Some of the main results for OH and O_2H processes of SO_2 in the atmosphere are summarized in Tab. 1 (1), (2). It is evident that the radical concentration is a function of solar irradiation, since these radicals are formed by irradion (eg. $HNO_2 + h\cdot\nu \longrightarrow NO + OH$). The radical concentration is also depending on NO_x and ozone concentration. These data are necessary for concentration calculations.The measured OH radical concentration (C.C. WANG, 1975) are only slightly different from calculated ones (LEVY 1973).

1.1.2 Quite simular experiments are used for the simulation of polluted urban atmospheres (3), where the reaction of ozone with unsaturated hydrocarbons (Olefins) yields a reactive oxidizing intermediate. Measuring the decrease of SO_2 or the increase of sulfuric acid particles leads to nearly the same removal rates (Tab. 2). It is well known that SO_2 can be oxidized in simulated photochemically smog systems. There is evidence of correlation between high ozone levels and elevated sulphate aerosol concentration, which is presented in Fig. 1 (Radiation was in the range of solar intensity of a summer day). Since this mechanism is also a radical chain process, extrapolation to atmospheric conditions (generally lower concentrations of the added pollutant) is rather questionable. The authors gave a rough estimate by 0.4%/h removal of SO_2. Another experiment was carriedout with ambient air, sampled in transparent plastic bags and irradiated by natural sunlight during a longer time of period. It was found (2), that during summer month (June-August) in a rural area oxidation rate was in the order of 1%/h. During winter und early spring (Feb.-March) the rates were approximately a factor of 3 to 5 slower. Ozone was also produced, in a rate, which correlated well with the SO_2-oxidation rate.

1.2.1 In a real atmosphere we are concerned with a very heterogeneous system: a gas phase loaded with particles, which can be fog and rain droplets or dry particles,mostly inorganic salts and oxides with more or less water vapour absorbed. Here too simulation experiments are very difficult to perform. Results obtained are therefore only applicable to specific cases, like simple droplets or droplet system (cloud,fog).

The controlling process for SO_2 oxidation within an atmospheric droplet is the oxidation of the Sulfite ion ($SO_3^=$) to Sulfate ion ($SO_4^=$). The Sulfite ion is formed by absorption of SO_2 from the gas phase into the aqueous phase, which is conrolled by the pH (concentration of the H^+-ions in the aqueous phase). The pH of a droplet is controlled by the formation of Sulfuric acid (H_2SO_4) during the oxidation, by pre-existing acidic aerosols as shown under 1.1., by Hydrochloric acid (HCl), by Ammonia (NH_3) and other atmospheric components with acidic or basic properties.

Since continental cloud and rain water has a pH normally between 4 and 5 the following calculations have been done,presented in Tab.3.Although the rates are remarkably differing changing the liquid water content (LWC) by a factor of 10, they are evidently almost negletable for the atmosphere (4).

1.2.2. The situation in water droplets is different, if trace-concentrations of metal ions are added to the aqueous system. Transition metals like iron (Fe) and Manganese (Mn) are known to be very effective catalysts for the oxidation of in water dissolved SO_2.Measurements of metal components in rainwater (5) yielded a concentration of 10^{-8}-10^{-6}Mole/L for Manganese and 10^{-7}-10^{-5}Mole/L for iron, both components completely dissolved in rainwater. The insoluble fractions are not considered. A quantitative estimate for the catalytic oxidation in cloud water is made in Tab.4. The rates are thought to be typical for a cloud situation. Effects of other trace constituents which could promote or inhibit the catalytic oxidation are not taken into account.

The capacity of dry aerosols to oxidize SO_2 was subject of various research work. Due to the special experimental arrangements, necessary for these studies, results were obtained at rather high SO_2concentration as well as aerosol concentration, which might be encountered only in stack plumes. Fig.2. shows some of the data for Manganesesulfate aerosols (6). At low humidity the SO_2 concentration in the gas phase is not influencing the conversion rate. A first order reaction rate is given at higher relative humidity. No dependence of temperature on reaction rate in the range of 20 - 50 °C was observed.

2.ABSORPTION ON VARIOUS MATERIALS

Atmospheric trace constituents are generally absorbed by different surfaces with a different efficiency. These processes are often called "wet and dry depostion".Only dry deposition is considered in this paper.

A parameter often used to decribe this process is the deposition velocity v. This transfer velocity of SO_2 is quite commonly expressed (8) as

$$v = \frac{1}{R\ (z)}$$

where R(z) is the total resistence to tranfer from a height z in the atmosphere to the ground. The total resistence is the sum of three separate resistances:

$$R(z) = r(z) + r_m + r_s$$

turbulent diffusion resistance r(z) - meteorological influences,

molecular diffusion resistance r_m - influence of the paticular properties of the boundary layer surface/gaseous phase,

suface resistence r_s - influence of the chemical,physical properties of the considered surface.

It is obvious, that experimental values for the deposition velocity of SO_2 must be different for different surfaces.For example (7a):

grass	o.36 - 2,2 cm/sec
snow	o.o4 - o.33 cm/sec

Laboratory studies have been done to investigate the influence of different soils on SO_2 absorption (9). Values for surface resistance ranged between o.4 - 3.8 sec/cm for dry soils and from o.2 - 1.2 sec/cm for moist soils (Payrissat 1974), which are corresponding to a deposition velocity of (other parameters neglected):

dry soil	o.25 - 2.5 cm/sec
moist soil	o.83 - 5.o cm/sec.

For plants the role of stomata and the influence of SO_2 on their function has been invetigated (10). This study indicates the high variability in the reaction of plant material with SO_2, metabolic activity, state of growth etc.. For example, the deposition velocity decreased from o.4 in the morning to o.14 cm/sec in the late afternoon, according to experiments with a pine tree (7a)

As it was already pointed out for chemical reactions, the extrapolation of results obtained in laboratory studies to atmospherical conditions is very questionable, due to the high complexity of the problem.

	OH-radicals per cm^3	Molecular rate constants at 1 atm 300 ^oK	SO_2-Oxidation rate
			% h^{-1}
Winter	o.62 10^6	1.3 10^{-12} $\frac{cm^3}{\text{molecule sec}}$	
	max. 3.2 10^6		1.1
Summer	4.2 10^6		
	max. 6.2 10^6		2.2
	O_2H-radicals per cm^3		
	o.48 10^9	8.5 10^{-16} "	≈ 0.003
	max. 1.43 10^9		

Tab.1.SO_2-oxidation rates due to radical reactions (Troposphere 50°N Latitude).

Ozone Conc. (ppb) / Propene Conc. (ppb)	100	40	10
50	o.35	o.14	o.o35
10	o.o7	o.o3	o.oo7
2	o.o14	o.oo6	o.oo1

Tab.2. SO_2-removal rates (% h^{-1}).

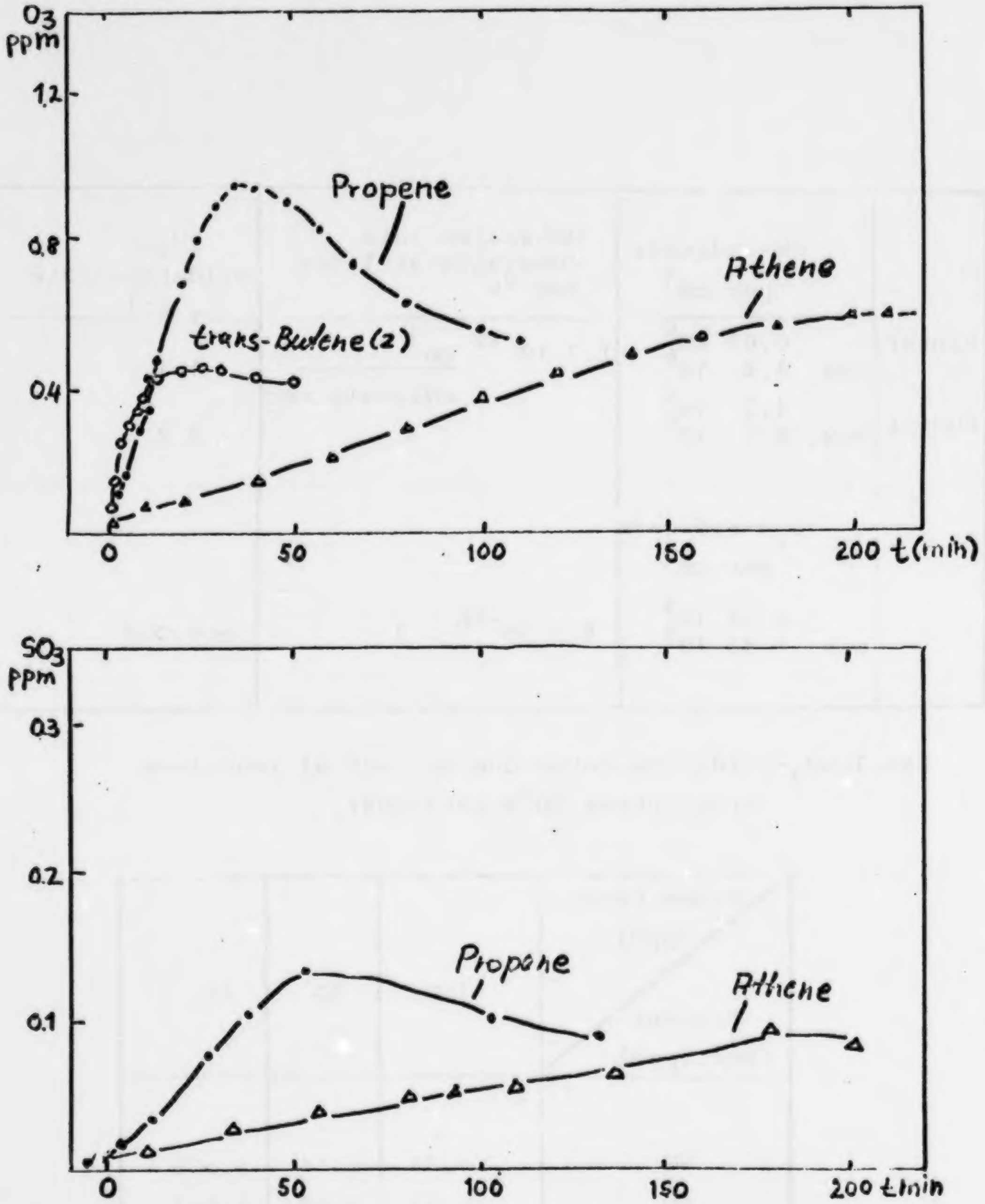

Fig.1. Increase of O_3 and SO_3 during smog simulation experiment. (initial conc. 2ppm Olefine, 0.75ppm NO_2, 0.85ppm SO_2)

LWC	$(pH)_o$	$(SO_2)_o$	$(NH_3)_o$	Temp. °C	SO_2-removal rates
0.1 g/m^3	3.1 3.5 3.1	1 ppb 1 ppb 2 ppb	1 ppb 2 ppb 1 ppb	3 3 3	10^{-6} %/h 10^{-5} %/h 10^{-6} %/h
1 g/m^3	3.8 4.1 3.8	1 ppb 1 ppb 2 ppb	1 ppb 2 ppb 1 ppb	3 3 3	4 10^{-4} %/h 2 10^{-3} %/h 4 10^{-4} %/h

Tab.3.Calculated SO_2-Removal Rates

LWC	pH	SO_2Conc.	Mn^{2+}	Fe^{2+}	T °C	Removal rates %/h
0.1	3.5	100 ppb	10^{-5}M/L	10^{-5}M/L	8	1 urban cloud
	3.5	100 ppb			25	1
	3.5	1 ppb	10^{-6}M/L	10^{-5}M/L	8	0.25 country cloud
	3.4	1 ppb			25	0.75
	4.0	1 ppb	10^{-5}M/L	10^{-5}M/L	25	3

Tab.4. SO_2-Removal Rates due to Catalytic Oxidation.

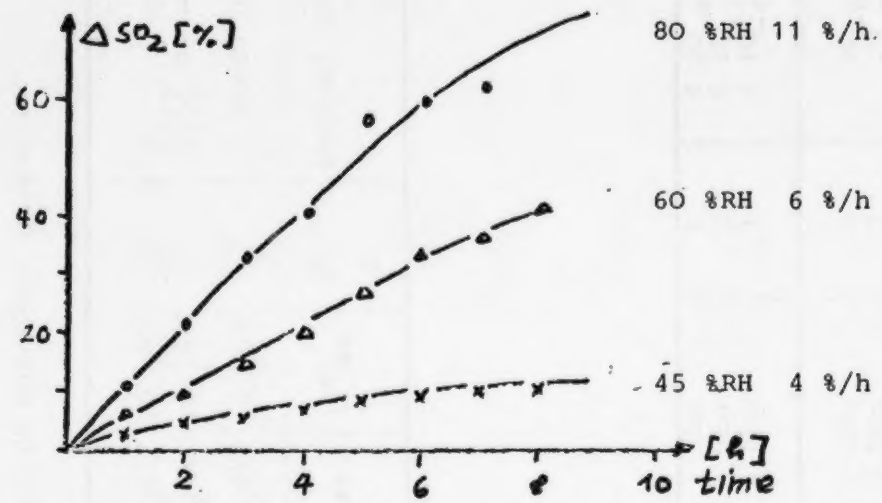

Fig.2. SO_2-removal by $MnSO_4$-aerosol.(Aerosolconc.30mg/m^3, 10^6-10^7 particles/cm^3,mean radius 1.2μ)

(1) R.A. COX "Gasphase Oxidation of Atmospheric Sulfur Dioxide" EUCO/SO_2/I/1/76

(2) R.A. COX, A.E.J. EGGLETON "Rate measurements of Aerosol Formation from the Photooxidation of SO_2 in sunlight" presented at the 3rd Technical Symposium on Research into the Physico-chemical behaviour of SO_2 in the Atmosphere, COST 61a, at ISPRA, Nov. 18-20, 1975

(3) K.H.BECKER, J. LÖBEL, U.SCHURATH, H. SEITZ "Oxidation of SO_2 in the Natural Atmosphere by Homogeneous Gasphase Reactions." Presented at the 3rd Technical Symposium on Research into the Physico-chemical behaviour of SO_2 in the Atmosphere. COST 61a at ISPRA, Nov. 18-20, 1975

(4) S.BEILKE, G. GRAVENHORST Position Paper on "Aqueous phase SO_2-Oxidation in the Atmosphere". EUCO/SO_2/I/1/76

(5) S.A. PENKETT (EUCO/SO_2/I/1/75)

(6) G. HAURY, S. JORDAN "Experimentelle Untersuchungen zur katalytischen Oxidation von SO_2 an Mangansulfataerosolen bei verschiedenen Temperaturen und relativen Feuchten." Presented at the Technical Symposium of COST 61a, at Ispra, Nov.18-20, 1975

(7a) Third Annual Report of the Management Committee Nov.1, 1974 - Okt.31, 1975

EUCO/SO_2/59/76 - XII/276/76

(7b) Report on a Meeting of Study Group "Absorption", EUCO/SO_2/54/75

C.C.WANG et al.,Science 189,797 (1975)

H.LEVY, Planet.Space.Scie.21, 575 (1973)

M.PAYRISSAT,S.BEILKE, "Uptake of SO_2 by different European Soils, Atm.Environm.9, 211 (1974)

(8) R.STEENKIST "Influences of the Deposition velocity on the Dispersion of SO_2 from High Sources.

(9) M.PAYRISSAT, A.HOFFMANN, P.REINIGER "SO_2 Uptake by Plants and Soils".

(10) J.BONTE,L. de CORMIS, A. TISNE "Interaction Végétaux - Dioxyde de Souffre"

(8). (9), (10), all papers presented at the "3rd Technical Symposium on Research into the Physico-Chemical Behaviour of SO_2 in the Atmosphere. COST 61a at ISPRA, Nov. 18 - 20, 1975.

DISCUSSION OF TOPIC 5

TALL STACK PLUMES, INCLUDING SULPHATE TRANSFORMATION AND REMOVAL PROCESSES

(WARREN B. JOHNSON, RAPPORTEUR)

PAPER 1: "IMPROVED TECHNIQUES FOR MODELING THE DISPERSION OF TALL STACK PLUMES," BY H. E. CRAMER

DISCUSSION:

Bowne: What range of source sizes in terms of heat output are covered by your plume rise equation?

Cramer: Source heat output is not a variable in our equation, but so far this has not caused problems.

Fortak: What was the nature of the experimental program used to obtain plume rise values?

Cramer: Two observational studies were conducted in which measurements of plume rise were obtained by means of EPA helicopters.

Fortak: How do you determine the plume centerline when there is substantial vertical mixing?

Cramer: We use the measured maximum SO_2 concentration to delineate the plume centerline.

Egan: Why do you use the old Briggs formula, when Briggs has now changed it from 3.5 x^* to 10h?

Cramer: The advantage in using the old formula is that it is simpler and easier to extrapolate.

Keddie: Have you compared Briggs' plume rise formula with Dr. Moore's results?

Cramer: No, but I believe the Briggs formula is satisfactory and would reproduce Moore's results well.

Turner: Have you have any success in predicting ground-level concentrations for unstable looping plumes?

Cramer: Our short-term formula gives a good estimate.

PAPER 2: "PLUME RISE AND BEHAVIOR OF EMISSIONS FROM A TALL STACK," BY F. FANAKI

PAPER 3: "DIFFUSION PARAMETERS FROM TALL STACK PLUMES," BY H. E. TURNER

PAPER 4: "A COMPARISON OF 'STAR' AND MEASURED LAPSE-RATE STABILITY CLASSIFICATIONS WITH OBSERVED TALL STACK PLUME DISPERSION PARAMETERS," BY R. V. PORTELLI

DISCUSSION:

Wendell: Were there any other cases when smoke plumes were observed by satellites?

Fanaki: No, this was a rather exceptional occasion; we have no other satellite observations of plumes that were transported over hundreds of kilometers.

Knox: With regard to the case of plume entrainment into a cumulonimbus cloud that you mentioned, have you observed this to happen frequently?

Fanaki: Entrainment into cumulus clouds does happen fairly frequently, but cumulonimbus clouds are not usually involved.

PAPER 5: "MATHEMATICAL MODELING OF CHEMICAL REACTIONS IN A PLUME, WITH APPLICATION TO A TALL STACK," BY M. LUSIS

DISCUSSION:

Hilst: How was your application of Friberg's theory affected by the sensitivity of the theory to relative humidity?

Lusis: This is one problem in getting good agreement; however, we used ambient relative humidity, which is very close to the plume relative humidity after a few kilometers of travel.

Hilst: What did you do about the ammonia values required by the theory?

Lusis: We used Friberg's values.

Veigele: Did you take into account the fact that Friberg's formulation is restricted to linear, non-meandering plumes?

Lusis: Yes, we applied this restriction in our work.

PAPER 6: "ON SO_2 REMOVAL AND SULPHATE FORMATION PROCESSES IN THE ATMOSPHERE," BY D. R. KALTHOFF

DISCUSSION:

Knox: There appears to be good agreement between your results and those obtained at Lawrence Livermore Laboratory by Dr. Deuwer. What pH value is associated with the conversion of 80% per hour which you mentioned?

Kalthoff: About 6.5.

Wendell: What size of experimental chambers were used to obtain the measurements that you reported?

Kalthoff: The chambers were of various sizes, with the average size perhaps about 400 liters.

Wendell: How about wall effects in the chambers?

Kalthoff: Wall effects have been taken into consideration, and were included in the analysis.

Hilst: It appears that you have considered mainly ambient level pollution concentrations. Have you considered the higher concentrations that occur during the early portions of plume travel?

Kalthoff: I believe there are some results on this in the original literature.

PAPER 7: "SULPHATE TRANSFORMATION AND REMOVAL PROCESSES IN POWER PLANT PLUMES," BY W. E. WILSON

DISCUSSION:

Fortak: What was the speed of the aircraft used to sample SO_2 and O_3, and what are the instrumentation response times?

Wilson: The aircraft travelled at about 60 mi/hr (96 km/hr) through narrow plumes. The SO_2 instrument gave 90% response in 5 seconds; the O_3 and NO_x instruments gave 90% response in 2 seconds. Values were digitized and recorded each 0.4 seconds.

Wendell: Was there a visible plume, indicating that liquid-phase conversion was taking place?

Wilson: No, normally the plumes were not visible. However, occasionally a plume merged with cumulus clouds.

Hoffnagle: Did you take into account instrument response times, which must be considered in order to obtain accurate values of mass flux as a function of downwind distance?

Wilson: Yes, this has been taken into consideration in our analysis.

Knox: Can we conclude from your observations, which show B-scat is high at the sides of the plume during the daytime, that homogeneous gas phase reactions are responsible?

Wilson: One might draw that conclusion.

Johnson: It is interesting that the results from the OECD project show fast conversion of SO_2 to sulphate initially, while your results indicate the opposite. Can you shed any light on this?

Wilson: All I can say is that our results are based on field experiments which we believe to be valid.

Lusis: Our results in Canada appear to confirm the OECD findings. Perhaps the difference in the St. Louis results can be explained on the basis of the existence of significant concentrations of ozone in the background air around the plume.

Wilson: Yes, that is possible; we think, therefore, that metal catalysts in the plume may not therefore be very important in the conversion process for this plume.

Hilst: Might a relative humidity effect be responsible?

Wilson: The plume data obtained by Brookhaven typically show a low dependence upon relative humidity, so I think not.

7 th NATO/CCMS
International Technical Meeting
on Air Pollution Modeling

TOPIC VI

DIFFUSION PARAMETERS AND STABILITY CATEGORIES

7 th NATO/CCMS
International Technical Meeting
on Air Pollution Modeling
and its Application

COMPARISON BETWEEN EXPERIMENTALLY MEASURED DIFFUSION PARAMETERS AND THE MAIN STABILITY CRITERIA.

L. Santomauro[+], D. Anfossi[+++], P. Bacci[++], A. Longhetto[++]

+ Osservatorio Meteorologico di Brera , Milano, Italy
++ Laboratorio Ricerca Ambientale - ENEL - Trino Vc., Italy
+++ Laboratorio di Cosmo-geofisica del CNR, Torino, Italy

AIRLIE HOUSE, Airlie, Virginia
U.S.A.
7 - 10 September, 1976

1. INTRODUCTION.

Between the main theories of atmospheric diffusion, the normal (or Gaussian) distribution function has shown to be a fundamental solution to the Fickian diffusion equation. Combined with the results of the statistical theory of turbulent dispersion, i.e.

$$\begin{aligned} \sigma_j &= \overline{(u_j')^2_T}\, T^2 \qquad && T \text{ small} \\ & && \qquad\qquad (1) \\ \sigma_j &= 2KT && T \text{ large} \end{aligned}$$

(with j = y, z and T indicating travel time), it has been considered the basis for most of the practical plume-diffusion formulas for the last forty years.

So, a lot of work has been devoted to the determination of suitable values for the diffusion coefficients σ_j, as a function of downwind distance and atmospheric stability in particular, allowing diffusion equations to be easily applied to practical problems.

From a theoretical point of view, the most noticeable expressions have been the models of Bosanquet and Pearson (1936), of Calder (1949), of Sutton (1953) and the one of the moving average variance (Hay and Pasquill, 1959).

By far more numerous have been empiric and experimental estimates; among these last, Cramer (1957) and Pasquill's diffusion curves (1961, 1962), these latter revised by F.A. Gifford (1961), Turner's criteria (1964), Singer and Smith's classification (1966) and Singer, Smith and Frizzola scheme (1966) represent a very remarkable patrimony of classical models, allowing the most different practical problems of diffusion to be tackled.

Notwithstanding this, it is a generally accepted opinion (Pasquill and Smith 1970) that theoretical and experimental estimates of pollution concentrations at different points downwind of emission sources are still needed, accounting as best as possible for features of environmental conditions, terrain and emission. This has been compelling people working in atmospheric pollution field to obtain more and more information regarding turbulent dispersion of airborne substances, through a variety of experiments of different kind, in order to improve (or review) earlier estimates or to propose some new procedures to evaluate diffusion parameters.

Among all new estimates added to the older ones, we would mention here the modified model of F. B. Smith (1972), which represents a generalization of the Pasquill model, the Mooore's model (1974), which accounts for plume spreading due both to self-induced and atmospheric turbulence, and the Bultynck-Mallet model (1969), in which a physically satisfactory definition of stability is given.

The present study aims at experimentally determining diffusion coefficients at two different sites (a flat country,chosen in order to calibrate diffusion coefficient estimates, obtained by our experimental methodology, with classical dispersion curves, and an irregular coastal site) and at comparing them both to classical and recent dispersion estimates.

2. DESCRIPTION OF METHODOLOGY AND EXPERIMENTS.

Experimental techniques adopted to evaluate dispersion estimates generally relied upon diffusion of tracers, both from expecially planned releases and from usual pollution sources. Only a few experiments with Lagrangian tracers (single elements or pairs), like balanced or tetroon balloons, have been carried out; except Gifford's experiments (1955) with balanced balloons their information generally related to meso - and large-scale dispersions (Angell 1962 - Angell and Pack 1965-1967). Since in a few cases, mainly when terrain aspect is irregular, information on diffusion at small scale becomes important, we turned our attention to measure dispersion coefficients with Lagrangian tracers in the range of downwind distances from 100 to 1000 m.

The interest in using Lagrangian tracers arises from the fact that atmospheric diffusion depends on Lagrangian statistics of air motions, which in most cases can hardly be evaluated by fixed point, or Eulerian, statistics, expecially when air trajectories change, as an effect of surface topography irregularities or of variations in thermodynamic equilibria. Lagrangian tracers allow both "smoke-plume" and "smoke-puff" type of diffusion to be investigated. As to the first one, which we are concerned to in this paper, lateral and vertical diffusion estimates can be obtained from three methods, i.e. from successive tracer releases, from pairs of tracers and from running averages of single trajectories (Angell,1962; Longhetto, 1976).

We selected, for analyzing our experimental results, the last method, in that standard deviations so derived refer to sampling times corresponding to sampling times utilized by previous investigators and comparable to travel times of tracers.

The collected data were processed by a computer, which calculated the variances of filtered time series data of Lagrangian velocities with filtering time given by travel time T. The lateral and vertical standard deviations were obtained by equation:

$$\sigma_j = \overline{u'_{j}}^{\,2}_{T,\tau} \quad T^2 \qquad (2)$$

where τ is the sampling time of each trajectory. Evaluation of σ_j

were limited to travel times as large as 10% of the lenght of u'_j statistics.

Instead of tetron balloons, aerological pilot balloons, made no-lift by suitable ballasts, positioned by pairs of photo-theodolites on a 2 km basis, have been used. In order to avoid unbalancing due to gas leakage, a mixture of two gases, the one more dense (CO_2) and the other less dense (H_2) than air, has been used, which allowed balloons to be kept no-lift for about two hours. The technique to fill and balance the balloons has been described in a previous paper (Longhetto, 1971). Positioning was effectued by recording photographycally azimuthal and zenithal angles every 15 sec, with an error of ± 0.1 . Stability conditions of lower layers of atmosphere were evaluated in all sites through vertical profiles of air temperature and wind speed. These information were obtained with a radio thermosonde towed by a captive balloon, as far as 600 m (range -20° C to 50° C, accuracy 0.2° C), and pi-bals (as far as 1500 m).

3. EXPERIMENTAL RESULTS.

Trajectories of balloons, released at heights between 100 and 200 m, were obtained during five 15 days field experiments, respectively at Trino Vercellese in June 1970, at Ostiglia in September 1971 and in May 1972 and at La Spezia in July and May 1975. The first two sites are flat countries in the Po Valley (Northern Italy), about 300 km apart but climatologically very similar, characterized by continental type climate with low ventilation (Santomauro, 1972); the last site is a coastal region, on the Northern Tyrrhenian Sea, with irregular topographycal contours surrounding the bay.

All of campaigns were carried out under fair weather conditions, with anticyclonic weak circulation, allowing development of local flows: at Trino and Ostiglia, valley breezes very shallow (about 200 m), while at La Spezia sea-land breezes, which could extend as far as 1000 m during daytime and 300 m during nightime (Anfossi, 1976).

Lateral and vertical standard deviations of balloons, evaluated through equation (2), were grouped into two categories, according to whether they referred to continental or coastal regions; travel times T have been transformed, for camparing our results to other estimates, in downwind distances x, by using average Lagrangian wind speeds measured by each balloon.

3.1 - Continental tests.

As far as continental flat areas are concerned, Fig. 1 shows the average curves we obtained of σ_y and of σ_z as a function of downwind distance x in the first 1000 m, grouped so as a Pasquill stability category could reasonably be defined for each series on the ground of weather conditions.

Since a noticeable scattering among single diffusion curves has been found, expecially under A and A/B conditions (something like that was also observed by Luna, 1972, and Olsson, 1972), we attempted to reduce it by considering diurnal evolution of equilibrium conditions of lower layers of atmosphere. In fact, the Po Valley region exhibits, under fair weather situations, a well-reproducible development of diurnal mixed layers and nocturnal inversion layers (Bacci, 1975), which leads one to think of different spreading of tracers, under a same bulk stability category.

As Fig. 2 shows, a trend during daytime in σ_z values as a function of local time, and then of mixing layer heights, has been found, which seems quite reasonable (in fact, σ_z attained its largest values in midday hours and the smallest ones early in the morning and before sunset); the trend shown by σ_z is in a quite good agreement with the one suggested by F.B. Smith (1972), exhibiting a change of about a factor of two between midday hours and sunset or dawn hours; also σ_y shows a similar trend.

3.2 - Coastal sites.

As far as the coastal region is concerned, Fig. 3 shows the σ_y and σ_z curves, obtained in the same way as those presented in Fig. 1.

Also in this case, as large a scattering as in the previous tests has been found among single diffusion curves, which has not been reduced when separating groups of trajectories according to different time intervals in the day. In this connection, it is to be remembered (Van der Hoven, 1967 - Anfossi, 1976) that during daytime a shallow mixing layer develops in the fairly stable air flow, blowing from the sea inland, whose depth (100 -200m) depends on air stability, solar radiation flux, wind speed and downwind distance from coastal line (our testing site was at 1800 m inland). As a consequence, the diurnal modulation brought about by solar radiation flux is only one of the four factors acting on the depth of mixing layer, and it can be hidden by larger fluctuations in these other factors.

4. DISCUSSION OF RESULTS.

A first remark with reference to Fig. 1 is that the σ_y values for stable conditions (E category) are larger, at all downwind distances, than the other horizontal dispersion parameters under neutral and unstable conditions (from D to A). The limited number of trajectories obtained under stable conditions, however, makes difficult establish whether this was due to decoupling of air layers with height, or to meandering or to any other reason. As to σ_z curves, on the contrary, all things behave properly, in that the stronger stability gets the smaller vertical dispersion coefficients become.

Another remark relates to the dependence of σ_y and σ_z on downwind distance under different stability conditions. Singer-Smith (1966) expected a similar trend for both horizontal and vertical dispersion coefficients as a function of downwind distance x, while our σ_y, for our continental sites, show an average trend proportional to a 0.8 power of x and σ_z proportional to a 0.6 power of x. Moore (1974), on the other hand, assumed a linear dependence of σ_y on x and a 0.5 power dependence of σ_z on x.

As the stability conditions change, our coefficient of regression curves changes too.

Looking at Fig. 3 shows the same departure, as in Fig. 1, of σ_y values during stable conditions, and here also we can't ascertain the true origin of this onservation.

In addition horizontal and vertical dispersion coefficients don't behave properly as in continental areas in that σ_y and σ_z values are not monotic functions of stability categories; this could be due both to irregular topography of the site (Fig. 4) and to different vertical thermodynamic structure of sea-breezes, what could make not reasonable extrapolate classical stability criteria to such kind of sites.

As to the downwind distance dependence of σ_y and σ_z under stability categories ranging from A to E, a trend similar to that expected at Brookhaven by Singer - Smith has been found in this series of tests. This seems to show a similarity in the behaviour of cross-wind dispersion parameters in sites topographically different, but characterized by fairly stable sea-breeze regimes.

In Moore's experiments, although carried out in coastal sites (Tilbury and Northfleet), this similarity is lost, due likely to synoptic channeling brought about by strong winds which forbid the onset of more stable breeze circulations.

In order to assess the reliability of our methodology in giving lateral and vertical dispersion parameters in the range 10^2-10^3 m downwind, our curves have been compared to other estimates and experimental results. Figs. 5-8 show the comparison between our data and Pasquill's curves, Moore's dispersion data and Singer-Smith's curves respectively.

As σ_y values (Fig. 5), our data over-estimate, mainly in the first 500 m. Pasquill's curves under all stability conditions; a similar trend, expecially under stable condition, is found if Moore's data are extrapolated to the $10^2 \div 10^3$ m range. This could likely be a consequence of persistence of stagnation situation in the Po Valley, supporting conditions favourable to air trajectory meanderings.

As to σ_z values (Fig. 6), our data agree with the ones of Moore under neutral and fairly stable conditions, while they under-estimate Moore's extrapolated dispersions under unstable conditions. Pasquill's dispersion data are all overestimated by our curves, under all stability conditions, as far as 500 m downwind; after, the agreement improves for stable, neutral and fairly unstable conditions, while A and B Pasquill's curves are strongly over-estimating our dispersion data.

At last, the comparison between our coastal data and Singer-Smith's curves (Figs. 7-8) shows that dispersion curves we obtained under all stability conditions all assemble along the b_1 and b_2 curves, in that they differ very little from one another with changing stability.

REFERENCES

Anfossi D. , Bacci P. , Giraud C. , Longhetto A. , Piano A. , (1976) Meteorological surveys at La Spezia site - 12émé Colloque Int. sur les atm. pollues, IRCHA, Paris, in press

Angell J. K. , (1962) - On the use of tetroons for the estimation of atmospheric dispersion on the mesoscale - Montly Weather Rev. 90 (7) - 263-270

Angell J.K. , Pack D.H. , (1965) - Atmospheric lateral diffusion estimate from tetroons- J. Appl. Meteorol. 4 (3) ; 418-425

Angell J.K. , Pack D.H. , (1967) - Proceeding of USAEC Meteorological Information Meeting - Chalk River

Bacci P. , Longhetto A. , Anfossi D. , (1975) - Modes of temperature profiles under convective and inversion condition, connected to air pollution - 6th NATO/CCMS , Int. Tech. Meeting on Air Poll. Modeling, Frankfurt

Bosanquet C. H. and Pearson J. L. , (1936) - The spread of smoke and gases from chimney stacks - Proc. Inst. Mech. Eng. 162 , 355

Bultynck H. , Mallet L. , (1969) - Diffusion turbulente des effluents emis dans l'atmosphere par une source elevèe à emission continue - Internal Report BLG 434 - Centre Etudes de l'Energie Nucleere - Belgique

Calder K. L. , (1949) - Eddy diffusion and evaporation in flow over aerodinamically smooth and rough surfaces : a treatment based on laboratory laws of turbulent flow with special reference to conditions in the lower atmosphere. - Quart. J. Mech. and Applied Math. , II, 153

Cramer H.E. , (1957) - A practical method for estimating the dispersal of atmospheric contaminants. - Proceedings of the Conference on Applied Meteorology, Am. Met. Soc.

Gifford F. , (1955) - A simultaneous Lagrangian-Eulerian turbulence experiment. - Monthly Weather Review, 81, 179

Gifford F. A. , (1961) - Use of routine meteorological observation for estimating atmospheric dispersion. - Nuclear Safety , 2 , 47-51

Hay J. S. , Pasquill F; , (1959) - Diffusion from a continuous source in relation to the spectrum and scale of turbulence. - Atmospheric Diffusion and Air Pollution, Advances in Geophysics, 345, Academic Press

Longhetto A. , (1971) - Some improvements in the balanced pilot balloons technique. - Atm. Env. , 5 , 327

Longhetto A. , Anfossi D. , Bacci P. , (1976) - Lagrangian dispersion parameters determined by tracking of balanced aerological balloons. - Third Symposium on Atmospheric Turbulence, Diffusion and Air Quality, October 19-22, Raleigh, N. C. , (U.S.A.), in press

Luna R.E. , Church H.W. - (1972) - A comparison of turbulence intensity and stability ratio measurement to Pasquill stability classes - Journ. Appl. Met. , II ; 663-669

Moore D; J; , (1974) - Observed and calculated magnitudes and distances of maximun ground level concentration of gaseous effluent material downwind of a tall stack. - Turbulent diffusion in environmental pollution, Advances in Geophysics , 18B , 201 Academic Press.

Olsson L. E. , (1972) - A comparison of stability measurements to Pasquill - Turner stability classes. - III Meeting of Panel on Modeling of the NATO/CCMS (XXI - 2) - Paris.

Pasquill F. , (1961) - The estimation of dispersion of windborne material. - Met. Mag. , 90 , 636

Pasquill F. , (1962) - Atmospheric diffusion. - Van Nostrand, London

Pasquill F. , Smith F. B. , (1970) - The Physical and meteorological basis for the estimation of the dispersion. - II IUAPPA International Clean Air Congress - Washington.

Santomauro L. , (1972) - Proposal for a mathematical model of air pollution survey in Milan. - III Meeting of Panel on Modeling of the NATO/CCMS (V - 1), Paris.

Singer I.A. , Frizzola J.A. and Smith M.E., (1966) - J. Air Pollution Control Assoc., 16, 594-597

Singer I.A. and Smith M.E. , (1966) - Intern. J. Air. Water Pollution, 10, 125-135

Smith F.B. (1972) - A scheme for estimating the vertical dispersion of a plume from source near ground level - III CCMS/NATO Meeting (XVII-I) - Paris

Sutton O.G. (1953) - Micrometeorology - Mc Graw-Hill, New York

Turner D.B. (1964) - A diffusion model for an urban area - J. Appl. Meteorol. 3, 83-91

Van der Hover I (1967) - Atmospheric transport and diffusion at coastal site - Nuclear Safety, 8, 490-9

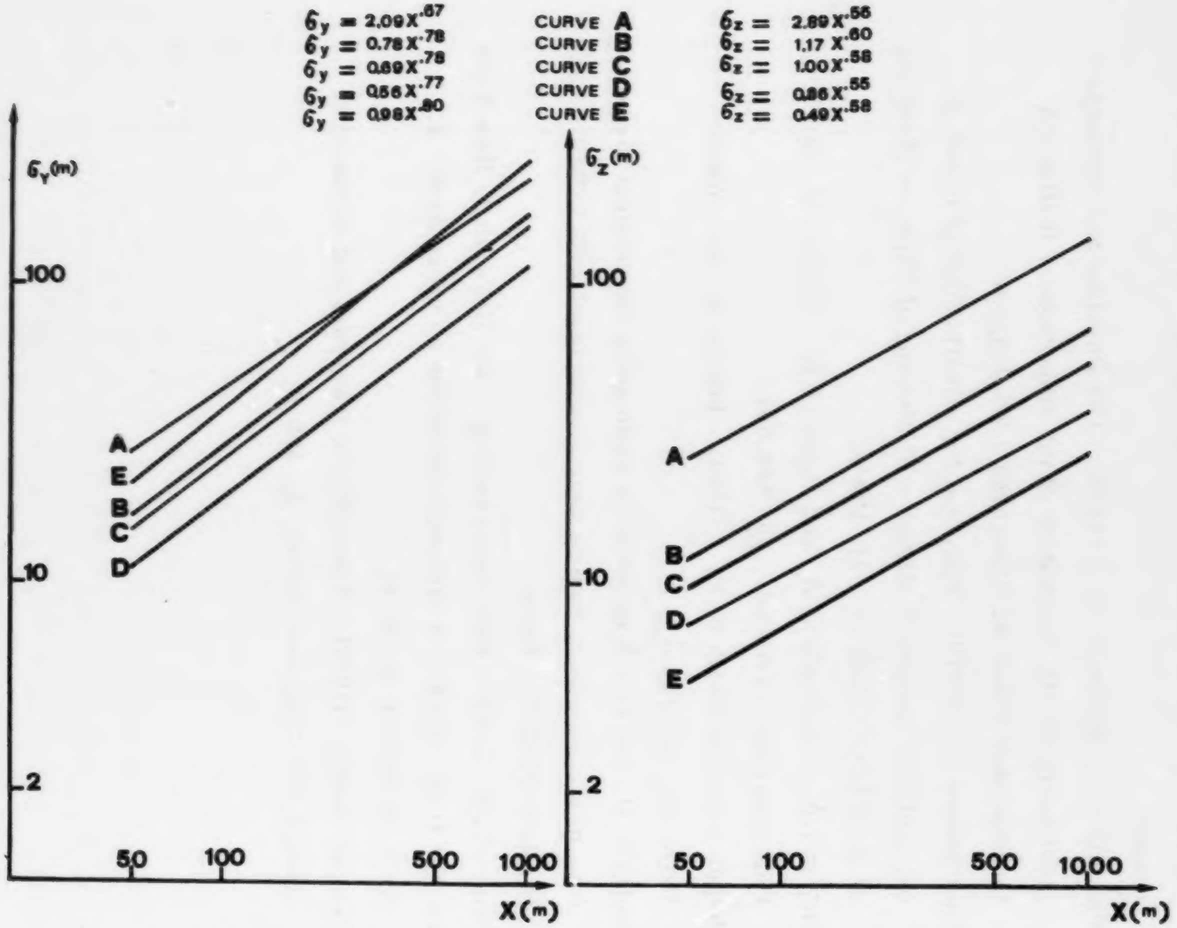

FIG. 1 : Experimental σ_y and σ_z, versus down wind distance, in continental flat sites

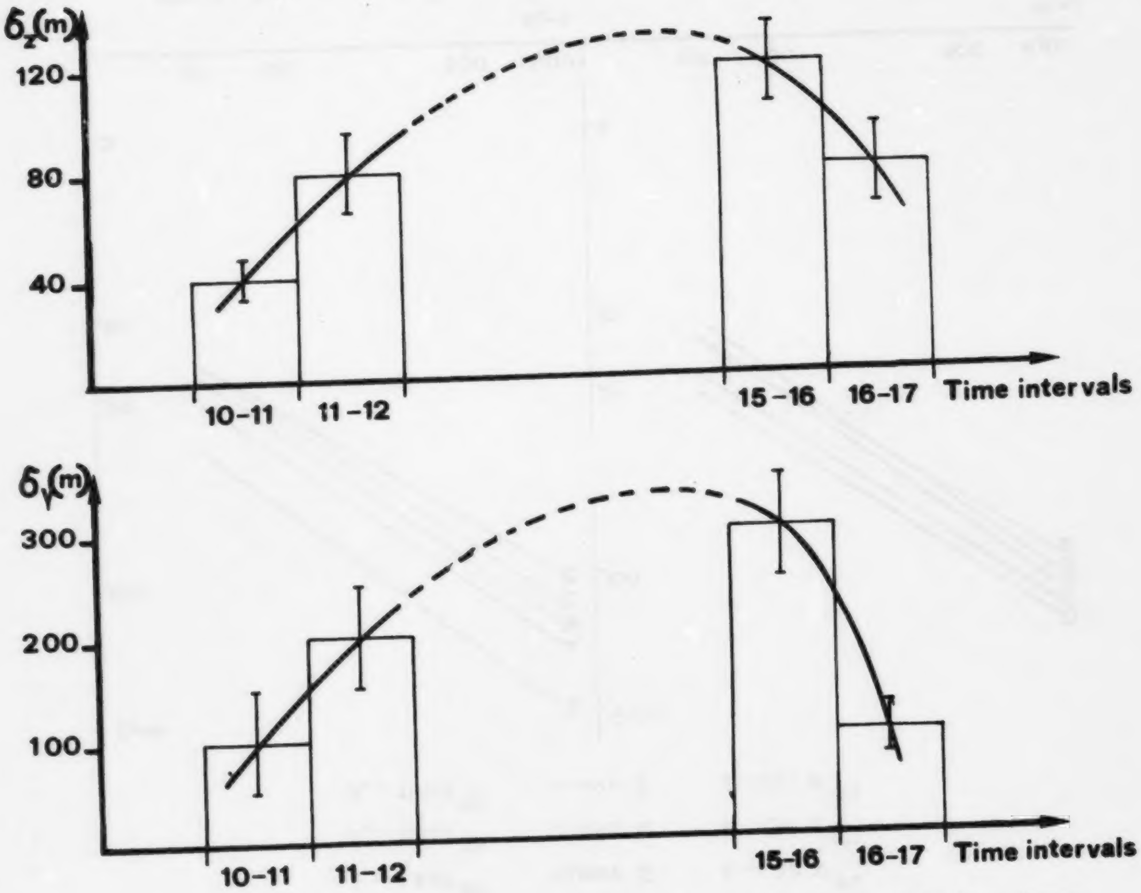

FIG. 2: Dispersion coefficients trends as a function of daytime hours

$\sigma_y = 1.19X^{.74}$	CURVE A	$\sigma_z = 0.70\,X^{.75}$
$\sigma_y = 0.99X^{.73}$	CURVE B	$\sigma_z = 0.61\,X^{.75}$
$\sigma_y = 1.43X^{.62}$	CURVE C	$\sigma_z = 1.23\,X^{.69}$
$\sigma_y = 1.02X^{.70}$	CURVE D	$\sigma_z = 1.52\,X^{.67}$
$\sigma_y = 1.55X^{.78}$	CURVE E	$\sigma_z = 2.37\,X^{.53}$

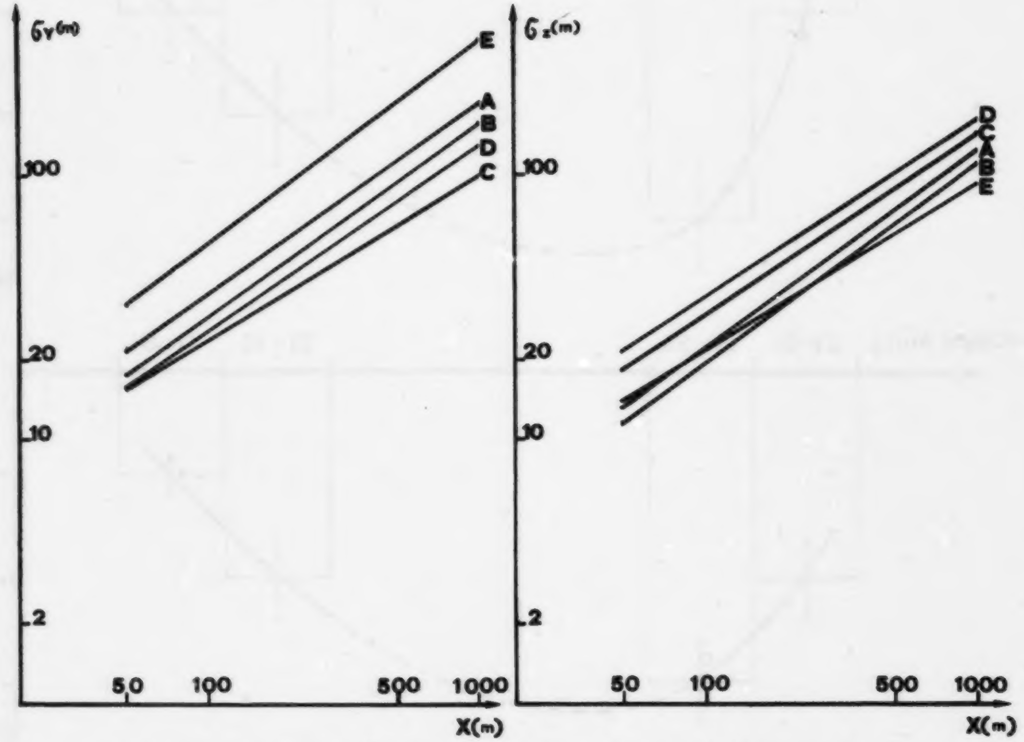

FIG. 3 : Experimental σ_y and σ_z ,versus downwind distance, in coastal site

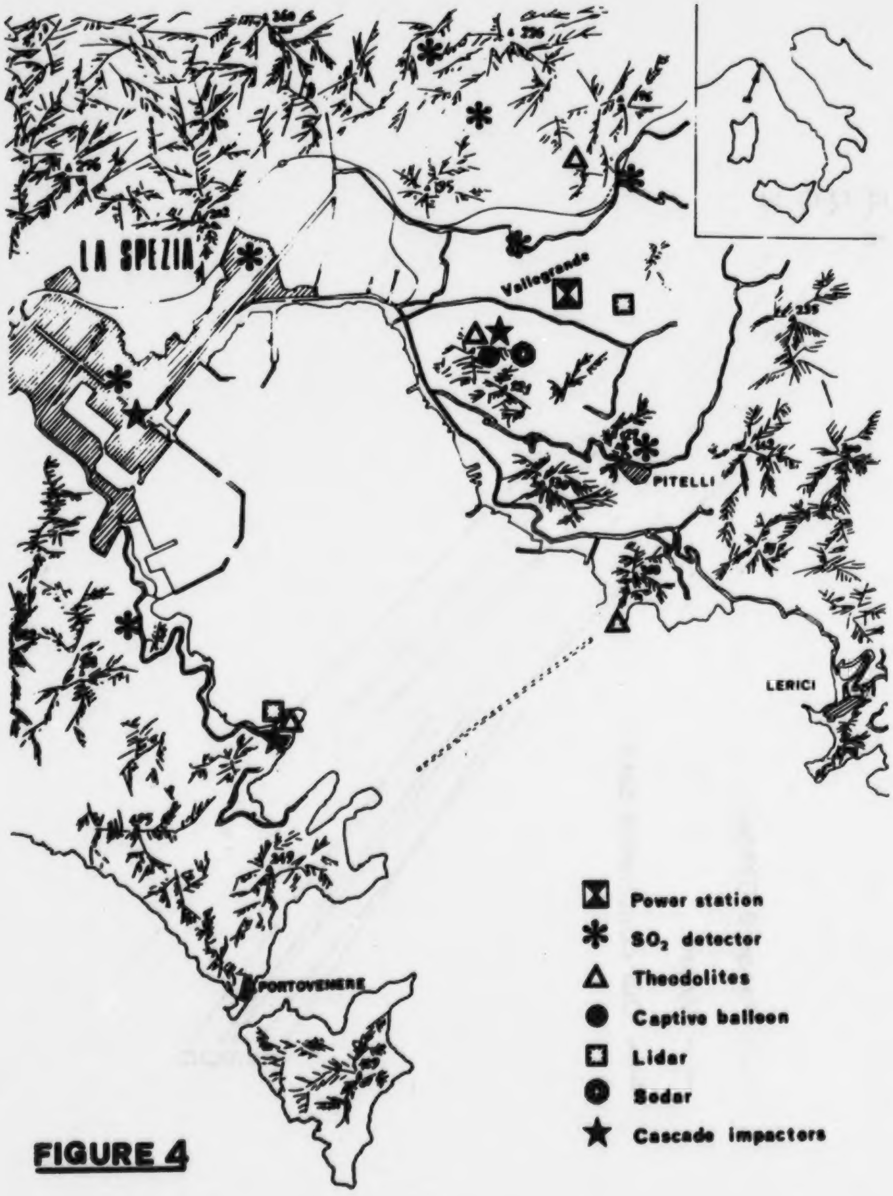
LA SPEZIA
Vallegrande
PITELLI
LERICI
PORTOVENERE
Power station
SO_2 detector
Theodolites
Captive balloon
Lidar
Sodar
Cascade impactors

FIGURE 4

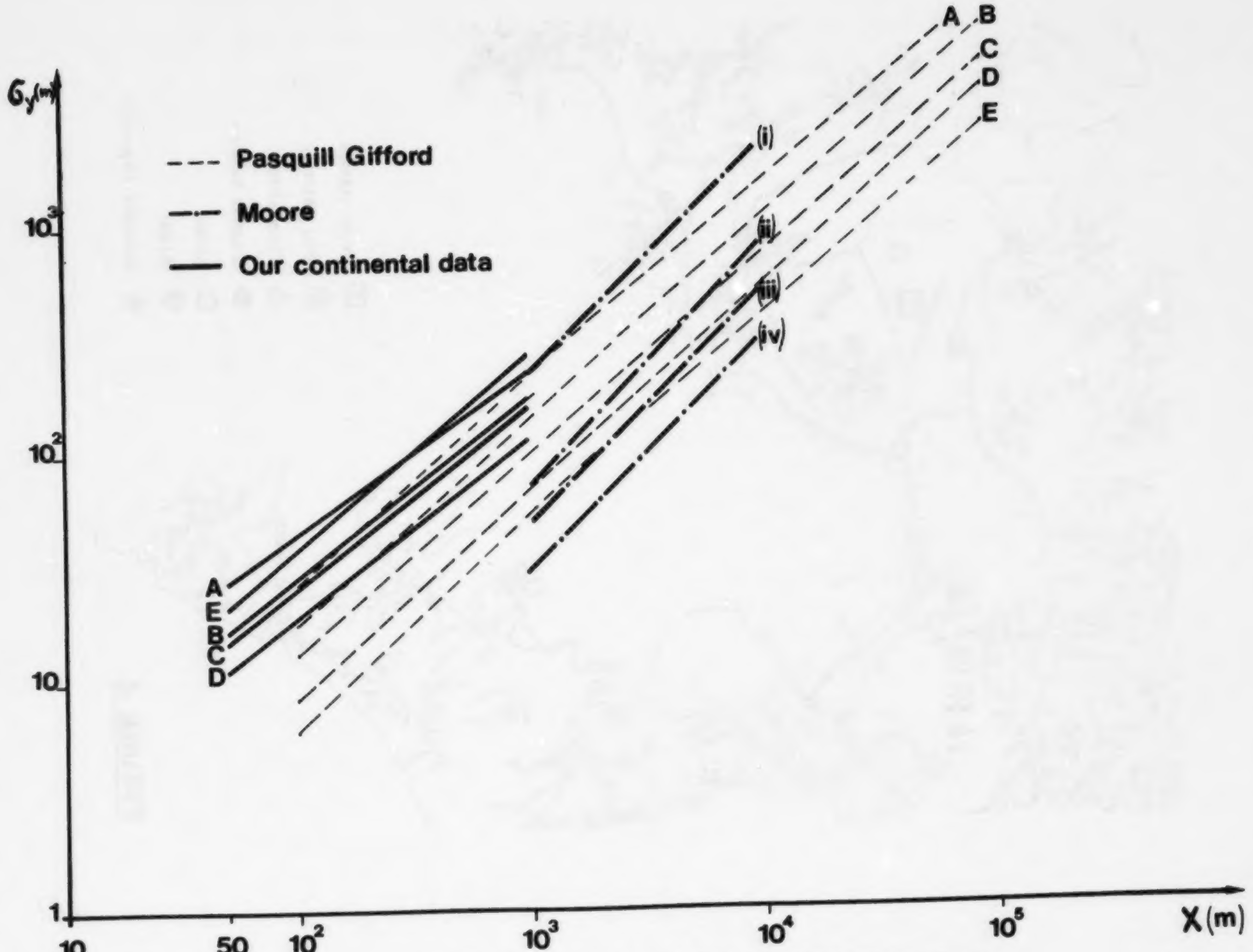

Fig. 5: Comparison between our σ_y continental data and Pasquill's and Moore's estimates

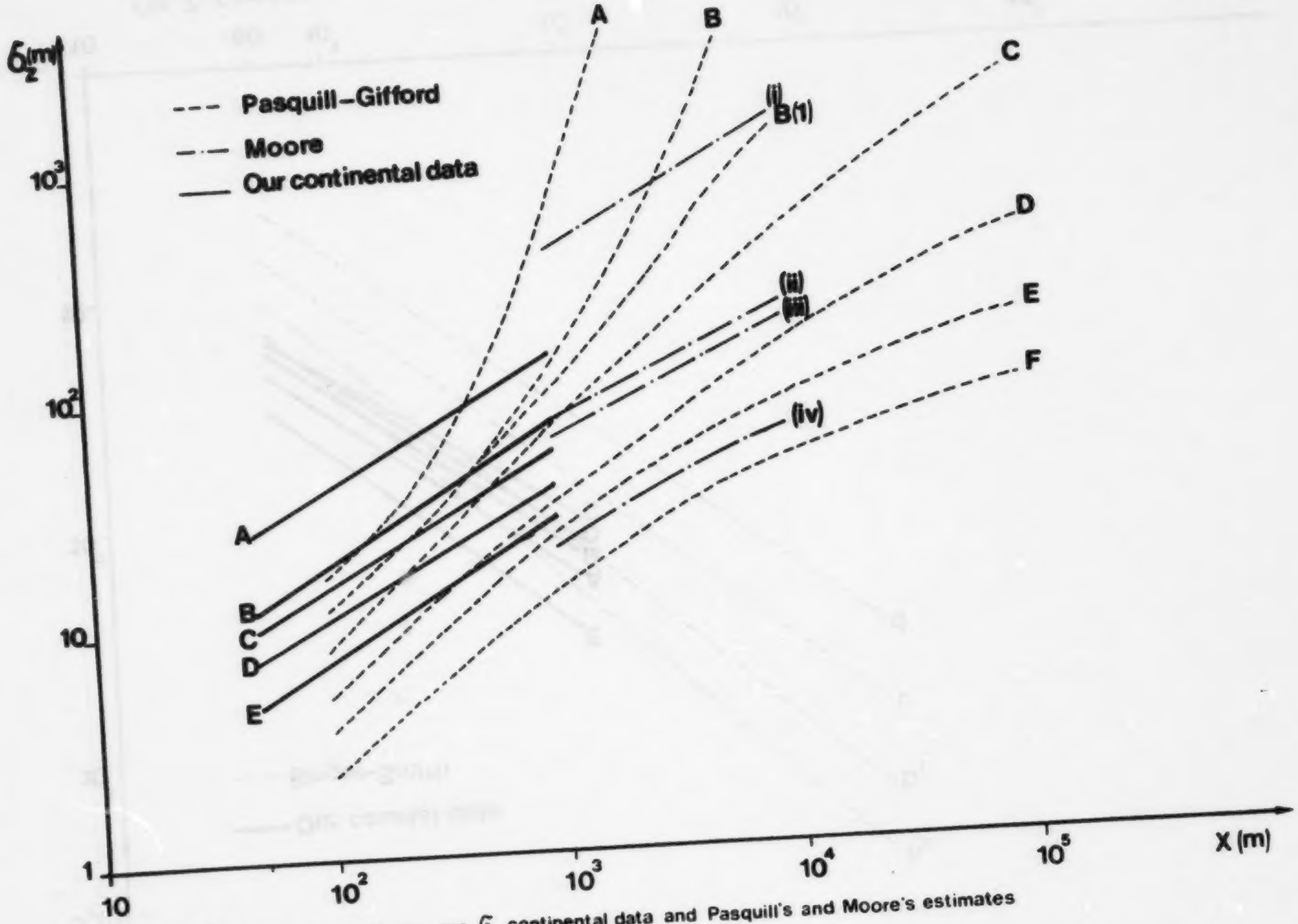

Fig. 6 : Comparison between our σ_z continental data and Pasquill's and Moore's estimates

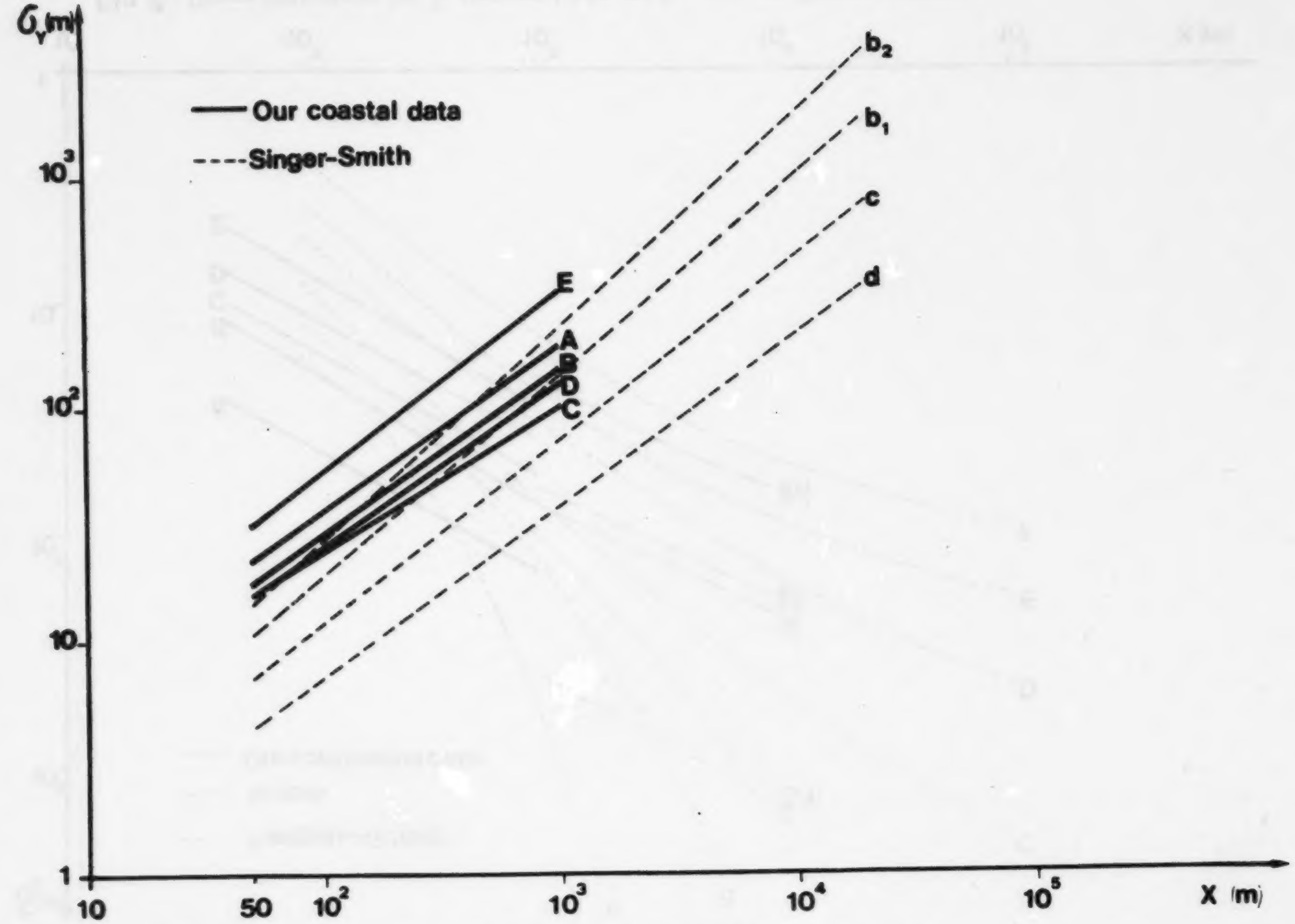

Fig. 7: Comparison between our σ_y coastal data and Singer-Smith's estimates

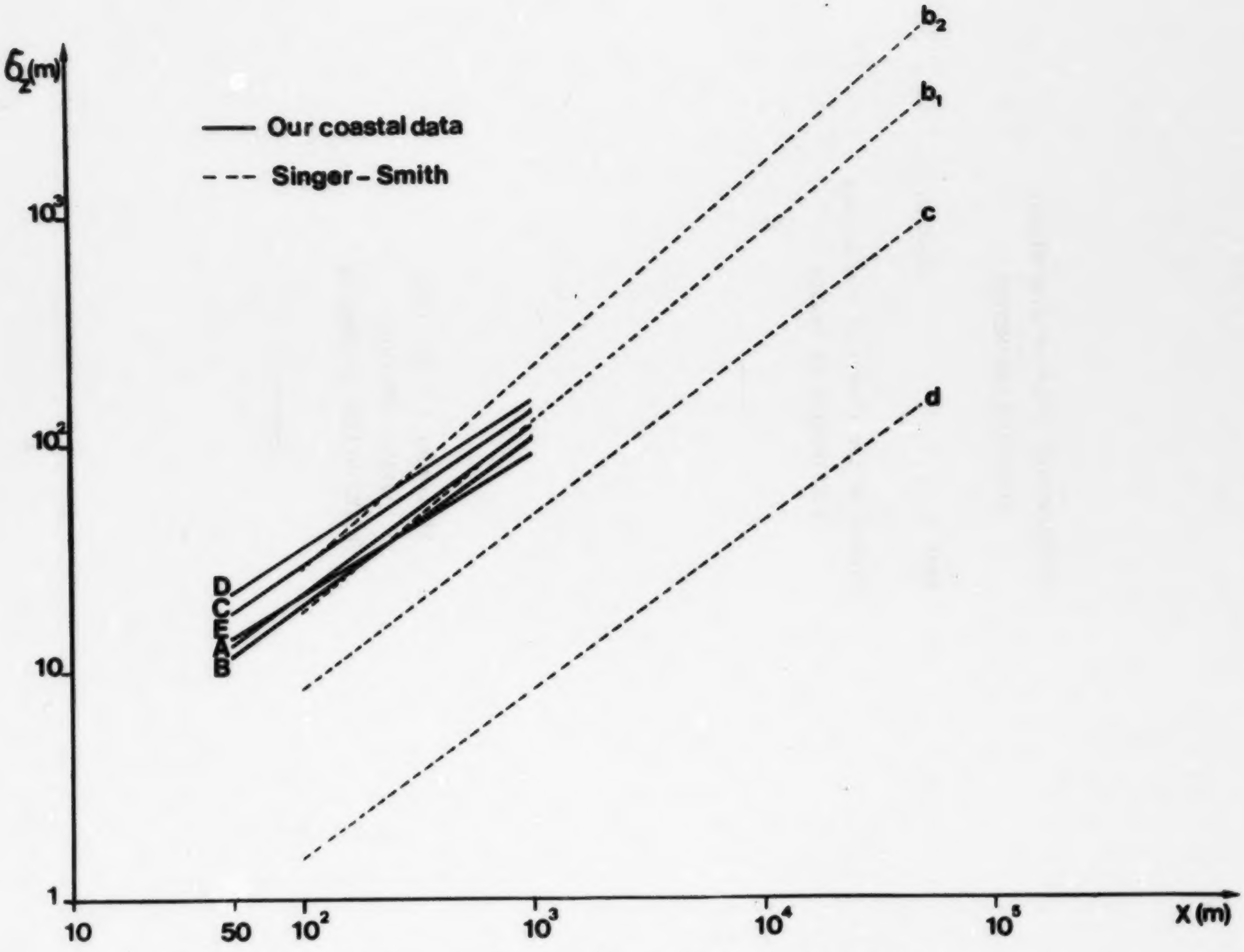

Fig.8: Comparison between our σ_z coastal data and Singer-Smith estimates

7 th International Technical Meeting
on Air Pollution Modeling and its Application

EXPERIMENTAL STUDY OF ATMOSPHERIC DIFFUSION PARAMETERS

SAAB A. RIBON M.

Direction des Etudes et Recherches
ELECTRICITE DE FRANCE

September 7 - 10, 1976
AIRLIE VIRGINIA
UNITED STATES OF AMERICA

EXPERIMENTAL STUDY OF ATMOSPHERIC DIFFUSION PARAMETERS

1 - INTRODUCTION

In spite of conceptual weakness, the "Gaussian Plume Model" provides a practical diffusion modeling tool for calculating concentrations of non reactive air pollutants down wind from an elevated point source. Yet the application of this model in design of power plant stacks and environmental impact analysis necessitates continuing adjustments to incorporate the maximum knowledge of the atmospheric turbulent structure representative of a specified site.

The important point is to dispose of the dilution factors and consequently of the dispersion parameters - expressed in terms of the standard deviations of plume spread - relating to the various meteorological conditions.

Considering the most widely used scheme proposed by PASQUILL-GIFFORD, it is essential to select a parameter which is characteristic of a state of atmospheric stability and to estimate the corresponding dispersion parameters as a function of the turbulent structure of the atmosphere and the time of travel from the source.

As EDF intends to equip all subsequent power plant sites with 80 m meteorological tower, our ideal is to develop a useful diffusion modeling approach that allows to incorporate to the maximum extent our observational knowledge of thermal and dynamic structure within the 80 m layer. Such an approach consists in deriving new equivalence criteria to select appropriate stability classes representing thermal structures and to bring into evidence a relationship between the dispersion parameters and the Eulerian Turbulence data obtained on a meteorological tower.

.../...

2 - THE EXPERIMENTAL SYSTEM

We have used the results of a special field study program on turbulent diffusion process developped by E.D.F. to validate this approach.

Two sets of fourteen tracer release experiments from a 100 m meteorological tower were conducted on the "JUMEAUVILLE SITE" on september 1974 and june 1975, in various types of meteorological conditions. During each experiment, tracers (SF6 and FREON) were released simultaneously from two different levels (48, 72 or 100 m) ; and 100 to 120 collectors were placed near the ground along four or five arcs centred on the presumed plumes axis and distant of 300 to 10000 m in terms of wind speed and direction, thermal stratification and height of emission. The concentrations were obtained for sampling time intervals of 1 hour and 1/4 hour.

Tower instrumentation is designed to provide temperature, wind speed and direction and their fluctuations at eight levels selected on a logarithmic spacing. In addition, turbulence characteristics were measured by means of GILL UVW tridimensional anemometers, set at three levels 18, 36, 72 m ; solar radiation was measured at 2 m level by means of a high sensitive pyranometer.

3 - VALIDITY OF STABILITY CRITERIA

Several schemes have been used to incorporate mateorological data for selecting stability categories. The Pasquill-Turner method was compared to different classifications :

- A E C and Gifford vertical temperature gradient ranges
- Hino incoming solar radiation method
- $\sigma \vartheta$ lateral wind fluctuations classes

The different schemes used are given in Table 1.

.../...

The validation included two steps. A first, a comparison between measured and calculated concentration - from Gaussian Plume Model - is made in order to analyse the fitness of the different criteria to estimate ground level centerline concentrations at different distances from the source. In a second step, we made sure that the selected criteria were in accordance with the measured and estimated crosswind and vertical dispersion parameters representative of stability categories.

In Table 2, we summarize the results of the analysis of our tests during the two tracer experiments. We designate by a double cross a good fitness when the ratio of the calculated concentrations to the one observed in the field experiments varies in the range 0,5 - 2, by a simple cross an acceptable fitness when this ratio varies in the range 0,3 - 3.

We can now point out that the most representative criteria are : Hino's Method (80 per 100), Gifford's vertical gradient ranges (66 per 100) and lateral wind fluctuations classes at 12 and 48 m levels (66 per 100). The lateral wind fluctuations at the highest levels - 72 and 96 m are only representative for the stable case.

A good complementarity exists between Hino's and Gifford's criteria. The Hino method gives good results for the most stable cases without rotation of wind direction, the Gifford classes describe well the unstable cases in the range :

$- 1.9 < \Delta T/\Delta z < - 1 \qquad u < 5,5$ m/s

$- 1.9 < \Delta T/\Delta z < - 0.7 \qquad u > 5,5$ m/s

4 - DIFFUSION DATA

In a previous meeting, we presented Taylor's approach as appropriate and useful to describe the major part of our experiments and to give simple working formulae for diffusion modeling.

.../...

The knowledge of the intensity and time scale of turbulence appears sufficient to describe the magnitude of the plume spread.

Referring to our field tests, we deduced the couple of values - lateral intensity and time scale - and - vertical intensity and time scale - which yield to the best adjustment with experimental results assuming stationary and homogeneous turbulence. In Table 3 we summarize the different turbulent fluctuations values at 18 and 72 m levels and time scale values for microscale (0-2km) and local spatial scale (0-10km) at different atmospheric stabilities.

The dispersion parameters σ y and σ z based on Taylor's original scheme are then described near the source (0 - 2 km), by the couples σ_v, σ_w at 18 m level and t_{L_1} and on local scale (2 - 10 km), by the couples σ_v, σ_w at 72 m level and t_{L_2} (See Fig. 1-2-3).

However let us note that no direct measurements of the vertical dispersion have been made but, assuming a Gaussian vertical distribution, a reasonably good vertical standard deviation, σ_z, can be estimated from a knowledge of the crosswind dispersion parameters and the source strength.

Significant departures from a Gaussian distribution appeared in a few tests (a) in a stable atmosphere, due to the variation in mean wind direction with altitude (b) in an unstable atmosphere, due to the meander light wind effect. We have not theorical arguments to estimate the dispersion in these complicated structures, but we expect some progress from a three dimensional numerical model based on statistical theory of turbulence.

5 - PRACTICAL ADAPTATIONS OF THE TAYLOR APPROACH

An objective system of classifying intensity and time scale of turbulence from current observations on meteorological towers is now being developed. It is based on a fine description of the basic parameters - intensity and time scale - as a function of friction velocity and stability.

In keeping with conventional methods, the standard deviations of the wind velocities normalized by the friction velocity are presented as a function of stability and height. In Table 4, a simplified summary of the magnitudes of turbulence expressed in terms of intensities or ratios of σ_u, σ_v, σ_w to u_* is presented as a function of stability and three height levels - 18, 36 and 72 m.

The classification considered in Table 3 for the time scale as a function of stability and JUMEAUVILLE rugosity (open country 2 - 10 cm) may be regarded as a more practical specification of emission conditions than a general relationship . In particular, it is necessary to investigate the vertical component of turbulence which is essentially related to the stability, and the implication of variation of time scale with height.

6 - DISCUSSION

From turbulence data measured at a meteorological tower, an effort is now made to compute Lagrangian statistical parameters from fixed point data using Eulerian time scale derived from the auto-correlation coefficient and energy dissipation rate. It is hoped that it will also help in the determination of the ratio of Lagrangian to Eulerian time scales for different atmospheric stabilities.

Let us note that there were systematic differences among the Eulerian turbulence data obtained on different heights during the extreme stabilities. It would be desirable to have adequate correlations between simultaneous Eulerian and Lagrangian measurements obtained on the same levels. Therefore a complementary field study is being developed using a tracer teledetection system - Barringer Correlation Spectrometer - to measure NO_2 gas, released from the JUMEAUVILLE tower, in both lateral and vertical directions.

Besides, gathering lateral and vertical concentration data can be an efficient and effective way of studying validity of stability classifications. Effects of atmospheric stability are indeed most clearly defined for the vertical dispersion which is essentially determined by the effects of aerodynamic friction and buoyancy in the boundary layer. For the horizontal components the problem is more complicated in that there are contributions of wind meandering and shear effects.

.../...

7 - REFERENCES

HAUGEN D., 1973 Workshop on Micrometeorology.
BOSTON, A.M.S. ed

LUMLEY J.L., TENNEKES H. 1973 A first course in turbulence.
M.I.T. press

PASQUILL, 1974 Atmospheric diffusion 2° ed.
N.Y. John WILEY

GIFFORD F., PASQUILL F., 1975 Workshop on Atmospheric Diffusion.
BOSTON A.M.S.

SAAB A., RIBON M. MERY P. 1975 Some features of turbulent diffusion process resulting from experimental field tests
6th NATO/CCMS International Meeting
FRANKFURT

TABLE 1 : KEYS TO STABILITY CATEGORIES

PASQUILL STABILITY CLASS	VERTICAL TEMP GRADIENT deg/100 m		$\sigma\theta$ (deg)
	A E C	GIFFORD	
A	- 1.9	- 1.73	25
B	- 1.9 to - 1.7	- 1.73 to - 1.36	20
C	- 1.7 to - 1.5	- 1.36 to - 1	15
D	- 1.5 to - 0.5	- 1 to - 0.64	10
E	- 0.5 to + 1.5	- 0.64 to 0	5
F	1.5 to 4	0	2.5

THE HINO METHOD

INCOMING SOLAR RADIATION mW/cm2 / U m/s	60	$45<I<60$	$30<I<45$	$15<I<30$	$5<I<15$
$u < 2.5$	A	B	B	C	D
$2.5 < u < 5$	B	B	C	C	D
$u > 5$	C	C	C	D	D

Observations : $I < 5$ mW/cm2 → { $I \geq R$ Class E

R = Reflected { $I < R$ Class F

Solar radiation

TABLE 2 : VALIDITY OF THE DIFFERENT STABILITY CRITERIA

OPERATION	CLASS	PASQUILL	AEC	GIFFORD	HINO	σ_θ 12	σ_θ 48	σ_θ 72	σ_θ 96
A 1	C	XX			XX	XX	XX		
A 2	C-D	X	X	XX	X	XX	X	X	
A 3	C-D	X	X	XX	X	XX	X	X	
A 4	B-C	X		XX	X				
A 6	B-C			X					
A 9	D	X	X	X		X	X		
A 11	D	XX			XX	XX	XX		
A 13	E				X		X		
A 14	D-E	X	X	X	X	X	X	X	X
B 1	C				X	X			
B 3	F				X		X	X	X
B 4	C	X	X	X	XX	XX			
B 5	E	-	-	-	-	-	X	X	X
B 6	B				XX				
B 10	B	X		XX	X				
B 11	B		X	X					
B 13	A			X		X	X	X	
B 14	E	-	-	-	-	-	-	X	X

XX Indicates a good fitness

X Indicates an acceptable fitness

TABLE 3 : INTENSITY AND SCALE OF TURBULENCE

	σ_v 18 m m/s	σ_v 72 m m/s	σ_w 18 m m/s	σ_w 72 m m/s	t_{L} 1 0-2 km s	t_{L} 2 2-10 km s
UNSTABLE HIGH SOLAR RADT	1.4	1.25	1.15	1.6	≃ 150	≃ 150
UNSTABLE MOD SOLAR RADT	1.1	0.95	0.85	0.8	150-200	250-300
NEUTRAL STRONG WIND	0.84	0.65	0.55	0.35	200-300	300-400
STABLE	0.4	0.15	0.10	0.04	variable	≃ 500

TABLE 4 : SIMPLIFIED SUMMARY OF MAGNITUDES OF TURBULENCE

HEIGHT	18 m				36 m				72 m			
σ_u/u_*	3-5		2-3	< 2	3-4		1.5-3	< 1.5	3-4		1.5-2.5	< 1.5
σ_v/u_*	4-7		2-4	< 2	3.5-5		2-3.5	< 2	3-5		2-3	< 2
σ_w/u_*	2.5-4		1-2	~ 1	2.5-3.5		1-1.5	< 1	2.5-3.5		1-1.5	< 1
σ_u/u	0.15-0.25		0.10-0.15	0.05-010	0.11-0.20		0.10-0.15	0.04-0.10	0.11-0.20		0.10-0.15	0.04-0.10
σ_v/u	0.2-0.35		0.15-0.20	0.10-0.15	0.17-0.30		0.10-0.17	0.05-0.10	0.15-0.20		0.10-0.15	0.04-0.10
σ_w/u	0.15-0.25		0.10-0.15	0.05-0.08	0.15-0.25		0.10-0.12	0.04-0.06	0.15-0.25		0.08-0.12	0.03-0.05
STABILITY	VERY UNSTABLE	UNSTABLE	NEUTRAL	STABLE	VERY UNSTABLE	UNSTABLE	NEUTRAL	STABLE	VERY UNSTABLE	UNSTABLE	NEUTRAL	STABLE

Fig. 1

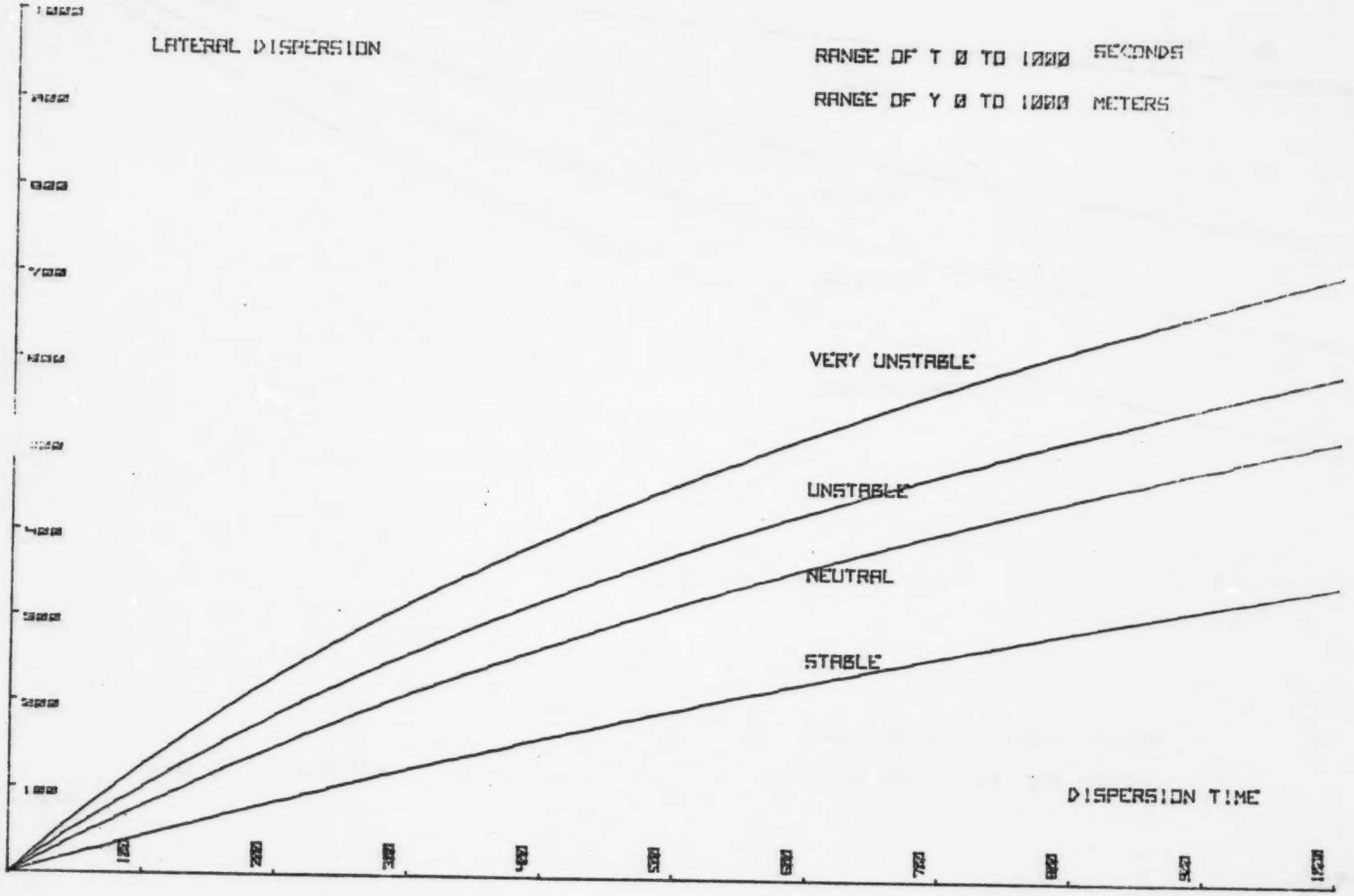
LATERAL DISPERSION
RANGE OF T 0 TO 1000 SECONDS
RANGE OF Y 0 TO 1000 METERS
VERY UNSTABLE
UNSTABLE
NEUTRAL
STABLE
DISPERSION TIME
100
200
300
400
500
600
700
800
900
1000

Fig. 2

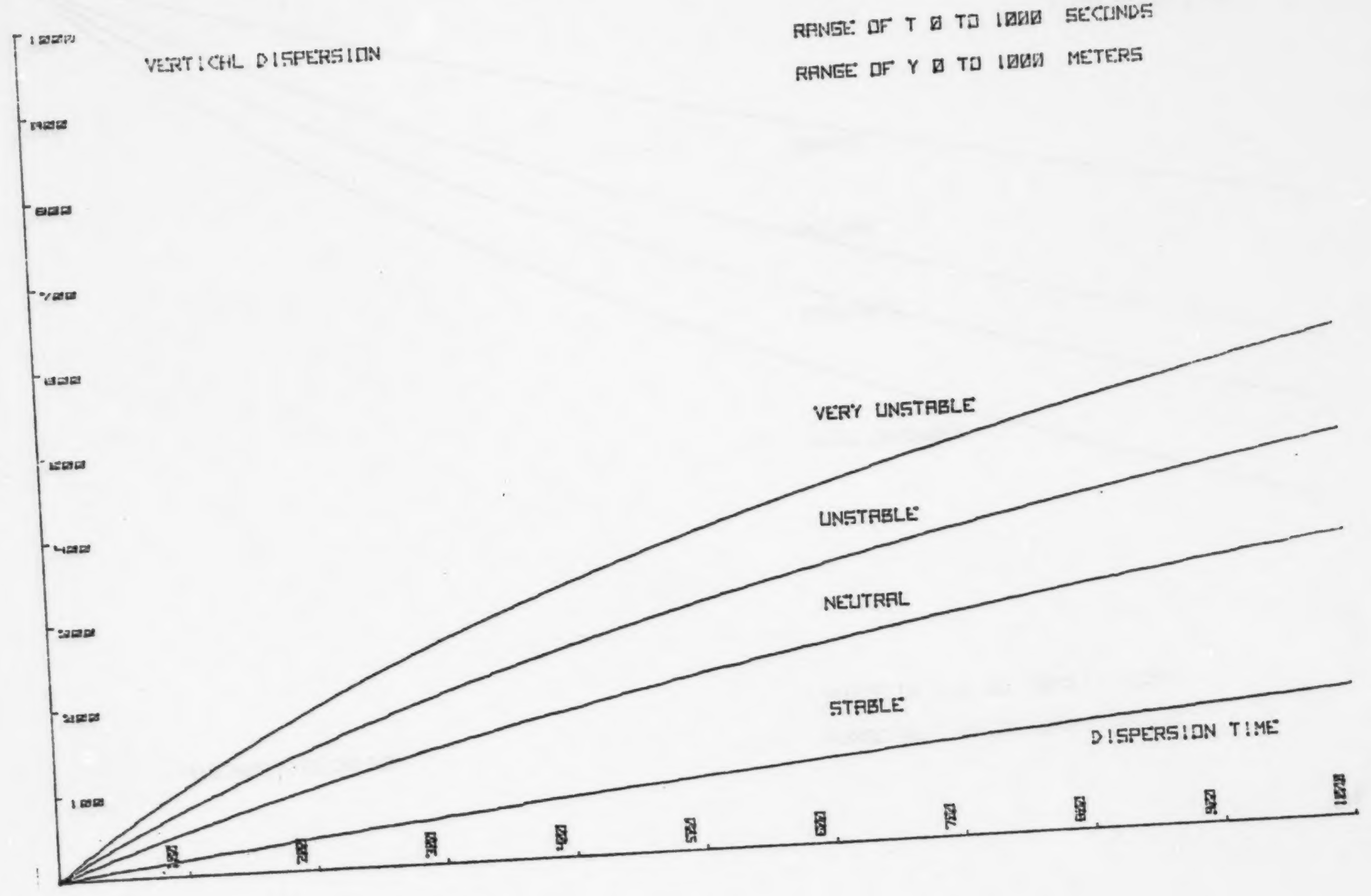
VERTICAL DISPERSION
RANGE OF T 0 TO 1000 SECONDS
RANGE OF Y 0 TO 1000 METERS
VERY UNSTABLE
UNSTABLE
NEUTRAL
STABLE
DISPERSION TIME
100
200
300
400
500
600
700
800
900
1000

Fig. 3

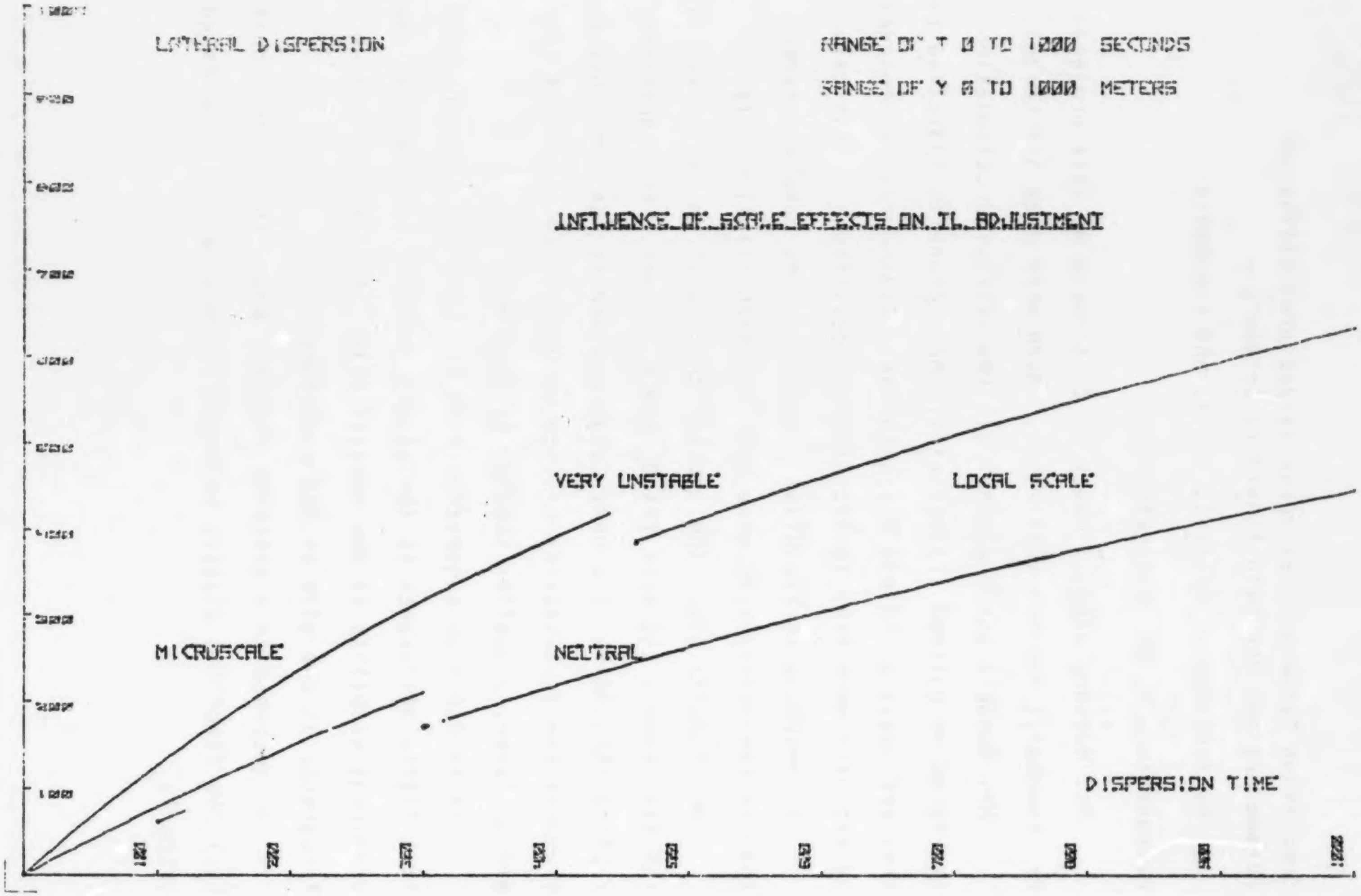
LATERAL DISPERSION
RANGE OF T 0 TO 1000 SECONDS
RANGE OF Y 0 TO 1000 METERS
INFLUENCE OF SCALE EFFECTS ON IL ADJUSTMENT
VERY UNSTABLE
LOCAL SCALE
MICROSCALE
NEUTRAL
DISPERSION TIME
100
200
300
400
500
600
700
800
900
1000
100
200
300
400
500
600
700
800
900
1000

Rapporteur - Russ Lee

Comparison Between Experimentally Measured Diffusion Parameters and the Main Stability Criteria -

by Santomauro, Anfossi, Bacci, and Longhetto

Presentation by Mr. Longhetto -

Mr. Mahoney asked if work is continuing on this project. Mr. Longhetto replied that it is. Much more data are needed.

Mr. Wendell asked whether all the diffusion calculations are based on balloon trajectories. Mr. Longhetto indicated that they are based on baloon trajectories. Procedures recommended by Pasquill were used to fit standard deviations to the data.

In response to Mr. Hilst's question, the speaker stated that 50 trajectory runs were made for each stability class.

Mr. Mahoney asked the speaker to comment on the spread of the data around the best fit σ_y and σ_x curves. Mr. Longhetto replied that there is a very large scatter of the data, but by grouping the trajectories by time of day and by height of the mixing layer, a smaller scatter is obtained.

In response to a question from Mr. Lee, the speaker noted that little difference in the sigmas could be seen between the different stability at the coastal site. Part of the reason is the topography at the site of the experiment.

In response to a question from Mr. Rote, the speaker noted that the stability classes referred to were based on the Pasquill criteria.

Mr. Johnson noted that the sigma-y curve for E stability was higher than the curves for the other stabilities, and suggested that meandering of the wind could play a role in producing this. Mr. Longhetto agreed that meandering could play a role; however, the data show a large amount of scatter. More data are needed before reliable curves can be determined.

Mr. Shenfeld asked if vertical temperature profiles were taken. They were not.

Rapporteur - Russ Lee

Experimental Study of Atmospheric Diffusion Parameters -
by Saab and Mery

Presentation by Mr. Ribon

Discussion:

In response to a question from Mr. Mahoney, Mr. Ribon described the experiment site as being relatively flat terrain.

Mr. Fanaki asked how the friction velocity was determined. The speaker stated that the friction velocity was determined from wind speed measured on the tower at 3m and 48m levels.

In response to Dr. Cramer's question, Mr. Ribon noted that the duration of the tests were about three hours. Measurements from the tower were made continuously for the duration of the test. The averaging time for individual data values was 15 seconds.

Mr. Mahoney asked if the climatology of the turbulence intensity would be more useful for model applications than a climatology of the Pasquill-Gifford stability categories. Mr. Ribon agreed and commented that this would be the next development. Data are generally not now available.

Mr. Turner is definitely in favor of this but, in urban sites, it is difficult to find a representative site to make the measurements.

Mr. Mahoney noted that the σ_θ determinations at the 72 meter level was much less good than at the lower levels.

In response to Mr. Nieuwstadt's question, the speaker noted that the stability (stable, unstable and neutral) were defined by the vertical temperature gradient. Unstable conditions did occur during the experiment.

7 th NATO/CCMS
International Technical Meeting
on Air Pollution Modeling

TOPIC VII

INNOVATIVE MODELING TECHNIQUES

7th International Technical Meeting
on Air Pollution Modeling and its Application

MODELLING THE ATMOSPHERIC DISPERSAL OF RADIOACTIVE POLLUTANTS BEYOND THE FIRST FEW HOURS OF TRAVEL

H.M. ApSimon and A.J.H. Goddard

Nuclear Power Section,
Mechanical Engineering Department,
Imperial College of Science and Technology,
London, United Kingdom.

September 7-10, 1976
Airlie, Virginia,
United States of America.

ABSTRACT

The importance of taking into account the spatial and temporal changes in the atmospheric boundary layer as pollutant material disperses is discussed. A model is described which has been designed to include these changes; the application of this model in simulating the travel and dispersal of radioactive material over Europe following routine release from nuclear power installations, and in calculating the exposure and population doses resulting from inhalation, is illustrated.

The model considers releases of a few hours duration from any chosen site, and uses pressure fields over Europe at six hour intervals during and after release, together with quasi-geostrophic forecasting techniques, to track the meandering paths taken by a series of discrete puffs of radioactive material until they leave the map area. Along the path of each puff, local meteorological data including cloud cover and rainfall at the time of passage are used to assess the likely state of the boundary layer and the resulting spreading and dilution of each puff, taking into account the time of day and the underlying surface of land or sea. The effects of changes in the depth of the mixing layer and its diurnal variation on vertical dispersion of the pollutants are described. Loss mechanisms due to natural decay, dry deposition at the ground, and wash out are also included.

INTRODUCTION

Because there is no threshold dose below which exposure to radiation has been proved harmless, it is important in the field of nuclear safety to consider the large numbers of people exposed at considerable distances from the sources although their individual exposure and risk is small. One of the difficulties in estimating long range transport and dispersal of atmospheric pollutants is that meteorological conditions at the source become less and less relevant as the travel times increase. Special modelling techniques have therefore been developed, which take into account spatial and temporal changes in the boundary layer and which will permit the study of the consequences of routine small releases from nuclear power installations in Europe at distances of up to one or two thousand kilometres. In this context we have relatively few isolated, near ground sources that can be treated individually and then superimposed, rather than a general widespread distribution of area sources.

We thus attempt to model the dispersal of releases of a few hours duration at a time from a specific site by studying in detail a series of discrete puffs of material released at intervals through the release period. Puffs of material released in between these particular puffs are assumed to follow intermediate tracks and dispersion. At a selected grid of points the time integrated atmospheric concentrations are accumulated as material passes overhead, and are subsequently combined with population data to obtain population dose. By applying the model in a wide range of synoptic weather conditions we hope to estimate the effects of a long term continuous release from particular sites.

Initially simulation of the behaviour of a discrete puff of polluted air is described; this falls under two headings - first predicting the track followed and secondly how the puff dilutes and disperses. It is then shown how this information is used for a series of puffs, to calculate the integrated atmospheric concentrations at a grid of points across the European map area. Finally application of the model is illustrated for a hypothetical release.

STAGES OF DEVELOPMENT OF A DISCRETE PUFF OF POLLUTED AIR

The development of each individual puff can be divided into four stages which roughly coincide with the different orders of magnitude of distance travelled, as illustrated in Figure 1.

Within the first ten kilometres or so, ground level concentrations within a puff will depend sensitively on source height, and puff dimensions will probably not be large compared with the mean free path of gamma radiation. Puff shape will therefore be important for gamma submersion doses, making invalid simple infinite cloud approximations. For releases in persistent stable conditions this phase may extend further depending on source height. Existing Gaussian plume models based on source meteorology are valid at these short distances. Beyond this, during the second stage, the puff gradually spreads vertically until it is fairly uniformly distributed through the depth of the mixing layer and is limited by an inversion; this will usually happen within about the first 100 kilometres from the source, in travel times of less than a day. Changes in meteorology affecting the puff become important on these time scales and ground level concentrations within a puff can vary quite rapidly during this phase. Subsequently, in the third stage, dispersal and depletion will depend on variations in the mixing layer in the course of its diurnal variation; also lateral dispersion is affected by divergence of wind direction on a synoptic scale. Finally, after the first overhead passage of the material across Europe, the material will continue to spread out and mix up through the troposphere. Here a different type of box model is used to estimate the residual effects of global circulation.

TRACKING PUFFS

To track the movements of discrete puffs during the second and third stages quasi-geostrophic forecasting techniques are used. At the top of the mixing layer, shearing stresses are negligible and the flow of air adjusts to the geostrophic flow between the isobars as determined by the pressure field. Lower down in the atmosphere the horizontal shearing stresses increase, turning the mean wind at an angle to the geostrophic wind direction and reducing the strength. The velocity profile in the mixing layer depends on the geostrophic wind speed and on stability and turbulence in the atmosphere as well as the type of terrain over which flow is taking place. Our model therefore calculates the tracks followed by the centre of a puff in a series of time steps using a mean wind proportional to the geostrophic wind in strength, and turned at an angle of ten degrees or more, according to whether the puff is over land or sea, and to atmospheric conditions and time of day. Some adjustment is also made according to the stage of development of the puff since initially the puffs will move in accordance with winds nearer the surface, rather than an average wind throughout the mixing layer.

To estimate the geostrophic winds we use grids of surface pressure data over the map area of interest at six hour intervals until all the puffs released have left the map area. The grid covers 30 degrees of longitude by 18 degrees of latitude and pressures are specified every two degrees of longitude and one degree of latitude, that is at intervals of just over 100 kilometres in each direction.

Figure 2 gives an illustration of the tracks of two hypothetical puffs released six hours apart in February 1973 from a site in Britain using these quasi-geostrophic techniques; the puffs linger for a few hours in light winds and are then swept off to the East by strengthening Westerly winds, leaving the map area about 2½ days after release. During this period an anticyclone was moving slowly Eastwards across Southern United Kingdom and France. There was cloud over the Northern half of the map area most of the time with a high proportion of near neutral stabibility in the boundary layer. The two puffs left the map area at latitudes differing by just over a degree or about 120 kilometres apart, the second puff just overtaking the first.

To test the tracking techniques, predicted winds at 10 metres were compared with surface observations at 19 weather stations chosen at random in the United Kingdom. Wind strengths agreed quite well for those stations in flat open areas, but there was considerable variation for stations with greater characteristic roughness or hilly terrain, as one might expect. There appeared to be a definite correlation between the ratio of 10 metres wind speed to geostrophic wind speed and the average roughness of the terrain up to 30 kilometres upwind. Predicted wind directions were satisfactory bearing in mind the variations between neighbouring stations; the worst agreement usually coincided with light winds or definite swings of wind direction. In general topographical effects should become less important in our model as travel time of a puff increases and the material disperses higher above the sheared surface layers.

GROWTH AND DEVELOPMENT OF PUFFS

To model the growth and development of puffs, each puff is treated as though material was confined in a vertical rectangular column moving with a mean velocity as described. Each column spreads in width as it mixes with more air in the small scale turbulent eddies of the atmosphere, but this lateral spreading is usually dwarfed by the divergence between puff tracks.

VERTICAL DISPERSION

To simulate vertical dispersion, the atmosphere is considered as a turbulent boundary layer of variable depth which is well mixed by mechanical stirring and convective mixing, surmounted by a series of stably stratified layers, each 100 metres thick and with relatively little mixing between layers. Initially the puff material is confined to the bottom of the column and vertical dispersion is based on conventional Pasquill dispersion parameters and stability categories but jumping from one stability category to another in a series of time steps according to local conditions at the time of passage along the puff track. At the beginning of each time step, usually an hour, the current dispersion to date is used to estimate dispersion over the ensuing time interval in the relevant conditions, rather than the travel distance from the source and source meteorology as in conventional models. Over land we use the revised dispersion parameters of

Pasquill and Smith which take into account surface roughness, and more accurately predict the daytime behaviour of the boundary layer through the energy input from insolation as a function of time of day and year. Cloud cover data is supplied over a relatively course grid at six hour intervals over the map area, as for the pressure grid. Over sea, near neutral conditions are currently assumed at all times.

In principle lateral spreading could be treated in the same way, but an average spreading rate of about 1 kilometre an hour in the width of the puff column seems sufficiently accurate since the eventual population exposure generally depends more on divergence between puff tracks.

Eventually the material penetrates up throughout the mixing layer and the vertical dispersion then depends on changes in the depth of this layer. If the mixing layer increases in depth subsequently the material is diluted and mixed with air up to the increased height. If the mixing layer becomes shallower some of the material becomes isolated in stable layers aloft and cannot be depleted by processes such as dry deposition at the ground. Every time the mixing layer depth changes in the history of a puff, interchange takes place between the mixing layer and the sequence of stable layers which is incorporated in the model. The concentration of material in the mixed layer is uniform with height as a result of mixing, but above this nuclides eventually become distributed in a series of strata as the changes in mixing layer depth erode and return material at different levels of concentration to the upper layers.

DEPTH OF MIXING LAYER

Typically the mixing layer will be relatively shallow at night over land, of the order of a few hundred metres, and will gradually increase in depth during the day, dropping sharply at dusk. To predict the depth of mixing over land during the day we use the model of Carson and Smith. This predicts the development of a dry convectively unstable boundary layer as a result of time dependent surface heating and entrainment of air from the stable layers above, and can also be made to allow for large scale vertical motion and the slow sinking of air in regions of anticyclone. If mechanical stirring from fast flow over rough terrain is more effective than convective mixing then the depth of the mixing layer is adjusted for this. Unfortunately the model does not take into account such processes as advection and the situations which occur when warm and cold air masses meet across a front. Also radiosonde data on the heights of inversions, which would be helpful in this context, are not readily available in a suitable form like the other meteorological data used, but it may be possible to improve the situation by providing extra data on cloud type and height.

DEPLETION OF ACTIVITY IN PUFFS

Apart from dilution of a puff, the quantity of a radioactive nuclide in suspension is reduced by natural decay, washout and dry deposition at the ground. In contrast to the rate of change of puff dimensions these loss rates depend strongly on the particular nuclide and its chemical form, and lead to different distributions of material between the mixing layer and the stable overlying layers for different nuclides. In order to include wash out, data on the occurrence of rain may be included at six hour intervals as for cloud cover and pressure data, but this is necessarily very approximate.

EXPOSURE

Having traced the evolution of a series of discrete puffs in hourly time steps, the release between two tracked puffs may be considered as a series of puffs which follow intermediate tracks: this leads to exposure at all grid points between the paths of the tracked puffs. The exposure at a general grid point G in the population grid is found by interpolation as illustrated in Figure 4, and is proportional to the fraction of puffs which pass over the point times the time integrated atmospheric concentration due to overhead passage of a single puff, $I(t_0,t)$.

$$E_G = f_G \times I(t_o,t)$$

where

$$I(t_o,t) = \frac{Q_g(t_o,t)}{B(t_o,t)H_g(t_o,t) \cdot \bar{u}(t_o,t)}$$

f_G = fraction passing over point

t_o = time of release of puff

t = time of passage overhead

$Q_g(t_o,t)$ is the quantity of a radioactive nuclide in the mixing layer (or the lowest stable layer in the case of a surface inversion)

$B(t_o,t)$ is the width of the puff

$H_g(t_o,t)$ is the depth of the mixing layer (or surface stable layer)

$\bar{u}(t_o,t)$ is the speed of translation of the puff

The fraction of puffs passing overhead at G is proportional to puff breadth, but since concentration within a puff is inversely proportional to puff breadth, the resulting exposure is relatively insensitive to puff spreading.

ILLUSTRATION

The application of the model is illustrated by some results obtained with a prototype computer model for a hypothetical release of 1 Ci of I^{131} during the six hours between the release of the two puffs whose tracks are shown in Figure 2, that is around dawn on a February morning. Figure 5 gives the time integrated concentrations due to overhead passage of the release in units of $\mu Ci/m^3$ x hours. In this prototype model, exposure from the first three hours after release is ignored and it is assumed that material has then mixed up to the top of the mixing layer; thus detailed development of the puffs over the first few hours has been omitted. A dry deposition velocity of 0.3 cm/sec has been assumed over land and the nuclide has a half life of about 8 days so that decay is also showing some effect by the time the release leaves the map area.

These integrated atmospheric concentrations may be combined with population dose over the map area. Illustrated in Figure 6 is the thyroid dose arising from inhalation of the hypothetical release of I^{131}. The dominance of the region close to the source of release is enhanced in this particular case due to the relatively rapid development of the mixing layer after dawn and to the strengthening of the wind. However it is expected that even when the model has been applied in a wide range of synoptic conditions at different times of day and year, the average trend will be to predict a faster rate of convergence of collective dose with increasing distance from the source than has been given by the conventional methods using continuous source meteorology. The main emphasis now will be to study the transitional phases up to the range of 100 km or so when puffs are still diffusing up through a turbulent boundary layer which is itself changing and evolving at the same time.

ACKNOWLEDGEMENTS

The authors would like to acknowledge the help of Dr. F.B. Smith and the staff of the Metererological Office at Bracknell, Berkshire, England, who have provided most of the ingredients for this model and without whose continued assistance this work would not have been possible.

This work has been supported in part under a EURATOM contract and the authors acknowledge the encouragement of G. Lacourly, Association EURATOM - C.E.A., Fortenay-aux-Roses, France.

REFERENCES

1. Carson, D.J. 'The development of a dry inversion capped convectively unstable boundary layer'. Quart.J.R.Met.Soc., (1973), 99, p.450-467.

2. Pasquill, F. 'Atmospheric diffusion'. 2nd (revised) Edition, Ellis Horwood Ltd., Chichester, (1974).

3. Smith, F.B. 'Brief notes on the specification of the boundary layer in terms of external readily assessed parameters'. Met.Office Boundary Layer Research Branch Turbulent Diffusion Note - TDN 63, (1975).

4. Smith, F.B. and Jeffreys, G.H. (1974), 'Airborne transport of sulphur dioxide from the United Kingdom'. Atmos.Env., 9, p.643-659.

5. Sykes, I. 'Computation of 2-dimensional trajectories based on surface geostrophic wind'. Met.Office Boundary Layer Research Branch Turbulence and Diffusion Note - TDN 71, (1975).

Stage of Development	Timespan and Range	Characteristics	Type of model and Computer Programs available
1. Puff diffuses down to ground level	First few hours range up to 10 km	Source height is very important. Puff shape and dimensions affect gamma dose from submersion	Gaussian plume models Programs WEERIE or FLAIR
2. Puff diffuses up to top of mixing layer	Up to a day Range up to 100 km	Changes in meteorology become important. Concentrations and rates of dilution can vary rapidly	Moving columnar puff model. Programs MESOS 3 + PEOPLE 1
3. Synoptic scale development	A few days Range up to 1 or 2 x 1000 km	Dilution depends on changes in depth of the mixing layer, and divergence of wind on a synoptic scale	Moving columnar puff model Programs MESOS 3 + PEOPLE 2
4. Global Circulation beyond first pass over the map area	From a few days to possibly a few times the ½ life of the nuclide Global range	Dispersion depends on transfer rates between global compartments including stratosphere, ocean, geosphere and biosphere	Box model Program GLOBAL

Figure 1. Stages of Development of Puffs

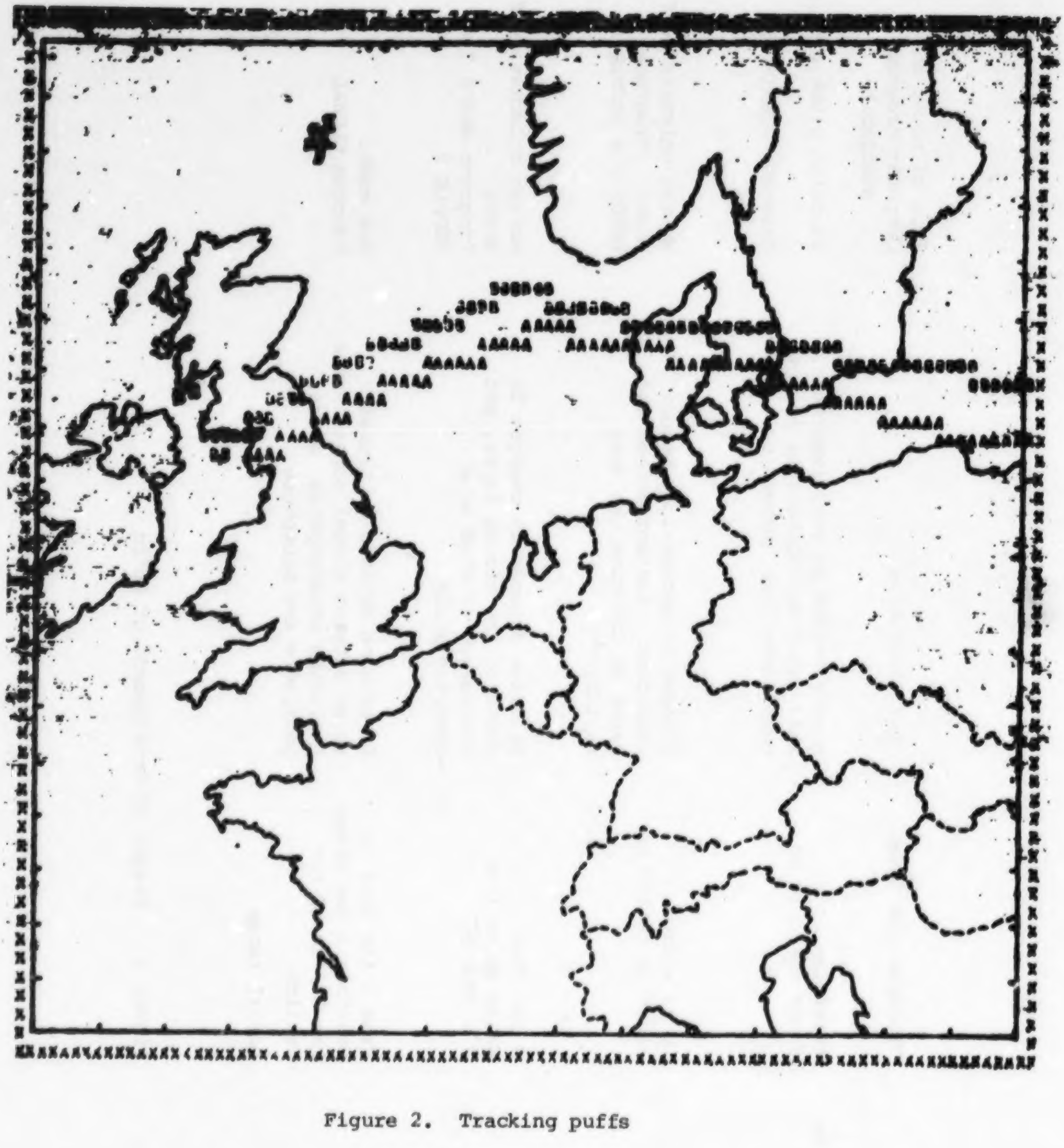

Figure 2. Tracking puffs

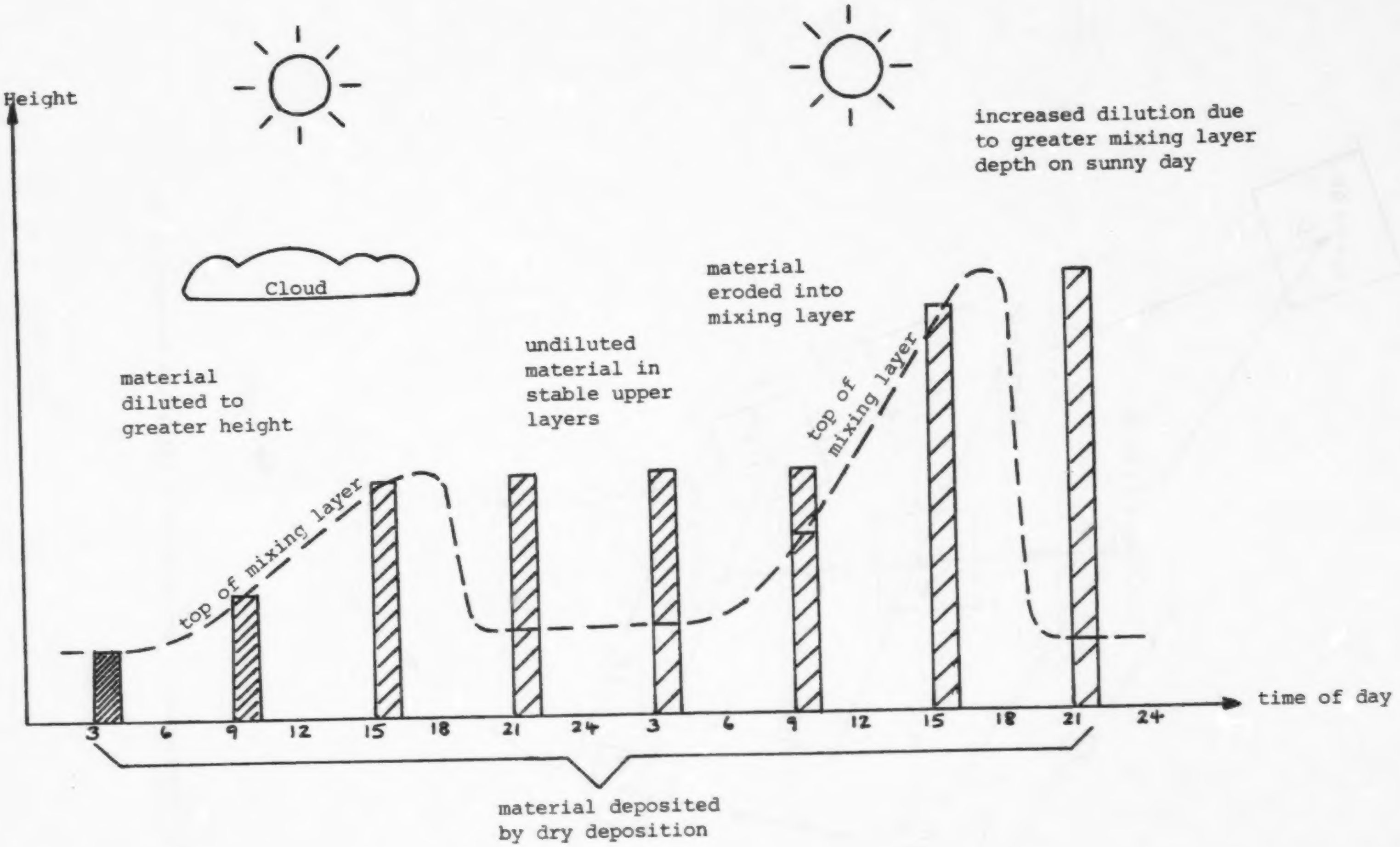
Height
Cloud
material
diluted to
greater height
top of mixing layer
undiluted
material in
stable upper
layers
material
eroded into
mixing layer
top of
mixing layer
increased dilution due
to greater mixing layer
depth on sunny day
3
6
9
12
15
18
21
24
3
6
9
12
15
18
21
24
time of day
material deposited
by dry deposition

Fig. 3. Illustration of model for strongly depositing nuclide for 48 hours following release at midnight. (density of shading indicated concentration)

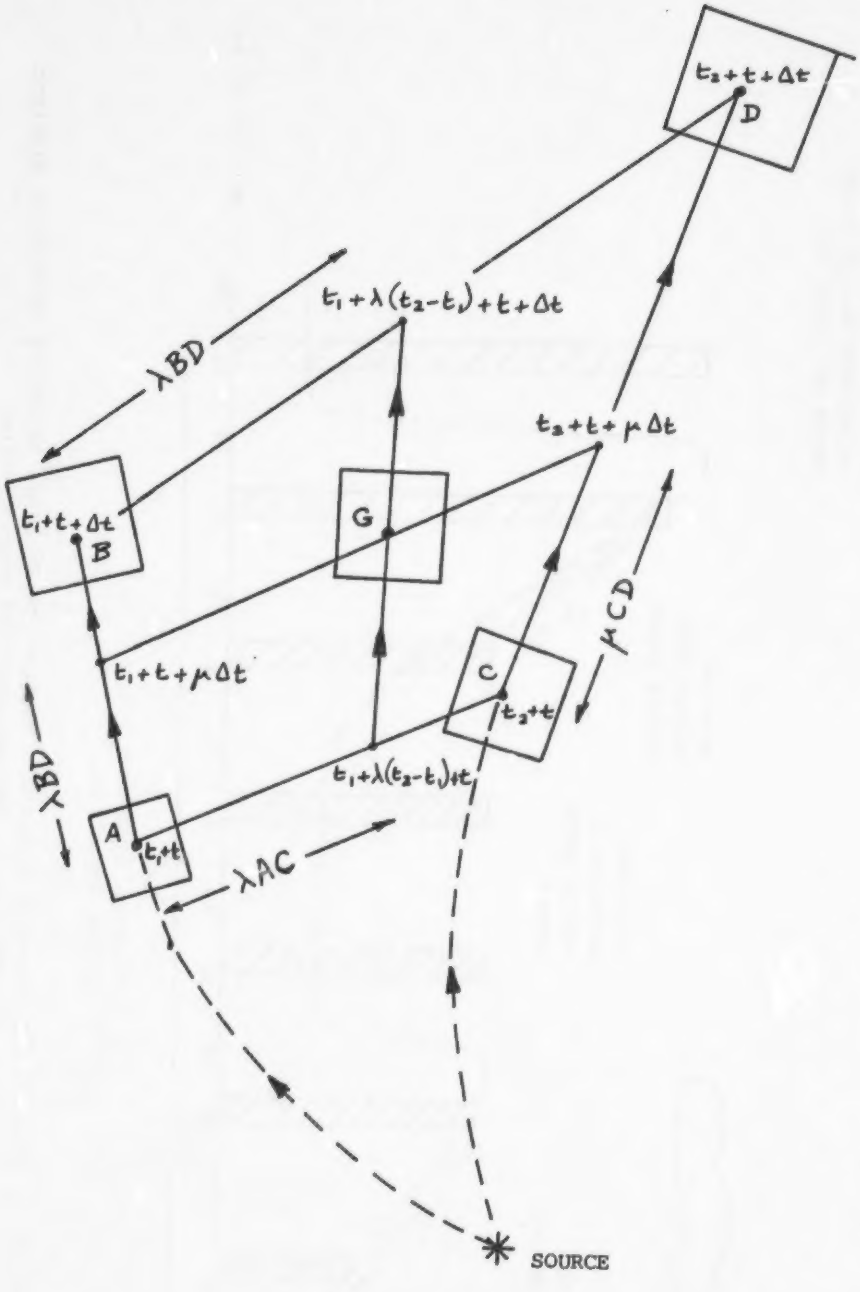
$t_2+t+\Delta t$
D
$t_1+\lambda(t_2-t_1)+t+\Delta t$
λBD
$t_2+t+\mu\Delta t$
$t_1+t+\Delta t$
B
G
μCD
$t_1+t+\mu\Delta t$
C
t_2+t
λBD
$t_1+\lambda(t_2-t_1)+t$
A
t_1+t
λAC
SOURCE

Fig. 4. Interpolation procedure for intervals between puffs.

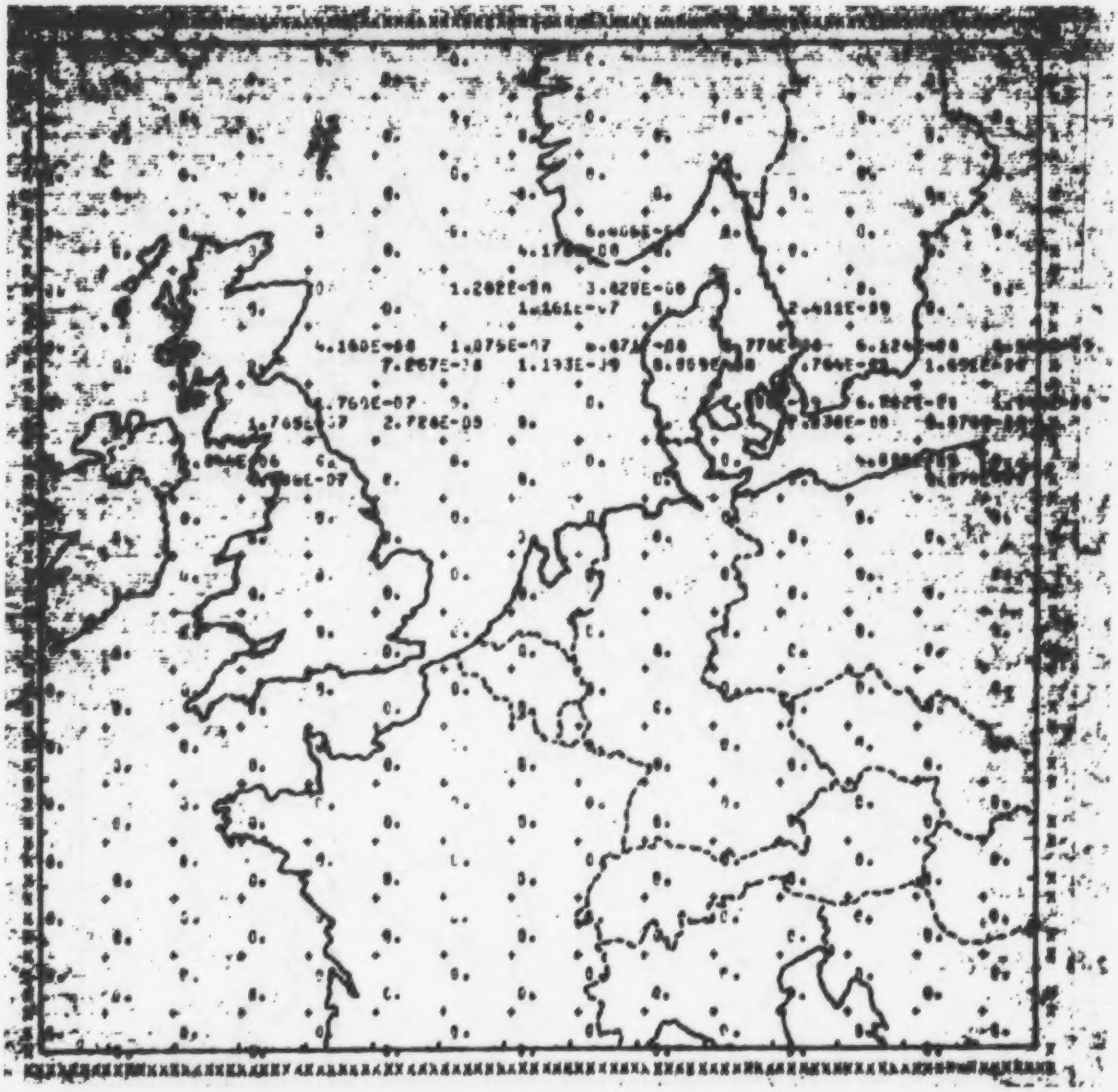

Figure 5. Time integrated atmospheric concentrations over map area for a hypothetical 6 hour release of I^{131} (μCi m^{-3} x hours)

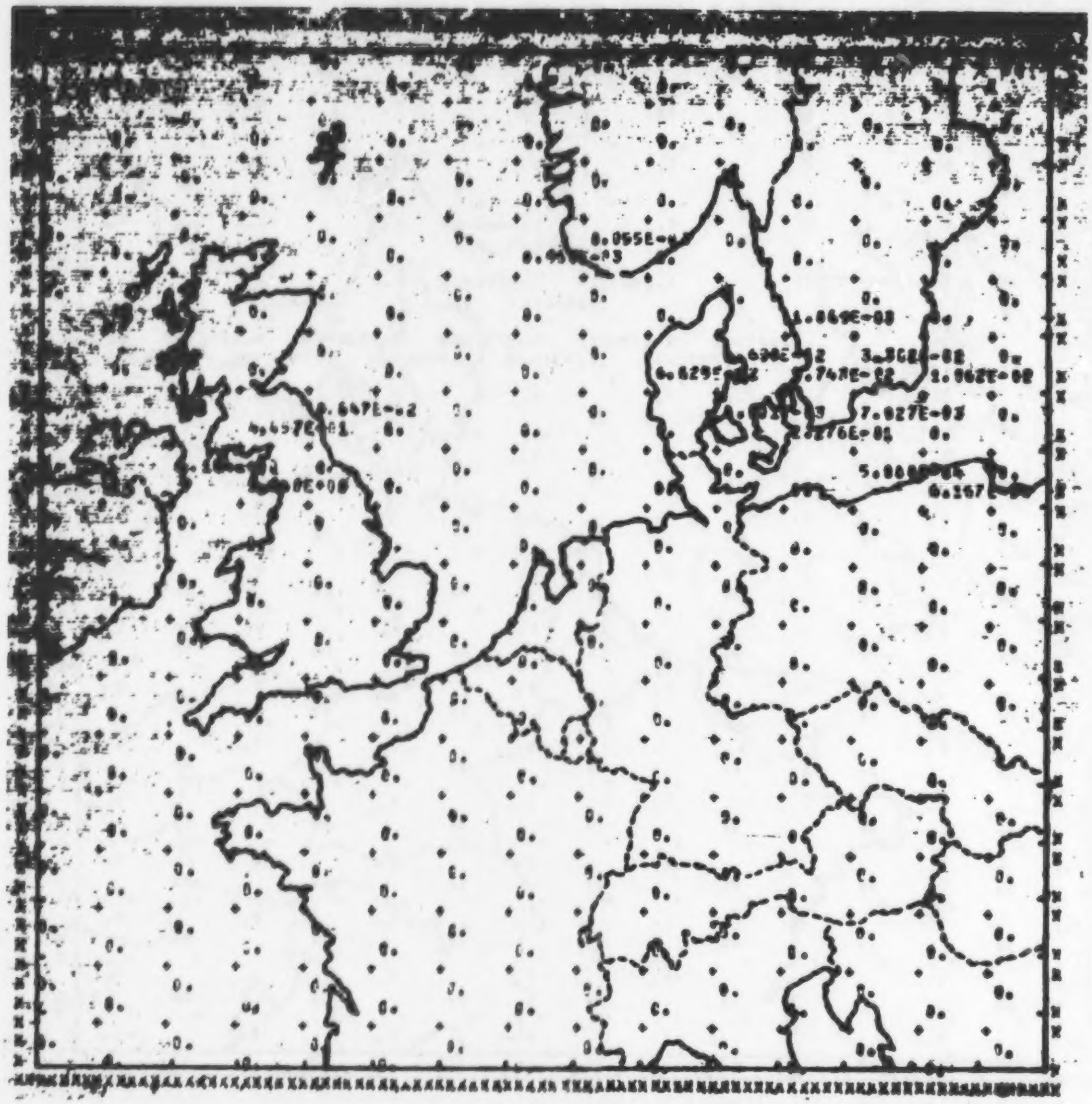
6.055E-04
1.869E-03
3.368E-03
6.629E-02
1.062E-02
7.027E-03
4.457E-01
5.868E-04
6.267

Figure 6. Population dose distribution for hypothetical release of I^{131} (man-rems in each grid square)

Reproduced from best available copy.

7th International Technical Meeting
on Air Pollution Modeling and its Application

Diffusion and Transport of a Passive Contaminant Over Complex Terrain Under Stable and Unstable Conditions

Richard A. Anthes
Nelson Seaman
Daniel Keyser

The Pennsylvania State University

September 7 - 10, 1976
Airlie, Virginia
United States of America

1. Introduction

The prediction of wind and the diffusion of pollutants over complex terrain is one of the most difficult problems facing the air pollution meteorologist. Variations in terrain produce significant small-scale perturbations to the larger-scale flow in the planetary boundary layer under both stable and unstable conditions. Local eddies in the vicinity of mountains or hills may even flow in an opposite direction to the synoptic scale flow. Ventilation of valleys associated with the diurnal variation of winds over sloping terrain may greatly affect the dispersion of pollution over a region during critical light-wind situations.

Even if the local winds over complex terrain are known (either through measurements or model predictions), the prediction of the pollutant concentration at a point is complicated by variations in terrain elevation. Simple models such as the Gaussian plume models are not designed to accommodate variable elevations downwind of the source.

This paper describes two experiments which forecast the diffusion and transport of a passive contaminant in the vicinity of steep terrain on a small regional scale (horizontal domain size approximately 60 km with a horizontal resolution of 3 km).

First, the wind and temperature structure in the lowest half of the atmosphere are predicted with the vertical cross section version of the Penn State mesoscale dynamic model (Anthes et al., 1974). The forecast is made over a three hour period beginning 1 hour before sunrise. The output from this model is saved and used in a subsequent transport and diffusion model designed for use over variable terrain. The results indicate a plausible behavior of both models under stable and unstable conditions over mountainous terrain.

2. Review of dynamic model

Space permits only a brief description of the dynamic forecast model; a complete description of the basic model is given by Anthes et al., 1974. The model is written in terrain-following σ coordinates, where

$$\sigma = \frac{p - p_t}{p_s - p_t} \tag{1}$$

Here p is pressure, p_s is the surface pressure, and p_t is the pressure at the top of the model. The basic prognostic equations consist of the equation of motion and the thermodynamic equation. Diagnostic equations include the hydrostatic equation, equation of state, and the continuity equation, from which the vertical velocity is derived.

In this version of the model, the turbulent fluxes of heat and momentum are modeled according to K-theory, where the eddy diffusivities for heat and momentum are time-dependent functions of the height of the mixed layer, static stability, and local wind shear (Busch et al., 1976). The diffusivity for heat is saved from the dynamic model for use in the calculation of the vertical diffusion of the pollutant in the transport and diffusion model.

For this experiment, the model consists of 12 prediction levels for velocity and temperature (Table 1), with most of the levels concentrated near the ground. The horizontal resolution is 3 km over most of the domain; near the lateral boundaries the horizontal grid is stretched to increase the distance of the lateral boundaries from the region of interest. The time step is 7 seconds.

Table 1

Vertical Levels in Dynamic Model

Vertical Index	σ	Pressure (mb) (p_s = 862 mb on valley floor)	Approximate height above valley floor (m)
1	0.13	547	3150
2	0.38	638	2240
3	0.56	703	1590
4	0.69	750	1120
5	0.77	779	830
6	0.80	790	720
7	0.83	800	620
8	0.86	811	510
9	0.89	822	400
10	0.92	833	290
11	0.95	844	180
12	0.98	855	70

3. The transport and diffusion model

The transport and diffusion model is a combination of the particle-in-cell (PIC) and Eulerian diffusion model modified for the terrain-following coordinate system defined by (1). Teuscher and Hauser (1974) give a description of the basic PIC model. The conservation equation solved by this model is

$$\frac{\partial q}{\partial t} = - \underset{\sim}{V}_H \cdot \nabla q - \dot{\sigma} \frac{\partial q}{\partial \sigma} + \frac{\partial}{\partial z} \left(K \frac{\partial q}{\partial z} \right) + S \qquad (2)$$

where q is the concentration of the pollutant (μg/kg)*, $\underset{\sim}{V}_H$ is the horizontal velocity, $\dot{\sigma}$ is the "vertical velocity" in σ-coordinates, z is height, K is the vertical diffusion coefficient and S is the source rate (μg/kg/s). The advective (transport) terms in (2) are treated by the Lagrangian PIC approach, in which a collection of particles representing concentrations of the contaminant are followed through the domain by the calculation of the particle trajectories. In the absence of the source and sink terms, this part of the forecast conserves the mass of the pollutant exactly and preserves extremely sharp gradients of q; in other words, there is no false numerical dispersion associated with the transport part of the model.

---

*Near the ground where the density is approximately 1 kg m^{-3}, the numerical value of the volume concentration (μg/m^3) is nearly equal to the numerical value of the mass concentration (μg/kg).

The vertical diffusion term in (2) is calculated on an Eulerian grid. A schematic diagram of this grid and three typical particles is shown in Figure 1. The "volume" associated with each Eulerian cell is (in three dimensions) $\Delta x \Delta y \Delta \sigma$ where Δx and Δy are the horizontal grid lengths in the west-east and north-south directions and $\Delta \sigma$ is the vertical grid increment. This same volume is arbitrarily associated with each particle.

It is important to note that the horizontal and vertical resolutions of the transport and diffusion model need not coincide with the corresponding resolutions of the dynamic model. In the vicinity of strong sources, for example, it might be useful to predict the transport and diffusion of a pollutant on a finer scale than that used to predict (or observe) the winds.

The vertical coordinate, σ, in the transport model used in this experiment is defined by (1) with p_t = 700 mb. This upper level was chosen because the height, h, of the planetary boundary layer (PBL) in the dynamic model never exceeded this level. With this definition, the terrain surface coincides with the lowest level of the Eulerian grid. This coincidence greatly simplifies the calculations of the lower boundary. However, the intersection of h with the σ-levels complicates the interpolation from particles to cells and back again near the top of the PBL, and introduces errors in this region. A preferable vertical coordinate, which would circumvent the these difficulties when a well-defined and nearly steady-state height to the mixed layer exists, would be

$$\sigma' = \frac{p - p_h}{p_s - p_h} \tag{3}$$

where p_h is the space-dependent pressure at h. In this modified σ-system, all particles and cells would be rectangular "volumes" in the computational domain.

In the transport part of the calculation, at each time step, τ, the position of each particle at τ + 1 is obtained by a forward extrapolation of the particle with the local wind field.

$$x^{\tau+1} = x^{\tau} + u^{\tau} \Delta t \tag{4}$$

$$\sigma^{\tau+1} = \sigma^{\tau} + \dot{\sigma}^{\tau} \Delta t \tag{5}$$

where u^{τ} and $\dot{\sigma}^{\tau}$ are obtained by interpolation in time and space from the dynamic model. The particles are now in their new locations. To ensure that each cell has a sufficient number of particles at time τ+1, all cells within the mixed layer are checked. If a cell is deficient in particles, new particles are added and these particles receive a concentration based on a linear interpolation from nearby cells. Special cases occur with cells on the lateral boundary when inflow exists and with new cells that are activated as the height of the mixed layer grows. If the empty cell is an inflow boundary, the particle is assigned a value that depends on the assumed concentration upwind of the domain. New cells that are generated at the top of the growing PBL are assigned a background concentration.

For the diffusion calculation, concentrations are interpolated from the particles to grid points by the formula

$$q_{jk} = \frac{\sum_{n=1}^{N} q^n f_{jk}^n}{\sum_{n=1}^{N} f_{jk}^n} \qquad (6)$$

where j and k are the horizontal and vertical indices of the Eulerian grid point, q^n is the concentration of the n^{th} particle in the neighborhood of a grid point (j,k) and f_{jk}^n is the fraction of the grid volume occupied by the n^{th} particle. After the concentration values are obtained on the Eulerian grid, the diffusion step is completed utilizing an implicit scheme (Richtmyer, 1957), which permits the use of a larger time step than do explicit schemes. Finally, the change associated with the vertical diffusion step at each grid point is interpolated back to the neighboring particles.

The accuracy of the transport and diffusion model increases with finer horizontal and vertical resolution associated with the Eulerian grid, and with the number of particles. Some limited sensitivity tests were made with varying the number of particles. These tests showed that approximately four particles per cell produced consistent results without a prohibitive amount of computer time. An increase of particles beyond four per cell did not significantly affect the forecasts. On the other hand, use of only one particle per cell did not preserve strong gradients as well as four per cell and introduced larger errors in the total mass budget of the pollutant. In these experiments, the original Eulerian cells were initialized with four particles. As the depth of the boundary layer grew and additional cells were incorporated into the PBL, these cells were initialized with two particles.

4. Results from the dynamic model

To illustrate the combined behavior of the dynamic and transport models under light-wind conditions, a forecast was made during the transition from stable to unstable conditions over the terrain profile shown in Figure 2 with a geostrophic wind of 2 m s^{-1}. This terrain is a smoothed version of the San Andres range, New Mexico, and varies in elevation from 1370 m to 2150 m.

The initial conditions consist of a stable atmosphere ($\frac{\partial\theta}{\partial z} = \frac{4.4°C}{km}$, where θ is potential temperature) with a west wind of 2 m s^{-1} at all levels. During the first hour of the forecast the surface heat flux was zero. After 1 hour, the heat flux, H_o, was given by

$$H_o = \begin{cases} A\ (t - 1.0) & 1 \leq t \leq 2 \\ A & t \geq 2 \end{cases}, \qquad (7)$$

where A = 349 w m^{-2} (1/4 of solar constant) and t is in hours. The heat flux given by (7) simulates sunrise and the subsequent sensible heat flux over arid terrain.

During the first hour, the wind field in the model is dramatically affected by the steep terrain. The static stability is great enough to prevent the low-level air from flowing across the ridge. By 0.5h the lifting of the stable air on the upwind side has produced a sufficiently large westward-directed pressure gradient to stall the initial westerly flow. By 1 hour, weak (0.5 m s^{-1}) easterly winds are blowing down the west slope (Fig. 2). Along the east slopes, the subsidence in the stable air during the first half hour has also produced a westward-directed pressure gradient force and a shallow layer of east winds has developed. Both of these shallow layers of east winds are manifestations of gravitational oscillations in a stably stratified fluid. In this experiment, they are primarily results of the arbitrary initial conditions of constant west winds of 2 m s^{-1}.

Above the low-level easterlies, the streamlines do cross the mountain, although the obstacle produces a large perturbation which extends great distances upwind and downwind of the mountain. Note, however, that the wind speeds associated with this wave are light, generally under 2 m s^{-1}.

At 1 hour, heating commences at the surface and the height of the PBL begins to grow. By 3h, it has grown to approximately 800m above the surface. As the layer of unstable air near the ground thickens, the nature of the wind perturbation near the mountain changes considerably (Fig. 3). The perturbation associated with the stable gravitational oscillation gradually disappears near the surface and an upslope component to the wind along both the east and the west slopes is generated by the elevated heat source. Above the PBL, a significant perturbation remains in the stable flow as it encounters the variable height of the mixed layer and is lifted over the mountain. Wind speeds remain light, however, with maximum upslope winds of about 0.5 m s^{-1} existing at 3h.

The trajectories of several particles over the period from 0 to 2.5h and the height of the mixed layer at 0, 1.5, 2, and 2.5h are depicted in Fig. 4. The rapid development of easterly flow near the valley floors is indicated by the reversals in the trajectories in this region. The trajectories near the 825 mb level show that westerlies persist until the height of the mixed layer grows above this level. Then the mean wind decreases and the particles move very slowly. Above the 800 mb level, westerlies continue throughout the entire forecast and particles are able to flow over the mountain. Fig. 4 illustrates the blocking affect of large mountains on low-level air parcels, and also demonstrates the difference between trajectories and streamlines (compare Fig. 4 with Figs. 2 and 3).

Figure 5 shows the cross section of the vertical mixing coefficient, K, at 3h. Maximum values of K in this strong convective situation exceed 250 $m^2\ s^{-1}$ near the middle of the PBL over the valleys where the depth of the PBL is greatest. Over the mountain, the depth of the PBL is less and the mixing length, from which K is determined in the dynamic model, is correspondingly reduced. However, values still exceed 80 $m^2\ s^{-1}$ in this region. A strong vertical gradient of K exists near the top of the PBL, which occurs about 25 mb above the 50 $m^2\ s^{-1}$ isoline. In contrast to the large values of K shown in Figure 5, the values during the stable portion of the experiment (0-1h) do not exceed 2 $m^2\ s^{-1}$.

5. Results from the transport and diffusion model

Two experiments were conducted with the meteorological data generated in the experiment described in Section 4. In the first, a uniform concentration of 100 µg/kg was assumed in the PBL. There were no sources or sinks during this experiment, only vertical diffusion. This experiment mainly illustrates the vertical dispersion of a contaminant over complex terrain as the PBL grows with time. In the second experiment, a constant flux of pollutant is assumed at the base of the mountain on the west side. This experiment illustrates the vertical and horizontal spread of a highly concentrated plume under a light-wind, convective situation in the vicinity of steeply sloping terrain.

The Eulerian grid for these experiments consisted of 26 levels with a $\Delta\sigma$ equal to 0.04. This resolution corresponds to a pressure increment of about 6 mb or a height increment of approximately 60 m over the valleys. The time step was varied during the calculation to preserve computational stability. Since the vertical diffusion in the lowest level of the model is calculated explicitly (because the lower boundary condition consists of the flux of q rather than a time-dependent value of q itself), the time step had to be decreased as K increased at this level. In these experiments, the time step varied from 105 s during the first hour to 7 s at 3.0h.

The concentration after 3h in the first experiment, in which the initial concentrations were 100 μg/kg, is shown in Figure 6. The major effect on the initially uniform concentration during the 3 hours is the strong vertical mixing. The average concentration in the PBL has been reduced to around 15 μg/kg by dilution. However, horizontal variations have developed as a result of horizontal variations in the mixing depth. Thus the concentrations are a maximum over the mountain, where the depth of the mixed layer is smallest.

The relative minima of the concentration on either side of the mountain are, to some extent, the result of numerical errors introduced by the vertical interpolation of the diffusion tendencies $(\frac{\partial q}{\partial t}_D)$ from the Eulerian cells to the particles. Vertical diffusion in a given column on the Eulerian grid affects all particles whose volumes overlap that column. Therefore, it is possible to interpolate erroneous changes due to diffusion wherever strong horizontal gradients of q exist. One remedy to this problem is to increase the horizontal resolution on the Eulerian grid in the vicinity of large horizontal gradients. Another is to increase the number of particles and reduce the size of the volume assigned to each particle.

In the second simulation, the initial concentration is zero. A constant area source of 35 $\mu g/m^2/s$ is assumed at x = 48 km (at the base of the slope on the west side). During the first hour, the concentration in this region increases rapidly, reaching a maximum of nearly 1000 μg/kg at sunrise. The horizontal wind during this time is too light to ventilate significantly the region. After sunrise, the rapidly growing PBL allows an upward diffusion of the pollutant, and the low-level concentrations are rapidly reduced (Fig. 7). By 3.0h, the maximum concentration is about 300 μg/kg at the source. Because of the constant surface flux, a fairly strong vertical gradient of q is maintained, in spite of the strong vertical mixing. For example, the concentration at the middle of the PBL over the source is about half that near the ground.

The weak alternating westerly and easterly circulations in the vicinity of the mountain have produced some horizontal spreading of the plume in both directions. However, the horizontal gradient of q remains quite large.

6. Summary

This paper has presented forecasts of pollution under light-wind conditions over very steep terrain using a combination of a general meteorological model and a modified particle-in-cell transport and diffusion model. The meteorological model was integrated first for 1 hour before and two hours after sunrise. During the first hour, air near the surface was blocked by the mountain and vertical mixing was very small.

After sunrise, the planetary boundary layer began to grow rapidly, vertical mixing increased by two orders of magnitude, and a weak mountain-valley circulation was induced by the differential heating on the mountainsides.

The wind, depth of the PBL, and mixing coefficients data obtained from the meteorological model were then used in a 3h forecast of pollution. This prediction was made using a particle-in-cell model modified for use over variable terrain. In this model, diffusion was done on an Eulerian grid while the transport of the diffusion was done through the computation of particle trajectories. Because the winds were light in this case (generally under 1 m s^{-1}) and surface heating was strong, vertical diffusion dominated the pollution predictions.

7. Acknowledgments

This research was supported by the Environmental Protection Agency through Contract 800-397-03. We thank Gail Maziarz for typing the manuscript.

References

Anthes, R. A., N. Seaman, J. Sobel and T. Warner, 1974: "The Development of Mesoscale Models Suitable for Air Pollution Studies." Select Research Group in Air Pollution Meteorology, Second Annual Progress Report: Volume 1, EPA-650/4-74-045-a, pp. 6-233.

Busch, Niels E., Simon W. Chang and Richard A. Anthes, 1976: "A High-Resolution Model of the Planetary Boundary Layer Suitable for Use with Mesoscale Dynamic Models," Journal of Applied Meteorology, 15, (September issue).

Richtmeyer, R. D., 1957: Difference Methods for Initial Value Problems, New York, Interscience, p. 101-104.

Teuscher, L. H. and L. E. Hauser, 1974: Development of Modeling Techniques for Photochemical Air Pollution, EPA-650/4-74-003, pp. 91.

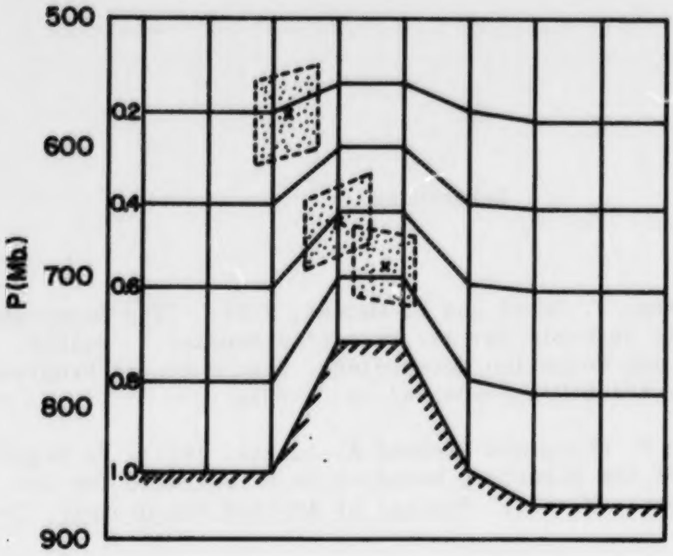
500
600
700
800
900
P(Mb.)
0.2
0.4
0.6
0.8
1.0

Fig. 1: Schematic diagram of particle-in-cell transport model. The dotted volumes are associated with the moving particles.

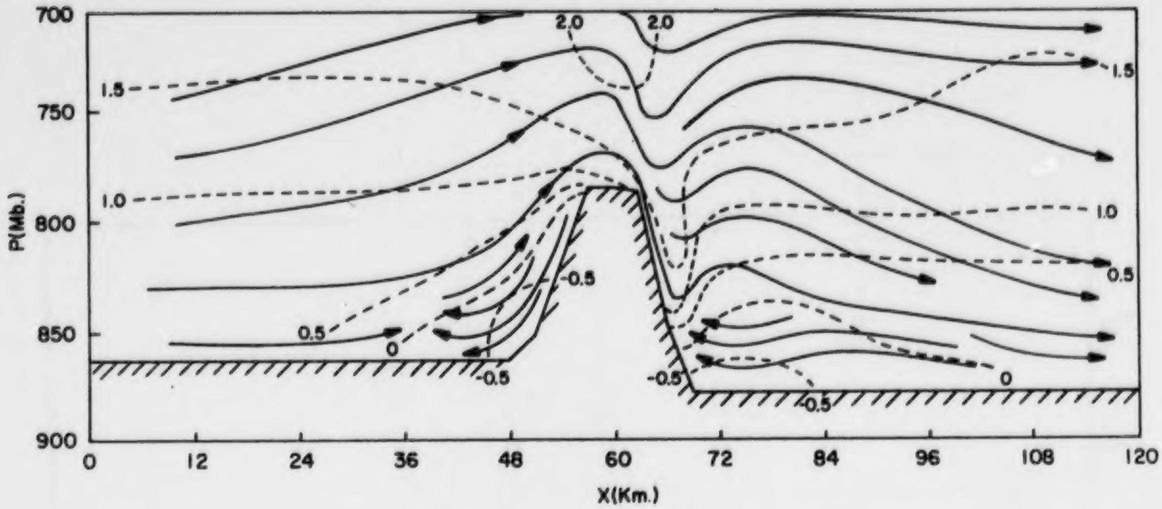

Fig. 2: Streamlines and isotachs (m/s) at 1.0 h (sunrise) of dynamic model's forecast.

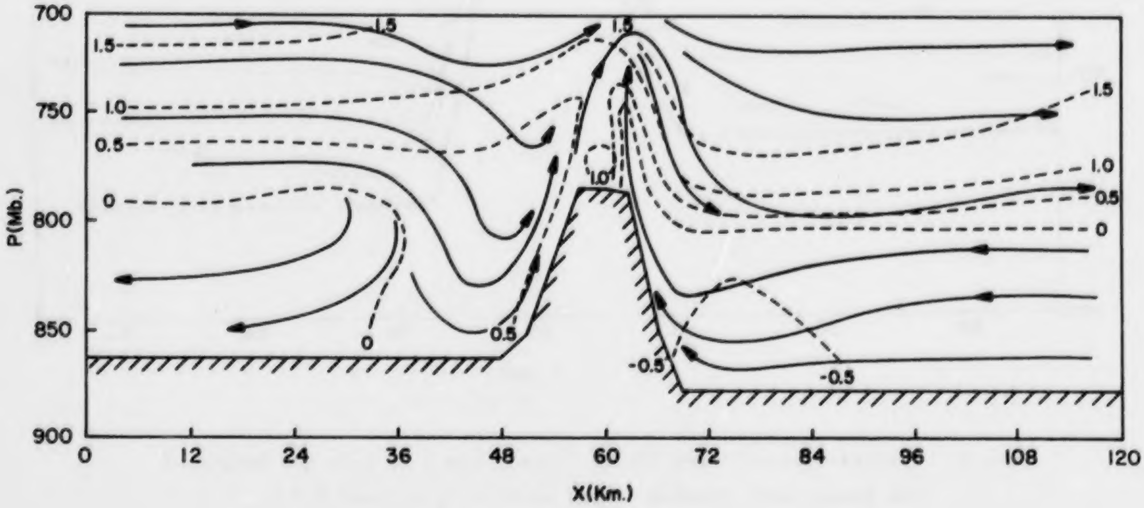

Fig. 3: Streamlines and isotachs (m/s) at 3.0 h of dynamic model's forecast.

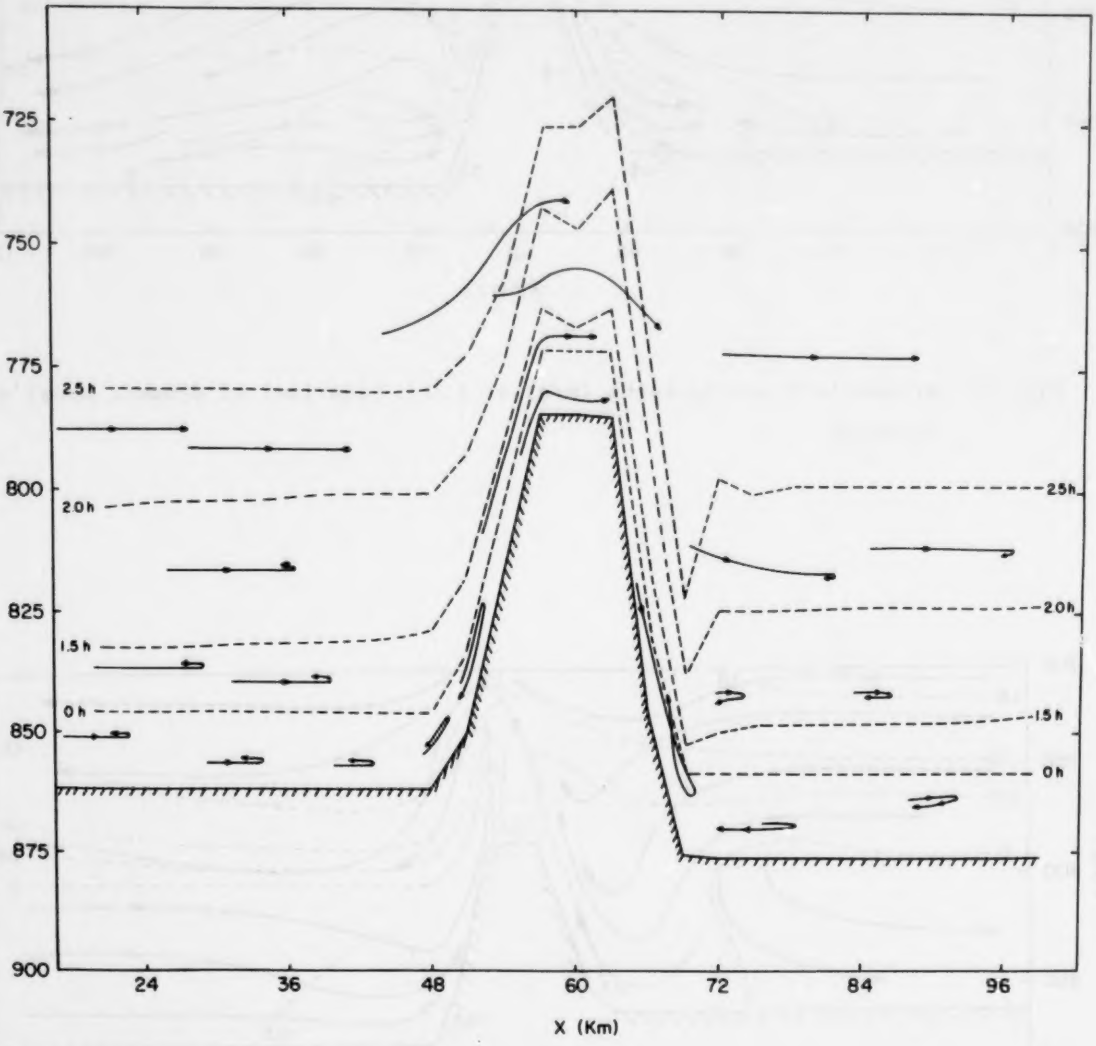

Fig. 4: Particle trajectories (solid lines) from 0 to 2.5h and height of the mixed layer (dashed lines) at 0, 1.5, 2.0 and 2.5 h.

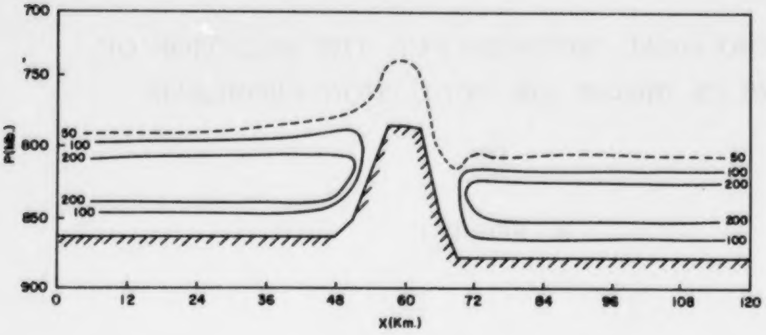

Fig. 5: Coefficient of eddy viscosity for heat ($m^2 s^{-1}$) at 3.0 h of forecast.

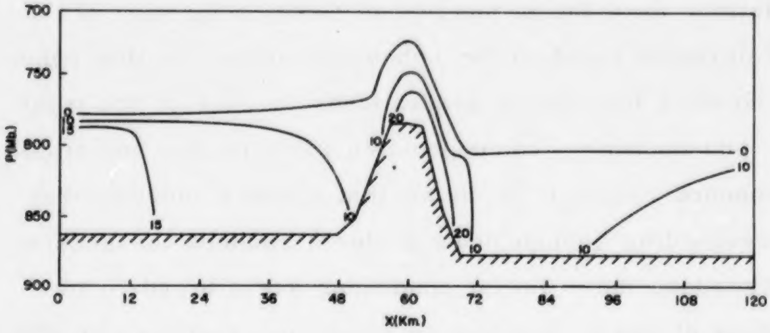

Fig. 6: Concentration (g/kg) at 3 h. Initial concentration was 100 g/kg throughout shallow PBL.

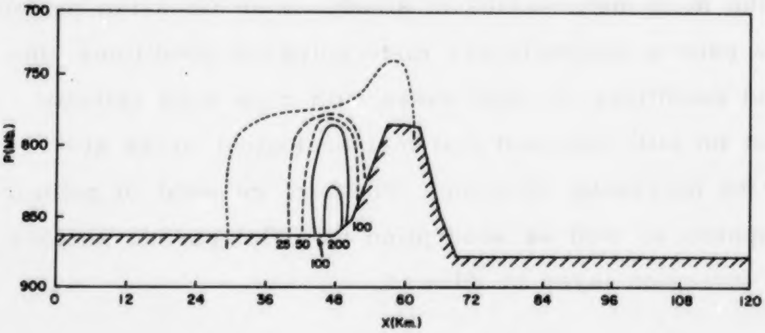

Fig. 7: Concentration (g/kg) at 3 h. Initial concentration was 0. A constant area source rate of 35 $g/m^2/s$ is assumed at x= 48 km.

ON THEORETICAL METHODS FOR THE SOLUTION OF COMPLEX URBAN AIR POLLUTION PROBLEMS

BY

H. FORTAK

ABSTRACT

Singular point sources of unit strength as are utilized in most air pollution calculations have the properties of Green's function of special type of diffusion equation for unbounded space. In this paper, the concept of Green's function is generalized. In case of the most general initial- and boundary-value problem for diffusion and transport within a bounded region it is shown that Green's function that fulfills the corresponding homogeneous problem reduces the general problem to integrations only. Initial conditions are allowed to be arbitrary functions of space, sources in space and sources (or sinks) at the boundary of a closed domain may be arbitrary functions of space and time. This statement is shown to be true in case of the most general budget equation for turbulent transport and diffusion in the atmosphere.

With regard to the many deficiencies of steady-state Gaussian models, main attention is paid to nonstationary meteorological conditions, including light wind conditions or even cases with zero wind velocity. However, it must be still assumed that meteorological fields are homogeneous in the horizontal direction. Further, removal of pollution within the atmosphere as well as absorption at a flat earth's surface and at an upper inversion layer is allowed.

In case of no variation of meteorological parameters with height this K - theory model allows to construct Green's function for the horizontally not bounded domain. Because of its otherwise quite general structure, the model is proposed for air pollution modeling of urban or regional scale.

The difficulties in constructing Green's function in cases of height - dependent meteorological parameters are discussed. All proposed methods lead to inherent complex Sturm - Liouville problems that can be solved only numerically. This is true for the methods of integral transformation, for the spectral method, and for the method that calculates moments of concentration.

As main result, it is proposed to use mixed analytical - numerical (only numerical solutions of integrals) models for very complex source distributions in space and time for urban air pollution modeling.

INTRODUCTION

The general structure of problems in air pollution modeling has not changed much during the last decade. The main goal of air pollution modeling is, as it is generally in meteorology, to predict the state of the atmosphere (here the chemical composition of the atmosphere) in terms of real-time short-term prediction and in terms of prediction of climatic changes within the atmosphere (here of climatic changes of air pollution).

The prediction of man-made climatic changes of air pollution for a given region was in some sense the first success in climate forecast of an important parameter of the atmosphere. This is especially true for air pollution models which predict frequency distributions of concentrations for as many grid points in an urban area or a region as necessary [1], [2], [3], [4]. This is the fact according to the definitions of climatology, because at a location not only the mean value but also the distribution of a meteorological parameter is predicted in case that man-made changes of the normal atmospheric input, i.e. the sources, are predicted.

We are now in a position to predict the long-term changes of air pollution sources fairly well. This may be an increase of sources, a planned decrease, a change of source arrangement, a change to other types of fuel, for example. It is surprising enough that simple Gaussian plume-type models seem to be able to predict climatic changes of air pollution sufficiently well, and now can be used for planning purposes in many regions in the world. This fact was known and validated almost ten years ago and the method is now used in some countries by several research groups. This type of forecast is a purely statistical one, not only because an empirical statistical distribution (the Gaussian plume model) is used. In addition, the statistics of meteorological conditions of transport and diffusion during a normal meteorological year is utilized, that is also based on statistics of at least five years of meteorological data. Further statistics of ground level concentration fields, that constitute the concentration inventory of the region, are utilized to calculate a detailed climatology of air pollution for many locations within the area of a city or a region.

There is, however, a certain number of problems left unsolved. First, the problem of air pollution transport and diffusion above irregular terrain. Secondly is the problem of finding a suitable model for treating light wind conditions, that are associated with temperature inversions occurring above the ground.

The effects of irregular terrain are not very well understood theoretically, although considerable empirical field studies and studies in the laboratory have been performed for several years. In the case of irregular terrain the vertical and horizontal wind-shear structure is distorting the actual plume such, that neither a Gaussian plume model nor common types of puff models will be applicable. It seems, that from a practical point of view, only numerical models using K-theory together with dynamical models for air flow over such terrain would be able to guarantee some progress in that field.

With regard to light wind conditions that are associated with inversions, observations from aircraft as well as laboratory and numerical investigations [5] indicate that, especially under conditions of convective instability below inversions, these layers are layers of extremely high concentrations. If the inversion layers are broken-up by thermal convection, one always finds strong downward turbulent diffusion and concentration peaks for shorter periods of time at the ground.

It seems to be extremely important to develop comprehensive time-dependent models, which describe the transition from normal conditions, for which the Gaussian plume theory eventually can be applied, to windless conditions (with built-up inversions) and vice versa. In this respect it is believed that time-dependent K-theories which do not use entirely numerical methods of solution, could be used, especially in order to avoid numerical diffusion effects.

Much have been said about other complications in modeling. For example about the validity of the Gaussian plume model at large distances from the sources, and about the departures from passive diffusion. However, if for a given area the appropriate type of model for prediction of climatology of air pollution has been developed, an almost unlimited number of useful applications in the field of environmental planning can be handled.

Examples are the analysis of environmental impact caused by changes in the source arrangement, by changes of the types of sources or of the types of fuel. Another example is the planning of land use and, therefore, the possibility of deciding where new industrial installations can be built or not be built.

Up to now, an almost unsolved problem is the problem of predicting air pollution in a given region on a real-time basis. Real-time prediction of air pollution requires real-time prediction of the behaviour of complicated atmospheric properties, which are responsible for transport and diffusion within the planetary boundary layer. Up to now, we don't have satisfactory numerical models for these scales involved. Most investigations on predictability of atmospheric processes indicate that deterministic forecasts for regions of 100 x 100 km in size are possible only for short periods of time, say less than 6 hours in advance. Most urban areas and regions are smaller than this. Therefore, one finds in principle a limit of deterministic predictability, even though we might have good nesting models within a steering large - scale model that would describe the physics of the planetary boundary layer sufficiently well. However, there is some indication that modern dynamic - stochastic forecasting models will be able to predict the state of the atmosphere in a statistical sense much further [6], [7]. In the scale that we are considering here, prediction almost one day in advance seems to be feasible.

Even if this problem of forecasting of time series of properties of the planetary boundary layer could be solved in Eulerian sense, there remains the solution of additional equations for transport and diffusion which obtains meteorological input time - step by time - step from the forecasting model. In this case, Eulerian models for transport and diffusion of pollutants should be used, and these are essentially models belonging to the group of time - dependent K - type theories. Although various attempts to solve this problem come to mine, not much progress in the direction described previously have been achieved so far. However, solutions to these problems are urgently needed, not only to forecast high - level air pollution episodes and, therefore, to build up a warning and control system, but also for testing many assumptions made in statistical models for the prediction of climatic changes of air pollution.

In this paper it is attempted to eliminate the assumption of a certain minimum wind velocity and provide even formulae for the case of windless conditions. In addition, instationary meteorological conditions are incorporated in a step-wise manner and full generality is assumed with regard to time-dependent distributions of sources in space and at boundaries. In full generality only height-independent meteorological parameters allow closed solutions in terms of Green's function. This will be the main part of the paper. The problem of finding Green's function for the case of height-depending meteorological parameters is touched only by discussing several attempts to solve the problem.

1. FORMULATION OF THE GENERAL PROBLEM

Assuming scales for which the classical equations of hydrodynamics are valid, then the budget equations for density ρ of unpolluted air and for the densities ρ^n of N pollution components are given by

$$(1)\qquad \begin{aligned} &\frac{\partial \rho}{\partial t} + \nabla \cdot \rho \mathbf{v} = 0 \\ &\frac{\partial \rho^n}{\partial t} + \nabla \cdot \rho^n \mathbf{v}^n = Q^n(\cdots, \rho^\mu, \cdots; \mathbb{R}, t) . \end{aligned}$$

Here, $\mathbf{v}$ and $\mathbf{v}^n$ are the velocity vectors of air and of all other pollution components of air, and Q^n defines space - time distribution of sources and sinks of density ρ^n, depending also on some or all components of pollution.

The major component of air, the unpolluted component, is used as reference component. Then, by introducing concentrations $c^n = \rho^n/\rho$ and relative velocity vectors $\mathbf{v}^n_{rel} = \mathbf{v}^n - \mathbf{v}$ and redefining Q^n by ρq^n, the budget equations for pollution components are

$$(2)\qquad \frac{\partial \rho c^n}{\partial t} + \nabla \cdot \rho c^n (\mathbf{v} + \mathbf{v}^n_{rel}) = \rho q^n .$$

Space - time distributions of sources in urban areas are given mainly by three types: A large number of point sources, area or space sources, and sources (or sinks) related to chemical reactions between components of polluted air. Allowing point sources to move in space (e.g. traffic sources) one finds

$$(3)\qquad q^n_1 = \sum_{r=1}^{R} p_r(t)\, \delta(\mathbb{R} - \mathbb{R}_r(t)) .$$

Here, $p_r(t)$ are source strengths, $\mathbf{R}_r(t)$ are trajectories of sources, and $\delta(\mathbf{R}-\mathbf{R}_r)$ is Dirac's delta function. Area or space sources are assumed to be known functions in space and time, i.e. $q_2^n = q_2^n(\mathbf{R},t)$. Sources (sinks) due to chemical reactions are determined by chemical reaction rates [8]

$$q_3^n = (M^n/M) \sum_{s=1}^{S} \beta_s^n k_s \prod_{\sigma=1}^{N} \left[(M/M^\sigma) c^\sigma\right]^{\nu_{s\sigma}} .$$

In the following we will consider the problem of chemical reactions in the most simple manner by assuming only one chemical component being removed during transport and diffusion according to

$$q_3^1 = -\lambda c^1 .$$

Applying ordinary and weighted averaging, Eqs. (1) and (2) become

$$\text{(4)} \qquad \frac{\partial \bar\rho}{\partial t} + \nabla \cdot \bar\rho \hat{\mathbf{v}} = 0$$

$$\text{(5)} \qquad \frac{\partial \bar\rho \hat c}{\partial t} + \nabla \cdot \bar\rho \hat c \hat{\mathbf{v}} = \bar\rho \left(\frac{\partial \hat c}{\partial t} + \hat{\mathbf{v}} \cdot \nabla \hat c \right) = \bar\rho \frac{\hat d \hat c}{dt} =$$

$$= -\nabla \cdot \left[\bar\rho \hat c \hat{\mathbf{v}}_{rel} + \overline{\rho c'' \mathbf{v}''} + \overline{\rho c'' \mathbf{v}''_{rel}} \right] + \bar\rho (q_1 + q_2) - \lambda \bar\rho \hat c .$$

In equation (5) Eq. (4) has been used for the transformation of the left hand side. In addition, the source distribution functions were assumed not to be random functions.

In case of sedimentation of the air pollution component we have $\hat{\mathbf{v}}_{rel} = \hat{\mathbf{v}}^1 - \hat{\mathbf{v}} = -\hat w \mathbf{k}$, where $\mathbf{k}$ is vertical unit vector, and, therefore, $-\nabla \cdot \bar\rho \hat c \hat{\mathbf{v}}_{rel} = \partial \bar\rho \hat c \hat w / \partial z$.

It remains the parametrization of turbulent transports of pollutants, i.e.

$$\bar\rho \hat{\mathbf{C}} = -\overline{\rho c'' \mathbf{v}''} \quad ; \qquad \bar\rho \hat{\mathbf{C}}_{rel} = -\overline{\rho c'' \mathbf{v}''_{rel}} .$$

This is a problem in the so-called K-theory, where utilization of the unknown tensor of turbulent diffusivity, $\mathbb{K}$, formally leads to

$$(6) \qquad \hat{\mathbb{C}} = \mathbb{K} \cdot \nabla \hat{c} \quad ; \quad \hat{\mathbb{C}}_{rel} = \mathbb{K}_{rel} \cdot \nabla \hat{c} \; .$$

Additionally it is assumed $\mathbb{K} = K_h (\mathbf{ii} + \mathbf{jj}) + K_z \mathbf{kk}$ with K_h and K_z being horizontal and vertical eddy diffusivities respectively.

Another approach [7] is to derive prognostic equations for the turbulent transport vector $\hat{\mathbb{C}}$ itself:

$$(7) \qquad \bar{\rho} \frac{\hat{d} \hat{\mathbb{C}}}{dt} = -\bar{\rho} [\hat{\mathbb{R}} \cdot \nabla \hat{c} + (\hat{\mathbf{v}} \nabla) \cdot \hat{\mathbb{C}}] + \nabla \cdot \overline{\rho c'' \mathbf{v}'' \mathbf{v}''} - \overline{\rho \frac{d\mathbf{v}}{dt} c''} - \overline{\rho \mathbf{v}'' \frac{dc}{dt}}$$

where we need, in addition, the set of hydrodynamic equations

$$\rho \frac{d\mathbf{v}}{dt} = \rho \mathbf{f} + \nabla \cdot \mathbb{F}$$

$$\bar{\rho} \frac{\hat{d} \hat{\mathbf{v}}}{dt} = \bar{\rho} \hat{\mathbf{f}} + \nabla \cdot [\overline{\mathbb{F}} + \bar{\rho} \hat{\mathbb{R}}]$$

and an equation for Reynolds' stress tensor $\bar{\rho} \hat{\mathbb{R}} = -\overline{\rho \mathbf{v}'' \mathbf{v}''}$, i.e.

$$(8) \qquad \bar{\rho} \frac{\hat{d} \hat{\mathbb{R}}}{dt} = -\bar{\rho} [\hat{\mathbb{R}} \cdot \nabla \hat{\mathbf{v}} + (\hat{\mathbf{v}} \nabla) \cdot \hat{\mathbb{R}}] + \nabla \cdot \overline{\rho \mathbf{v}'' \mathbf{v}'' \mathbf{v}''} - \overline{\rho \frac{d\mathbf{v}}{dt} \mathbf{v}''} - \overline{\rho \mathbf{v}'' \frac{d\mathbf{v}''}{dt}}$$

Closure assumptions are required with regard to the third moments (parametrization) or with regard to higher moments if new prognostic equations for these are derived. Such attempts proved to be quite promising but will not be followed in this paper, instead, conventional K-theory will be applied.

Disregarding relative motion of pollution ($\mathbf{v}_{rel} \equiv 0$), Eq. (5) reads

$$\frac{\partial \bar{\rho} \hat{c}}{\partial t} + \nabla \cdot \bar{\rho} \hat{c} \hat{\mathbf{v}} = \bar{\rho} \frac{\hat{d} \hat{c}}{dt} = \nabla \cdot \hat{\mathbb{C}} + \bar{\rho} (q_1 + q_2) - \lambda \bar{\rho} \hat{c}$$

Since within the planetary boundary layer Boussinesq' approximation ($\nabla \cdot \hat{\mathbf{v}} \approx 0$, $\hat{d}\bar{\rho}/dt \approx 0$) holds, we can write

$$(9) \qquad \frac{\partial \hat{c}}{\partial t} + \nabla \cdot \hat{c}\hat{\mathbf{v}} = \frac{\partial \hat{c}}{\partial t} + \hat{\mathbf{v}} \cdot \nabla \hat{c} = \frac{\hat{d}\hat{c}}{dt} = \nabla \cdot \hat{\mathbf{c}} + (q_1 + q_2) - \lambda \hat{c}$$

$$\hat{\mathbf{c}} = -\overline{c''\mathbf{v}''} = \mathbb{K} \cdot \nabla \hat{c}$$

In the following, $\mathbf{R}$ is position vector in observers space and $\mathbf{R}'$ the same in source space. A given space domain is V with closed surface S . The position vectors on S are $\mathbf{R}_s$ and $\mathbf{R}_s'$ respectively.

Initial conditions for Eq. (5) are

$$(10) \qquad \hat{c}(\mathbf{R}, 0) = \hat{c}_0(\mathbf{R})$$

or, if an instantaneous point source is the only source in $\mathbf{R} = \mathbf{R}'$

$$(11) \qquad \lim_{t \to 0} [\hat{c}(\mathbf{R}, t)] = p\,\delta(\mathbf{R} - \mathbf{R}')$$

With regard to boundary conditions, Eq. (9) is integrated over the domain V and Green's theorem is applied:

$$(12) \qquad \frac{\partial}{\partial t}\left[\iiint dV \hat{c}\right] = \oiint dS(-\mathbf{n} \cdot [\hat{c}\hat{\mathbf{v}} - \hat{\mathbf{c}}]) + \iiint dV[(q_1 + q_2) - \lambda \hat{c}]$$

where $\mathbf{n}$ is the outer normal vector on S. The total amount of $\hat{c}$ in V increases if one has sufficient large sources q_1 and q_2 to compensate removal and if the total transport of $\hat{\mathbf{c}}$, i.e. $\hat{c}\hat{\mathbf{v}} - \hat{\mathbf{c}}$ has a negative value if integrated over S . Knowledge of the normal total transport across the surface S of the domain V, i.e. of $\mathbf{n} \cdot (\hat{c}\hat{\mathbf{v}} - \hat{\mathbf{c}})|_{\mathbf{R} = \mathbf{R}_s}$ establishes the necessary boundary condition on S. If there are sources (or sinks) on S we have inhomogeneous boundary conditions. The most general type of such boundary condition is given by

$$-\mathbf{n}\cdot[\alpha\hat{c}\hat{\mathbf{v}}-\beta\hat{c}]\Big|_{\mathbf{R}=\mathbf{R}_s} = q_s(\mathbf{R}_s,t) - A\hat{c}\Big|_{\mathbf{R}=\mathbf{R}_s} \tag{13}$$

allowing for simple absorption at the boundary with deposition velocity A.

We will show that the general initial - value and boundary - value problem (Eqs. (9), (10), and (13)) can be reduced to the solution of similar but homogeneous equations for Green's function [9], [10].

Green's function $G(\mathbf{R},t\,|\,\mathbf{R}',t')$ is singular at $t=t'$ and $\mathbf{R}=\mathbf{R}'$, i.e. it is a singular point source of unit source strength:

$$\lim_{t\to t'}\left[G(\mathbf{R},t\,|\,\mathbf{R}',t')\right] = \delta(\mathbf{R}-\mathbf{R}') \qquad : t \geqq t' \tag{14}$$

Moreover the principle of causality requires

$$G(\mathbf{R},t\,|\,\mathbf{R}',t') = 0 \qquad : t < t' \tag{15}$$

Further, there is a principle of reciprocity in a Lagrangian sense

$$G(\mathbf{R},t\,|\,\mathbf{R}',t') = G(\mathbf{R}',-t'\,|\,\mathbf{R},-t) \tag{16}$$

with

$$\frac{\partial G}{\partial t} + \hat{\mathbf{v}}\cdot\nabla G = \frac{\hat{d}G}{dt} = -\frac{\hat{d}G}{dt'} = -\left(\frac{\partial G}{\partial t'} + \hat{\mathbf{v}}\cdot\nabla' G\right) \tag{17}$$

where the distinction between differentiation in observers space and that in source space, i. e.

$$\nabla \equiv \frac{\partial}{\partial \mathbf{R}} \quad , \quad \nabla' \equiv \frac{\partial}{\partial \mathbf{R}'}$$

have been made. According to Eq. (17) the principle of reciprocity is fulfilled if source - point and observers point are connected by a trajectory of fluid motion. Therefore, in this context time reversal means reversal of the fluid motion, i.e. of the trajectory. The situation here is much more complex as it is in case of diffusion (or heat conduction) in resting media.

In addition to the already mentioned properties of Green's function, Eqs. (14) to (17), it is assumed that G fulfills to a certain extent the same parabolic diffusion equation as $\hat{c}$ does:

$$\frac{\hat{d}G}{dt} = \frac{\partial G}{\partial t} + \hat{\mathbf{v}}\cdot\nabla G = \nabla\cdot\mathbb{G} + \delta(\mathbf{R}-\mathbf{R}')\,\delta(t-t') - \lambda G \quad , \tag{18}$$

where

$$\mathbb{G} = \mathbb{K}\cdot\nabla G \qquad (\mathbb{K}\text{ symmetric}), \tag{19}$$

together with homogeneous boundary conditions on S. We will prove later that in case of boundary condition Eq. (13) for concentration, Green's function should fulfill the homogeneous boundary condition

$$-\mathbf{n}\cdot\left[(\alpha-\beta)G\hat{\mathbf{v}} - \beta\mathbb{G}\right]\Big|_{\mathbf{R}=\mathbf{R}_s} = -AG\Big|_{\mathbf{R}=\mathbf{R}_s} \tag{20}$$

The principle of causality is a trivial one. It follows from Eq. (14), the definition of a singular point source. The principle of reciprocity requires special attention. Utilizing Eq. (18) for $G(\mathbf{R},t|\mathbf{R}',t')$ as well as for $G^* = G(\mathbf{R},-t|\mathbf{R}'',-t'')$, where time t'' should be within the region of the following integration over time, one obtains the set of equations

$$\frac{\hat{d}G}{dt} = \nabla\cdot\mathbb{G} + \delta(\mathbf{R}-\mathbf{R}')\,\delta(t-t') - \lambda G$$

$$-\frac{\hat{d}G^*}{dt} = \nabla\cdot\mathbb{G}^* + \delta(\mathbf{R}-\mathbf{R}'')\,\delta(t-t'') - \lambda G^*$$

Now, multiply the first of these by G^* and the second by G, subtract, and integrate over the domain V and over time from $-(t'+\Delta t)$

to $t'+\varepsilon$. By virtue of Eq. (19) we have

$$G^*\nabla\cdot\mathbb{G} - G\nabla\cdot\mathbb{G}^* = \nabla\cdot[G^*\mathbb{G} - G\mathbb{G}^*]$$

and therefore, using in addition Green's theorem,

$$\int_{-(t'+\Delta t)}^{t'+\varepsilon} dt \iiint dV \frac{\hat{d}GG^*}{dt} = \int_{-(t'+\Delta t)}^{t'+\varepsilon} dt \oiint dS\, \mathbf{n}\cdot[G^*\mathbb{G} - G\mathbb{G}^*] + \int_{-(t'+\Delta t)}^{t'+\varepsilon} dt \iiint dV G^*\delta(\mathbb{R}-\mathbb{R}')\delta(t'-t) -$$

$$- \int_{-(t'+\Delta t)}^{t'+\varepsilon} dt \iiint dV G\, \delta(\mathbb{R}-\mathbb{R}'')\delta(t''-t)$$

(It should be noted that the removal term $-\lambda G$ does not contribute to the preceeding equation).

Now,

$$\int_{-(t'+\Delta t)}^{t'+\varepsilon} dt \iiint dV\, G(\mathbb{R},-t\,|\,\mathbb{R}'',-t'')\,\delta(\mathbb{R}-\mathbb{R}')\,\delta(t'-t)$$

$$= \int_{-(t'+\Delta t)}^{t'+\varepsilon} dt\, G(\mathbb{R}',-t\,|\,\mathbb{R}'',-t'')\,\delta(t'-t) = G(\mathbb{R}',-t'\,|\,\mathbb{R}'',-t'') \quad .$$

An analogous expression holds for the last integral on the right hand side. Utilizing the homogeneous boundary condition Eq. (20) ($\beta \neq 0$) for both G and G^*, it is seen immediately that the first integral on the right hand side vanishes. Therefore, we have up to now

$$\int_{-(t'+\Delta t)}^{t'+\varepsilon} dt \iiint dV \frac{\hat{d}GG^*}{dt} = G(\mathbb{R}',-t'\,|\,\mathbb{R}'',-t'') - G(\mathbb{R}'',t''\,|\,\mathbb{R}',t')$$

The principle of reciprocity would be fulfilled if the left hand side of this equation would vanish. For fixed domain V we interchange the order of integration and write

$$\iiint dV \int_{-(t'+\Delta t)}^{t'+\varepsilon} dt \frac{\hat{d}GG^*}{dt} = \iiint dV\, GG^*\Big|_{t'+\varepsilon} - \iiint dV\, GG^*\Big|_{-(t'+\Delta t)} \quad ,$$

where integration along fluid trajectories has been performed. Now, from the principle of causality, Eq. (15),

$$G''\big|_{t'+\varepsilon} = G(\mathbb{R},-t|\mathbb{R}'',-t'')\big|_{t=t'+\varepsilon} = G(\mathbb{R},-(t'+\varepsilon)|\mathbb{R}'',-t'') = 0 \quad \text{since } t'' < t'+\varepsilon$$

and

$$G\big|_{-(t'+\Delta t)} = G(\mathbb{R},t|\mathbb{R}',t')\big|_{t=-(t'+\Delta t)} = G(\mathbb{R},-(t'+\Delta t)|\mathbb{R}',t') = 0 \quad \text{since } -(t'+\Delta t) < t'$$

Therefore, the principle of reciprocity is proved in Lagrangian interpretation.

We now show that Green's function solves the inhomogeneous initial-value and boundary-value problem, Eqs. (9), (10), and (13), for concentration $\hat{c}$. Writing these equations again

(9) $$\frac{\hat{d}\hat{c}}{dt} = \nabla\cdot\hat{\mathbf{c}} + q(\mathbb{R},t) - \lambda\hat{c}$$

(10) $$\hat{c}(\mathbb{R},0) = \hat{c}_o(\mathbb{R})$$

(13) $$-\mathbf{n}\cdot[\alpha\hat{c}\hat{\mathbf{v}} - \beta\hat{\mathbf{c}}]\big|_{\mathbb{R}=\mathbb{R}_s} = q_s(\mathbb{R}_s,t) - A\hat{c}\big|_{\mathbb{R}=\mathbb{R}_s}$$

the corresponding homogeneous problem for Green's function is given by Eqs. (18) and (20), i.e. by

(18) $$\frac{\hat{d}G}{dt} = \nabla\cdot\mathbb{G} + \delta(\mathbb{R}-\mathbb{R}')\,\delta(t-t') - \lambda G$$

(20) $$-\mathbf{n}\cdot[(\alpha-\beta)G\hat{\mathbf{v}} - \beta\mathbb{G}]\big|_{\mathbb{R}=\mathbb{R}_s} = -AG\big|_{\mathbb{R}=\mathbb{R}_s}$$

Formulating Eqs. (9) and (18) in source-space and utilizing Eq. (17), this leads to

$$\frac{\hat{d}\hat{c}}{dt'} = \nabla'\cdot\hat{\mathbf{c}}' + q(\mathbb{R}',t') - \lambda\hat{c} \qquad ; \ \hat{c} = \hat{c}(\mathbb{R}',t') \qquad ; \ \hat{\mathbf{c}}' = \mathbb{K}\cdot\nabla'\hat{c}$$

$$-\frac{\hat{d}G}{dt'} = \nabla'\cdot\mathbb{G}' + \delta(\mathbb{R}'-\mathbb{R})\,\delta(t'-t) - \lambda G \quad ; \ G = G(\mathbb{R},t|\mathbb{R}',t') \ ; \ \mathbb{G}' = \mathbb{K}\cdot\nabla' G$$

Multiply the first of these by G and the second by $\hat{c}$, subtract, integrate over the domain V and over time from 0 to $t+\varepsilon$, and further use Green's theorem, it follows successively

$$\frac{\hat{d}G\hat{c}}{dt'} = \nabla'\cdot[G\hat{\mathbf{c}}' - \hat{c}\mathbf{G}'] + Gq - \hat{c}\,\delta(\mathbf{R}'-\mathbf{R})\,\delta(t'-t)$$

$$\frac{\partial G\hat{c}}{\partial t'} + \nabla'\cdot[G\hat{c}\hat{\mathbf{v}} - G\hat{\mathbf{c}}' + \hat{c}\mathbf{G}'] = Gq - \hat{c}\,\delta(\mathbf{R}'-\mathbf{R})\,\delta(t'-t)$$

$$\iiint dV'\frac{\partial G\hat{c}}{\partial t'} + \oiint dS'\mathbf{n}\cdot[G\hat{c}\hat{\mathbf{v}} - G\hat{\mathbf{c}}' + \hat{c}\mathbf{G}'] = \iiint dV'Gq - \hat{c}(\mathbf{R},t')\,\delta(t'-t)$$

$$\iiint dV'\int_0^{t+\varepsilon} dt'\frac{\partial G\hat{c}}{\partial t'} + \int_0^{t+\varepsilon} dt'\oiint dS'\mathbf{n}\cdot[G\hat{c}\hat{\mathbf{v}} - G\hat{\mathbf{c}}' + \hat{c}\mathbf{G}'] = \int_0^{t+\varepsilon} dt'\iiint dV'Gq - \hat{c}(\mathbf{R},t)$$

since

$$\int_0^{t+\varepsilon} dt'\frac{\partial G\hat{c}}{\partial t'} = G(\mathbf{R},t|\mathbf{R}',t+\varepsilon)\,\hat{c}(\mathbf{R}',t+\varepsilon) - G(\mathbf{R},t|\mathbf{R}',0)\,\hat{c}(\mathbf{R}',0) \quad .$$

The first term on the right hand side vanishes according to the principle of causality. One obtains

$$\begin{aligned}\hat{c}(\mathbf{R},t) = \iiint dV'G(\mathbf{R},t|\mathbf{R}',0)\,\hat{c}_o(\mathbf{R}') &+ \int_0^{t+\varepsilon} dt'\iiint dV'G(\mathbf{R},t|\mathbf{R}',t')\,q(\mathbf{R}',t') + \\ &+ \int_0^{t+\varepsilon} dt'\oiint dS'(-\mathbf{n}\cdot[G\hat{c}\hat{\mathbf{v}} - G\hat{\mathbf{c}}' + \hat{c}\mathbf{G}'])\end{aligned}$$

With regard to boundary conditions on S, the case $\beta \neq 0$ is considered first. Multiplying Eq. (13) by G and Eq. (20) by $\hat{c}$ (all formulated in source space) and subtracting both equations, one obtains

$$-\mathbf{n}\cdot[G\hat{c}\hat{\mathbf{v}} - G\hat{\mathbf{c}}' + \hat{c}\mathbf{G}']\Big|_{\mathbf{R}'=\mathbf{R}_s'} = \frac{1}{\beta}\,G(\mathbf{R},t|\mathbf{R}_s',t')\,q_s(\mathbf{R}_s',t')$$

In case $\beta = 0$ Eq. (13) reads

$$-\alpha\,\mathbf{n}\cdot\hat{\mathbf{v}}\hat{c}\Big|_{\mathbf{R}'=\mathbf{R}_s'} = q_s(\mathbf{R}_s',t')$$

and Eq. (20)

$$G\Big|_{\mathbb{R}'=\mathbb{R}_s'} = 0$$

provided $\mathbf{n}\cdot\hat{\mathbf{v}}\Big|_{\mathbb{R}'=\mathbb{R}_s'} \neq 0$. Therefore,

$$-\mathbf{n}\cdot[G\hat{c}\hat{\mathbf{v}} - G\hat{c}' + \hat{c}\,\mathbb{G}']\Big|_{\mathbb{R}'=\mathbb{R}_s'} = \frac{1}{\alpha}\,\frac{\mathbf{n}\cdot\mathbb{G}'}{\mathbf{n}\cdot\hat{\mathbf{v}}}\Big|_{\mathbb{R}'=\mathbb{R}_s'} q_s(\mathbb{R}_s',t')$$

The final solution of the quite general inhomogeneous initial- and boundary-value problem for concentration is now given in terms of Green's function as follows:

$$\boxed{\begin{aligned} \hat{c}(\mathbb{R},t) = {} & \iiint dV'\,G(\mathbb{R},t\,|\,\mathbb{R}',0)\,\hat{c}_0(\mathbb{R}') + \int_0^{t+\varepsilon} dt' \iiint dV'\,G(\mathbb{R},t\,|\,\mathbb{R}',t')\,q(\mathbb{R}',t') + \\ & + \begin{cases} \displaystyle\int_0^{t+\varepsilon} dt' \oiint dS'\,\frac{1}{\beta}\,G(\mathbb{R},t\,|\,\mathbb{R}_s',t')\,q_s(\mathbb{R}_s',t') & : \beta \neq 0 \\ \displaystyle\int_0^{t+\varepsilon} dt' \oiint dS'\,\frac{1}{\alpha}\,\frac{\mathbf{n}\cdot\mathbb{K}\cdot\nabla' G}{\mathbf{n}\cdot\hat{\mathbf{v}}}\Big|_{\mathbb{R}'=\mathbb{R}_s'} q_s(\mathbb{R}_s',t') & : \beta = 0 \end{cases} \end{aligned}} \tag{21}$$

The first term on the right hand side of Eq. (21) is the contribution to $\hat{c}(\mathbb{R},t)$ due to the initial condition, the second is due to the action of sources in space ($q(\mathbb{R}',t') = q_1(\mathbb{R}',t') + q_2(\mathbb{R}',t')$ with q_1 according to Eq. (3)), and the third is due to the special conditions at the boundary S. The coefficients α and β are allowed to be functions of $\mathbb{R}_s'$ and t' and kept under the integrals for this reason. It should be noted that the removal term appears in Eq. (18) but not in the final solution for $\hat{c}$.

The main result included in Eq. (21) is the following: Once the homogeneous boundary-value problem (Eqs. (18) and (20)) for Green's function has been solved, an unlimited number of general inhomogeneous initial-value and boundary-value problems for concentration $\hat{c}$ can be solved just by simple integrations. This fact is well known from the theory of heat conduction in solids [11], but it has been proved again in this section for turbulent diffusion within a moving fluid in a more rigorous manner as it was done in previous papers [9], [10].

This fact has been utilized in some Lagrangian models of turbulent diffusion [12] (puff models as well as plume models). A reason for this is the fact that instantaneous puffs or plumes have exactly the properties of Green's function and are solutions of similar parabolic diffusion equations as were utilized so far.

Concluding this section, some special cases of boundary conditions will be mentioned. In many cases the earth's surface is flat within the domain of transport and diffusion. Additionally a temperature inversion frequently is present in a certain height $\mathbf{z} = H$ above the ground ($\mathbf{z} = 0$). In such cases the kinematic boundary condition requires $\mathbf{n} \cdot \hat{\mathbf{v}} = \mathbf{k} \cdot \hat{\mathbf{v}} = 0$ ($\mathbf{z} = H$) and $\mathbf{n} \cdot \hat{\mathbf{v}} = -\mathbb{k} \cdot \hat{\mathbf{v}} = 0$ ($\mathbf{z} = 0$), $\mathbb{k}$ being the vertical unit vector. From Eq. (13) it follows

$$\beta\, \mathbf{k} \cdot \mathbb{K} \cdot \nabla \hat{c} \Big|_{z=H} = q_s(\mathbf{r}_s, H, t) - A\hat{c} \Big|_{z=H} \tag{22}$$

$$-\beta\, \mathbb{k} \cdot \mathbb{K} \cdot \nabla \hat{c} \Big|_{z=0} = q_s(\mathbf{r}_s, 0, t) - A\hat{c} \Big|_{z=0} \tag{23}$$

where absorption with deposition velocity A has been subtracted from the area source functions q_s utilizing the already mentioned most simple assumption regarding the mechanism of absorption at surfaces. Due to the definitions in the formulation of boundary conditions, $q_s > 0$ acts as a source for the interior of S. $q_s = -A\hat{c}$ ($A > 0$) indicates the fact that absorption at boundaries acts as a sink.

In all numerical solutions lateral boundaries are required since the domain of integration must be limited. This fact limits the applicability of numerical solutions of the general problem considerably. At lateral boundaries the horizontal transport of pollution by wind, and eventually even the turbulent transport, must be prescribed. The most simple case is given if lateral boundaries are far from regions of sources. Then, at these

$$-n_h \cdot \hat{v}_h \hat{c} \Big|_{\mathbf{R}=\mathbf{R}_s} = q_s(R_s, t) \tag{24}$$

i.e. import and export of air pollution by wind motion have to be known. Import from other regions on the luff side can eventually be obtained by measurements. Export to other regions is obtained by solution of Eq. (21) in which q_s principally is not known on the lee side of the region. This is true although Green's function can be constructed even for this case because it vanishes at lateral boundaries if boundary condition Eq. (24) is valid.

2. K - THEORY OF TURBULENT TRANSPORT AND DIFFUSION

Since modern approaches towards the solution of air pollution problems increasingly use the so called K - theory of turbulent diffusion in connection with numerical methods of solution we start with that theory.

It cannot be assumed that general solutions for irregular terrain are obtainable. Therefore, we consider only the case of flat terrain. If allowance is made for diverging or converging horizontal wind fields,

$$\nabla \cdot \hat{v} = \nabla_h \cdot \hat{v}_h + \frac{\partial \hat{v}_z}{\partial z} \approx 0$$

indicates that vertical motions do exist. These vertical motions eventually may penetrate temperature - inversion layers. Eq. (9) now reads as

$$\frac{\partial \hat{c}}{\partial t} + \hat{v}_h(\mathbf{r},z,t) \cdot \nabla_h \hat{c} + \hat{v}_z(\mathbf{r},z,t)\frac{\partial \hat{c}}{\partial z} = \nabla_h \cdot [K_h(\mathbf{r},z,t)\nabla_h \hat{c}\,] + \frac{\partial}{\partial z}\left[K_z(\mathbf{r},z,t)\frac{\partial \hat{c}}{\partial z}\right] + q(\mathbf{r},z,t) - \lambda(\mathbf{r},z,t)\hat{c} \quad , \tag{25}$$

the initial condition Eq. (10) as

$$\hat{c}(\mathbf{r},z,0) = \hat{c}_o(\mathbf{r},z)$$

and the boundary condition Eq. (22) generalized according to Eq. (13)

$$\left[(A - \alpha \hat{v}_z)\hat{c} + \beta K_z \frac{\partial \hat{c}}{\partial z}\right]_{z=H} = q_s(\mathbf{r}_s,H,t) \; ; \quad \begin{array}{l} A = A(\mathbf{r}_s,H,t) \\ \beta = \beta(\mathbf{r}_s,H,t) \end{array} \tag{26}$$

Further

$$\left[A\hat{c} - \beta K_z \frac{\partial \hat{c}}{\partial z}\right]_{z=0} = q_s(\mathbf{r}_s,0,t) \; ; \quad \begin{array}{l} A = A(\mathbf{r}_s,0,t) \\ \beta = \beta(\mathbf{r}_s,0,t) \end{array} \tag{27}$$

at the earth's surface, and

$$(24) \qquad -(n_h \cdot \hat{v}_h)\hat{c}\Big|_{\mathbf{R}=\mathbf{R}_s} = q_s(\mathbf{R}_s,t) \quad ; \quad n_h \cdot \hat{v}_h \neq 0$$

at lateral boundaries.

The corresponding system of equations for Green's function, Eqs. (18) and (20), is given by

$$(28) \qquad \frac{\partial G}{\partial t} + \hat{v}_h(\mathbf{r},z,t)\cdot\nabla_h G + \hat{v}_z(\mathbf{r},z,t)\frac{\partial G}{\partial z} = \nabla_h\cdot[K_h(\mathbf{r},z,t)\nabla_h G] +$$

$$+ \frac{\partial}{\partial z}\left[K_z(\mathbf{r},z,t)\frac{\partial G}{\partial z}\right] + \delta(\mathbf{r}-\mathbf{r}')\delta(z-z')\delta(t-t') - \lambda(\mathbf{r},z,t)G$$

$$(29) \qquad \left[(A-(\alpha-\beta)\hat{v}_z)G + \beta K_z\frac{\partial G}{\partial z}\right]_{z=H} = 0$$

$$(30) \qquad \left[AG - \beta K_z\frac{\partial G}{\partial z}\right]_{z=0} = 0$$

$$(31) \qquad G\Big|_{\mathbf{R}=\mathbf{R}_s} = 0$$

In full generality "only" the external parameters $\hat{v}_h$, $\hat{v}_z$, K_h, K_z, λ, should be known at all points in space and for all times $t > 0$. Parameters α, β and A should be known at all boundary points and also for all times $t > 0$ in order to find a solution of Eqs. (28) to (31) for Green's function. It is well known, however, that no closed analytical solution can be obtained if arbitrary external parameters are allowed.

The only possibility, at least in principle, is provided by means of numerical methods. However, there are serious problems involved in this context: 1. It is difficult to represent the singularity of Green's function in a numerical scheme. 2. It is difficult to conserve the total (unit) amount of injected mass of air pollution. 3. In many numerical schemes artificial diffusion is produced and hardly can be controlled. Points 2. and 3. also are valid if the problem Eqs. (24) to (27) is solved directly by numerical integration [13], [14]. Although such attempts are much promising in the future, computing time on existing large and fast computers is unrealistic high even if relatively simple models are used. We will not follow these lines of research in this paper. Instead, it will be attempted to investigate methods of mixed analytical - numerical kind.

In all what follows, main attention is paid, as was mentioned in the introduction, to nonstationary problems, to cases with weak wind or even windless conditions, and to cases with time dependent heights of temperature inversion layers. Therefore, turbulent diffusion in the direction of the momentary wind vector cannot be disregarded.

3. GREEN's FUNCTION FOR MODELS THAT ARE SIMPLE WITH REGARD TO METEOROLOGICAL CONDITIONS

It seems that analytical solutions of the general problem are feasible only under simplifying assumptions with regard to the set of external parameters. We shall consider first the case of constant coefficients. Special assumptions are the following:

1. Homogeneous wind field: $\nabla_h \hat{v}_h \equiv 0$, $\hat{v}_z = 0$, i.e. straight trajectories (streamlines) which are equally spaced. This wind field is assumed not to change with time during a time interval $t_{n+1} - t_n = \Delta t_n$. However, it should be allowed that there are discontinuous changes from one time interval to the next one. Therefore, $\hat{v}_h = \hat{v}_h(t) = \hat{v}_h(t_n) = const$: $t_n < t < t_{n+1}$.

2. The same is assumed to be valid for all other parameters: $\{K_h, K_z, A, H\} \equiv \psi = \psi(t) = \psi(t_n) = const$: $t_n < t < t_{n+1}$.

The time sequence in Green's function $G(\mathbf{R},t|\mathbf{R}',t')$ is given by $t_{n+1} \geqq t > t' \geqq t_n$. We will see that the structure of Green's function makes it easy to change the meteorological parameters during the calculation from one finite time interval to the next one.

According to Eqs. (28) to (31) we find

$$\frac{\partial G}{\partial t} + \hat{v}_h(t_n) \cdot \nabla_h G = K_h(t_n) \nabla_h^2 G + K_z(t_n) \frac{\partial^2 G}{\partial z^2} + \delta(\mathbf{r}-\mathbf{r}')\delta(z-z')\delta(t-t') - \lambda(t_n) G \tag{32}$$

$$A(H,t_n) G + \beta(H,t_n) K_z(t_n) \left.\frac{\partial G}{\partial z}\right|_{z=H(t_n)} = 0 \tag{33}$$

$$A(0,t_n) G - \beta(0,t_n) K_z(t_n) \left.\frac{\partial G}{\partial z}\right|_{z=0} = 0 \tag{34}$$

assuming an infinite domain in horizontal direction.

In what follows we will omit the argument t_n and will put $A(H,t_n) = A$ $\beta(H,t_n) = \beta_H$, and $A(0,t_n) = A_0$, $\beta(0,t_n) = \beta_0$. Solutions can be found by various methods of mathematical physics. One possibility is, first to apply two-dimensional Fourier-integral transformation with respect to $\mathbf{r}$, secondly to apply Laplace transformation with respect to time t , and then solve the remaining boundary-value problem in z by conventional methods, or even with integral transformations again.

The structure of Eq. (32) allows, however, application of the simple method of separation that splits Green's function according to

$$G(\mathbf{R},t\,|\,\mathbf{R}',t') = G_h(\mathbf{r},t\,|\,\mathbf{r}',t')\,G_z(z,t\,|\,z',t') \tag{35}$$

into two separate functions. We now find

$$\frac{\partial G_h}{\partial t} + \hat{v}_h \cdot \nabla_h G_h = K_h \nabla_h^2 G_h + \delta(\mathbf{r}-\mathbf{r}')\,\delta(t-t') - \lambda G_h \tag{36}$$

and

$$\frac{\partial G_z}{\partial t} = K_z \frac{\partial^2 G_z}{\partial z^2} + \delta(z-z')\,\delta(t-t') \tag{37}$$

with

$$\begin{aligned} A_H G_z + \beta_H K_z \frac{\partial G_z}{\partial z}\bigg|_{z=H} &= 0 \\ A_0 G_z - \beta_0 K_z \frac{\partial G_z}{\partial z}\bigg|_{z=0} &= 0 \end{aligned} \tag{38}$$

It is easy to prove (by means of the above mentioned integral transformations or by direct verification), that for the unbounded domain Green's function G_h is given by

$$(39)\quad G_h(\mathbf{r},t|\mathbf{r}',t') = \exp[-\lambda(t-t')]\,\frac{\exp\left[-\dfrac{\{(\mathbf{r}-\mathbf{r}')-\hat{\mathbf{v}}_h(t-t')\}^2}{4K_h(t-t')}\right]}{4\pi K_h(t-t')} = G_h(\mathbf{r}-\mathbf{r}',t-t')$$

It should be mentioned that this solution fulfills both, the principle of causality as well as the principle of reciprocity (Eqs. (15), (16), and (17)).

Green's function $G_z(z,t|z',t')$ is well known from the theory of conduction of heat in solids [11] (see also [9], [10]). We find

$$(40)\quad G_z(z,t|z',t') = \sum_{n=1}^{\infty} Z_n(z)\,Z_n(z')\,\exp[-K_z\alpha_n^2(t-t')]$$

where

$$(41)\quad Z_n(z) = \frac{\sqrt{2(\beta_H^2K_z^2\alpha_n^2+A_H^2)}\,\{\beta_o K_z\alpha_n\cos\alpha_n z + A_o\sin\alpha_n z\}}{\sqrt{(\beta_o^2K_z^2\alpha_n^2+A_o^2)[H(\beta_H^2K_z^2\alpha_n^2+A_H^2)+\beta_H K_z A_H]+\beta_o K_z A_o(\beta_H^2K_z^2\alpha_n^2+A_H^2)}}$$

and $\pm\alpha_n$, $n = 1,2,\cdots$ are the roots of

$$(42)\quad \tan[\alpha H] = \alpha\,\frac{\beta_o K_z A_H + \beta_H K_z A_o}{\beta_o\beta_H K_z^2\alpha^2 - A_o A_H}$$

If there is no absorption at the boundaries ($A_o = A_H = 0$) a term $1/H$ is to be added to Eq. (40). In this special case

$$Z_n(z) = \sqrt{\frac{2}{H}}\cos\left(\frac{n\pi}{H}z\right) \quad ; \quad \alpha_n = \frac{n\pi}{H}\,,\ n = 1,2,\cdots$$

and

$$G_z(z,t|z',t') = \frac{1}{H}\left\{1 + 2\sum_{n=1}^{\infty}\cos\left(\frac{n\pi}{H}z\right)\cos\left(\frac{n\pi}{H}z'\right)\exp\left[-\left(\frac{n\pi}{H}\right)^2K_z(t-t')\right]\right\}$$

$$= \frac{1}{H}\left\{1 + \sum_{n=1}^{\infty}\left(\cos\frac{n\pi}{H}(z-z') + \cos\frac{n\pi}{H}(z+z')\right)\exp\left[-\left(\frac{n\pi}{H}\right)^2K_z(t-t')\right]\right\}$$

$$(43)\quad G_z(z,t|z',t') = \frac{1}{2H}\left\{\Theta_3\left(\frac{z-z'}{2H},K_z\frac{t-t'}{H^2}\right) + \Theta_3\left(\frac{z+z'}{2H},K_z\frac{t-t'}{H^2}\right)\right\}$$

with Jacobi's third Theta function

$$\Theta_3(z,t) = 1 + 2\sum_{n=1}^{\infty} \cos(2\pi n z)\exp[-(\pi n)^2 t] \tag{44}$$

$$= \frac{1}{\sqrt{\pi t}} \sum_{n=-\infty}^{\infty} \exp\left[-\frac{(z+n)^2}{t}\right]$$

Multiplying Eqs. (39) and (40) one obtains Green's function for a quite general boundary-value problem (Eqs. (32) to (34)), i.e.

$$G(\mathbf{R},t|\mathbf{R}',t') = \frac{\exp\left[-\frac{((\mathbf{r}-\mathbf{r}')-\hat{\mathbf{v}}_h(t-t'))^2}{4K_h(t-t')}\right]}{4\pi K_h(t-t')} \sum_{n=1}^{\infty} Z_n(z) Z_n(z') \exp[-(K_z\alpha_n^2+\lambda)(t-t')] \tag{45}$$

It is well known that the series converges rapidly. Therefore, it is no serious problem to calculate G on a desk computer.

The case of windless conditions causes no trouble. Putting $\hat{\mathbf{v}}_h \equiv 0$ in Eq. (45), this just simplifies the computations. Therefore, if a homogeneous wind field during time interval Δt_n dies out, during time interval Δt_{n+1} $\hat{\mathbf{v}}_h$ is put equal to zero together with changes of the other external parameters.

It might have been strange to carry along coefficients $\beta(H,t_n)$ and $\beta(0,t_n)$ in the boundary conditions. With this it was intended to take care of the fact that at the earth's surface as well as at the upper temperature inversion turbulent diffusivity gradually approaches zero. Here, it is assumed that K_z is constant with height but assumes smaller values ($\beta < 0$) almost discontinuously at the boundaries.

If Eq. (45), i.e. Green's function, is introduced into Eq. (21) one obtains ($t_{n+1} > t > t_n$)

$$\begin{aligned}\hat{c}(\mathbf{r},z,t) = & \iint_{-\infty}^{\infty} d\mathbf{r}' \int_0^H dz' G_h(\mathbf{r},t|\mathbf{r}',t_n)\, G_z(z,t|z',t_n)\, \hat{c}(\mathbf{r}',z',t_n) + \\ & + \int_{t_n}^{t+\varepsilon} dt' \iint_{-\infty}^{\infty} d\mathbf{r}' \int_0^H dz' G_h(\mathbf{r},t|\mathbf{r}',t')\, G_z(z,t|z',t')\, q(\mathbf{r}',z',t') + \\ & + \int_{t_n}^{t+\varepsilon} dt' \iint_{-\infty}^{\infty} d\mathbf{r}_s' \frac{1}{\beta_0} G_h(\mathbf{r},t|\mathbf{r}_s',t')\, G_z(z,t|0,t')\, q_s(\mathbf{r}_s',0,t') + \\ & + \int_{t_n}^{t+\varepsilon} dt' \iint_{-\infty}^{\infty} d\mathbf{r}_s' \frac{1}{\beta_H} G_h(\mathbf{r},t|\mathbf{r}_s',t')\, G_z(z,t|H,t')\, q_s(\mathbf{r}_s',H,t')\end{aligned} \tag{46}$$

The computational procedure is the following: During time interval $t_1 > t \geqq 0$ initial condition $\hat{c}(\mathbf{r},z,0)$ is assumed to be known. The same should be true for all source functions in space and at the boundaries. These are functions of time within $[0,t_1]$. By selecting all external parameters $\hat{v}_h$, K_h, K_z, λ, A_0, β_0, A_H, H, and β_H, taken to be constant during time interval $[0,t_1]$, Green's function, Eq. (45), is known. Then, Eq. (46) predicts concentration in space as a function of time. Especially, of course, for time $t = t_1$ when it seems to be necessary to take care of time changes of all (or some) external parameters. Then, $\hat{c}(\mathbf{r},z,t_1)$ is initial condition for next time step, the new Green's function is easily obtained, and by virtue of Eq. (46) the continuation of diffusion process is simulated until at time $t = t_2$ a further correction of external parameters seems to be necessary. Since meteorological conditions often show persistent behaviour, in many cases only a few of such steps are needed to take care of nonstationary meteorological conditions. On the other hand, the changes in time of source functions belong to a much smaller time scale (especially during one day in winter time). These changes are taken care of analytically and continuously with regard to time.

The only computational difficulty occurs in the first term on the right hand side of Eq. (46). There, integration is performed over initial condition $\hat{c}(\mathbf{r},z,t_n)$ which is not obtainable in terms of continuous functions. Even if with $\hat{c}(\mathbf{r},z,0) = 0$ and analytical solutions of the remaining integrals in Eq. (46) a continuous solution is obtained, the first integral on the right hand side of Eq. (46) certainly has to be solved numerically if the solution for the next time step is desired.

There are circumstances in which integrations in Eq. (46) can be carried out analytically. First, consider point sources in space. At $\mathbf{r} = \mathbf{r}_m$ and $z = z_m$ (effective stack height) the time-dependent source strength may be a function of time. According to Eq. (3) the contribution of M such sources to space sources is given by

$$q_1(\mathbf{r},z,t) = \sum_{m=1}^{M} p_m(t)\,\delta(\mathbf{r}-\mathbf{r}_m)\,\delta(z-z_m)\ . \tag{47}$$

If only these sources were present, the second integral on the right hand side of Eq. (46) reads

$$\begin{aligned}
&\sum_{m=1}^{M} \int_{t_n}^{t+\varepsilon} dt'\, p_m(t') \iint_{-\infty}^{\infty} d\mathbf{r}' \int_{0}^{H} dz'\, G_h(\mathbf{r},t|\mathbf{r}',t')\, G_z(z,t|z',t')\, \delta(\mathbf{r}'-\mathbf{r}_m)\,\delta(z'-z_m) \\
(48)\quad &= \sum_{m=1}^{M} \int_{t_n}^{t+\varepsilon} dt'\, p_m(t')\, G_h(\mathbf{r},t|\mathbf{r}_m,t')\, G_z(z,t|z_m,t') \\
&= \sum_{m=1}^{M} \sum_{n=1}^{\infty} Z_n(z) Z(z_m) \int_{t_n}^{t+\varepsilon} dt'\, p_m(t')\, \exp[-(K_z\alpha_n^2+\lambda)(t-t')]\, \frac{\exp\left[-\dfrac{((\mathbf{r}-\mathbf{r}_m)-\hat{v}_h(t-t'))^2}{4K_h(t-t')}\right]}{4\pi K_h(t-t')}
\end{aligned}$$

In most urban air pollution problems a number M of individual point sources is known with respect to their location $\mathbf{r}_m$, their physical height h_m, and with respect to source strength $p_m(t)$. Other parameters of the stack together with meteorological parameters that are relevant for transport and diffusion determine plume rise Δh_m. Therefore, effective stack height z_m is calculated in a subroutine for each individual stack.

In principle, it is possible to solve the convolution integral in Eq. (48) analytically under certain circumstances, i.e. constant source strengths $p_m(t) = p_m = \text{const} : t_{n+1} > t > t_n$. However, numerical integration proved to be much more convenient, and, in addition, faster with regard to computing time.

Another possibility to integrate terms in Eq. (46) analytically exists if the boundary sources (area sources) are assumed to be constant within small areas of a cartesian grid with grid distances $\Delta x_s = x_{i+1} - x_i$ and $\Delta y_s = y_{j+1} - y_j$. Let $\mathbf{r}_s(i,j)$ be position vector to point $x_s = x_i$, $y_s = y_j$, then $q_{ij}(t)$ is mean area source strength of the small area $(\Delta x_s \, \Delta y_s)_{i,j}$. Taking for example the lower boundary condition (at the earth's surface) one obtains

$$\begin{aligned}
&\int_{t_n}^{t+\varepsilon} dt' \iint_{-\infty}^{\infty} d\mathbf{r}_s' \frac{1}{\beta_0} G_h(\mathbf{r},t \mid \mathbf{r}_s',t')\, G_z(z,t \mid 0,t')\, q_s(\mathbf{r}_s',0,t) = \\
&= \sum_{n=1}^{\infty} Z_n(z) Z_n(0) \sum_{i=-\infty}^{\infty} \sum_{j=-\infty}^{\infty} \int_{t_n}^{t+\varepsilon} dt' \frac{1}{\beta_0} q_{ij}(t') \frac{\exp[-(K_z\alpha_n^2+\lambda)(t-t')]}{4\pi K_h(t-t')} \times \\
&\qquad \times \int_{x_i}^{x_{i+1}} dx_s' \int_{y_j}^{y_{j+1}} dy_s' \exp\left[-\frac{((x-x_s')-U(t-t'))^2+((y-y_s')-V(t-t'))^2}{4K_h(t-t')}\right] \\
&= \sum_{n=1}^{\infty} Z_n(z) Z_n(0) \sum_{i=-\infty}^{\infty} \sum_{j=-\infty}^{\infty} \int_{t_n}^{t+\varepsilon} dt' \frac{1}{\beta_0} q_{ij}(t') \exp[-(K_z\alpha_n^2+\lambda)(t-t')] \times \\
&\times \frac{1}{4}\left\{\operatorname{erf}\left[\frac{x-x_i-U(t-t')}{\sqrt{4K_h(t-t')}}\right] - \operatorname{erf}\left[\frac{x-x_{i+1}-U(t-t')}{\sqrt{4K_h(t-t')}}\right]\right\}\left\{\operatorname{erf}\left[\frac{y-y_j-V(t-t')}{\sqrt{4K_h(t-t')}}\right] - \operatorname{erf}\left[\frac{y-y_{j+1}-V(t-t')}{\sqrt{4K_h(t-t')}}\right]\right\}
\end{aligned} \tag{49}$$

It should be noted that in case of $q_{ij} = \text{const}$ during time interval $[t_n, t_{n+1}]$ integration over time also can be performed.

In urban air pollution problems it proved reasonable to divide area sources into small areas of just that kind mentioned above [1], [2], [3]. Apart from the assumption of Fickian diffusion (constant diffusivities), the model developed here (Eq. (46) with Eqs. (45), (48), and (49)) is a considerable extension of existing urban air pollution models. It provides not only for realistic incorporation of time dependent external parameters but describes many other effects that are important from a practical point of view. It may be mentioned again that windless conditions can be approached continuously within certain periods of integration over time, and, further, that removal within the atmosphere as well as at the upper and lower boundary can be taken into account. Finally, there are several possibilities available for model calibration, i.e. parameters like $\beta(H,t)$ and $\beta(0,t)$, and also $A(H,t)$ and $A(0,t)$ can be used for this purpose.

The usefulness of such a generalized urban air pollution model has not been investigated so far. In the author's opinion, the precise incorporation of source properties (geometrical configuration, time-dependent behaviour) together with large-scale changes of meteorological parameters ($\hat{v}_h, K_h, K_z, H$) seem to have main influences on the concentration fields. Contrary to this statement, refined incorporation of boundary layer properties (e.g. vertical wind profile) but poor representation of the above mentioned properties seem to be less advantageous. In addition, the problem becomes very complex as will be seen in the next section.

4. METEOROLOGICAL CONDITIONS THAT ARE HORIZONTAL HOMOGENEOUS BUT VARY WITH HEIGHT

A generalization of boundary value problem Eqs. (32) to (34) with regard to height-dependent meteorological parameters is the following:

$$\frac{\partial G}{\partial t} + \hat{\mathbf{v}}_h(z,t_n)\cdot\nabla_h G = K_h(z,t_n)\nabla_h^2 G + \frac{\partial}{\partial z}\left[K_z(z,t_n)\frac{\partial G}{\partial z}\right] + \delta(\mathbf{r}-\mathbf{r}')\delta(z-z')\delta(t-t') - \lambda(z,t_n)G \tag{50}$$

$$A(H,t_n)G\Big|_{z=H(t_n)} + \beta(H,t_n)\left[K_z(z,t_n)\frac{\partial G}{\partial z}\right]_{z=H(t_n)} = 0 \tag{51}$$

$$A(0,t_n)G\Big|_{z=0} - \beta(0,t_n)\left[K_z(z,t_n)\frac{\partial G}{\partial z}\right]_{z=0} = 0 \tag{52}$$

It is seen immediately that separation of variables is not possible due to the fact that we have height-dependent coefficients. There are, however, methods for reducing the above stated problem to simpler ones. The first one to be mentioned here is the method of integral-transformation.

Applying Fourier's integral transformation first, one obtains with the pair of transformation relationships

$$\widetilde{G} = \iint_{-\infty}^{\infty} d\mathbf{r}\, e^{-i\mathbf{k}\cdot\mathbf{r}}\, G \quad ; \quad G = \frac{1}{(2\pi)^2}\iint_{-\infty}^{\infty} d\mathbf{k}\, e^{i\mathbf{r}\cdot\mathbf{k}}\, \widetilde{G} \tag{53}$$

and with

$$\widetilde{\nabla_h G} = -i\mathbf{k}\widetilde{G} \quad ; \quad \widetilde{\nabla_h^2 G} = \mathbf{k}^2\widetilde{G} \quad ; \quad \widetilde{\delta(\mathbf{r}-\mathbf{r}')} = e^{-i\mathbf{k}\cdot\mathbf{r}'}$$

$$\frac{\partial\widetilde{G}}{\partial t} - \left[i\mathbf{k}\cdot\hat{\mathbf{v}}_h(z,t_n) + \mathbf{k}^2 K_h(z,t_n) - \lambda(z,t_n)\right]\widetilde{G} = \frac{\partial}{\partial z}\left[K_z(z,t_n)\frac{\partial\widetilde{G}}{\partial z}\right] + e^{-i\mathbf{k}\cdot\mathbf{r}'}\delta(z-z')\delta(t-t') \tag{54}$$

With regard to time, Laplace's integral transformation, especially the two-sided transformation [15], can be applied only, if meteorological parameters are constant with regard to time. In that special case the pair of transformation relationships is given by

$$\begin{aligned} \bar{G} &= p\int_{-\infty}^{\infty} dt\, e^{-pt}\, G && : \alpha < \operatorname{Re} p < \beta \\ G &= \frac{1}{2\pi i}\int_{c-i\infty}^{c+i\infty} dp\, e^{pt}\, \frac{\bar{G}}{p} && : \alpha < c < \beta \quad , \end{aligned} \tag{55}$$

further

$$\overline{\frac{\partial G}{\partial t}} = p\bar{G} \quad ; \quad \overline{\delta(t)} = p$$

Transforming Eq. (54) in this manner one obtains instead

$$\frac{d}{dz}\left[K_z(z)\frac{d\tilde{\bar{G}}}{dz}\right] + \left\{ i\mathbf{k}\cdot\hat{\mathbf{v}}_h(z) + \mathbf{k}^2 K_h(z) - \lambda(z) - p \right\}\tilde{\bar{G}} = \\ = p\exp\left[-(i\mathbf{k}\cdot\mathbf{r}' + pt')\right]\delta(z-z') \tag{56}$$

Even in this much simplified version the solution of a highly complicated Sturm - Liouville problem has to be found which is given by the self - adjoint Liouville equation Eq. (56) together with the transformed boundary conditions, Eqs. (51) and (52). For special cases classes of analytical solutions can be obtained. These, however, are too complicated to be transformed back from $\mathbf{k}, p$ - space to $\mathbf{r}, t$ - space. Therefore, numerical solutions of Eq. (54), obeying the transformed boundary conditions, for a sufficient large number of wave - number vectors $\mathbf{k}$ is the only possibility to construct Green's function for the domain under consideration.

It is interesting to observe that several other methods of solution end almost all at the same point, i.e. at a Sturm - Liouville - problem. We will demonstrate this by means of two more examples.

First, we investigate the so called spectral method. Consider a finite domain and an orthonormal set of eigenfunctions $F_{\mathbf{k}}(\mathbf{r})$ that fulfills lateral boundary conditions. Furthermore, the condition of orthonormality

$$\iint d\mathbf{r}\, F_k(\mathbf{r})\, F_j^*(\mathbf{r}) = \overline{F_k F_j^*} = \delta_{kj} \quad ; \qquad F^*: \text{conjugate complex}$$

holds for each two members of the set.

Expanding $G = \Sigma F_k(\mathbf{r})\, G_k \equiv F_k G_k$ (summation convention)

and $\delta(\mathbf{r}-\mathbf{r}') = \Sigma\, \gamma_k F_k(\mathbf{r})\, F_k^*(\mathbf{r}') = \gamma_k F_k F_k^*$,

further, multiplying Eq. (50) by F_j^*, and integrating over the finite domain leads to

$$\overline{F_j^* F_k}\, \frac{\partial G_k}{\partial t} + \hat{v}_h \cdot \overline{F_j^* \nabla_h F_k}\, G_k = K_h\, \overline{F_j^* \nabla_h^2 F_k}\, G_k + \overline{F_j^* F_k}\, \frac{\partial}{\partial z}\left[K_z \frac{\partial G_k}{\partial z}\right] +$$
$$+ \overline{\gamma_k F_j^* F_k F_k'^*}\, \delta(z-z')\delta(t-t') - \lambda\, \overline{F_j^* F_k}\, G_k$$

or

$$\frac{\partial G_j}{\partial t} + \left\{\hat{v}_h \cdot \overline{F_j^* \nabla_h F_k} - K_h \overline{F_j^* \nabla_h^2 F_k} + \lambda \delta_{jk}\right\} G_k = \frac{\partial}{\partial z}\left[K_z \frac{\partial G_j}{\partial z}\right] + D_j\, \delta(z-z')\, \delta(t-t') \tag{57}$$

This is an infinite system of equations for the spectral components G_j that has to be solved for each meteorological time step $[\, t_{n+1}, t_n \,]$ together with boundary conditions, Eqs. (51) and (52), formulated in spectral domain. Compared with the method of complex Fourier-transformation there is the disadvantage of a finite domain, and, in addition, the fact that Eq. (57) leads to a coupled system of Liouville's equations.

An interesting method of solution is given by the technique of calculating moments [16], [17]. A higher order moment, say of concentration, is defined by

$$C^{\alpha,\beta} = \iint_{-\infty}^{\infty} d\mathbf{r}\, x^{\alpha} y^{\beta}\, \hat{c}(\mathbf{r},z,t) \tag{58}$$

The same notation will be used for Green's function. Multiplying Eq. (50) by $x^\alpha y^\beta$ and integrate, the following relationships are needed:

$$\hat{v}_h \cdot \iint_{-\infty}^{\infty} d\mathbf{r}\, x^\alpha y^\beta \nabla_h G = -(\alpha U C^{\alpha-1,\beta} + \beta V C^{\alpha,\beta-1}) \qquad ; \quad \hat{v}_h \equiv \{U,V\}$$

$$\iint_{-\infty}^{\infty} d\mathbf{r}\, x^\alpha y^\beta \nabla_h^2 G = \alpha(\alpha-1) C^{\alpha-2,\beta} + \beta(\beta-1) C^{\alpha,\beta-2}$$

$$\iint_{-\infty}^{\infty} d\mathbf{r}\, x^\alpha y^\beta \delta(\mathbf{r}-\mathbf{r}') = x'^\alpha y'^\beta$$

From Eq. (50) the following system of equations is obtained:

$$\frac{\partial C^{\alpha,\beta}}{\partial t} - [\alpha U C^{\alpha-1,\beta} + \beta V C^{\alpha,\beta-1}] = K_h [\alpha(\alpha-1) C^{\alpha-2,\beta} + \beta(\beta-1) C^{\alpha,\beta-2}] + \frac{\partial}{\partial z}\left[K_z \frac{\partial C^{\alpha,\beta}}{\partial z}\right] + x'^\alpha y'^\beta \delta(z-z')\delta(t-t') - \lambda C^{\alpha,\beta} \tag{59}$$

The first few members of this set of equations are given by

$$\frac{\partial C^{0,0}}{\partial t} = \frac{\partial}{\partial z}\left[K_z \frac{\partial C^{0,0}}{\partial z}\right] + \delta(z-z')\delta(t-t') - \lambda C^{0,0}$$

$$\frac{\partial C^{1,0}}{\partial t} - U C^{0,0} = \frac{\partial}{\partial z}\left[K_z \frac{\partial C^{1,0}}{\partial z}\right] + x'\delta(z-z')\delta(t-t') - \lambda C^{1,0}$$

$$\frac{\partial C^{0,1}}{\partial t} - V C^{0,0} = \frac{\partial}{\partial z}\left[K_z \frac{\partial C^{0,1}}{\partial z}\right] + y'\delta(z-z')\delta(t-t') - \lambda C^{0,1}$$

$$\frac{\partial C^{2,0}}{\partial t} - 2U C^{1,0} = 2K_h C^{0,0} + \frac{\partial}{\partial z}\left[K_z \frac{\partial C^{2,0}}{\partial z}\right] + x'^2 \delta(z-z')\delta(t-t') - \lambda C^{2,0} \tag{59}$$

$$\frac{\partial C^{0,2}}{\partial t} - 2V C^{0,1} = 2K_h C^{0,0} + \frac{\partial}{\partial z}\left[K_z \frac{\partial C^{0,2}}{\partial z}\right] + y'^2 \delta(z-z')\delta(t-t') - \lambda C^{0,2}$$

$$\frac{\partial C^{1,1}}{\partial t} - [U C^{0,1} + V C^{1,0}] = \frac{\partial}{\partial z}\left[K_z \frac{\partial C^{1,1}}{\partial z}\right] + x'y'\delta(z-z')\delta(t-t') - \lambda C^{1,1}$$

A finite set of moments determines the distribution the better the more members are included in the set.

Repeating what was mentioned in [16], statistical properties of the distributions are $C^{0,0}$: total amount of material per unit depth of layer, $\{C^{1,0}/C^{0,0}, C^{0,1}/C^{0,0}\} \equiv \{X,Y\}$: position vector of the centroid of material in the layer, $C^{2,0}/C^{0,0} - X^2 = \sigma_x^2$ and $C^{0,2}/C^{0,0} - Y^2 = \sigma_y^2$: variances of material with respect to the coordinate axes, $C^{1,1}/C^{0,0} - XY = \sigma_{xy}$: a measure of cross-correlation of the material in the layer.

Singular point sources show Gaussian behaviour near the source point and for small $\Delta t = t - t'$. Therefore, it might be sufficient to construct Green's function with the help of solutions of the first five members of Eqs. (59).

A modification of this method is the following which shows how the complete distribution is built up by all moments. For this the pair of Fourier-integraltransforms

$$\tilde{G}(\mathbf{k}) = \iint_{-\infty}^{\infty} d\mathbf{r}\, e^{-i\mathbf{k}\cdot\mathbf{r}} G(\mathbf{r}) \quad ; \quad (2\pi)^2 G(\mathbf{r}) = \iint_{-\infty}^{\infty} d\mathbf{k}\, e^{i\mathbf{k}\cdot\mathbf{r}} \tilde{G}(\mathbf{k})$$

is considered and the first member is expanded into a Taylor-series:

$$\tilde{G}(\mathbf{k}) = \sum_{n=1}^{\infty} \frac{(-i)^n}{n!} \iint_{-\infty}^{\infty} d\mathbf{r} (\mathbf{k}\cdot\mathbf{r})^n G(\mathbf{r})$$

From this, generalized moments, moments with regard to axes having direction of wave-number vector $\mathbf{k}$, are defined:

(60) $$M_n(\mathbf{k}) = \iint_{-\infty}^{\infty} d\mathbf{r} (\mathbf{k}\cdot\mathbf{r})^n G(\mathbf{r})$$

By virtue of

(61) $$\begin{aligned}(2\pi)^2 G(\mathbf{r}) &= \iint_{-\infty}^{\infty} d\mathbf{k}\, e^{i\mathbf{k}\cdot\mathbf{r}} \left[\sum_{n=1}^{\infty} \frac{(-i)^n}{n!} M_n(\mathbf{k}) \right] \\ &= \sum_{n=1}^{\infty} \frac{(-i)^n}{n!} \iint_{-\infty}^{\infty} d\mathbf{k}\, e^{i\mathbf{k}\cdot\mathbf{r}} M_n(\mathbf{k})\end{aligned}$$

it is seen how $G(\mathbf{r})$ is constructed by all moments $M_n(\mathbf{k})$. It is now possible to obtain a system of equations for the moments $M_n(\mathbf{k})$ out of Eq. (50). Multiplying Eq. (50) by $(\mathbf{k}\cdot\mathbf{r})^n$ and integrating over the entire domain one is first led to expressions like

$$\iint_{-\infty}^{\infty} d\mathbf{r}\,(\mathbf{k}\cdot\mathbf{r})^n \nabla_h G = -\mathbf{k}\, n\, M_{n-1}(\mathbf{k})$$

$$\iint_{-\infty}^{\infty} d\mathbf{r}\,(\mathbf{k}\cdot\mathbf{r})^n \nabla_h^2 G = \mathbf{k}^2 n(n-1) M_{n-2}(\mathbf{k})$$

$$\iint_{-\infty}^{\infty} d\mathbf{r}\,(\mathbf{k}\cdot\mathbf{r})^n \delta(\mathbf{r}-\mathbf{r}') = (\mathbf{k}\cdot\mathbf{r}')^n$$

Introducing this all into Eq. (50) one obtains

$$\text{(62)}\qquad \frac{\partial M_n}{\partial t} - \left[\mathbf{k}\cdot\hat{\mathbf{v}}_h\, n\, M_{n-1} + \mathbf{k}^2 K_h\, n(n-1) M_{n-2}\right] = \frac{\partial}{\partial z}\left[K_z \frac{\partial M_n}{\partial z}\right] + \\ + (\mathbf{k}\cdot\mathbf{r}')^n \delta(z-z')\delta(t-t') - \lambda M_n$$

For given wave-number vector $\mathbf{k}$, the first few members of this system are the following:

$$\frac{\partial M_0}{\partial t} = \frac{\partial}{\partial z}\left[K_z \frac{\partial M_0}{\partial z}\right] + \delta(z-z')\delta(t-t') - \lambda M_0$$

$$\text{(63)}\qquad \frac{\partial M_1}{\partial t} - \mathbf{k}\cdot\hat{\mathbf{v}}_h M_0 = \frac{\partial}{\partial z}\left[K_z \frac{\partial M_1}{\partial z}\right] + (\mathbf{k}\cdot\mathbf{r}')\,\delta(z-z')\delta(t-t') - \lambda M_1$$

$$\frac{\partial M_2}{\partial t} - 2\left[\mathbf{k}\cdot\hat{\mathbf{v}}_h M_1 + \mathbf{k}^2 K_h M_0\right] = \frac{\partial}{\partial z}\left[K_z \frac{\partial M_2}{\partial z}\right] + (\mathbf{k}\cdot\mathbf{r}')^2 \delta(z-z')\delta(t-t') - \lambda M_2$$

As was the case in system Eqs. (59), this is not a coupled system of equations, instead, each equation for higher moments depends only on already calculated moments. In both cases, the inherent Sturm-Liouville problem causes difficulties, although successful numerical integrations of Eqs. (59) have been performed [16].

It is interesting to derive some further relationships as e.g. the

the relationship between the M_n and the $C^{\alpha,\beta}$. Writing Eq. (61) explicitly

$$M_n(\mathbf{k}) = \iint_{-\infty}^{\infty} dx\,dy\,(k_x x + k_y y)^n\, G(x,y)$$

and applying the binomial theorem

$$(\mathbf{k}\cdot\mathbf{r})^n = (k_x x + k_y y)^n = \sum_{r=0}^{n} \binom{n}{r} (k_x x)^{n-r} (k_y y)^r$$

one obtains immediately

$$M_n(\mathbf{k}) = \sum_{r=0}^{n} \binom{n}{r} k_x^{\,n-r} k_y^{\,r}\, C^{n-r,r} \tag{64}$$

The moment theorem is obtained as follows: Consider as before

$$\begin{aligned}\widetilde{G}(\mathbf{k}) &= \sum_{n=1}^{\infty} \frac{(-i)^n}{n!} \iint_{-\infty}^{\infty} d\mathbf{r}\,(\mathbf{k}\cdot\mathbf{r})^n\, G(\mathbf{r}) \\ &= \sum_{n=1}^{\infty} \frac{(-i)^n}{n!} \sum_{r=0}^{n} \binom{n}{r} k_x^{\,n-r} k_y^{\,r}\, C^{n-r,r}\end{aligned}$$

and compare with Taylor-expansion of $\widetilde{G}(\mathbf{k})$ about $\mathbf{k} = 0$, i.e.

$$\begin{aligned}\widetilde{G}(\mathbf{k}) &= \sum_{n=1}^{\infty} \frac{1}{n!} \left[\mathbf{k}\cdot\frac{\partial}{\partial \mathbf{k}}\right]^n \widetilde{G}(0) \\ &= \sum_{n=1}^{\infty} \frac{1}{n!} \left[k_x \frac{\partial}{\partial k_x} + k_y \frac{\partial}{\partial k_y}\right]^n \widetilde{G}(0) \\ &= \sum_{n=1}^{\infty} \frac{1}{n!} \sum_{r=0}^{n} \binom{n}{r} k_x^{\,n-r} k_y^{\,r} \left[\frac{\partial^{n-r}}{\partial k_x^{\,n-r}} \frac{\partial^{r} \widetilde{G}(\mathbf{k})}{\partial k_y^{\,r}}\right]_{\mathbf{k}=0}\end{aligned}$$

Equating coefficients of equal powers of $k_x k_y$ we deduce the moment theorem

$$(-i)^n C^{n-r,r} = \left[\frac{\partial^{n-r}}{\partial k_x^{\,n-r}} \frac{\partial^{r} \widetilde{G}(\mathbf{k})}{\partial k_y^{\,r}}\right]_{\mathbf{k}=0} \tag{65}$$

Concluding this section, it is believed that the method of calculating moments as described in combination with finite difference schemes with regard to vertical coordinate seems to be a very promising one. It is to be hoped that it will be possible to construct Green's function sufficiently well in the future, such that solutions for inhomogeneous problems can be found as was mentioned in this paper. Many disadvantages of entirely numerical methods then could be passed by.

REFERENCES

[1] Fortak, H.G. (1966). "Rechnerische Ermittlung der SO_2 - Grundbelastung aus Emissionsdaten". Inst. f. Theoretische Meteorologie der Freien Universität Berlin.

[2] -- (1969). "Numerical Simulation of the Temporal and Spatial Distributions of Urban Air Pollution Concentration". Proc. of Symp. on Multiple-Source Urban Diffusion Models. Washington, D.C., U.S.E.P.A., APCO Publ. AP - 86.

[3] -- (1972). "Anwendungsmöglichkeiten von mathematisch-meteorologischen Diffusionsmodellen zur Lösung von Fragen der Luftreinhaltung". Min. Arbeit, Gesundheit und Soziales, Duesseldorf.

[4] -- (1975). "Application of an Air Pollution Model to the Problem of Feasible Industrialization of a Planned Deep - Sea Harbor." 6th NATO - CCMS International Technical Meeting on Air Pollution Modeling, Frankfurt.

[5] Deardorff, J.W., and G.E. Willis (1974). "Computer and laboratory modeling of the vertical diffusion of non - buoyant particles in the mixed layer". Adv. in Geophys., Vol. 18, New York, Academic Press.

[6] Fortak, H.G. (1973). "Mathematical Models for Air Pollution Abatement". In "Models for Environmental Pollution Control" (R.A. Deininger, Editor). Ann Arbor Science Publ. Inc., Ann Arbor, Mich.

[7] -- (1974). "Mathematical Modeling of Urban Pollution". Adv. in Geophys., Vol. 18, New York, Academic Press.

[8] Eschenroeder, A., and J.R. Martinez (1971). Conf. Air Pollut. Meteorol., Amer. Meteorol. Soc., Boston, Mass.

[9] Fortak, H.G. (1957). "Zur allgemeinen Berechnung von Suspensionsverteilungen in turbulenten Strömungen". Gerlands Beiträge zur Geophysik, Vol. 66, Akad. Verl. Ges., Leipzig.

[10] -- (1957). "Sinkstofftransport in geraden Kanälen als Randwertproblem". Acta Hydrophysica, Vol. IV, Inst. f. Physikalische Hydrographie, Dt. Akad. Wiss. zu Berlin. Akademie - Verlag, Berlin.

[11] Carslaw, H.S., and I.C. Jaeger (1948). "Conduction of heat in solids". Oxford.

[12] Fortak, H.G. (1969). " Bodenimmissionsverteilungen im Lee eines Schornsteins für den Fall beliebiger Formen der Rauchfahnenachse". Veröff. Inst. f. Theoretische Meteorologie der Freien Universität Berlin.

[13] Richtmyer, R.D., and K.W. Morton (1967). "Difference Methods for Initial - Value Problems". Interscience, New York.

[14] Shir, C.C., and L.I. Shieh (1973). "A generalized urban air pollution model and its application to the study of SO_2 distribution in the St. Louis metropolitan area". Techn. Rep. RJ 1227, IBM San Jose Res. Center, California.

[15] Van der Pol, B., and H. Bremmer (1955). "Operational Calculus". Cambridge Univ. Press.

[16] Wallington, C.E. (1968). "Numerical Solution of Atmospheric Diffusion Equations". Scientific Paper No. 28, Met. Office, London.

[17] Tyldesley, J.B., and C.E. Wallington (1965). "The effect of wind shear and vertical diffusion on horizontal dispersion". Quart. Journ. Roy. Met. Soc., London.

7th International Technical Meeting
on Air Pollution Modeling and its Application

POLLUTANT DISPERSION SIMULATION BY MONTE CARLO TECHNIQUES

K.-H. Müller
European Community
JRC Ispra/Italy

September 7-10, 1976
Airlie, Virginia
United States of America

1. Dispersion Mechanism

From turbulence research one knows that an air stream usually contains temporarily stable air parcels, eddies, which lead an independent life during finite time periods and afterwards decay. These eddies vary in size. Obviously as well as the drift component the eddy motion also has a stochastic component. One observes smooth pieces of path and abrupt changes in direction. In macroscopic stationary flows, there are regions with a practically unvarying spectrum of eddy sizes. This, however, does not mean that the eddies have an infinite life- and residence-time, but that there are a lot of individual histories (birth, stability phase, decay) phase-shifted against another.

In such a continuum interspersed by eddies a gas-cloud enriched with pollutants will be released. At this time point, it can be considered as a single parcel. One observes that it undergoes the same fate as the other eddies: it has a certain stability phase, it decays afterwards into smaller "quasi-stable" units which, in their turn, decay again after a certain life-time and which, finally, lose their macroscopic particle structure (RICHARDSON (1922)). Thus, the entrained pollutant will be distributed more or less homogeneously over a certain volume containing, as a rule, yet other eddies of different "ages". If the individual constituents enter a region where eddy-birth takes place, they will be partially joined with constituents of other decaying eddies to form new bigger quasi-stable units (coagulation), and the transport- and decay process continues. In this way, the pollutant is dispersed much faster and more extensively than by molecular diffusion. The eddies thus act as vehicles and the atmosphere as the carrier.

The cascade of pollutant eddies emerging from a decaying waste-gas cloud is, outside the "effective source domain" which has still to be defined, numerically small, in comparison with the number of turbulence-elements there. An interaction between pollutant eddies will therefore be rarer by far than the interaction between pollutant eddies and carrier. Consequently, the ensemble of pollutant eddies, outside the effective source domain, will hardly modify the turbulence field of the atmosphere. This fact is of fundamental significance for the mathematical description of the pollutant dispersion process (→ linearization). After a certain relaxation time, both the polluted eddies and the turbulence elements will have the same size-spectrum, the same velocity-distribution and the same decay-behaviour. There is equilibrium.

Inside the effective source domain, however, a process of accomodation takes place: the elements of the polluted cloud will be "thermalized". One will, therefore, distinguish between a phase of thermalization and a phase of equilibrium.

The observable abrupt changes in direction could be assumed to be "collisions" between eddies. The corresponding interaction mechanism, however, is up to now unknown. Only an intensive study of the eddy structure can give some insight. This however concerns turbulence research and is for us of peripheral interest only. We are not at all interested in the fate of the single eddy, since we need only the space-time dependent density distribution of the atmospheric pollution.

There exist, in the literature, many attempts to use a mechanism, taken from another domain of physics, to describe the dispersion process, such as e.g. that used in the theory of Brownian motion (CHADRASEKHAR (1943)). One should try, however, to combine such a mechanism with the concept of "mean life-time".

The statistical distributions of life-times determining the cascade-decay have to be taken from experimental data; they are probability- or frequency-distributions, like all experimental results in this field, since the observations register only realizations of statistical quantities or sample means. Life-times of polluted eddies depend on

$$\left.\begin{array}{l}\text{density}\\ \text{size-spectrum}\\ \text{velocity-distribution}\end{array}\right\}\ \text{of the turbulence elements}$$

and on the

$$\left.\begin{array}{l}\text{size}\\ \text{velocity}\end{array}\right\}\ \text{of the polluted eddy.}$$

It seems reasonable to interpret each collision as an absorption followed by an emission. If, at the collision point, the eddy is absorbed, it automatically enriches the carrier with pollutant. If there is, an instant later, an emission, the new eddy may have a gain or loss of pollutant content in comparison with the incoming eddy. We then speak of a "up- or down-scattering".

There are two different models to deal with the decay and coagulation: either the eddy is assumed to be a cluster of uniform "atoms", or an air parcel, homogeneous inside but of irregular shape, to which arbitrary masses can be added or taken away. Another assumption fundamental for the modelling is, that the interactions do not possess any memory effects. Consequently, the velocity direction of an emitted eddy is equally distributed, if the eddy distribution of the carrier is on average isotropic. Without turbulence elements there are, obviously, no collisions.

Between the collisions the eddies follow curved paths, since the buoyancy- and gravity-forces act on them continuously. In view of the need for a mathematical simulation one may ask whether such a trajectory could be approximated sufficiently well by a chain of straight paths, joined together at the collision points. This seems to be permissible, if the corresponding force-field does not noticeably change along the "mean collision-free path". In this case, one can apply the concept of "free paths" fruitful elsewhere; i.e. velocity changes are assumed to occur at discrete space points only, in the form of collisions.

Finally, one should point out that single eddies are always representatives of a turbulence spectrum and that eddies of different sizes have different mobility. Quantitative relations must be taken from turbulence theory.

During the phase of equilibrium the mathematical effort of simulation is considerably smaller than during that of the thermalization. In the case of equilibrium one could assume the kinetic energy of the turbulence elements to be e.g. Maxwellian-distributed. The parameters characterizing such a distribution have to be fixed by fitting experimental data.

The question whether the eddies, emerging a puff later, are already preformed during the puff emission (cluster model) and are travelling together for a while or whether the mode of decay will be decided only at the moment where the eddy hits an obstacle, seems to be irrelevant, but largely determines the mathematical structure of the simulation model.

In the case of a cluster structure of the puffs representing the emission of a point source, the number of the uniform cluster components is proportional to the intensity of the source; the rate of release can vary with time.

At the space-time point where the eddy emission takes place both the eddy and the carrier have an identical concentration spectrum of chemical substances. During the free flight, the eddy represents a closed system without any contact with the carrier material permeated. Because of this, the chemical reactions occurring inside the eddy are independent of the situation outside. At the point of absorption, the local concentration spectrum of the absorbing material becomes modified by the chemicals carried by the eddy. Other more or less simultaneously arriving eddies contribute in a similar way. Obviously each eddy born and starting there carries with itself, the actual concentration spectrum of the birth place, and so forth.

In the vicinity of chimneys the micro-meteorology is governed by the emission process itself. Released hot gases create a buoyancy zone into which surrounding cold air is drawn. That mixing region is the "effective source region" of an emitter. There, the eddies carrying the discharged pollutants start their way through the laminar or turbulent moving atmosphere. In the course of time, the eddies decay and coagulate. Precipitations and chemical reactions change the pollutant concentration in the air, absorption and reflection along solid and fluid surfaces. Because of eddy diffusion and convection caused by the local aerodynamics the polluted air will be distributed through an increasing volume.

2. Simulation Techniques

A stochastic simulation model is required which makes use of a submodel for each of the relevant phenomena (local turbulence, buoyancy, wash-out etc.) governing the transport-, dispersion- and dilution processes, which can be replaced by a more sophisticated one, if measurements require it.

Since a regional air monitoring network has only a finite number of stations at its disposal, one will interpret the atmosphere of a region as a 3-dimensional system of compartments, each with its own homogeneous micro-meteorology. All meteorological information belonging to the corresponding compartments is called the meteorological inventory of the region. Defective inventories have to be completed either by interpolation or by additional measurements. A dispersion simulation is only applicable to a region for which complete inventories of meteorology and emission are available.

Only a model simulation of the pollutant dispersion can check the relevance of the single parameters characterizing the different submodels and distinguish between parameters of the local and universal significance. Evidently, both the construction and the validation of such a simulation model need a rather large number of experiments both on the laboratory and the city scale. These experiments serve two different purposes: to determine the dispersion characteristics of a city and to test the model structure. Finally, sensitivity analysis must be used to find the range of values for the different model parameters and to minimize the model input. The decisive minimization, however, can be done only using measured data obtained from dispersion experiments both on the laboratory and on the city scale.

Last but not least, it should be guaranteed that the model has a sound theoretical basis, that a particularly lucid simulation results, and thatthis approach can conveniently be performed on a computer with economical use of computer time, if one follows the pollutant dispersion from emission to the end of a given observation interval.

Given a set of air quality standards, the complete emission inventory of the region to be controlled and the corresponding meteorological inventory containing a sufficiently detailed description of the local meteorology. Determine a computerized pollutant level forecast indicating the pollutant concentration distribution in adequate detail in space and time, paying regard, in the first instance, to the dangerous situations usually accompanied by irregular or weak winds.

An inspection of smoke diffusing near the ground gives the impression that the dispersion is brought about primarily by the relative motion with the wind but otherwise seems to move at random. An examination of the record of wind speed shows that the oscillations are caused by the passage of whirls and vortices which, like molecules, appear to have distinct identities. The idea that molecular formalism can describe in an empirical fashion the transport of pollutants within a turbulent atmosphere is taken for granted by many researchers even though there is no proof that this is generally justifiable. Whether this approximation is appropriate can be judged only on the basis of the particular application.

Fundamentally, the pollutant dispersion can be described from both the Eulerian and the Lagrangian points of view.

a. Eulerian Models

The transport mechanism for a diluted eddy gas is governed by the linear Boltzmann equation[1]:

$$\frac{df}{dt} = -\alpha f + \underset{m',\vec{v}'}{S} \beta(m',\vec{v}'; m,\vec{v}) f(m',\vec{v}') + S \qquad (1)$$

This is a balance equation. The left-hand side is the substantial derivative of f, which is the number of eddies of type m per phase-space volume element, whereas the right-hand side represents the sum of gains and losses there. Using the "free path concept", i.e. polygonial trajectories consisting of straight paths interrupted by instantaneous deviations, we get

---

[1] S denotes a superposition, a discrete summation $\sum$ or a continuous integration $\int$ or both.

(2) $$\frac{df}{dt} = \frac{\partial f}{\partial t} + \vec{v} \cdot \mathrm{grad}\, f$$

$\vec{v}$ denotes the velocity vector of the individual, α the "total interaction coefficient" and $L = 1/\alpha$ the "mean life-time", β the "scattering coefficient". To solve the transport equation (1), a Monte Carlo approach has been developed, in the past, which constructs a series of random walks for a stochastically selected but representative sample of members of an expanding particle cloud. For a more detailed explanation see, for instance DAVISON (1957).

A simultaneous treatment of chemical reactions, however, requires a more complex kernel β, that is a kernel which depends on the density f itself. The classical Monte Carlo techniques here meet difficulties. One, therefore, tries to change eq. (1) into a more convenient form. To do so, one takes the so-called "first collision concept" successfully applied to reactor physics (DAVISON (1957)).

All collision can be treated as first collision by assuming that an eddy suffering any collision is absorbed. In this picture the collision density

(3) $$\Psi(\vec{r},t) = v\alpha \mathop{S}_{m,\vec{v}} f(m,\vec{v}) = v\alpha\, \chi(\vec{r},t)$$

satisfies the equation

(4) $$\begin{cases} \Psi(\vec{r},t) = \mathop{S}_{\vec{\rho}} K(|\vec{r}-\vec{\rho}|)\left[S(\vec{\rho},\tau) + h(\vec{\rho},\tau)\,\Psi(\vec{\rho},\tau)\right] \\ \tau = t - |\vec{r}-\vec{\rho}|/v \end{cases}$$

$K(|\vec{r} - \vec{\rho}|)$ is the probability for an eddy starting from $\vec{\rho}$ to suffer its first collision at $\vec{r}$, e.g.

$$K(|\vec{r}-\vec{\rho}|) \sim \frac{v^{-1}\alpha}{4\pi|\vec{r}-\vec{\rho}|^2}\, \exp\left(-v^{-1}\alpha|\vec{r}-\vec{\rho}|\right)$$

$h(\vec{r},t)$ new eddies appear at the absorption point, provided that the emission is isotropic.

Nonlinearities characteristic for chemical reactions enter here via the "multiplication factor", $h(\vec{r},t)$, which is now dependent on the densities of all the substances involved in the chemical transformation and which has to be derived from the kinetic equations taken from the literature (e.g. LEIGHTON (1961)). Eq. (2) can be solved by an iteration starting from plausible density distributions. Eqs. (1) and (4) represent the basis of our considerations.

We shall now discuss the dispersion of inert substances and come back to the chemical transformations at the end of this paper.

The space-time dependent number of eddies $\chi(\vec{r},t)$ satisfies the differential equation

$$\text{(5)} \qquad \operatorname{div}(\mathbb{D}\operatorname{grad})\chi = a\chi + \frac{\partial\chi}{\partial t} + T\frac{\partial^2\chi}{\partial t^2} + \sum_{k=3}^{\infty}\varepsilon_k\frac{\partial^k\chi}{\partial t^k} + Q$$

where the ε_k's, the absorption coefficient a, the relaxation time T and the eddy diffusion tensor $\mathbb{D}$ depend on $\alpha, \beta, \vec{v}$ and space-time $(\vec{r},t)$. (SOODAK (1962); MÜLLER (1975)).

To keep the mathematics within reasonable bounds, we shall, in a first step, confine ourselves to discrete eddy-classes and to the so-called "hyperbolic approximation" characterized by

$$\text{(6)} \qquad \varepsilon_k \equiv 0 \qquad \text{for} \qquad k \geq 3$$

Only when it turns out that this approximation is not sufficient for the interpretation of an experiment, shall we take into consideration higher time derivatives also.

The hyperbolic approximation leads to classical equations of mathematical physics. In the past, numerous integration approaches have been developed which we can use. (See e.g. FRANK - v. MISES (1961)).

Equation (1) degenerates, for n different types of eddies, to the set of wave equations

$$(7) \qquad T_i \frac{\partial^2 \chi_i}{\partial t^2} + \frac{\partial \chi_i}{\partial t} + \sum_{j=1}^{n} b_{ij} \chi_j = \nabla \cdot (\mathbb{D}_i \nabla \chi_i) + Q_i$$

with i = 1,2,...,n.

Since the solution χ_i^{as} of the parabolic equations, i.e. the diffusion equations

$$(8) \qquad \frac{\partial \chi_i^{as}}{\partial t} + \sum_{j=1}^{n} b_{ij} \chi_j = \nabla \cdot (\mathbb{D}_i \nabla \chi_i) + Q_i$$

converges, for increasing t, to χ_i, i.e.

$$(9) \qquad \chi_i^{as} \approx \chi_i \qquad \text{for} \qquad t > T$$

one shall also test the solutions of (8) by experiments, to find their practical usefulness.

Several attempts have been made to justify the application of both the wave equations (7) and the diffusion equations (8) to pollutant dispersion (e.g. MONIN (1959), LAMB-SEINFELD (1973), PASQUILL (1974)). The a priori free parameters of the derived equations can be fixed either by fitting their solutions to experimentally measured concentrations χ_i or by theoretical reasoning.

For solving codes for the equations (7) and (8) see e.g. OECD-NEA (1976).

It should be said here that the solutions of all the dispersion equations mentioned above can - via syllogisms from other domains of physics - be interpreted as a sum of stochastic micro-processes and mathematically be solved by Monte Carlo techniques (e.g. MÜLLER (1975)).

b. Lagrangian Models

One has here two different possibilities of interpreting the pollutant dispersion, that is, by allowing the eddies

- to be "interwoven" in the turbulence field, to move in harmony with it, or
- to lead an autonomous existence there (within the meaning of the Brownian motion).

The choice will be influenced mainly by the measured data available, such as frequency distributions of wind-speed and direction, of eddy energies and sizes, and two- or more-point correlations and turbulence scales of type (e.g. ROTTA (1972))

$$(10)\qquad \left\{ \begin{aligned} L_{ijk}(\vec{r},t) &= \gamma_{ij}\int_{-\infty}^{+\infty} R_{ij}(\vec{r},t;\varrho_k,0)\,d\varrho_k \\ T_{ij}(\vec{r},t) &= \gamma_{ij}\int_{-\infty}^{+\infty} R_{ij}(\vec{r},t;0,\tau)\,d\tau \\ \gamma_{ij} &= \left[2\,\overline{u_i'(\vec{r},t)\,u_j'(\vec{r},t)}\right]^{-1} \\ R_{ij}(\vec{r},t;\vec{\varrho},\tau) &= \frac{\overline{u_i'(\vec{r},t)\,u_j'(\vec{r}+\vec{\varrho},t+\tau)}}{\left[\overline{u_i'^2(\vec{r},t)}\;\overline{u_j'^2(\vec{r}+\vec{\varrho},t+\tau)}\right]^{1/2}} \end{aligned} \right.$$

Continuum Theory

The Eulerian velocity field $\vec{u}$ composed into $\vec{u} = \vec{u}_m + \vec{u}'$ possesses, apart from the mean velocity $\vec{u}_m$, a so-called "stochastic component"

$$(11)\qquad \vec{u}'(\vec{r},t) = \mathop{\mathrm{S}}_{\vec{k},\omega} \vec{U}(\vec{k},\omega)\exp(i\omega t + i\vec{k}\cdot\vec{r})$$

which is a superposition of all the air motions not describable up to now in a deterministic sense. Usually the amplitude $\vec{U}$, the wave number $\vec{k}$ and the frequency ω will be taken from long-time observations. As one knows, the moving atmosphere carries air masses behaving like lumps of a certain consistency and moving as units during finite time intervals, i.e. clusters of submasses having nearly identical histories of motion and highly correlated velocity vectors. Two- and more-point correlations allow the identification of such "air parcels" experimentally. Within the framework of a mathematical modelling of pollutant dispersion the possibility of calculating one or more of the quantities $\vec{U},\vec{k}$ and ω by the aid of random generators and to simulate, finally, the eddy trajectories as random walks suggests itself.

KRAICHNAN (1970) developed a model for eddy diffusion in which the velocity field was represented by a Fourier series

$$\vec{u}(\vec{r},t) = \sum_{-\infty}^{+\infty} \vec{V}_n \times \vec{k}_n \, exp(i\omega_n t + i\vec{k}_n \cdot \vec{r}) \tag{12}$$

where the $\vec{V}_n$ and ω_n were taken from Gaussian distributions and the $\vec{k}_n$ from classical energy spectra. ORZAG (1969), McCOY (1975) and others used similar approaches. PATTERSON/CORRSIN (1966) established a random field of velocities on a predetermined space-time lattice. As a particle moves, it obeys the velocity instructions that it finds as it arrives at lattice points. TOMPSON (1971) created particle trajectories directly in $\vec{r}$-space by generating $\vec{u}'$ according to measured or theoretically calculated statistical means like $\sigma_i^2 = \langle u_i'^2 \rangle$.

The diversity of measured frequency distributions and disposable turbulence scales, like (10), offers a multiplicity of similar structured models for eddy diffusion and thus automatically for pollutant dispersion. (e.g. JOYNT-BLACKMAN (1976)).

RICHARDSON (1922) developed the hypothesis that fully developed turbulence consists of a continuous hierarchy of eddies of various orders of size and energy content. The eddies have a characteristic life-time, after which larger eddies give up their energy to smaller ones. The lowest order eddies dissipate their energy heating up the atmosphere. This decay, sometimes locally accompanied by eddy coagulations, makes a realistic modelling rather complicated. The literature contains few appropriate references.

Particle Theory

One interprets the turbulence as a cloud of particles interspersed in a continuous air flow and leading an individual existence. Thus, one concedes to the atmospheric motion a degree of freedom higher than usual, with the aim of equiping the model with an ample set of free parameters and granting a greater flexibility which, in its turn, permits us to take into account dispersion relevant information inherent in the flood of meteorological data continuously registered over many years and characterizing the local situation. The simplest type of such a description is, to concede an individual existence only to the polluted eddies and to interprete the "clean" turbulence field as a continuum in the above mentioned sense. The situation resembles a set of pearls (eddies) dancing about a deforming "flying carpet" (turbulence field). It is obviously a sort of Brownian motion.

Wind- and temperature-field fluctuations expressed by frequency distributions, correlation coefficients etc. supply both statistical measures like $\vec{u}_m$; $\sigma_u^2 = \langle \vec{u}'^2 \rangle$ and Θ_m; $\sigma_\Theta^2 = \langle \Theta'^2 \rangle$ chracterizing, in their turn, statistical distributions like the Gaussian and, in addition, particle properties like sizes, free paths and free flight times, in short, basic information to construct particle trajectories in the form of random paths. The variety of these gives us the opportunity to calculate a "plume axis", a "plume rise" and "dispersion parameters (σ_1, σ_2, σ_3)" as a set of ensemble means. These parameters determined by small-scale experiments can, sometimes, be used as input to city-scale pollutant dispersion models like these of TURNER (1964), FORTAK (1970) etc.

A more sophisticated simulation assumes that the "clean" turbulence field is composed, at least partially, of an eddy cloud also, migrating in an ocean of air, such as ring- and spherical-shaped vortices or clusters of such units (MILNE-THOMSON (1960)). The gas of polluted eddies permeates the turbulence gas. Whether the eddies under consideration are really identical with these classical vortices or not has still to be clarified, but this is a task for turbulence research. Pollutant dispersion modellers will, with thanks, accept such results and apply them in their business.

Now some remarks concerning the mathematization of the dispersion processes.

One usually starts here from the Newton equation

$$\frac{d\vec{v}}{dt} = -\mathbb{A}\vec{v} + \vec{a} \tag{13}$$

where $\mathbb{A}$ is the friction tensor and $\vec{a}$ any acceleration acting on the particle as a whole. $\vec{v}$ and $\vec{a}$ are mean values representative for the eddy motion. A formal integration leads to

$$\vec{v}(t) = e^{-\mathbb{A}t}\vec{v}(t_0) + \int_{t_0}^{t} e^{-\mathbb{A}(t-\tau)}\vec{a}(\tau)\,d\tau \tag{14}$$

This result shows that the velocity $\vec{v}$ consists of two additive components, one dependent on the initial velocity $\vec{v}(t_o)$ and decreasing in time. The remaining component is the end-result of all the influences affecting the particle during the time-interval $(t - t_o)$.

The classical theory of Brownian motion interprets $\vec{a}$ as a series of randomly spaced Dirac-impulses caused by collisions between the Brównian particle and the molecules of the carrier. As a result of the particle bombardments, the velocity of the diffusing Brownian particle at any instant is random in magnitude and direction, its velocity-history being thus a stochastic process. The time-integral of the velocity-history is the displacement-history which is necessarily again a stochastic process. The corresponding random-walk approach divides the total displacement of a Brownian particle into a number of independent steps

(15) $$\Delta \vec{x} = \int_{\Delta t} \vec{v}(\tau)\,d\tau$$

The probability distribution of a particle executing such random steps is a standard problem of probability theory with an extensive literature (e.g. CRAMER (1946), BARTLETT (1956), FELLER (1957)).

According to (15) the random step can be taken in the form

(16) $$\Delta x_i = p_i(t)\Delta t + q_i(t)\, r_i(t)\Delta t$$

where $r_i(t)\Delta t$ is any random process with independent increments, e.g. a Gaussian white noise, and where p_i and q_i are Eulerian quantities which can be obtained either from measurements of the flow conditions or from theoretical or empirical correlations.

BULLIN-DUKLER (1974) simulated this method on a hybrid computer. Time-varying fluctuating velocities were simulated using white noise generators filtered in a specific manner. The procedure can readily accomodate time-varying boundary conditions and source strenghts as well as time and position dependent flow conditions. The computer time required is very short.

CHANDRASEKHAR (1943), GOLDSTEIN (1951), MONIN (1959), KIRMSE (1964), RILEY-CORRSIN (1971) and the already cited authors relate the coefficients of equation (16) to the physics of the problem and adopt the "free path concept" already mentioned above. They follow an ensemble of uniform and unchanging particles over a series of equal time intervals, but they do not consider the life-time, the decay and the coagulation conditioned by the local structure of the atmosphere. The simultaneous existence of eddies of different sizes and pollutant content are also neglected. One wonders whether this deficiency can be compensated for by a more refined consideration of meteorological quantities only.

Most of these authors show that their "Lagrangian model" is equivalent to a Eulerian "diffusion equation" or a "telegrapher's equation", at least asymptotically. The cascade decay, however, already demonstrates that instead of a single dispersion differential equation (parabolic or hyperbolic) one has to apply a set of those equations and that the pollutant concentration calculated by the superposition of the different particle densities does not necessarily have to satisfy such a second-order differential equation.

3. Eddy Diffusion

Flying balloons or tetroons move along polygonial trajectories composed of free paths some meters in length. Quasi-stable parcels of air show similar random walks. Profiting from this similarity we construct an analogous Monte Carlo approach corresponding to the linear Boltzmann equation (1) and thus solve it.

A local turbulence field induced by an obstacle or by thermal effects in a laminar meso-wind field will be interpreted as an eddy cloud. The eddy velocity is composed of a drift-component and a stochastic one; outside the cloud the eddy density is much lower. A polluted air-parcel entering the turbulence field will be thermalized there.

Polluted eddies are assumed to be particles of a diluted gas, released from a known position in space and time. Let $x_i(t)$ be the coordinate of this moving particle. Such coordinates are random variables. Each such release of a particle can be expected to result in a different time function $x_i(t)$. Its location is recorded at $t = T$. This is repeated many times for each T and for a series of values of T of interest. The local concentration χ can be found from a sample mean by dividing the number of particles recorded as being in some small volume by that volume. $x_i(t)$ is assumed to be a Markovian process. Thus, the statistics of the particle locations at time t in the future depends only on its position at the present and is independent of the past. This implies in our case, that the location of the eddy is independent of the history of the turbulence.

a. Life-time

These particles interact with the gas of the turbulence elements characterized by a given particle density δ and a given velocity distribution $g(V)dV$. The interaction is a sort of scattering or moderation. Let the particles of the moderating gas have a velocity-independent cross-section σ and the trajectories of the colliding particles, before the interaction, an angle ε ($\cos \varepsilon = \mu$). Since all directions are equally likely for both the particles, the probability of a collision angle between ε and $(\varepsilon + d\varepsilon)$ is $d\mu/2$. Thus the number of such collisions per space-time volume element is given by

$$d\chi = v_r \, \sigma \delta \, g(V) dV \, d\mu/2 = v \delta \, ds = v \, d\alpha \tag{17}$$

where v_r = relative velocity between the colliding particles and ds = differential cross section for a particle of velocity v.

In the centre-of-mass system the velocity only changes its direction; the scattering is assumed to be isotropic here. The total scattering cross-section $\alpha(v)$ can now be obtained by integrating $d\alpha$ over V and μ. If we assume, in addition, that a particle cloud decays according to a first-order rate law, the "life-time" of an individual particle is exponentially distributed. The probability that the particle will not decay in the time interval Δt is, therefore, $\exp(-\alpha \Delta t)$, where α is the decay-coefficient. The corresponding "mean life-time" is given by $L = 1/\alpha$.

In the case of a gas-mixture entered by a polluted particle, one will obtain a decay coefficient linearly composed of the decay-coefficients α_i corresponding to all the gas-components i representing the mixture. The (partial) densities δ_i have to be taken from the eddy-size spectrum offered by turbulence theory.

Example: If the moderating gas consists of uniform particles of mass M (= multiple of the incoming eddy mass) and if the gas particles have a Maxwellian velocity distribution

(18) $$g(V)\,dV = 4a^2V^2 \exp(-a^2V^2)\,dV$$

where $a^2 = M/2k\Theta$ and Θ = gas temperature, we obtain for the decay-coefficient

(19) $$\alpha(v) = \sigma\delta\left[\frac{\exp(-b^2)}{\sqrt{\pi}\,b} + \left(1 + \frac{1}{2b^2}\right)\operatorname{erf}(b)\right]$$

where $b = v/a$ (WIGNER-WILKINS (1944)).

Such a description of the turbulence field is called a "temperature concept" of turbulence. Let us now look at the collision process itself.

We base our model upon the following hypotheses:

1) The streaming air will be characterized by the velocity vector $\vec{u}_m$. The interspersed turbulence elements possess known size-spectra and particle-densities, and a velocity $V\vec{\Omega}$ relative to $\vec{u}_m$, where V satisfies the distribution $g(V)dV$ and $\vec{\Omega}$ is a uniformly distributed random-variable.

2) All the eddies are clusters.

3) Inside the effective source domain (ESD), the life-time of a polluted eddy is longer than the time of the free flight (TFF) between two collisions, i.e. each collision is a scattering without change of pollutant content.

4) Outside the ESD, the life-time and the TFF are identical, i.e. at each collision point the chain will be passed through:

absorption → disintegration → coagulation → emission.

The pollutant content is usually changed thereby.

b. Equilibrium

The eddies will be classified according to their sizes. At the collision point each polluted eddy disintegrates into its constituents, the "atoms" and consequently augments the local pollutant density. All the atoms simultaneously accumulated in the volume element including the collision point are at this moment disjoint, but coagulate afterwards in a manner specific for the collision point, and finally leave the volume element, so reducing the pollutant density there. The same process occurs at each collision point.

For the mathematical description one assumes that there are eddies of different size-categories, characterized by the number of atoms involved. Each polluted atom of an incoming eddy may be attached to any category during the collision. The corresponding probability has to be chosen from the local eddy size-spectrum. The attachment takes place via a linear indexing of the arriving polluted atoms by a random address. The interaction mechanism of the next collision is characterized again according to both the local situation and the category to which the respective atom belongs. The pollutant concentration at the collision point increases instantaneously but only by the quantum carried by the polluted atom under consideration, since the eddy to which it belongs is only a temporary vehicle. The other polluted atoms travelling in company with it will be separately followed along their way from emission point to detector. The mean local expansion velocity of an eddy cloud depends essentially on both the local eddy size-spectrum and the "mean turbulence temperature", Θ_i, there. This model also allows one to pay regard to a loss of pollutant, as caused by a wash-out, chemical transformations etc. The tool best suited here is the so-called space-time dependent "importance factor".

c. Thermalization

The puff leaving a chimney is part of a hot-gas stream which possesses a considerable vertical momentum being transmitted over time to the surrounding atmosphere. There is a mixing domain with a strong turbulence, a pronounced mean vertical velocity, a higher mean turbulence temperature and a specific eddy size-spectrum: the so-called "effective source domain" of the chimney. From here, the pollutant eddies start their way through the phase of equilibrium. An estimate of the dimensions of this source domain is of importance for practical purposes. One could take here a so-called "plume rise formula" which, in general, will be determined in an experimental way (BRIGGS (1969)). In stationary cases the velocity field near to the source is governed almost exclusively by the hot waste gas stream. Turbulence theory gives corresponding information subsumed under the key words "the turbulent hot free jet". This given velocity field is entered by a pollutant puff, i.e. an eddy cloud. Scattering mechanisms can be constructed there on different hypotheses, e.g. with the picture of inelastically colliding particles, or with that of interacting vortex rings (THOMSON (1883), FOHL-TURNER (1975)).

d. Buoyancy

Buoyancy effects modify the momentum of the eddies according to the thermal stratification of the atmosphere. One refers to it as "stable" (unstable) if the stratification damps (intensifies) the vertical motions of air parcels and "neutral" if it does not influence the motions. Along the relatively short flight between two consecutive collisions the buoyancy K itself usually does not change significantly; as modification of the velocity vector $\vec{v}$ we can take $d\vec{v} = (0,0,Kdt)$. The literature gives the expression

$$K = \frac{g}{\Theta}\left(\frac{\partial \Theta}{\partial z} + \Gamma\right) = R_i \left(\frac{\partial \bar{u}}{\partial z}\right)^2 \qquad (20)$$

coupling the force K with the Richardson number R_i, i.e. with the gradient of the ln Θ - vertical profile (ELIASSEN-KLEINSCHMIDT (1957)).

e. Boundary Conditions

At solid and liquid interfaces the particles are partly reflected and partly absorbed. Because of surface roughness the reflection is mostly diffuse. The use of an isotropic angular distribution seems to be adequate. If the characteristic length of surface roughness is smaller than the eddy size the surface is assumed to be smooth.

The space-time domain under consideration is, in general, finite. Its boundary shape and the particle behaviour there can be chosen arbitrarily. It may happen, that a particle moving around crosses the space boundaries of the region several times (in ↔ out), before it (1) finally leaves the region or (2) is absorbed or (3) the observation time is over. All these possibilities represent - for the observer - a suitable termination of the single-particle history. To avoid unnecessary use of computer time, we shall construct a cut-off mechanism to treat multiple crossings. The so-called "albedo", i.e. a certain reflection factor, $q < 1$, seems to be best suited here.

Every particle emitted bears the "weight" $w = 1$. After n boundary crossings (in ↔ out), however, $w = q^n$. By the introduction of a lower-limit q_{min}, we shall judge the history finished when $q^n \leq q_{min}$ (MÜLLER (1975)).

At thermal inversion layers one can also observe a partial reflection. Here too the albedo concept is a good way to parametrize the rejection phenomenon. Corresponding measurements are inevitable.

Some attention should be paid to time-dependent boundary conditions, which are usually associated with inversion layers. Since the inversion dynamics is of lower frequency than the reflection process, the albedo concept mentioned above can be applied without any change. One needs only be aware of the actual position and spacing of the layer.

4. Chemical Reactions

The concentrations of the different chemicals relevant to air pollution change in time and according to the local concentration ratios which, in their turn, change in space and time due to eddy diffusion The adequate mathematical tool is, as already said, the "first collision concept". Another fact to be taken into account is, that the chemical concentrations inside an eddy "grow older" in the same way as the concentrations remaining at the birth place of the eddy do. The corresponding formalism is given by the iteration system

$$
(21)\quad \begin{cases} \chi_i^{j}(\vec{r},0) = \lim\limits_{t\to 0} \chi_i^{j-1}(\vec{r},t) \\[2ex] \dfrac{\partial \chi_i^{j}(\vec{r},t)}{\partial t} = F_i(\chi_1^{j}\ \chi_2^{j} \ldots .) \\[2ex] \chi_i^{j+1}(\vec{r},t) = \chi_i^{j}(\vec{r},t) + \mathop{\mathrm{S}}\limits_{\vec{\xi},\tau} \varphi(\vec{r}-\vec{\xi},t-\tau)\, p(\vec{\xi},\tau)\, \chi_i^{j}(\vec{\xi},t) \end{cases}
$$

where the index j counts the collisions and $\chi_i^{o}(\vec{r},0) = \chi_o(\vec{r})$ gives the known background distribution of substance i, and $\varphi(\vec{r}-\vec{\xi},\ t-\tau)$ denotes the transfer function between birth place $(\vec{\xi},\tau)$ and first collision point $(\vec{r},t)$. The φ has to be calculated, $\varphi(\vec{r},t) = \mathop{\mathrm{S}}\limits_{m,\vec{v}} g(m,\vec{v})$, from the solution g of the version, $\beta \equiv 0$, of equation (1), for a Dirac source, $S \sim \delta(r)\,\delta(t)$; $p \cdot \chi_i$ is the amount of substance i carried away from $(\vec{\xi},\tau)$ by eddies. The quantity p depends on the eddy density. Stationary turbulence means $\frac{\partial p}{\partial t} \equiv 0$. The concentrations χ_i after n collisions result from n repetitions of system (21). This procedure represents for an increasing n a successive approximation to the measurable Eulerian concentrations, i.e.

$$
(22)\qquad \chi_i(\vec{r},t) = \lim_{n\to\infty} \chi_i^{n}(\vec{r},t)
$$

A first order approximation can be obtained by taking the mean lifetime L instead of the real life-time, i.e. replacing the statistical distribution by its mean value.

5. References

BRIGGS, G.A. (1969) USAC-TID 25075

BULLIN, J.A. & DUKLER, A.E. (1974) Env. Sci. Technol. 8, 156

BARTLETT, M.S. (1960) "An Introduction to Stochastic Processes" University Press Cambridge

CHANDRASEKHAR, S. (1943) Rev. Mod. Phys. 15, 1

CHANG, J.S. et al. (1973) UCRL-7[illegible]323

CRAMER, H. (1946) "Mathematical Methods of Statistics" University Press, Princeton

DAVISON, B. (1957) "Neutron Transport Theory", Oxford

ELIASSEN, A. & KLEINSCHMIDT, E. (1957, 1963) Enc. Phys. 48, 1 Springer, Berlin

FELLER, W. (1957) "An Introduction to Probability Theory and its Applications", John Wiley, N.Y.

FOHL, T. & TURNER, J.S. (1975) The Physics of Fluids 18, 433

FORTAK, H. (1970) NAPCA-Sympo. "Mult. Source Urban Diff. Models", Chapel Hill NC.

FRANK, P. & V. MISES, R. (1961) "Die Differential- und Integralgleichungen", Dover Publ., NY.

GOLDSTEIN, S. (1951) Quart. J. Mech. Appl. Math. 4, 129

JOYNT, R.C., & BLACKMAN, D.R. (1976) Atm. Env. 10, 433

KRAICHNAN, R.H. (1970) Phys. Fluids 13, 22

LAMB, R.G. & SEINFELD, J.H. (1973) Env. Sci. Technol. 7, 253

LEIGHTON, P.A. (1961) "Photochemistry of Air Pollution", Academic Press, N.Y.

McCOY, M.G. (1975) UCRL-51962

MILNE-THOMSON, L.M. (1960) "Theoretical Hydrodynamics", Mac Millan, N.Y.

MONIN, A.S. (1959) "Advances Geophysics" 6, Academic Press, N.Y.

MÜLLER, K.H. (1975) Proc. NATO/CCMS-Panel, Frankfurt
Proc. IBM Seminar "Air Poll. Modelling", Venice

OECD-NEA (1976) "Computer Program Library" Ispra/Italy

ORZAG, S. (1969) Phys. Fluids, Suppl. II, 12, 257

PASQUILL, F. (1974) "Atmospheric Diffusion", John Wiley, N.Y.

PATTERSON, G.S. & CORRSIN, S. (1966) "Dynamics of Fluids and Plasmas" (ed. Pai, S.I.), Academic Press, N.Y.

RICHARDSON, F.L. (1922) "Weather Prediction by Numerical Processes", Cambr. Univ. Press, London

RILEY, J. & CORRSIN, S. (1971) "Conf. Air Pollution Meteorology", Raleigh, N.C.

ROTTA, J.C. (1972) "Turbulente Strömungen", Teubner, Stuttgart

SOODAK, H. (1962) "Reactor Handbook", 3A, Interscience N.Y.

THOMSON, J.J. (1883) "A Treatise on the Motion of Vortex Rings", Mc Millan, London

THOMPSON, R. (1971) Quart. J. Roy. Met. Soc. 97, 93

TURNER, D.B. (1964) J. Appl. Met. 3, 83

WIGNER, E.P. & WILKINS, J.E. (1944) AECD-2275

7th NATO/CCMS International Technical
Meeting on Air Pollution Modeling and
its Application

MATHEMATICAL MODEL FOR URBAN DIFFUSION OF CARBON MONOXIDE FROM MOTOR VEHICLES

FEEMAS* - AIR QUALITY WORKING GROUP

P.P. Gaddo, F. Corazzari, R. Borgialli (FIAT - Rapporteurs)
G. Marcenaro (ESSO)
G. Marchesi (ENI)
F. Carbone, G. Ferrante (MOBIL)
D. Casella, A. Piccone (A. Romeo)
S. Chiaiso, E. Damasio (SHELL- now I.P.)

September 7 - 10 , 1976
Airlie , Virginia
United States of America

---

* FEEMAS is an Association of Research Centres set up by FIAT, ESSO, ENI, MOBIL, ALFA ROMEO, IP with the purposes of common research programmes in the fields of fuels, engines and air pollution.

Abstract

The need for a tool capable of predicting air quality changes as a consequence of measures taken to control emissions from mobile sources, prompted FEEMAS to verify the applicability of a mathematical model for CO diffusion to the city of Turin where an extended network of air quality monitoring stations is available.

The model input data (traffic hourly distribution and its qualitative and quantitative composition, specific emissions, meteorological parameters) were obtained through surveys and experimental determinations. Hence, they represent the true urban area conditions referred to town arterial plan, traffic and meteorological conditions.

The output data were checked on the base of CO concentration levels observed at the Monitoring Station of the FIAT Network.

Substantially, the model proved suitable to simulate the pollution levels induced by motorized traffic in a town like Turin: namely, the trends of calculated and observed levels are quite similar.

From this point of view, the model performance is satisfactory, even if some discrepancies are noticed.

The model is quite versatile too, taking into account the wide variety of input parameters and their uncertainty degree.

Checked the model outputs validity, a peculiar data processing has been made, assuming the ipothesis of establishment of a pedestrianized area in the old town center of Turin.

An average 90% reduction of pollution levels was calculated within such area, and no reduction or significant benefits was found for the adjacent areas, with traffic volume at par.

MATHEMATICAL MODEL FOR URBAN DIFFUSION OF CARBON MONOXIDE FROM MOTOR VEHICLES

1. Application of a Mathematical Model to the city of Turin

Among its research activities, FEEMAS undertook a study for the development of a tool permitting the prediction of changes in the urban center air quality as a result of actions aimed at motorvehicle emission control.

As the investigation subject, Turin was chosen for which FIAT set up an extended network for air quality monitoring that permits the truth of the results obtained from the simulation to be correlated.

In consideration of the urban configuration of Turin and keeping in mind the scope of the work to be undertaken, a synoptic mesomodel was chosen for this city.

A similar simulation scheme was already set up by the Stanford Research Institute for some American centers.

The selected model calculates the distribution of carbon monoxide pollution in the urban area, at ground level and on an hourly basis.

The elements on which data processing is based are :

- The recording points (receptors) where pollutant concentration is calculated
- The amount of emissions from the vehicles on the road
- Meteorological parameters
- Correlation equations of the input values

This group of elements which enter directly in model formulation is supplemented by the host of data collected by the monitoring stations.

This permits the calibration of the model and a verification of the calculated data, i.e. ultimately, the reliability of the selected calculation method.

Receptor Points

These points represent the stations at which CO concentrations are calculated.

They are identified through the subdivision of the urban areas into telescopic squares with side of 600 m city edge areas and 200 m (central areas) respectively.

The receptor points, whose total is about 500, are located at the center of each square.

The subdivision grid is oriented NS-EW and includes the area limited by the city municipality boundaries.

Computation of Active Emissions for Pollution Calculation at Receptor Points

The pollution calculated at a receptor point is given, logically, also by the emissions coming from up wind areas.

In-depth studies on this subject led to the development of an oriented receptor (Clarke Gifford) which encloses an area whose emissions can actually contribute to receptor pollution. (Fig. 1)

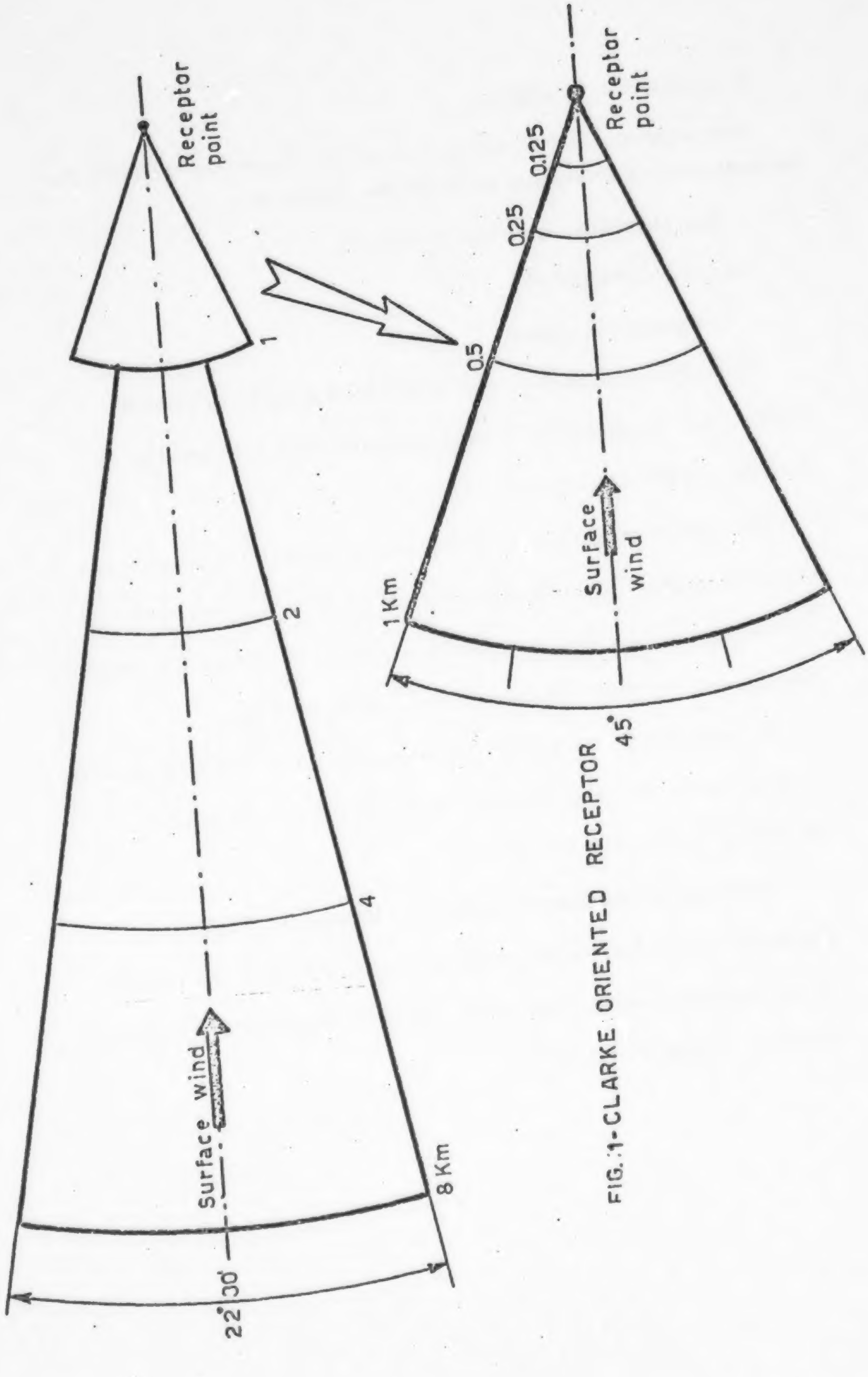
Receptor point
1
2
4
Surface wind
8 Km
22°30'
Receptor point
0.125
0.25
0.5
Surface wind
1 Km
45°

FIG.1-CLARKE ORIENTED RECEPTOR

Metereological Parameters

The meteorological parameters which are required to calculate the concentration at a receptor point are the following :

- Wind direction, speed and variability
- Mixing depth (HMD)
- Atmospheric stability

Anemological parameter data, wind direction and speed, wind shifts about the prevalent blowing direction, have been provided by the FIAT Air Quality Control stations.

No statistical data on mixing depth, as well as the astronomical and meteorological parameters for its calculation, are available for city of Turin: those used here were provided by the Atmosphere Dynamics Institute of the Brera (Milan) Astronomical Observatory.

The adoption of the typical Milan parameters for the city of Turin is justified by the geographical, climatological and anemological similitudes between the two cities.

Regarding the atmospheric stability classes, the Brookhaven method was chosen for the mathematical model input data, its classification principles being based on the amount of wind shifts about the prevalent blowing direction.

Emission Parameters

Traffic

Vehicular flow distribution parameters were deducted from the city traffic through an investigation conducted with the aid of direct transit recordings in sampled areas of the arterial network.

The investigation was aimed at acquiring data on the hourly distribution of traffic flow in the streets.
The flow hourly rates were obtained by taking the flow daily rates of each link and multiplying them by the vehicle percent hourly subdivision of the zone to which each link belonged.

Specific Emissions

The specific emissions of the vehicles in circulation were determined as follows :

- Definition of the driving modes characteristic of the city of Turin.
- Selection of sample vehicles representative of the vehicle park.
- Submittal of sample vehicles on engine test stand to the defined driving modes and emission measurements.

The study for the definition of the driving modes for the city of Turin was carried out on the basis of an investigation made on the utilization of mechanical units during trips in urban areas.

Statistical processing of the cycles relevant to the different areas led to the definition of a typical cycle-illustrated in the three charts-for each area (see Figs. 2, 3, 4).

ACTUAL DRIVING CYCLES IN TURIN

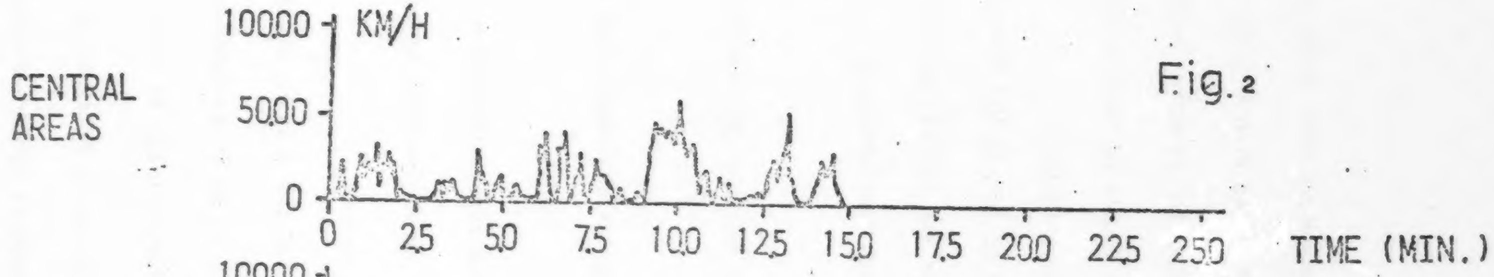

Fig. 2

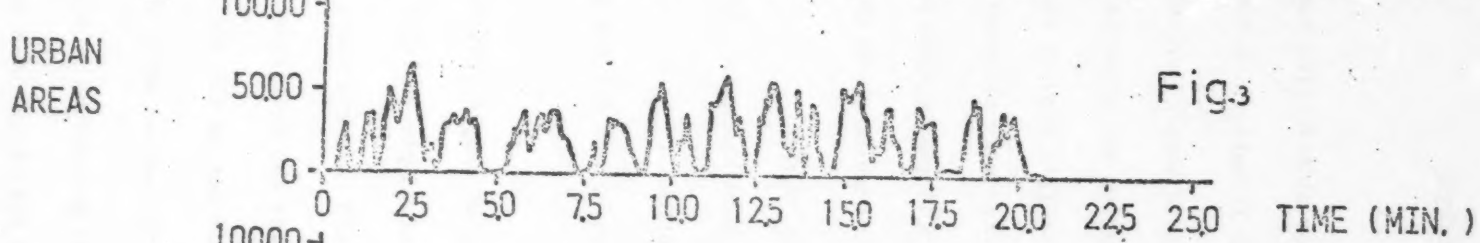

Fig. 3

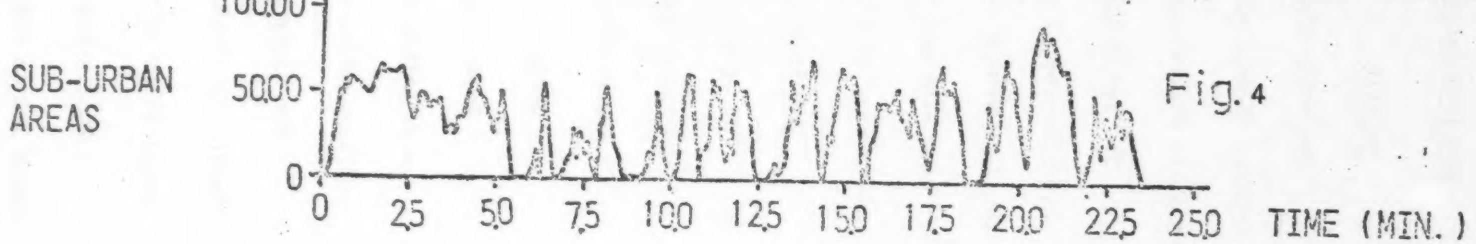

Fig. 4

Such driving modes have been coupled to the urban area partitioning zones.

The measurement of the specific emissions from the sample vehicles was made by repeating on chassis dynamometer for each sample vehicle, the three typical cycles of the city of Turin.

Basic Equations for Correlation of Input Data

The basic overall equation for computing CO concentrations is :

$$C = \frac{1}{U}\left\{\sum_{i=1}^{N-1} Q_i \left[\frac{0{,}8\left(r_{i+1}^{1-b_{ij}} - r_i^{1-b_{ij}}\right)}{a_{ij}(1-b_{ij})}\right] + Q_N \left[\frac{08\left(r_T^{1-b_{ij}} - r_N^{1-b_{ij}}\right)}{a_{ij}(1-b_{ij})} + \frac{r_{N+1} - r_T}{h}\right] + \sum_{i=N+1}^{8} Q_i \left[\frac{r_{i+1} - r_i}{h}\right]\right\}$$

The following parameters are included in this equation :

C = Carbon monoxide concentration at receptor

U = Average wind speed

ij = Constants identified by the atmospheric stability classes, bound to meteorological parameters and distance from receptor

r = Distance of sources from receptor

ij = Indixes identifying, respectively, the urban area zone considered and the existing climatic stability class.

h = Mixing depth

Q_i = Vehicle park emission strength referred to the i th segment

Q_N = Vehicle park emission strength referred to the N th segment area within which the transition radius is located.

2- Model Application - Check and Processing of Results

Processing of the mathematical model was so programmed as to have available a pollution level pattern as follows :

- Under the present urban traffic conditions, assuming they are representative of the various experimental driving modes.
- In the assumption of a pedestrianized island in the city center.

In order to verify the validity of mathematical model outputs, a comparison was made, in the time span considered, between the calculated pollution levels and those recorded at the Monitoring Stations.

As can be seen on the charts of Fig. 5 thru 8

the calculated values reliably reflect the actual concentration level patterns on a typical day;

pollution peak levels occur at peak traffic hours and minimum levels at off-peak traffic hours.

The model showed its ability to perceive such variations and to express them in terms of CO concentrations sufficiently close to reality.

As far as the recorded deviations are concerned, in some cases they may be of a certain extent but on the average their values remaine within acceptable limits.

CARBON MONOXIDE: COMPARISON BETWEEN CALCULATED AND OBSERVED LEVELS AT FIAT MONITORING STATIONS

Fig. 5

JANUARY 13/17 - 1975

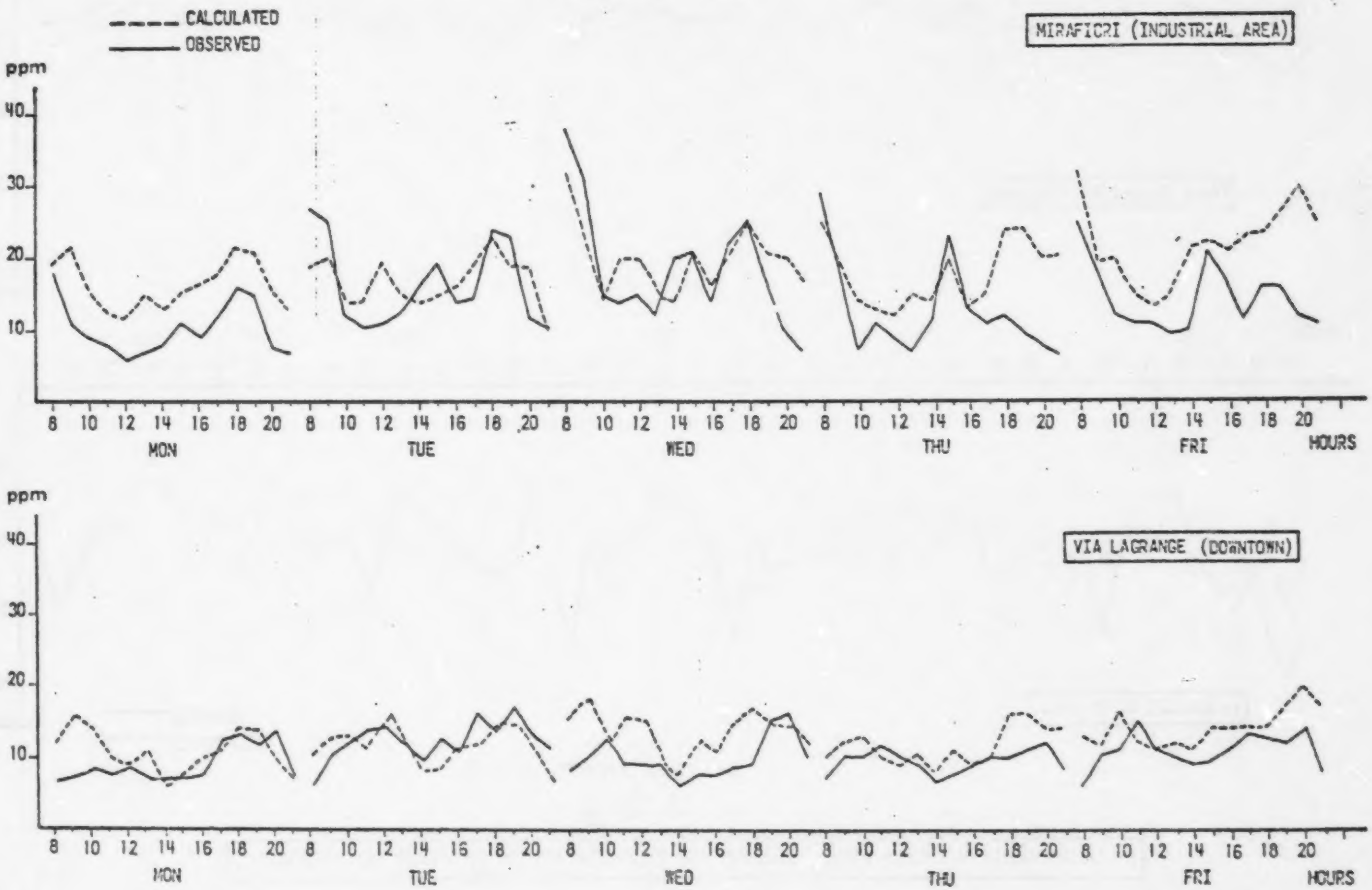

CARBON MONOXIDE: COMPARISON BETWEEN CALCULATED AND OBSERVED LEVELS AT FIAT MONITORING STATIONS

Fig. 6

JANUARY 13/17 - 1975

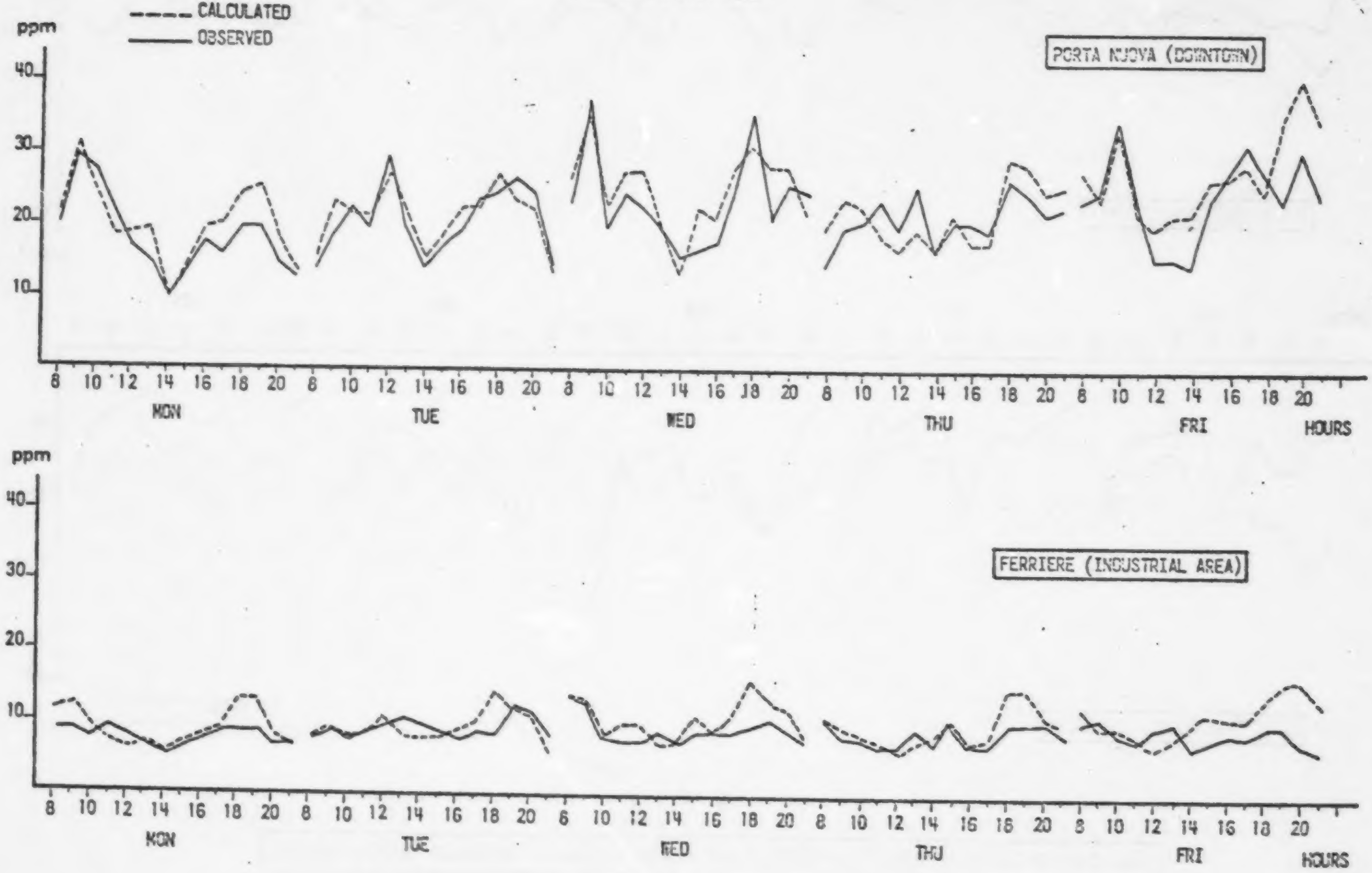

CARBON MONOXIDE: COMPARISON BETWEEN CALCULATED AND OBSERVED LEVELS AT FIAT MONITORING STATIONS

Fig. 7

SEPTEMBER 22/26 - 1975

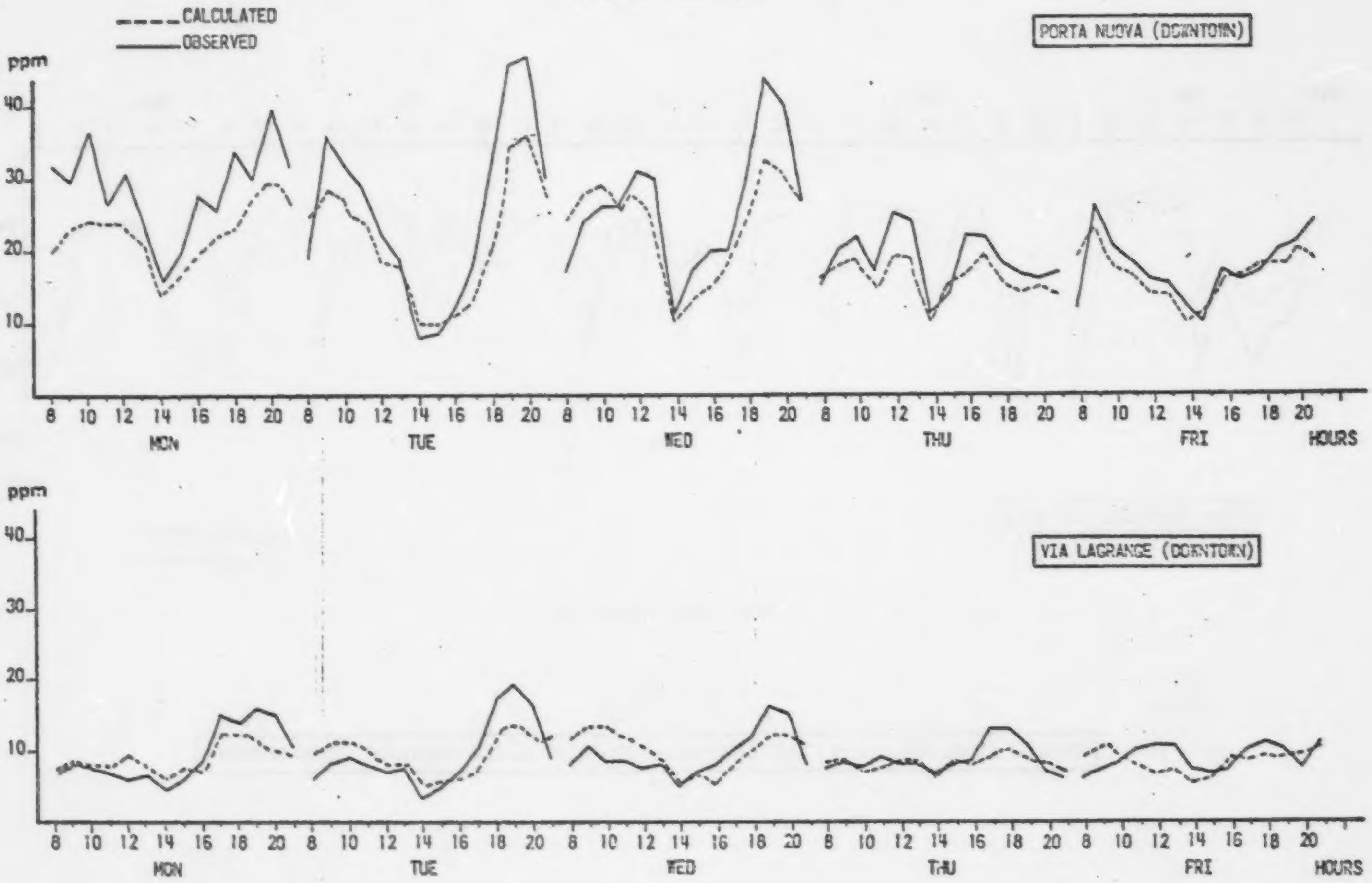

CARBON MONOXIDE: COMPARISON BETWEEN CALCULATED AND OBSERVED LEVELS AT FIAT MONITORING STATIONS

Fig. 8

SEPTEMPBER 22/26 - 1975

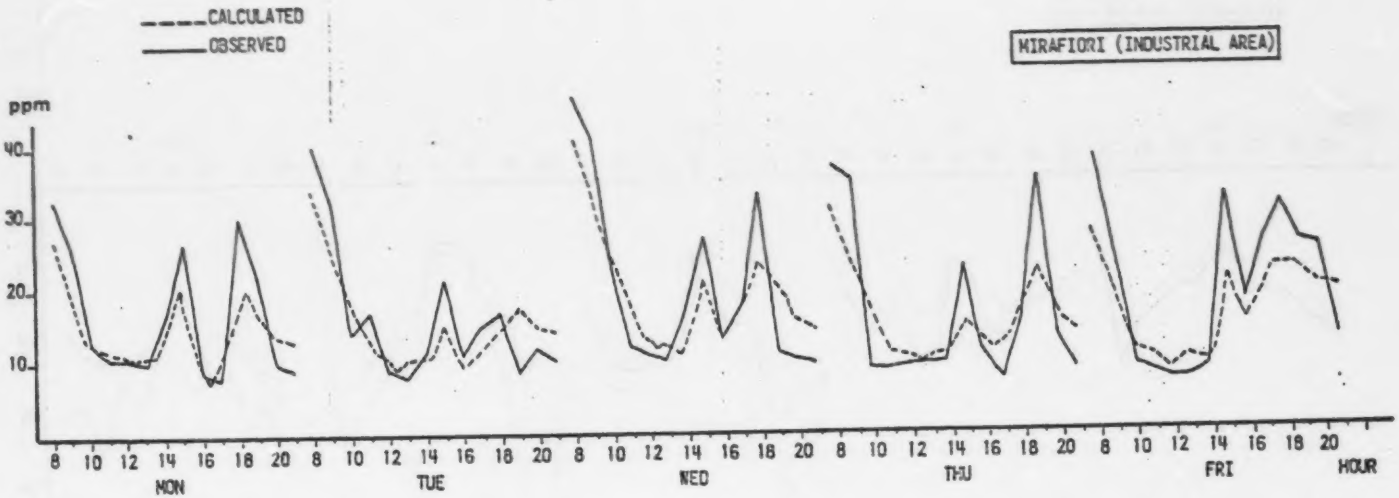

On the basis of the results obtained from the first series of processing, a program was set up for further use of the model to simulate particular pollution conditions such as those consequent to the adoption of a pedestrianized island in the city center.

The results of processing performed assuming a pedestrianized island in down town Turin are of great interest. This simulation proved to be suitable for evaluating the ecological impact of an urban planning provision that the Public Authorities looked upon with increasing favor to solve the problems of traffic in the urban areas.

It was therefore assumed that private vehicle traffic flow would be banned in 20 squares of the grid corresponding to the city center and that, therefore, emissions from vehicles would be eliminated.

Processing was made by evaluating the pollution levels that can be reached during a peak traffic hour of a typical day.

Processing results have shown that in the pedestrian zone there would be an 80-90% decrease in the pollution rate with respect to the actual values (see Fig. 9 - 10)

Residual concentration levels would be minimum (1.6 to 3.4 ppm).

In some boundary squares the recorded decrements are lower (50-60%) inas such as these areas are evidently affected by the emissions of nearby areas where traffic is allowed.

In the areas next to the pedestrian zone that are little affected by the provision, pollution levels are almost unchanged with respect

TURIN DOWNTOWN AREA

Fig. 9

DISTRIBUTION OF CO CONCENTRATION PEAK-HOUR UNDER NORMAL CONDITIONS

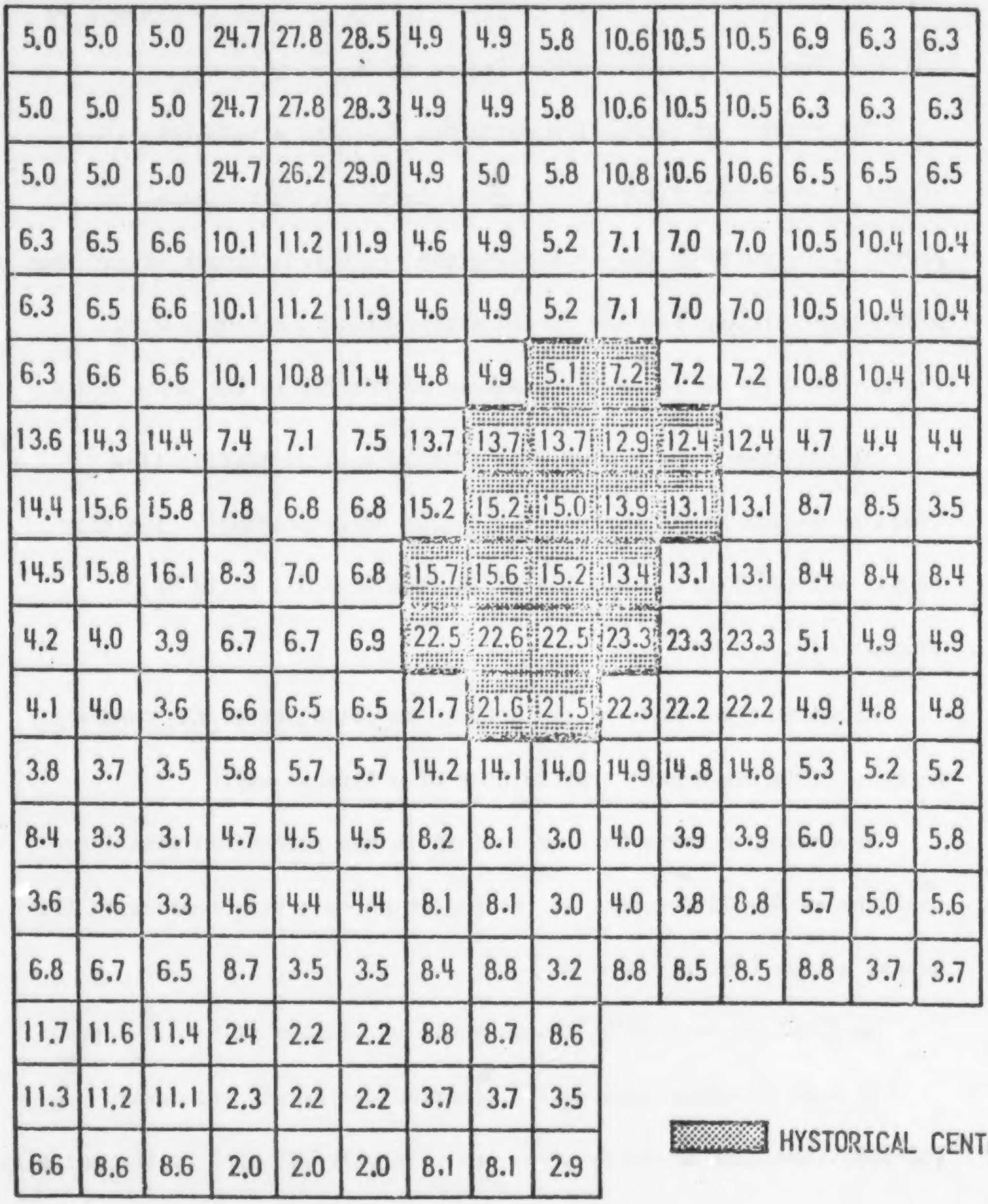

5.0	5.0	5.0	24.7	27.8	28.5	4.9	4.9	5.8	10.6	10.5	10.5	6.9	6.3	6.3
5.0	5.0	5.0	24.7	27.8	28.3	4.9	4.9	5.8	10.6	10.5	10.5	6.3	6.3	6.3
5.0	5.0	5.0	24.7	26.2	29.0	4.9	5.0	5.8	10.8	10.6	10.6	6.5	6.5	6.5
6.3	6.5	6.6	10.1	11.2	11.9	4.6	4.9	5.2	7.1	7.0	7.0	10.5	10.4	10.4
6.3	6.5	6.6	10.1	11.2	11.9	4.6	4.9	5.2	7.1	7.0	7.0	10.5	10.4	10.4
6.3	6.6	6.6	10.1	10.8	11.4	4.8	4.9	5.1	7.2	7.2	7.2	10.8	10.4	10.4
13.6	14.3	14.4	7.4	7.1	7.5	13.7	13.7	13.7	12.9	12.4	12.4	4.7	4.4	4.4
14.4	15.6	15.8	7.8	6.8	6.8	15.2	15.2	15.0	13.9	13.1	13.1	8.7	8.5	3.5
14.5	15.8	16.1	8.3	7.0	6.8	15.7	15.6	15.2	13.4	13.1	13.1	8.4	8.4	8.4
4.2	4.0	3.9	6.7	6.7	6.9	22.5	22.6	22.5	23.3	23.3	23.3	5.1	4.9	4.9
4.1	4.0	3.6	6.6	6.5	6.5	21.7	21.6	21.5	22.3	22.2	22.2	4.9	4.8	4.8
3.8	3.7	3.5	5.8	5.7	5.7	14.2	14.1	14.0	14.9	14.8	14.8	5.3	5.2	5.2
8.4	3.3	3.1	4.7	4.5	4.5	8.2	8.1	3.0	4.0	3.9	3.9	6.0	5.9	5.8
3.6	3.6	3.3	4.6	4.4	4.4	8.1	8.1	3.0	4.0	3.8	8.8	5.7	5.0	5.6
6.8	6.7	6.5	8.7	3.5	3.5	8.4	8.8	3.2	8.8	8.5	8.5	8.8	3.7	3.7
11.7	11.6	11.4	2.4	2.2	2.2	8.8	8.7	8.6						
11.3	11.2	11.1	2.3	2.2	2.2	3.7	3.7	3.5						
6.6	8.6	8.6	2.0	2.0	2.0	8.1	8.1	2.9						

▨ HYSTORICAL CENTRE

TURIN DOWNTOWN AREA

Fig. 10

DISTRIBUTION OF CO CONCENTRATION DURING A PEAK-HOUR TRAFFIC BAN INSIDE HYSTORICAL CENTRE

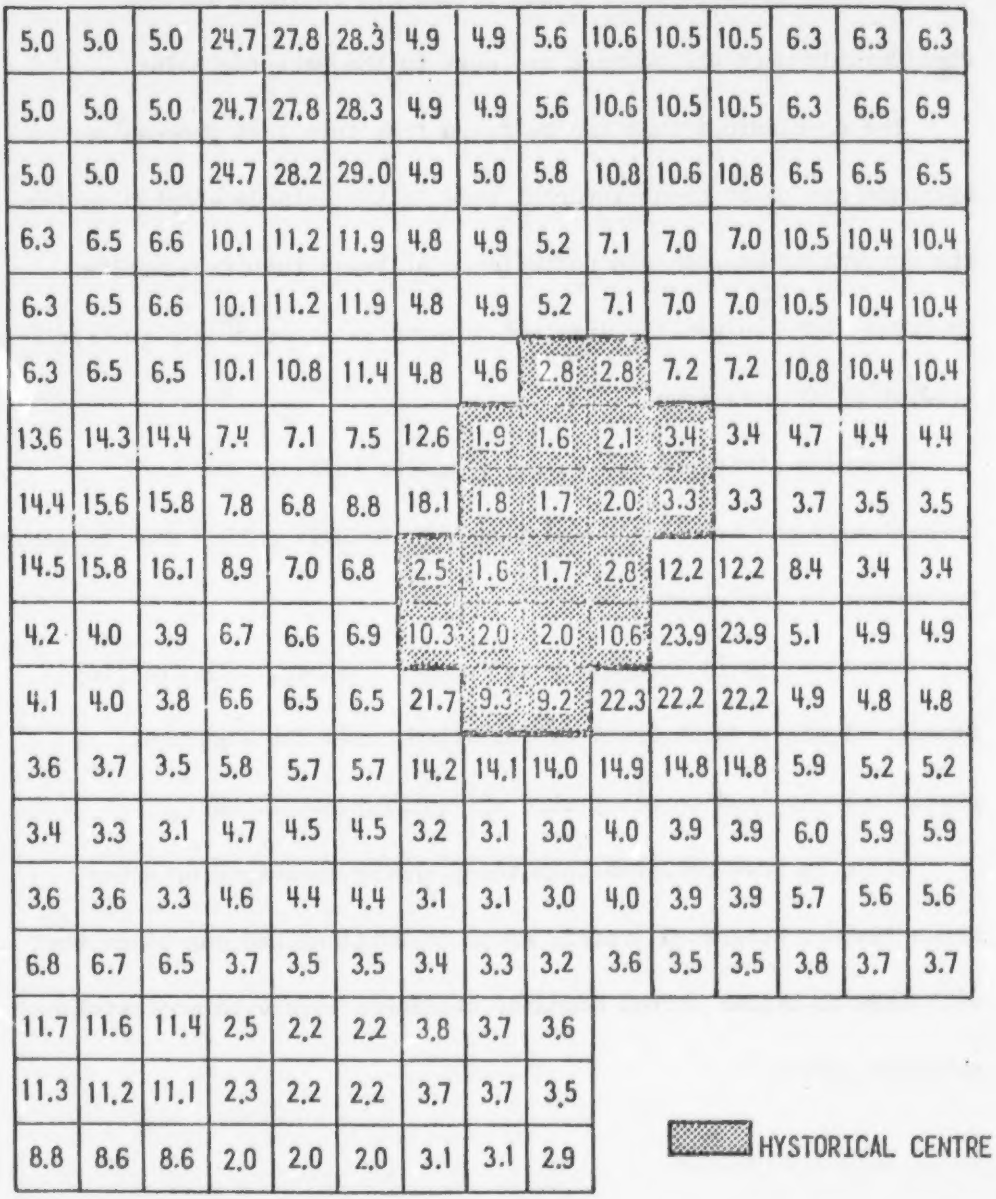

5.0	5.0	5.0	24.7	27.8	28.3	4.9	4.9	5.6	10.6	10.5	10.5	6.3	6.3	6.3
5.0	5.0	5.0	24.7	27.8	28.3	4.9	4.9	5.6	10.6	10.5	10.5	6.3	6.6	6.9
5.0	5.0	5.0	24.7	28.2	29.0	4.9	5.0	5.8	10.8	10.6	10.8	6.5	6.5	6.5
6.3	6.5	6.6	10.1	11.2	11.9	4.8	4.9	5.2	7.1	7.0	7.0	10.5	10.4	10.4
6.3	6.5	6.6	10.1	11.2	11.9	4.8	4.9	5.2	7.1	7.0	7.0	10.5	10.4	10.4
6.3	6.5	6.5	10.1	10.8	11.4	4.8	4.6	2.8	2.8	7.2	7.2	10.8	10.4	10.4
13.6	14.3	14.4	7.4	7.1	7.5	12.6	1.9	1.6	2.1	3.4	3.4	4.7	4.4	4.4
14.4	15.6	15.8	7.8	6.8	8.8	18.1	1.8	1.7	2.0	3.3	3.3	3.7	3.5	3.5
14.5	15.8	16.1	8.9	7.0	6.8	2.5	1.6	1.7	2.8	12.2	12.2	8.4	3.4	3.4
4.2	4.0	3.9	6.7	6.6	6.9	10.3	2.0	2.0	10.6	23.9	23.9	5.1	4.9	4.9
4.1	4.0	3.8	6.6	6.5	6.5	21.7	9.3	9.2	22.3	22.2	22.2	4.9	4.8	4.8
3.6	3.7	3.5	5.8	5.7	5.7	14.2	14.1	14.0	14.9	14.8	14.8	5.9	5.2	5.2
3.4	3.3	3.1	4.7	4.5	4.5	3.2	3.1	3.0	4.0	3.9	3.9	6.0	5.9	5.9
3.6	3.6	3.3	4.6	4.4	4.4	3.1	3.1	3.0	4.0	3.9	3.9	5.7	5.6	5.6
6.8	6.7	6.5	3.7	3.5	3.5	3.4	3.3	3.2	3.6	3.5	3.5	3.8	3.7	3.7
11.7	11.6	11.4	2.5	2.2	2.2	3.8	3.7	3.6						
11.3	11.2	11.1	2.3	2.2	2.2	3.7	3.7	3.5						
8.8	8.6	8.6	2.0	2.0	2.0	3.1	3.1	2.9						

▨ HYSTORICAL CENTRE

to the present levels.

This fact can be explained with the rapid diffusion of CO whose recorded values are practically negligible when its sources are far from the monitoring point CO amounts increase instead considerably when the sources are next to the receptor point.

The conclusions that can be drawn from this last processing approach can be of great interest because the methods adopted so far the control of atmospheric pollution - at least that from mobile sources - were univocally directed to ward an increasingly restrictive limitation of emissions.

The more stringent the emission limits enforced the more economically and tecnically exacting will be this policy that is perhaps the easier to implement.

Moreover, it is impossible to foresee whether, with traffic density at the present level or increased, emission abatement provisions may lead to acceptable air quality standards.

It is in fact possible that the planning structure of urban areas feature congested traffic areas or bottlenecked junctions that will lead to higher carbon monoxide standards even with more stringent emission limits.

Seventh International Technical Meeting on Air Pollution Modeling and Its Application

Airlie, Virginia

September 7-10, 1976

Topic 7: Innovative Modeling Techniques

Rapporteur's Report

Donald M. Rote, Rapporteur

Papers given by:

1. Mrs. H. Apsimon (Speaker), A.J.H. Goddard, Nuclear Power Section, Mechanical Engineering Department, Imperial College of Science and Technology, London S. W. 7, UK.
2. R. A. Anthes (Speaker), N. Seaman, D. Kayser, Penn. State University, Dept. of Meteorology, 543 Deike Bldg., University Park, PA 16802, USA.
3. H. G. Fortak, Deutsche Forschungs-und Versuchsanstalt fur Luft- and Raumfahrt E. V. Institut fur Physik der Atmosphare, 8031 Oberpfaffenhofen, Post Wessling, 088, FRG.
4. K. H. Muller, CCR Euratom, 21020 Ispra, Italia.

In the first paper Mrs. Apsimon described a model for simulating the dispersal of radioactive pollutants beyond the first few hours of travel and gave the results of a calculation for a hypothetical 6-hour release of I_{131}. The model takes into account both spatial and temporal changes in the planetary boundary layer that affect the transport and fate of the pollutants. The transport of a continuous release is simulated by a series of discrete puffs, one released every 6 hours, whose trajectories are computed from grids of surface pressure data covering 30 degrees of longitude and 18 degrees of latitude. The computation of the trajectories uses mean wind speeds proportional to the geostrophic wind speed and wind directions rotated thru an angle from the geostrophic wind direction depending on surface and atmospheric conditions and time of day. Comparison of the results of 10 meter winds computed by their "pseudo-geostrophic" technique and measurements showed that wind speeds agreed quite well over open, flat areas, but not so well for other surface conditions. Agreement with 400m winds was much better.

Mrs. Apsimon pointed out that because there is no threshold dose below which exposure to radiation has been shown to be harmless, it is necessary to consider the exposure of large numbers of people to low dose levels corresponding to large distances from the source. Consequently, as part of the model computation, dose values are folded into population distributions. Because of the large travel times involved, loss mechanisms including natural decay and wet and dry depositure are incorporated in the model. Future work will emphasize the transitional phases of development of the dicrete puffs for ranges up to 100 km during which time the puffs have not yet become uniformly distributed in the vertical in the mixed layer which is itself rapidly changing with time. During these phases of development ground level concentrations are highest and strongly dependent on time.

D. Fox: What do you do about stable conditions?

H. Apsimon: The stable layer was allowed to come to the ground at night for low wind speeds and no deposition was considered under such conditions.

W. Klug: Was baroclynicity taken into consideration in computing surface winds?

H. Apsimon; No. However, the model is flexible enough to allow such effects to be treated.

R. Anthes: Is vertical settling important?

H. Apsimon: Such effects were not examined. However, the Carson and Smith model used for the development of the mixed layer could account for settling and such investigations are planned.

In the second paper, R. Anthes described two numerical experiments to forecast the diffusion and transport of an inert pollutant in the vicinity of steep terrain. The experiments involved the use of a 2-D (vertical-downwind cross section) version of the Penn. State Mesoscale Dynamic Model. This latter model was used to make a 3-hour forecast of the meteorological variables which in turn served as input data for a transport and diffusion model designed for use over variable terrain. The diffusion model was a modified version of the particle-in-cell model described by Teuscher and Hauser in which the vertical diffusion term is calculated on an Eulerian grid.

The basic problem was to forecast pollutant concentrations during the transition from stable to unstable conditions given only the terrain (a smoothed version of the San Andres range in New Mexico) and a 2m/sec geostrophic wind. The circulation is an output of the dynamic model.

The first experiment began with an initially uniform concentration field with no additional sources or sinks and was supposed to illustrate the effects of growth of the PBL on the vertical distribution. The calculation showed that horizontal variations in the mixing depth due to terrain variations resulted in significant horizontal variations in the concentration after 3 hours.

The second experiment included a constant flux of pollutant near the base but upwind of the mountain and illustrated the vertical and horizontal spreading of a plume under a light-wind, convective situation. In spite of strong vertical mixing and an alternating wind circulation pattern, both horizontal and vertical concentration gradients remained large near the source.

The Author felt that the results of both models were plausible but had no observations for comparison.

G. Hofnagle: Was the surface temperature a function of X?

R. Anthes: Ordinarily, insolation is the input variable but for these experiments surface heat flux was input. In general either can be a function of position.

A. Venkatram: If the memory of the system is short, why not use a diagnostic model instead of a predictive model?

This question precipitated some discussion regarding the definition of terms. The author, in his paper, used the term "prognostic" to refer to the equation of motion and the thermo-dynamic equation and the term "diagnostic" to refer to the hydrostatic and continuity equations and the equation of state.

W. Johnson offered the following "off-the-cuff" definitions:

Diagnostic - use of measurements and simplified relations in lieu of the use of full dynamical equations.

Predictive - use external forcing and full dynamical equations.

In a subsequent communication A. Venkatram provided the following elaboration on the definitions of these terms which are not in disagreement with W. Johnson's "off-the-cuff" comments:

1. A diagnostic model is a steady state model. Diagnostic models can be used when a system reacts with a negligible time lag to changes imposed on the system, i.e., the sytem has a very short memory. Then, it is possible to relate system variables such as temperature and velocity to variables at the boundaries of the system. For example, the drag law which relates surface shear stress to the geostrophic wind is the result of diagnostic modelling. In essence, a diagnostic model is valid when the time scale of the system is small relative to the time scales we are interested in.

2. A prognostic model is an unsteady state model. A prognostic model is needed when the system reacts to external forcing with a time lag which cannot be neglected; it has a relatively long memory and it is necessary to trace its history before we can relate boundary variables to system variables.

In the present case it was not clear how the "memory" as Venkatram put it, compared with the rates of change of the meteorological quantities driving the diffusion and transport model. In any case,using the full set of dynamical equations did provide a convenient means of obtaining the complex data required to apply the diffusion and transport model.

G. Marziano: Can the model be applied to costal regions and if so, what circulation data is required?

R. Anthes: Yes. The dynamical equations would generate the local circulation given the mean geostrophic wind, surface roughness and time of year.

Hilat: Have you investigated close up separation and turbulent wake phenomena?

Anthes: No, because you need non-hydrostatic effects.

In the third paper, H. Fortak discussed the use of Green's functions in air pollution modelling. Provided that the Green's functions can be written down for the homogeneous form of the transport equation, the solution for quite general inputs and boundary conditions reduces to the solution of integrals. He points out that whereas finite difference methods yield rough concentration fields the Green's function approach leads to smoothed out fields. He examined, with care, the general properties that the Green's functions must possess including causality and reciprocity. He then discussed an application of the method to the special time dependent case of a homogenous wind field.

Wendell: Have any computations been performed?

Fortak: Yes. It turns out that most integrations can be done analytically. Often one gets error functions which only require a desk calculator for evaluation.

Runca: Are you limited in your choice of K coefficients?

Fortak: Yes, Z-dependent K's lead to complicated Sturm Liouville problems. These equations would require finite differencing.

Reddie: Have comparisons been made with other model outputs?

Fortak: No, aside from simple checking.

The fourth paper was given by K. Muller. In this paper Muller described the use of Monte Carlo techniques for simulation of dispersion of pollutants. In his rather novel approach, he regards a pollutant puff or cloud as a single large eddy which undergoes the same fate as other eddies in that after some initial relaxation time during which collisions cause a breakup of the original eddy into many smaller eddies, the pollution eddies and turbulence elements have the same spectral and decay behavior. He assumes that the frequency distribution of the pollutant eddies is governed by the linear Boltzman equation and discusses its solution with Monte Carlo techniques. These techniques are discussed in general and the literature is reviewed. Then the nature of the collision mechanism was discussed and he commented on the possibility of incorporating chemical transformations into the approach.

J. Knox: Would you do chemistry in each eddy independently?

K. Muller: Yes.

H. Fortak: Do you limit the turbulence field of motion with some model?

K. Muller: Yes.

D. Jost: Up to which wave length of the turbulence spectrum do you go?

K. Muller: Answer not clear.

7th NATO/CCMS International Technical Meeting
on Air Pollution Modeling and its Application

SOME CONSIDERATIONS ABOUT THE STABILITY CATEGORIES IN THE CASE OF SHORT RANGE DIFFUSION OF ATMOSPHERIC RELEASES

Pietro CAGNETTI
Lab.Contaminazione Continentale CNEN - CSN Casaccia, ROMA, Italy

Sept. 7-10, 1976, Airlie, Virginia, United States of America

SOME CONSIDERATIONS ABOUT THE STABILITY CATEGORIES IN THE CASE OF SHORT RANGE DIFFUSION OF ATMOSPHERIC RELEASES

SUMMARY

A series of about 30 atmospheric diffusion experiments, using a chemical tracer was carried out to study the effect of the turbulence induced by buildings of a nuclear research center on the diffusion of contaminants over short distances.

It is pointed out that, on a wide range of stability situations practically analyzed the results do not confirm the variety of estimates generally suggested for flat terrain by the literature.

Some practical rules are given to evaluate the dilution of contaminants over short distances at the Casaccia Nuclear Research Center site for situations ranging from instability to light stability.

1 - INTRODUCTION

At the Casaccia Nuclear Research Center several experiments of atmospheric diffusion on short distances were carried out with the aim of investigating the influence on diffusion either of the turbulence induced by a single building or of the general increase of turbulence due to the natural obstacles present in the Center.

An aerosol of uranine dye, produced by atomization and with 99.9 per cent of the particles less than 1 μm dia. (1) was utilized as a chemical tracer.

A first series of 11 experiments was performed with release heights of 10 and 20 m, and sampling points at 315 and 500 m of distance downwind.

A second series of 11 experiments was then carried out with a release height of 40 m, and with sampling points up to the same max. distance. At last a third series of 9 releases was performed upwind of a building of about 1600 m^2 cross sectional area, and with crosswind sampling points up to a distance of 850 m (2).

2 - EXPERIMENTAL DATA FROM RELEASES FAR FROM BUILDINGS

The site is characterized by a rather flat terrain; several buildings with a mean height of 10 m, and different kinds of strewn trees, are present in the Center (see Fig.2, ref.(2)). Such natural and artificial obstacles induce a great turbulence in the near ground air-layer, which may justify the experimental results.

For a more detailed relation of all the experiments and of the meteorological data collected, we refer to publications (1) and (2).

In Fig.1 the crosswind air concentrations are shown, for a sampling arc at a distance of 315 m and for a release height of 20 m. The release lasted about 20 minutes; the dashed line represents the theoretical values of concentrations obtained from the Pasquill estimates of the diffusion parameters, and taking into account the lateral spread of the wind.The diffusion situation was characterized by a "B" category, according to Pasquill's theory (7).

Fig.2 refers to an experiment similar to the previous one, but during a "C" category situation; the release lasted half an hour. The same sampling distance, and a height of release of 10 m, characterize the experimental data shown in Fig.3, collected during a "B", category situation, and for a release lasting 1 hour.

It must be remarked that the crosswind peak values of air concentration are about the same indipendently of the height of release (10-20 m) or of the category. Those values are sistematically less than the theoretical ones, even if the effect of the lateral dispersion, consequent to the prolonged time release, is taken into account (1). It was first supposed that the non significancy of the categories distinction was caused by the turbulence induced by the site asperities. This was why a series of releases from 10 and 40 m of height was performed, first with a single sampling arc at 500 m then with an additional arc at 265 m.

Figures 4 and 5 refer to a release from an height of 10 m, and to 2 situations characterized by categories "C" and "B", respectively. The difference shown in those two cases between the theoretical estimates (dashed lines) and the experimental data is greater than shown in the previous experiments at lower distance.

A great number of releases were carried out from a height of 40 m involving also categories of neutrality "D" and slight stability "E".

Figures 6-7-8-9 refer to examples of categories B,C,D and E-F. It can be seen that the theoretical values are higher than the experimental ones during instability situations, lower during stability, and about the same during neutrality. But in all cases the experimental values for the crosswind peak concentrations are the same at about $5 \cdot 10^{-6}$ s/m^3 (at 500 m of distance and for a release height of 40 m). The other experiments confirm such a result.

It has been possible, at last, through the calculation of the product $\sigma_\theta \cdot \bar{U}$ (where σ_θ= horizontal standard deviation of the wind direction, $\bar{U}$ = mean wind velocity), to estimate by means of the method proposed by Watson (3), the σ_y values (σ_y = horizontal standard deviation of crosswind ground level air concentrations).

Fig.10 shows the comparison between such theoretical values and the experimental data collected at the Casaccia Center:a very good agreement can be observed.

3 - EXPERIMENTAL RESULTS FOR RELEASES IN PROXIMITY OF A BUILDING

The preceding results lead us to suppose that the turbulence in the layer near the ground, induced by the elevated value of the surface roughness, is responsible of the homogeneity shown by the data collected during situations characterized by different stability categories. However this can hardly explain the homogeneity shown by the data collected from 40 m releases. This is why a new series of experiments were carried out to see whether a single building, in the lee of the release, would introduce an additional effect in the turbulence and therefore in the downwind dilution.

A series of nine experiments, with a sampling network around the building (of which the cross-sectional area is about 1600 m^2) and on two arcs at 450 and 850 m was performed (2). The results (dashed line)are shown in Fig.11, were the dotted line refers to the data collected far from buildings, but always in the Center (those are the experimental data we discussed in the previous paragraphs). We can see that the dilution effect of the building implies a factor of about 4 at 300 m from the release point. As the distance increases the factor falls rapidly to about 2 at 550 m, and probably to 1 at 800-1000 m. These results are in good agreement with the measurements made by Islitzer at Idaho Falls (4) and confirm the difficulty of justifing the homogeneity of the different categories only by the assumption of the increased turbulence in the layer near the ground. In effect, if the near ground turbulence were sufficient to produce the almost constant dilution factors, only a little difference should be seen between the air concentration values downwind of a release in the wake induced by a building and far from buildings.

- SOME PRACTICAL CONSIDERATIONS

If we group all the data concerning near ground releases (10-20 m) during instability categories (see Fig.12) we can compare them with the estimates given by Pasquill for a short time of release. From an inspetion of the graph it can be seen that, during instability categories, the real concentration values for a near ground release could be foreseen taking the Pasquill data from a category between "A" and "B" (dashed line) and then correcting them for the prolonged time of release by means of the law proposed by Hinds (5) ($\chi_1/\chi_2 =$ $= (t_2/t_1)^{0.5}$) and confirmed by Moore (6).

This implies the assumption that the estimates of Pasquill would be valid for a release time of about 5 minutes. For a 1 hour release the correction factor would be about 3.5 (dotted line). The mean wind velocity for all the experiments, fell in the range from 2.5 to 4.5 m/s. Furthermore, when the height of release is 40 m (see Fig.13), always during instability categories ("B" and "C"), the experimental data agree with the estimates of Pasquill for a category between "C" and "D" (dashed line) with a mean wind velocity of 4 m/s, and taking into account the duration of the release with the Hinds formula (dotted line), as in the previous case.

It must be said indeed that the experiments carried out during neutrality or light stability, with a 40 m release height, had given concentration values, at the ground level and at a distance of 500 m, similar to those shown during instability situations. However no experiments were carried out during high stability situations, as in the early morning after a clear night with very light winds. This would be a very interesting case, but it is known that it is very difficult to realize some experiments during very light wind situations. The only case we tested (Fig.9, moderate stability, about one hour after sunset) was in effect characterized by a surface mean wind velocity of 0.6 m/s.

CONCLUSIONS

The analysis of the data from 30 diffusion experiments carried out at the Casaccia Center site, during different categories, from instability to moderate stability, and up to a maximum distance of 850 m, shows that, at least for this particular site:

a) the crosswind peak concentration at low distances seems not to be a function of the surface wind velocity (in the range 0.6 - 4.5 m/s actually tested) and of the stability category, as generally stated for free and flat terrain;

b) the experimental crosswind peak concentration values for a near ground level release and during a wide range of situation from instability to neutrality are well fitted by the theoretical data from a category intermediate between "A" and "B", after that a correction is made for the release duration, with the aid of the Hinds formula, and supposing $\bar{V}= 4$ m/s;

c) for a release height of 40 m, a good fit of the experimental data is given by the theoretical data for a category between "C" and "D", elaborated as in the previous case b);

d) the concentration values from near-building diffusion are in quite good agreement with other authors experimental data;

e) the lateral spread values as a function of the travel time and of the standard deviation of the horizontal wind direction are in good agreement with the Hanford theory.

REFERENCES

1 - CAGNETTI P.: "Influenza della turbolenza indotta dalle infrastrutture di un Centro di ricerche nucleari sulla diffusione atmosferica a breve distanza di contaminanti radioattivi" CNEN Report RT/PROT(76)8

2 - CAGNETTI P.: "Downwind concentrations of an airborne tracer released in the neighbourhood of a building" Atmospheric Environment, vol.9, pages 739-747, 1975

3 - WATSON E.C., SIMPSON C.L.: "Effect of wind variability on environmental consequences of prolonged releases of radioactive contaminants" BNWL-SA-1058, 1967

4 - ISLITZER N.F.: "Aerodynamic effect of large reactor complexes upon atmospheric turbulence and diffusion" IDO-12041, U.S. Weather Bureau, N.R.T.S. Idaho Falls, Idaho

5 - HINDS W.T.: " On the variation of concentration in plumes and building wakes " BNWL-SA-1400, 1967

6 - MOORE D.J.: "SO_2 concentration measurements near Tilbury Power Station" Atmospheric Environment 1967, vol1, pag.389

7 - PASQUILL F.: "Atmospheric Diffusion" Van Nostrand, London 1961

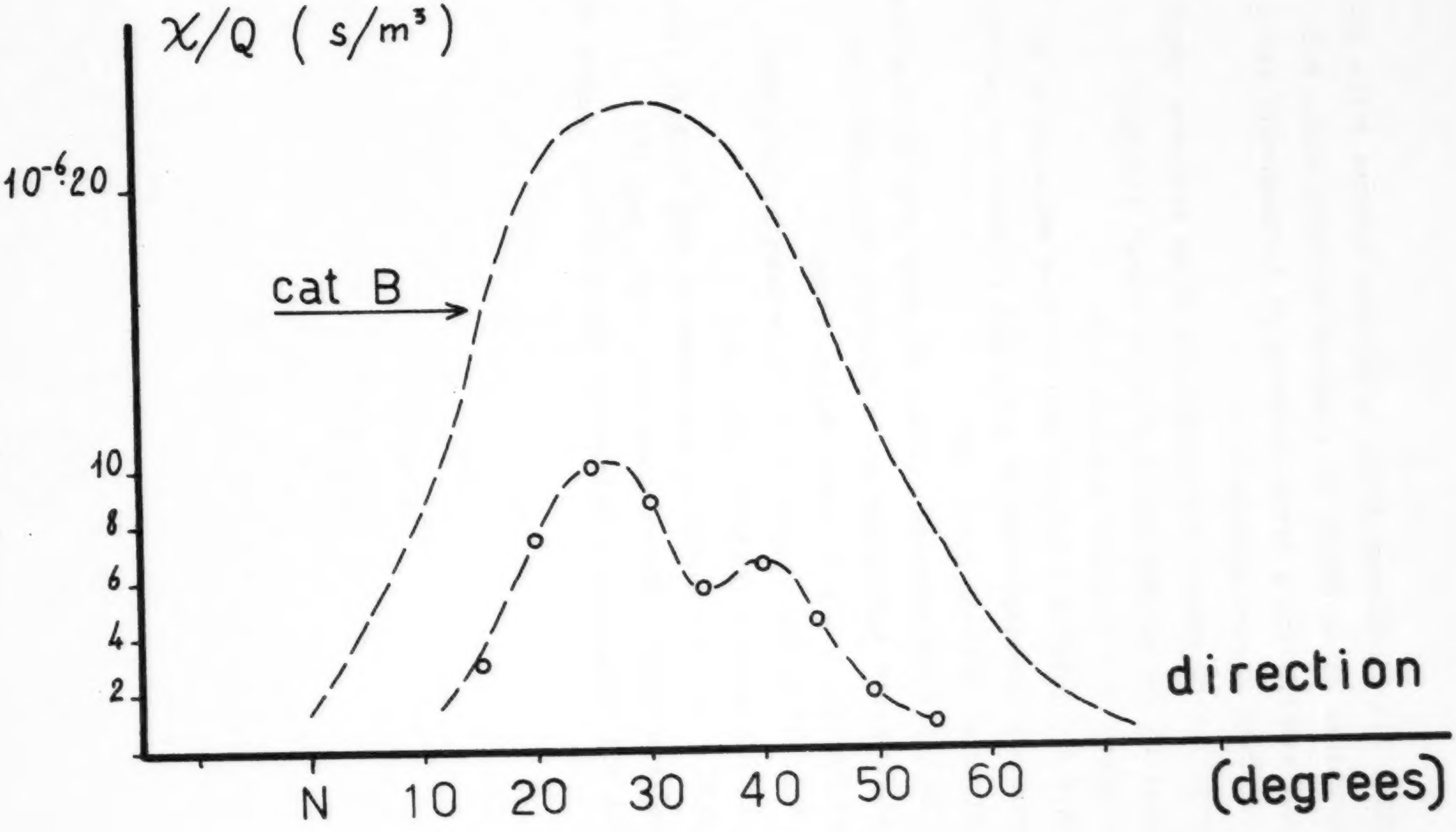
χ/Q (s/m³)
10⁻⁶ 20
10
8
6
4
2
cat B
direction
(degrees)
N
10
20
30
40
50
60

FIG. 1

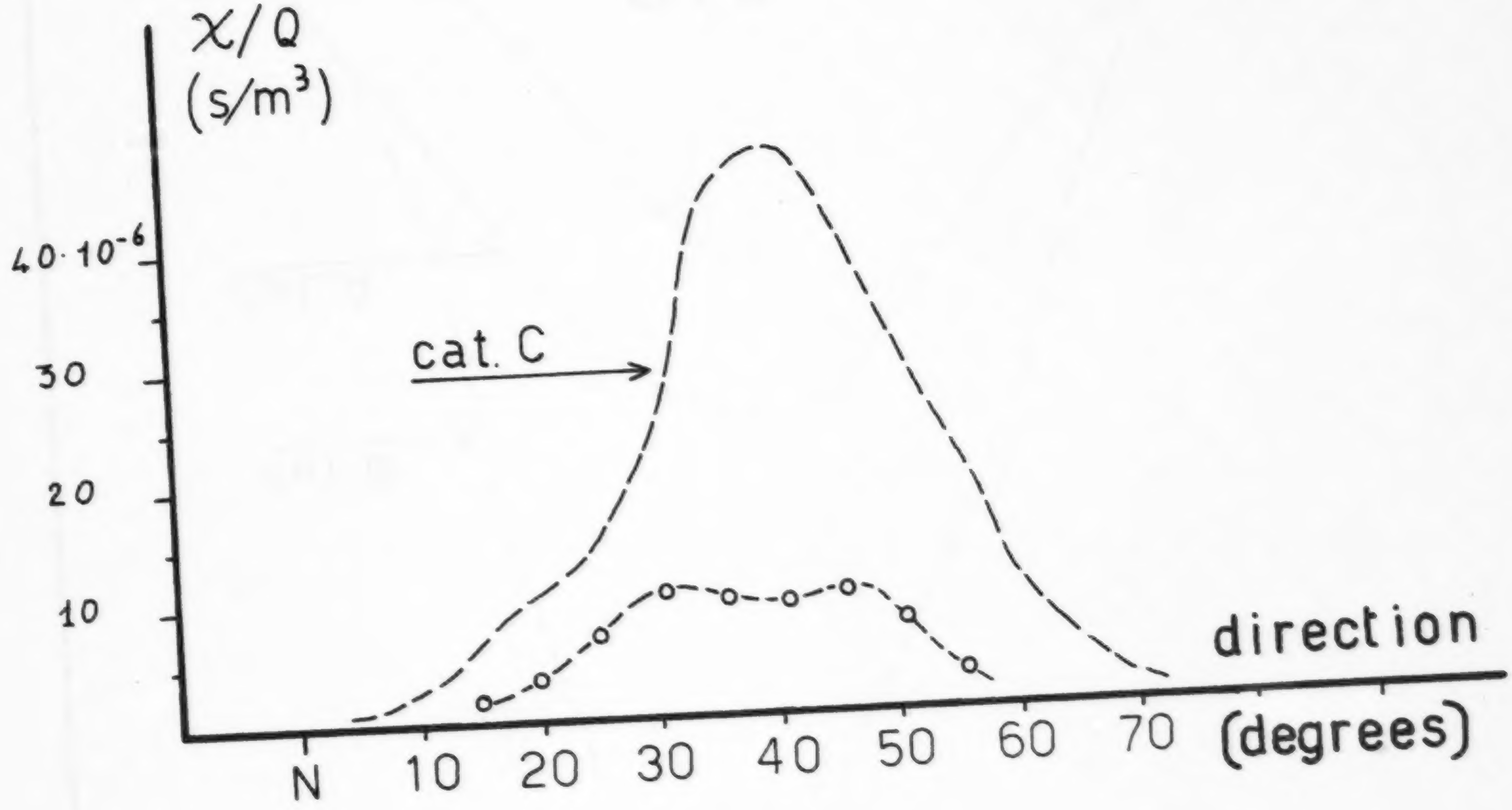
χ/Q
(s/m^3)
40·10^{-6}
30
20
10
cat. C
N
10
20
30
40
50
60
70
direction
(degrees)

FIG. 2

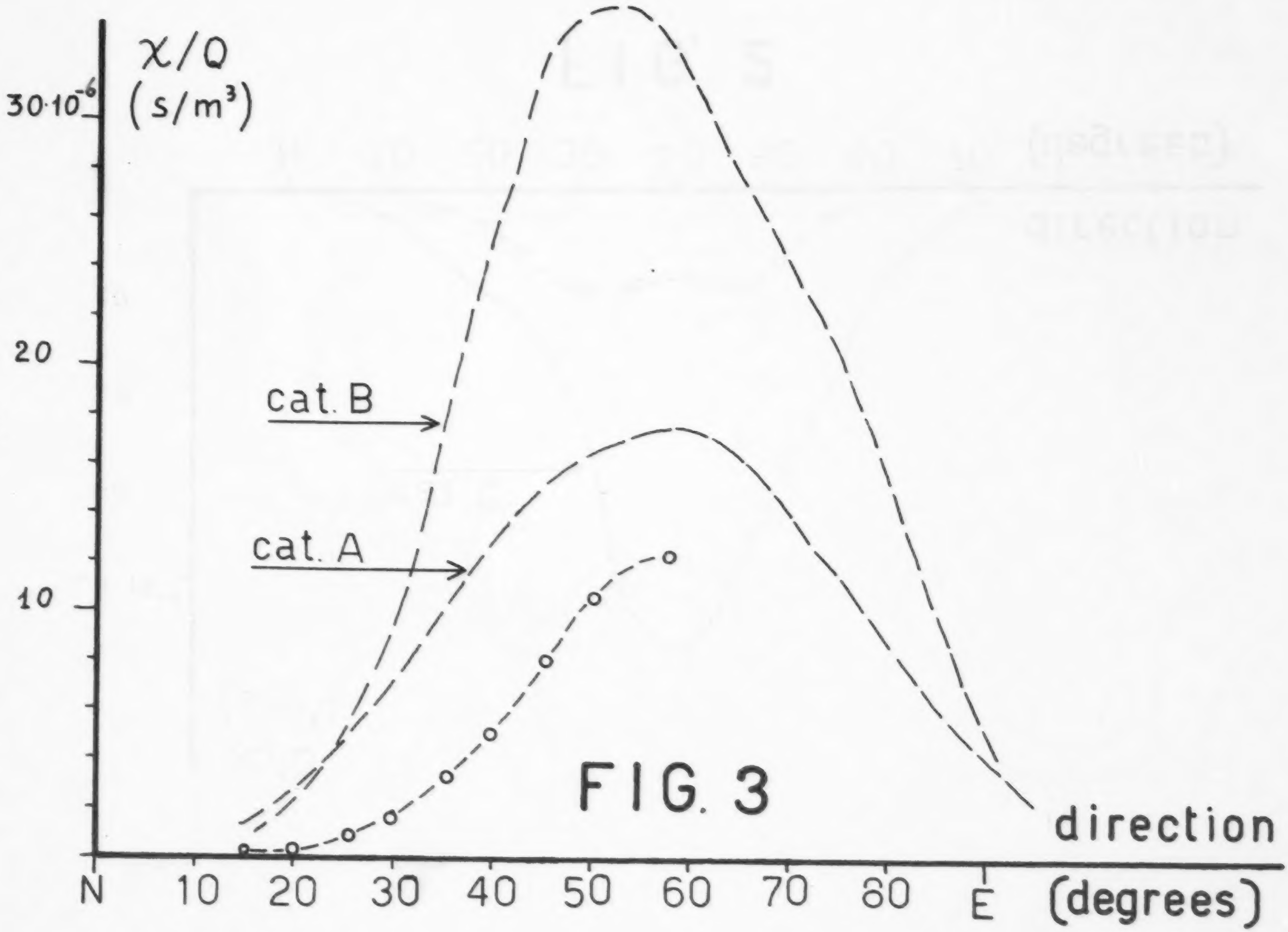
χ/Q
(s/m³)
30·10⁻⁶
20
10
cat. B
cat. A
N
10
20
30
40
50
60
70
80
E
direction
(degrees)

FIG. 3

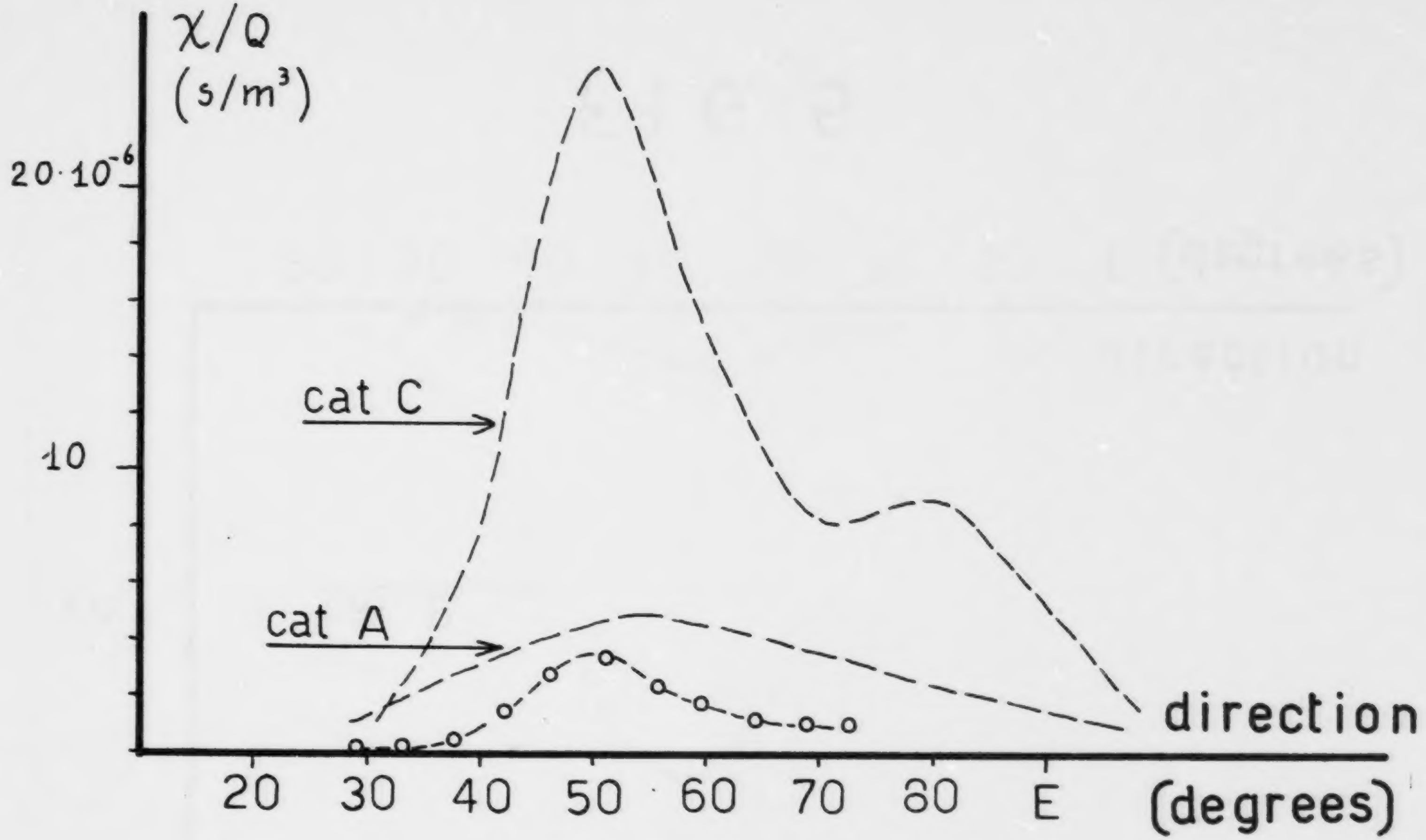
χ/Q
(s/m³)
20·10⁻⁶
10
cat C
cat A
direction
(degrees)
20
30
40
50
60
70
80
E

FIG. 4

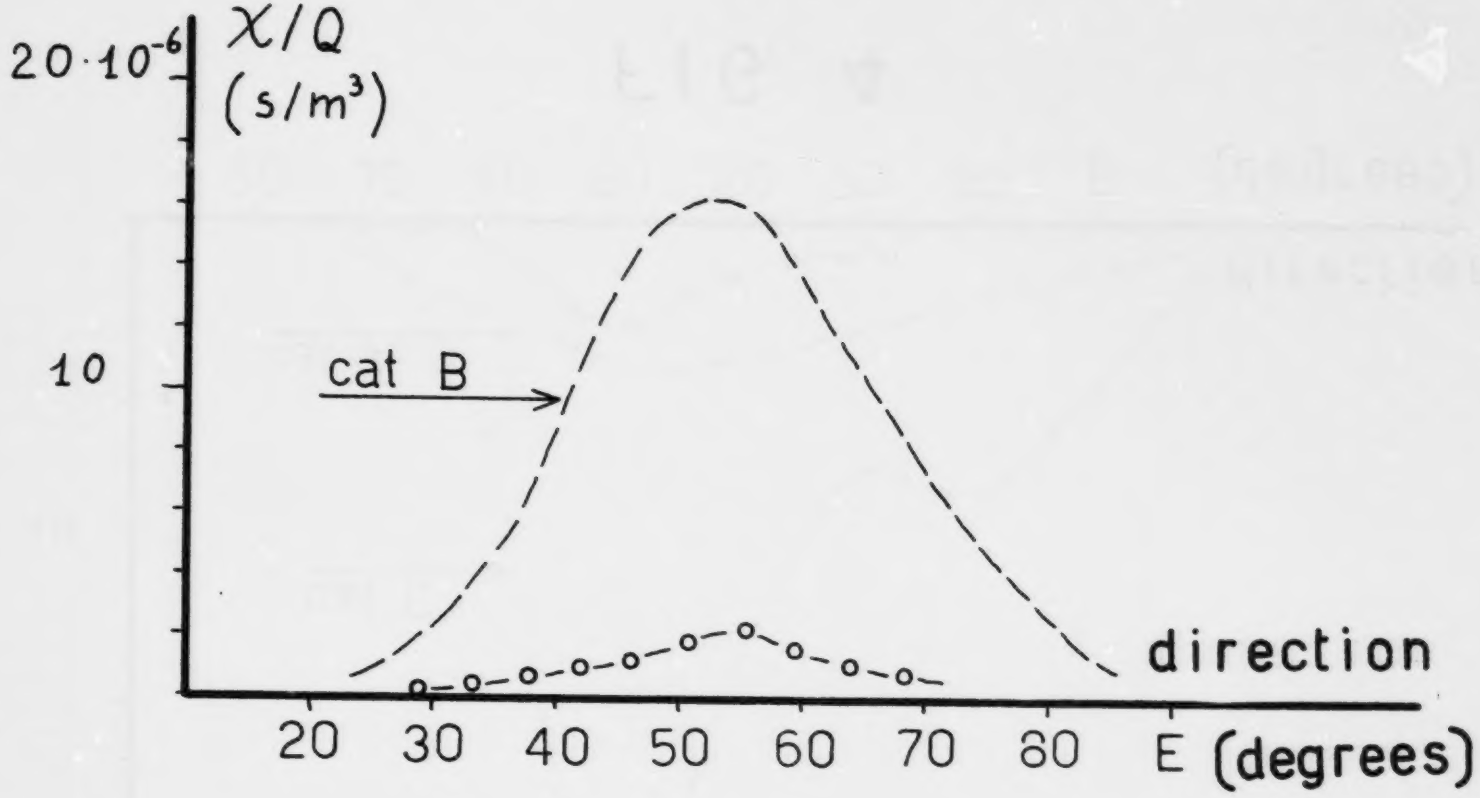

FIG. 5

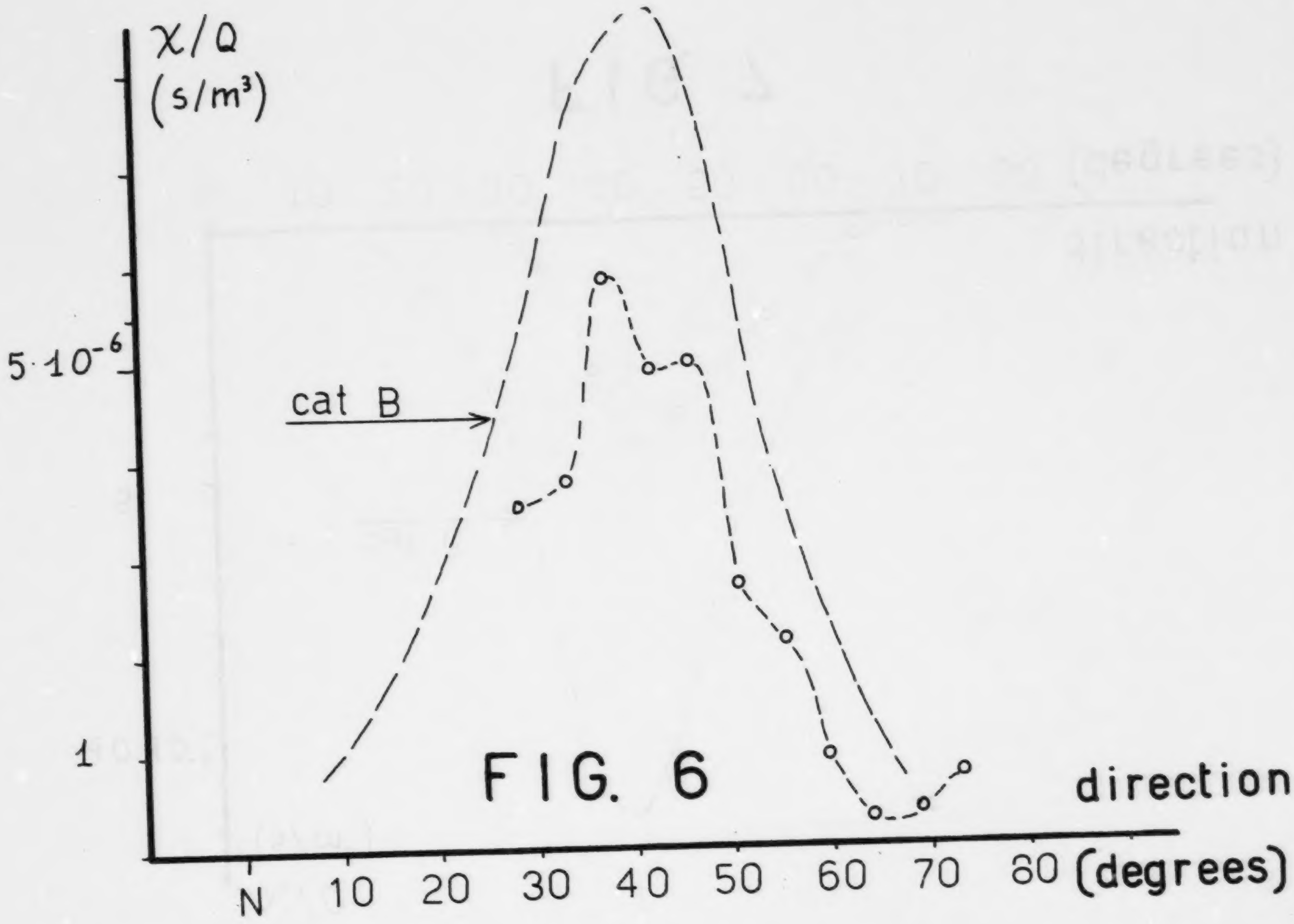

FIG. 6

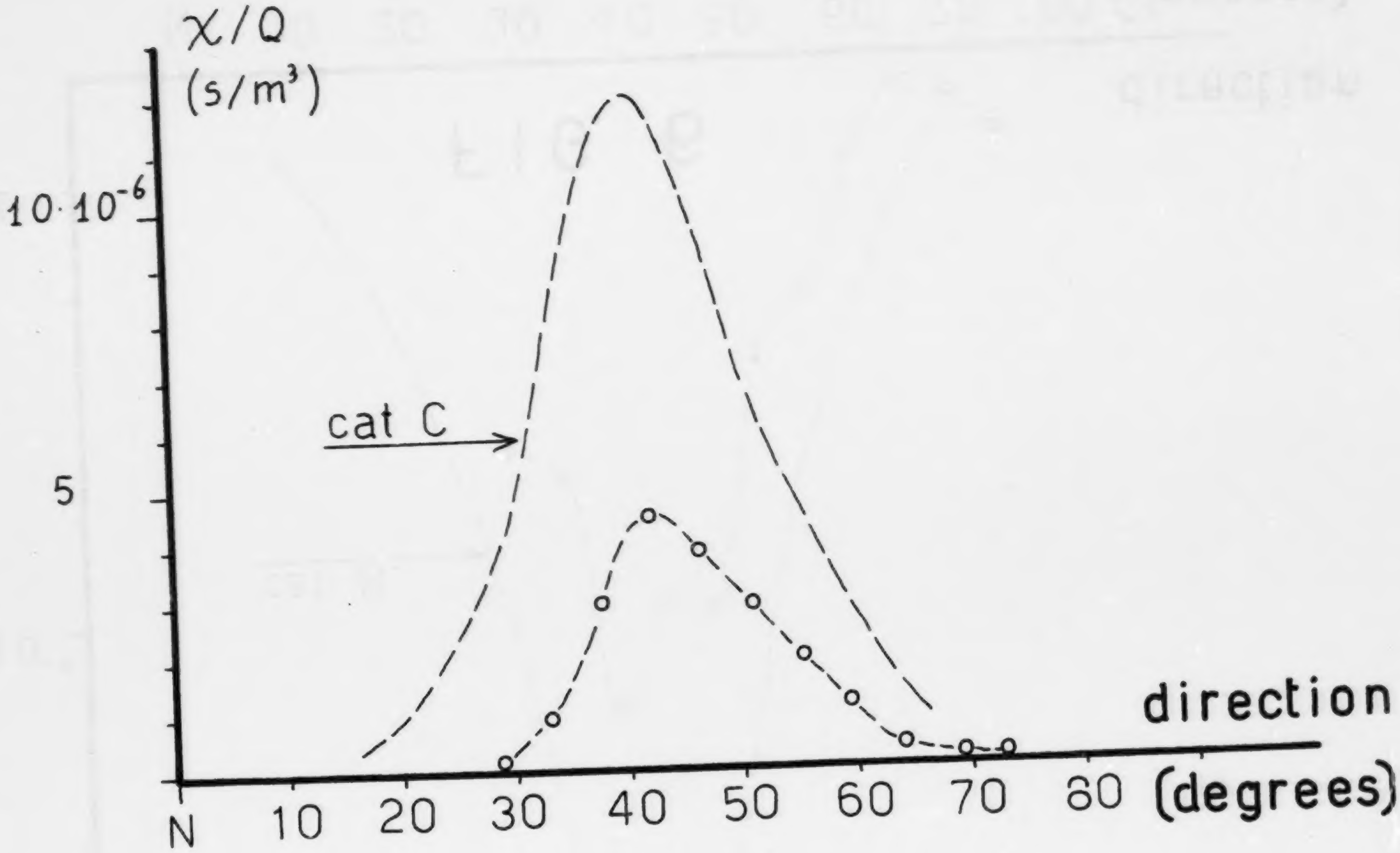
χ/Q
(s/m^3)
$10 \cdot 10^{-6}$
5
cat C
direction
(degrees)
N
10
20
30
40
50
60
70
80

FIG. 7

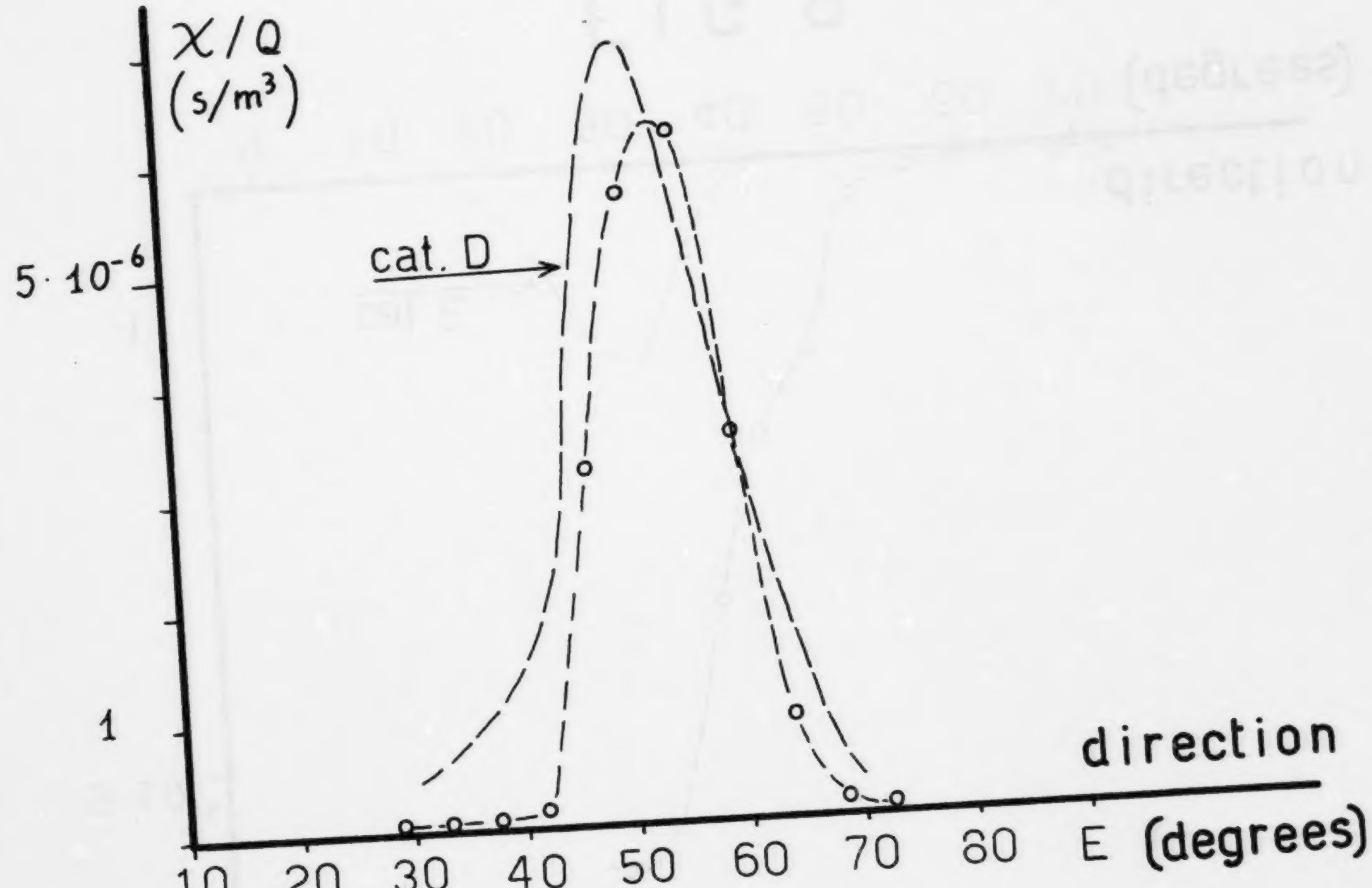

FIG. 8

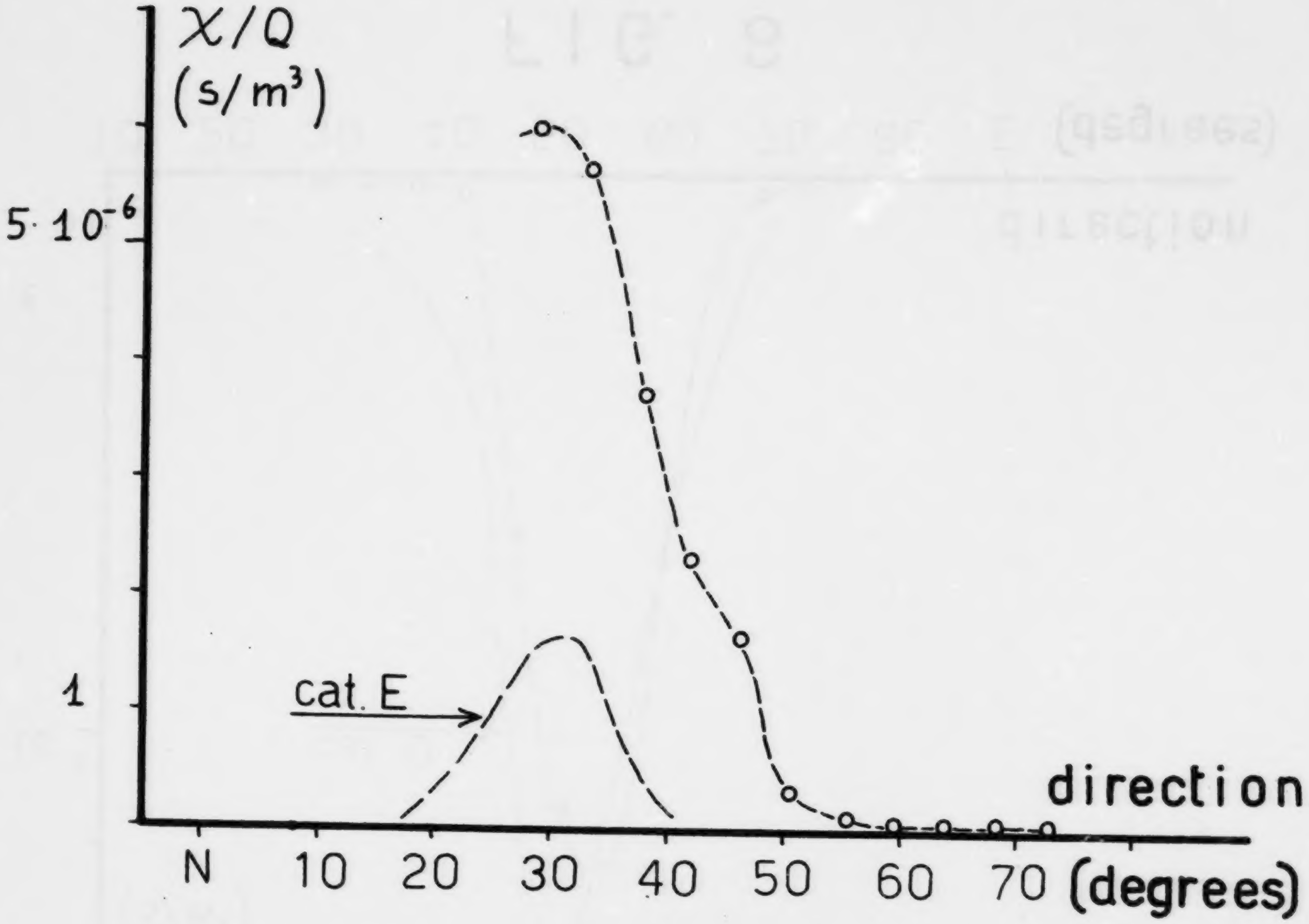
χ/Q
(s/m^3)
$5 \cdot 10^{-6}$
1
cat. E
direction
N
10
20
30
40
50
60
70
(degrees)

FIG. 9

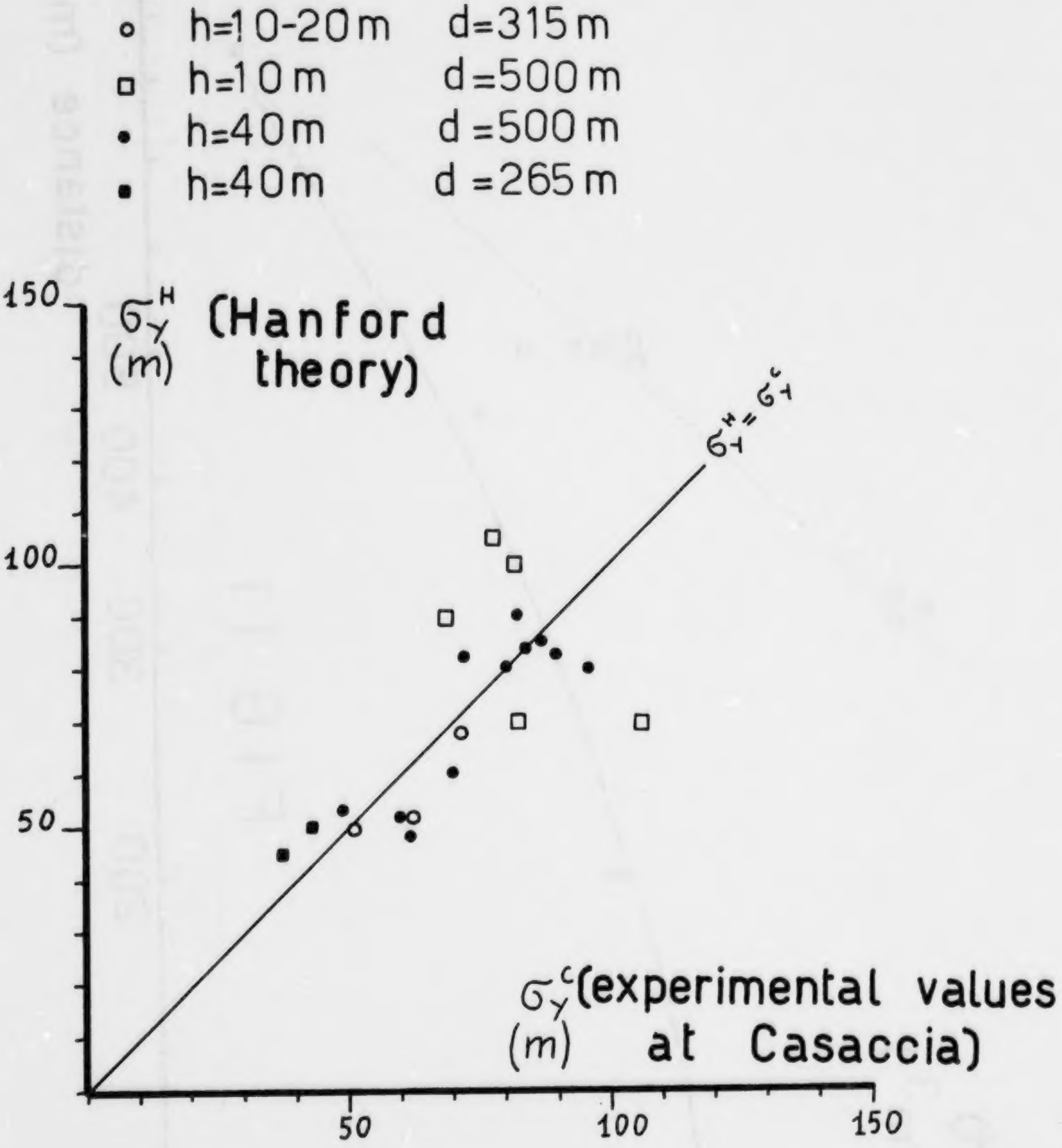
○ h=10-20m d=315m
□ h=10m d=500m
• h=40m d=500m
■ h=40m d=265m
150
100
50
σ_y^H (m) (Hanford theory)
$\sigma_y^H = \sigma_y^c$
σ_y^c (m) (experimental values at Casaccia)
50
100
150

FIG. 10

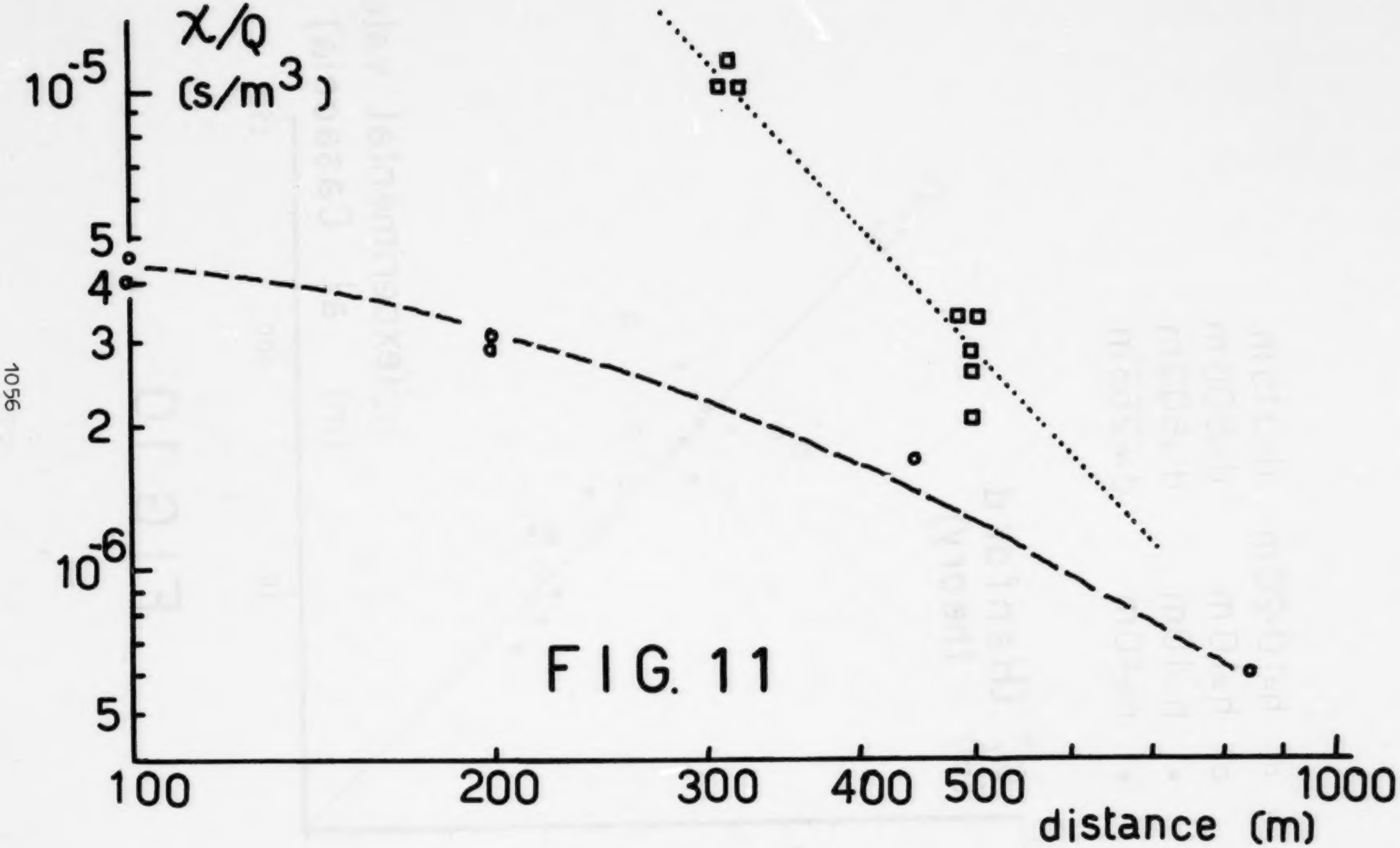

FIG. 11

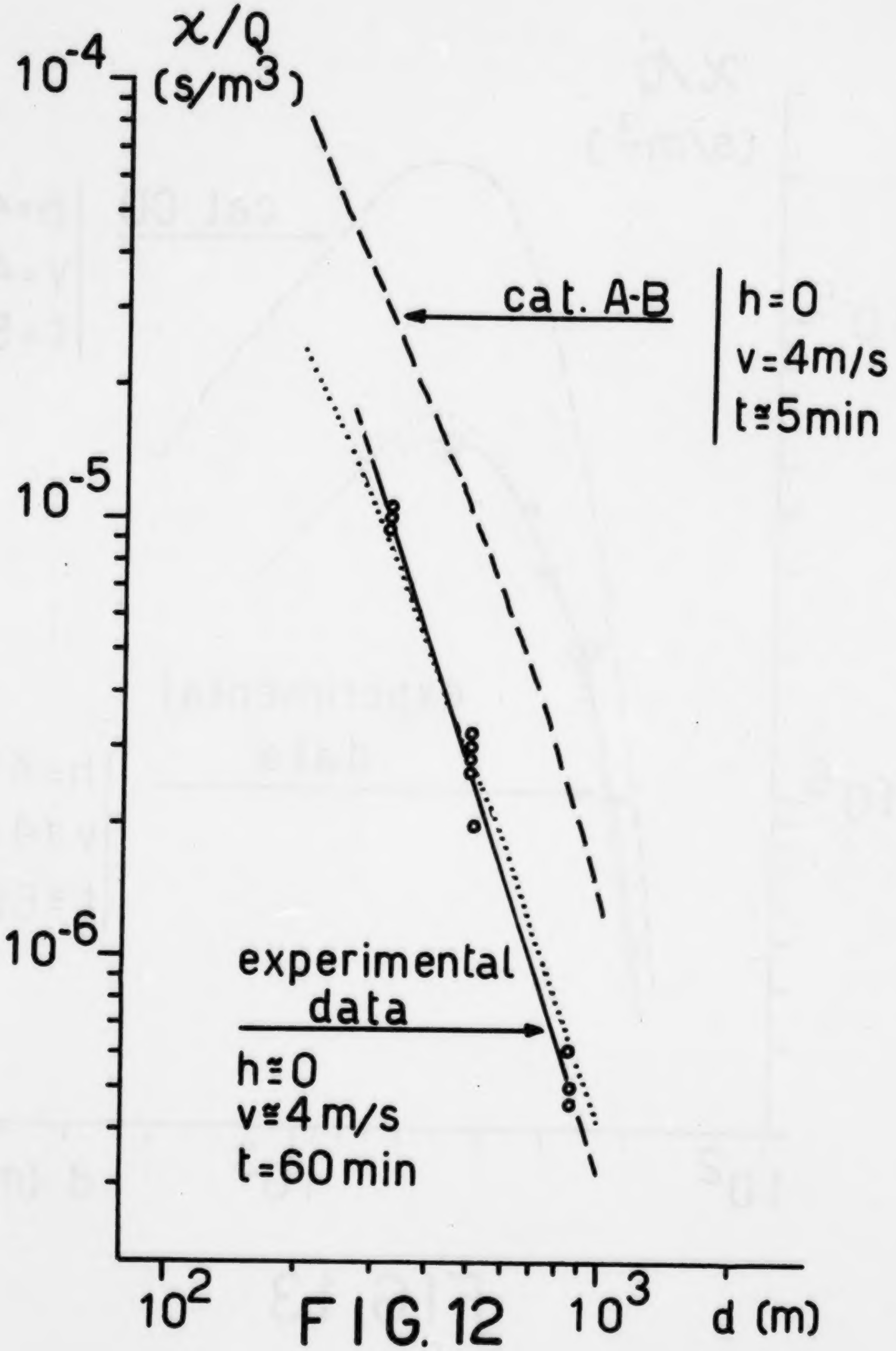
χ/Q
(s/m³)
10^{-4}
10^{-5}
10^{-6}
cat. A-B
h=0
v=4m/s
t≅5min
experimental
data
h≅0
v≅4 m/s
t=60 min
10^2
10^3
d (m)

FIG. 12

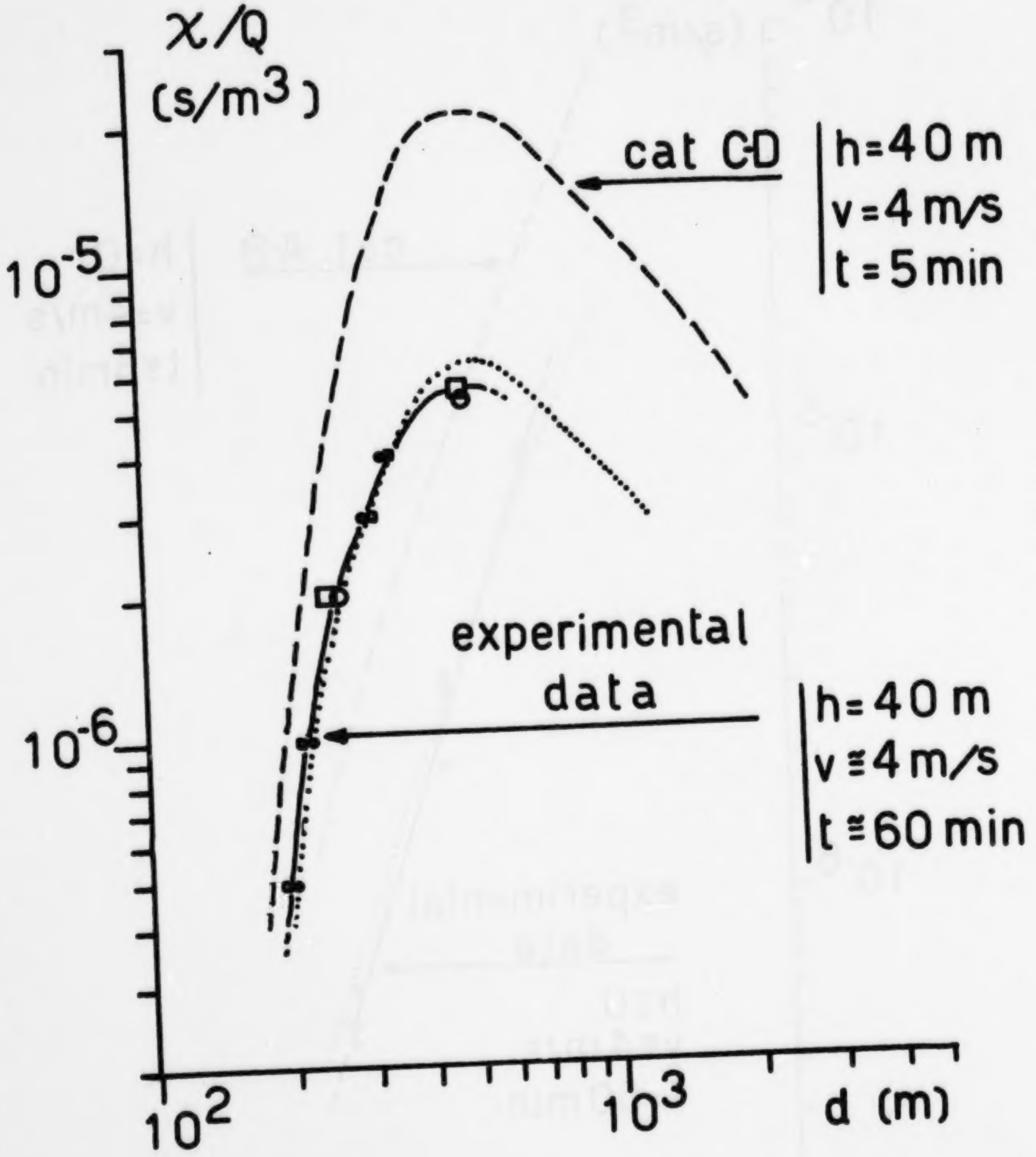
χ/Q
(s/m3)
10-5
10-6
cat C-D
h=40 m
v=4 m/s
t=5 min
experimental data
h=40 m
v≅4 m/s
t≅60 min
10²
10³
d (m)

FIG. 13

7th International Technical Meeting on Air Pollution Modeling and its Application

Application of the Tennekes-Carson Slab Model of the PBL to the Prediction of Internal Boundary Layer Development

A. Venkatram
Atmospheric Environment Service
Toronto, Canada

September 7-10, 1976

Airlie, Virginia

United States of America

1. Introduction

There has been some recent interest (Meroney et al., 1975; Peters, 1975; Weisman, 1976; Raynor et al., 1974; Sethuraman and Cermak, 1974) in the occurrence of fumigation as related to the development of the internal boundary layer when cold stable air flows from water onto warmer land. The depth of the mixed layer as a function of the distance from the land-water boundary determines the location of fumigation of elevated pollutant plumes from shoreline stacks. Meroney et al. (1975) have studied mixed layer growth in a wind tunnel and their results show that in the initial stages of development the mixed layer height shows a half power dependence on fetch. Most observational evidence (Van der Hoven, 1967; Raynor et al., 1974; Weisman and Hirt, 1975) seem to support this result.

At the level of sophistication required for operational prediction of mixed layer growth, a number of thermal boundary layer models have been proposed (Priestley, 1959; Peters, 1975). Although these models provide reasonable estimates of mixed layer height, they rely heavily on the concept of eddy diffusivity which, apart from being inapplicable in a strongly convective atmosphere, cannot be estimated in an objective manner.

We suggest that a physically realistic model of internal boundary layer development can be constructed by using the Tennekes (1973) or Carson (1973) mixed layer model in a Langrangian framework. One advantage of such an approach is that the much maligned eddy diffusivity is not used. The assumptions about the temperature and velocity fields have been experimentally verified (Willis and Deardorff, 1975; Lenschow, 1974). Furthermore, the dynamics of the mixed layer is not very sensitive to the closure hypothesis (Mahrt and Lenschow, 1976).

In this paper we present a computationally simple advective mixed layer model, which in some ways is similar to the successful urban boundary layer model proposed by Summers (1965).

2. Physical Model

A schematic of the physical situation being considered is shown in Fig. 1. Cold stable air flows onto warmer land, and the resulting upward heat flux gives rise to the mixed internal boundary layer. We assume that the land temperature is uniform and does not vary significantly over the time scale of the model (∿ 3 hrs). This implies steady state conditions; we are looking at an "equilibrium state" lasting for a few hours. This assumption might not be satisfactory during the hours around sunrise and sunset when surface temperatures change rapidly.

Fig. 2 gives a schematic representation of the potential temperature profile in the developing convective internal boundary layer. Velocity and potential temperature gradients are confined to the shallow superadiabatic surface layer which is typically of the order of tens of meters in depth. The turbulent layer above the surface layer is buoyancy dominated and is assumed to produce uniform profiles of potential temperature and wind. While the well-mixed assumption is satisfactory for the potential temperature, it is not clear that vertical gradients of velocity are always negligible in the mixed layer. However, there is some evidence to show that wind shear may be small even with baroclinicity (Arya and Wyngaard, 1975). The inversion layer which separates the convective boundary layer from the non-turbulent stable atmosphere above is taken to be thin enough to be represented by a first order discontinuity in potential temperature.

In the figure, the potential temperature gradient in the stable layer is seen to be independent of height. However, this is not a necessary assumption for the formulation of the model. It will be shown later on that the proposed model is capable of handling changes in γ (see Fig. 2).

3. Formulation of the Model

We choose a right-handed co-ordinate system with the x-axis oriented in the direction of the mixed layer wind at the land-water boundary. Then, the energy equation for the mixed layer can be written as (Tennekes, 1973)

$$h \frac{d\theta_m}{dt} = (\overline{w'\theta'})_s - (\overline{w'\theta'})_h \qquad (1)$$

where h is the mixed layer height, θ_m is the potential temperature and the subscripts 's' and 'h' refer to the surface and the top of the mixed layer respectively. The substantial derivative term in (1) can be expanded as

$$\frac{d\theta_m}{dt} = u\frac{\partial\theta_m}{\partial x} + v\frac{\partial\theta_m}{\partial y} \qquad (2)$$

where u and v are the mixed layer winds.

Using the thermal energy equation, the following equation for the rate of inversion rise can be derived (Tennekes, 1973; Carson, 1973)

$$\frac{dh}{dt} = - \frac{(\overline{w'\theta'})_h}{\Delta} + w_h \qquad (3)$$

where Δ is the temperature jump across the inversion, w_h is the vertical velocity at the top of the mixed layer.

In this study, we assume that the vertical velocity, w_h, can be neglected in comparison with the thermal entrainment velocity w_e $(= -(\overline{w'\theta'})_h/\Delta)$.

This assumption would be most reasonable in the initial stages of mixed layer growth when the relatively large surface heat fluxes give rise to large entrainment rates.

To close the set of equations we require an equation for the inversion heat flux, $(\overline{w'\theta'})_h$ or equivalently Δ. To keep the analysis as simple as possible we write Δ as follows

$$\Delta = F\gamma h \tag{4}$$

where F is a constant less than one. Eq. (4) was first suggested by Betts (1973). By combining (1), (3) and (4) we can show that it is equivalent to the commonly used (Tennekes, 1973; Carson, 1973) expression

$$(\overline{w'\theta'})_h = -A(\overline{w'\theta'})_s \tag{5}$$

where $A = F/(1-2F)$.

There have been some recent studies (Carson, 1973; Zilitinkevich, 1975) which show that (5) is not entirely satisfactory as A varies during the growth of the mixed layer. However, this is not critical as estimates of mixed layer height made using formulations of the type given by (5) have compared very favourably with observational data (Tennekes and Van Ulden, 1974). Furthermore, Mahrt and Lenshow (1976) show that if A increases from 0.15 to 0.25, an expected typical variation in A, the mixed layer height is changed by 7%. We will provide additional justification for this assertion at a later stage.

Referring to Fig. 2 we can express the mixed layer depth h as follows

$$h = (\theta_m - \theta_v)/\gamma(1-F) \tag{6}$$

where θ_v is the temperature obtained by extrapolating the stable profile above the mixed layer to the land surface. As γ varies from layer to layer, θ_v need not be equal to the water temperature θ_w.

We parameterize the surface heat flux using the bulk aerodynamic method (Deardorff, 1972). Following Deardorff's notation we write

$$(\overline{w'\theta'})_s = C_\theta u_* (\theta_\ell - \theta_m) \tag{7}$$

where C_θ is the heat transfer coefficient, and u_*, the surface friction velocity is parameterized using C_u, the friction coefficient

$$u_* = C_u u_m \tag{8}$$

where $u_m = (u^2+v^2)^{1/2}$

If we assume that the land surface is characterized by a constant roughness length, we can take C_θ and C_u to be uniform. Although C_θ and C_u do depend on surface stratification, there is some evidence (Priestley, 1959) to show that the variation of the bulk transfer coefficients can be neglected. As we do not expect the horizontal velocity to vary significantly over the horizontal scale (tens of kilometers) being considered, we take u_* to be constant.

Combining (1), (5) and (7) and using non-dimensional quantities we obtain

$$\frac{\bar{\theta}}{(1-\bar{\theta})}\frac{d\bar{\theta}}{d\bar{t}} = 1 \tag{9}$$

where $\bar{\theta} = (\theta_m - \theta_v)/(\theta_\ell - \theta_v)$ (10)

and $\bar{t} = C_\theta t u_*(1-F)/(1-2F)H$ (11)

and $H = (\theta_\ell - \theta_v)/\gamma(1-F)$ (12)

With the initial condition $\bar{\theta} = \bar{\theta}_i$; $\bar{t} = 0$, the solution of (9) is straightforward

$$\bar{\theta} = 1 - (1-\bar{\theta}_i)\exp\left[-(\bar{t} + \bar{\theta} - \bar{\theta}_i)\right] \tag{13}$$

and using (6) we can write

$$\bar{h} = \bar{\theta}; \quad \bar{h} = h/H \tag{14}$$

From the above discussion, we can readily see that the model can handle step changes in γ. All we need to do is change the initial condition and redefine θ_v.

We note that H represents the maximum mixed layer height. In the next section we will discuss the solution given by (13) in more detail.

4. Discussion

If we assume that the boundary layer is stably stratified over the water, one would expect the depth of the mixed layer being advected onto the land to be of the order of the Monin-Obukhov length (∿ 10 m), and we are justified in neglecting $\bar{\theta}_i$ in (13). Then, sacrificing some generality for elegance, we can rewrite (13) as follows

$$\bar{h} = 1 - \exp\left[-(\bar{t} + \bar{h})\right] \tag{15}$$

We have plotted the curve given by (15) in Fig. 3. We note from the log-log graph that h is proportional to the half power of $\bar{t}$ in the initial stages of growth. This behaviour can be readily clarified by expanding the exponential term in (15) around $\bar{t} = 0$.

$$\bar{h} \sim \sqrt{2\bar{t}} \tag{16}$$

We can gain some appreciation for (16) by replacing the time co-ordinate with the horizontal space co-ordinate x. It can be easily shown that over the time scale (∿ 3 hrs) of the physical situation under consideration, the change in wind direction will be small in the absence of significant surface temperature gradients perpendicular to the wind direction or topographical variations. Then, as the x-axis is along the initial direction of the wind, v can be justifiably neglected and u_m can be replaced by u. With these simplications the variable $\bar{t}$ becomes

$$\bar{t} = C_\theta C_u x(1-F)/(1-2F)H \tag{17}$$

and (16) can be rewritten as

$$h \sim \left[2C_\theta C_u x(\theta_\ell - \theta_v)/\gamma(1-2F)\right]^{1/2} \tag{18}$$

In assuming a constant γ in (18) we have neglected the effect of the surface based stable layer in which the potential temperature gradient is considerably greater than in the layer above it. We can estimate the error involved by calculating the distance at which a typical surface inversion is filled up. Let us assign some values to the variables in (18)

$C_\theta = C_u = 0.1$ (Deardorff, 1972); $\theta_v = \theta_w = 300$ K; $\theta_\ell = 310$K

$\gamma = 0.02$ K/m (Carson, 1973); $F = 1/7$ (Tennekes, 1973)

$h = 100$ m.

Using the above values, the distance at which the surface based stable layer is eroded is around 0.70 km. As we are interested in scales of the order of tens of kilometers, we might get away by using a γ corresponding to the atmosphere above the surface inversion. However, there is no difficulty in accounting for the varying γ.

At this point it is appropriate to examine the sensitivity of mixed layer growth to the assumed value of F. From (18) we can see that the factor $1/(1-2F)^{1/2}$ determines this sensitivity. A typical variation of A from 0.15 to 0.25 corresponds to F changing from 0.115 to 0.167 (see [5]). This variation in F translates into a mere 4% change in h. Thus, we can safely conclude that the assumption regarding the value of F is not terribly important insofar as estimating the mixed layer height is concerned.

As γ of the surface inversion over the water is usually larger than that of the atmosphere above it, $\theta_v > \theta_w$, and we can write

$$(\theta_\ell - \theta_v) = f(\theta_\ell - \theta_w) \qquad (19)$$

where f is a fraction (< 1) that can be as small as 1/3 (Carson, 1973).

Substituting (19) into (18) yields

$$h \sim \left[\frac{2f}{(1-2F)} C_\theta C_u \frac{(\theta_\ell - \theta_w)}{\gamma} x\right]^{1/2} \tag{20}$$

As f is less than 1 we can probably take $(2f/[1-2F])^{1/2} \sim 1$. Then, making the reasonable assumption that $C_\theta \sim C_u$ and replacing C_u by u_*/u we can re-express (20) as follows

$$h \sim \frac{u_*}{u} \left[\frac{(\theta_\ell - \theta_w)}{\gamma} x\right]^{1/2} \tag{21}$$

It is very encouraging to note that (21) is virtually identical to the empirical equation presented by Raynor et al. (1974) to fit their observational data. It might be useful to point out again that the initial dependence of h on the square root of the fetch has been confirmed by a number of observational studies (Van der Hoven, 1967; Meroney et al., 1975; Weisman and Hirt, 1975).

In examining Fig. 3 we note that (16) is applicable for $\bar{h}$ as great as 0.3 corresponding to $\bar{t} = 6 \times 10^{-2}$. In fact the error involved in using (16) instead of (15) to compute $\bar{h}$ is around 12% which might well be within the limits of error acceptable in environmental studies. To determine the horizontal extent over which (21) can be reasonably used we will assign some typical values to the variables in (17)

$$C_\theta = C_u = 0.1; \quad F = 1/7; \quad H = 1000 \text{ m}; \quad \bar{t} = 6 \times 10^{-2} \quad \text{(Fig. 3)}.$$

Then, (17) yields $x \sim 6$ km. Clearly, the range of applicability of (21) increases with H (= $[\theta_\ell - \theta_w]/\gamma[1-F]$). The square root dependence of $\bar{h}$ on $\bar{t}$ does not hold for large $\bar{t}$ (or x). In fact, for large $\bar{t}$, $\bar{h}$ behaves like

$$h \sim 1 - \exp(-\bar{t}) \qquad (22)$$

The preceding exercise demonstrates the importance of formulating a model such as the one described in this paper. It is evident that the model gives us considerably more insight into the physical situation than dimensional analysis can. The arguments about the range of applicability of (21) show that one has to be careful about postulating relationships between h and x.

It is necessary to emphasize the convenience afforded by the utilization of (15) in predicting mixed layer growth. The estimation of the bulk transfer coefficients C_θ and C_u is facilitated by the fact that they do not vary significantly over a wide range of conditions (Priestley, 1959). As the transfer coefficients are surface related, they can be readily measured. Alternatively, they can be reliably estimated from formulae such as those developed by Deardorff (1972). In any event, it is much easier to deal with the bulk transfer coefficients than with an average eddy diffusivity, a quantity which has little meaning in a strongly convective boundary layer.

The relevance of the model to the prediction of fumigation is self-evident and need not be elaborated here. It is only necessary to point out that fumigation cannot occur if the height of the elevated plume exceeds the maximum mixed layer height H.

References

Arya, S.P.S., and J.C. Wyngaard, 1975: Effect of baroclinicity on wind profiles and geostrophic drag law for the convective planetary boundary layer. *J. Atmos. Sci.*, *32*, 767-778.

Carson, D.J., 1973: The development of dry inversion-capped convectively unstable boundary layer. *Quart. J. Roy. Meteorol. Soc.*, *99*, 450-467.

Deardorff, J.W., 1972: Parameterization of the planetary boundary layer for use in general circulation models. *Mon. Wea. Rev.*, *100*, 93-106.

Lenschow, D.H., 1974: Model of the height variation of the turbulence kinetic energy budget in the unstable planetary boundary layer. *J. Atmos. Sci.*, *31*, 465-474.

Mahrt, L., and D.H. Lenschow, 1976: Growth dynamics of the convectively mixed layer. *J. Atmos. Sci.*, *33*, 41-51.

Meroney, R.W., J.E. Cermak and B.T. Yang, 1975: Modeling of atmospheric transport and fumigation at shoreline sites. *Boundary-Layer Meteorology*, *9*, 69-90.

Peters, L.K., 1975: On the criteria for the occurrence of fumigation inland from a large lake. *Atmospheric Environment*, *9*, 809-816.

Priestley, C.H.B., 1959: Turbulent Transfer in the Lower Atmosphere. The University of Chicago Press, 130 pp.

Raynor, G.S., P. Michael, R.M. Brown and S. Sethuraman, 1974: A research program on atmospheric diffusion from an oceanic site. Symposium on Atmospheric Diffusion and Air Pollution, Santa Barbara, Calif., 289-295.

Sethuraman, S. and J.E. Cermak, 1974: Mean temperature distributions over a physically modelled three-dimensional heat island for different stability conditions. Symposium on Atmospheric Diffusion and Air Pollution, Santa Barbara, Calif., 381-386.

Summers, P.W., 1965: An urban heat island model, its role in air pollution problems with application to Montreal. Paper presented at the 1st Canadian Conference in Micrometeorology, Toronto 12-14, 1965.

Tennekes, H., 1973: A model for the dynamics of the inversion above a convective boundary layer. *J. Atmos. Sci.*, *30*, 558-567.

Tennekes, H., 1975: Reply to Zilitinkevich, 1975: *J. Atmos. Sci.*, *32*, 992-995.

Van der Hoven, I., 1967: Atmospheric transport and diffusion at coastal sites. *Nucl. Safety*, *8*, 490-499.

Weisman, B., and M.S. Hirt, 1975: Dispersion governed by the thermal internal boundary layer. Paper presented at the 68th Annual Meeting of APCA, Boston, June 1975.

Willis, G.E., and J.W. Deardorff, 1974: A laboratory model of the unstable planetary boundary layer. *J. Atmos. Sci.*, *31*, 1297-1307.

Zilitinkevich, S.S., 1975: Comments on a "A Model for the Dynamics of the Inversion Above a Convective Boundary Layer. *J. Atmos. Sci.*, *32*, 991-992.

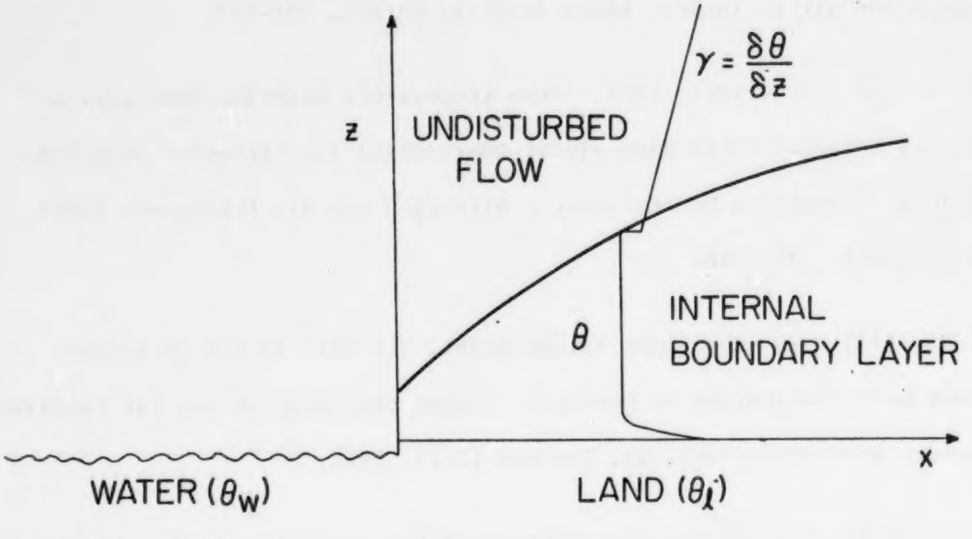
$\gamma = \frac{\delta\theta}{\delta z}$
z
UNDISTURBED FLOW
θ
INTERNAL BOUNDARY LAYER
x
WATER (θ_W)
LAND (θ_l)

Figure 1 - Schematic of Physical System

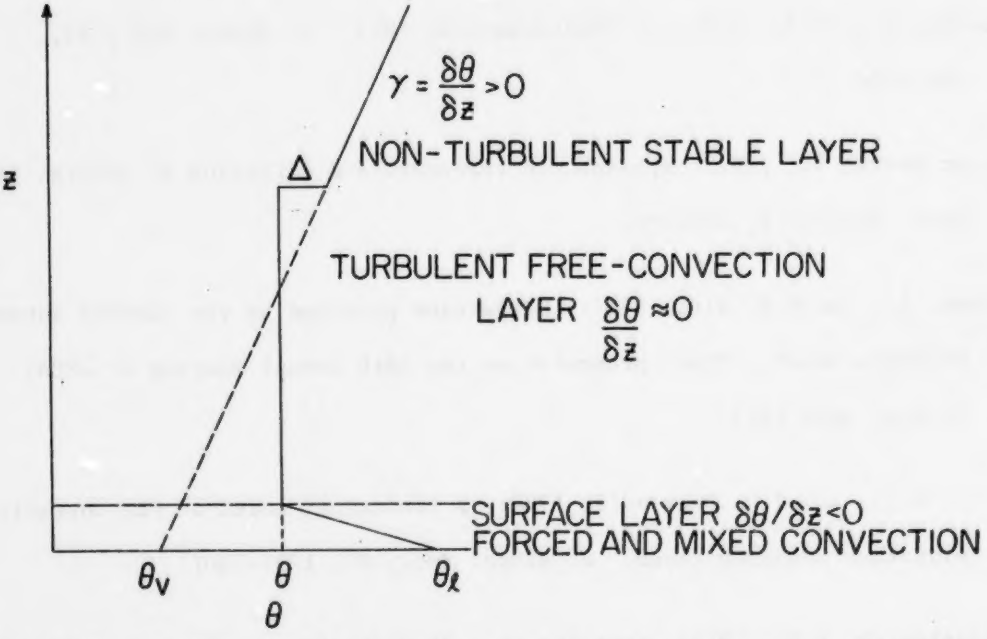
$\gamma = \frac{\delta\theta}{\delta z} > 0$
z
Δ
NON-TURBULENT STABLE LAYER
TURBULENT FREE-CONVECTION LAYER $\frac{\delta\theta}{\delta z} \approx 0$
SURFACE LAYER $\delta\theta/\delta z < 0$
FORCED AND MIXED CONVECTION
θ_V
θ
θ_l
θ

Figure 2 - Schematic Representation of Idealized Potential Temperature Profile.

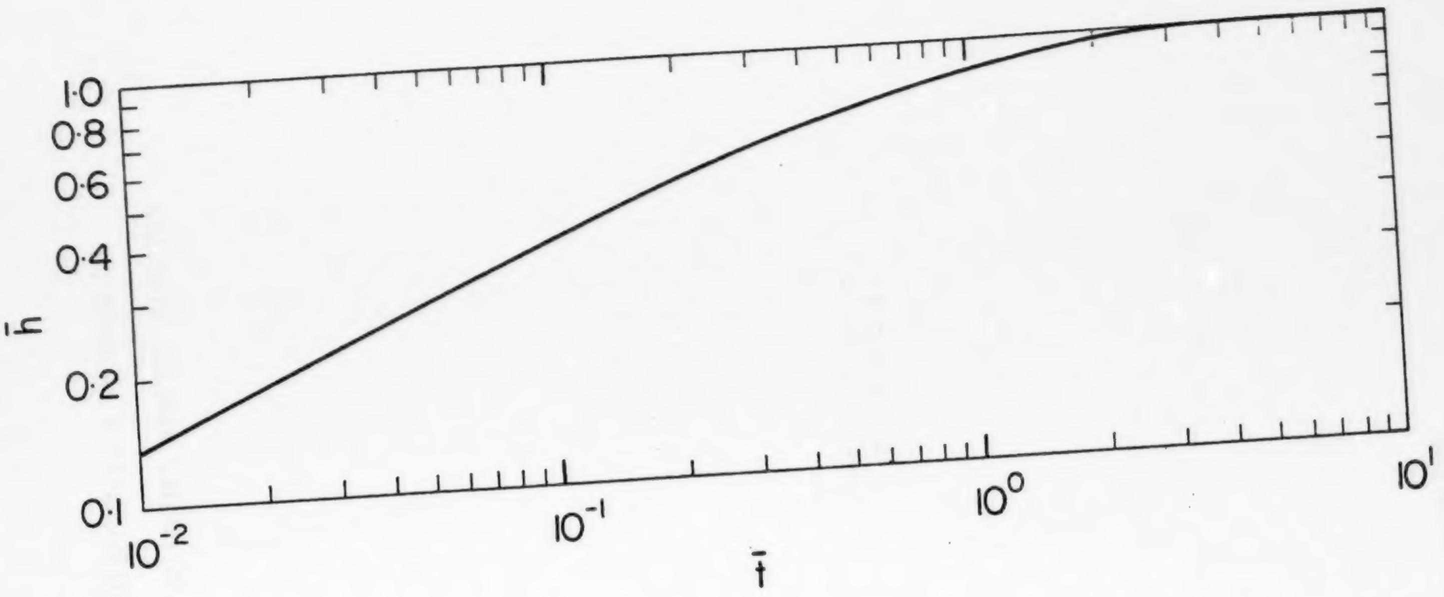

FIGURE 3 - VARIATION OF $\bar{h}$ WITH $\bar{t}$

7 th NATO/CCMS
International Technical Meeting
on Air Pollution Modeling

AGENDA

AIRLIE HOUSE, AIRLIE, VIRGINIA
UNITED STATES OF AMERICA

Tuesday, September 7, 1976

Registration of Participants

Wednesday, September 8, 1976

Opening Remarks (Federal Republic of Germany and U.S.A.)
Short address by Cameron Sanders (U.S. State Department)

Presentation and Discussion of Topic 1:

Examples of Model Validation and Model Application

Chairman: H. H. SLATER
Rapporteur: J. B. KNOX

1. R. A. Porter:

   Two Efficient Gaussian Plume Models Developed at the Texas Air Control Board

   (R. A. Porter, P. E. Meteorology Section,
   J. H. Christiansen, Data Processing Section,
   Texas Air Control Board, 8520 Shoal Creek Blvd.,
   Austin, Texas, 78758, U.S.A.)

Rapporteur: B. A. EGAN

2. D. M. Rote:

   Air Quality Management Utilizing Air Quality Models

   (D. M. Rote, EES, Argonne National Laboratory,
   9700 South Cass Avenue, Argonne, Illinois
   60439, U.S.A.)

3. R. Gualdi

   Mathematical Models Applications in Air Quality Network Planning and Management

   (A. Cavallaro, R. Gualdi, G. Laneve,
   G. Tebaldi, Provincia di Milano,
   Laboratorio Igiene e Profilassi, Reparto Chimico,
   Via Juvara 22, Milano, Italia)

4. L. L. Schulman:

   Validation of Gaussian Plume Point Source Diffusion Model in a Lake Shore Environment

   (L. L. Schulman, T. F. Lavery, S. Penansky,
   Environmental Research and Technology, Inc.,
   696 Virginia Road, Concord, Mass. 01742, U. S. A.)

5. G. F. Hoffnagle:

Diffusion Model Comparisons to Measured Data in Complex Terrain

(R. B. Lantz, G. F. Hoffnagle and S. B. Pahwa, INTERA, Environmental Consultants, Ltd., 1201 Dairy Ashford, Houston, Texas, 77079, U.S.A.)

6. B. Sivertsen:

The Use and Validation of Dispersion Models in a Fjord Valley Area of Norway

(B. Sivertsen, Norwegian Institute of Air Research, N - Kjeller)

7. F. Nieuwstadt:

The Validation of a Gaussian Plume Model for Long-term Averaged Concentrations in the Rijnmond Area

(F. Nieuwstadt, Koninklijk Netherlands Meteorologisch Instituut, Utrechtseweg 297, NL - De Bilt)

8. W. E. Wilson:

A Dual Tracer Study for the Validation of Models with Respect to High and Low Altitude Sources

(W. E. Wilson, U.S. Environmental Protection Agency, Research Triangle Park, N. C.; F. Shair, California Institute of Technology; J. Overton, Northrop Services, Inc., U.S.A.)

9. J. G. Kretzschmar:

Validation of the Emission Frequency Distribution Models in the Region of Antwerp

(J. G. Kretzschmar, G. de Baere, F. Vandervee, SCK, CEN, Boerentang 200, B-2400 Mol, Presentation and Discussion of Topic 2:

Interregional and Regional Models

Chairman: M. KWIZAK

Rapporteur: H. E. TURNER

1. B. Dietzer:

   Preliminary Results of the Application of a Statistical Model on Interregional Transport of SO_2

   (B. Dietzer, Sektion Meteorologie der
   TH Darmstadt, Hochschulstr. 1,
   D - 6100 Darmstadt)

2. W. B. Johnson:

   The European Regional Model of Air Pollution (EURMAP) and its Application to Transfrontier Air Pollution

   (W. B. Johnson, D. E. Wolf, R. L. Mancuso
   Stanford Research Institute, Menlo Park,
   California 94025, USA)

3. J. B. Knox

   Recent Advances in the Simulation of Regional Air Quality

   (J. B. Knox, Atmospheric and Geophys. Sciences
   Div. Physical Department, Lawrence Livermore,
   Lab., Univ. of California, Livermore, Calif.
   94550, U.S.A.)

Rapporteur: A. W. C. KEDDIE

4. D. G. Fox:

   Modeling Mountain Air Quality for Land Use Planning

   (D. G. Fox, U.S. Department of Agriculture,
   Forest Service, Rocky Mountain Forest and
   Range Experiment Station, 240 West Prospect St.,
   Fort Collins, Colo. 80521, U.S.A.)

5. L. L. Wendell:

A Regional Scale Model for Computing Deposition and Ground Level Air Concentration of SO_2 and SO_4 from Elevated and Ground Sources

(L. L. Wendell, D. C. Powell, R. L. Drake,
Battelle Pacific Northwest Lab., Battle Blvd.,
Richland, Washington 99352, U.S.A.)

6. N. V. Gillani:

1. Analytical-Numerical Model for Mesoscale Transport, Transformation and Removal of Air Pollutants
2. A Study of Long Range Transport from Visibility Observations, Trajectory Analysis and Local Air Pollution Monitoring Data

(R. B. Husar, N. V. Gillani, J. D. Husar,
Washington, Univ., Dept. of Mechanical
Engineering, St. Louis, Missouri, 63130, USA)

Thursday, September 9, 1976

Presentation and Discussion of Topic 3:

Sensitivity Analysis and Dispersion under Low Wind Speeds

Chairman: K. L. CALDER

Rapporteur: R. A. PORTER

1. R. F. Lee:

   A Sensitivity Analysis of the Single Source (CRSTER) Model

   (W. P. Freas, R. F. Lee, Source Receptor Analysis Branch, OAQPS, U.S. Environmental Protection Agency, Research Triangle Park, N. C. 27711, USA)

2. R. L. Clayson

   Concentration and Index Sensitivity of Gaussian Plume Model

   (W. J. Veigele, R. L. Clayson, Resource Science Institute of Kappa Systems, Inc., 1409 Potter Drive, Colorado Springs, Colorado 80909, USA)

3. R. J. Yamartino:

   An Air Quality Dispersion Model Applicable to Calm Conditions

   (R. J. Yamartino, Jr., Energy and Environmental Systems Div., Argonne National Lab., 9700 S. Cass Ave., Argonne, Ill., 60439, USA)

4. K. Herrmann:

   The Role of Turbulent Diffusion in the Direction of the Mean Wind in a Numerical AQSM

   (K. Herrmann, Institut für Meteorologie der TH Darmstadt, Hochschulstr. 1, D - 6100 Darmstadt)

5. L. Kropp:

   Influences of Model Parameters and Sensibility to their Variation within the Emissions Forecasting

   (L. Kropp, H. Bresser, Technischer Überwachungsverein Rheinland, Postfach 101750, 5 Köln 1)

Presentation and Discussion of Topic 4:

Numerical Grids and Physical Modeling

Chairman: H. G. FORTAK

Rapporteur: D. G. FOX

1. R. S. Thompson:

   Dispersion of Roof-Top Emissions from Isolated Buildings - A Wind Tunnel Study

   (R. S. Thompson, Meteor. and Assess. Div.,
   Environmental Sciences Research Lab.,
   D. J. Lombardi, Northrop Services Inc.,
   Research Triangle Park, N. C. 27711, USA)

2. E. Runca:

   An Efficient Quality K-Model and its Application to Venice

   (E. Runca, Centro Scientifico IBM,
   Palazzo Giustiniani, Dorsoduro 3228,
   30123 Venezia, Italia)

3. G. L. Marziano:

   Further Developments in the Application of Shir's Model to the Venice Area

   (G. L. Marziano, A. Sutera, L. Gianolio,
   Instituto Ricerche "G. Donegani", Soc.
   Montedison, Via del Lavoro, 4,
   I - 28100 Novara)

4. B. A. Egan:

   A Three-Dimensional Advective-Diffusive Model for Long-Range Sulphate Transport and Transformation

   (B. A. Egan, K. S. Rao and A. Bass,
   Environmental Research and Technology Inc.,
   696 Virginia Road, Concord, Mass. 01742, USA)

5. J. Giebel:

   An empirical equation for simulating maximum concentration values occurring at buildings projecting into the path of a plume in the immediate vicinity of an emission source.

   (J. Giebel, Landesanstalt für Immissions- und Bodennutzungsschutz, Wallneyer Str., D - 43 Essen-Bredeney)

Presentation and Discussion of Topic 5:

Tall Stack Plume, including Sulphate Transformation and Removal Processes

Chairman: L. KROPP

Rapporteur: W. B. JOHNSON

1. H. E. Cramer

   Improved Techniques for Modeling the Dispersion of Tall Stack Plumes

   (H. E. Cramer, H. E. Cramer Co., Inc.
   P.O.B. 8049, Salt Lake City, Utah, 84108, USA)

2. F. Fanaki, H. E. Turner
   R. V. Portelli, M. Lusis:

   a) Plume Rise and Behaviour of Emissions from a Tall Stack

   b) Diffusion Parameters from Tall Stack Plumes

   c) A Comparison of "STAR" and Measured Lapse-Rate Stability Classifications with Observed Tall Stack Plume Dispersion Parameters

   d) Mathematical Modeling of Chemical Reactions in a Plume, with Application to a Tall Stack

   (F. Fanaki, H. E. Turner, R. V. Portelli,
   M. M. Millan, M. Lusis, Atmospheric Environment
   Service Canada, 4905 Dufferin Street,
   Downsview, Ontario, M3H 5T4, Canada)

3. D. R. Kalthoff:

   On SO_2 Removal and Sulphate Formation Processes in the Atmosphere

   (Mrs. D. Kalthoff, Institut für Meteorologie
   und Geophysik, Feldbergstr. 47, D-6000 Frankfurt/M. 1,)

4. W. E. Wilson:

   Sulfate Transformation and Removal Processes in Power Plant Plumes

   (W.E. Wilson, U.S. Environmental Protection Agency,
   Research Triangle Park, N.C., 27711, R. Husar,
   Washington University, K. T. Whitby, University
   of Minnesota, U.S.A.)

Friday, September 10, 1976

Presentation and Discussion of Topic 6:

Diffusion Parameters and Stability Categories

Chairman: J. R. MAHONEY

Rapporteur: R. F. LEE

1. A. Longhetto:

   Comparison between Experimentally Measured Diffusion Parameters and the Main Stability Criteria

   (L. Santomauro, Osservatorio Meteorologico di Brera, Milano, D. Anfossi Laboratorio di Cosmogeofisica del CNR, Torino; P. Bacci, A. Longhetto, ENEL, Centro Ricerca Termica e Nucleare, Milano, Italia)

2. M. Ribon:

   Experimental Study of Atmospheric Diffusion Parameters

   (A. Saab, M. Ribon, Electricité de France, Direction des Etudes et Recherches, 6, Quai Watier, F-78400 Chatou, France)

Presentation and Discussion of Topic 7:

Innovative Modeling Techniques

Chairman: A. W. C. KEDDIE

Rapporteur: D. M. ROTE

1. H. ApSimon:

   Modeling the Atmospheric Dispersal of Radioactive Pollutants beyond the First Few Hours of Travel

   (Mrs. H. ApSimon, A. J. H. Goddard, Nuclear Power Section, Mechanical Engineering Department, Imperial College of Science and Technology, GB - London S. W. 7)

2. R. A. Anthes:

   Diffusion and transport of a Passive Contaminant over Complex Terrain under Stable and Unstable Conditions

(R. A. Anthes, N. Seaman, D. Kayser, Pennsylvania State University, Dept. of Meteorology, 543 Deike Bldg., University Park, Pennsylvania, USA)

3. H. G. Fortak:

   On Theoretical Methods for the Solution of Complex Urban Air Pollution Problems

   (H. G. Fortak, Deutsche Forschungs- und Versuchsanstalt für Luft- und Raumfahrt e.V., Institut für Physik der Atmosphäre, and Free Univ. of Berlin, D - 8031 Oberpfaffenhofen, Post Wessling, Obb)

4. K. H. Muller:

   Pollutant Dispersion Simulation by Monte Carlo Techniques

   (K. H. Muller, CCR EURATOM, I 21020 Ispra)

5. F. Corazzari:

   Mathematical Model for Urban Diffusion of Carbon Monoxide from Motor Vehicles

   (F. Corazzari, Laboratori Centrali Fiat, Strada Torino 50, I - 10043 Orbassano, Torino)

7 th NATO/CCMS
International Technical Meeting
on Air Pollution Modeling

ATTENDEES

AIRLIE HOUSE, AIRLIE, VIRGINIA
UNITED STATES OF AMERICA

Richard Anthes
Department of Meteorology
Pennsylvania State University
543 Deike Building
University Park, Pennsylvania 16802

Hella Bartels
Deutscher Wetterdienst
Zentralamt, Ref. K 8
605 Offenbach,
Frankfurter Str. 135
FEDERAL REPUBLIC OF GERMANY

Andre L. Berger
Institut d'Astronomie et de
Geophysique
University of Louvain
2, Chemin du Cyclotron
1348 Louvain-La-Neuve
BELGIUM

Anton Braig
Battelle-Institut e.V.
Am Römerhof 35
6000 Frankfurt a. Main
FEDERAL REPUBLIC OF GERMANY

Reid L. Clayson
Kappa Systems, Inc.
1409 N. Potter Drive
Colorado Springs, Colorado 80909

Harrison E. Cramer
H. E. Cramer Co., Inc.
P. O. Box 8049
Salt Lake City, Utah 84108

Bruce Egan
Environmental Research and
Technology, Inc.
3 Militia Drive
Lexington, Mass. 02173

Helen ApSimon
Mechanical Engineering
Imperial College of Science and Technology
Prince Consort Road
London SW 7, ENGLAND

Robert Bauman (MD-12)
Strategies and Air Standards Division
U.S. Environmental Protection Agency
Research Triangle Park, NC 27711

Norman Bowne
TRC - Research Corporation of New England
125 Silas Deane Highway
Wethersfield, Connecticut 06109

Kenneth L. Calder
Meteorology and Assessment Division(MD-80)
U.S. Environmental Protection Agency
Research Triangle Park, N.C. 27711

F. Corazzari
Laboratori Centrali Fiat
Strada Torino 50
I-10043 Orbassano (Torino)

Bernd Dietzer
TH Darmstadt
Sektion Meteorologie
Hochschulstr. 1
D-6100 Darmstadt
FEDERAL REPUBLIC OF GERMANY

Fouad Fanaki
Atmospheric Environment Service
4905 Dufferin Street
Downsview, Ontario
CANADA M3H5T4

H. Fortak
Deutsche Forschungs- und Versuchsanstalt
für Luft- und Raumfahrt e.V.
Institut für Physik der Atmosphäre
D-10831 Oberpfaffenhofen
Post Wessling/OBB
FEDERAL REPUBLIC OF GERMANY

Douglas Fox
Rocky Mountain Forest and Range
Experiment Station
240 W. Prospect Street
Fort Collins, Colorado 80521

Friedhelm Gerold
Technischer Überwachungs-Verein
Rheinland e.V.
Postfach 101750
D-5000 Köln 1
FEDERAL REPUBLIC OF GERMANY

Josef Giebel
Landesanstalt f. Immissions-
u. Bodennutzungsschutz des
Landes NRW
Wallneyer Str. 6
D-4300 Essen-Bredeney
FEDERAL REPUBLIC OF GERMANY

Noor Gillani
Department of Mechanical Engineering
Washington University
Box 1185
St. Louis, Missouri 63130

H. Goumans
Ministerie van Volksgezondheit
and Milieuhygiene
DG-MH Sanering Rijnmondgebred
Doctor Reyerstraat 12
DAL 31, Leidschendam
THE NETHERLANDS

Roberto Gualdi
Laboratorio Provinciale di Igiene
E Profilassi
Via Juvara 22
Milano, ITALY

Peter Guldberg
Walden Research
Division of ABCOR
850 Main Street
Wilmington, Massachusetts 01887

James Hammerle (MD-14)
Monitoring and Data Analysis Division
U.S. Environmental Protection Agency
Research Triangle Park, NC 27711

Klaus Herrmann
Technische Hochschule Darmstadt
Institut f. Meteorologie
Hochschulstr. 1
D-6100 Darmstadt
FEDERAL REPUBLIC OF GERMANY

Glenn R. Hilst
TRC - Research Corporation of New England
125 Silas Deane Highway
Wethersfield, Connecticut 06109

John Irwin
Meteorology & Assessment Division (M
(MD-80)
U.S. Environmental Protection
Agency
Research Triangle Park, N.C. 27711

Warren B. Johnson, jr.
Atmospheric Sciences Laboratory
Stanford Research Institute
333 Ravenswood Avenue
Menlo Park, California 94025

Dieter Jost
Umweltbundesamt
Bismarckplatz 1
D-1000 Berlin 33
FEDERAL REPUBLIC OF GERMANY

Dagmar Kalthoff
Universitätsinstitut für
Meteorologie und Geophysik
Feldbergstr. 47
6000 Frankfurt a. Main
FEDERAL REPUBLIC OF GERMANY

Alistair Keddie
Department of Industry
Warren Spring Laboratory
Gunnels Wood Road
Stevenage, Herts, 2G1 2 BX
UNITED KINGDOM

Werner Klug
Institut für Meteorologie
Technische Hochschule Darmstadt
D-6100 Darmstadt
FEDERAL REPUBLIC OF GERMANY

Joe Knox
Lawrence Radiation Laboratory
P. O. Box 808
Livermore, California 94550

J. G. Kretzschmar
SCK/CEN - 200 Beoretang Mol
B-2400
BELGIUM

L. Kropp
Technischer Überwachungsverein
Rheinland e.V.
Postfach 101750
D-5000 Köln 1
FEDERAL REPUBLIC OF GERMANY

Michael Kwizak
Atmospheric Environment Service
4905 Dufferin Street
Downsview, Ontario
CANADA M3H 5T4

Gale Hoffnagle
INTERA Environmental Consultants,
Ltd.
1201 Dairy Ashford Road
Houston, Texas 77079

R. F. Lee
Environmental Protection Agency
Office of Air Quality Planning and
Standards
Research Triangle Park
North Carolina 27711

Arnoldo Longhetto
Osservatorio
Meteorologico di Brera
Via Brera, 28
I-20121 Milano
ITALY

Maris Lusis
Atmospheric Environment Service
4905 Dufferin Street
Downsview, Ontario
CANADA M3H 5T4

Louis M. Malet
Royal Meteorological Institute
of Belgium
Avenue Circulaire 3
B 1180 Brussels
BELGIUM

G. L. Marziano
Instituto Richerche "G. Donegani"
Soc. Montedison
Via del Lavoro, 4
28100 Novara
ITALY

H. Meinl
Dornier-System GmbH
Postfach
7990 Friedrichshafen
FEDERAL REPUBLIC OF GERMANY

K. H. Müller
Eurotom - Ispra
Division Physik
I-21020 Centro Euratom
Di Ispra (Varese)
ITALY

Lewis Nagler
EPA, Region IV
1421 Peachtree Street, N.E.
Atlanta, Georgia 30309

Christer Persson
Swedish Meteorological and
Hydrological Inst.
Fack S-60101
Norrkoping, SWEDEN

Richard A. Porter
Texas Air Control Board
8520 Shoal Creek Blvd.
Austin, Texas 78758

Donald Rote
Argonne National Laboratory
Argonne, Illinois 60439

Ronald C. Salley
AFCEC/EVP
Tyndall AFB, Florida 32401

T. Schneider
National Institute of Public
Health
P. O. Box 1
Bilthoven, NETHERLANDS

Lloyd L. Schulman
Environmental Research and
Technology, Inc.
696 Virginia Road
Concord, Maine

Louis Shenfield
Supervisor, Air Quality and
Meteorology
Environment Ontario
Air Resources Branch
880 Bay Street, 4th Floor
Toronto, Ontario
CANADA M4V1P5

Hersch Slater
Monitoring and Data Analysis
Division (MD-12)
Environmental Protection Agency
Research Triangle Park, N.C.27711

Frans Nieuwstadt
Royal Netherlands
Meteorological Institute
Utrechtseweg 297
DeBilt, NETHERLANDS

Ronald Portelli
Atmospheric Environment Service
4905 Dufferin Street
Downsview, Ontario
CANADA M3H5T4

Michel Ribon
Electricité de France
Direction des Etudes et Recherches
6, Quai Watier
F-78400 Chatou
FRANCE

Eliodoro Runca
IBM Centro Scientifico
Dorsoduro 3228
30123 Venezia
ITALY

Luigi Santomauro
Director, Osservatorio Meteorologico
di Brera
Via Brera 28
20121 Milano
ITALY

Heinrich Schultz
Theodor Storm Str. 5
3007 Gehrden
FEDERAL REPUBLIC OF GERMANY

Bjarne Sivertsen
Norwegian Institute for Air Research
P. O. Box 130
N-2001 Lillestrom
NORWAY

Winston A. Smith
EPA, Region IV
1421 Peachtree St., N.E.
Atlanta, Georgia 30309

R. Stern
Freie Universität Berlin
Institut für Theor. Meteorologie
D-1000 Berlin
FEDERAL REPUBLIC OF GERMANY

Roger S. Thompson
Environmental Sciences Research
Lab. (MD-81)
U. S. Environmental Protection
Agency
Research Triangle Park, N.C.27711

D. Bruce Turner
Meteorology and Assessment
Division (MD-80)
U. S. Environmental Protection
Agency
Research Triangle Park, N.C.27711

William Veigele
Vice President
Kappa Systems, Inc.
1409 No. Potter Drive
Colorado Springs, Colorado 80909

Erich Weber
Regierungsdirektor
Bundesministerium des Innern
Rheindorfer Str. 198
5300 Bonn/Rhein
FEDERAL REPUBLIC OF GERMANY

William Wilson
U.S. Environmental Protection
Agency (MD-59)
Research Triangle Park
North Carolina 27711

J. A. Wisse
Royal Netherlands Meteorological
Inst.
Utrechtseweg 397
DeBilt, NETHERLANDS

A. Venkatram
Atmospheric Environment Service
Environment Canada
4905 Dufferin Street
Downsview, Toronto
Ontario, CANADA M3H5T4

Frank Trivero
FIAT Research & Development
One Parklane Blvd.
Parklane Towers West Suite 1210
Dearborn, Michigan 48126

Edward Turner
Atmospheric Environment Service
Environment Canada
4905 Dufferin Street
Downsview, Ontario
CANADA M3H5T4

Alexander von Hesler
Regionale Planungsgemeinschaft Untermain,
Zeil 127
6000 Frankfurt a. Main
FEDERAL REPUBLIC OF GERMANY

Larry Wendell
Battelle Pacific N.W. Labs.
Battelle Blvd.
Richland, Washington 99352

Ken Wiltsee
Walden Research
Division of ABCOR
850 Main Street
Wilmington, MA 01887

Robert J. Yamartino, jr.
Energy and Environmental Systems Division
Argonne National Laboratory
9700 South Cass Avenue
Argonne, Illinois 60439

*U.S.GOVERNMEI ' PRINTING OFFICE:1977 740 -110/309 REGION NO. 4